QUANTIFYING THE EFFECT OF A FATIGUE CRACK ON THE RESIDUAL STRESS FIELD INDUCED BY THE SPLIT SLEEVE COLD EXPANSION PROCESS IN 2024-T351 AND 7075-T651 ALUMINUM ALLOYS

by

Scott Spencer Carlson

A dissertation submitted to the faculty of
The University of Utah
in partial fulfillment of the requirements for the degree of

Doctor of Philosophy

Department of Mechanical Engineering

The University of Utah

May 2018

The University of Utah Graduate School

STATEMENT OF DISSERTATION APPROVAL

The dissertation of **Scott Spencer Carlson**

has been approved by the following supervisory committee members:

David W. Hoeppner	, Chair	**Nov. 6, 2017** Date Approved
Kenneth L. DeVries	, Member	**Nov. 6, 2017** Date Approved
Daniel O. Adams	, Member	**Nov. 6, 2017** Date Approved
Mark L Thomsen	, Member	**Nov. 6, 2017** Date Approved
Michael R. Hill	, Member	**Nov. 6, 2017** Date Approved
Paul N. Clark	, Member	**Nov. 6, 2017**

and by **Tim A. Ameel** , Chair/Dean of

the Department/College/School of **Mechanical Engineering**

and by David B. Kieda, Dean of The Graduate School.

ABSTRACT

In fatigue and fracture critical aerospace structure, fastener holes represent one of the most highly prone locations for the nucleation and propagation of fatigue cracks. The Split Sleeve Cold Expansion^{TM} (SSCx) process was developed to help reduce the probability of fatigue crack propagation at fastener locations. The SSCx process has been demonstrated to provide a dramatic improvement in the fatigue life at processed hole, however within the current fatigue life paradigms there is limited ability to take analytical advantage of this process when calculating an inspection interval. One of the concerns related to the implementation of this type of deep, engineered residual stress into a fatigue life calculation is whether or not a fatigue crack that propagates through the residual stress/strain field is changed due to the presence of the fatigue crack. In order quantify the effect a fatigue crack has on the residual stress field around a cold expanded (Cxed) hole within two common aluminum alloys (2024-T351 and 7075-T651), first a series of baseline uncracked coupons were developed. From these groups of replicate coupons, the two-dimensional residual stress fields were quantified using the contour method.

In the second phase of this program, fatigue cracks were then developed and propagated within identical coupons to specific cold expansion (Cx) mandrel entrance surface lengths, ranging from 0.08 inch to 0.50 inch. The contour method was used to

determine the residual stresses within these fatigue-cracked coupons. With a statistical understanding of the baseline, uncracked condition, the effect of the presence of the fatigue crack spatial throughout the coupon was able to be quantified.

The effect of the fatigue crack was then integrate into a range of FEA simulation processed used to calculate SIFs and provide a prediction of a given test condition. Predictions were made using the legacy, static residual stress field, as determined by the baseline, uncracked coupons. We then utilized the information gained through the residual stressed determined in the fatigue-cracked coupons to make another prediction. Through the integration of the determined effect of the fatigue crack a more accurate prediction of the test condition was able to be developed.

TABLE OF CONTENTS

ACKNOWLEDGEMENTS

I would like to first and foremost thank my amazing wife, Catherine, and our now seven wonderful children for all their support throughout this project. When I started down this path we only had three children, so this has been a family project for sure, and that family has changed a lot as we have progressed through this. You are all truly the light in my life. I would also like to thank my parents and all of their support and encouragement throughout this process.

I would like to thank my graduate committee, Dr. David Hoeppner, Dr. Mark Thomsen, Dr. Dan Adams, Dr. Larry DeVries, Dr. Paul Clark, and Dr. Mike Hill for all of their support and leadership throughout this process. It has taken quite a long time to complete and their patience has been incredibly valuable to me.

I would also like to thank the A-10 Aircraft Structural Integrity Program (ASIP) office for being willing to put on contract this effort. Without which this program would have never been able to be accomplished. Thank you, Dr. Mark Thomsen! I would also like to thank AP/ES Incorporated for the manufacturing, and fatigue crack growth testing, of the coupons used for this research. Thank you, Dr. Tom Mills for your attention to detail during the manufacturing and testing of them. I would also like to thank Marcus Stanfield for all of his assistance in helping to update and debug the contour method code that we were provided by Dr. TJ Spradlin. Marcus, without your help there is no way

that I could have ever been able to overcome the challenges that were presented through this work. My deepest thanks goes to you. Thank you, Dr. Spradlin, for allowing me access to the code that you used on your dissertation. I also need to thank Dr. Michael R. Hill (University of California, Davis) for allowing me access to the displacement data produced under contracts from the USAF.

I need to especially thank Dr. David Hoeppner, my chair. There is no way to express the influence you have had on me. Through sitting at your feet and listening to your life experiences I have come to love learning and it is because of that love for learning that I have pushed this far to try and understand this question and gain this degree. Thank you Dr. Hoeppner, from the bottom of my soul.

This has been a long program to complete and through it I have gained many wonderful friends. It has also caused much contention amongst some in and out of my committee, and that has been the sources of some of the darkest times of my life. I have had the opportunity to grow quite a bit through this experience. It would seem that out of the darkest times can come one of the greatest sources of light.

1 INTRODUCTION

1.1 Hypothesis

It is well known that the Split Sleeve Cold Expansion™ (SSCx)* can provide a significant fatigue life improvement when applied to tension dominated fatigue and fracture critical structure. However, there are many questions that must still be answered in order to allow government agencies and the commercial aerospace industry to take analytical advantage of this fatigue life advantage in the calculation of initial and recurring inspection intervals within the damage tolerance lifing paradigm. One of these key questions is whether a fatigue crack effects the residual stress field that is introduced by the Cold Expansion (Cx) process.

Within the damage tolerance paradigm, it is assumed that a "rogue" flaw is present within the structure, in the most critical location, and orientation possible. The rogue flaw is defined at holes as being a 0.05 inch x 0.05 inch circular corner flaw. If a critical fastener hole has been Cold Expanded (Cxed) it is possible to reduce this rogue flaw down to a size of 0.005 inch x 0.005 inch. This reduction in the initial flaw size (IFS) must be validated through test to ensure the conservative nature of this change, when applied to the given critical structural location. [1,2] The rogue flaw assumption

---

* The term Split Sleeve Cold Expansion™ (SSCx) is commonly referred to as just the Cold Expansion (Cx) process, and will be referred to as this from here on.

within the damage tolerance paradigm requires a quantification of the behavior of a fatigue crack as it propagates through the residual stress field at a Cxed hole. If the effect of the fatigue crack on the residual stress field can be well understood, it may enable a more accurate life prediction for critical airframe structure. In order to quantify the effect a fatigue crack has on the residual stress field imposed by the Cx process, this work focused on the quantification of the baseline, uncracked residual stress field which was introduced into two common aluminum alloys, 2024-T351 and 7075-T651. These two aluminum alloys represent a typical range of the strength and fracture toughness for aerospace structural materials, thus helping to bound the scope of this work.

In an effort to minimize the scatter that would be in the residual stress/strain field introduced into the material by the Cx process a targeted level of applied expansion was developed. Within the Fatigue Technology Incorporation (FTI) Cx specification there is a range of applied expansion levels for these two aluminum alloys at the final hole diameter of 0.5 inch.[3] This ranges from 3.16% to 4.16% applied expansion. All of the coupons that will be investigated will be machined to a goal tolerance level which was 3.16%. The goal of this was to minimize the repeatability uncertainty associated with the Cx process.

In order to develop a baseline residual stress field understanding, multiple replicates were developed at the specified applied expansion level. For the 2024-T351 material five coupons were developed and for the 7075-T651 material three were manufactured. From these the residual stresses were determined using the contour method. Through the understanding of these baseline, uncracked Cxed coupons it was possible to determine the repeatability and single measurement uncertainties associated

with the determined stress fields.

As stated, one of the fundamental assumptions of the damage tolerance paradigm is the presence of a rogue flaw at critical locations. As previously mentioned, at Cxed holes this would be defined as a semicircular corner flaw. Thus, in an effort to apply this work within the damage tolerance paradigm, additional replicate coupons to the baseline, uncracked coupons were manufactured and fatigue cracks were developed as corner cracks and propagated to a range of corner crack and through-thickness crack lengths. For most of these coupons two replicates were produced, but for the longer cracks, 0.25 inch and 0.50 inch, only a single coupon was produced. From these fatigue-cracked coupons the residual stress field was determined following the exact same contour method process as that developed and implemented for the baseline, uncracked coupons. Thus, residual stresses were determined using the same method for both the baseline, uncracked condition, and for a range of fatigue-cracked conditions. With a statistically based quantification of the baseline, uncracked condition available, it was possible to compare and quantify, from a statistical perspective, the effect of a fatigue crack on the residual stress field introduced by the Cx process in these two aluminum alloys.

With this now quantified, fatigue crack growth predictions can be performed at a range of statistical distributions of the defined residual stress fields for both the baseline, uncracked condition along with the fatigue-cracked condition. These fatigue crack growth predictions would provide an additional basis to quantify the effect of the fatigue crack on the residual stress field. One of the difficulties associated with the determination of residual stresses within a body is that there is no measurement method by which one can know the “true” residual stress field within a given body. Once a

measurement of any kind is taken it potentially disturbs the system, and thus has the potential to influence the accuracy of the measurement. Due to the process associated with residual stress determination methods there is no way to know the accuracy of the residual stresses. Thus it is often useful to incorporate the residual stresses into another model form, such as a fatigue crack growth model. Through this it is possible to make a fatigue prediction, with and without the inclusion of the determined residual stress field, and to compare those results to a test condition. If the inclusion of the determined residual stresses allows for a more accurate prediction of the given fatigue test, then this can increase the confidence one has in the determined, and integrated residual stress field. For this program, residual stress fields were determined for both the baseline, uncracked and the fatigue-cracked conditions. Both sets of residual stress data were then included into a fatigue crack growth prediction, with the goal of determining if the integration of the effect of the fatigue crack on the residual stress field would improve the accuracy of the life prediction. If it did, this would add an additional layer of confidence to answer the question of whether or not the presence of a fatigue crack changes the residual stress field that is introduced into 2024-T351 and 7075-T651 by the Cx process, by allowing for a more accurate prediction of the given test condition, in which a fatigue crack was propagated through a replicate residual stress field.

Through this work it is hoped that future analytical methods will be able to take into account the effect of a fatigue crack on the residual stress field imposed through the Cx process resulting in more accurate fatigue life predictions. In addition, this work would allow for an advancement of the state of the art within not only linear elastic fracture mechanics (LEFM) but also this information would effect how non-destructive

inspections (NDI) are performed on critical structures which contain compressive residual stresses. It is often accepted that the presence of a fatigue crack has an affect on the residual stress field imposed by the Cx process, however limited work has been performed to quantify this effect in a statistical manner.

1.2 Application of the Cold Expansion (Cx) Process to Critical Aerospace Fastener Holes

In fatigue and fracture critical aircraft structures, fastener holes represent one of the most critical geometric notches/discontinuities. Under far-field tension-loading these stress concentrations are often the locations where fatigue cracks nucleate/form and propagate from. Due to this, often field and heavy depot maintenance is scheduled under the prediction that fatigue cracks have propagated from these critical fastener holes. In an effort to increase the length of time before an initial inspection, and between recurring inspections, the Cx process was developed in the early 1970s by the Boeing Company, then later patented and marketed by Fatigue Technology Incorporation (FTI).[4,5] The Cx process is performed by hydraulically pulling a tapered mandrel and lubricated sleeve through the critical fastener hole. The combined maximum diameter of the mandrel and the sleeve is greater than the diameter of the hole, thus when the mandrel is pulled through the hole it expands radially, introducing a region of plastic strain closely around the hole.[6,7] These plastic strains introduce a broader region of elastic strain that can reach up to one diameter away from the hole. The combination of these two strain regions is what produces the residual stress field within the processed material. Fig. 1 provides a simple schematic of the Cx process.

Through the Cx process a beneficial residual, or self-stress, is introduced at the

critical fastener hole. The magnitude and depth of the residual stress field varies due to many factors, such as material, initial hole diameter, and thickness. However, a general "rule of thumb" is that the near hole bore the compressive residual stresses are close to the material yield strength (σ_{yield}) and from there they decrease to where it becomes a positive stress at around one radius away from the edge of the hole.[8,9,10] A photo-elastic image of this general self-stress field can be seen in Fig. 2 and a legacy three-dimensional (3D) representation of the residual stress field, as determined by neutron diffraction, is provided in Fig. 3.

Much research and testing has been performed, from the simple coupon, to the major component level, that demonstrates the fatigue life benefits that can be obtained by applying the Cx process to fatigue and fracture critical structure.[11,12,13,14] However, there has been limited success in the prediction of fatigue life and crack shape evolution at Cx holes.[15,16,17,18,19,20,21]

1.3 Historical Perspective on the Implementation of the Residual Stress Field from the Cx Process into Fatigue Crack Growth Predictions

In order to more accurately model the fatigue crack evolution at a Cx hole it was necessary that two major improvements be made. First is the ability to model and calculate/develop SIFs at multiple points along a simulated crack front. Legacy methods often only solve for the SIF at two locations for a semicircular crack propagating from the edge of a fastener hole, near the surface of the part, and at the bore of the hole.[22] The ability to calculate SIFs at multiple points along the crack front allows for a more holistic understanding of the crack driving force for the entire crack. Since the crack front acts as a whole within a body, each point along the crack striving to find its lowest energy level,

"pulling" and or "pushing" the locations along the crack front. Thus, if one is only able to calculate two points along the crack front it is unlikely that it would be possible to quantify the crack front shape and driving force accurately. The second major improvement was the ability to impose within the finite element analysis (FEA) an "accurate" residual stress field.[19] Currently there are two major methods for the development of this "accurate" residual stress field.

The first method by which a residual stress can be determined is through the use of a finite element analysis (FEA) process simulation of the Cx process.[23,24,25,26,27] The other method is to utilize a residual stress "measurement" process by which the residual stress field within the material can be determined through a displacement or strain measurement.[28,29,30,31,32,33,34]

The term "residual stress measurement" is ubiquitous within the residual stress field and a short discussion of the author's perspective on this is needed. Many definitions exist for the terms "measure" and "measurement" and they do not all seem to relay the same information. For instance, the Oxford's English Dictionary, from 1971, defines "measure" in twenty-two different ways and "measurement" in four different ways.[35] Provided are the first few for context.

Measure

1. "*The action or process of measuring, measurement.*"
2. *"Size or quantity as ascertained or ascertainable by measuring."*

Measurement

1. *"The action or an act of measuring."*
2. *"A dimension ascertained by measuring, size or extent measured by a standard."*
3. *"A system of measuring or of measure."*

The 1994 Webster's II New Riverside University dictionary has nine definitions of the

word “measure”.[36] For this I will only provide the first two of them as follows:

Measure

1. *“Dimensions, capacity, or quantity as determined by measuring.”*
2. *“A reference sample or standard used for the quantitative comparison of properties.”*

The term “measurement” has three different definitions contained within the Webster’s II New Riverside University. They are provided as follows:

Measurement

1. *“The act of measuring or process of being measured.”*
2. *“A system of measuring.”*
3. *“The dimension, capacity, or quantity determined by measuring.”*

It can be seen from these two examples that the terms “measure” and “measurement” have a requirement of the act of measuring a specific defined quantity. The contour method does perform this action directly by measuring the topography of the specific surfaces of interest. Some have called this action a “fundamental” measurement.[37] Examples of quantities that may be directly measured are number, mass, volume, length, angle, period of time, force, electrical resistance, current, and voltage. Those measurements that require additional calculations can be called “dependent” or “derived.” These include dimensions such as temperature, hardness, density, magnetic permeability, and stress.[38] Many of the measurements that are performed within the scientific and philosophical communities require both fundamental and derived quantities. The contour method is no different. Thus it would be proper to state that the residual stress within a body is a derived measurement, or even an “indirect measurement,” requiring the fundamental measurement of the surface topography and from the residual stress is able to be determined via a secondary derived measurement.

This is possibly the reason that the current version of the Oxford English Dictionary provides a definition for the term “measurement” as:

Measurement

1. *“The action or an act of measuring or calculating a length, quantity, value, etc.”*

This definition of measurement allows for the inclusion of the act of a “derived” measurement in which a quantity is calculated. Thus through the inclusion of the philosophy that there are both “fundamental” and “derived” measurements it is possible to include the term measurement to the method by which the residual stress is quantified. If possible it would be more correct to state that the residual stress is a “derived” or “indirect” measurement, but often for simplicity when communicating it is shortened to just measurement. The author will work to clarify within this document the term used for the quantification of the residual stress within a body by using the term “determined.” This word is defined within the current in Oxford English Dictionary in nineteen different ways. The eleventh form of the word best suits the purposes of this work:[39]

Determine

1. *“To ascertain definitely by observation, examination, calculation, etc., (a point previously unknown or uncertain); to fix as known.”*

It is hoped that through the proper vocabulary it will be possible to clarify the results obtained within this document and also the process. It is said that “the first step to wisdom is getting things by their right names.”[40]

Back to the development of residual stresses through both a FEA-based approach and through the use of residual stress determination methods. Each of the two methods used for the quantification of the internal residual stress field, imposed by the Cx process,

have their own shortcomings and difficulties. In order to obtain accurate results, the FEA simulation requires very accurate material models for both the elastic and plastic behavior of the material curve, along with an accurate representation of the entire Cx process. The use of weight functions is also another approach that has been developed and used.[41,42,43] This approach also requires an accurate understanding of the residual stress field and then must also be implemented under the appropriate constraints.

The quantification of a residual stress field via any of the many residual stress determination processes produces an estimate of the residual stress with some level of spatial uncertainty associated with it. There is no way to determine the "true" residual stress or stain field that is contained within the body and so some quantification of the spatial uncertainty is necessary in order to provide a bound on the accuracy of the given quantity. In addition, for many of the residual stress determination processes there are no community-accepted standards for taking the measurements or processing data, akin to what is available for other material response quantification methods, such as the development of tensile strength, fracture toughness, or crack growth data.[44,45,46]

In addition to the spatial uncertainty, many of the methods lack the spatial resolution needed to implement within a fatigue crack growth prediction. Due to the steep gradient, over a relatively short distance, it is essential that the determined residual stress field has the ability to capture this radial gradient, as well as the through-thickness change. These requirements limit the number of residual stress determination processes that are available to provide a 2D residual stress field that can be utilized within a fatigue crack growth prediction.

1.4 Limitations of Current Approaches to the Implementation of Deep Residual Stresses into Fatigue Life Predictions for Fatigue and Fracture Critical Structure

1.4.1 Quantification of the Uncertainty of Determined Residual Stresses via the contour method

One residual stress determination method that has presented a very promising means by which the spatial density and accuracy can be overcome is the contour method. Through this method a 2D residual stress "map" can be provided.[47] This method allows for residual stresses to be provided at a spatial resolution of approximately 0.005 inch x 0.005 inch across the area of interest. However, no effort has been placed to quantify the spatial uncertainty associated with this method when used to determine the residual stresses around a Cxed hole. If the contour method were to be used as the means for implementing residual stresses at Cxed holes into fatigue crack growth predictions, it would be necessary to quantify the spatial uncertainty associated with this method. This would allow for statistical confidence in both the residual stress fields that are produced and the final predicted fatigue life.

1.4.2 Implementation of Deep Engineered Residual Stress Fields into Fatigue crack Growth Predictions

With the current capabilities to determine or predict the residual stress within the material that has been Cxed, there still exists limitations in the ability to integrate the residual stress field into life prediction software. Legacy methods for predicting the fatigue crack shape evolution along with the total life of a part have commonly provided only two SIFs when solving for crack progression at a corner crack next to a hole. This is often sufficient to allow for accurate predictions of fatigue cracks when there is no deep residual stress field within the material adjacent to the hole.[48] This is because the corner

crack often propagates at an aspect ratio (bore crack length (a)/surface crack length (c)) between 1 and 1.5.[49,50,51,52] However, for cracks that propagate from Cx holes, the aspect ratio does not stay within these bounds.[53] Fatigue cracks that propagate out of Cx holes can take on very unique shapes as seen in Fig. 4.[54,55] In order to capture this type of fatigue crack growth shape evolution it is essential that the crack growth analysis software has the ability to calculate SIF at multiple points along the crack front. Through this process it will then allow the crack growth rate to be applied to each individual nodal location within the analysis.[56] This is now possible through the integration of AFGROW (a fatigue crack growth software) and StressCheck® (a p-version FEA software package that can be used to calculate SIF).[57] The Visual Basic Plug-in, Broad Application for Modeling Failure (BAMF), allows for the integration of a two-dimensional (2D) residual stress field as a crack-face traction, entitled the Contour Integral Method for Loaded Cracks (CIM-LC).[58] Currently there are additional software choices that provide a similar ability to calculate SIFs across the crack front. These include BEASY, and FRANC3D.[59,60,61,62,63]

Through the use of BAMF, it is possible to overcome the challenge of defining the crack shape with only two points. With BAMF it is possible to have up to forty-five points along the crack front, for which a SIF can be calculated and propagated, individually, based on the SIF and material file stored within AFGROW. Through this capability it is possible to predict fatigue crack shapes that can match the example shown in Fig. 4.

1.5 Investigation into the Effect of a Fatigue Crack on the Residual Stress Field Introduced by the Cx Process in 2024-T351 and 7075-T651

With the ability now to quantify the residual stress field via the contour method, and the ability to understand the spatial uncertainty associated with that residual stress determination technique, it is now possible through BAMF to more accurately allow the crack shape to evolve (based on SIF). With a more sound understanding of these inputs into a fatigue crack growth prediction it is now possible to begin looking at other essential questions regarding the implementation of deep engineered residual stresses into a life prediction. These questions include the quantification of the effect of applied expansion, material thickness, edge margin, fastener pitch, pin load, over and under loads within a spectrum, usage, and the presence of a fatigue crack on the residual stress field.[64,65,66,67,68] Through funding from the United States Air Force's A-10 Aircraft Structural Integrity Program (ASIP) Office hundreds of residual stress conditions have been determined via the contour method.[56] This work has focused on gathering residual stress conditions within a "real-life" design box, capturing profiles for multiple materials, thicknesses, hole diameters, edge margins, and applied expansions. In addition to this, work is currently underway to quantify the effect of usage on the residual stress fields imposed by the Cx process. This will be done by removing sections from used aircraft that were Cxed either during production of the aircraft or at some point during its service life. These sections, holes will then have the residual stress determined via the contour method and these datasets will be compared to newly manufactured parts that match the same material and other essential geometric characteristics. The goal of this future work is to quantify the effect of usage on the residual stress field and to state with confidence this effect across the residual stress field.

This extensive data repository has allowed for many conclusions to be drawn concerning the residual state introduced by the Cx process. However, there has been no work performed to statistically quantify the spatial uncertainty associated with the residual stress determination technique or the Cx process repeatability. This work is essential if statistically-based conclusions are to be made concerning any effect a perturbation to the baseline condition has on the residual stress state.

As the structural integrity organizations within aerospace industry move towards the implementation of residual stresses in the calculations used to define the initial and recurring inspection intervals, one of the major questions that is posed by those that accept the risk is whether or not the presence of a fatigue crack changes a residual stress field. The current methodology that has been established for individual analyses is to impose a baseline residual stress field that was developed from an uncracked coupon into a model and predict the effect of this residual stress field on the life, without any change to the residual stress condition that was applied. The concern with this approach is that it is likely that a change in the residual stress/strain state occurs do to the development and propagation of a fatigue crack. Some have postulated that the effect of the fatigue crack on the Cx residual stress field should be determined and accounted for in crack growth predictions.[33,34,67,69,70] However, the historical methods that were used to quantify this effect often over-simplified the problem or lacked the technology to determine the residual stress field at a spatial resolution, and with a level of defined statistical uncertainty that would be necessary to establish an answer for this question in the context of damage tolerance, as applied to aerospace structure. In addition to this new understanding of the spatial residual stress field's statistical characteristics, additional

analytical tools have now been developed to allow for the integration of this knowledge into a more holistic prediction of fatigue life of critical structure.

The contour method is one method which can be used to determine the impact of a fatigue crack on the residual stress field introduced by the Cx process. This method also allows the spatial resolution to allow for the residual stress fields to be used, both in the baseline, uncracked condition, and in the fatigue-cracked condition, to produce a fatigue crack growth prediction of a given condition at a desired level of accuracy. These fatigue life predictions could then act as a method for validation of the residual stresses that were determined via the contour method.

1.6 Methodology for the Quantification and Impact of a Fatigue Crack on the Residual Stress Field Imposed by the Cold Expansion Process

In order to isolate the effect of a fatigue crack on the residual stress/strain field introduced into two aluminum alloys (2024-T351 and 7075-T651), the following steps were performed.

1. Manufacture residual stress determination coupons in 2024-T351 and 7075-T651 to the “low” end of the applied expansion specification from FTI (3.16%).
2. Perform the contour method on coupons to determine the residual stress condition.
3. Develop single measurement and repeatability spatial uncertainty for the full-field residual stresses.
4. Manufacture identical residual stress coupons in 2024-T351 and 7075-T651 aluminum alloys at the “low” end of applied expansion.

5. Fatigue load residual stress coupons using constant amplitude loading.
6. Determine the residual stress state within the fatigue-cracked coupons using the contour method, following the identical process as was developed for the baseline, uncracked coupons.
7. Perform fatigue crack growth predictions using the baseline, uncracked residual stress fields, with the applied statistical distribution for a given fatigue test conditions.
8. Perform fatigue crack growth predictions with the implementation of residual stresses determined from fatigue-cracked coupons, with the applied statistical distribution, for a given fatigue test condition.
9. Perform validation fatigue crack growth fatigue testing using marker banding to document the fatigue crack shape evolution from the crack size.
10. Compare results to determine if the inclusion of the determined effect of the fatigue crack more accurately models the fatigue crack growth shape evolution and total life.

Through this methodology it is possible to statistically quantify the effect of a fatigue crack on the residual stress field introduced at the “low” applied expansion level on two commonly used aluminum alloys, 2024-T351 and 7075-T651. The quantified effect of the fatigue crack could then be used to predict the fatigue life and crack shape evolution of a given test condition, and thus used to validate the approach.

1.7 Preface to Document

The author would like to provide some information to allow the reader to understand the purpose of the format of the document. This dissertation is laid out in a manner that documents the overarching programmatic flow, which was followed to develop experimental coupons, enhance the current available state of the art for the data reduction, smoothing and fitting of surface topology for the determination of residual stresses, via the contour method, and finally to test the hypothesis that a fatigue crack effects the residual stress field introduced by the SSCx^{TM} process within two aerospace-grade aluminum alloys. Thus the chapter flow allows the reader to understand the experimental set, including the coupon metrology, for the development of Cxed measurement coupons which were engineered to have a very specific applied expansion. The methods used to do this are not common knowledge within the aerospace community.

The dissertation then goes into significant detail regarding the development of residual stresses via the contour method. There is a desire of the author to bring into the light some of the more obscure aspects of this method in an effort to allow for greater discussion and advancement of the state of the art and for possibly the standardization of this method for the determination of residual stresses used in structural analysis.

The dissertation then focuses on the statistical quantification of the spatial uncertainty associated with the residual stress which is imposed by the Cx process. The methods used to quantify this spatial uncertainty were published during the time of this work but were never used to capture the spatial uncertainty that is associated with the complex residual stress field imposed by the Cx process. These two methods allowed for

the quantification of the repeatability and single measurement spatial uncertainty. These two published methods were used to quantify both types of spatial uncertainty for a series of replicate Cxed coupons which were produced to a specific level of applied expansion. These coupons did not have any fatigue cracks in them and represented the baseline residual stress condition for the two materials. For each material multiple replicates were produced and the residual stresses were determined in each. In addition to determining the residual stresses within each coupon, the single measurement and repeatability uncertainties were calculated. The dissertation provides multiple contour and line plots for each of the individual coupons as well as a comparison of each individual coupon to the average residual stresses for the group.

Now with a statistical understanding of the spatial residual stress within the baseline uncracked conditions, the dissertation documents the development of another series of identical coupons that had fatigue cracks formed and propagated in them. These coupons again had the residual stresses determined in them using the identical contour method procedures used for the baseline condition. The dissertation again provides individual contour and line plots for one of the coupons within each fatigue crack length group.

With the residual stresses determined for both the baseline and fatigue-cracked condition, the dissertation then compares the fatigue-cracked coupons to the baseline to allow for conclusions to be made as to the effect of the fatigue crack on the residual stresses.

The final portion of this dissertation documents the integration of the determined residual stresses into a state-of-the-art methodology for the calculation of SIFs along a

simulated crack front within a FEA. Through the use of the software plug-in known as the Broad Application for Modeling Failure (BAMF) it was possible to integrate the residual stresses determined from both the baseline and the fatigue-cracked coupons to provide a prediction for a given test condition. These predictions were made using the average residual stress field and also a statistically based bound of one standard deviation on that average. Thus for each test condition, three individual predictions were developed and provided. The methods for the development of these predictions are provided in detail. The dissertation then provides a method for capturing the effect of the fatigue crack, as provided by the contour method results, into the BAMF prediction for the fatigue life of the same test condition. Again a statistical representation of the residual stress fields for each group of crack sizes is provided and utilized within a given prediction. Thus, again, three predictions were developed for each material and are provided.

Thus this dissertation flows in a way in which it is hoped that the reader will understand the experimental process by which the stated conclusions were determined. In addition, the dissertation documents in visual detail the results of the extensive residual stress dataset which was developed through this program. For this experimental program a total of twenty-four Cxed coupons were processed to determine the residual stress. For each of those coupons the single measurement spatial uncertainty was calculated, and then compared to the repeatability uncertainty of that given material. Thus a large statistical dataset was developed to enable the reader to gain confidence in the results and conclusions obtained by this work.

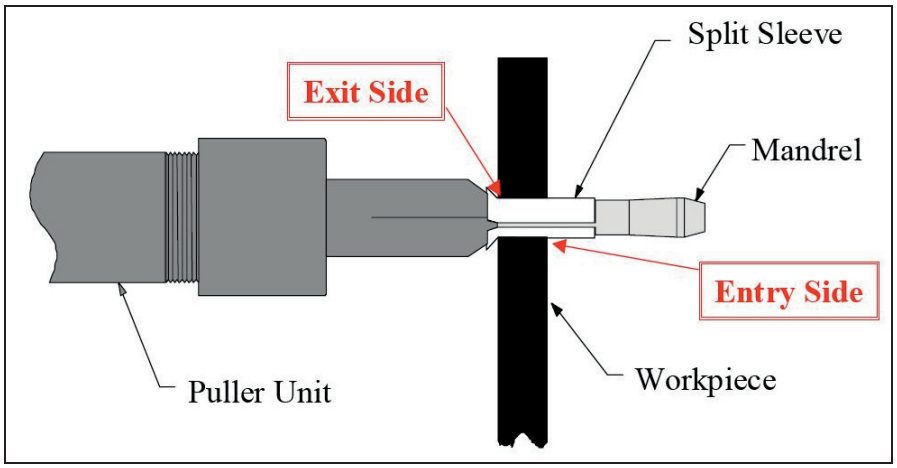

Fig. 1 FTI's Split Sleeve Cold Expansion™ (SSCx) Set-Up with Mandrel, Sleeve and Workpiece Shown – Highlighting the Entrance and Exit Side of the Cx Process.[3]

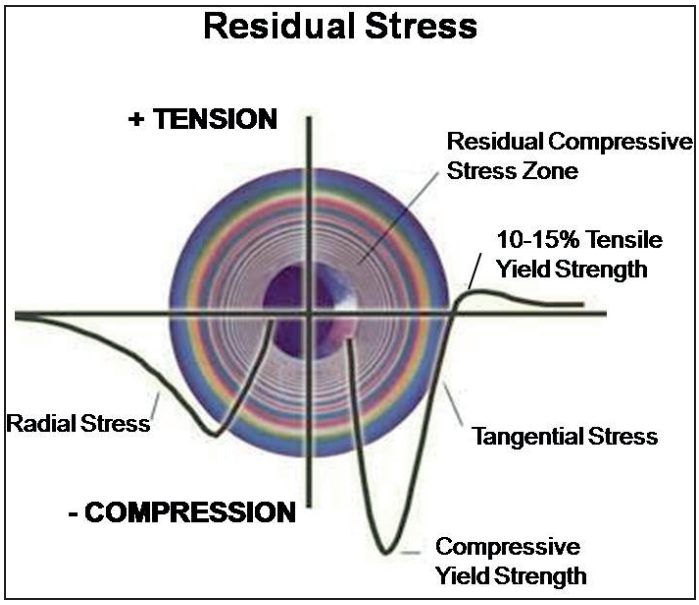

Fig. 2 Photoelastic Image of the Residual “Stress” Field Around a Cxed Hole (It Should be Noted that Photoelastic Images do not Capture Stress but Strain).[3]

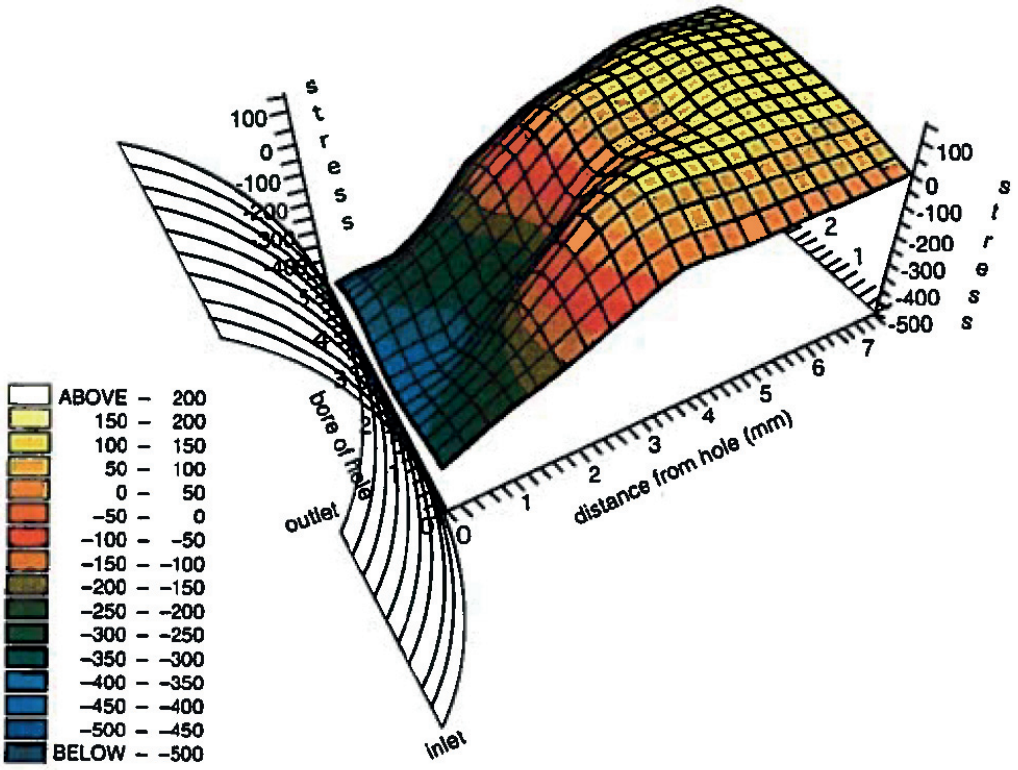

Fig. 3 3D Representation of the Residual Stress Field at a Cxed Hole, as Determined by Neutron Diffraction.[71]

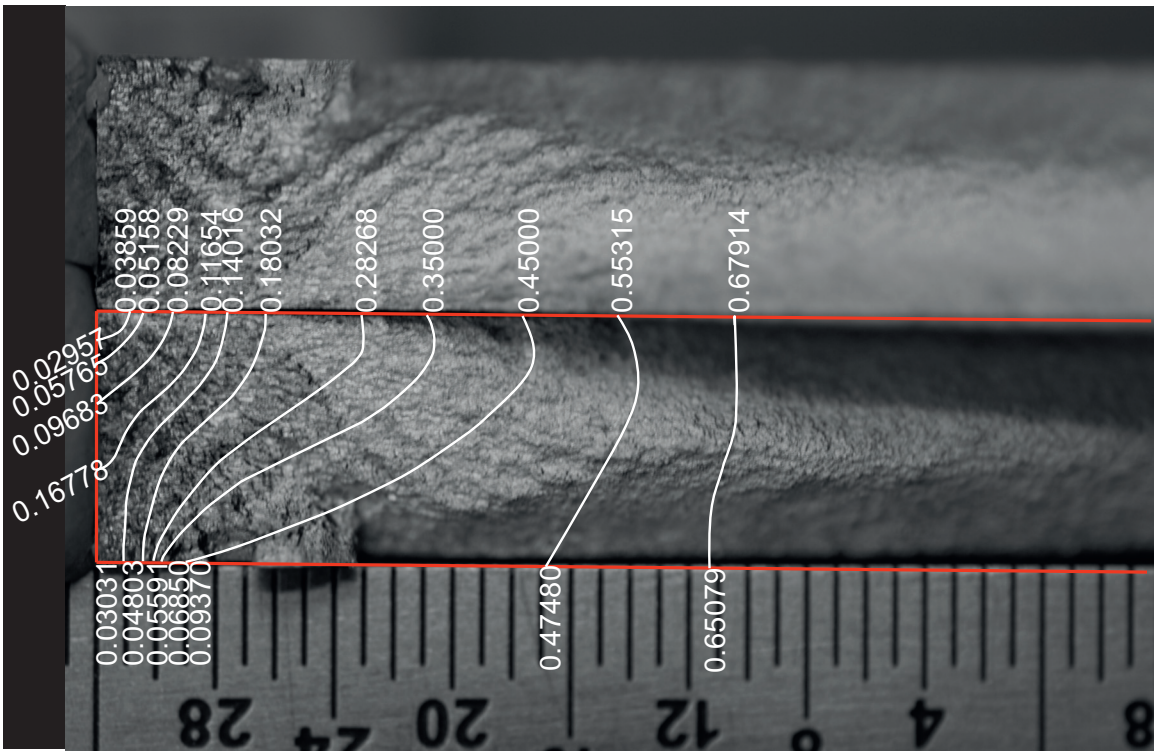

Fig. 4 Image of Marker Banded Specimen Cx 2024-18 with Marker Bands Highlighted with Surface and Bore Lengths (All Dimensions in Inches).[54]

2 DEVELOPMENT OF BASELINE COLD EXPANDED COUPONS FOR RESIDUAL STRESS DETERMINATION

2.1 Fabrication of Baseline Cold Expanded Residual Stress Coupons

The initial set of baselines Cx coupons were manufactured from fatigue coupons used for the Carlson, Pilarczyk master's dissertation work.[54,72] The fatigue coupons used for that work were manufactured from 2024-T351 and 7075-T651 plate, as shown in Fig. 5, Fig. 6, and Fig. 7. For their work nineteen Cx coupons were manufactured, along with two ASTM Standard E647 coupons, and four coupons that were Non-Cold Expanded (Non-Cxed). From these coupons, new residual stress determination coupons were developed. All of the residual stress determination coupons that were used for this research were extracted from the four Non-Cx coupons, in both the 7075 and the 2024 material. For these coupons there were not bonded on tabs so it was possible to create a new residual stress coupon that was 4.0 inches wide by 0.25 inch thick by 5.0 inches long. An image of where the residual stress determination coupons were extracted is shown in Fig. 8.

Within the FTI specification for the Cx process there is a range of potential applied expansions for a given hole size. For both the 2024-T351 and 7075-T651 material a final hole diameter of 0.50 inch was chosen. For this final hole diameter there is a range of potential applied expansions, due to the tolerance stack-ups of the mandrel

nose diameter, initial hole diameter, and sleeve thickness.[3] For a 0.50 inch final diameter hole the applied expansion range is 3.15% for the "low", 3.67% for the "Mid", and 4.16% for the "High" applied expansion. All of the holes, in both the 2024 and 7075 material were processed to the Low applied expansion level.

2.2 Cold Expansion of Baseline Residual Stress Coupons

In order to reach this specific level of applied expansion, unique Cx mandrels were manufactured at and purchased from FTI. The mandrels started from the standard 16-0-N tool and were then ground down to have a maximum major diameter of 0.4684+0.0002-0.0000 inch. The major mandrel diameter is defined as the largest diameter of the mandrel near the tip, as shown in Fig. 9.

The following steps were performed while manufacturing these coupons.

1. Drill initial hole diameter to 0.4770+0.0000-0.0002 inch
2. Cx hole using specific mandrel for low applied expansion with maximum diameter of 0.4684 inch
3. Ensure that split sleeve is orientated in the 12'O-clock position to coupon length
4. Final ream to diameter of 0.498±0.002 inch

These residual stress coupons were given the following nomenclature, and this will be carried through. The 2024-T351 coupons, with a 0.50 inch final diameter hole size, were name CxA2, and the 7075-T651 coupons, with the same final hole diameter, were designated as CxD2. The drawings for these coupons are provided in Fig. 10 and Fig. 11. provides a reference for applicable FTI parts, dimensions, and notes for the manufacturing of the CxA2 and CxD2 residual stress coupons.

2.3 Tribology of Baseline CxA2 and CxD2 Residual Stress Coupons

As the CxA2 and CxD2 coupons were being manufactured hole dimensions were carefully measured. Each hole was measured using a Fowler/Bowers Holematic. This tool is able to measure hole diameters to a resolution of ±0.00005 inch, thus being sufficient for the requirements within the part drawing. An image of the Fowler/Bowers Holematic is shown in Fig. 12. The physical measurements of the holes were taken during the Cx process and are shown in Table 1, Table 2, and Table 3.

As shown in Table 2 and Table 3, the applied expansions for the CxA2 coupons ranged from a maximum of 3.23% to a minimum of 3.14%. The average applied expansion for these five coupons was 3.18% with a standard deviation of 0.038%. For the CxD2 coupons all of them were machined and processed such that they all had the same amount of applied expansion, 3.23%.

After coupons were processed, each coupon was then wrapped and shipped to Hill Engineering, LLC., in Rancho Cordova, CA for them to be processed via the contour method to provide surface displacements for processing into residual stresses that were imposed into the material via the Cx process.

Table 1 Tooling and Reference Drawings for CxA2 (2024-T351) and CxD2 (7075-T651) Residual Stress Coupons

Tool/Product	Material	Dimensions (inch)	Part #	Tolerance (inch)	Test Matrix Applicability	Quantity	Spares	Notes
Coupon Blanks	2024-T351	4 inch(LT) x 5 inch (L) x 0.250 inch thick	N/A		A2	21	8	Reference Drawings
Coupon Blanks	7075-T651	4 inch(LT) x 5 inch (L) x 0.250 inch thick	N/A		D2	9	5	Reference Drawings
Starting Drills		29/64 (0.4531 inch)	Double Margin Drill? (FTI has P/N CBSD-16-0-N-1)		A2,D2	2		For 16-0-N (0.500"final dia)
Starting Drills		15/32 (0.4687 inch)	Double Margin Drill? (FTI has P/N CBSD-16-0-N-1)		A2, D2	2		For 16-0-N (0.500"final dia)
Pre-CX Reamers		0.4770 inch diameter	N/A	+0.0000-0.0002	A2, D2	2		Ground to tolerance - For 16-0-N (0.500"final dia)
Mandrels		0.4684 inch major diameter	Start with CBM-16-0-N-1-60-V2	+0.0002-0.0000	A2, D2	1		For 16-0-N (0.500"final dia)
Sleeves		0.012 inch thick	CBS-16-0-N-16F		A2, D2	30	5	For 16-0-N (0.500"final dia)
Finish Reamers		0.500 inch diameter	Any Reamer will work (FTI has P/N CBR-16-0-N-1-.XXXX)	+0.002-0.002	A2, D2	2		For 16-0-N (0.500"final dia)

Table 2. Physical Measurements of CxA2 (2024-T351) Residual Stress Coupons During Cx Processing

COUPON #	Parent Coupon	Pre-Cx Diameter (inch)	Honed/Butterflied to size?	Mandrel Diameter (inch)	Sleeve Thickness (inch)	Applied Expansion	Post Cx Diamether LT Orientation (inch)	Post CX Dia L-LT Orientation (inch)	Avg Post Cx Diameter (inch)	Residual Expansion
A2-1	NCX2024-2	0.4772	No	0.4684	0.0120	3.19%	0.4884	0.4883	0.48835	2.34%
A2-2	NCX2024-2	0.4774	No	0.4684	0.0120	3.14%	0.4884	0.4883	0.48835	2.29%
A2-3	NCX2024-1	0.4772	No	0.4684	0.0120	3.19%	0.4876	0.48805	0.48783	2.23%
A2-4	NCX2024-6	0.4770	No	0.4684	0.0120	3.23%	0.4892	0.48835	0.48878	2.47%
A2-5	NCX2024-5	0.4774	No	0.4684	0.0120	3.14%	0.48885	0.4883	0.48858	2.34%

Table 3. Physical Measurements of CxD2 (7075-T651) Residual Stress Coupons During Cx Processing

COUPON #	Parent Coupon	Pre-Cx Diameter (inch)	Honed/Butterflied to size?	Mandrel Diameter (inch)	Sleeve Thickness (inch)	Applied Expansion	Post CX Dia LT Orientation (inch)	Post CX Dia L-LT Orientation (inch)	Avg Post Cx Diameter (inch)	Residual Expansion
D2-1	NONCX7075-3	0.4770	No	0.4684	0.0120	3.23%	0.4857	0.4862	0.4859	1.87%
D2-2	NONCX7075-2	0.4770	No	0.4684	0.0120	3.23%	0.4857	0.4867	0.4862	1.92%
D2-3	NONCX7075-3	0.4770	No	0.4684	0.0120	3.23%	0.4857	0.4867	0.4862	1.92%

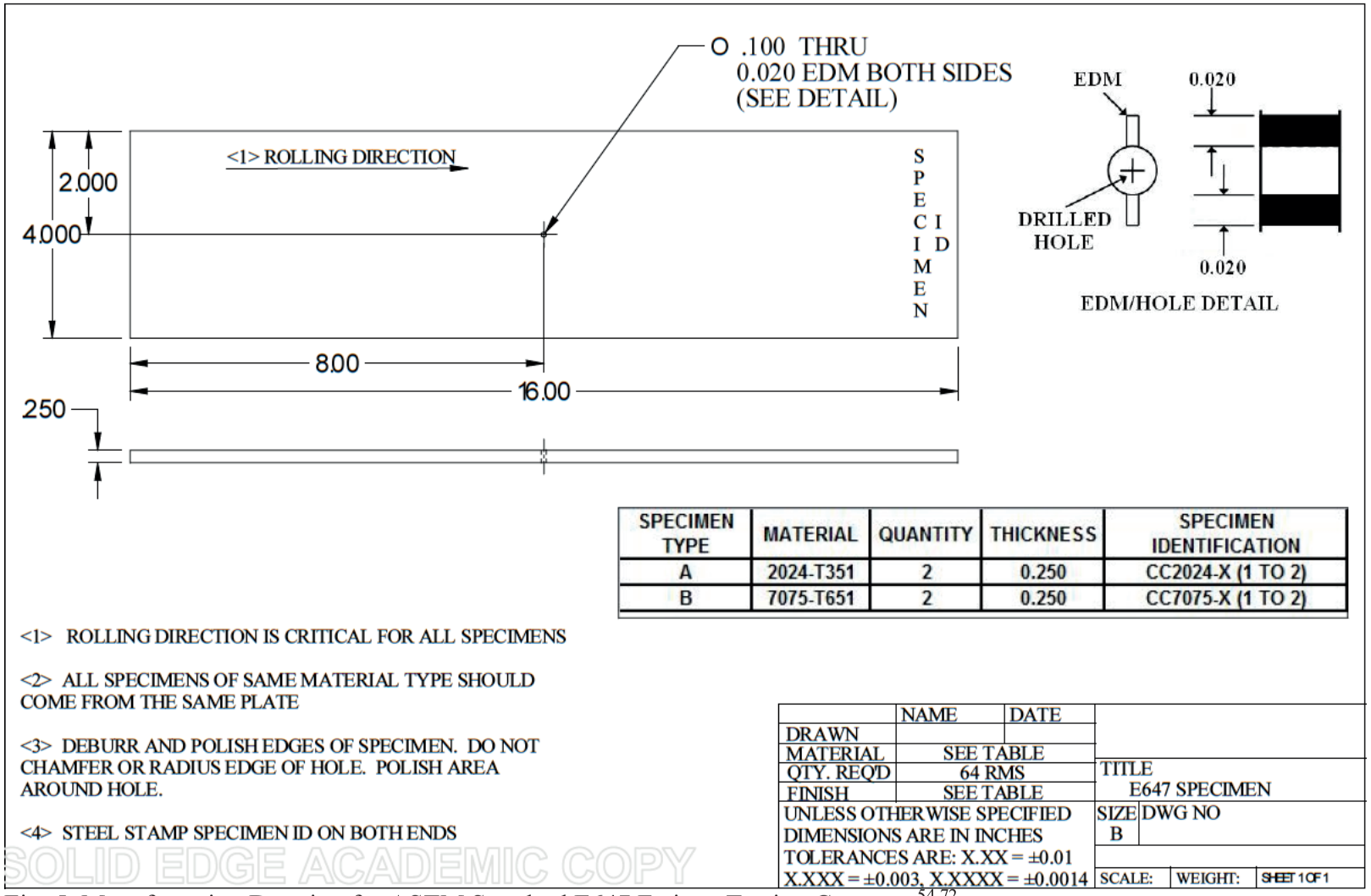

SPECIMEN TYPE	MATERIAL	QUANTITY	THICKNESS	SPECIMEN IDENTIFICATION
A	2024-T351	2	0.250	CC2024-X (1 TO 2)
B	7075-T651	2	0.250	CC7075-X (1 TO 2)

<1> ROLLING DIRECTION IS CRITICAL FOR ALL SPECIMENS

<2> ALL SPECIMENS OF SAME MATERIAL TYPE SHOULD COME FROM THE SAME PLATE

<3> DEBURR AND POLISH EDGES OF SPECIMEN. DO NOT CHAMFER OR RADIUS EDGE OF HOLE. POLISH AREA AROUND HOLE.

<4> STEEL STAMP SPECIMEN ID ON BOTH ENDS

	NAME	DATE	
DRAWN			
MATERIAL	SEE TABLE		
QTY. REQ'D	64 RMS		TITLE E647 SPECIMEN
FINISH	SEE TABLE		
UNLESS OTHERWISE SPECIFIED DIMENSIONS ARE IN INCHES TOLERANCES ARE: X.XX = ±0.01 X.XXX = ±0.003, X.XXXX = ±0.0014			SIZE B DWG NO
			SCALE: WEIGHT: SHEET 1 OF 1

Fig. 5. Manufacturing Drawing for ASTM Standard E647 Fatigue Testing Coupons.[54,72]

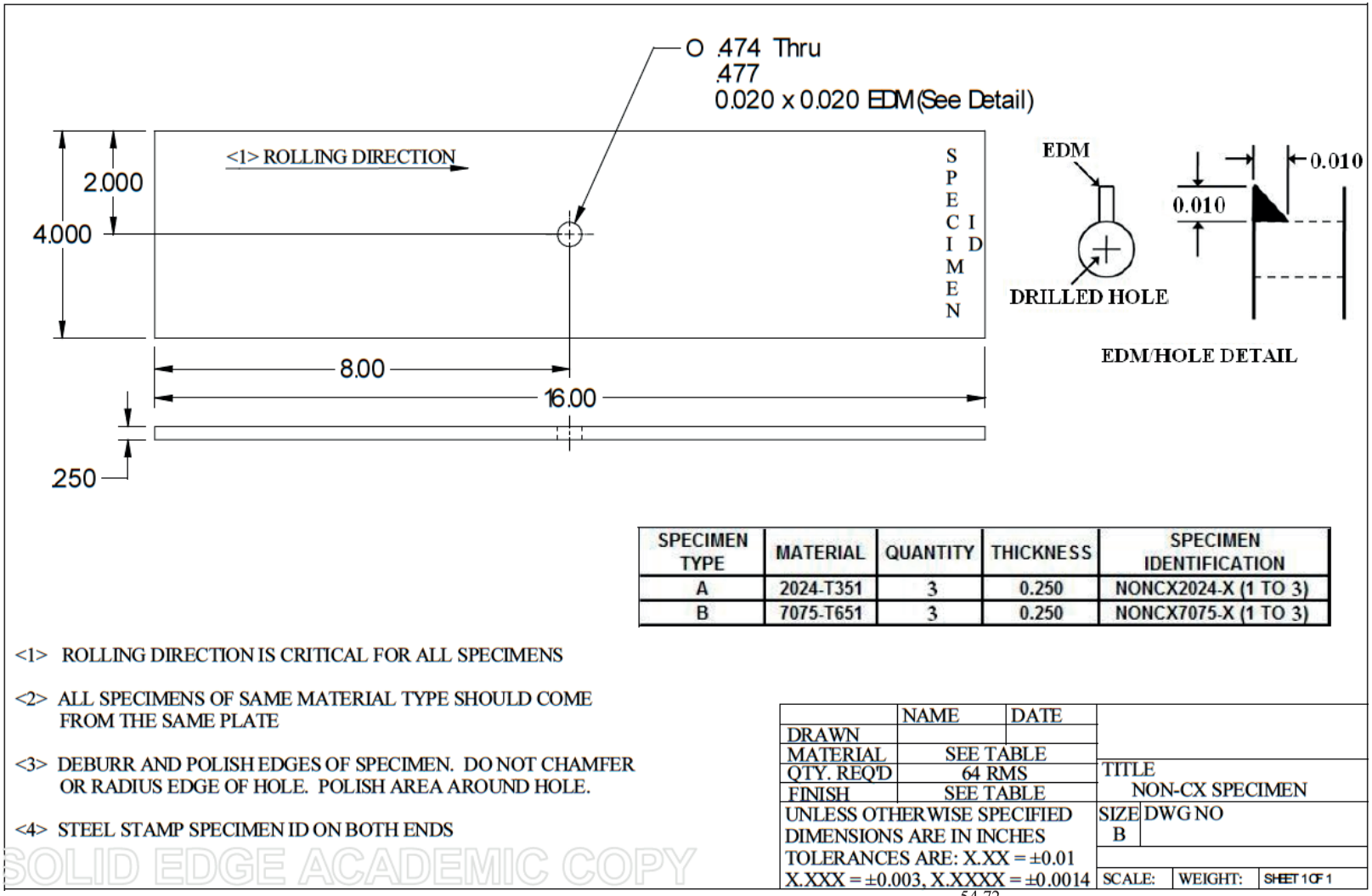

SPECIMEN TYPE	MATERIAL	QUANTITY	THICKNESS	SPECIMEN IDENTIFICATION
A	2024-T351	3	0.250	NONCX2024-X (1 TO 3)
B	7075-T651	3	0.250	NONCX7075-X (1 TO 3)

<1> ROLLING DIRECTION IS CRITICAL FOR ALL SPECIMENS

<2> ALL SPECIMENS OF SAME MATERIAL TYPE SHOULD COME FROM THE SAME PLATE

<3> DEBURR AND POLISH EDGES OF SPECIMEN. DO NOT CHAMFER OR RADIUS EDGE OF HOLE. POLISH AREA AROUND HOLE.

<4> STEEL STAMP SPECIMEN ID ON BOTH ENDS

	NAME	DATE
DRAWN		
MATERIAL	SEE TABLE	
QTY. REQ'D	64 RMS	
FINISH	SEE TABLE	
UNLESS OTHERWISE SPECIFIED DIMENSIONS ARE IN INCHES TOLERANCES ARE: X.XX = ±0.01 X.XXX = ±0.003, X.XXXX = ±0.0014		

TITLE: NON-CX SPECIMEN

SIZE: B | DWG NO

SCALE: | WEIGHT: | SHEET 1 OF 1

Fig. 6. Manufacturing Drawings for Non-Cold Expanded (Non-Cxed) Fatigue Coupons.[54,72]

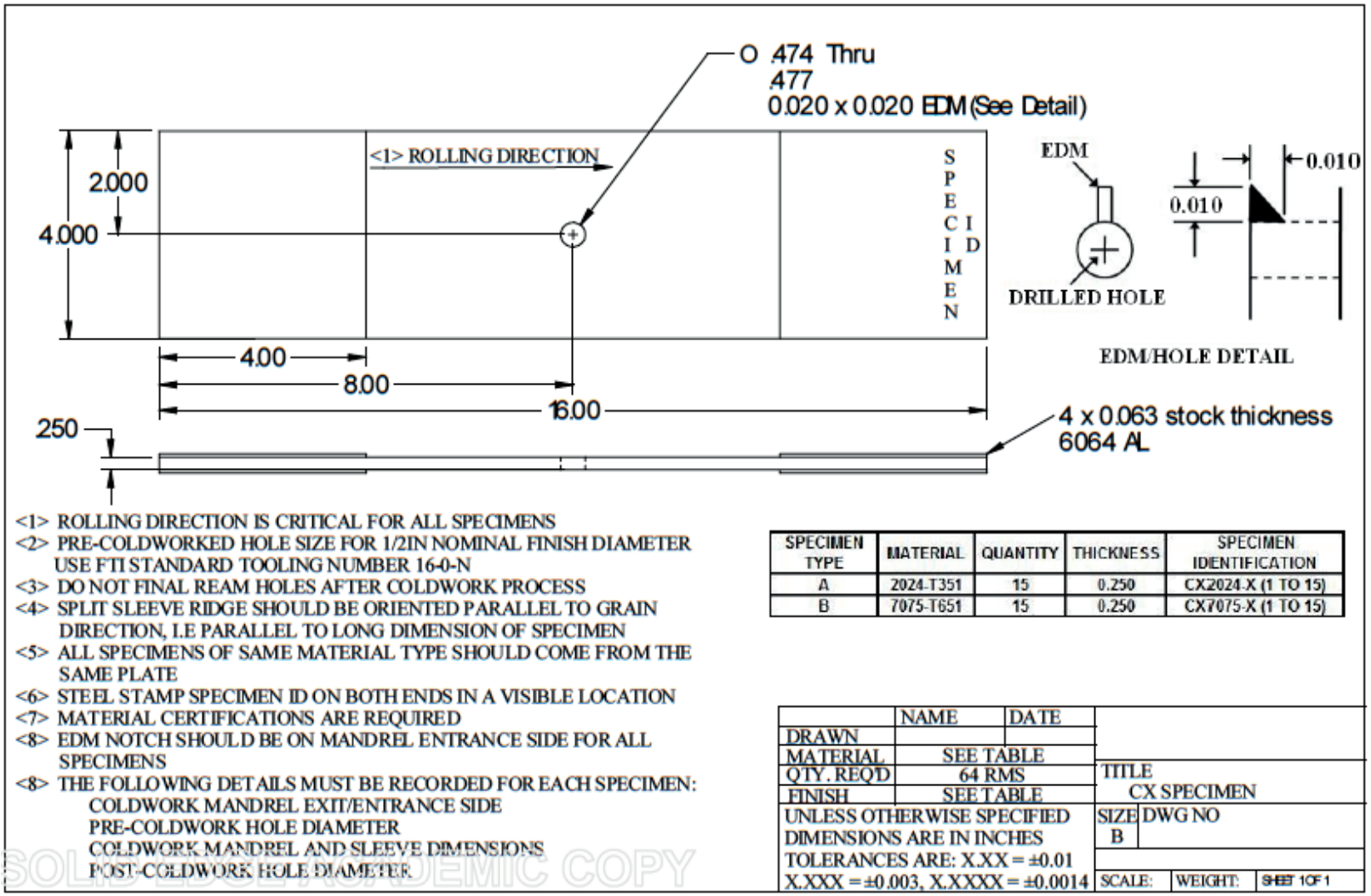

Fig. 7. Manufacturing Drawing for Cold Expanded (Cx) Fatigue Coupons.[54,72]

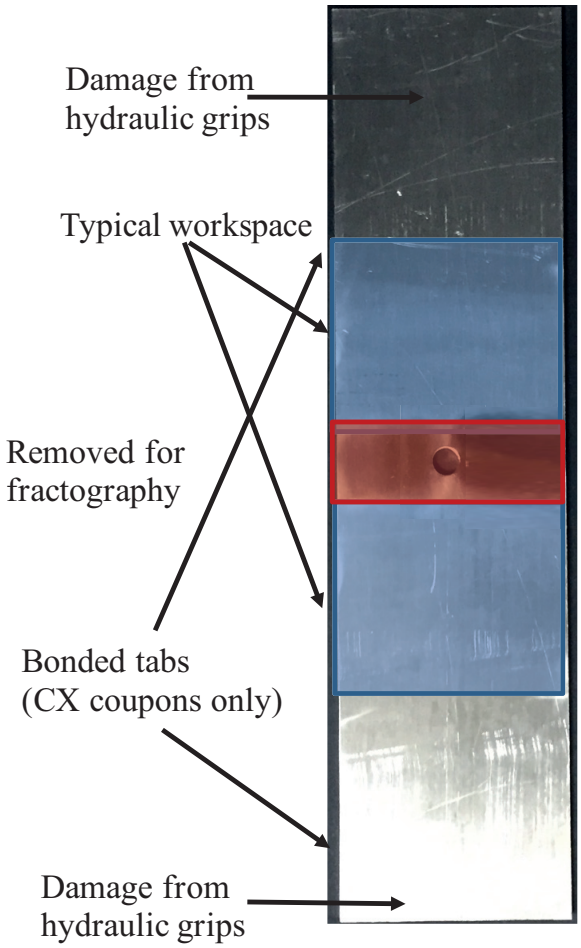

Fig. 8. Image of Non-Cold Expanded (Non-Cxed) Fatigue Coupon Showing Locations where Residual Stress Coupons Were Extracted.

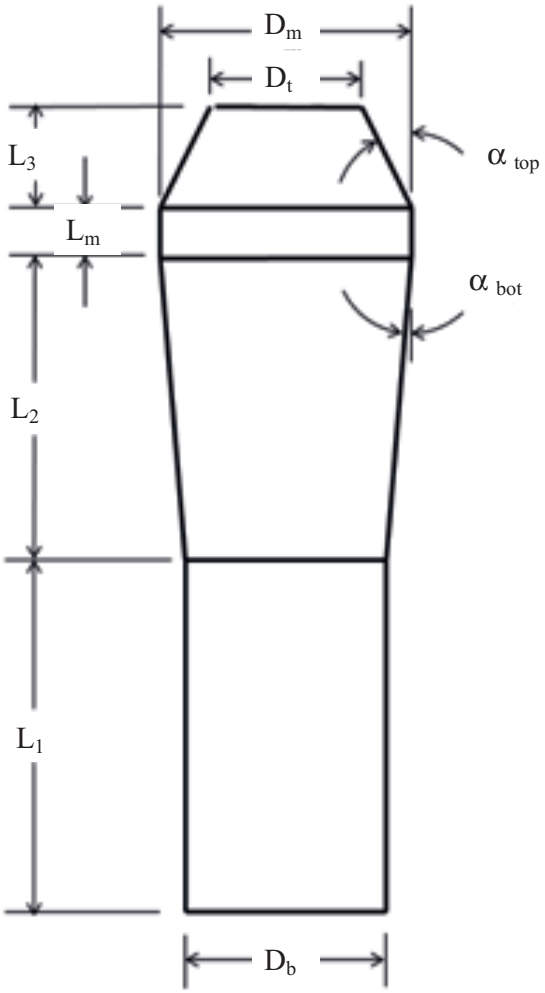

Fig. 9. Basic Drawing of Cx Mandrel Tip Showing Call-outs for Specific Dimensions.

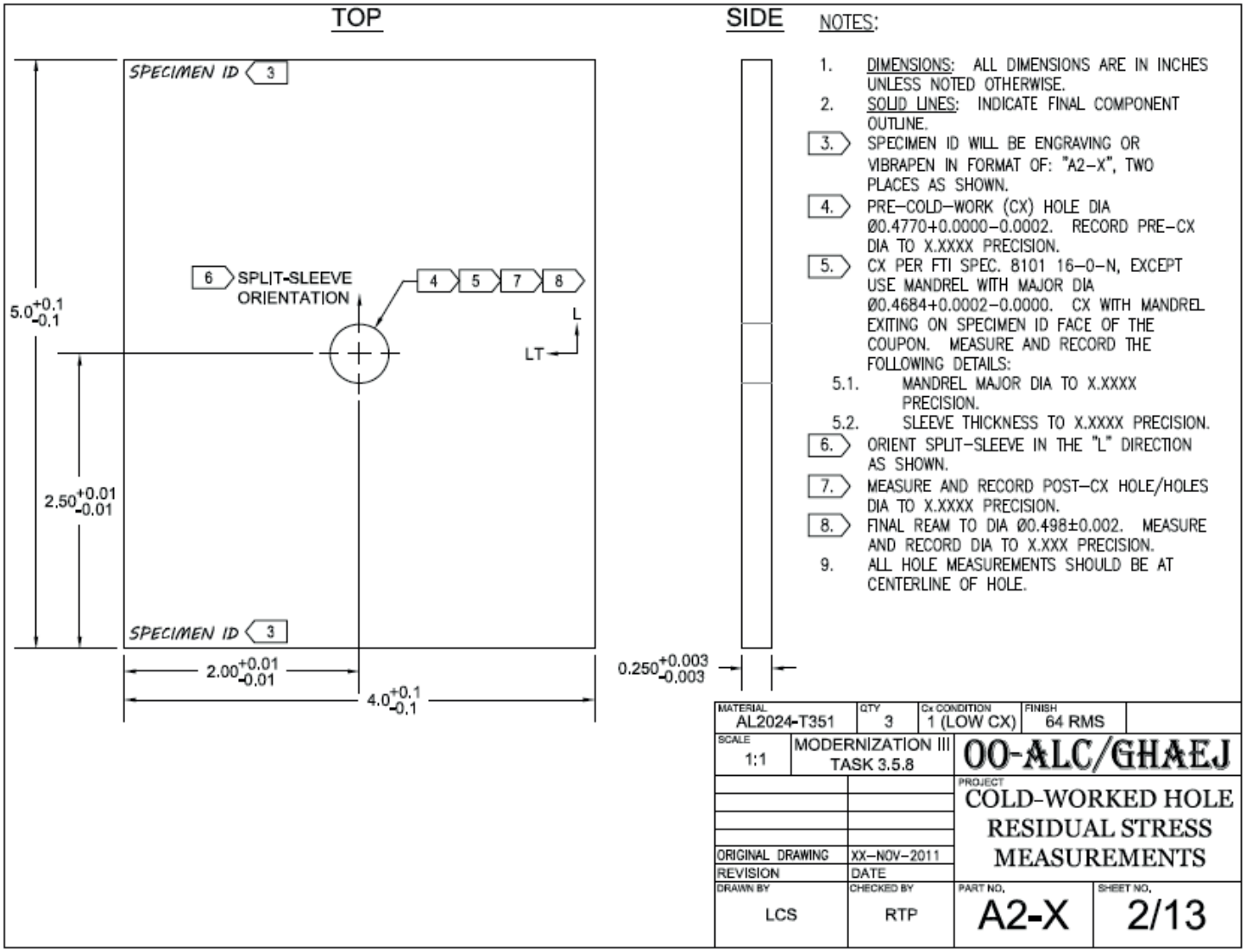

Fig. 10. Drawing for 2024-T351 Residual Stress Coupons, Showing Process Steps in Notes.

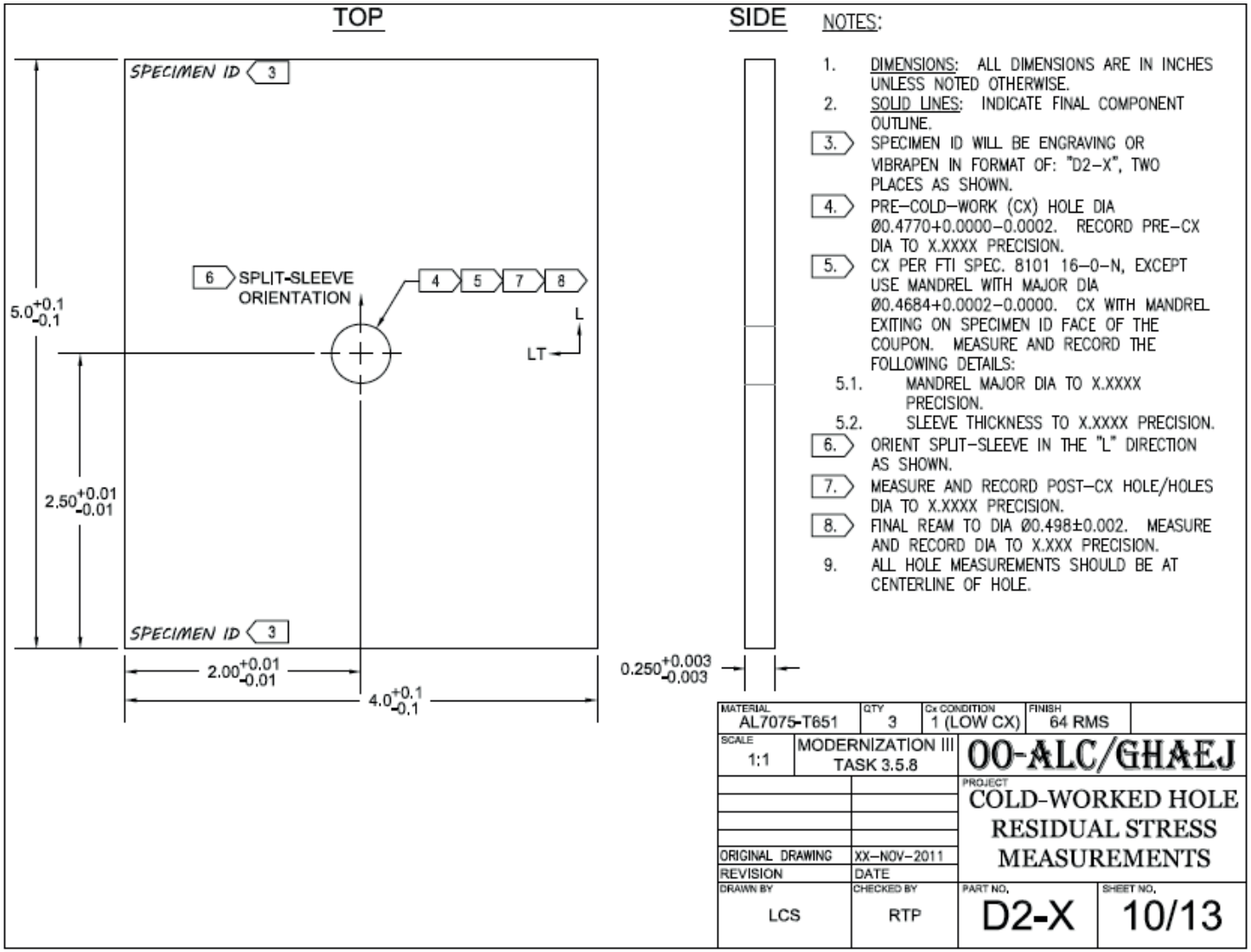

Fig. 11. Drawing for 7075-T651 Residual Stress Coupons, Showing Process Steps in Notes.

Fig. 12. Image of Fowler/Bowers Holematic Hole Measuring Tool. Image Courtesy of Dallen Andrew.

3 CONTOUR METHOD FOR RESIDUAL STRESS DETERMINATION AT COLD EXPANDED HOLES

3.1 Overview of Contour Method for Determining Residual Stresses

The purpose of this work was to determine the residual stress field that was produced by the Cx process in baseline coupons and then to compare those results to another series of coupons that was produced under the same manufacturing constraints, and Cxed to the same level of applied expansion. However, these coupons would have a fatigue crack developed and propagated in them under constant amplitude loading. The contour method was selected for determining the residual or self-stresses within the coupons that had been Cxed. The contour method was selected because it provides a 2D residual stress field, or map along a plane of interest. This plane of interest is defined by the user and for this work the plane of interest was defined as the plane 90 degrees from the orientation of the split sleeve produced during the Cx process. In addition, the contour method provides a residual stress spatial resolution that is required for integration into a fatigue crack growth analysis for fatigue life prediction purposes.[56,73,74]

3.1.1 General Theory of Contour Method

The contour method was first presented and published by Dr. Mike Prime in the years 2000 – 2001 as a method for determining residual stresses within a body by

measuring the strains released after a surface has been cut.[75,76]

The contour method is based on Bueckner's superposition principle. This principle was defined in 1958 by Bueckner and then further refined by others.[77,78,79] The method has been used to determine a variety of residual stress conditions for a wide range of residual stress problems.[80,81] The method has been very eloquently defined in multiple sources and it does not seem necessary to define the overall process within this paper, only to define how the coupons of interest were processed here.[82,83,84,85]

The contour method is broken down into five major components, each of which will be discussed in greater detail below.

3.1.2 Surface Strain Release Measurement Procedures

3.1.2.1 Fixturing the Part

First the part is clamped for the cutting operation. It is essential that the part is fixtured in a way that prevents rigid body motion from occurring. The method often used is to clamp the part on both sides of the planned cut-plane. A backing plate can be also used, as seen in Fig. 13.

For the most part, and for all of the coupons in which residual stresses were determined for this work, the cut was made with a wire electro-discharge machine (EDM). This type of cutting operation often is used because of the limited plastic deformation that can be developed during the cut.[86] The ideal method for machining the part would result in a straight cut, one that would remove as little material as possible from the body, and would result in no plastic deformation. Wire EDM is currently the process of choice.

All of the coupons for this program were clamped in the same manner as shown in Fig. 14. This clamping method eliminated all potential rigid body motion.

3.1.2.2 Cutting the Part along the Plane of Interest

Once the part is installed in the cutting fixture, the part is cut. For all of the coupons within this body of work the cutting method was the same and all cutting parameters of the wire EDM were held constant. The wire EDM process is thermo-electrical, in which the material is eroded away by a series of repetitive spark discharges from a pulsed direct-current power supply between the workpiece and the wire.[87] All parts were cut using a Mitsubishi FA-10 wire EDM with a 0.004 inch diameter brass wire. There are many other settings that must be held to very strict parameters to ensure that issues such as wire breaking or improper flushing of the cut material does not happen.[85,88] These settings are specific to material type and many other specimen parameters.[89] These parameters are proprietary to Hill Engineering, LLC. However, they have a standard protocol for cutting Cx holes that has been used for many years.

The cutting method used on these coupons is performed in the exact same manner for all of the coupons. Each coupon was placed on the clamping fixture with the Cx mandrel entrance face up, as shown in Fig. 15, and was cut along the plane of interest.

Through this process, the coupon was cut into two pieces with two new surfaces produced along the cut plane. An image of a post-cut part is shown in Fig. 16 and Fig. 17.

Systematic errors can be introduced into the contour method through the cutting process and should be noted.[90] These errors can be introduced if the wire EDM is not set

to the proper cutting feed rate, wire diameter, cooling parameters, and many other specific settings required for a consistent cut. Other errors can occur during the cutting process, such as a wire breaking or over-burn of the material due to some foreign particle in the material's matrix. In addition, wire vibration or drag can cause a "bowed" cut.[75,91] This type of error often can be avoided by specific set-up and execution parameters.[92] One additional source of systematic error that can be introduced into the contour method is when additional stresses are introduced into the part from the cutting process itself. These sources of error have been studied by use of incremental slitting, or crack compliance.[86] For all of the wire EDM cuts that were performed there were no indications of any sources of systematic error or effects from plasticity.[93] All cuts were performed without any documented problems that would impact the residual stress determination process.

3.1.2.3 Measuring the Displacements along the Cut Surfaces

With the part now cut in two pieces along the plane of interest the residual strains that were introduced into the part via the Cx process are now released because of the presence of a new, free surface. Any displacements that are measured on these new surfaces are assumed to be produced by the normal stresses to the cut plane. Shear stresses within the part are not able to be determined through this method. Any shear effects produced by the cutting are eliminated by averaging the displacements on both sides.75 It is important to note that the contour method is only able to provide the normal stress, σx, as shown graphically in Fig. 18. For a released surface, via cutting with a normal stress in the x-direction, as shown in Fig. 18, the equivalent surface traction per

unit thickness, T, is provided by Equation 1,

$$T_x = -\sigma_{xnx} \text{ and } T_y = -\tau_{xynx} \qquad \text{Equation 1}$$

where n is the unit surface normal vector, and $n_{Y=0}$ is the case shown in Fig. 18.

Because, in the case shown in Fig. 18, and that of the Cx hole, the normal traction is symmetric and the transverse traction is antisymmetric, with respect to the cut plan and because it is assumed that the problem is elastic and superposition holds, the average deformations from the two cut and measured surfaces will represent the contour shape as if only the normal stresses were present in the body.

Historically, there have been two major categories of methods used to measure the surface displacements produced after cutting. These two methods are contact and noncontact. The contact method involves the use of a coordinate measuring machines (CMM). The optical methods include triangulating and confocal lasers, interferometry and confocal imaging microscopes. Each of these methods had usage trade-offs that were considered prior to the measurement of the surface displacements. All of the coupons had their cut surfaces measured using a Taylor-Hobson Talyscan 250 scanning laser profilometer. The coupons were measured at a lab temperature of 73 deg F. Each of the scans had a spacing of 0.007 inch in the X direction and 0.0004 inch in the Y direction (orientations are shown in Fig. 17). The scanner has a reasonable vertical precision to 0.00004 inch. All surface topography measurements followed industry best practices.[94]

3.1.3 Determination of Residual Stresses from Measured Surface Displacements

Laser profilometry surface measurements provide a dataset in X, Y, and U_{zz} (displacement height) of the measured surface (this axis reference is provided in Fig. 16 and Fig. 17). This data was then processed to determine the residual strains and ultimately to the residual stress state that was in the body prior to the cutting of the part.[95] In order to process the data, a set of Matlab scripts was provided by the United States Air Force's Research Laboratory.[96] The code was updated to include additional scripts to grid the data and also to assist in the alignment of the two sides and the removal of data points that were outside of the defined coupon geometry. Additions to the code had to be developed to allow for processing shapes that represented the cross-section of those for this work.

3.1.3.1 Determination of Part Edge

Displacement data were provided in three columns: X, Y, and Uzz. Data density for the X and Y directions was at 0.004 inch, so each file had approximately two million specific data points with displacement data associated with each point. Each coupon had two text files associated with it, providing all of the measured displacement data for that individual face. Each surface was processed separately up to a specific point where they were then averaged. When the data file is read into the Matlab code, it is possible to see all of the data associated with the surface scan, see Fig. 19. All datasets had their origin at the center of the hole and at the mandrel entrance surface. The outline of the part would need to be defined. This was done by carefully tracing along the outer edge of the part and deleting all data that were inside of a single pixel edge, as shown in Fig. 20.

If multiple data points were to be left at a given edge it would be difficult to determine the boundary of the part and errors would occur in the solution. Once the outline was defined the data appeared as shown in Fig. 21.

3.1.3.2 Alignment of Data to X and Y Coordinate Axes

After establishing an outline of the part it is essential that new reference coordinate axes be established at a given edge. For all of the coupons, the new coordinate system origin was moved from the lower surface and center of the hole. In order for this to be accomplished a new X and Y alignment axis had to be selected. To accomplish this all of the data were removed to only show the desired new X axis alignment data, for all of these coupons this was the lower horizontal line, the Y=0 line, as shown in Fig. 22. Then the Y axis data was retained in order to define this new Y frame, this is shown in Fig. 23.

After the dataset had the outline defined and was aligned to a new X and Y axis, a least squares plane was fit through the data and aligned to a new coordinate axis, as shown in Fig. 24. The purpose of fitting a plane through the data was to establish the 0 displacement location throughout the space. Thus it was possible to define positive or negative displacement and a magnitude to that displacement.

Within Matlab this fit was performed using the lsplane function. Once the least squares plane was fit to the data the edges of the data set were redefined and the final output was provided for viewing and review, as shown in Fig. 25. The fitting of this least squares plane to the data field is essential to allow for an orientation of what is a positive or negative displacement. This then will correlate to compressive on tensile residual

stress.

3.1.3.3 Averaging of the Two Datasets Representing the Measured Faces

This process was again followed for the opposing side of the cut, named the "floating" dataset within the Matlab code. Just like for the "static" face dataset, the "floating" dataset edges were defined to a single pixel, aligned to new X and Y coordinate axes, and finally fit with a least squares plane. Once this was accomplished, the two faces, and the defined outline for the part, were brought back for further processing. The center of the hole was found and then the max. and min. values of the left and right sides were found for both the X and Y axes. With both halves now available, the data within each half were linearly interpolated to a common gridspacing using the "meshgrid" function within MatLab. This created a 2D grid with spacing of 0.0004 inch x 0.0004 inch for the X and Y direction.[97] The "griddata" function was then used to interpolate the "static" and "floating" data to that specific grid spacing.[98] Now that all of the data for the "static" and "floating" datasets were on the same grid spacing in the X and Y direction, it was possible to average both datasets. Averaging of each matching data point is required to remove any displacements induced by shear stresses.[75,99] If there were data points that did not have a match on one of the two sides this was defined as a "NaN" (Not a Number) and were dropped from the final averaged dataset. An example of a final averaged dataset is presented in Fig. 26.

3.1.3.4 Determination of and Removal of Statistically Significant Outliers

One of the most critical aspects of the data reduction process is the removal of "noise" within the data. This noise can be a result of many factors, to include measurement error, surface roughness, and effects of the wire EDM processes.[82] Currently there are no standard methods for removing noise from the averaged dataset prior to fitting.[75,76] As can be seen in Fig. 27 there are areas within this averaged dataset that visually would represent an outlier within the surface.

In order to determine what an outlier is, the Modified Thompson Tau method for determining a statistical outlier was employed.[100,101,102] With the data fit to a least-squares plane, the mean and standard deviation of the misfit between the averaged surface and any fit can be calculated across the surface. A significance level for an outlier was set to 5%, which is recommended for practical applications.[103] With the mean, standard deviation, and a significance level established, it was possible to determine for each point on the averaged surface if that point was outside of the acceptance criteria. The Modified Thompson Tau method for quantifying outliers has been used across multiple disciplines, from the medical to the financial industry.[104,105] The code used for this is provided within the Appendix.

3.1.3.5 Apply a Mathematical Fit to Averaged and De-Noised Data

It is now essential that the averaged surface be fit because any sharp variation in the surface contour will be dramatically amplified as a sharp stress gradient determined by the FEA. Many different techniques are available for the fitting of the displacement surfaces. These techniques include fitting by a Fourier series, a sine or cosine function, a

high order polynomial, or through the use of bivariate cubic splines (B-Splines) fit through specific knot locations.[75,82,85,95,106,107,108,109] A B-spline curve consists of a sequence of polynomial curve segments, which are used to fit along a given segment between knot locations.[110,111] The "spap2" function within Matlab was used to perform this spline fitting.[112]

The process used is outlined within Fig. 28 in which the initial surface was fit using a least-squares fit to the averaged surface. The user then selected the number of knots that would be used to join the spline pieces together. The code allows for a different knot density to be selected for the X and Y coordinate axes. The spacing for the knots was defined by the number of knots evenly spaced through the thickness of the part. This spacing was then used to place knots along the X axis of the part. Thus, an evenly spaced knot mesh is made through the surface data.

In order to determine the "optimal" fit of the data, a range of knot densities for both the X and Y axes were investigated. The through-thickness stress gradient at a Cx hole is not very complex, thus requiring a lower number of knots to provide the optimal fit. The radial stress, in the X direction for all of these coupons, was more complex, with the potential of having two inflexion points, one close to the edge of the hole, and the other where the stress field turns from compressive to tensile. This type of residual stress field can be seen as calculated through the FEA simulation in Fig. 29.

For each iteration of the Modified Thompson Tau a calculation of the Euclidean Normal (L2) error was determined between the fit surface and the averaged displacements. The L2 Normal error is defined from Equation 2 and provides the summation of the root sum square (RSS) of the residual, between the fit surface and the

actual displacements on the averaged surface.

$$L_{2_{norm}} = \sqrt{\sum_{i=1}^{n} \left(z_{displacement} - z_{fit}\right)^2} \qquad \text{Equation 2}$$

This L2 error was then plotted as a function of knot density for the X, or radial direction away from the hole. A series of knot densities was plotted and is shown in Fig. 30.

In order to determine the optimal fit the change in slope of the line within Fig. 30 was investigated. From the data for these Cx holes, the two major slope changes occurred at a 4-knot spacing and then at 10. This allowed for a focus to be placed on the radial knot spacing as the process was moved forward.

3.1.3.6 Building of Finite Element Model of Part

Now that a series of knot spacings have been developed and fits for those knots spacing were developed, the FEM was built. There are two methods that can be employed to make the FEM for these coupons. Each coupon had individual metrology performed for the basic parameter dimensions, and these dimensions could be taken from the measurements taken by the laser. Thus, for each individual coupon a unique FEM could be produced. It would allow for the exact implementation of measured displacements to the exact coupon dimensions. This would eliminate any minor extrapolations that would need to be performed if an average coupon FEM geometry was used. This is the process often used when stresses are to be determined in a single part, without multiple replicates. However, one of the major difficulties of this method is that when the FEM is built and meshed each coupon will have a unique mesh and nodal placement, thus it would require additional interpolation to allow for future statistical

analysis at the exact same location across replicates of a given condition.

The method for this work utilized the drawing dimensions of the coupons. Each of the coupon sets were machined to the same tolerance requirements. Thus, all of the FEMs were built from the same average machining, as shown in Fig. 10 and Fig. 11. The elastic parameters of Modulus of Elasticity (E) and Poisson's Ratio (ν) for all of the simulations for the 2024-T351 material were set to $E = 10.5x10^3$ ksi (73773 MPa), and $\nu = 0.33$.[113] For all of the 7075-T651 simulations $E = 10.3x10^3$ ksi (71016 MPa), and $\nu = 0.33$.[114]

With a series of surface fits developed, they were used to solve for the residual stress that would produce the measured deformations in the material. Surface fits developed from a range of knot densities (knot densities of 3, 4, and 5 for the Y direction and 4,8, and 20 in the X direction) were used to solve for these residual stresses. To do this each surface fit was inverted and applied to a FEM as a series of displacement boundary conditions. Three constraints were applied to restrain rigid body motion, which were defined by Abaqus. The model was meshed entirely using Abaqus's C3D8R elements. These are general purpose, linear brick elements that are fully integrated with 2x2x2 integration points. All elements were also run using Abaqus's "Standard" element type. Partitioning of the mesh followed the guidelines to minimize element distortion.[115] An image of the meshed part with typical rigid body constraints and displacement boundary conditions is shown in Fig. 31. The model was then allowed to reach equilibrium and the resulting stresses in the body represented the residual stresses along the cut plane, which were in the part due to the Cx process.

With the ability to solve for one given knot density the next phase was to define

the “optimal” fit for both the X and Y directions in the part. Therefore, the FEA portion of the process was performed for all of the knot combinations determined to represent the maximum shift in the L2 error plot shown in Fig. 30.

3.1.3.7 Convergence Study of Optimal Knot Densities

FEA simulations were performed for nine combinations of X and Y direction knot densities. These included three knots in the Y direction with four, eight, and twenty knots in the X direction. The same X direction knot density was replicated for both four and five knots in the Y direction. The resulting residual stresses from these calculations were plotted as a series mid thickness, and through-thickness stress plots. Features within these stress line plots were compared to determine an “optimal” knot spacing. Features of interest were those near the edge of the hole, the transition area from compression to tension, the “hump”, the amount of oscillations in the data needed to be investigated (at higher knot densities the amount of oscillations increased). Finally the “optimal” fit did not have a significant fitting effect at the end of the sample (X = 0, or 4 inch). A series of plots are provided below to provide insight into the selection of the “optimal” fit for the residual stress produced at a Cx hole. The first series of plots are of a knot density of three through the thickness (Y direction) and knot densities of four, eight, and twenty knots radially away from the hole (X direction). These can be seen in Fig. 32 through Fig. 35.

The next series of plots is for four knots through the thickness and also the same four, eight, and twenty knots radially away from the hole, as seen in Fig. 36 through Fig. 39.

The final series of plots is for five knots through the thickness and four, eight, and twenty knots radially away from the hole, these can be seen in Fig. 40 through Fig. 43.

Plotting these knot densities made it possible to determine that a four knot spacing for the radial direction would be optimal due to the limited oscillations in the stress as it moves away from the tension point at approximately 0.25 inch away from the edge of the hole. With that selected, a plot of the through thickness knot densities, of three, four, and five, were plotted, as seen in Fig. 44.

From the comparison shown in Fig. 44 it was determined that for the through-thickness direction (Y direction) a knot density of four would be best. This decision was based on the smoother fit at each edge of the part and also through the thickness. The radial (X direction) knot densities were then plotted with the through-thickness direction locked at four knots. This stress plot can be seen in Fig. 36 through Fig. 39. One of the main reasons for selecting this knot density was due to the limited oscillations in the stress field as it moves away from the edge of the hole and out past the peak tension portion at the mid plane.

3.1.3.8 Mesh Density Convergence Study

With a proper knot density defined, a mesh convergence study was performed. The mesh density was parametrized by the number of elements through the thickness. This parameterization method allowed for the calculation of the partitions sizes around the circumference of the hole to ensure that minimal distortion in the element was maintained. An element bias was developed around the hole, radially away from the hole on the plane of interest, and then from that plane through the part. All biasing followed

standard FEA guidlines.[115] Images of the mesh biasing and difference in mesh density for the range of elements covered in the convergence study is shown Fig. 45 through Fig. 48 for 16 elements through the thickness.

Images of the mesh at four elements through the thickness are also provided in Fig. 49 through Fig. 52.

Mesh densities of two through thirty-two elements through the thickness, doubling the number of elements at each step, were investigated and a convergence study was performed on the final stress output across the face. The average absolute error across the entire face was used to determine convergence of the model. Fig. 53 provides this plot and shows that at sixteen elements through the thickness the average absolute error is 0.15 ksi. It was determined that this was sufficient and also represented the maximum allowable model size to be run on the computer used, with 128 gigabytes of random access memory (RAM). Models over this size required a dramatic increase in solve time and were not sustainable for the number of models run for this program.

3.1.3.9 Displacement Data Processing Conclusions

All of the parameters needed to process the displacement data provided for both the baseline, no fatigue crack, and also the data from the coupons with fatigue cracks has been summarized. The process for aligning, averaging, removal of statistical outliers for smoothing, fitting (both spline order and knot density), and finally FEA mesh density was optimized for the given geometric condition and residual stress fields produced by the Cx process.

All of the twenty-four total Cx holes, eight coupons for which there were no

fatigue cracks developed and sixteen for which fatigue cracks were developed in one side of the coupon, were processed using identical parameters. Knot densities, spline order, outlier threshold (α), and mesh densities were locked for all datasets. This allowed for the process variation to be minimal and allowed for all residual stresses to be extracted at the exact same nodes for each replicate produced in this research program. The purpose of this was to minimize the level of systematic uncertainty that would be introduced into the data processing method by changes made within the process for a given material or coupon condition. In addition, it allowed for statistical analysis to be performed at the same geometric location for each replicate condition. This would allow for the repeatability and single measurement uncertainty quantification to be performed.

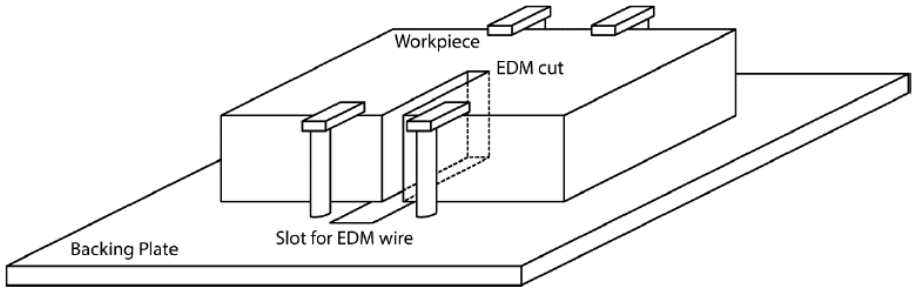

Fig. 13 Basic Illustration of Double Clamping of Part During Wire EDM Cutting for Contour Method.[82]

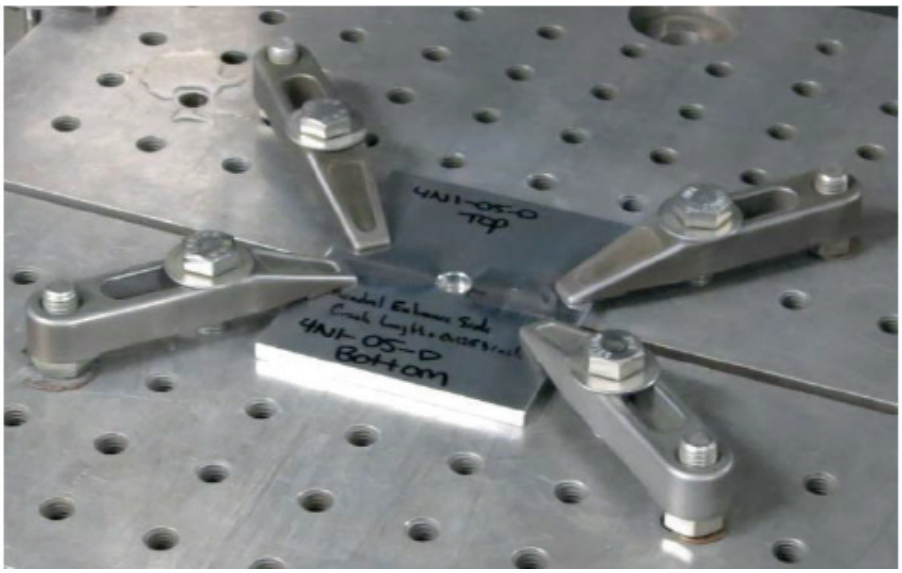

Fig. 14 Photograph of Cx Coupon Clamped in Wire EDM Cutting Machine. Photo Courtesy of Hill Engineering, LLC.

Fig. 15 Basic Drawing of Wire EDM Cutting Set-up for Contour Method.

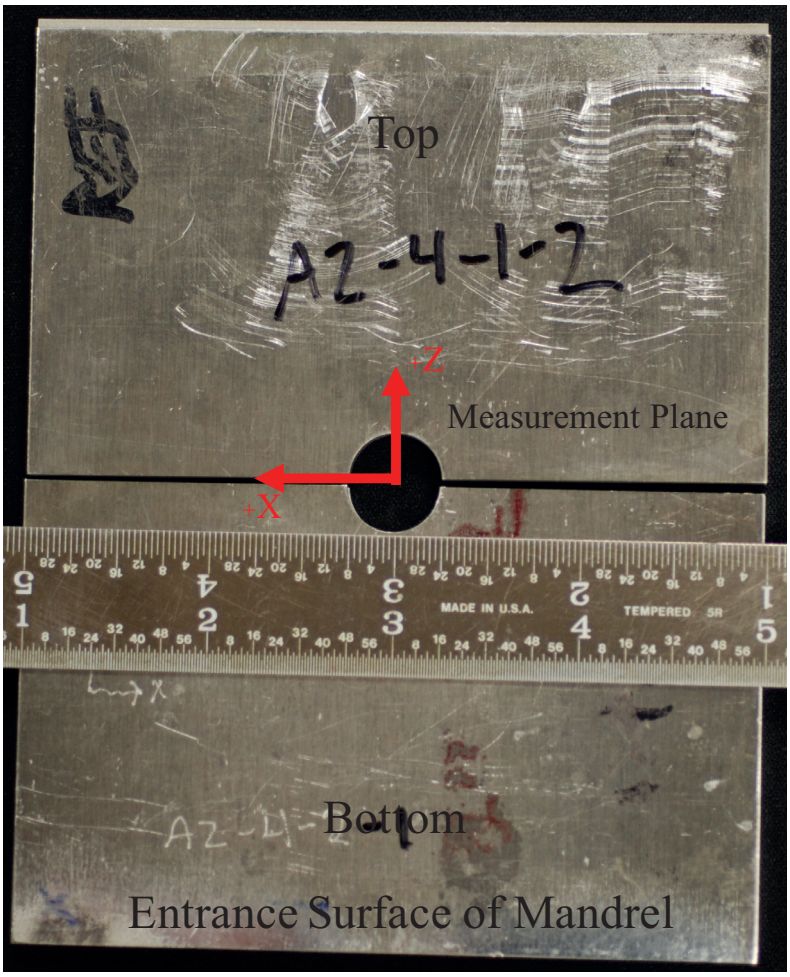

Fig. 16 Image of Residual Stress Coupon with Reference Coordinate Axes after the Wire EDM Cut Was Performed.

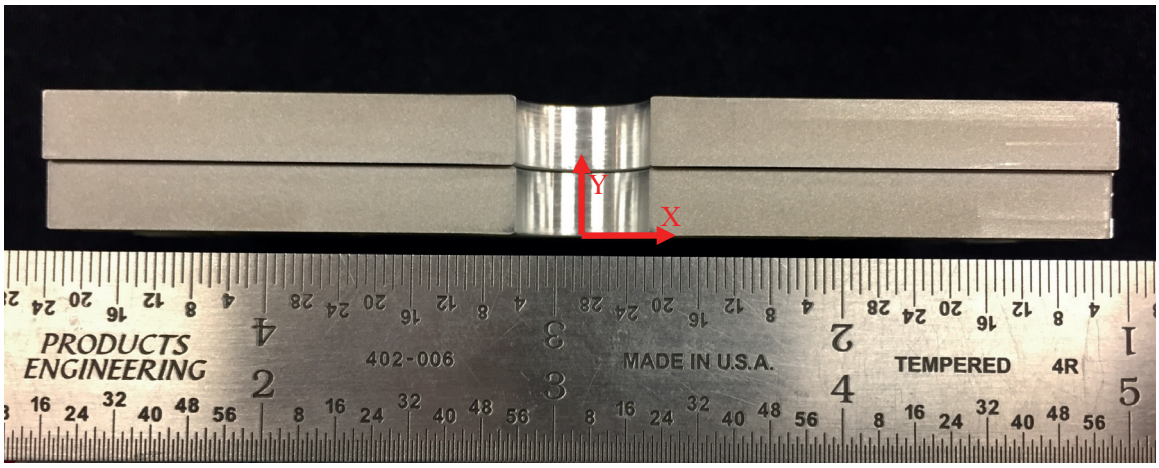

Fig. 17 Image of Residual Stress Coupon Showing Orientation Coordinate Axes for the Cut Surfaces and the Surface Features after Being Cut Using a Wire EDM.

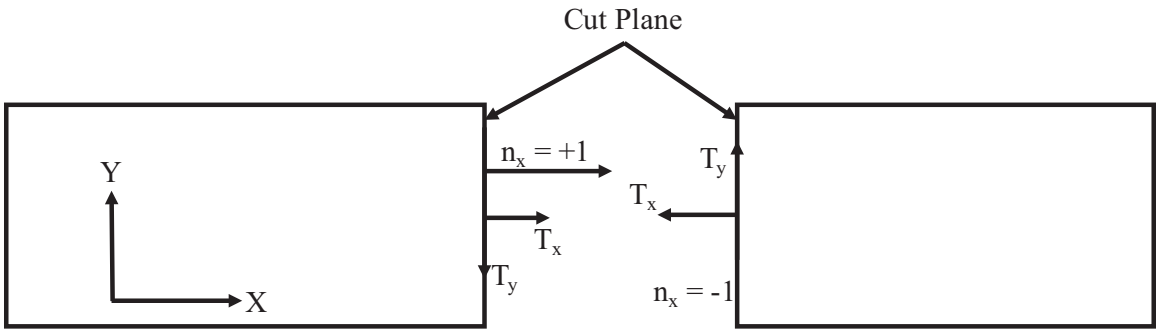

Fig. 18 Basic Schematic Showing Tractions Equivalent to Released Residual Stresses on Cut Surface. Normal Traction, T_x is Symmetric About the Cut Plane, Transverse T_y is Antisymmetric.

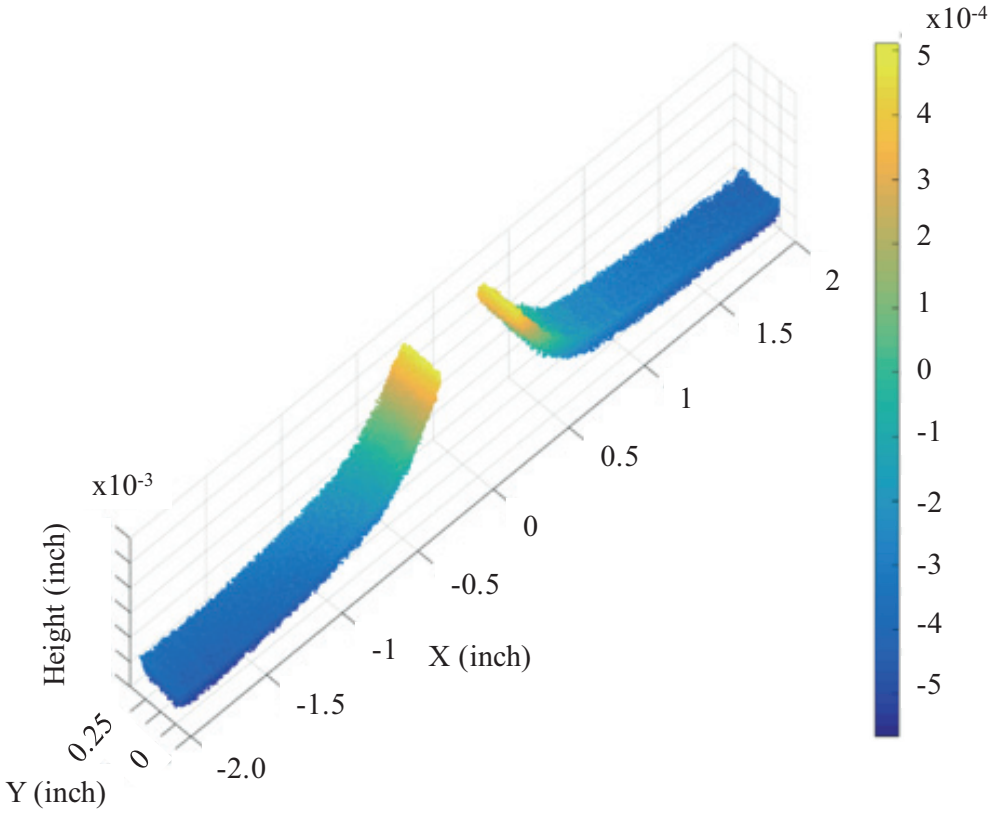

Fig. 19 Image of Laser Displacement Data Showing Basic Shape of Displacements with Reference to the Origin.

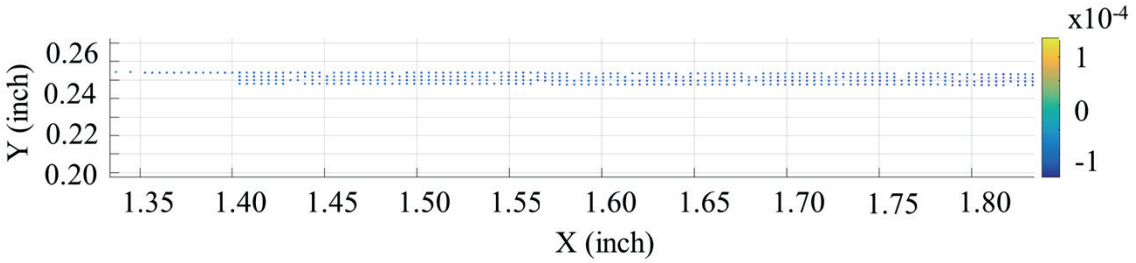

Fig. 20 Image of Laser Displacement Data Showing Edge Topography.

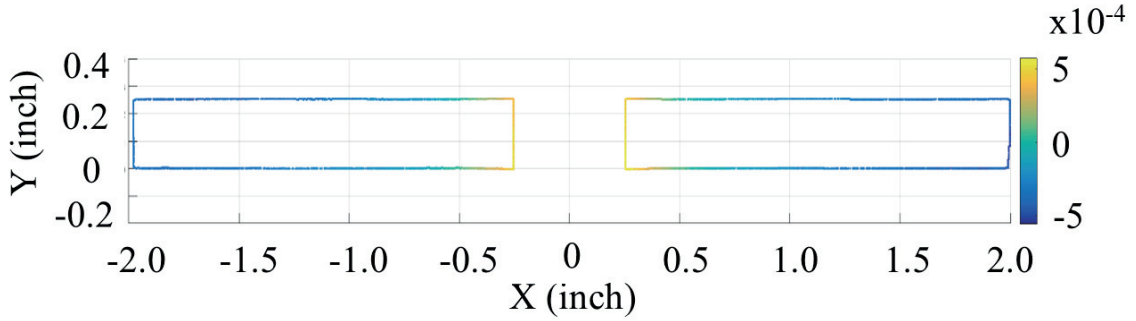

Fig. 21 Outline of Laser Displacement Data with Reference to Origin.

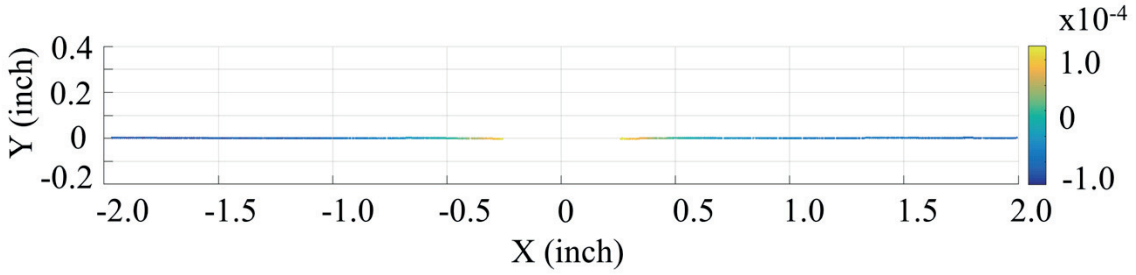

Fig. 22 Image of Data Used for Alignment for X Axis for Translation to New Coordinate Axes.

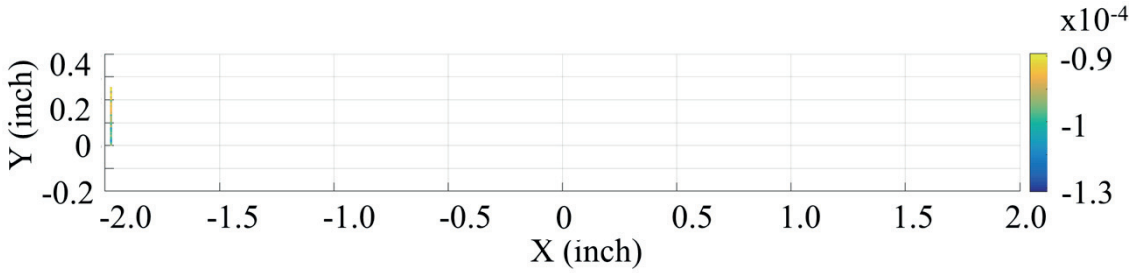

Fig. 23 Image of Data Used for Alignment for Y Axis for Translation to New Coordinate Axes.

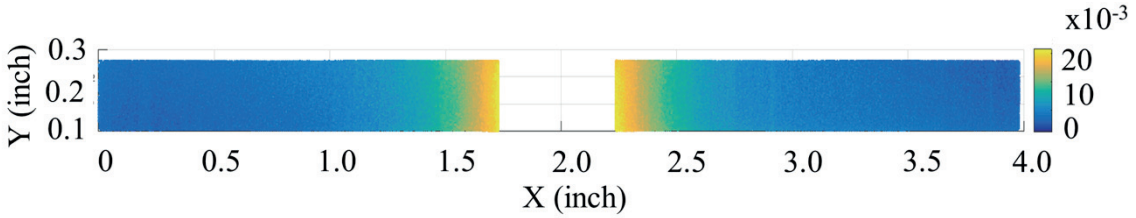

Fig. 24 Image of Laser Displacement Data Showing Shift in Origin to Lower Left Corner of Coupon.

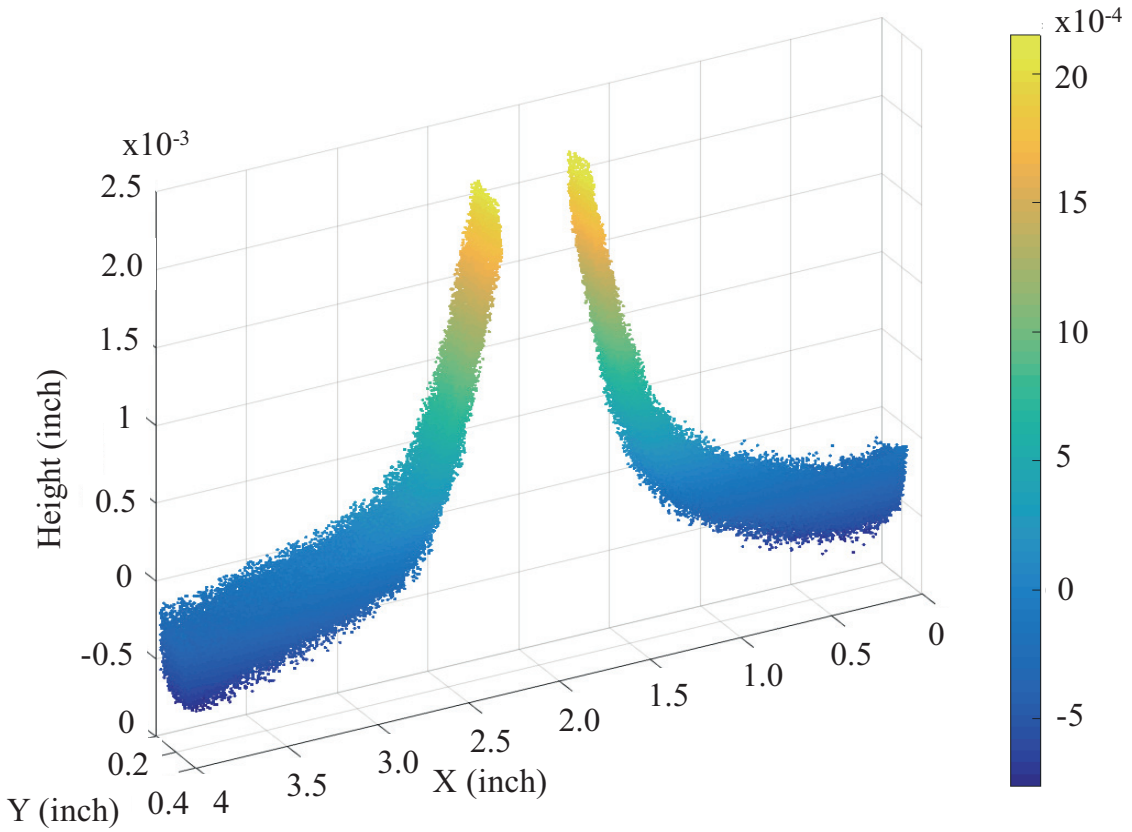

Fig. 25 Image of Laser Displacement after Edge was Defined, Alignment to New Coordinate Axes, Least Squares Plane Fit to Data, and Edge was Again Defined.

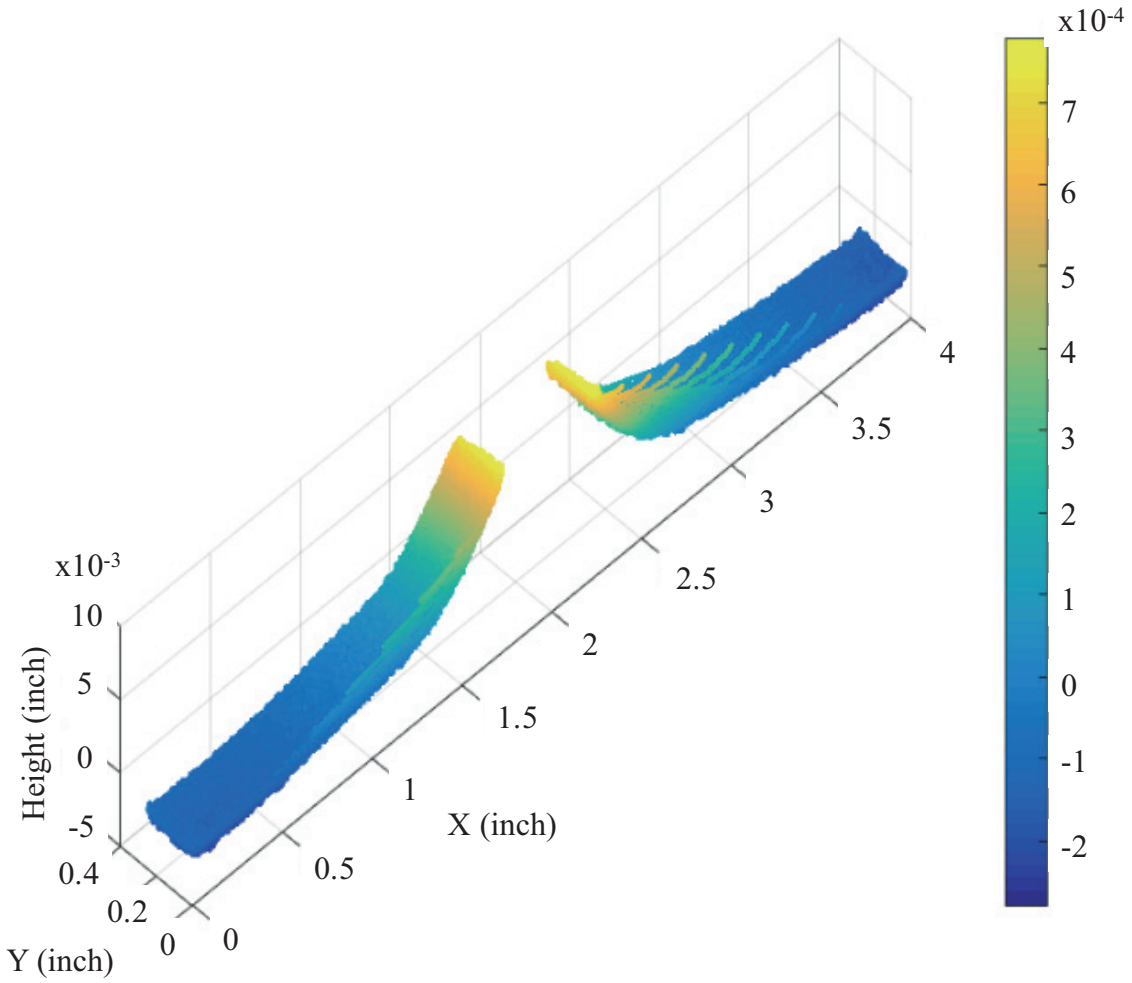

Fig. 26 Image of Laser Displacement after Both "Static" and "Floating" Datasets Have Been Interpolated to a New Grid Spacing and Averaged.

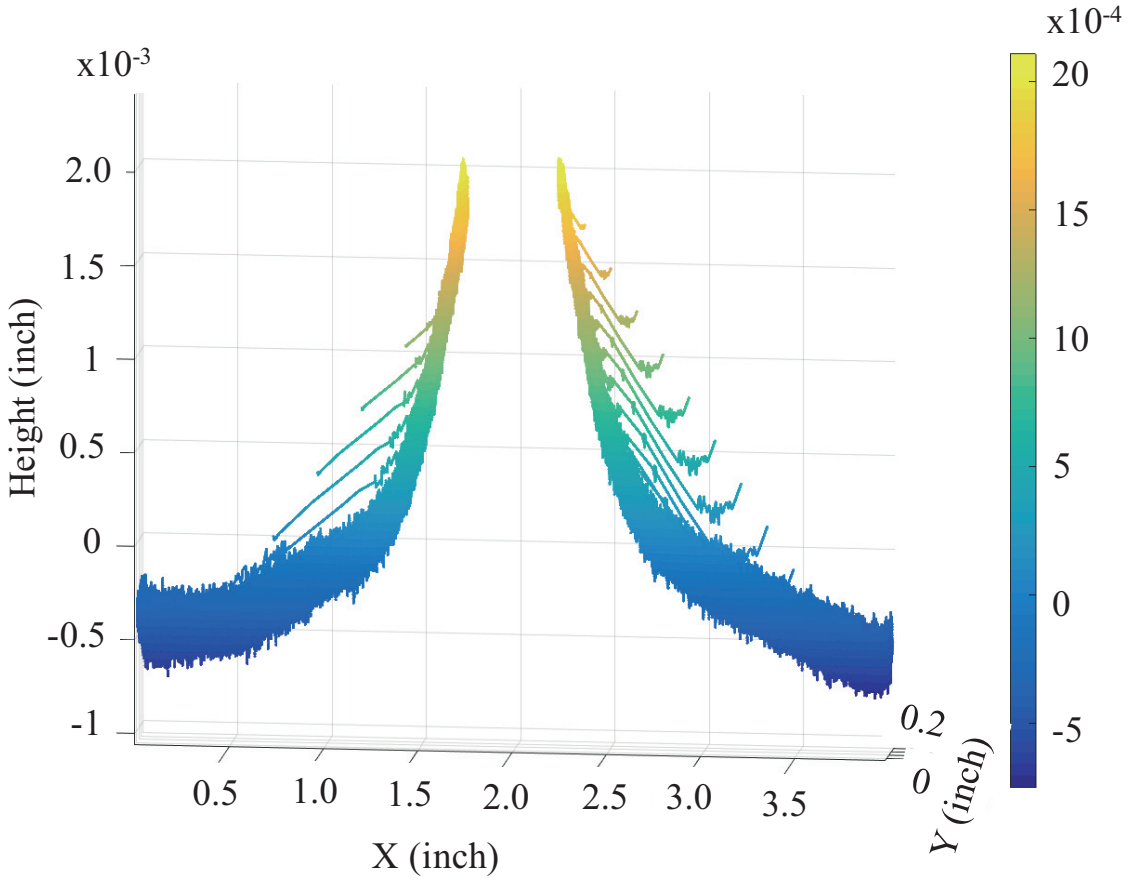

Fig. 27 Image of Laser Displacement Data Showing Level of "Noise" within Dataset after Averaging and Gridding.

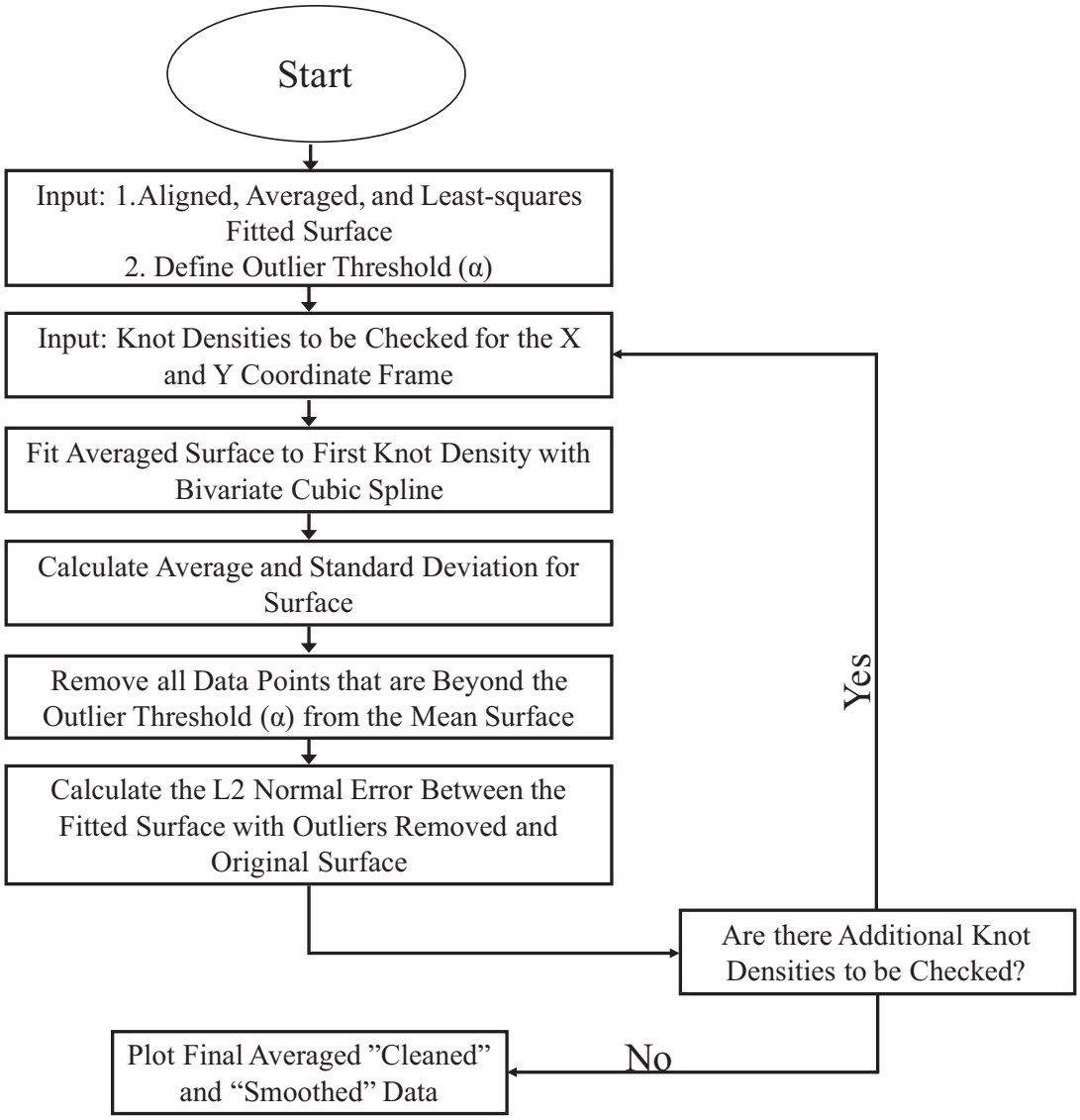

Fig. 28 Flowchart Illustration of Process Used for the Removal of Statistical Outliers and the Fitting of the Remaining Surface.

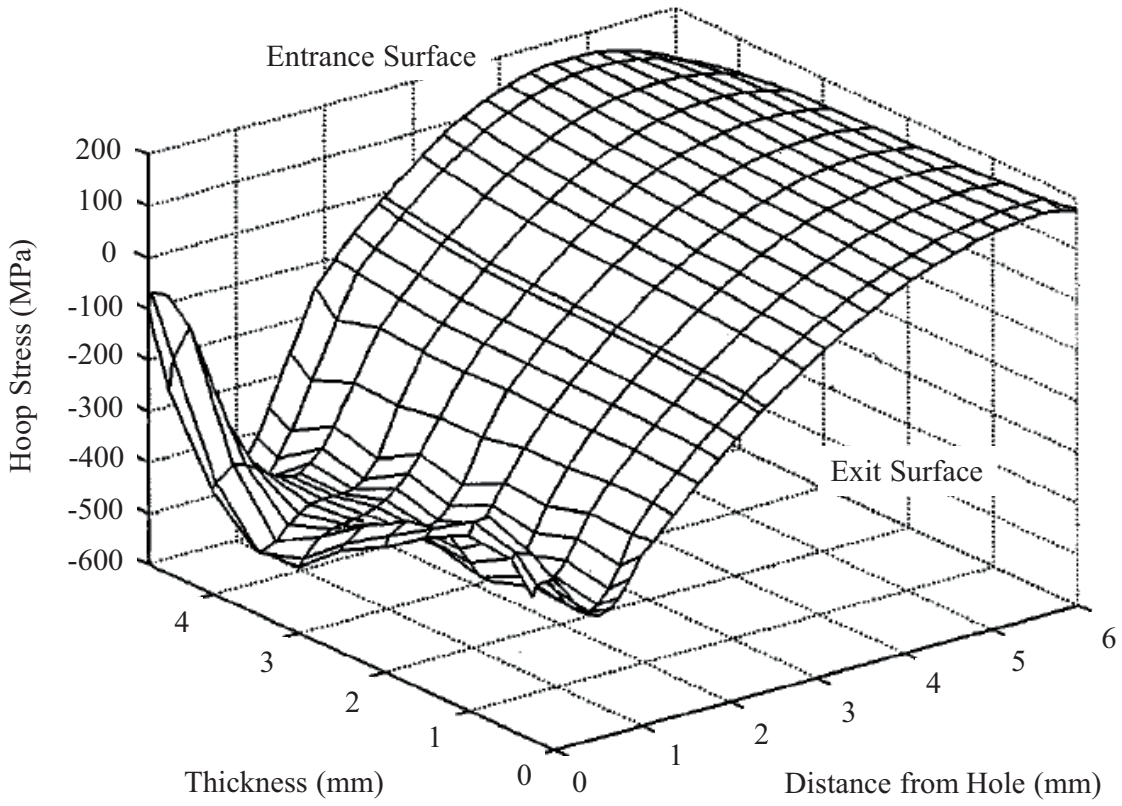

Fig. 29 Three-dimensional Residual Hoop Stress for a 4% Applied Expansion Cx Hole.[116]

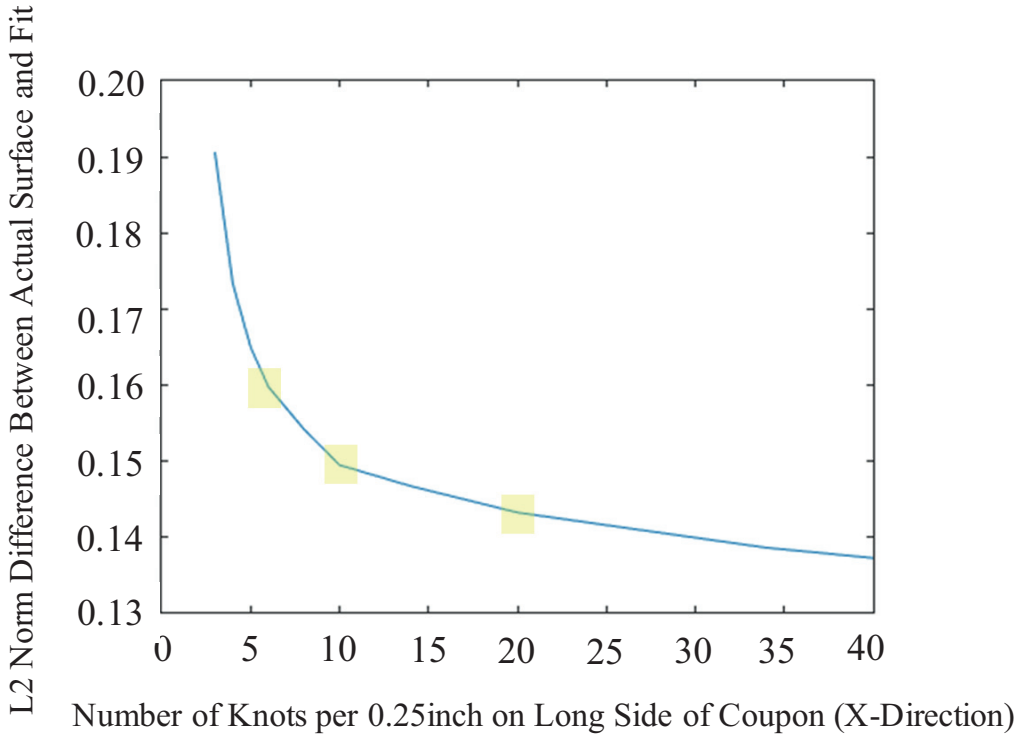

Fig. 30 Plot of L2 Normal Error of Fit vs. Displacement from Cx Hole.

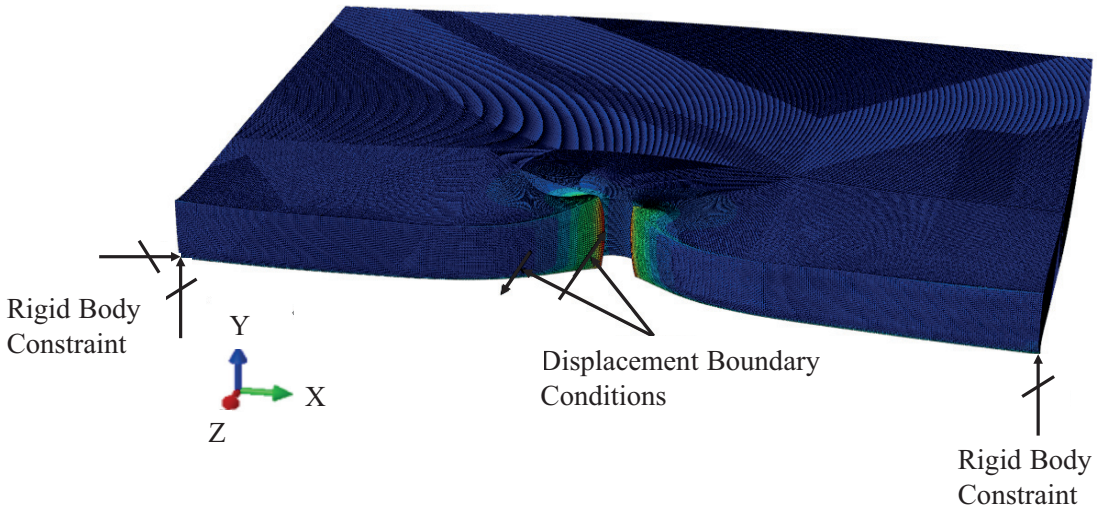

Fig. 31 Finite Element Mesh of Cold Expanded Hole after Displacement Boundary Constraints Have Been Applied, Showing Locations of Rigid Body Constraints - Deformations are Exaggerated by a Factor of 187.

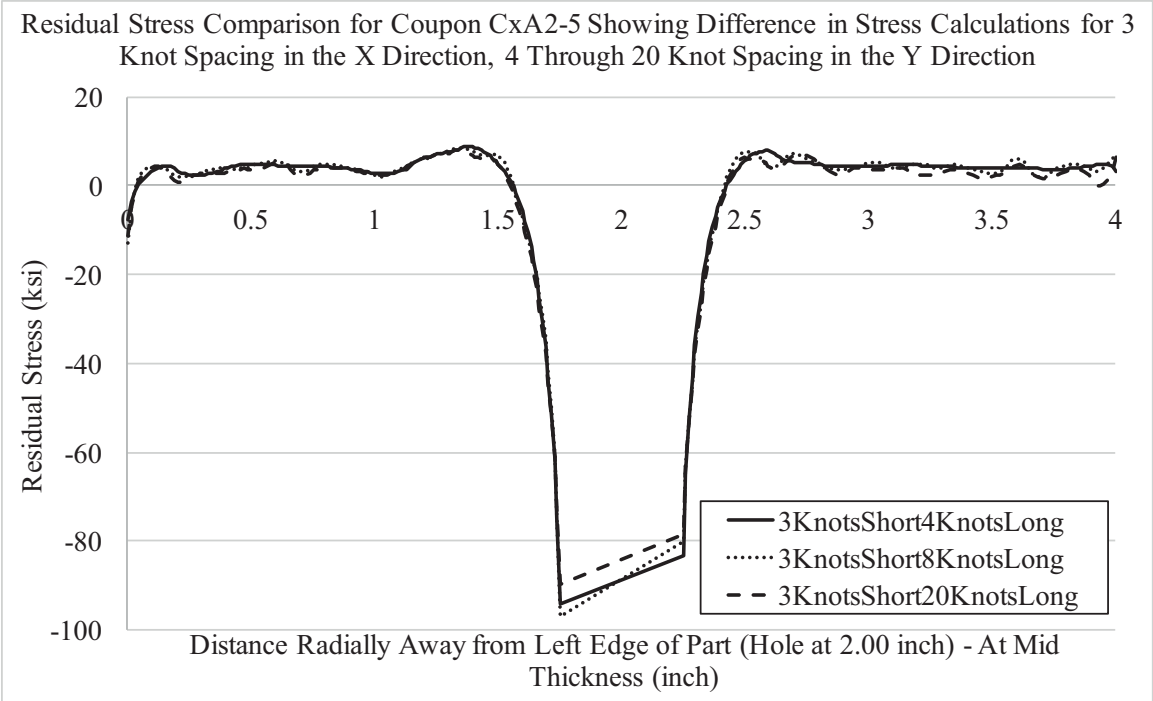

Fig. 32 Line Plot of Residual Stress at Mid Thickness Plane for Knot Densities of Three Through-Thickness and Four, Eight, and Twenty Knots Radially away from Hole.

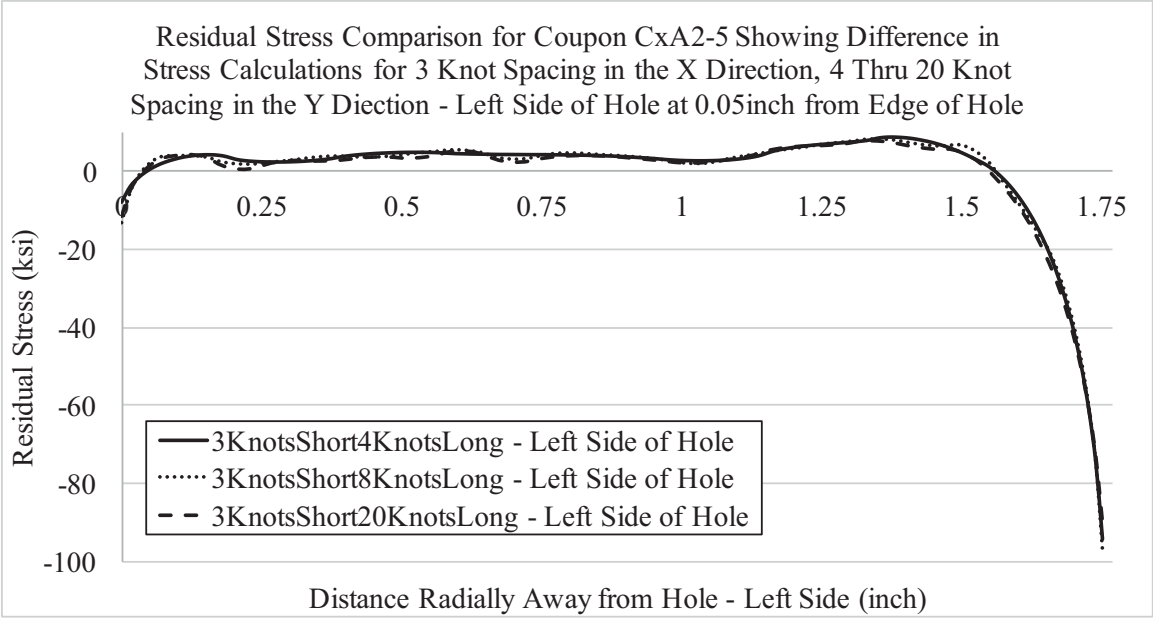

Fig. 33 Line Plot of Residual Stress at Mid Thickness Plane for Coupon CxA2-5 for Knot Densities of Three Through-Thickness and Four, Eight, and Twenty Knots Radially away from Hole – Showing Left Side of Hole.

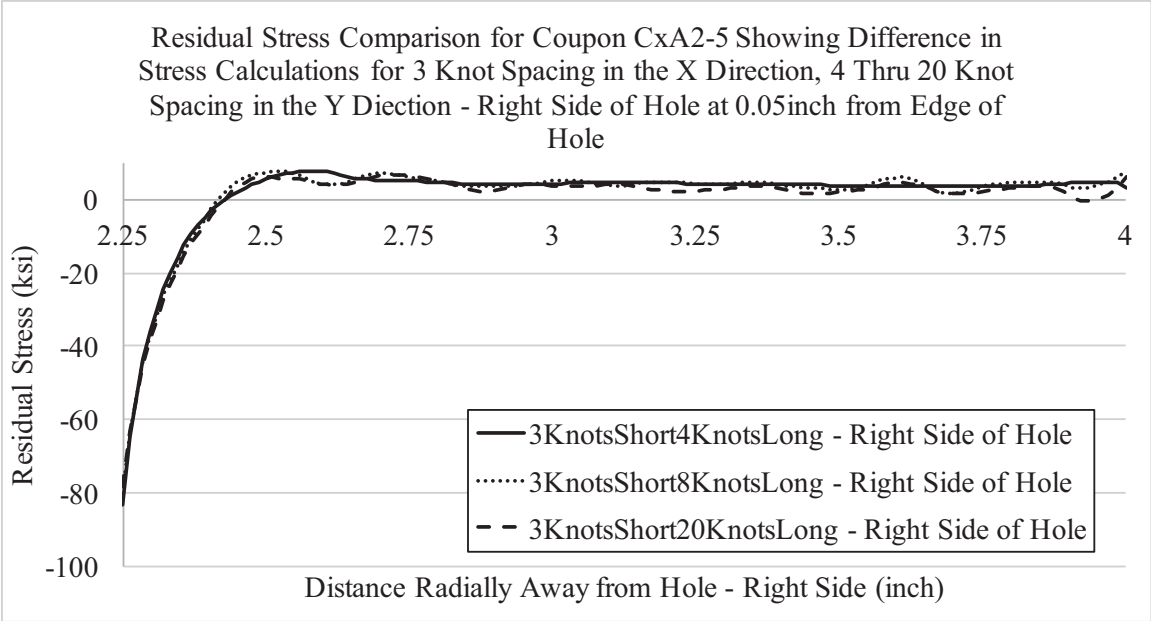

Fig. 34 Line Plot of Residual Stress at Mid Thickness Plane for Knot Densities of Three Through-Thickness and Four, Eight, and Twenty Knots Radially away from Hole – Showing Right Side of Hole.

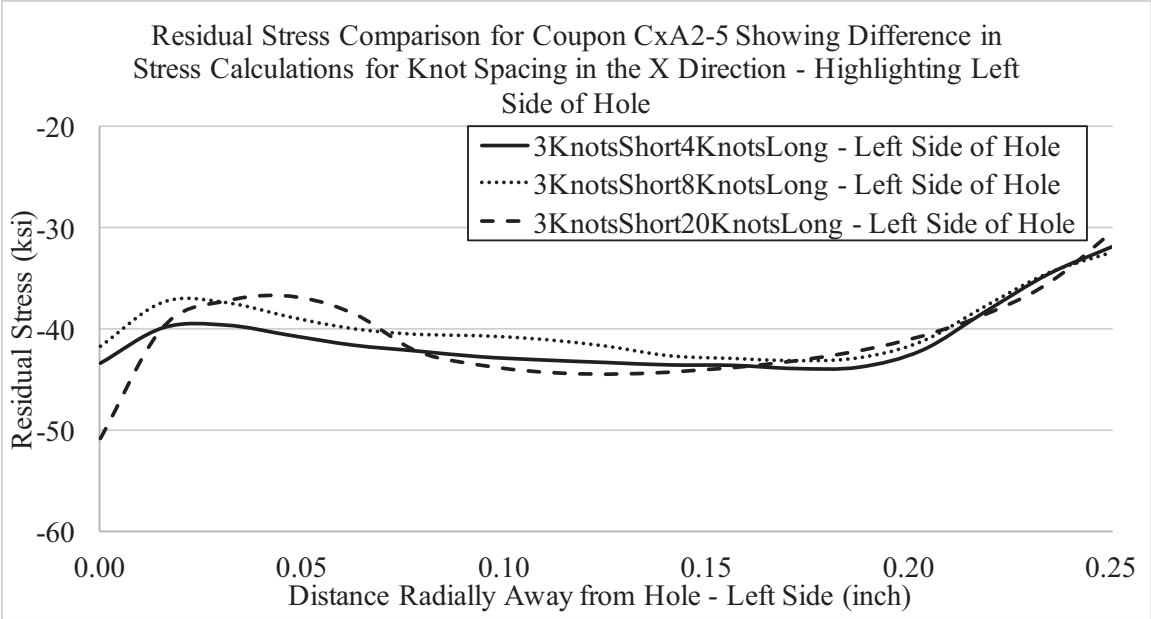

Fig. 35 Line Plot of Residual Stress at 0.05 inch from Left Side of Hole for Knot Densities of Three Through-Thickness and Four, Eight, and Twenty Knots Radially away from Hole.

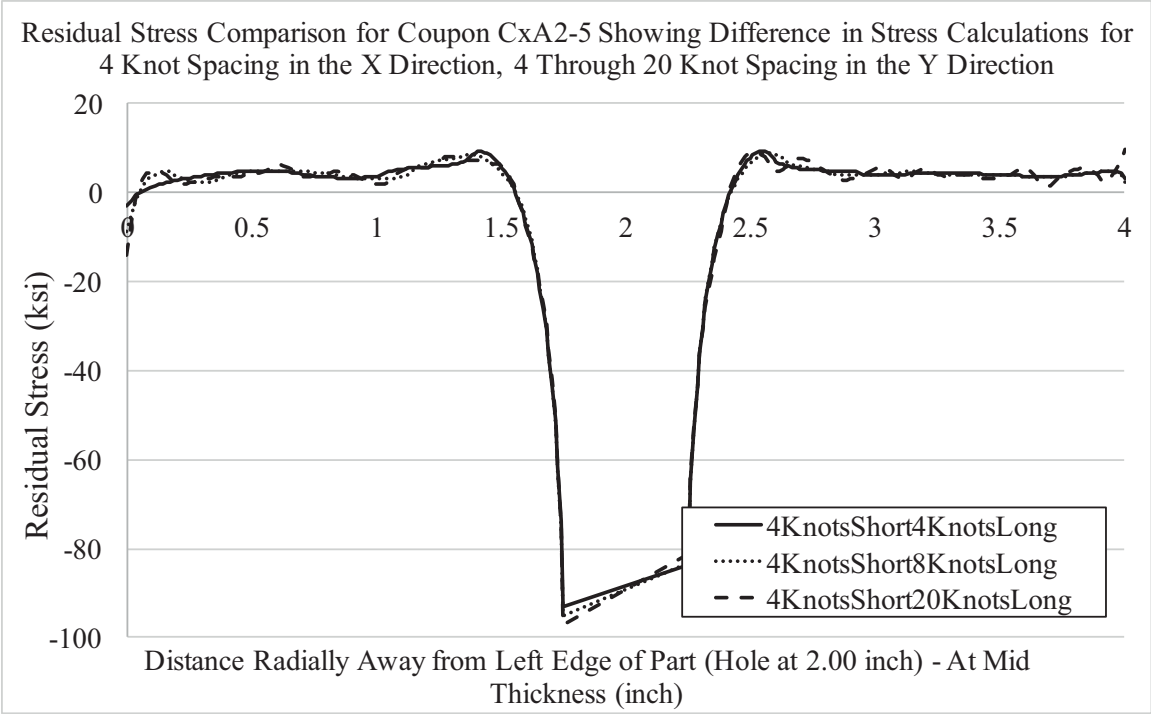

Fig. 36 Line Plot of Residual Stress at Mid Thickness Plane for Knot Densities of Four Through-Thickness and Four, Eight, and Twenty Knots Radially away from Hole.

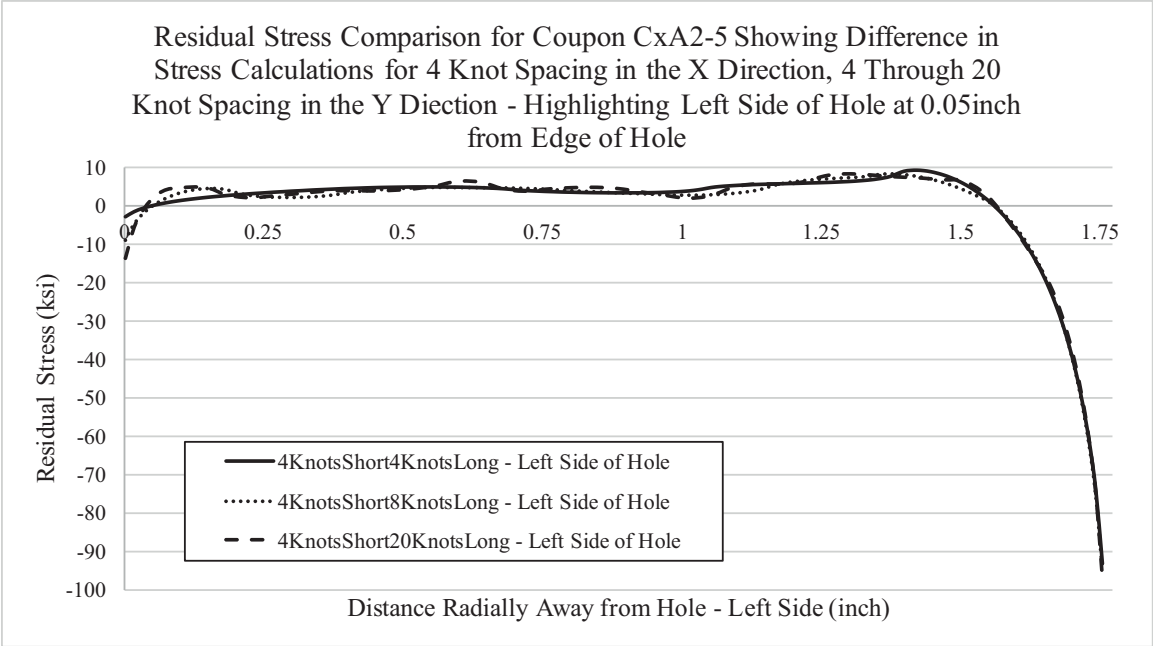

Fig. 37 Line Plot of Residual Stress at Mid Thickness Plane for Knot Densities of Four Through-Thickness and Four, Eight, and Twenty Knots Radially away from Hole – Showing Left Side of Hole.

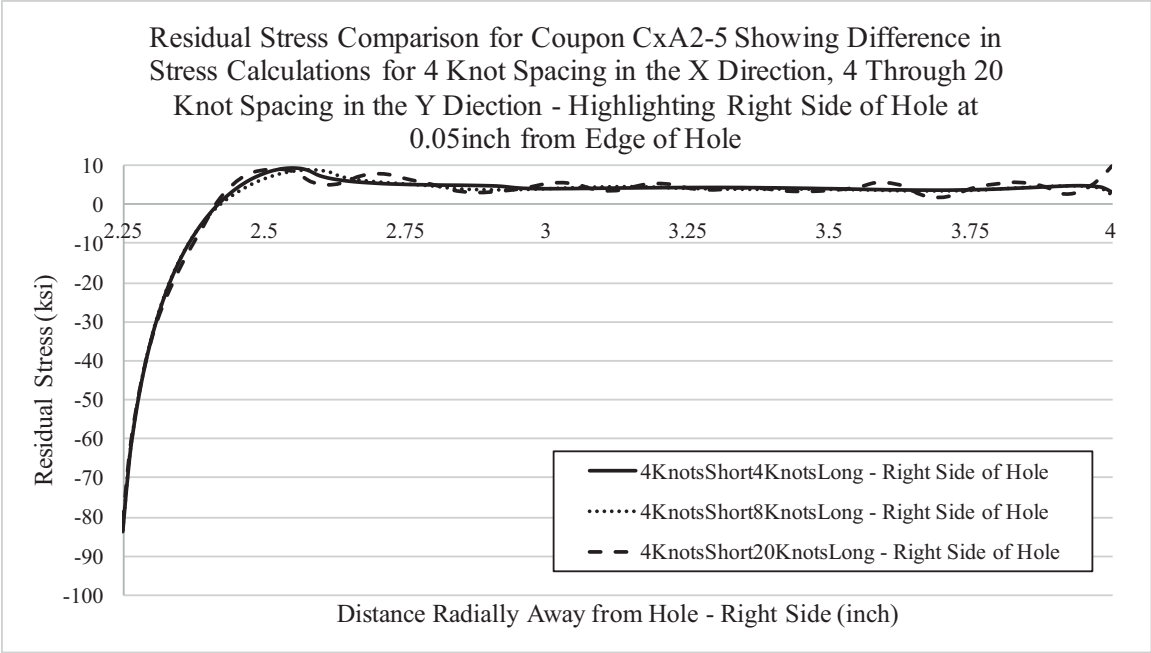

Fig. 38 Line Plot of Residual Stress at Mid Thickness Plane for Knot Densities of Four Through-Thickness and Four, Eight, and Twenty Knots Radially away from Hole – Showing Right Side of Hole.

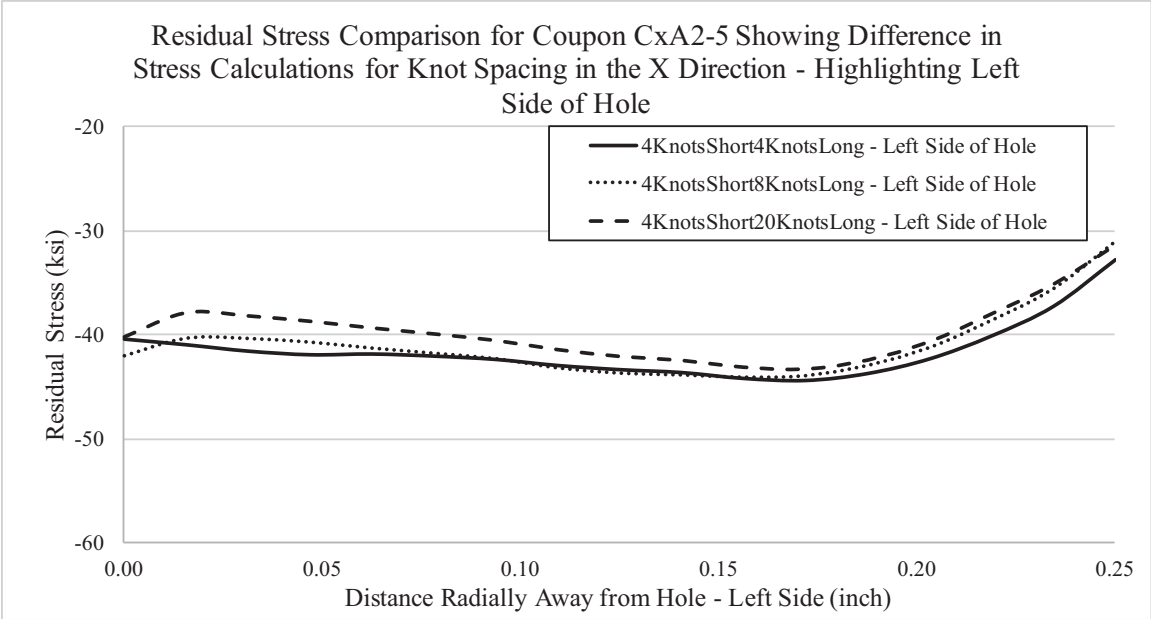

Fig. 39 Line Plot of Residual Stress at 0.05 inch from Left Side of Hole for Coupon CxA2-5 for Knot Densities of Four Through-Thickness and Four, Eight, and Twenty Knots Radially away from Hole.

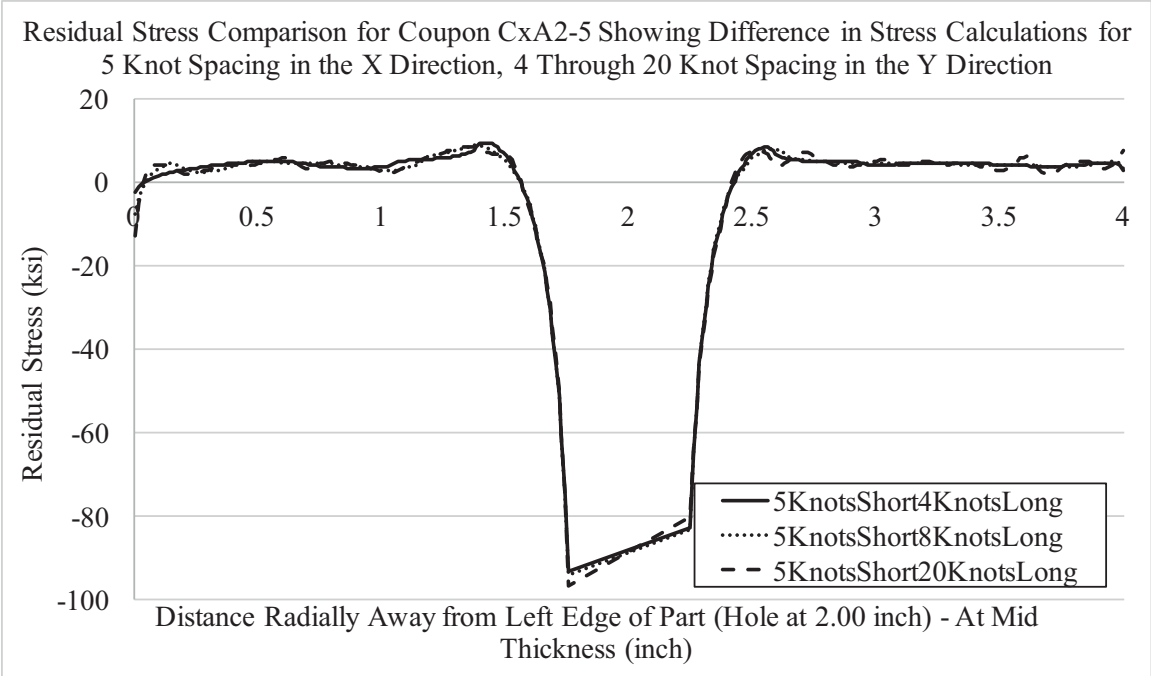

Fig. 40 Line Plot of Residual Stress at Mid Thickness Plane for Knot Densities of Five Through-Thickness and Four, Eight, and Twenty Knots Radially away from Hole.

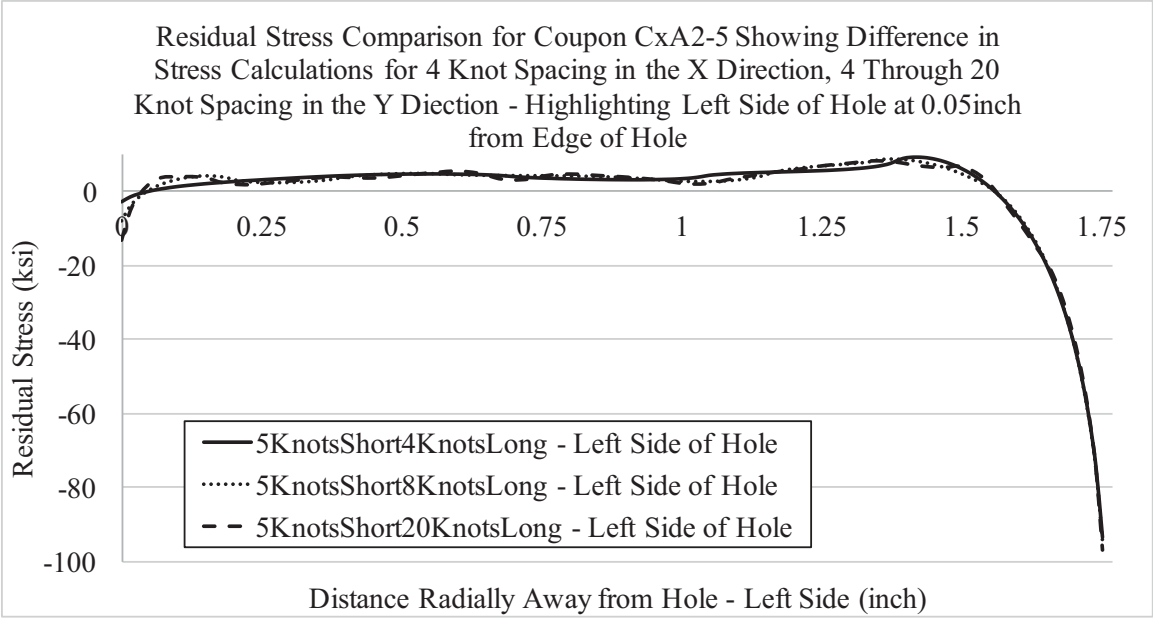

Fig. 41 Line Plot of Residual Stress at Mid Thickness Plane for Knot Densities of Five Through-Thickness and Four, Eight, and Twenty Knots Radially away from Hole – Showing Left Side of Hole.

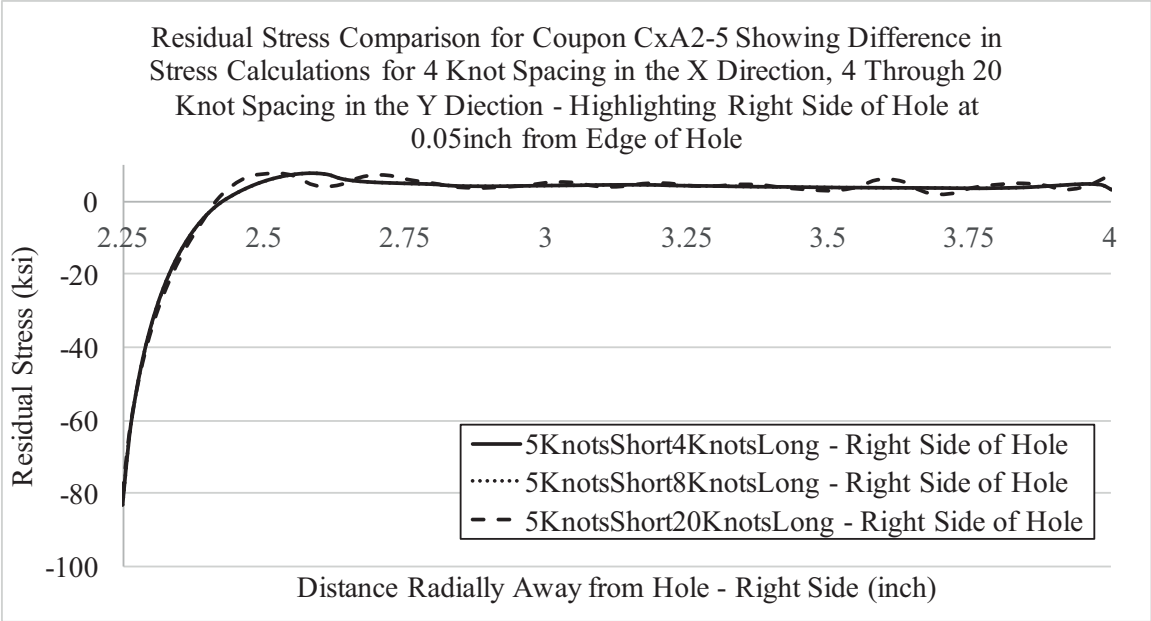

Fig. 42 Line Plot of Residual Stress at Mid Thickness Plane for Knot Densities of Five Through-Thickness and Four, Eight, and Twenty Knots Radially away from Hole – Showing Right Side of Hole.

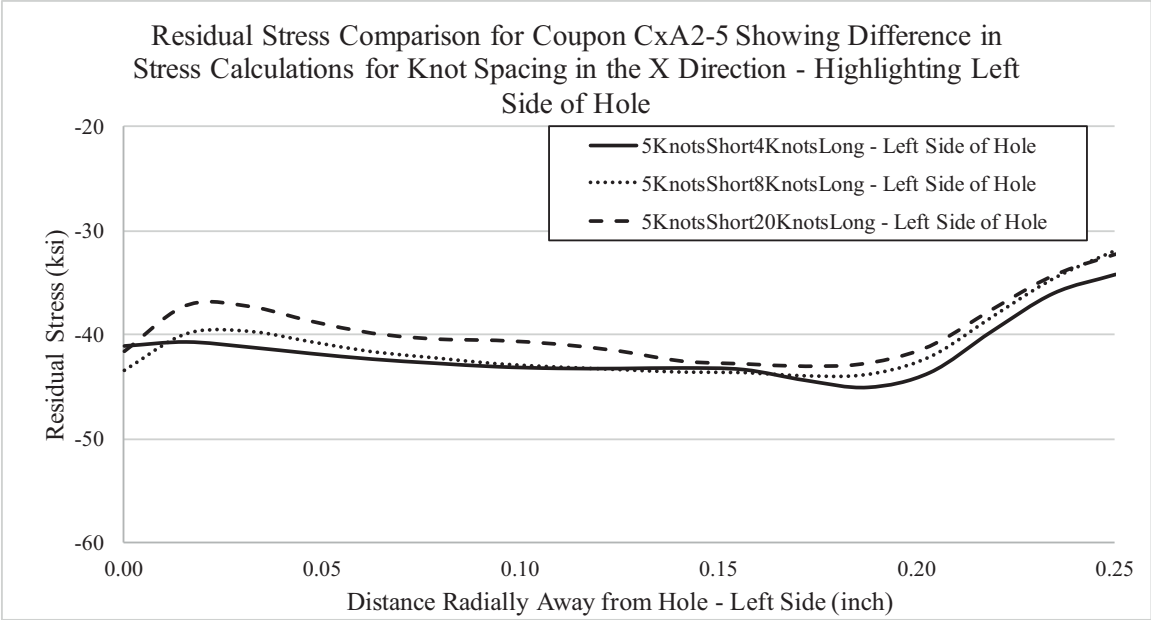

Fig. 43 Line Plot of Residual Stress at 0.05 inch from Left Side of Hole for Knot Densities of Five Through-Thickness and Four, Eight, and Twenty Knots Radially away from Hole.

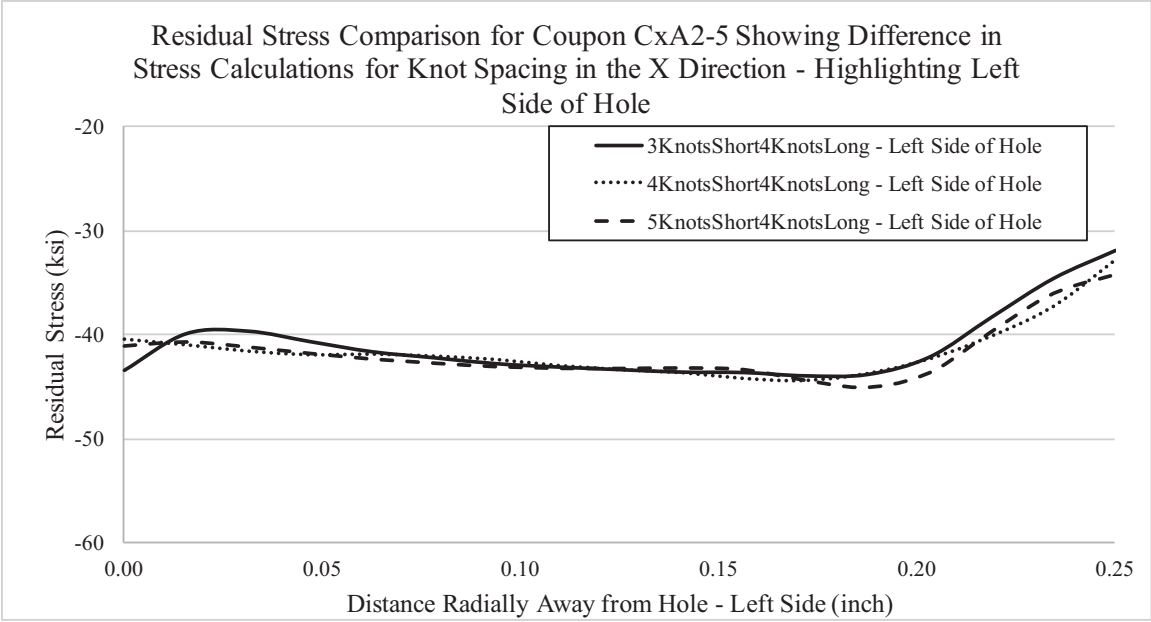

Fig. 44 Line Plot of Residual Stress at 0.05 inch from Left Side of Hole for Coupon CxA2-5 for Knot Densities of Three, Four, and Five Through-Thickness and Four Knots Radially away from Hole.

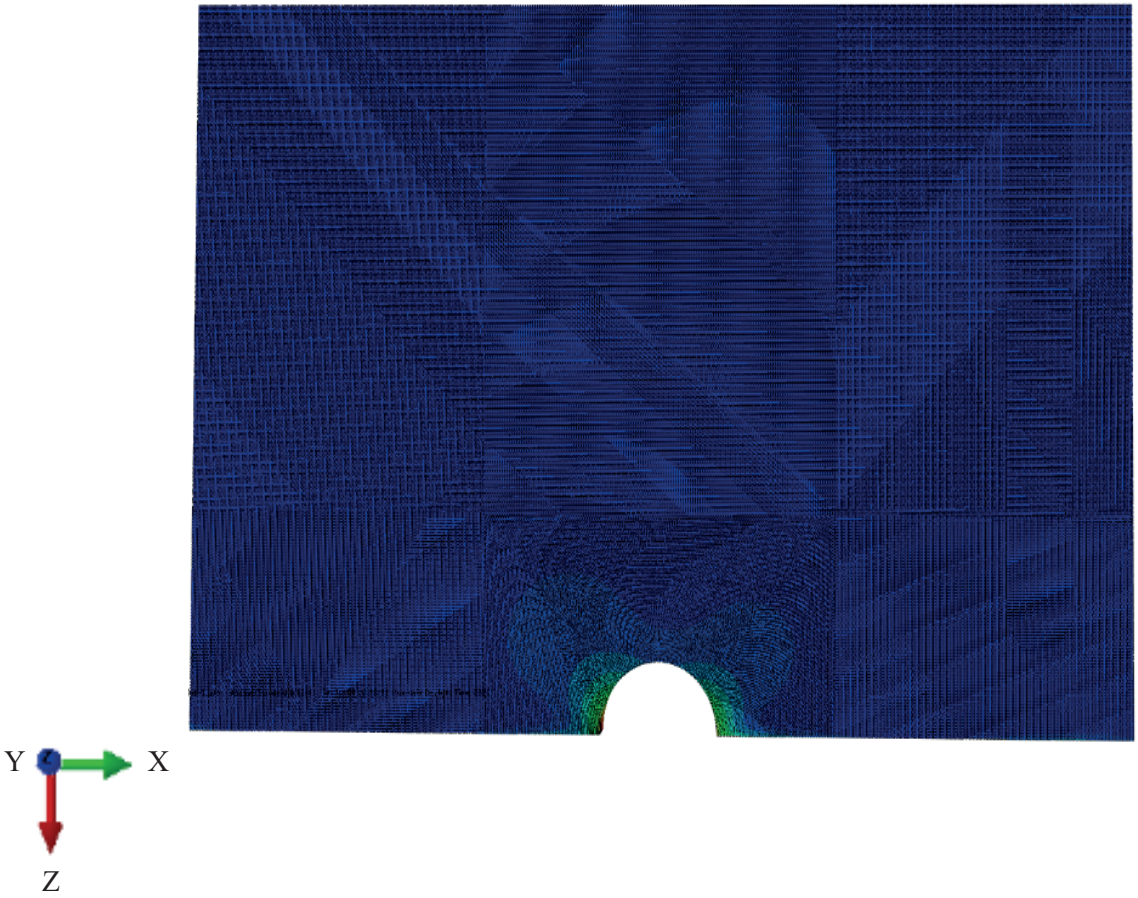

Fig. 45 View Looking Down at FEA Mesh with Sixteen Elements Through the Thickness – Showing Partitioning and Element Bias.

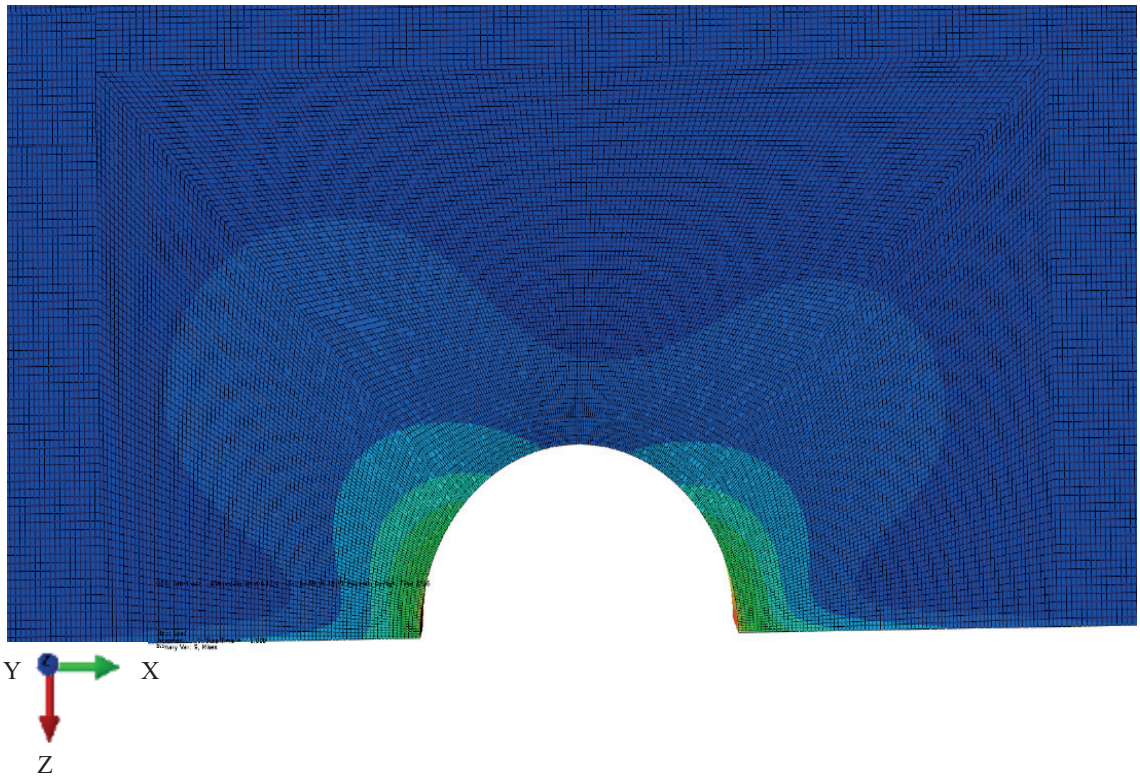

Fig. 46 Close-up View Looking Down at FEA Mesh with Sixteen Elements Through the Thickness – Showing Partitioning.

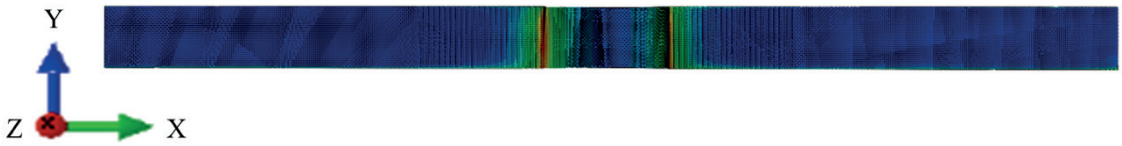

Fig. 47 View Looking at Hole in Finite Element Analysis Mesh with Sixteen Elements Through the Thickness – Showing Bias Radially away from Edge of Hole.

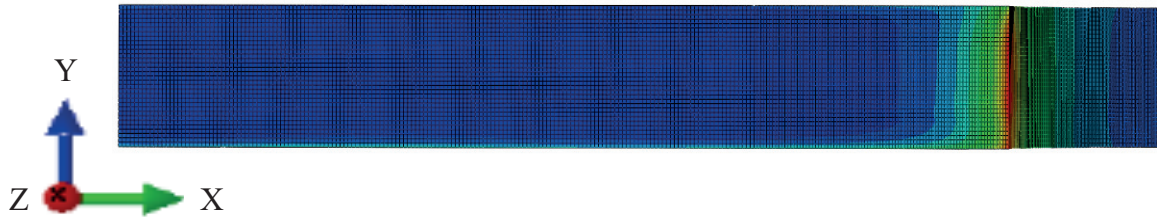

Fig. 48 Close-up View Looking at Hole in FEA Mesh with Sixteen Elements Through the Thickness – Showing Bias Radially away from Left Edge of Hole.

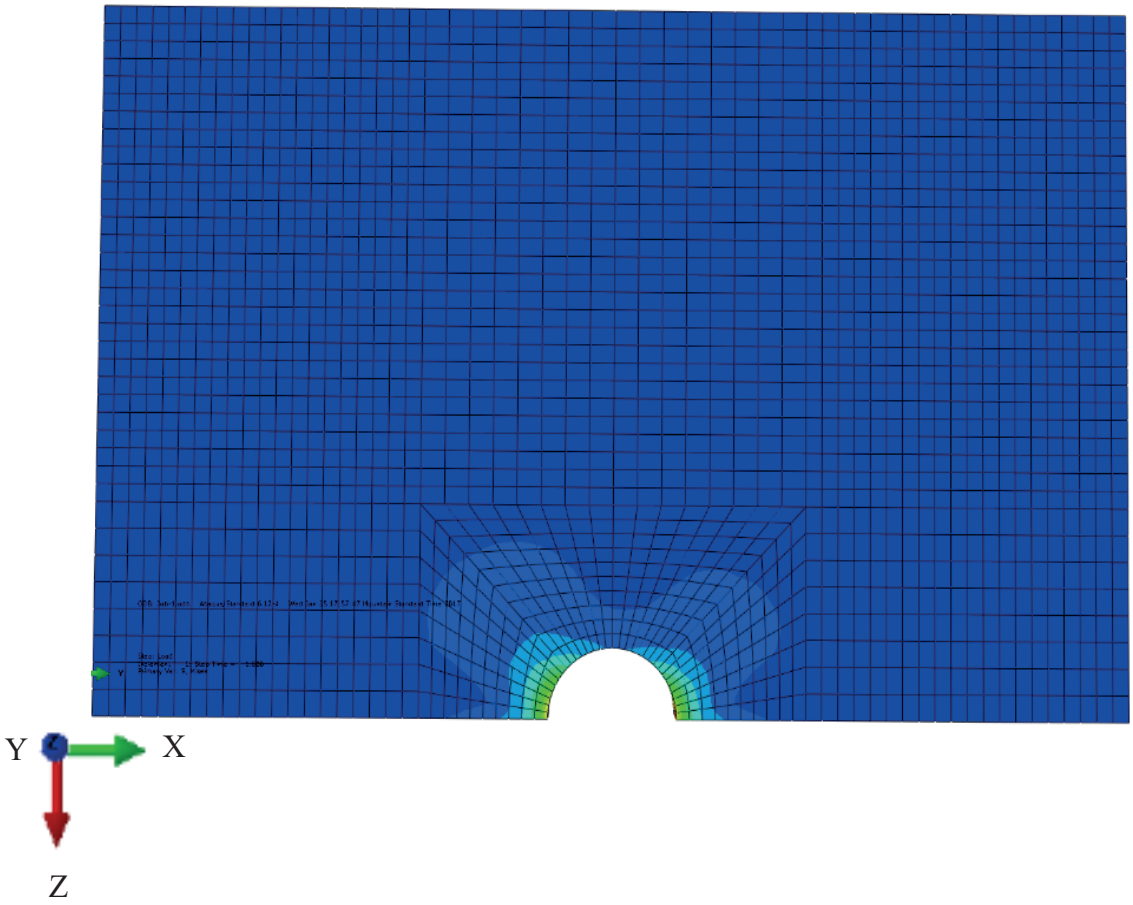

Fig. 49 View Looking Down at FEA Mesh with Four Elements Through the Thickness – Showing Partitioning and Element Bias.

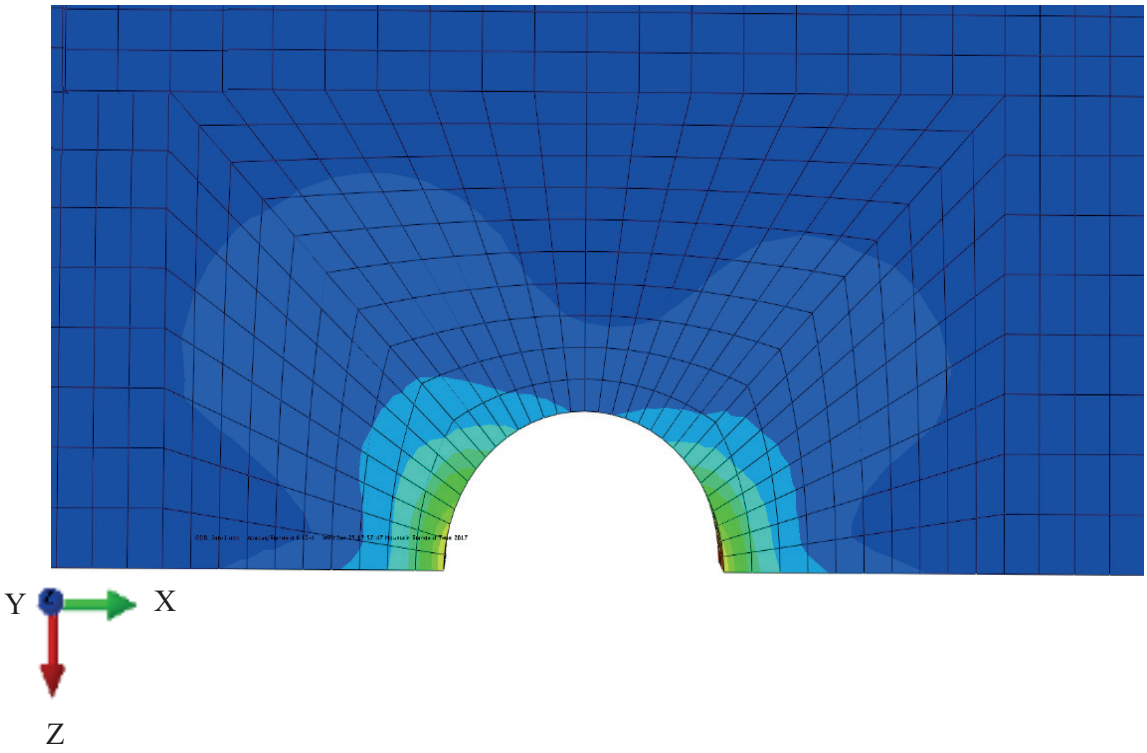

Fig. 50 Close-up View Looking Down at FEA Mesh with Four Elements Through the Thickness – Showing Partitioning.

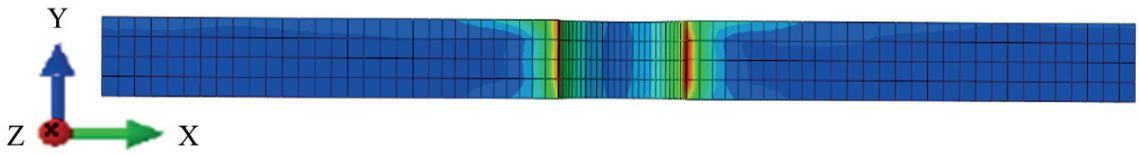

Fig. 51 View Looking at Hole in FEA Mesh with Four Elements Through the Thickness – Showing Bias Radially away from Edge of Hole.

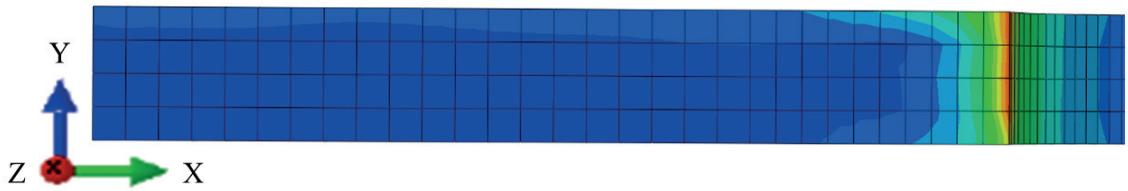

Fig. 52 Close-up View Looking at Hole in FEA Mesh with Four Elements Through the Thickness – Showing Bias Radially away from Left Edge of Hole.

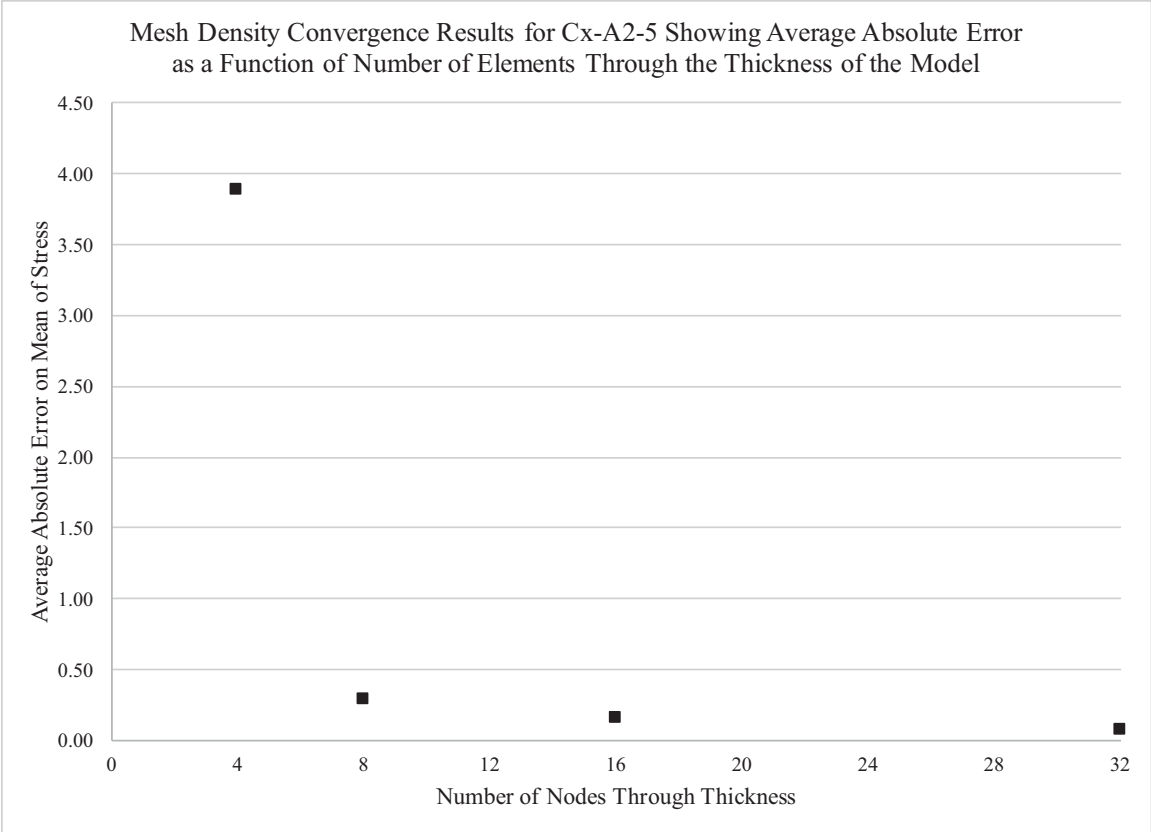

Fig. 53 Mesh Density Convergence Plot of Average Absolute Error vs. Number of Nodes Through the Thickness.

4 RESULTS OF RESIDUAL STRESSES FOR BASELINE UNCRACKED CX HOLES AS DETERMINED VIA THE CONTOUR METHOD

4.1 Residual Stress Results for 2024-T351 (A2) Coupons

4.1.1 Contour Plots of Residual Stress for 2024-T351 (A2) Coupons

Residual stresses will be presented in a variety of methods in order to provide the overall picture of the residual stresses that are in a material after it has been processed via the Cx process. Often contour plots are used to allow for a full-field visualization of the stress field. Residual stress contour plots will be provided for each of the five 2024-T351 coupons that were processed to produce residual stresses. For all coupons, the Cx process mandrel entrance location is at the Y=0 location. Residual stresses for all 2024-T351 (A2) coupons are provided in Fig. 54 through Fig. 63. Zoomed in contour plots are provided that allow for additional investigation near the edge of the hole.

From these contour plots it can be seen that, like that shown in the past, the stress gradient near the edge of the hole is very steep. In addition, there is a difference in the through thickness gradient from the left to right side of the hole. For these 2024-T351 coupons it seems that the left side of the hole has a near surface effect at the Cx mandrel entrance surface (Y=0). This effect is such that the highest level of compression doesn't seem to make it all the way down to the edge of the part. On the right side of the hole the deepest level of compression seems to follow a straight line from the entrance to the exit

surfaces. It is also important to note that the highest level of tension occurs on the exit side of the coupon away from the edge of the hole. These areas occur at similar locations on both sides of the hole.

4.1.2 Line Plots of Stress Radially away from Hole for CxA2 Group

Line plots of the residual stress are provided at five locations through the thickness of the part. These locations are at specific nodal locations within the mesh. For all of the coupons, line plots will be provided in reference to the Cx mandrel entrance surface. The locations for these line plots are at 0.00 inch (Entrance Surface), 0.05 inch, 0.09 inch, 0.125 inch (Mid Thickness), 0.16 inch, 0.20 inch, and 0.25 inch (Exit Surface) from the mandrel entrance surface. Line plots were produced for all individual replicates, and can be found in the Appendix. Line plots for these locations are found in Fig. 64 through Fig. 77. All line plots of stress show the stress for each individual sample, CxA2-1 – 5 and also the average and standard deviation for the group of measurements.

For all of the line plots for the 2024-T351 there showed a bias in the depth of the residual stress. For all of the coupons the left side of the hole had a slightly deeper residual stress at the edge of the hole. It is currently unknown why this bias exists. It is possibly due to the cutting of the coupons, for it is known that one side of the hole was cut first, from the edge of the hole to the edge of the part, and then back to the other side. It is also possible that this effect is due to the Cx process itself, or the application of it. That the puller was not perfectly square with the hole when it was pulled. Finally, it could be due to some clocking misalignment during the Cx process. Such that the split sleeve was not exactly aligned with the 12 o'clock position, causing there to be, along the

cut plane, a region of asymmetry. This is an area of investigation that needs to have further work.

There is a significant level of repeatability, however, shown in these five coupons. The depth of the deepest compression is within 10 ksi, the location where the stress crosses the 0 ksi line is very close to being the same on each side of the hole and the maximum tension level is similar at each cross sectional cut at the hole.

4.1.3 Line Plots of Stress Through the Thickness of the Part for CxA2 Group

Line plots were also produced through the thickness of the part. These plots provide additional insight into the residual stress state within the part. Line plots were produced for both the left and right side of the hole, with the Cx process mandrel entrance being at X=0. All line plots of stress show the stress for each individual sample, CxA2-1 – 5 and also the average and standard deviation for the group of measurements.

4.1.3.1 Line Plots of Stress Through the Thickness for CxA2 – Left Side of the Hole

Line plots of stress are provided for the left side for a range of distances away from the hole, to include 0.01 inch, 0.05 inch, 0.10 inch, and 0.15 inch, as provided in Fig. 78 through Fig. 93. Two sets of figures will be provided for the through-thickness residual stresses. The first set will have the Y axis set to the maximum compressive stress and the maximum tensile stress, and this will be held constant. This helps to see the general trends of the residual stress. The second plot at each location will have the Y axis set to auto, thus that the stress will be more focused. This allows for a more

zoomed-in view of the residual stresses, at the specific range they are at that cross section.

4.1.3.2 Line Plots of Stress Through the Thickness for CxA2 – Right Side of the Hole

Line plots of stress are provided for the right side for a range of distances away from the hole, to include 0.01 inch, 0.05 inch, 0.10 inch, and 0.15 inch, as provided in Fig. 86 through Fig. 92.

It can be noticed from these residual stress line plots that as the traces move away from the edge of the hole the depth of the compressive residual stress decreases, to where at 0.15 inch away from the edge of the hole there is a significant region that is near zero (0) stress. Also, from these line plots it can be seen that the highest levels of variability between the replicates is at the edges of the part. Also, it can be seen that as the line plots moves towards the edges of the part there can be a significant shift in the slope of the residual stress field. This effect seems to be most pronounced at the exit surface of the part. It is known that at the edges of the part the contour method has a higher level of uncertainty, thus it is likely that these stresses are less accurate and are highly influenced by this edge effect. The coupon repeatability shows that even close to the edges of the part, one element away, the variability decreases significantly and thus a higher level of trust can be given to these values.

4.2 Residual Stress Results for 7075-T651 (D2) Coupons

4.2.1 Contour Plots of Residual Stress for 7075-T651 (D2) Coupons

Residual stress contour plots will be provided for each of the three 7075-T651 coupons that were processed to produce residual stresses. For all coupons, the Cx process mandrel entrance location is at the Y=0 location. Residual stress contour plots are provided in Fig. 94 through Fig. 99. In addition to the full-field contour plots, like those provided for the CxA2 (2024-T351) coupons, a zoomed in contour plot of the area close to the edge of the hole will be provided.

Like that seen in the CxA2 (2024-T351) coupons, the 7075-T651 coupons show some amount of asymmetry right at the edge of the hole. The location of the highest level of tension is similar to that seen in the CxA2 (2024-T351) coupons but there is a difference in the orientation of that higher tension field. The maximum level of compression in the CxD2 (7075-T651) coupons, is significantly higher than that seen in the CxA2 (2024-T351) coupons. This is reasonable if one compares the static allowables of the material, with the 7075 material having much higher tension and compression allowables.

4.2.2 Line Plots of Stress Radially away from Hole for CxD2 Group

Line plots of the residual stress radially away from the hole are plotted at the same locations as provided in the A2 condition. Line plots of the residual stress radially away from the hole are shown in Fig. 100 through Fig. 113.

From these line plots it is possible to gain an understanding of the differences in the compressive residual stresses between the left and right sides of the hole. It can again

be seen that for all of these parts there seems to be a bias on the depth of the residual stress from the left side of the hole to the right side. Again, all coupons were cut the same way, the left side first and then the right. However, it is unclear if this cutting methodology is the reason for this bias.

4.2.3 Line Plots of Stress through the Thickness of the Part for CxD2 Group

4.2.3.1 Line Plots of Stress through the Thickness for CxD2 – Left Side of the Hole

For the CxD2 (7075-T651) coupons line plots were developed for the left side of the hole. The spacing for these line plots is the same as was provided for the CxA2 configuration. The residual stress line plots for the left side of the hole for all CxD2 coupons are provided in Fig. 114 through Fig. 121. For all of the through-thickness plots there will again be provide two scales for viewing the images. The goal is not only to enable the reader to gain a greater understanding of the variation in the residual stress along these lines, but also to understand how they compare to each other on the same scale.

From these through-thickness plots it is possible to see that the highest level of variability from these three replicates occurs at the Cx mandrel exit surface and at some locations on that exit surface that level of variability reaches ±35 ksi. This high level of variability is quite localized and is highest near the edge of the hole. As these residual stress line plots trace out away from the edge of the hole the level of variability decreases across the face. The Cx mandrel entrance side of the hole has less variability then the exit side, and the cause of this is not currently known.

4.2.3.2 Line Plots of Stress through the Thickness for CxD2 – Right Side of the Hole

For the CxD2 (7075-T651) coupons line plots were developed for the right side of the hole. The spacing for these line plots is the same as was provided for the CxA2 configuration. The residual stress line plots for the left side of the hole for all CxD2 coupons is provided in Fig. 122 through Fig. 129.

For the right side of the hole there are similar trends as provided for the left side, however, the level of variability on the right side seems to be less. Again the maximum regions of variability are on the exit surface and closer to the edge of the hole. The maximum variability is approximately ±15 ksi, rather than the ±35 ksi as seen on the left side.

4.3 Statistical Analysis of Residual Stresses Determined via the Contour Method at Cold Expanded Holes

4.3.1 Repeatability Uncertainty of Residual Stress Determined via the Contour Method at Cold Expanded Holes in 2024-T351 and 7075-T651 Aluminum Alloys

With multiple replicates of each condition developed for both the 2024-T351 and 7075-T651 coupon configuration it was possible to determine the repeatability uncertainty associated with the Cx process. This statistical analysis approach had never been applied to the residual stress fields introduced via the Cx process, however it has been applied to other more simplistic residual stress fields determined via the contour method.[117,118] It should be noted that the coupons developed for this research were held to a much higher tolerance level in order to optimize the applied expansion level at the hole.[119] This applied expansion was controlled for the A2 and D2 by the pre-Cx hole

diameter and the mandrel's major diameter (D_m), per Fig. 9, Table 2, and Table 3. Thus, the final applied expansion for the A2 (2024-T351) condition had an average of 3.18% ±0.04% and the D2 (7075-T651) condition had an average applied expansion of 3.28% ±0.03%. The allowable range for the applied expansion within the FTI spec for this hole diameter, in these two alloys, ranges from the "low" end at 3.16% to 4.16% at the "high" end of the applied expansion level. Thus the amount of statistical variation that was calculated herein is smaller than that which would be present within the residual stress field produced by the Cx process when performed within tolerances of the FTI process specifications.

The repeatability uncertainty was calculated spatially across the entire face of each coupon at the same points. This was possible because the final dimensional configuration and nodal density was set to be exactly the same for each coupon. Thus, each coupon was represented by 4,182 nodal stress locations, with multiple replicates for each material, five for the 2024-T351 and three for the 7075-T651 aluminum alloy. For both the CxA2 (2024-T351) and the CxD2 (7075-T651) configurations the average and repeatability standard deviation were calculated as a function of the in-plane nodal position. The repeatability standard deviation was calculated as shown in Equation 3

$$s(x,y) = \sqrt{\frac{1}{N-1}\sum_{i=1}^{N}\left(\sigma_i(x,y) - \bar{\sigma}(x,y)\right)^2} \qquad \text{Equation 3}$$

where $s\,(x, y)$ is the repeatability standard deviation at a given in-plane spatial location (x, y), N is the number of specimens for which a residual stress was determined (for the CxA2 condition this is five and for the CxD2 condition this is three), $\sigma(x, y)$ is the

residual stress determined for that in-plane nodal (x, y) location, and $\bar{\sigma}(x, y)$ is the mean stress determined via the contour method.[120,121]

4.3.1.1 Average and Repeatability Standard Deviation Contour Plots of CxA2 (2024-T351) Coupon Configuration

Residual stress contour plots for each of the five CxA2 conditions were provided in Fig. 54 through Fig. 62. The average residual stress from these five coupons are provided in Fig. 130 and Fig. 131 and the spatial standard deviation is provided in Fig. 132 and Fig. 133. From the contour plots of the standard deviation it can be seen that the highest standard deviations can be seen at the Cx mandrel exit surface and are away from the edge of the hole, along the exit surface.

4.3.1.2 Average and Repeatability Standard Deviation Contour Plots of CxD2 (7075-T651) Coupon Configuration

Residual stress contour plots for each of the three CxD2 conditions were provided in Fig. 94 through Fig. 98. The average residual stress from these three coupons is provided in Fig. 134 and Fig. 135. Two contour plots of the spatial standard deviation of the residual stress can be found inFig. 136 and Fig. 137.

4.3.1.3 Conclusions from Repeatability Uncertainty of Residual Stress Determined via the Contour Method at Cold Expanded Holes in 2024-T351 and 7075-T651 Aluminum Alloys

4.3.1.3.1 Conclusion from Average and Repeatability Uncertainty of CxA2 (2024-T351) Residual Stress Fields

From the calculation of the repeatability standard deviation it is possible to see that the residual stress field has the highest level of uncertainty at the exit surface on both

the left and right side of the hole, with a peak standard deviation equal to ±13 ksi, which is equal to 14% of the peak average stress of the CxA2 (2024-T351) condition. At the edge of the hole the uncertainty was held relatively constant between ±3 ksi to ±6 ksi, this is between 3.2% and 6.5% of the maximum average residual stress within these coupons. In addition to the high zones of uncertainty on the exit surfaces there are small locations on the entrance hole surface on both the left and right sides of the hole. In these locations, there is a peak uncertainty of between ±8 ksi to ±10 ksi, which represents a 8.6% to 9.3% uncertainty in reference to the maximum average residual stress for these 2024-T351 parts.

It should be noted that it is often stated that the contour method is less accurate at the edges of a part. The work performed within this research helps to quantify the uncertainty of the residual stress state across the entire plan of interest.

4.3.1.3.2 Conclusion from Average and Repeatability Uncertainty of CxA2 (2024-T351) Residual Stress Fields

The maximum standard deviation within the CxD2 coupon configuration was ±36 ksi. This amount of uncertainty was very localized to the exit surface, near the edge of the hole, and represented a much higher percentage of the maximum stress within the part, 29.3%, which is more than three times (3x) the level of uncertainty that was calculated within the CxA2 (2024-T351) coupons. However, within these CxD2 (7075-T651) coupons it can be seen that the overall level of uncertainty is much lower, with very localized peaks of uncertainty. Near the edge of the hole, on both the left and right sides of the hole, the standard deviation ranges between ± 4ksi to ±6 ksi, which is only 3.2% to 4.9% of the maximum average residual stress determined for the CxD2 (7075-

T651) coupon configuration. It is possible that this is due to the material upset that is a result of the Cx mandrel as it exits the hole. This additional resultant deformation may complicate the determination of the final residual stress state near the Cx mandrel exit surface.

One other difference between the CxD2 (7075-T651) and the CxA2 (2024-T351) condition is that within the CxD2 (7075-T651) configuration this high amount of uncertainty is very localized, mainly on corners of the hole at the exit surface. Whereas, for the CxA2 (2024-T351) configuration, the higher levels of uncertainty continued across almost the entire exit surface of the part.

Through the core of each material configuration the level of repeatability uncertainty remained within a level of ±2 ksi to ±4 ksi, representing a relatively low degree of uncertainty related to the maximum average residual stress measured for both the CxD2 (7075-T651) and the CxA2 (2024-T351) condition.

4.3.2 Development of a Single Measurement Uncertainty for the Residual Stress Determined via the Contour Method at Cold Expanded Holes in 2024-T351 and 7075-T651 Aluminum Alloys

In addition to developing a repeatability uncertainty for each of the two Cx configurations, a method was followed to develop an uncertainty for each individual residual stress calculation/determination. The quantification of this single measurement uncertainty would allow for an assessment of the quality of the measurement technique.[120,122] This work would allow for a spatial single measurement uncertainty to be developed and applied to the residual stress fields that were developed via the contour method.

Two sources of random error have been stated to exist within the contour method.[123] These include a "modeling" error, or a fit error, and "displacement" error. The fit error takes into account any error that may be introduced by not selecting the optimal numeric fit for the displacement field. As shown in Fig. 30, the L2 error was used to try and determine the "optimal" knot density for both the X and Y coordinate axes, however it is possible that this optimal fit was not truly the most accurate fit for the surface that could have been selected. The quantification of this fit error enables an estimation of the error within the data processing that is associated with the potential of either over or under fitting the displacement field. The displacement error captures the random noise that would be included in the measured displacement field. This source of noise could be introduced to the wire cutting operation, dust on the cut surface during scanning, or other random sources of error that are present in the displacement measuring source.[118]

4.3.2.1 Modeling/Fit Error Estimation within the Contour Method as Applied to the Residual Stress Field at Cx Holes

In order to estimate the spatial uncertainty associated with the order of fit that is applied to the aligned, averaged and de-noised displacement field, the optimal fit must first be established. For all of the Cx coupons processed in this work that final spacing was four knots in the Y direction, through the thickness. This would define a knot ever 0.0625 inch. This spacing was then used in the X direction, radially away from the hole. Therefore placing thirty-two knots in the X direction, every 0.0625 inch, starting at the edge of the hole and ending at the outer surface. With this optimal knot density in both the X and Y coordinate frame determined, the knot density in both the X and Y directions

were adjusted up and down one level from the optimal fit. This method for quantifying the modeling/fit error has been successfully applied to residual stresses determined via the slitting method.[124]

The knot spacing was adjusted down to three knots and up to five knots through the thickness (Y direction), which corresponded to a knot density radially away from the hole (X direction) of twenty-four knots at the low end to forty knots at the high end. Thus, a total of five surface fits were developed for the averaged, de-noised surface, with knot spacings of three, four, and five through the thickness, and twenty-four, thirty-two, and forty radially away from the hole.

In order to determine the modeling/fit error the average and standard deviation of the residual stress was taken at every nodal location across the spatial domain. This modeling/fit error was thus defined in Equation 4.

$$U_{FitError} = STD\left(\sigma_{x,y}, \sigma_{x+1,y}, \sigma_{x-1,y}, \sigma_{x,y+1}, \sigma_{x,y-1}\right) \qquad \text{Equation 4}$$

Within Equation 4 the $U_{FitError}$ represents the fit error and σ is the residual stress at the individual nodal location as determined via the contour method at a given knot density for both the X and Y directions along the plane of interest. It was determined that this model/fit error has a Gaussian, or Normal, distribution at each of the points along the plane of interest, and thus would imply that one standard deviation would capture 68.4% of the data on each side of the mean.[120]

4.3.2.2 Displacement Error Estimation within the Contour Method as Applied to the Residual Stress Field at Cx Holes

The displacement error associated with this single measurement uncertainty quantification is intended to capture the random errors that are introduced by the surface roughness of the measured coupon, and the inherent measurement error that is associated with the laser profilometer system. In order to capture this source of random error a Monte Carlo approach was used.[125] To quantify the noise that is present within the displacement data due to these effects, the average and standard deviation were calculated of the difference between the optimal fit of the displacement data and the actual displacement data. It is assumed that the noise has a Gaussian (Normal) distribution, and thus it was possible to add random noise that was defined by the mean and standard deviation of the residual/difference between the fit and the actual noise.

This random noise was added to each displacement point within the final averaged and de-noised surface. This surface was then fit using the optimal knot spacing of four knots through the thickness and thirty-two knots radially away from the hole, with the same order of B-spline. This fitted surface was again applied as a boundary condition and the FEA was solved at the defined mesh density, as outlined. The output residual stresses at each node were tabulated as a function of the number of runs. For each individual coupon CxA2-1 – CxA2-5 and CxD2-1 – CxD2-3, fifty Monte Carlo simulations were performed.

Once all of the simulations were completed and performed, a nodal average and standard deviation was calculated. This standard deviation represents the displacement error associated with a single contour method residual stress determination.

4.3.2.3 Total Error within the Contour Method as Applied to the Residual Stress Field at Cx Holes

With the model/fit error and the displacement error now calculated for each individual coupon, a total error was calculated by RSS the individual sources of error at each spatial, nodal location. This total error therefore would represent the single measurement total uncertainty of the contour method.

4.3.3 Results of Single Measurement Uncertainty for the Residual Stress Determined via the Contour Method at Cold Expanded Holes in 2024-T351 and 7075-T651 Aluminum Alloys

4.3.3.1 Total Single Measurement Uncertainty Contour Plots for CxA2-1 (2024-T351) Coupon Configuration

The single measurement uncertainty was calculated for each individual coupon for which residual stresses were determined. The results from coupon CxA2-1 will be provided, and the other four coupon results are provided within the Appendix. In order to understand the spatial uncertainty associated with the model/fit error and the displacement error, contour plots were developed for their individual contribution to the total uncertainty. The component of the total uncertainty associated with the model/fit error for Coupon CxA2-1 is provided in Fig. 138.

The component of the total uncertainty associated with the displacement uncertainty developed via Monte Carlo simulation is shown in Fig. 139, and the RSS of these two errors is provided for coupon CxA2-1.

4.3.3.2 Total Single Measurement Uncertainty Line Plots Radially from Hole for CxA2-1 (2024-T351) Coupon Configuration

In addition to the contour plots provided in Fig. 138 through Fig. 140, line plots were developed along seven radial lines through the thickness, and five through thickness stress lines, emanating radially away from the hole. These locations are identical in position as the line plots provided within Fig. 64 through Fig. 77. For each of the line plots the knot spacing is provided. Three, four, and five knots through the thickness is the exact number of knots placed along the "short," or Y direction. For the "long," X direction the knot spacing is stated as three, four, and five. This corresponds to the spacing and the number of knots along the radial direction being twenty-four, thirty-two, and forty. These line plots are provided in Fig. 141 through Fig. 147. For each of the line plots the individual knot density stress is provided, along with the average of all five knot densities. The standard deviation at each point is provided via error bars.

4.3.3.3 Total Single Measurement Uncertainty Line Plots Through-Thickness for CxA2-1 (2024-T351) Coupon Configuration

Line plots of the stress through the thickness were also plotted on both the left and right sides of the holes.

4.3.3.3.1 Total Single Measurement Uncertainty Line Plots Through-Thickness at Left Side of Hole for CxA2-1 (2024-T351) Coupon Configuration

Residual stresses are plotted for the left side of the hole at five locations radially away from the hole. These are plotted in Fig. 148 through Fig. 151.

4.3.3.3.2 Total Single Measurement Uncertainty Line Plots Through-Thickness at Right Side of Hole for CxA2-1 (2024-T351) Coupon Configuration

Similar plots were developed for the right side of the hole, as shown in Fig. 152 through Fig. 155.

It can be seen from these plots that the shift in the knot density has a very small effect on the variability in the final stress field. This is due to the small shift in the fit developed through the splines. If the knot density was to be shifted up and down ten knots it would have a significantly more effect on the residual stress field. However, due to the low number knots that seems to most accurately fit the surface, this level of adjustment isn't possible. It is also somewhat unrealistic to place that much additional uncertainty into the process, when it is possible to define a "best fit" for the surface and it is assumed that the practitioners that perform the contour method have established methods to establish this fit.

4.3.3.4 Total Single Measurement Uncertainty Contour Plots for CxD2-1 (7075-T651) Coupon Configuration

The same process was performed for each of the three replicates of the CxD2 7075-T651 material condition. Contour plots of the model/fit, displacement, and total uncertainty for coupon CxD2-1 are provided in Fig. 156 through Fig. 158. The contour plots for coupons CxD2-2 and CxD2-3 are provided in the Appendix.

4.3.3.5 Total Single Measurement Uncertainty Line Plots Radially from Hole for CxD2-1 (7075-T651) Coupon Configuration

Line plots were developed at the same spatial locations as those provided for the CxA2 conditions. Each location on the line plot provides the stress for the given knot

density along with the average and standard deviation at that location. Line plots for these seven locations, going radially away from the hole, are provided in Fig. 159 through Fig. 165.

4.3.3.6 Total Single Measurement Uncertainty Line Plots Through-Thickness for CxD2-1 (7075-T651) Coupon Configuration

Line plots of the stress through the thickness were also plotted on both the left and right sides of the holes.

4.3.3.6.1 Total Single Measurement Uncertainty Line Plots Through-Thickness at Left Side of Hole for CxD2-1 (7075-T651) Coupon Configuration

Residual stresses are plotted for the left side of the hole at five locations radially away from the hole. These are plotted in Fig. 166 through Fig. 169.

4.3.3.6.2 Total Single Measurement Uncertainty Line Plots Through-Thickness at Right Side of Hole for CxD2-1 (7075-T651) Coupon Configuration

Similar plots were developed for the right side of the hole, as shown in Fig. 170 through Fig. 173.

4.3.4 Comparison of Single Measurement Uncertainty to Repeatability Uncertainty for Residual Stresses Developed via the Contour Method at Cold Expanded Holes in 2024-T351 and 7075-T651 Aluminum Alloys

One of the fundamental questions quantified within this work is whether the single measurement uncertainty quantification method is able to capture the uncertainty that is present due to the residual stress-inducing process. The Cx process tolerances for these holes were held to an order of magnitude higher level of precision than those that

would be processed by following the general guidelines within the FTI process specification. Thus, if the single measurement uncertainty methodology was able to statistically capture the uncertainty that was present in the replicate statistical analysis it would be possible to perform the contour method on a single part, and apply the single measurement uncertainty estimator to that residual stress field. This residual stress field, along with the calculated total uncertainty, would provide a statistical bound that would capture the repeatability uncertainty found within the replicate data set.

In order to determine this the line plots through the thickness and distributed radially away from the hole are provided for the CxA2-1 and CxD2-1 coupon configuration.

4.3.4.1 Radial Line Plots Comparing the Single Measurement Uncertainty to Repeatability Uncertainty for Coupon CxA2-1 (2024-T351)

Radial line plots are provided for the CxA2-1 coupon configuration that provide the CxA2 repeatability average with error bars representing one standard deviation, as shown in red. In addition to this, the single measurement total uncertainty is also plotted in black, with the average solution from the five knot densities, with error bars representing one standard deviation from the average. Line plots for the other four CxA2 coupons, comparing the single measurement uncertainty to the repeatability uncertainty are contained within the Appendix. Line plots along three transects through the thickness of the coupon, emanating radially away from the hole, are provided in Fig. 174 through Fig. 176.

4.3.4.2 Through-Thickness Line Plots Comparing the Single Measurement Uncertainty to Repeatability Uncertainty for Coupon CxA2-1 (2024-T351)

Through-thickness line plots of the residual stresses are provided, comparing the single measurement uncertainty (in black) to the repeatability uncertainty (in red) for the same through-thickness spatial locations as presented earlier.

4.3.4.2.1 Through-Thickness Line Plots Comparing the Single Measurement Uncertainty to the Repeatability Uncertainty for the Left Side of the Hole in Coupon CxA2-1 (2024-T351)

Through-thickness line plots of the average CxA2 stress at the left side of the hole, with the repeatability standard deviation as error bars is compared to the single measurement uncertainty for CxA2-1 are shown in Fig. 177 through Fig. 180.

4.3.4.2.2 Through-Thickness Line Plots Comparing the Single Measurement Uncertainty to the Repeatability Uncertainty for the Right Side of the Hole in Coupon CxA2-1 (2024-T351)

Line plots also are provided for the right side of the hole in Fig. 181 through Fig. 184.

4.3.4.3 Radial Line Plots Comparing the Single Measurement Uncertainty to Repeatability Uncertainty for Coupon CxD2-1 (7075-T651)

Radial line plots are provided for the CxD2-1 coupon configuration that provide the CxD2 repeatability average with error bars representing one standard deviation, as shown in red. In addition to this, the single measurement total uncertainty is also plotted in black, with the average solution from the five knot densities, with error bars representing one standard deviation from the average. Line plots for the other two CxD2

coupons, comparing the single measurement uncertainty to the repeatability uncertainty are contained within the Appendix. Line plots along the same three transects through the thickness of the coupon, emanating radially away from the hole, are provided in Fig. 185 through Fig. 187.

4.3.4.4 Through-Thickness Line Plots Comparing the Single Measurement Uncertainty to Repeatability Uncertainty for Coupon CxD2-1 (7075-T651)

Through-thickness line plots of the residual stresses are provided, comparing the single measurement uncertainty (in black) to the repeatability uncertainty (in red) for the same through-thickness spatial locations as presented earlier.

4.3.4.4.1 Through-Thickness Line Plots Comparing the Single Measurement Uncertainty to the Repeatability Uncertainty for the Left Side of the Hole in Coupon CxD2-1 (7075-T651)

Through-thickness line plots of the average CxD2 stress at the left side of the hole, with the repeatability standard deviation as error bars, is compared to the single measurement uncertainty for CxD2-1 and are shown in Fig. 188 through Fig. 191.

4.3.4.4.1 Through-Thickness Line Plots Comparing the Single Measurement Uncertainty to the Repeatability Uncertainty for the Right Side of the Hole in Coupon CxD2-1 (7075-T651)

Line plots also are provided for the right side of the hole in Fig. 192 through Fig. 195.

4.3.5 Conclusions from Comparison of Single Measurement Uncertainty to Repeatability Uncertainty for Residual Stresses Developed via the Contour Method at Cold Expanded Holes in 2024-T351 and 7075-T651 Aluminum Alloys

For the CxA2 coupons (2024-T351) it can be seen from the contour plot of the total single measurement uncertainty, Fig. 138 as compared to the repeatability uncertainty as shown in Fig. 132, that the relative locations and magnitudes of the uncertainties are similar, as shown in Fig. 196. However, the single measurement uncertainty is not able to capture the maximums and provides a lower level of spatial uncertainty when compared to that produced by the repeatability uncertainty estimator.

This also can be said for the CxD2-1 (7075-T651) coupon as compared to the CxD2 average. The relative magnitude of ±36 ksi is calculated, however the repeatability standard deviation is much more constant through the part, except at the exit surface, right at the edge of the hole. The single measurement uncertainty, however, shows a higher level of uncertainty from the edge of the hole to about 0.50 inch away from the edge of side of the hole. The two contour plots are shown side by side in Fig. 197.

However, when the line plots are used to compare the two methods for quantifying uncertainty it can be seen that the single measurement uncertainty method often has a smaller magnitude and at many locations the standard deviations do not overlap. This can be seen in Fig. 198 and Fig. 199 for coupon CxA2-1 as compared to the CxA2 average for the right and left sides of the hole, thus representing a statistical difference in the uncertainty quantified by the two methods.

Therefore it can be said that the single measurement uncertainty is not always capable of capturing the level of process variability that may be introduced by a given residual stress process. Thus, it is recommended that replicate measurements should

always be made for a given residual stress condition. Through this it will be possible to not only establish the single measurement uncertainty associated with the process used to determine the residual stresses within the body, but also to quantify the process uncertainty associated with the residual stress-inducing process. Both are important pieces of information to help establish the potential statistical dispersion of future static or fatigue life predictions.

Comparing the single measurement uncertainty and the repeatability uncertainty for the CxD2-1 (7075-T651) and the average CxD2 to the CxA2-1 (2024-T351) and the average CxA2 that the repeatability uncertainty it is possible to say that generally across the face the two materials have roughly the same level of uncertainty. The CxD2 coupons have a higher magnitude of both single measurement uncertainty and repeatability uncertainty, within very specific locations, when compared to the CxA2 coupon configuration. This higher magnitude of uncertainty could be due to the higher strength of the 7075-T651, as compared to the 2024-T351 aluminum material. Additional research should be placed into this area to determine if it is possible to define the spatial uncertainty for one of the materials and then through a transfer function quantify accurately the spatial uncertainty in the other material.

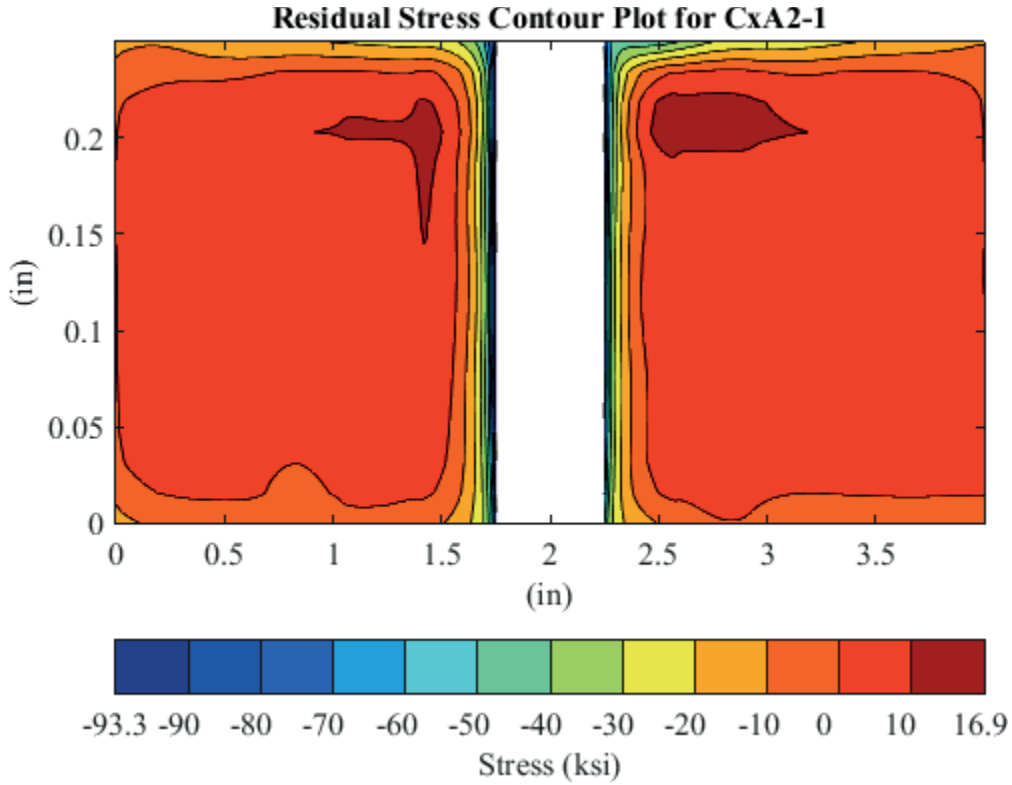

Fig. 54 Residual Stress Contour Plot of Coupon CxA2-1 (2024-T351) – Mandrel Entrance Surface at Y=0.

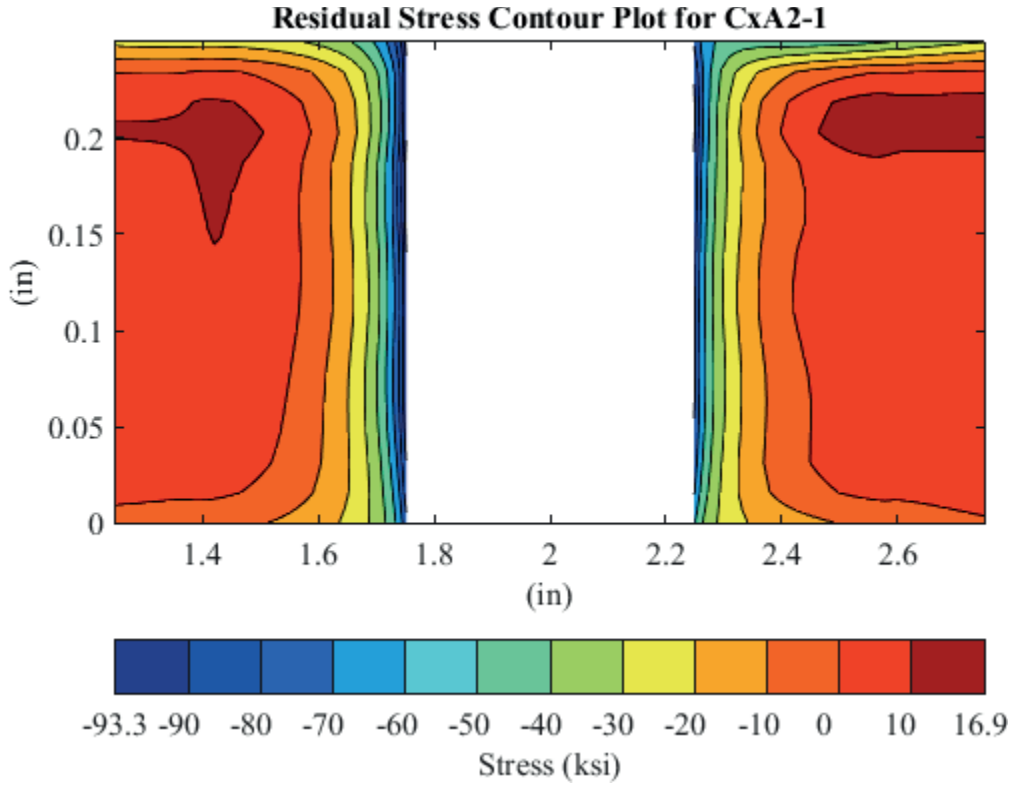

Fig. 55 Residual Stress Contour Plot of Coupon CxA2-1 (2024-T351) – Mandrel Entrance Surface at Y=0 – Zoomed in Next to Hole.

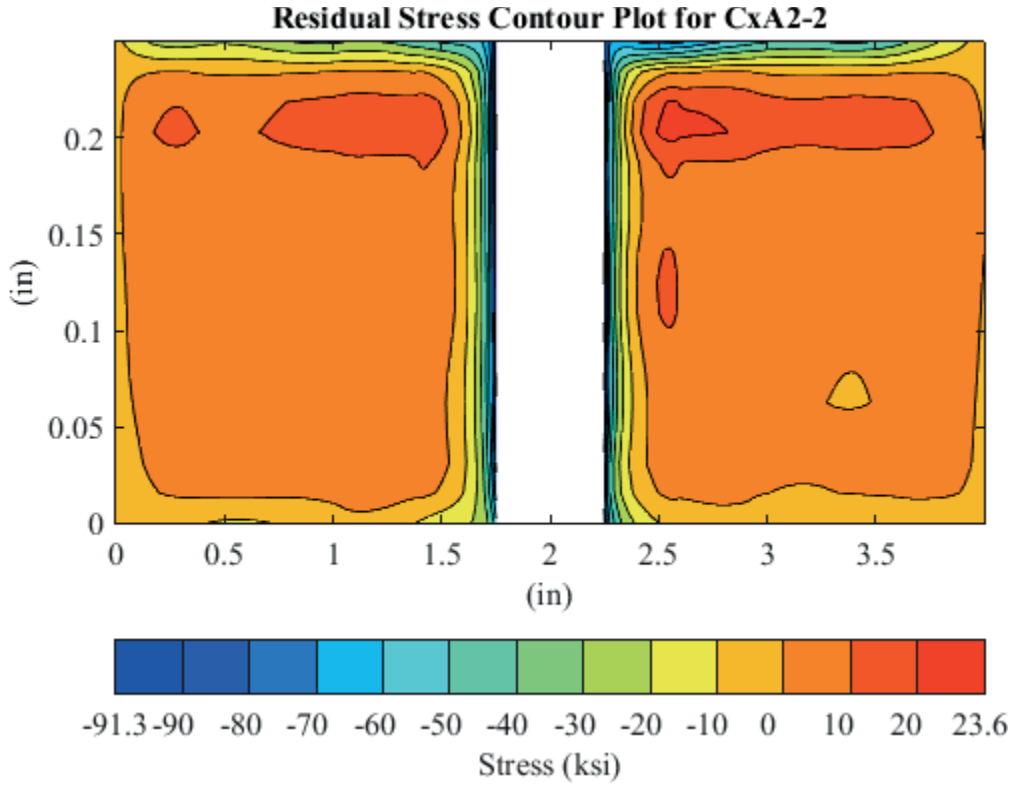

Fig. 56 Residual Stress Contour Plot of Coupon CxA2-2 (2024-T351) – Mandrel Entrance Surface at Y=0.

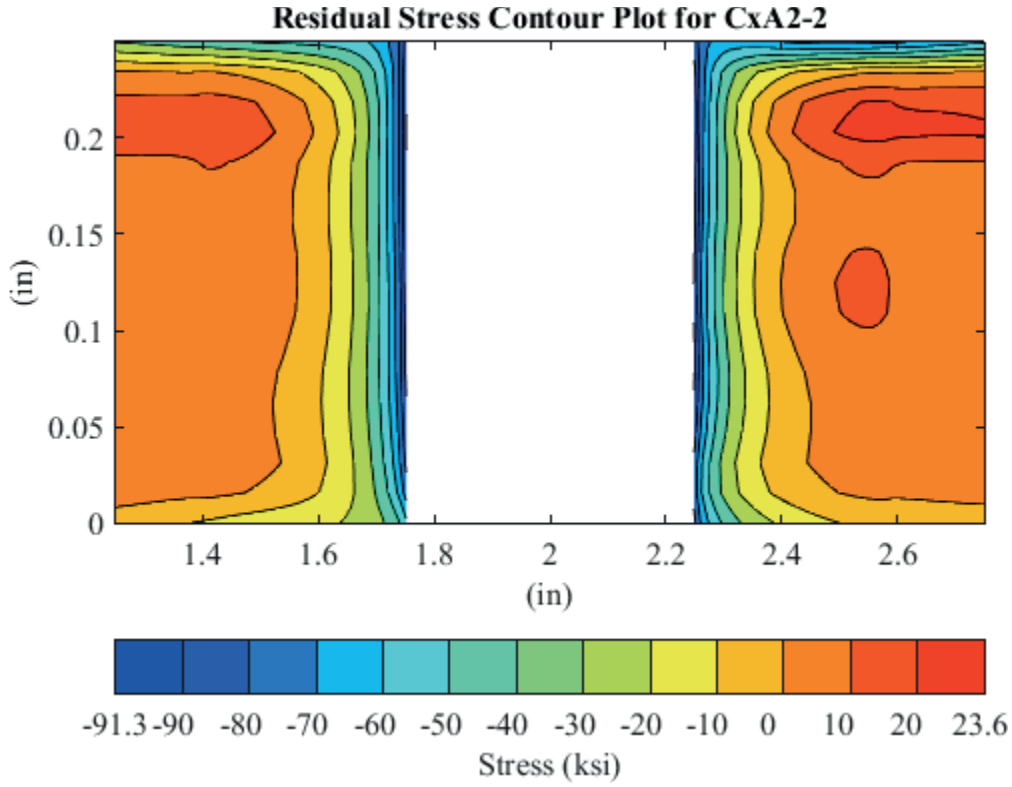

Fig. 57 Residual Stress Contour Plot of Coupon CxA2-2 (2024-T351) – Mandrel Entrance Surface at Y=0 – Zoomed in Next to Hole.

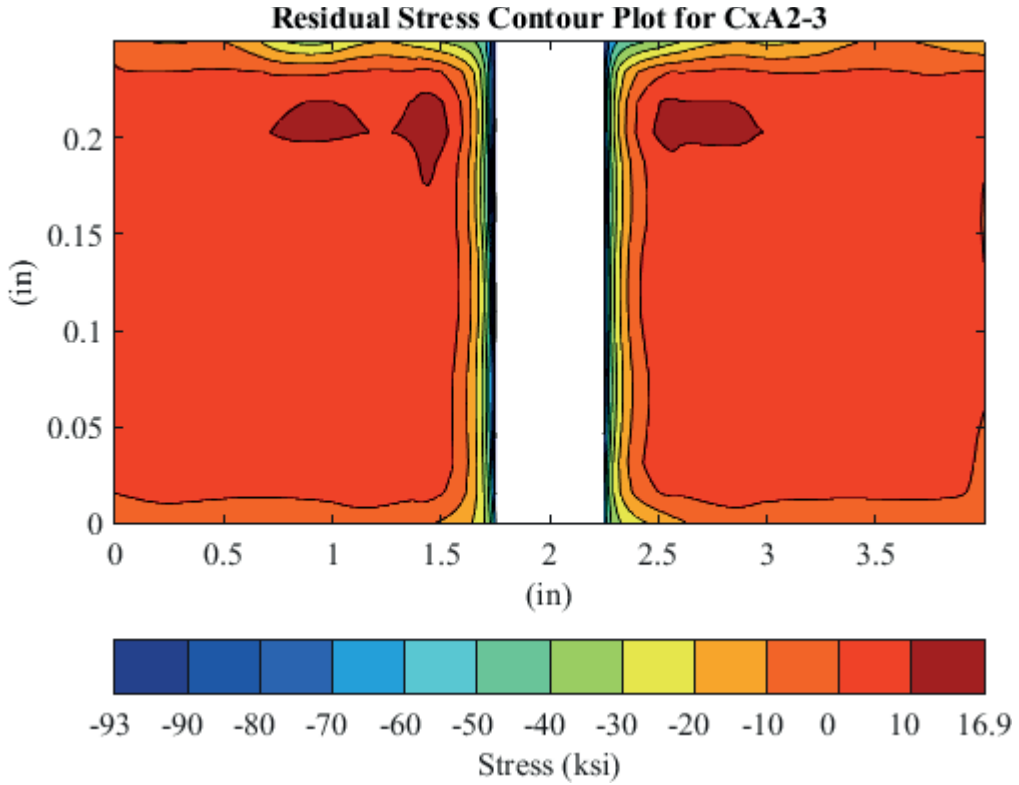

Fig. 58 Residual Stress Contour Plot of Coupon CxA2-3 (2024-T351) – Mandrel Entrance Surface at Y=0.

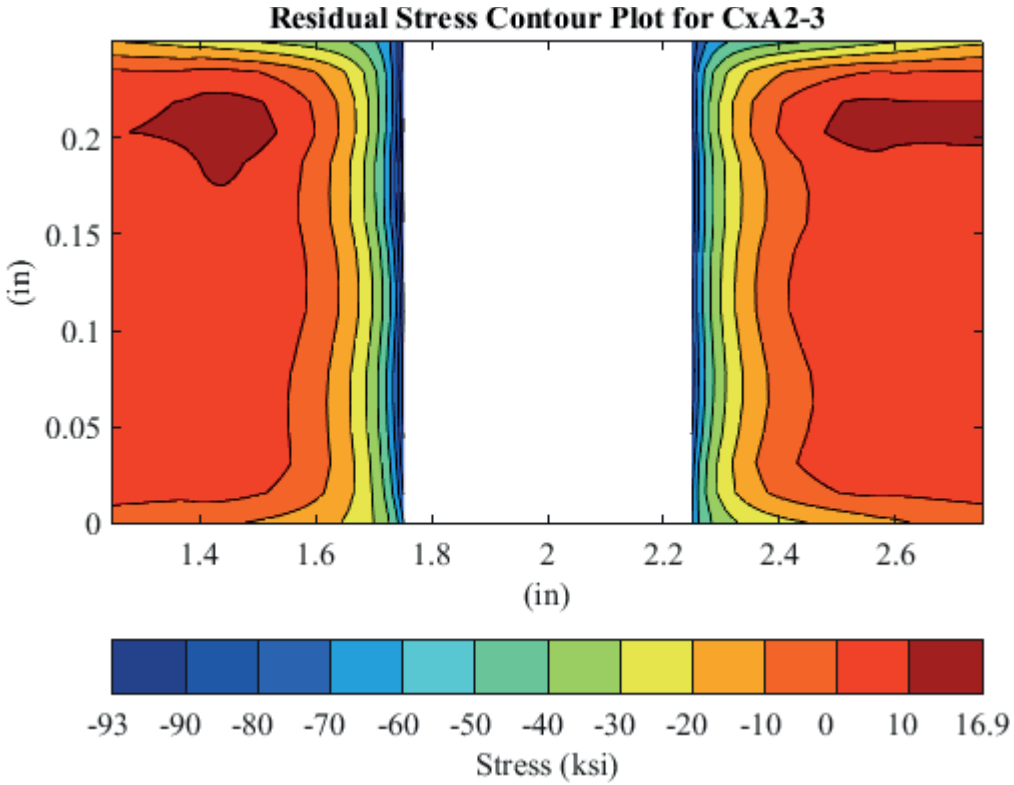

Fig. 59 Residual Stress Contour Plot of Coupon CxA2-3 (2024-T351) – Mandrel Entrance Surface at Y=0 – Zoomed in Next to Hole.

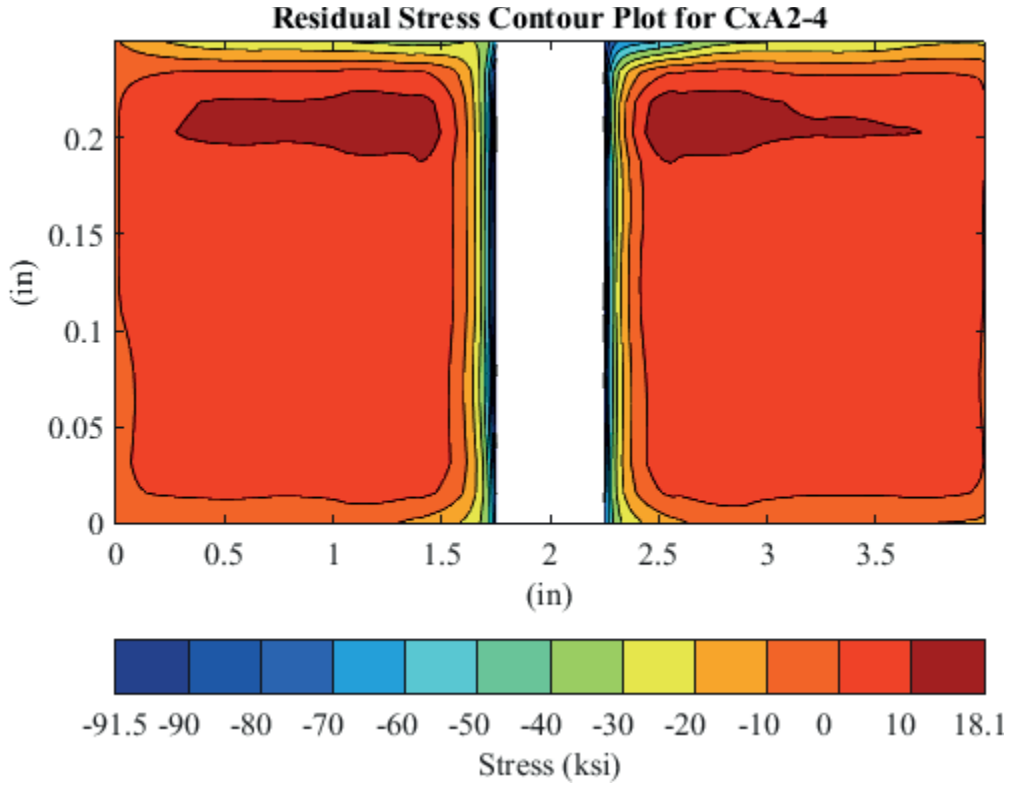

Fig. 60 Residual Stress Contour Plot of Coupon CxA2-4 (2024-T351) – Mandrel Entrance Surface at Y=0.

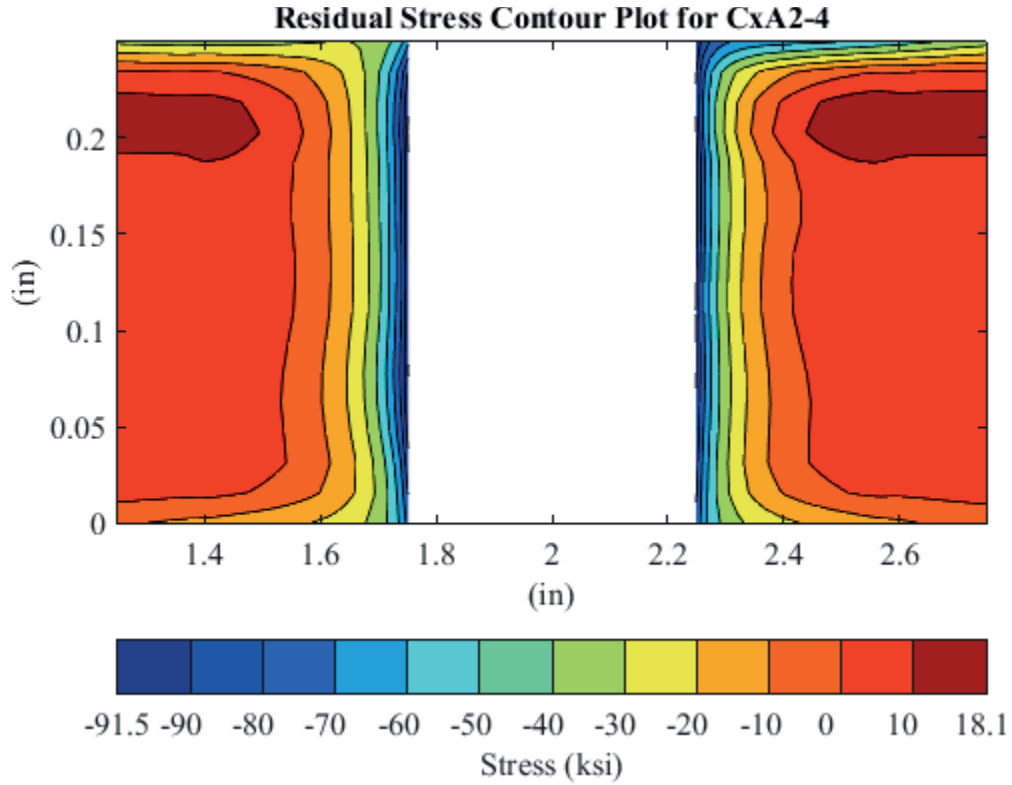

Fig. 61 Residual Stress Contour Plot of Coupon CxA2-4 (2024-T351) – Mandrel Entrance Surface at Y=0 – Zoomed in Next to Hole.

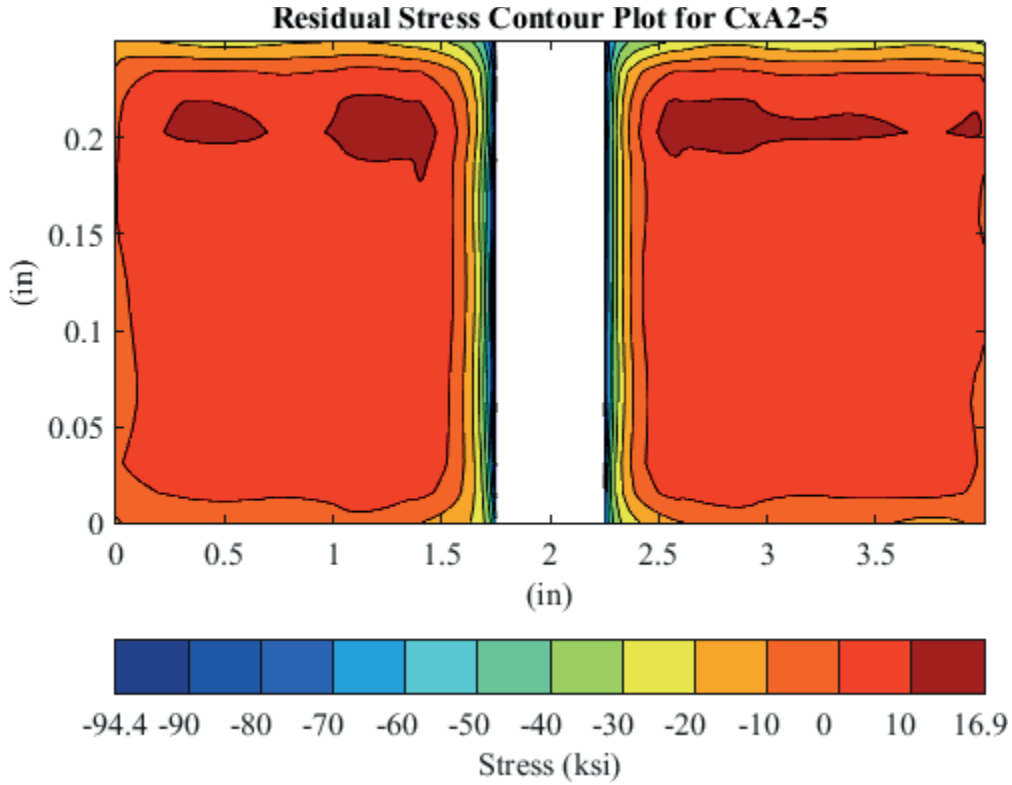

Fig. 62 Residual Stress Contour Plot of Coupon CxA2-5 (2024-T351) – Mandrel Entrance Surface at Y=0.

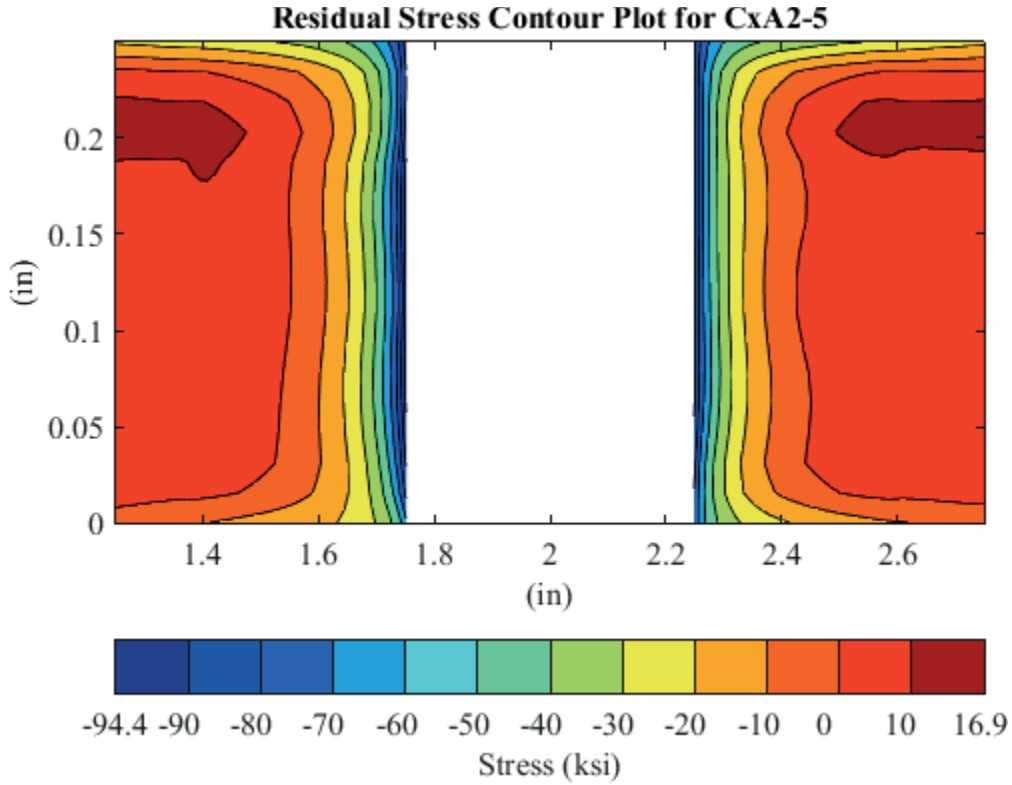

Fig. 63 Residual Stress Contour Plot of Coupon CxA2-5 (2024-T351) – Mandrel Entrance Surface at Y=0 – Zoomed in Next to Hole.

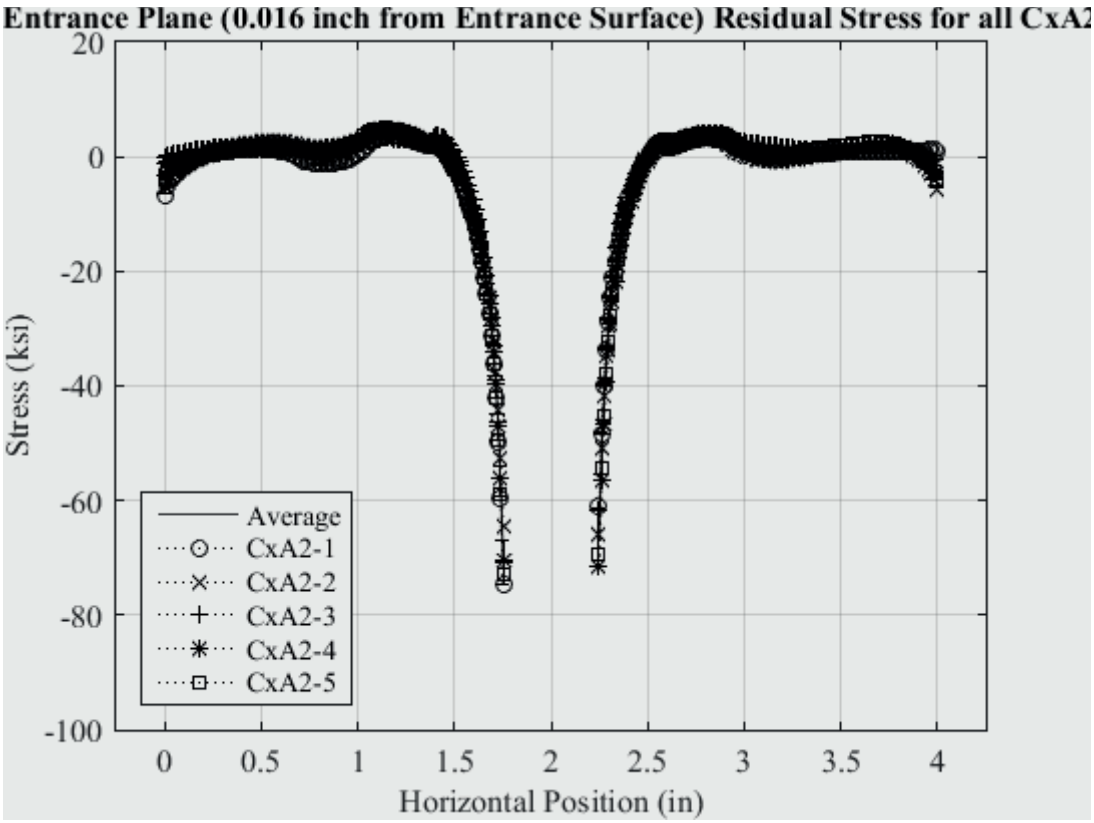

Fig. 64 Residual Stress Line Plot of all CxA2 (2024-T351) Replicates and Average Residual Stress at a Distance of 0.016 inch (Entrance Surface) from the Entrance Surface.

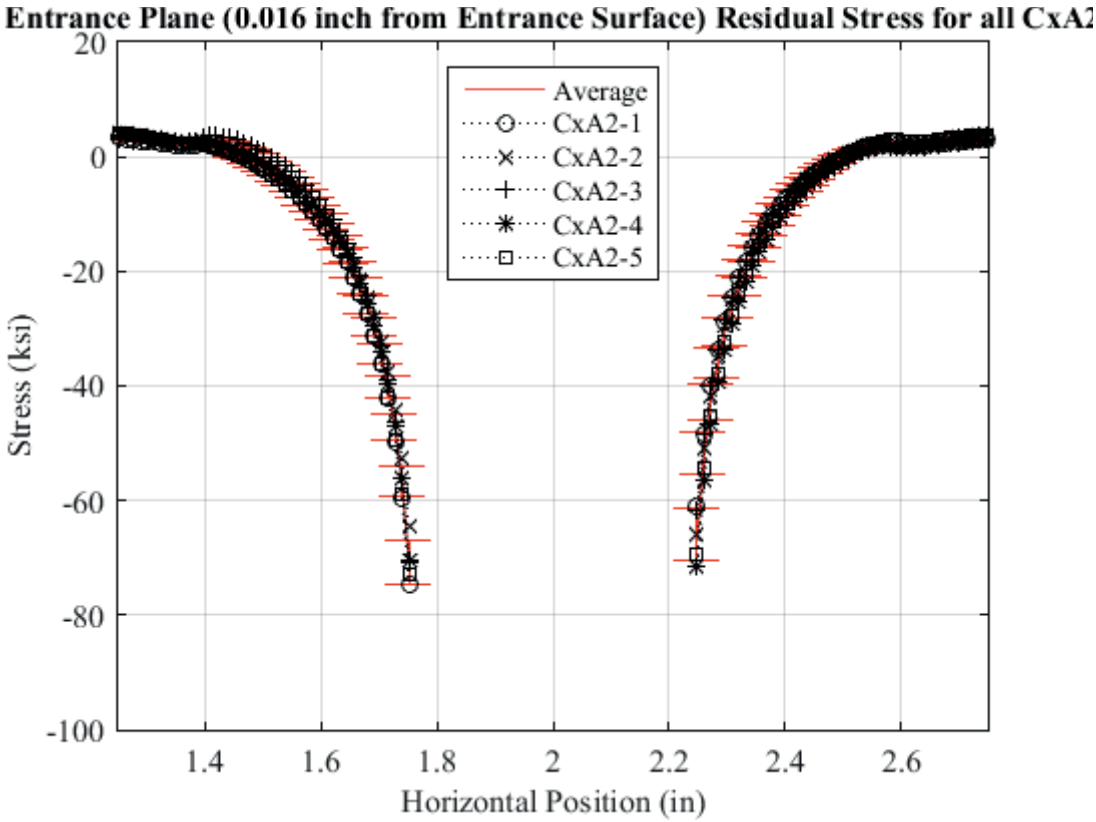

Fig. 65 Residual Stress Line Plot of all CxA2 (2024-T351) Replicates and Average Residual Stress at a Distance of 0.016 inch (Entrance Surface) from the Entrance Surface – Zoomed in Next to Hole.

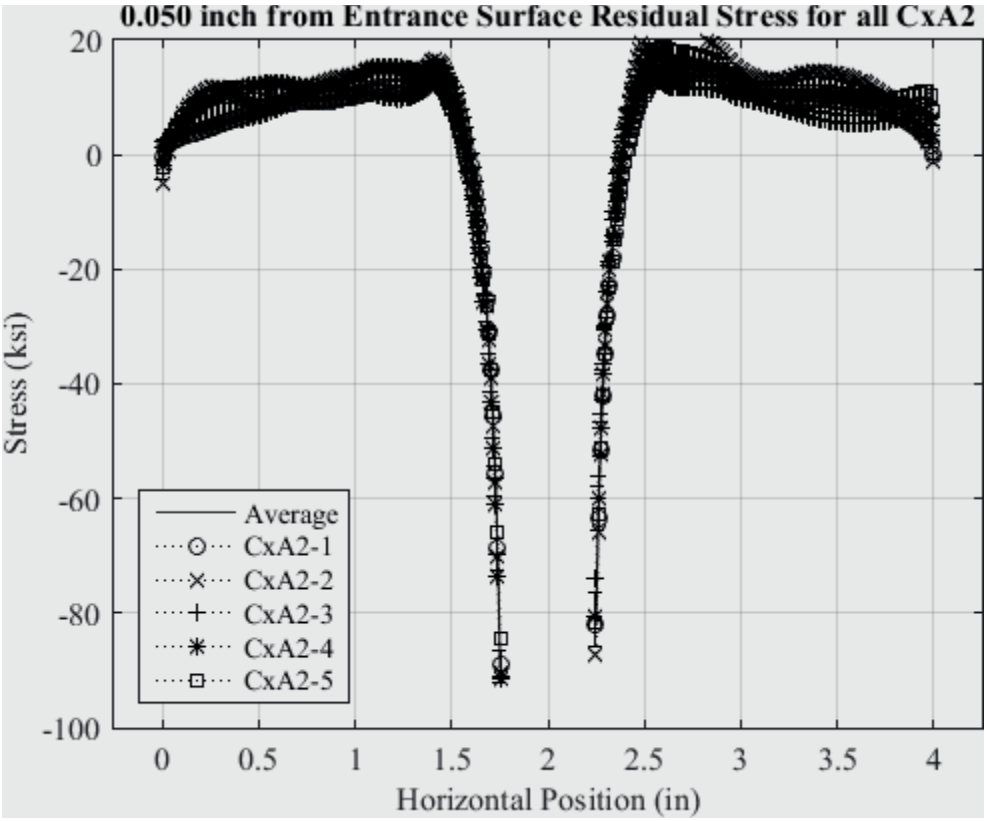

Fig. 66 Residual Stress Line Plot of all CxA2 (2024-T351) Replicates and Average Residual Stress at a Distance of 0.050 inch from the Entrance Surface.

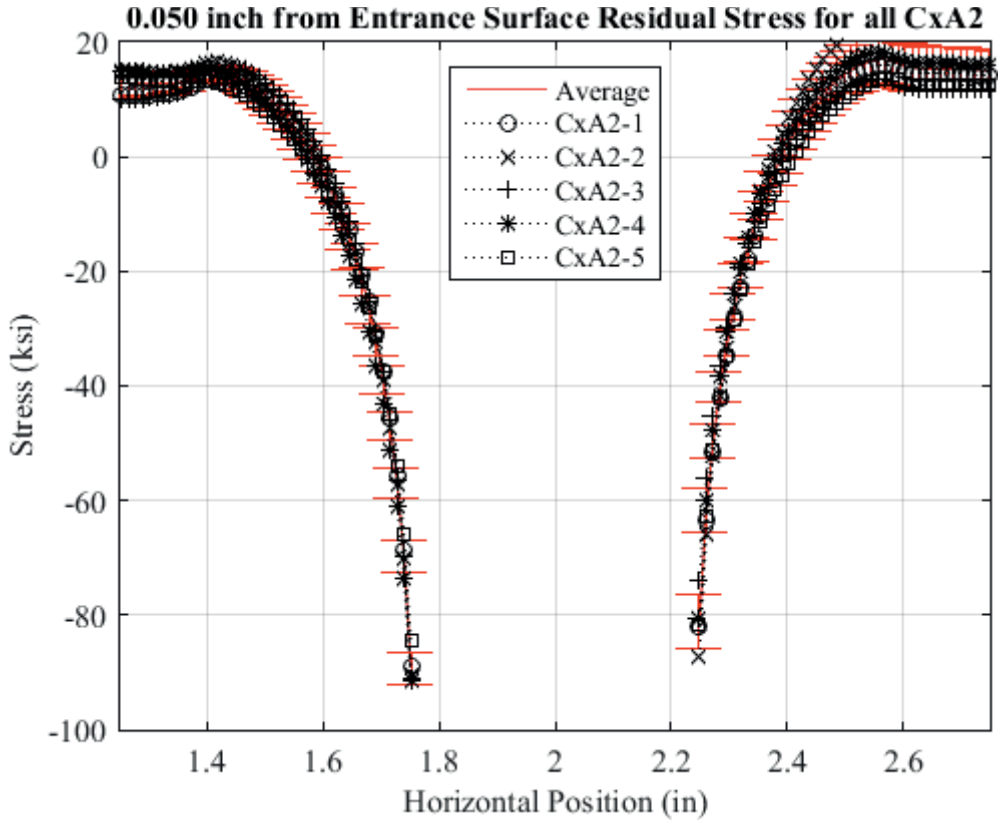

Fig. 67 Residual Stress Line Plot of all CxA2 (2024-T351) Replicates and Average Residual Stress at a Distance of 0.050 inch from the Entrance Surface – Zoomed in Next to Hole.

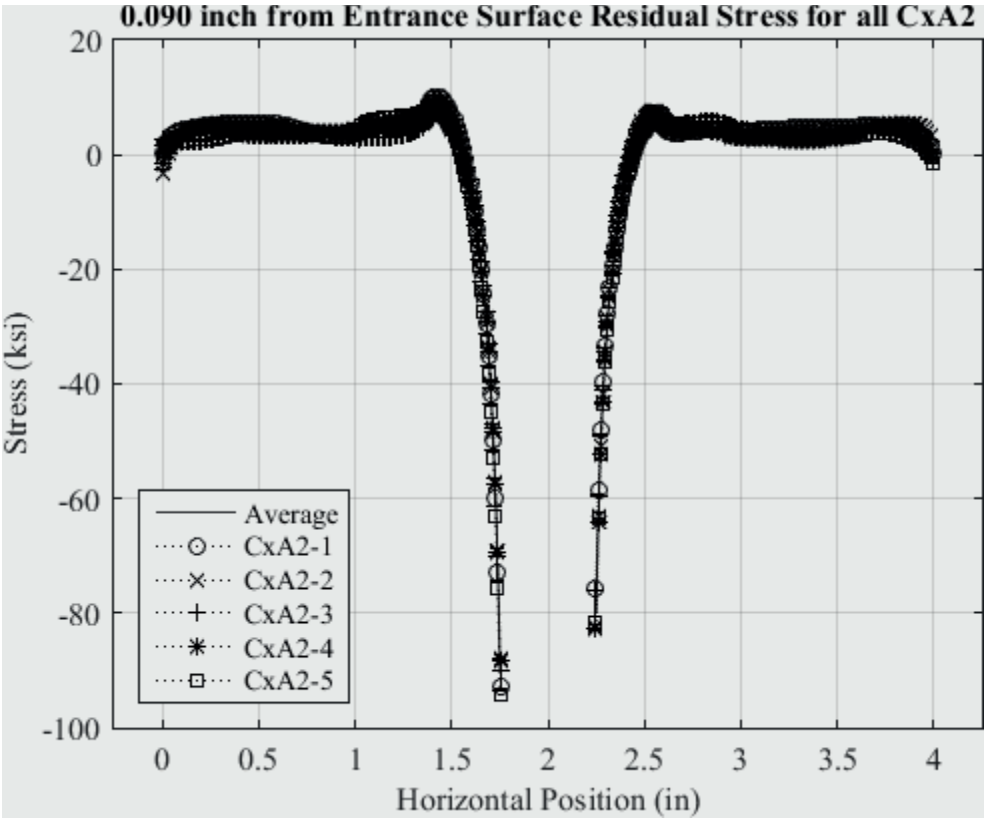

Fig. 68 Residual Stress Line Plot of all CxA2 (2024-T351) Replicates and Average Residual Stress at a Distance of 0.090 inch from the Entrance Surface.

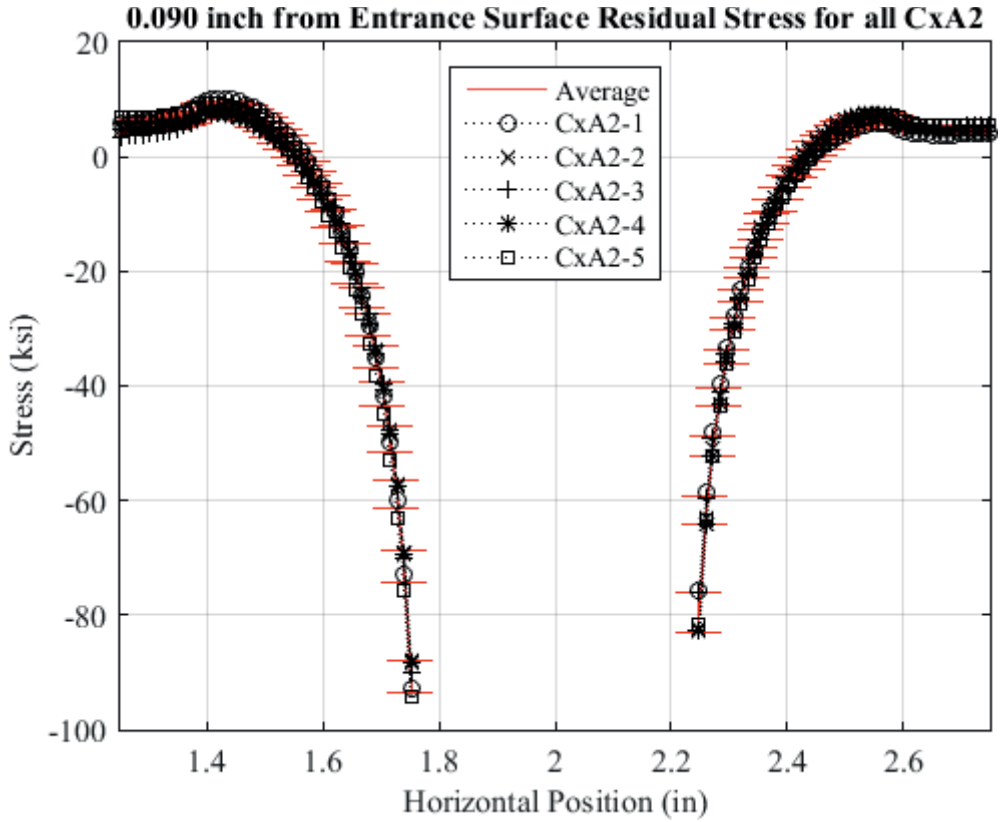

Fig. 69 Residual Stress Line Plot of all CxA2 (2024-T351) Replicates and Average Residual Stress at a Distance of 0.090 inch from the Entrance Surface – Zoomed in Next to Hole.

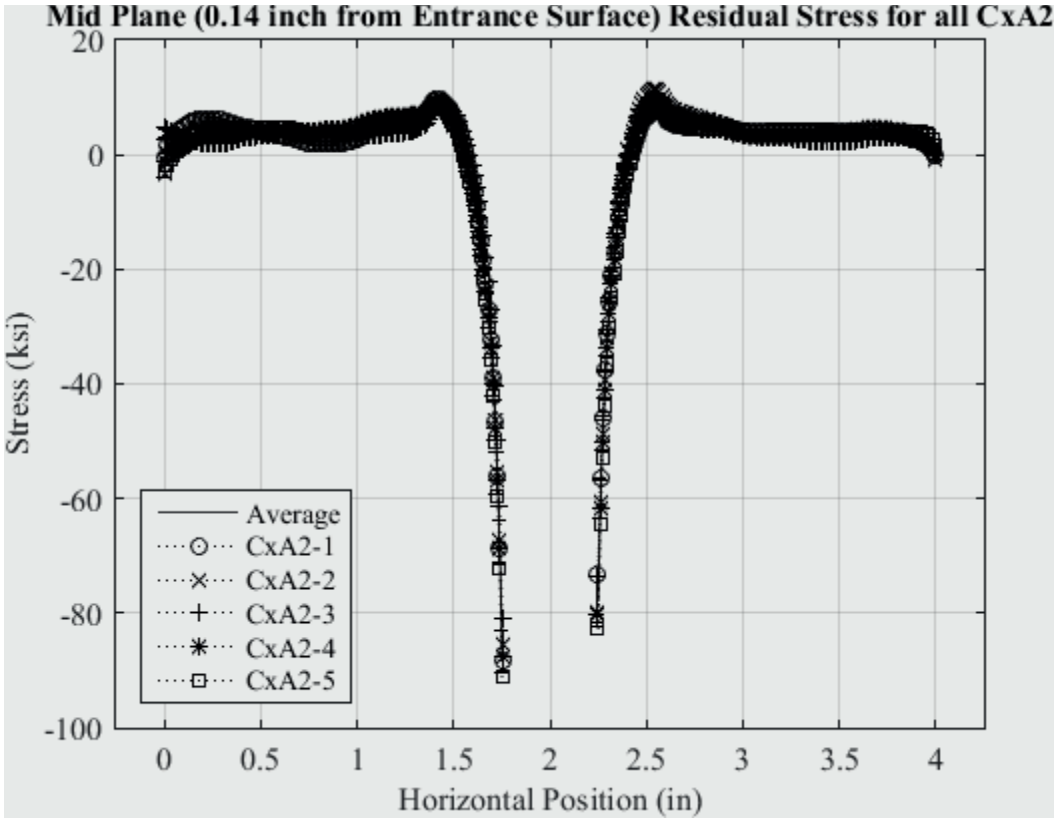

Fig. 70 Residual Stress Line Plot of all CxA2 (2024-T351) Replicates and Average Residual Stress at a Distance of 0.140 inch (Mid Thickness) from the Entrance Surface.

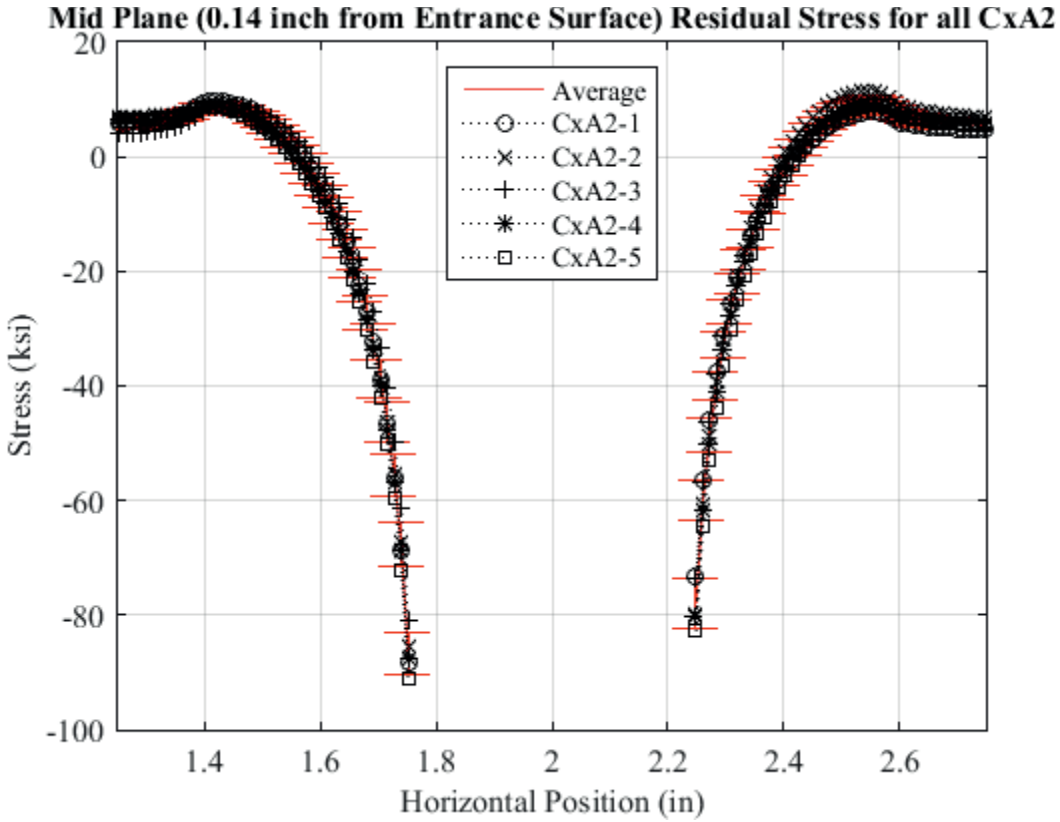

Fig. 71 Residual Stress Line Plot of all CxA2 (2024-T351) Replicates and Average Residual Stress at a Distance of 0.140 inch (Mid Thickness) from the Entrance Surface – Zoomed in Next to Hole.

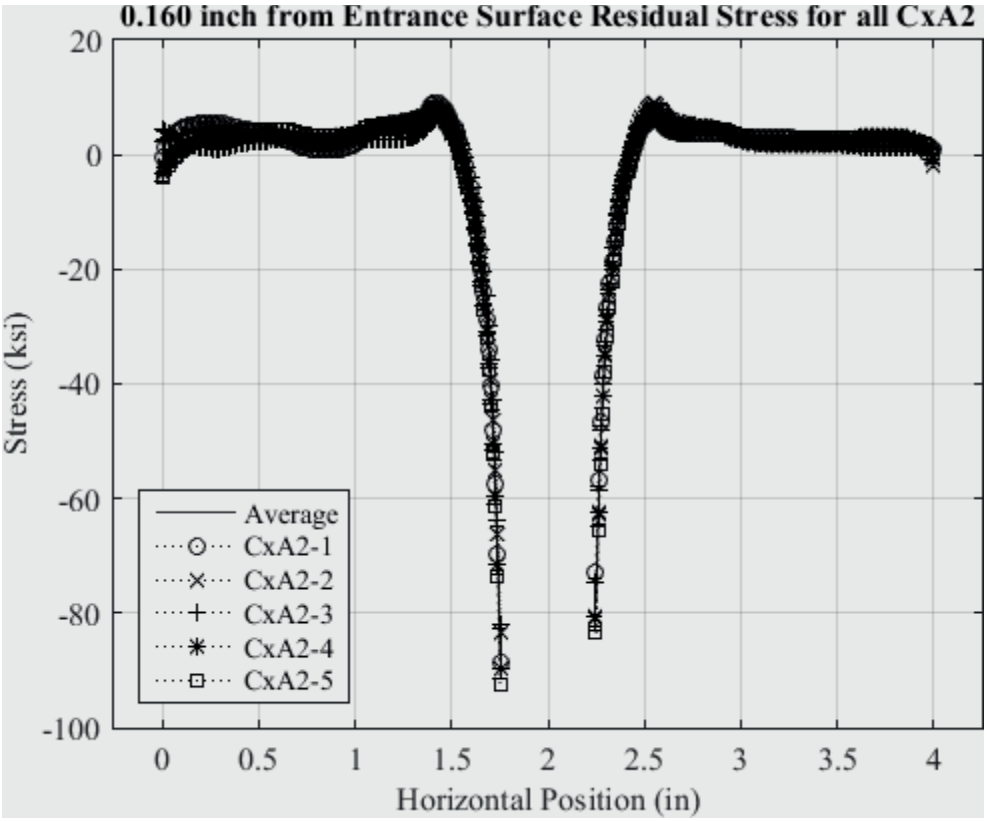

Fig. 72 Residual Stress Line Plot of all CxA2 (2024-T351) Replicates and Average Residual Stress at a Distance of 0.160 inch from the Entrance Surface.

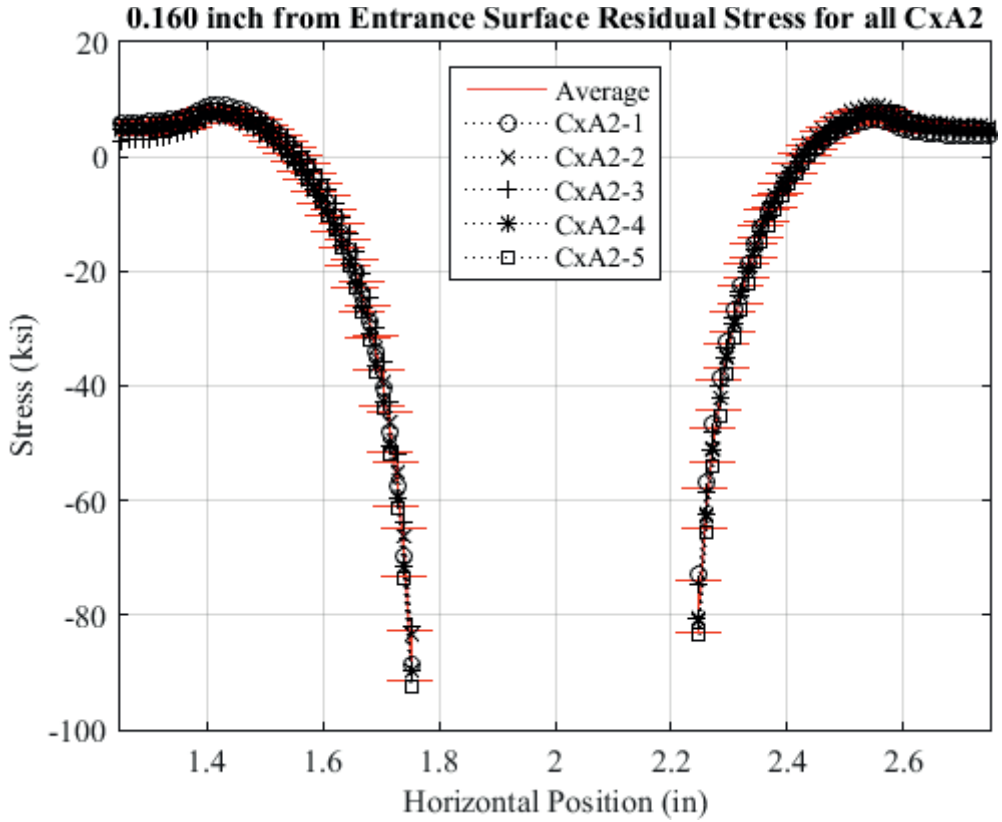

Fig. 73 Residual Stress Line Plot of all CxA2 (2024-T351) Replicates and Average Residual Stress at a Distance of 0.160 inch from the Entrance Surface – Zoomed in Next to Hole.

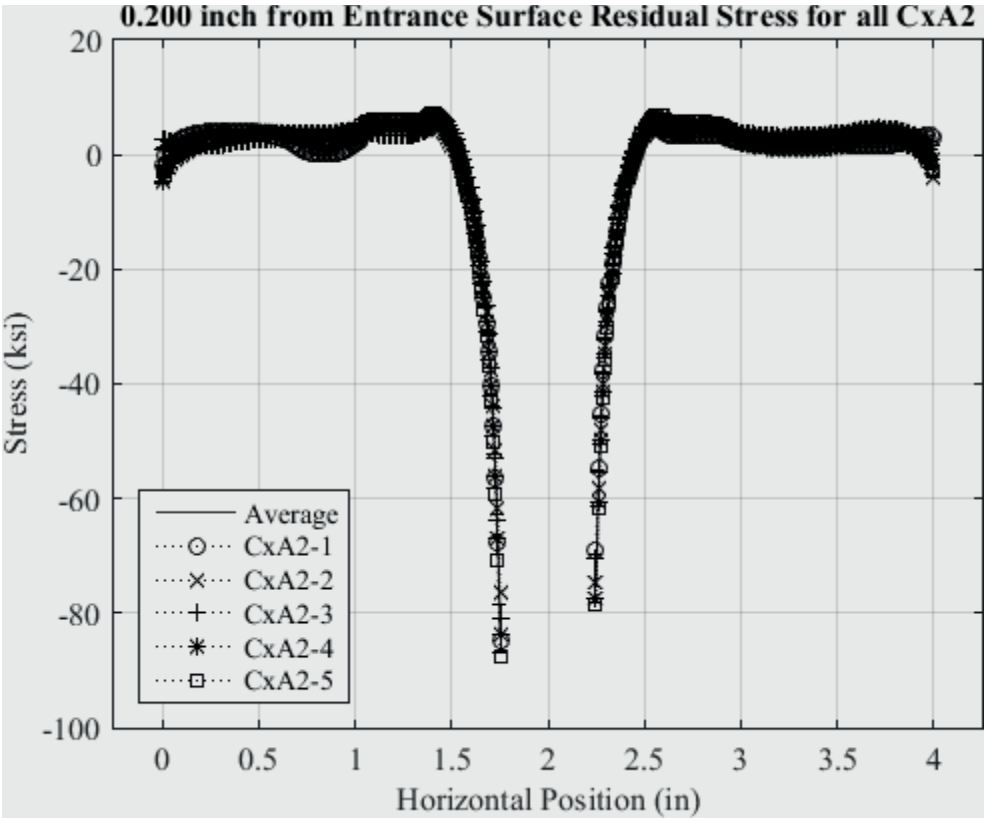

Fig. 74 Residual Stress Line Plot of all CxA2 (2024-T351) Replicates and Average Residual Stress at a Distance of 0.020 inch from the Entrance Surface.

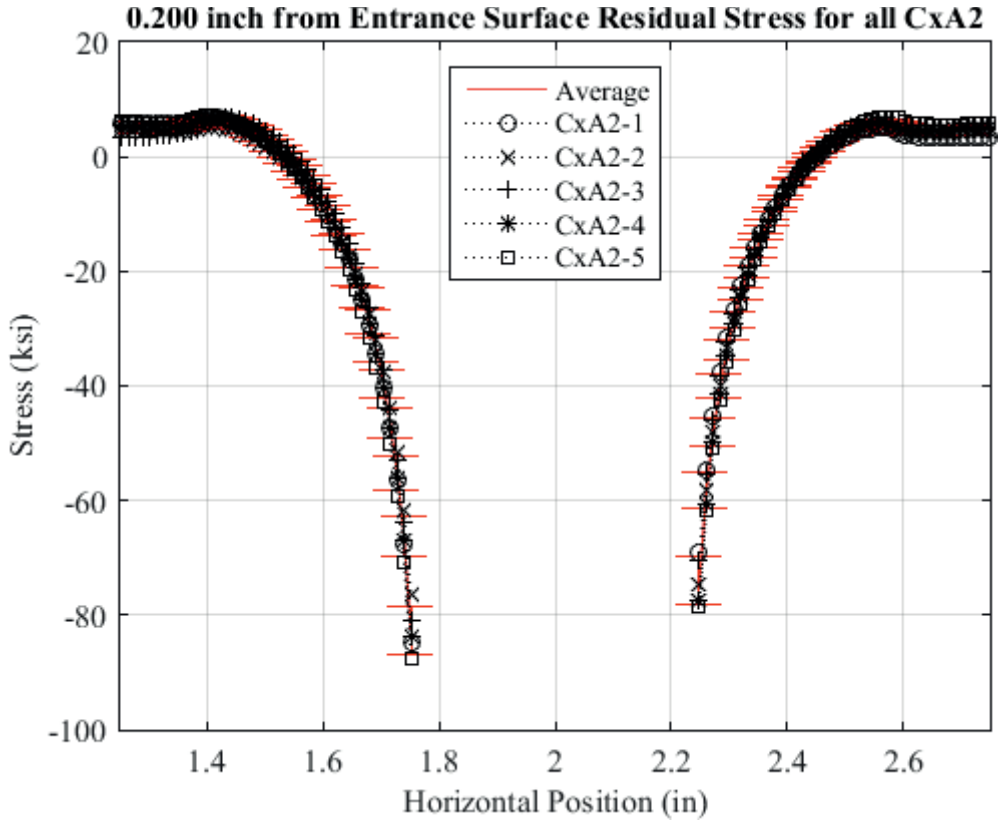

Fig. 75 Residual Stress Line Plot of all CxA2 (2024-T351) Replicates and Average Residual Stress at a Distance of 0.020 inch from the Entrance Surface – Zoomed in Next to Hole.

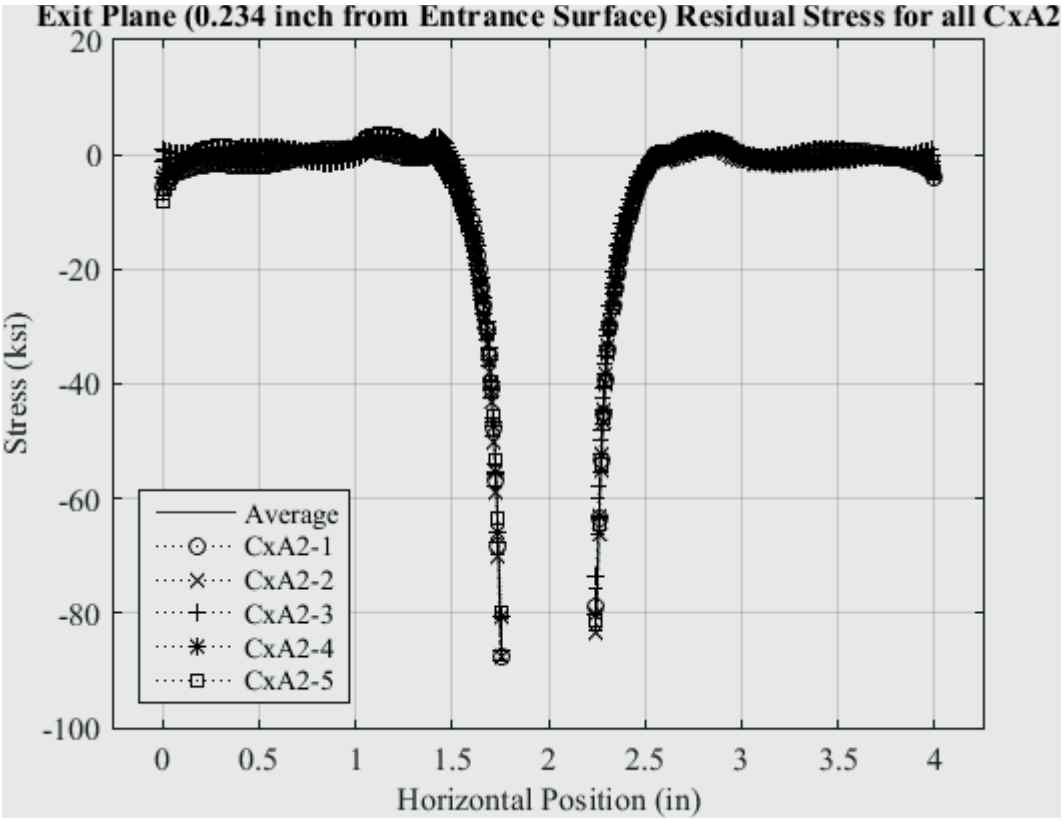

Fig. 76 Residual Stress Line Plot of all CxA2 (2024-T351) Replicates and Average Residual Stress at a Distance of 0.234 inch (Exit Surface) from the Entrance Surface.

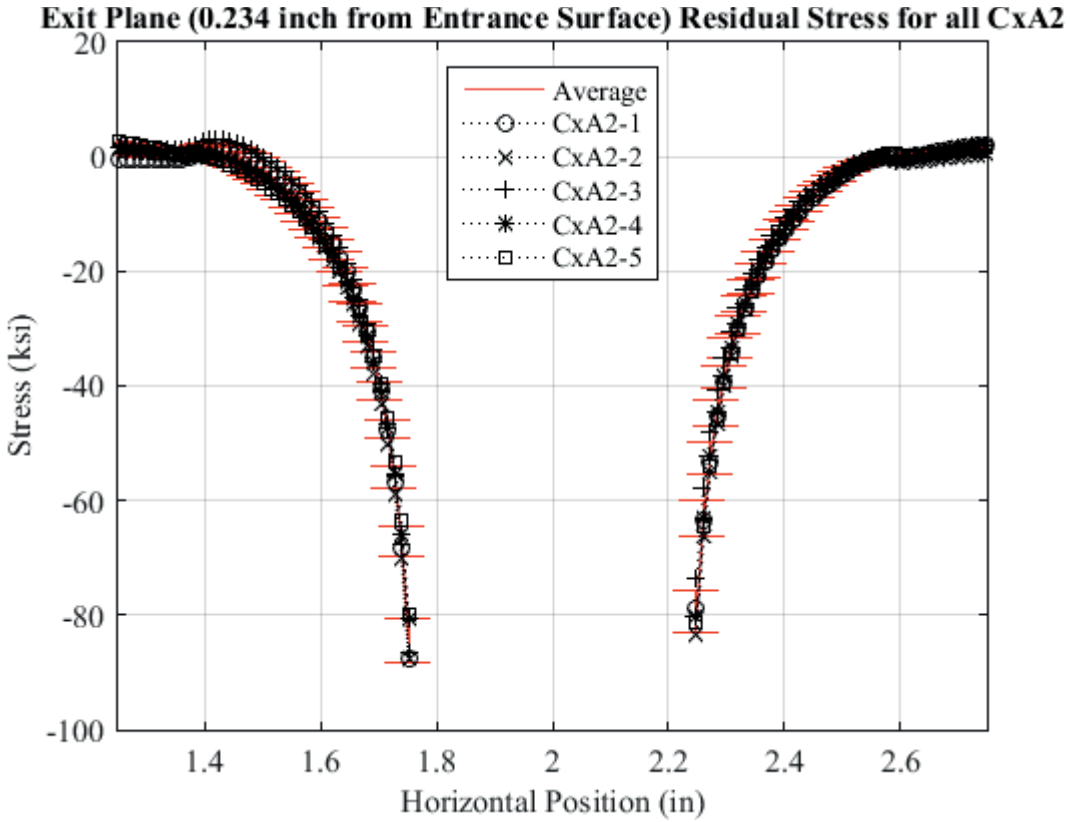

Fig. 77 Residual Stress Line Plot of all CxA2 (2024-T351) Replicates and Average Residual Stress at a Distance of 0.234 inch (Exit Surface) from the Entrance Surface – Zoomed in Next to Hole.

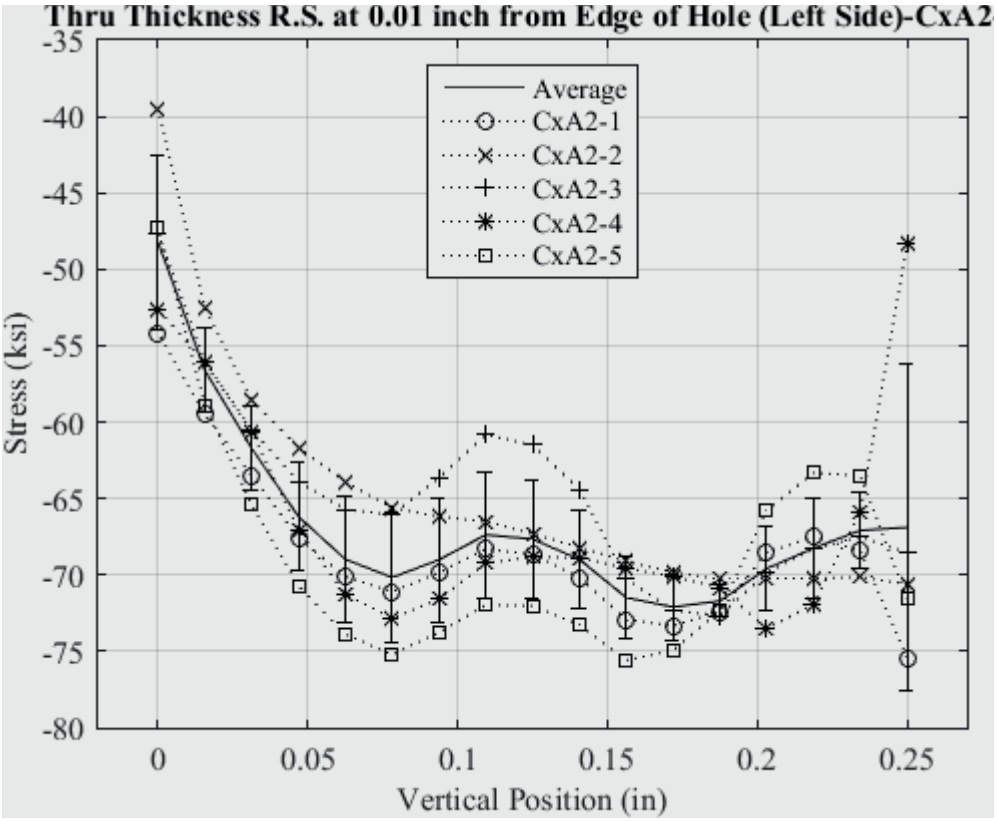

Fig. 78 Line Plot of Residual Stress at 0.01 inch from the Left Edge of the Hole for all CxA2 (2024-T351) Replicates.

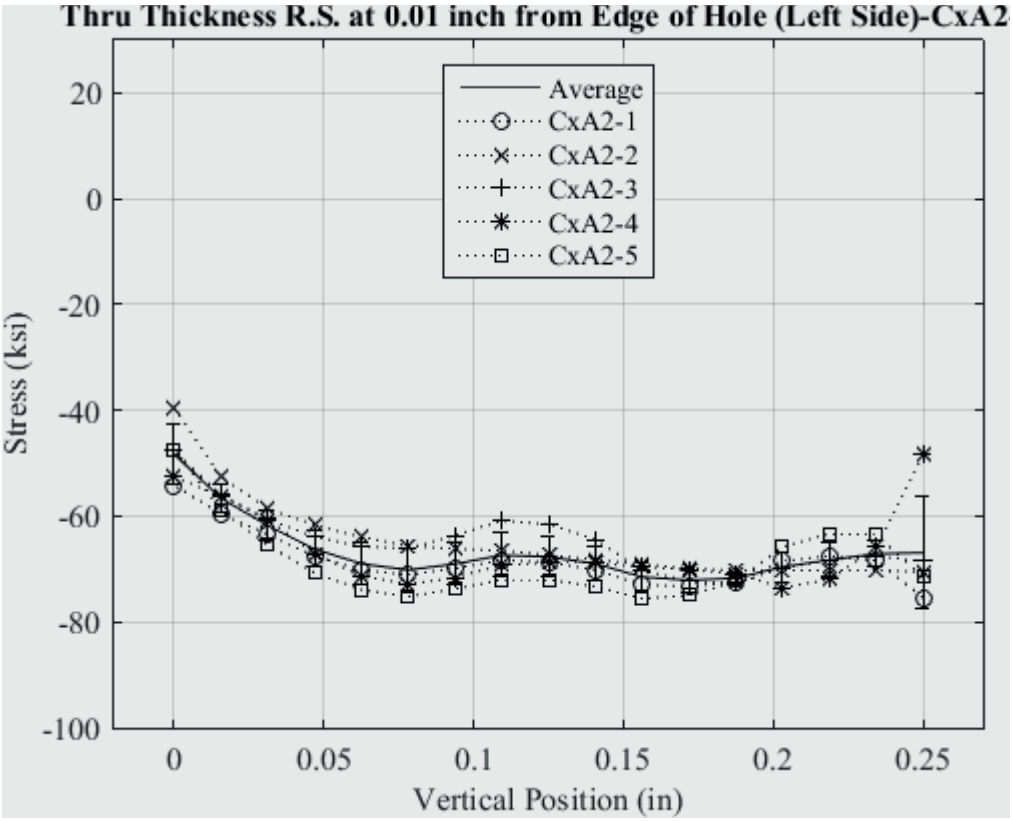

Fig. 79 Line Plot of Residual Stress at 0.01 inch from the Left Edge of the Hole for all CxA2 (2024-T351) Replicates – Locked Stress Scale.

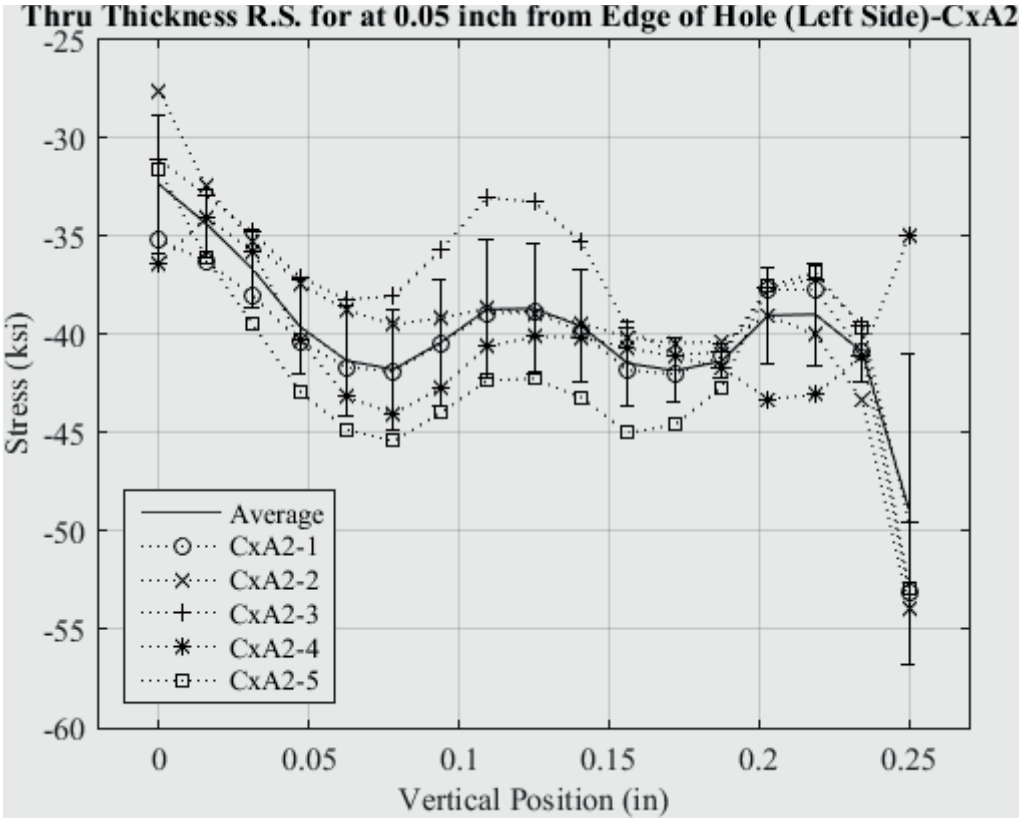

Fig. 80 Line Plot of Residual Stress at 0.05 inch from the Left Edge of the Hole for all CxA2 (2024-T351) Replicates.

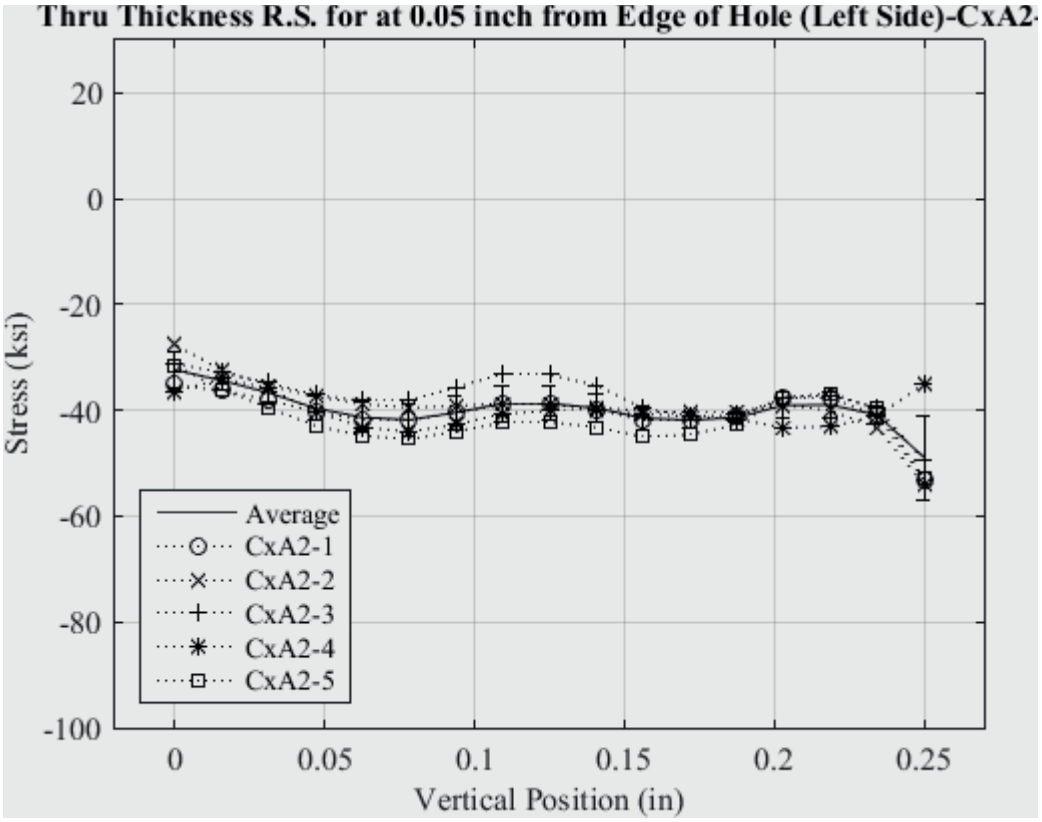

Fig. 81 Line Plot of Residual Stress at 0.05 inch from the Left Edge of the Hole for all CxA2 (2024-T351) Replicates – Locked Stress Scale.

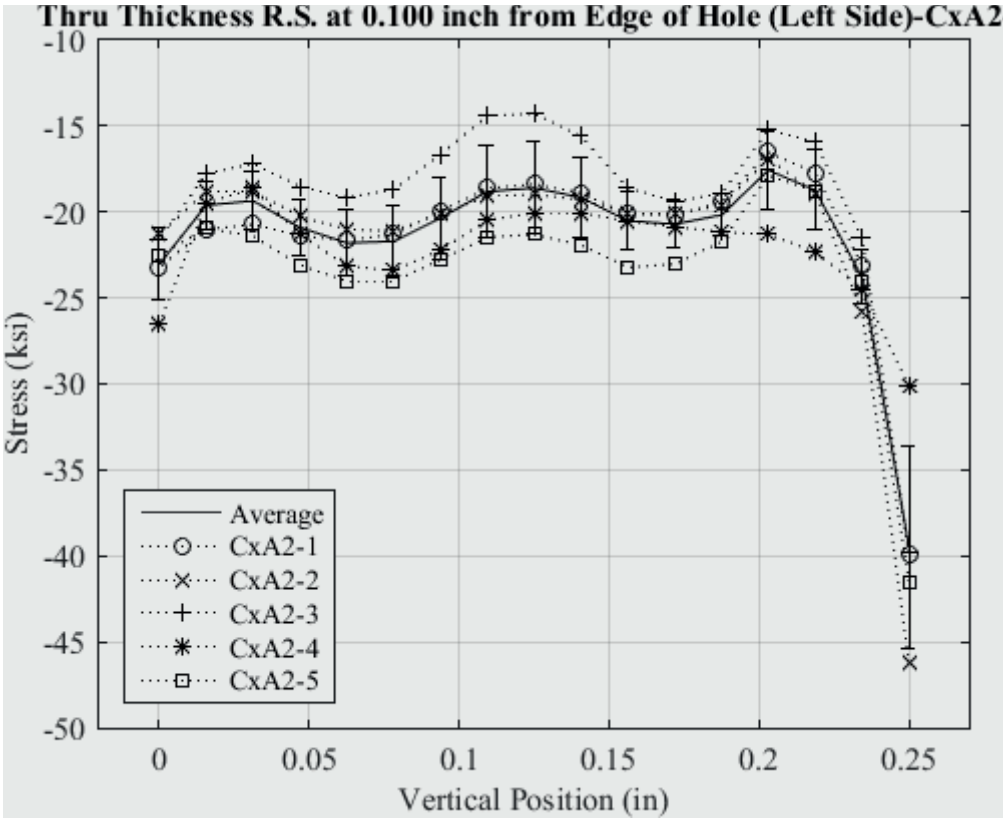

Fig. 82 Line Plot of Residual Stress at 0.10 inch from the Left Edge of the Hole for all CxA2 (2024-T351) Replicates.

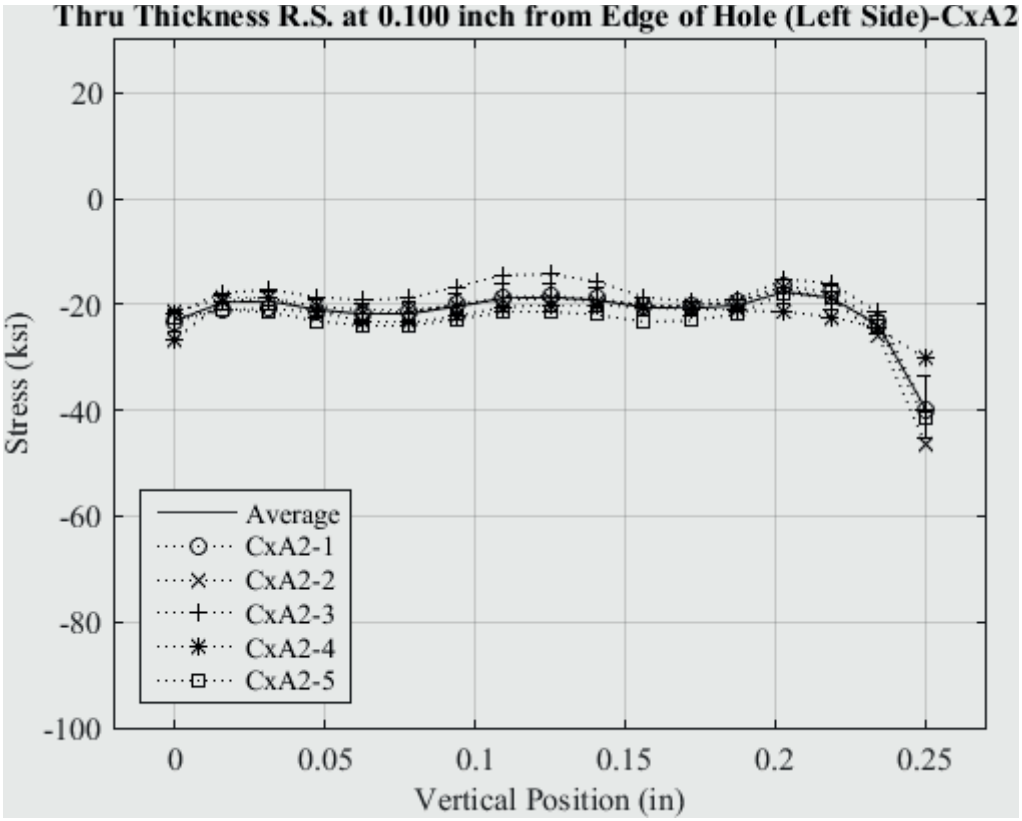

Fig. 83 Line Plot of Residual Stress at 0.10 inch from the Left Edge of the Hole for all CxA2 (2024-T351) Replicates – Locked Stress Scale.

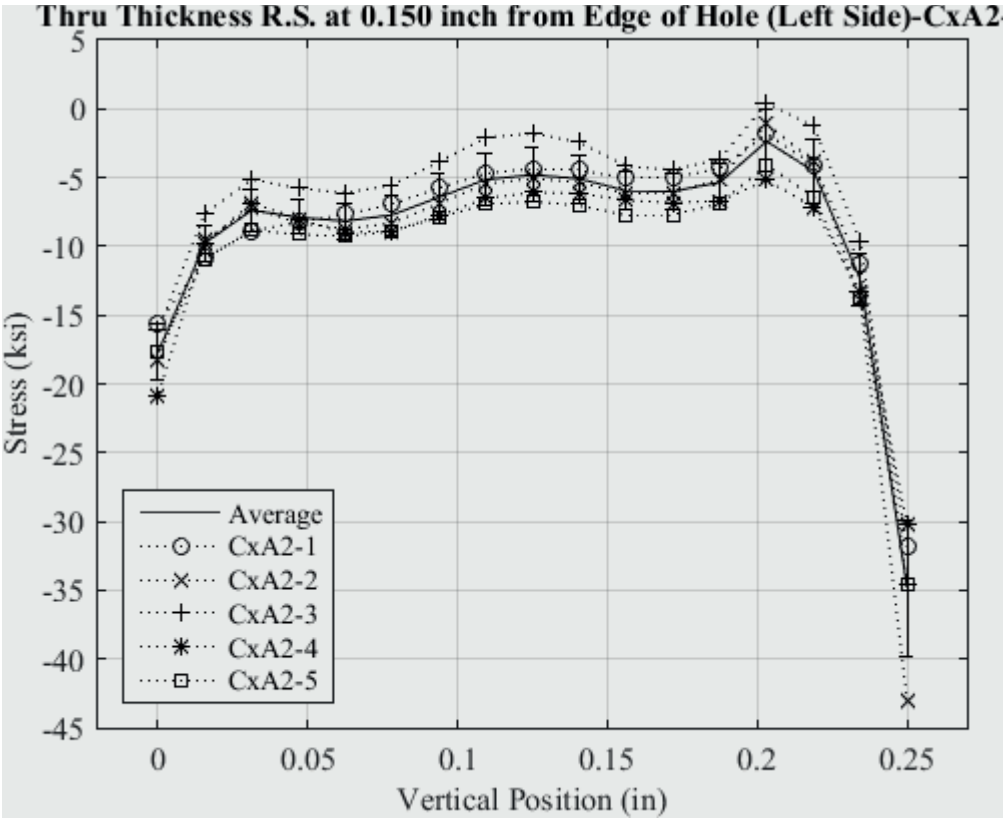

Fig. 84 Line Plot of Residual Stress at 0.15 inch from the Left Edge of the Hole for all CxA2 (2024-T351) Replicates.

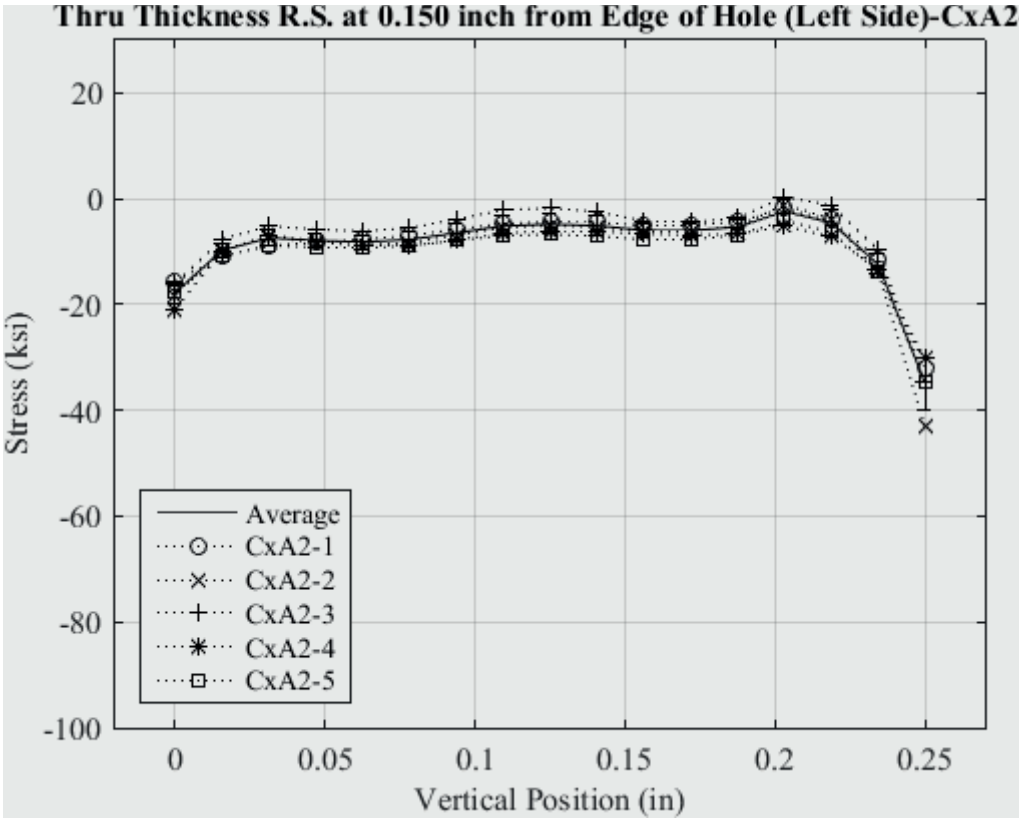

Fig. 85 Line Plot of Residual Stress at 0.15 inch from the Left Edge of the Hole for all CxA2 (2024-T351) Replicates – Locked Stress Scale.

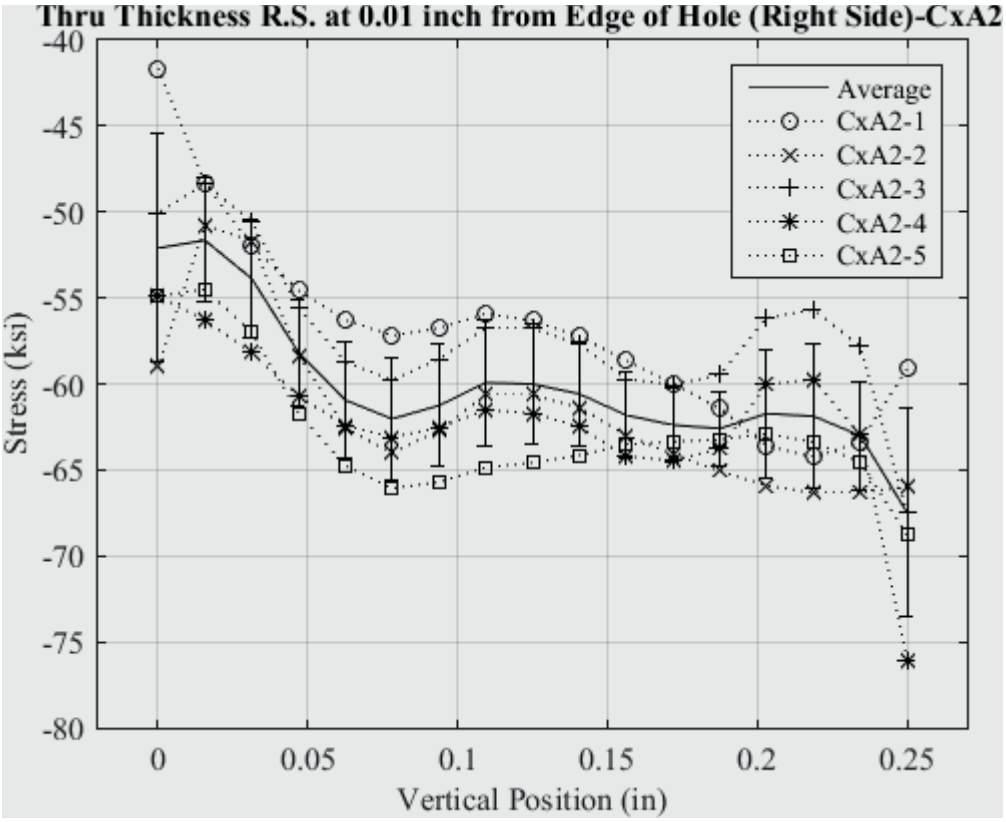

Fig. 86 Line Plot of Residual Stress at 0.01 inch from the Right Edge of the Hole for all CxA2 (2024-T351) Replicates.

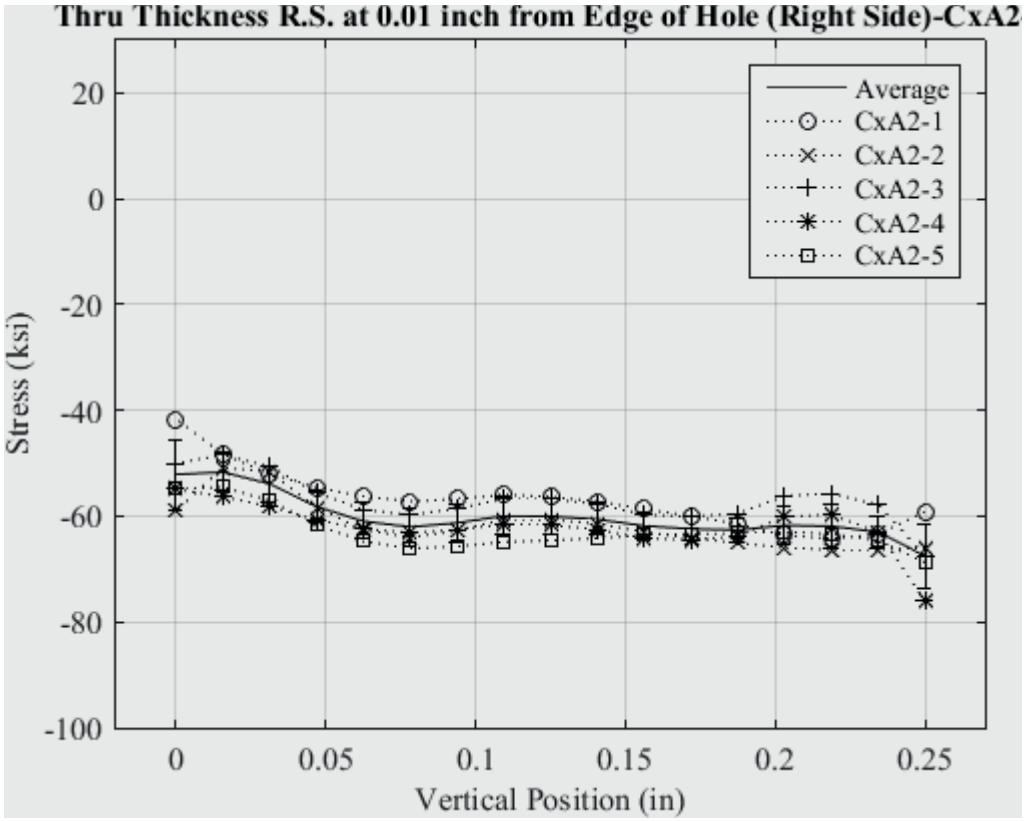

Fig. 87 Line Plot of Residual Stress at 0.01 inch from the Right Edge of the Hole for all CxA2 (2024-T351) Replicates – Locked Stress Scale.

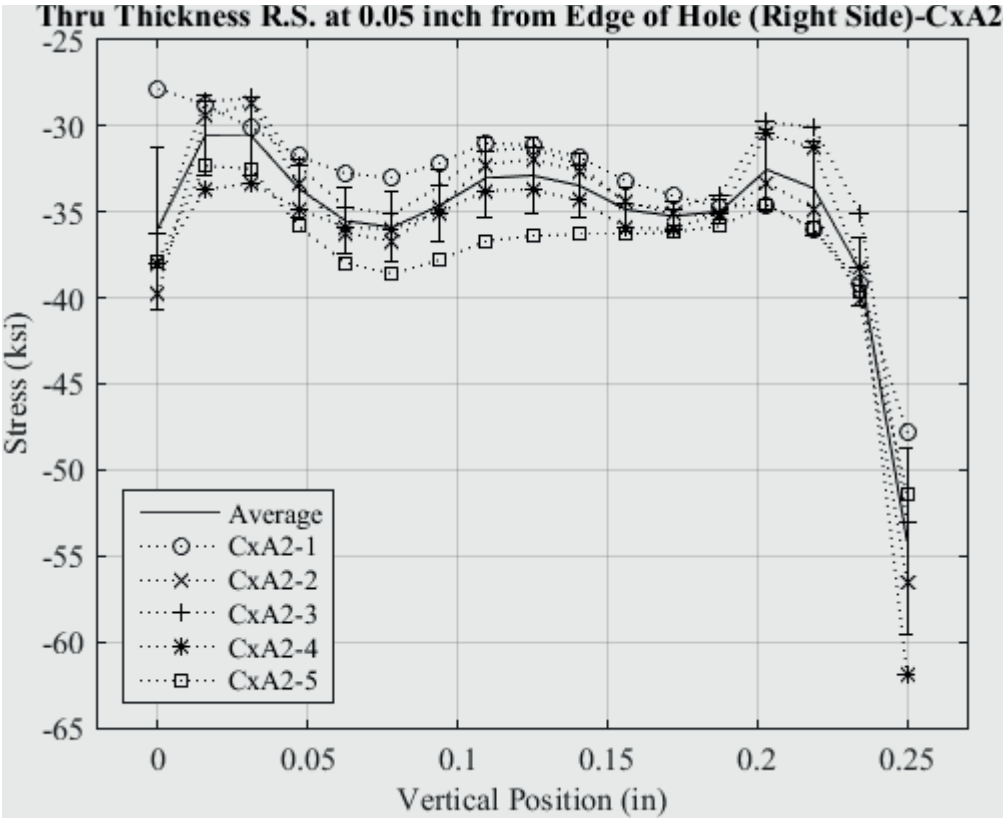

Fig. 88 Line Plot of Residual Stress at 0.05 inch from the Right Edge of the Hole for all CxA2 (2024-T351) Replicates.

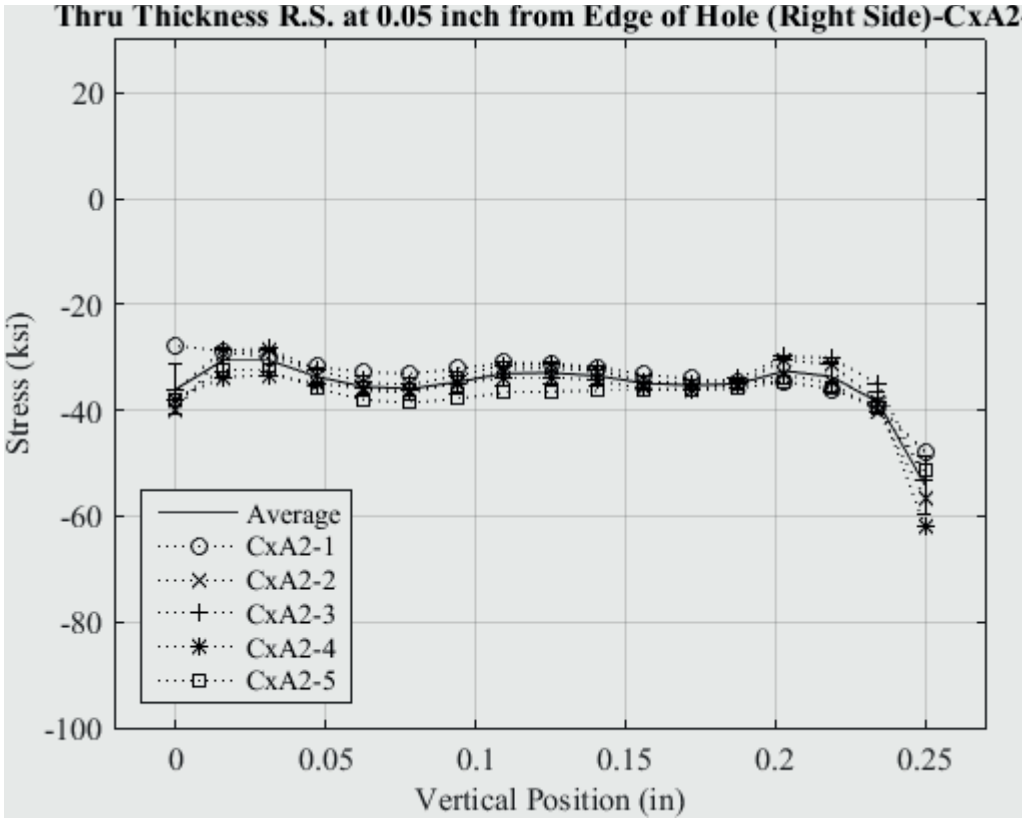

Fig. 89 Line Plot of Residual Stress at 0.05 inch from the Right Edge of the Hole for all CxA2 (2024-T351) Replicates – Locked Stress Scale.

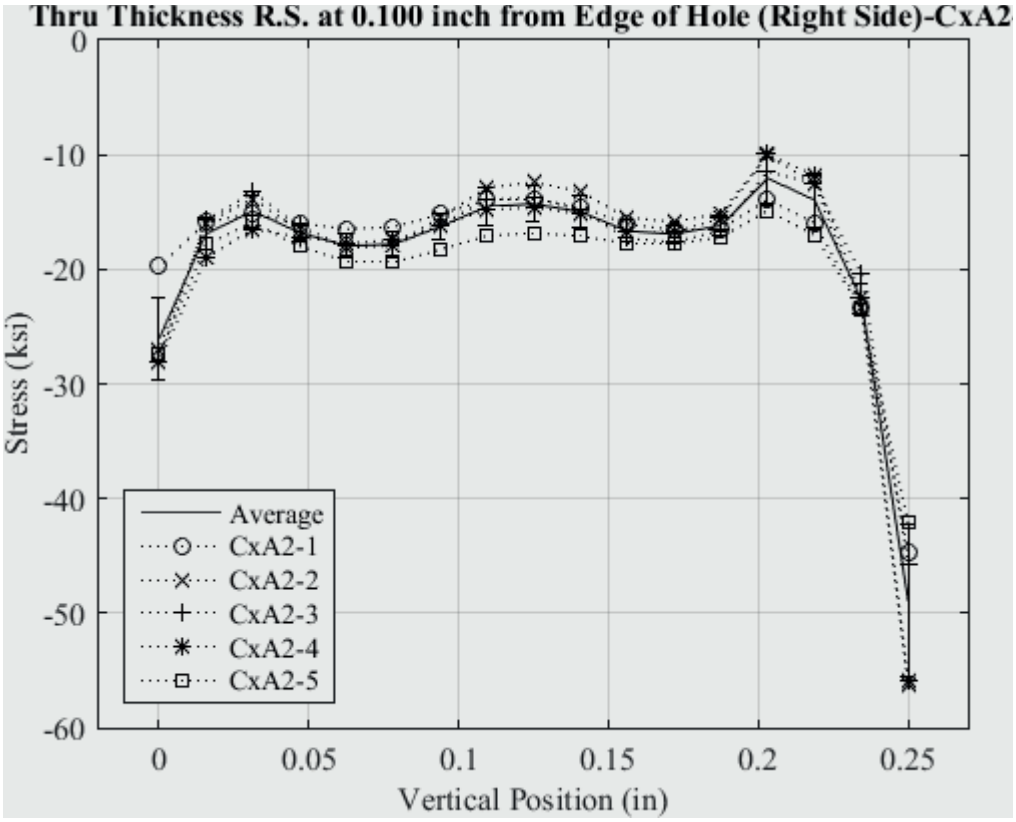

Fig. 90 Line Plot of Residual Stress at 0.10 inch from the Right Edge of the Hole for all CxA2 (2024-T351) Replicates.

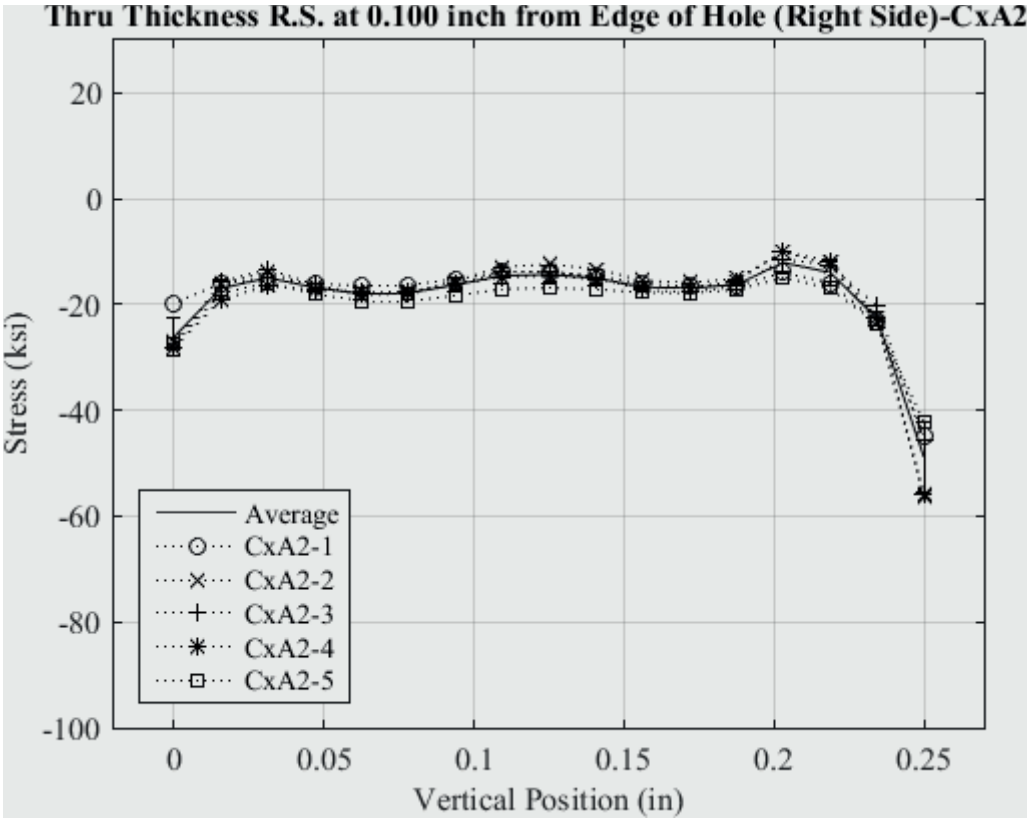

Fig. 91 Line Plot of Residual Stress at 0.10 inch from the Right Edge of the Hole for all CxA2 (2024-T351) Replicates – Locked Stress Scale.

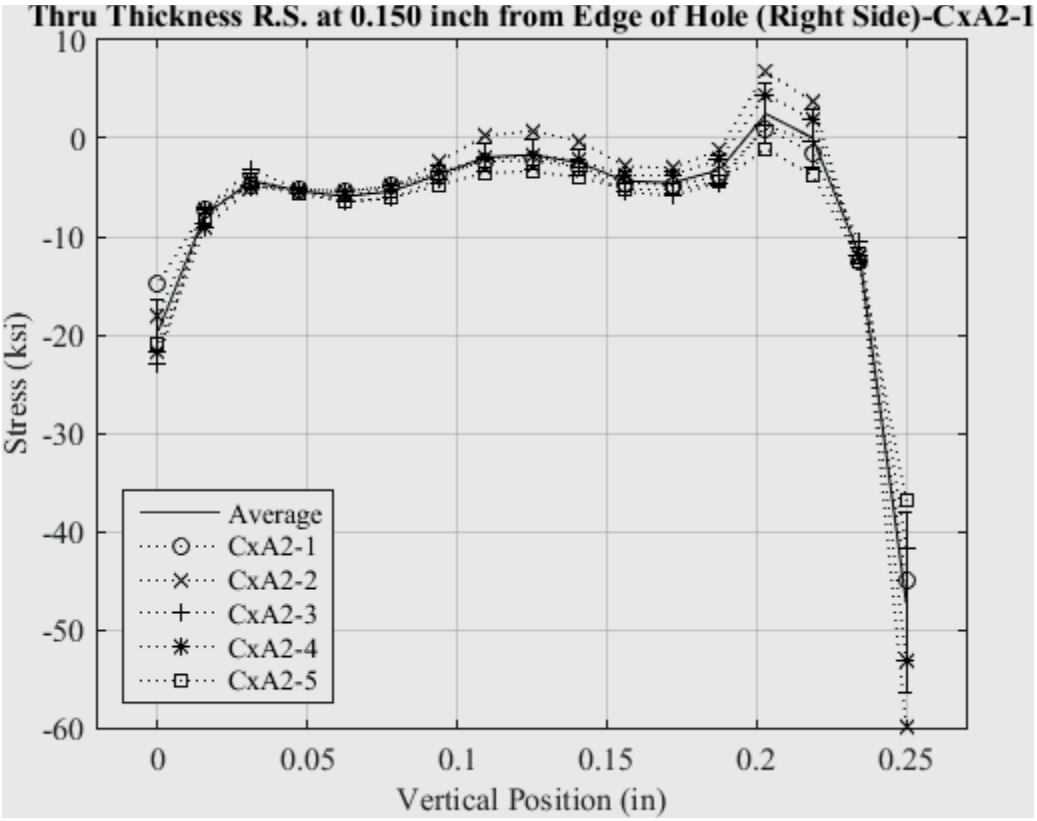

Fig. 92 Line Plot of Residual Stress at 0.15 inch from the Right Edge of the Hole for all CxA2 (2024-T351) Replicates.

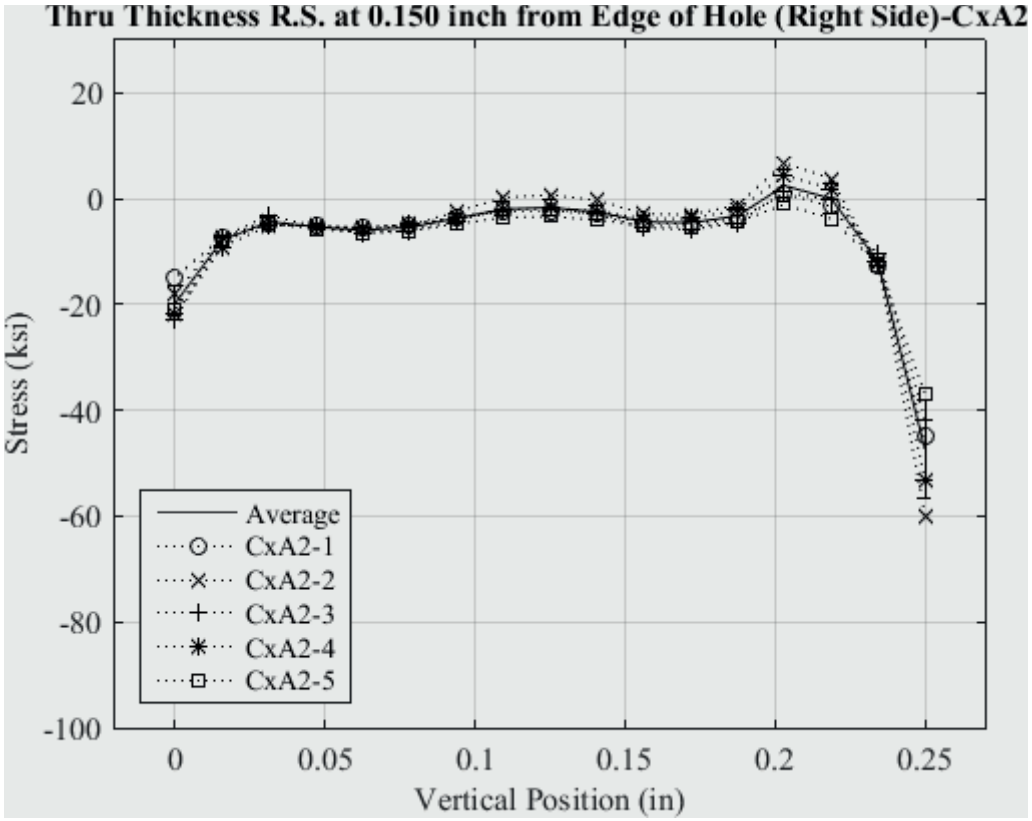

Fig. 93 Line Plot of Residual Stress at 0.15 inch from the Right Edge of the Hole for all CxA2 (2024-T351) Replicates – Locked Stress Scale.

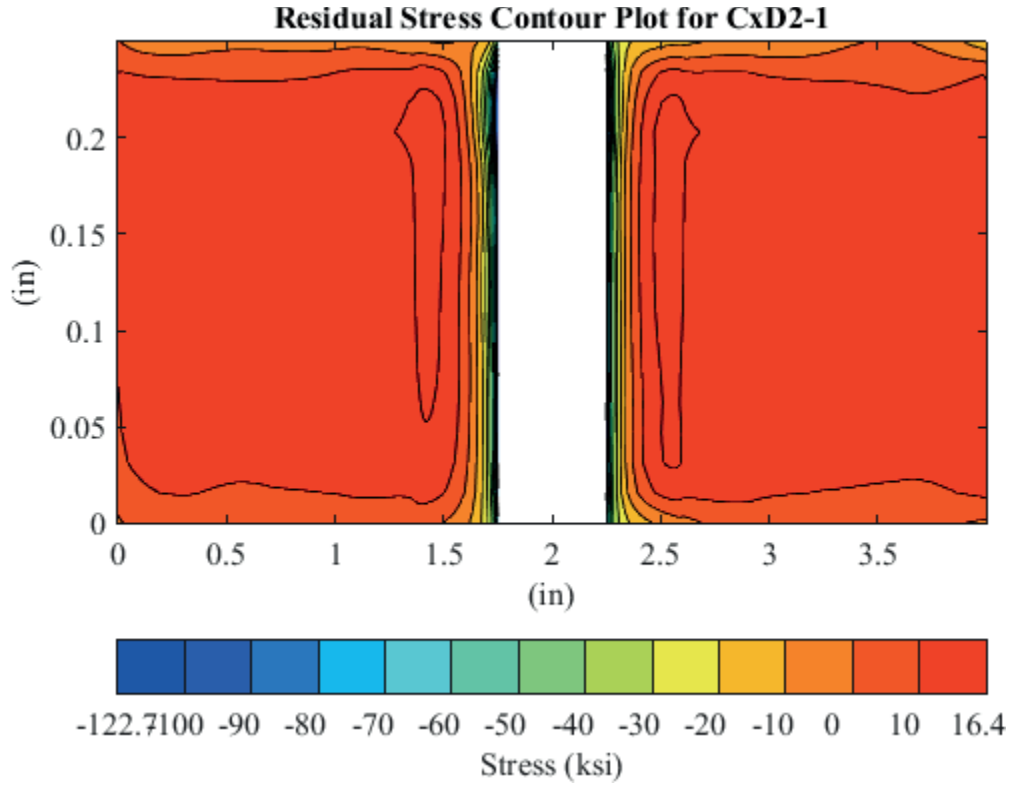

Fig. 94 Residual Stress Contour Plot of Coupon CxD2-1 (7075-T651) – Mandrel Entrance Surface at Y=0.

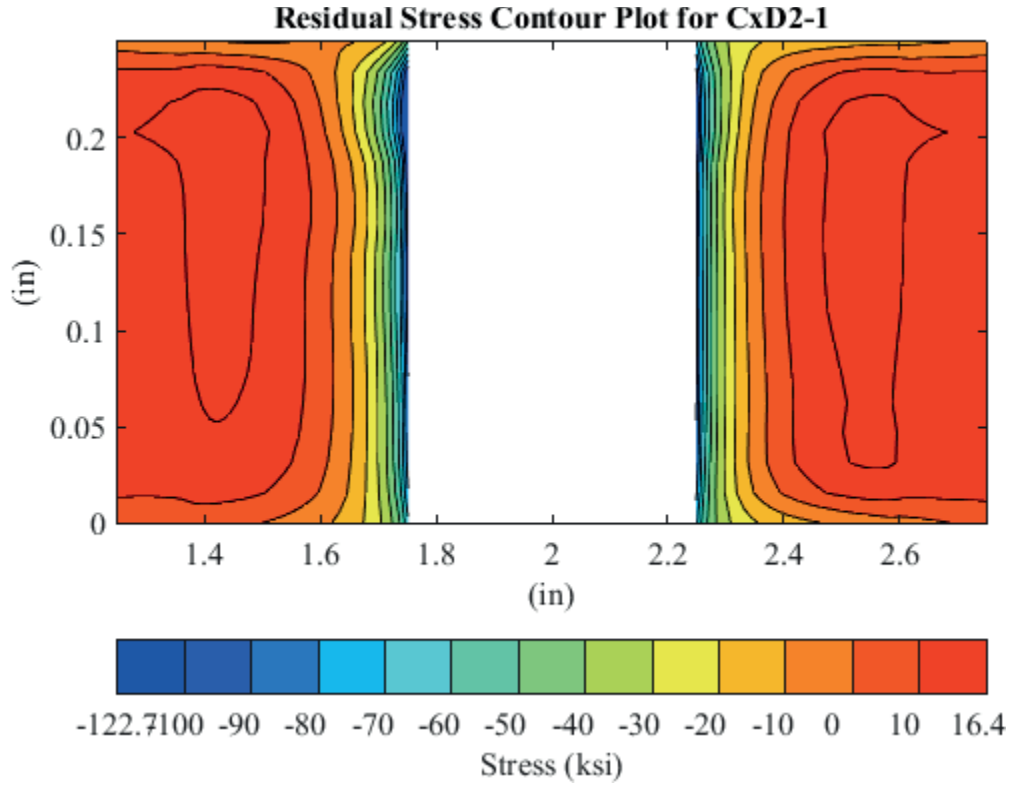

Fig. 95 Residual Stress Contour Plot of Coupon CxD2-1 (7075-T651) – Mandrel Entrance Surface at Y=0 – Zoomed in Next to Hole.

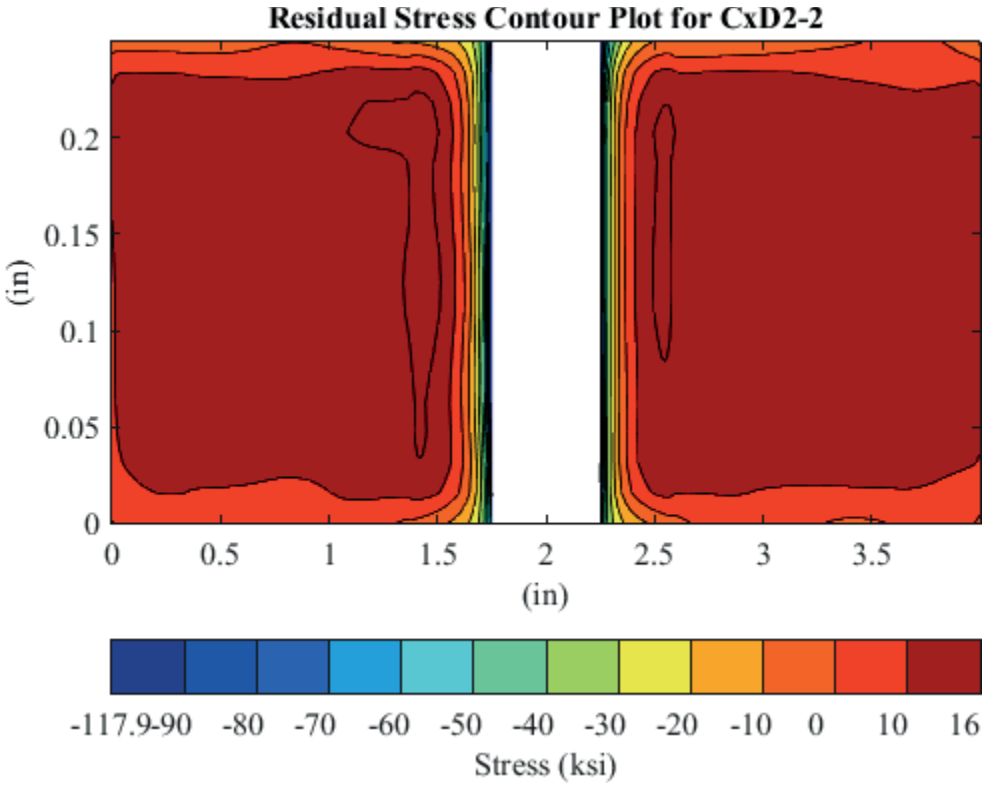

Fig. 96 Residual Stress Contour Plot of Coupon CxD2-2 (7075-T651) – Mandrel Entrance Surface at Y=0.

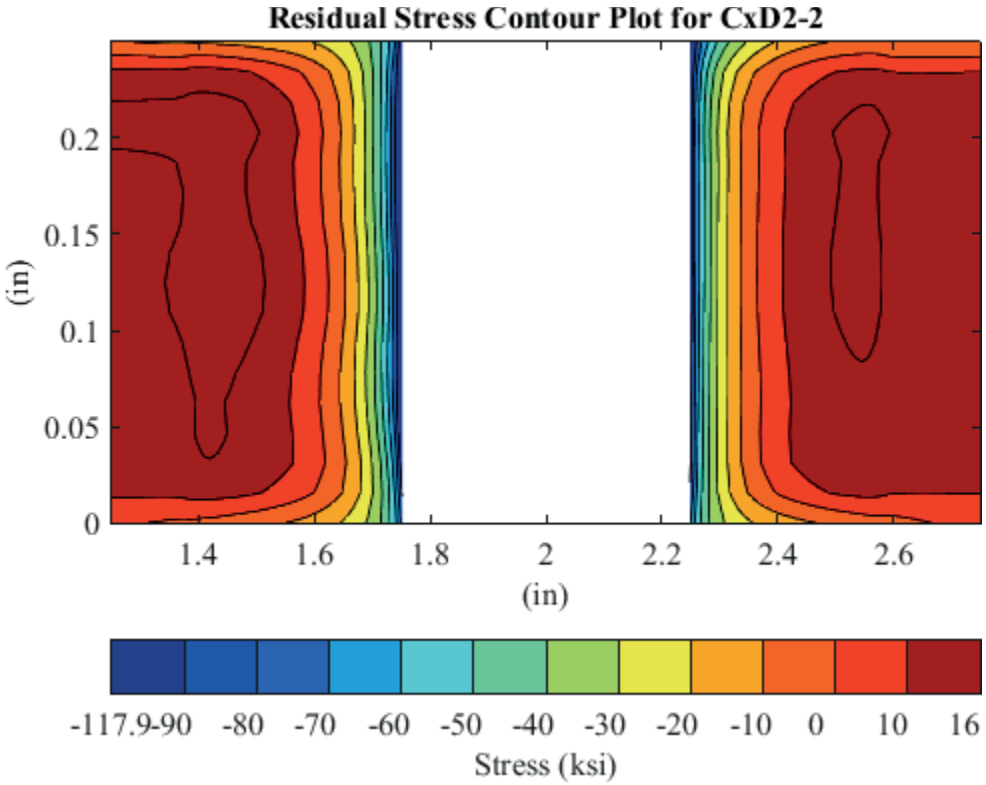

Fig. 97 Residual Stress Contour Plot of Coupon CxD2-2 (7075-T651) – Mandrel Entrance Surface at Y=0 – Zoomed in Next to Hole.

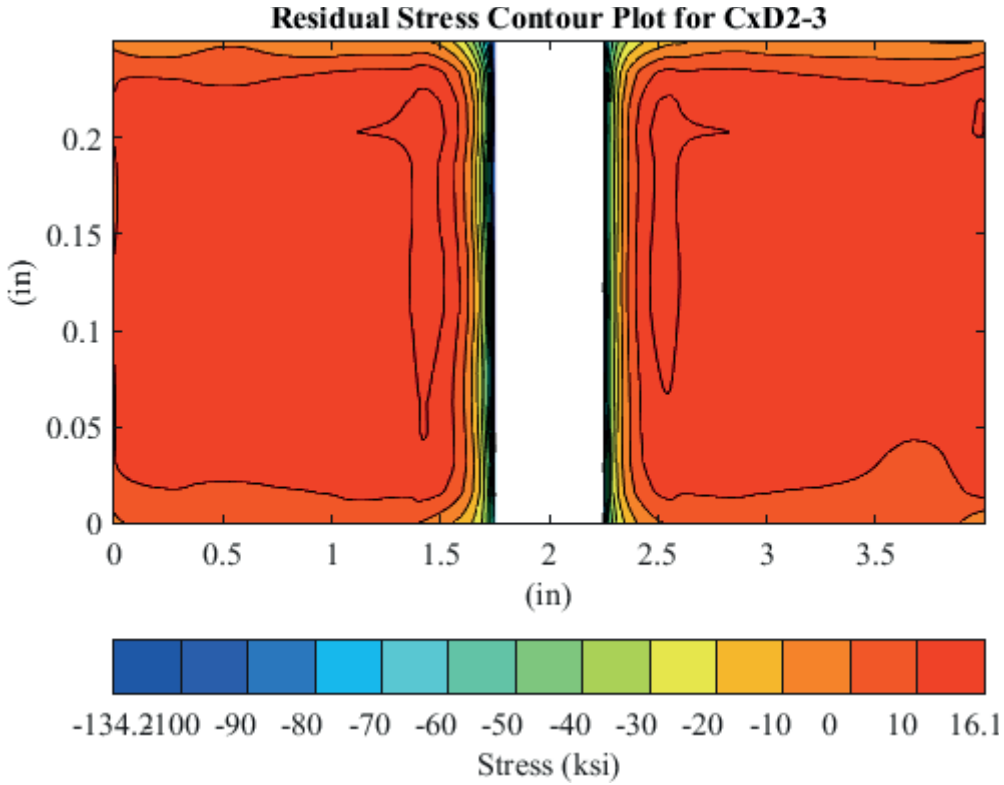

Fig. 98 Residual Stress Contour Plot of Coupon CxD2-3 (7075-T651) – Mandrel Entrance Surface at Y=0.

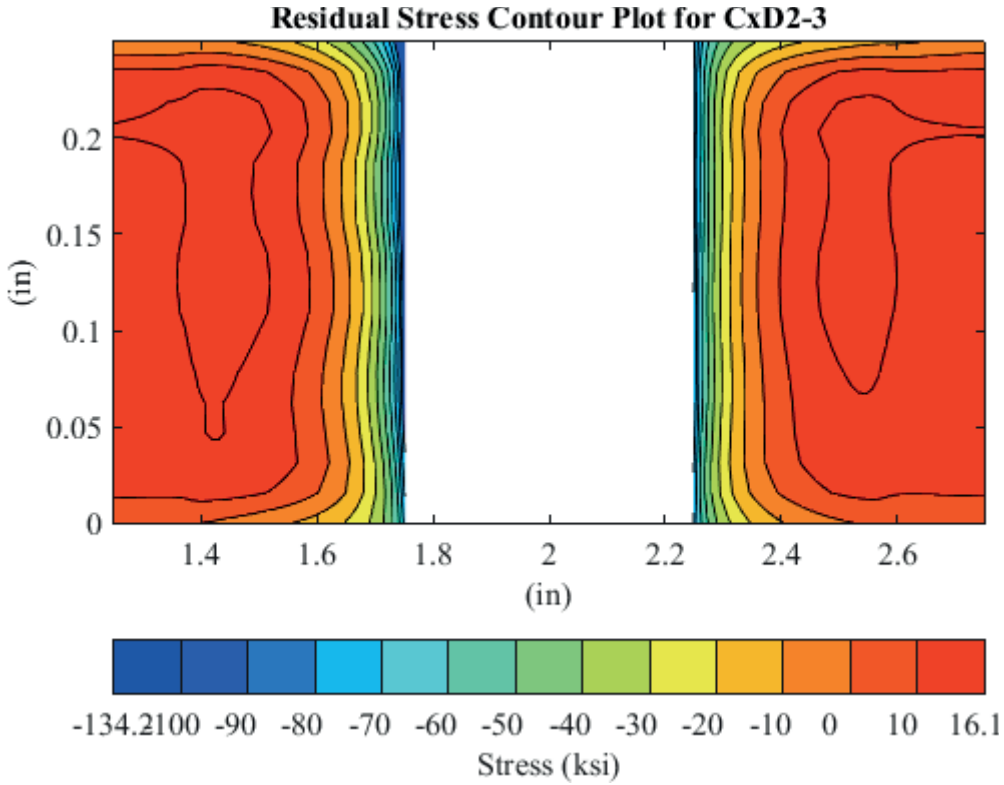

Fig. 99 Residual Stress Contour Plot of Coupon CxD2-3 (7075-T651) – Mandrel Entrance Surface at Y=0 – Zoomed in Next to Hole.

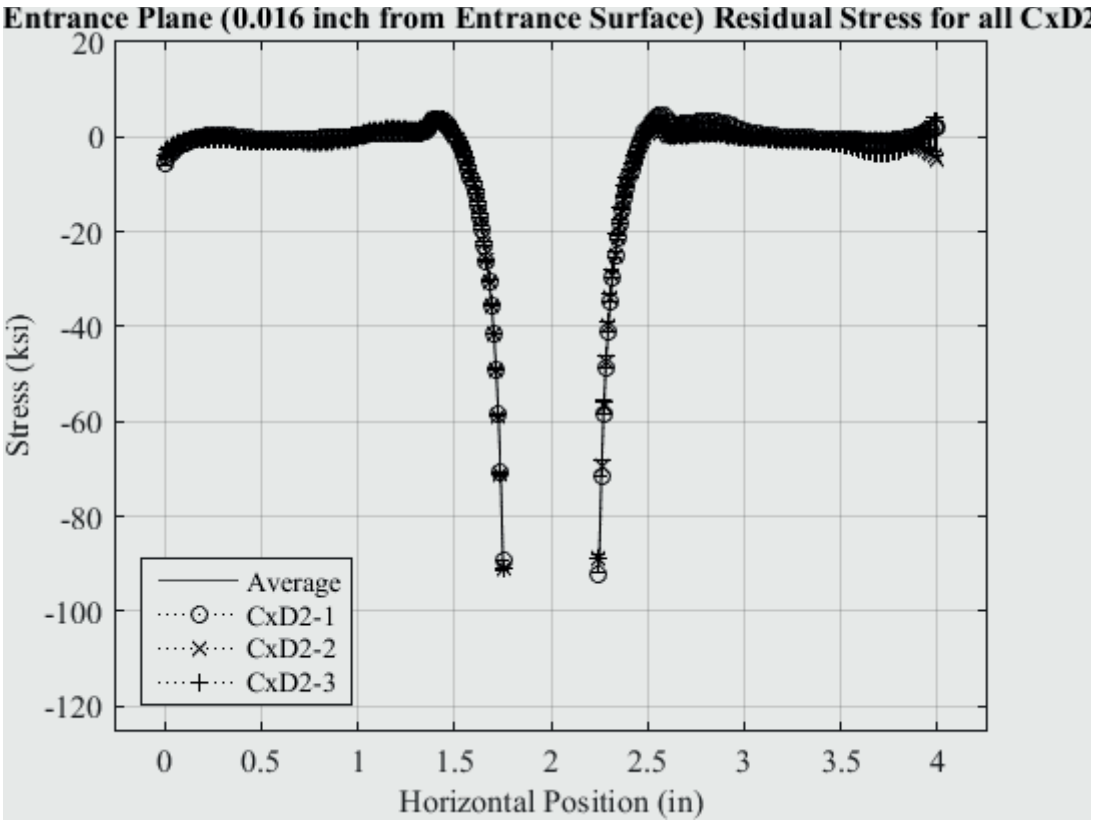

Fig. 100 Residual Stress Line Plot of all CxD2 (7075-T651) Replicates and Average Residual Stress at a Distance of 0.016 inch (Entrance Surface) from the Entrance Surface.

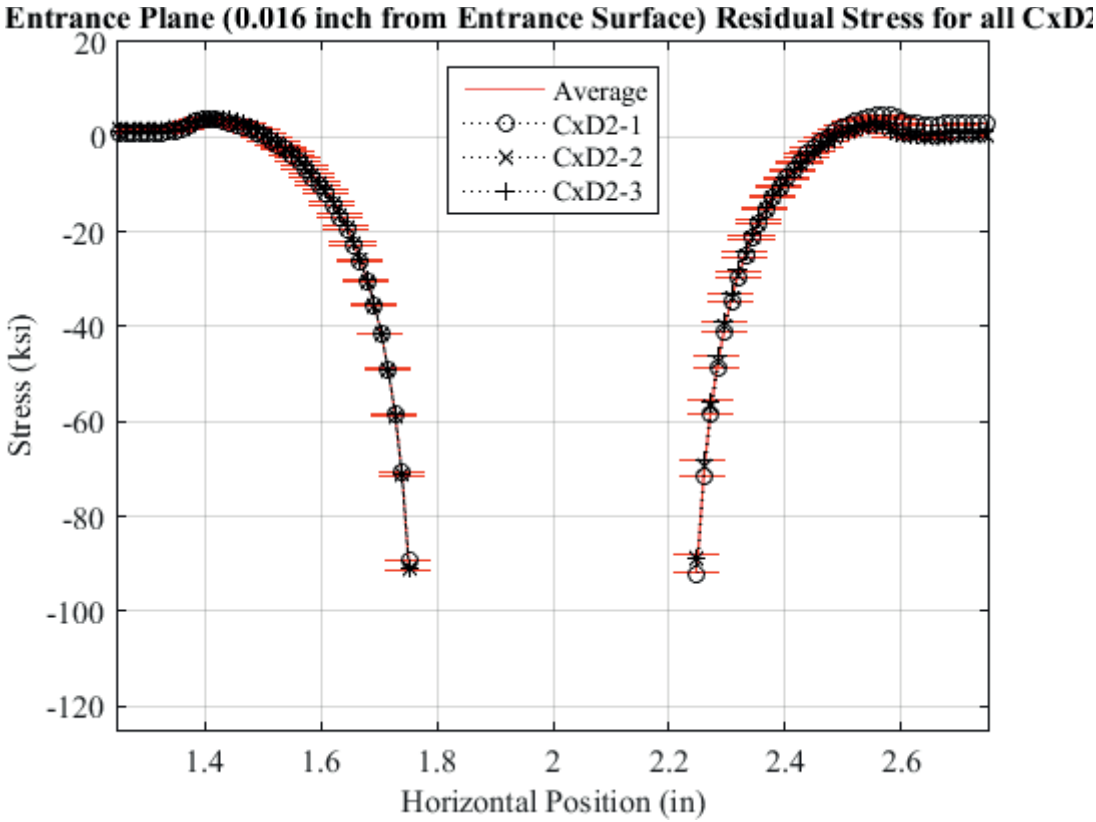

Fig. 101 Residual Stress Line Plot of all CxD2 (7075-T651) Replicates and Average Residual Stress at a Distance of 0.016 inch (Entrance Surface) from the Entrance Surface – Zoomed in Next to Hole.

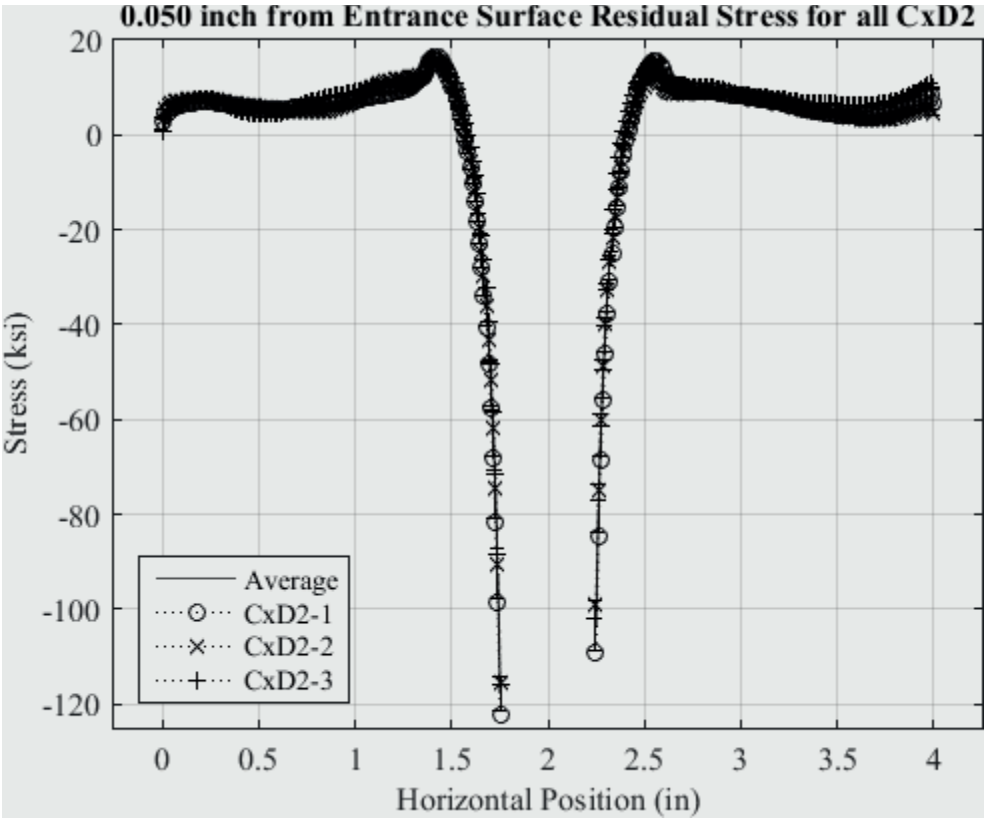

Fig. 102 Residual Stress Line Plot of all CxD2 (7075-T651) Replicates and Average Residual Stress at a Distance of 0.050 inch from the Entrance Surface.

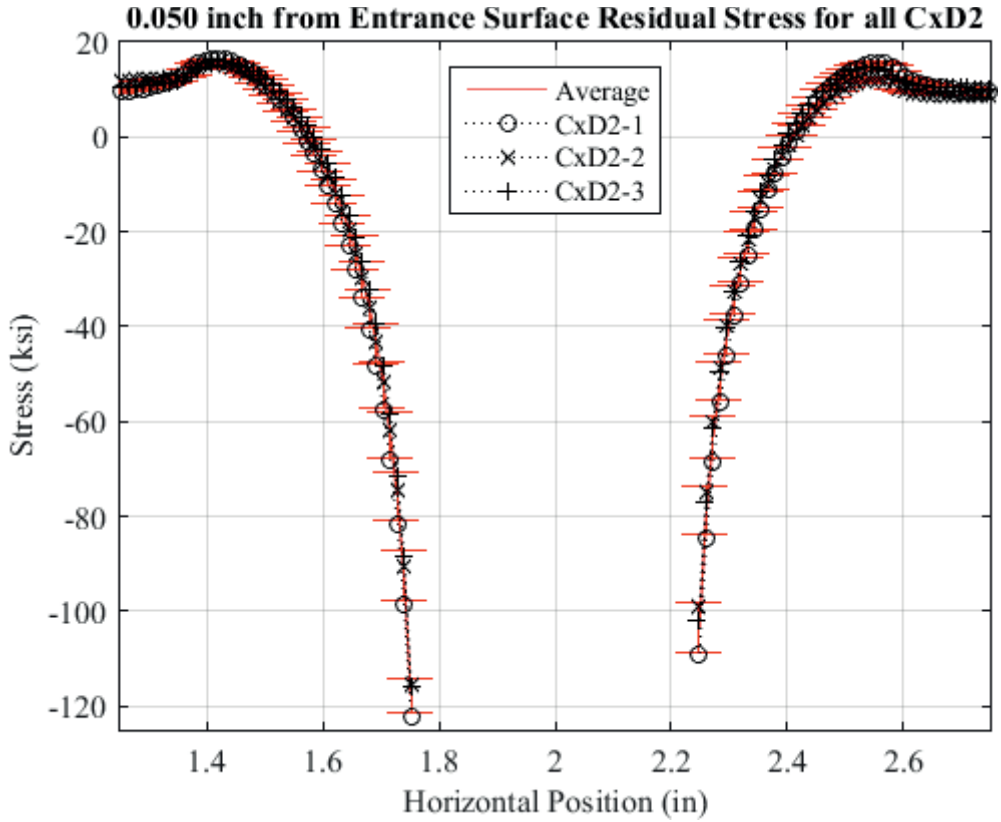

Fig. 103 Residual Stress Line Plot of all CxD2 (7075-T651) Replicates and Average Residual Stress at a Distance of 0.05 inch (Entrance Surface) from the Entrance Surface – Zoomed in Next to Hole.

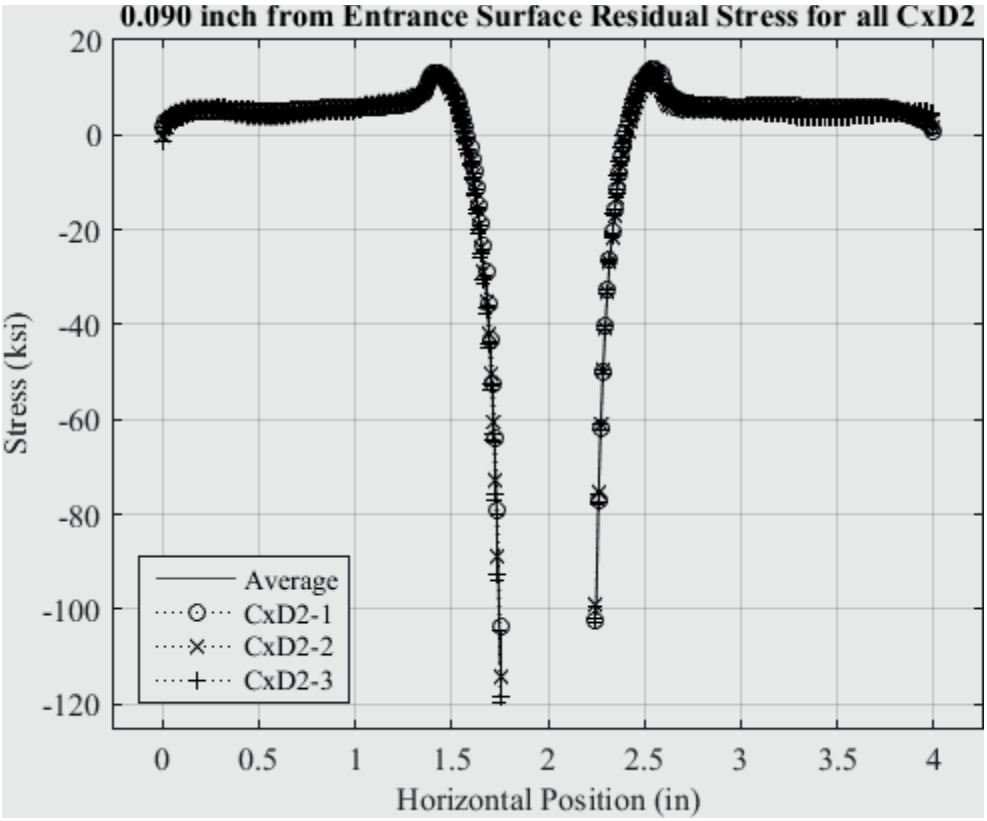

Fig. 104 Residual Stress Line Plot of all CxD2 (7075-T651) Replicates and Average Residual Stress at a Distance of 0.090 inch from the Entrance Surface.

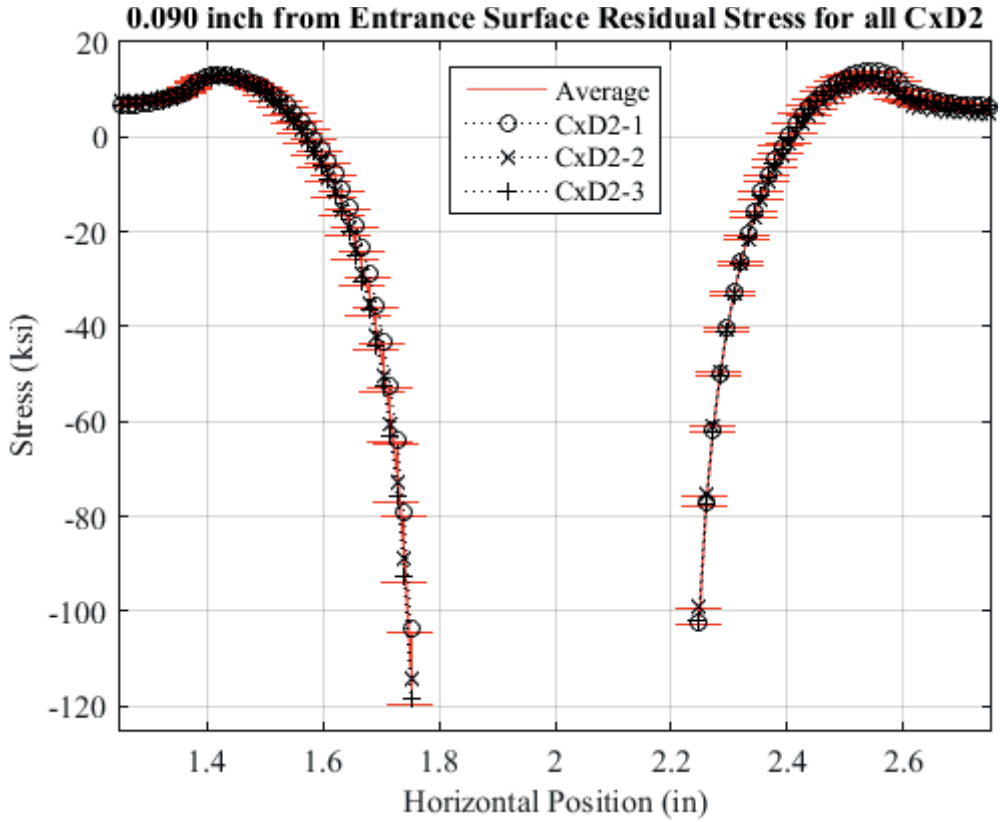

Fig. 105 Residual Stress Line Plot of all CxD2 (7075-T651) Replicates and Average Residual Stress at a Distance of 0.090 inch (Entrance Surface) from the Entrance Surface – Zoomed in Next to Hole.

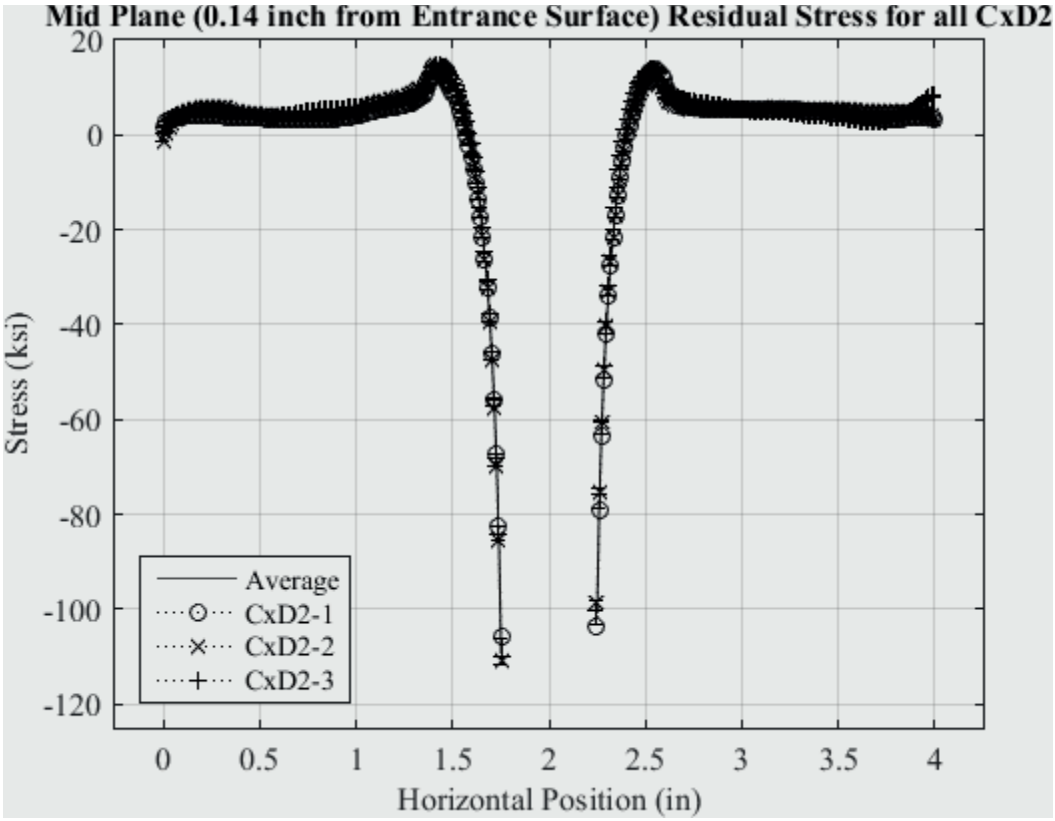

Fig. 106 Residual Stress Line Plot of all CxD2 (7075-T651) Replicates and Average Residual Stress at a Distance of 0.140 inch (Mid Thickness) from the Entrance Surface.

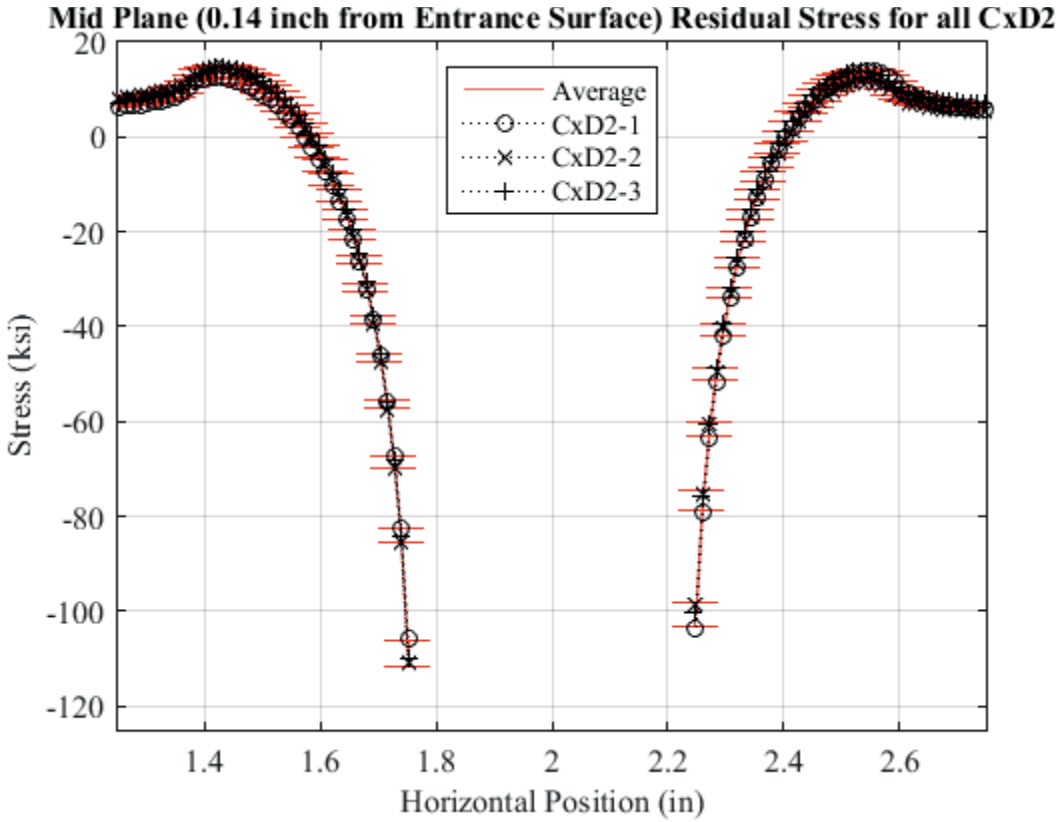

Fig. 107 Residual Stress Line Plot of all CxD2 (7075-T651) Replicates and Average Residual Stress at a Distance of 0.140 inch (Mid Thickness) from the Entrance Surface – Zoomed in Next to Hole.

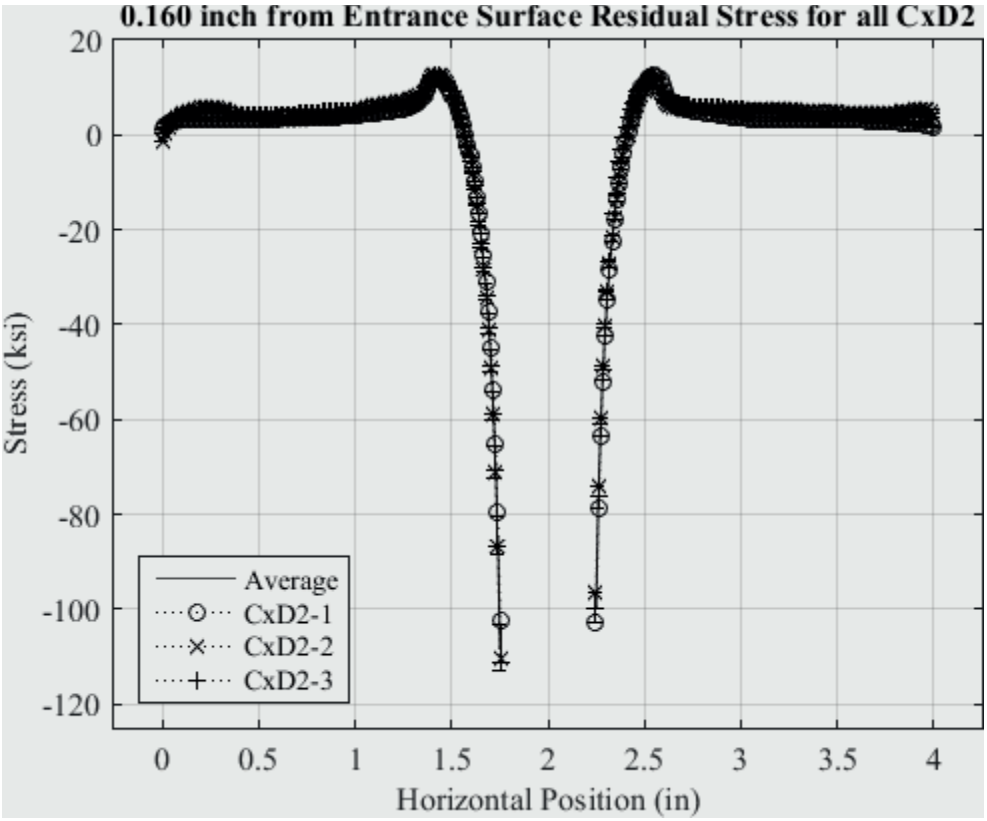

Fig. 108 Residual Stress Line Plot of all CxD2 (7075-T651) Replicates and Average Residual Stress at a Distance of 0.160 inch from the Entrance Surface.

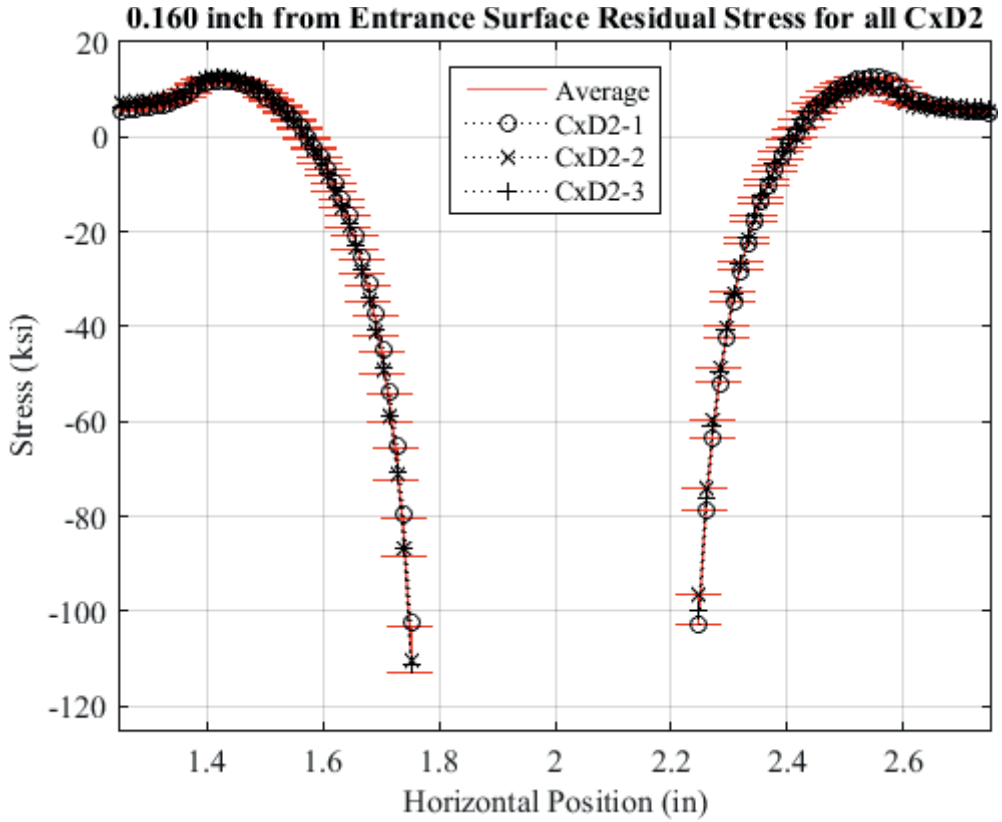

Fig. 109 Residual Stress Line Plot of all CxD2 (7075-T651) Replicates and Average Residual Stress at a Distance of 0.160 inch from the Entrance Surface – Zoomed in Next to Hole.

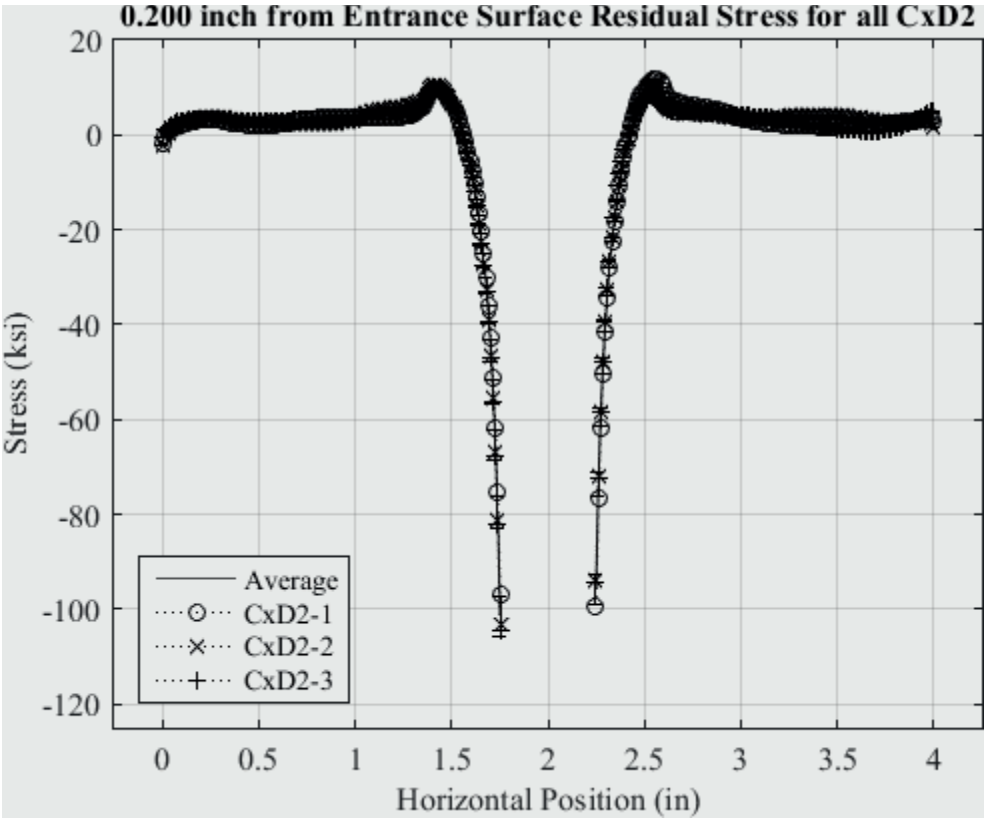

Fig. 110 Residual Stress Line Plot of all CxD2 (7075-T651) Replicates and Average Residual Stress at a Distance of 0.200 inch from the Entrance Surface.

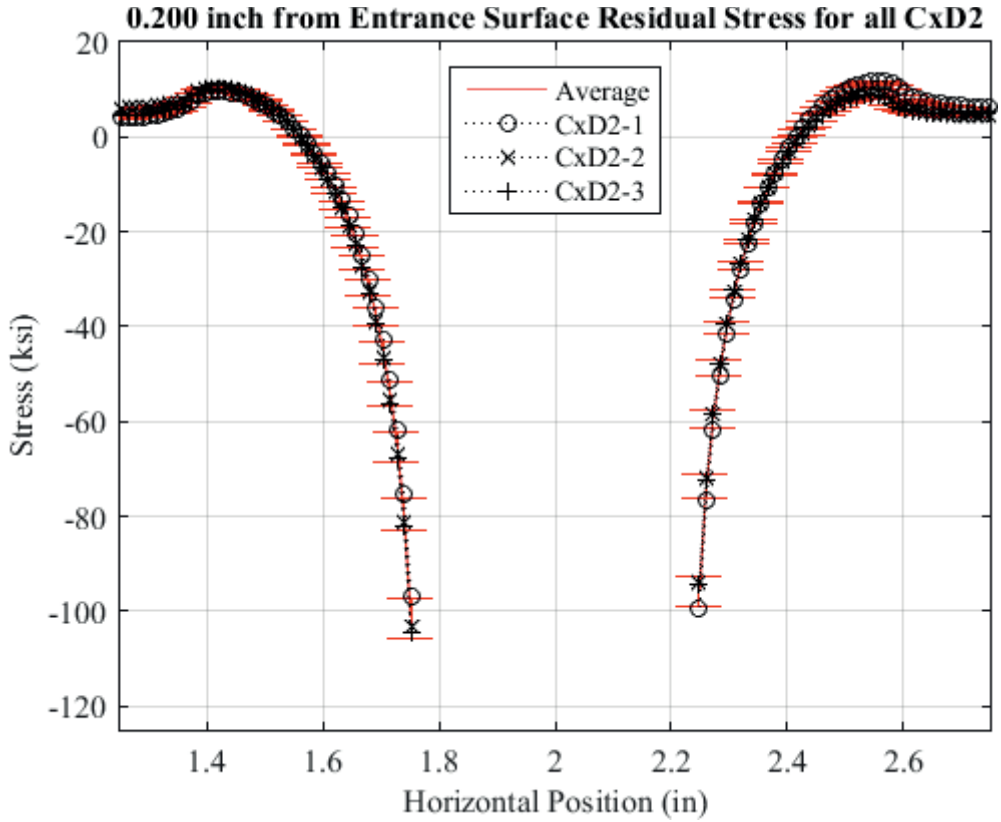

Fig. 111 Residual Stress Line Plot of all CxD2 (7075-T651) Replicates and Average Residual Stress at a Distance of 0.200 inch from the Entrance Surface – Zoomed in Next to Hole.

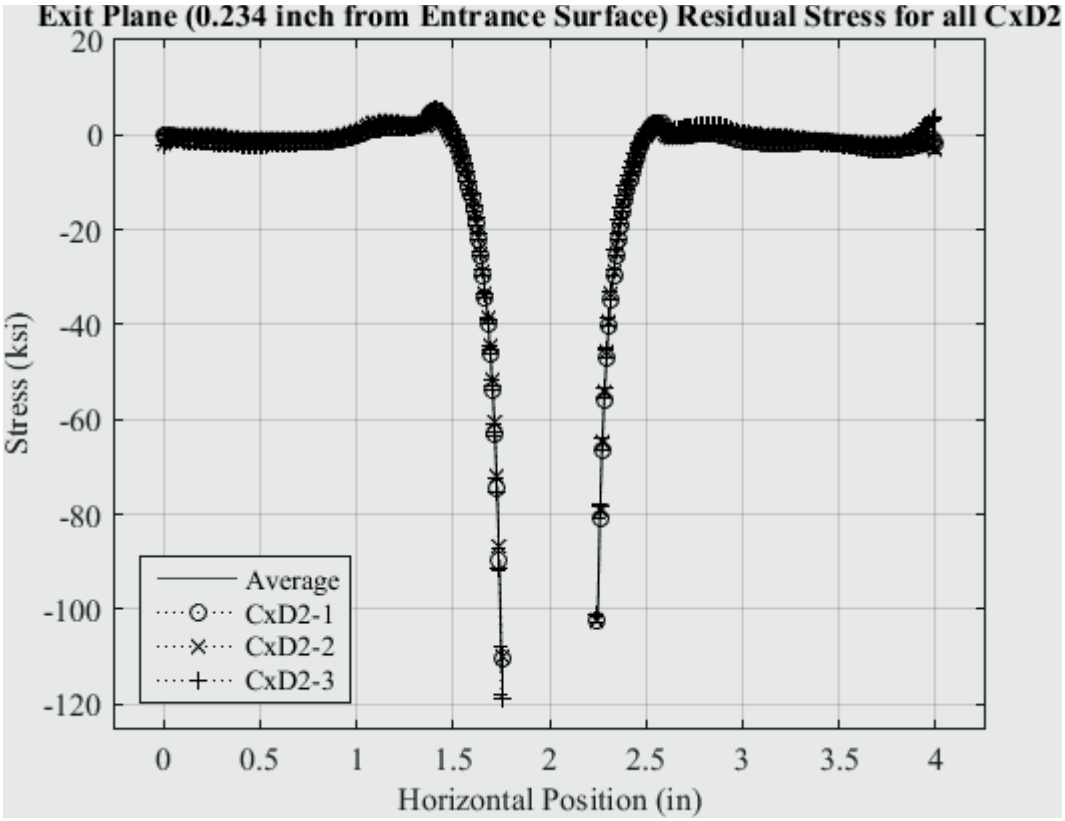

Fig. 112 Residual Stress Line Plot of all CxD2 (7075-T651) Replicates and Average Residual Stress at a Distance of 0.234 inch (Exit Surface) from the Entrance Surface.

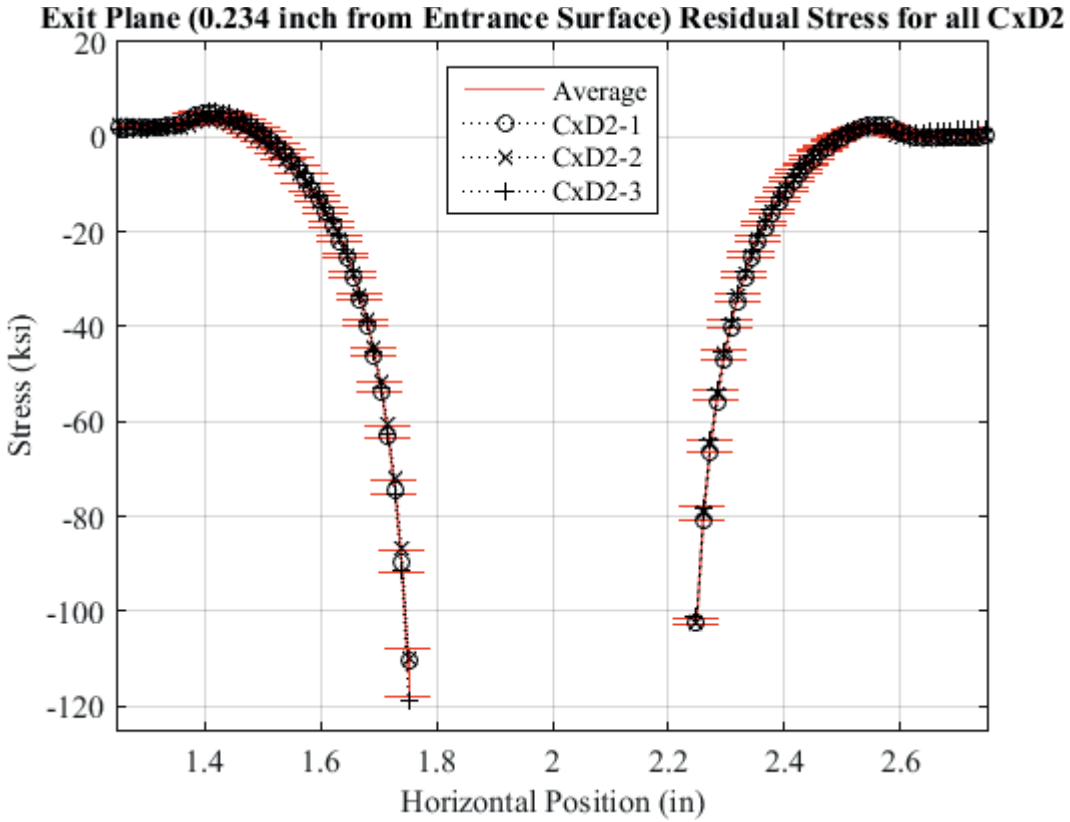

Fig. 113 Residual Stress Line Plot of all CxD2 (7075-T651) Replicates and Average Residual Stress at a Distance of 0.234 inch (Exit Surface) from the Entrance Surface – Zoomed in Next to Hole.

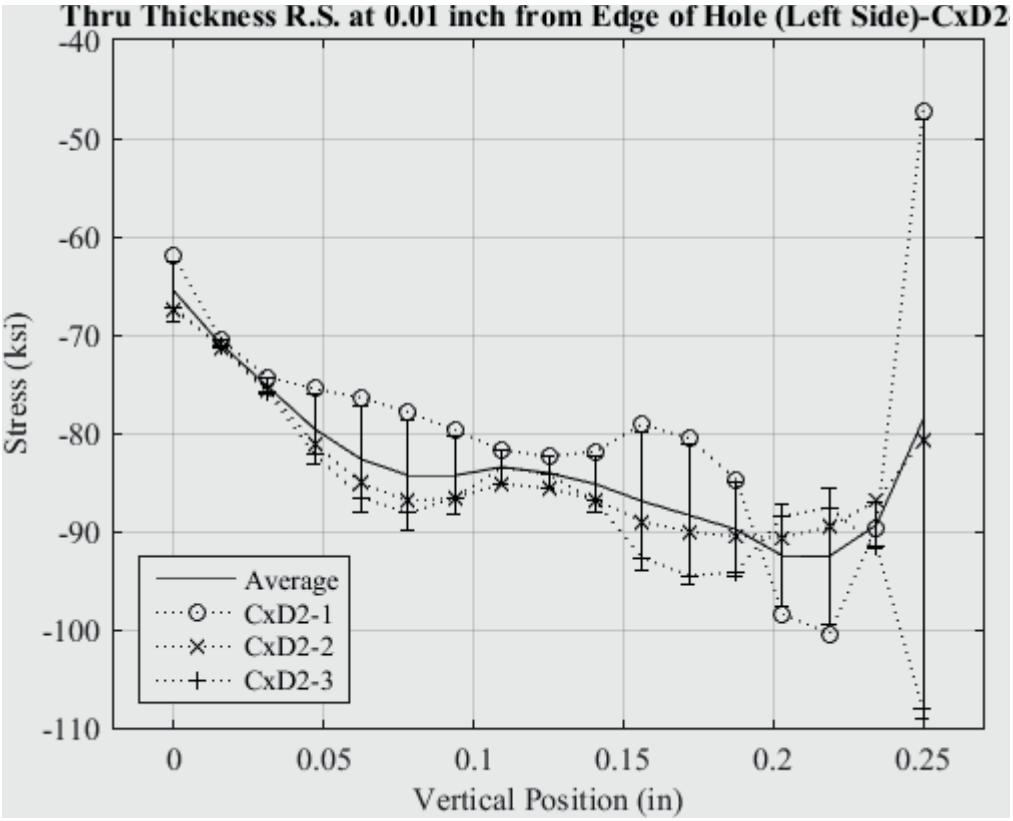

Fig. 114 Line Plot of Residual Stress at 0.010 inch from the Left Edge of the Hole for all CxD2 (7075-T651) Replicates.

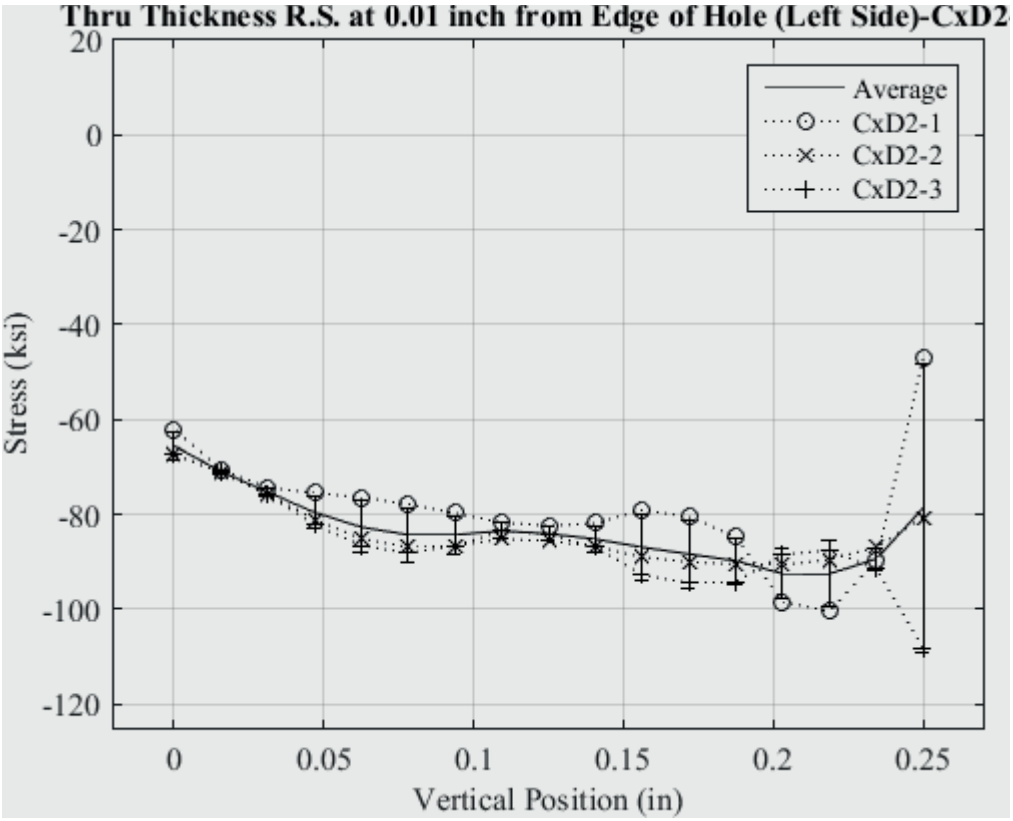

Fig. 115 Line Plot of Residual Stress at 0.010 inch from the Left Edge of the Hole for all CxD2 (7075-T651) Replicates – Stress Scale Locked.

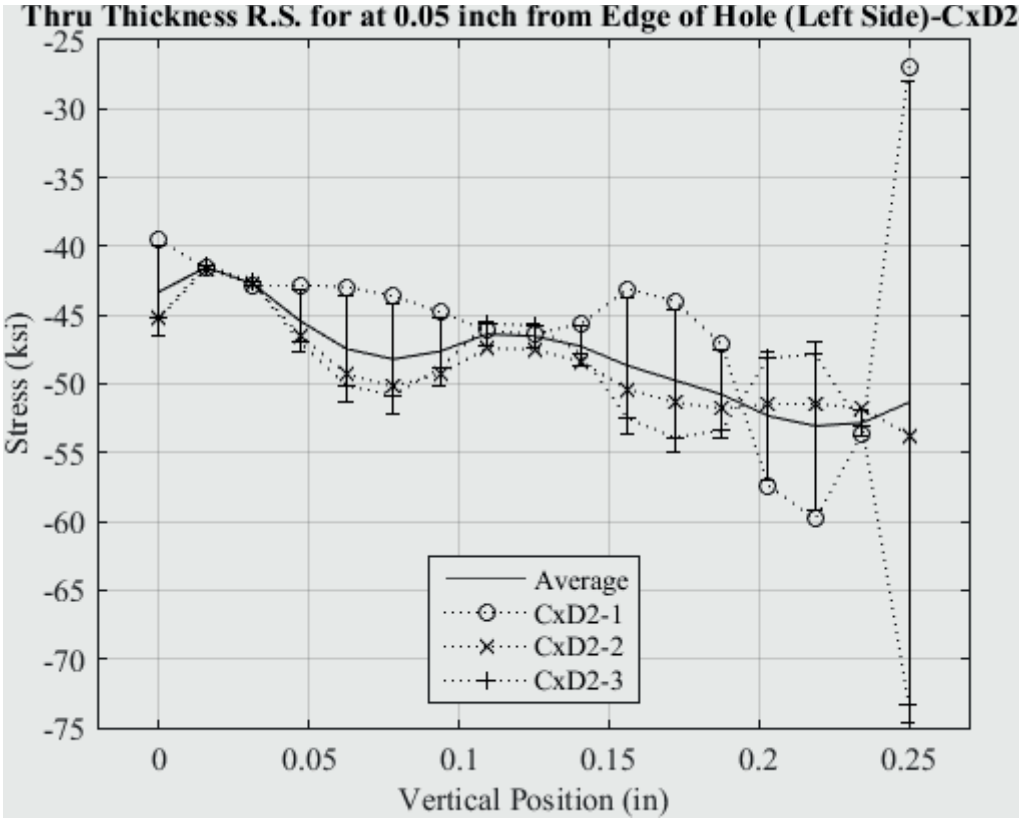

Fig. 116 Line Plot of Residual Stress at 0.050 inch from the Left Edge of the Hole for all CxD2 (7075-T651) Replicates.

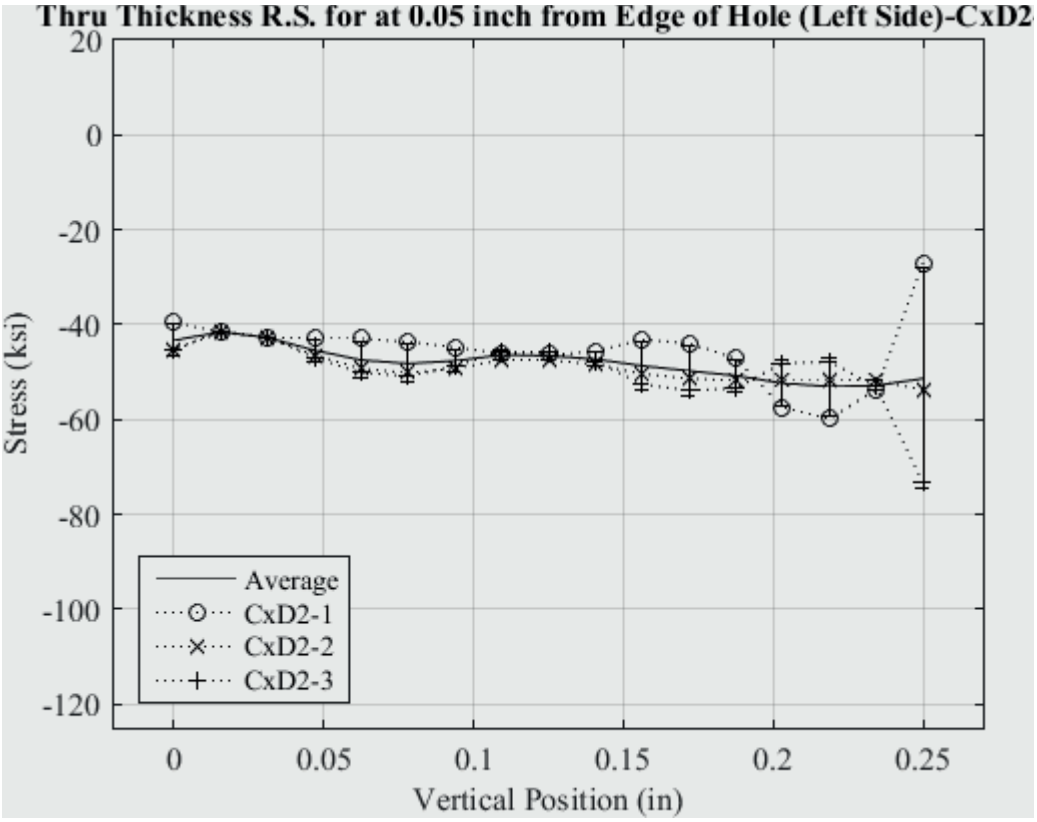

Fig. 117 Line Plot of Residual Stress at 0.050 inch from the Left Edge of the Hole for all CxD2 (7075-T651) Replicates – Stress Scale Locked.

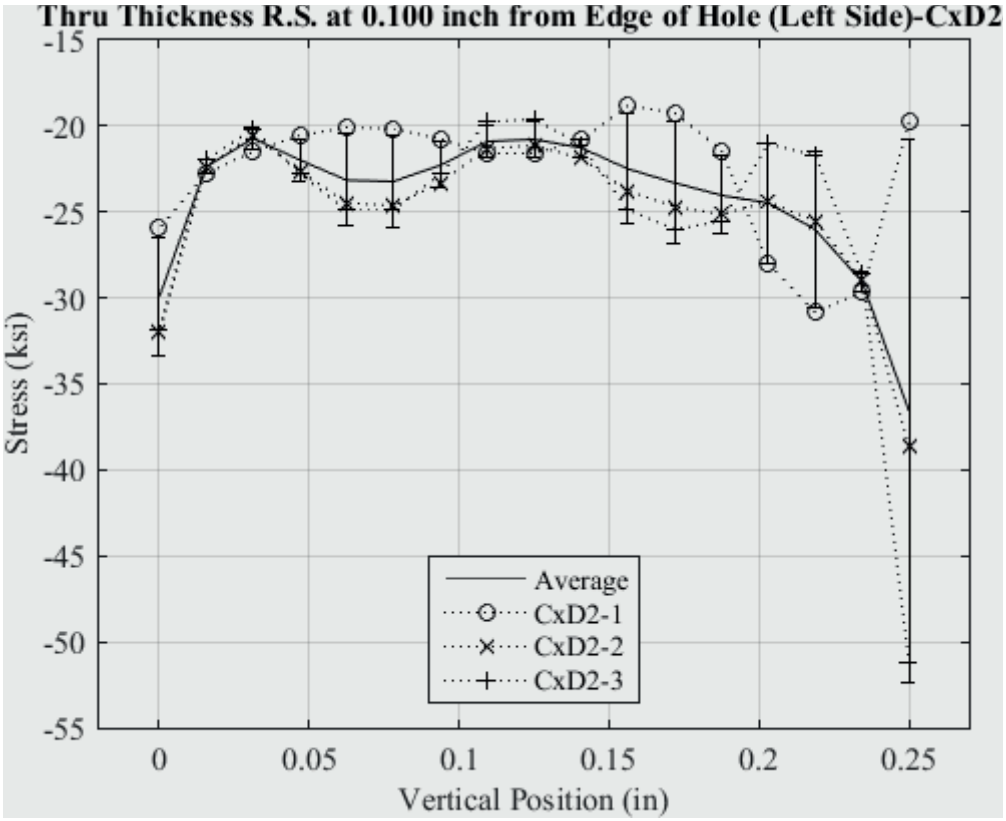

Fig. 118 Line Plot of Residual Stress at 0.100 inch from the Left Edge of the Hole for all CxD2 (7075-T651) Replicates.

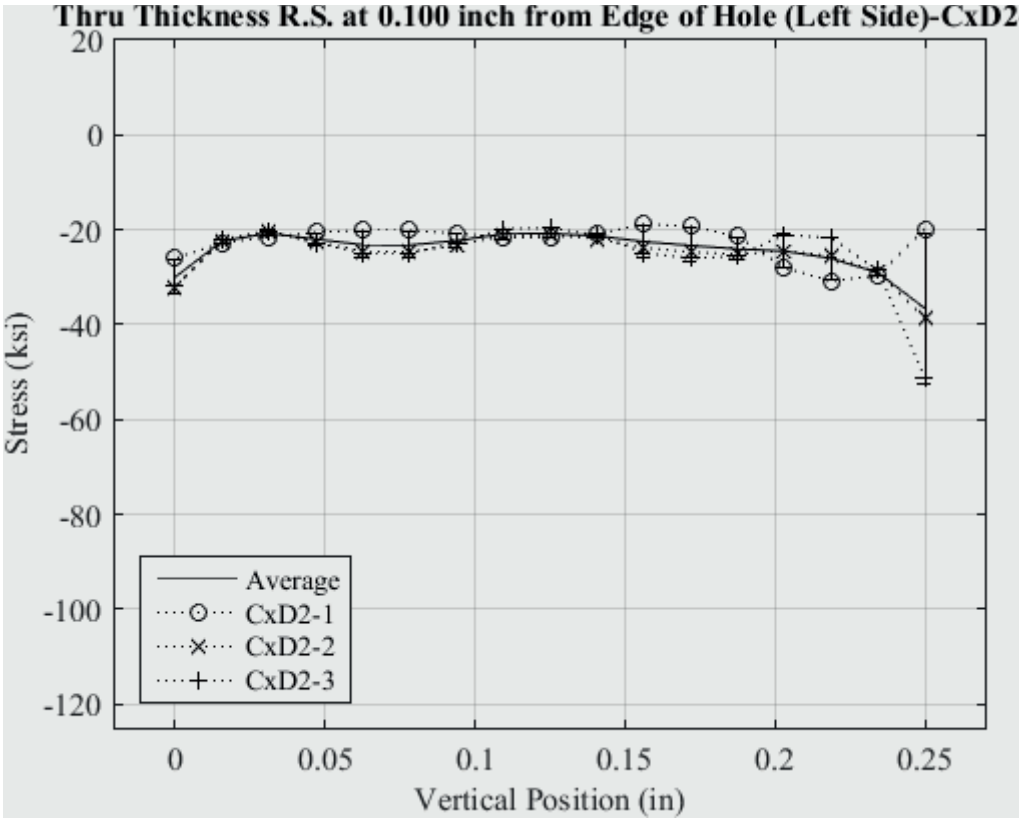

Fig. 119 Line Plot of Residual Stress at 0.100 inch from the Left Edge of the Hole for all CxD2 (7075-T651) Replicates – Stress Scale Locked.

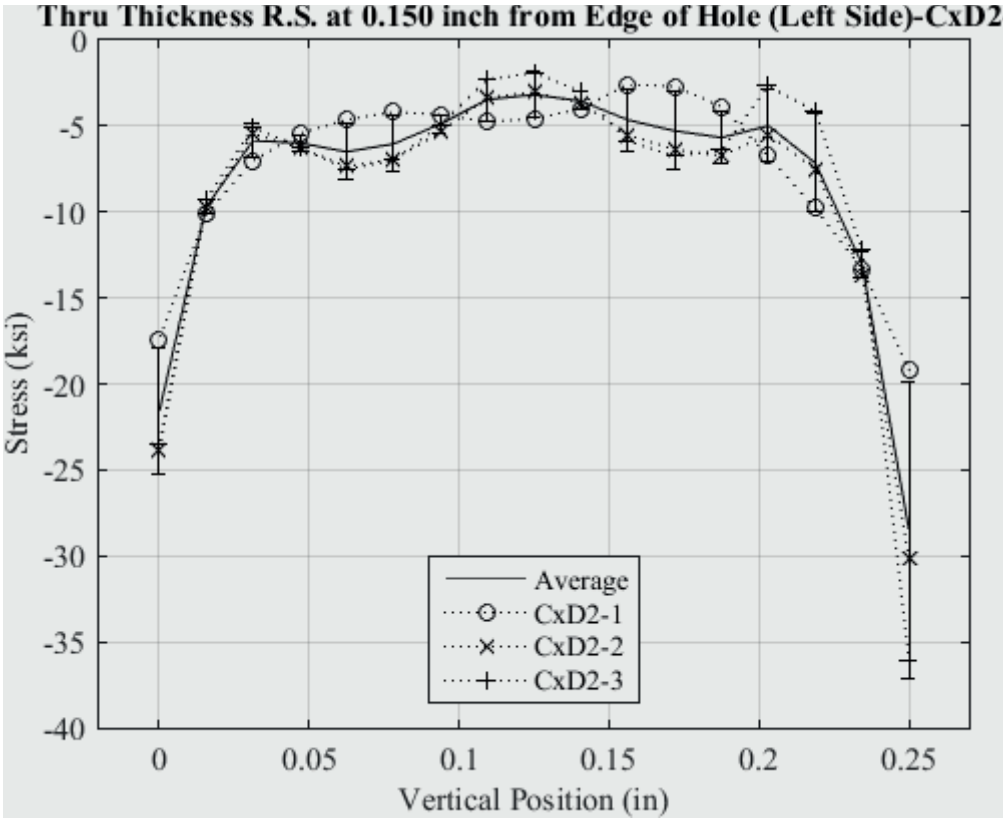

Fig. 120 Line Plot of Residual Stress at 0.150 inch from the Left Edge of the Hole for all CxD2 (7075-T651) Replicates.

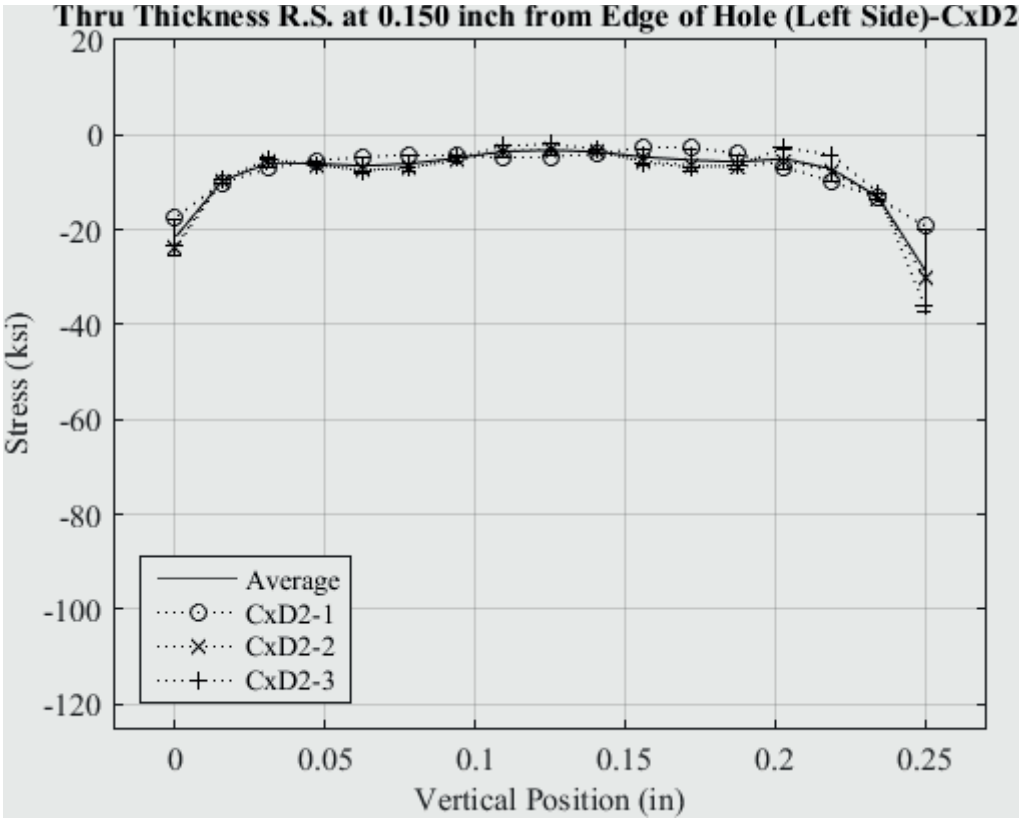

Fig. 121 Line Plot of Residual Stress at 0.150 inch from the Left Edge of the Hole for all CxD2 (7075-T651) Replicates – Stress Scale Locked.

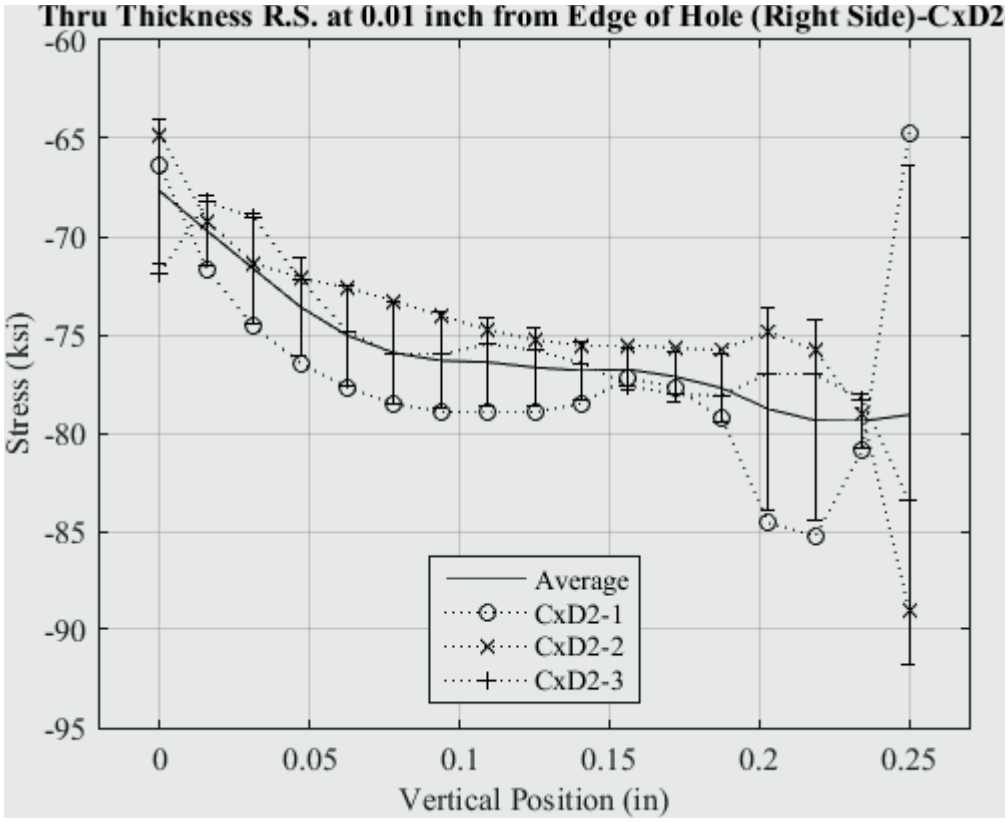

Fig. 122 Line Plot of Residual Stress at 0.010 inch from the Right Edge of the Hole for all CxD2 (7075-T651) Replicates.

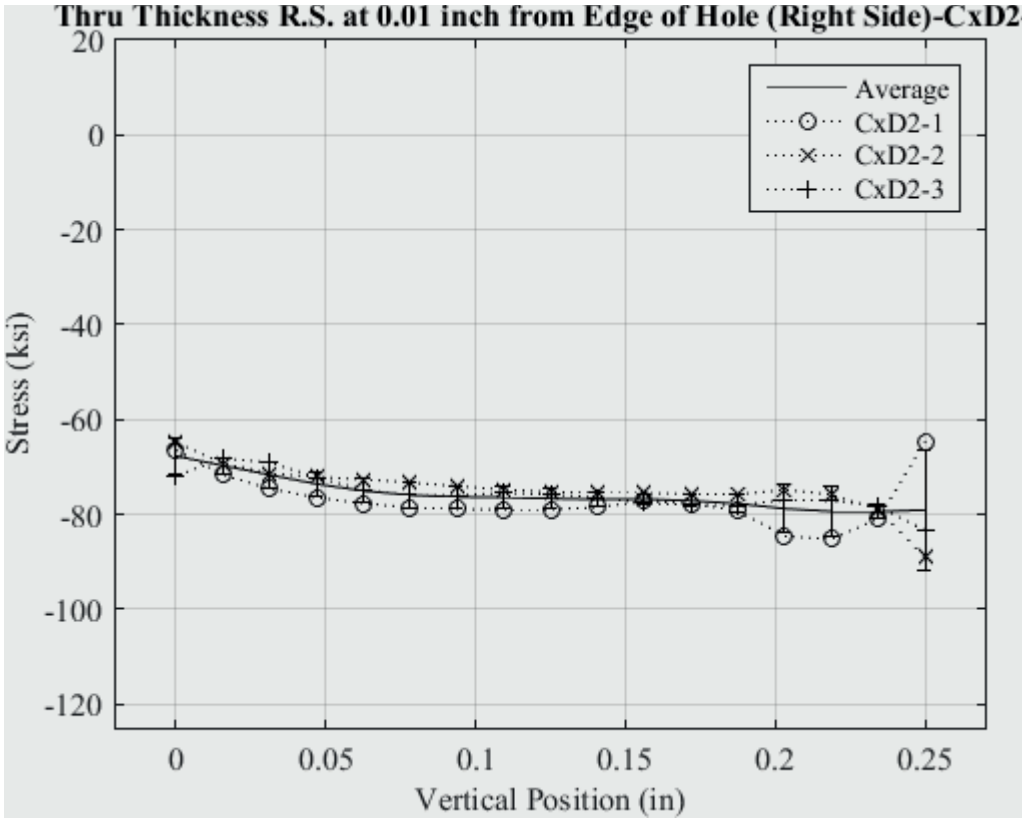

Fig. 123 Line Plot of Residual Stress at 0.010 inch from the Right Edge of the Hole for all CxD2 (7075-T651) Replicates – Stress Scale Locked.

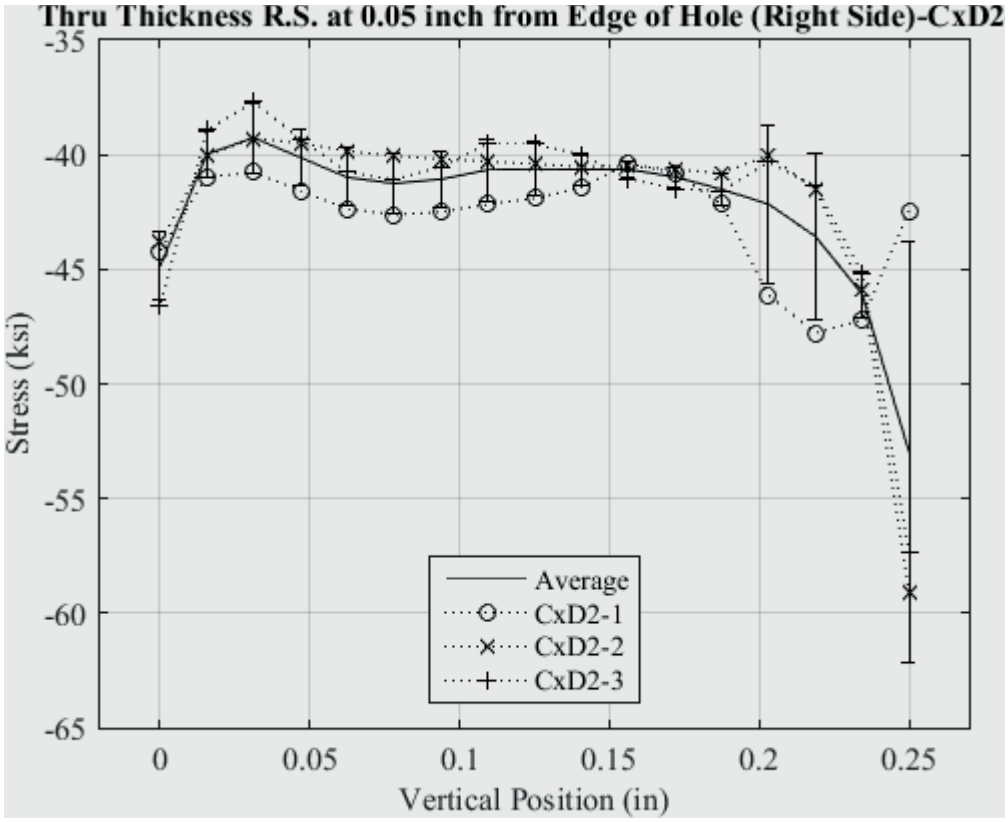

Fig. 124 Line Plot of Residual Stress at 0.050 inch from the Right Edge of the Hole for all CxD2 (7075-T651) Replicates.

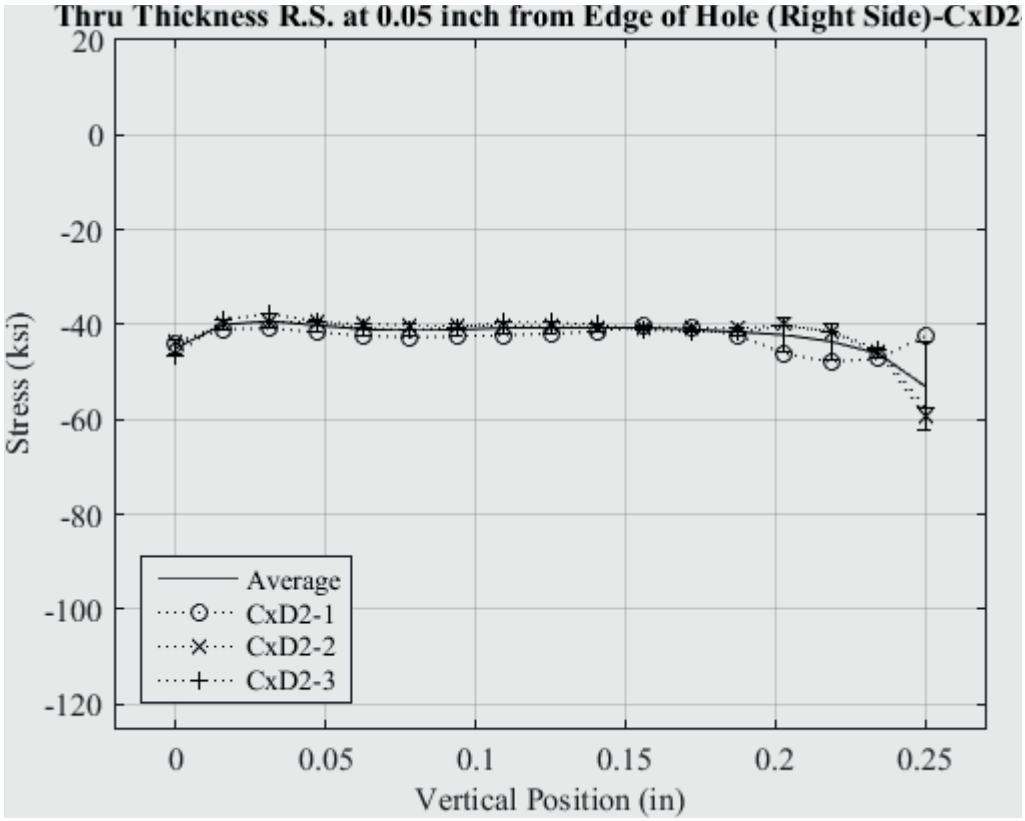

Fig. 125 Line Plot of Residual Stress at 0.050 inch from the Right Edge of the Hole for all CxD2 (7075-T651) Replicates – Stress Scale Locked.

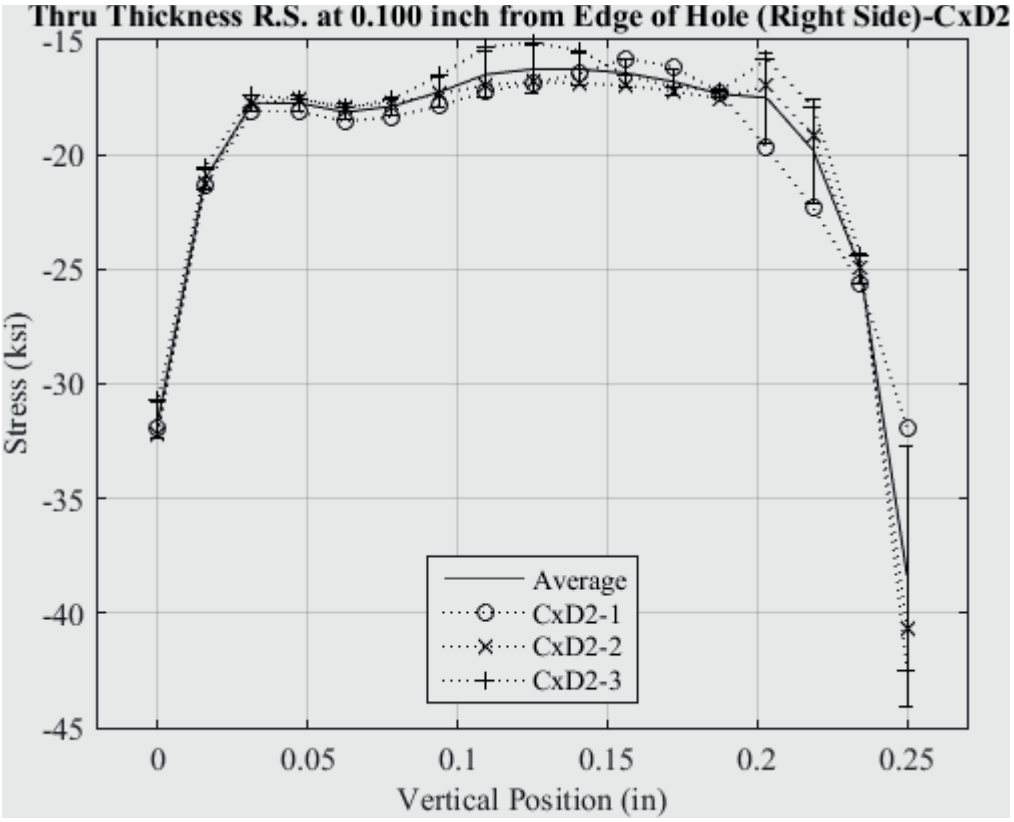

Fig. 126 Line Plot of Residual Stress at 0.100 inch from the Right Edge of the Hole for all CxD2 (7075-T651) Replicates.

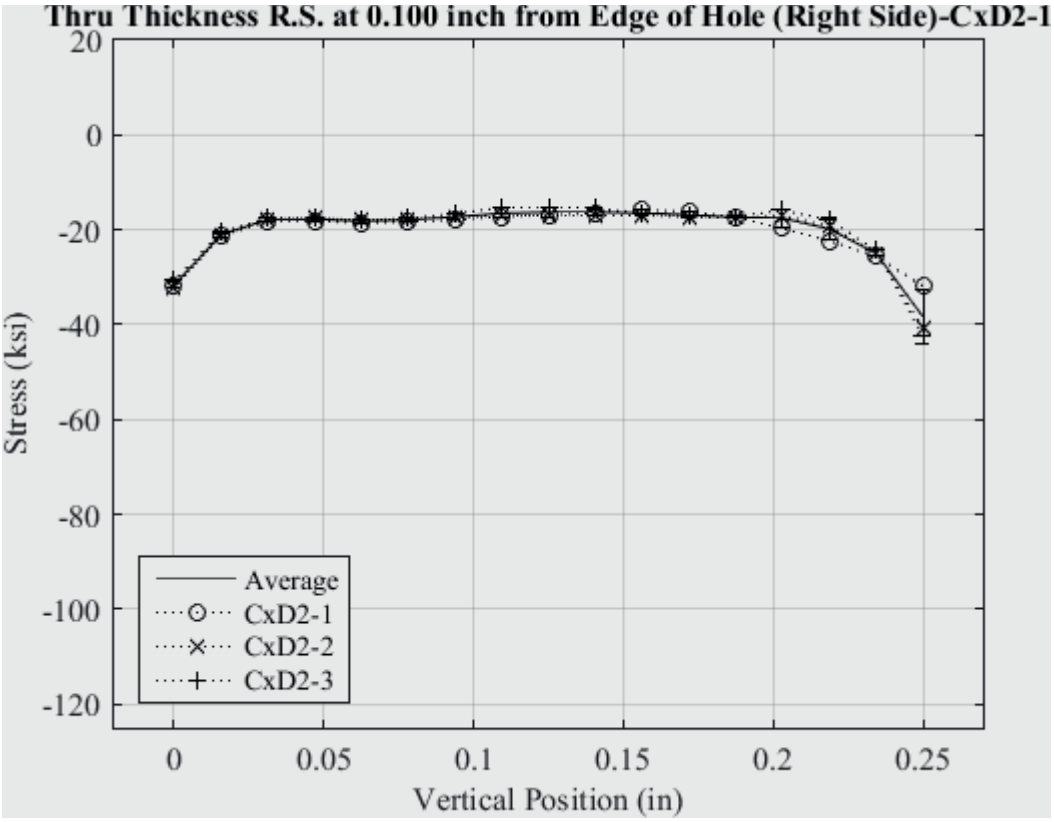

Fig. 127 Line Plot of Residual Stress at 0.100 inch from the Right Edge of the Hole for all CxD2 (7075-T651) Replicates – Stress Scale Locked.

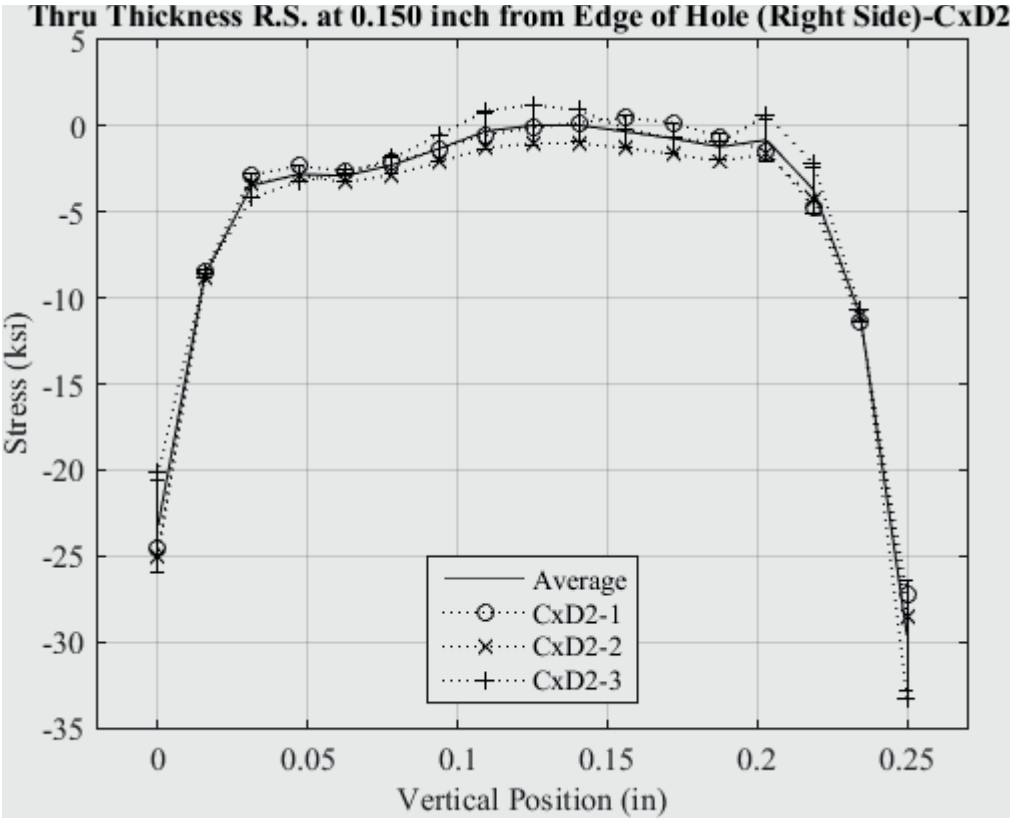

Fig. 128 Line Plot of Residual Stress at 0.150 inch from the Right Edge of the Hole for all CxD2 (7075-T651) Replicates.

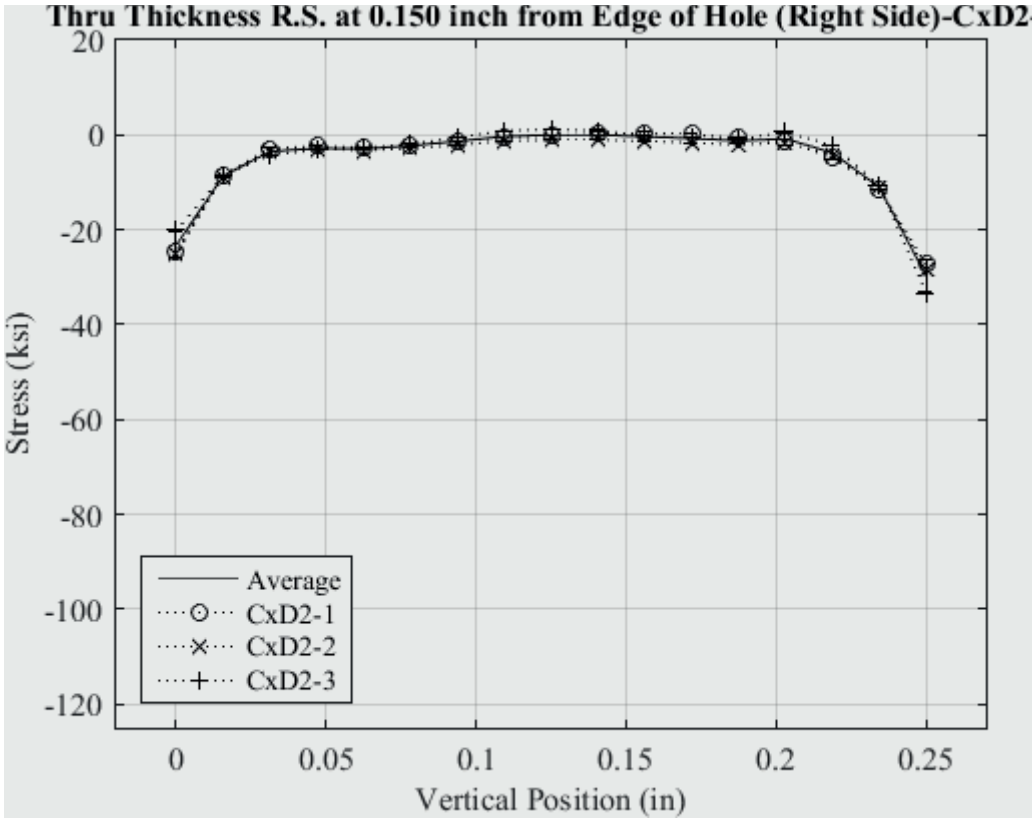

Fig. 129 Line Plot of Residual Stress at 0.150 inch from the Right Edge of the Hole for all CxD2 (7075-T651) Replicates – Stress Scale Locked.

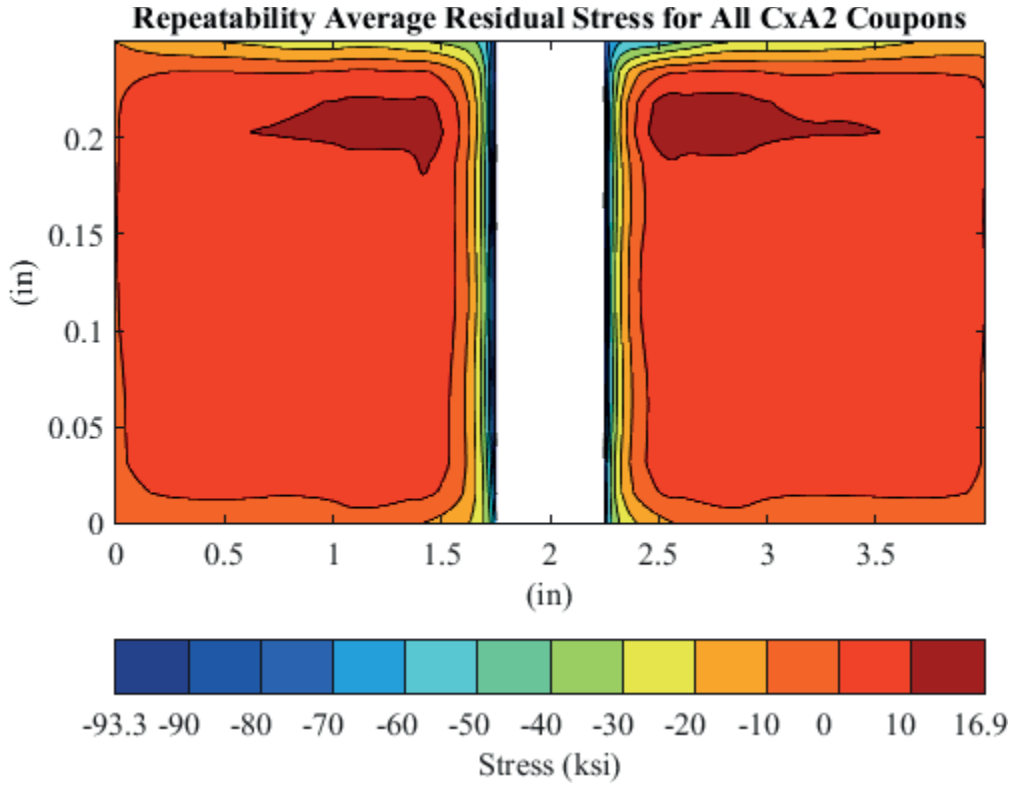

Fig. 130 Residual Stress Contour Plot of the Average CxA2 (2024-T351) Coupon Configuration Five Replicates Produced – Mandrel Entrance Surface at Y=0.

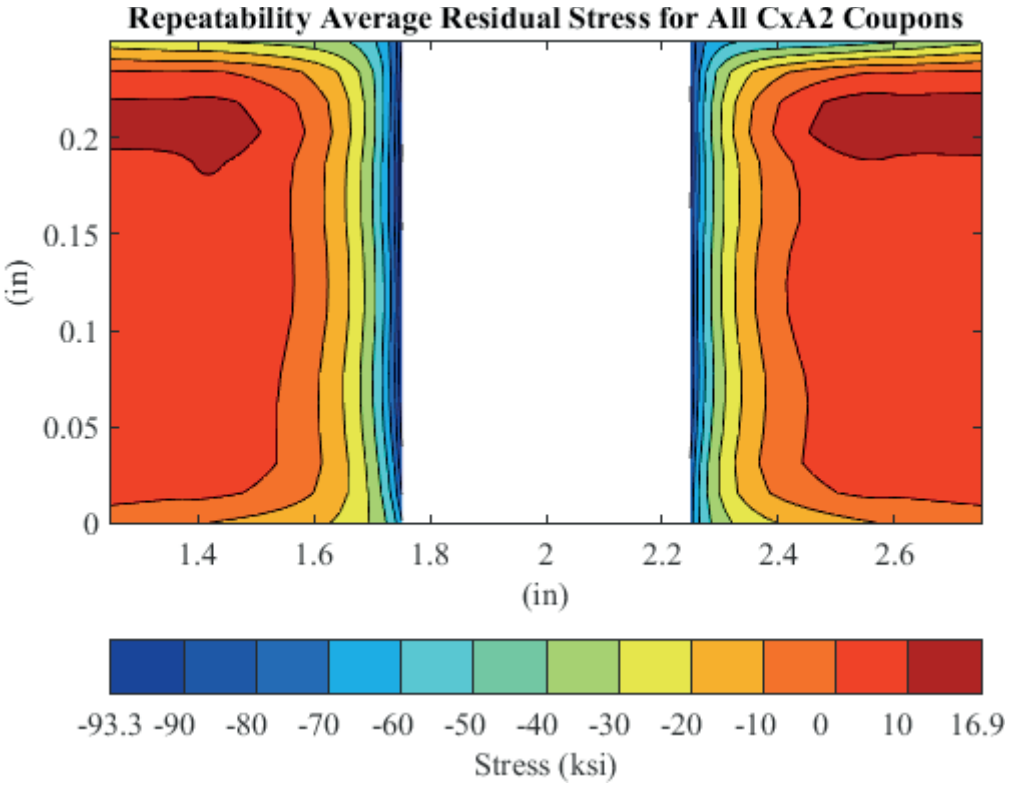

Fig. 131 Residual Stress Contour Plot of the Average CxA2 (2024-T351) Coupon Configuration Five Replicates Produced – Mandrel Entrance Surface at Y=0 – Zoomed in Next to Hole.

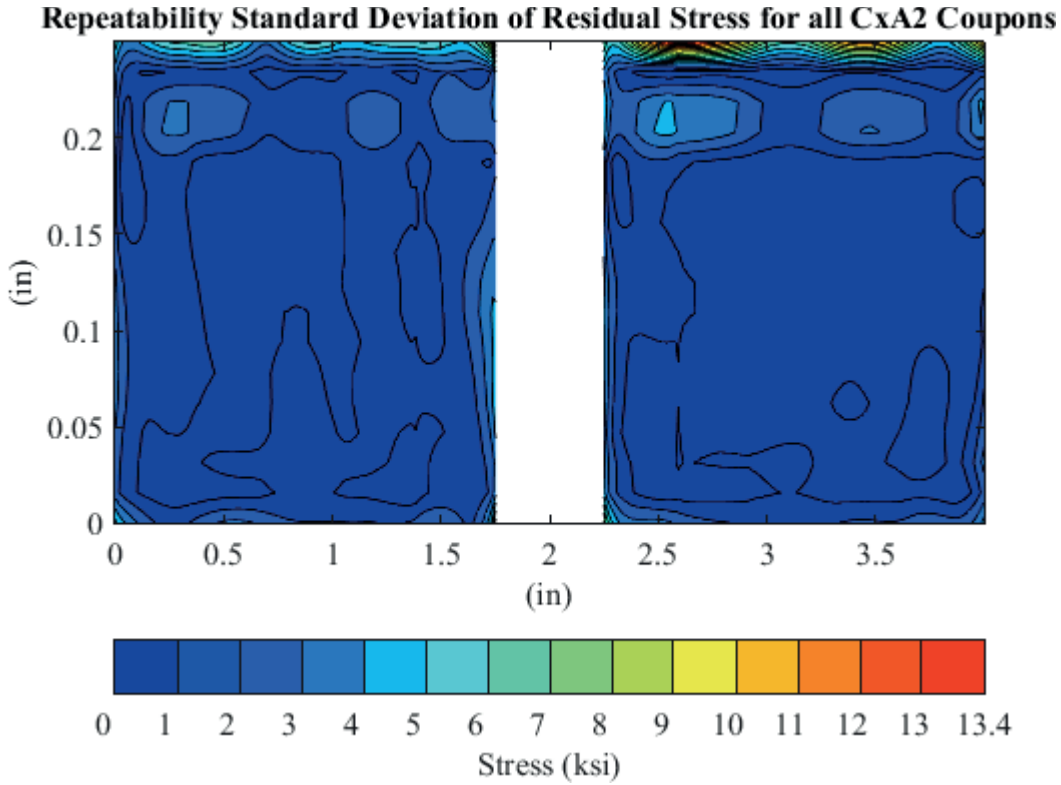

Fig. 132 Contour Plot of the Residual Stress Standard Deviation for the CxA2 (2024-T351) Coupon Configuration Five Replicates Produced – Mandrel Entrance Surface at Y=0.

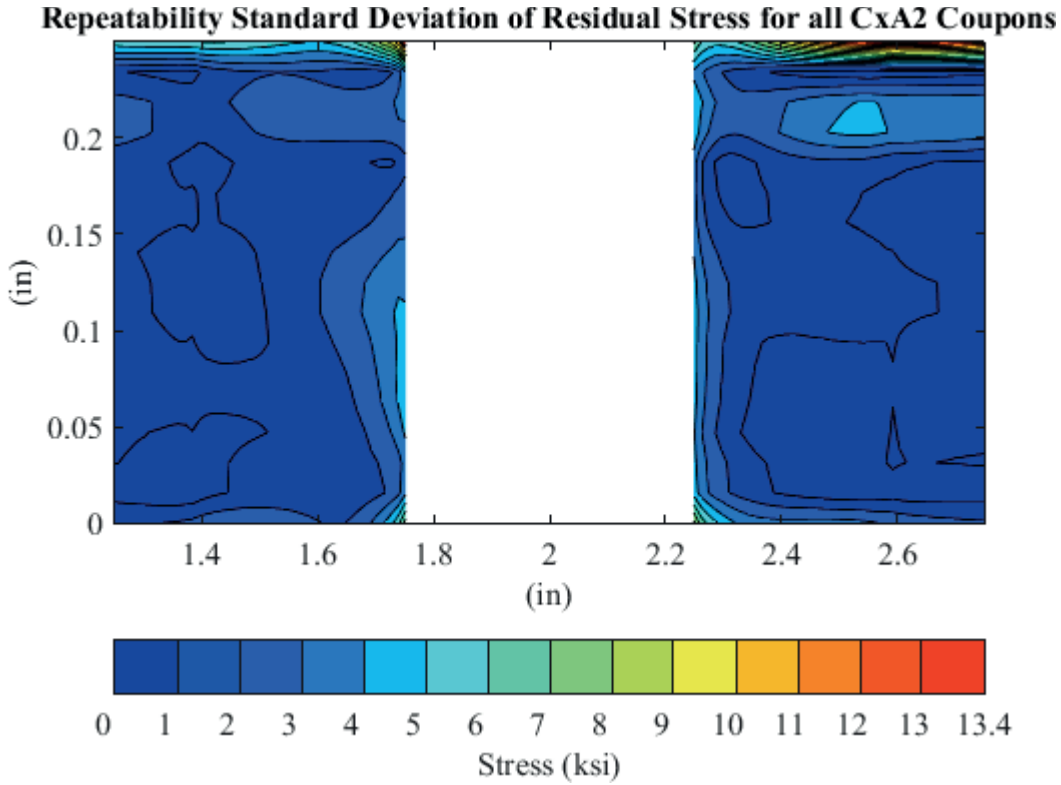

Fig. 133 Contour Plot of the Residual Stress Standard Deviation for the CxA2 (2024-T351) Coupon Configuration Five Replicates Produced – Mandrel Entrance Surface at Y=0 – Zoomed in Next to Hole.

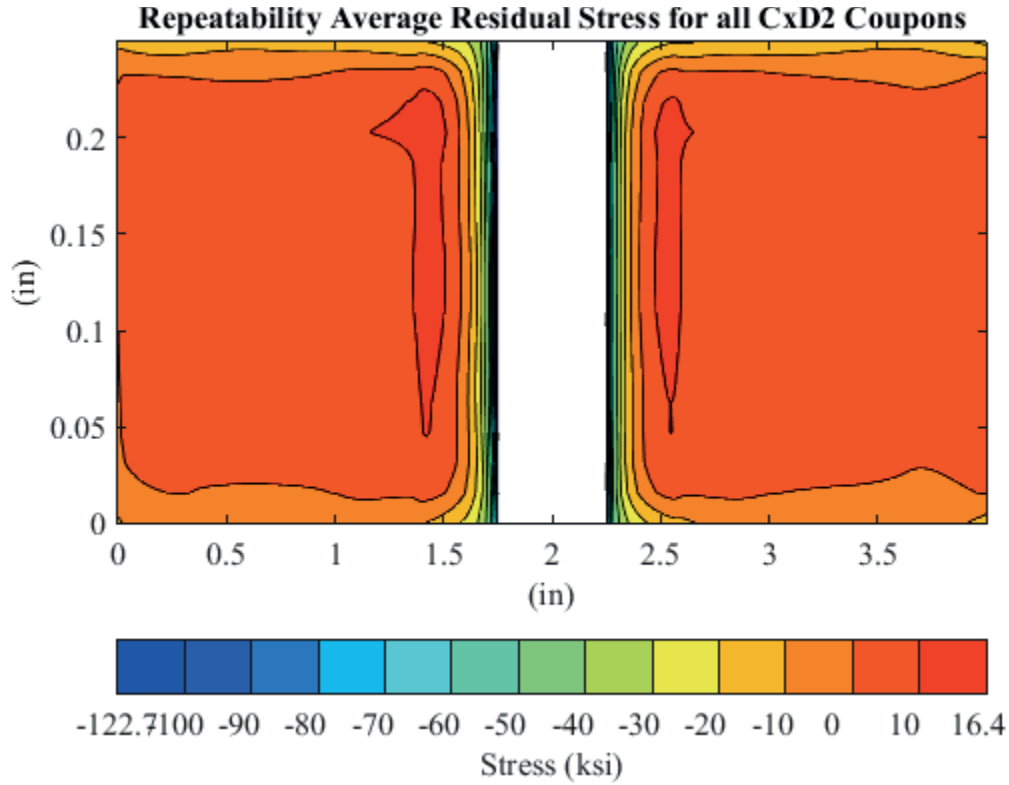

Fig. 134 Residual Stress Contour Plot of the Average CxD2 (7075-T651) Coupon Configuration Three Replicates Produced – Mandrel Entrance Surface at Y=0.

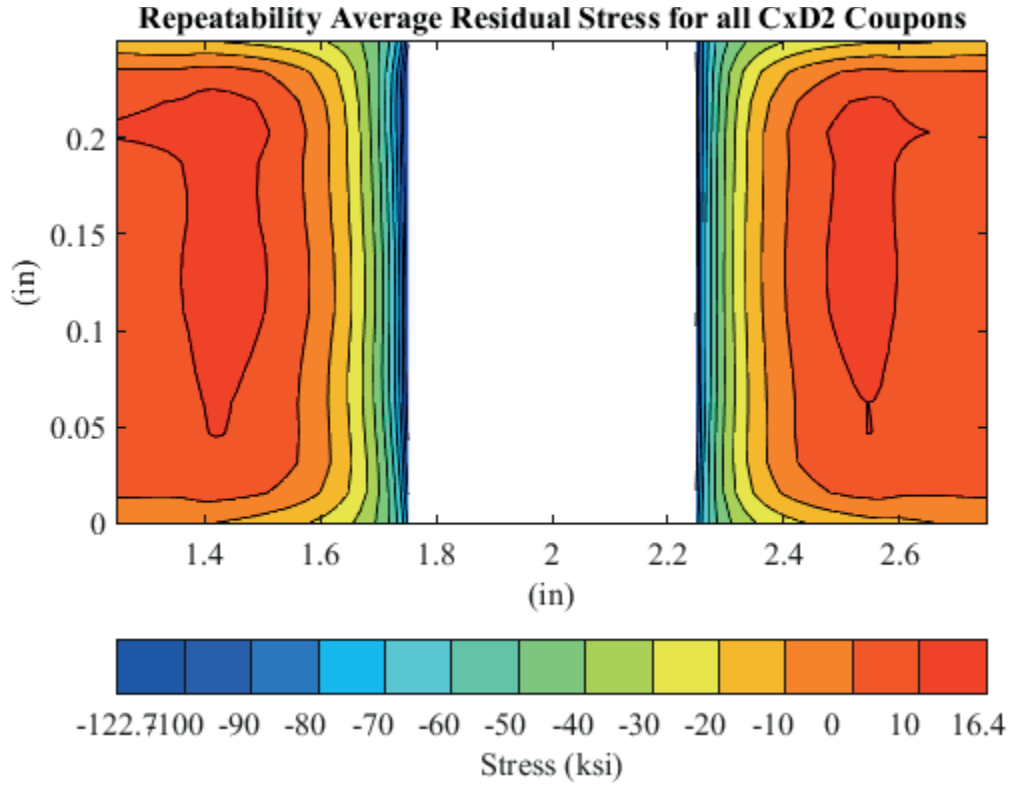

Fig. 135 Residual Stress Contour Plot of the Average CxD2 (7075-T651) Coupon Configuration Three Replicates Produced – Mandrel Entrance Surface at Y=0 – Zoomed in Next to Hole.

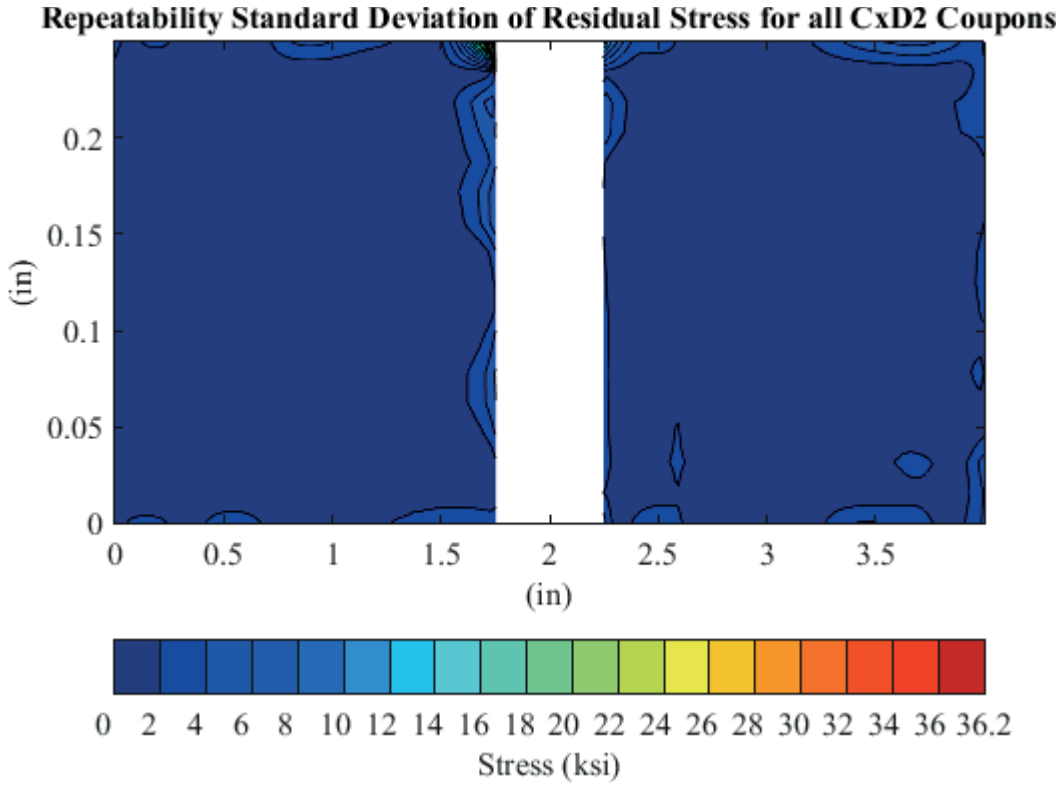

Fig. 136 Contour Plot of the Residual Stress Standard Deviation for the CxD2 (7075-T651) Coupon Configuration Three Replicates Produced – Mandrel Entrance Surface at Y=0.

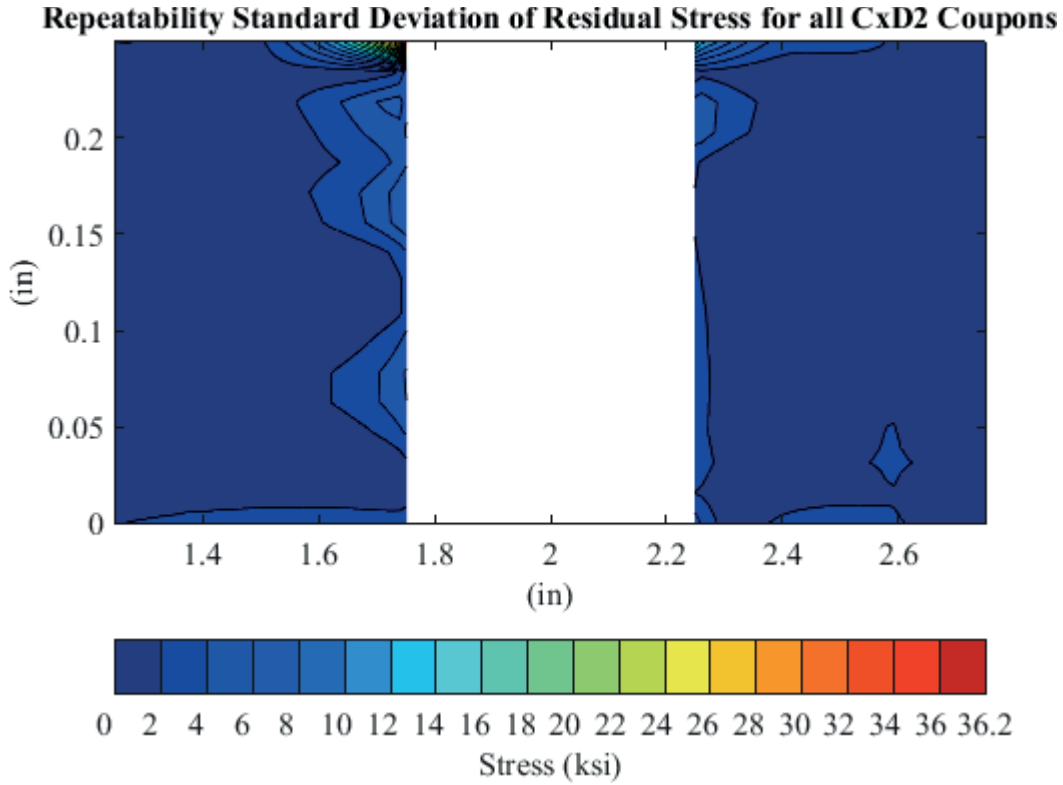

Fig. 137 Contour Plot of the Residual Stress Standard Deviation for the CxD2 (7075-T651) Coupon Configuration Three Replicates Produced – Mandrel Entrance Surface at Y=0 – Zoomed in Next to Hole.

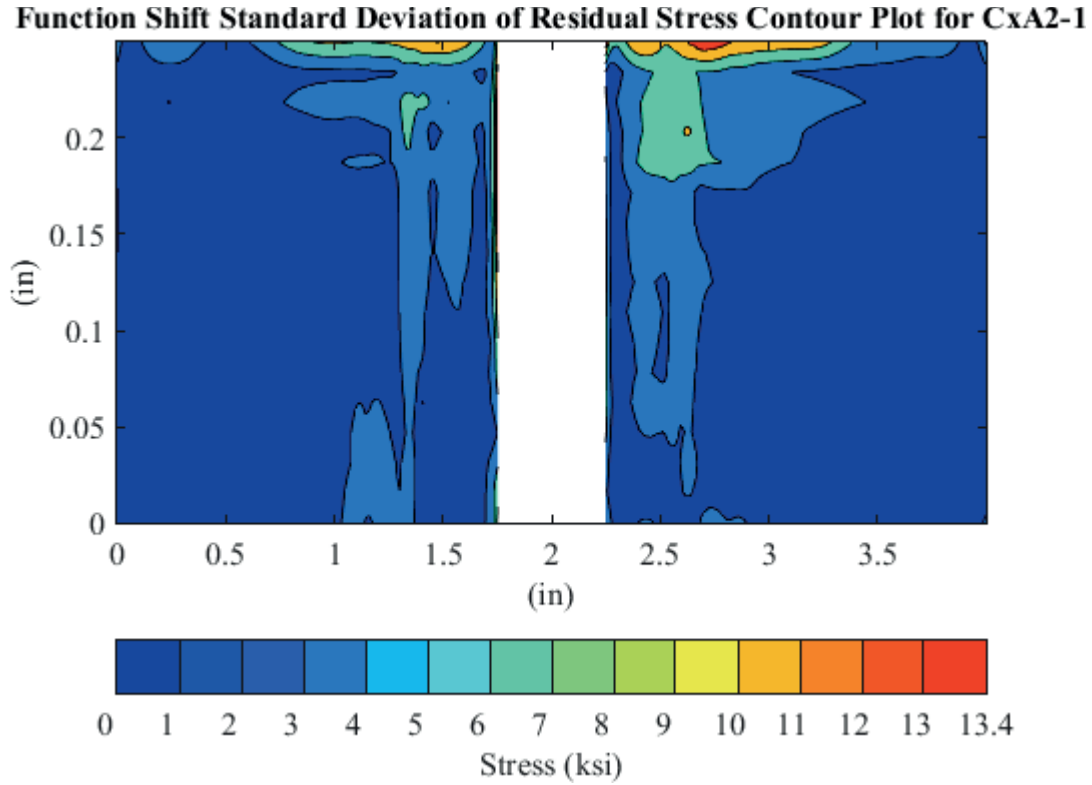

Fig. 138 Contour Plot of Model/Fit Error Developed via Knot Shift in both the X and Y Coordinate Frame for Coupon CxA2-1 – Mandrel Entrance Surface at Y=0.

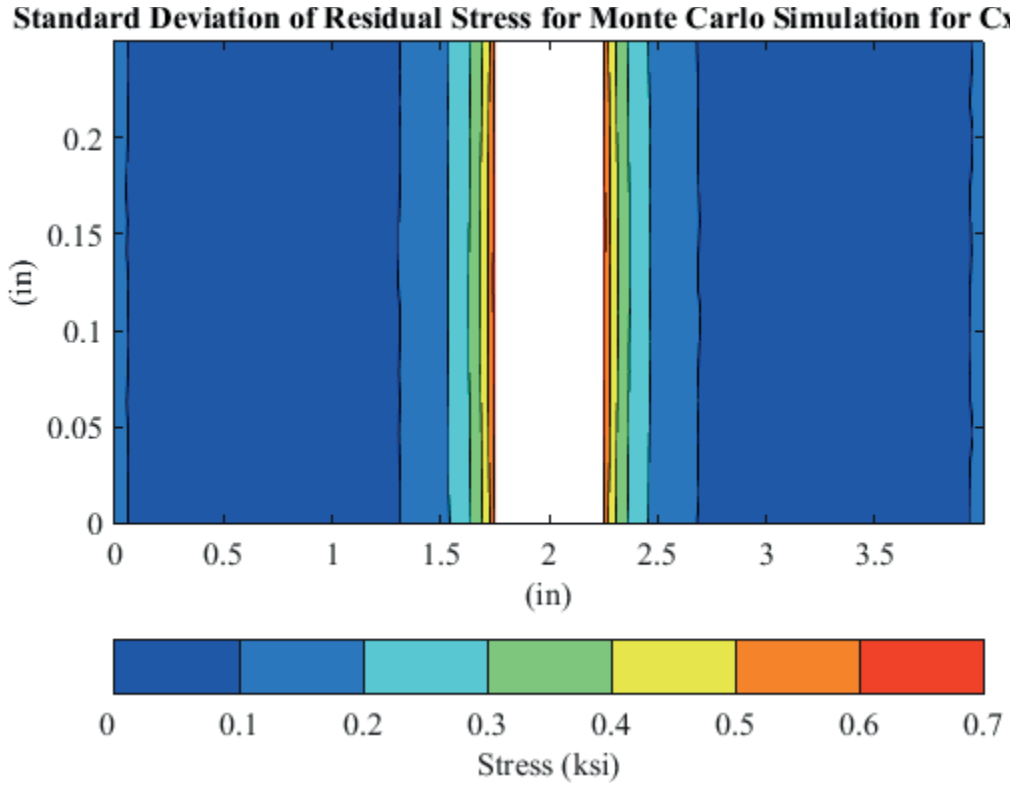

Fig. 139 Contour Plot of Displacement Uncertainty Developed via Monte Carlo Simulation for Coupon CxA2-1 – Mandrel Entrance Surface at Y=0.

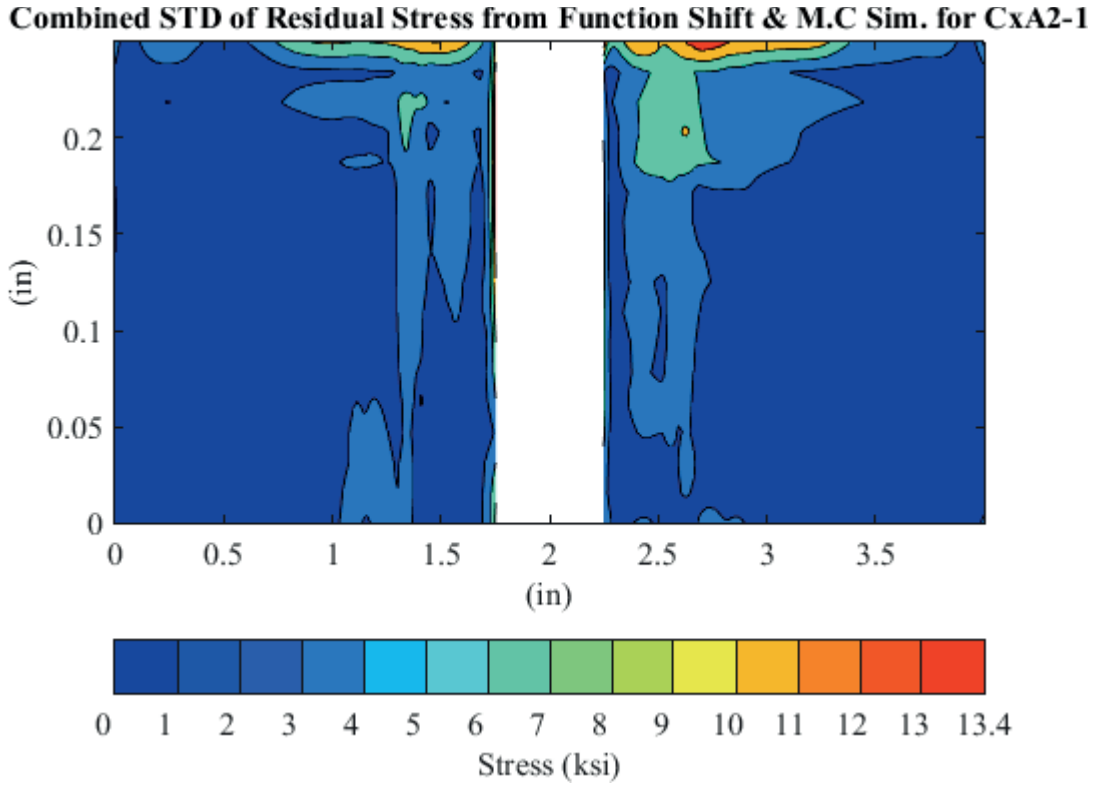

Fig. 140 Contour Plot of Root Sum Square (RSS) of Model/Fit and Displacement Uncertainties for Coupon CxA2-1 – Mandrel Entrance Surface at Y=0.

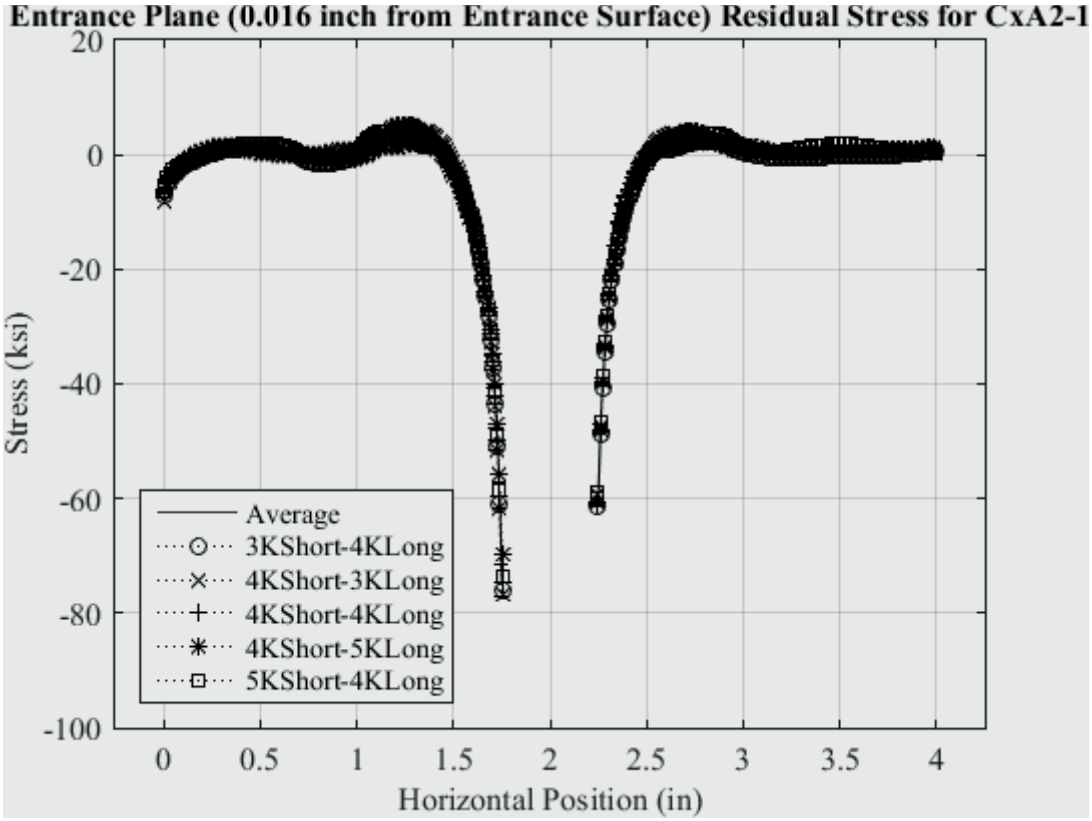

Fig. 141 Residual Stress Line Plot for all Five Knot Densities to Determine Model/Fit Error for CxA2-1 (2024-T351) at a Distance of 0.016 inch (Entrance Surface) from the Entrance Surface.

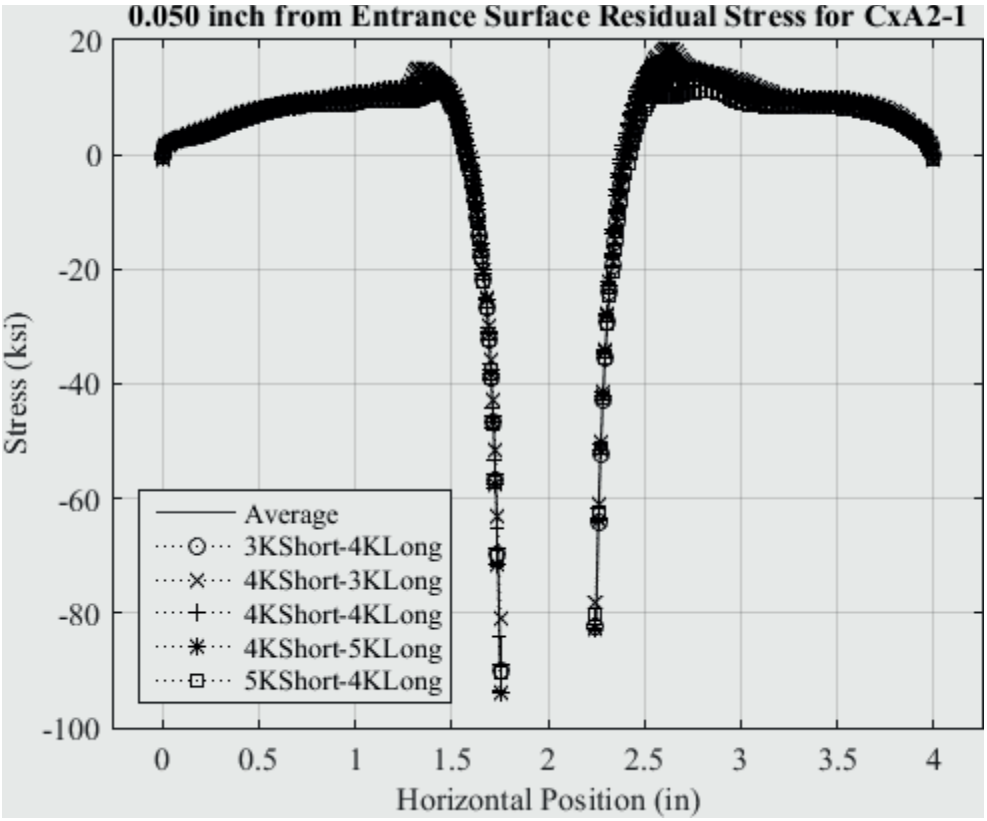

Fig. 142 Residual Stress Line Plot for all Five Knot Densities to Determine Model/Fit Error for CxA2-1 (2024-T351) at a Distance of 0.050 inch from the Entrance Surface.

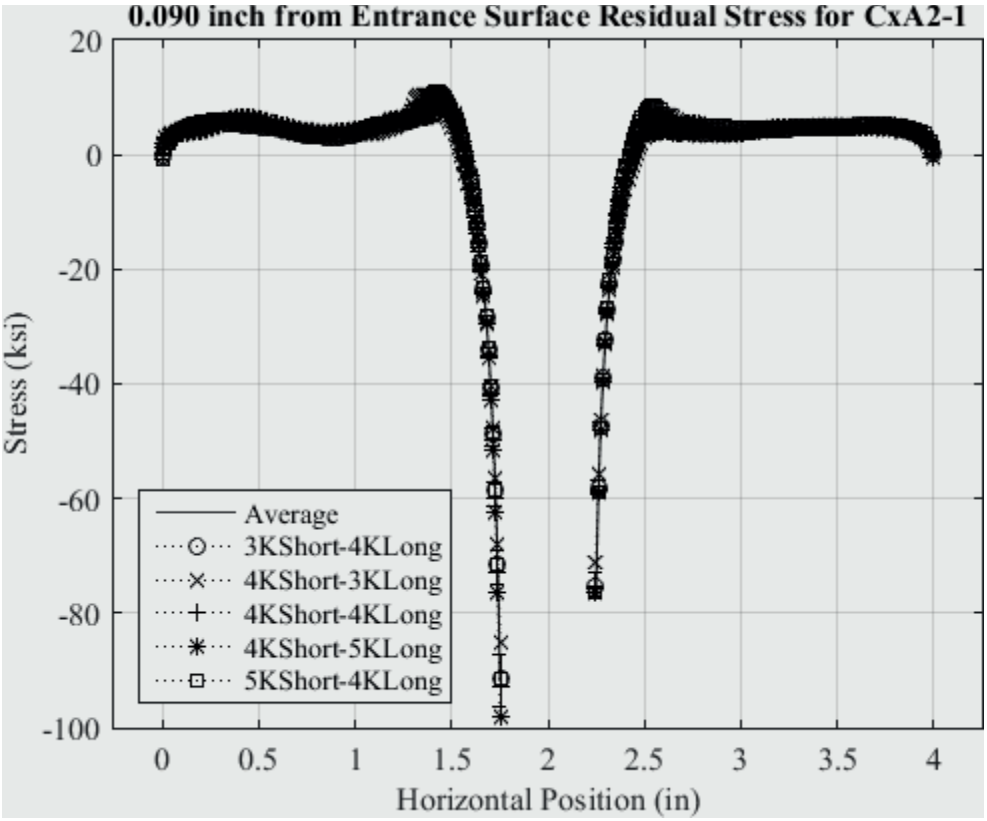

Fig. 143 Residual Stress Line Plot for all Five Knot Densities to Determine Model/Fit Error for CxA2-1 (2024-T351) at a Distance of 0.090 inch from the Entrance Surface.

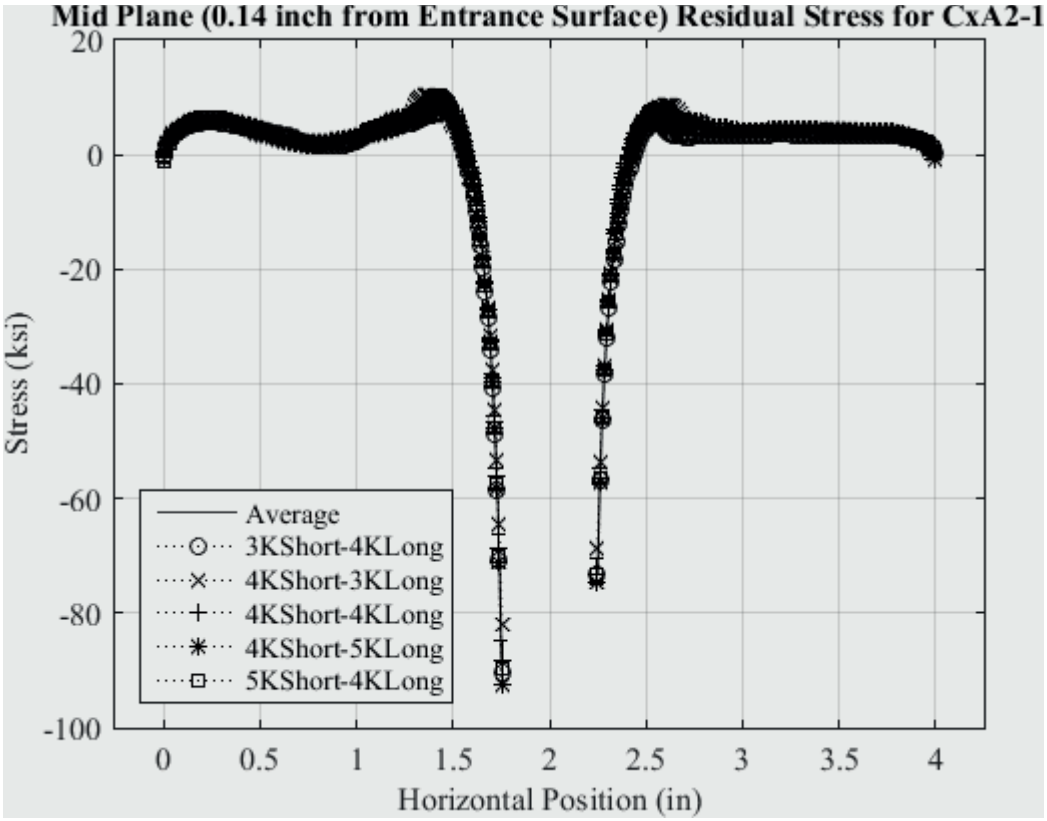

Fig. 144 Residual Stress Line Plot for all Five Knot Densities to Determine Model/Fit Error for CxA2-1 (2024-T351) at a Distance of 0.140 inch, (Mid Plane Surface) from the Entrance Surface.

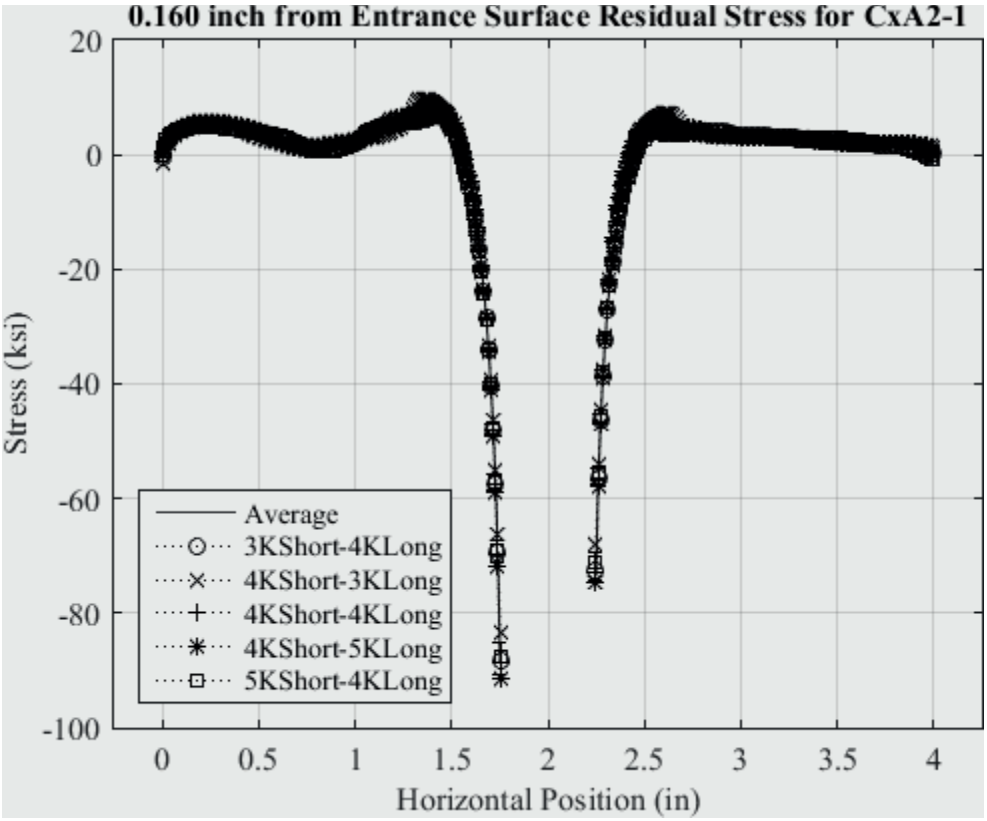

Fig. 145 Residual Stress Line Plot for all Five Knot Densities to Determine Model/Fit Error for CxA2-1 (2024-T351) at a Distance of 0.160 inch from the Entrance Surface.

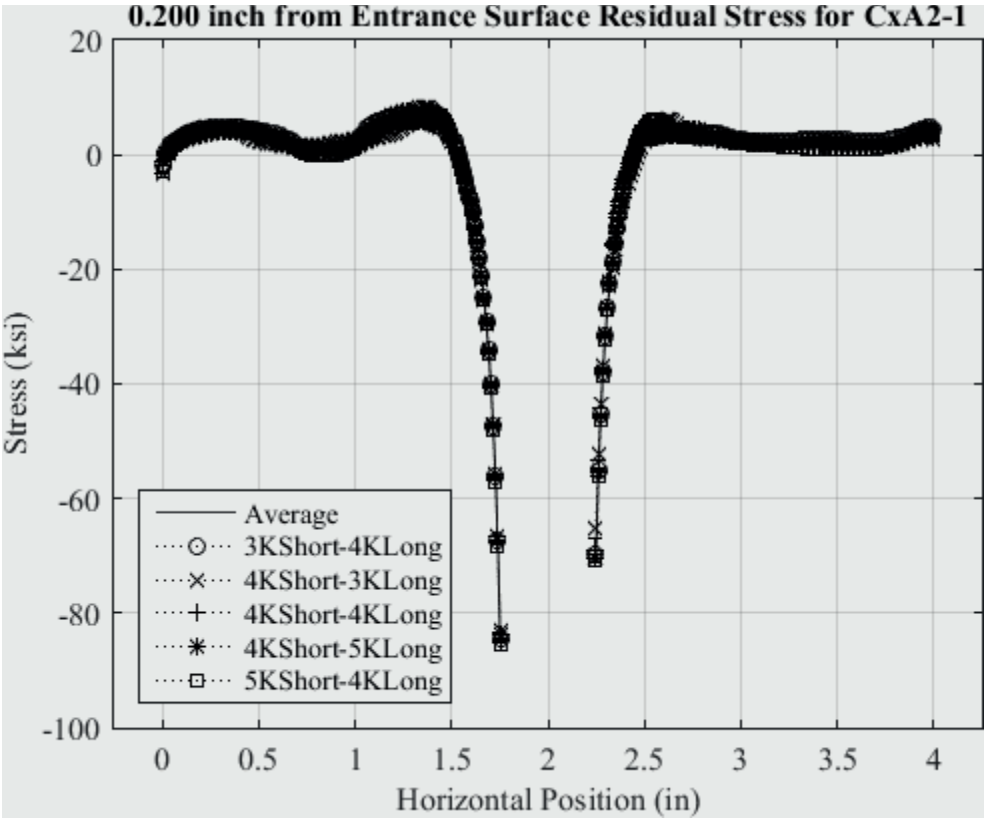

Fig. 146 Residual Stress Line Plot for all Five Knot Densities to Determine Model/Fit Error for CxA2-1 (2024-T351) at a Distance of 0.200 inch from the Entrance Surface.

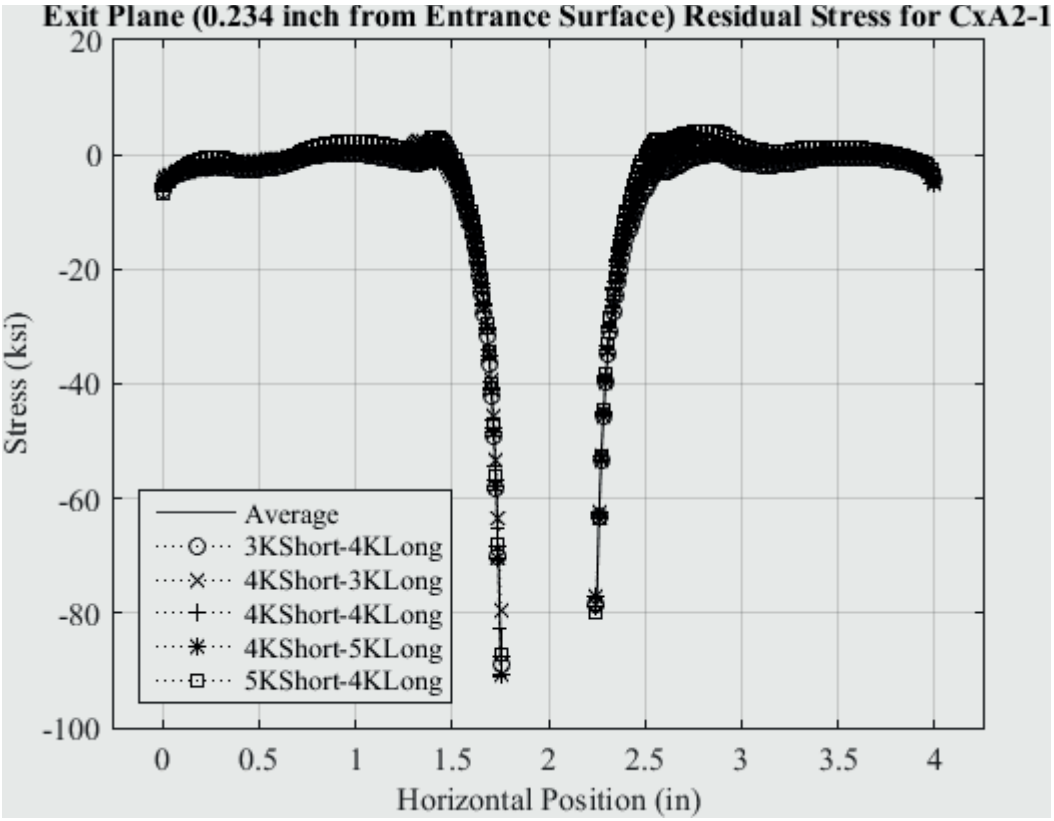

Fig. 147 Residual Stress Line Plot for all Five Knot Densities to Determine Model/Fit Error for CxA2-1 (2024-T351) at a Distance of 0.234 inch (Exit Surface) from the Entrance Surface.

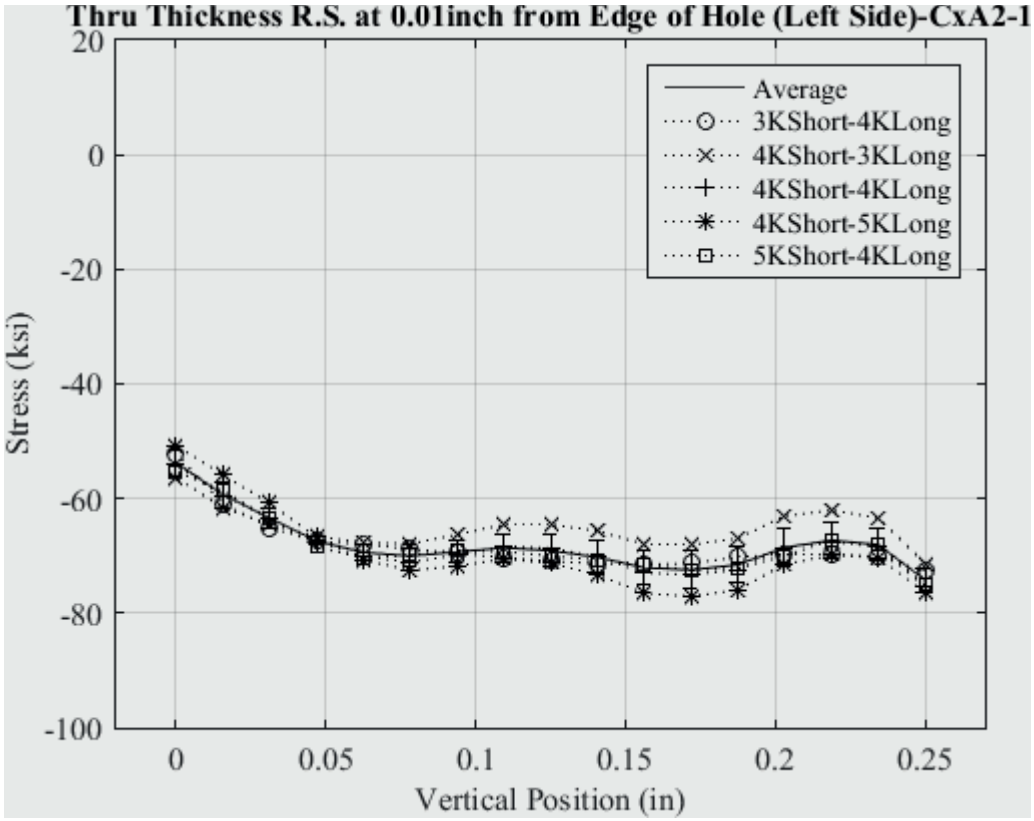

Fig. 148 Line Plot of Residual Stress at 0.01 inch from the Left Edge of the Hole for all Five Knot Densities to Determine Model/Fit Error CxA2-1 (2024-T351) – Stress Scale Locked.

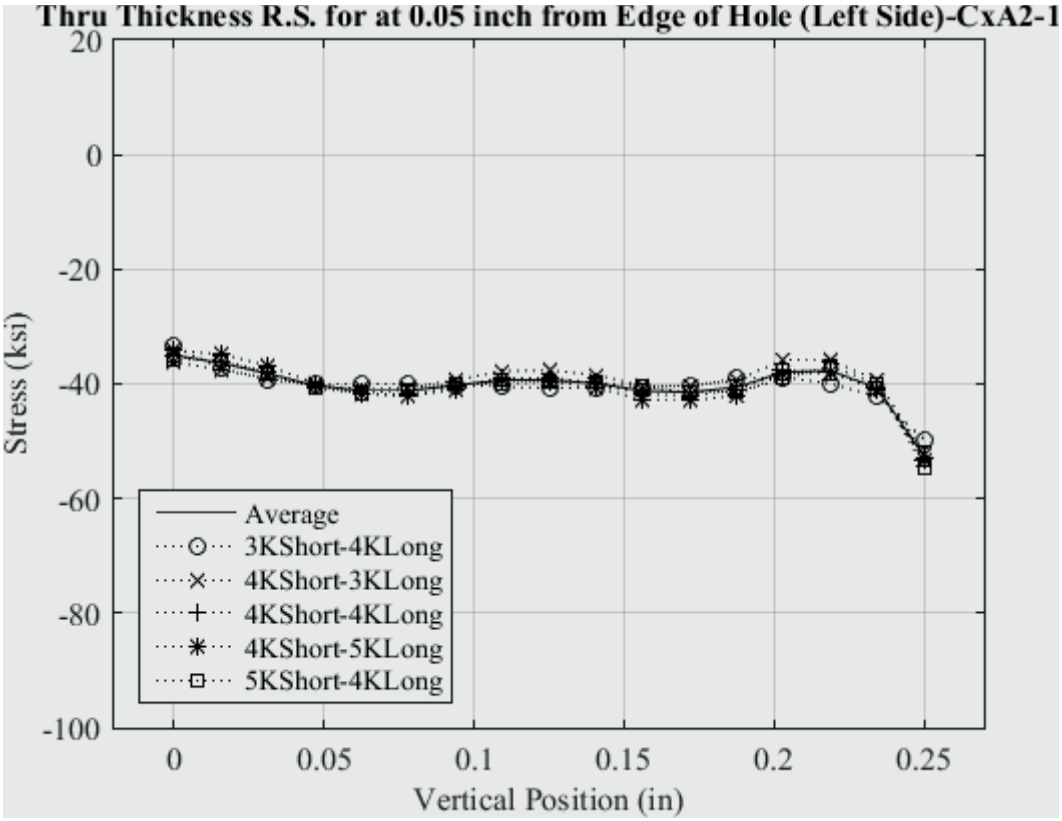

Fig. 149 Line Plot of Residual Stress at 0.05 inch from the Left Edge of the Hole for all Five Knot Densities to Determine Model/Fit Error CxA2-1 (2024-T351) – Stress Scale Locked.

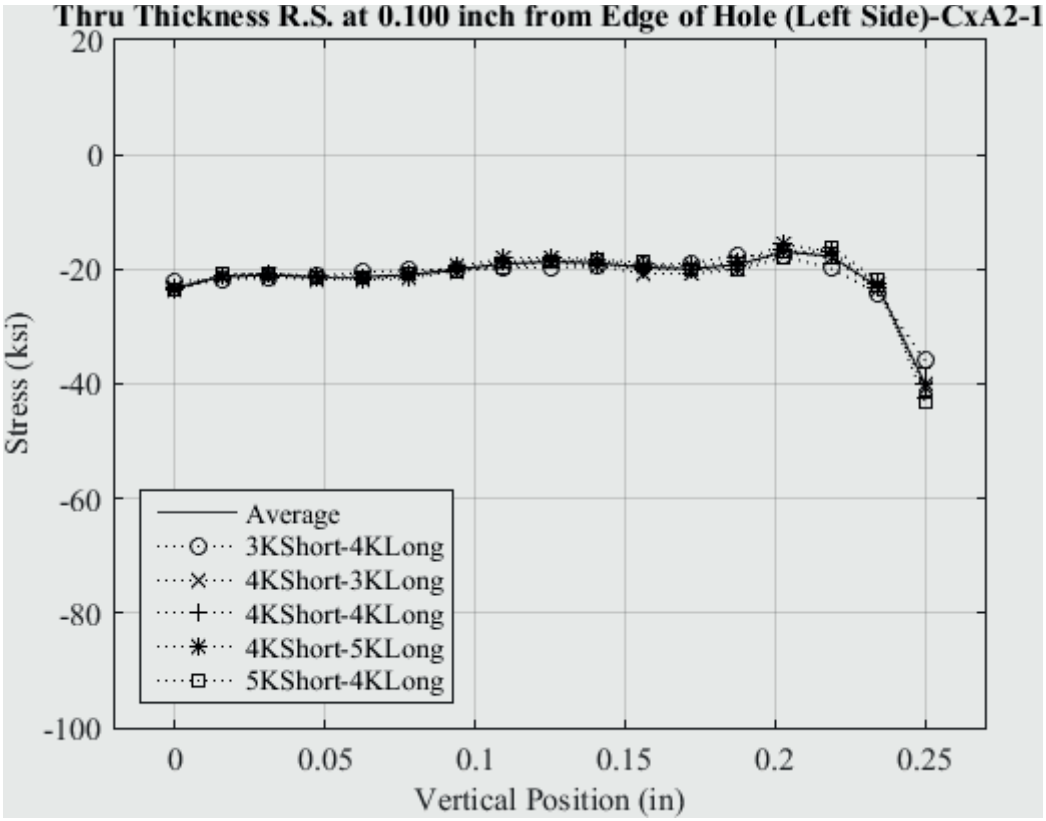

Fig. 150 Line Plot of Residual Stress at 0.10 inch from the Left Edge of the Hole for all Five Knot Densities to Determine Model/Fit Error CxA2-1 (2024-T351) – Stress Scale Locked.

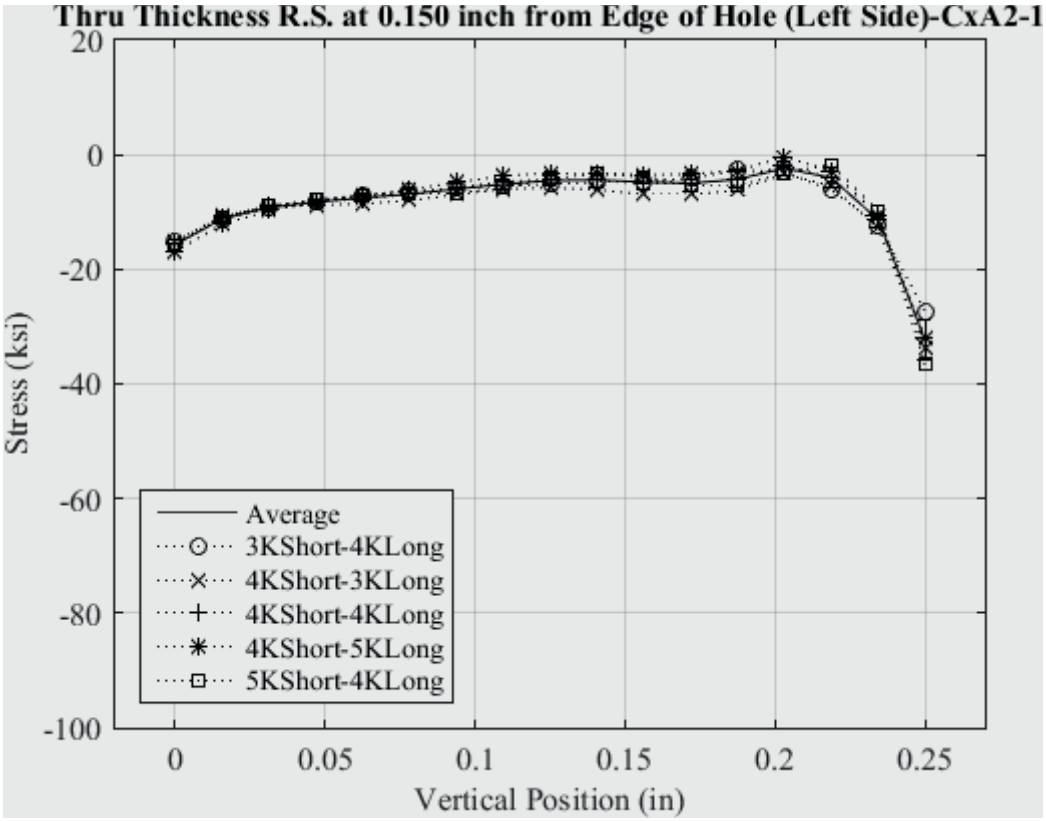

Fig. 151 Line Plot of Residual Stress at 0.150 inch from the Left Edge of the Hole for all Five Knot Densities to Determine Model/Fit Error CxA2-1 (2024-T351) – Stress Scale Locked.

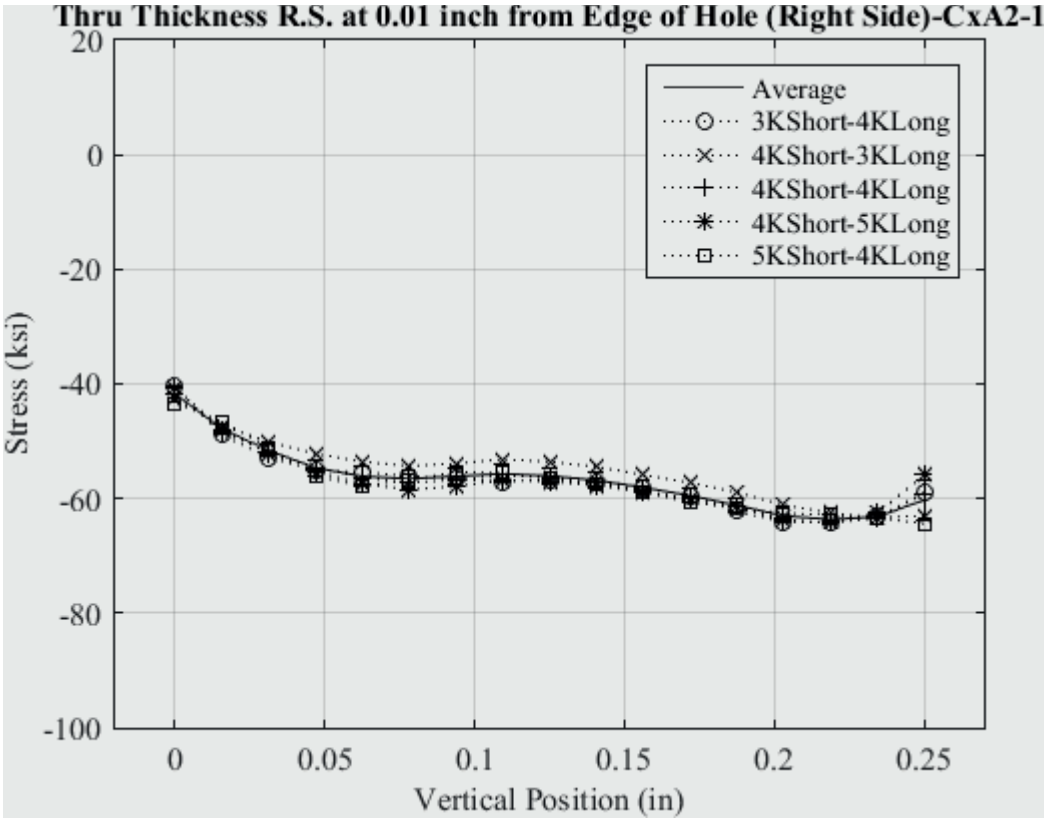

Fig. 152 Line Plot of Residual Stress at 0.01 inch from the Right Edge of the Hole for all Five Knot Densities to Determine Model/Fit Error CxA2-1 (2024-T351) – Stress Scale Locked.

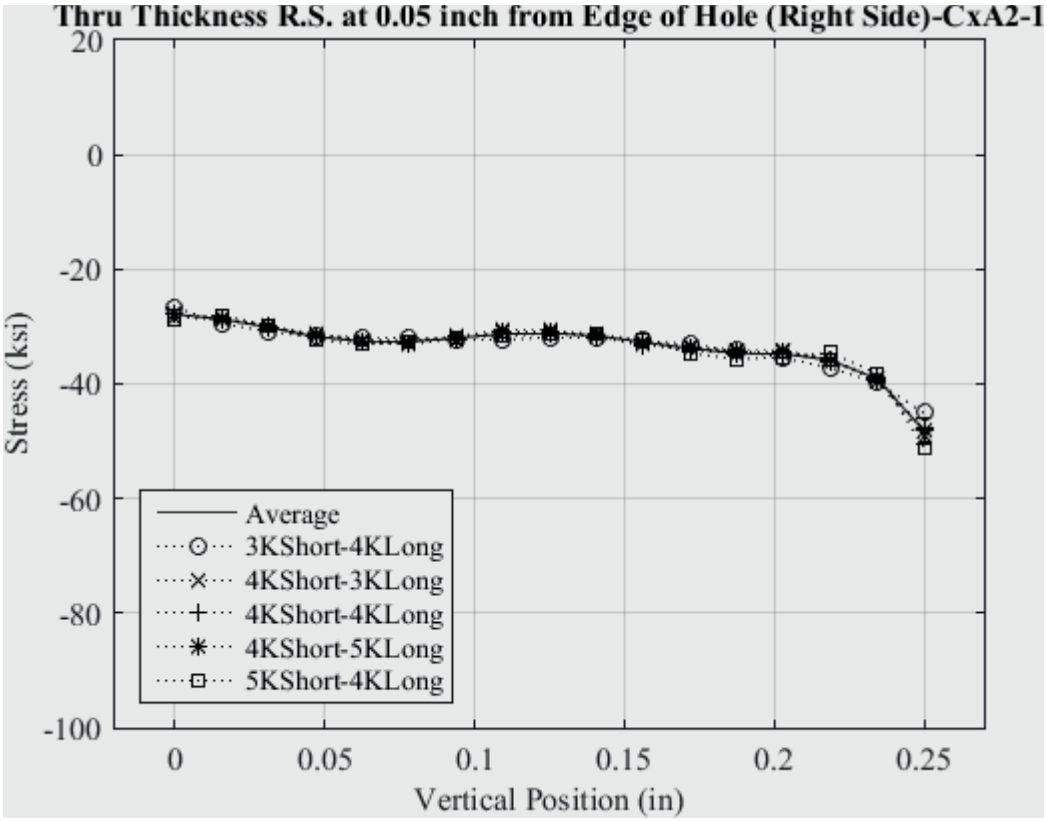

Fig. 153 Line Plot of Residual Stress at 0.05 inch from the Right Edge of the Hole for all Five Knot Densities to Determine Model/Fit Error CxA2-1 (2024-T351) – Stress Scale Locked.

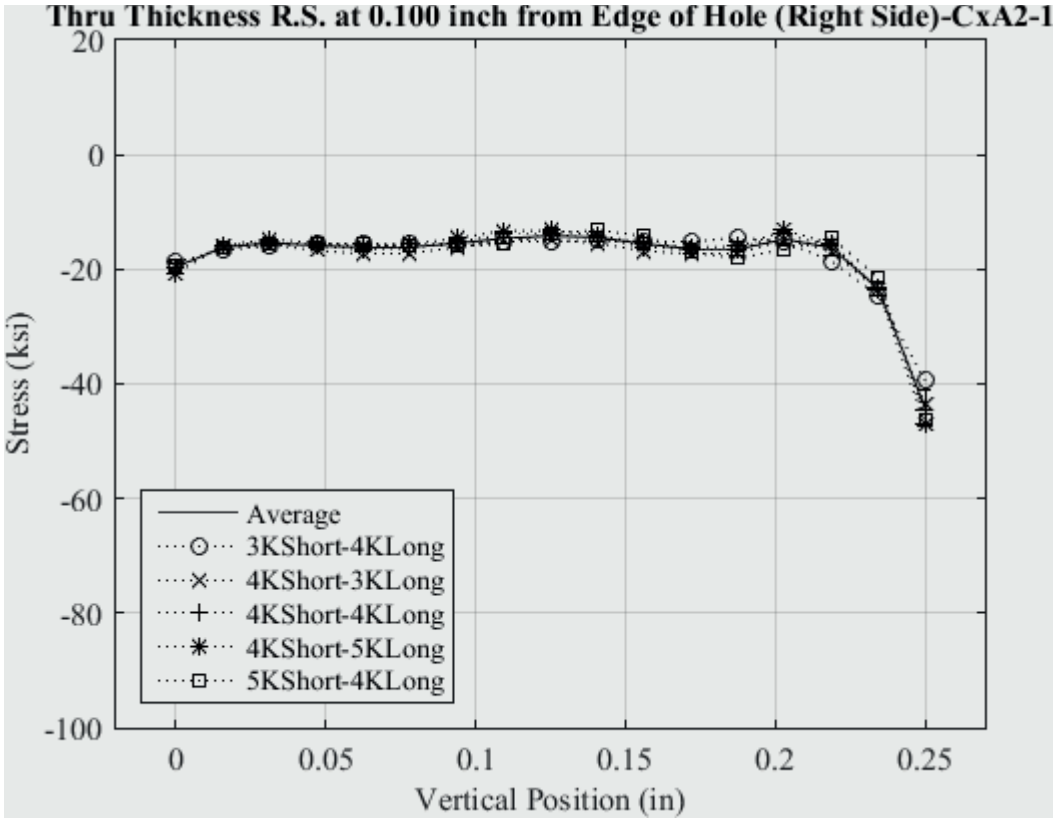

Fig. 154 Line Plot of Residual Stress at 0.10 inch from the Right Edge of the Hole for all Five Knot Densities to Determine Model/Fit Error CxA2-1 (2024-T351) – Stress Scale Locked.

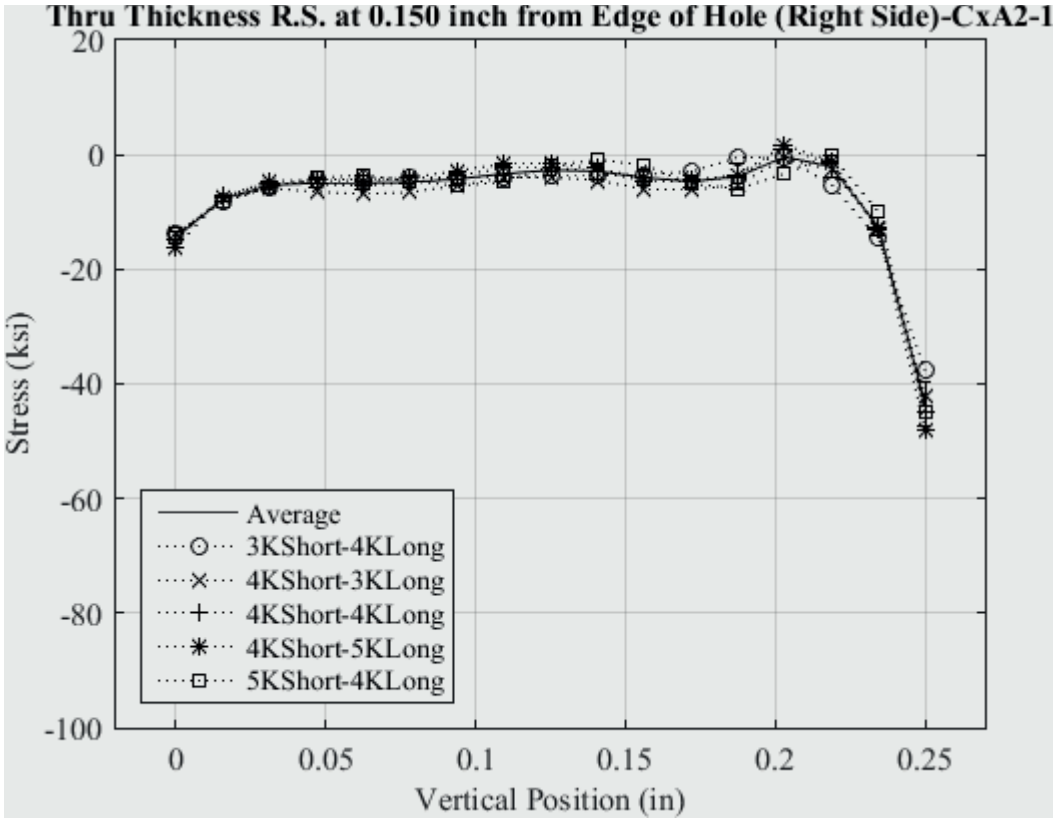

Fig. 155 Line Plot of Residual Stress at 0.150 inch from the Right Edge of the Hole for all Five Knot Densities to Determine Model/Fit Error CxA2-1 (2024-T351) – Stress Scale Locked.

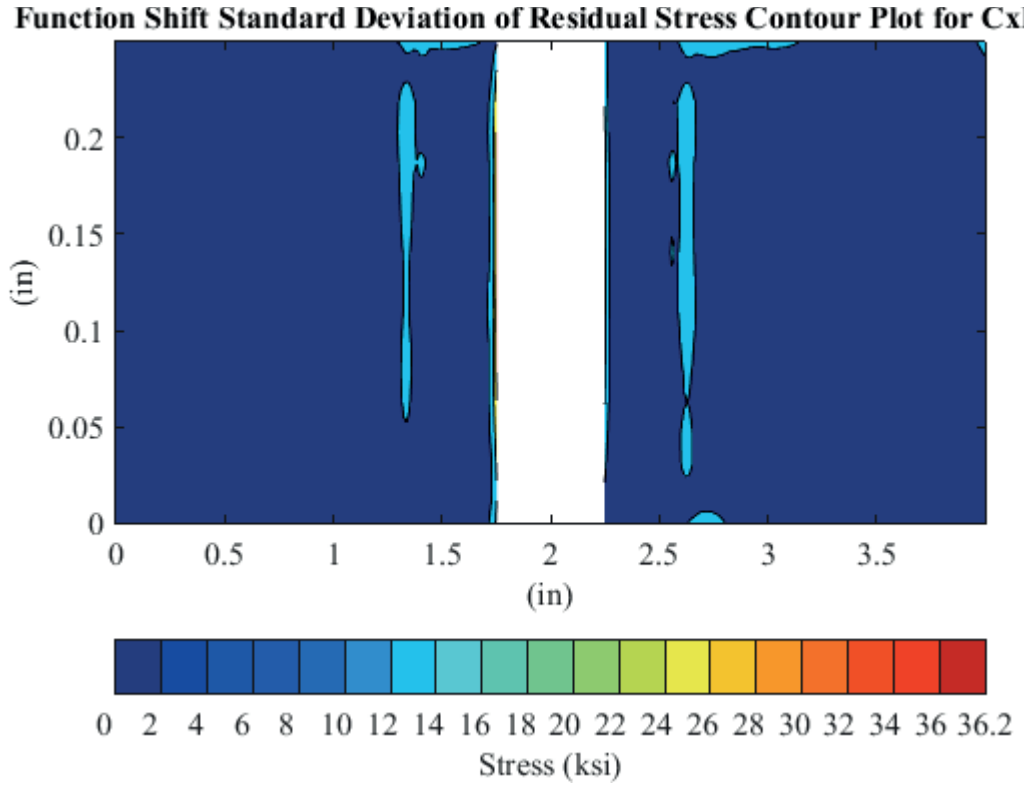

Fig. 156 Contour Plot of Model/Fit Error Developed via Knot Shift in both the X and Y Coordinate Frame for Coupon CxD2-1.

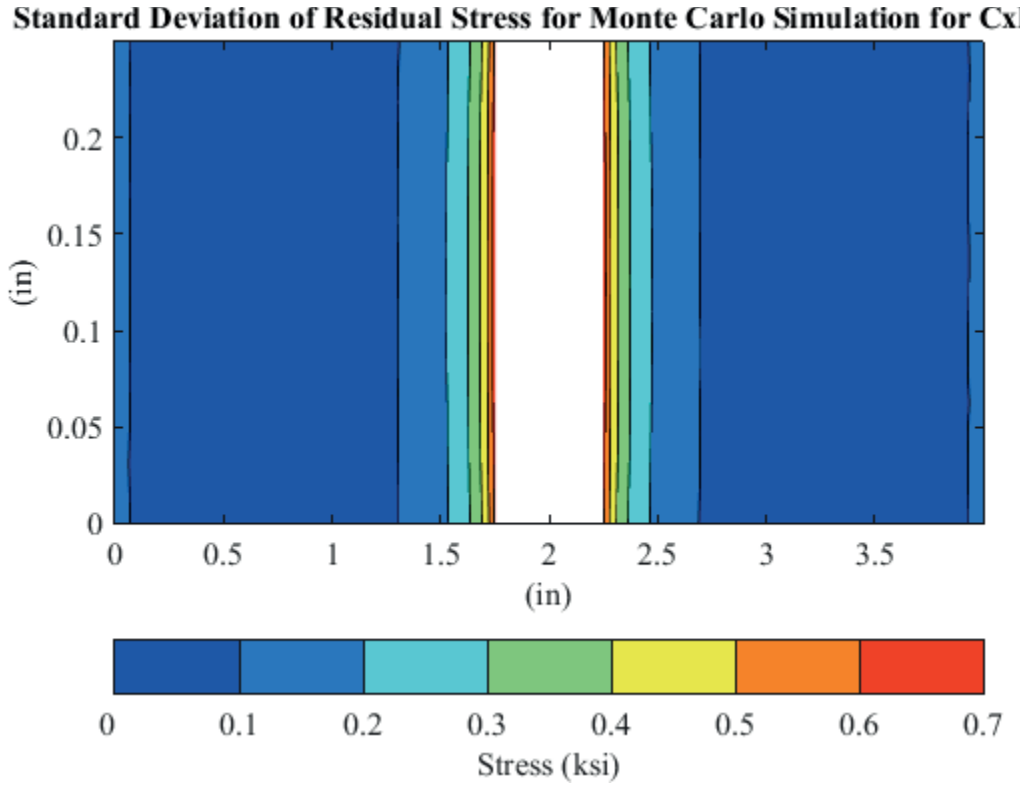

Fig. 157 Contour Plot of Displacement Uncertainty Developed via Monte Carlo Simulation for Coupon CxD2-1.

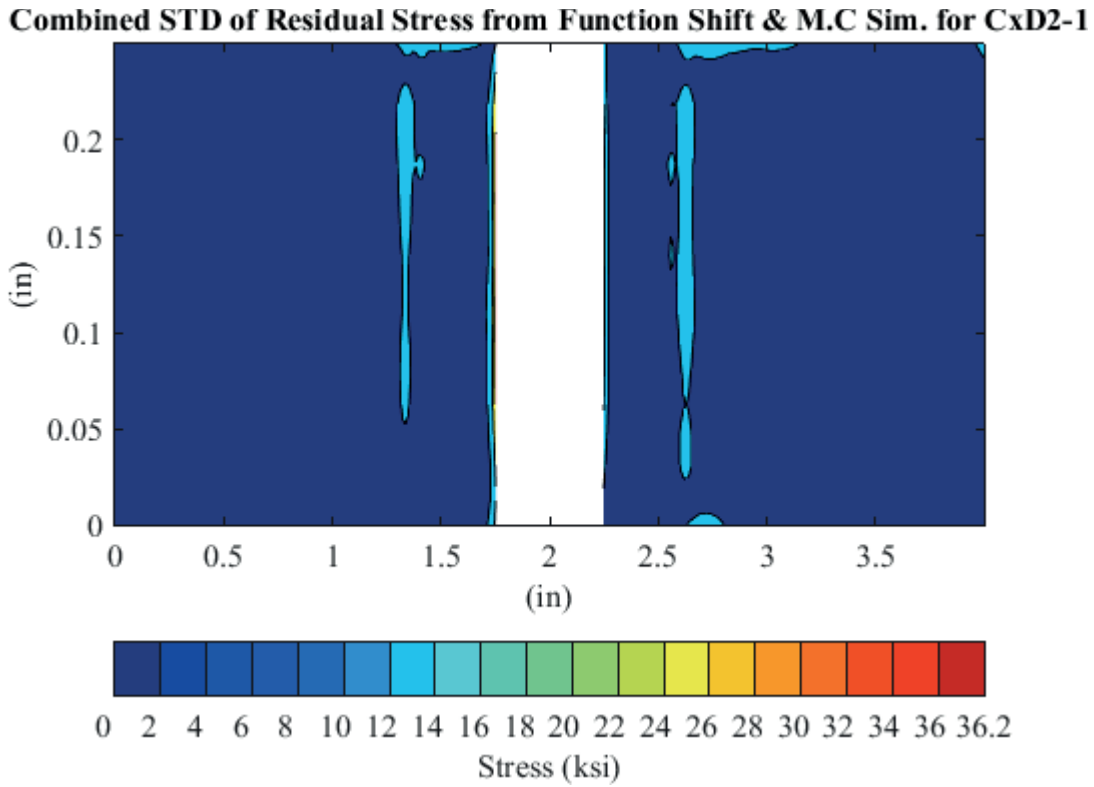

Fig. 158 Contour Plot of Root Sum Square (RSS) of Model/Fit and Displacement Uncertainties for Coupon CxD2-1.

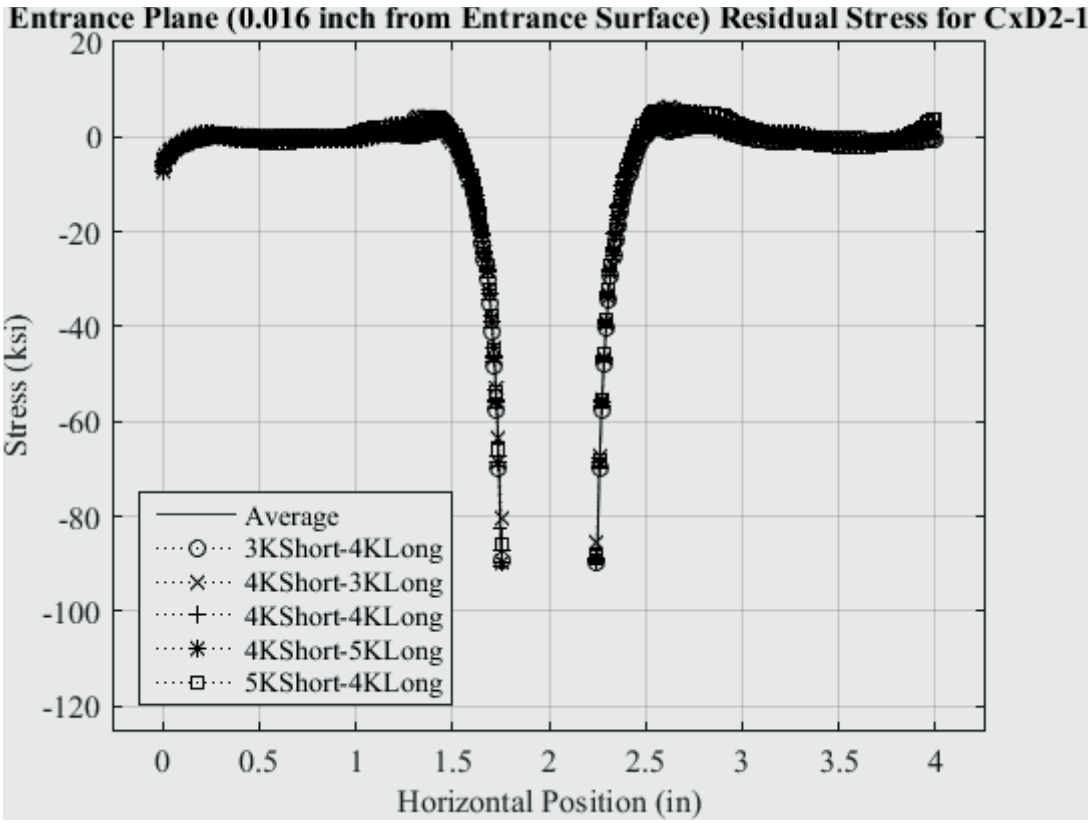

Fig. 159 Residual Stress Line Plot for all Five Knot Densities to Determine Model/Fit Error for CxD2-1 (7075-T651) at a Distance of 0.016 inch (Entrance Surface) from the Entrance Surface.

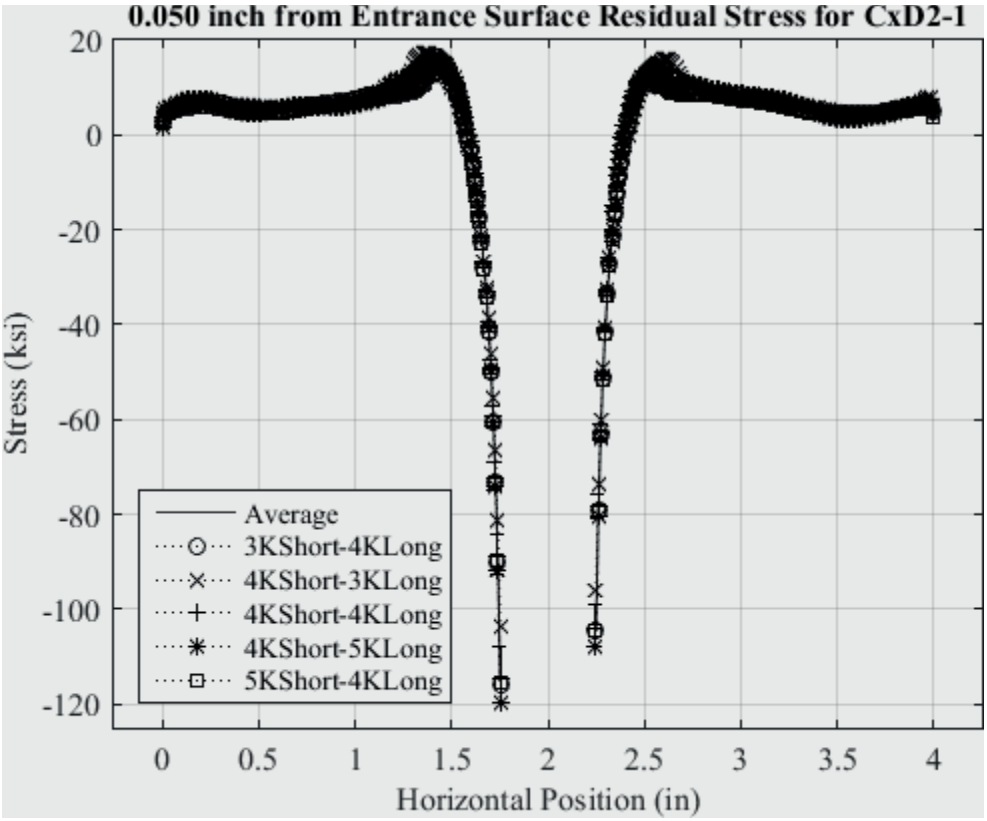

Fig. 160 Residual Stress Line Plot for all Five Knot Densities to Determine Model/Fit Error for CxD2-1 (7075-T651) at a Distance of 0.050 inch from the Entrance Surface.

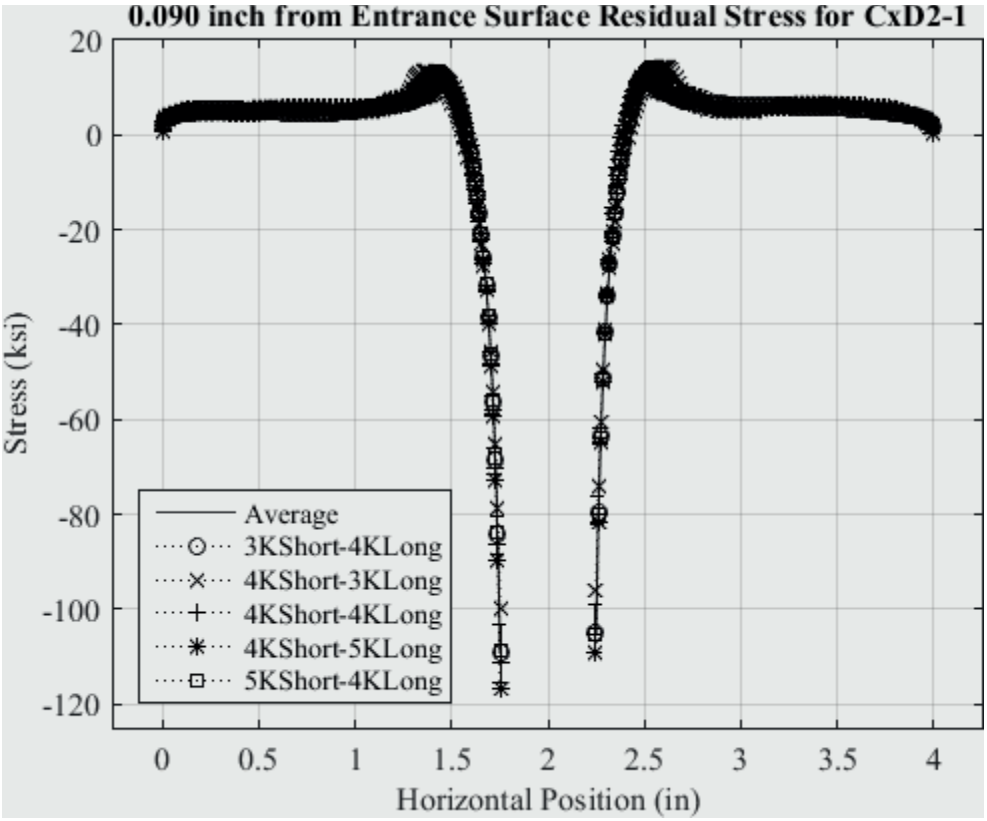

Fig. 161 Residual Stress Line Plot for all Five Knot Densities to Determine Model/Fit Error for CxD2-1 (7075-T651) at a Distance of 0.090 inch from the Entrance Surface.

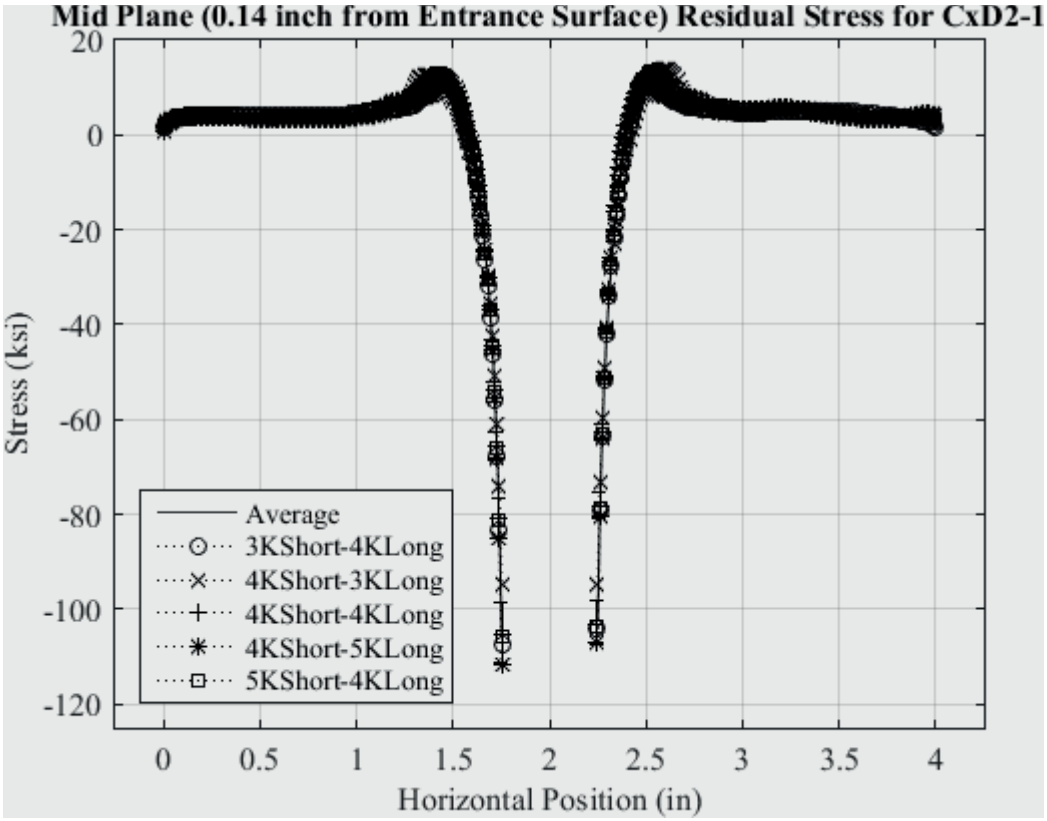

Fig. 162 Residual Stress Line Plot for all Five Knot Densities to Determine Model/Fit Error for CxD2-1 (7075-T651) at a Distance of 0.140 inch (Mid Plane Surface) from the Entrance Surface.

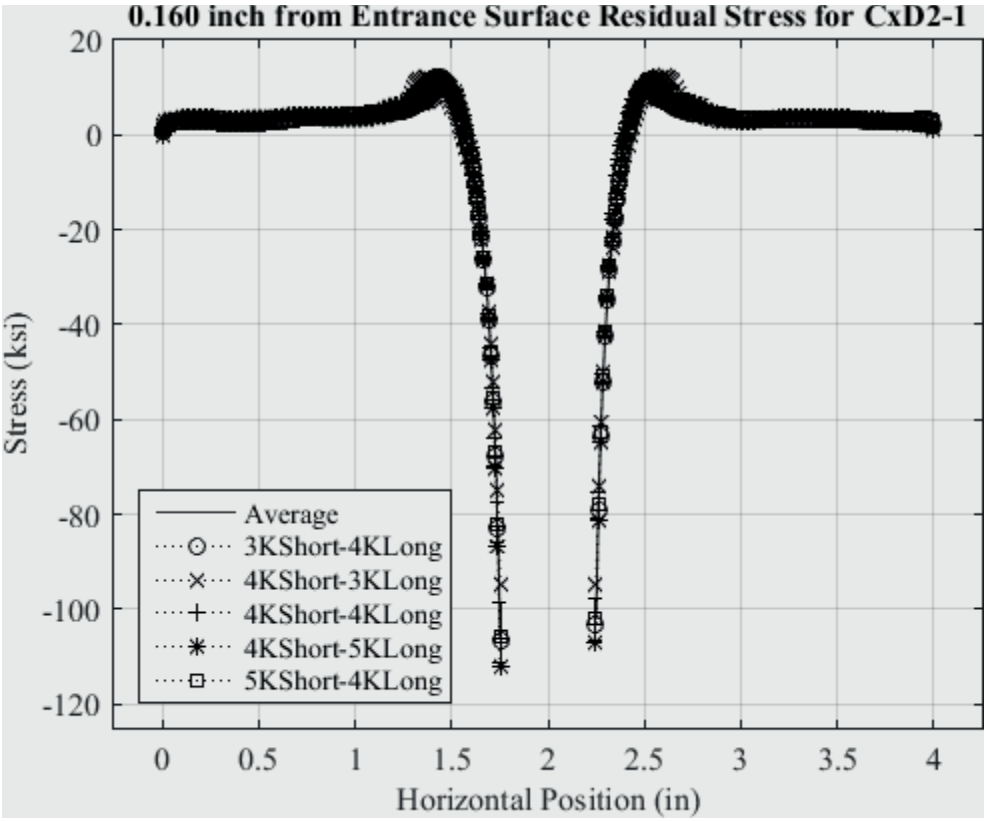

Fig. 163 Residual Stress Line Plot for all Five Knot Densities to Determine Model/Fit Error for CxD2-1 (7075-T651) at a Distance of 0.160 inch from the Entrance Surface.

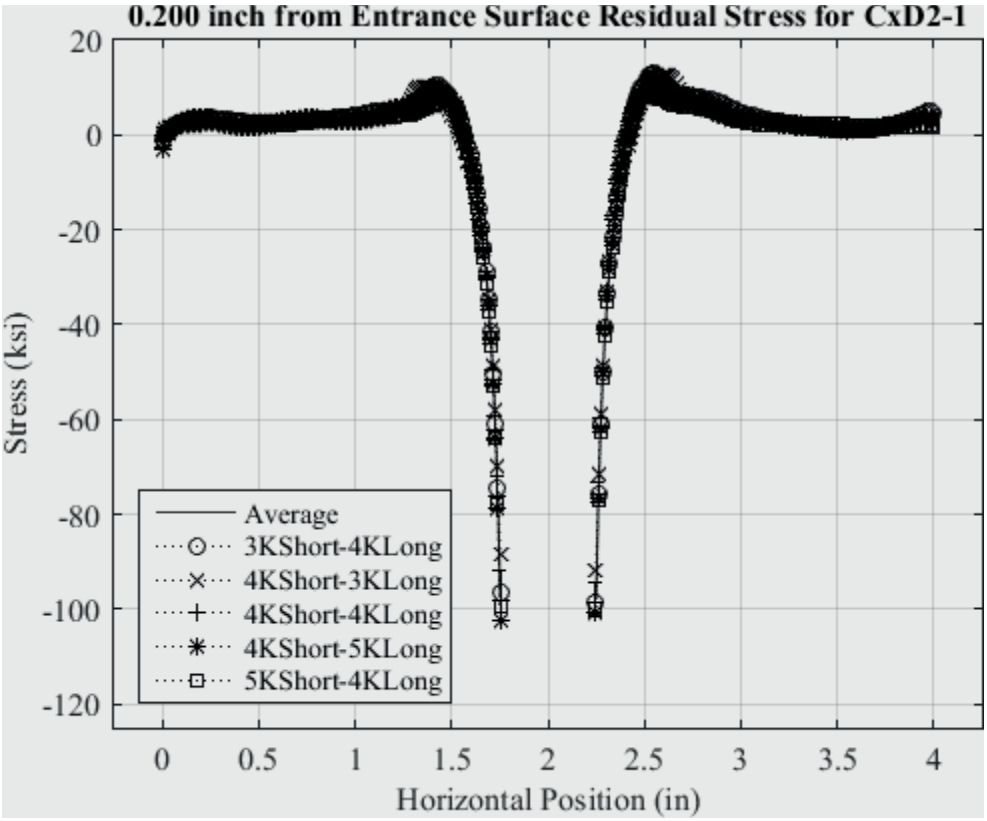

Fig. 164 Residual Stress Line Plot for all Five Knot Densities to Determine Model/Fit Error for CxD2-1 (7075-T651) at a Distance of 0.200 inch from the Entrance Surface.

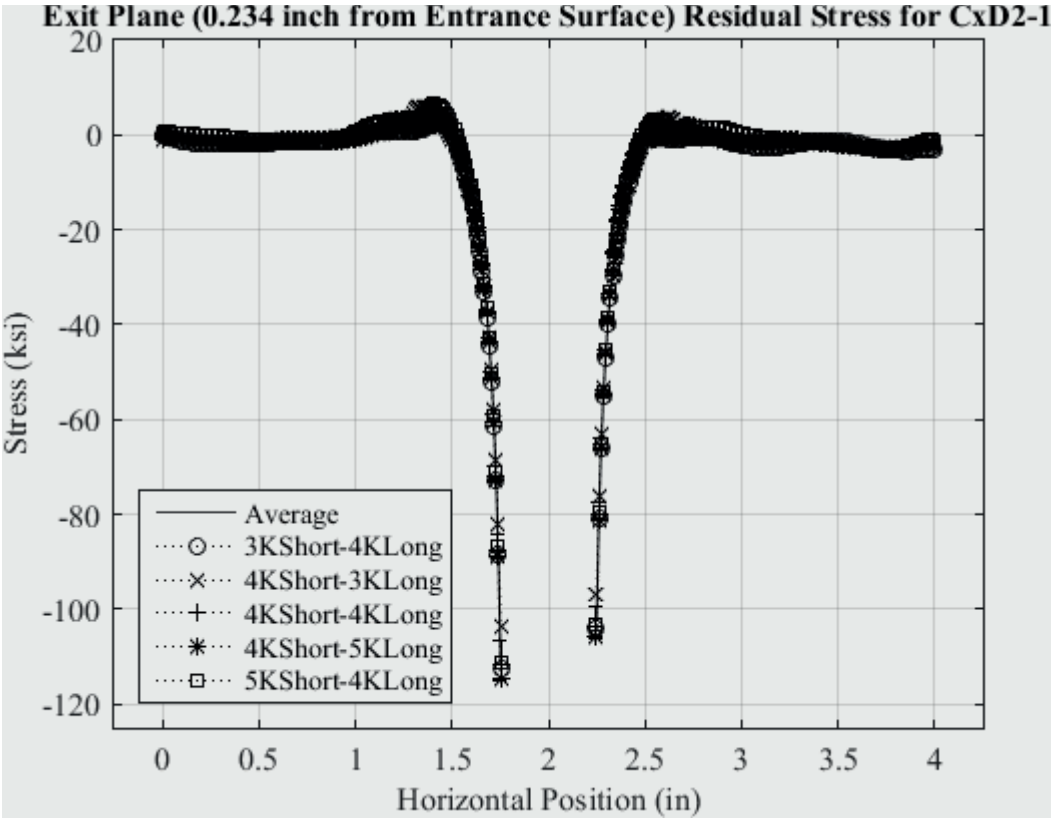

Fig. 165 Residual Stress Line Plot for all Five Knot Densities to Determine Model/Fit Error for CxD2-1 (7075-T651) at a Distance of 0.234 inch (Exit Surface) from the Entrance Surface.

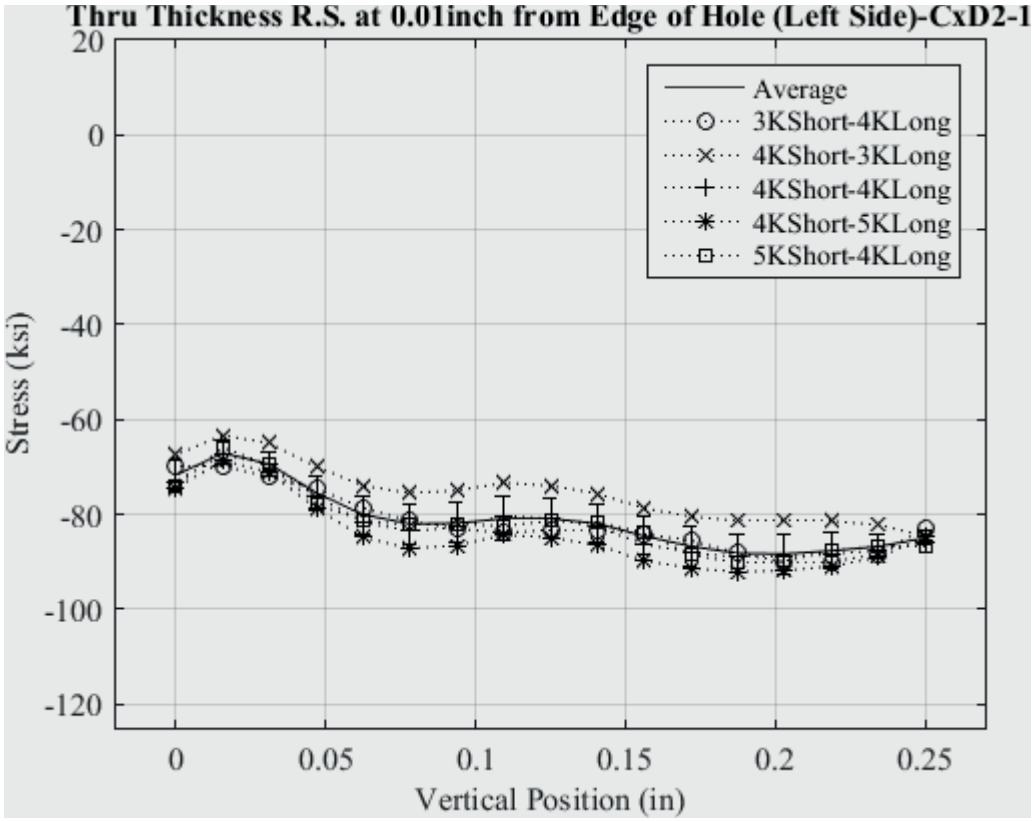

Fig. 166 Line Plot of Residual Stress at 0.01 inch from the Left Edge of the Hole for all Five Knot Densities to Determine Model/Fit Error CxD2-1 (7075-T651) – Stress Scale Locked.

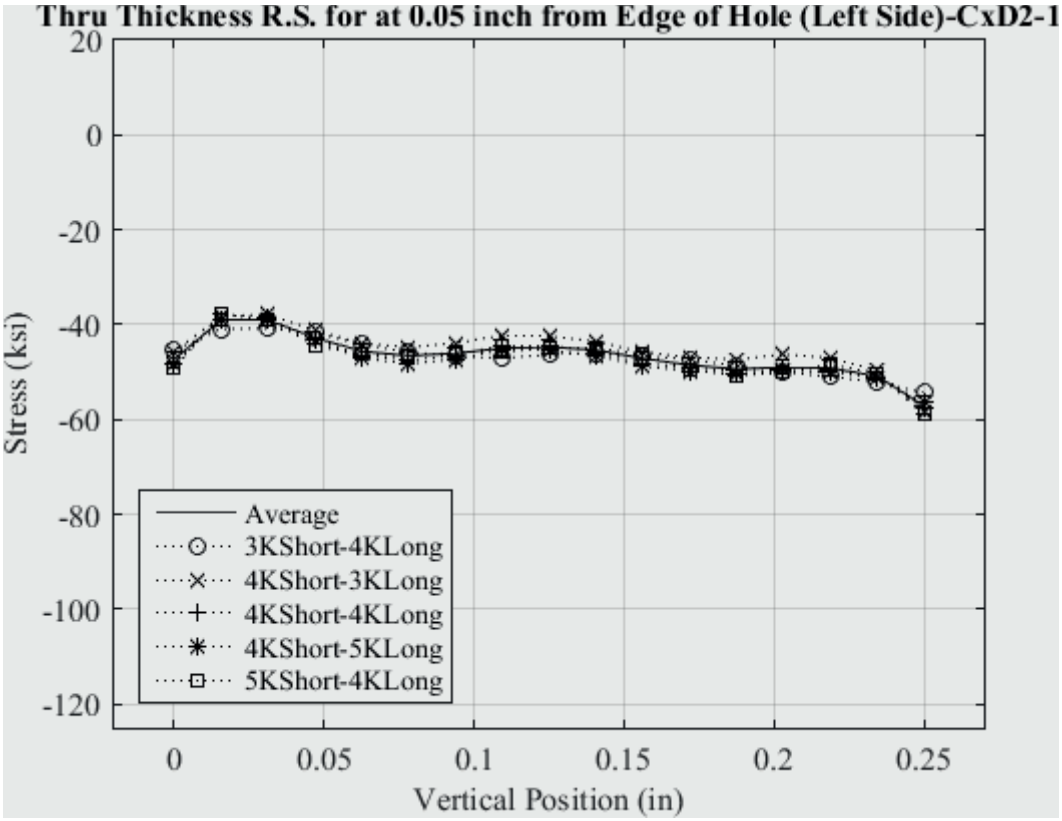

Fig. 167 Line Plot of Residual Stress at 0.05 inch from the Left Edge of the Hole for all Five Knot Densities to Determine Model/Fit Error CxD2-1 (7075-T651) – Stress Scale Locked.

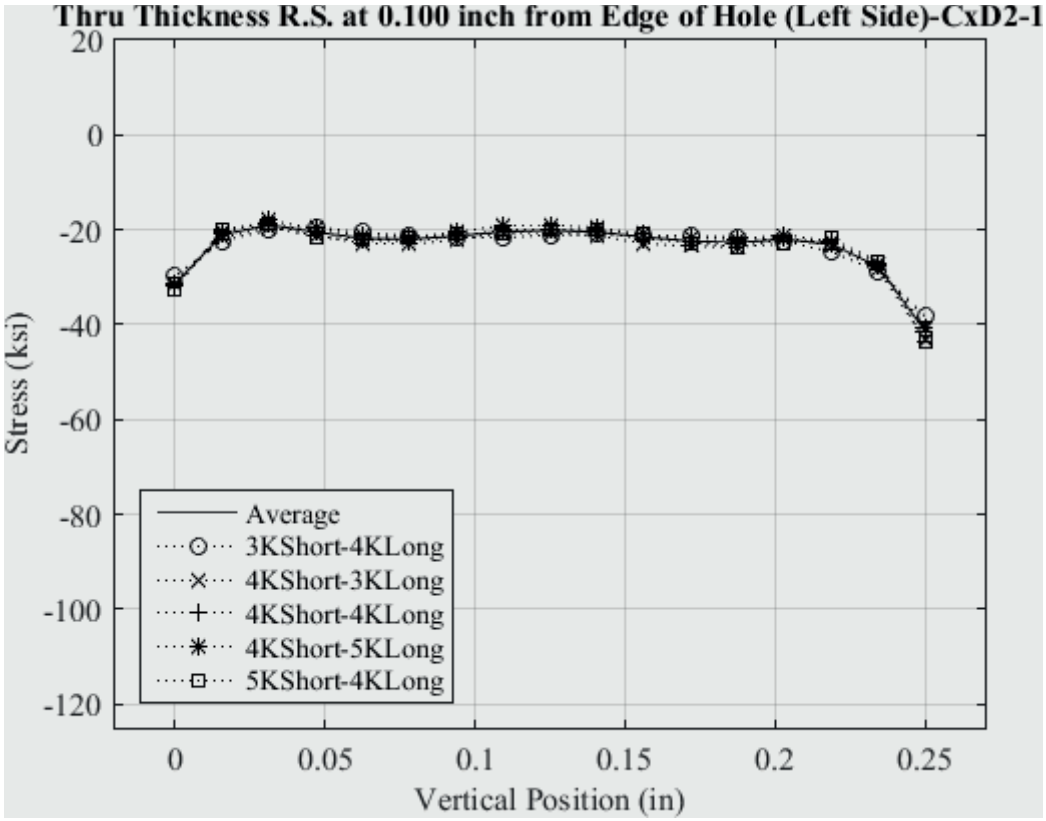

Fig. 168 Line Plot of Residual Stress at 0.10 inch from the Left Edge of the Hole for all Five Knot Densities to Determine Model/Fit Error CxD2-1 (7075-T651) – Stress Scale Locked.

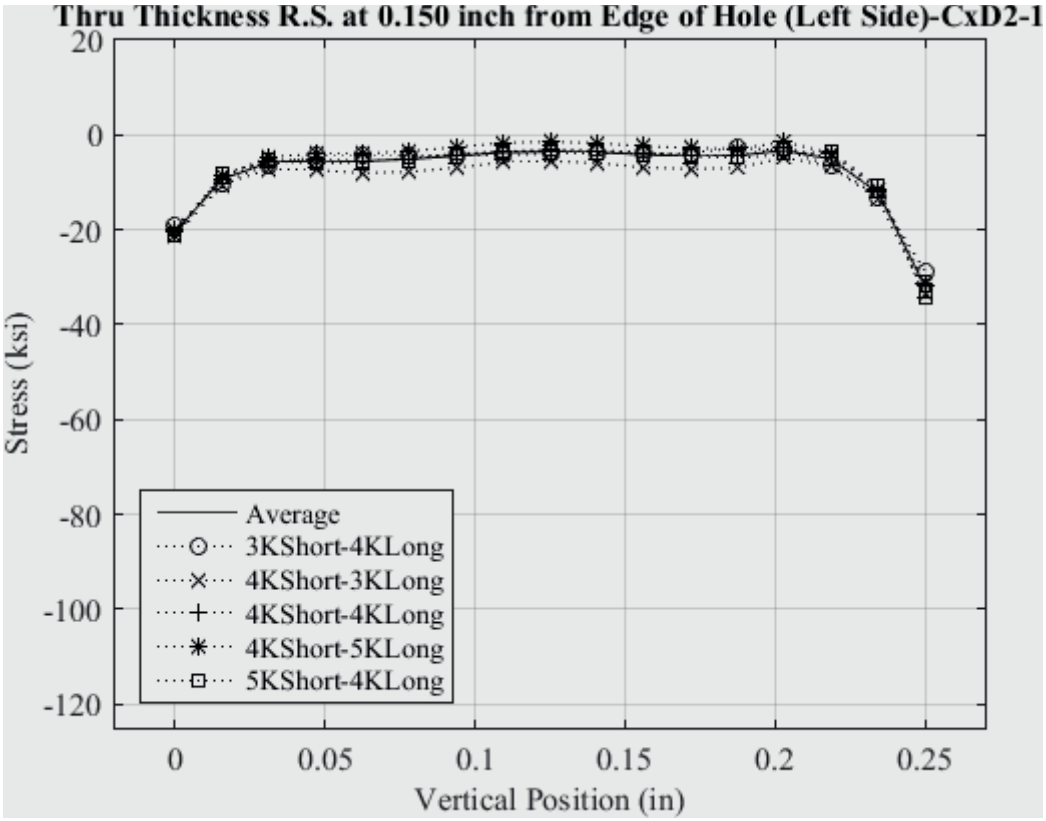

Fig. 169 Line Plot of Residual Stress at 0.150 inch from the Left Edge of the Hole for all Five Knot Densities to Determine Model/Fit Error CxD2-1 (7075-T651) – Stress Scale Locked.

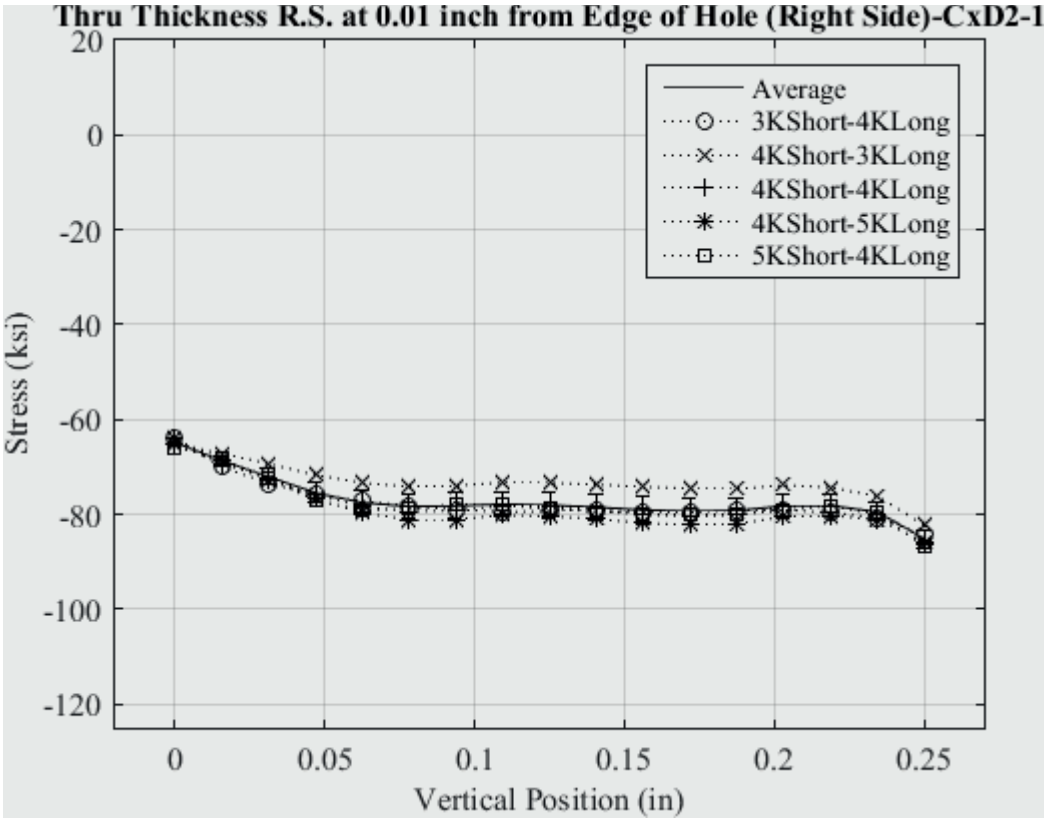

Fig. 170 Line Plot of Residual Stress at 0.01 inch from the Right Edge of the Hole for all Five Knot Densities to Determine Model/Fit Error CxD2-1 (7075-T651) – Stress Scale Locked.

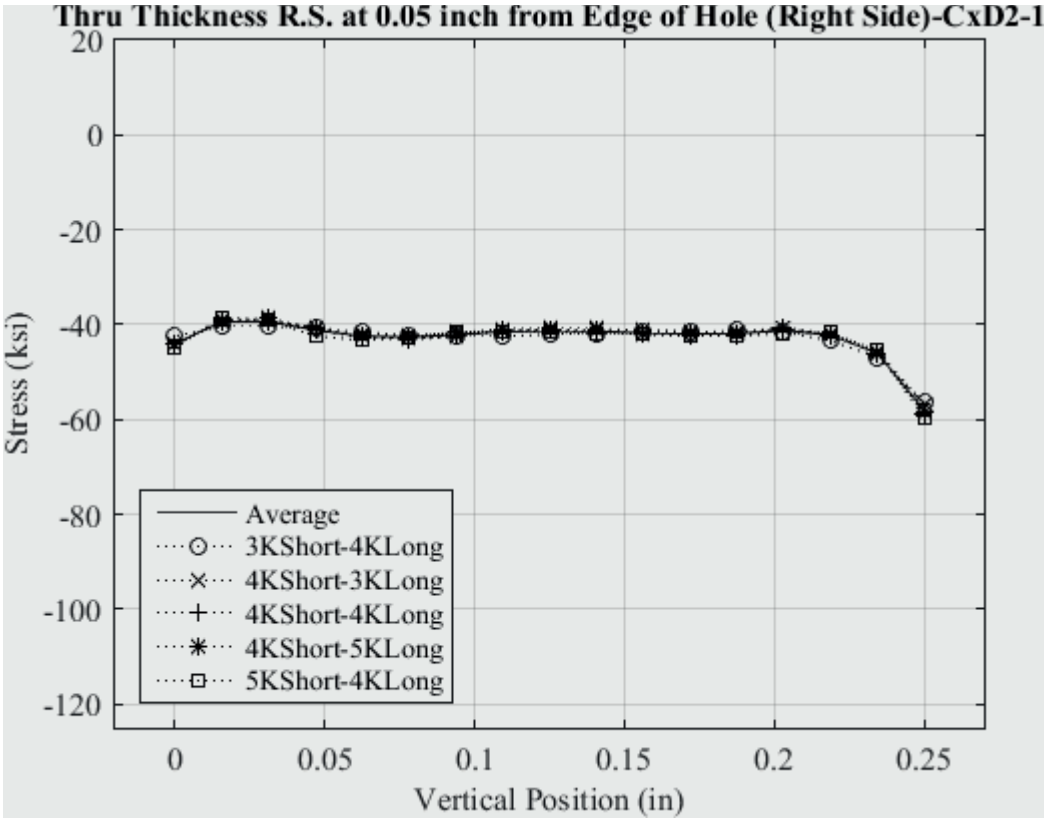

Fig. 171 Line Plot of Residual Stress at 0.05 inch from the Right Edge of the Hole for all Five Knot Densities to Determine Model/Fit Error CxD2-1 (7075-T651) – Stress Scale Locked.

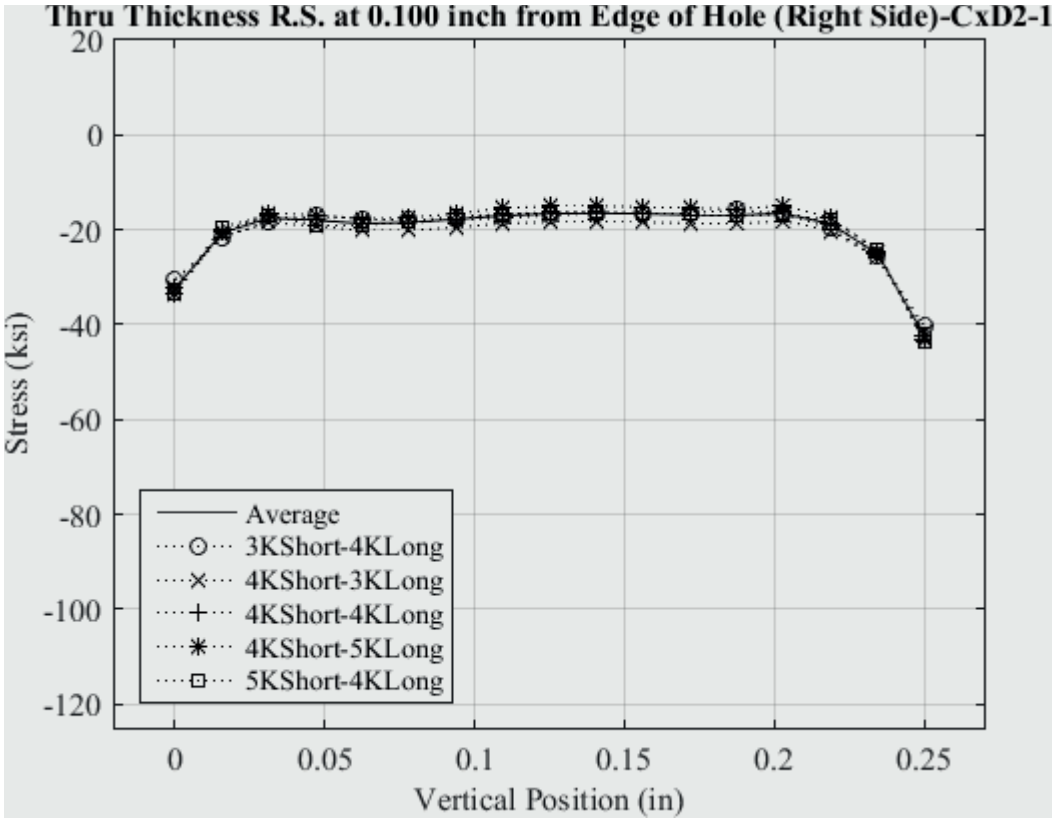

Fig. 172 Line Plot of Residual Stress at 0.10 inch from the Right Edge of the Hole for all Five Knot Densities to Determine Model/Fit Error CxD2-1 (7075-T651) – Stress Scale Locked.

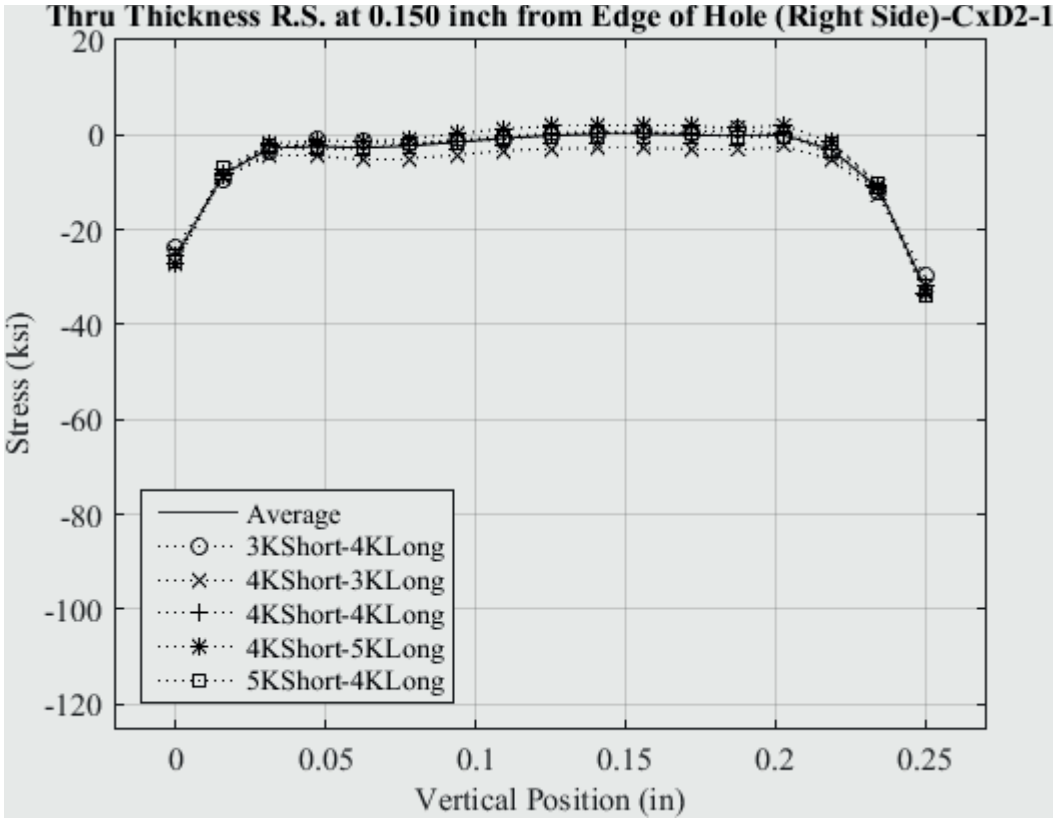

Fig. 173 Line Plot of Residual Stress at 0.150 inch from the Right Edge of the Hole for all Five Knot Densities to Determine Model/Fit Error CxD2-1 (7075-T651) – Stress Scale Locked.

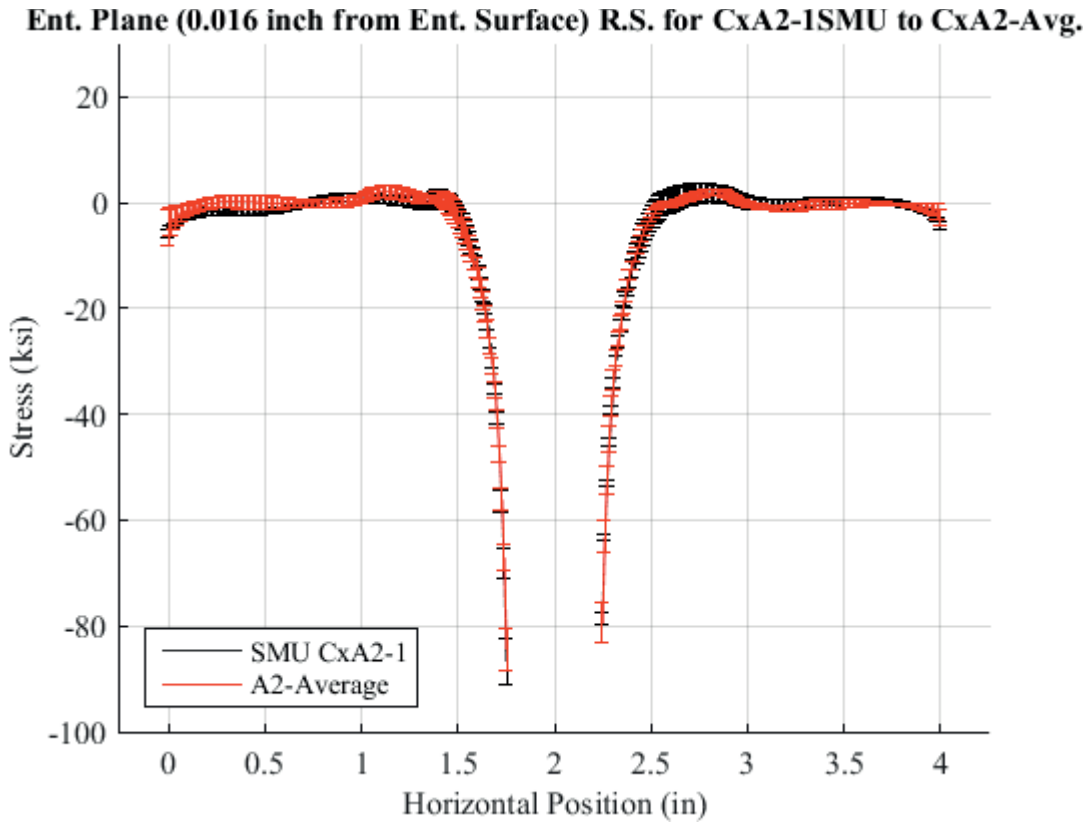

Fig. 174 Residual Stress Line Plot Comparing the CxA2-1 Single Measurement Average Residual Stress with its Associated Total Uncertainty as Error Bars (in Red) to the CxA2 Average Residual Stress with the Repeatability Uncertainty as Error Bars (in Black) at a Distance of 0.016 inch (Entrance Surface) from the Entrance Surface.

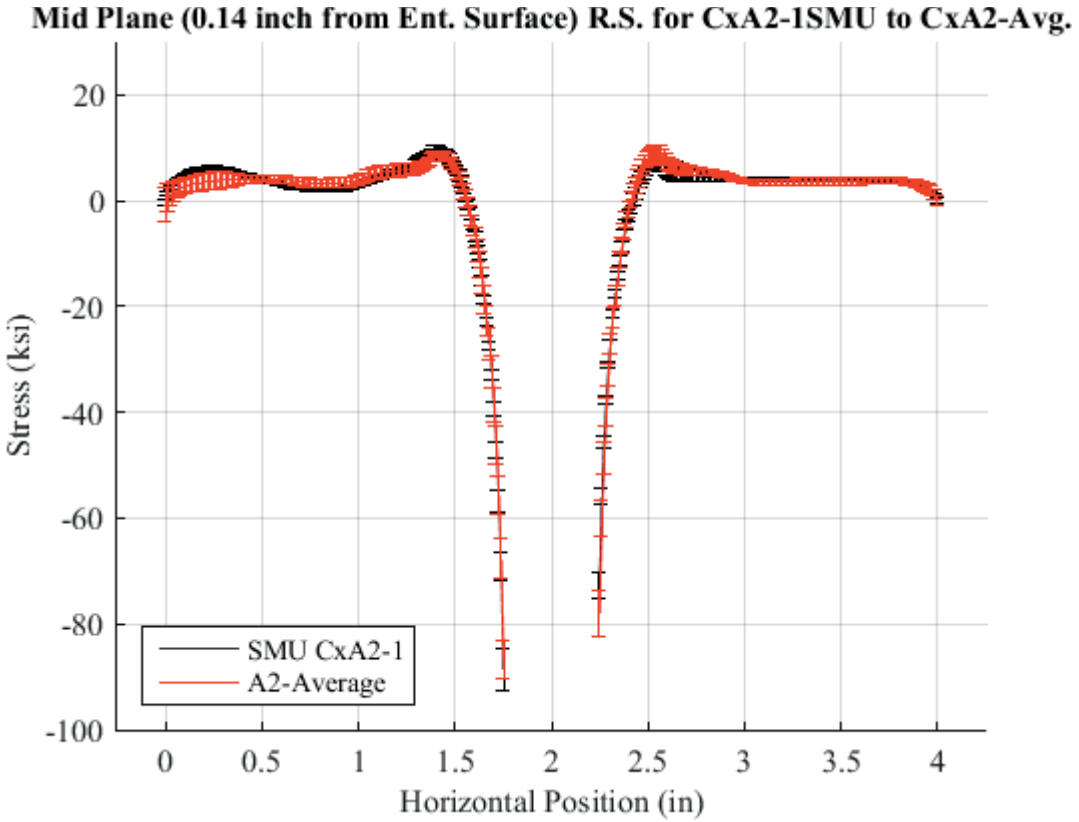

Fig. 175 Residual Stress Line Plot Comparing the CxA2-1 Single Measurement Average Residual Stress with its Associated Total Uncertainty as Error Bars (in Red) to the CxA2 Average Residual Stress with the Repeatability Uncertainty as Error Bars (in Black) at a Distance of 0.0140 inch (Mid Plane Surface) from the Entrance Surface.

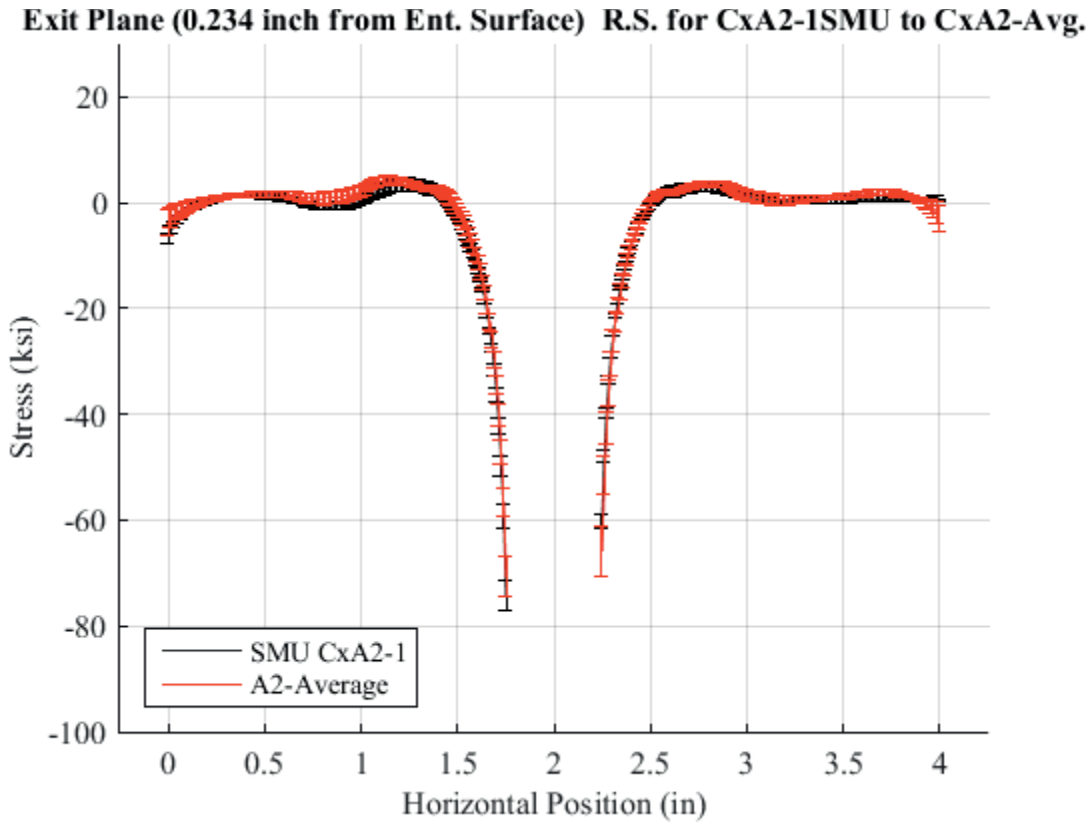

Fig. 176 Residual Stress Line Plot Comparing the CxA2-1 Single Measurement Average Residual Stress with its Associated Total Uncertainty as Error Bars (in Red) to the CxA2 Average Residual Stress with the Repeatability Uncertainty as Error Bars (in Black) at a Distance of 0.234 inch (Exit Surface) from the Entrance Surface.

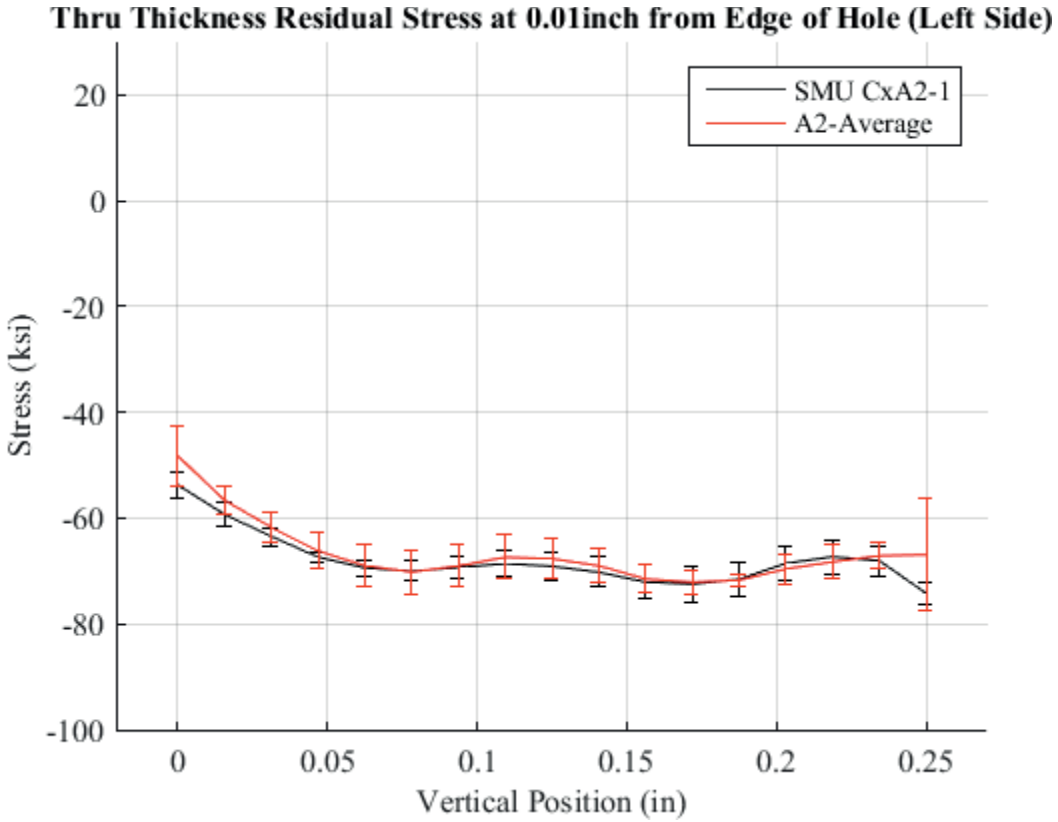

Fig. 177 Residual Stress Line Plot Comparing the CxA2-1 Single Measurement Average Residual Stress with its Associated Total Uncertainty as Error Bars (in Red) to the CxA2 Average Residual Stress with the Repeatability Uncertainty as Error Bars (in Black) at 0.01 inch from the Left Edge of the Hole – Stress Scale Locked.

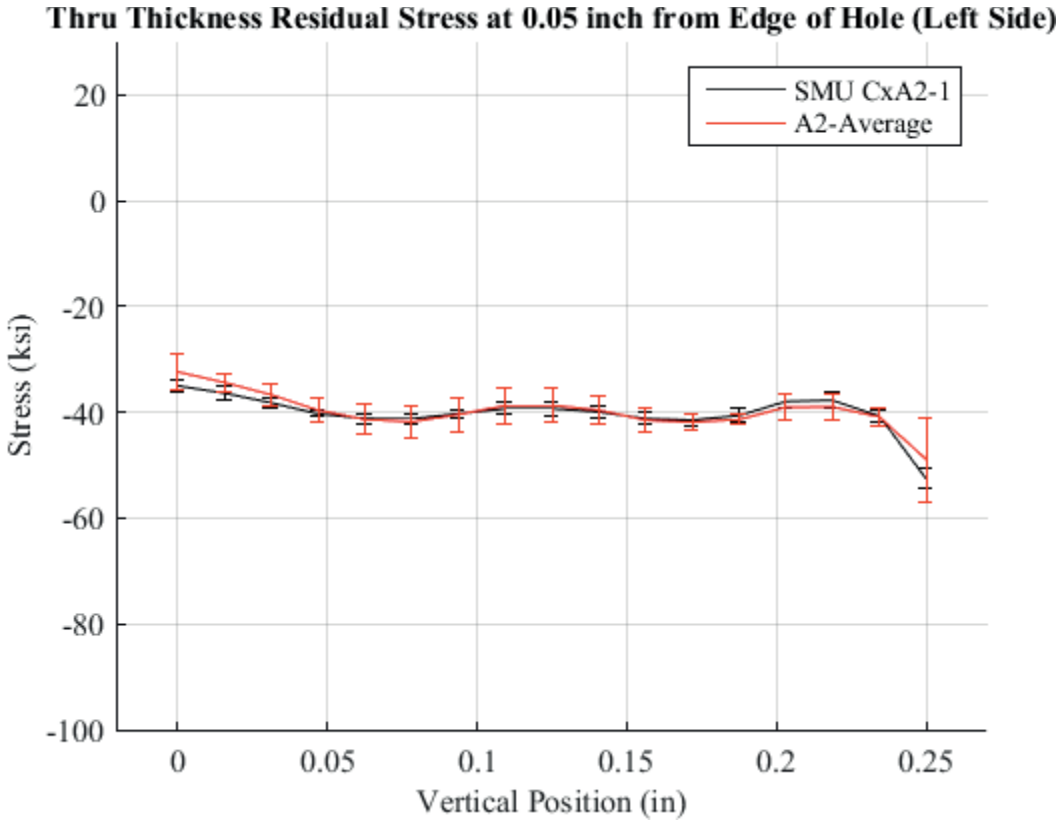

Fig. 178 Residual Stress Line Plot Comparing the CxA2-1 Single Measurement Average Residual Stress with its Associated Total Uncertainty as Error Bars (in Red) to the CxA2 Average Residual Stress with the Repeatability Uncertainty as Error Bars (in Black) at 0.05 inch from the Left Edge of the Hole – Stress Scale Locked.

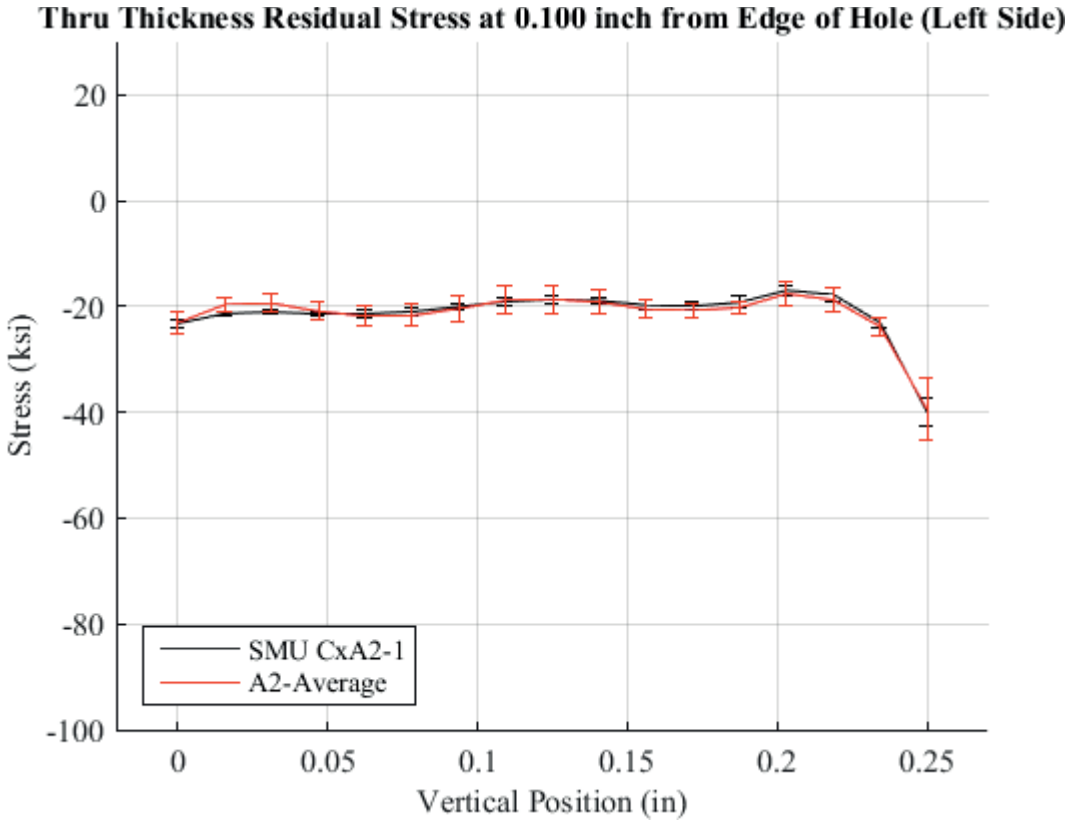

Fig. 179 Residual Stress Line Plot Comparing the CxA2-1 Single Measurement Average Residual Stress with its Associated Total Uncertainty as Error Bars (in Red) to the CxA2 Average Residual Stress with the Repeatability Uncertainty as Error Bars (in Black) at 0.10 inch from the Left Edge of the Hole – Stress Scale Locked.

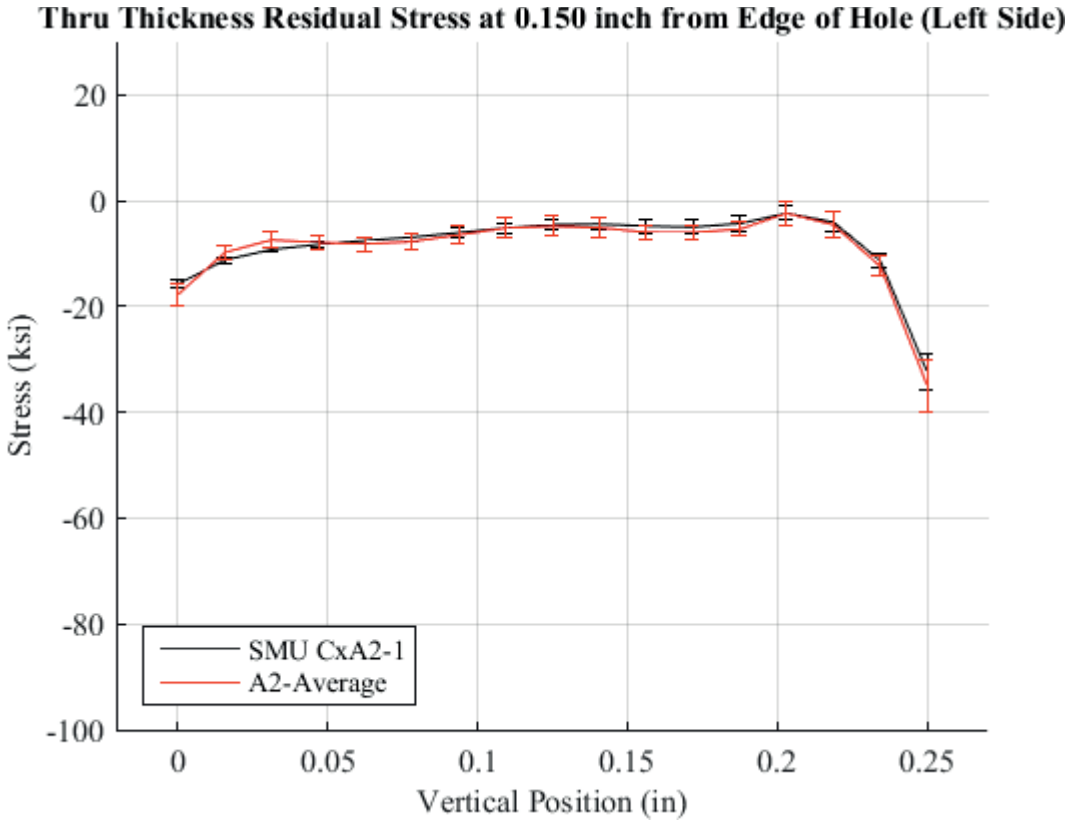

Fig. 180 Residual Stress Line Plot Comparing the CxA2-1 Single Measurement Average Residual Stress with its Associated Total Uncertainty as Error Bars (in Red) to the CxA2 Average Residual Stress with the Repeatability Uncertainty as Error Bars (in Black) at 0.150 inch from the Left Edge of the Hole – Stress Scale Locked.

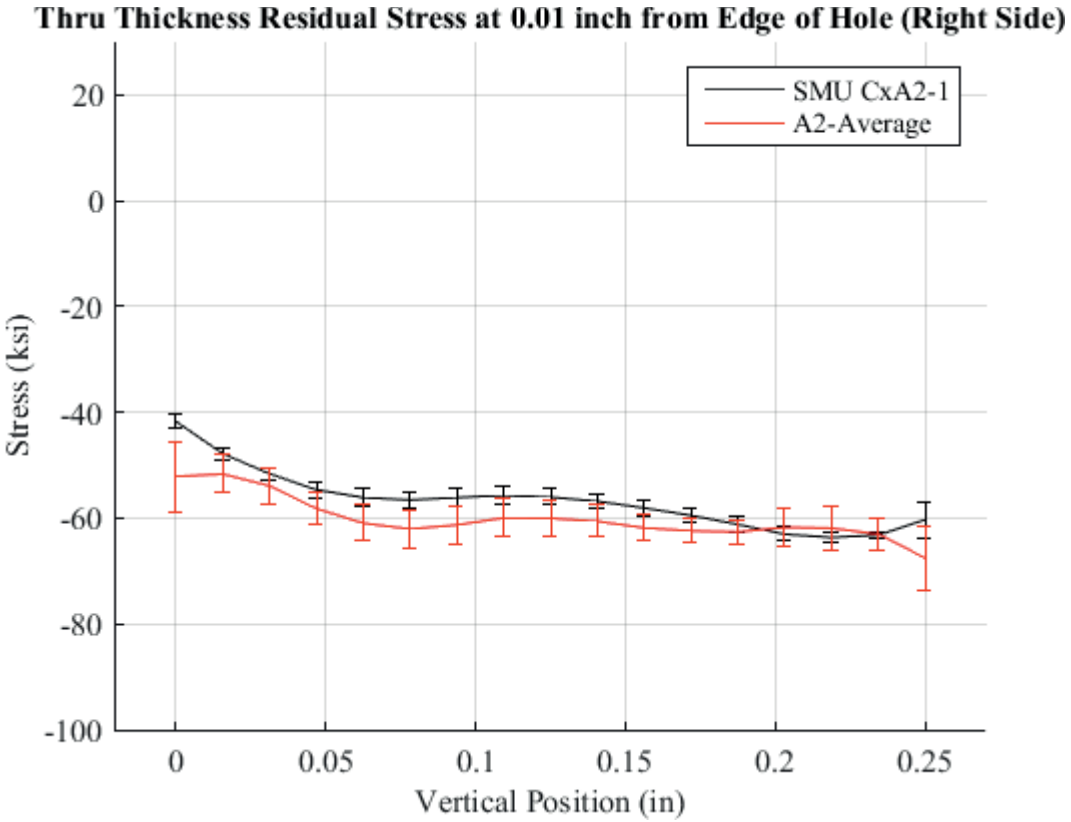

Fig. 181 Residual Stress Line Plot Comparing the CxA2-1 Single Measurement Average Residual Stress with its Associated Total Uncertainty as Error Bars (in Red) to the CxA2 Average Residual Stress with the Repeatability Uncertainty as Error Bars (in Black) at 0.01 inch from the Right Edge of the Hole – Stress Scale Locked.

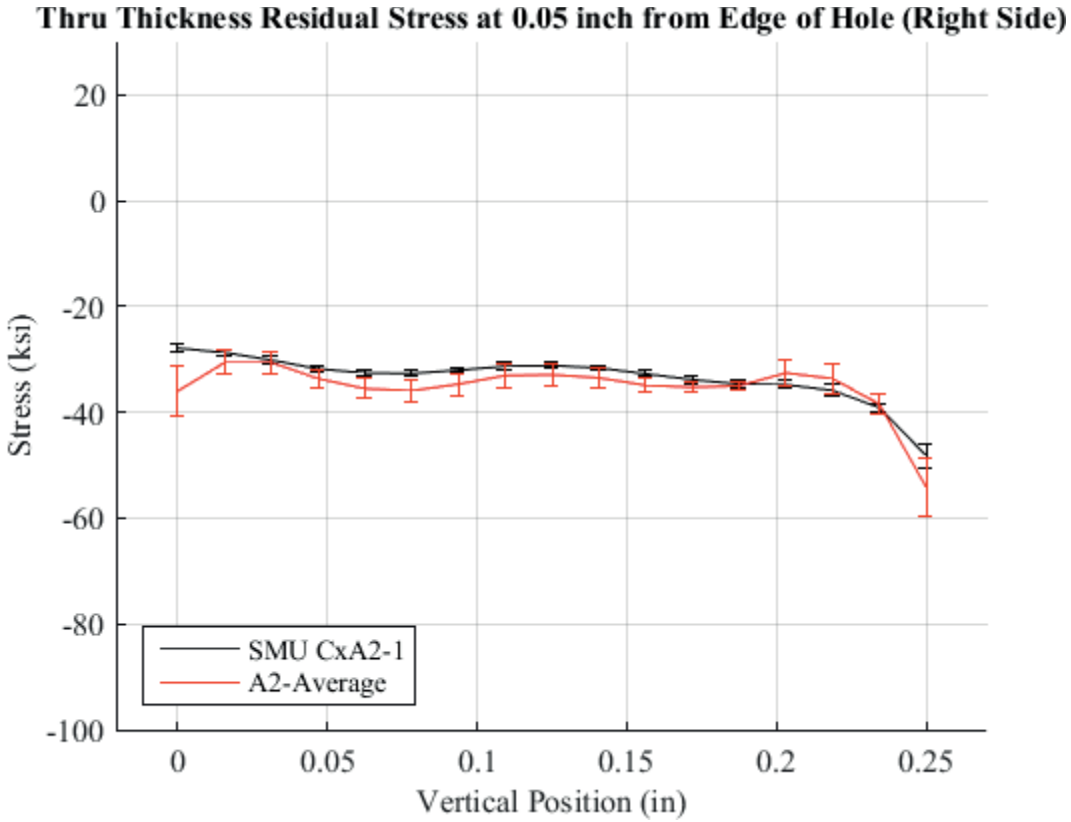

Fig. 182 Residual Stress Line Plot Comparing the CxA2-1 Single Measurement Average Residual Stress with its Associated Total Uncertainty as Error Bars (in Red) to the CxA2 Average Residual Stress with the Repeatability Uncertainty as Error Bars (in Black) at 0.05 inch from the Right Edge of the Hole – Stress Scale Locked.

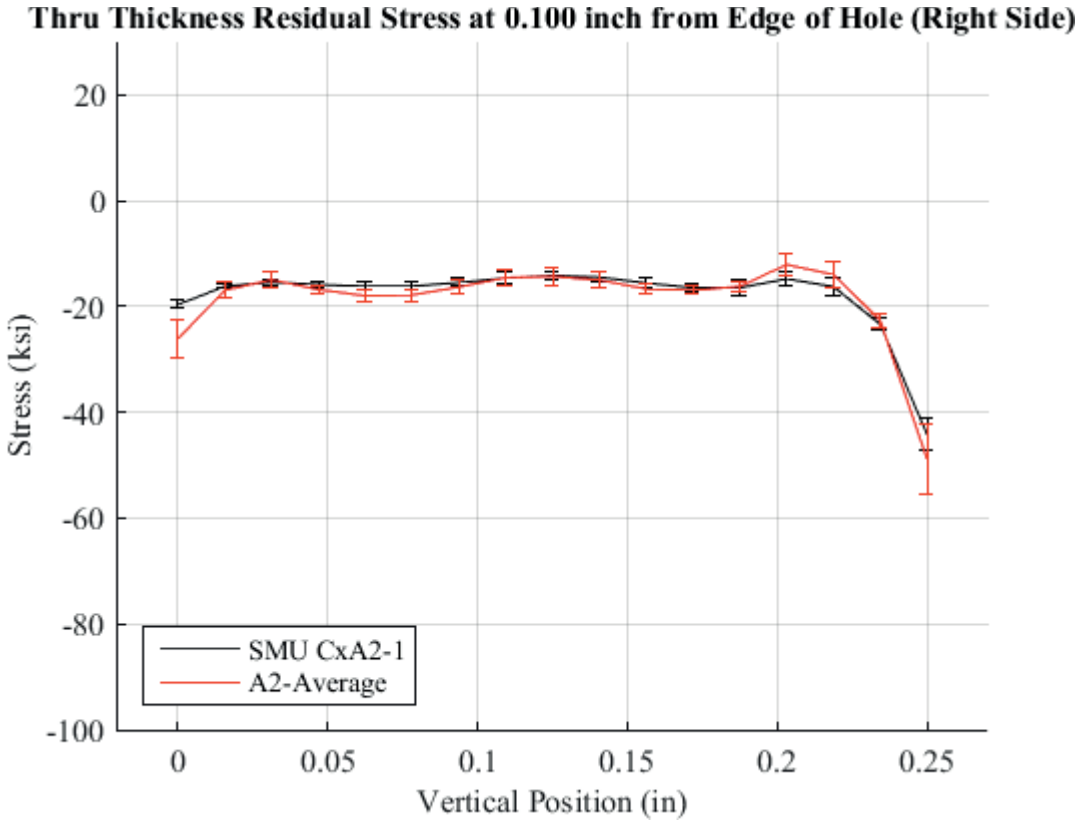

Fig. 183 Residual Stress Line Plot Comparing the CxA2-1 Single Measurement Average Residual Stress with its Associated Total Uncertainty as Error Bars (in Red) to the CxA2 Average Residual Stress with the Repeatability Uncertainty as Error Bars (in Black) at 0.10 inch from the Right Edge of the Hole – Stress Scale Locked.

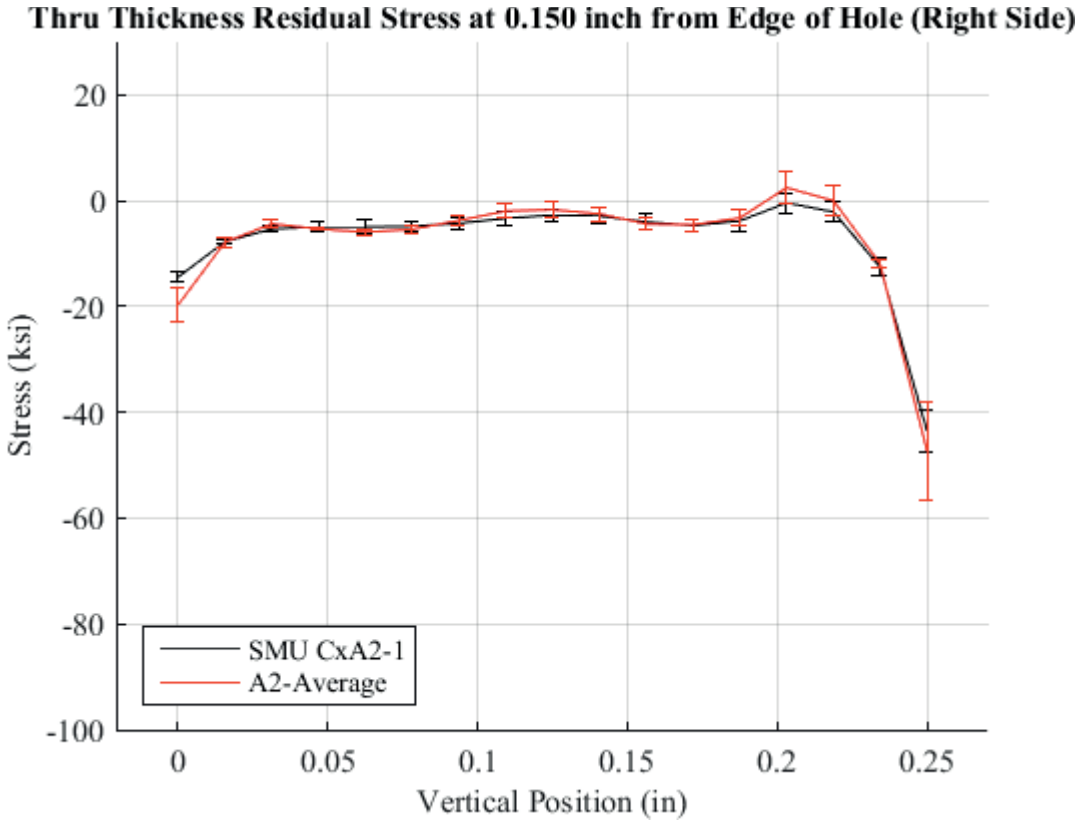

Fig. 184 Residual Stress Line Plot Comparing the CxA2-1 Single Measurement Average Residual Stress with its Associated Total Uncertainty as Error Bars (in Red) to the CxA2 Average Residual Stress with the Repeatability Uncertainty as Error Bars (in Black) at 0.15 inch from the Right Edge of the Hole – Stress Scale Locked.

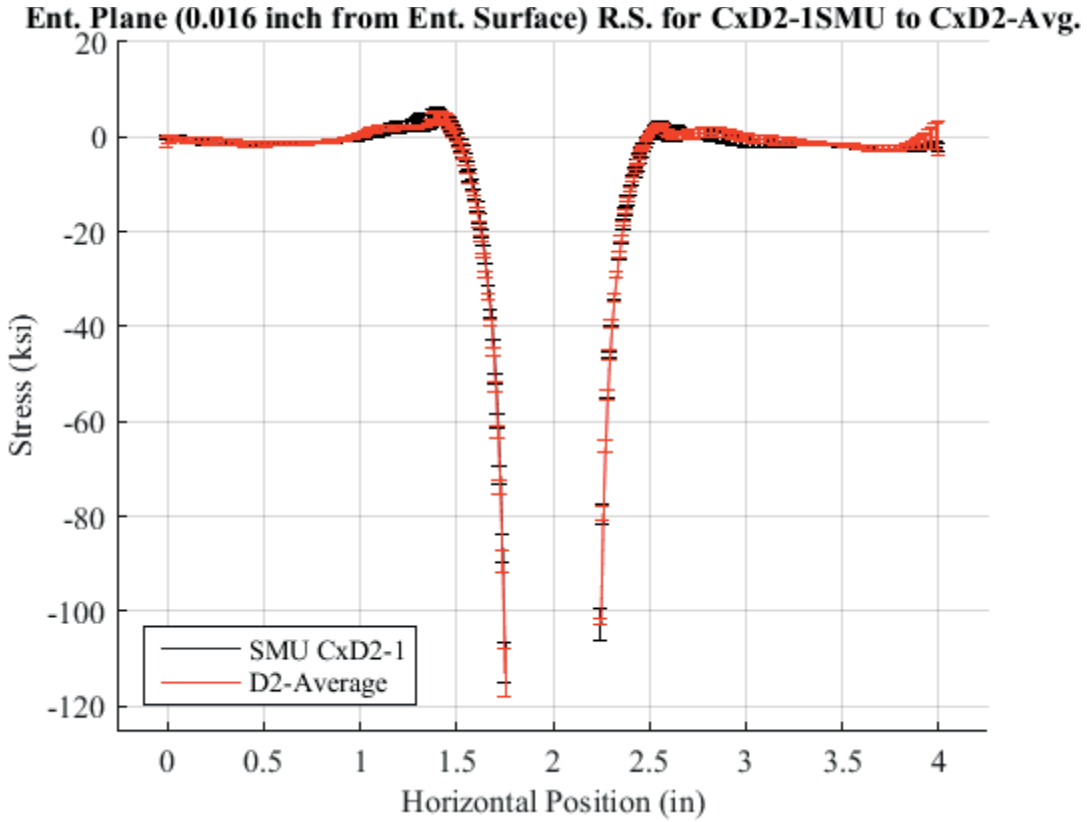

Fig. 185 Residual Stress Line Plot Comparing the CxD2-1 Single Measurement Average Residual Stress with its Associated Total Uncertainty as Error Bars (in Red) to the CxD2 Average Residual Stress with the Repeatability Uncertainty as Error Bars (in Black) at a Distance of 0.016 inch (Entrance Surface) from the Entrance Surface.

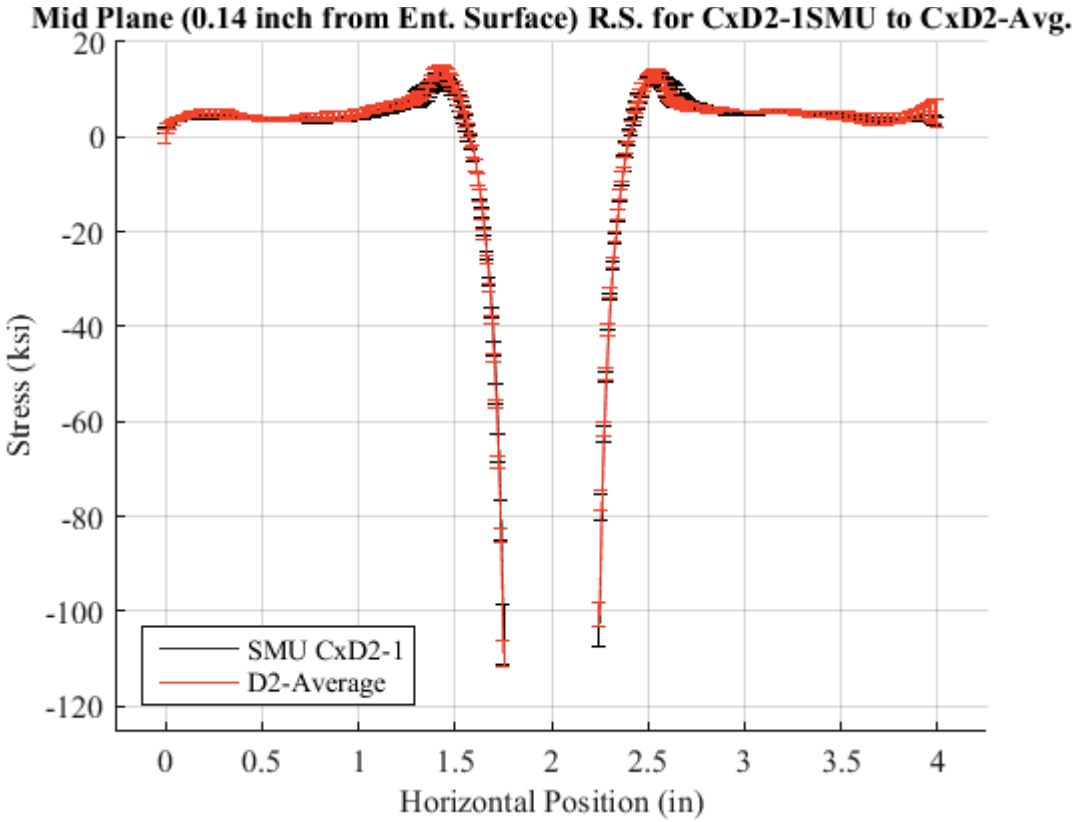

Fig. 186 Residual Stress Line Plot Comparing the CxD2-1 Single Measurement Average Residual Stress with its Associated Total Uncertainty as Error Bars (in Red) to the CxD2 Average Residual Stress with the Repeatability Uncertainty as Error Bars (in Black) at a Distance of 0.140 inch (Mid Plane Surface) from the Entrance Surface.

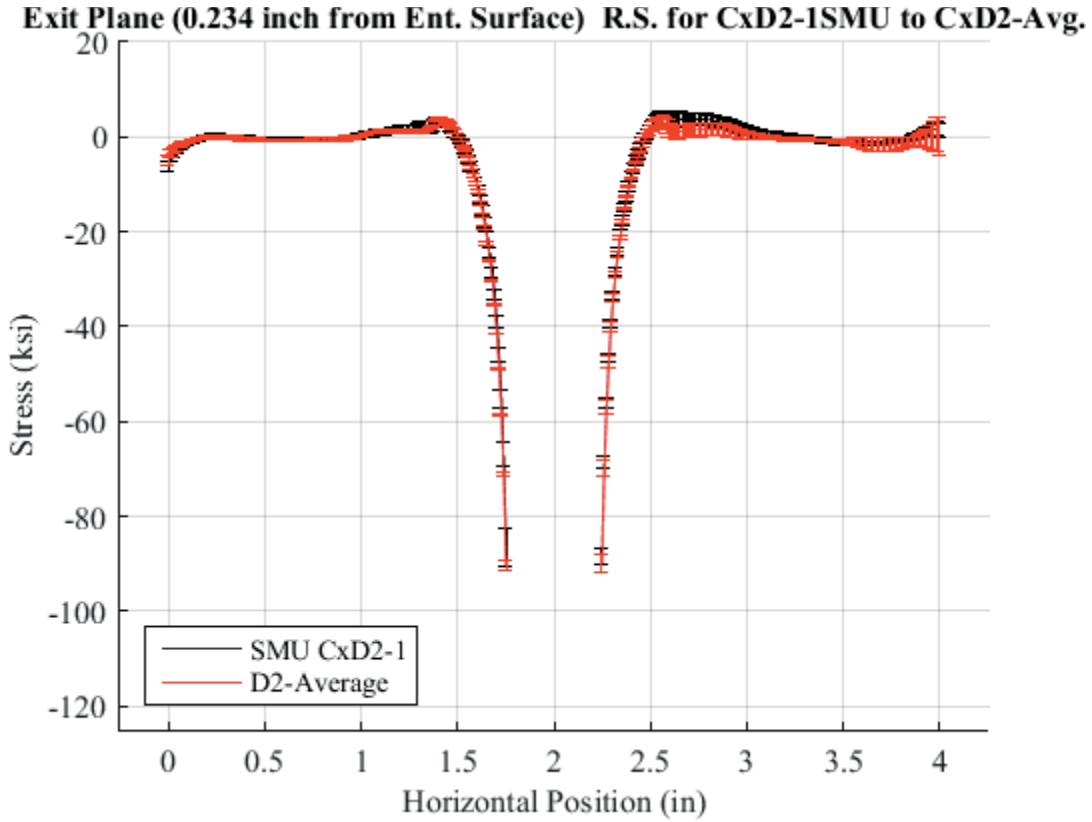

Fig. 187 Residual Stress Line Plot Comparing the CxD2-1 Single Measurement Average Residual Stress with its Associated Total Uncertainty as Error Bars (in Red) to the CxD2 Average Residual Stress with the Repeatability Uncertainty as Error Bars (in Black) at a Distance of 0.234 inch (Exit Surface) from the Entrance Surface.

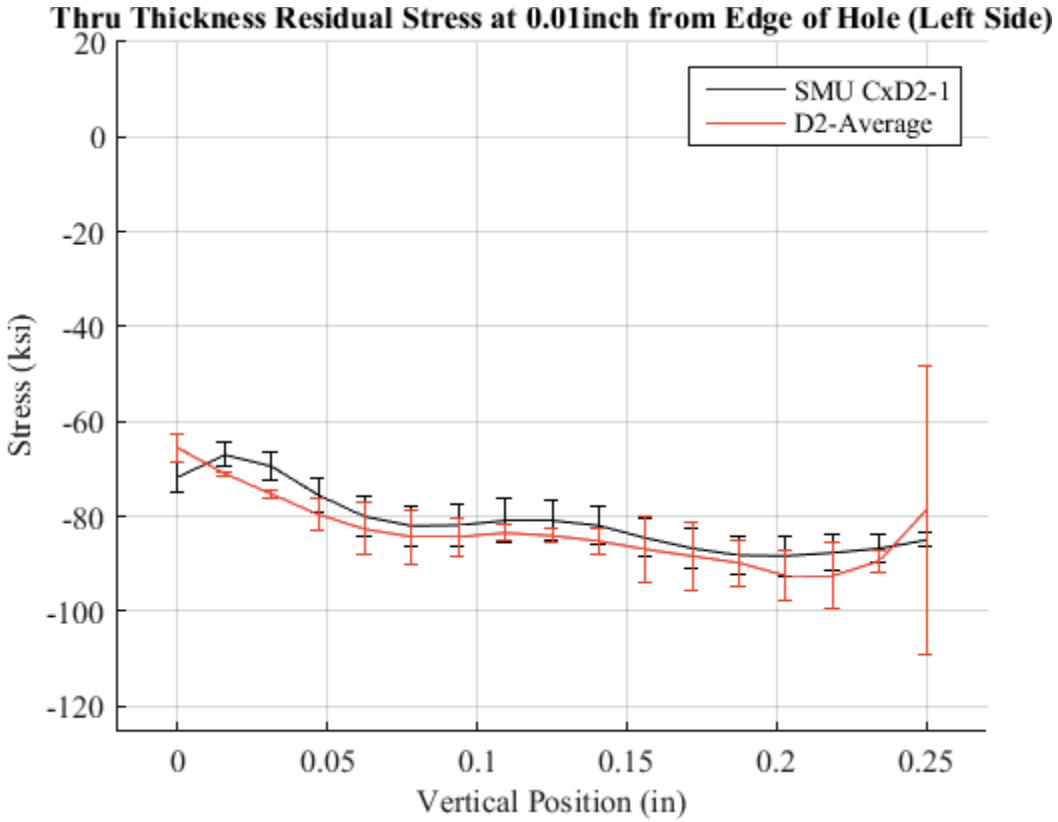

Fig. 188 Residual Stress Line Plot Comparing the CxD2-1 Single Measurement Average Residual Stress with its Associated Total Uncertainty as Error Bars (in Red) to the CxD2 Average Residual Stress with the Repeatability Uncertainty as Error Bars (in Black) at 0.01 inch from the Left Edge of the Hole – Stress Scale Locked.

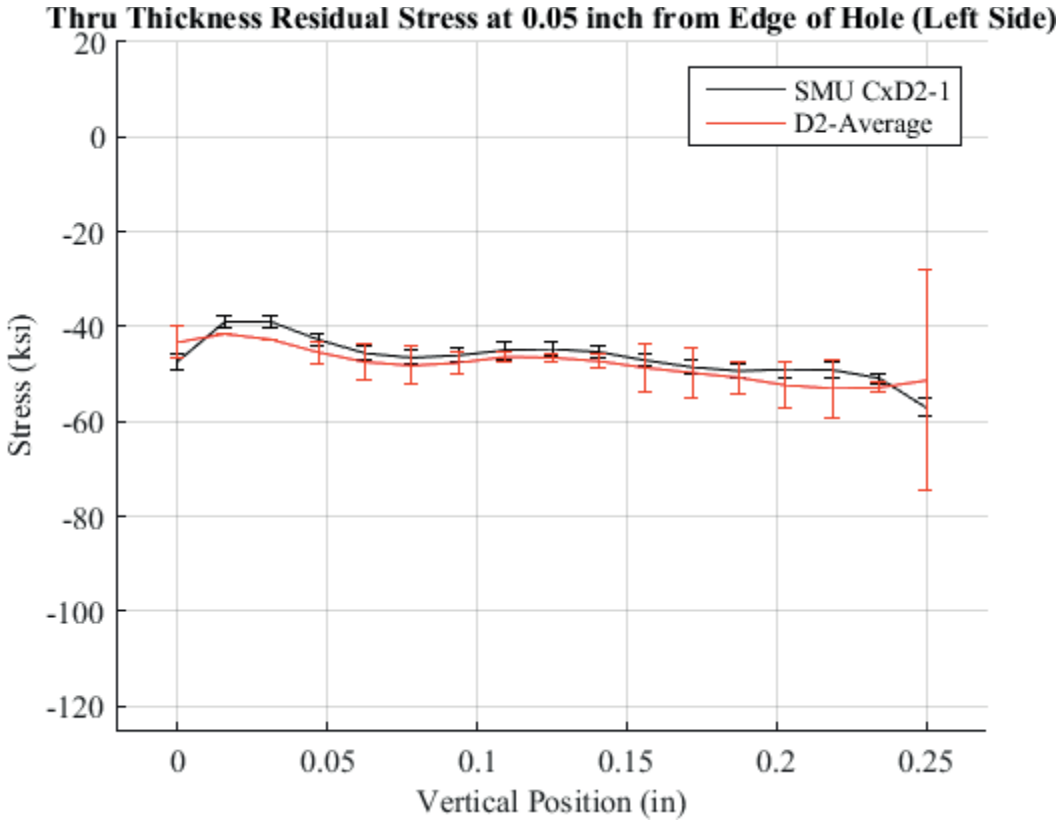

Fig. 189 Residual Stress Line Plot Comparing the CxD2-1 Single Measurement Average Residual Stress with its Associated Total Uncertainty as Error Bars (in Red) to the CxD2 Average Residual Stress with the Repeatability Uncertainty as Error Bars (in Black) at 0.05 inch from the Left Edge of the Hole – Stress Scale Locked.

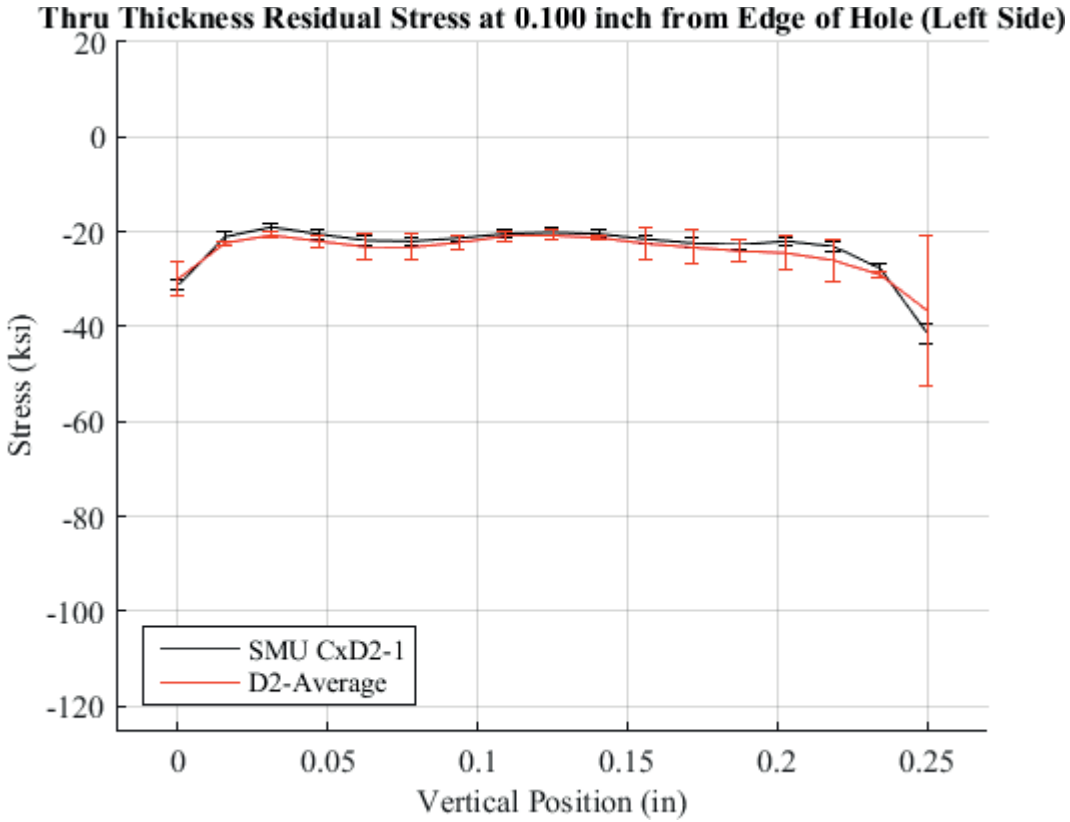

Fig. 190 Residual Stress Line Plot Comparing the CxD2-1 Single Measurement Average Residual Stress with its Associated Total Uncertainty as Error Bars (in Red) to the CxD2 Average Residual Stress with the Repeatability Uncertainty as Error Bars (in Black) at 0.10 inch from the Left Edge of the Hole – Stress Scale Locked.

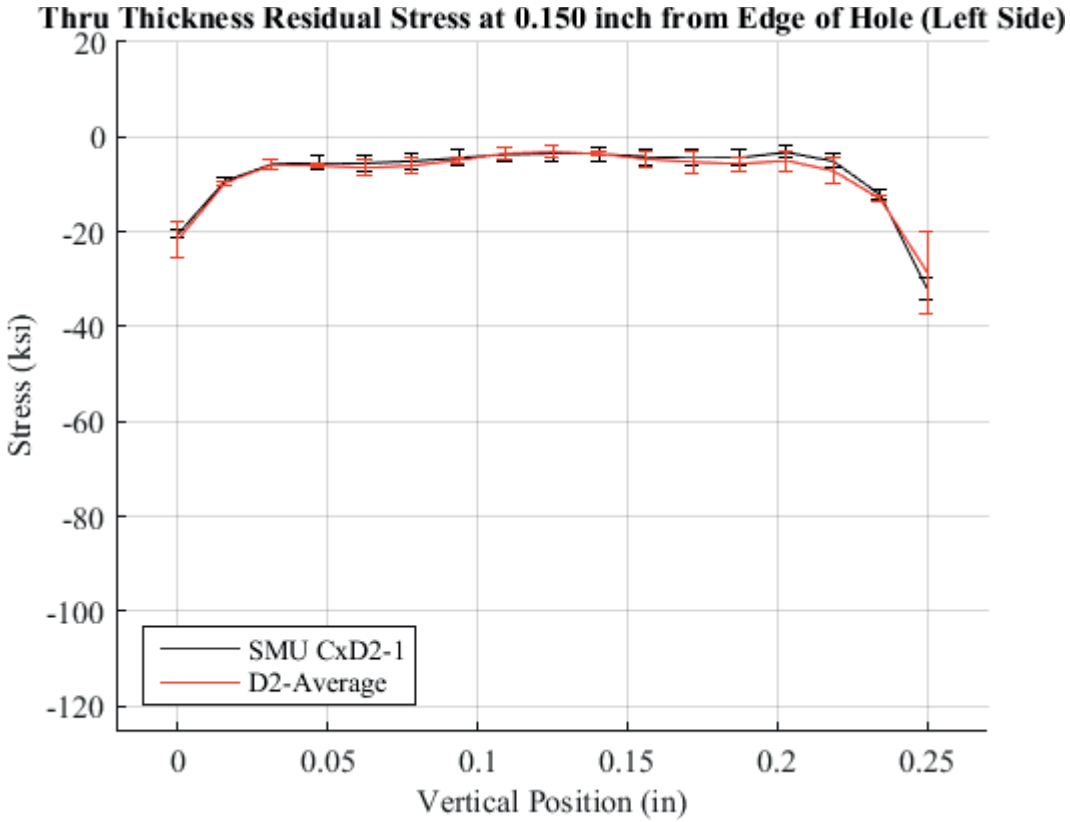

Fig. 191 Residual Stress Line Plot Comparing the CxD2-1 Single Measurement Average Residual Stress with its Associated Total Uncertainty as Error Bars (in Red) to the CxD2 Average Residual Stress with the Repeatability Uncertainty as Error Bars (in Black) at 0.150 inch from the Left Edge of the Hole – Stress Scale Locked.

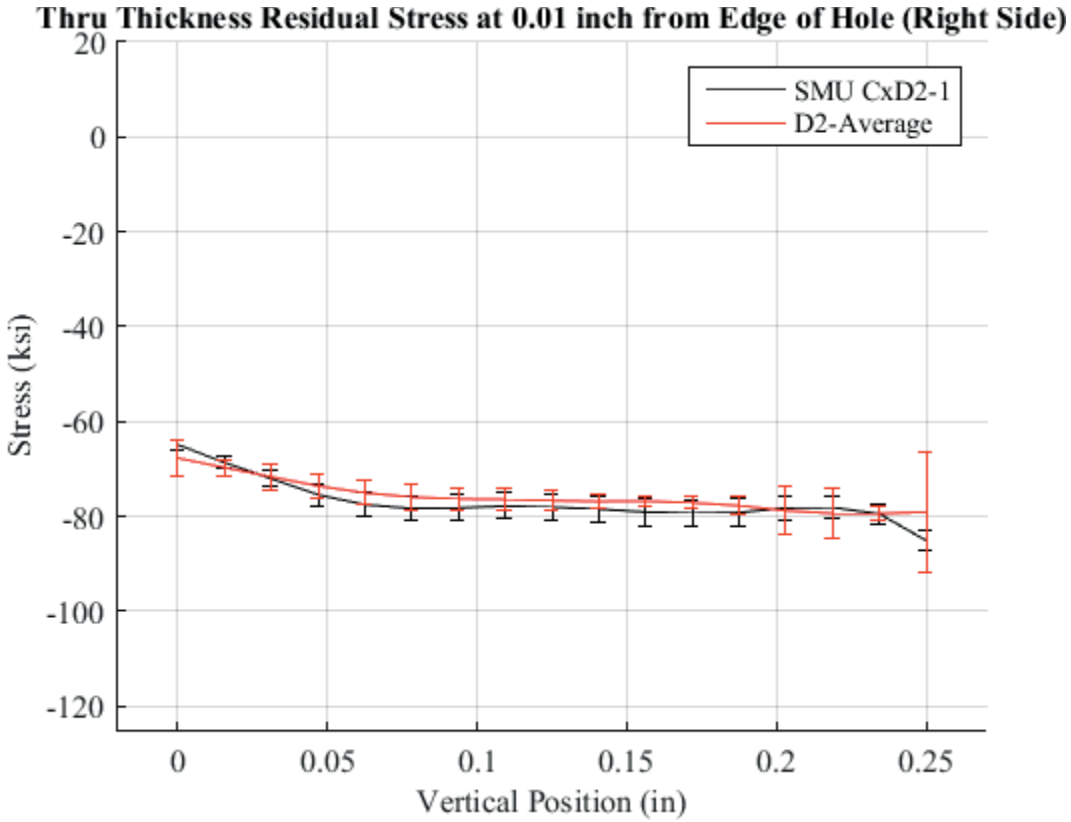

Fig. 192 Residual Stress Line Plot Comparing the CxD2-1 Single Measurement Average Residual Stress with its Associated Total Uncertainty as Error Bars (in Red) to the CxD2 Average Residual Stress with the Repeatability Uncertainty as Error Bars (in Black) at 0.01 inch from the Right Edge of the Hole – Stress Scale Locked.

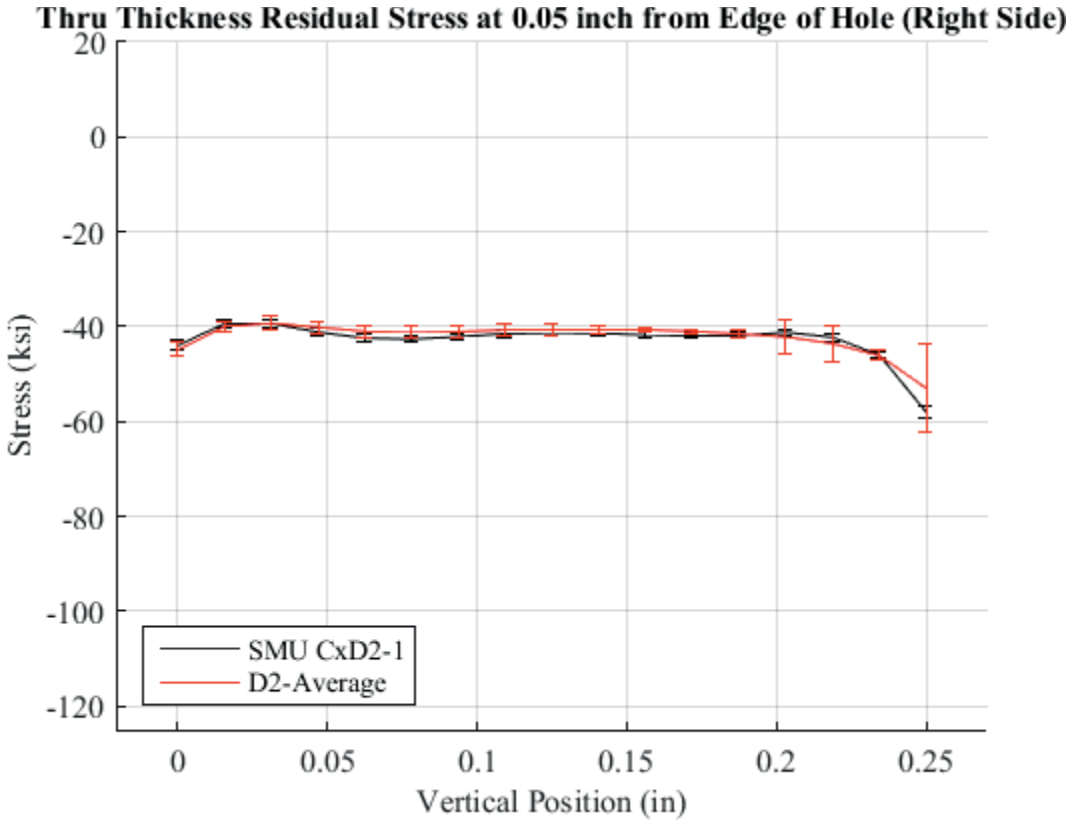

Fig. 193 Residual Stress Line Plot Comparing the CxD2-1 Single Measurement Average Residual Stress with its Associated Total Uncertainty as Error Bars (in Red) to the CxD2 Average Residual Stress with the Repeatability Uncertainty as Error Bars (in Black) at 0.05 inch from the Right Edge of the Hole – Stress Scale Locked.

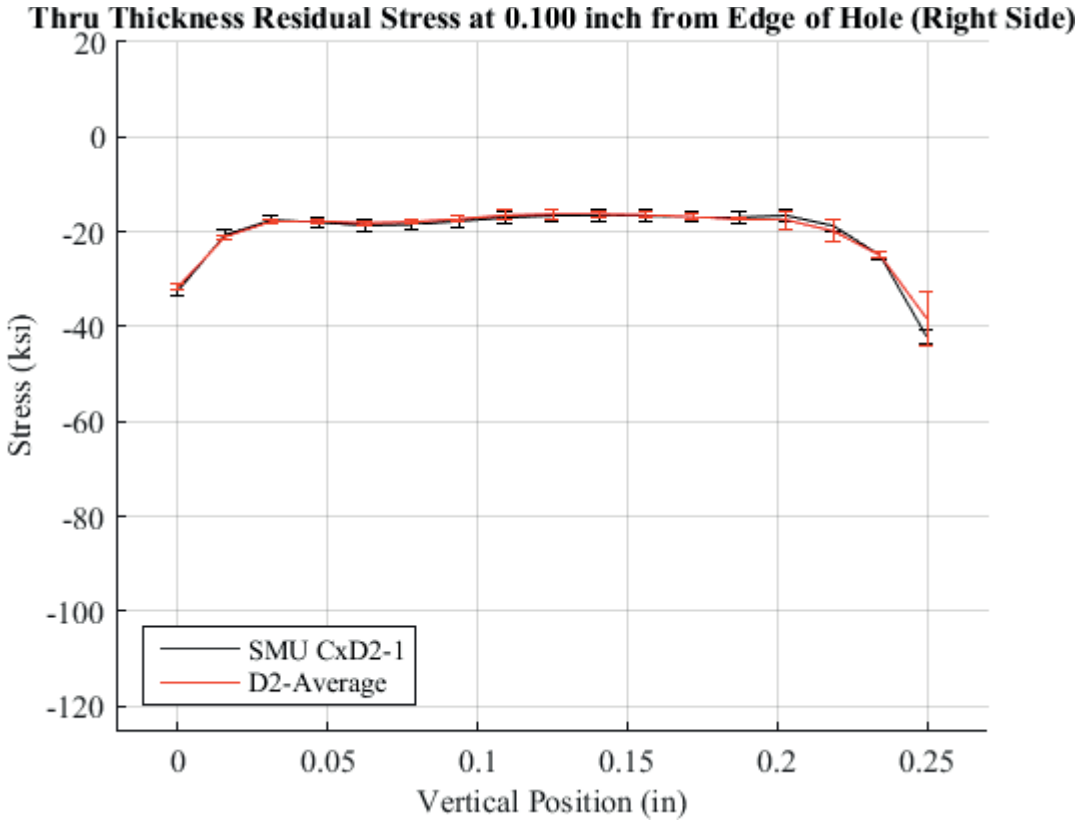

Fig. 194 Residual Stress Line Plot Comparing the CxD2-1 Single Measurement Average Residual Stress with its Associated Total Uncertainty as Error Bars (in Red) to the CxD2 Average Residual Stress with the Repeatability Uncertainty as Error Bars (in Black) at 0.10 inch from the Right Edge of the Hole – Stress Scale Locked.

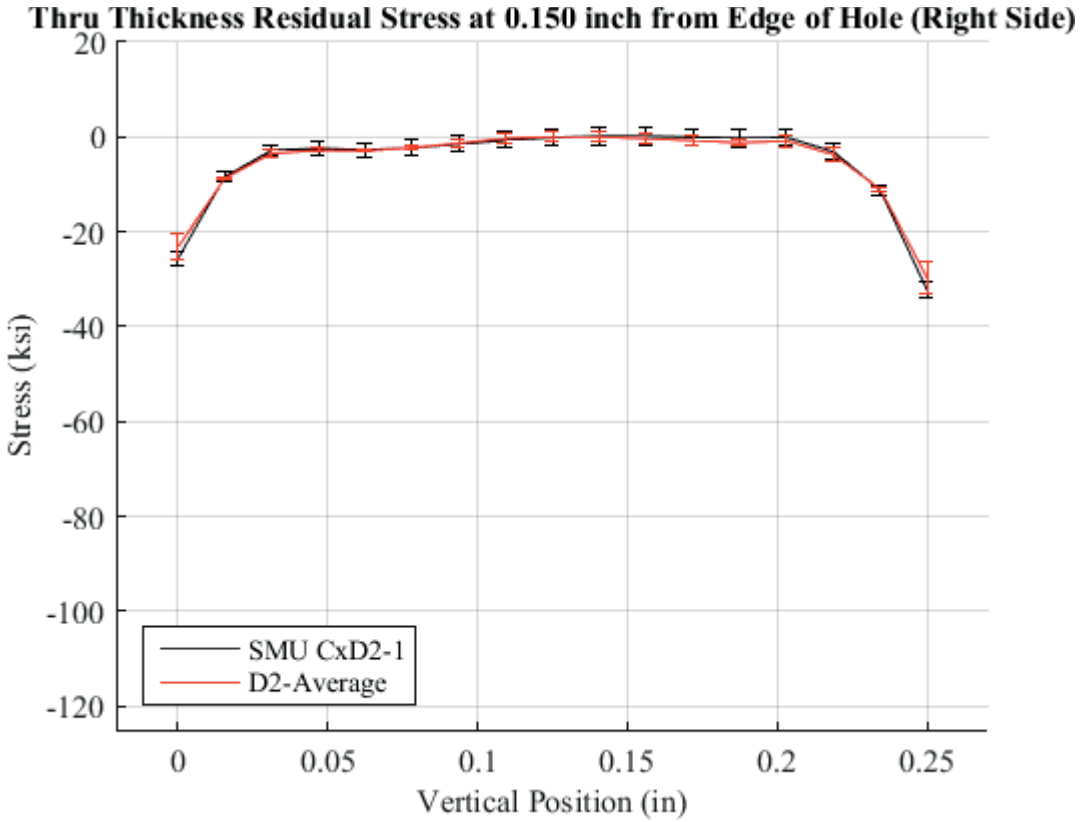

Fig. 195 Residual Stress Line Plot Comparing the CxD2-1 Single Measurement Average Residual Stress with its Associated Total Uncertainty as Error Bars (in Red) to the CxD2 Average Residual Stress with the Repeatability Uncertainty as Error Bars (in Black) at 0.150 inch from the Right Edge of the Hole – Stress Scale Locked.

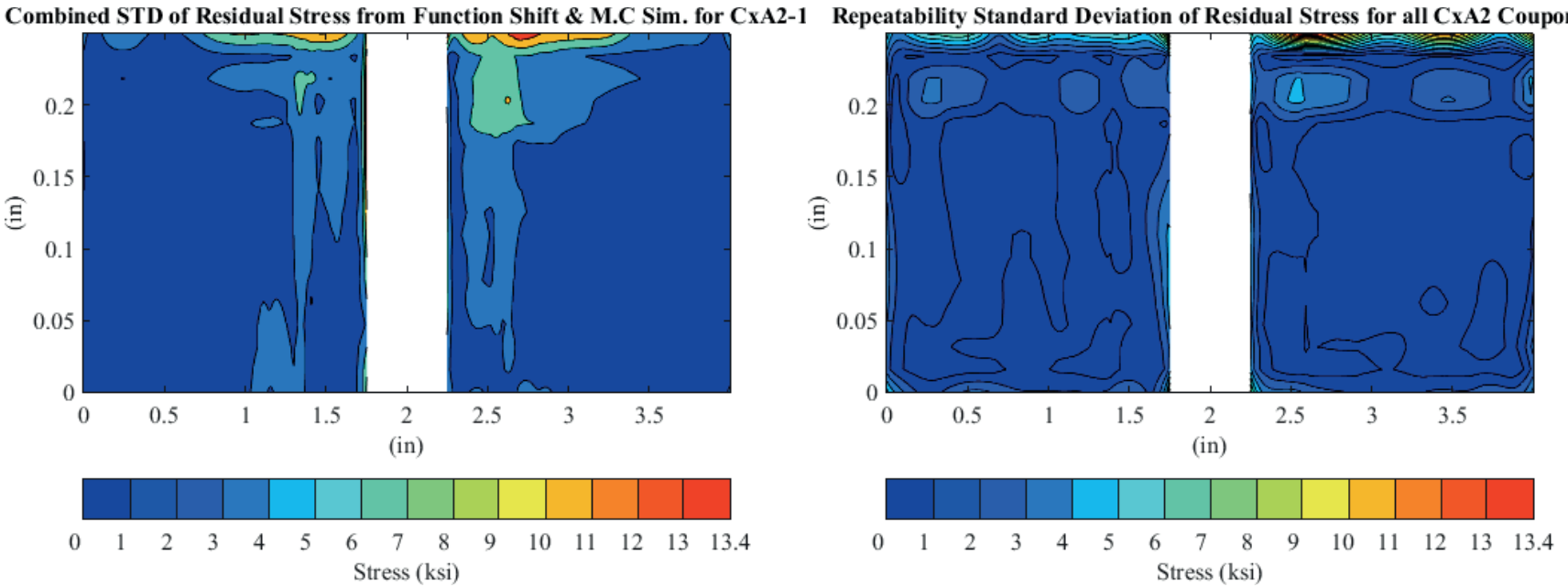

Fig. 196 Comparison of Single Measurement Uncertainty Contour Plot (Left Plot) for CxA2-1 (2024-T351) and the Repeatability Uncertainty Contour Plot (Right Plot) for all of the CxA2 (2024-T351) Coupon Replicates.

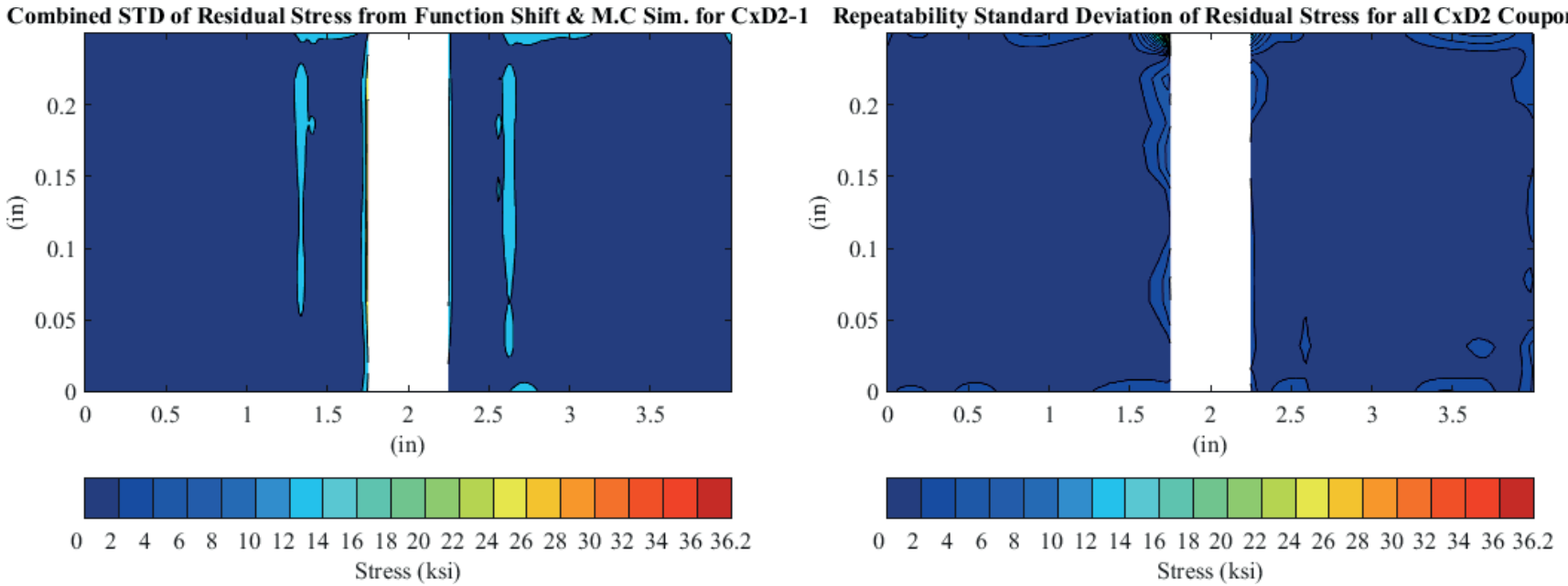

Fig. 197 Comparison of Single Measurement Uncertainty Contour Plot (Left Plot) for CxD2-1 (7075-T651) and the Repeatability Uncertainty Contour Plot (Right Plot) for all of the CxD2 (7075-T651) Coupon Replicates.

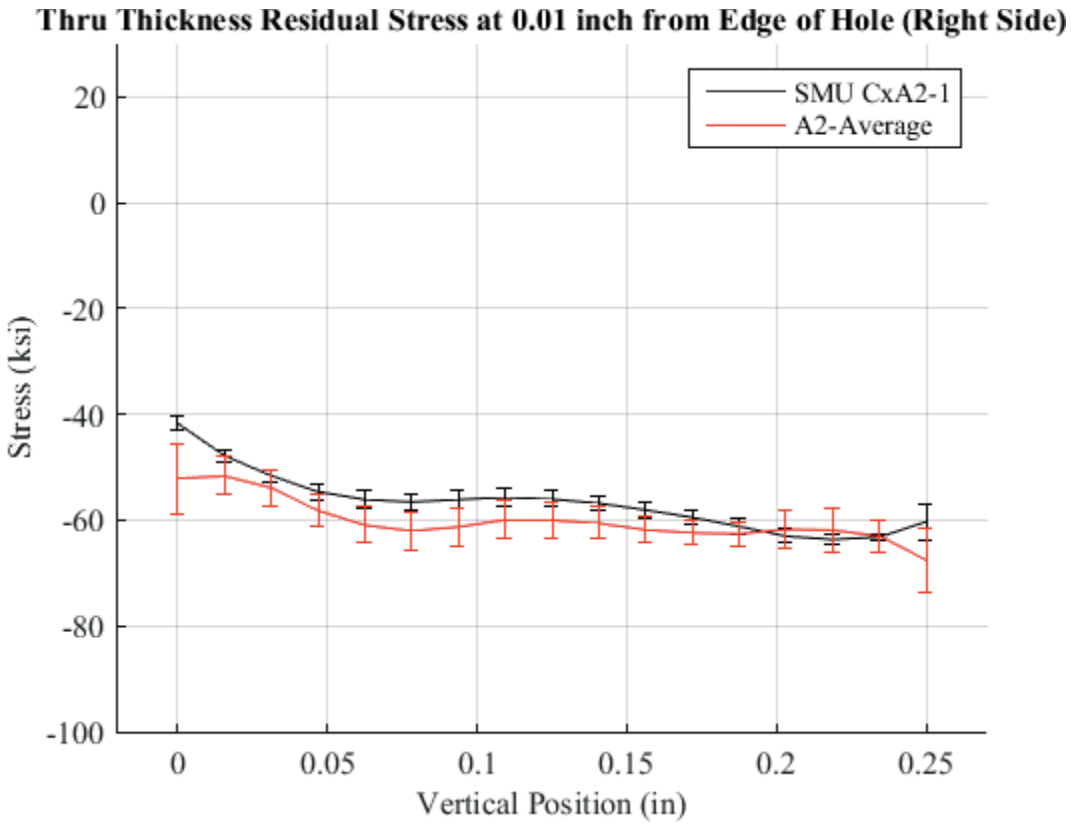

Fig. 198 Line Plot of Residual Stress Through the Thickness at 0.01 inch from the Right Side of the Hole for CxA2-1 Showing the Total Single Measurement Uncertainty Applied to the Average Stress Produced by the Five Knot Densities used as Compared to the CxA2 Repeatability Uncertainty as Applied to the Average Stress.

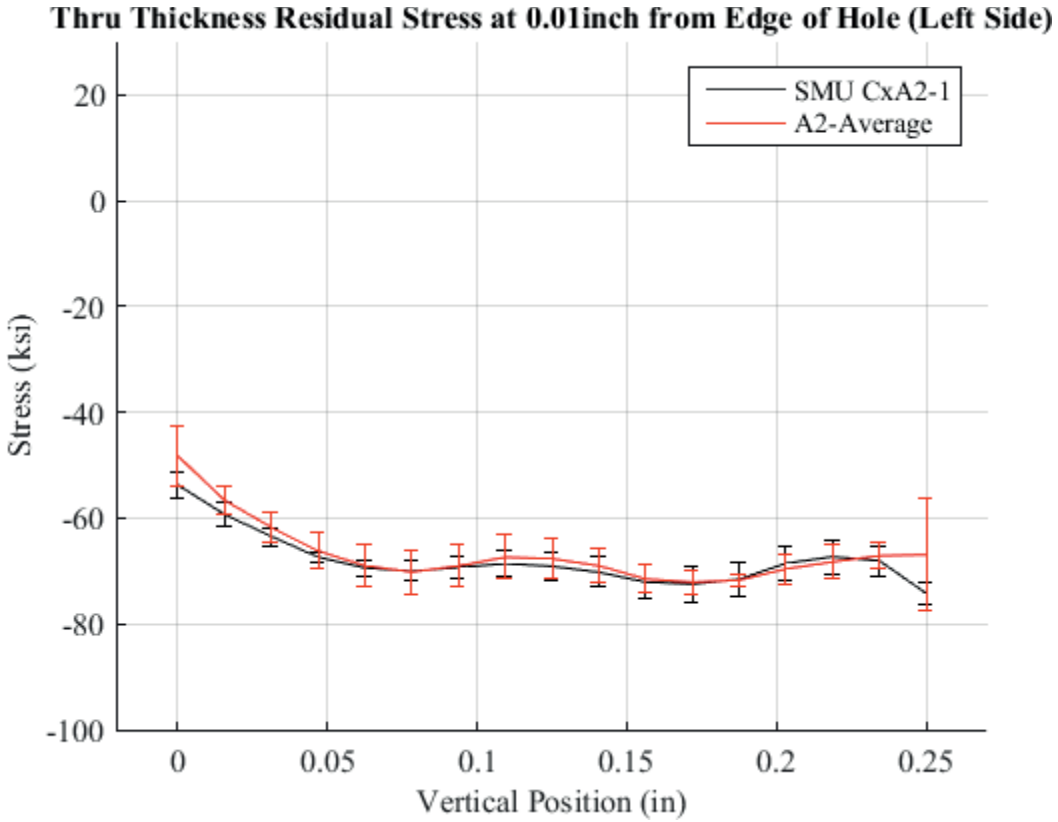

Fig. 199 Line Plot of Residual Stress Through the Thickness at 0.01 inch from the Left Side of the Hole for CxA2-1 Showing the Total Single Measurement Uncertainty Applied to the Average Stress Produced by the Five Knot Densities used as Compared to the CxA2 Repeatability Uncertainty as Applied to the Average Stress.

5 DEVELOPMENT OF FATIGUE-CRACKED COLD EXPANDED COUPONS FOR RESIDUAL STRESS DETERMINATION

5.1 Fabrication of Fatigue-Cracked Cold Expanded Residual Stress Coupons

An additional set of sixteen coupons were fabricated, eight both 2024-T351 and an additional eight 7075-T651 aluminum. These coupons were not fabricated out of the same lot of material from which the CxA2 (2024-T351) and CxD2 (7075-T651) were manufactured. For these experiments, it was assumed that the lot-to-lot variability was not statistically significant. The material certifications for both sets of materials are provided in Fig. 200 through Fig. 202. A comparison of the material properties for these Cx4N1 coupons, as compared to that defined within MMPDS-06 can be found within Table 4.[113,114]

As can be seen from Table 4, the values provided from the material specifications exceed that of the A-basis values for both the baseline, uncracked and the fatigue-cracked coupons. This is to be expected due to the statistical nature of the these MMPDS values.[126] It was determined that even though the values of the material specifications exceeded that defined within MMPDS, the conservative MMPDS values would be used for all analysis.

For these coupons, a new naming convention was developed because it was part of a larger test and residual stress determination program. For all of the coupons the first

three digits are Cx4N1. The next two are related to the crack length that was developed in them, followed by either a B or a D to delineate the specific alloy, 2024-T351 or 7075-T651, respectively. Therefore, the coupon condition will be defined within the text, Cx4N1-XX-B or Cx4N1-XX-D.

All sixteen of the coupons were developed and manufactured the same way. For these coupons, the same process was used to Cx each of the holes as was done for the CxA2 (2024-T351) and CxD2 (7075-T651) coupons. The same precision-ground Cx mandrels (maximum mandrel diameter of 0.4684 inch) were used for all of the Cx4N1 coupons, with same initial hole diameter and final ream size as was used for the CxA2 (2024-T351) and CxD2 (7075-T651) coupons. This would ensure that the Cx levels would be as close to the CxA2 (2024-T351) and CxD2 (7075-T651) coupons as possible.

Drawings for these coupons were broken into three parts. The first drawing was to define the initial hole size, the second defined the final ream, and the third was to cut the fatigue coupon down to a size more convenient for the contour method. The final ream process was performed after the coupon was precracked; after the surface crack reached the required length the coupons were cut down to only 5.00±0.02 inch. The drawings for the Cx4N1-XX-B (2024-T351) and Cx4N1-XX-D (7075-T651) coupons are provided in Fig. 203 through Fig. 206.

5.2 Cold Expansion Procedure for Fatigue-Cracked Cold Expanded Residual Stress Coupons

For all of the Cx4N1 coupons the same procedure was used to Cx the coupons. First the coupon blanks were prepared by a machine shop. Next the initial hole diameter was placed in the coupon using standard drill bits and final reamed using custom reamers

to provide a hole that met the drawing pre-Cx hole diameter of 0.4770±0.0005 inch. The hole then was deburred by hand using Scotch-Brite pads. This was done to help to ensure that the hole corner was as square as possible.[56] The hole diameter then was measured using a Nikon MM-60 measuring microscope and the hole diameter was documented to $1.96x10^{-5}$ inch (0.5 micron) precision.[127] The hole then was cleaned in preparation for the cold expansion process. The hole then was Cxed following the standard FTI split sleeve procedure, with the split sleeve orientated at the top of the hole (12 o'clock position). The mandrel entrance face was annotated on the coupon. The coupon's mandrel entrance and exit surfaces were then polished using multiple grits and finally a diamond slurry was used to get the final surface to an almost mirror finish. This was performed to help assist in crack detection via traveling microscope.[54] Fig. 207 provides an image of the coupon configuration for fatigue crack development. Tabs also were bonded to the coupons to help prevent premature failure of the coupons due to the test machine grips.[72]

5.3 Precracking Procedure for Fatigue-Cracked Cold Expanded Residual Stress Coupons

After the coupons were Cxed and the surfaces polished, a starter notch was introduced on the right side of the Cx mandrel entrance, as shown Fig. 207. This starter notch was made using a jeweler's saw, which produced a notch on the order of 0.01 inch – 0.015 inch symmetric corner cut in the material with a dimension of 0.009 inch wide. From this corner notch, the coupons were placed in a 55 kip MTS frame that was controlled by a MTS FlexTest 40 controller using Multipurpose TestWare. All testing, pre-cracking and fatigue crack growth was performed at the Analytical Processes Engineered Solutions (AP/ES) test facility in St. Louis, Mo. The facility where these

coupons were tested had relative humidity of <40% (air conditioned) and a temperature that was held at approximately 75-deg. F. The frequency of all testing was performed at 8 Hz. All crack lengths were monitored via optical traveling microscopes.

Precracking was performed at 25 ksi for the 2024-T351 coupons and at 26.5 ksi for the 7075-T651 coupons, with a Stress Ratio (R) of 0.1. Each of the coupons developed cracks from the jeweler's saw, at the mandrel entrance surface, on the right side of the hole. Once the crack was formed from the jeweler's saw it was monitored both along the right side of the entrance surface and down the bore on the right side. Cracks were allowed to propagate approximately 0.029 inch from the edge of the starter notch, which would give them a surface crack length of approximately 0.0465 inch. This surface length would allow for a final fatigue crack to be present in the coupon of between 0.030 – 0.040 inch at the surface when the final ream of 0.5000 ± 0.0002 inch per Fig. 204 and Fig. 206. A process flow for this is shown in Fig. 208.

The bore crack length was not required to match the surface crack length and often due to crack growth aspect ratio the bore crack length would be longer than the surface.[128,129,130,131] An image of coupon Cx4N1-10-B in the post precracked, final ream condition is shown in Fig. 209.

5.4 Propagation of Fatigue Cracks in Cold Expanded Residual Stress Coupons

The main purpose of this research program was to determine if the presence of a fatigue crack has an influence on the residual stress field produced by the Cx process, within two common aerospace aluminum alloy systems. The contour method was chosen as the method by which this determination would be made. In order to answer this

question a series of baseline non cracked, Cxed coupons were produced and the residual stresses within those coupons was determined via the contour method. These residual stresses would provide a statistical representation of the residual stress fields at the Cx hole, and allow for a comparison to the fatigue-cracked coupons.

Fatigue-cracked, Cxed coupons were developed with a range of crack lengths on the entrance, right side of the hole. Replicates of some of the fatigue-cracked conditions were produced. Coupon information for each of the Cx4N1-XX-B (2024-T351) coupons is provided in Table 5, with the Cx4N1-XX-D (7075-T651) provided in Table 6. All of the Cx4N1-XX-B (2024-T351) coupons were tested at a Stress Ratio (R) of 0.1 at a stress level of 25 ksi. The Cx4N1-XX-D (7075-T651) coupons were tested at the same (R), but at 26.5 ksi. All of the same lab conditions were held as when the precracking was performed, and the same equipment was used. The surface crack lengths were tracked using the same optical techniques as defined for precracking.

Through the fatigue testing, fatigue cracks were formed and propagated to the surface lengths defined within Table 7 and Table 8.

5.5 Surface Fatigue Cracks Morphology in Cold Expanded Residual Stress Coupons

Images were taken of the final surface crack for each of the coupons using a Nikon MM-60 measuring microscope. The Nikon MM-60 microscope is mounted to a stage that has a positional accuracy of 1.96×10^{-5} inch (0.5 micron) and has a magnification range from 50x to 1000x.[127] These images would aid in the definition of a plane upon which each of the coupons would later be cut for residual stress determination. Images of each of the Cx4N1-XX-B (2024-T351) coupons is provided

Fig. 210 through Fig. 217.

The Cx4N1-XX-D (7075-T651) coupons also were documented and the images of the surface cracks associated with them are provided in Fig. 218 through Fig. 225.

5.5.1 Conclusions from Surface Crack Morphology Images at Cold Expanded Holes in 2024-T351 and 7075-T651

From the images taken of the surface crack morphology it was possible to determine that for both of the aluminum alloy systems the crack grew in a fairly planar manner from the initial, post ream crack size of approximately 0.03 inch, through 0.125 inch, as seen in Fig. 214 and Fig. 215 for 2024-T351 and in Fig. 222 and Fig. 223 for 7075-T651. After the crack passed a surface crack length of 0.125 inch the crack began to become much more torturous. This can be seen in the 2024-T351 material in Fig. 216 and in the 7075-T651 alloy in Fig. 224. By the time the surface crack reached a surface length approximately 0.50 inch the cracks had transitioned to a new plane. This made it difficult to determine the appropriate cutting plane for the residual stress determination via the contour method. It was decided to cut each coupon through the center of the hole, hoping to be able to capture the effect of the crack for both smaller cracks and those that had transitioned to larger through cracks.

5.6 Final Machining of Fatigue-Cracked Cold Expanded Coupons Down to Size for Contour Method Processing

After each of the Cx4N1 coupons, both 2024-T351 and 7075-T651, reached the defined mandrel surface crack length they were cut down to a more manageable size for residual stress determination via the contour method. The residual stress coupons were

cut down per the coupon drawings in Fig. 226 and Fig. 227. After each coupon was cut down they were individually packaged to protect them from damage during transport to Hill Engineering, LLC. in Sacramento, California, where they were cut along the fatigue crack plan, and had the plane of interest measured for data processing via the contour method process developed to determine the residual stresses within the Baseline A2 (2024-T351) and D2 (7075-T651) coupon configuration.

Table 4: Comparison of Material Properties of Cx4N1 and Baseline CxA2 (2024-T351) CxD2 (7075-T651) Coupons versus MMPDS-06

	Average Values per Material Spec Sheet for Cx4N1 Coupons (Rounded)			Average Values per Material Spec Sheet for Baseline Coupons			A-Basis Values per MMPDS - 06		
	Ftu (ksi)	Fty (ksi)	E	Ftu (ksi)	Fty (ksi)	E	Ftu (ksi)	Fty (ksi)	E
2024-T351	69	48	18	69	48	18	64	48	10.7
7075-T651	86	77	12	86	76	11	77	69	10.3

KAISER ALUMINUM
FABRICATED PRODUCTS

Built in Class

CERTIFIED TEST REPORT
http://Online.KaiserAluminum.com

Kaiser Aluminum
Trentwood Works
Spokane, WA 99215-5108
(800) 367-2586

CUSTOMER PO NUMBER:	WORK PACKAGE:	CUSTOMER PART NUMBER:	PRODUCT DESCRIPTION:		
5400242076-10		ALFLR00822-60.5	Sawed Plate		
KAISER ORDER NUMBER:	LINE ITEM:	SHIP DATE:	ALLOY:	CLAD:	TEMPER:
1186765	1	03/16/2015	2024	BARE	T351
WEIGHT SHIPPED:	QUANTITY:	B/L NUMBER:	GAUGE:	WIDTH:	LENGTH:
4328 LB	19 PCS EST.	2052891	0.2500 IN	60.500 IN	144.500 IN

SHIP TO:	SOLD TO:
COPPER & BRASS SALES 5450 EAST HOME FRESNO, CA 93727 US	COPPER & BRASS SALES ATTN: ACCOUNTS PAYABLE P.O. Box 5116 SOUTHFIELD, MI 48086 US

MHU 1874823: LOT 121983B1: 19 pieces

Certified Specifications

AMS 4037/RevQ AMS-QQ-A-250/4/RevB ASTM B 209/Rev14

Test Code: 1504

Test Results:

LOT: 121983B1 CAST: 750 DROP: 14 INGOT: 4

Melted in USA
(ASTM E8/E557)
(EN 2002-1)

Tensile: Temper	Dir/#Tests	Ultimate KSI (MPA)	Yield KSI (MPA)	Elongation %
T351	LT / 02 (Min:Max)	69.2 : 69.2 (477 : 477)	47.3 : 47.6 (326 : 328)	17.3 : 17.8

(ASTM E1251)

Chemistry:	SI	FE	CU	MN	MG	CR	ZN	TI	V	ZR		OTHER
Actual	0.07	0.17	4.5	0.54	1.4	0.01	0.12	0.01	0.01	0.00	TOT	0.04

Chemistry:		SI	FE	CU	MN	MG	CR	ZN	TI	V	ZR		OTHER
2024	MIN	0.00	0.00	3.8	0.30	1.2	0.00	0.00	0.00	0.00	0.00	MAX	0.05
	MAX	0.50	0.50	4.9	0.9	1.8	0.10	0.25	0.15	0.05	0.05	TOT	0.15

Aluminum Remainder

Plant Serial: 4368263
Kaiser Order Number: 1186765
Line Item: 1

Page 1 of 2

From: ThyssenKrupp Materials NA
Cust. ONLINE METALS - TX Del.: 2403776145
CstAr 7859 CstOr 39106
Wgt.: 227.789 LB Date 03/31/2015

John R. Gaskotte

Fig. 200 Material Certification for 2024-T351 Aluminum Alloy Used for all Fatigue-Cracked, Cxed Coupons.

AMAG
ROLLING

Abnahmeprüfzeugnis 3.1 (EN 10204)
Inspection certificate - mill certificate

Nr.: 85198008 01 / 1
Rev.: 0
Seite / page: 1 von / of 2
Datum / date: 2014 08 06

Zertifiziert nach / certified to ISO 9001, ISO/TS 16949, EN/AS 9100, ISO 14001, NADCAP

Auftraggeber / customer: ThyssenKrupp Materials NA, Inc. ThyssenKrupp Steel Services 22355 W 11 Mile Road SOUTHFIELD MI 48033 USA	Bestell Nr. / order no.: 5400221439-R01
	Datum / date: 2014 04 21
	Auftragsbest. Nr. / order confirm no.: 674962
	Datum / date: 2014 04 22
Warenempfänger / consignee: ThyssenKrupp Materials NA Copper and Brass Sales Division 1137 Atlanta Ind Dr MARIETTA GA 30066-6604 USA	Lieferschein Nr. / delivery note: 85198008
	Datum / date: 2014 08 29

Produkt / product	Bedingungen / terms
Form / form: Plate, stretched Werkstoff / material: 7075 Zustand / temper: T651 Dim. / dim.: [inch]: 0,250x48,50x144,50 Kundenartikel Nr. / cust. article no.: ALFLR00983	Technische Lieferbedingungen / techn. spec.: AMS-QQ-A-250/12, 04.2007 ASTM B 209 - 10 AMS 4045K, 12.2010 Sondervorschrift / special terms:

AB-Pos. ord.-Item.	BNr/Los/Teilios Lot/No./Part	Guss Nr. cast no.	Werkstoff material	Kollo packno.	Gewicht netto weight net	Stk. pcs.
01	70721/01/00	01/0063785/4	7075	6749620004	2167,106 lbs	12
01	70721/01/00	01/0063785/4	7075	6749620006	2164,903 lbs	12

Chemische Zusammensetzung ([%] Gewichtsanteile) / Chemical composition ([%] weight proportion (OES))

Guss Nr. / cast no.	material		Si	Fe	Cu	Mn	Mg	Cr	Zn	Ti	Ti+ Zr	Others Each
01/0063785/4	7075	spec. min.	-	-	1,2	-	2,1	0,18	5,1	-	-	-
		spec. max.	0,40	0,50	2,0	0,30	2,9	0,28	6,1	0,20	0,25	0,05
		actual	0,07	0,13	1,3	0,02	2,6	0,18	5,8	0,04	0,05	0,02
		Others Total										
		spec. min.	-									
		spec. max.	0,15									
		actual	0,03									

Fig. 201 Material Certification for 7075-T651 Aluminum Alloy Used for all Fatigue-Cracked, Cxed Coupons, pg. 1.

AMAG
ROLLING

Abnahmeprüfzeugnis 3.1 (EN 10204)
Inspection certificate - mill certificate

Nr.: 85198008 01 / 1
Rev.: 0
Seite / page: 2 von / of 2
Datum / date: 2014 08 06

Zertifiziert nach / certified to ISO 9001, ISO/TS 16949, EN/MS 9100, ISO 14001, NADCAP

Zugprüfung LT / tensile-test LT

BN/Los	Zustand	Richtung	Tests		UTS	YS	A2"			
Lot/No.	temper	direction			[ksi]	[ksi]	[%]			
				spec.min.	78,0	67,0	9			
				spec.max.	-	-	-			
70721/01	T651	LT	11	from	85,3	76,4	10			
70721/01	T651	LT		to	86,0	77,6	13			

Sonstige Prüfungen / other tests

Maßkontrolle: OK. / Dimensional Check: OK.
Oberfläche: OK. / Surface inspection: OK.

Bemerkungen / notes

Gegossen und gefertigt in Österreich / Country of melt and manufactured in Austria

Es wird bestätigt, dass die Lieferung geprüft wurde und den Vereinbarungen bei der Bestellung entspricht.
We hereby certify that the material described above has been tested and complies with the terms of the order contract.

Werksachverständiger / factory specialist	E-Mail / e-mail
Josef Klampfer	josef.klampfer@amag.at

Herstellerland: Österreich / goods origin: The goods are of Austrian origin.
Maschinell erstellt - Gültig ohne Unterschrift / Automated - valid without being signed.

Fig. 202 Material Certification for 7075-T651 Aluminum Alloy Used for all Fatigue-Cracked, Cxed Coupons, pg. 2.

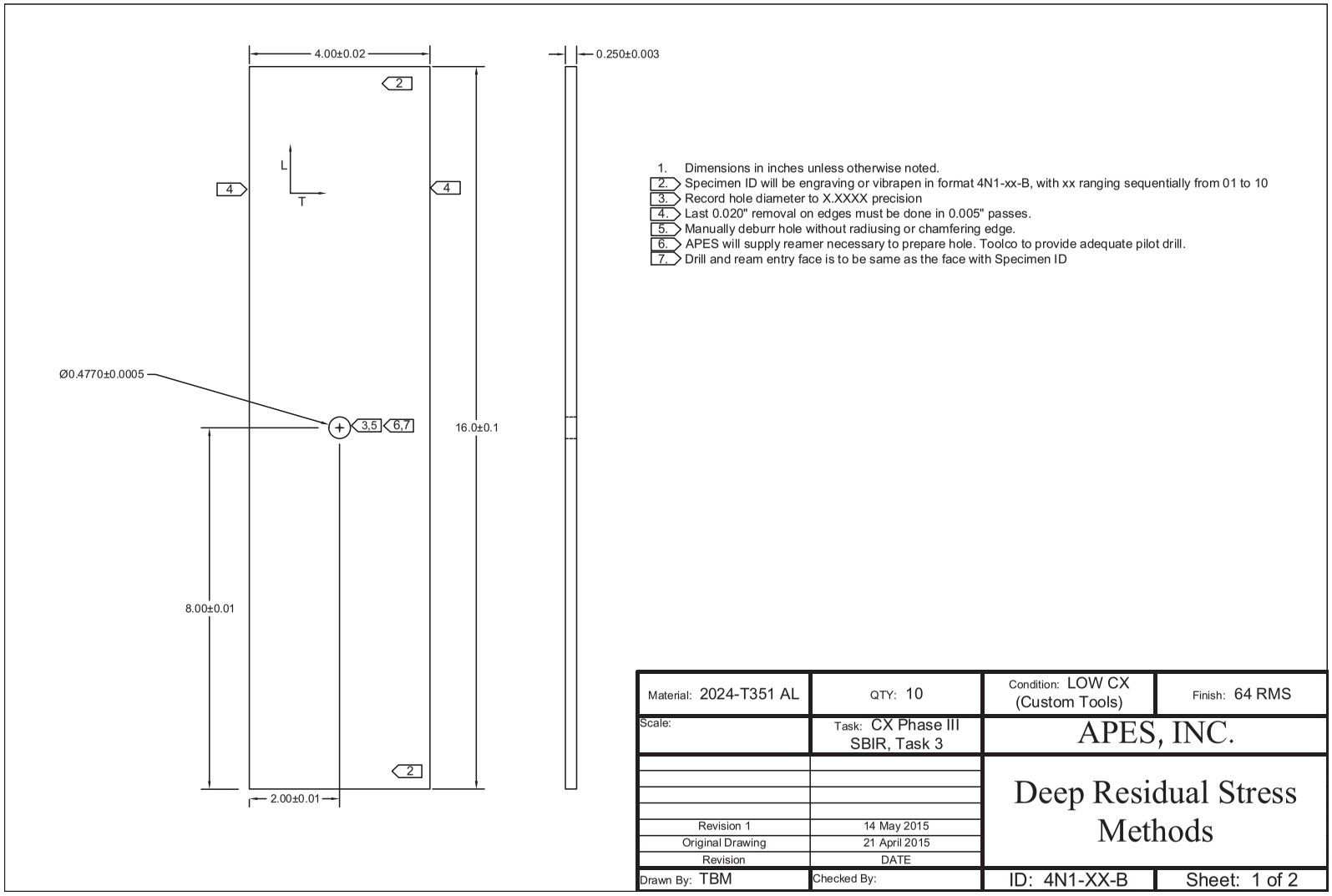

Fig. 203 Manufacturing Drawing for Cx4N1-XX-B (2024-T351) Coupons Defining Initial Hole Size for Specific Applied Expansion Level.

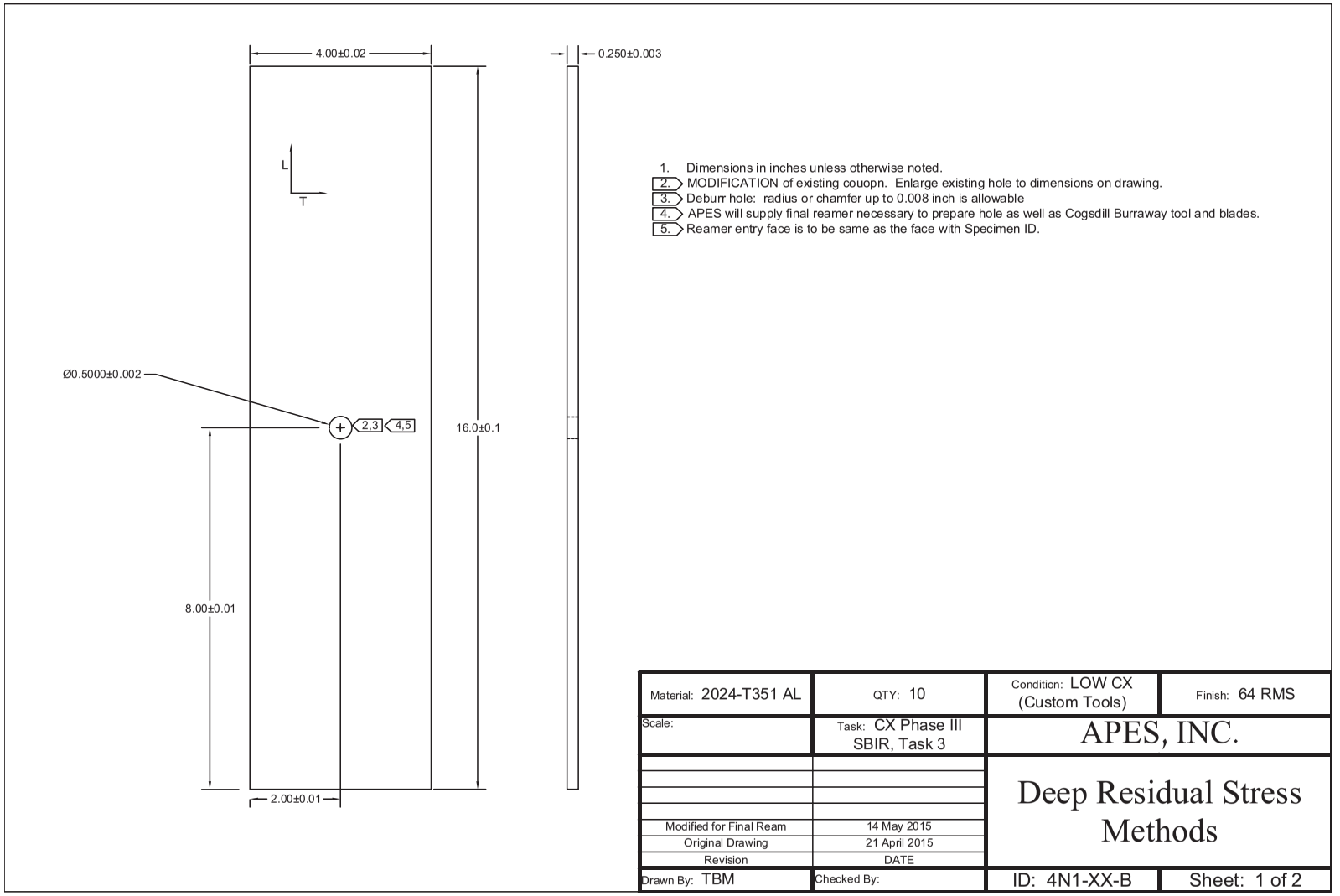

Fig. 204 Manufacturing Drawing for Cx4N1-XX-B (2024-T351) Coupons Defining Final Ream Diameter and Deburring Process.

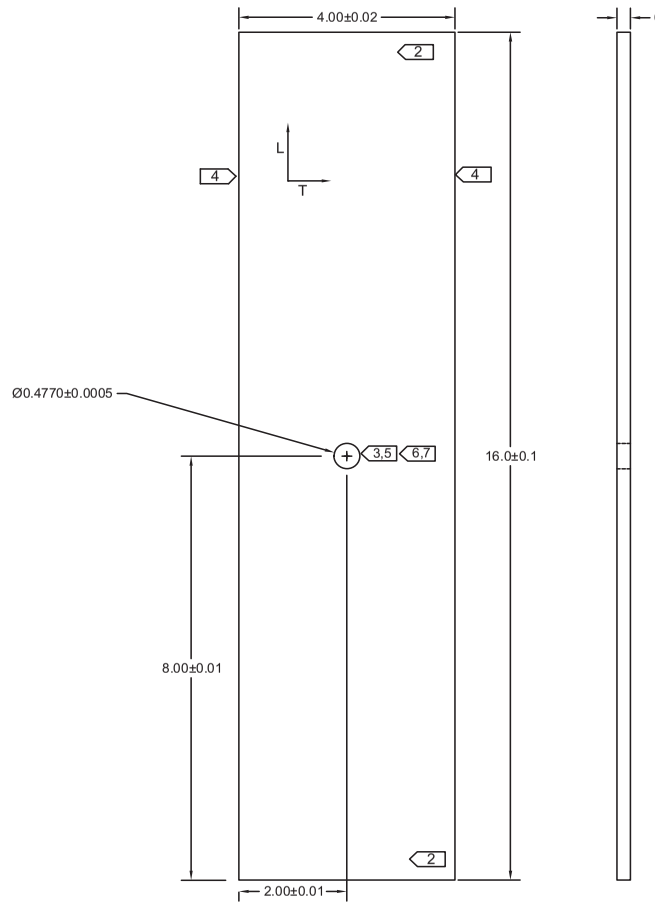

1. Dimensions in inches unless otherwise noted.
2. Specimen ID will be engraving or vibrapen in format 4N1-XX-D, with XX ranging sequentially from 01 to 10
3. Record hole diameter to X.XXXX precision
4. Last 0.020" removal on edges must be done in 0.005" passes.
5. Manually deburr hole without radiusing or chamfering edge.
6. APES will supply reamer necessary to prepare hole. Toolco to provide adequate pilot drill.
7. Drill and ream entry face is to be same as the face with Specimen ID

Material: 7075-T651 AL	QTY: 10	Condition: LOW CX (Custom Tools)	Finish: 64 RMS
Scale:	Task: CX Phase III SBIR, Task 3	APES, INC.	
		Deep Residual Stress Methods	
Revision 1	14 May 2015		
Original Drawing	21 April 2015		
Revision	DATE		
Drawn By: TBM	Checked By:	ID: 4N1-XX-D	Sheet: 2 of 2

Fig. 205 Manufacturing Drawing for Cx4N1-XX-D (7075-T651) Coupons Defining Initial Hole Size for Specific Applied Expansion Level.

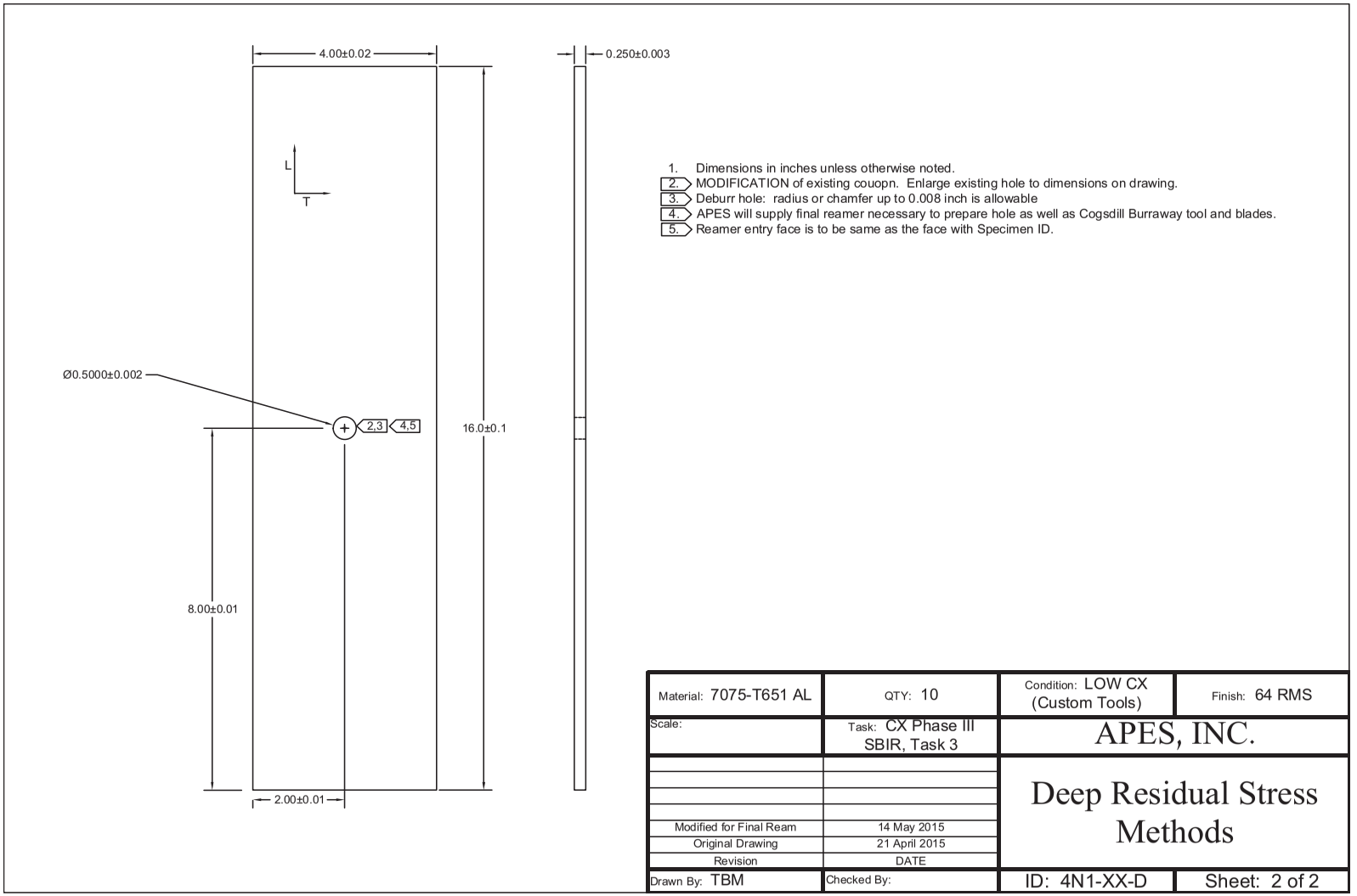

Fig. 206 Manufacturing Drawing for Cx4N1-XX-D (7075-T651) Coupons Defining Final Ream Diameter and Deburring Process.

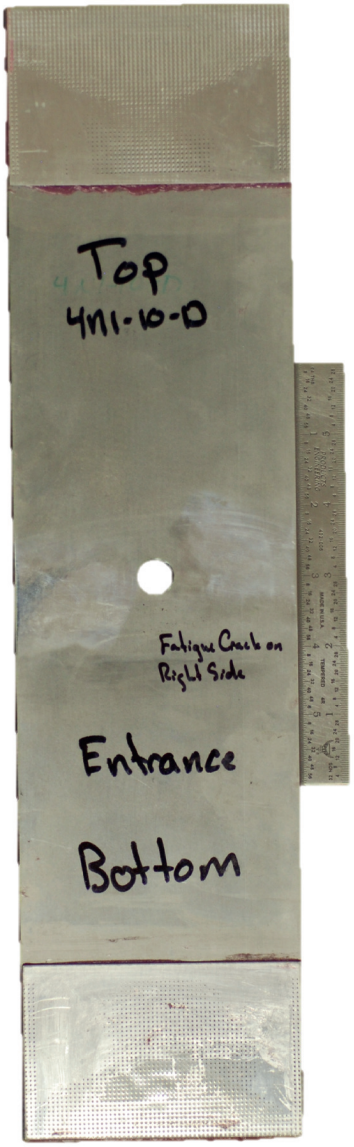

Fig. 207 Image of Coupon Cx4N1-10-D (7075-T651) – Representing the Cx4N1 Fatigue Coupon Configuration Used for Fatigue Crack Development.

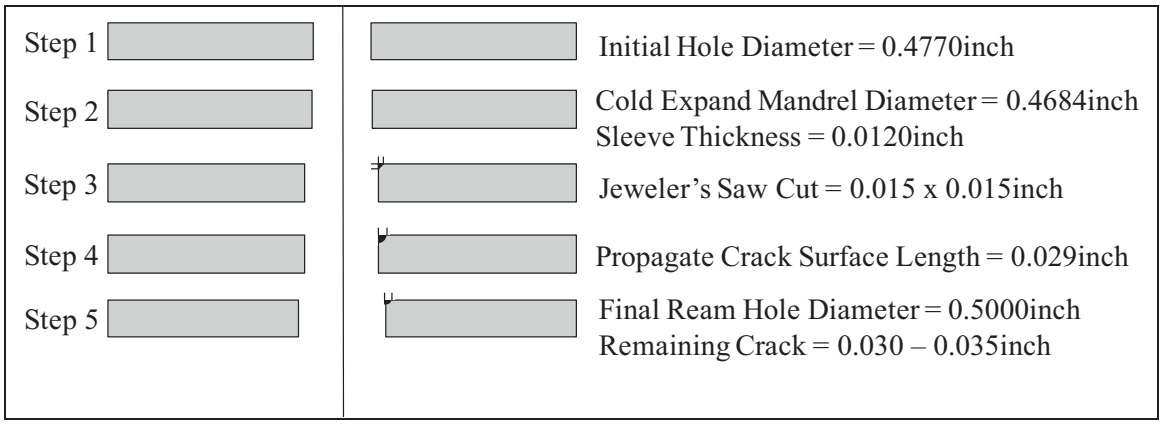

Fig. 208 Process Flow of Coupon Hole Development, Precracking, and Final Ream.

Fig. 209 Image of Coupon Cx4N1-09-B (2024-T351) Which Has Been Precracked and Final Reamed.

Table 5 Coupon Definition and Metrology for Cx4N1-XX-B (2024-T351) Cold Expanded Fatigue Crack Growth and Residual Stress Determination

4N1-XX-B (2024-T351) Coupons						
Specimen ID	**Defined Mandrel Entrance Surface Crack Length (inch)**	**Gauge Width (inch)**	**Material Thickness (inch)**	**Initial Ream Diameter (CMM) (inch)**	**% CX**	**Final Ream Diameter (inch)**
4N1-01-B	0.08	4.0000	0.2545	0.4771	3.23%	0.4990
4N1-02-B		4.0030	0.2550	0.4768	3.29%	0.4997
4N1-03-B	0.1	4.0025	0.2548	0.4772	3.21%	0.4997
4N1-04-B		4.0022	0.2555	0.4771	3.23%	0.4990
4N1-05-B	0.125	4.0027	0.2557	0.4771	3.23%	0.4980
4N1-06-B		4.0023	0.2555	0.4770	3.25%	0.4990
4N1-07-B	0.25	4.0020	0.2555	0.4770	3.25%	0.4995
4N1-08-B	0.5	4.0013	0.2550	0.4770	3.25%	0.4995
AVERAGE		***4.0020***	***0.2552***	***0.4770***	***3.24%***	***0.4992***
STDEV		***0.0009***	***0.0004***	***0.0001***	***0.03%***	***0.0006***

Table 6 Coupon Definition and Metrology for Cx4N1-XX-D (7075-T651) Cold Expanded Fatigue Crack Growth and Residual Stress Determination

4N1-XX-D (7075-T651) Coupons						
Specimen ID	**Defined Mandrel Entrance Surface Crack Length (inch)**	**Gauge Width (inch)**	**Material Thickness (inch)**	**Initial Ream Diameter (CMM) (inch)**	**% CX**	**Final Ream Diameter (inch)**
4N1-01-D	0.08	4.0028	0.2495	0.4766	3.34%	0.4988
4N1-02-D		4.0023	0.2510	0.4768	3.29%	0.4990
4N1-03-D	0.1	4.0017	0.2508	0.4769	3.27%	0.4993
4N1-04-D		4.0015	0.2500	0.4770	3.25%	0.4985
4N1-05-D	0.125	4.0020	0.2505	0.4769	3.27%	0.4992
4N1-06-D		4.0027	0.2507	0.4770	3.25%	0.4980
4N1-07-D	0.25	4.0020	0.2505	0.4767	3.31%	0.4983
4N1-08-D	0.5	4.0022	0.2512	0.4769	3.27%	0.4992
AVERAGE		***4.0021***	***0.2505***	***0.4769***	***3.28%***	***0.4988***
STDEV		***0.0005***	***0.0005***	***0.0001***	***0.03%***	***0.0005***

Table 7 Coupon Definition, Metrology, and Final Surface Crack Length for Cx4N1-XX-B (2024-T351) Cold Expanded Fatigue Crack Growth and Residual Stress Determination

4N1-XX-B (2024-T351) Coupons							
Specimen ID	**Defined Mandrel Entrance Surface Crack Length (inch)**	**Mandrel Entrance Face Crack (inch)**	**Gauge Width (inch)**	**Gauge Thickness (inch)**	**Initial Ream Diameter (CMM) (inch)**	**% CX**	**Final Ream Diameter (inch)**
4N1-01-B	0.08	0.0797	4.0000	0.2545	0.4771	3.23%	0.4990
4N1-02-B		0.0798	4.0030	0.2550	0.4768	3.29%	0.4997
4N1-03-B	0.1	0.0974	4.0025	0.2548	0.4772	3.21%	0.4997
4N1-04-B		0.0962	4.0022	0.2555	0.4771	3.23%	0.4990
4N1-05-B	0.125	0.1259	4.0027	0.2557	0.4771	3.23%	0.4980
4N1-06-B		0.1214	4.0023	0.2555	0.4770	3.25%	0.4990
4N1-07-B	0.25	0.2515	4.0020	0.2555	0.4770	3.25%	0.4995
4N1-08-B	0.5	0.4974	4.0013	0.2550	0.4770	3.25%	0.4995
AVERAGE			***4.0020***	***0.2552***	***0.4770***	***3.24%***	***0.4992***
STDEV			***0.0009***	***0.0004***	***0.0001***	***0.03%***	***0.0006***

Table 8 Coupon Definition, Metrology, and Final Surface Crack Length for Cx4N1-XX-D (7075-T651) Cold Expanded Fatigue Crack Growth and Residual Stress Determination

4N1-XX-D (7075-T651) Coupons							
Specimen ID	**Defined Mandrel Entrance Surface Crack Length (inch)**	**Mandrel Entrance Face Crack (inch)**	**Gauge Width (inch)**	**Gauge Thickness (inch)**	**Initial Ream Diameter (CMM) (inch)**	**% CX**	**Final Ream Diameter (inch)**
4N1-01-D	0.08	0.0793	4.0028	0.2495	0.4766	3.34%	0.4988
4N1-02-D		0.0807	4.0023	0.2510	0.4768	3.29%	0.4990
4N1-03-D	0.1	0.0972	4.0017	0.2508	0.4769	3.27%	0.4993
4N1-04-D		0.1015	4.0015	0.2500	0.4770	3.25%	0.4985
4N1-05-D	0.125	0.1253	4.0020	0.2505	0.4769	3.27%	0.4992
4N1-06-D		0.1235	4.0027	0.2507	0.4770	3.25%	0.4980
4N1-07-D	0.25	0.2505	4.0020	0.2505	0.4767	3.31%	0.4983
4N1-08-D	0.5	0.5017	4.0022	0.2512	0.4769	3.27%	0.4992
AVERAGE			***4.0021***	***0.2505***	***0.4769***	***3.28%***	***0.4988***
STDEV			***0.0005***	***0.0005***	***0.0001***	***0.03%***	***0.0005***

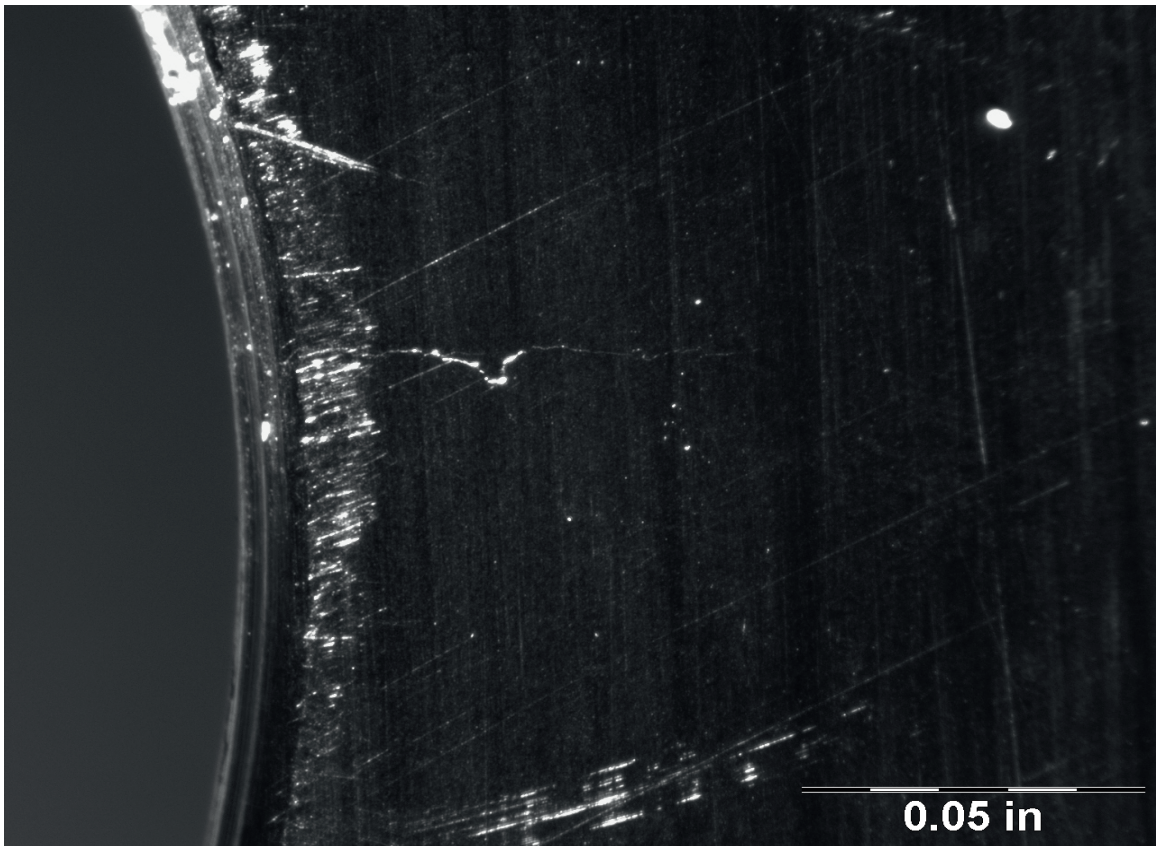

Fig. 210 Image of Surface Crack in Coupon Cx4N1-01-B, Surface Crack Length is 0.0797 inch.

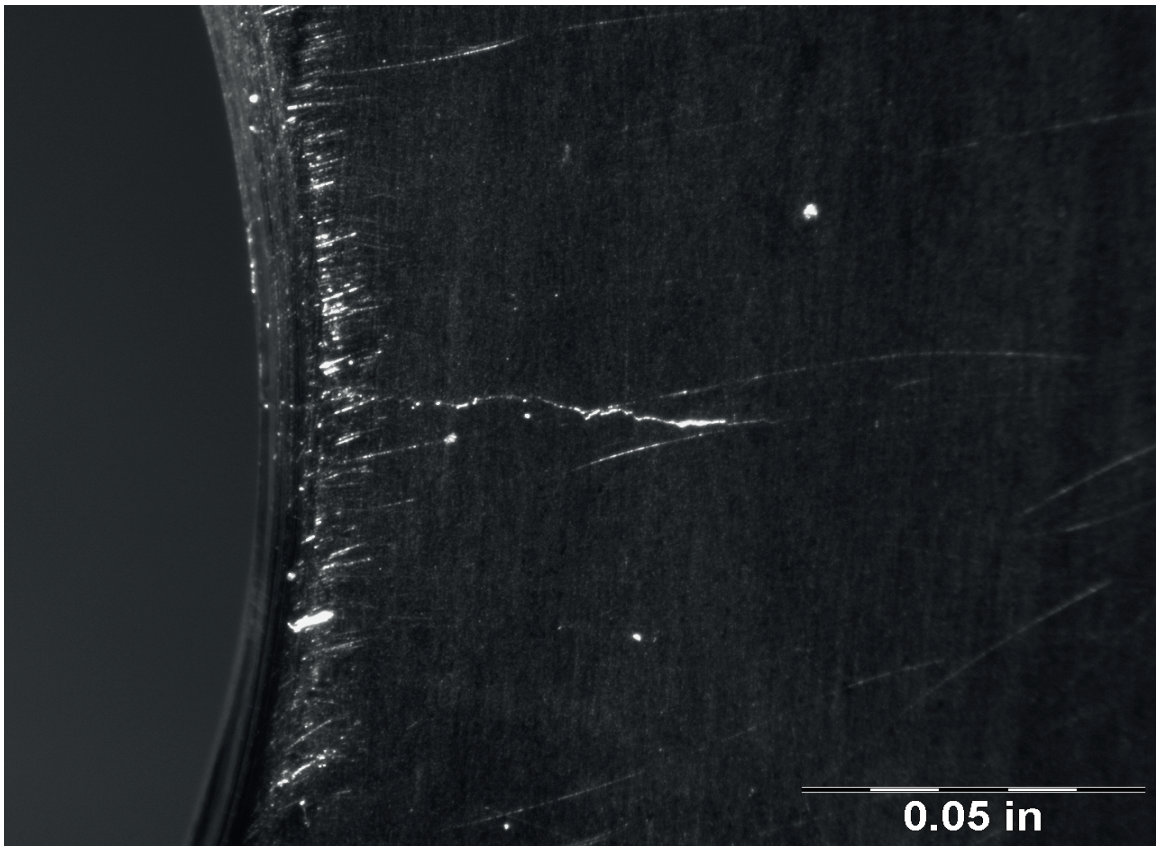

Fig. 211 Image of Surface Crack in Coupon Cx4N1-02-B, Surface Crack Length is 0.0798 inch.

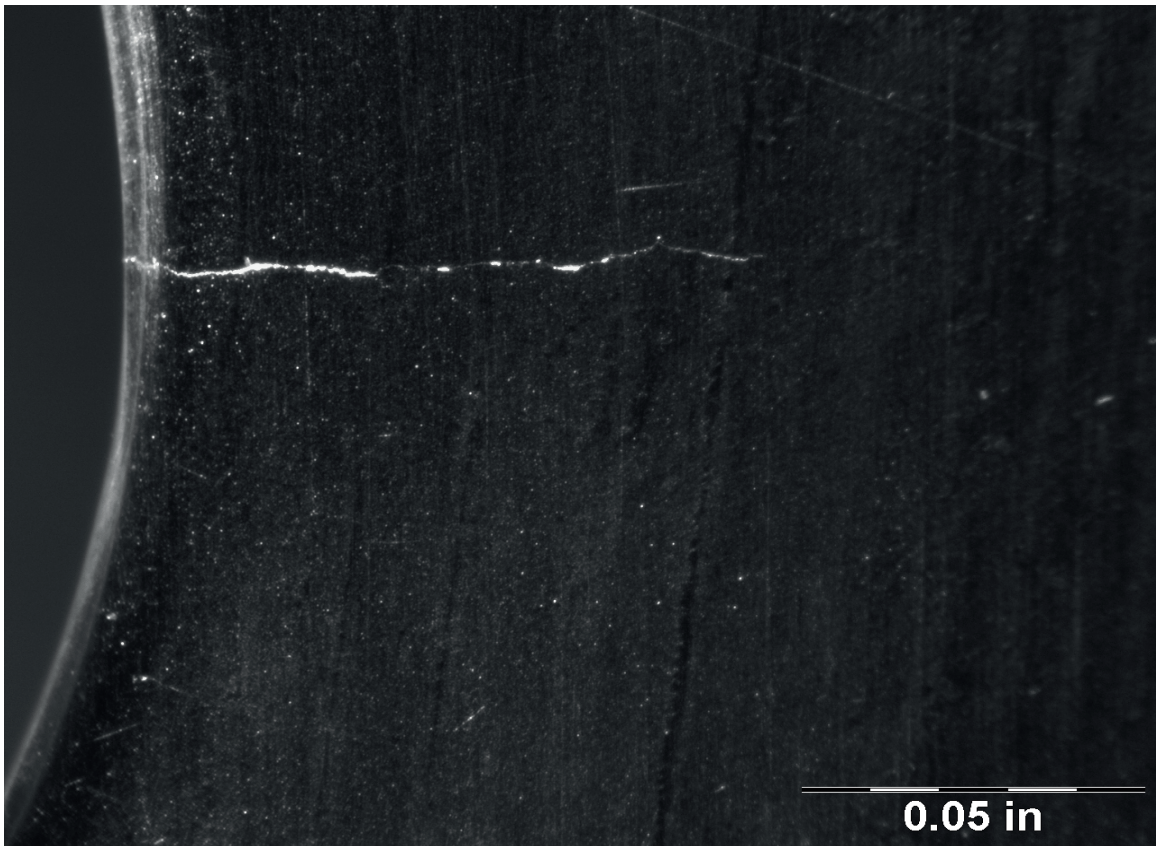

Fig. 212 Image of Surface Crack in Coupon Cx4N1-03-B, Surface Crack Length is 0.0974 inch.

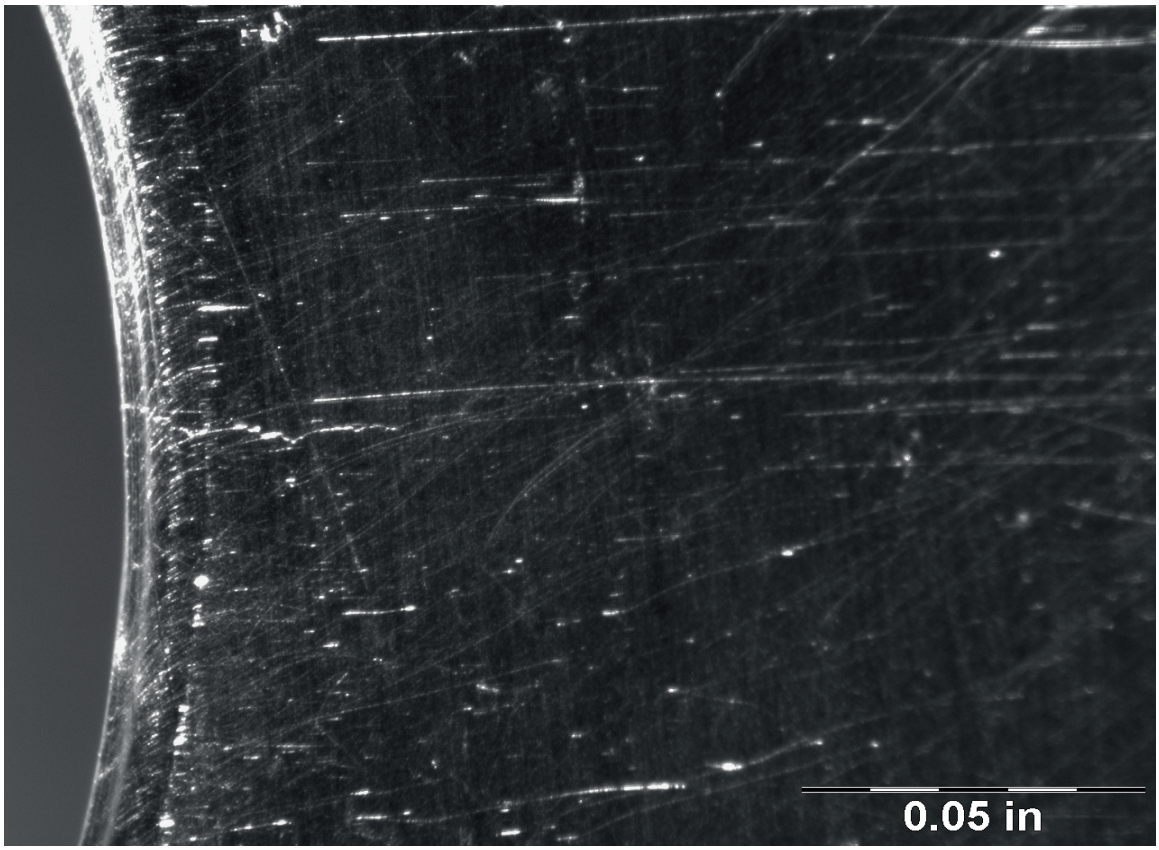

Fig. 213 Image of Surface Crack in Coupon Cx4N1-04-B, Surface Crack Length is 0.0962 inch.

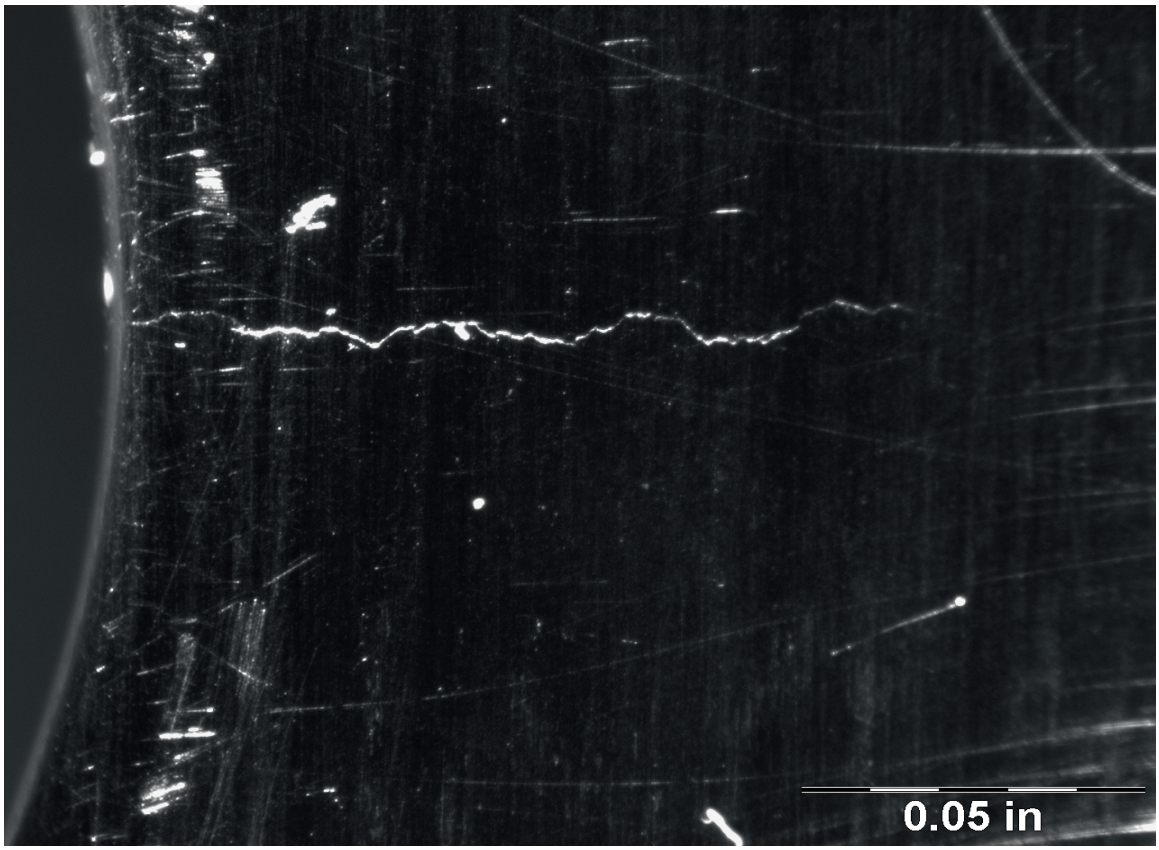

Fig. 214 Image of Surface Crack in Coupon Cx4N1-05-B, Surface Crack Length is 0.1259 inch.

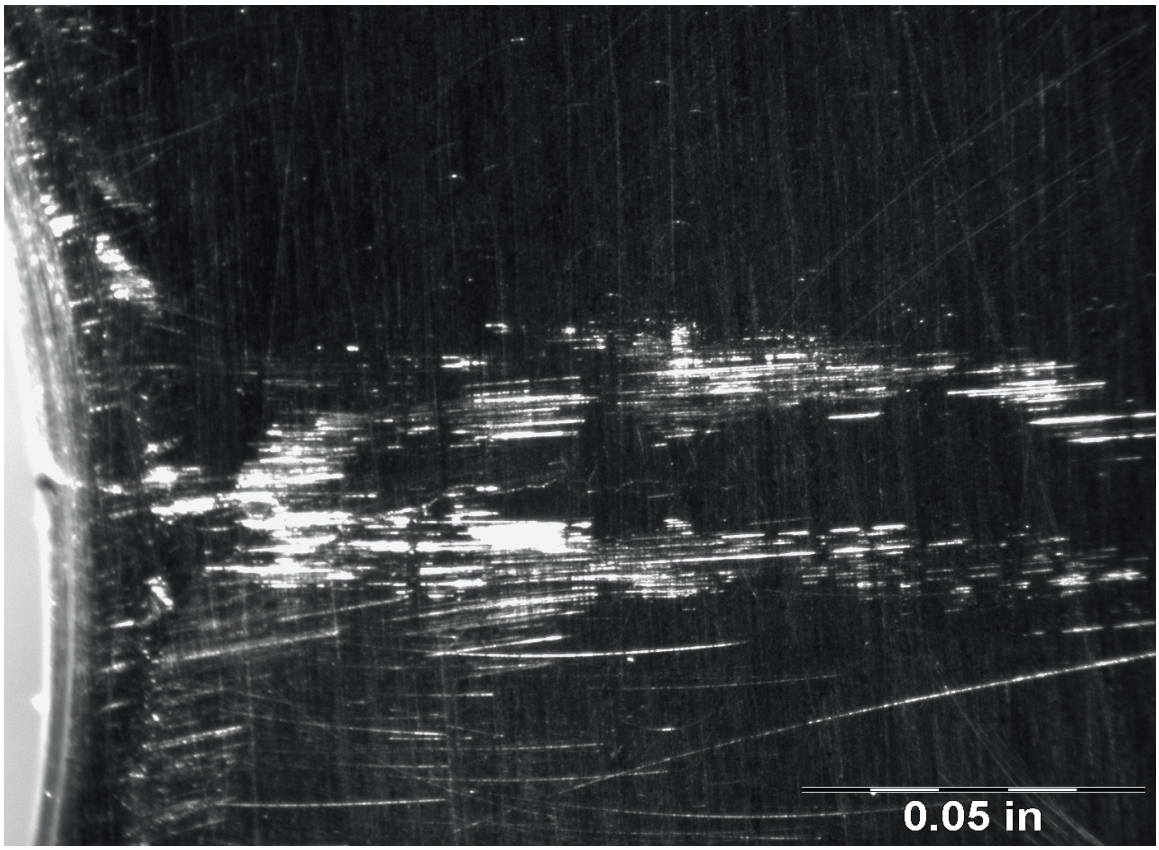

Fig. 215 Image of Surface Crack in Coupon Cx4N1-06-B, Surface Crack Length is 0.1214 inch.

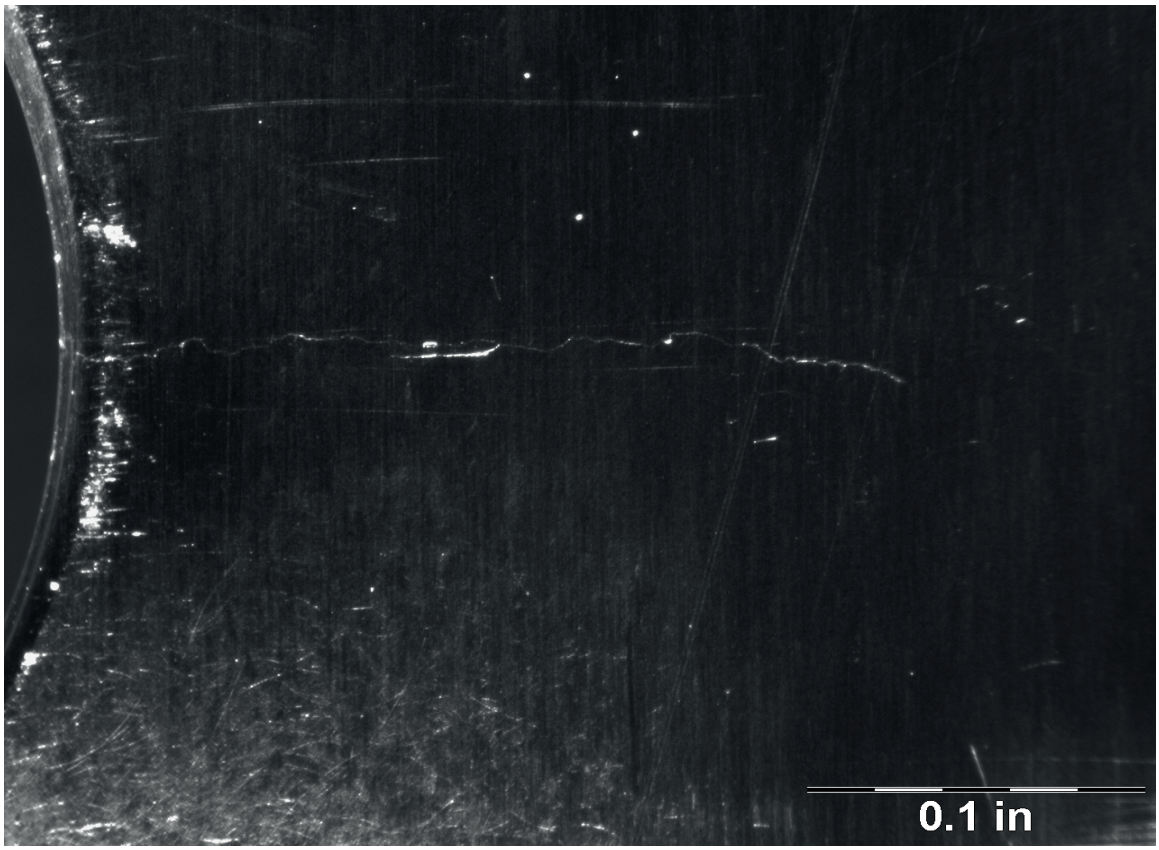

Fig. 216 Image of Surface Crack in Coupon Cx4N1-07-B, Surface Crack Length is 0.2515 inch.

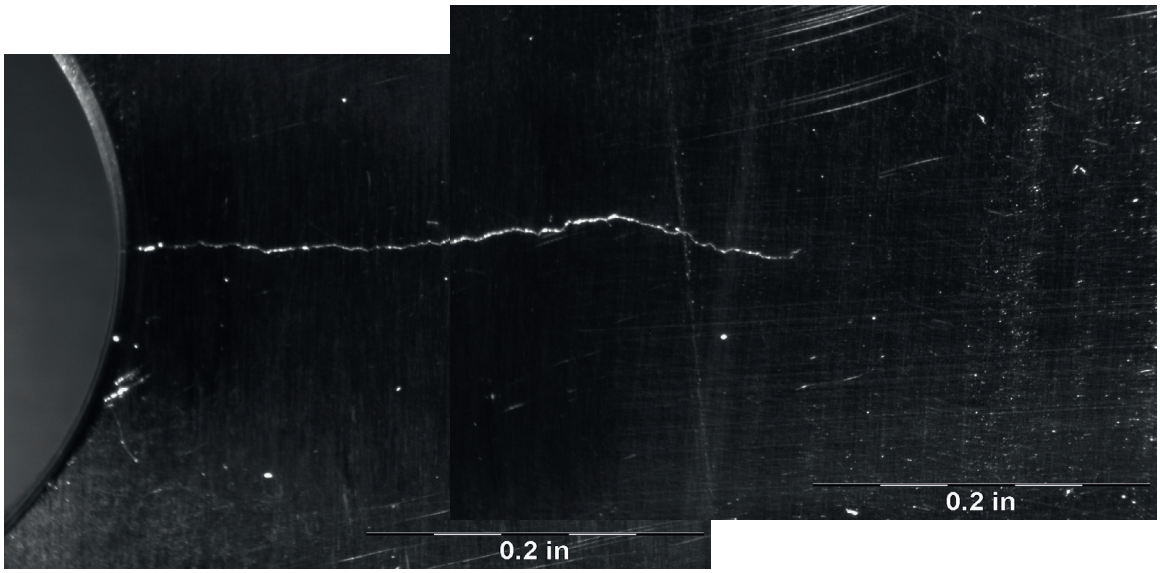

Fig. 217 Image of Surface Crack in Coupon Cx4N1-08-B, Surface Crack Length is 0.4974 inch.

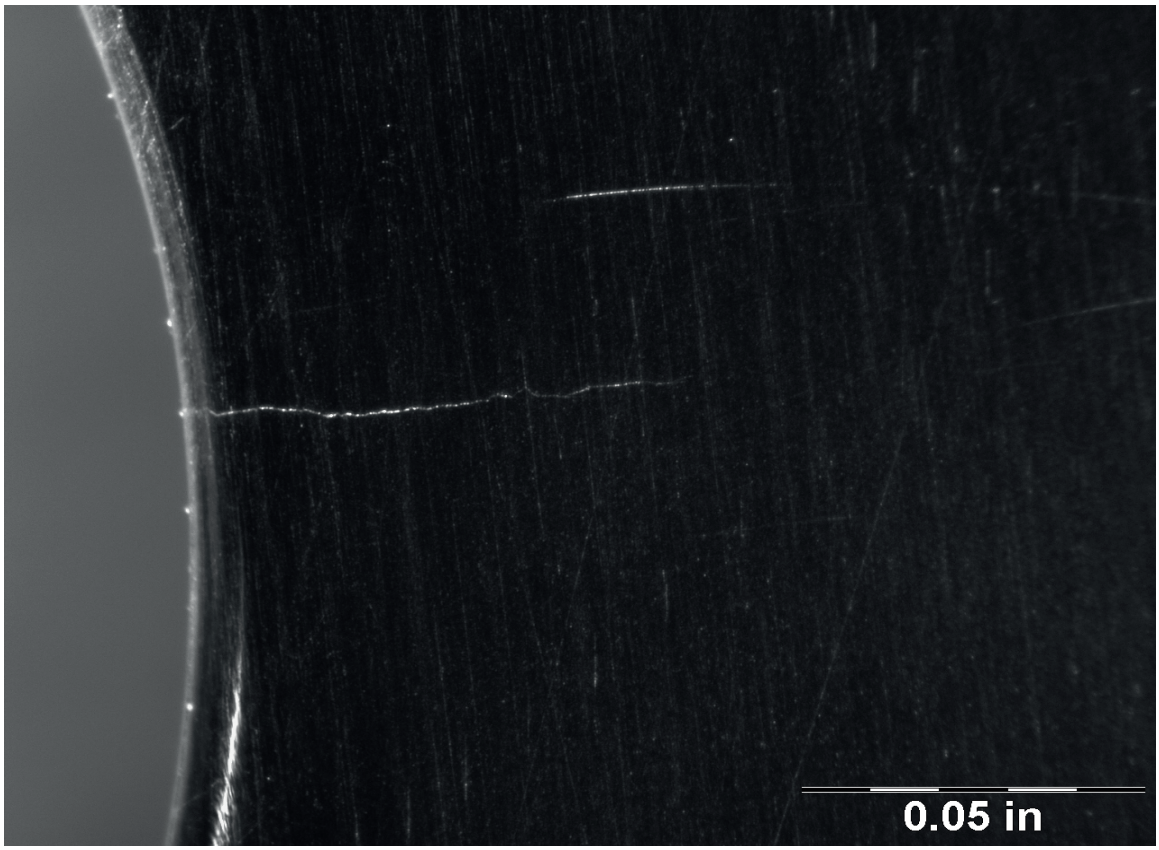

Fig. 218 Image of Surface Crack in Coupon Cx4N1-01-D, Surface Crack Length is 0.0793 inch.

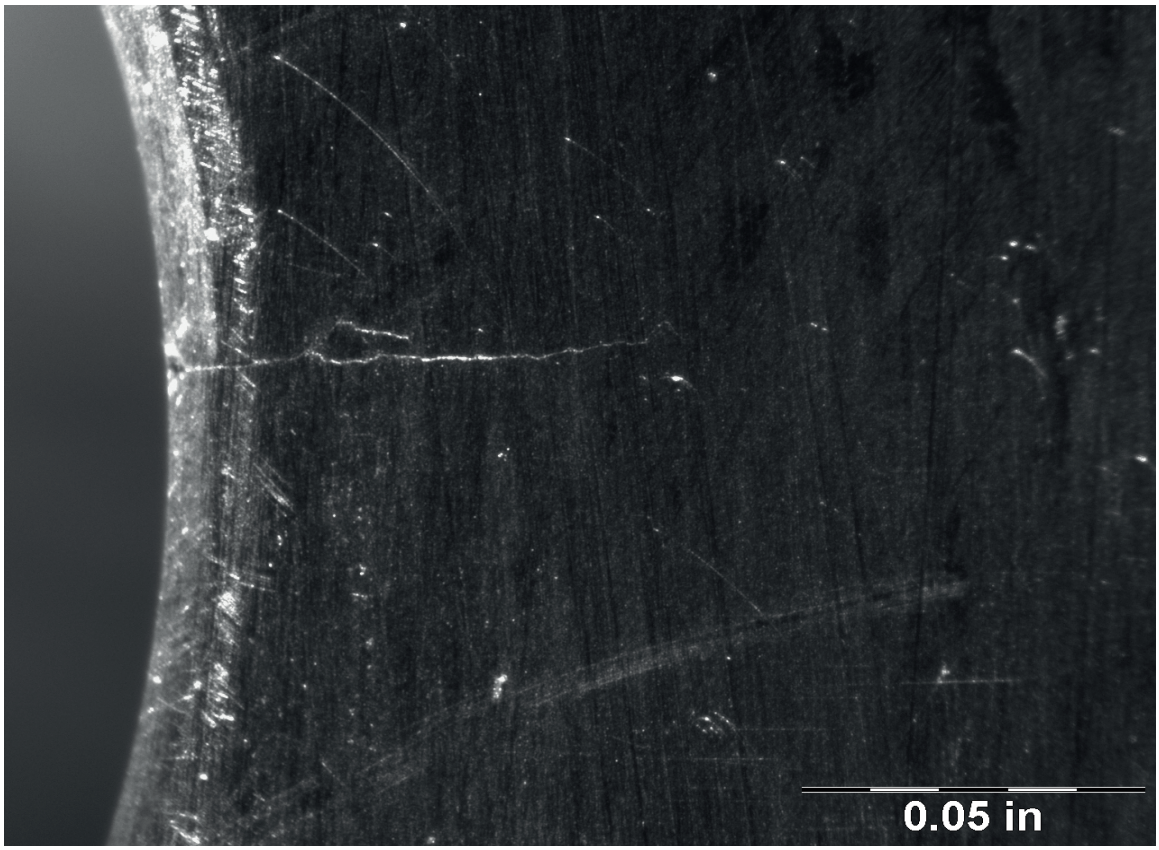

Fig. 219 Image of Surface Crack in Coupon Cx4N1-02-D, Surface Crack Length is 0.0807 inch.

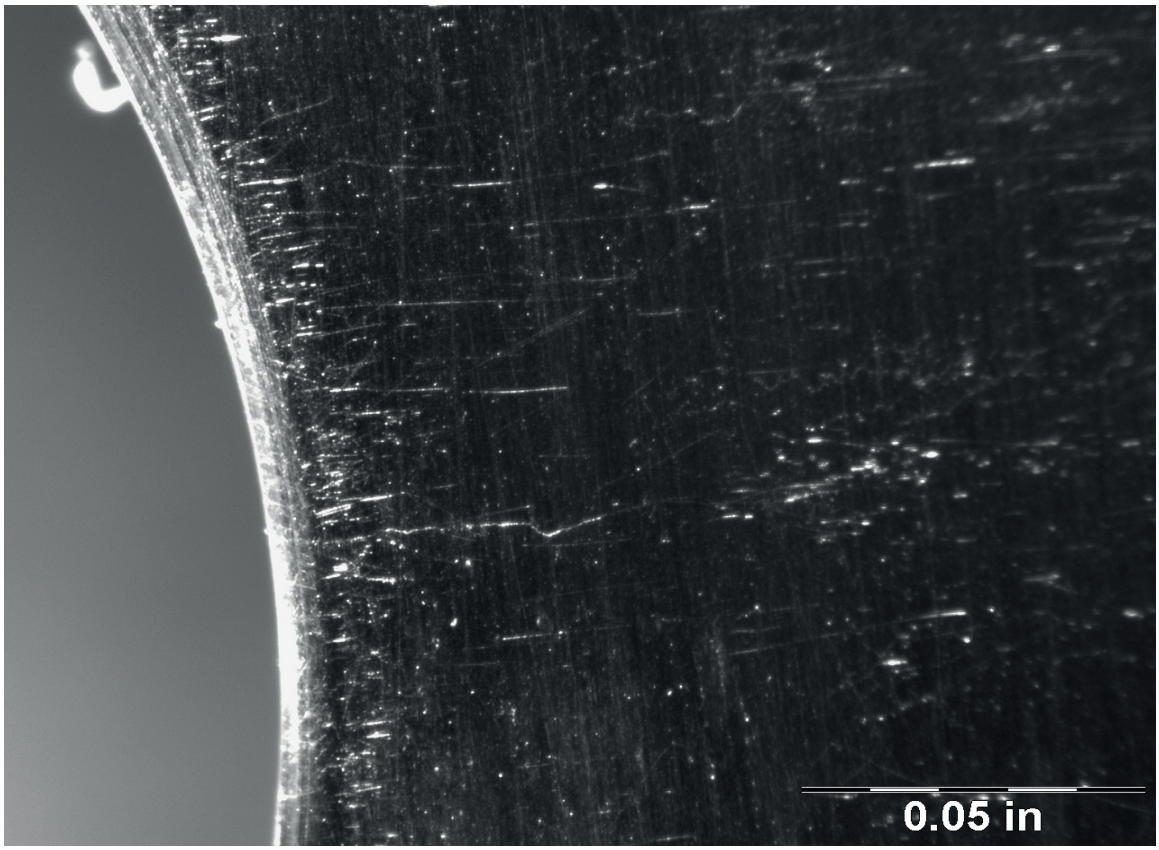

Fig. 220 Image of Surface Crack in Coupon Cx4N1-03-D, Surface Crack Length is 0.0972 inch.

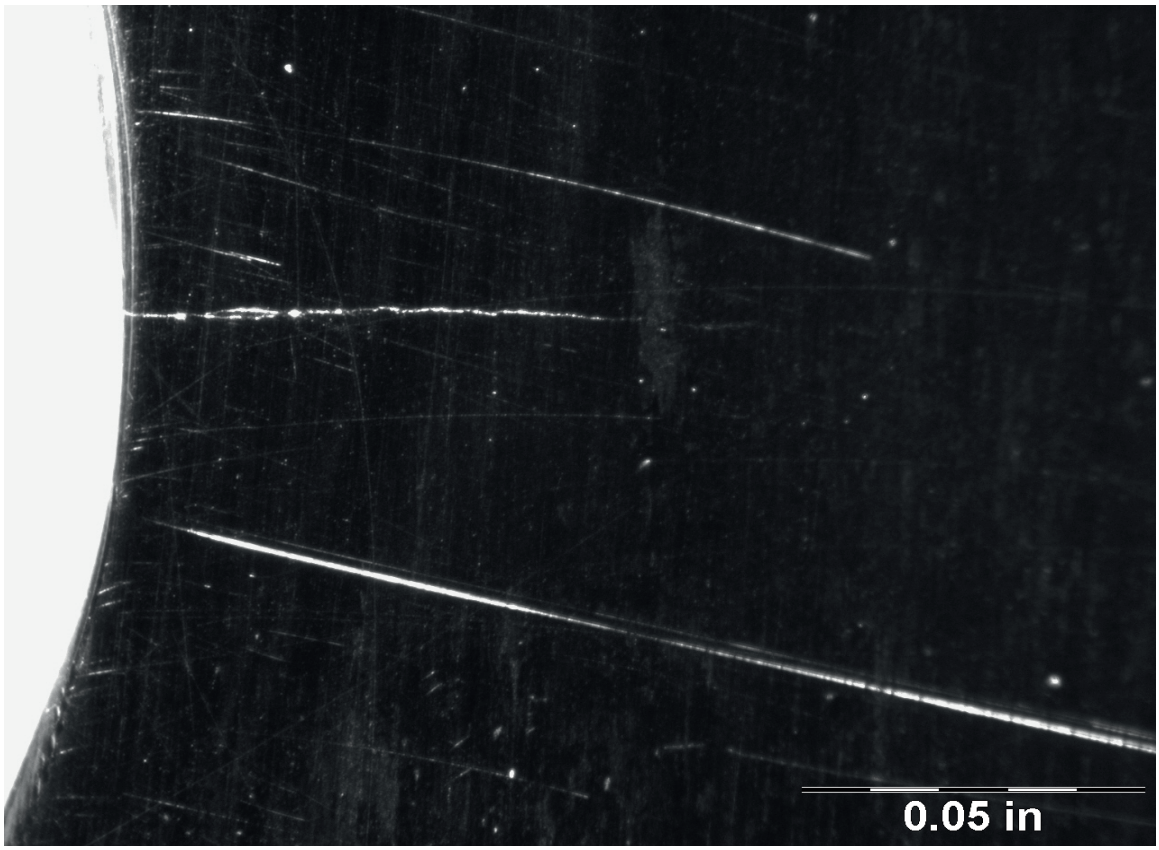

Fig. 221 Image of Surface Crack in Coupon Cx4N1-04-D, Surface Crack Length is 0.1015 inch.

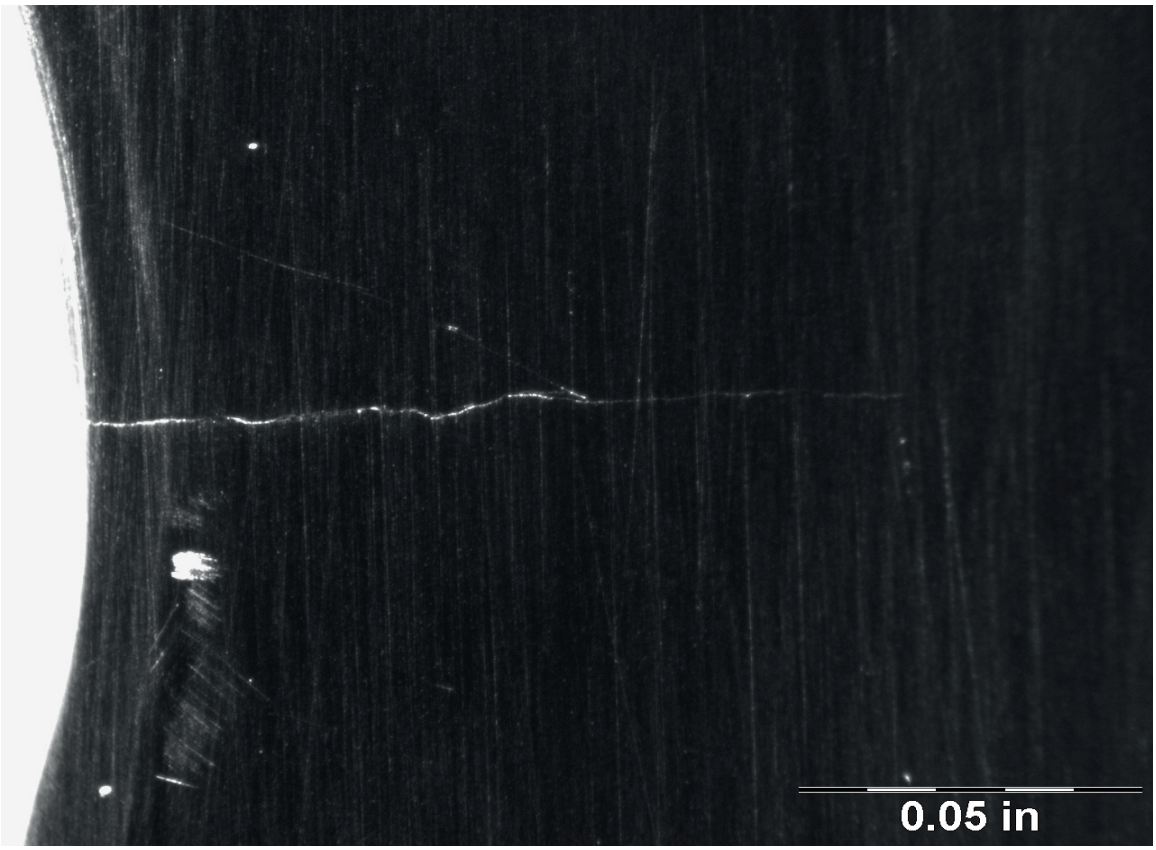

Fig. 222 Image of Surface Crack in Coupon Cx4N1-05-D, Surface Crack Length is 0.1253 inch.

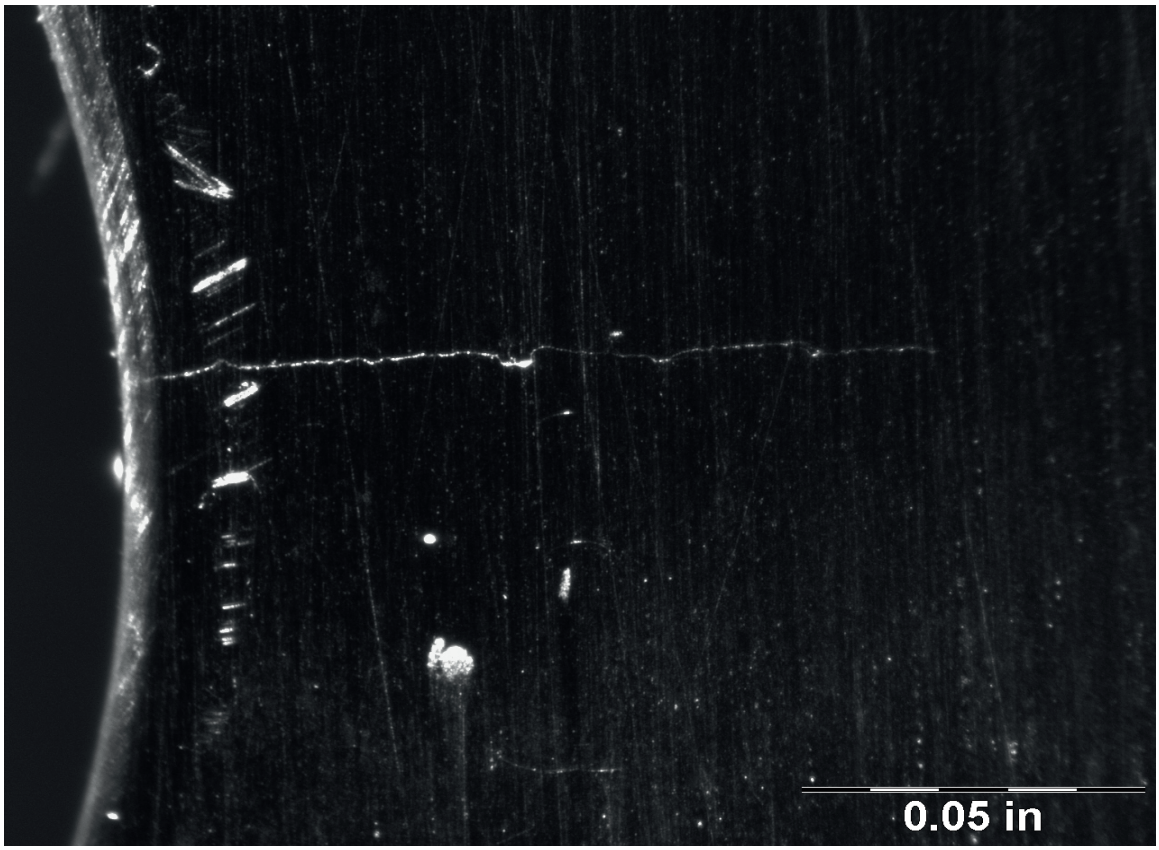

Fig. 223 Image of Surface Crack in Coupon Cx4N1-06-D, Surface Crack Length is 0.1235 inch.

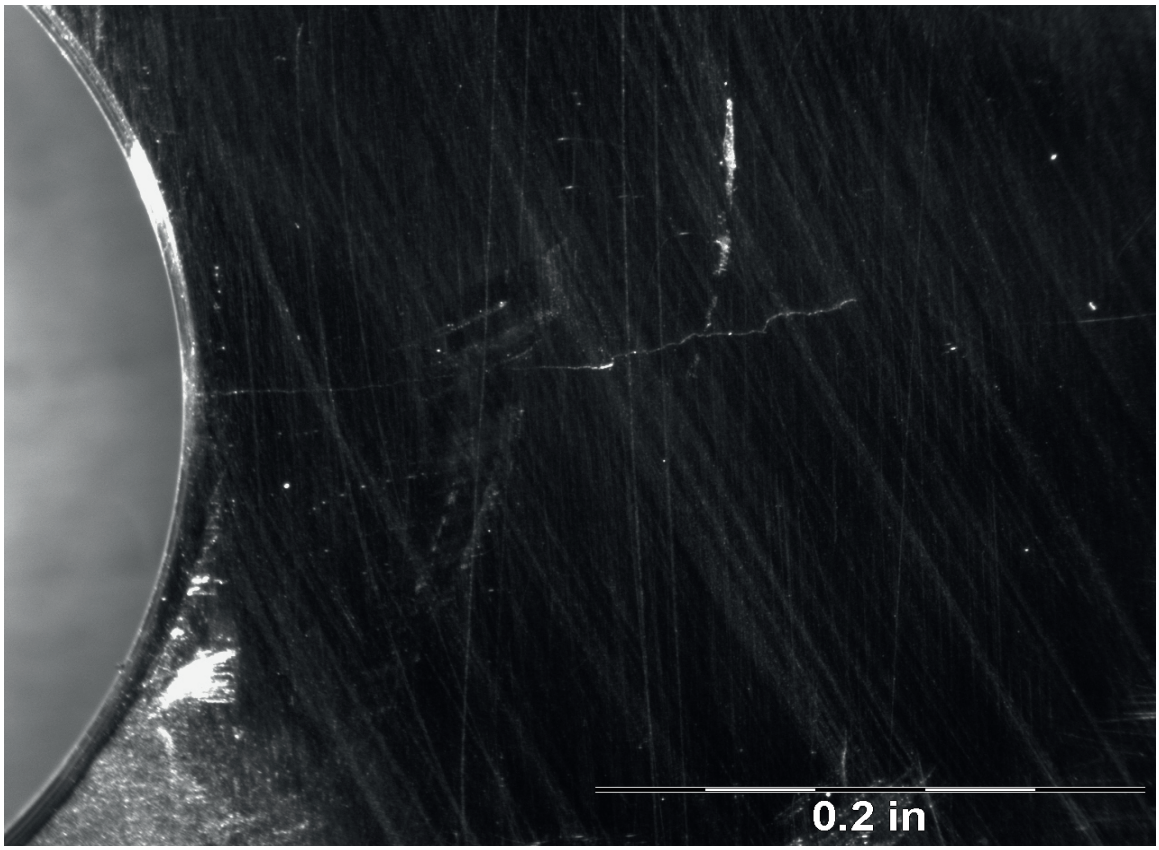

Fig. 224 Image of Surface Crack in Coupon Cx4N1-07-D, Surface Crack Length is 0.2505 inch.

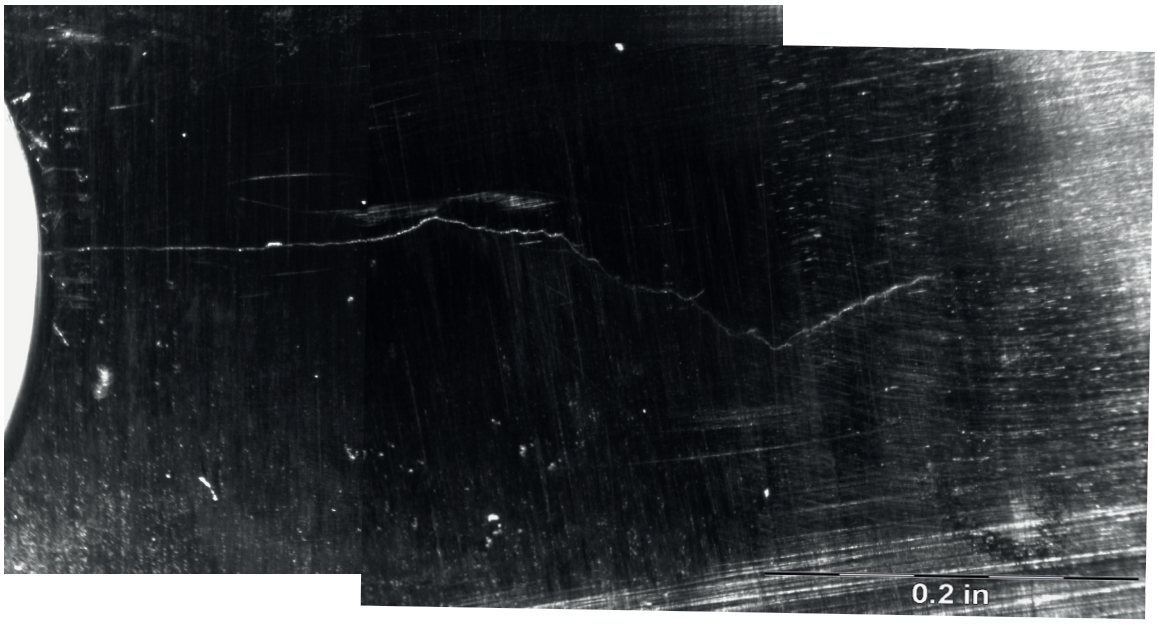

Fig. 225 Image of Surface Crack in Coupon Cx4N1-08-D, Surface Crack Length is 0.5017 inch.

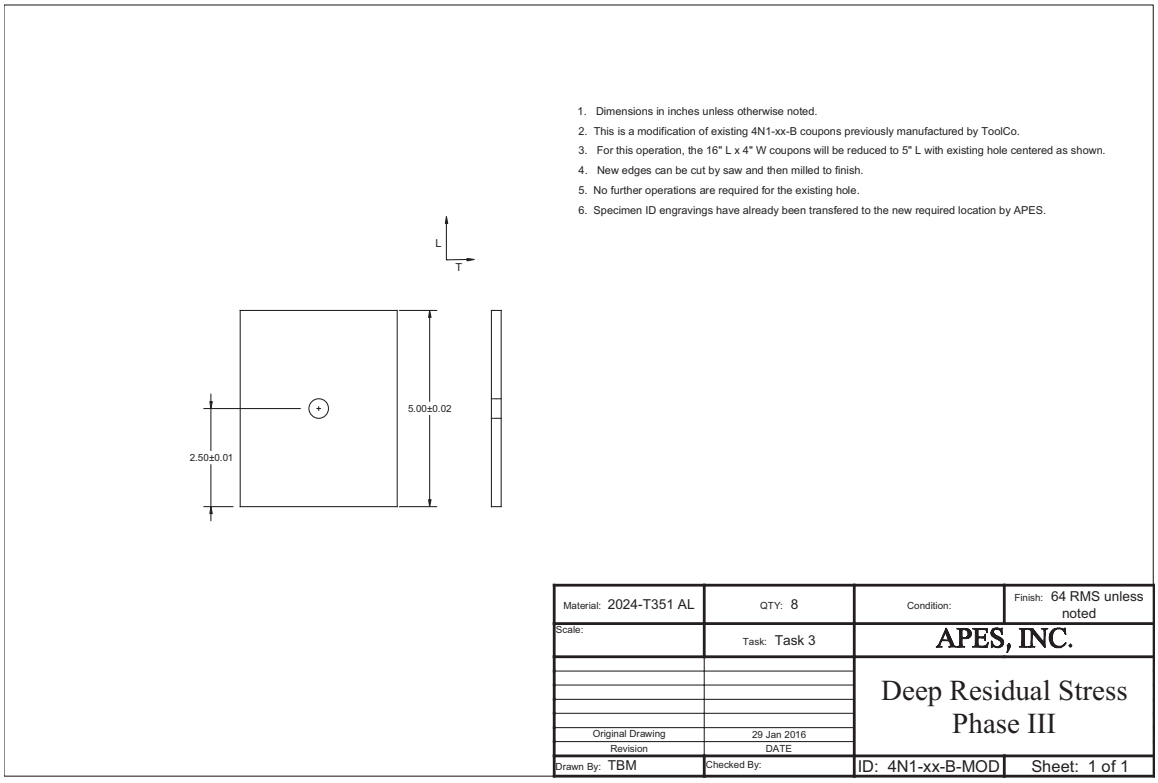

Fig. 226 Final Machining Drawings for Cutting Down Cx4N1-XX-B Fatigue Coupons Down for Residual Stress Determination via the Contour Method.

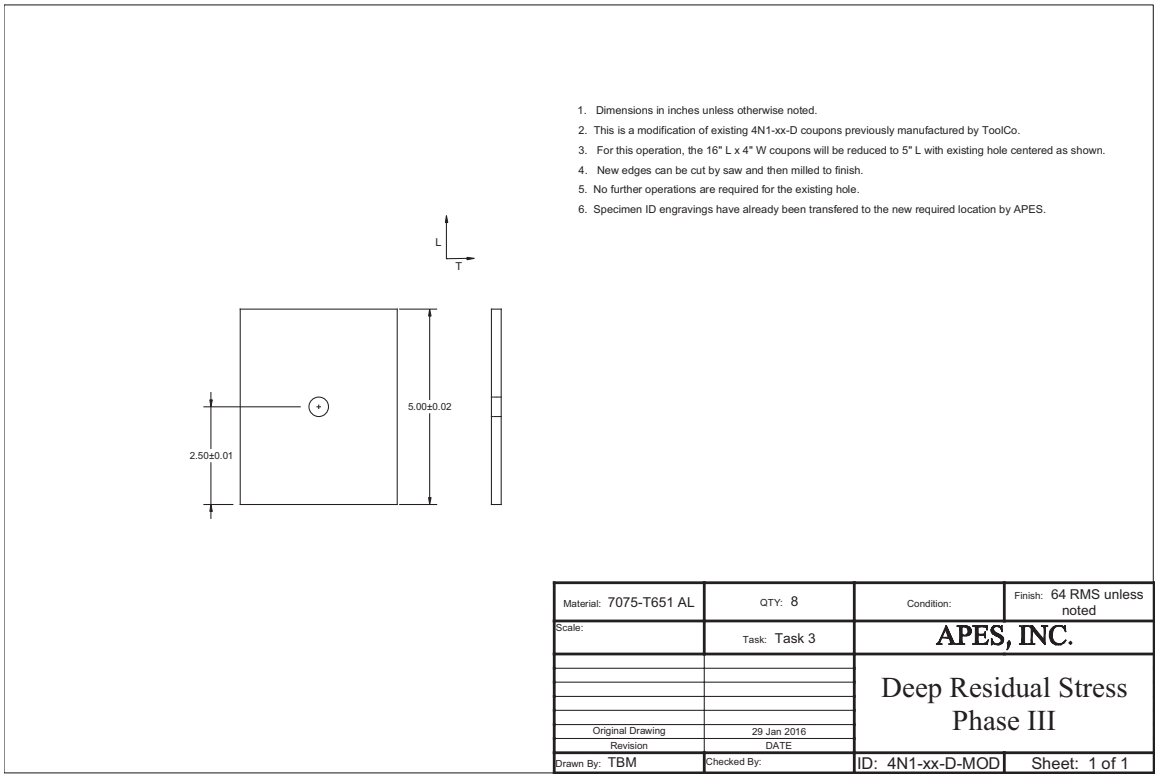

Fig. 227 Final Machining Drawings for Cutting Down Cx4N1-XX-D Fatigue Coupons Down for Residual Stress Determination via the Contour Method.

6 DETERMINATION OF RESIDUAL STRESSES IN FATIGUE-CRACKED COUPONS

6.1 Arrival Condition of Cold Expanded and Fatigue-Cracked Coupons for Contour Method Cutting and Displacement Measurement

All sixteen Cxed and fatigue-cracked coupons were received by Hill Engineering, LLC. with no damage annotated. The incoming condition of all of the coupons are provided in Fig. 228 and Fig. 229.

6.2 Fixturing and Cutting of the Cold Expanded and Fatigue-Cracked Coupons for Contour Method Displacement Measurement

These fatigue-cracked coupons matched the same geometry as the baseline, non cracked coupons; the same fixturing methods were used. The basic set-up for this fixturing was provided in Fig. 14. One requirement that differed from the baseline coupons was that for all of the fatigue-cracked coupons the side with the fatigue crack was always cut first. This cutting method was identical to that performed on the baseline coupons, an is shown in Fig. 230. The goal of this was to ensure that no additional systematic errors were introduced into the process.

In order to keep the cutting sequence, left side first, then right side, the same as the baseline coupons, each of the Cx4N1, fatigue-cracked coupons, was rotated 180-deg. so that the bottom of the coupon was now facing the top. This put the crack on the left

side of the hole for all of the displacement data produced for the Cx4N1 coupons. A basic schematic for this new orientation is provided in Fig. 231.

One of the unique aspects of this research is that this was the first time in which parts were cut, as part of the contour method, with known existing fatigue cracks within the part. It was decided that the parts would be cut through the fatigue crack plane on all of the coupons. For the coupons with larger cracks a cut plane was selected that would cut along the plane through the majority of the length of the crack and, with the exception of the end of the crack, there would be sections which would not be directly along the cut plane. Fig. 232 provides a representation of this for the worst case of the sixteen coupons, coupon Cx4N1-08-D (7075-T651) which had a surface crack length of 0.5017 inch.

There were no significant problems with cutting along the planes of interest for this research program. For the two largest crack sizes it was reported that due to the non planar aspect of the crack it was not possible to follow the crack path. This can be seen in Fig. 233. This is one of the limitations of the contour method, and thus if residual stress determinations are to be made with coupons having larger cracks the contour method might not be the best method for residual stress determination.

All of the post cut surfaces were documented via macro photography. An image of the Cx4N1-01-B (2024-T351) coupon with a 0.0797 inch surface crack is provided in Fig. 234 and Cx4N1-01-D (7075-T651) with a 0.0793 inch surface crack is provided in Fig. 235. All of the surfaces images for the Cx4N1-XX-B and Cx4N1-XX-D coupons are provided the Appendix.

6.3 Displacement Measuring of Cold Expanded and Fatigue-Cracked Coupons after Wire EDM Cut

The same methods were used to measure the post cut surfaces of the Cx4N1-XX-B and -D coupons as was used for the baseline, CxA2 and CxD2 coupon configurations. This was in an effort to reduce, as much as possible, the systematic uncertainties that could arise from using different equipment and methods when measuring the displacements upon the planes of interest after cutting.

The displacement field data was provided at the same grid spacing of 0.003 inch in the X and 0.001 inch in the Y direction, thus data files with approximately 1.3 million data points were developed for both the “static” and “floating” surfaces.

6.4 Development of Residual Stresses from Surface Displacement Data

The exact same process was used to develop residual stresses from the displacement data provided for all of the Cx4N1-XX-B and -D as was performed for CxA2 and CxD2 coupons. The process will be outlined again with limited images of the data as it was processed.

The raw displacement data for one side of the part (“static”) was opened and the outline of the part was defined for both sides of the hole. Then the part was aligned to a new X and Y coordinate axis, and a least-squares plane fit through the entire dataset, referenced to the new part orientation. Then the data were rotated to this new coordinate system. An image of this aligned “static” data set for coupon Cx4N1-01-B (2024-T351 with a 0.08 inch entrance surface crack) is provided in Fig. 236, and the opposite side of the cut part, the “floating” data set is shown in Fig. 237. The two sides then were averaged and the data density increased to a grid spacing of 0.0001 inch, an image of that

data set is shown in Fig. 238. This aligned and averaged dataset was then processed using the Modified Thompson Tau method for removing statistical outliers. The same alpha (α) of 0.05, or 5% was used as the threshold.

The data was then fit to a knot density of four knots through the thickness (Y axis) and thirty-two knots extending radially away from the hole (X axis). A third order B-Spline was used to fit the data between each knot location. After the smoothing and fitting was performed the data surface looked like that shown in Fig. 239.

Once the fit was produced a solid model was developed using the same parameters defined for the CxA2 (2024-T351) and CxD2 (7075-T651) coupons, as shown in Fig. 10 and Fig. 11. The meshing parameters were held constant in an effort to minimize the introduction of additional uncertainties into the residual stress determination. The mesh density was identical to that shown in Fig. 45 through Fig. 48 for 16 elements through the thickness. The boundary conditions were also identical to those for the baseline, uncracked CxA2 (2024-T351) and CxD2 (7075-T651) coupons, as shown in Fig. 31. Residual stresses then were extracted at each nodal location along the face of interest. It should be noted that no residual stress data were extracted along the exact edge of the coupon, both for the entrance and exit surface and along the bore. The residual stress plots provide data to the edge of the coupon but no line plots were developed along the edges. The first line plots were extracted at the first nodal location away from the edge of the part.

6.5 Residual Stress Results for Fatigue-Cracked Cx4N1-01-B and Cx4N1-02-B (2024-T351) Coupons 0.08 inch Fatigue Crack on Mandrel Entrance Surface

For the 0.08 inch fatigue crack condition there were two replicates produced, Cx4N1-01-B and Cx4N1-02-B. Residual stresses were determined for each of these conditions and contour plots of the residual stress and line plots along the same transects will be provided. For reference, all of the coupons were oriented such that the Cx mandrel entrance surface is at the Y=0, or the bottom, and all of the cracks that were formed in the coupons would be on the left side of the hole, at the mandrel entrance surface, X=1.75 inch.

6.5.1 Contour Plots of Residual Stress for Cx4N1-01-B and Cx4N1-02-B Coupons

Contour plots of the residual stress for coupon Cx4N1-01-B are provided in Fig. 240 and Fig. 241. For coupon Cx4N1-02-B the contour plots of the residual stress are provided in Fig. 242 and Fig. 243. There was a fatigue crack of surface length 0.0797 inch for the -01 coupon and 0.0798 inch for the -02. The average residual stress contour plot of Cx4N1-01-B and Cx4N1-02-B is provided in Fig. 244 and for a zoomed in region in Fig. 245.

For crack location and orientation, Fig. 240 provides an overlay of where the fatigue cracks were developed and propagated. The crack size, as shown within Fig. 240, is not to scale, but is there to provide orientation when discussing the location of the fatigue crack.

From these residual stress contour plots it is possible to see that there is a slight difference in the residual stress profile of the left side, next to the edge of the hole, versus

that which can be seen on the right side.

6.5.2 Line Plots of Stress Radially away from Hole for Cx4N1-01-B and Cx4N1-02-B Coupons

All of the line plots have both the -01 and the -02 plotted together. This allows for a greater ability to compare the two replicates. Line plots were produced at the same locations as those in the CxA2 (2024-T351) and the CxD2 (7075-T651) coupons, at specific distances from from the entrance surface. These locations include 0.016 inch (entrance surface), 0.05 inch, 0.09 inch, 0.14 inch (mid plane), 0.16 inch, 0.20 inch, and 0.234 inch (exit surface). Line plots are provided for each of these seven planes in Fig. 246 through Fig. 259. In addition to the individual residual stresses, the average residual stress was calculated and a standard deviation error bar was applied to each plot.

From these line plots it is possible to see that for both the left and the right sides of the holes the residual stresses are repeatable, with the highest level of repeatability being from the edge of the hole to 0.10 inch away from the edge. It can also be seen that the right side of the hole had a lower level of repeatability uncertainty than the left side. This could be due to the presence of the crack and the impact that a fatigue crack has on a residual stress field, making it have a higher level of variability.

6.5.3 Line Plots of Stress through the Thickness of the Part Cx4N1-01-B and Cx4N1-02-B Coupons

Line plots through the thickness of the part were produced for both the left and the right side of the hole, at four locations. These include at distances of 0.01 inch, 0.05 inch, 0.10 inch, and 0.150 inch from the edge of the hole. For each of the plots the

individual residual stress is plotted, with an average of the two sides, and error bars representing one standard deviation.

6.5.3.1 Line Plots of Stress through the Thickness for Cx4N1-01-B and Cx4N1-02-B – Left Side of the Hole

The left side of the hole had a 0.080 inch fatigue crack developed within these coupons. This fatigue crack was developed at the entrance surface and for all of these residual stress plots the fatigue crack was on the left side of the hole. Fig. 260 through Fig. 263 provide these line plots of stress.

6.5.3.2 Line Plots of Stress through the Thickness for Cx4N1-01-B and Cx4N1-02-B – Right Side of the Hole

Residual stress line plots for the right side of the hole, at the same intervals, are provided in Fig. 264 through Fig. 267. The right side of the hole on these coupons did not have a fatigue crack develop, and thus represented a Cx hole that has undergone cyclical loading.

6.6 Residual Stress Results for Fatigue-Cracked Cx4N1-03-B and Cx4N1-04-B (2024-T351) Coupons 0.10 inch Fatigue Crack on Mandrel Entrance Surface

Residual stress results for the Cx4N1-03-B and Cx4N1-04-B (2024-T351) coupons are provided below.

6.6.1 Contour Plots of Residual Stress for Cx4N1-03-B and Cx4N1-04-B Coupons

Residual stress contour plots of Cx4N1-03-B and Cx4N1-04-B are provided in Fig. 268 and Fig. 273. Each of these coupons had a fatigue crack that developed in the left side of the hole that was approximately 0.10 inch long on the mandrel entrance surface.

From the residual stress contour plots of the Cx4N1-03-04-B coupons it is possible to see a softening of the compressive residual stress field on the left side of the hole near the edge of the hole at the Cx mandrel entrance surface. The depth of the higher levels of compression are shorter than that seen on the right side of the hole. However, the general shape of the contour bands remains similar for both sides of the hole. From these contour plots it is possible to visualize the effect of the fatigue crack on the residual stress field, at the left side of the hole. This effect seems to decrease the depth of the maximum compression and also adjusts the residual stress contour lines, moving them farther away from the edge of the hole, and increasing the level of tension near the edge of the hole.

6.6.2 Line Plots of Stress Radially away from Hole for Cx4N1-03-B and Cx4N1-04-B Coupons

Line plots were produced for the 0.10 inch fatigue crack condition. Seven line plots were produced at the same locations as in the Cx4N1-01-B and Cx4N1-02-B (2024-T351) conditions, and are provided in Fig. 274 through Fig. 287. For each location, an average also was determined and error bars are plotted on the average to cover one standard deviation from the mean.

From these residual stress line plots it's possible to see that from the Cx mandrel entrance face through to the mid thickness the residual stress is less near the edge of the hole on the left side of the hole than that which is on the right side. This would correlate to the effect of the fatigue crack being present on the left side of the hole and extending to almost the mid thickness of the coupon.

6.6.3 Line Plots of Stress through the Thickness of the Part Cx4N1-03-B and Cx4N1-04-B Coupons

Line plots of the residual stress through the thickness of the part are provided in Fig. 288 through Fig. 295. Each line plot shows the residual stress for Cx4N1-03-B and Cx4N1-04-B (2024-T351) coupons. These coupons had a fatigue crack surface length of approximately 0.10 inch on the left side of the hole.

6.6.3.1 Line Plots of Stress through the Thickness for Cx4N1-03-B and Cx4N1-04-B – Left Side of the Hole

Residual stress line plots for the left side of the hole are provided at the same distances away from the hole as previously provided and are shown in Fig. 288 through Fig. 291. The average of each point was calculated and a standard deviation about that mean was plotted as error bars.

6.6.3.2 Line Plots of Stress through the Thickness for Cx4N1-03-B and Cx4N1-04-B – Right Side of the Hole

The right side of the hole had the same plots developed for it as was performed for the left side of the hole. These plots are provided in Fig. 292 through Fig. 295.

6.7 Residual Stress Results for Fatigue-Cracked Cx4N1-05-B and Cx4N1-06-B (2024-T351) Coupons with a 0.125 inch Fatigue Crack on Mandrel Entrance Surface

The Cx4N1-05-B and -06-B (2024-T351) conditions had a 0.125 inch corner crack at the mandrel entrance surface on the left side. Contour plots and line plots of the residual stress for these two coupons, along with the average and error bars representing one standard deviation of stress, are provided in order to gain an understanding of the effect of a crack of this size on the residual stress field.

6.7.1 Contour Plots of Residual Stress for Cx4N1-05-B and Cx4N1-06-B Coupons

Contour plots of the residual stress for Cx4N1-05-B, Cx4N1-06-B (2024-T351) along with the average of the two are provided in Fig. 296 through Fig. 301.

From the residual stress contour plots of Cx4N1-05-06-B (2024-T351) it can be seen that again there is a visible difference from the left to the right side of the Cxed hole. This difference is most noticeable at the Cx mandrel entrance surface, where there is a shifting of the residual stress field towards a more tensile residual stress. In addition, it can be seen in the average of the two coupons that the width of the compressive zones from -20 ksi to -10 ksi increases, along with the -10 kis to 0 ksi zone.

6.7.2 Line Plots of Stress Radially away from Hole for Cx4N1-05-B and Cx4N1-06-B Coupons

Line plots of the residual stress emanating radially away from the Cxed hole were produced at the same planar locations as in the other conditions. Each line plot provides the residual stress for the Cx4N1-05-B and Cx4N1-06-B (2024-T351) condition, the

average of the two conditions, and the standard deviation as expressed as error bars at each nodal location where the residual stress was produced. These radial line plots are provided in Fig. 302 through Fig. 315.

6.7.3 Line Plots of Stress through the Thickness of the Cx4N1-05-B and Cx4N1-06-B Coupons

Line plots of the through-thickness residual stress for both the left side of the hole (the location where a 0.125 inch corner crack had been developed) and the right side are provided. Each plot shows the residual stress for the individual conditions, Cx4N1-05-B and Cx4N1-06-B (2024-T351), along with the average of the two stresses and the standard deviation of the stress about the mean. Residual stresses were plotted at the same four locations as above.

6.7.3.1 Line Plots of Stress through the Thickness for Cx4N1-05-B and Cx4N1-06-B – Left Side of the Hole

Line plots of the through-thickness stress for the left side of the hole are provided in Fig. 316 through Fig. 319.

6.7.3.2 Line Plots of Stress through the Thickness for Cx4N1-05-B and Cx4N1-06-B – Right Side of the Hole

Through thickness residual stress line plots for the right side of the hole are provided in Fig. 320 through Fig. 323. It should be noted that no crack was present on this side of the hole, which is true for all of the previous conditions.

6.8 Residual Stress Results for Fatigue-Cracked Cx4N1-07-B (2024-T351) Coupons with a 0.25 inch Fatigue Crack on Mandrel Entrance Surface

For the Cx4N1-07-B condition a crack was propagated to a final surface length of 0.2515 inch. No replicate was developed for this condition so the stress plots represent only the single -07 (0.2515 inch) condition.

6.8.1 Contour Plots of Residual Stress for Cx4N1-07-B Coupons

The residual stress contour plot for the Cx4N1-07-B (2024-T351) cracked condition is provided in Fig. 324 and Fig. 325.

6.8.2 Line Plots of Stress Radially away from Hole for Cx4N1-07-B Coupons

Residual stress line plots along the same planes as outlined for the previous coupons were developed for the Cx4N1-07-B condition. This coupon had a fatigue crack that was developed and propagated to a length of 0.2515 inch. Since there was only one coupon developed each of the line plots will only have a single residual stress plotted. The radial residual stress line plots are provided in Fig. 326 through Fig. 347. Additional plots are provided for each condition that are focused in on the area next to the hole. This is to provide additional insights into the characteristics of the residual stress field and the differences between the cracked side (left side) and the uncracked side (right side) of the hole.

6.8.3 Line Plots of Stress for through the Thickness of the Cx4N1-07-B Coupons

Line plots were developed for both the left and the right side of the Cx hole. For the Cx4N1-07-B (2024-T351) there was a 0.2515 inch surface crack that was developed and propagated on the left side of the hole. There was only one of these coupons developed and so there was no average or standard deviation produced and plotted.

6.8.3.1 Line Plots of Stress through the Thickness for Cx4N1-07-B – Left Side of the Hole

Line plots of the residual stress through the thickness of the part for the left side of the coupon are provided in Fig. 340 through Fig. 343.

6.8.3.2 Line Plots of Stress through the Thickness for Cx4N1-07-B – Right Side of the Hole

The right side of the Cx4N1-07-B (2024-T351) had no fatigue crack and thus would represent a coupon that had been fatigue loaded but had no crack develop. Residual stress line plots were developed along the same through-thickness plans as for the left side. The through-thickness line plots are provided in Fig. 344 through Fig. 347.

6.9 Residual Stress Results for Fatigue-Cracked Cx4N1-08-B (2024-T351) Coupons with a 0.50 inch Fatigue Crack on Mandrel Entrance Surface

The Cx4N1-08-B (2024-T351) condition had a 0.4974 inch surface crack that was formed on the mandrel entrance surface. In addition to this there was a small fatigue crack that nucleated on the opposite side of the hole. This right-sided fatigue crack had propagated to a size of about 0.05 x 0.05 inch. Residual stresses for this cracked condition are provided below.

6.9.1 Contour Plots of Residual Stress for Cx4N1-08-B Coupons

A contour plot of the residual stress for the Cx4N1-08-B (2024-T351) condition is provided in Fig. 348 and Fig. 349. It can be seen that there is a visible difference in the residual stress field between the left side of the hole, the side with a 0.4974 inch crack and the right side, which had formed a smaller 0.05 inch corner crack.

6.9.2 Line Plots of Stress Radially away from Hole for Cx4N1-08-B Coupons

Residual stress line plots of the radial stress for coupon Cx4N1-08-B (2024-T351) are provided in Fig. 350 through Fig. 363. This coupon had a 0.4974 inch surface crack that was developed and propagated on the left entrance surface of this coupon. There was also a small fatigue crack on the right side of the coupon.

6.9.3 Line Plots of Stress through the Thickness of the Cx4N1-08-B Coupons

Additional line plots of the through-thickness residual stresses were produced along the same planes as provided in the previous coupons. Since there was only one of these coupons produced only the single line plot of residual stress is provided.

6.9.3.1 Line Plots of Stress through the Thickness for Cx4N1-08-B – Left Side of the Hole

Residual stress, through-thickness stresses for the left side of the hole are provided in Fig. 364 through Fig. 367. This side of the coupon had a 0.4974 inch through-thickness crack that had been developed and propagated.

6.9.3.2 Line Plots of Stress through the Thickness for Cx4N1-08-B – Right Side of the Hole

The right side of this coupon had a small fatigue crack that had formed during fatigue loading. The line plots for these are provided in Fig. 368 through Fig. 371.

6.10 Comparison of Residual Stress Line Plots for all Cx4N1-B (2024-T351) Coupons

In an effort to draw further conclusions from the residual stresses determined from these experiments a series of line plots are provided, which plot all of the fatigue-cracked coupons together. Through these it is possible to draw further conclusions regarding the effects of the fatigue crack on the residual stress field, as compared among the group of fatigue-cracked coupons, and also compared to the opposite side of the hole, which had no fatigue crack, except for coupon Cx4N1-08-B, which had the largest, 0.50 inch crack. For these comparisons, only three residual stress line plots for the radial stress will be provided. And three will be provided for the through-thickness residual stresses.

6.10.1 Residual Stress Radial Line Plots Comparing all Cx4N1-B (2024-T351) Coupons

Residual stress line plots of the radial stresses are provided for the Cx mandrel entrance, mid plane and exit surfaces. Two plots are provided for each location, the first provides the stress profile for the entire length of the coupon, and the second focuses in on the first 0.25 inch away from the edge of the hole. These plots are provided in Fig. 372 through Fig. 377.

6.10.2 Through-Thickness Residual Stress Line Plots Comparing all Cx4N1-B (2024-T351) Coupons

In addition to the radial line plots of the residual stresses, through-thickness line plots were developed. These help to provide a more focused view of the residual stress field's behavior. These through-thickness residual stress line plots are provided in Fig. 378 through Fig. 383.

Some general trends can be seen from these plots. First, the right side of the hole generally has a more compressive residual stress through the thickness at each of the provided line locations. In addition, for the left side of the hole, the one with the fatigue cracks, it can be seen that there is a general trend for which the residual stress moves towards to a more tensile stress as a function of crack size, and as the line plots move away from the edge of the hole the residual stresses begin to collapse onto each other, such that at a distance of 0.10 inch away from the edge of the hole it is difficult to distinguish the individual coupons and their crack sizes. Except for the Cx4N1-08-B (2024-T351) coupon, which had the 0.50 inch crack. The residual stresses for this coupon seem to demonstrate a significant difference due to the effect of the crack, as compared to each other. The right side of the hole does not show this same trend. The residual stresses on the right side of the hole seem to all fall within a similar ban, with little to demonstrate a difference. This would have the potential to show that cyclically loading the coupons did not cause a significant difference in the stress field, since coupons were cyclically loaded to a larger and larger number of cycles, due to the propagation of the fatigue crack on the other side of the hole.

6.11 Residual Stress Results for Fatigue-Cracked Cx4N1-01-D and Cx4N1-02-D (7075-T651) Coupons with a 0.08 inch Fatigue Crack on Mandrel Entrance Surface

Residual stress contour and line plots also were developed for all the same crack lengths in coupons manufactured from 7075-T651 plate. The Cx4N1-01-D and Cx4N1-02-D configurations had cracks that were formed with a surface length of approximately 0.08 inch.

6.11.1 Contour Plots of Residual Stress for Cx4N1-01-D and Cx4N1-02-D Coupons

Surface contour plots of the residual stress for the Cx4N1-01-D and Cx4N1-02-D (7075-T651) conditions are provided in Fig. 384 through Fig. 389. These coupons had a fatigue crack that was propagated on the mandrel entrance surface, lower left edge of the hole, to a surface length of approximately 0.08 inch.

6.11.2 Line Plots of Stress Radially away from Hole for Cx4N1-01-D and Cx4N1-02-D Coupons

Line plots of the residual stress were produced at seven locations, all referenced from the entrance surface. These include line plots at 0.016 inch (entrance plane), 0.05 inch, 0.09 inch, 0.14 inch (mid plane), 0.16 inch, 0.20 inch, and 0.234 inch (exit plane). These plots show both the left and the right side of the hole in one single plot. Each plot has the individual measurements for Cx4N1-01-D and Cx4N1-02-D (7075-T651), the average of the two measurements, and error bars at each nodal location, which represents one standard deviation about the mean. In addition to line plots showing the residual stresses for the entire distance away from the edge of the hole, figures are provided for

the stress profile for the first 0.25 inch away from the edge of the hole. Residual stress line plots for coupons Cx4N1-01-D and Cx4N1-02-D (7075-T651) are provided in Fig. 390 through Fig. 403.

6.11.3 Line Plots of Stress for through the Thickness of the Part Cx4N1-01-D and Cx4N1-02-D Coupons

Through-thickness line plots of the residual stress on both the left side and the right side of the hole were developed at four specific locations away from the edge of the hole: 0.01 inch, 0.05 inch, 0.10 inch, and 0.150 inch. For each plot the individual residual stresses are provided, along with the average stress value for the two measurements, and error bars, which represent one standard deviation on the mean.

6.11.3.1 Line Plots of Stress through the Thickness for Cx4N1-01-D and Cx4N1-02-D – Left Side of the Hole

The residual stress through-thickness line plots for the left side of the hole are provided in Fig. 404 through Fig. 407.

6.11.3.2 Line Plots of Stress through the Thickness for Cx4N1-01-D and Cx4N1-02-D – Right Side of the Hole

Residual stress line plots also are provided for the right side of the hole for these two coupons. The right side of the hole did not have a fatigue crack. These residual stress line plots are provided in Fig. 408 through Fig. 411.

6.12 Residual Stress Results for Fatigue-Cracked Cx4N1-03-D and Cx4N1-04-D (7075-T651) Coupons with a 0.10 inch Fatigue Crack on Mandrel Entrance Surface

Residual stress contour plots and line plots were developed for coupons Cx4N1-03-D and Cx4N1-04-D (7075-T651). These coupons had fatigue cracks that were propagated to a final crack size of approximately 0.10 inch. These fatigue cracks were nucleated/formed on the left side of the coupon, on the Cx mandrel entrance surface.

6.12.1 Contour Plots of Residual Stress for Cx4N1-03-D and Cx4N1-04-D Coupons

Residual stress contour plots of coupons Cx4N1-03-D and Cx4N1-04-D (7075-T651) are provided along with the average residual stress of the two replicate conditions. These residual stress contour plots are provided in Fig. 412 through Fig. 417.

6.12.2 Line Plots of Stress Radially away from Hole for Cx4N1-03-D and Cx4N1-04-D Coupons

Line plots were developed along the same planes and defined for the other coupons and these residual stress line plots are provided in Fig. 418 through Fig. 431. For each of these line plots the individual residual stress is provided along with the average residual stress for the two coupons. A standard deviation was developed from that average and the error bars represent that standard deviation bounding the average residual stress. In addition to the line plots that provide a full-width perspective, plots are provided for the first 0.25 inch away from the edge of the hole.

6.12.3 Line Plots of Stress through the Thickness of the Part Cx4N1-03-D and Cx4N1-04-D Coupons

Through thickness residual stress line plots were developed at four planes on both the left and the right side of the hole. For this condition the coupons had a 0.10 inch fatigue crack that was developed on the left side of the hole. For each of these line plots the individual residual stress is provided along with the average residual stress for the two coupons. A standard deviation was developed from that average and the error bars represent that standard deviation bounding the average residual stress.

6.12.3.1 Line Plots of Stress through the Thickness for Cx4N1-03-D and Cx4N1-04-D – Left Side of the Hole

Residual stress through-thickness line plots for the left side of the Cx hole are provided in Fig. 432 through Fig. 435. This side of the hole had a fatigue crack that was developed and propagated to a length of approximately 0.10 inch.

6.12.3.2 Line Plots of Stress through the Thickness for Cx4N1-03-D and Cx4N1-04-D – Right Side of the Hole

The right side of the hole for these coupons had no fatigue crack developed during cyclic loading. Residual stress line plots for the right side of the hole for these two coupons are shown in Fig. 436 through Fig. 439.

6.13 Residual Stress Results for Fatigue-Cracked Cx4N1-05-D and Cx4N1-06-D (7075-T651) Coupons with a 0.125 inch Fatigue Crack on Mandrel Entrance Surface

The Cx4N1-05-D and Cx4N1-06-D (7075-T651) conditions had fatigue cracks that were developed and propagated to a length of 0.1259 inch for the -05 and to 0.1214

inch for the -06 coupon. These fatigue cracks were nucleated at the Cx mandrel entrance surface, on the left side of the hole. All of the line plots provided show the individual residual stress along with an average for the two replicates. A standard deviation was calculated from the average that is shown with a double-sided error bar on the average residual stress.

6.13.1 Contour Plots of Residual Stress for Cx4N1-05-D and Cx4N1-06-D Coupons

Residual stress contour plots for these two coupons are shown in Fig. 440 through Fig. 443. An average of these two residual stress fields is provided in Fig. 444 and Fig. 445.

6.13.2 Line Plots of Stress Radially away from Hole for Cx4N1-05-D and Cx4N1-06-D Coupons

Line plots of the residual stress radially away from the hole for this fatigue-cracked condition are shown in Fig. 446 through Fig. 457.

6.13.3 Line Plots of Stress through the Thickness of the Cx4N1-05-D and Cx4N1-06-D Coupons

Line plots were taken at four through-thickness locations for both the left and right side of the hole. Each line plot has the residual stress at discrete nodal locations for the two coupons, along with the average of the two and the standard deviation, as represented by a double-sided error bar.

6.13.3.1 Line Plots of Stress through the Thickness for Cx4N1-05-D and Cx4N1-06-D – Left Side of the Hole

The through-thickness residual stress line plots for the left side of the hole are provided in Fig. 458 through Fig. 461. It should be noted that for these coupons a fatigue crack that had a surface crack length of approximately 0.125 inch was developed in the left side of the hole.

6.13.3.2 Line Plots of Stress through the Thickness for Cx4N1-05-D and Cx4N1-06-D – Right Side of the Hole

Through thickness plots for the right side are provided in Fig. 462 through Fig. 465. The right side of these coupons had no fatigue crack.

6.14 Residual Stress Results for Fatigue-Cracked Cx4N1-07-D (7075-T651) Coupons with a 0.25 inch Fatigue Crack on Mandrel Entrance Surface

The Cx4N1-07-D (7075-T651) coupon had a 0.2505 inch fatigue crack that had been formed and propagated on the Cx mandrel entrance surface, on the left side of the hole. For this condition there was only one coupon manufactured so no replicate information is available. Residual stress contour plots and line plots are provided for this condition.

6.14.1 Contour Plots of Residual Stress for Cx4N1-07-D Coupons

Residual stress contour plots of the Cx4N1-07-D (7075-T651) condition are provided in Fig. 466 and Fig. 467.

6.14.2 Line Plots of Stress Radially away from Hole for Cx4N1-07-D Coupons

Residual stress line plots were developed along the same planes through the thickness showing the radial stress away from the hole. The line plots of the radial stress are provided in Fig. 468 through Fig. 481.

6.14.3 Line Plots of Stress through the Thickness of the Cx4N1-07-D Coupons

Through-thickness line plots were developed for both the left and right sides of the Cx hole. The left side of the coupon had a fatigue crack that had a surface length of 0.2505 inch.

6.14.3.1 Line Plots of Stress through the Thickness for Cx4N1-07-D – Left Side of the Hole

Residual stress line plots for the left side of the hole are provide in Fig. 482 through Fig. 485.

6.14.3.2 Line Plots of Stress through the Thickness for Cx4N1-07-D – Right Side of the Hole

Line plots for the right side of the hole are provided in Fig. 486 through Fig. 489.

6.15 Residual Stress Results for Fatigue-Cracked Cx4N1-08-D (7075-T651) Coupons with a 0.50 inch Fatigue Crack on Mandrel Entrance Surface

A residual stress contour plot and line plots were developed for the Cx4N1-08-D (7075-T651) condition. This condition had a fatigue crack that was developed and propagated to a Cx mandrel surface length of 0.5017 inch. This fatigue crack had

propagated through the thickness of the part and an additional small (approx. 0.05 inch x 0.05 inch) corner crack had developed on the right side of the hole as well. This formed during fatigue loading and was not induced via any notching mechanism. For this condition there was only one coupon manufactured so no replicate information is available to determine an average and standard deviation.

6.15.1 Contour Plots of Residual Stress for Cx4N1-08-D Coupons

Residual stress contour plots of the Cx4N1-08-D (7075-T651) condition are provided in Fig. 490 and Fig. 491.

6.15.2 Line Plots of Stress Radially away from Hole for Cx4N1-08-D Coupons

Residual stress line plots for the Cx4N1-08-D (7075-T651) coupon were developed along the same through-thickness planes as the other coupons. These line plots are provided in Fig. 492 through Fig. 505.

6.15.3 Line Plots of Stress through the Thickness of the Cx4N1-08-D Coupons

Through-thickness line plots were produced for both the left and right side of the hole. For this condition the left side of the hole had a 0.5017 inch surface crack along the Cx mandrel entrance surface. The right side of the hole also had a small (0.05 inch x 0.05 inch) corner crack at the mandrel entrance surface.

6.15.3.1 Line Plots of Stress through the Thickness for Cx4N1-08-D – Left Side of the Hole

Through-thickness line plots of the residual stress state on the left side of the hole are provided in Fig. 506 through Fig. 509.

6.15.3.2 Line Plots of Stress through the Thickness for Cx4N1-08-D – Right Side of the Hole

Residual stress line plots for the right side of the hole are provided in Fig. 510 through Fig. 513.

6.16 Comparison of Residual Stress Line Plots for All Cx4N1-D (7075-T651) Coupons

6.16.1 Residual Stress Radial Line Plots Comparing all Cx4N1-B (2024-T351) Coupons

In an effort to capture and quantify the effect of the fatigue crack on the residual stress field introduced by the Cx process in this alloy, radial line plots were developed showing all of the coupons results. Line plots are provided at three of the through-thickness depths, the entrance, mid plane, and exit. In addition, plots are provided that capture the first 0.25 inch from each side of the hole. This helps to visualize the effects near the edge of the hole, where greatest impact occurs. These line plots are provided in Fig. 514 through Fig. 519.

It can be seen from these line plots that there is a general trend in which the side of the hole with the fatigue crack, the left side, shows a decrease in the residual stress from the Cx mandrel entrance surface through to the exit surface. This effect seems to decrease the magnitude of the residual stress by approximately 20 ksi. Unlike that which

is seen in the Cx4N1-B (2024-T351) coupons, this shift does not seem to correspond to the fatigue crack size on the left side of the hole, but seems to occur regardless of the crack size.

6.16.2 Through-Thickness Residual Stress Line Plots Comparing all Cx4N1-B (2024-T351) Coupons

In an effort to gain a greater understanding of the effect of the fatigue crack, several through-thickness residual stress line plots are provided for both the left side of the hole and the right side. As seen in the above residual stress line plots of the stress radially away from the hole, it is seen that the fatigue crack dramatically decreases the compressive residual stresses next to the processed hole. Through-thickness residual stress line plots for the left side of the hole are provided in Fig. 520 through Fig. 523, and the right side in Fig. 524 through Fig. 527.

From these figures there are some key findings. It can be seen in Fig. 520 as compared to Fig. 524 that the effect of the crack seems to decrease the average through-thickness residual stress to approximately 70 ksi from the right side of the hole, which had an approximate average residual stress of 80 ksi. One of the very unique findings from these coupons is that it seems that the size of the fatigue crack does not correlate to a shift in the residual stress field on the left side of the hole. All of the through-thickness residual stress lines show a similar trend in which the residual stresses are decreased, when compared to the right side of the hole. This shift is roughly a 10 ksi shift for all of the fatigue crack sizes. This effect is not what was shown in the Cx4N1-B (2024-T351) coupons. In that material there was still a shift in the residual stress field when compared to the uncracked, right, side of the hole, however, this shift was correlated to the size of

the fatigue crack. It is unknown why the 7075-T651 material exhibits this unique behavior and is something that needs further exploration.

Fig. 228 Image of all Cx4N1-XX-B (2024-T351) Cold Expanded and Fatigue-Cracked Coupons upon Arrival at Hill Engineering LLC.

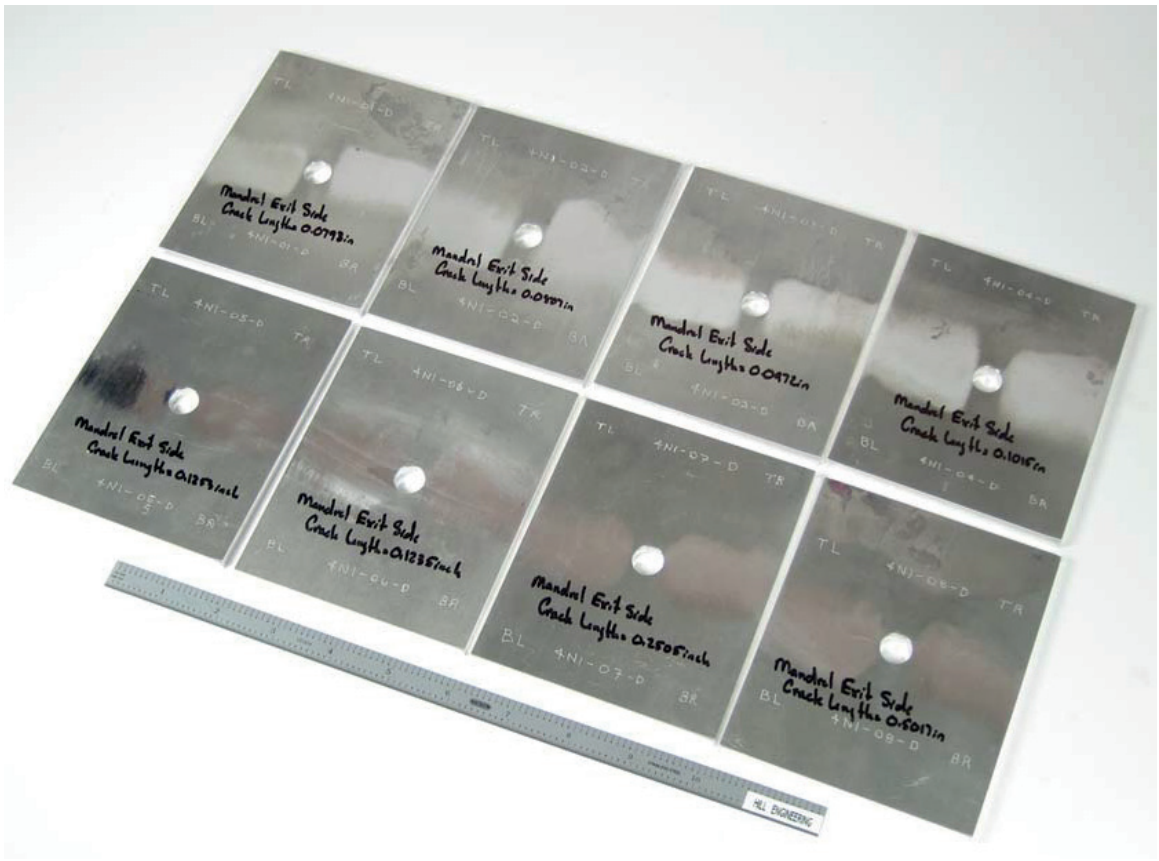

Fig. 229 Image of all Cx4N1-XX-D (7075-T651) Cold Expanded and Fatigue-Cracked Coupons upon Arrival at Hill Engineering LLC.

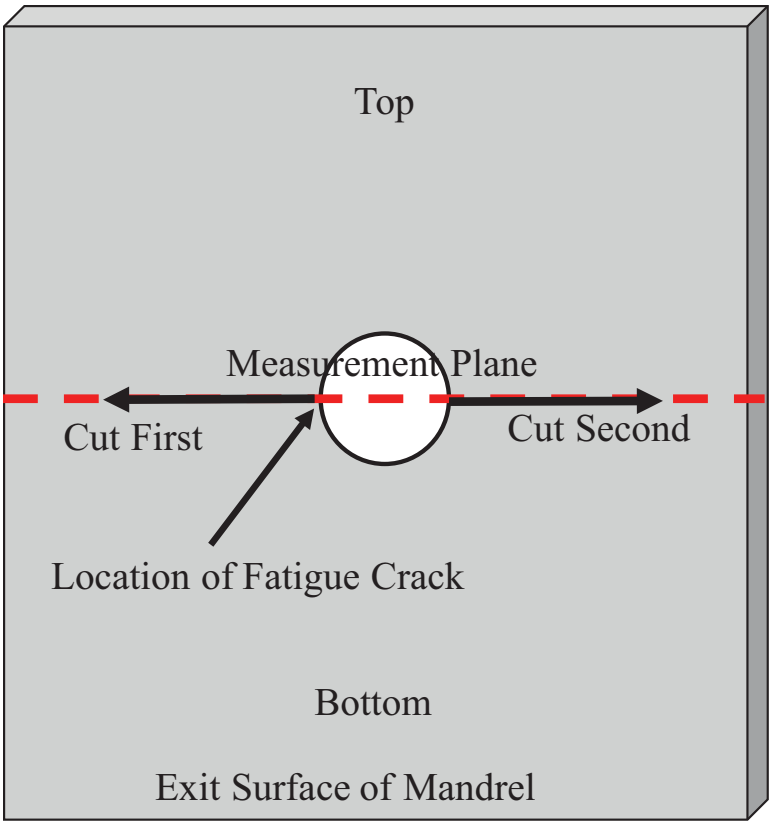

Fig. 230 Basic Schematic for Wire EDM Cutting Process for Cx4N1 Fatigue-Cracked Coupons.

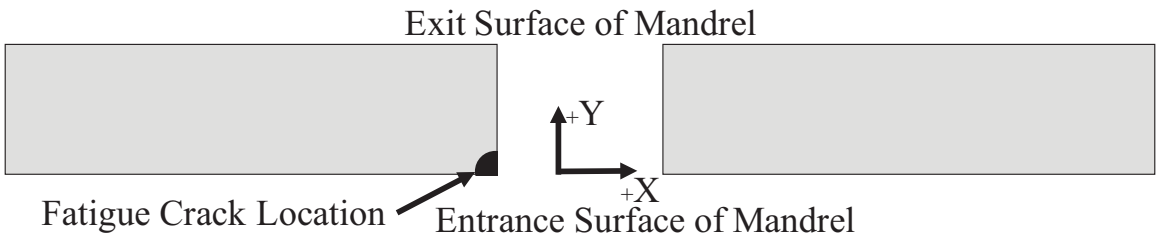

Fig. 231 Basic Schematic of all Cx4N1 Displacement Orientations – Showing Location of Fatigue Crack for all Coupons.

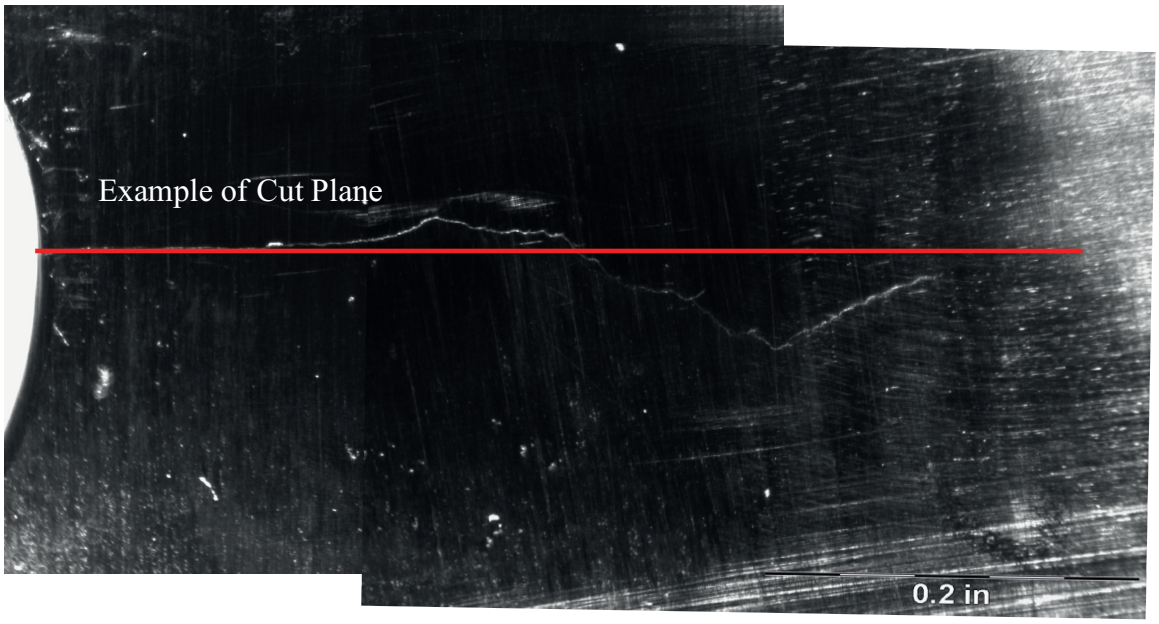

Fig. 232 Image of Coupon Cx4N1-08-D Showing the Nonplanar Surface Crack Tip Morphology with Representation of Wire EDM Cut Line.

Fig. 233 Image of Coupon Cx4N1-08-D, Which Had a 0.5017 inch Surface, after the Wire EDM Cut, Showing that the Crack Front Could not be Followed Throughout the Cut.

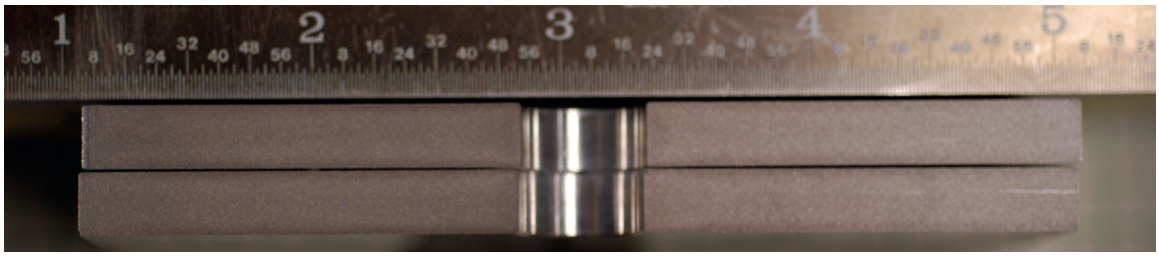

Fig. 234 Image of Post Wire EDM Cut for Coupon Cx4N1-01-B (2024-T351).

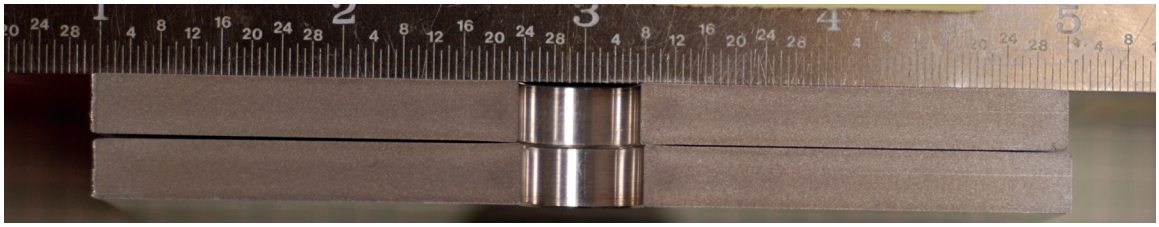

Fig. 235 Image of Post Wire EDM Cut for Coupon Cx4N1-01-D (7075-T651).

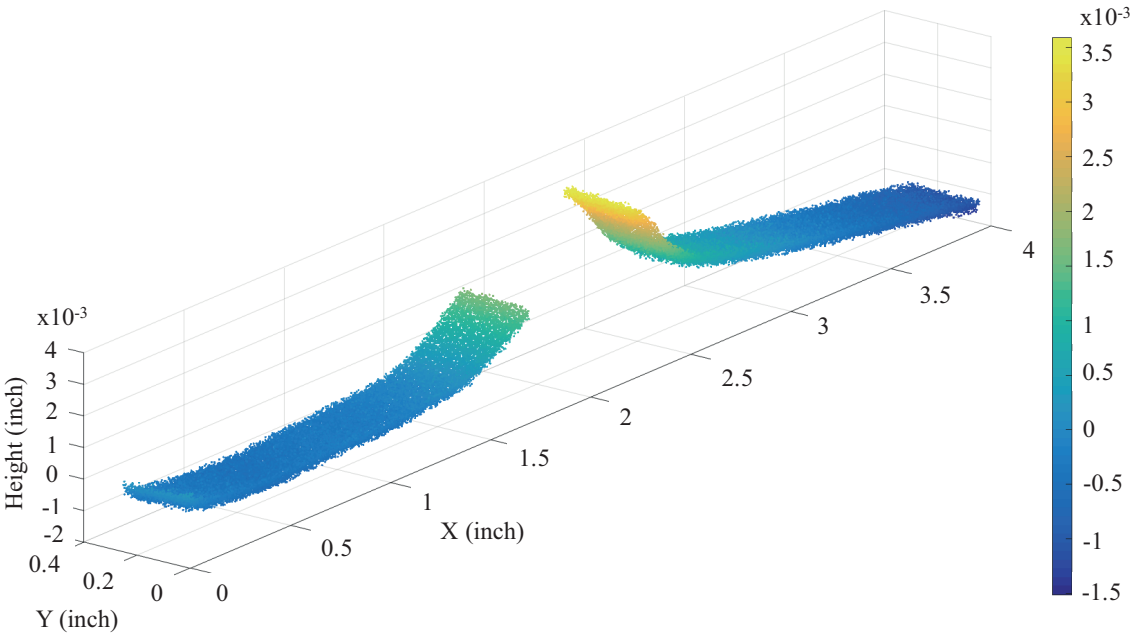

Fig. 236 Image of Displacement Data for Coupon Cx4N1-01-B (2024-T351) from the "Static" Side.

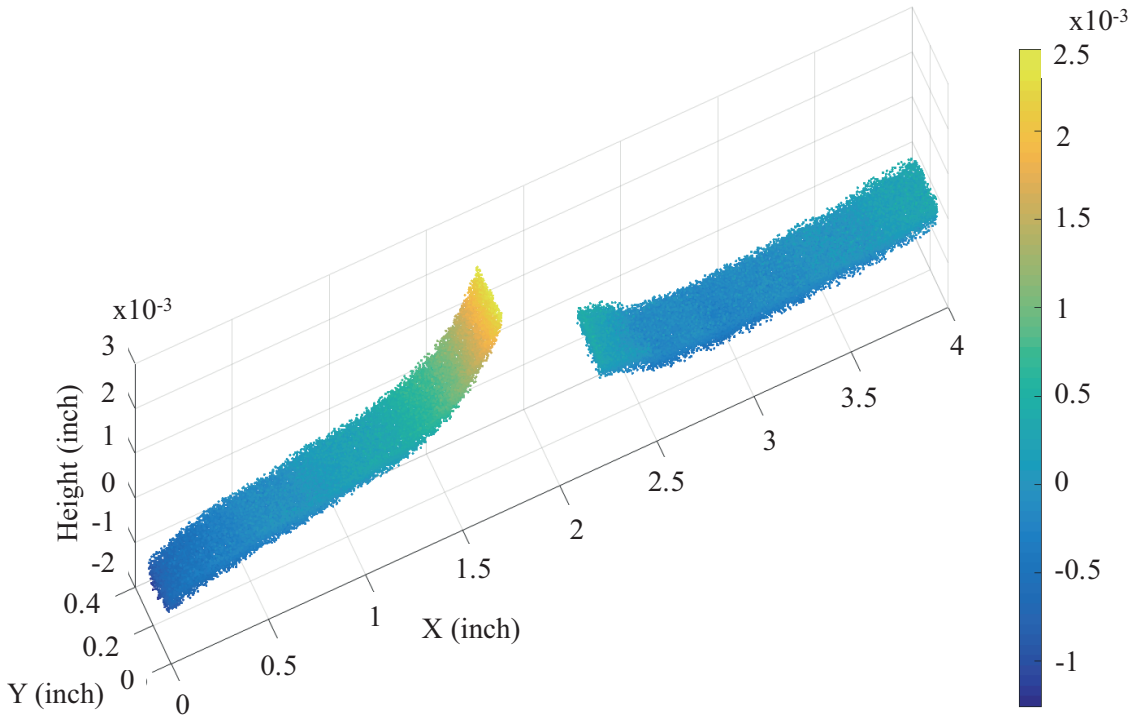

Fig. 237 Image of Displacement Data for Coupon Cx4N1-01-B (2024-T351) from the "Floating" Side.

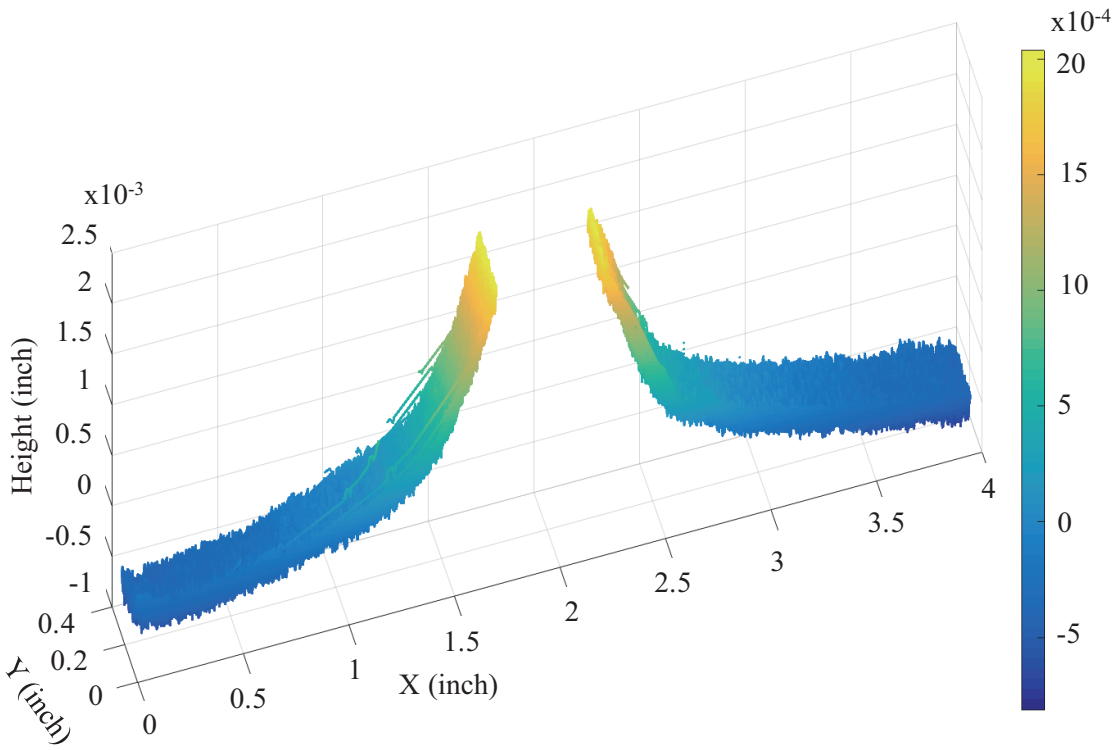

Fig. 238 Image of Displacement Data for Coupon Cx4N1-01-B (2024-T351) after Being Averaged and Data Density Increased.

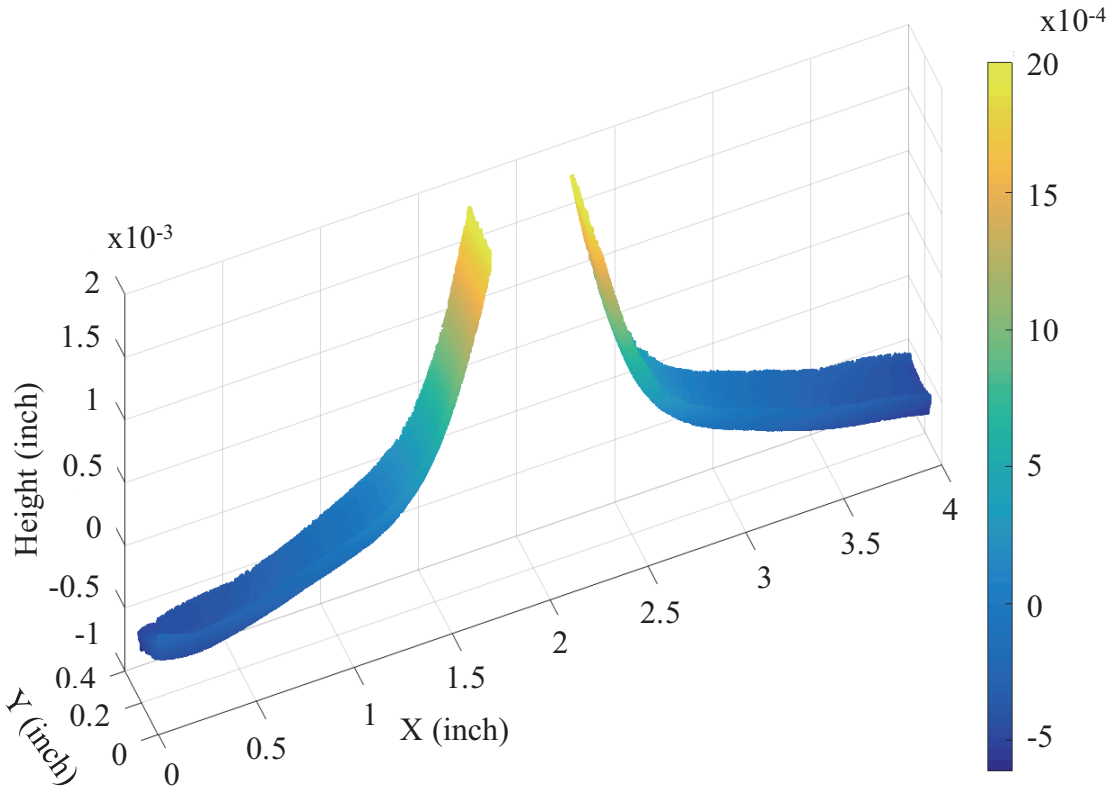

Fig. 239 Image of Displacement Data for Coupon Cx4N1-01-B (2024-T351) after the Modified Thompson Tau Method was Performed to Remove Outliers for a Knot Density of Four Through-Thickness and Thirty-Two Radially away from Hole.

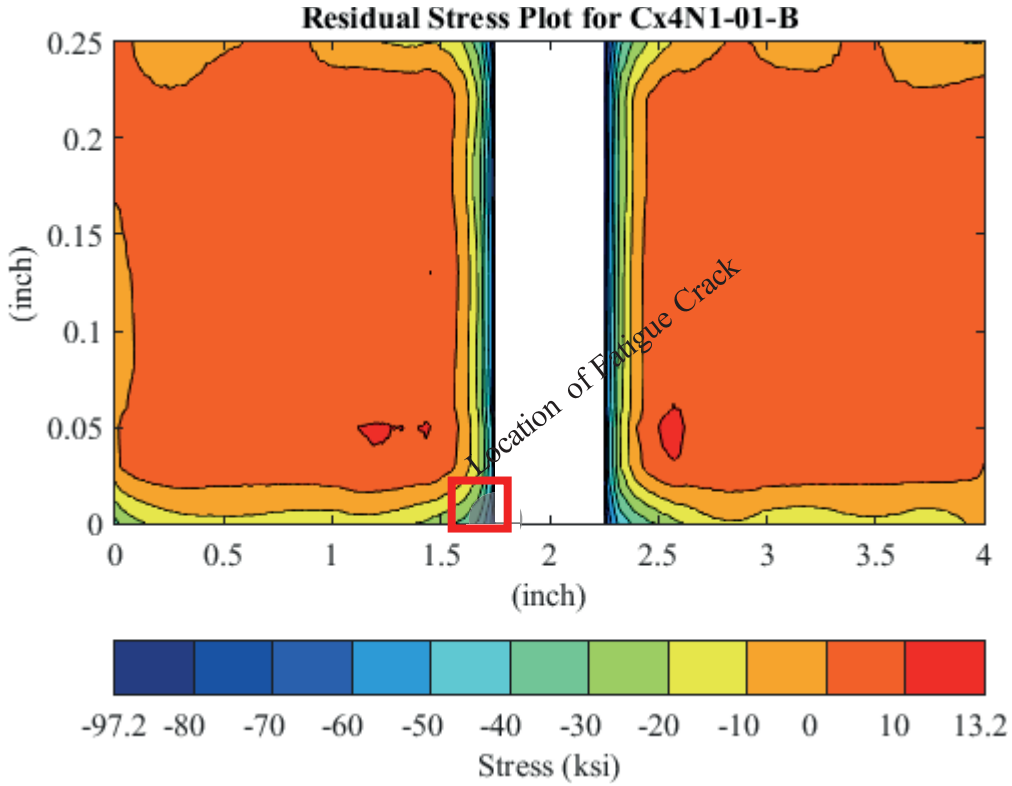

Fig. 240 Residual Stress Contour Plot of Coupon Cx4N1-01-B (2024-T351) – Mandrel Entrance Surface at Y=0, 0.080 inch Fatigue Crack on Left Side of Hole on Mandrel Entrance Surface.

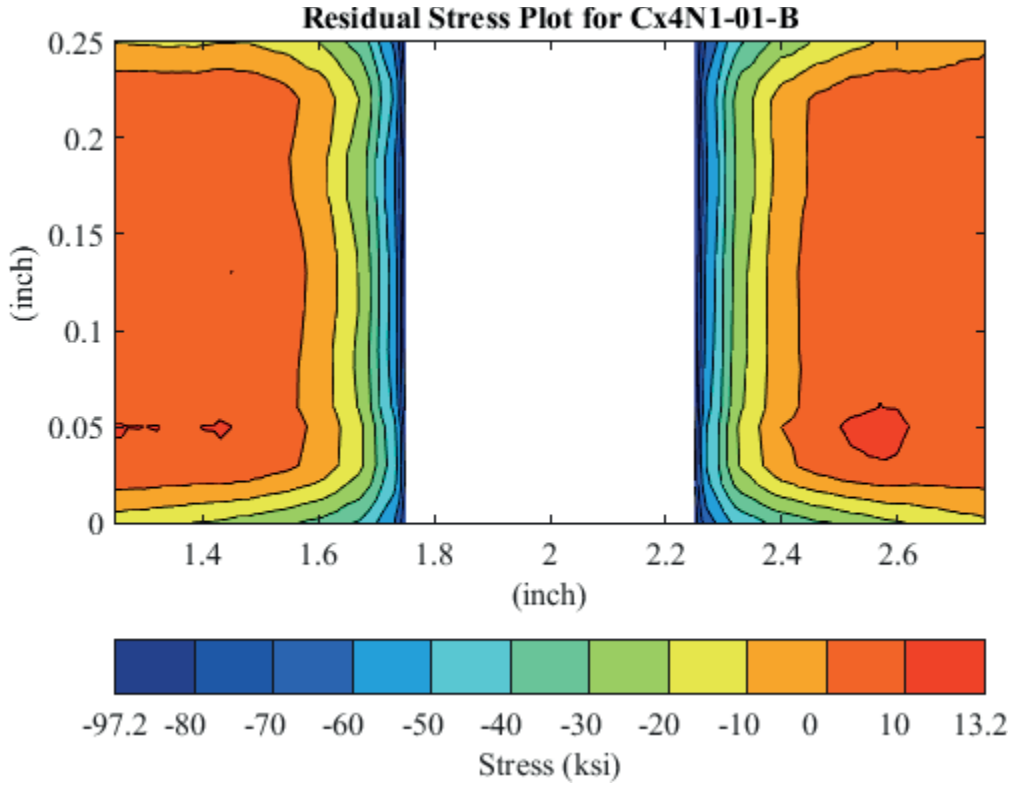

Fig. 241 Residual Stress Contour Plot of Coupon Cx4N1-01-B (2024-T351) – Mandrel Entrance Surface at Y=0, 0.080 inch Fatigue Crack on Left Side of Hole on Mandrel Entrance Surface – Zoomed in Next to Hole.

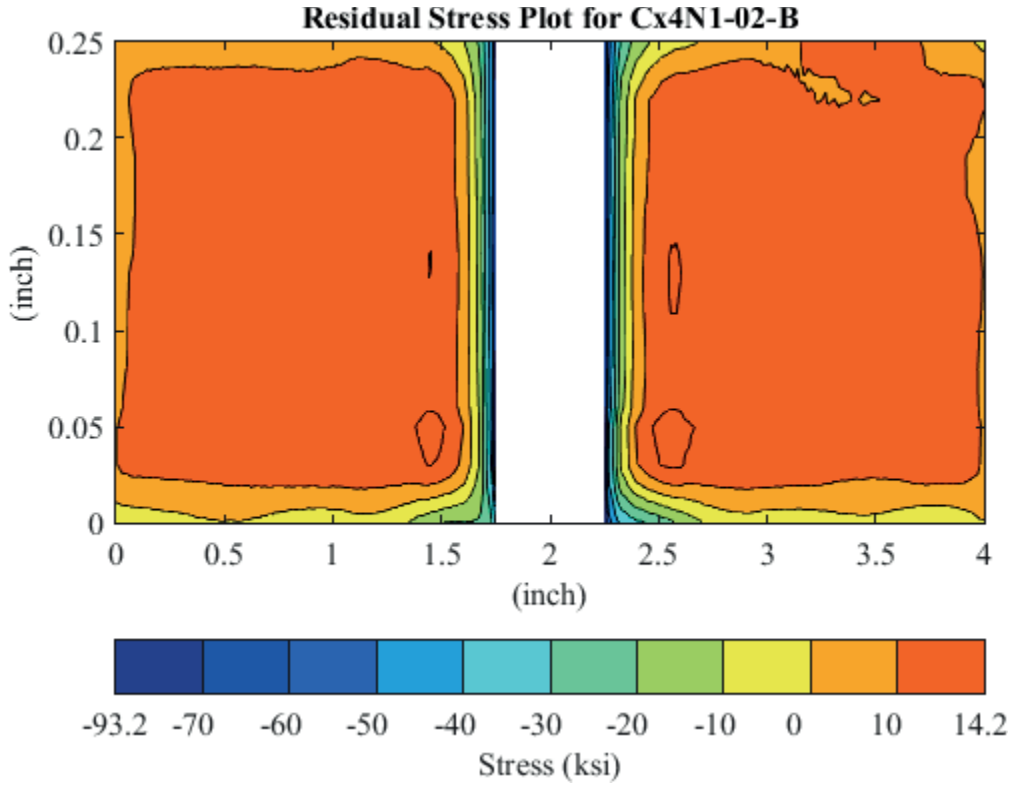

Fig. 242 Residual Stress Contour Plot of Coupon Cx4N1-02-B (2024-T351) – Mandrel Entrance Surface at Y=0, 0.080 inch Fatigue Crack on Left Side of Hole on Mandrel Entrance Surface.

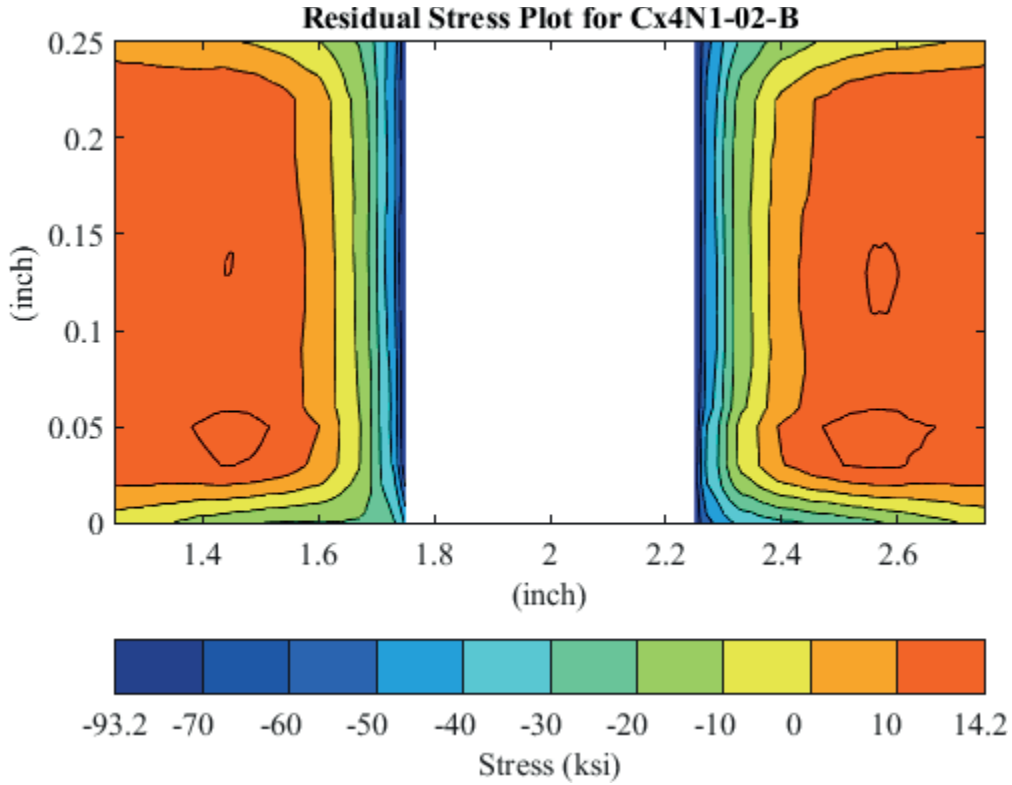

Fig. 243 Residual Stress Contour Plot of Coupon Cx4N1-02-B (2024-T351) – Mandrel Entrance Surface at Y=0, 0.080 inch Fatigue Crack on Left Side of Hole on Mandrel Entrance Surface – Zoomed in Next to Hole.

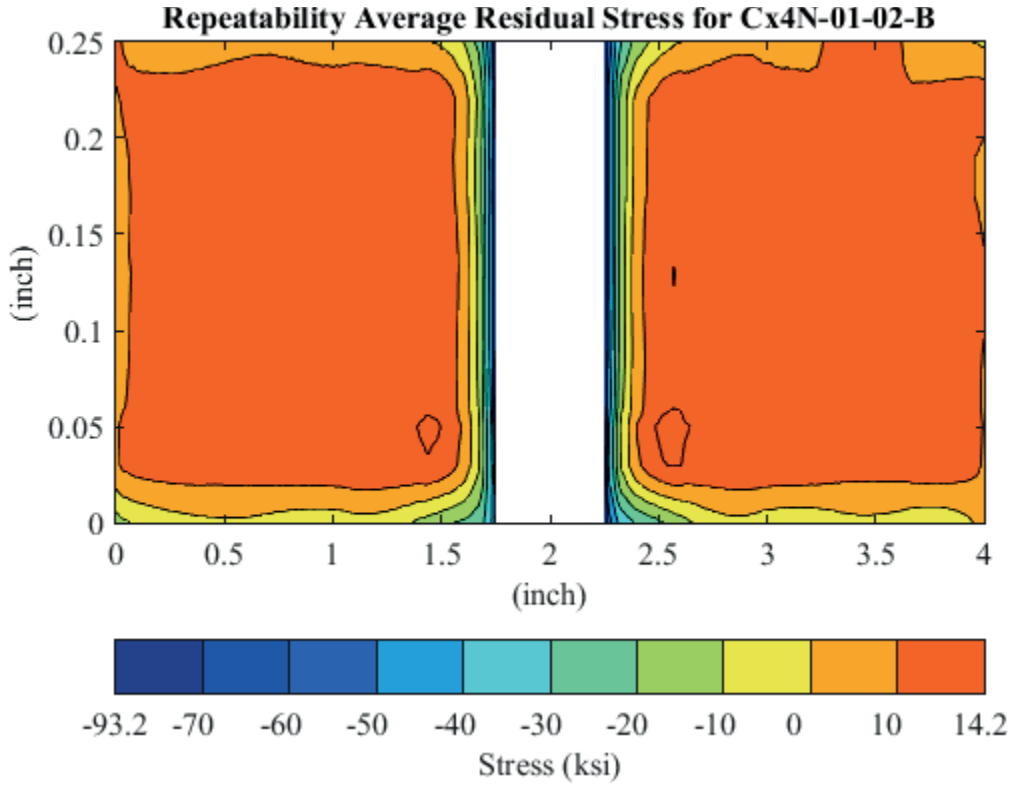

Fig. 244 Average Residual Stress Contour Plot of Coupons Cx4N1-01-B and Cx4N1-02-B (2024-T351) – Mandrel Entrance Surface at Y=0, 0.080 inch Fatigue Crack on Left Side of Hole on Mandrel Entrance Surface

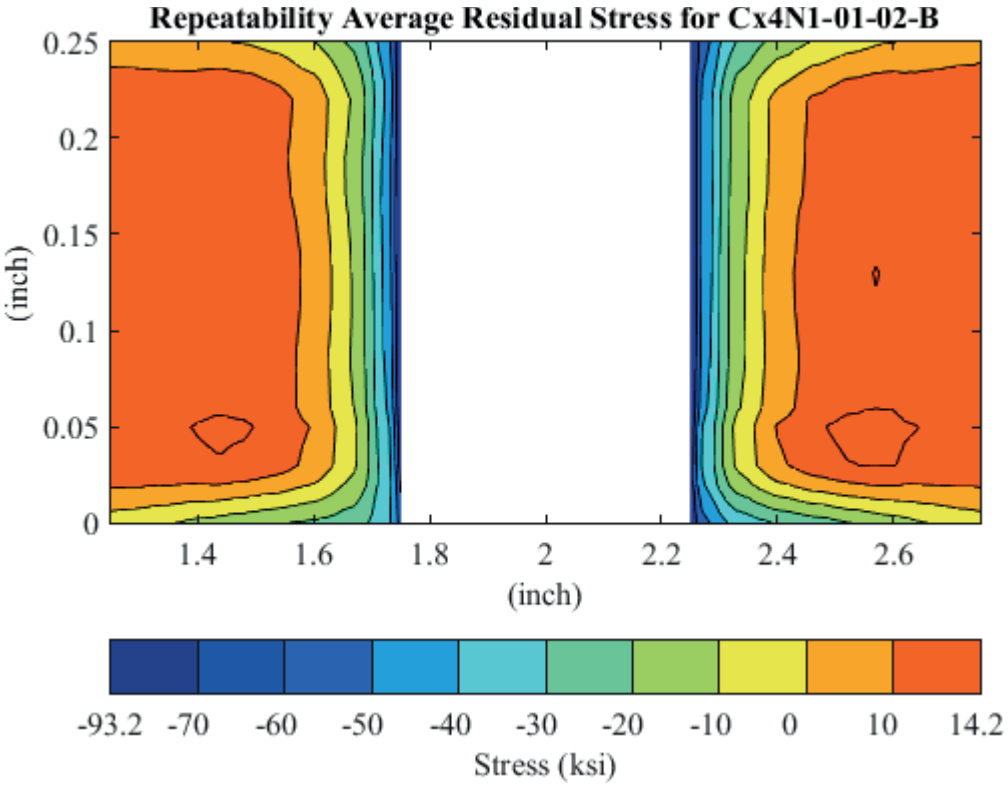

Fig. 245 Average Residual Stress Contour Plot of Coupons Cx4N1-01-B and Cx4N1-02-B (2024-T351) – Mandrel Entrance Surface at Y=0, 0.080 inch Fatigue Crack on Left Side of Hole on Mandrel Entrance Surface – Zoomed in Next to Hole.

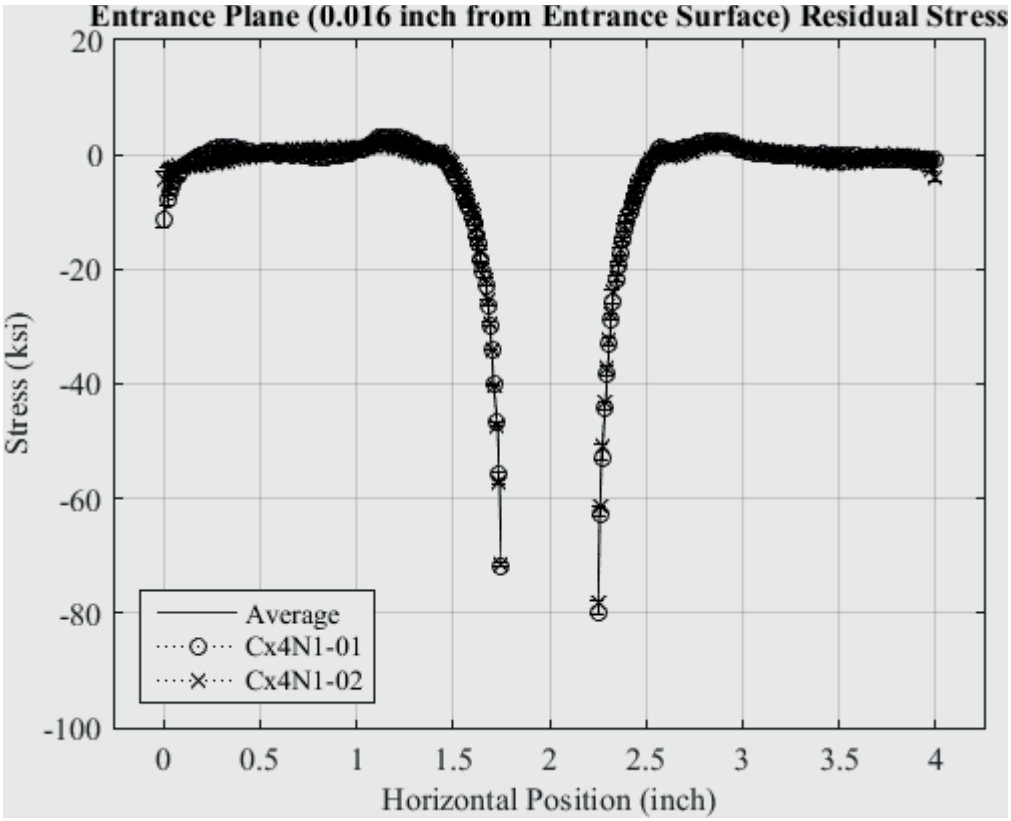

Fig. 246 Residual Stress Line Plot of Cx4N1-01-B and Cx4N1-02-B (2024-T351) at a Distance of 0.016 inch (Entrance surface) from the Entrance Surface – Coupons had a 0.08 inch Fatigue Crack at the Left Entrance Surface.

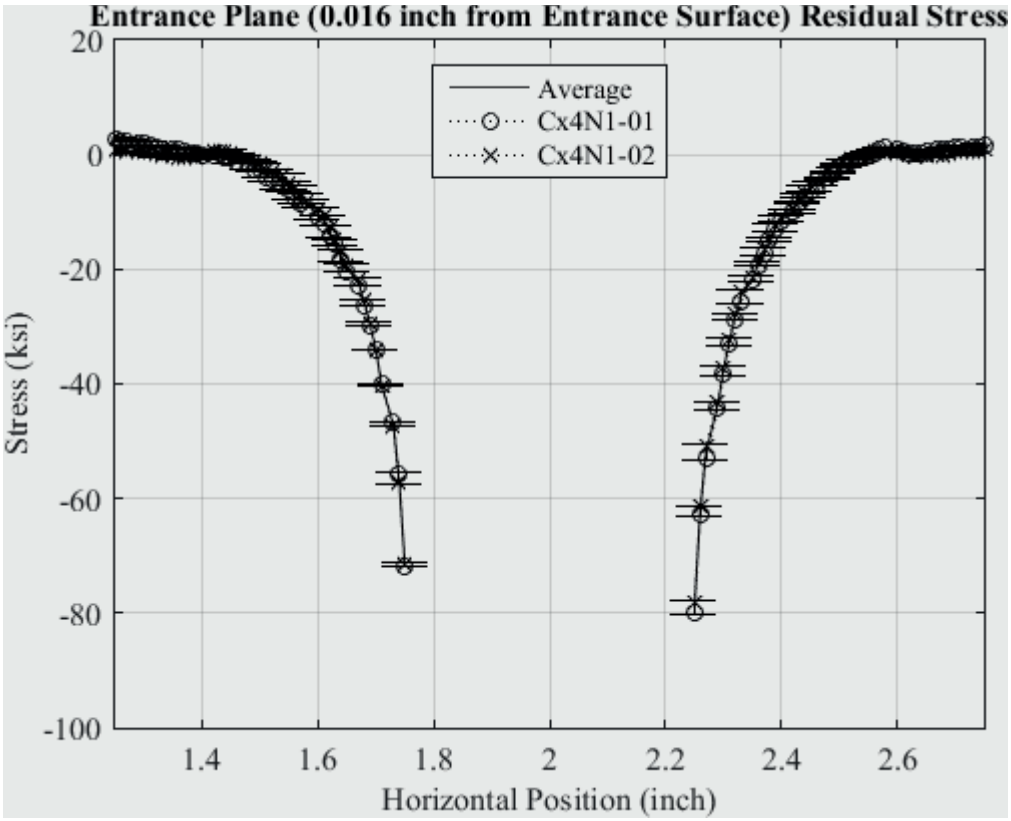

Fig. 247 Residual Stress Line Plot of Cx4N1-01-B and Cx4N1-02-B (2024-T351) at a Distance of 0.016 inch (Entrance surface) from the Entrance Surface – Coupons had a 0.08 inch Fatigue Crack at the Left Entrance Surface – Zoomed in Next to Hole.

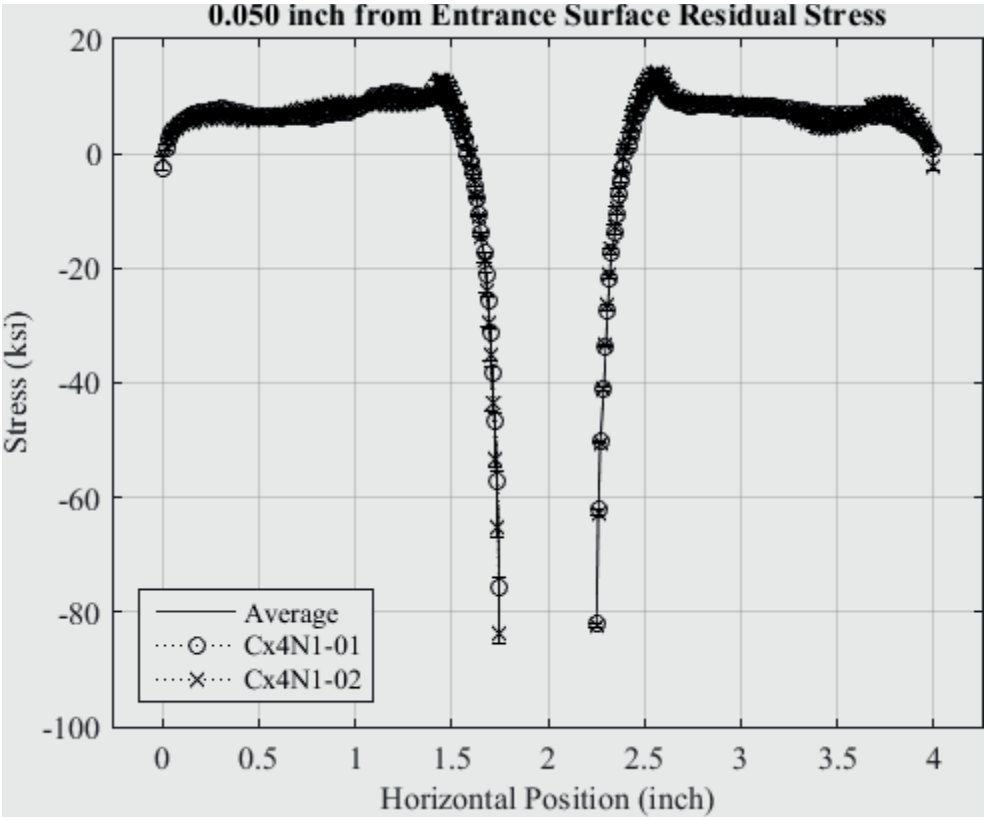

Fig. 248 Residual Stress Line Plot of Cx4N1-01-B and Cx4N1-02-B (2024-T351) at a Distance of 0.050 inch from the Entrance Surface – Coupons had a 0.08 inch Fatigue Crack at the Left Entrance Surface.

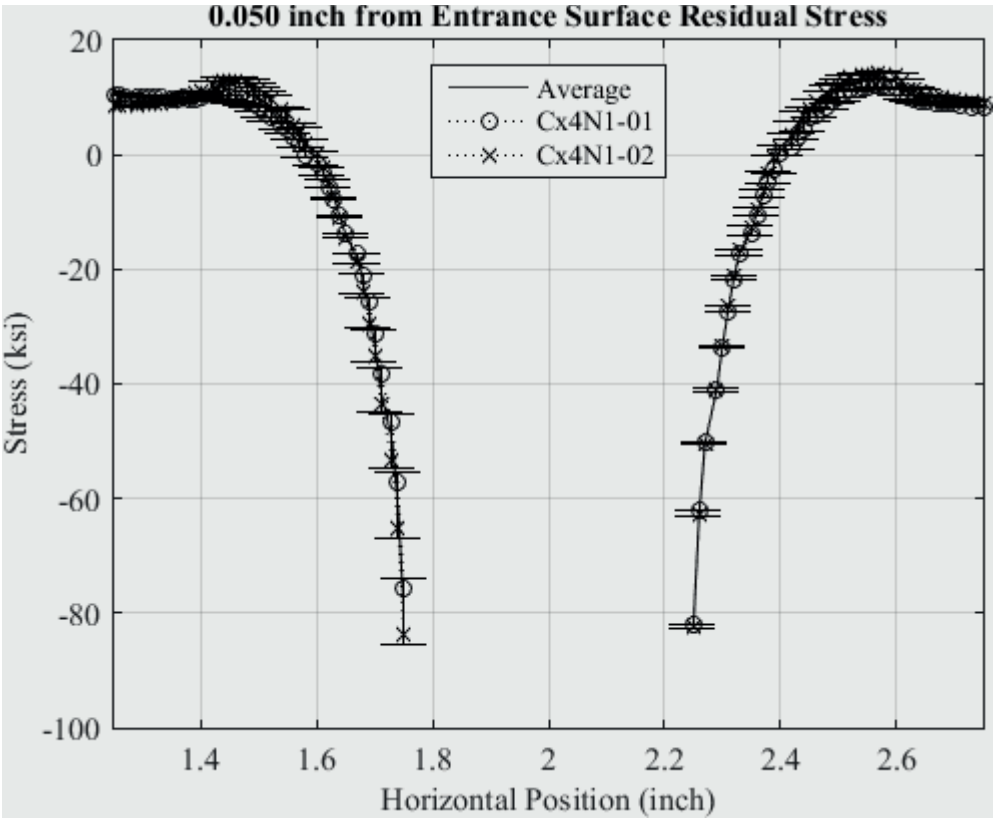

Fig. 249 Residual Stress Line Plot of Cx4N1-01-B and Cx4N1-02-B (2024-T351) at a Distance of 0.050 inch from the Entrance Surface – Coupons had a 0.08 inch Fatigue Crack at the Left Entrance Surface – Zoomed in Next to Hole.

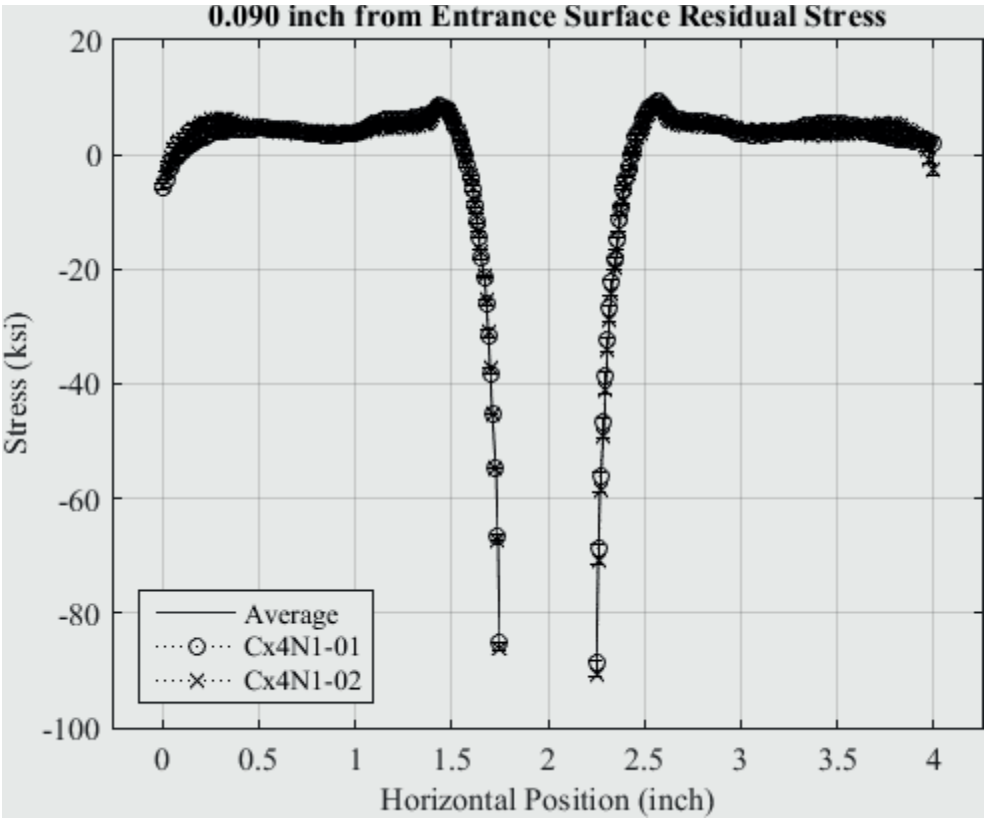

Fig. 250 Residual Stress Line Plot of Cx4N1-01-B and Cx4N1-02-B (2024-T351) at a Distance of 0.090 inch from the Entrance Surface – Coupons had a 0.08 inch Fatigue Crack at the Left Entrance Surface.

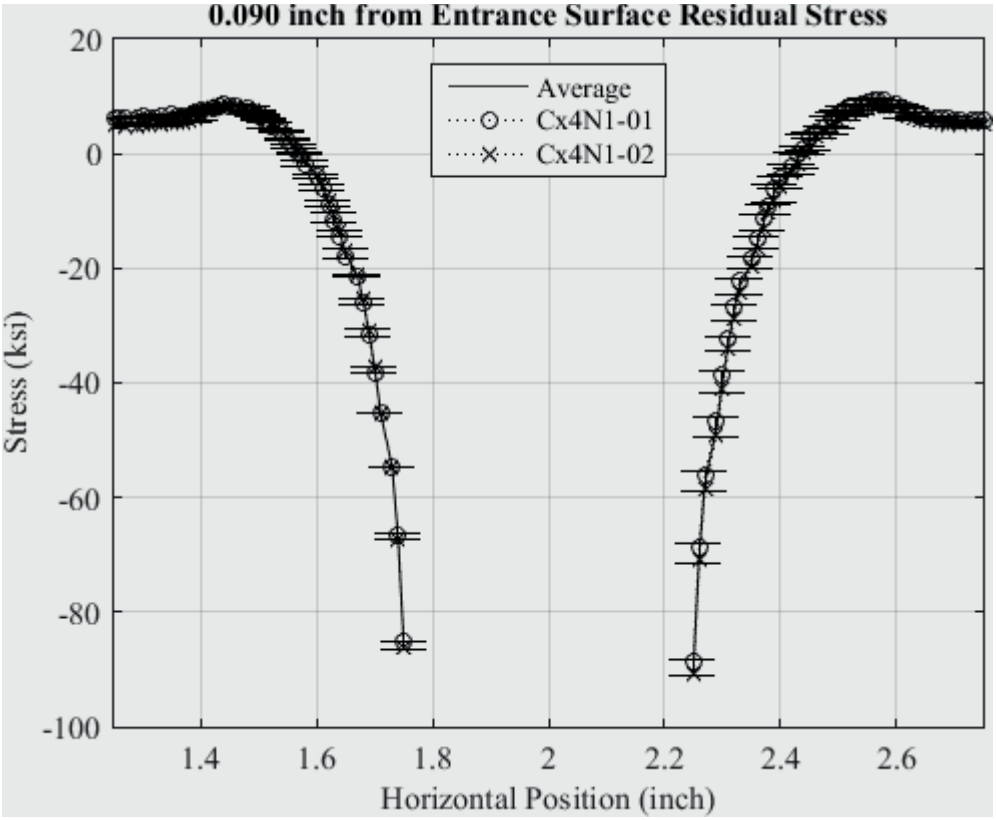

Fig. 251 Residual Stress Line Plot of Cx4N1-01-B and Cx4N1-02-B (2024-T351) at a Distance of 0.090 inch from the Entrance Surface – Coupons had a 0.08 inch Fatigue Crack at the Left Entrance Surface – Zoomed in Next to Hole.

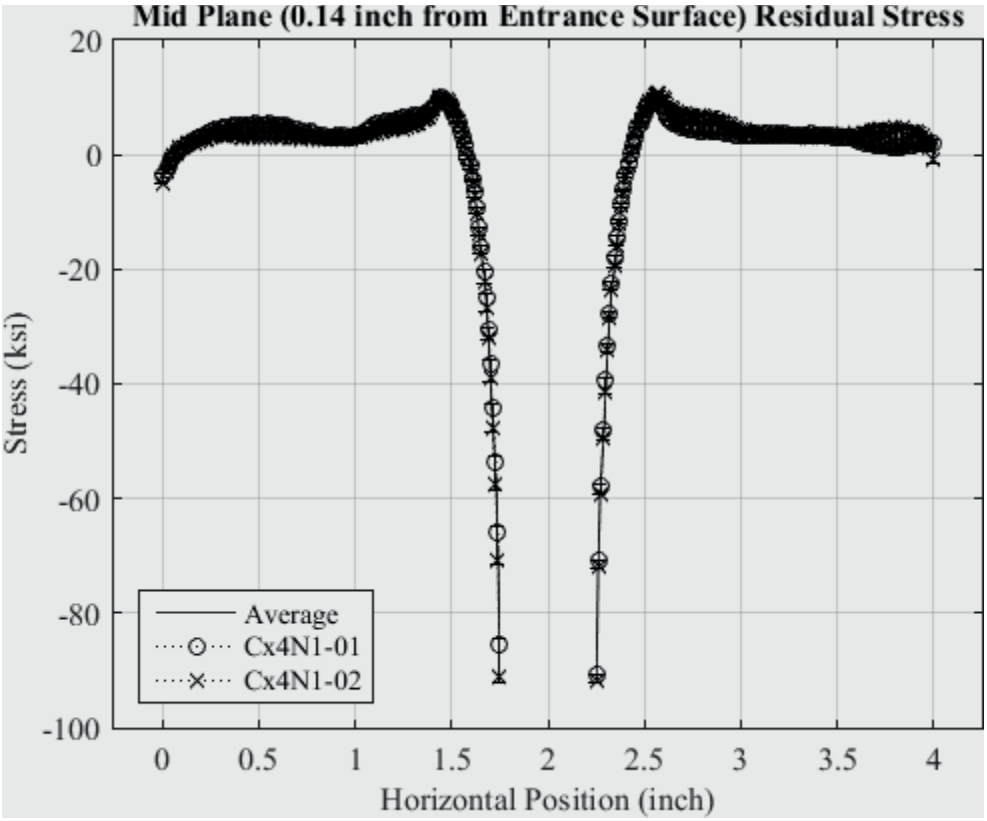

Fig. 252 Residual Stress Line Plot of Cx4N1-01-B and Cx4N1-02-B (2024-T351) at a Distance of 0.140 inch (Mid Plane Surface) from the Entrance Surface – Coupons had a 0.08 inch Fatigue Crack at the Left Entrance Surface.

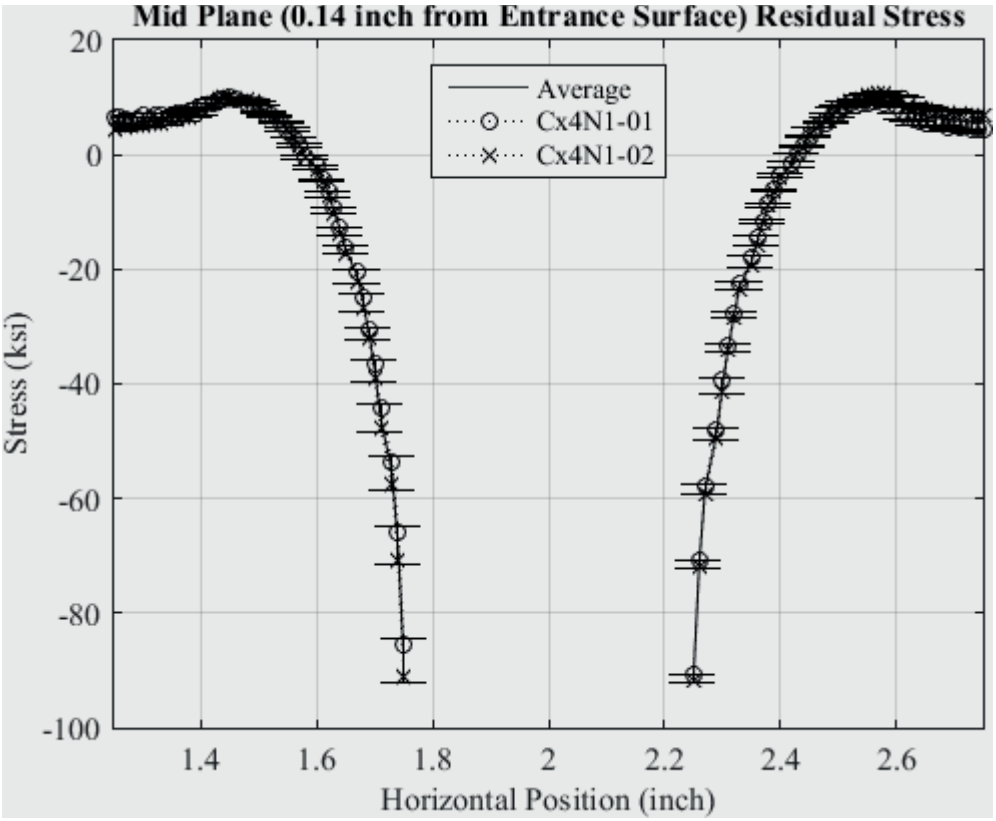

Fig. 253 Residual Stress Line Plot of Cx4N1-01-B and Cx4N1-02-B (2024-T351) at a Distance of 0.140 inch (Mid Plane Surface) from the Entrance Surface – Coupons had a 0.08 inch Fatigue Crack at the Left Entrance Surface – Zoomed in Next to Hole.

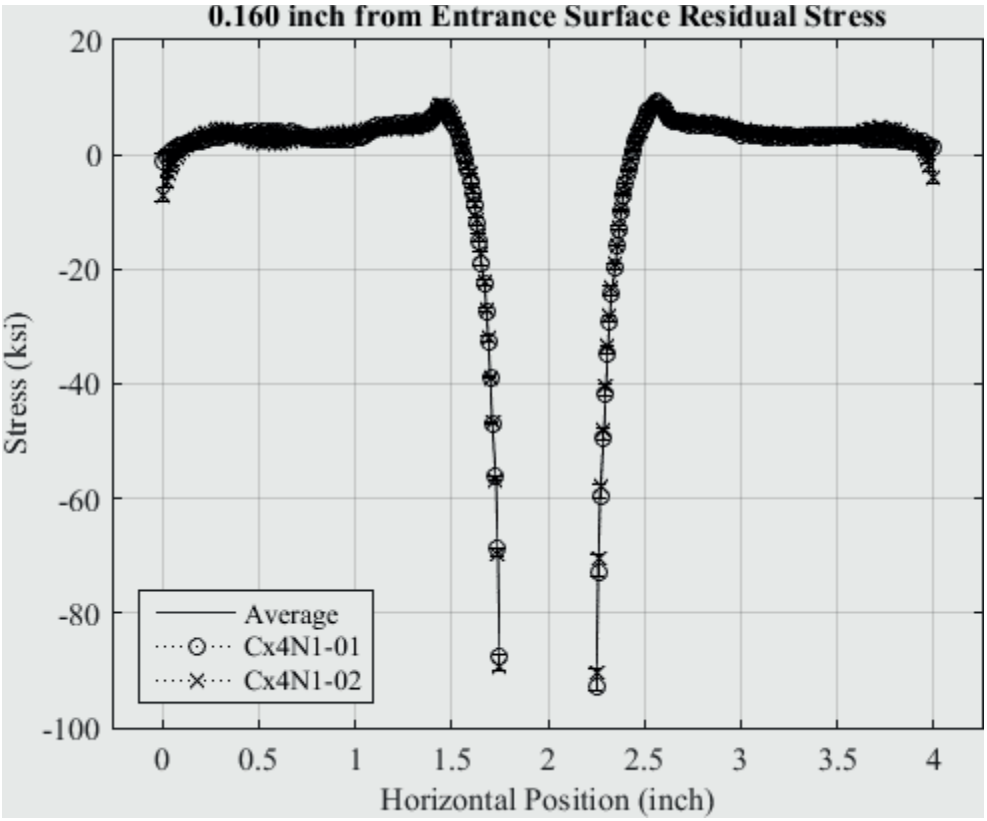

Fig. 254 Residual Stress Line Plot of Cx4N1-01-B and Cx4N1-02-B (2024-T351) at a Distance of 0.160 inch from the Entrance Surface – Coupons had a 0.08 inch Fatigue Crack at the Left Entrance Surface.

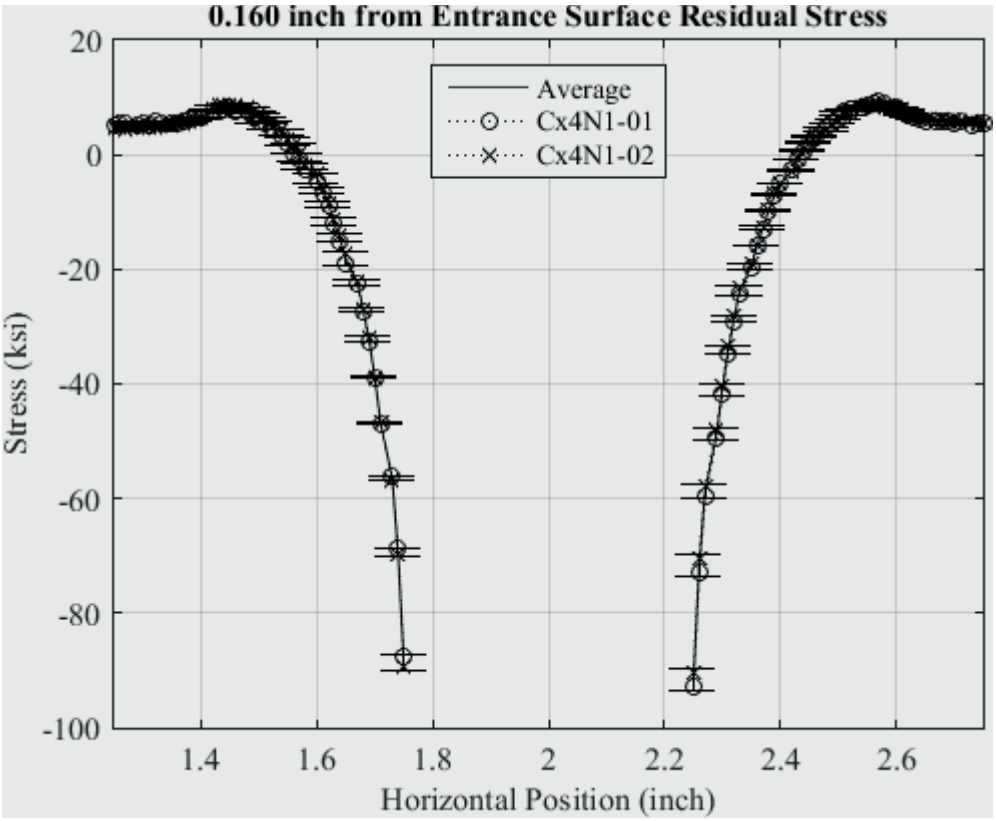

Fig. 255 Residual Stress Line Plot of Cx4N1-01-B and Cx4N1-02-B (2024-T351) at a Distance of 0.160 inch from the Entrance Surface – Coupons had a 0.08 inch Fatigue Crack at the Left Entrance Surface – Zoomed in Next to Hole.

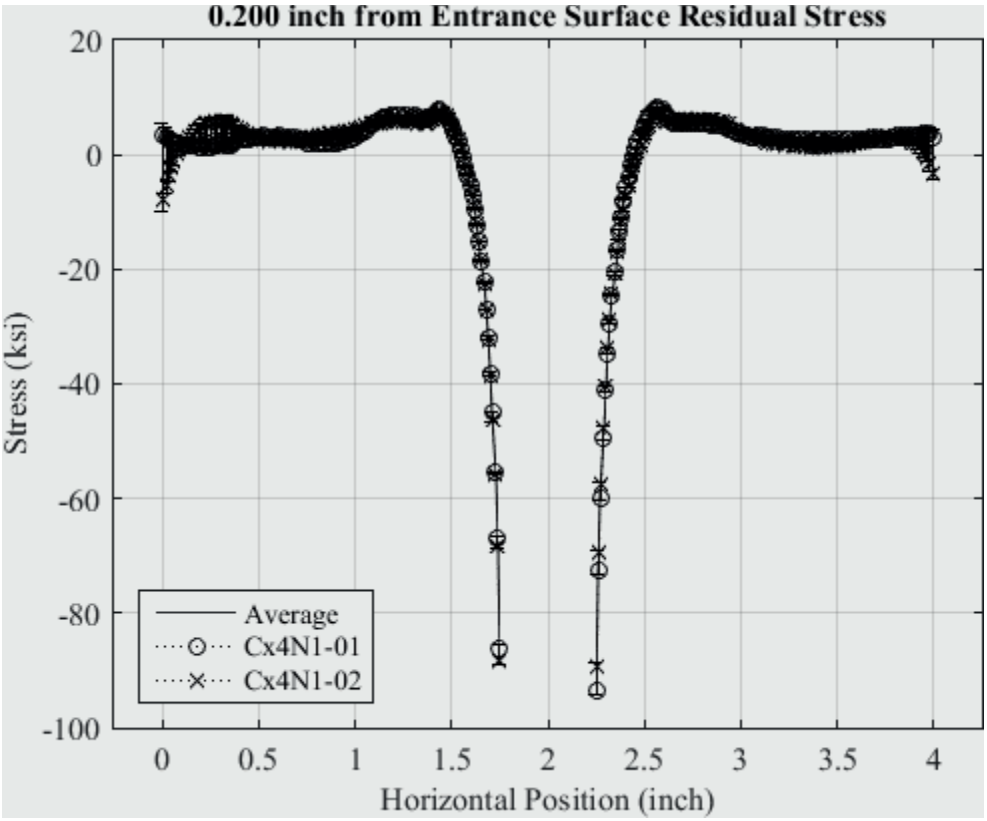

Fig. 256 Residual Stress Line Plot of Cx4N1-01-B and Cx4N1-02-B (2024-T351) at a Distance of 0.200 inch from the Entrance Surface – Coupons had a 0.08 inch Fatigue Crack at the Left Entrance Surface.

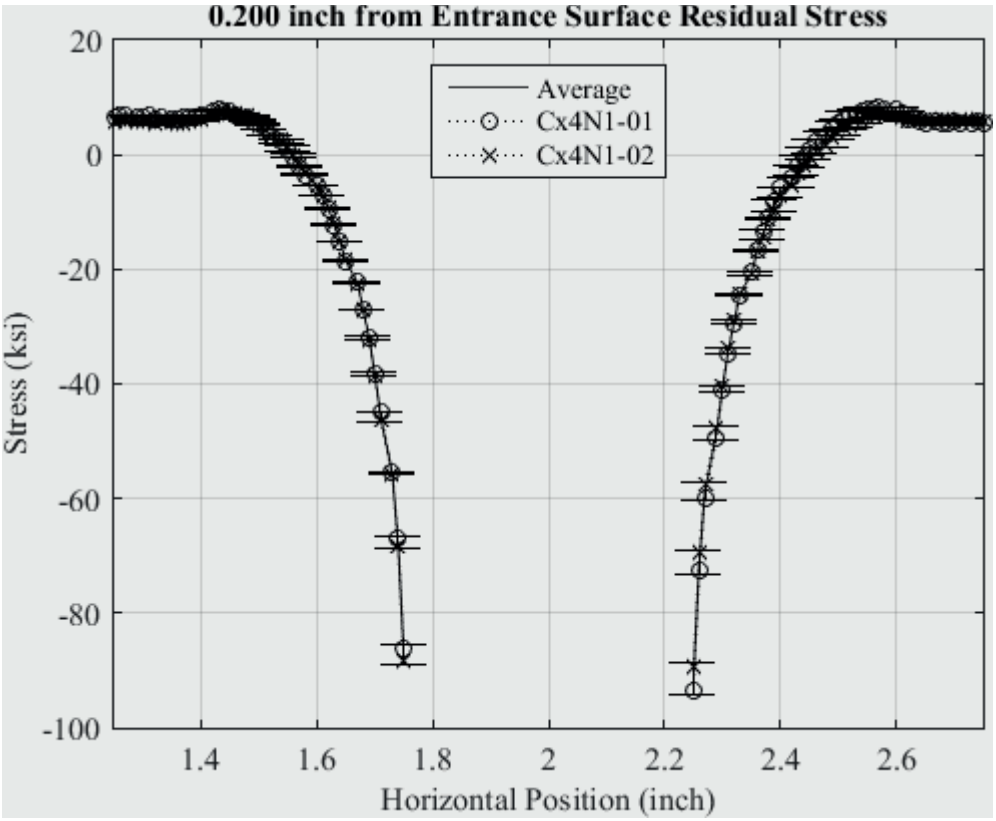

Fig. 257 Residual Stress Line Plot of Cx4N1-01-B and Cx4N1-02-B (2024-T351) at a Distance of 0.200 inch from the Entrance Surface – Coupons had a 0.08 inch Fatigue Crack at the Left Entrance Surface – Zoomed in Next to Hole.

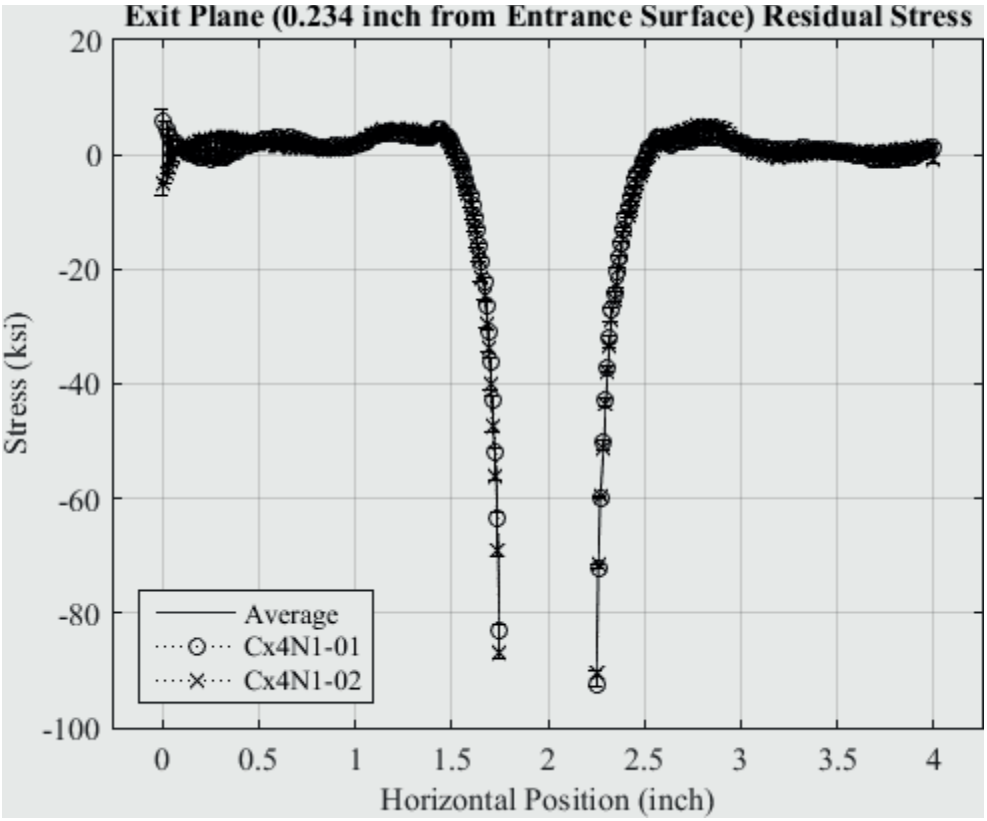

Fig. 258 Residual Stress Line Plot of Cx4N1-01-B and Cx4N1-02-B (2024-T351) at a Distance of 0.234 inch (Exit Surface) from the Entrance Surface – Coupons had a 0.08 inch Fatigue Crack at the Left Entrance Surface surface.

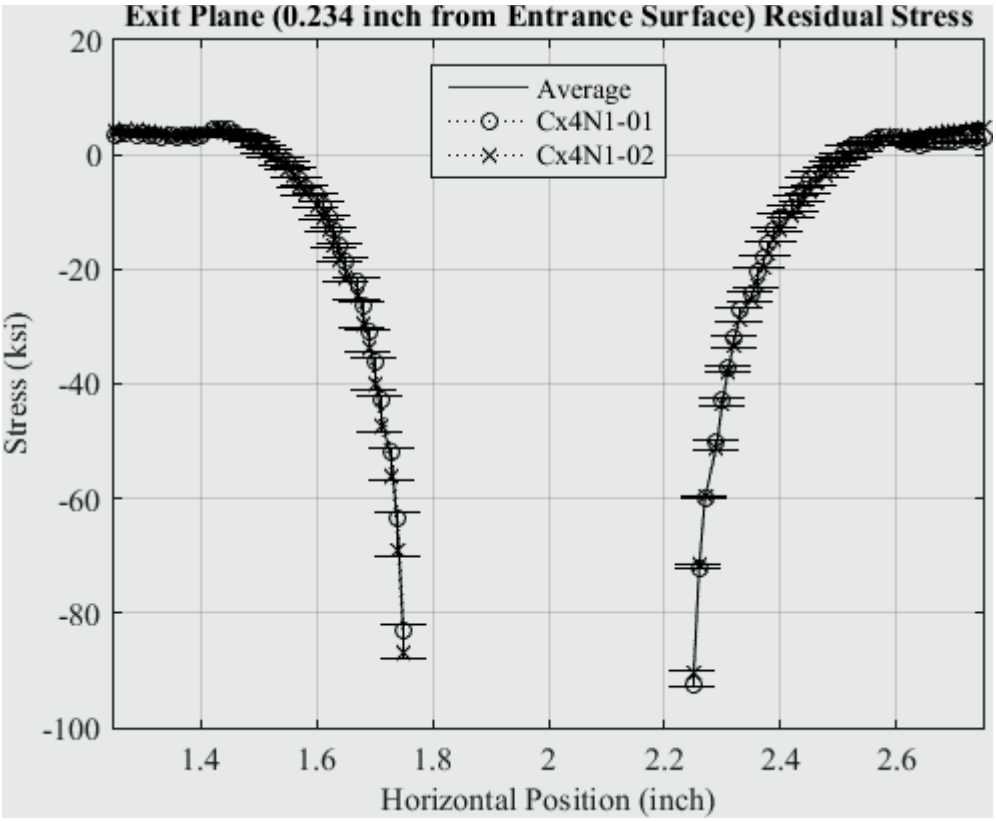

Fig. 259 Residual Stress Line Plot of Cx4N1-01-B and Cx4N1-02-B (2024-T351) at a Distance of 0.234 inch (Exit Surface) from the Entrance Surface – Coupons had a 0.08 inch Fatigue Crack at the Left Entrance Surface – Zoomed in Next to Hole.

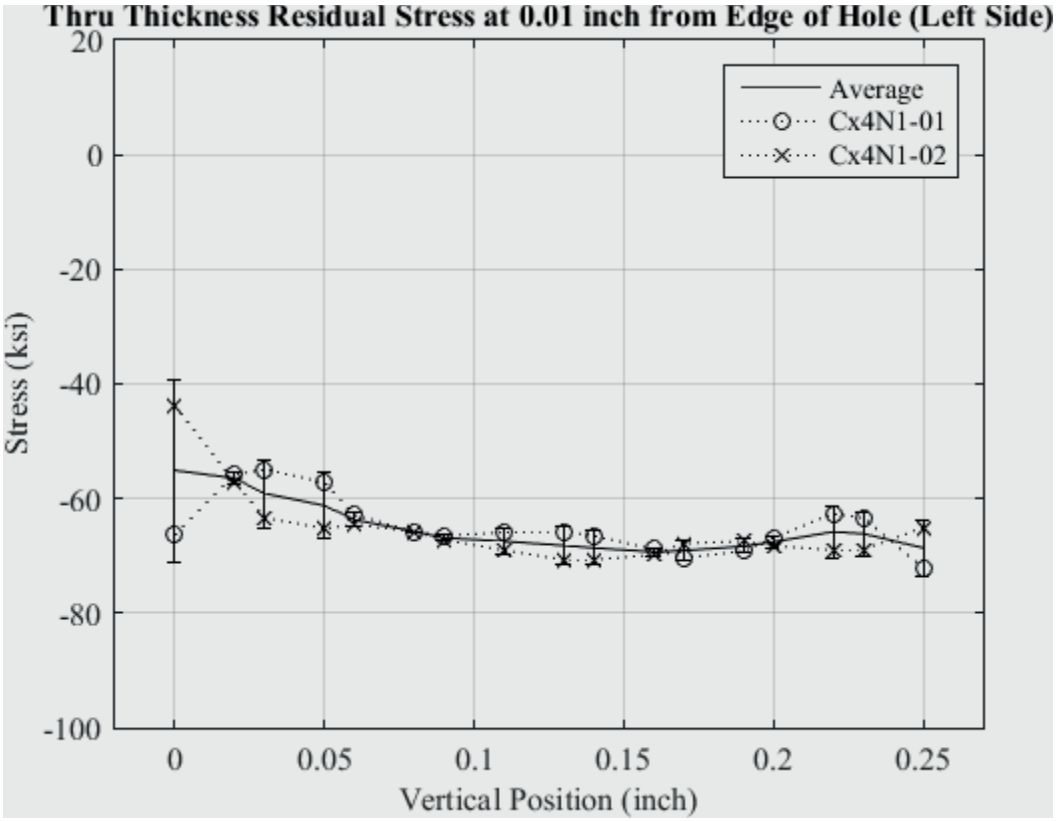

Fig. 260 Residual Stress Line Plot of Cx4N1-01-B and Cx4N1-02-B (2024-T351) Through the Thickness at 0.01 inch from Left Side of Hole – Coupons had a 0.08 inch Fatigue Crack at the Left Entrance Surface.

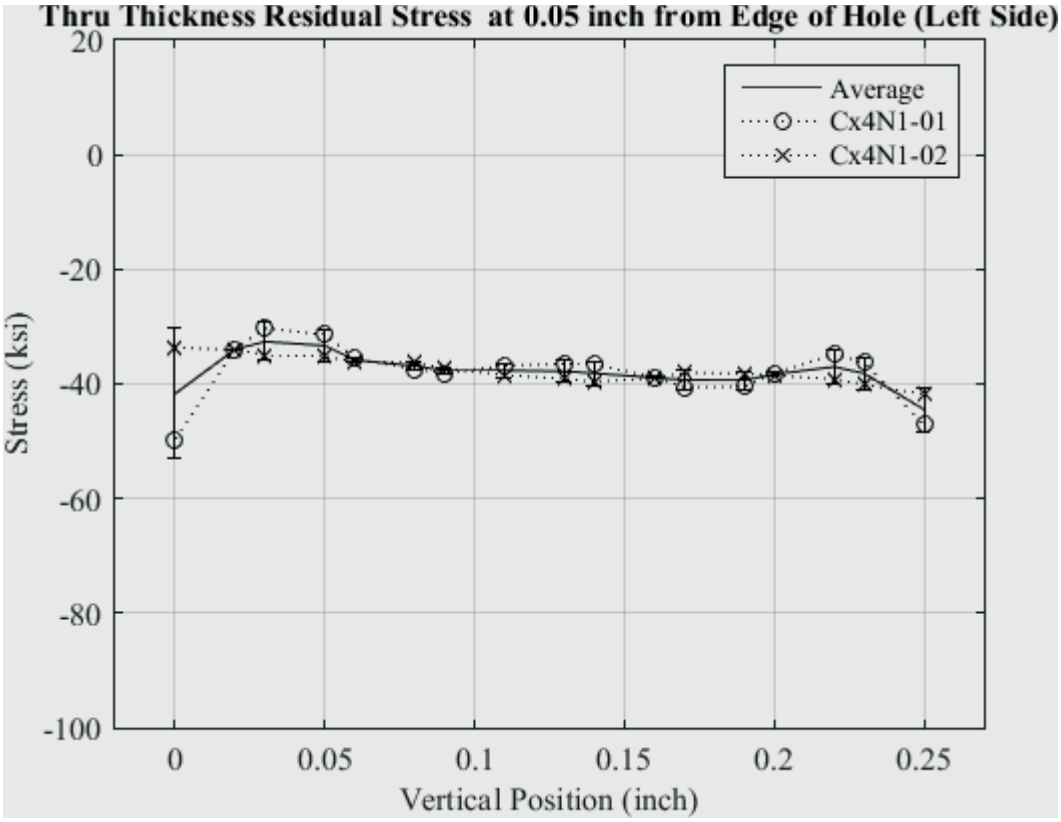

Fig. 261 Residual Stress Line Plot of Cx4N1-01-B and Cx4N1-02-B (2024-T351) Through the Thickness at 0.05 inch from Left Side of Hole – Coupons had a 0.08 inch Fatigue Crack at the Left Entrance Surface.

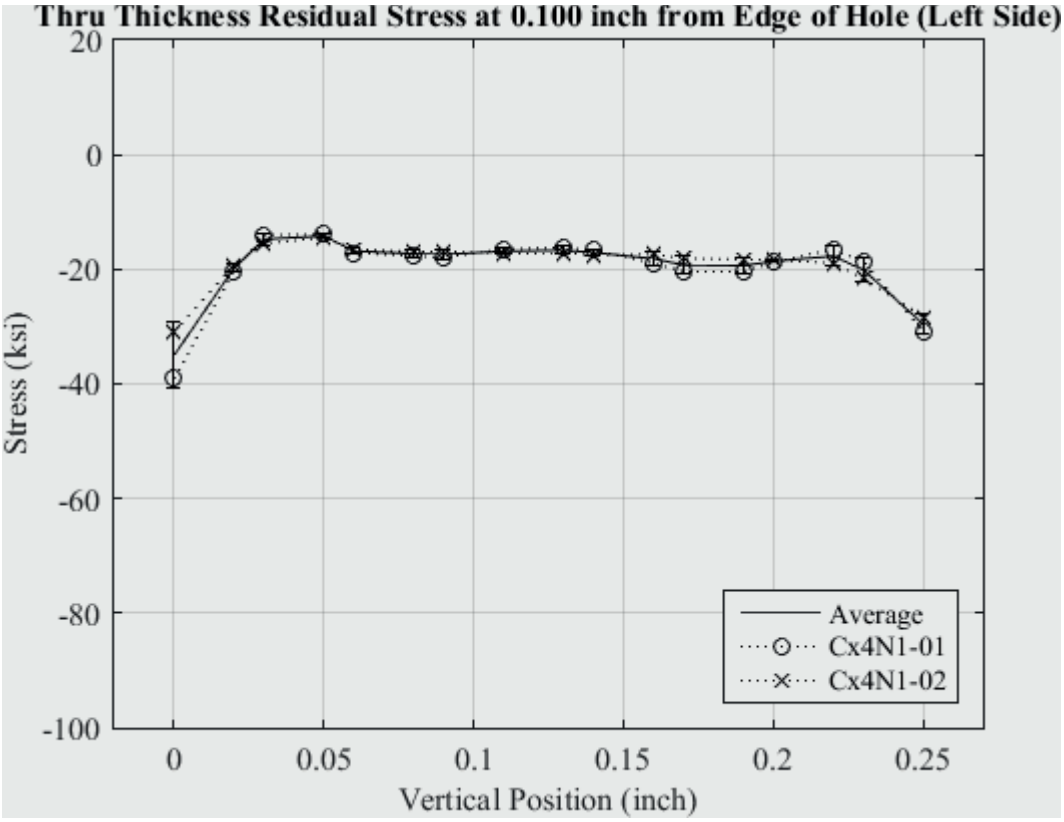

Fig. 262 Residual Stress Line Plot of Cx4N1-01-B and Cx4N1-02-B (2024-T351) Through the Thickness at 0.10 inch from Left Side of Hole – Coupons had a 0.08 inch Fatigue Crack at the Left Entrance Surface.

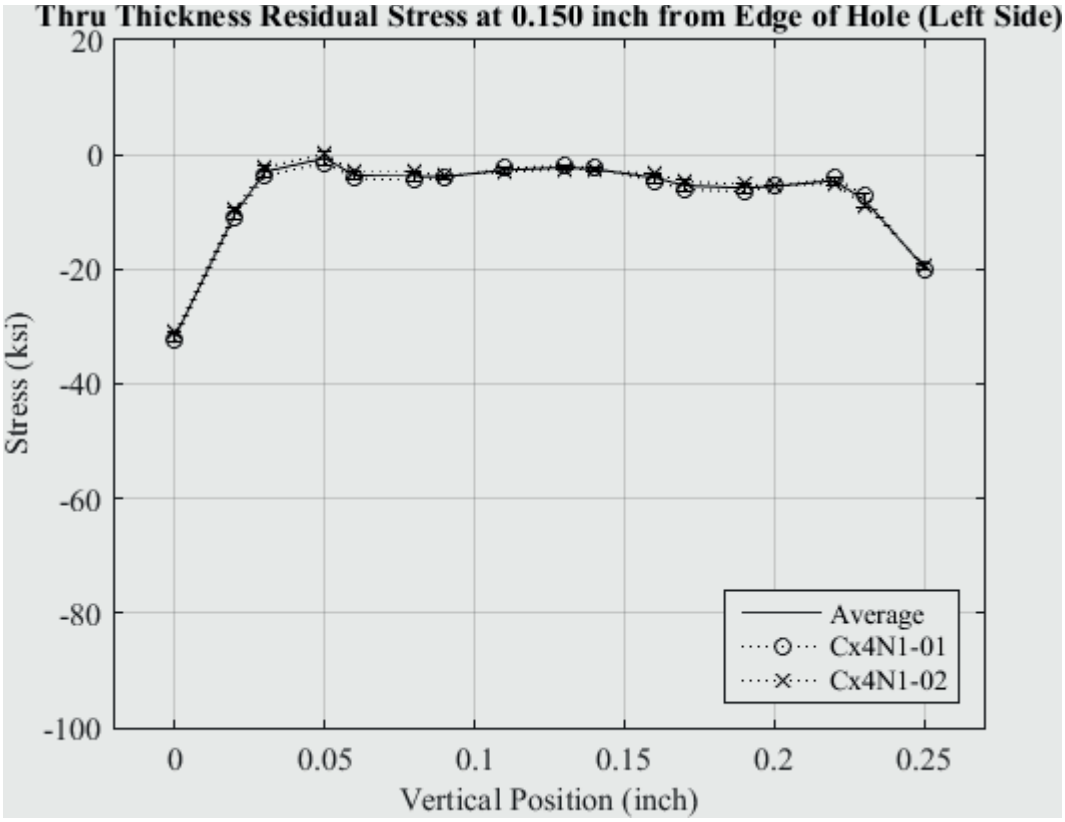

Fig. 263 Residual Stress Line Plot of Cx4N1-01-B and Cx4N1-02-B (2024-T351) Through the Thickness at 0.150 inch from Left Side of Hole – Coupons had a 0.08 inch Fatigue Crack at the Left Entrance Surface.

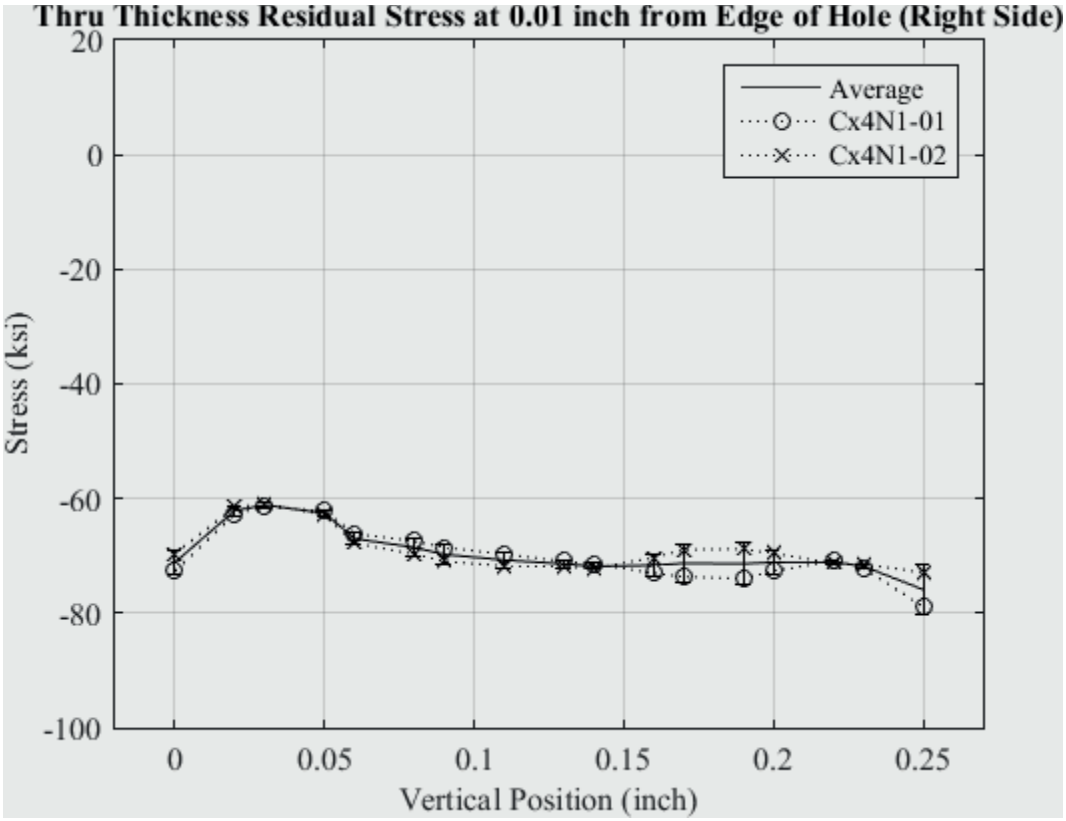

Fig. 264 Residual Stress Line Plot of Cx4N1-01-B and Cx4N1-02-B (2024-T351) Through the Thickness at 0.01 inch from Right Side of Hole – Coupons had a 0.08 inch Fatigue Crack on the Left Side of the Hole.

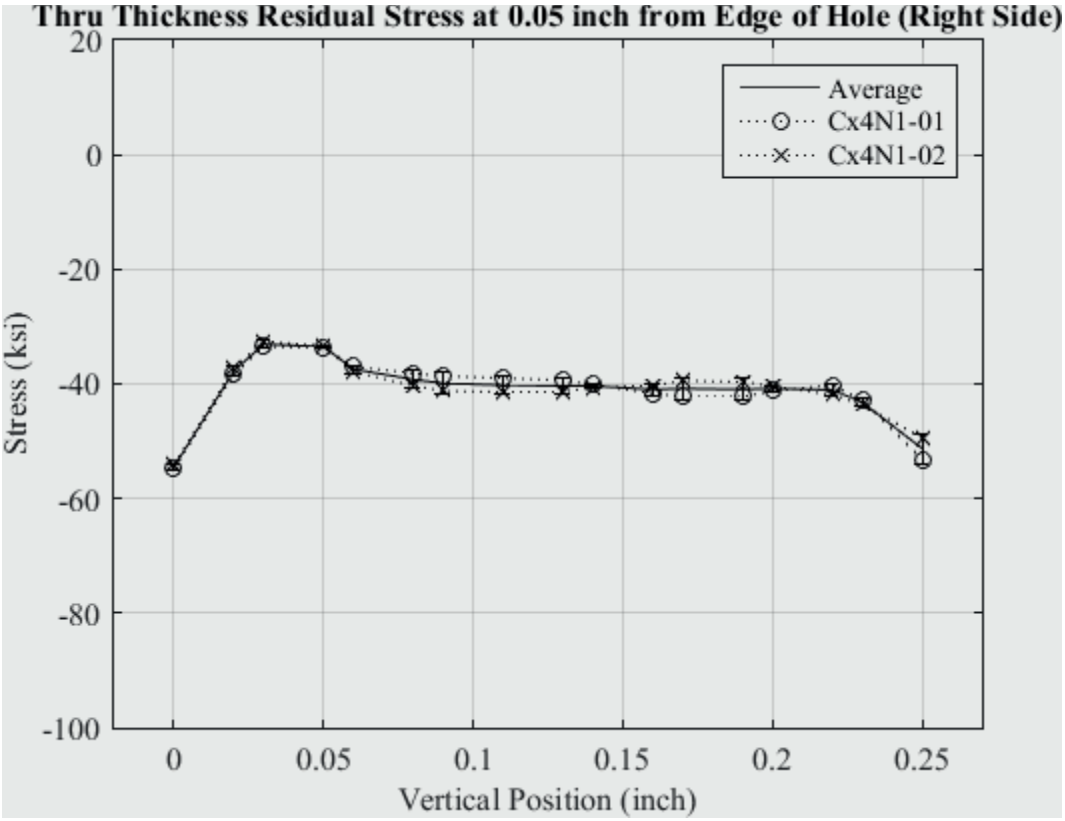

Fig. 265 Residual Stress Line Plot of Cx4N1-01-B and Cx4N1-02-B (2024-T351) Through the Thickness at 0.05 inch from Right Side of Hole – Coupons had a 0.08 inch Fatigue Crack on the Left Side of the Hole.

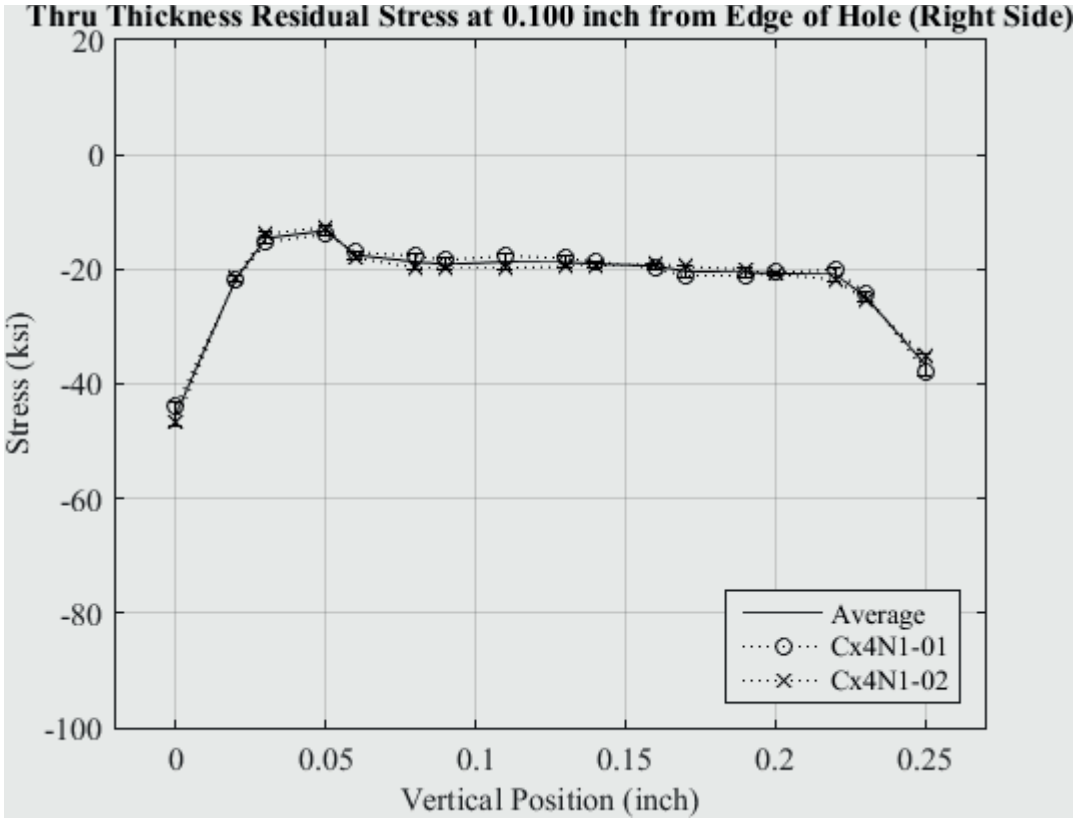

Fig. 266 Residual Stress Line Plot of Cx4N1-01-B and Cx4N1-02-B (2024-T351) Through the Thickness at 0.10 inch from Right Side of Hole – Coupons had a 0.08 inch Fatigue Crack on the Left Side of the Hole.

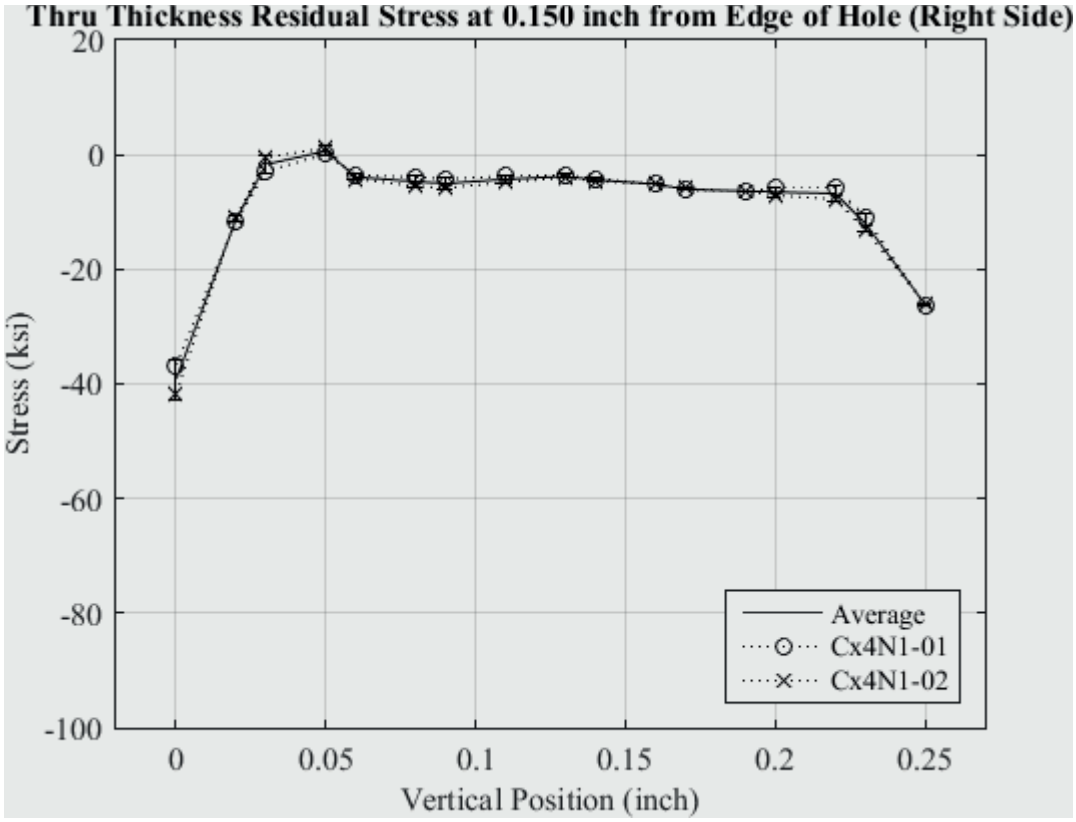

Fig. 267 Residual Stress Line Plot of Cx4N1-01-B and Cx4N1-02-B (2024-T351) Through the Thickness at 0.150 inch from Right Side of Hole – Coupons had a 0.08 inch Fatigue Crack on the Left Side of the Hole.

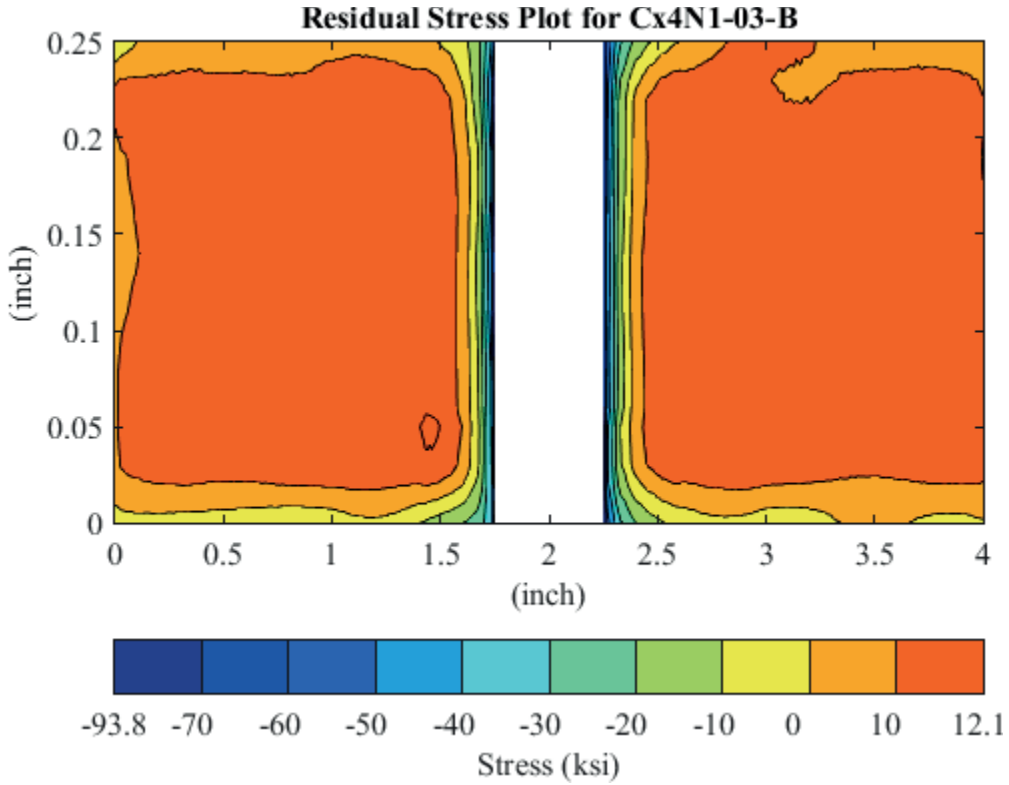

Fig. 268 Residual Stress Contour Plot of Coupon Cx4N1-03-B (2024-T351) – Mandrel Entrance Surface at Y=0, 0.10 inch Fatigue Crack on Left Side of Hole on Mandrel Entrance Surface.

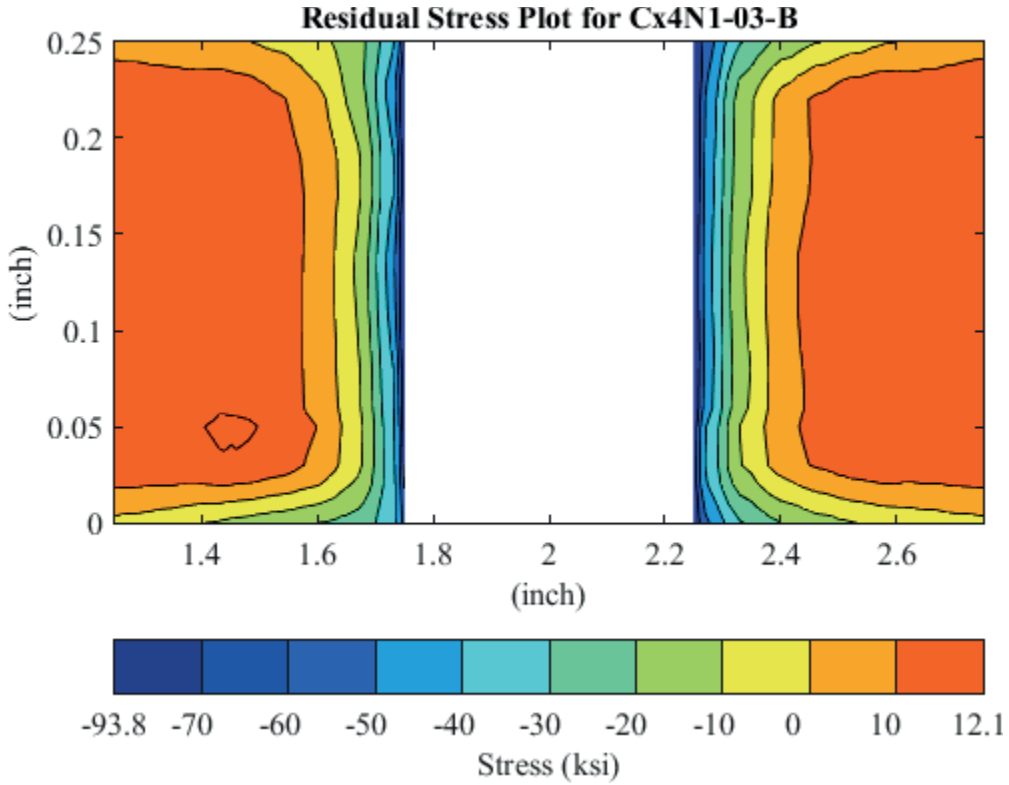

Fig. 269 Residual Stress Contour Plot of Coupon Cx4N1-03-B (2024-T351) – Mandrel Entrance Surface at Y=0, 0.10 inch Fatigue Crack on Left Side of Hole on Mandrel Entrance Surface – Zoomed in Next to Hole.

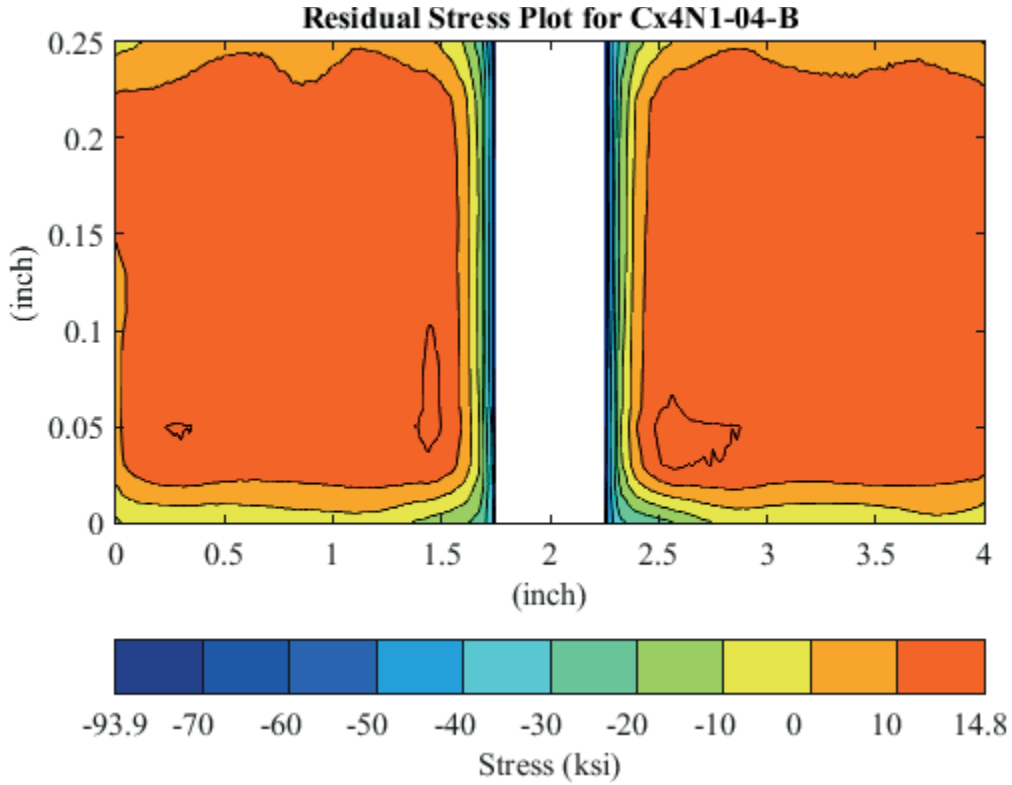

Fig. 270 Residual Stress Contour Plot of Coupon Cx4N1-04-B (2024-T351) – Mandrel Entrance Surface at Y=0, 0.10 inch Fatigue Crack on Left Side of Hole on Mandrel Entrance Surface.

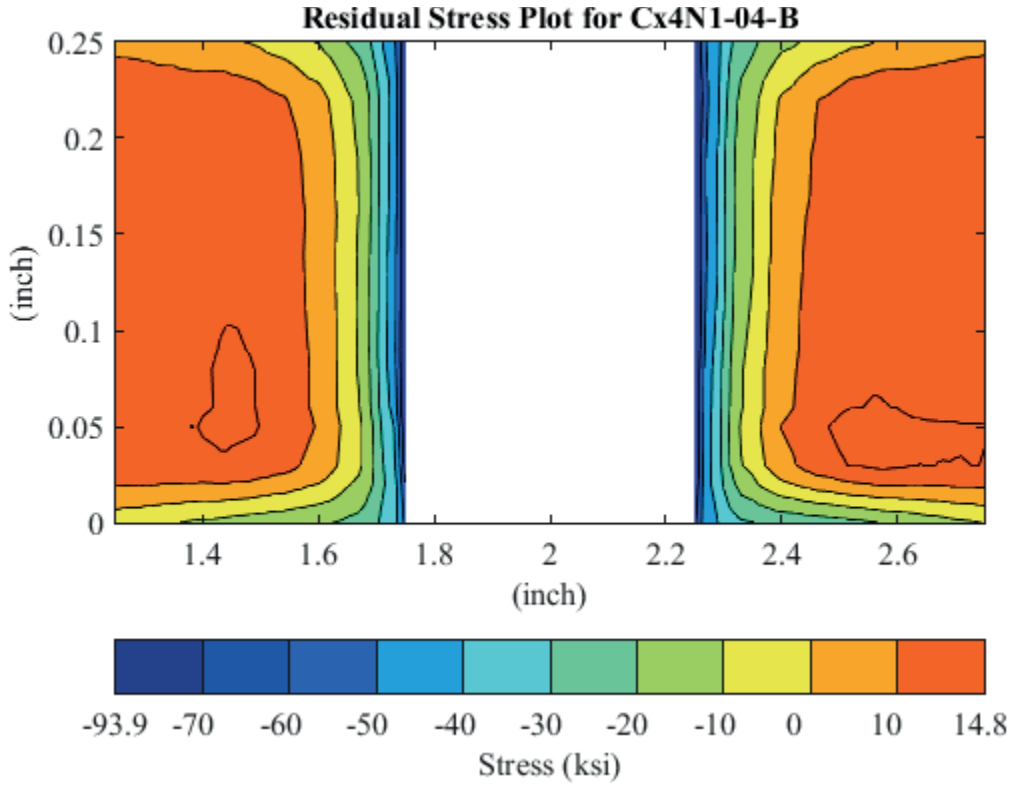

Fig. 271 Residual Stress Contour Plot of Coupon Cx4N1-04-B (2024-T351) – Mandrel Entrance Surface at Y=0, 0.10 inch Fatigue Crack on Left Side of Hole on Mandrel Entrance Surface – Zoomed in Next to Hole.

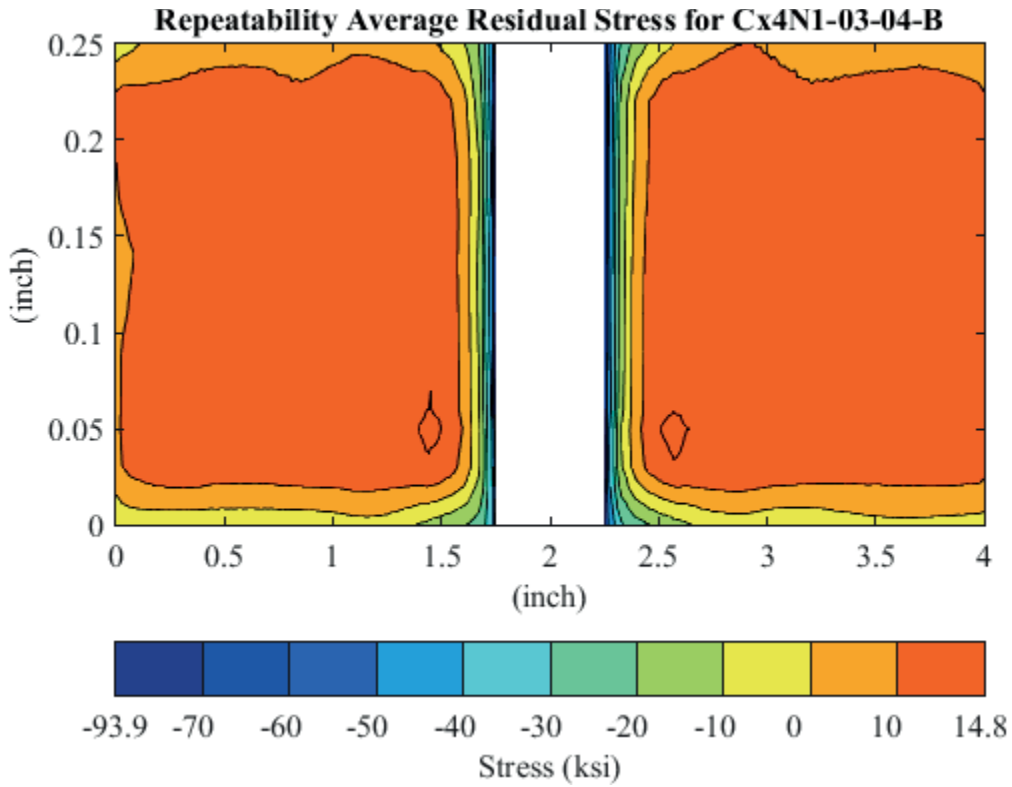

Fig. 272 Average Residual Stress Contour Plot of Coupons Cx4N1-03-B and Cx4N1-04-B (2024-T351) – Mandrel Entrance Surface at Y=0, 0.100 inch Fatigue Crack on Left Side of Hole on Mandrel Entrance Surface.

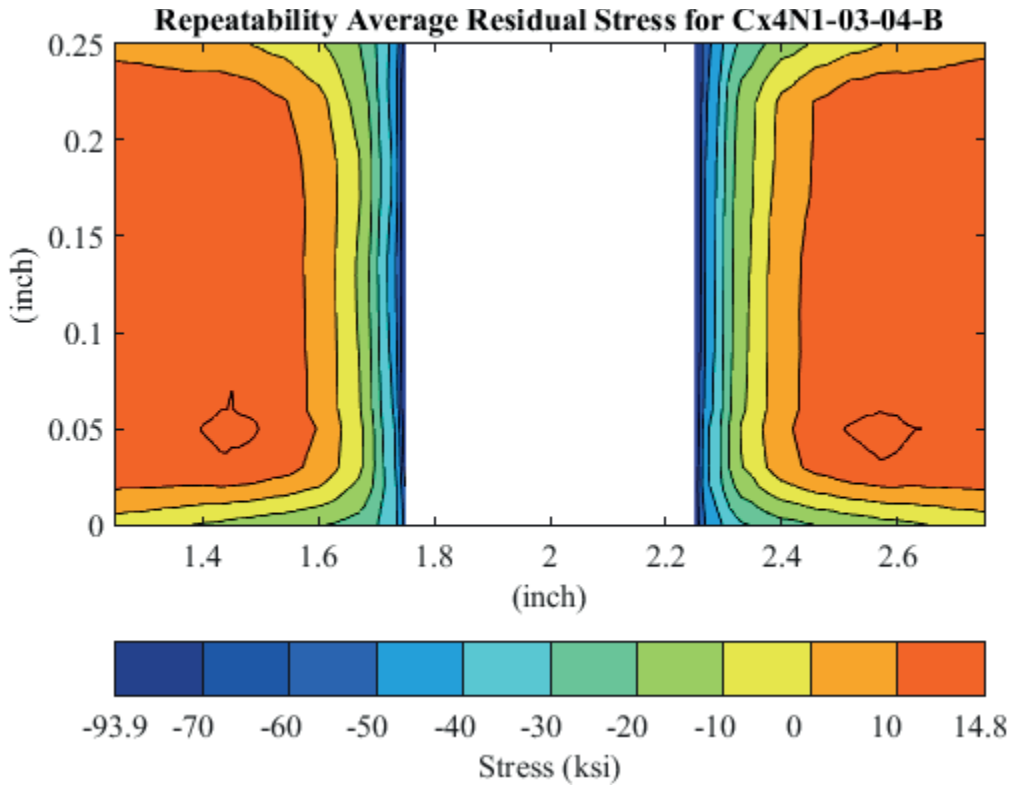

Fig. 273 Average Residual Stress Contour Plot of Coupons Cx4N1-03-B and Cx4N1-04-B (2024-T351) – Mandrel Entrance Surface at Y=0, 0.100 inch Fatigue Crack on Left Side of Hole on Mandrel Entrance Surface – Zoomed in Next to Hole.

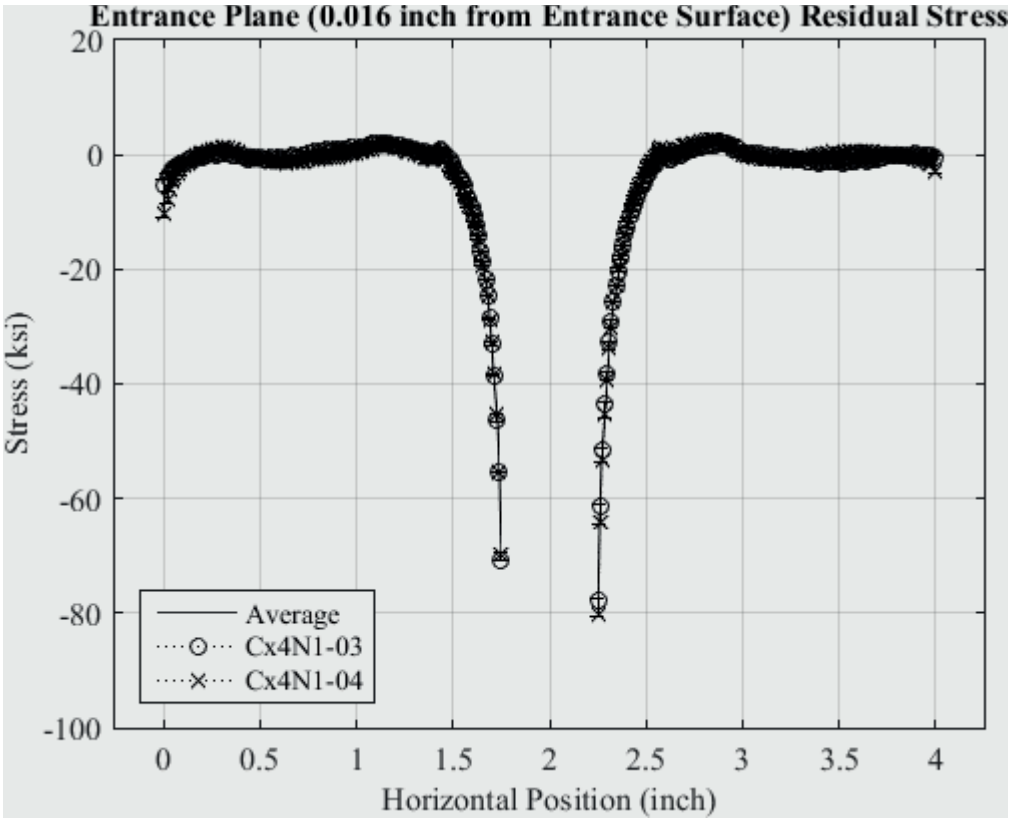

Fig. 274 Residual Stress Line Plot of Cx4N1-03-B and Cx4N1-04-B (2024-T351) at a Distance of 0.016 inch (Entrance Surface) from the Entrance Surface – Coupons had a 0.10 inch Fatigue Crack at the Left Entrance Surface.

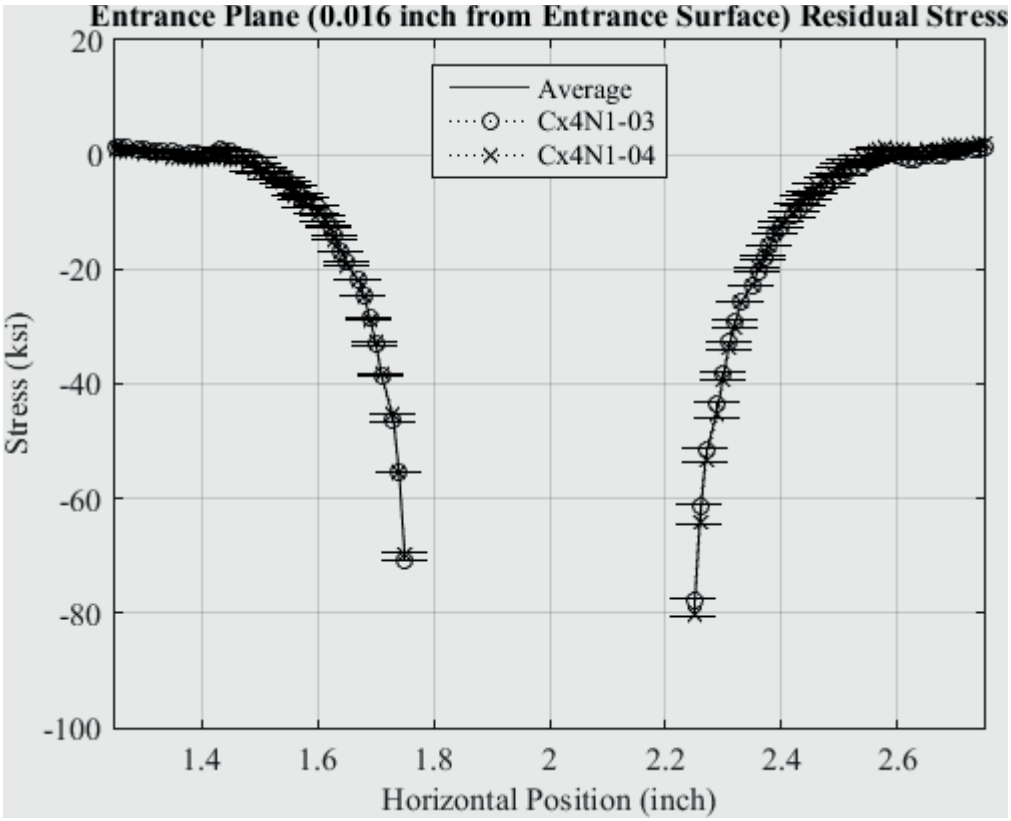

Fig. 275 Residual Stress Line Plot of Cx4N1-03-B and Cx4N1-04-B (2024-T351) at a Distance of 0.016 inch (Entrance Surface) from the Entrance Surface – Coupons had a 0.10 inch Fatigue Crack at the Left Entrance Surface – Zoomed in Next to Hole.

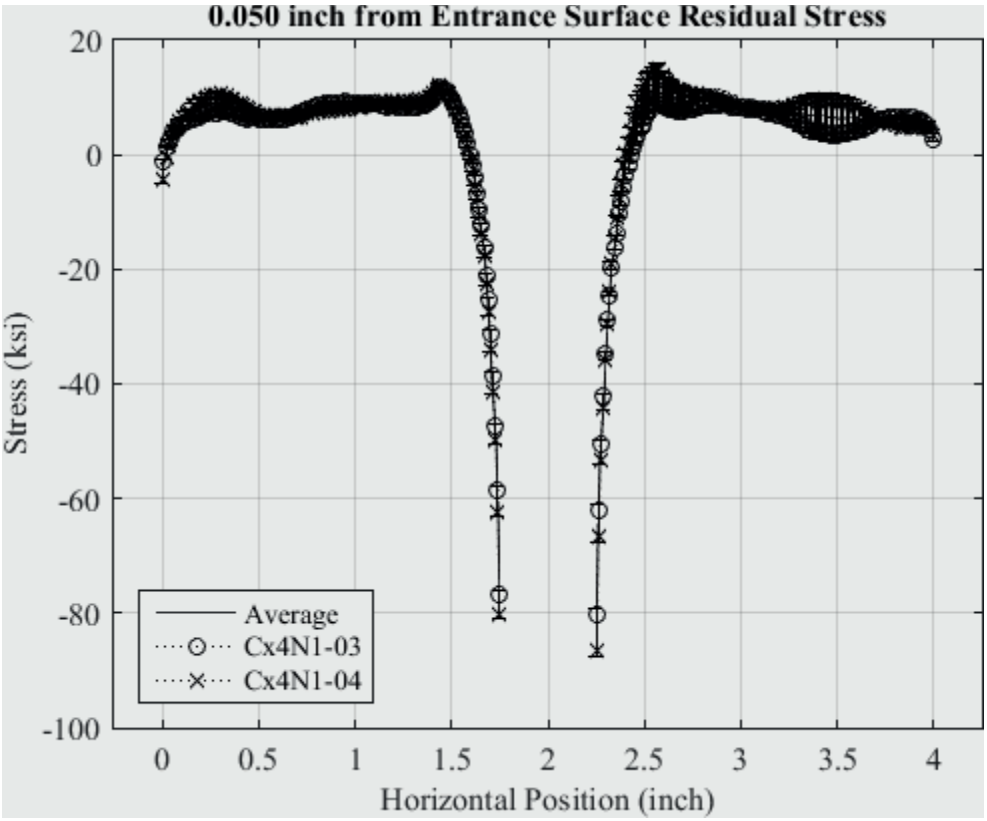

Fig. 276 Residual Stress Line Plot of Cx4N1-03-B and Cx4N1-04-B (2024-T351) at a Distance of 0.05 inch from the Entrance Surface – Coupons had a 0.10 inch Fatigue Crack at the Left Entrance Surface.

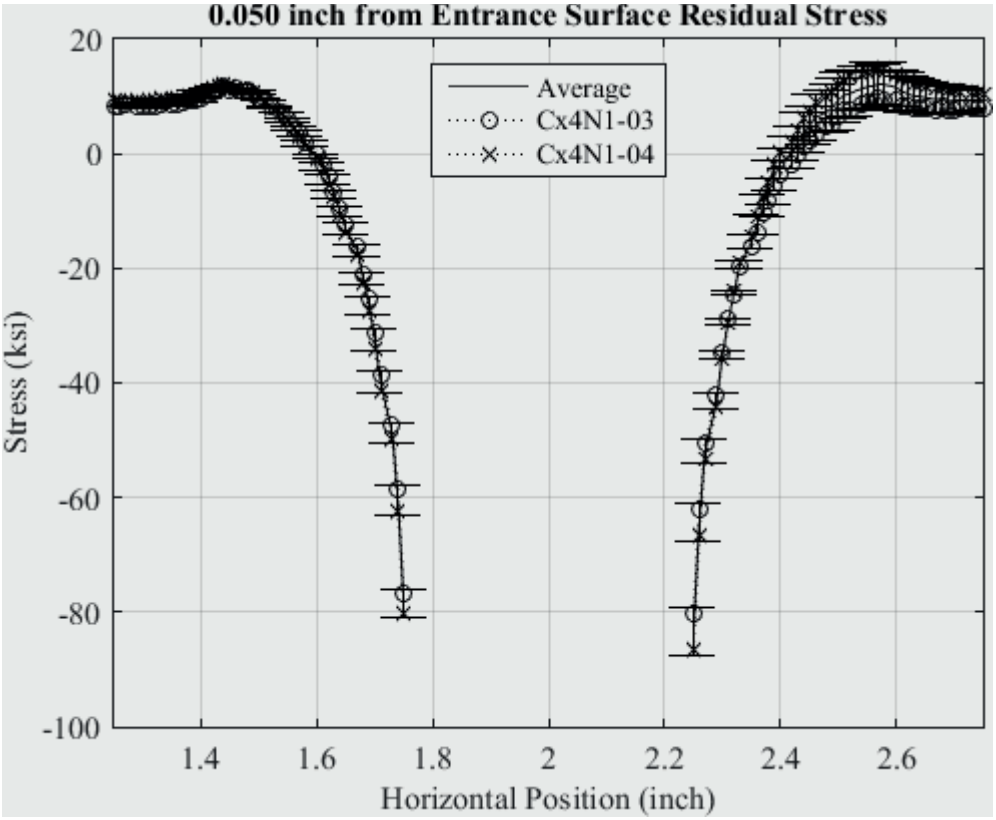

Fig. 277 Residual Stress Line Plot of Cx4N1-03-B and Cx4N1-04-B (2024-T351) at a Distance of 0.05 inch from the Entrance Surface – Coupons had a 0.10 inch Fatigue Crack at the Left Entrance Surface – Zoomed in Next to Hole.

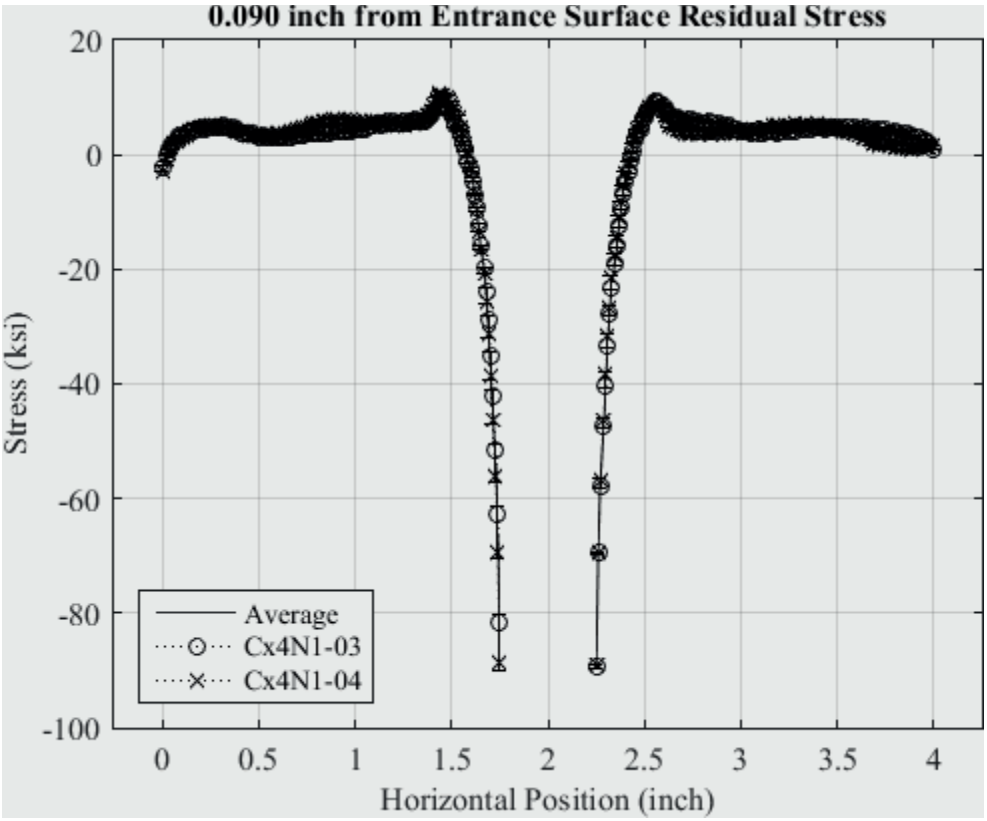

Fig. 278 Residual Stress Line Plot of Cx4N1-03-B and Cx4N1-04-B (2024-T351) at a Distance of 0.09 inch from the Entrance Surface – Coupons had a 0.10 inch Fatigue Crack at the Left Entrance Surface.

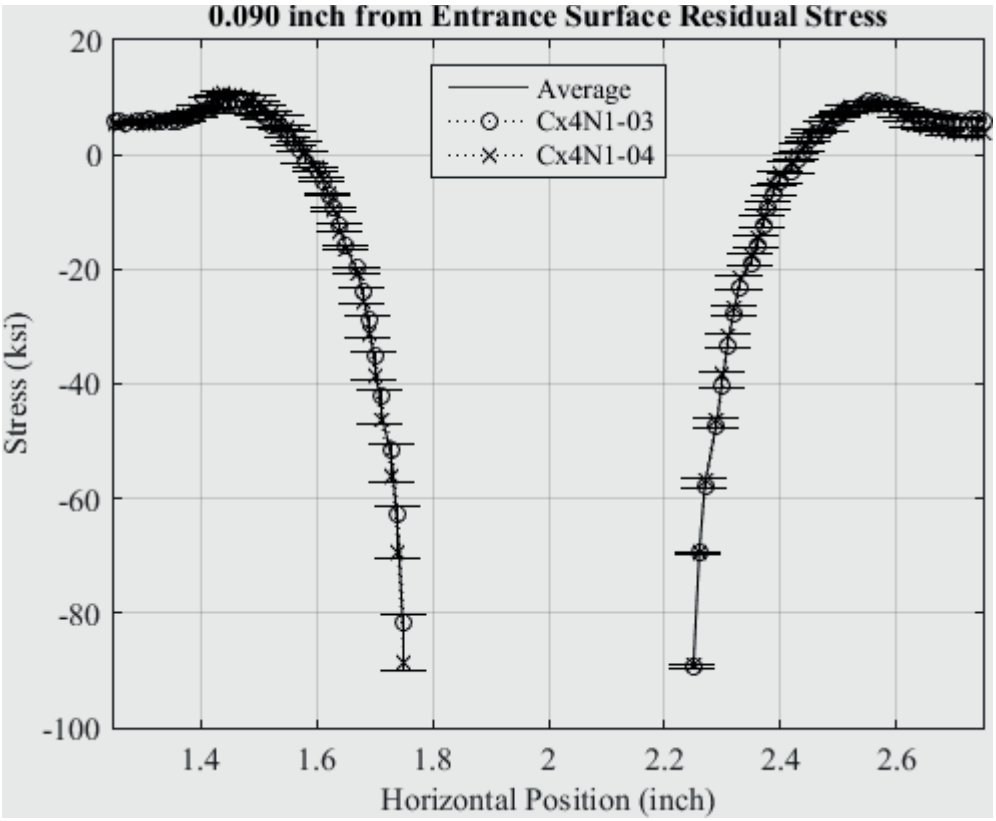

Fig. 279 Residual Stress Line Plot of Cx4N1-03-B and Cx4N1-04-B (2024-T351) at a Distance of 0.09 inch from the Entrance Surface – Coupons had a 0.10 inch Fatigue Crack at the Left Entrance Surface – Zoomed in Next to Hole.

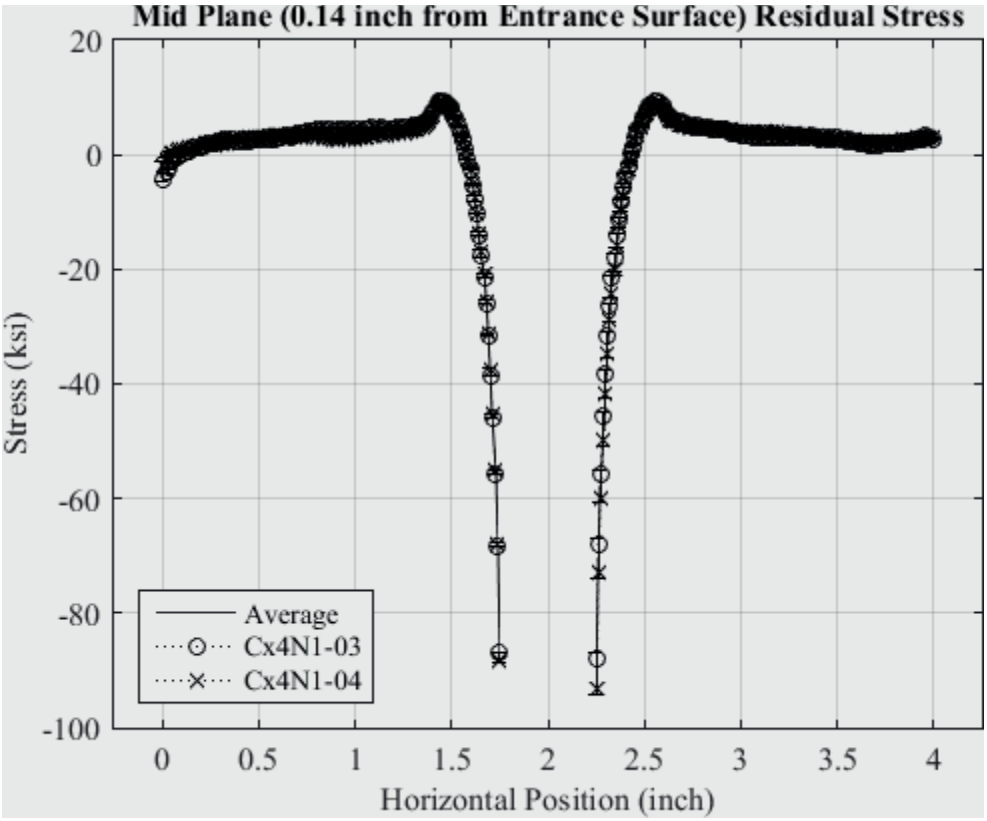

Fig. 280 Residual Stress Line Plot of Cx4N1-03-B and Cx4N1-04-B (2024-T351) at a Distance of 0.140 inch (Mid Plane Surface) from the Entrance Surface – Coupons had a 0.10 inch Fatigue Crack at the Left Entrance Surface.

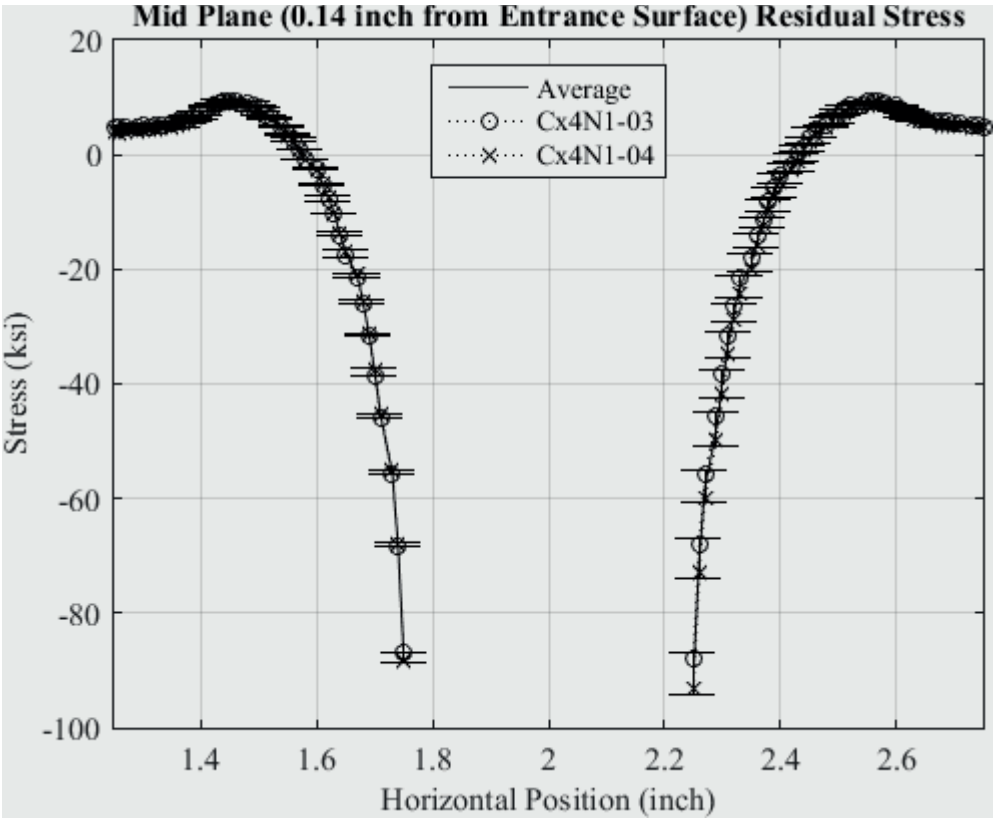

Fig. 281 Residual Stress Line Plot of Cx4N1-03-B and Cx4N1-04-B (2024-T351) at a Distance of 0.140 inch (Mid Plane Surface) from the Entrance Surface – Coupons had a 0.10 inch Fatigue Crack at the Left Entrance Surface – Zoomed in Next to Hole.

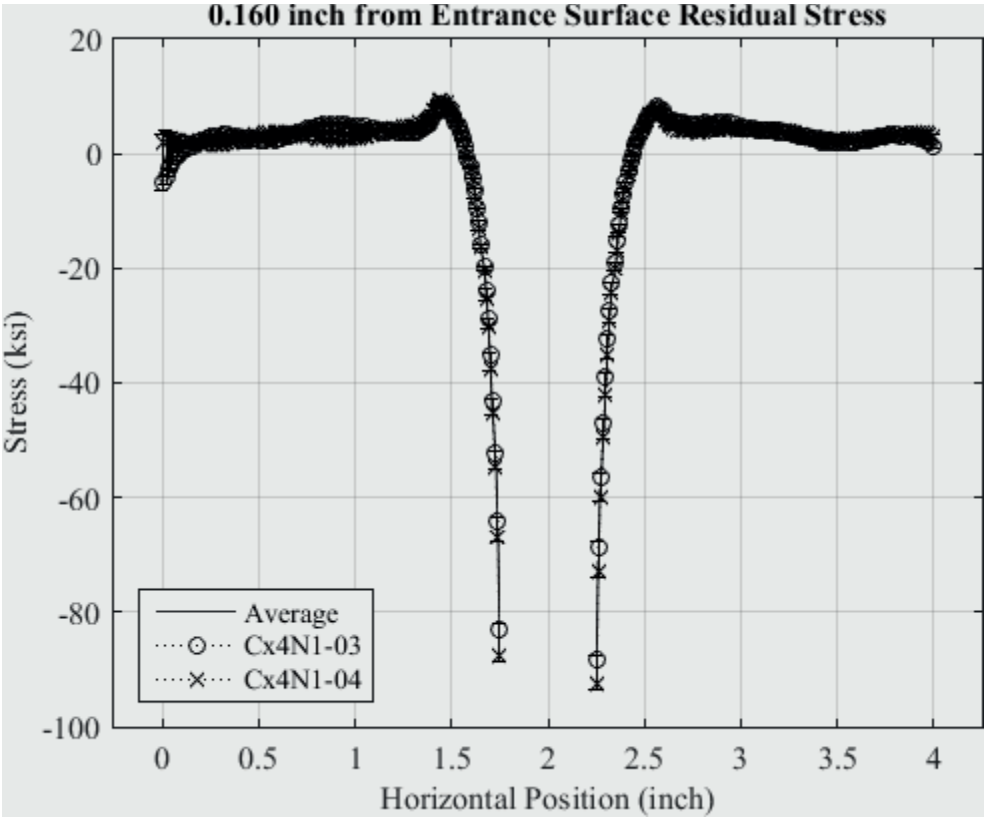

Fig. 282 Residual Stress Line Plot of Cx4N1-03-B and Cx4N1-04-B (2024-T351) at a Distance of 0.160 inch from the Entrance Surface – Coupons had a 0.10 inch Fatigue Crack at the Left Entrance Surface.

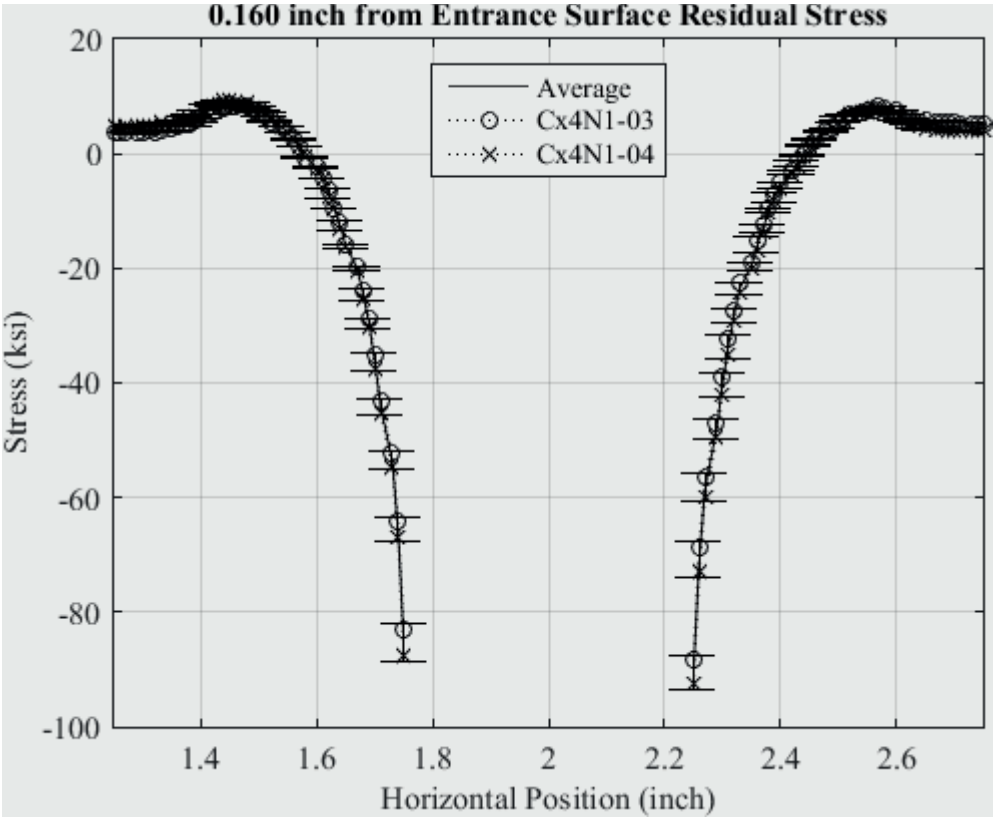

Fig. 283 Residual Stress Line Plot of Cx4N1-03-B and Cx4N1-04-B (2024-T351) at a Distance of 0.160 inch from the Entrance Surface – Coupons had a 0.10 inch Fatigue Crack at the Left Entrance Surface – Zoomed in Next to Hole.

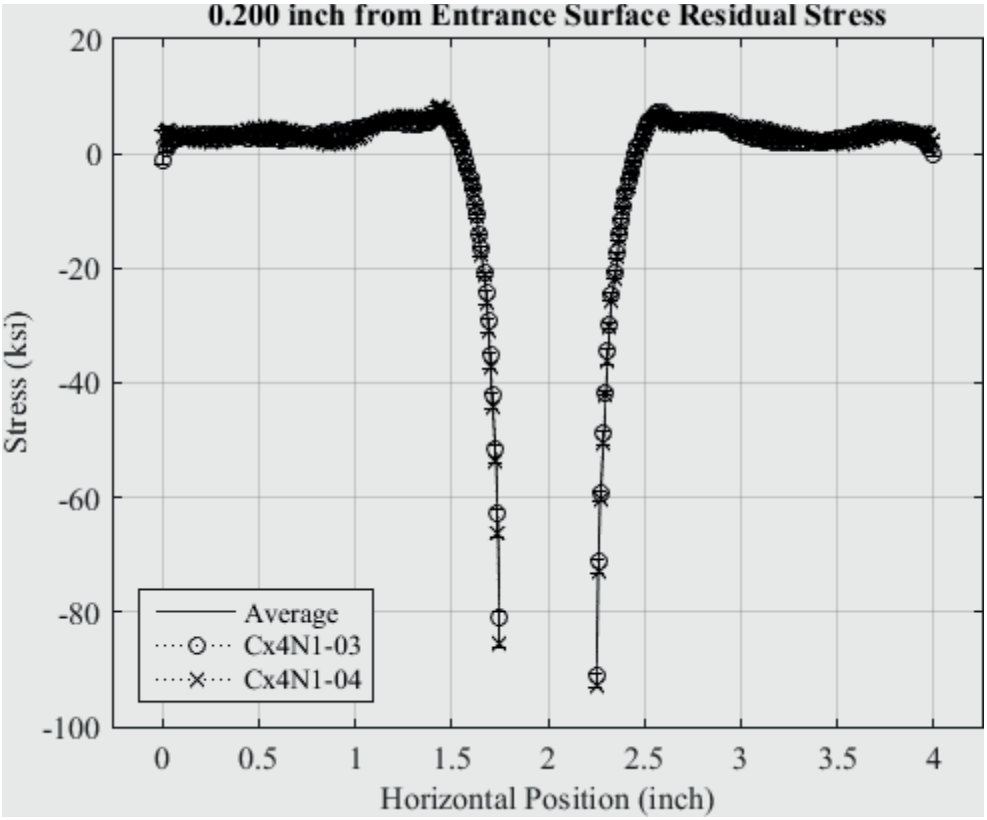

Fig. 284 Residual Stress Line Plot of Cx4N1-03-B and Cx4N1-04-B (2024-T351) at a Distance of 0.200 inch from the Entrance Surface – Coupons had a 0.10 inch Fatigue Crack at the Left Entrance Surface.

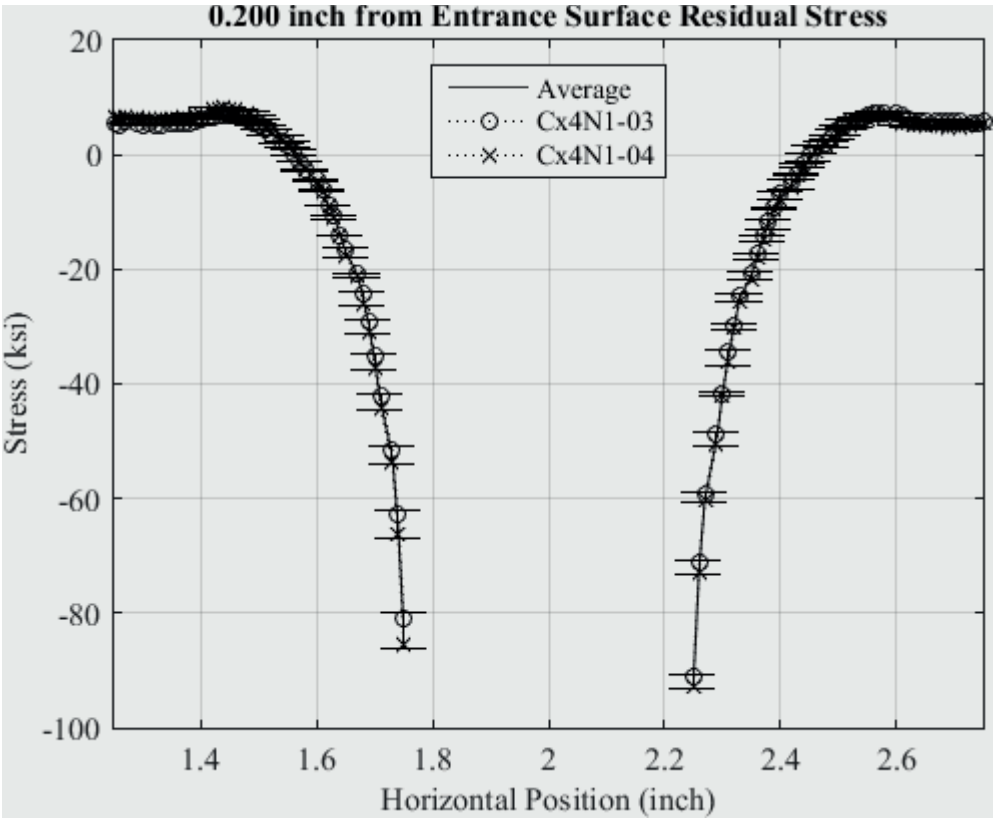

Fig. 285 Residual Stress Line Plot of Cx4N1-03-B and Cx4N1-04-B (2024-T351) at a Distance of 0.200 inch from the Entrance Surface – Coupons had a 0.10 inch Fatigue Crack at the Left Entrance Surface – Zoomed in Next to Hole.

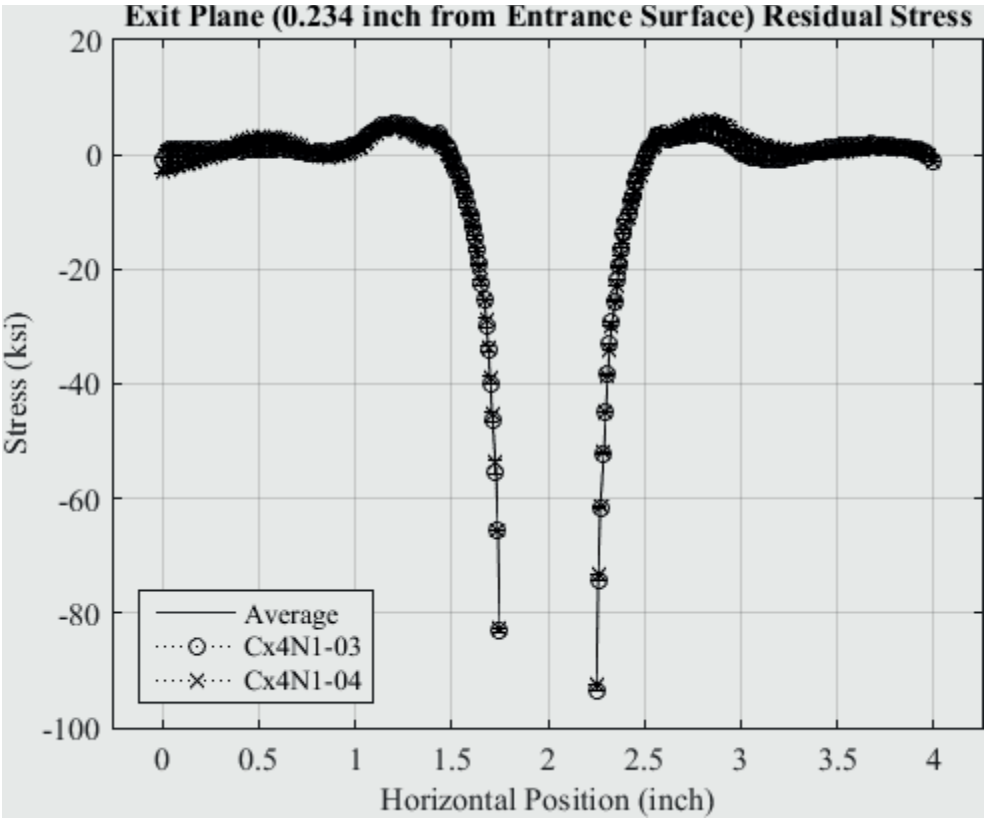

Fig. 286 Residual Stress Line Plot of Cx4N1-03-B and Cx4N1-04-B (2024-T351) at a Distance of 0.234 inch (Exit Plane Surface) from the Entrance Surface – Coupons had a 0.10 inch Fatigue Crack at the Left Entrance Surface.

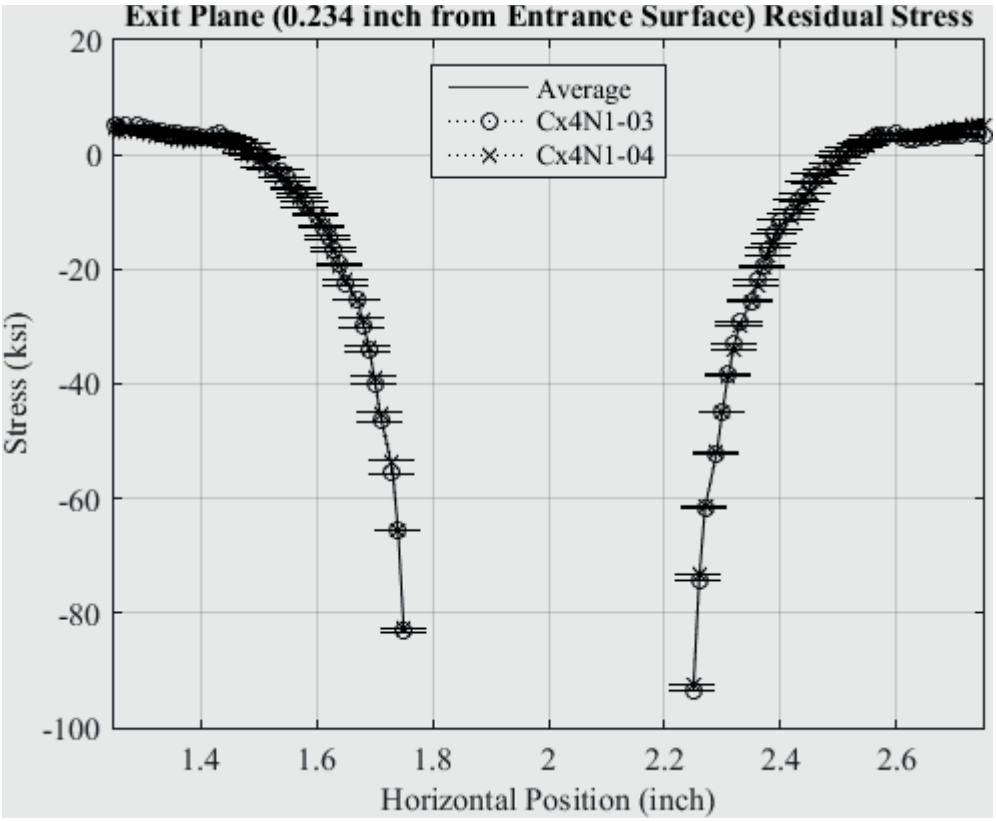

Fig. 287 Residual Stress Line Plot of Cx4N1-03-B and Cx4N1-04-B (2024-T351) at a Distance of 0.234 inch (Exit Plane Surface) from the Entrance Surface – Coupons had a 0.10 inch Fatigue Crack at the Left Entrance Surface – Zoomed in Next to Hole

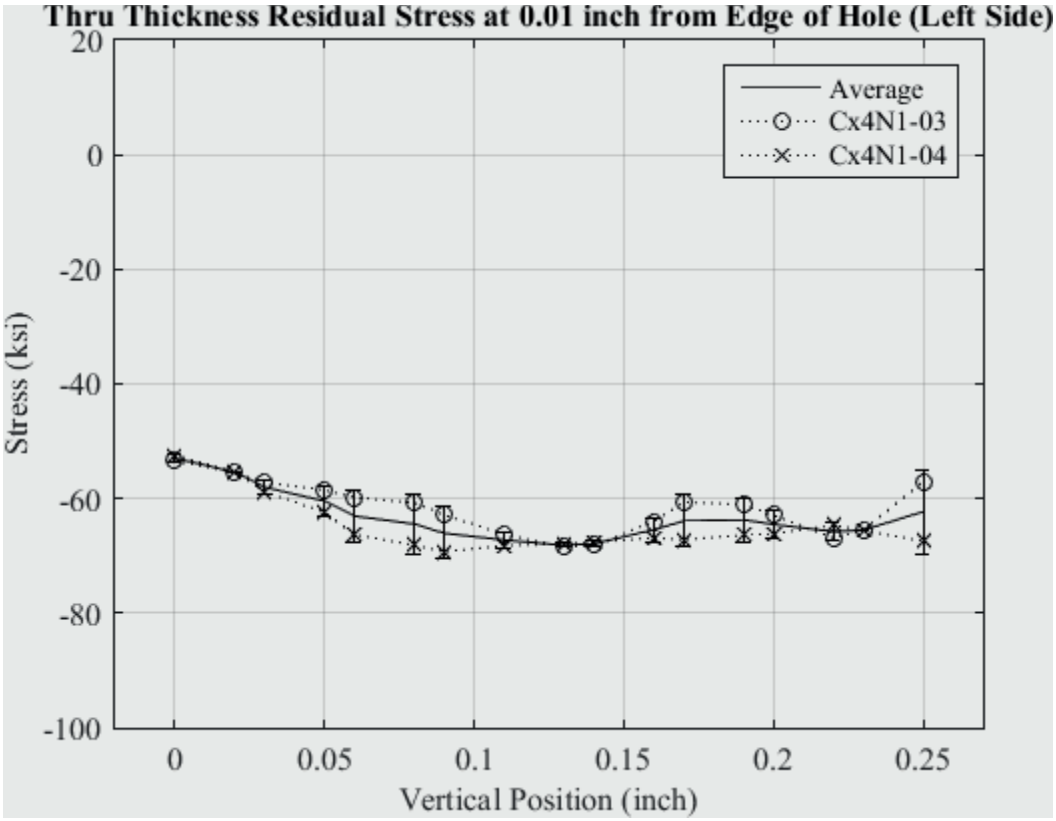

Fig. 288 Residual Stress Line Plot of Cx4N1-03-B and Cx4N1-04-B (2024-T351) Through the Thickness at 0.01 inch from Left Side of Hole – Coupons had a 0.10 inch Fatigue Crack at the Left Entrance Surface.

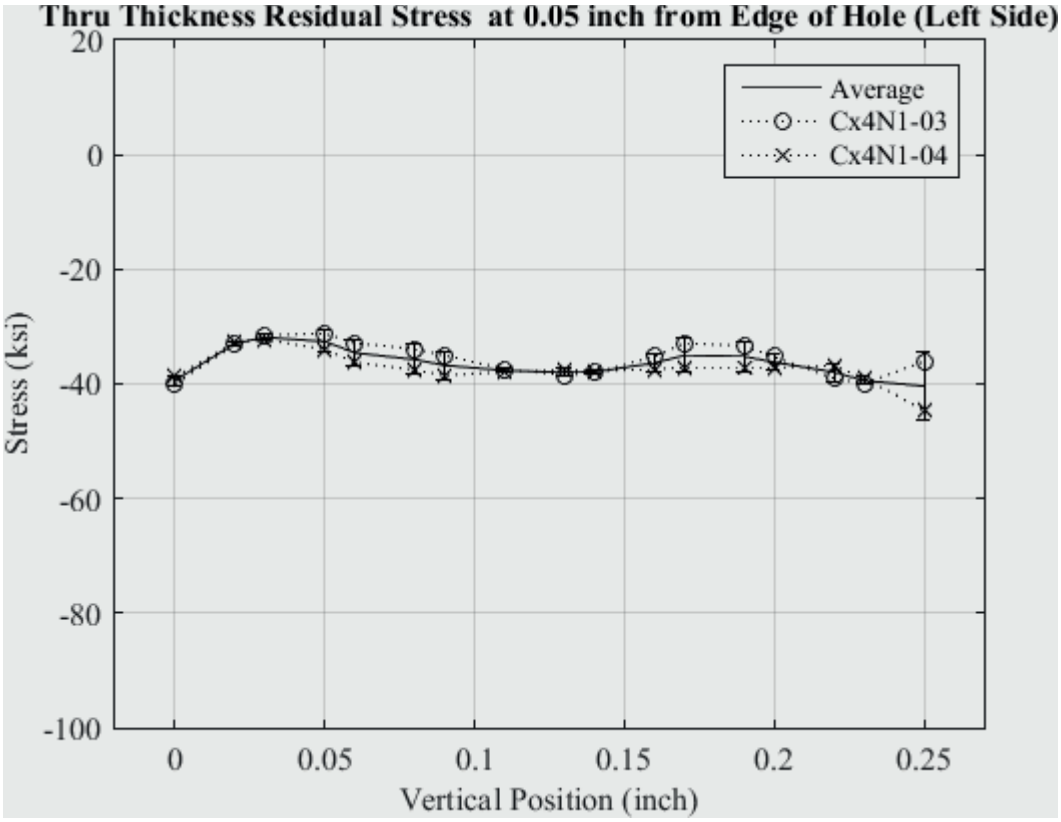

Fig. 289 Residual Stress Line Plot of Cx4N1-03-B and Cx4N1-04-B (2024-T351) Through the Thickness at 0.05 inch from Left Side of Hole – Coupons had a 0.10 inch Fatigue Crack at the Left Entrance Surface.

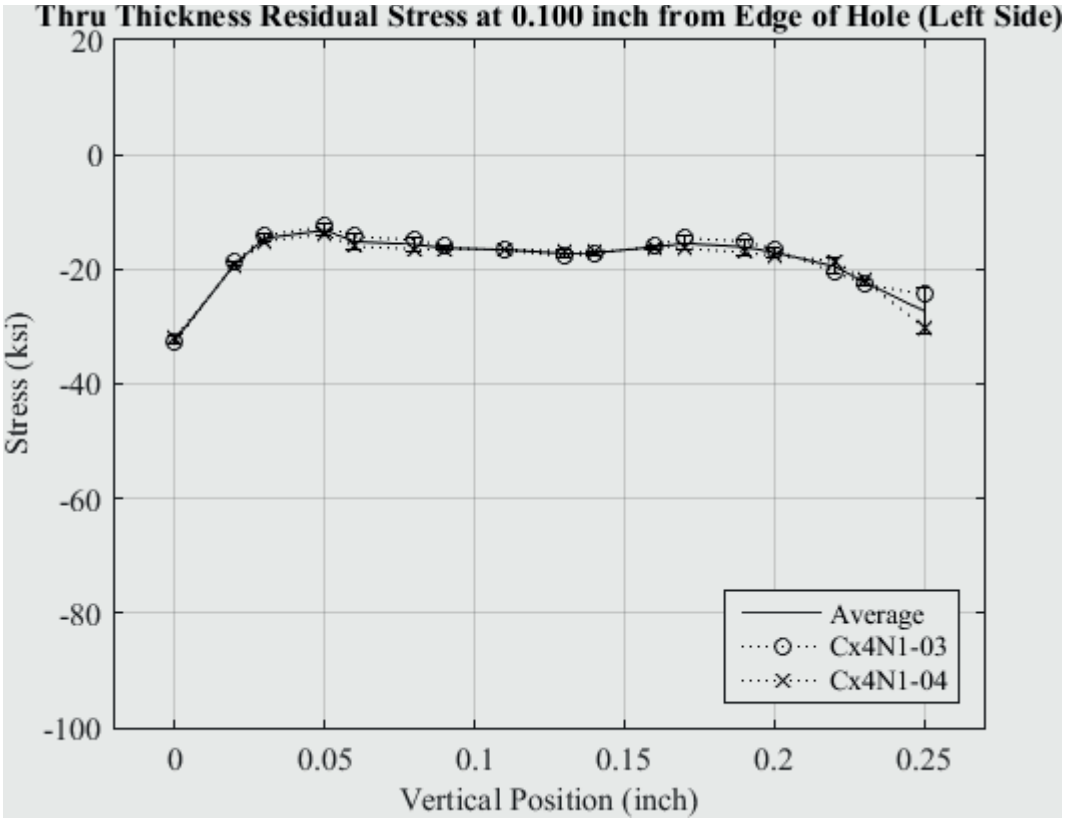

Fig. 290 Residual Stress Line Plot of Cx4N1-03-B and Cx4N1-04-B (2024-T351) Through the Thickness at 0.10 inch from Left Side of Hole – Coupons had a 0.10 inch Fatigue Crack at the Left Entrance Surface.

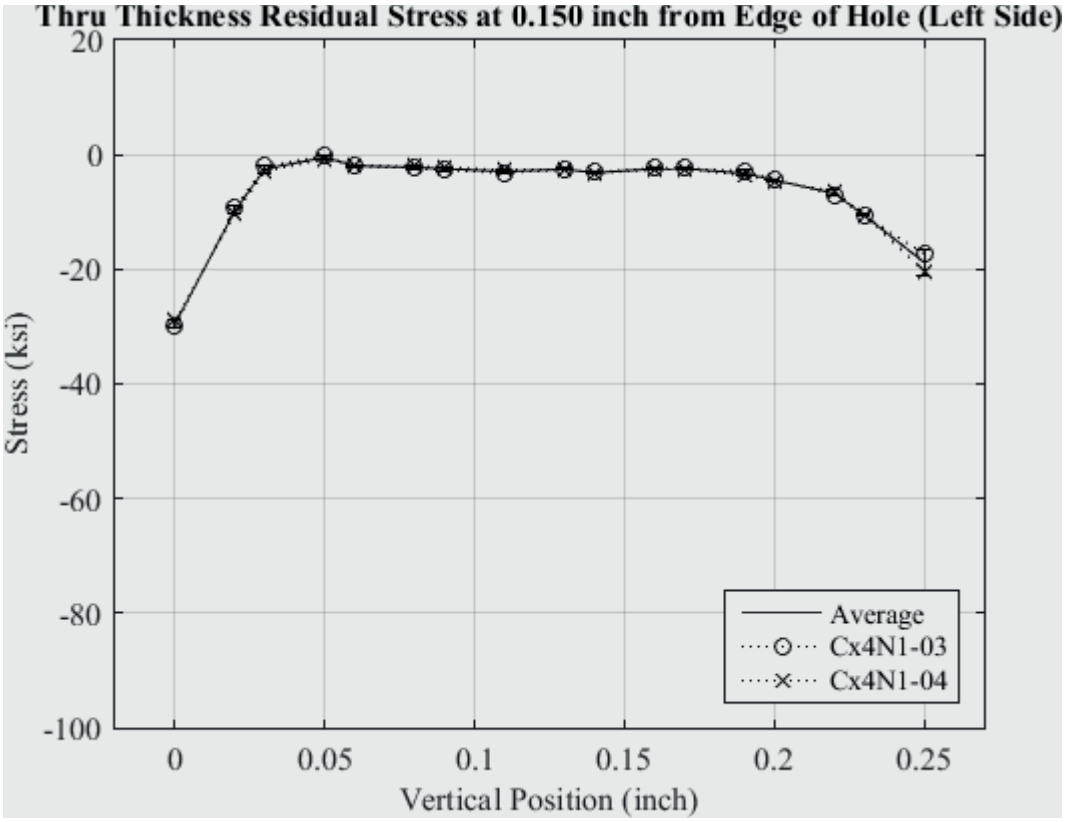

Fig. 291 Residual Stress Line Plot of Cx4N1-03-B and Cx4N1-04-B (2024-T351) Through the Thickness at 0.150 inch from Left Side of Hole – Coupons had a 0.10 inch Fatigue Crack at the Left Entrance Surface.

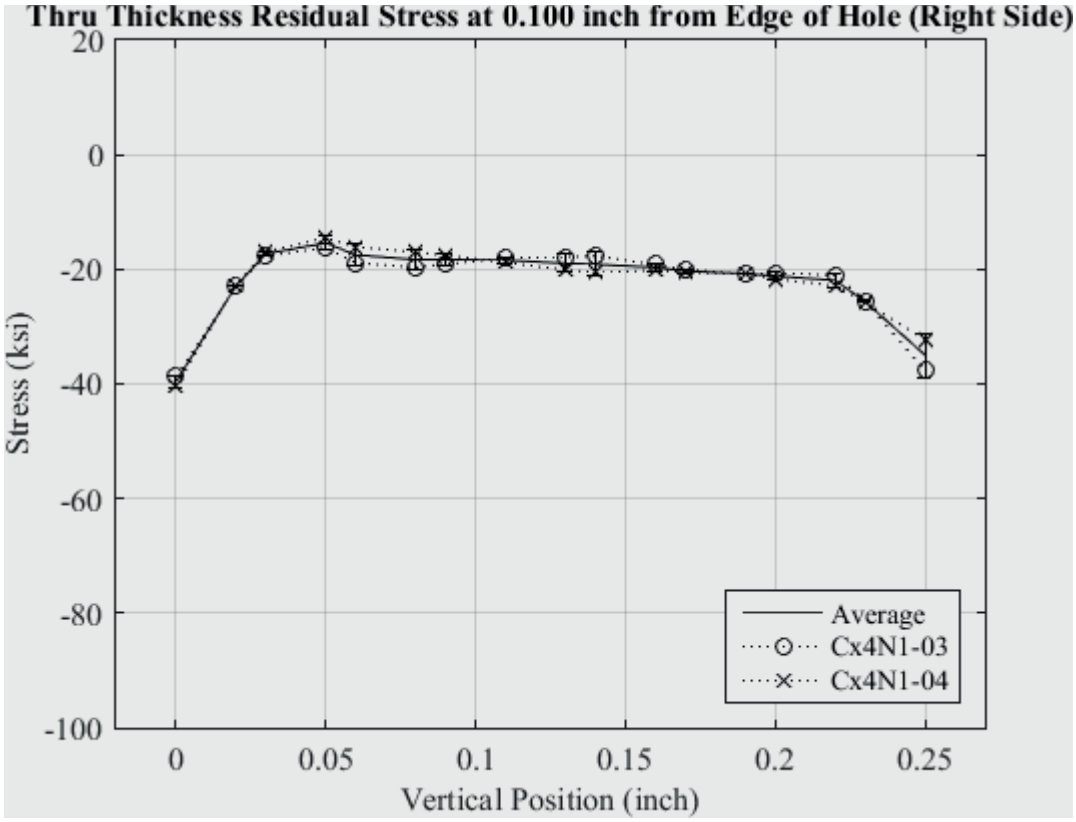

Fig. 292 Residual Stress Line Plot of Cx4N1-03-B and Cx4N1-04-B (2024-T351) Through the Thickness at 0.01 inch from Right Side of Hole – Coupons had a 0.10 inch Fatigue Crack at the Left Entrance Surface.

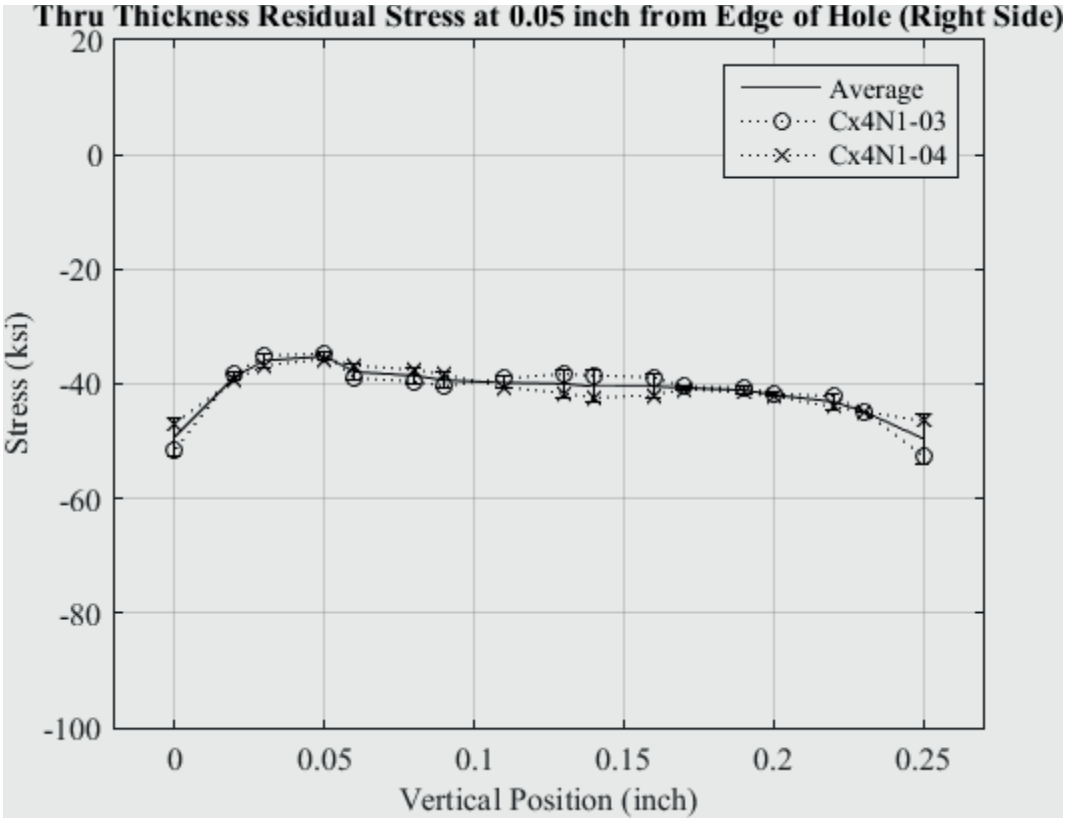

Fig. 293 Residual Stress Line Plot of Cx4N1-03-B and Cx4N1-04-B (2024-T351) Through the Thickness at 0.05 inch from Right Side of Hole – Coupons had a 0.10 inch Fatigue Crack at the Left Entrance Surface.

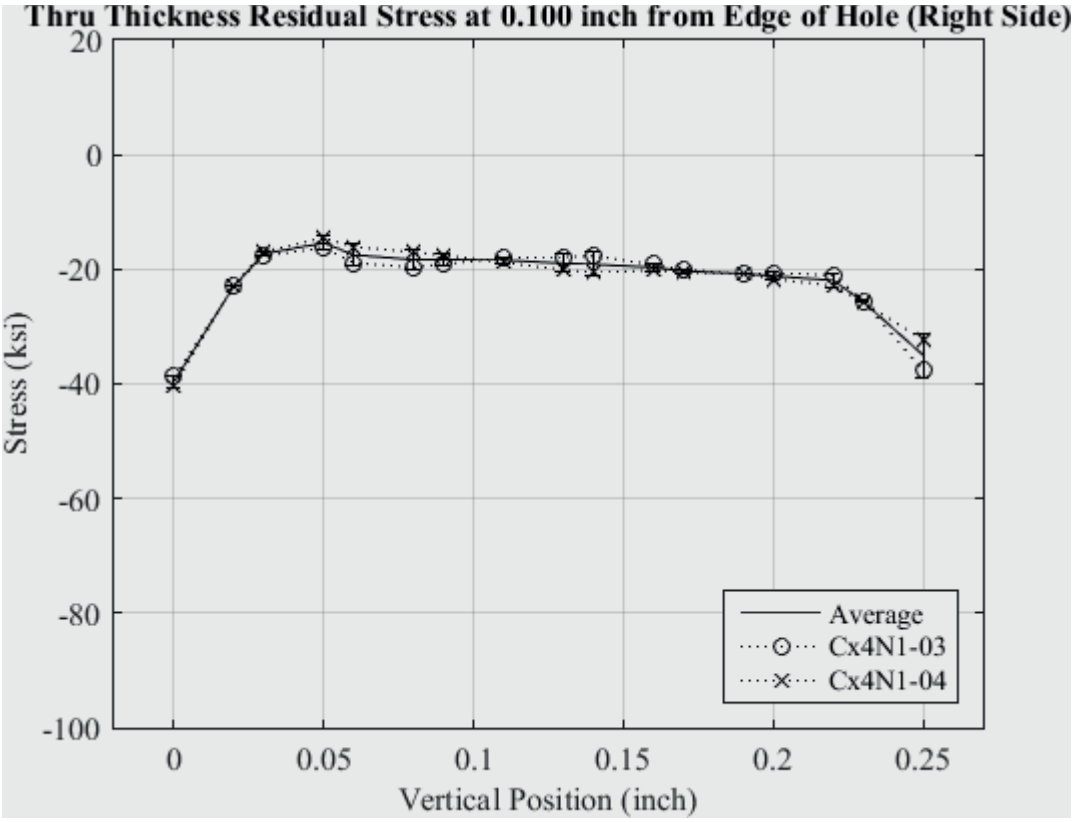

Fig. 294 Residual Stress Line Plot of Cx4N1-03-B and Cx4N1-04-B (2024-T351) Through the Thickness at 0.10 inch from Right Side of Hole – Coupons had a 0.10 inch Fatigue Crack at the Left Entrance Surface.

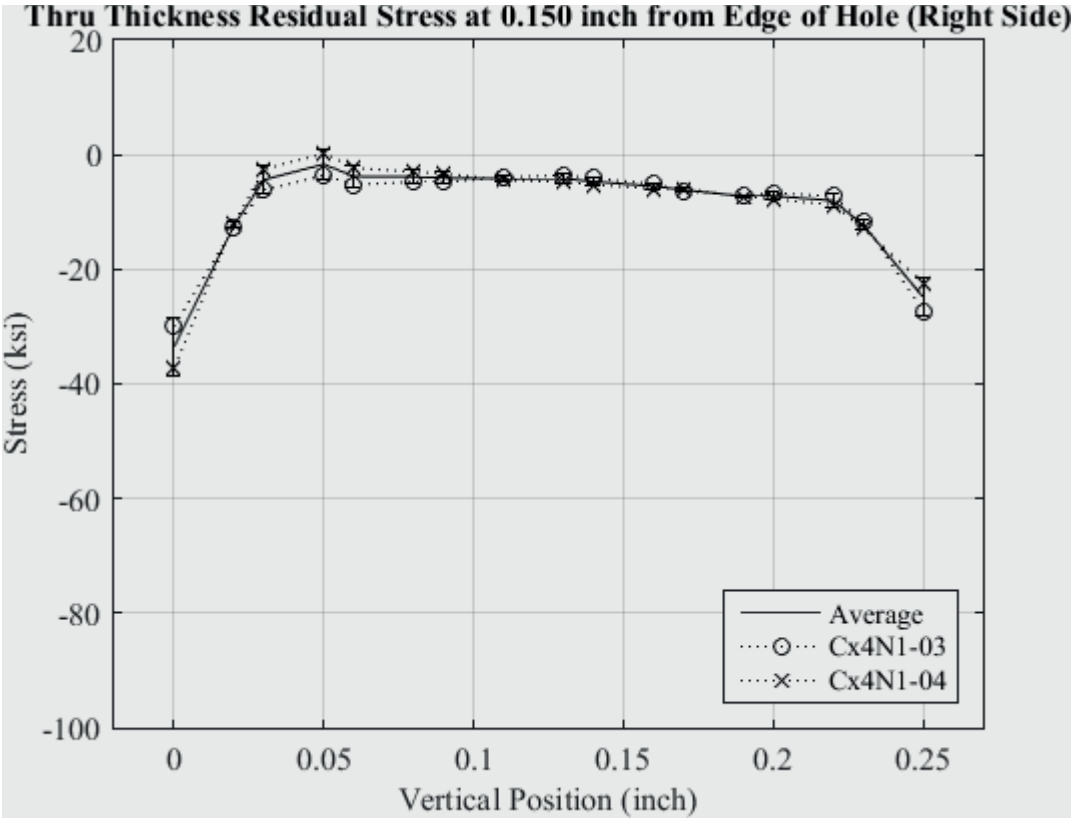

Fig. 295 Residual Stress Line Plot of Cx4N1-03-B and Cx4N1-04-B (2024-T351) Through the Thickness at 0.150 inch from Right Side of Hole – Coupons had a 0.10 inch Fatigue Crack at the Left Entrance Surface.

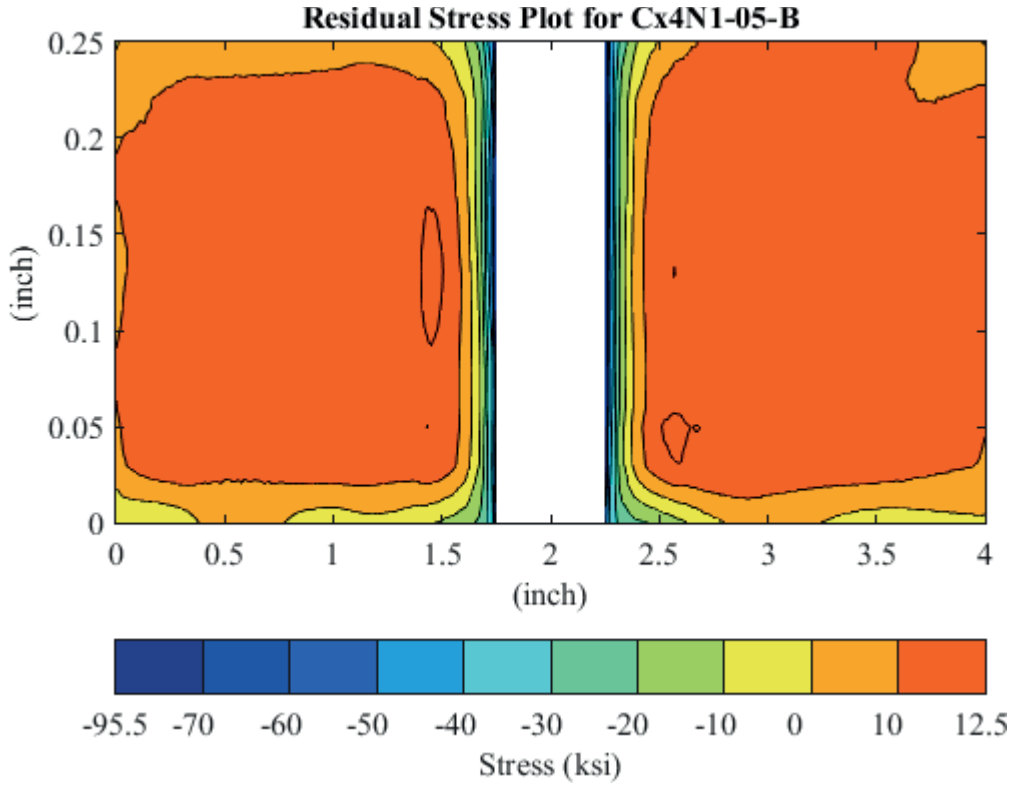

Fig. 296 Residual Stress Contour plot of Coupon Cx4N1-05-B (2024-T351) – Mandrel Entrance Surface at Y=0, 0.125 inch Fatigue Crack on Left Side of Hole on Mandrel Entrance Surface.

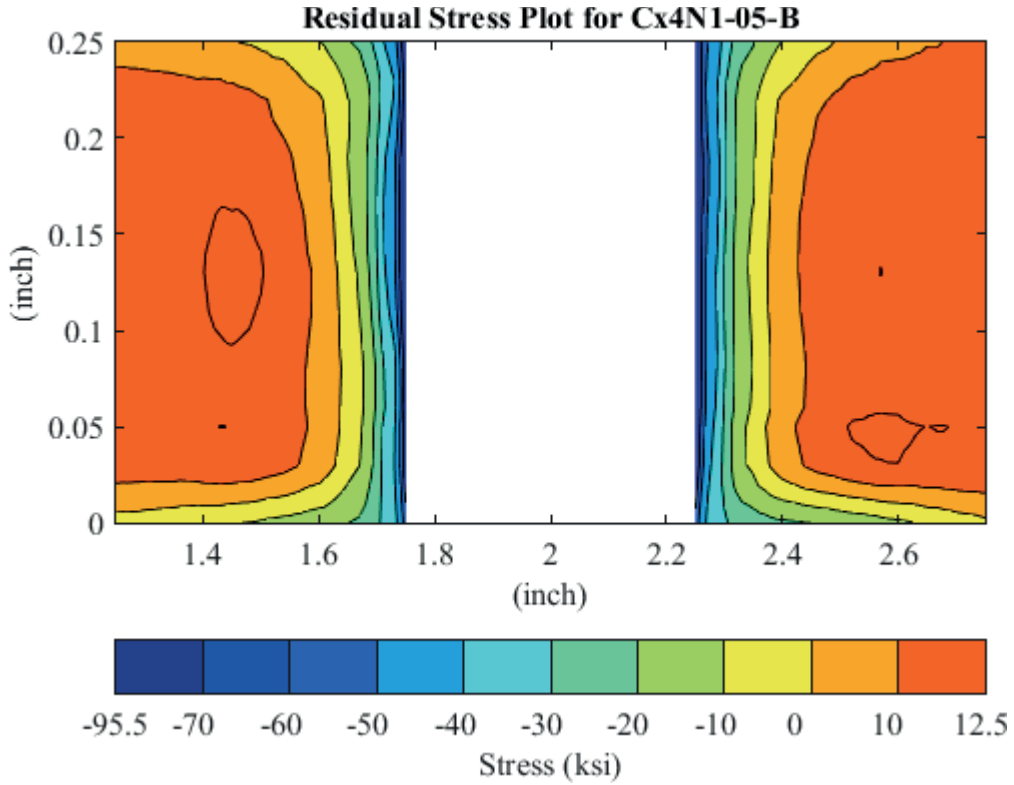

Fig. 297 Residual Stress Contour plot of Coupon Cx4N1-05-B (2024-T351) – Mandrel Entrance Surface at Y=0, 0.125 inch Fatigue Crack on Left Side of Hole on Mandrel Entrance Surface – Zoomed in Next to Hole.

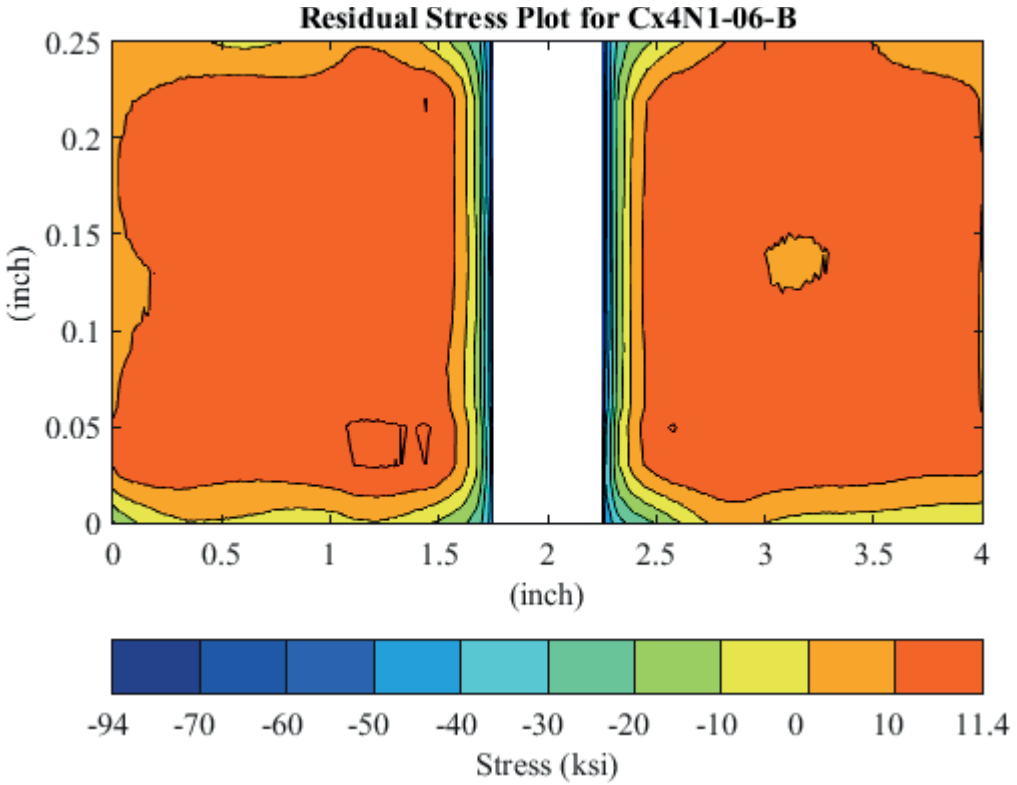

Fig. 298 Residual Stress Contour plot of Coupon Cx4N1-06-B (2024-T351) – Mandrel Entrance Surface at Y=0, 0.125 inch Fatigue Crack on Left Side of Hole on Mandrel Entrance Surface.

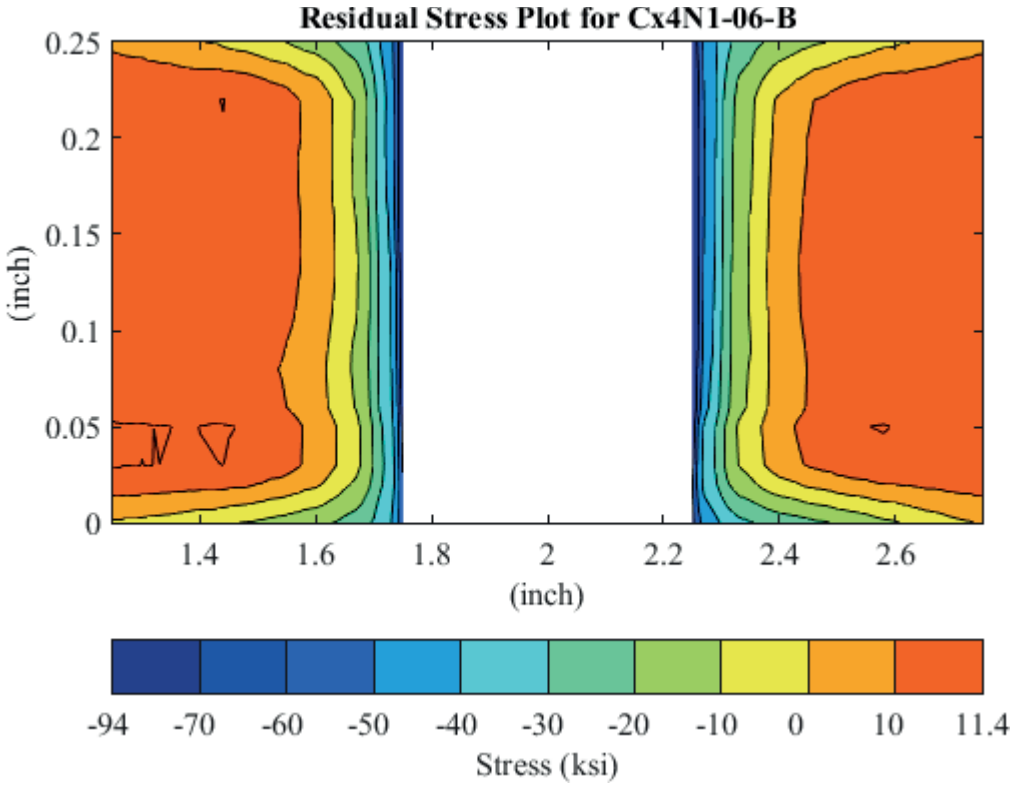

Fig. 299 Residual Stress Contour plot of Coupon Cx4N1-06-B (2024-T351) – Mandrel Entrance Surface at Y=0, 0.125 inch Fatigue Crack on Left Side of Hole on Mandrel Entrance Surface – Zoomed in Next to Hole.

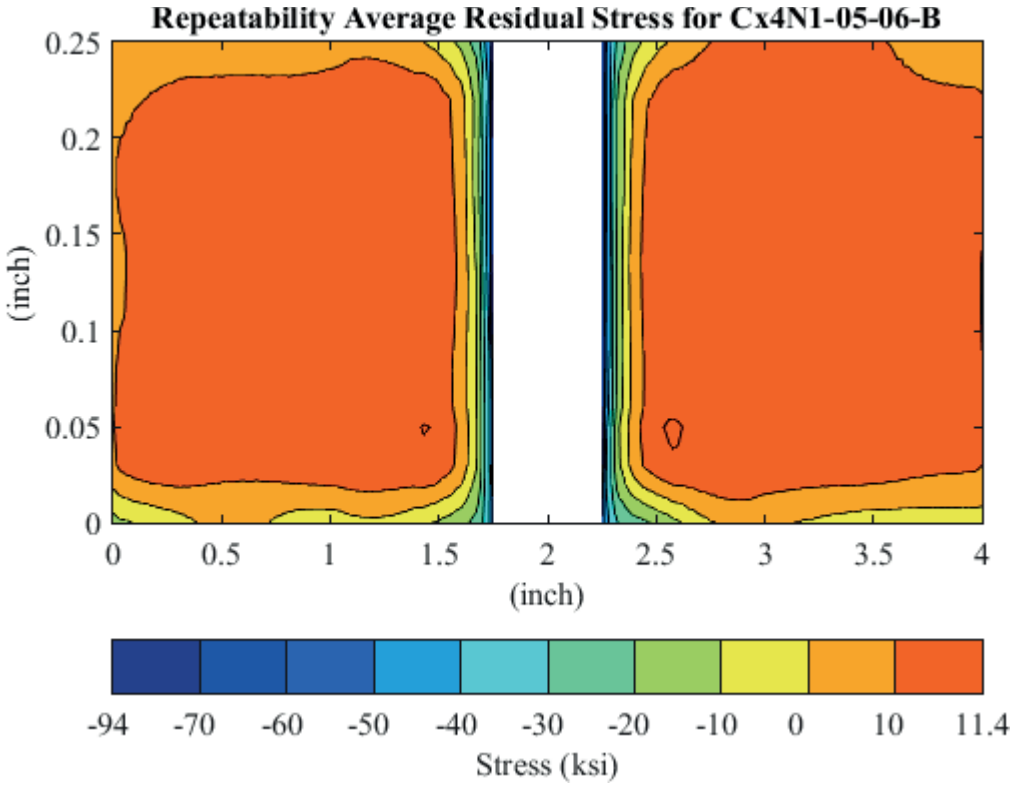

Fig. 300 Average Residual Stress Contour Plot of Coupons Cx4N1-03-B and Cx4N1-04-B (2024-T351) – Mandrel Entrance Surface at Y=0, 0.125 inch Fatigue Crack on Left Side of Hole on Mandrel Entrance Surface.

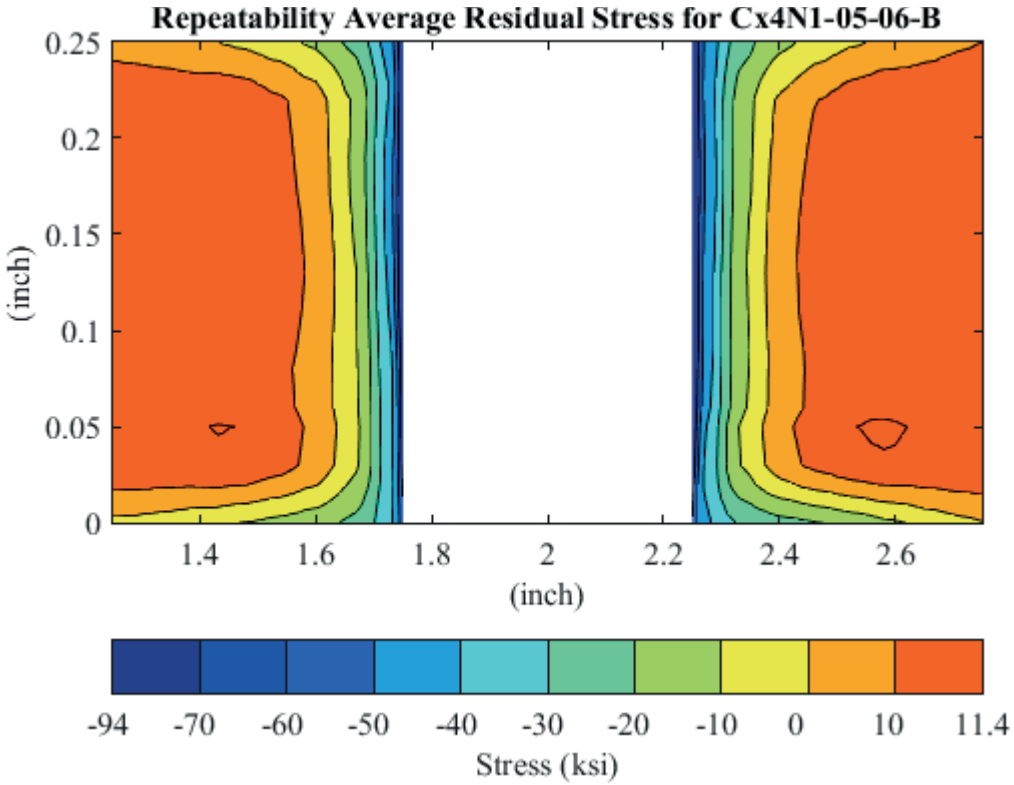

Fig. 301 Average Residual Stress Contour Plot of Coupons Cx4N1-03-B and Cx4N1-04-B (2024-T351) – Mandrel Entrance Surface at Y=0, 0.125 inch Fatigue Crack on Left Side of Hole on Mandrel Entrance Surface – Zoomed in Next to Hole.

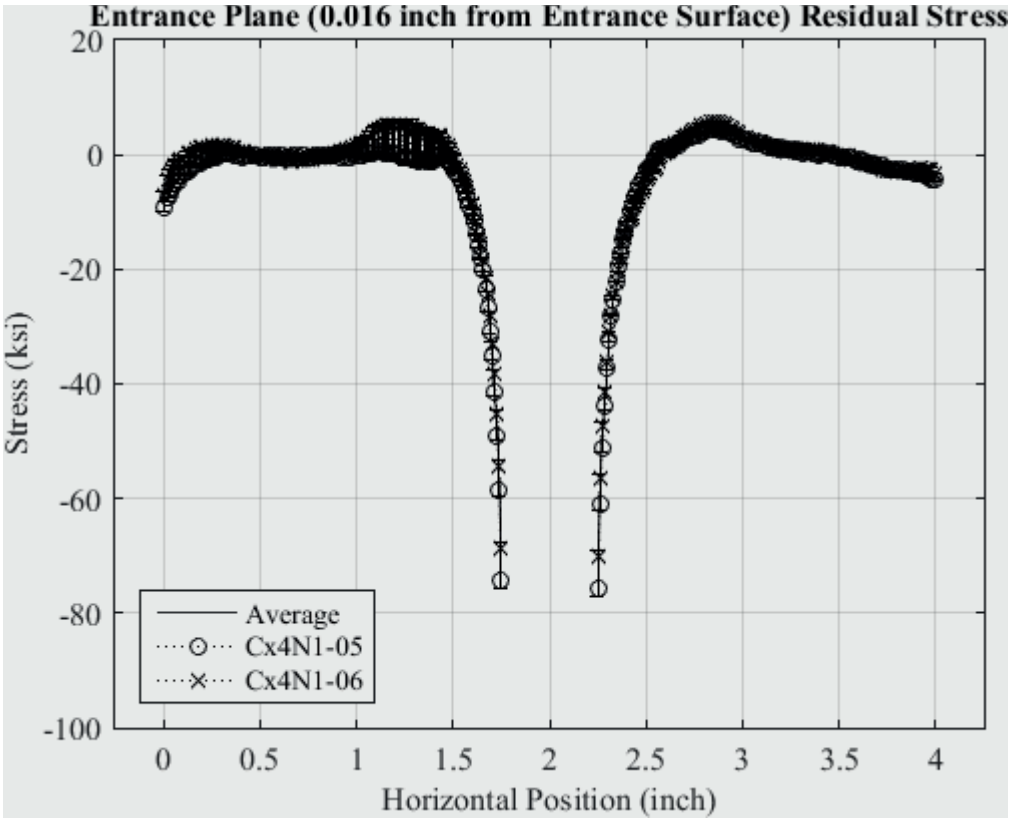

Fig. 302 Residual Stress Line Plot of Cx4N1-05-B and Cx4N1-06-B (2024-T351) at a Distance of 0.016 inch (Entrance Surface) from the Entrance Surface – Coupons had a 0.125 inch Fatigue Crack at the Left Entrance Surface.

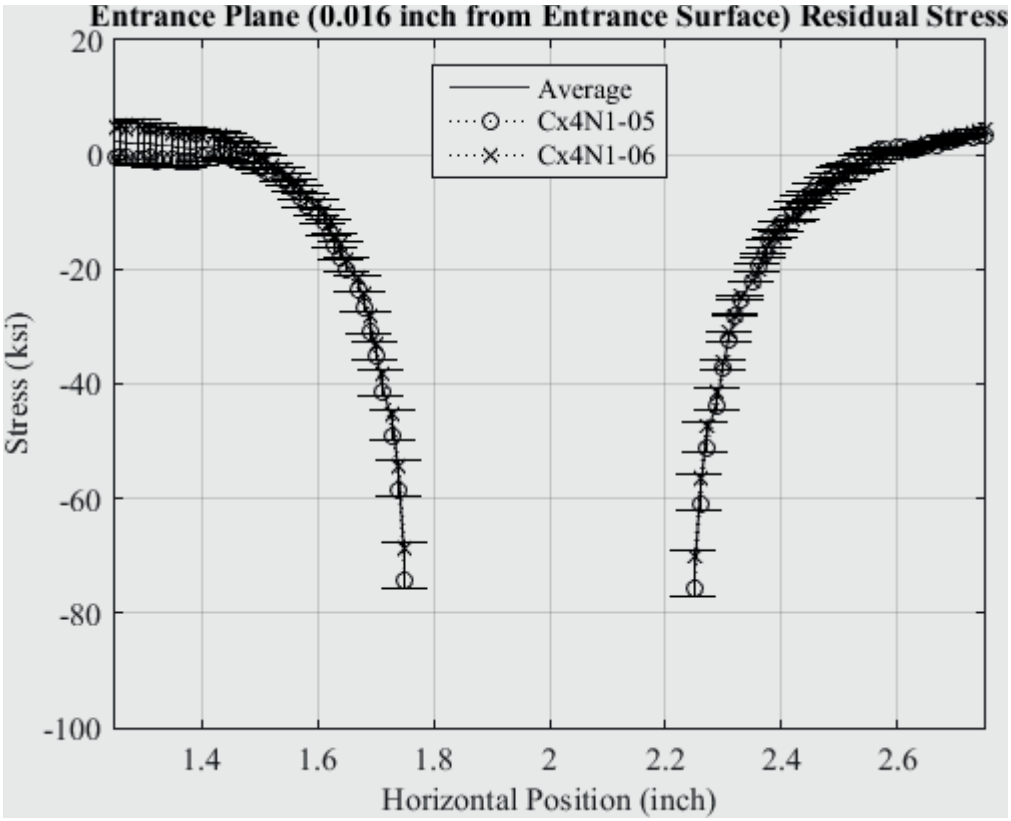

Fig. 303 Residual Stress Line Plot of Cx4N1-05-B and Cx4N1-06-B (2024-T351) at a Distance of 0.016 inch (Entrance Surface) from the Entrance Surface – Coupons had a 0.125 inch Fatigue Crack at the Left Entrance Surface – Zoomed in Next to Hole.

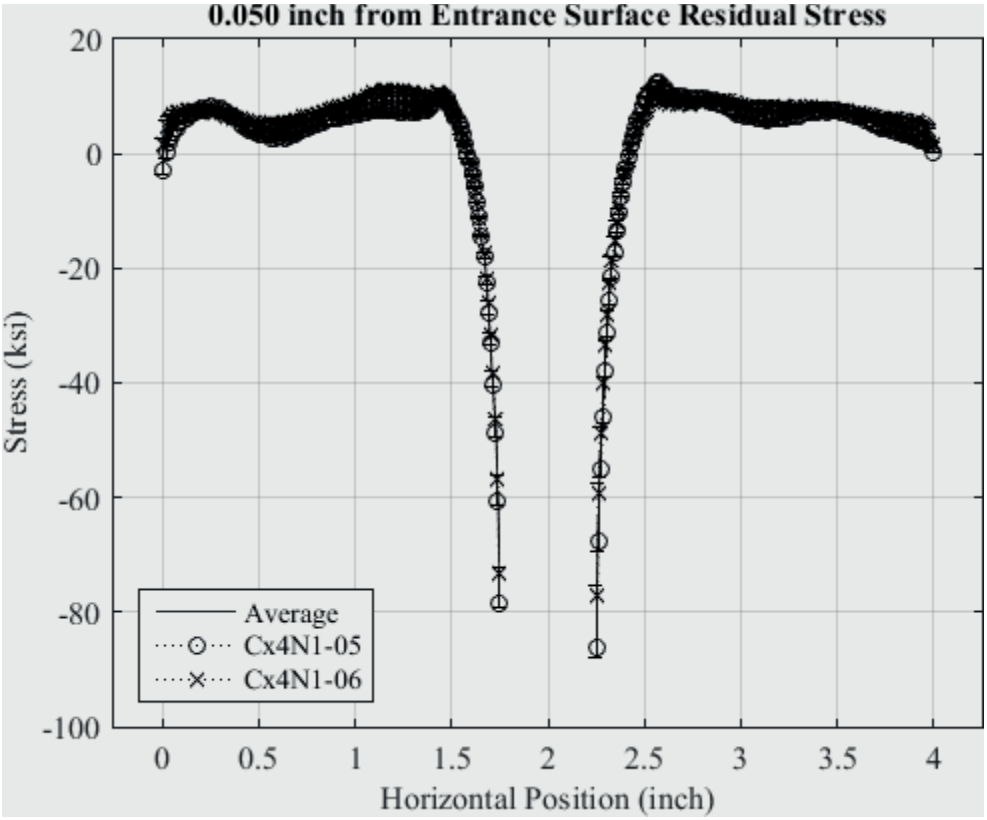

Fig. 304 Residual Stress Line Plot of Cx4N1-05-B and Cx4N1-06-B (2024-T351) at a Distance of 0.05 inch from the Entrance Surface – Coupons had a 0.125 inch Fatigue Crack at the Left Entrance Surface.

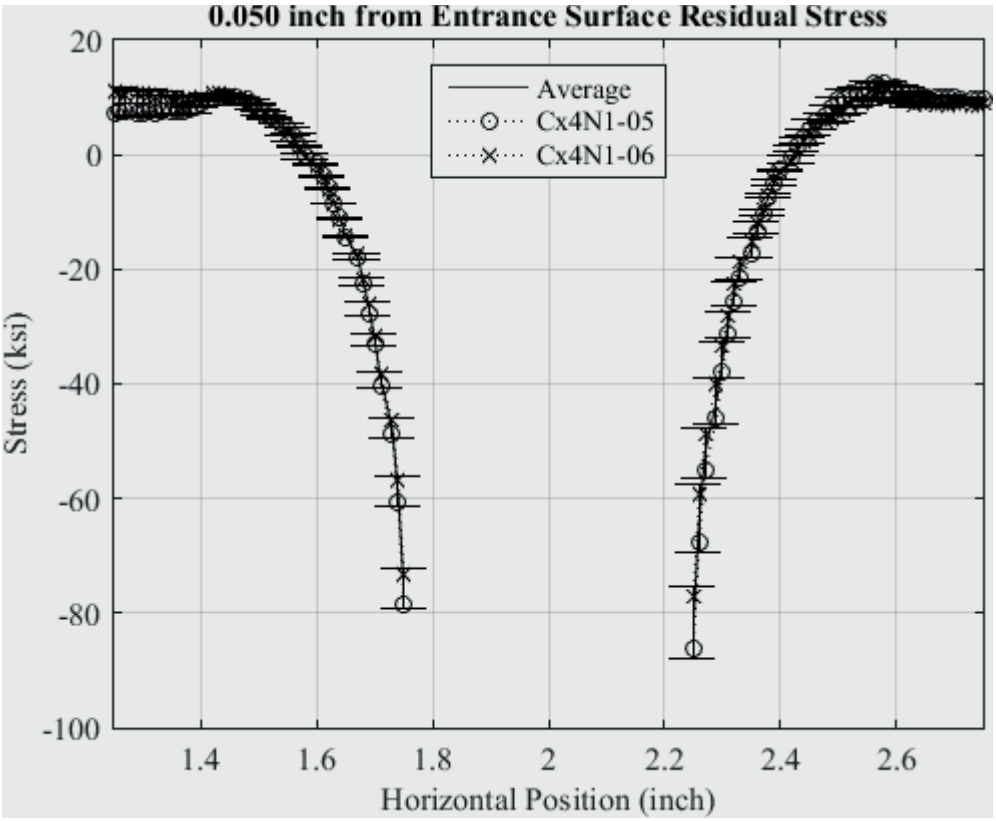

Fig. 305 Residual Stress Line Plot of Cx4N1-05-B and Cx4N1-06-B (2024-T351) at a Distance of 0.05 inch from the Entrance Surface – Coupons had a 0.125 inch Fatigue Crack at the Left Entrance Surface – Zoomed in Next to Hole.

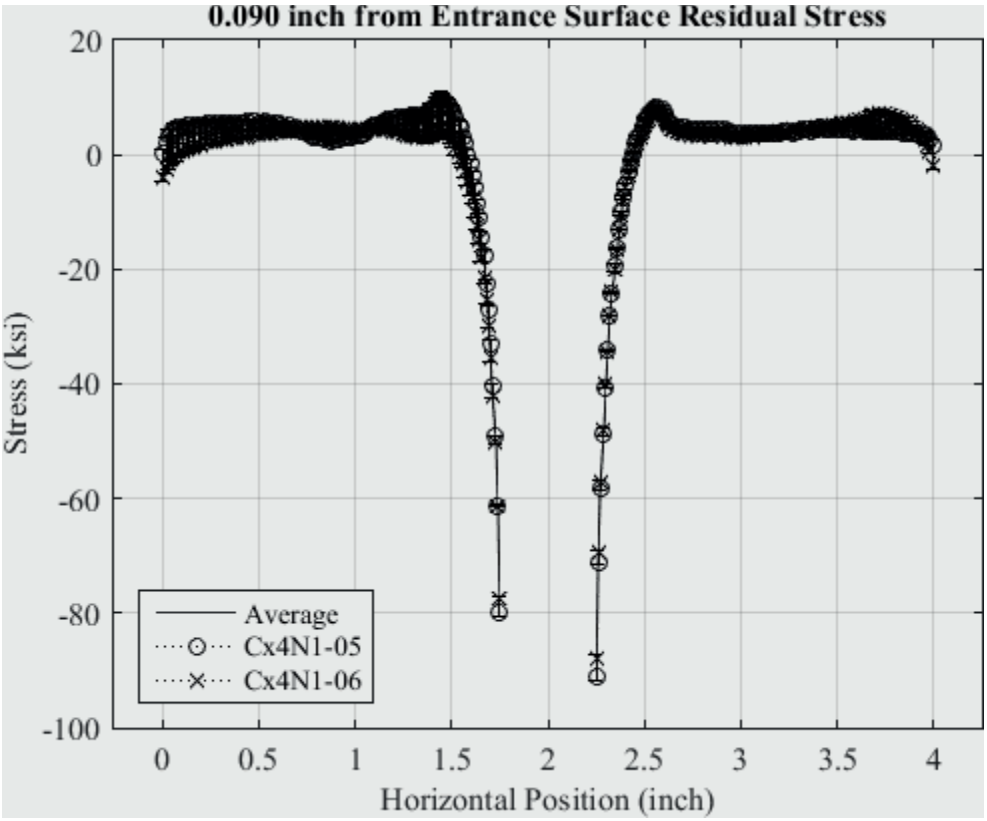

Fig. 306 Residual Stress Line Plot of Cx4N1-05-B and Cx4N1-06-B (2024-T351) at a Distance of 0.09 inch from the Entrance Surface – Coupons had a 0.125 inch Fatigue Crack at the Left Entrance Surface.

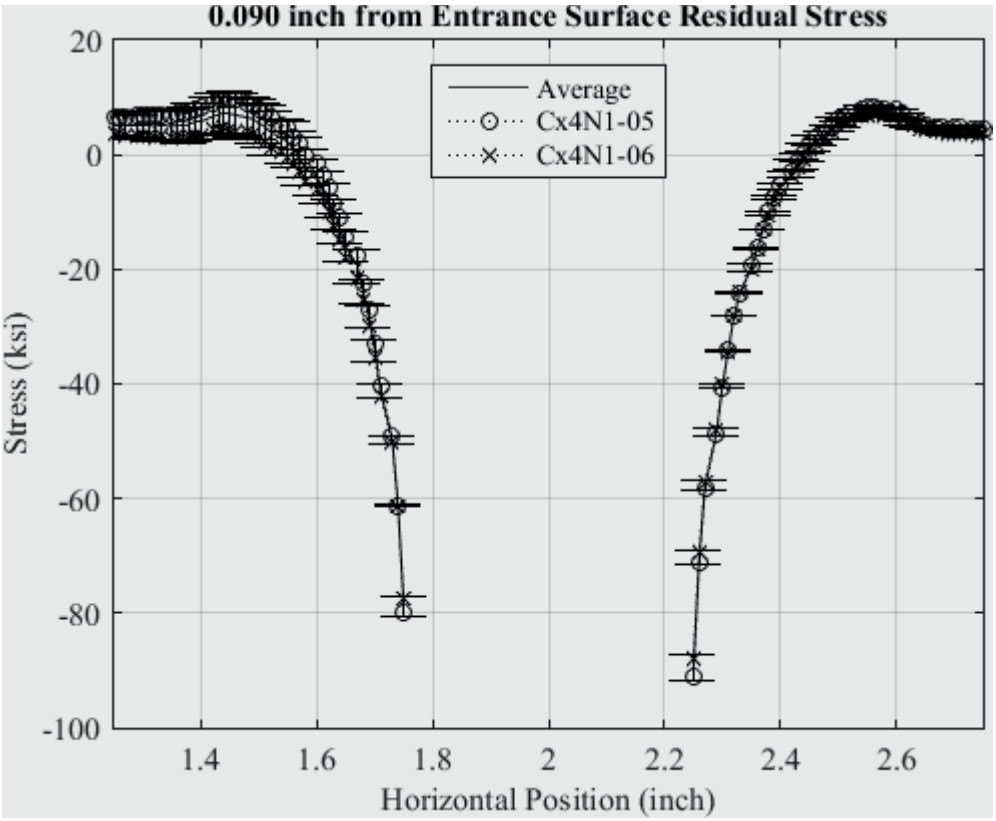

Fig. 307 Residual Stress Line Plot of Cx4N1-05-B and Cx4N1-06-B (2024-T351) at a Distance of 0.09 inch from the Entrance Surface – Coupons had a 0.125 inch Fatigue Crack at the Left Entrance Surface – Zoomed in Next to Hole.

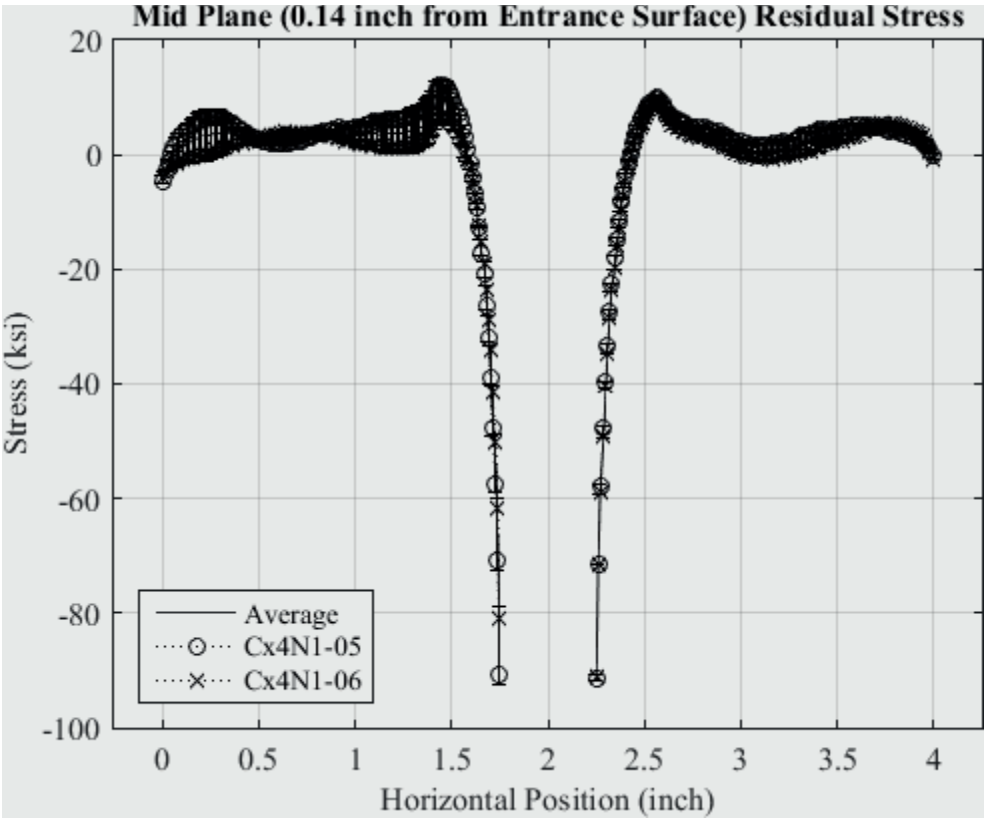

Fig. 308 Residual Stress Line Plot of Cx4N1-05-B and Cx4N1-06-B (2024-T351) at a Distance of 0.140 inch (Mid Plane Surface) from the Entrance Surface – Coupons had a 0.125 inch Fatigue Crack at the Left Entrance Surface.

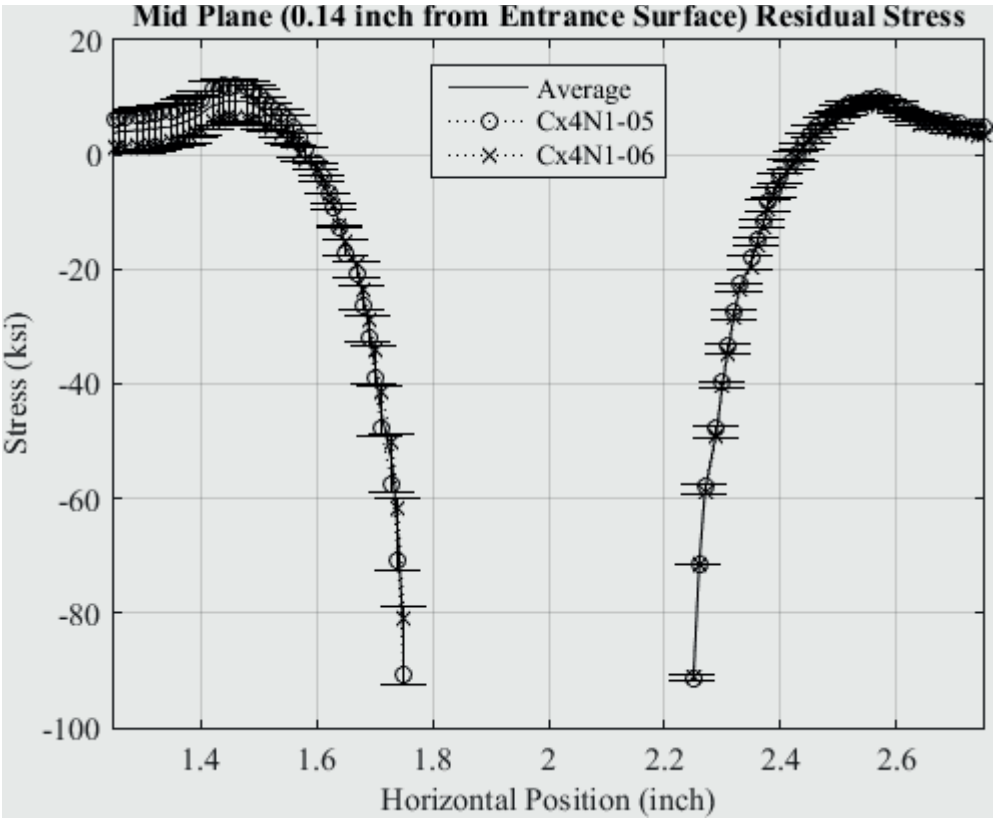

Fig. 309 Residual Stress Line Plot of Cx4N1-05-B and Cx4N1-06-B (2024-T351) at a Distance of 0.140 inch (Mid Plane Surface) from the Entrance Surface – Coupons had a 0.125 inch Fatigue Crack at the Left Entrance Surface – Zoomed in Next to Hole.

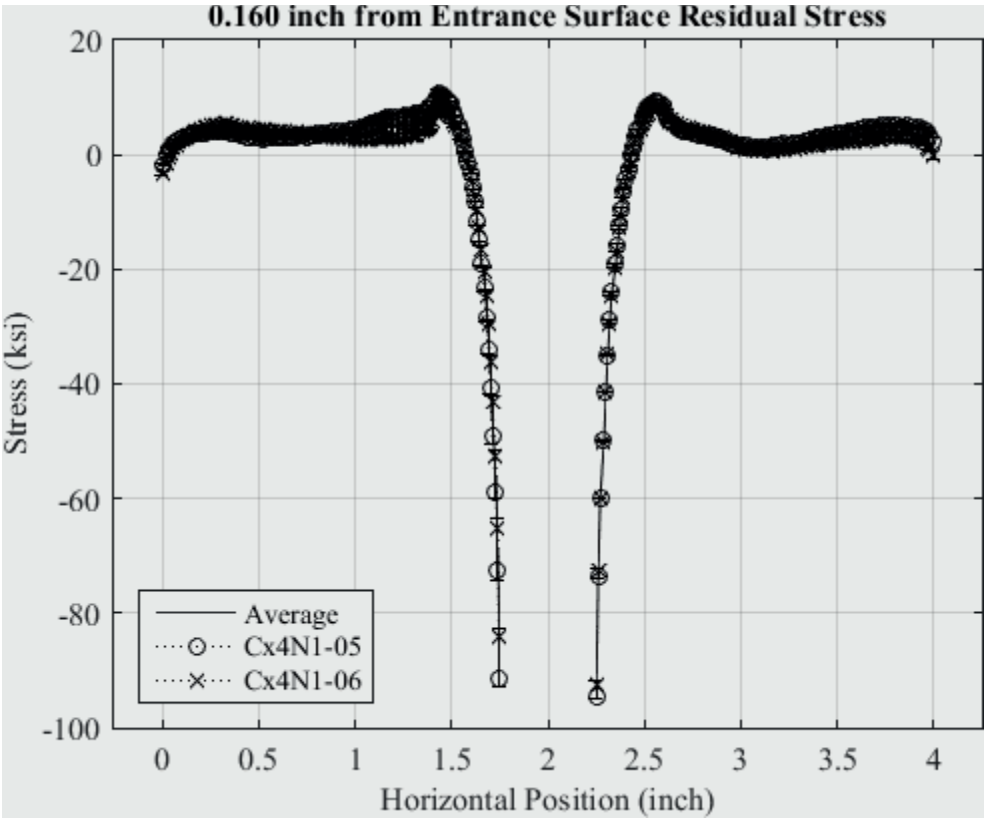

Fig. 310 Residual Stress Line Plot of Cx4N1-05-B and Cx4N1-06-B (2024-T351) at a Distance of 0.160 inch from the Entrance Surface – Coupons had a 0.125 inch Fatigue Crack at the Left Entrance Surface.

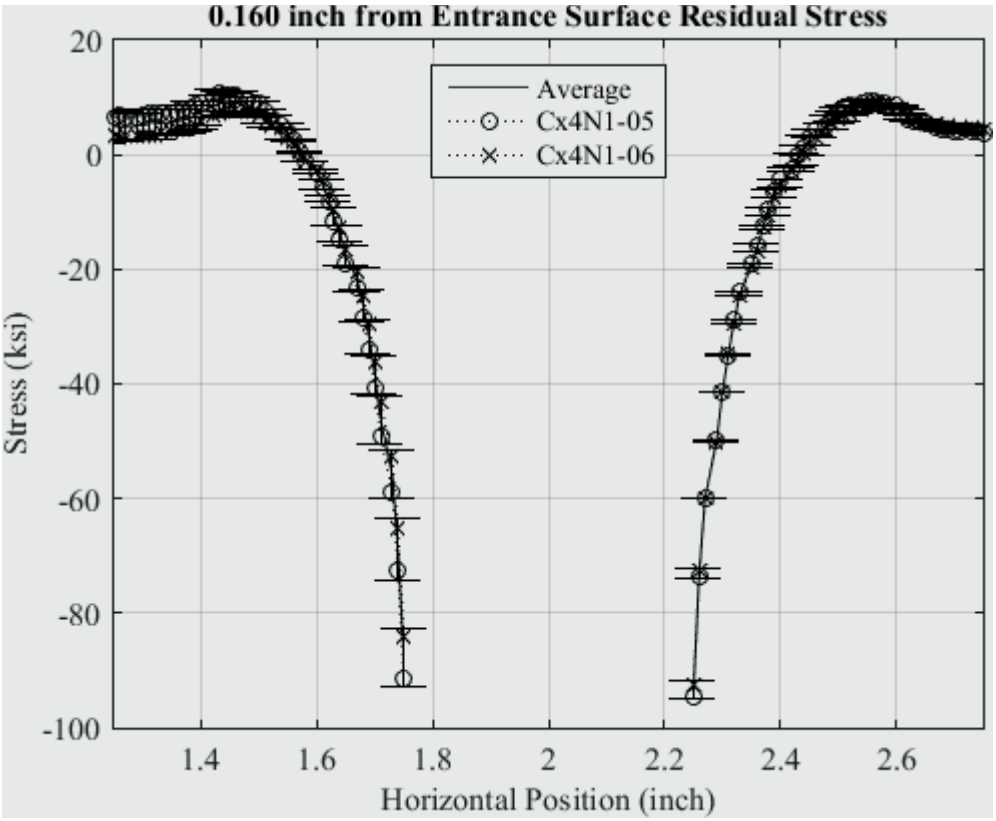

Fig. 311 Residual Stress Line Plot of Cx4N1-05-B and Cx4N1-06-B (2024-T351) at a Distance of 0.160 inch from the Entrance Surface – Coupons had a 0.125 inch Fatigue Crack at the Left Entrance Surface – Zoomed in Next to Hole.

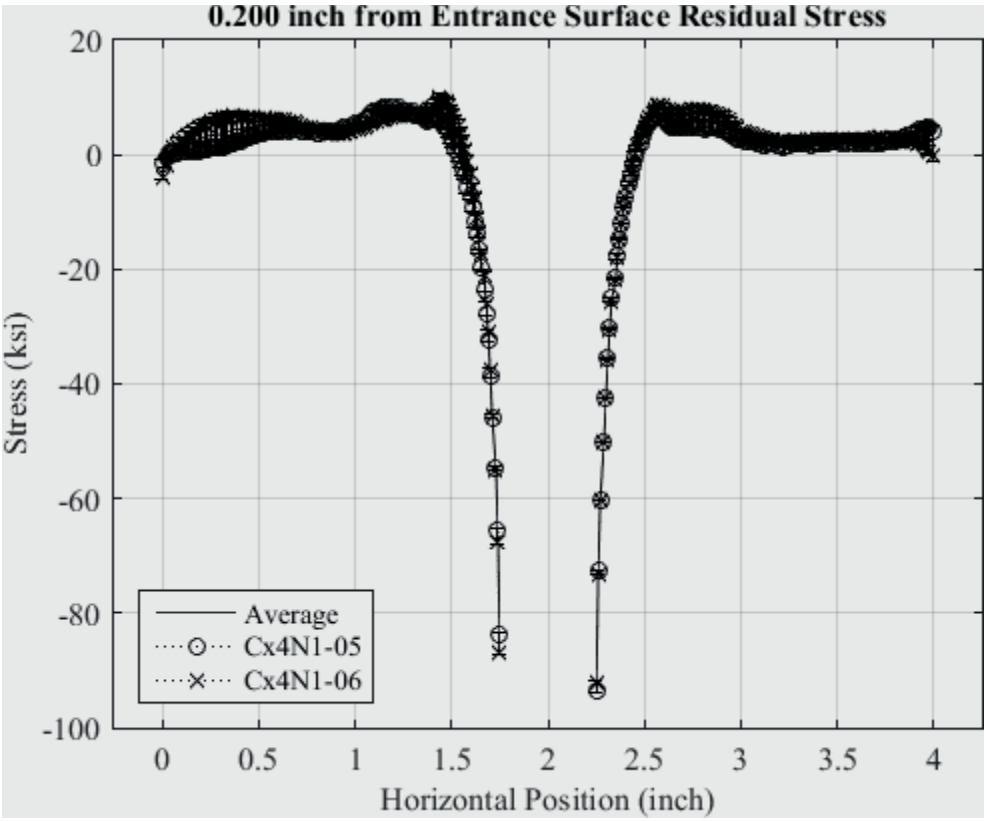

Fig. 312 Residual Stress Line Plot of Cx4N1-05-B and Cx4N1-06-B (2024-T351) at a Distance of 0.200 inch from the Entrance Surface – Coupons had a 0.125 inch Fatigue Crack at the Left Entrance Surface.

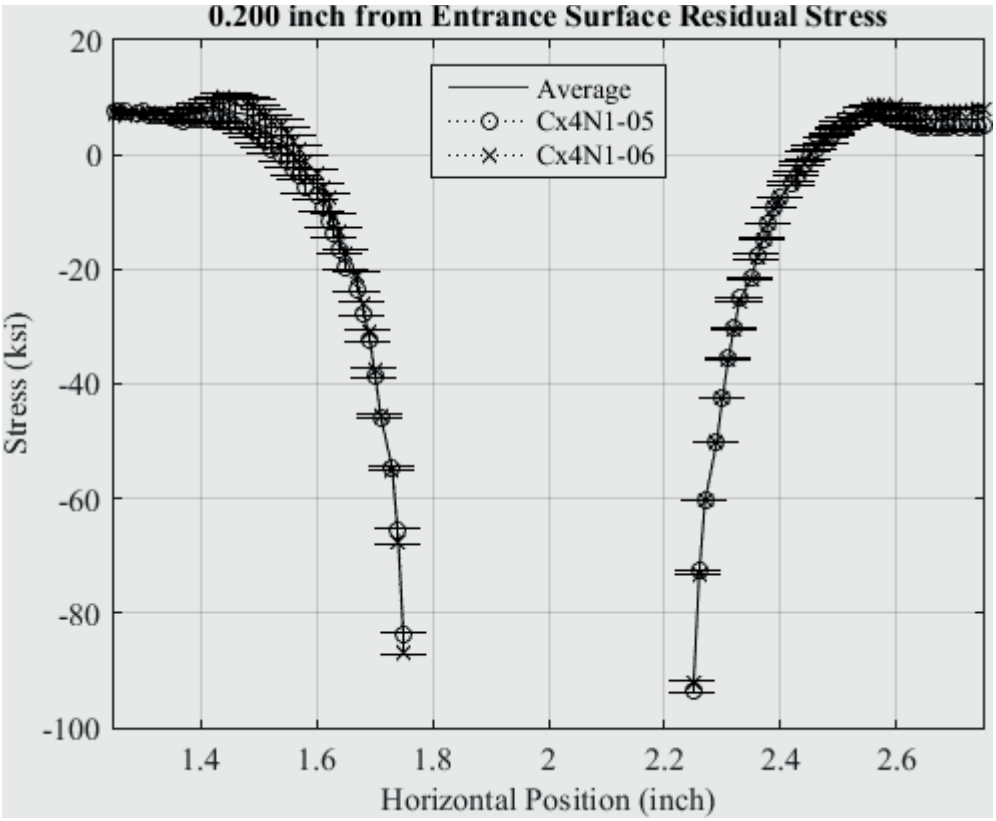

Fig. 313 Residual Stress Line Plot of Cx4N1-05-B and Cx4N1-06-B (2024-T351) at a Distance of 0.200 inch from the Entrance Surface – Coupons had a 0.125 inch Fatigue Crack at the Left Entrance Surface – Zoomed in Next to Hole.

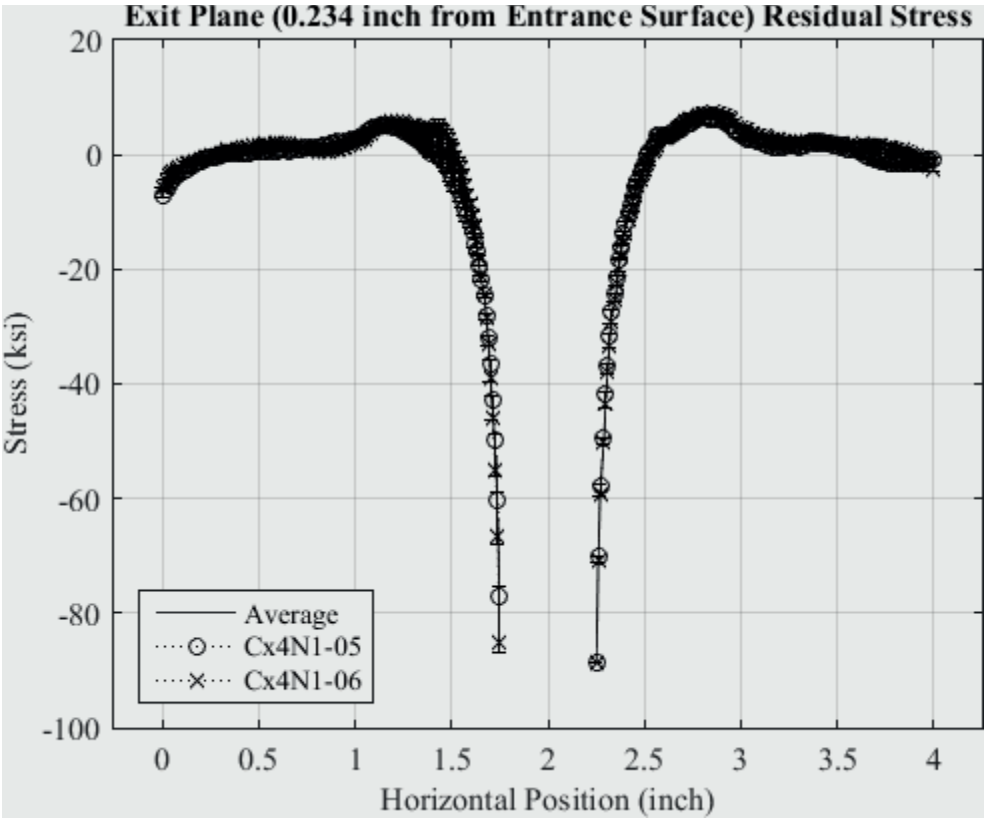

Fig. 314 Residual Stress Line Plot of Cx4N1-05-B and Cx4N1-06-B (2024-T351) at a Distance of 0.234 inch (Exit Surface) from the Entrance Surface – Coupons had a 0.125 inch Fatigue Crack at the Left Entrance Surface.

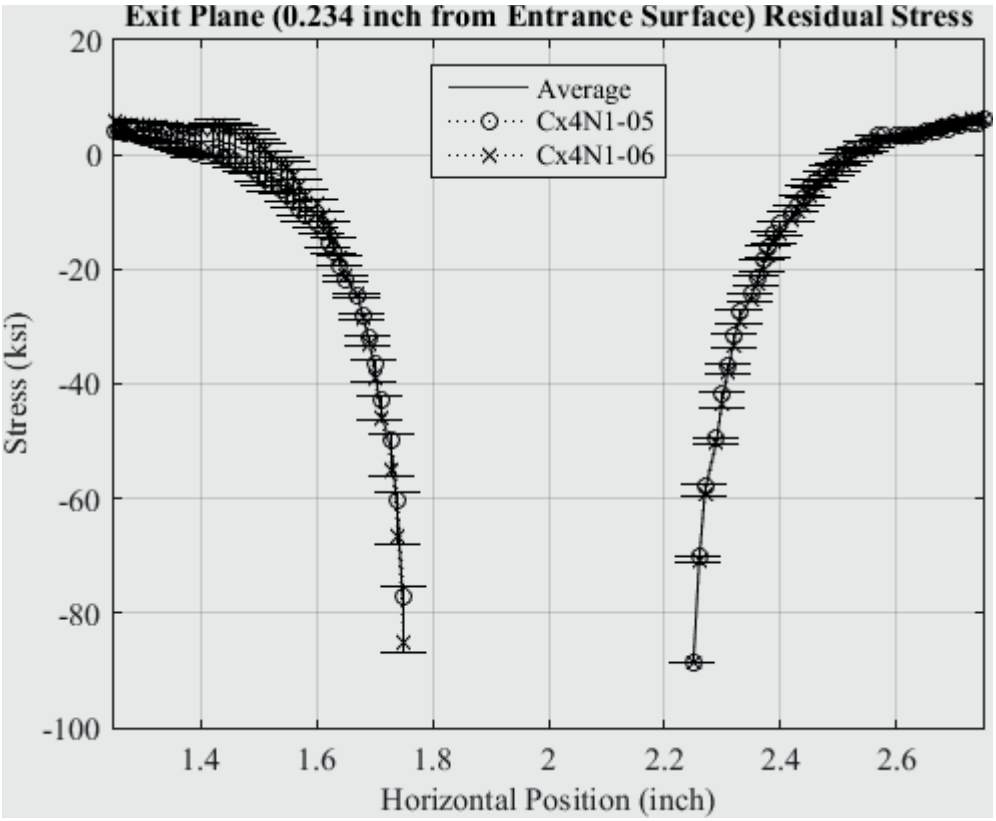

Fig. 315 Residual Stress Line Plot of Cx4N1-05-B and Cx4N1-06-B (2024-T351) at a Distance of 0.234 inch (Exit Surface) from the Entrance Surface – Coupons had a 0.125 inch Fatigue Crack at the Left Entrance Surface – Zoomed in Next to Hole.

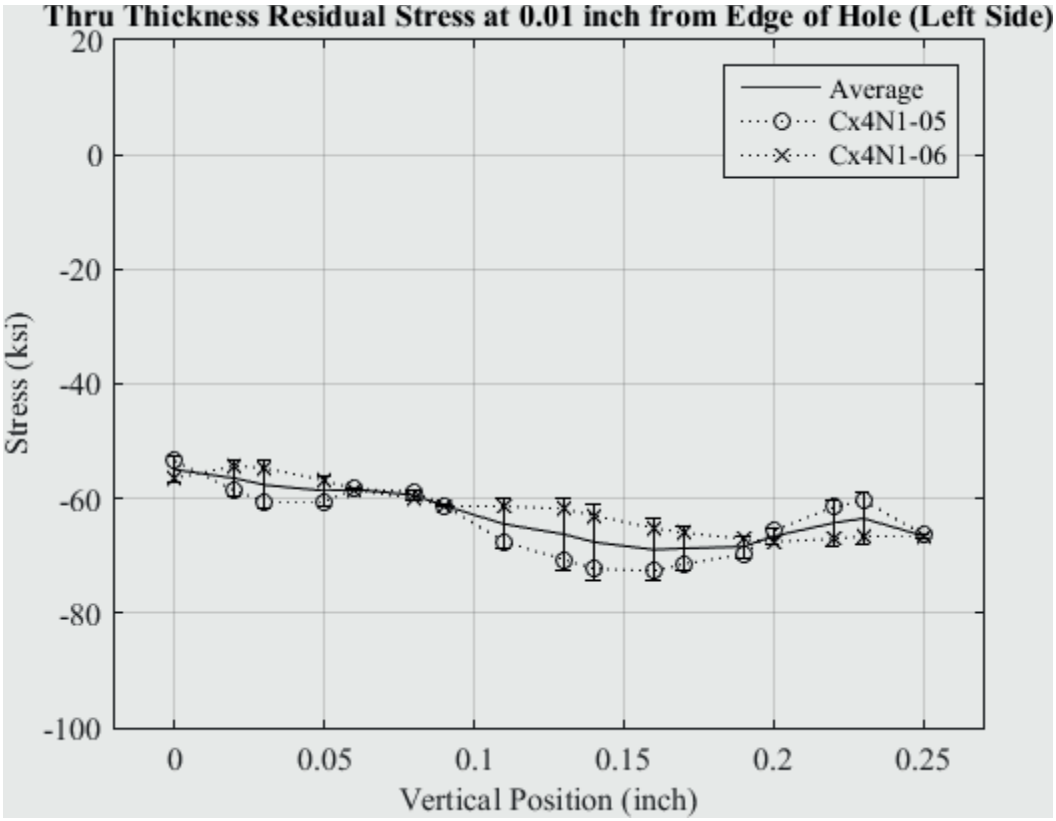

Fig. 316 Residual Stress Line Plot of Cx4N1-05-B and Cx4N1-06-B (2024-T351) Through the Thickness at 0.01 inch from Left Side of Hole – Coupons had a 0.125 inch Fatigue Crack at the Left Entrance Surface.

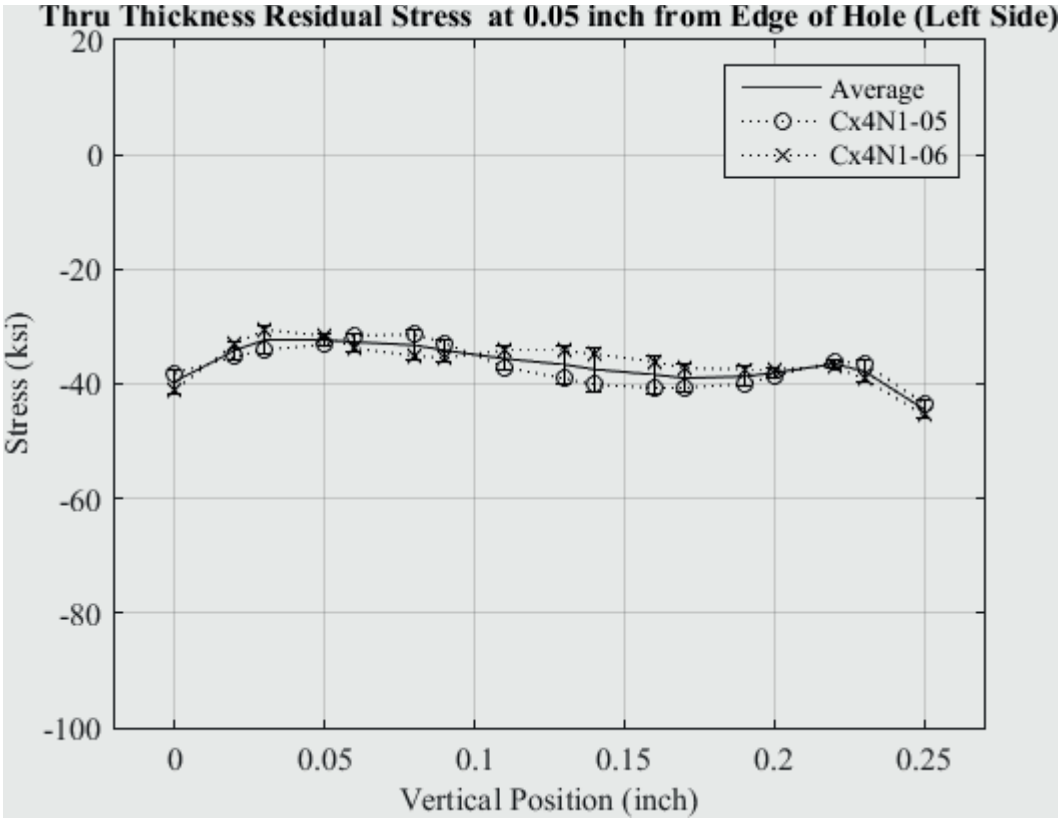

Fig. 317 Residual Stress Line Plot of Cx4N1-05-B and Cx4N1-06-B (2024-T351) Through the Thickness at 0.05 inch from Left Side of Hole – Coupons had a 0.125 inch Fatigue Crack at the Left Entrance Surface.

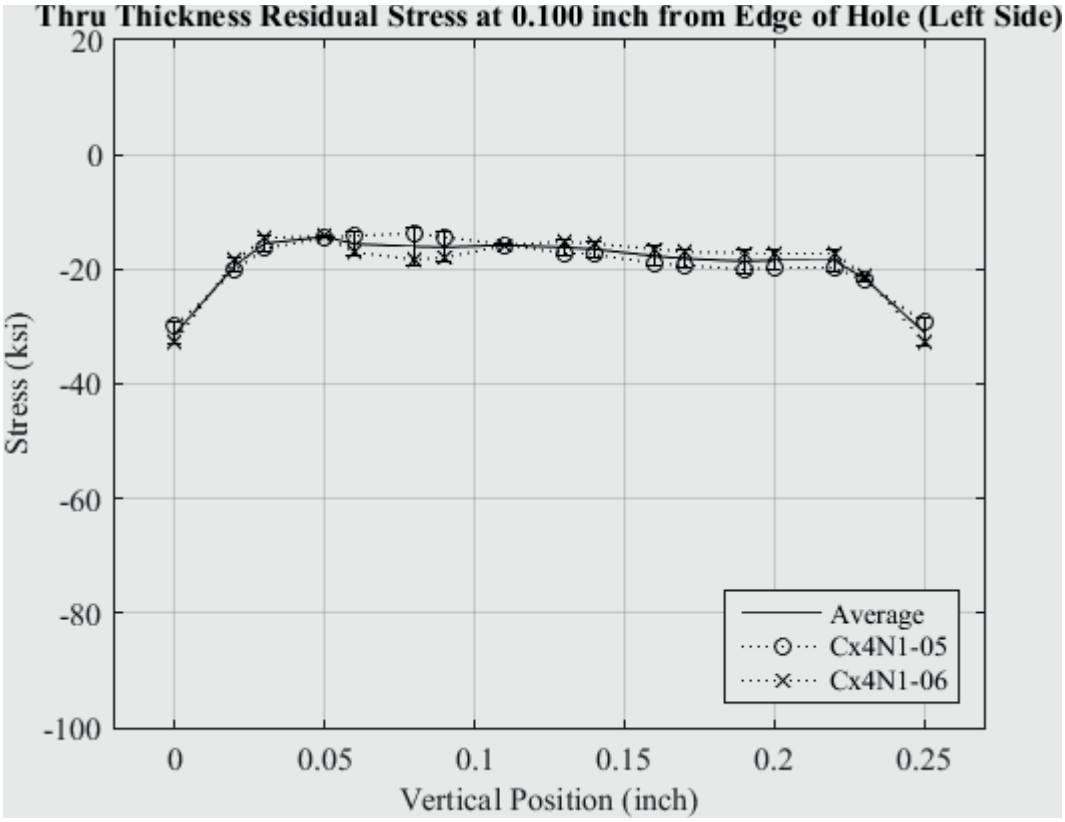

Fig. 318 Residual Stress Line Plot of Cx4N1-05-B and Cx4N1-06-B (2024-T351) Through the Thickness at 0.10 inch from Left Side of Hole – Coupons had a 0.125 inch Fatigue Crack at the Left Entrance Surface.

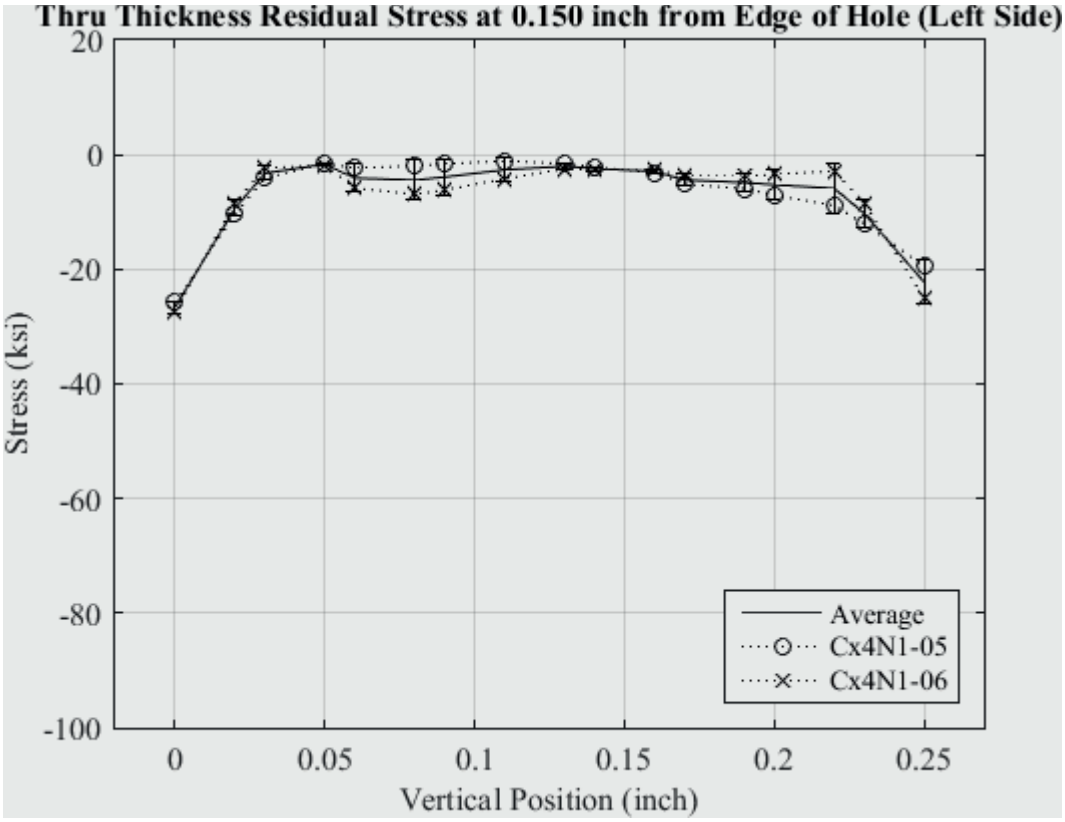

Fig. 319 Residual Stress Line Plot of Cx4N1-05-B and Cx4N1-06-B (2024-T351) Through the Thickness at 0.150 inch from Left Side of Hole – Coupons had a 0.125 inch Fatigue Crack at the Left Entrance Surface.

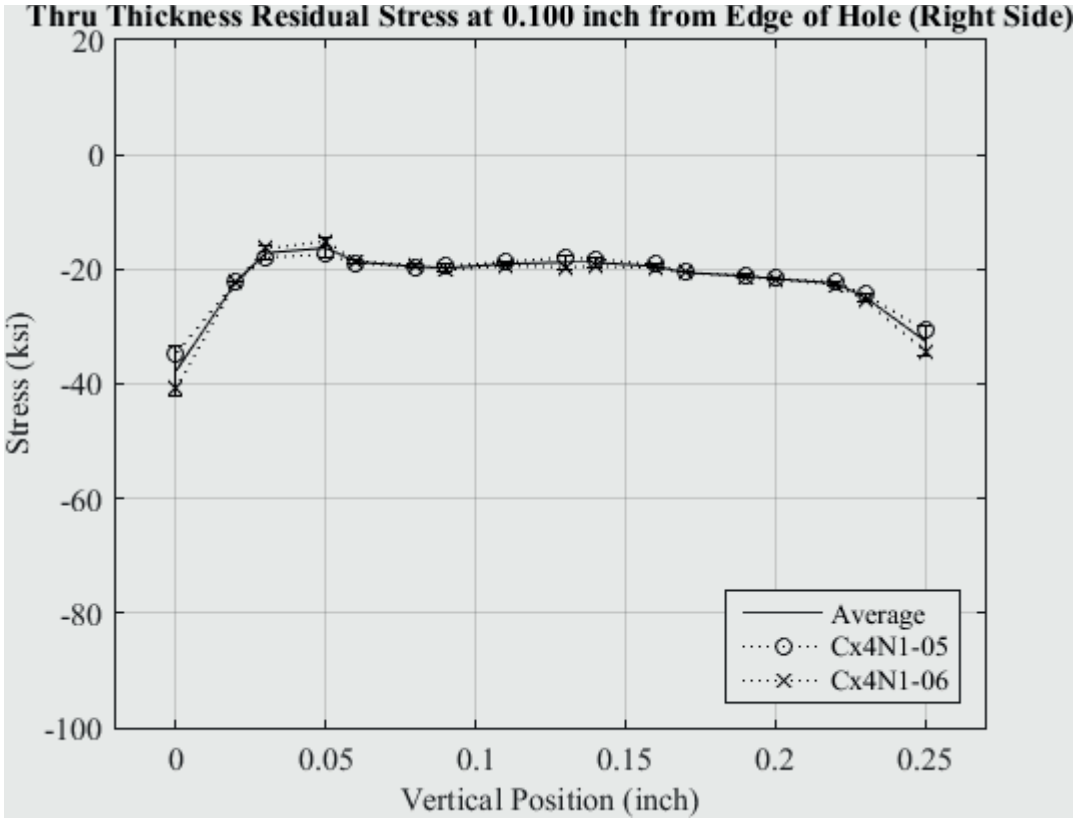

Fig. 320 Residual Stress Line Plot of Cx4N1-05-B and Cx4N1-06-B (2024-T351) Through the Thickness at 0.01 inch from Right Side of Hole – Coupons had a 0.125 inch Fatigue Crack at the Left Entrance Surface.

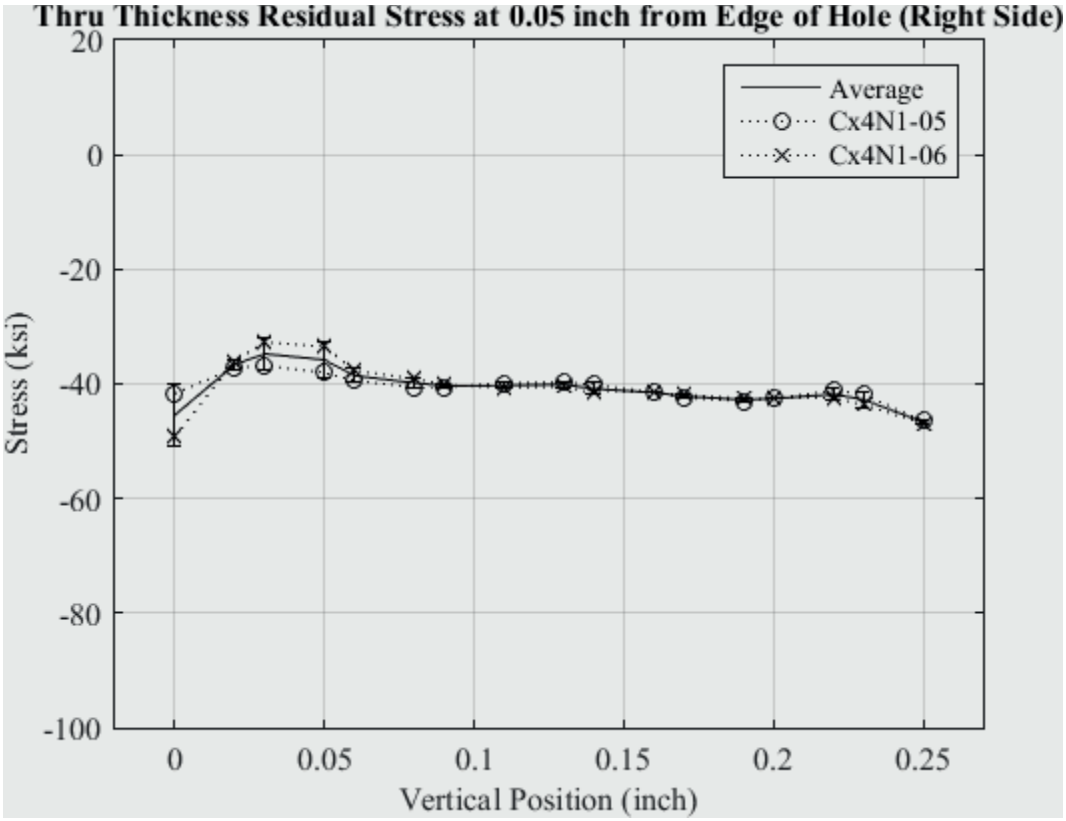

Fig. 321 Residual Stress Line Plot of Cx4N1-05-B and Cx4N1-06-B (2024-T351) Through the Thickness at 0.05 inch from Right Side of Hole – Coupons had a 0.125 inch Fatigue Crack at the Left Entrance Surface.

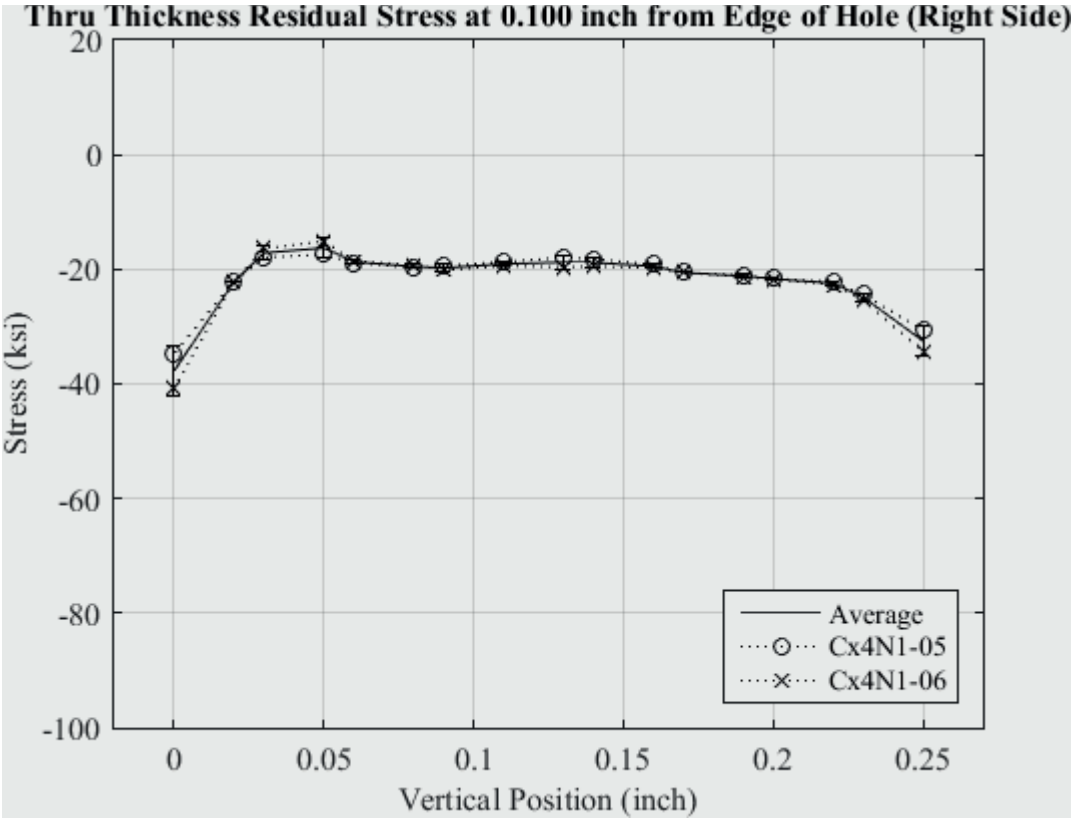

Fig. 322 Residual Stress Line Plot of Cx4N1-05-B and Cx4N1-06-B (2024-T351) Through the Thickness at 0.10 inch from Right Side of Hole – Coupons had a 0.125 inch Fatigue Crack at the Left Entrance Surface.

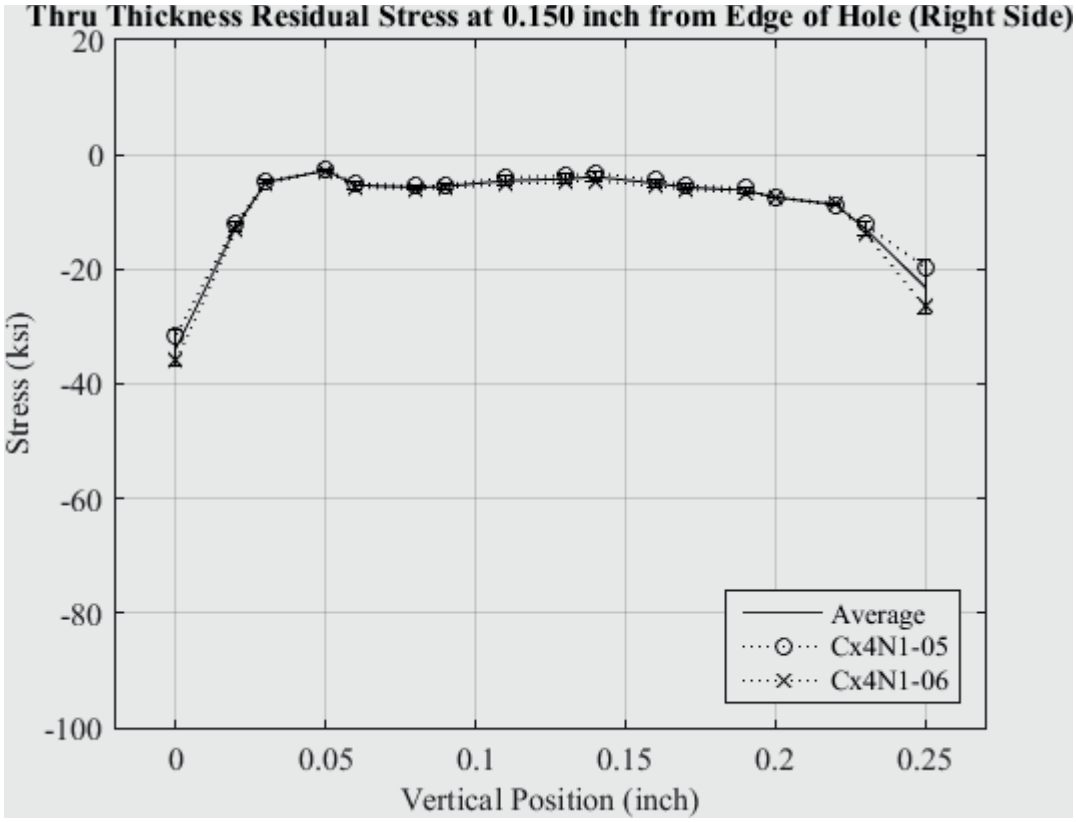

Fig. 323 Residual Stress Line Plot of Cx4N1-05-B and Cx4N1-06-B (2024-T351) Through the Thickness at 0.150 inch from Right Side of Hole – Coupons had a 0.125 inch Fatigue Crack at the Left Entrance Surface.

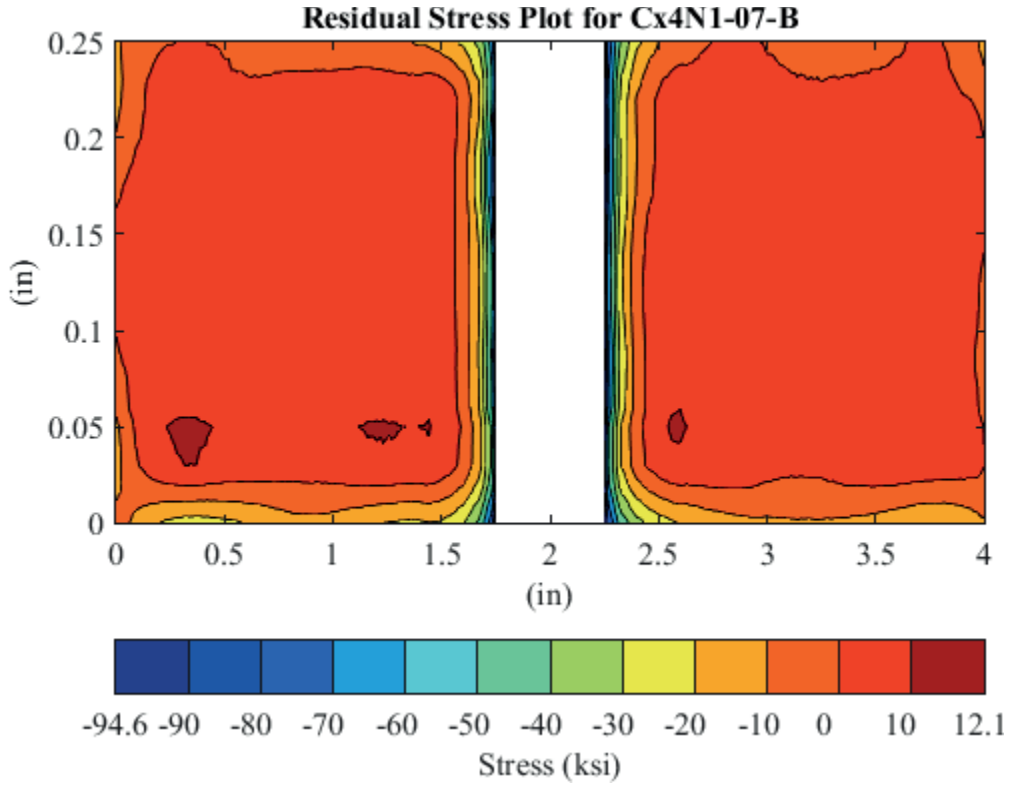

Fig. 324 Residual Stress Contour Plot of Coupon Cx4N1-07-B (2024-T351) – Mandrel Entrance Surface at Y=0, 0.2515 inch Fatigue Crack on Left Side of Hole on the Mandrel Entrance Surface.

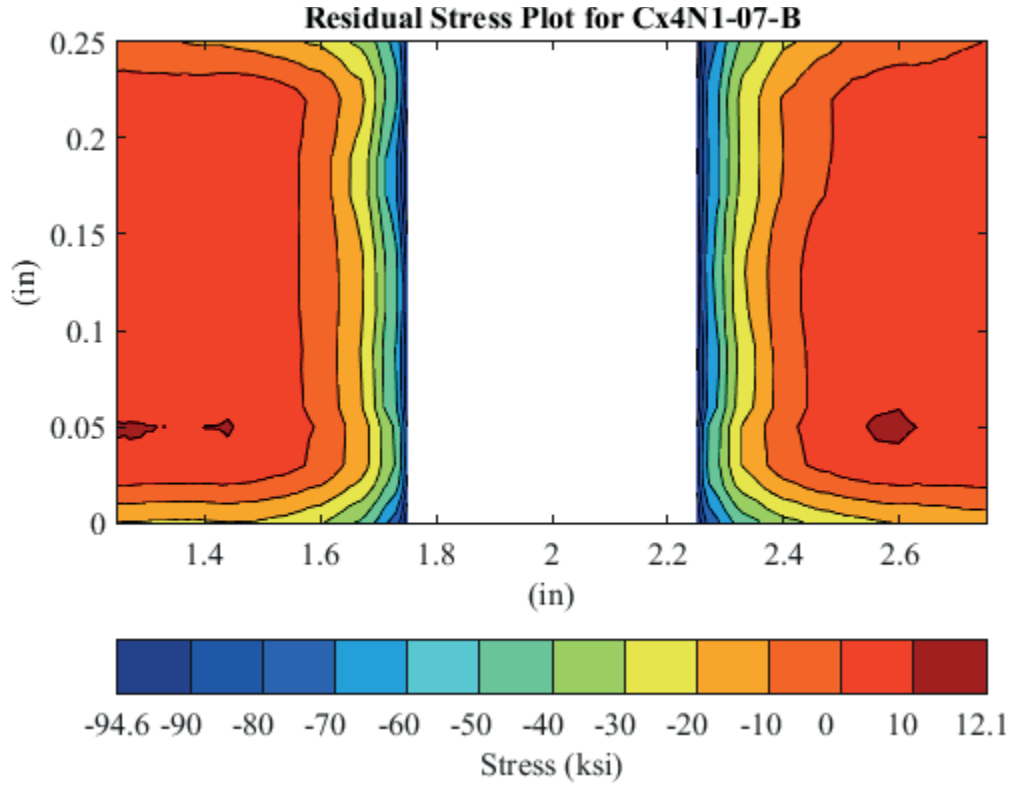

Fig. 325 Residual Stress Contour Plot of Coupon Cx4N1-07-B (2024-T351) – Mandrel Entrance Surface at Y=0, 0.2515 inch Fatigue Crack on Left Side of Hole on the Mandrel Entrance Surface – Zoomed in Next to Hole.

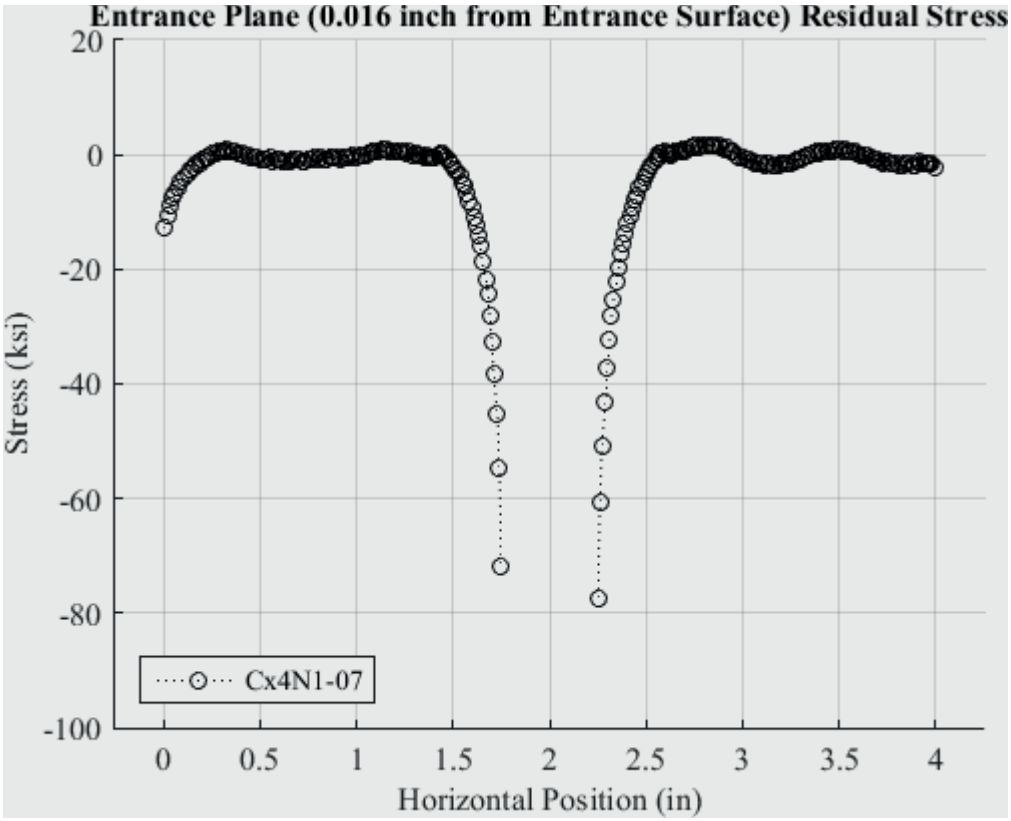

Fig. 326 Residual Stress Line Plot of Cx4N1-07-B (2024-T351) at a Distance of 0.016 inch (Entrance Surface) from the Entrance Surface – Coupons had a 0.2515 inch Fatigue Crack at the Left Entrance Surface.

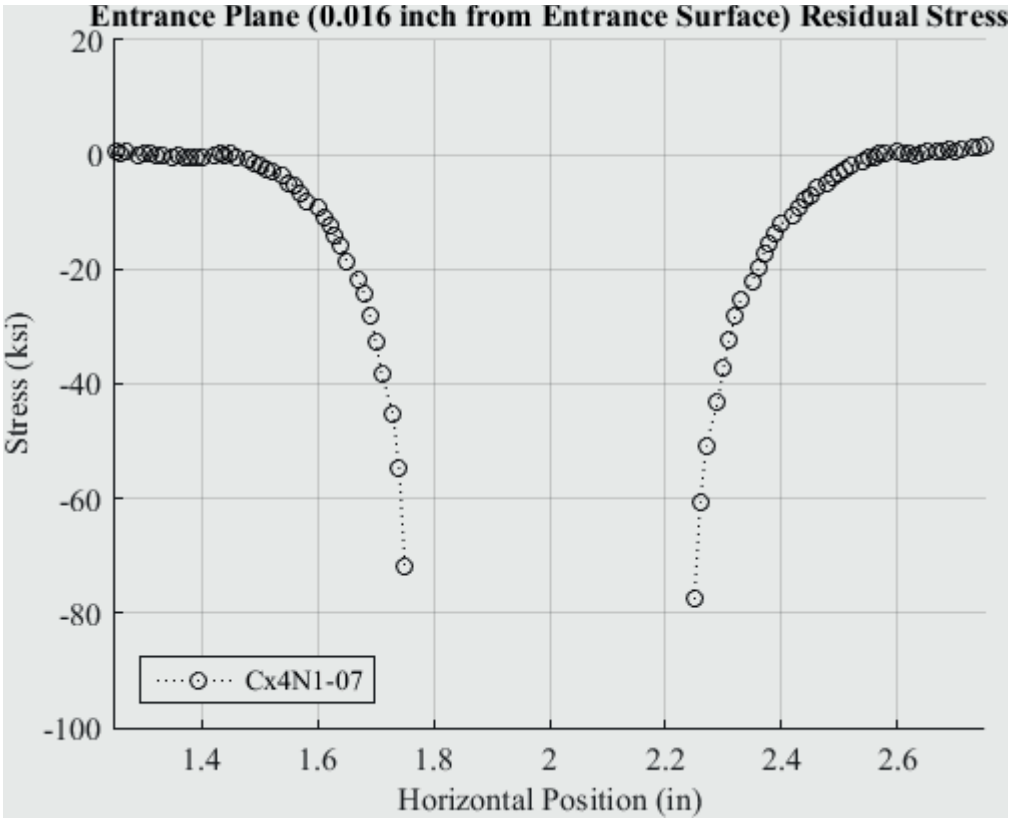

Fig. 327 Residual Stress Line Plot of Cx4N1-07-B (2024-T351) at a Distance of 0.016 inch (Entrance Surface) from the Entrance Surface – Coupons had a 0.2515 inch Fatigue Crack at the Left Entrance Surface – Zoomed in Next to Hole.

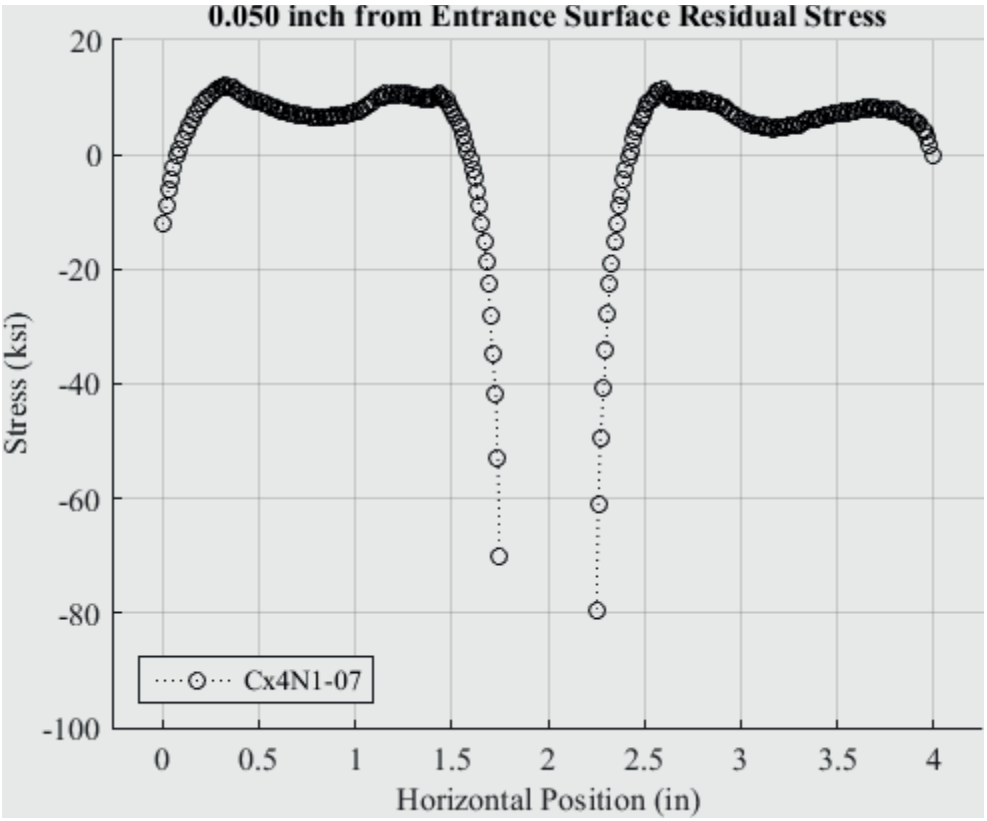

Fig. 328 Residual Stress Line Plot of Cx4N1-07-B (2024-T351) at a Distance of 0.05 inch from the Entrance Surface – Coupons had a 0.2515 inch Fatigue Crack at the Left Entrance Surface.

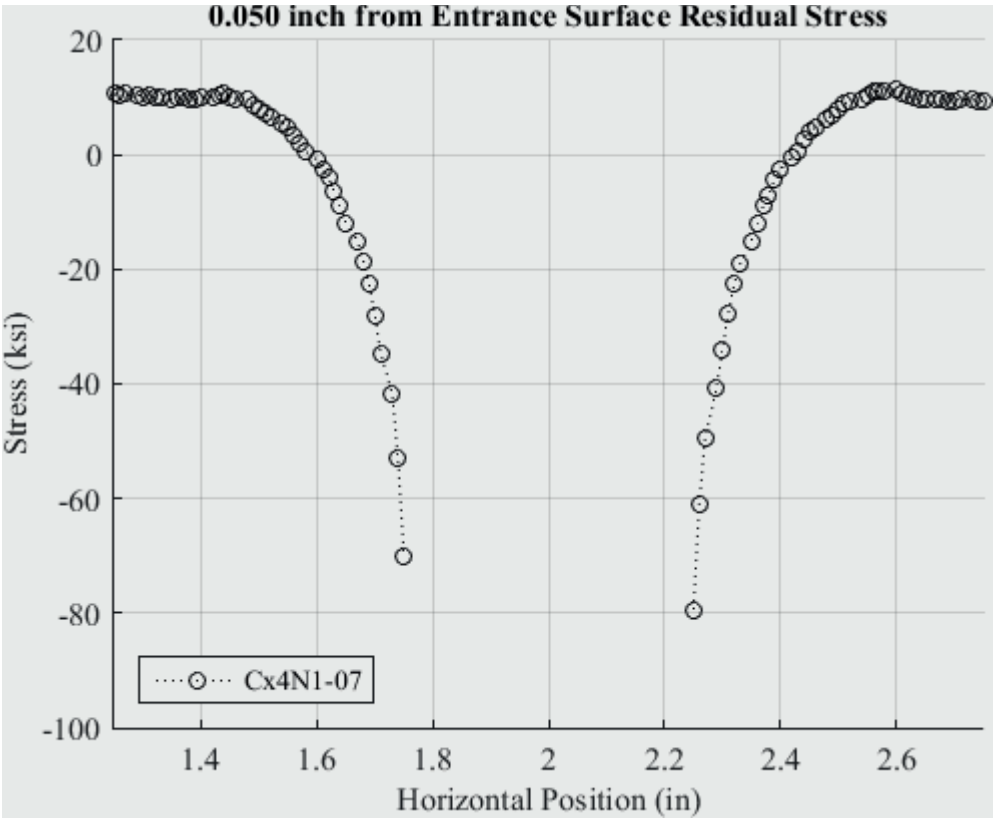

Fig. 329 Residual Stress Line Plot of Cx4N1-07-B (2024-T351) at a Distance of 0.05 inch from the Entrance Surface – Coupons had a 0.2515 inch Fatigue Crack at the Left Entrance Surface – Zoomed in Next to Hole.

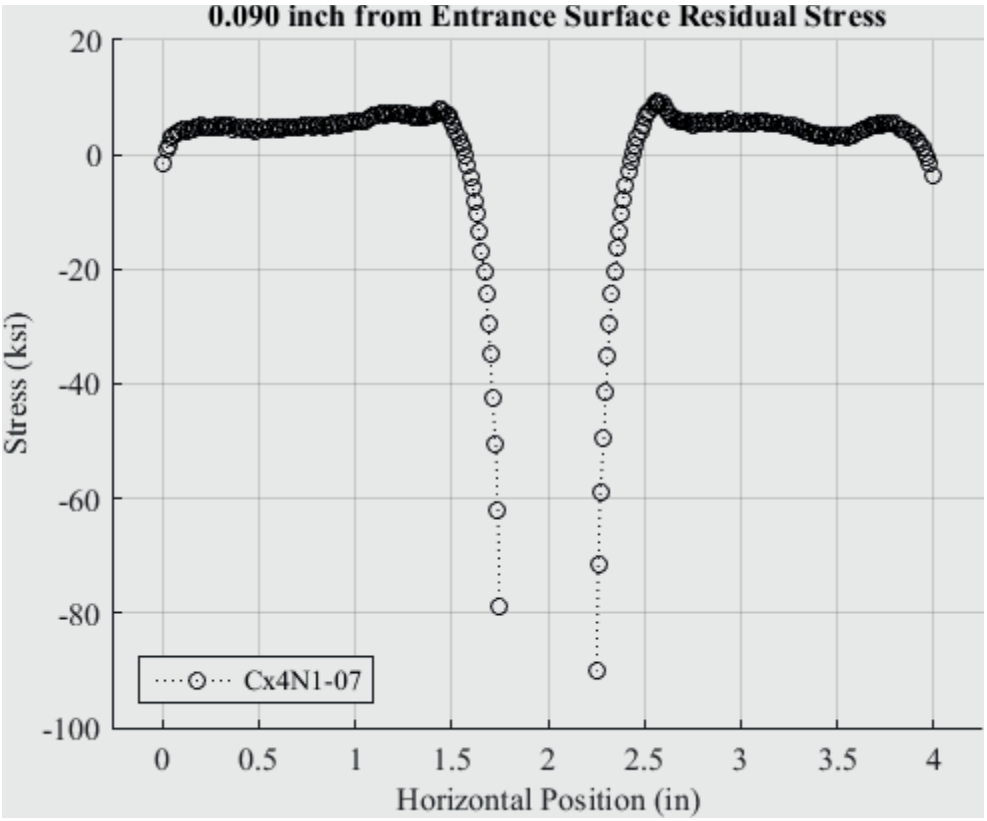

Fig. 330 Residual Stress Line Plot of Cx4N1-07-B (2024-T351) at a Distance of 0.05 inch from the Entrance Surface – Coupons had a 0.2515 inch Fatigue Crack at the Left Entrance Surface.

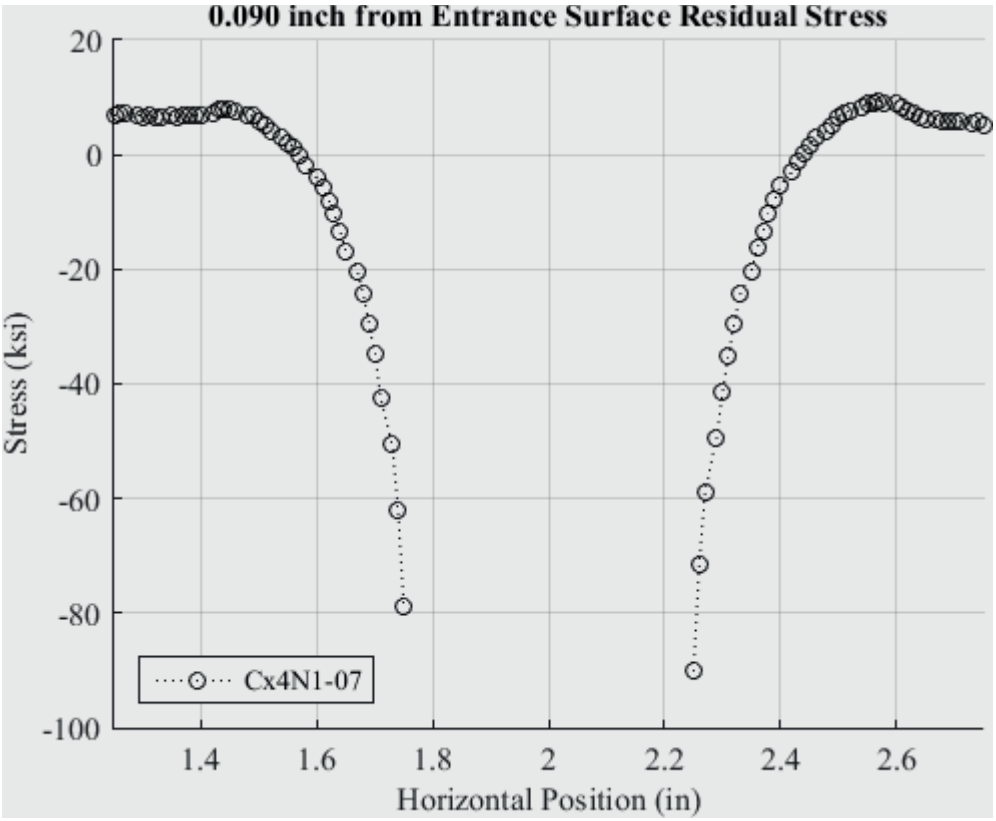

Fig. 331 Residual Stress Line Plot of Cx4N1-07-B (2024-T351) at a Distance of 0.09 inch from the Entrance Surface – Coupons had a 0.2515 inch Fatigue Crack at the Left Entrance Surface – Zoomed in Next to Hole.

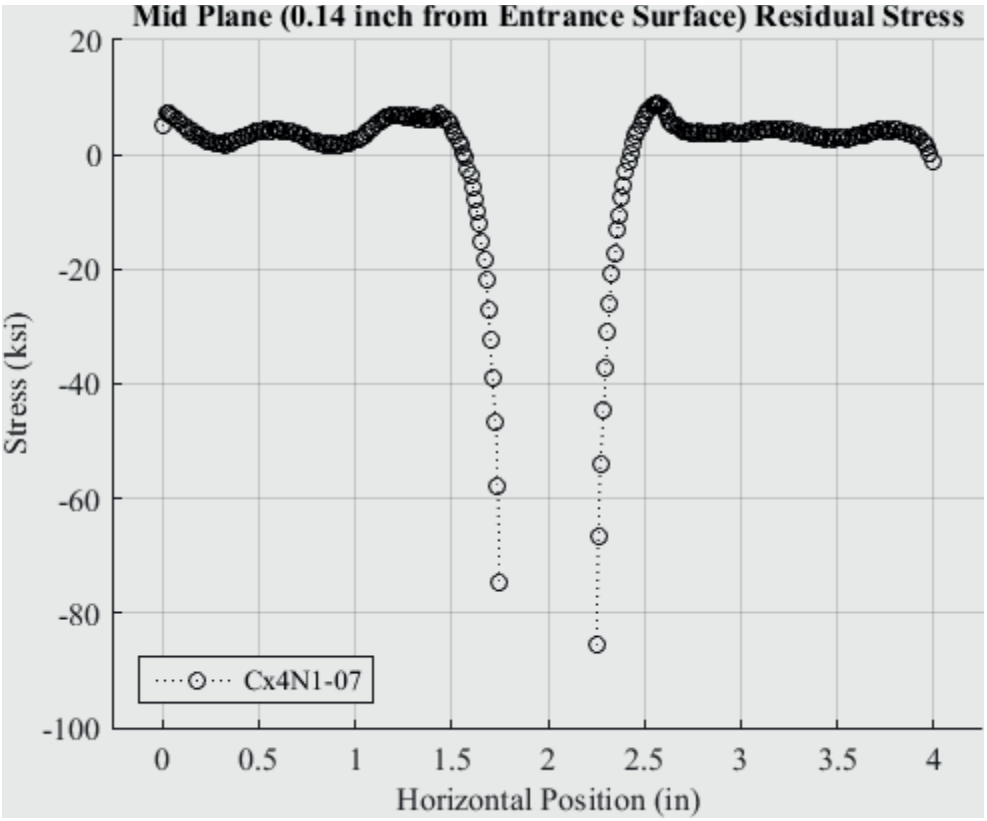

Fig. 332 Residual Stress Line Plot of Cx4N1-07-B (2024-T351) at a Distance of 0.140 inch (Mid Plane Surface) from the Entrance Surface – Coupons had a 0.2515 inch Fatigue Crack at the Left Entrance Surface.

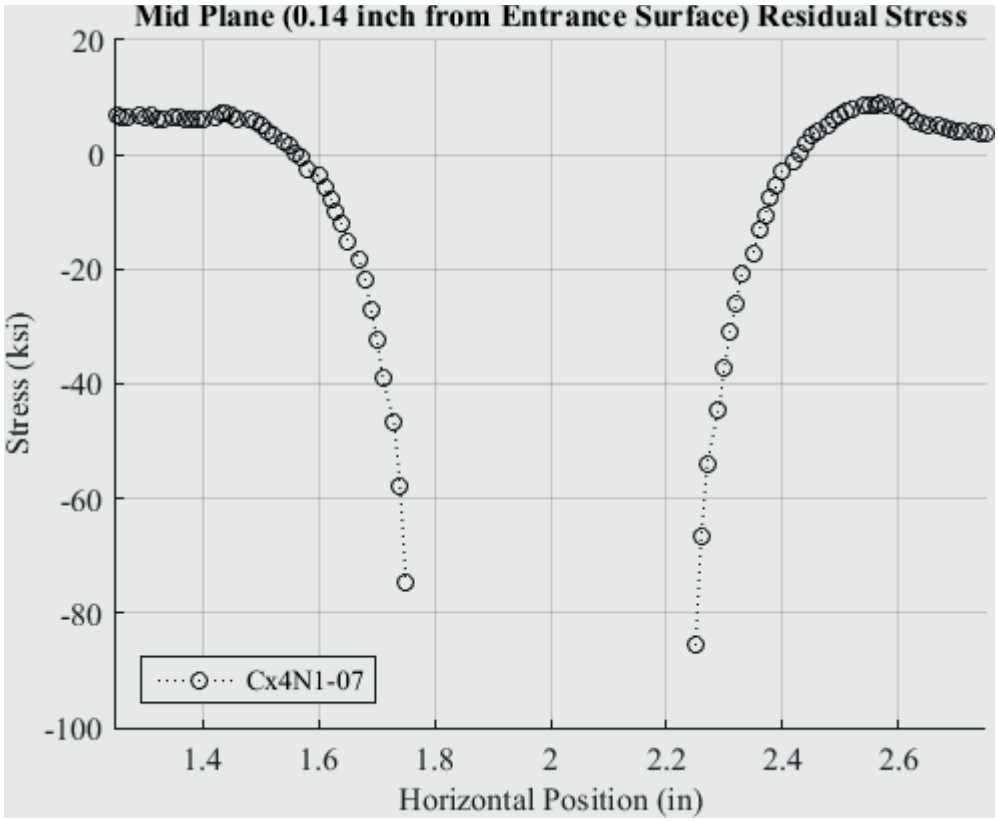

Fig. 333 Residual Stress Line Plot of Cx4N1-07-B (2024-T351) at a Distance of 0.140 inch (Mid Plane Surface) from the Entrance Surface – Coupons had a 0.2515 inch Fatigue Crack at the Left Entrance Surface – Zoomed in Next to Hole.

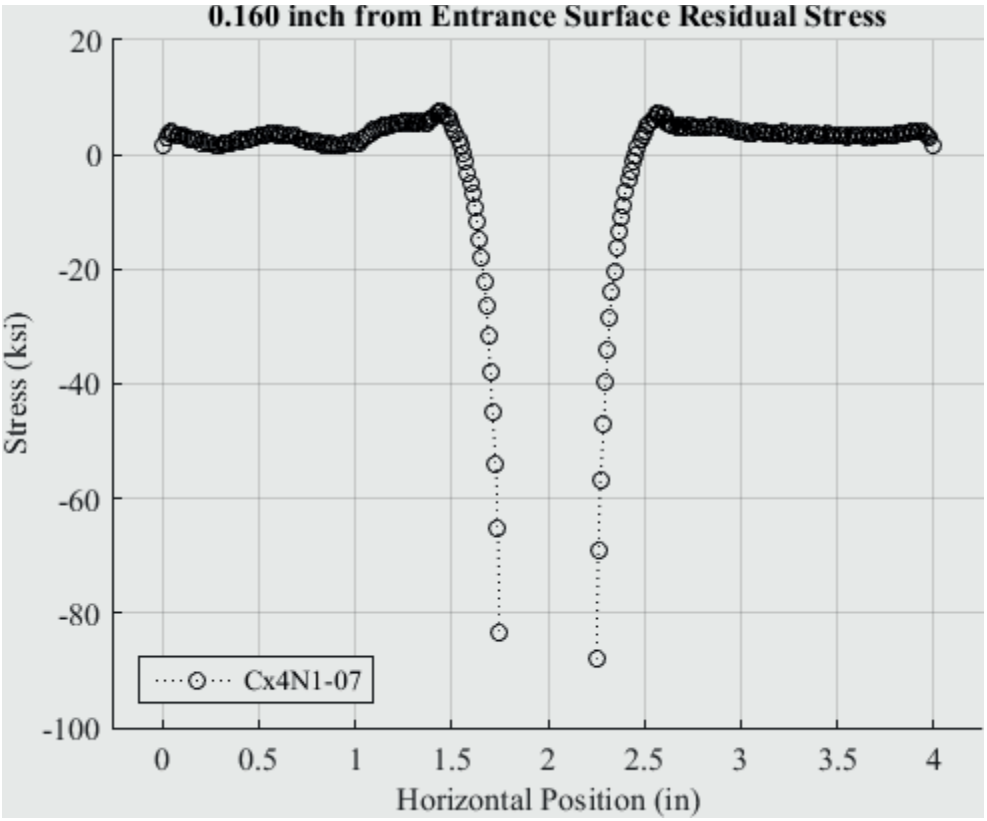

Fig. 334 Residual Stress Line Plot of Cx4N1-07-B (2024-T351) at a Distance of 0.160 inch from the Entrance Surface – Coupons had a 0.2515 inch Fatigue Crack at the Left Entrance Surface.

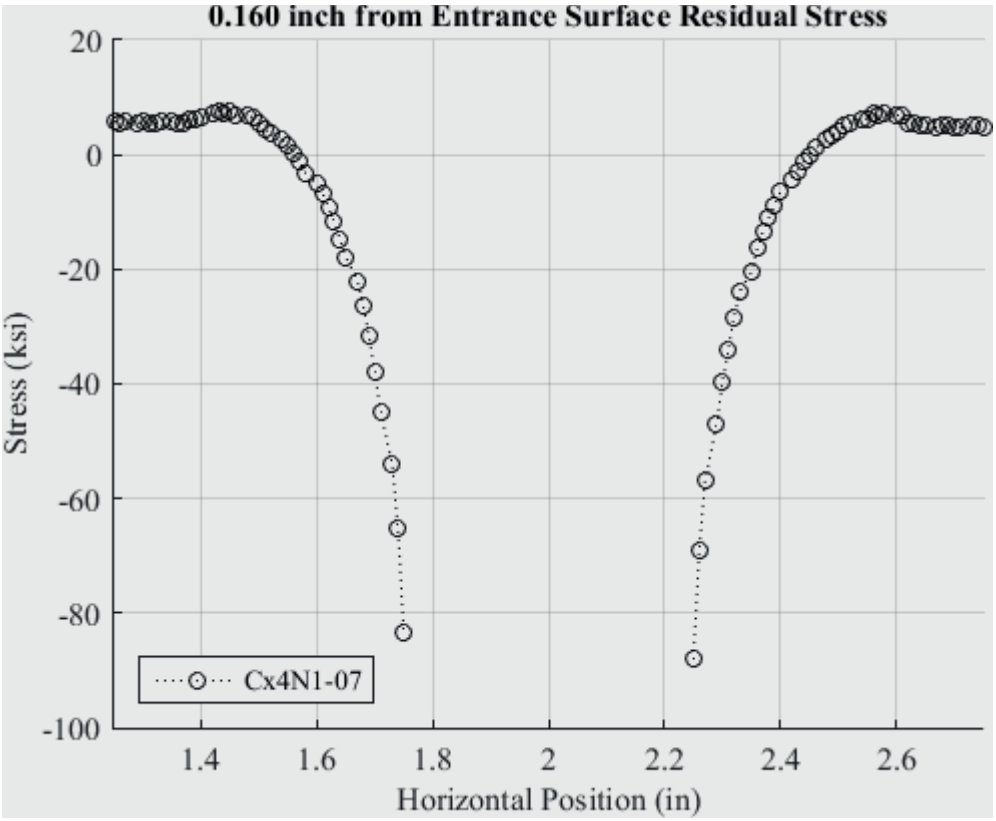

Fig. 335 Residual Stress Line Plot of Cx4N1-07-B (2024-T351) at a Distance of 0.160 inch from the Entrance Surface – Coupons had a 0.2515 inch Fatigue Crack at the Left Entrance Surface – Zoomed in Next to Hole.

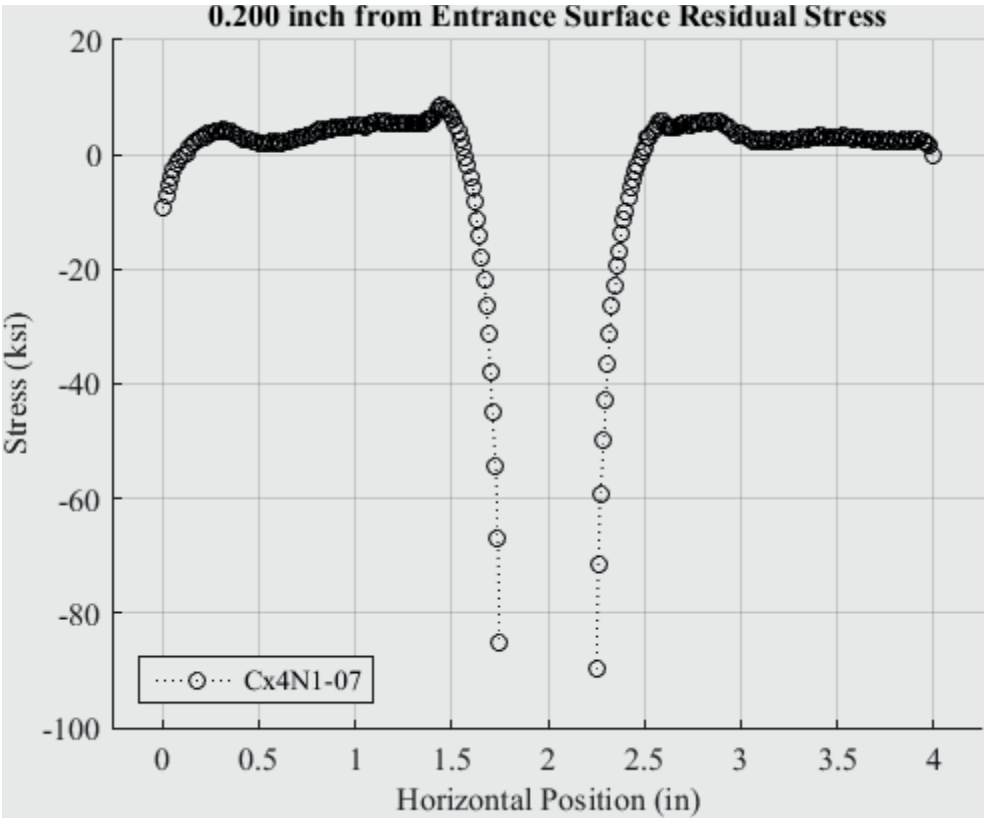

Fig. 336 Residual Stress Line Plot of Cx4N1-07-B (2024-T351) at a Distance of 0.200 inch from the Entrance Surface – Coupons had a 0.2515 inch Fatigue Crack at the Left Entrance Surface.

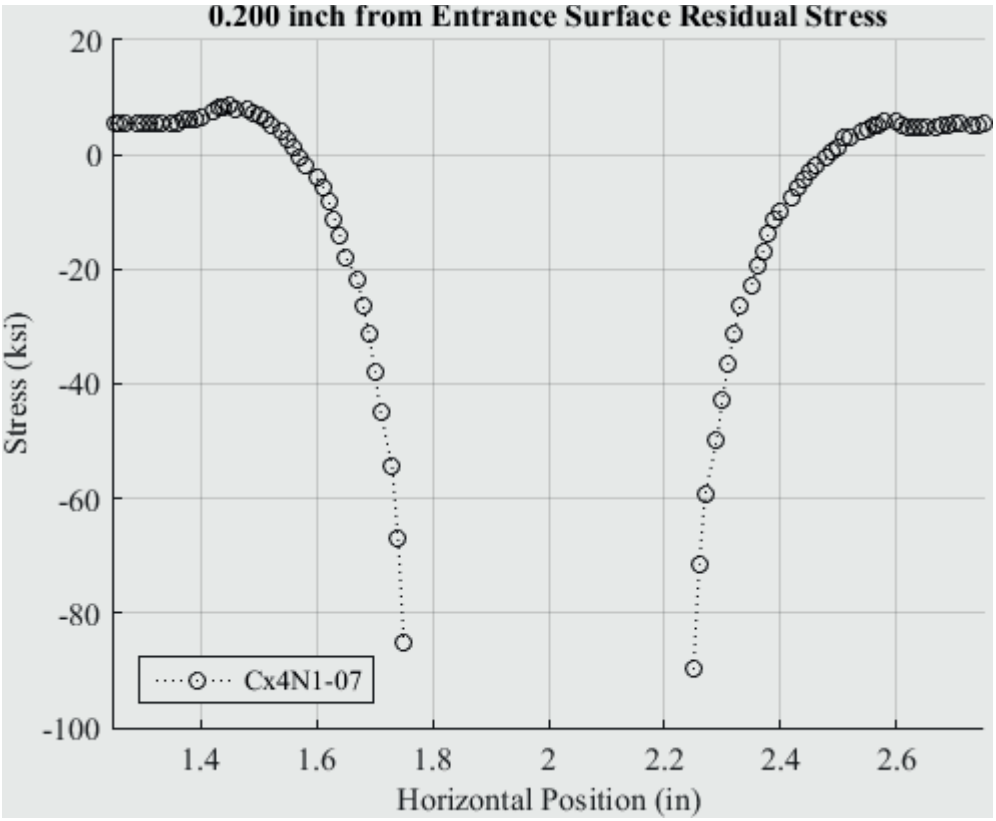

Fig. 337 Residual Stress Line Plot of Cx4N1-07-B (2024-T351) at a Distance of 0.200 inch from the Entrance Surface – Coupons had a 0.2515 inch Fatigue Crack at the Left Entrance Surface – Zoomed in Next to Hole.

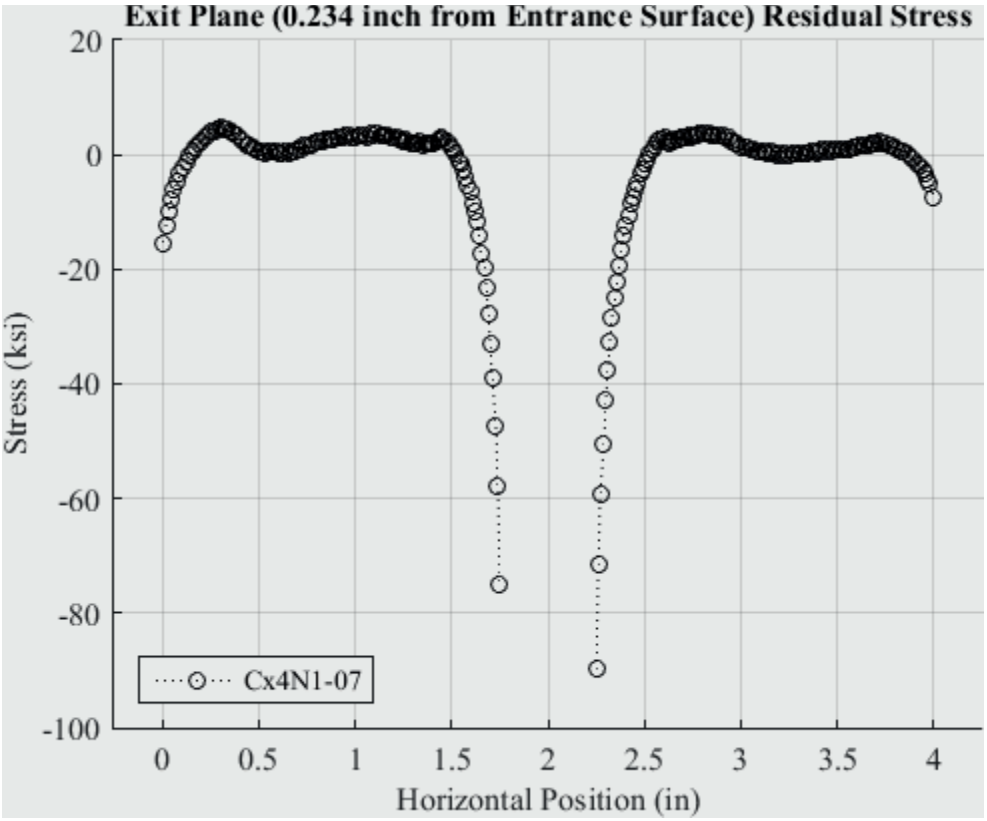

Fig. 338 Residual Stress Line Plot of Cx4N1-07-B (2024-T351) at a Distance of 0.234 inch (Exit Surface) from the Entrance Surface – Coupons had a 0.2515 inch Fatigue Crack at the Left Entrance Surface.

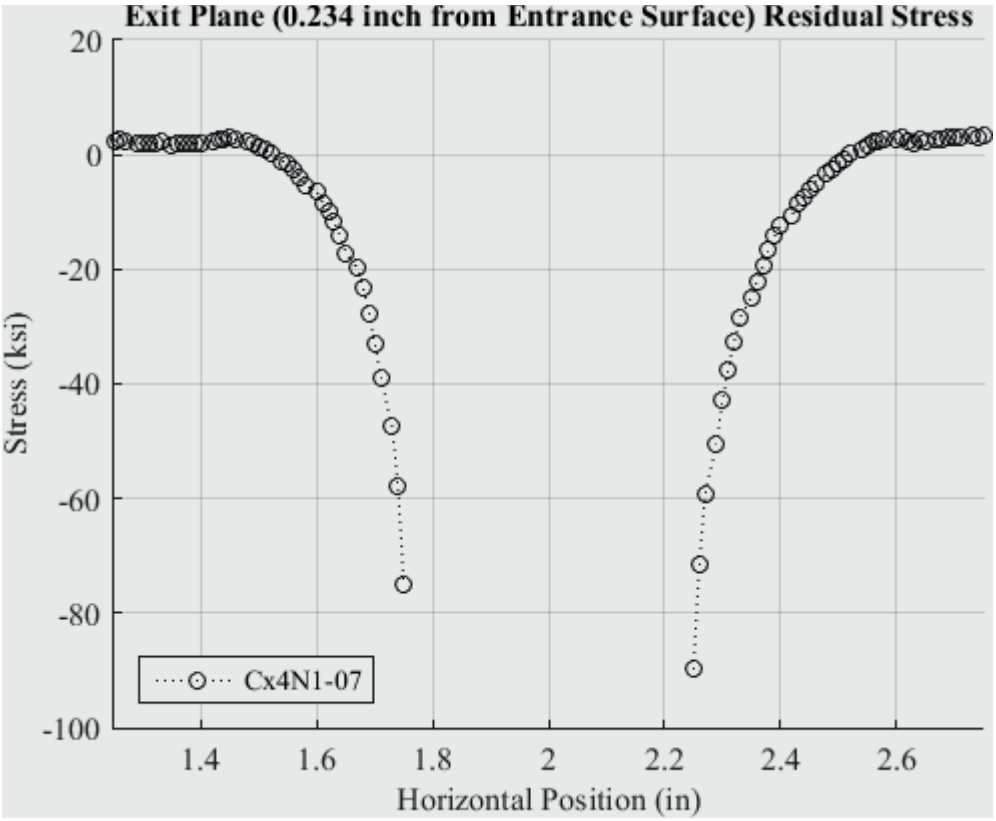

Fig. 339 Residual Stress Line Plot of Cx4N1-07-B (2024-T351) at a Distance of 0.234 inch (Exit Surface) from the Entrance Surface – Coupons had a 0.2515 inch Fatigue Crack at the Left Entrance Surface – Zoomed in Next to Hole.

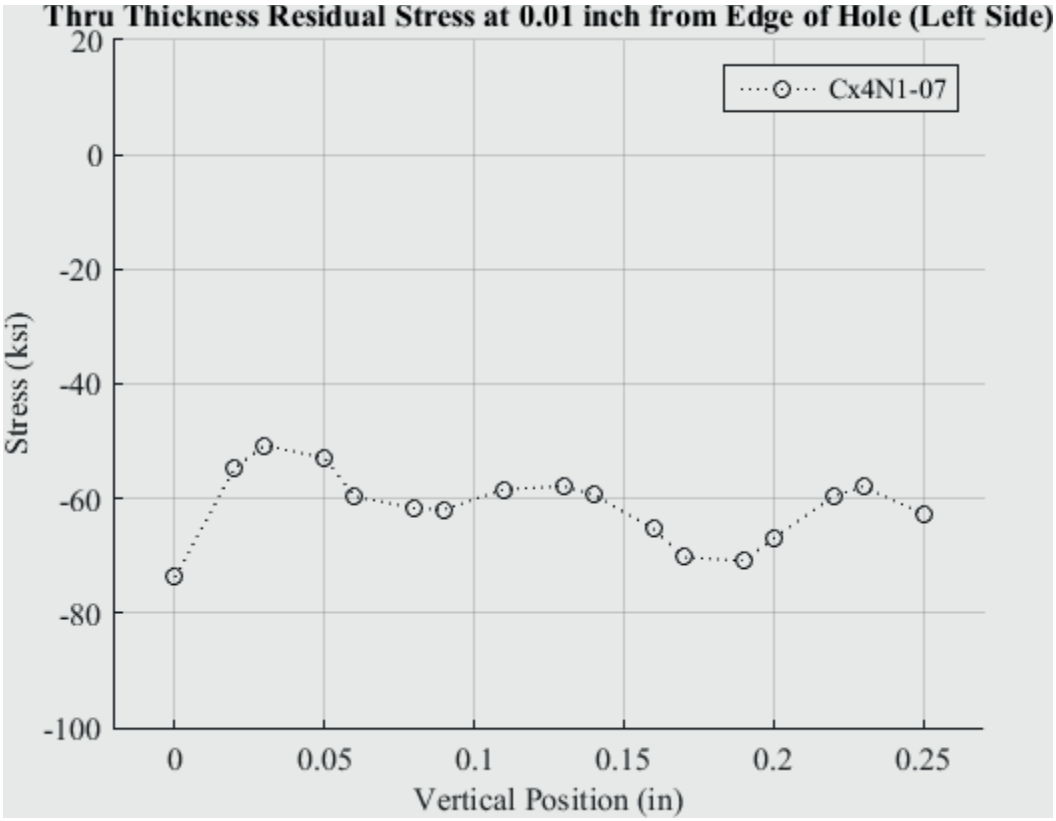

Fig. 340 Residual Stress Line Plot of Cx4N1-07-B (2024-T351) Through the Thickness at 0.01 inch from Left Side of Hole – Coupons had a 0.2515 inch Fatigue Crack at the Left Entrance Surface.

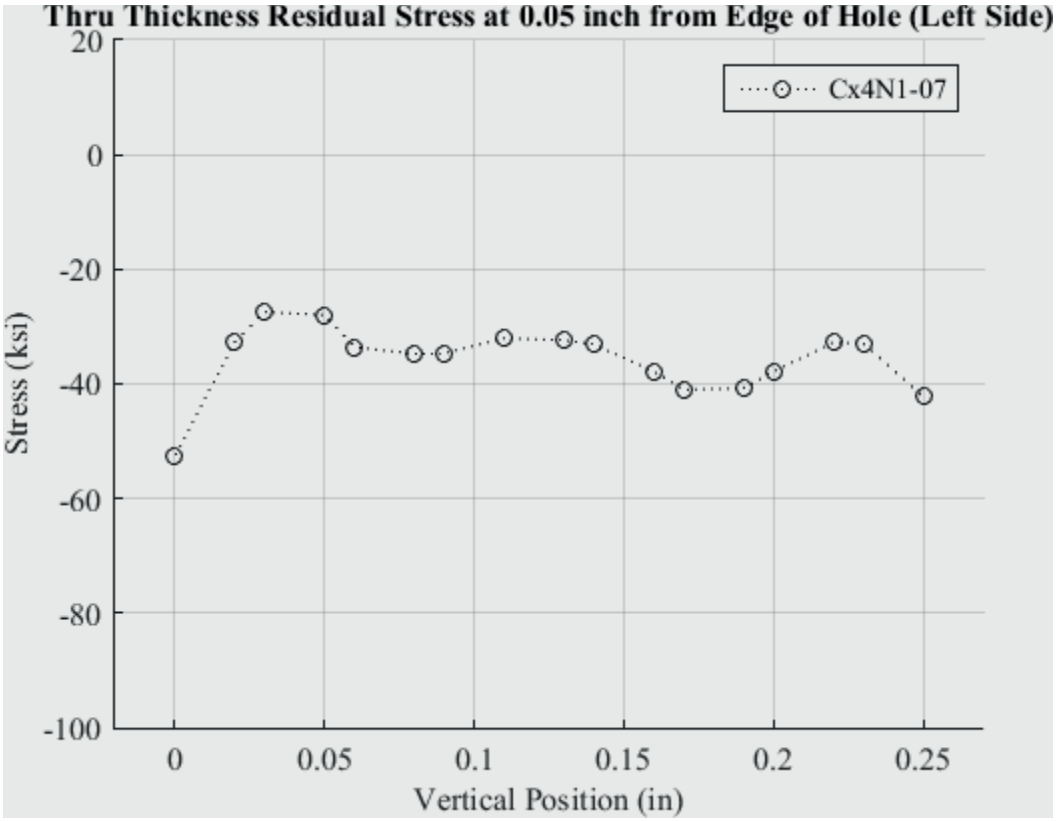

Fig. 341 Residual Stress Line Plot of Cx4N1-07-B (2024-T351) Through the Thickness at 0.05 inch from Left Side of Hole – Coupons had a 0.2515 inch Fatigue Crack at the Left Entrance Surface.

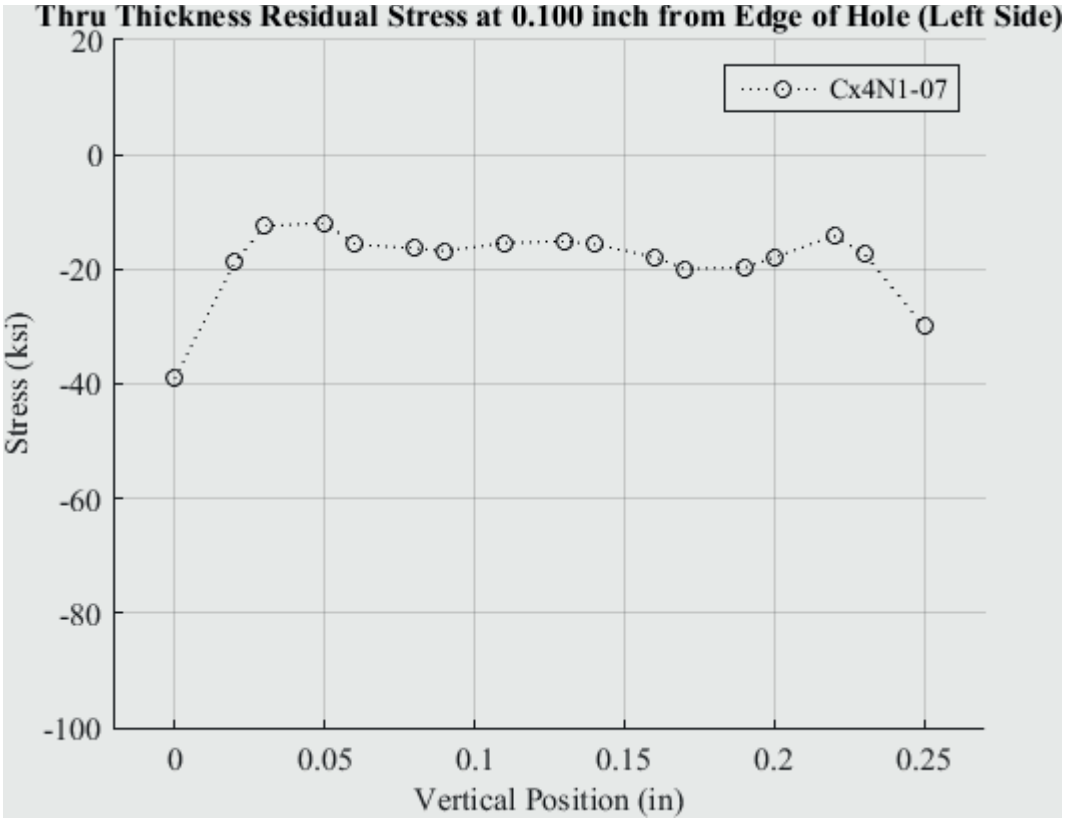

Fig. 342 Residual Stress Line Plot of Cx4N1-07-B (2024-T351) Through the Thickness at 0.10 inch from Left Side of Hole – Coupons had a 0.2515 inch Fatigue Crack at the Left Entrance Surface.

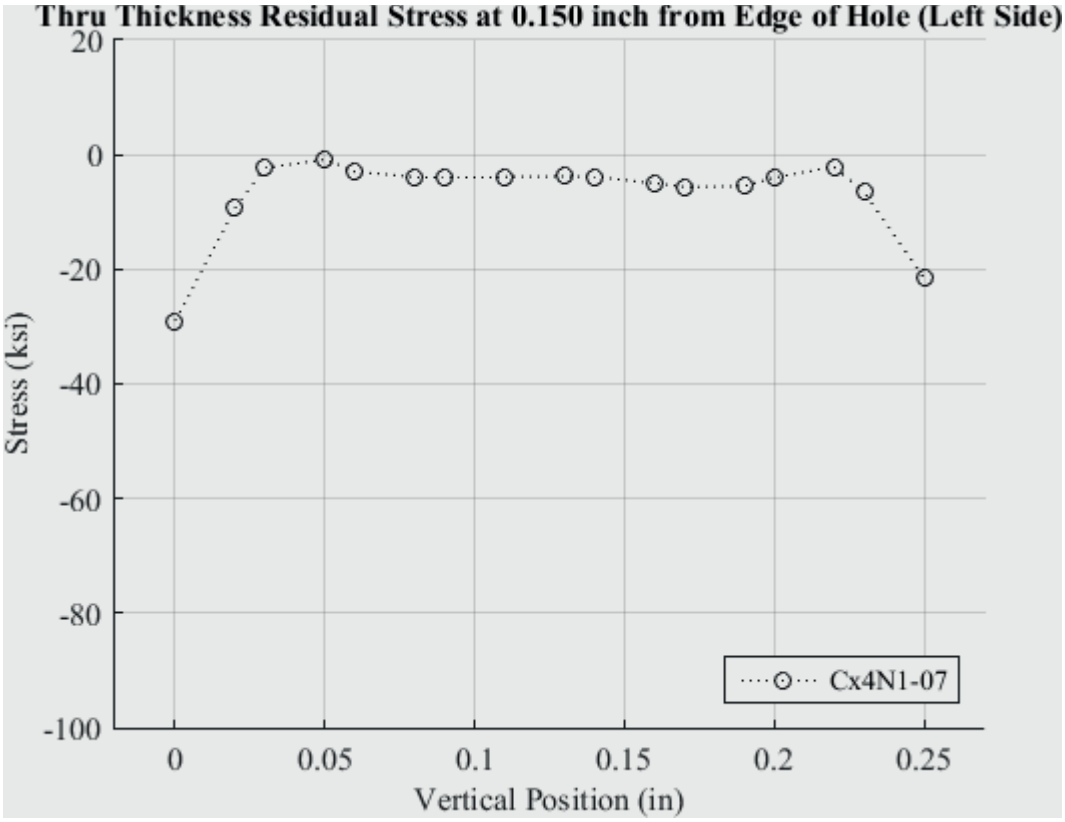

Fig. 343 Residual Stress Line Plot of Cx4N1-07-B (2024-T351) Through the Thickness at 0.150 inch from Left Side of Hole – Coupons had a 0.2515 inch Fatigue Crack at the Left Entrance Surface.

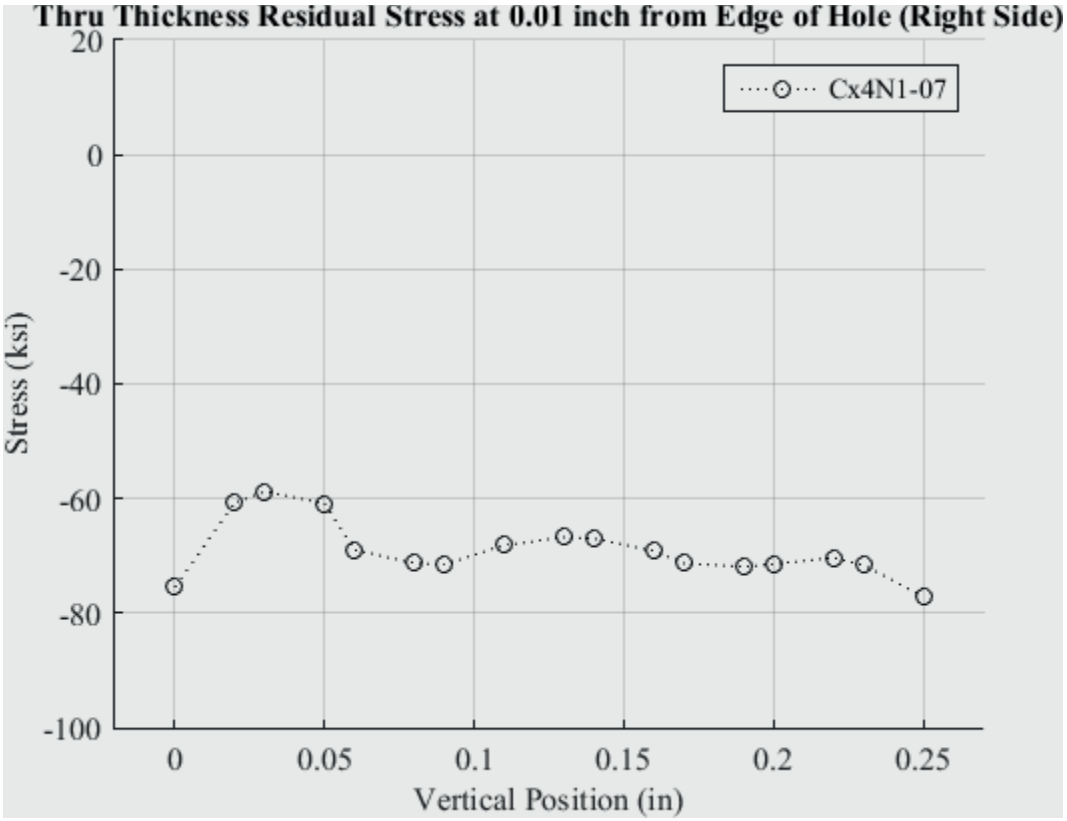

Fig. 344 Residual Stress Line Plot of Cx4N1-07-B (2024-T351) Through the Thickness at 0.01 inch from Right Side of Hole – Coupons had a 0.2515 inch Fatigue Crack at the Left Entrance Surface.

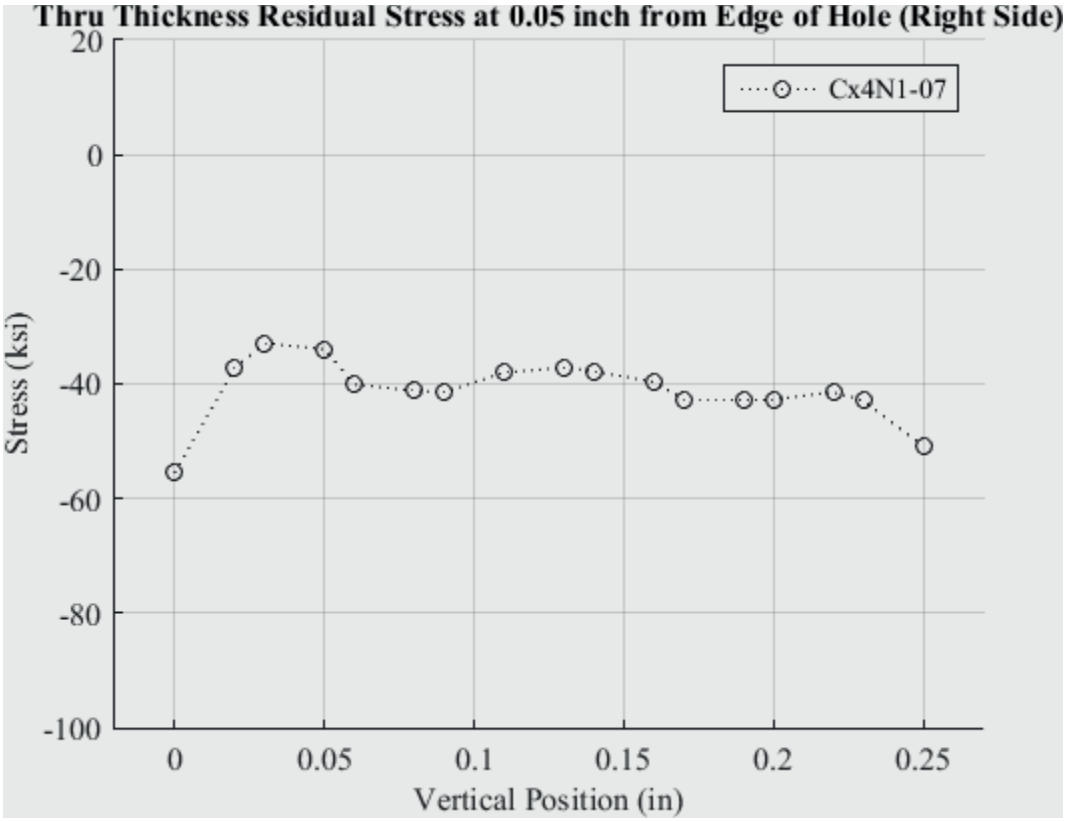

Fig. 345 Residual Stress Line Plot of Cx4N1-07-B (2024-T351) Through the Thickness at 0.05 inch from Right Side of Hole – Coupons had a 0.2515 inch Fatigue Crack at the Left Entrance Surface.

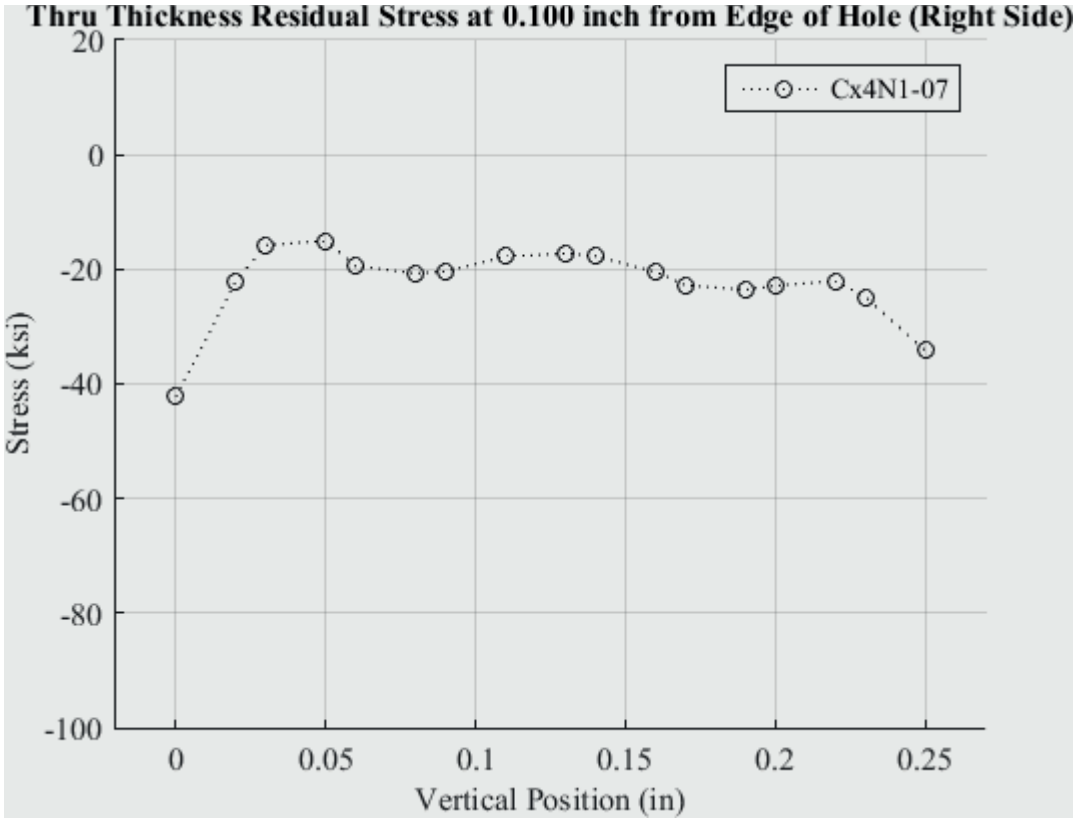

Fig. 346 Residual Stress Line Plot of Cx4N1-07-B (2024-T351) Through the Thickness at 0.10 inch from Right Side of Hole – Coupons had a 0.2515 inch Fatigue Crack at the Left Entrance Surface.

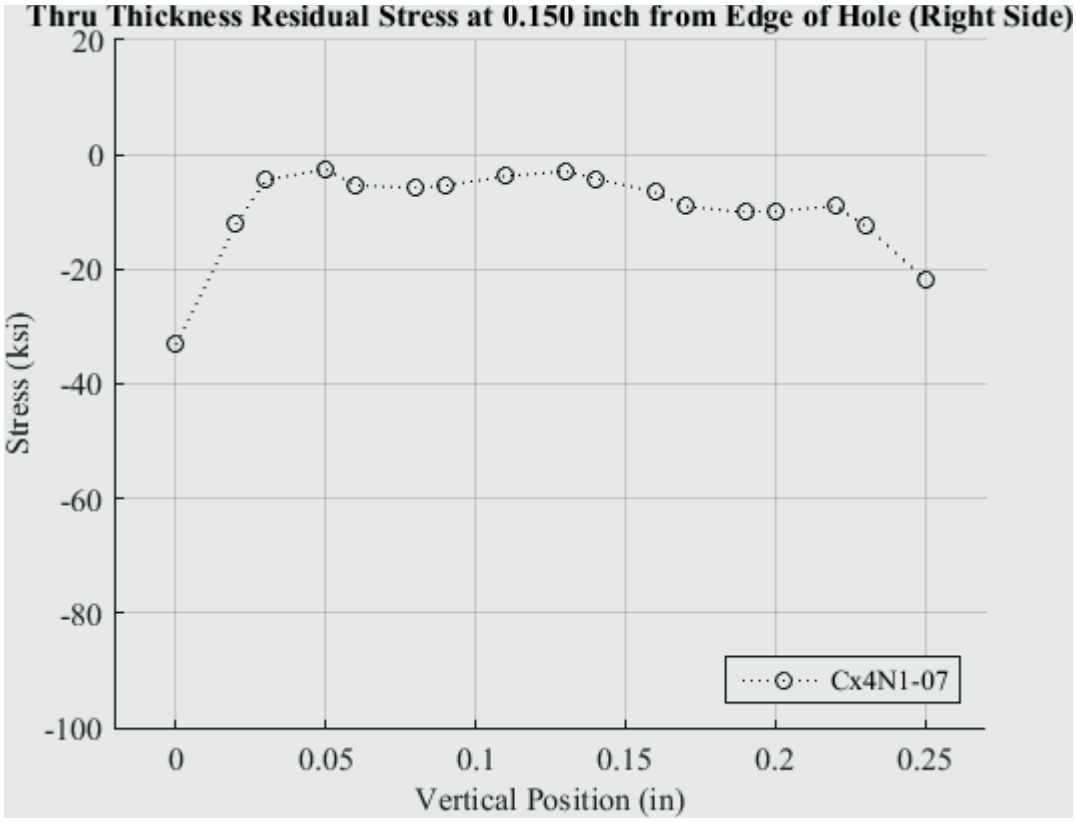

Fig. 347 Residual Stress Line Plot of Cx4N1-07-B (2024-T351) Through the Thickness at 0.150 inch from Right Side of Hole – Coupons had a 0.2515 inch Fatigue Crack at the Left Entrance Surface.

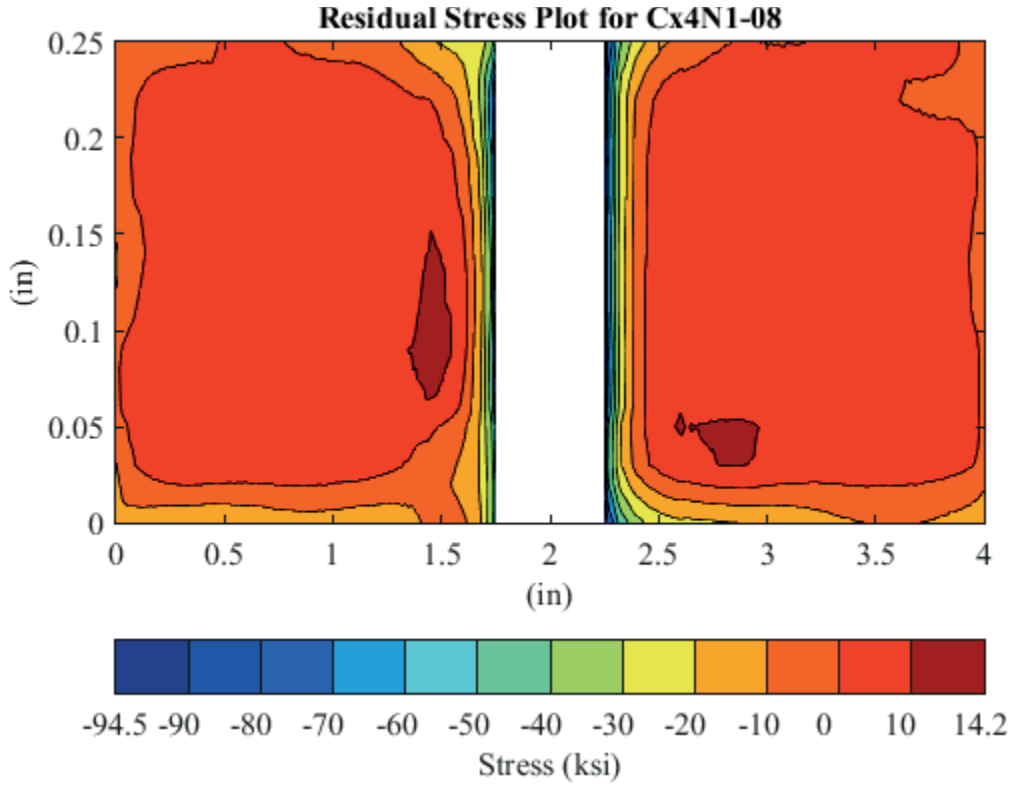

Fig. 348 Residual Stress Contour Plot of Coupon Cx4N1-08-B (2024-T351) – Mandrel Entrance Surface at Y=0, 0.4974 inch Fatigue Crack on Left Side of Hole on Mandrel Entrance Surface.

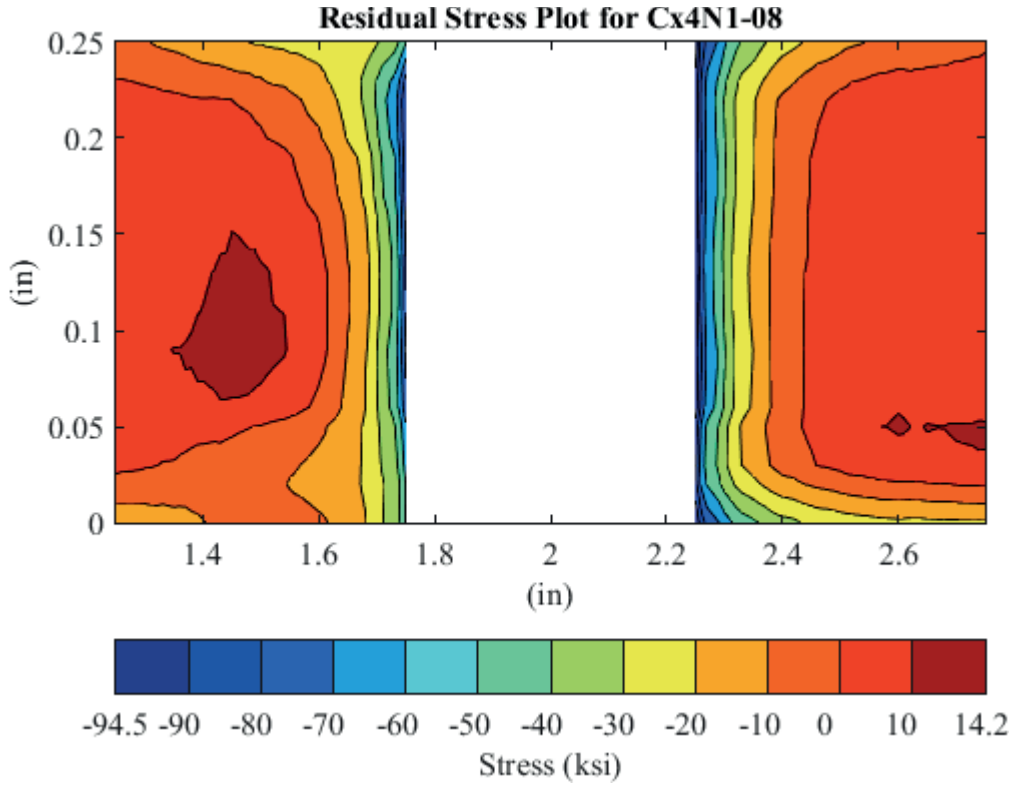

Fig. 349 Residual Stress Contour Plot of Coupon Cx4N1-08-B (2024-T351) – Mandrel Entrance Surface at Y=0, 0.4974 inch Fatigue Crack on Left Side of Hole on Mandrel Entrance Surface – Zoomed in Next to Hole.

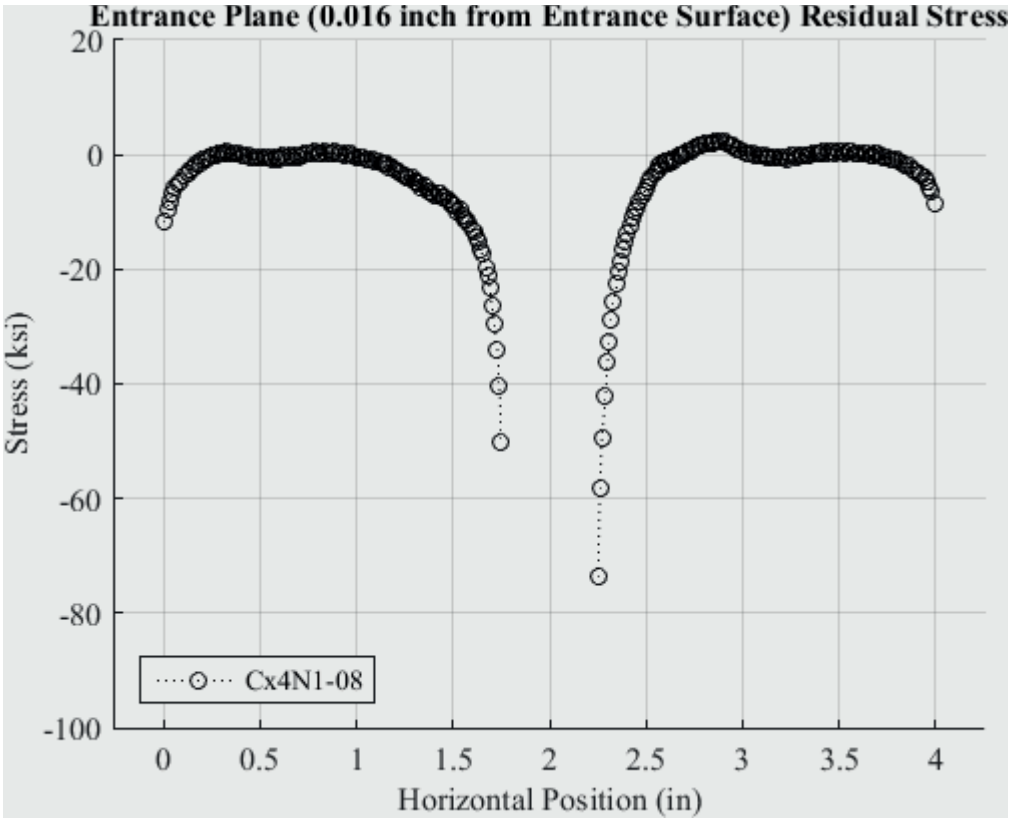

Fig. 350 Residual Stress Line Plot of Cx4N1-08-B (2024-T351) at a Distance of 0.016 inch (Entrance Surface) from the Entrance Surface – Coupons had a 0.4974 inch Fatigue Crack at the Left Entrance Surface.

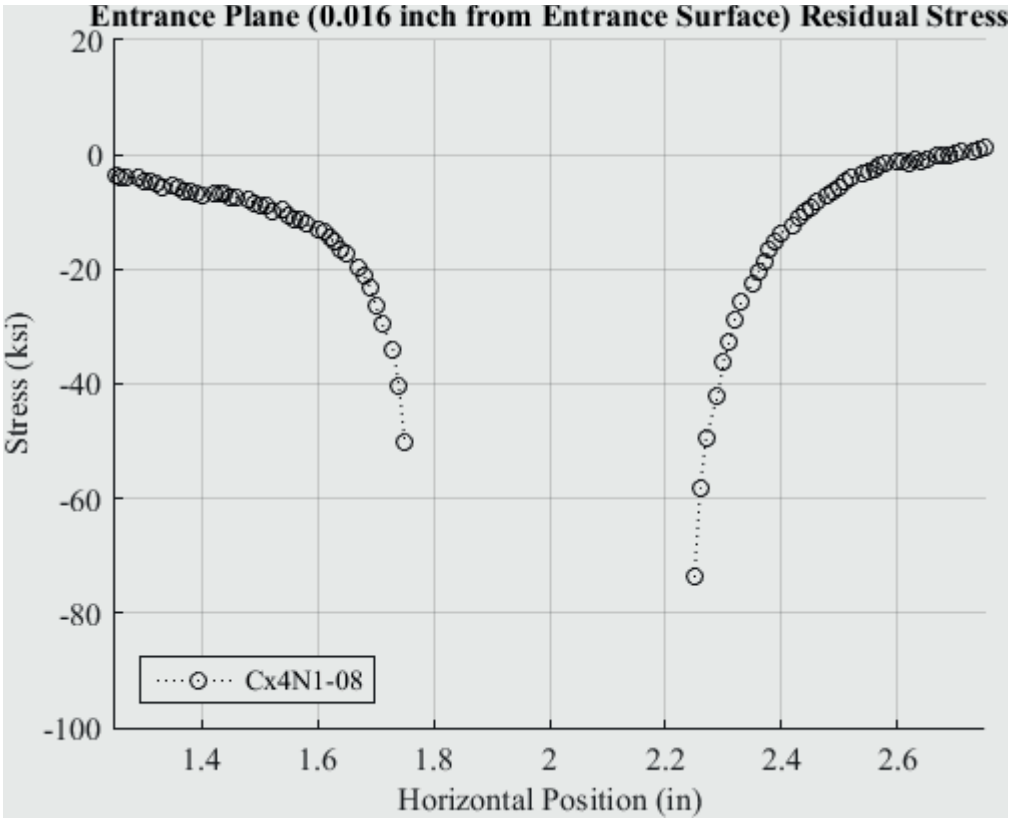

Fig. 351 Residual Stress Line Plot of Cx4N1-08-B (2024-T351) at a Distance of 0.016 inch (Entrance Surface) from the Entrance Surface – Coupons had a 0.4974 inch Fatigue Crack at the Left Entrance Surface – Zoomed in Next to Hole.

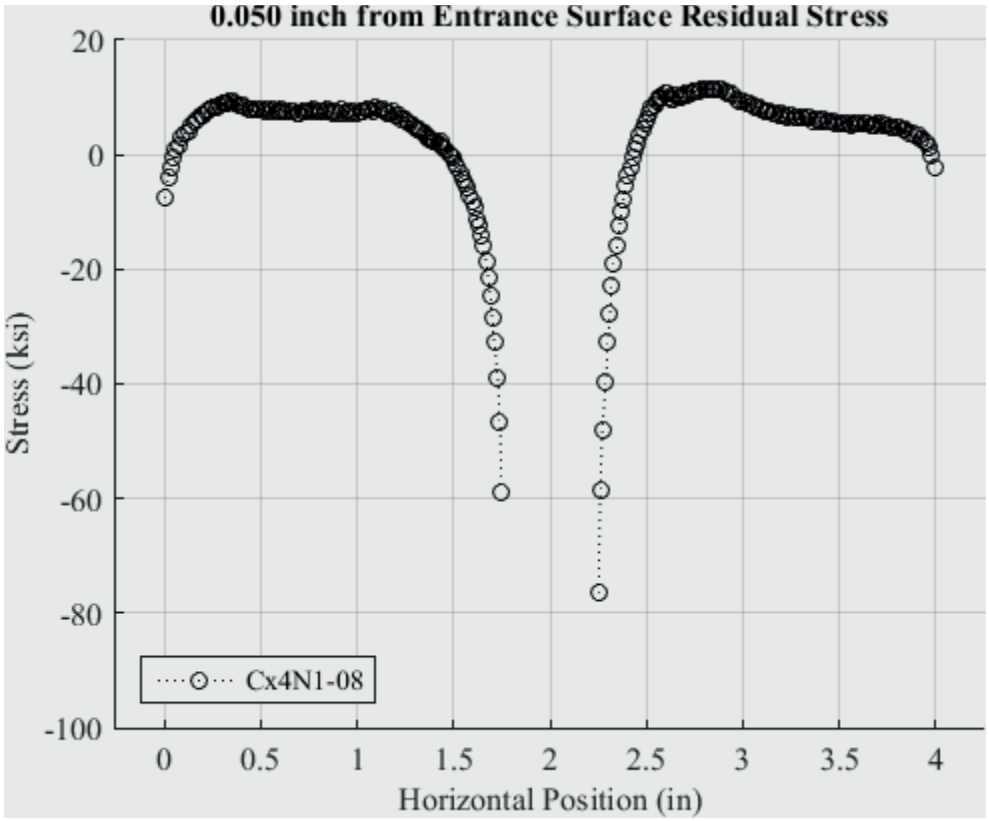

Fig. 352 Residual Stress Line Plot of Cx4N1-08-B (2024-T351) at a Distance of 0.05 inch from the Entrance Surface – Coupons had a 0.4974 inch Fatigue Crack at the Left Entrance Surface.

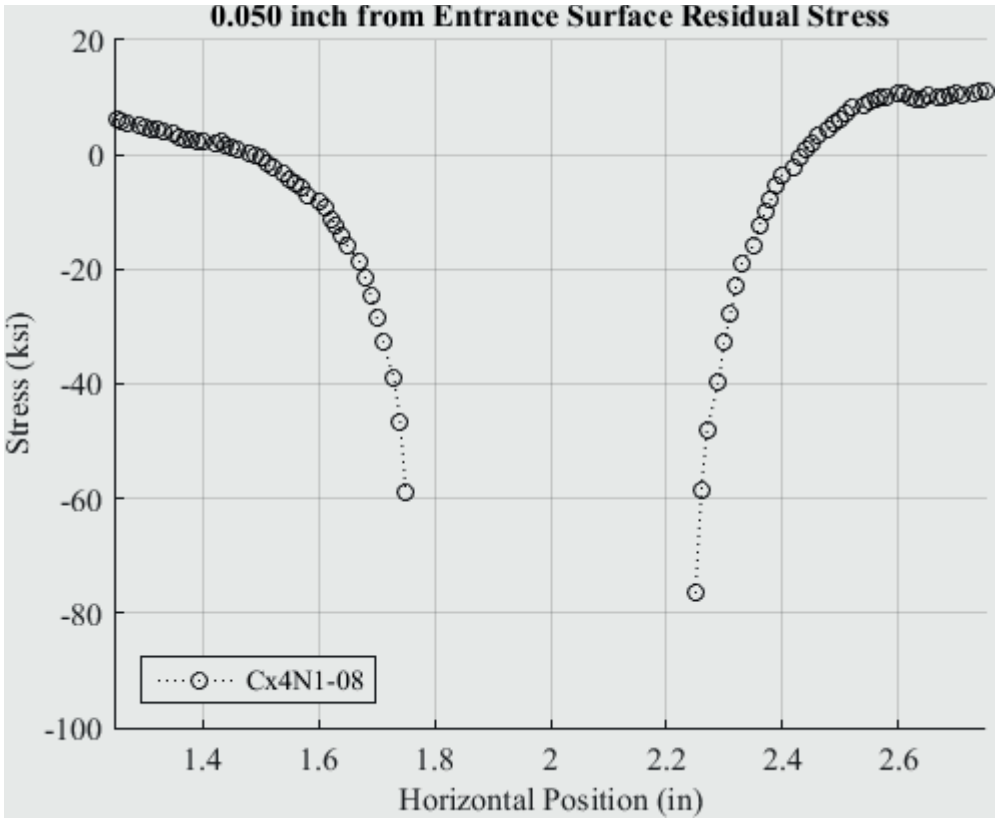

Fig. 353 Residual Stress Line Plot of Cx4N1-08-B (2024-T351) at a Distance of 0.05 inch from the Entrance Surface – Coupons had a 0.4974 inch Fatigue Crack at the Left Entrance Surface – Zoomed in Next to Hole.

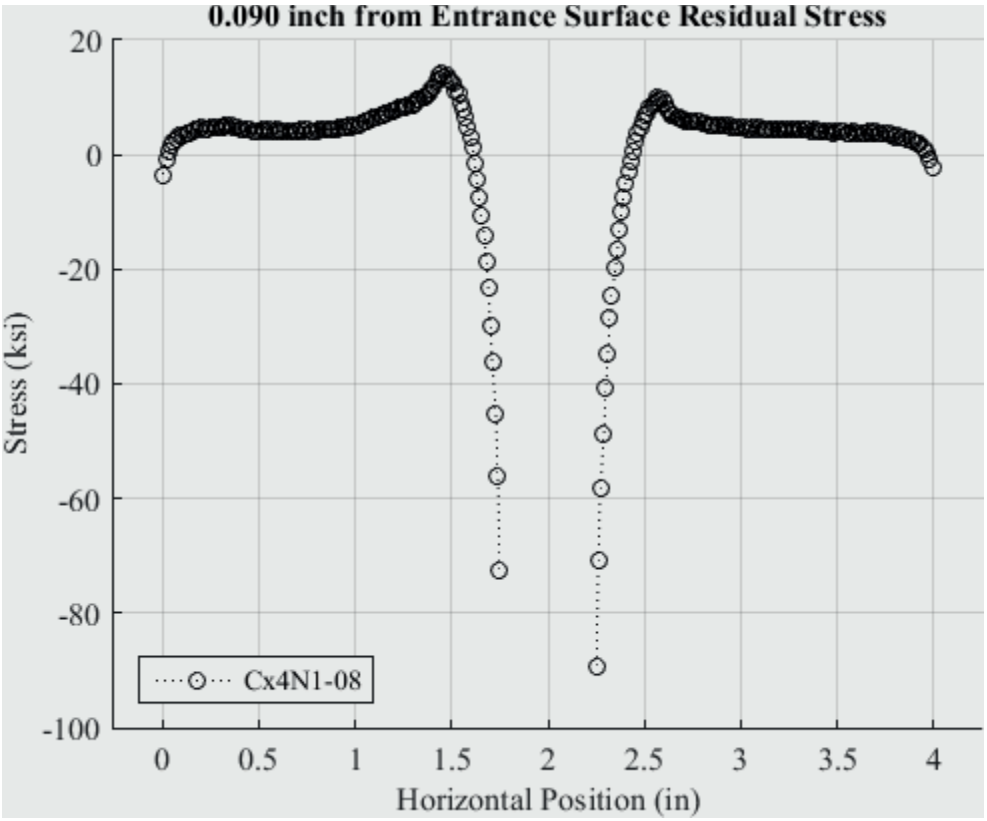

Fig. 354 Residual Stress Line Plot of Cx4N1-08-B (2024-T351) at a Distance of 0.09 inch from the Entrance Surface – Coupons had a 0.4974 inch Fatigue Crack at the Left Entrance Surface.

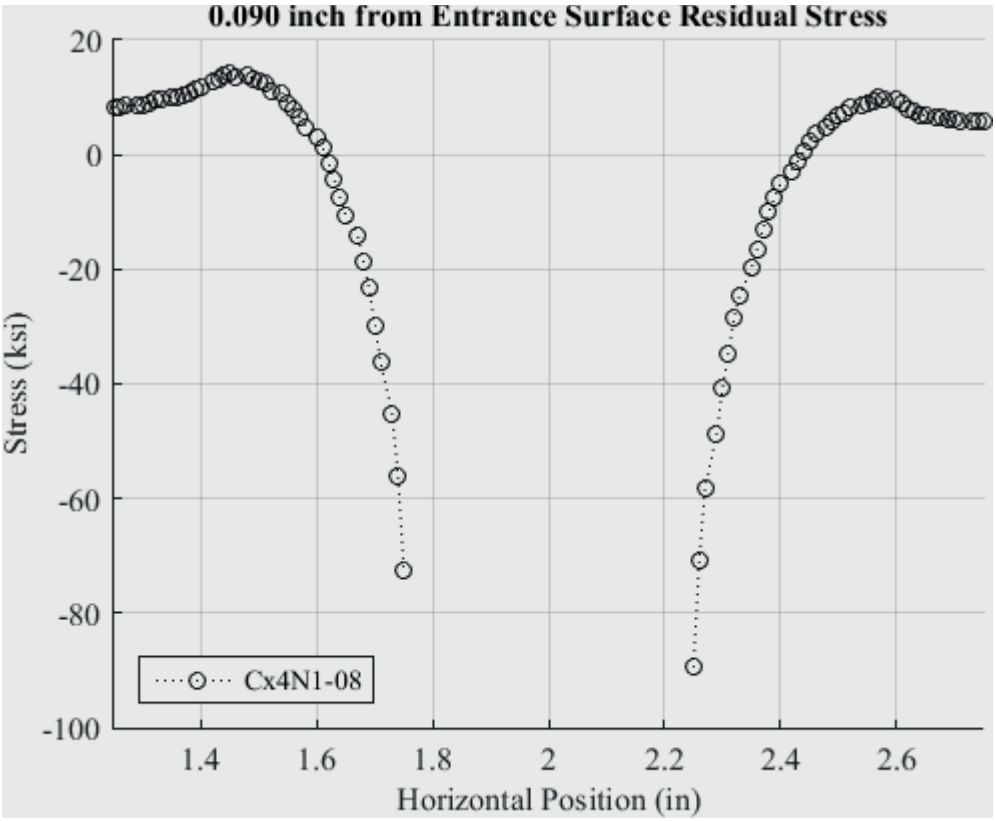

Fig. 355 Residual Stress Line Plot of Cx4N1-08-B (2024-T351) at a Distance of 0.09 inch from the Entrance Surface – Coupons had a 0.4974 inch Fatigue Crack at the Left Entrance Surface – Zoomed in Next to Hole.

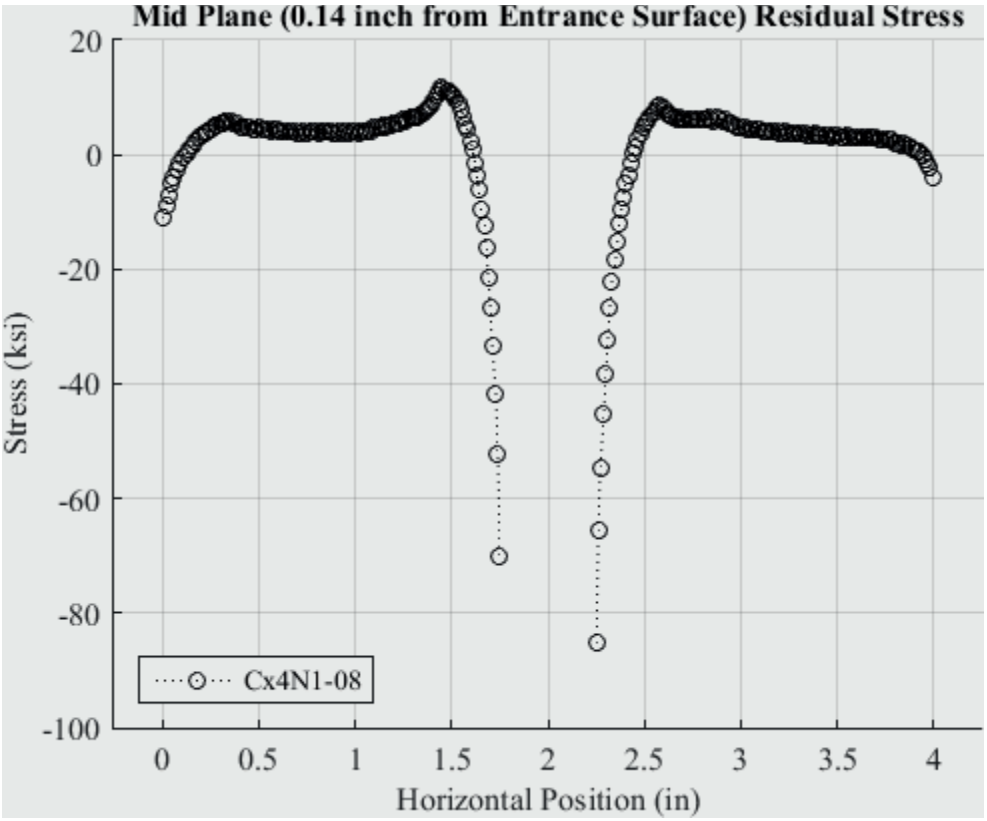

Fig. 356 Residual Stress Line Plot of Cx4N1-08-B (2024-T351) at a Distance of 0.140 inch (Mid Plane) from the Entrance Surface – Coupons had a 0.4974 inch Fatigue Crack at the Left Entrance Surface.

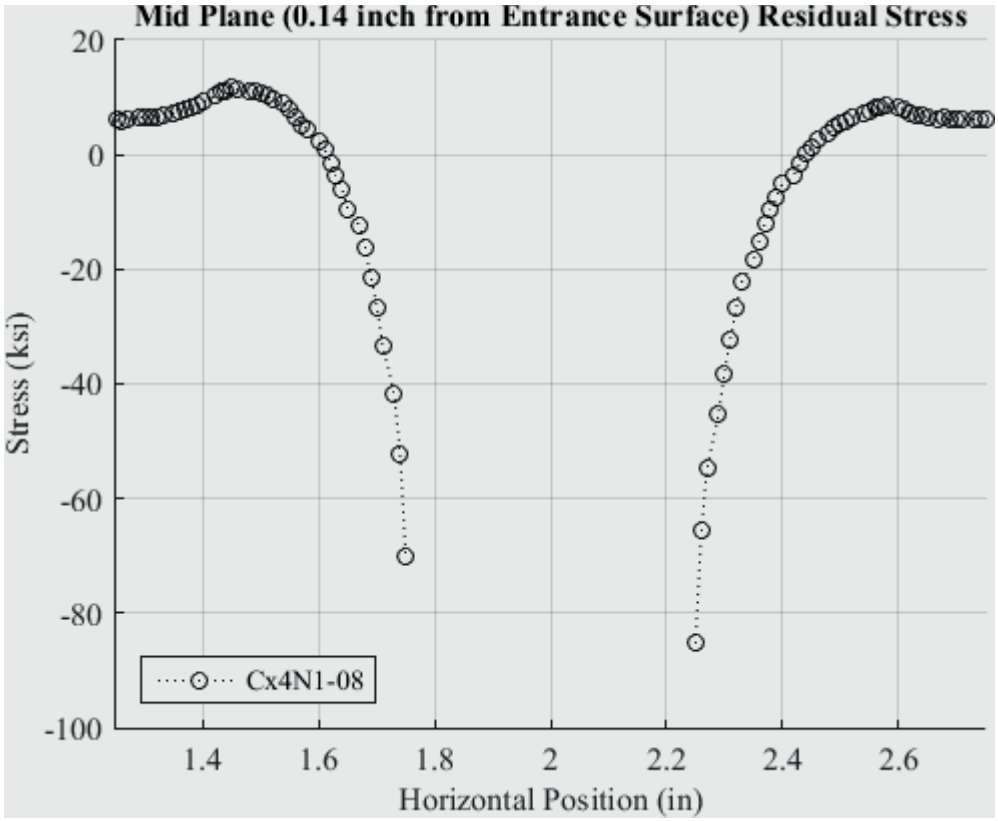

Fig. 357 Residual Stress Line Plot of Cx4N1-08-B (2024-T351) at a Distance of 0.140 inch (Mid Plane) from the Entrance Surface – Coupons had a 0.4974 inch Fatigue Crack at the Left Entrance Surface – Zoomed in Next to Hole.

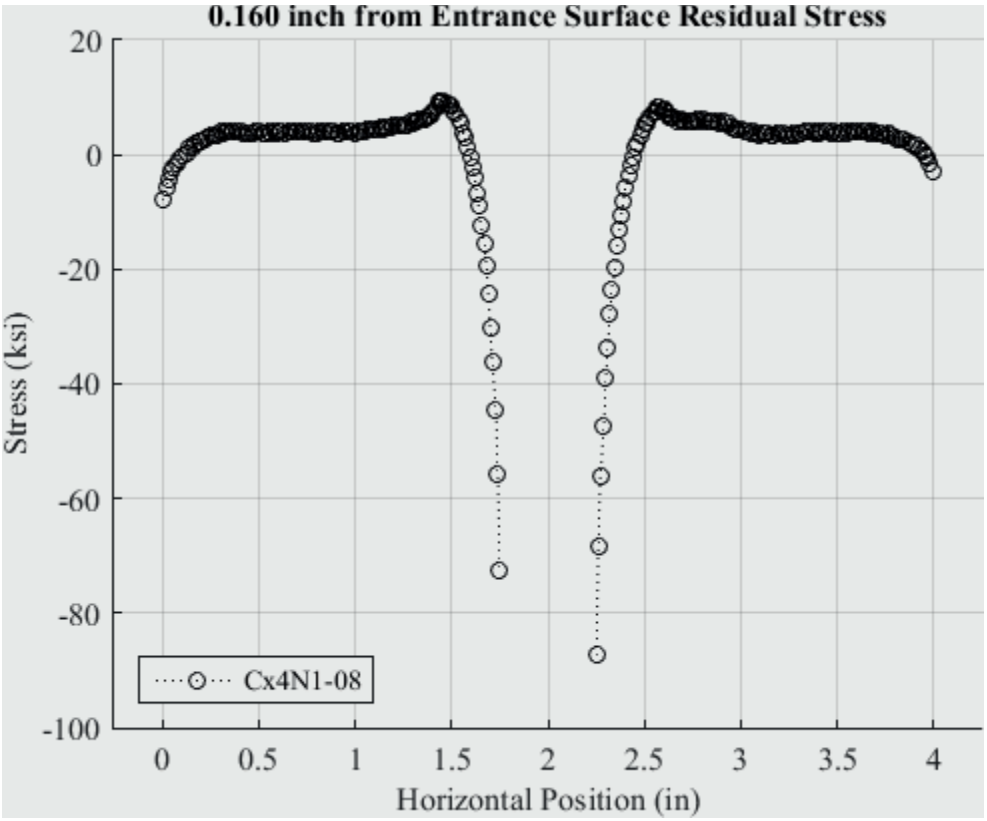

Fig. 358 Residual Stress Line Plot of Cx4N1-08-B (2024-T351) at a Distance of 0.160 inch from the Entrance Surface – Coupons had a 0.4974 inch Fatigue Crack at the Left Entrance Surface.

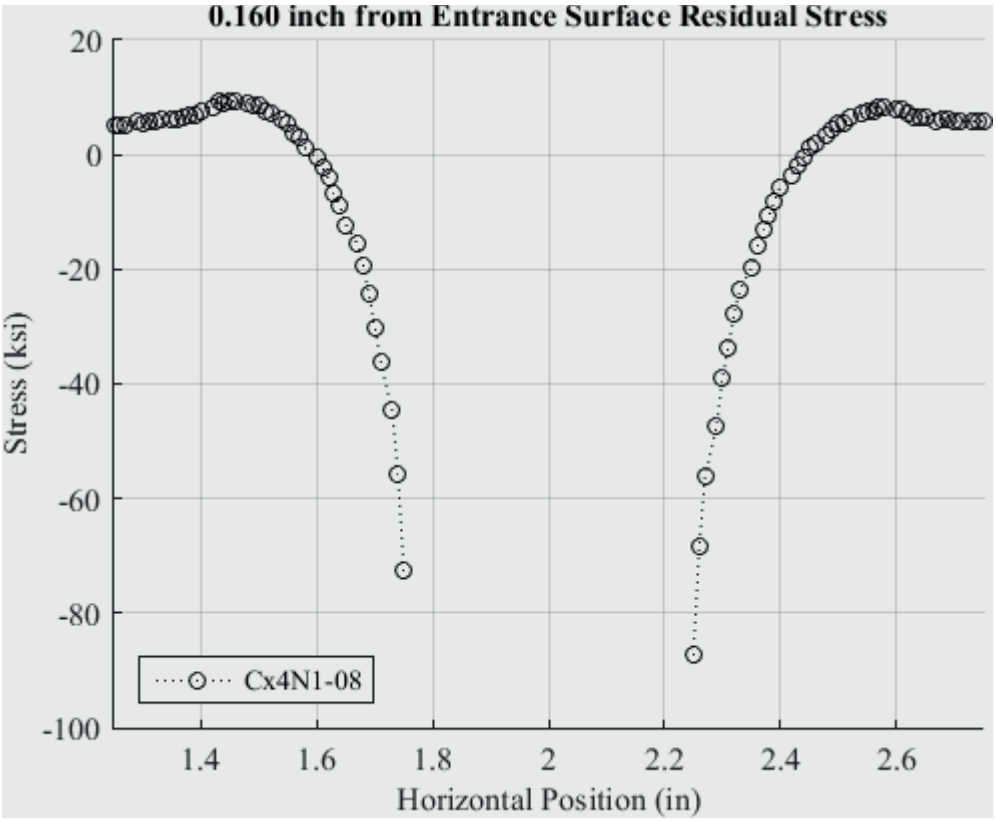

Fig. 359 Residual Stress Line Plot of Cx4N1-08-B (2024-T351) at a Distance of 0.160 inch from the Entrance Surface – Coupons had a 0.4974 inch Fatigue Crack at the Left Entrance Surface – Zoomed in Next to Hole.

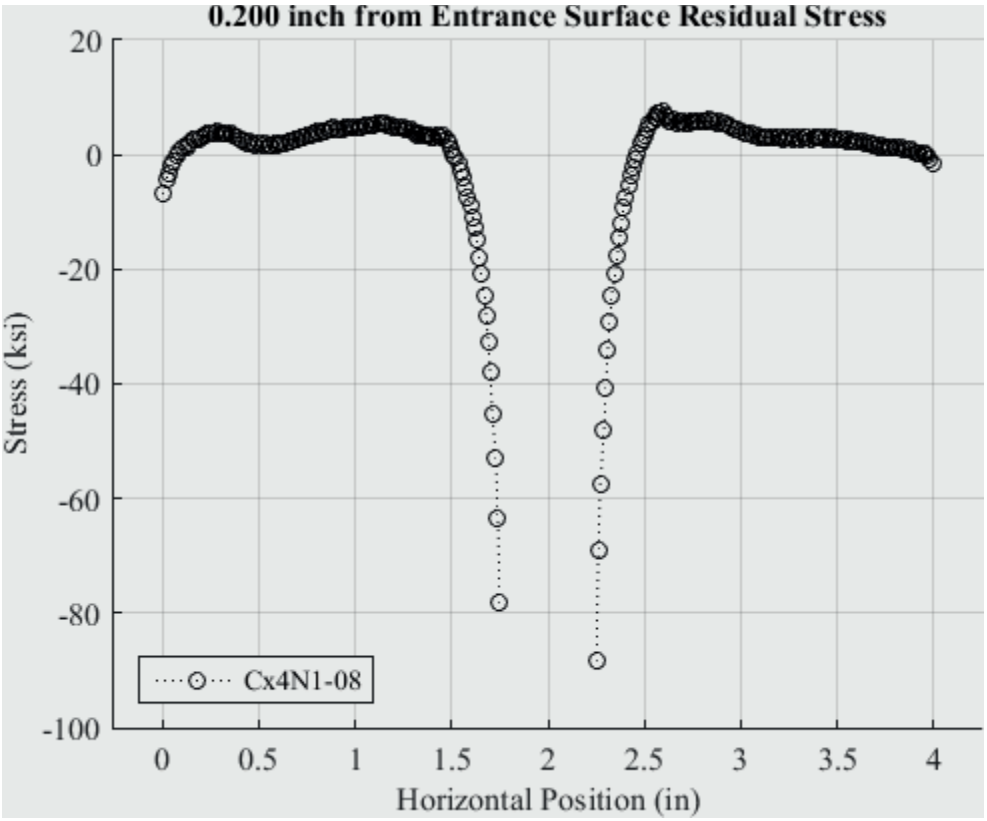

Fig. 360 Residual Stress Line Plot of Cx4N1-08-B (2024-T351) at a Distance of 0.200 inch from the Entrance Surface – Coupons had a 0.4974 inch Fatigue Crack at the Left Entrance Surface.

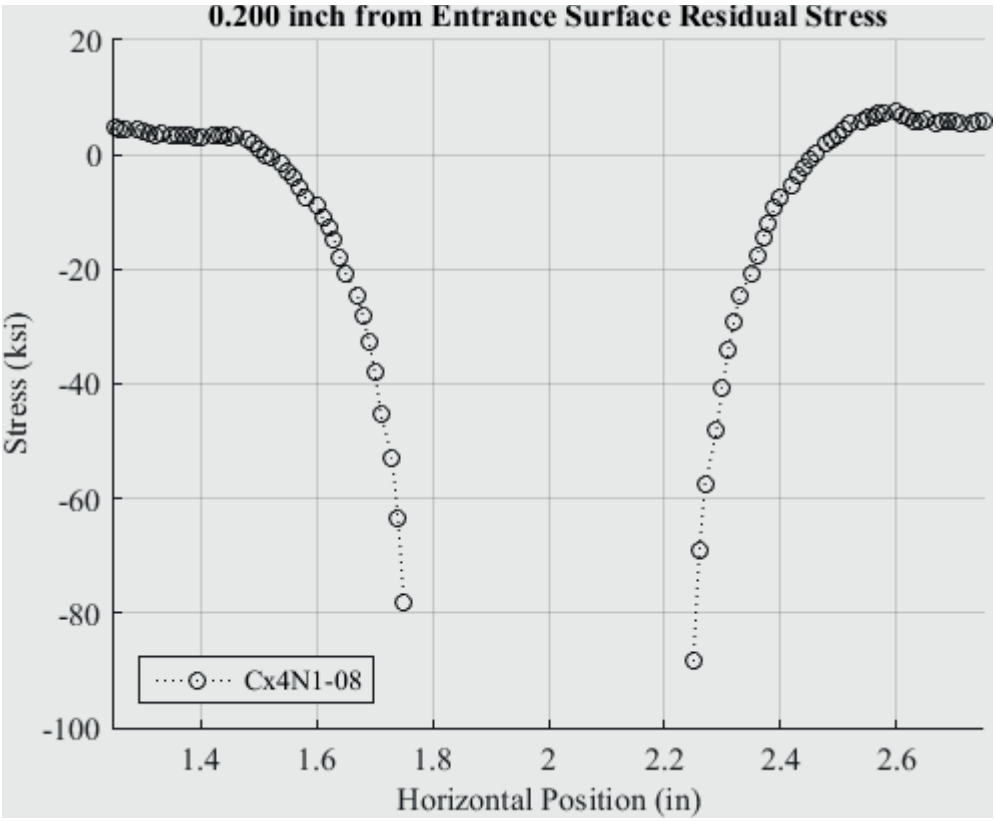

Fig. 361 Residual Stress Line Plot of Cx4N1-08-B (2024-T351) at a Distance of 0.200 inch from the Entrance Surface – Coupons had a 0.4974 inch Fatigue Crack at the Left Entrance Surface – Zoomed in Next to Hole.

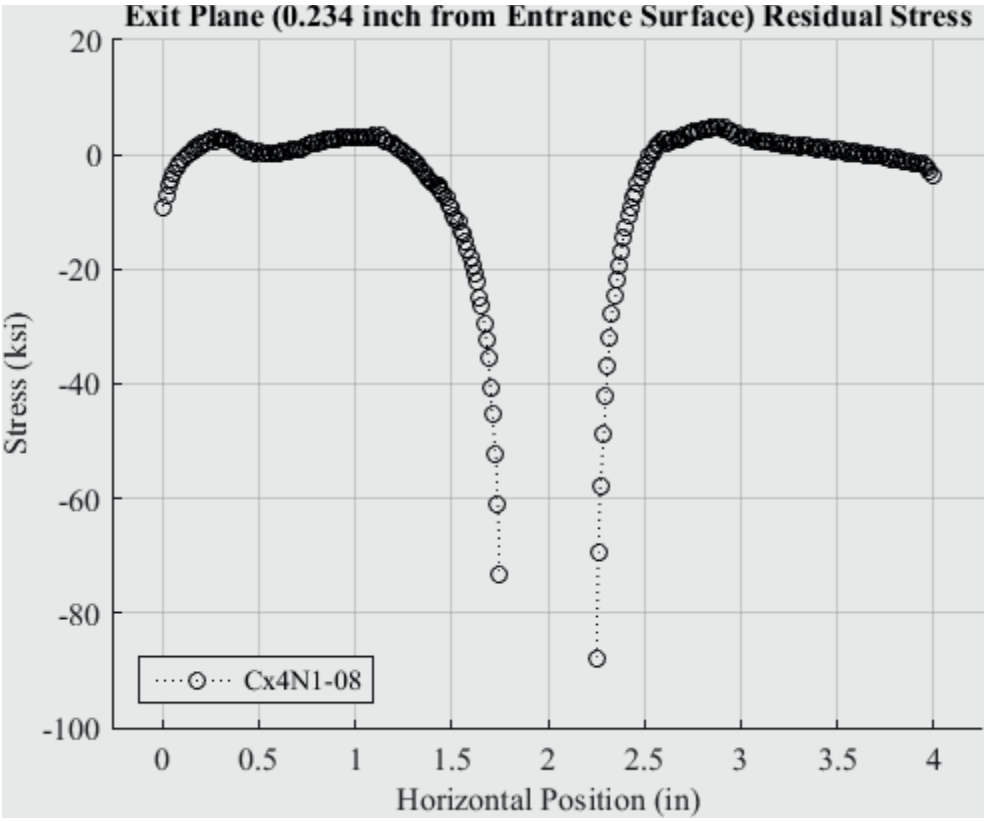

Fig. 362 Residual Stress Line Plot of Cx4N1-08-B (2024-T351) at a Distance of 0.234 inch (Exit Plane) from the Entrance Surface – Coupons had a 0.4974 inch Fatigue Crack at the Left Entrance Surface.

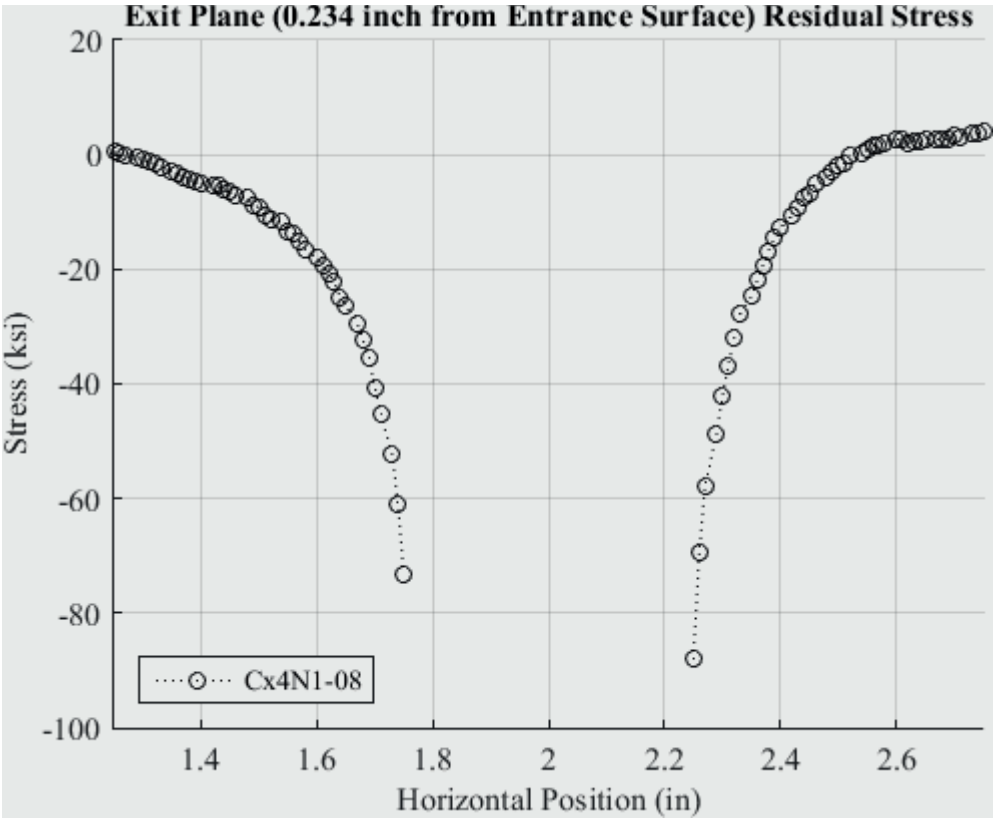

Fig. 363 Residual Stress Line Plot of Cx4N1-08-B (2024-T351) at a Distance of 0.234 inch (Exit Plane) from the Entrance Surface – Coupons had a 0.4974 inch Fatigue Crack at the Left Entrance Surface – Zoomed in Next to Hole.

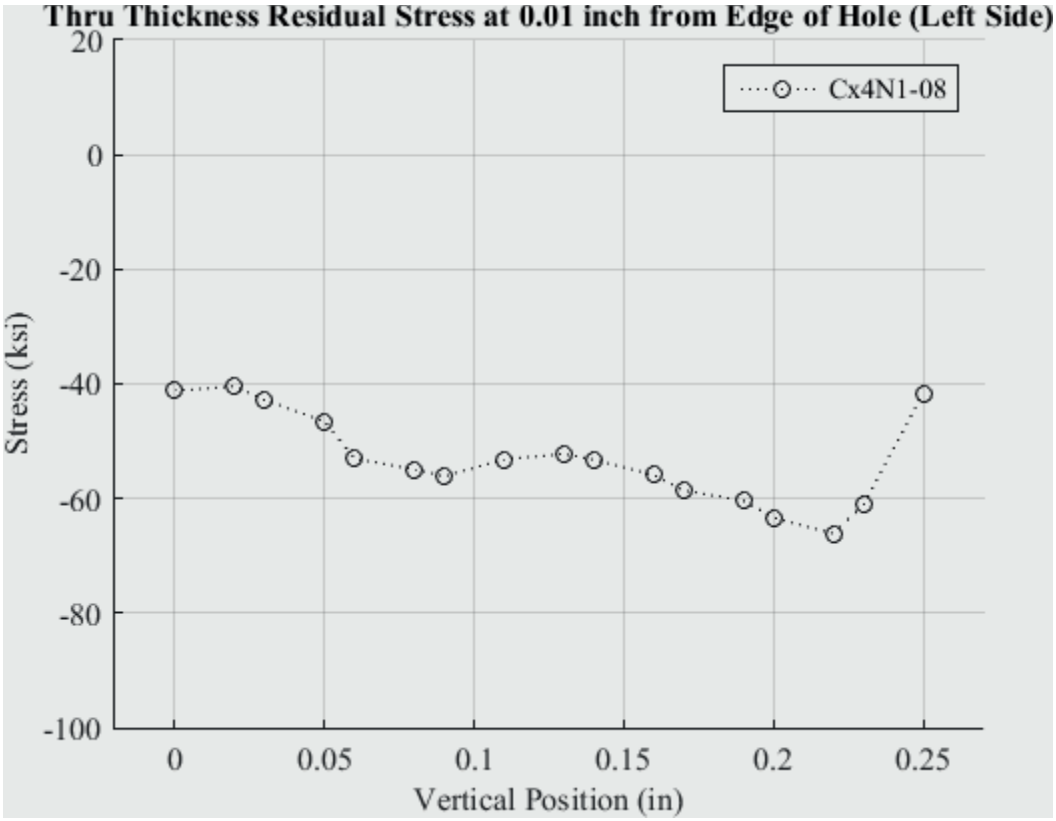

Fig. 364 Residual Stress Line Plot of Cx4N1-08-B (2024-T351) Through the Thickness at 0.01 inch from Left Side of Hole – Coupons had a 0.4974 inch Fatigue Crack at the Left Entrance Surface.

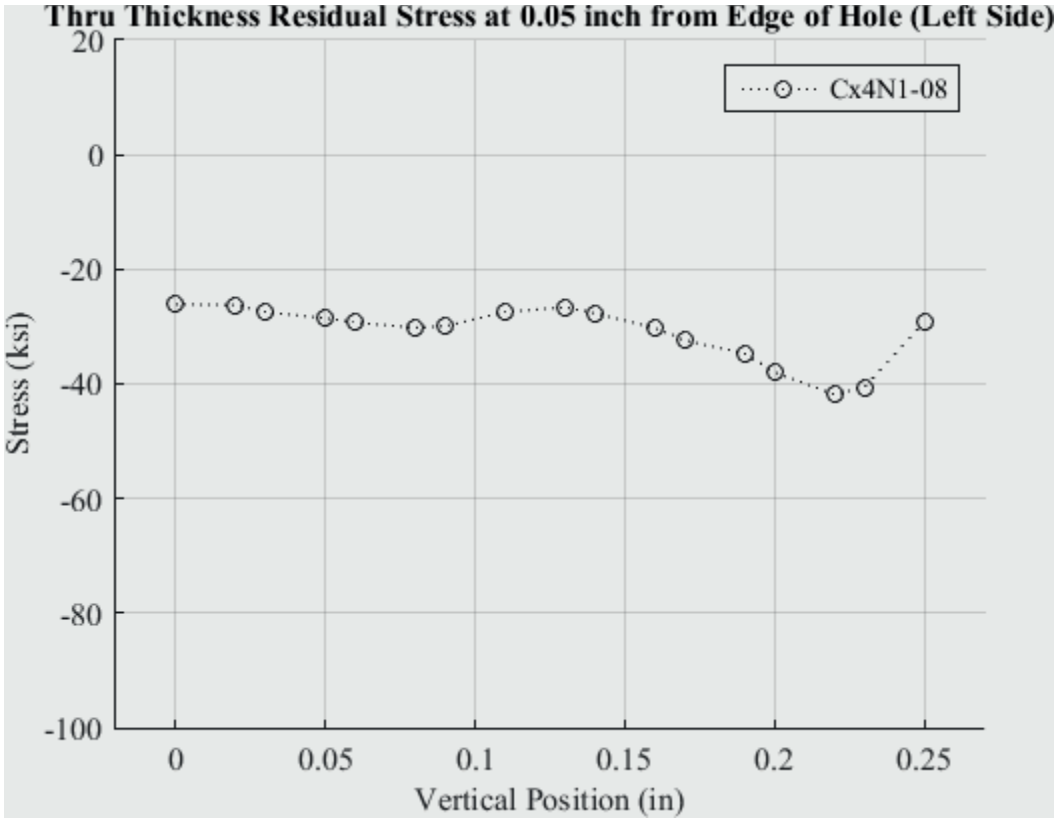

Fig. 365 Residual Stress Line Plot of Cx4N1-08-B (2024-T351) Through the Thickness at 0.05 inch from Left Side of Hole – Coupons had a 0.4974 inch Fatigue Crack at the Left Entrance Surface.

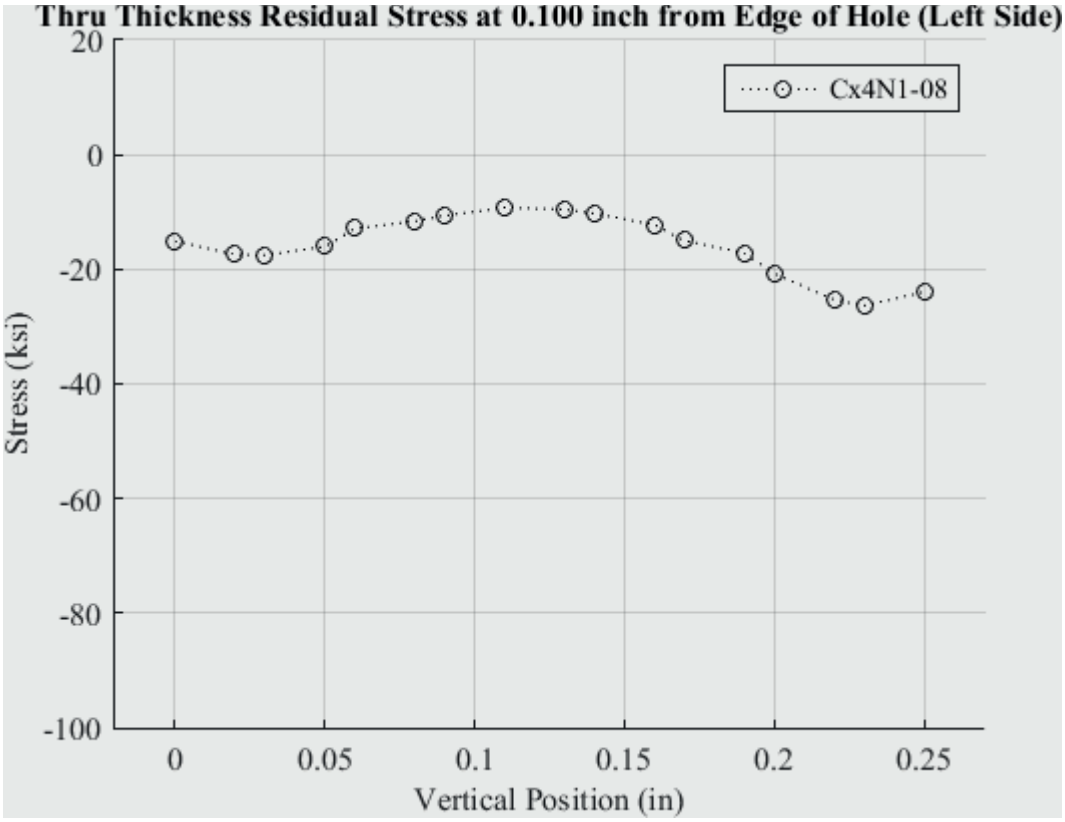

Fig. 366 Residual Stress Line Plot of Cx4N1-08-B (2024-T351) Through the Thickness at 0.10 inch from Left Side of Hole – Coupons had a 0.4974 inch Fatigue Crack at the Left Entrance Surface.

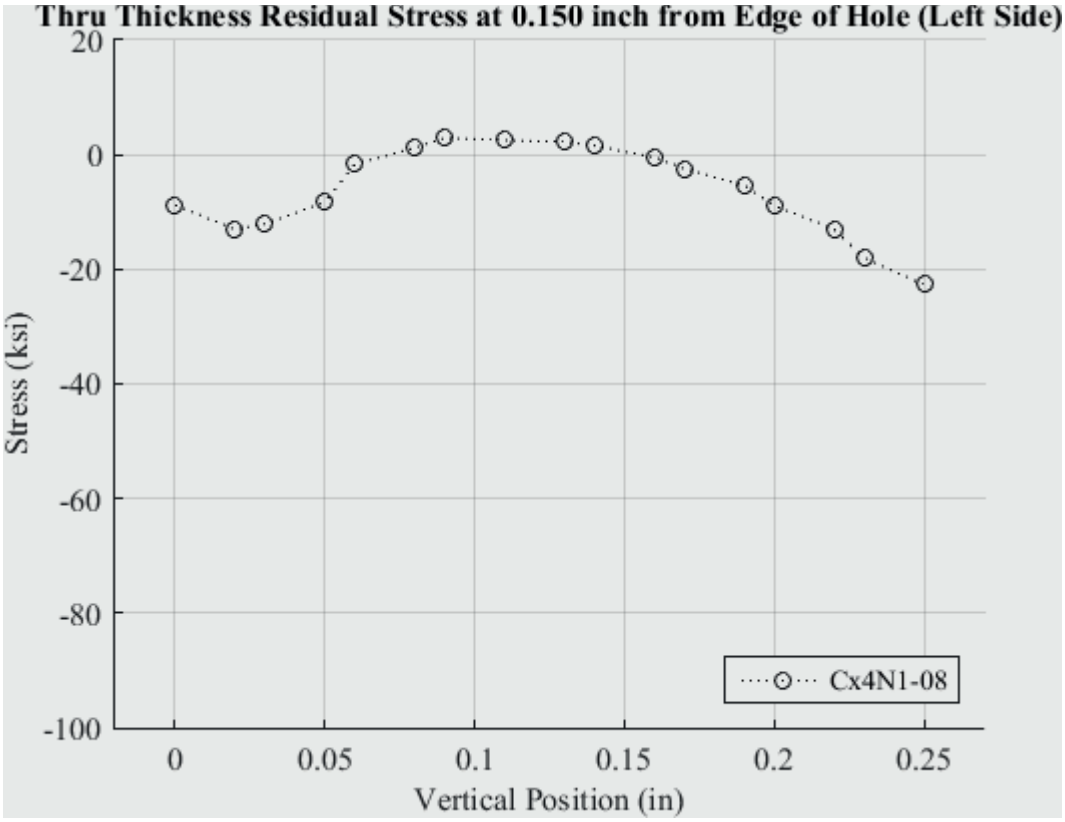

Fig. 367 Residual Stress Line Plot of Cx4N1-08-B (2024-T351) Through the Thickness at 0.150 inch from Left Side of Hole – Coupons had a 0.4974 inch Fatigue Crack at the Left Entrance Surface.

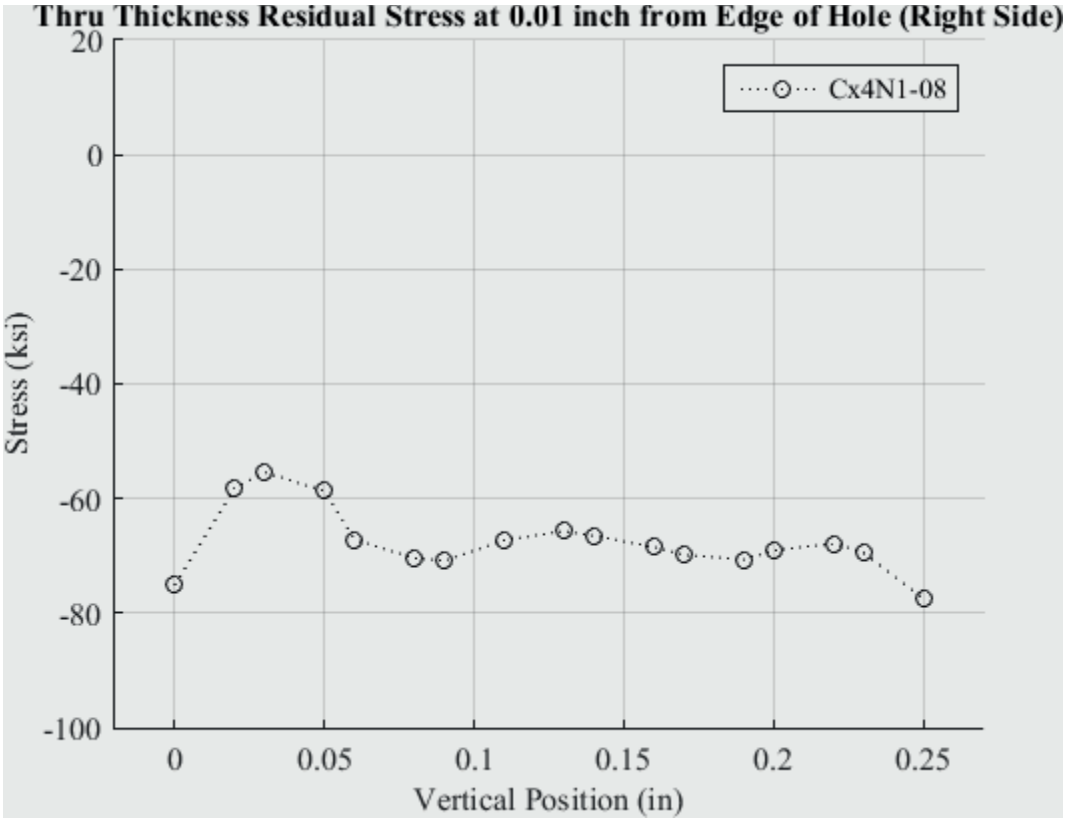

Fig. 368 Residual Stress Line Plot of Cx4N1-08-B (2024-T351) Through the Thickness at 0.01 inch from Right Side of Hole – Coupons had a 0.4974 inch Fatigue Crack at the Left Entrance Surface and a Small Fatigue Crack on the Right Side.

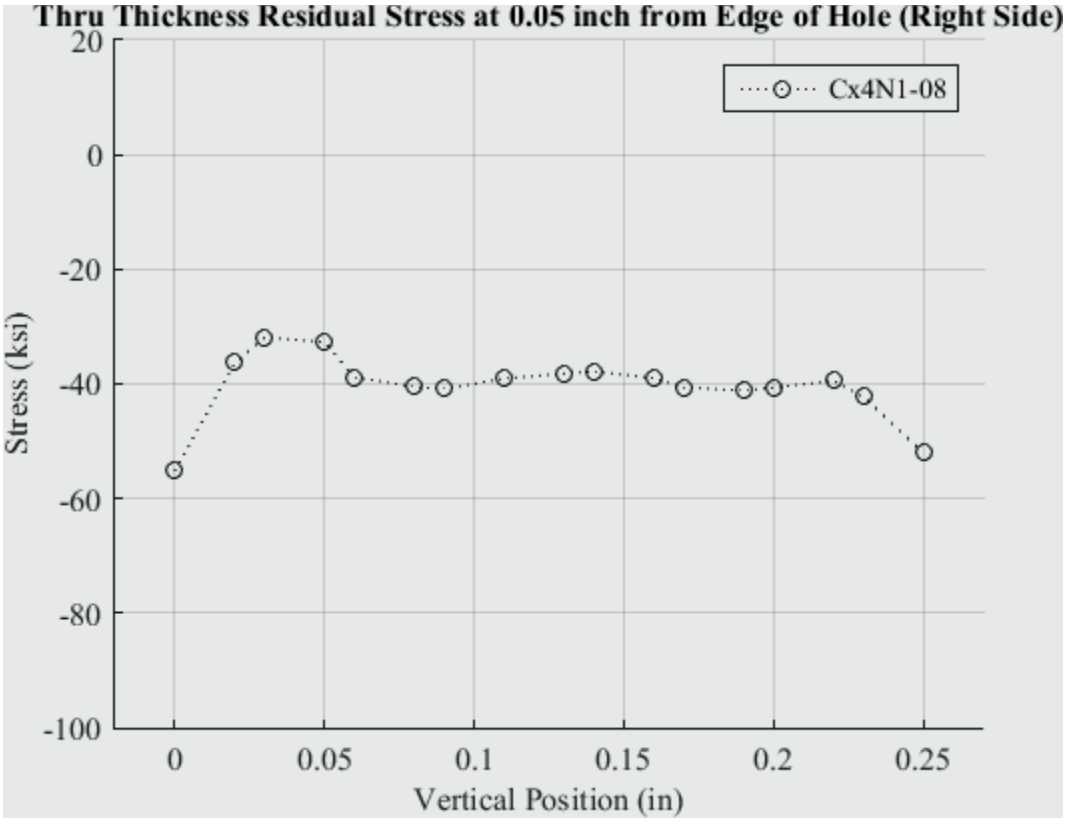

Fig. 369 Residual Stress Line Plot of Cx4N1-08-B (2024-T351) Through the Thickness at 0.05 inch from Right Side of Hole – Coupons had a 0.4974 inch Fatigue Crack at the Left Entrance Surface and a Small Fatigue Crack on the Right Side.

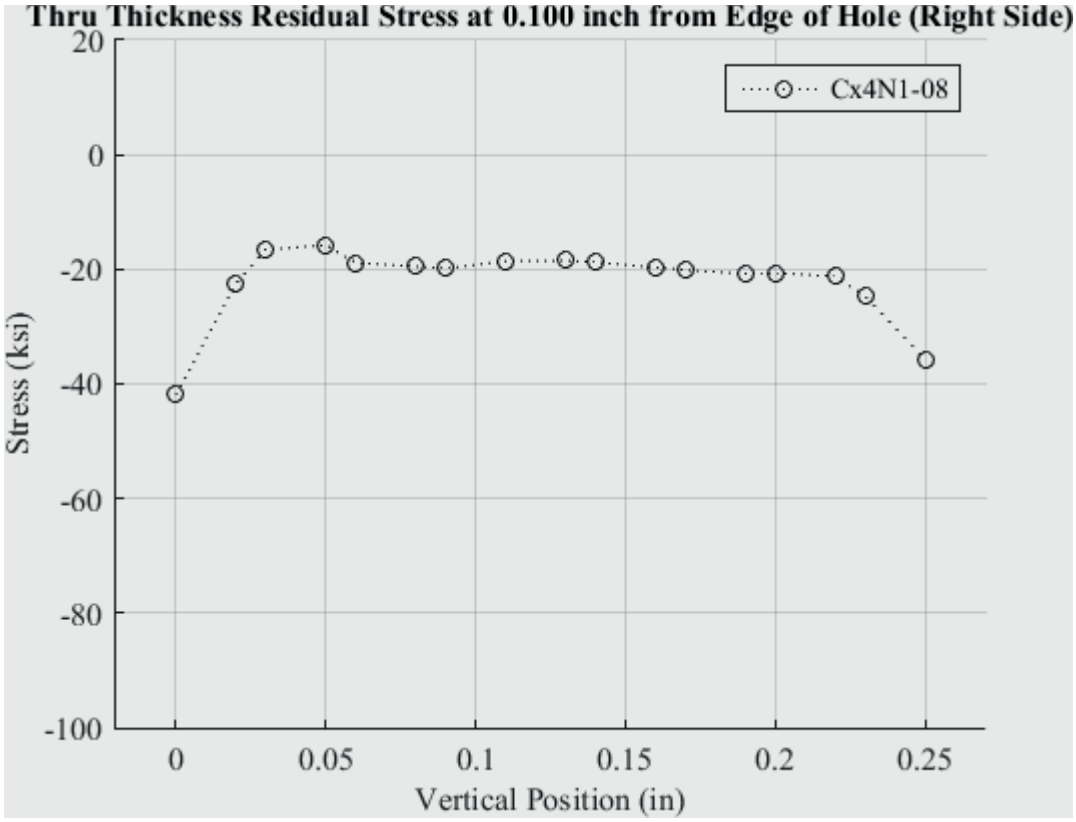

Fig. 370 Residual Stress Line Plot of Cx4N1-08-B (2024-T351) Through the Thickness at 0.10 inch from Right Side of Hole – Coupons had a 0.4974 inch Fatigue Crack at the Left Entrance Surface and a Small Fatigue Crack on the Right Side.

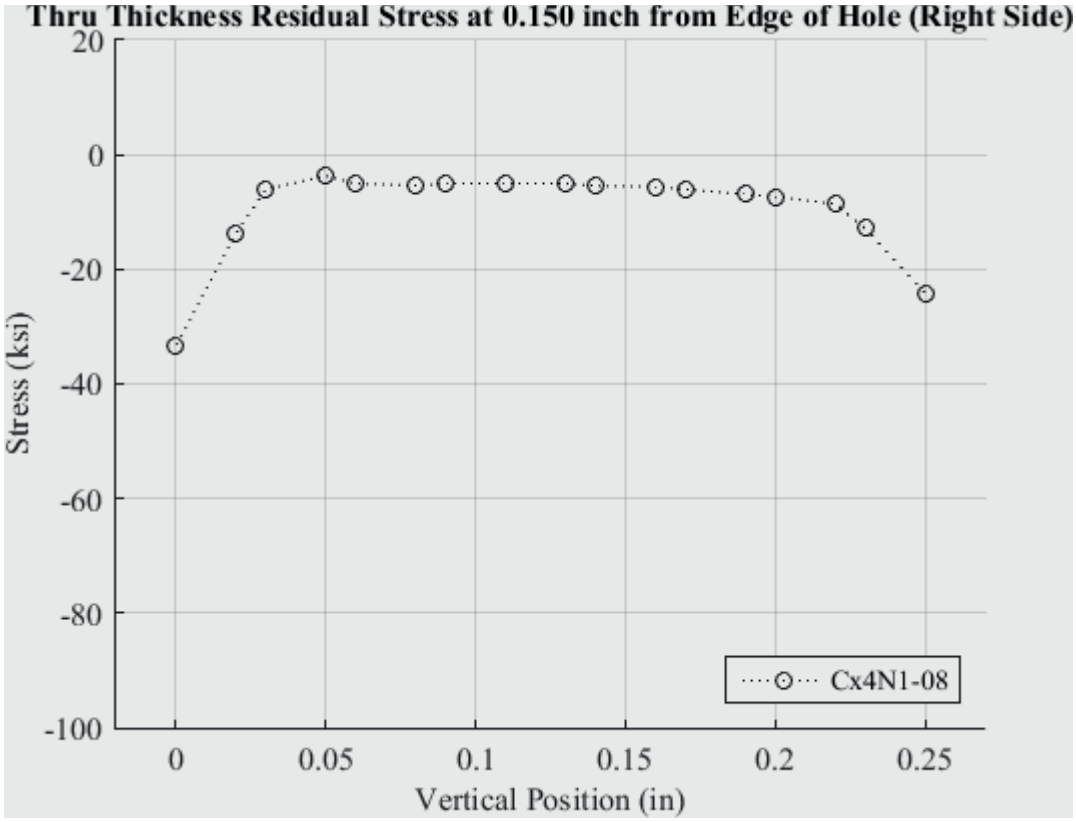

Fig. 371 Residual Stress Line Plot of Cx4N1-08-B (2024-T351) Through the Thickness at 0.150 inch from Right Side of Hole – Coupons had a 0.4974 inch Fatigue Crack at the Left Entrance Surface and a Small Fatigue Crack on the Right Side.

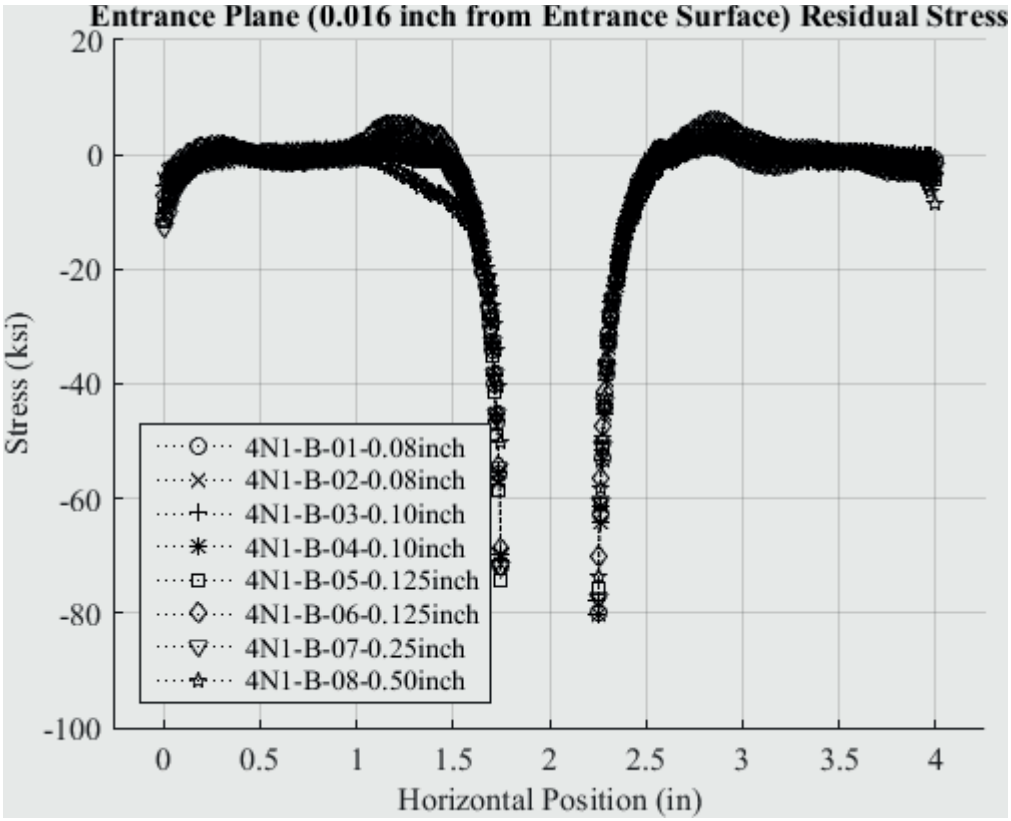

Fig. 372 Residual Stress Line Plot of All Cx4N1-B (2024-T351) Coupons at a Distance of 0.016 inch (Entrance Surface) from the Entrance Surface.

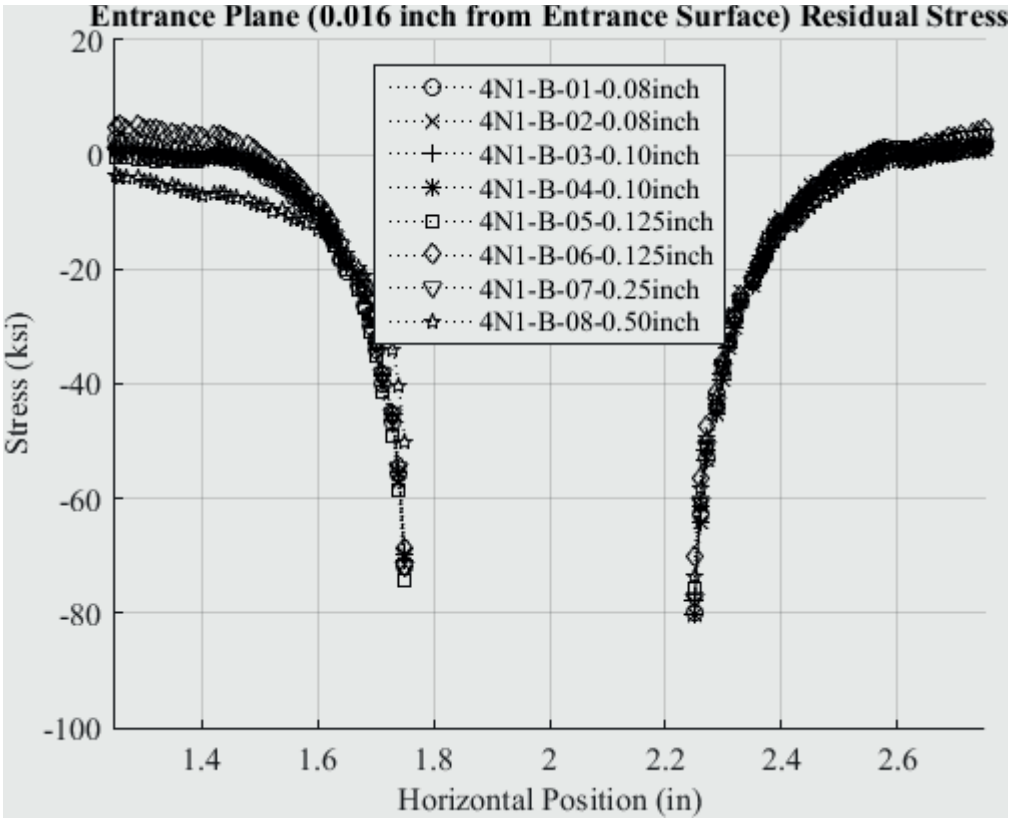

Fig. 373 Residual Stress Line Plot of All Cx4N1-B (2024-T351) Coupons at a Distance of 0.016 inch (Entrance Surface) from the Entrance Surface – Zoomed in Next to Hole.

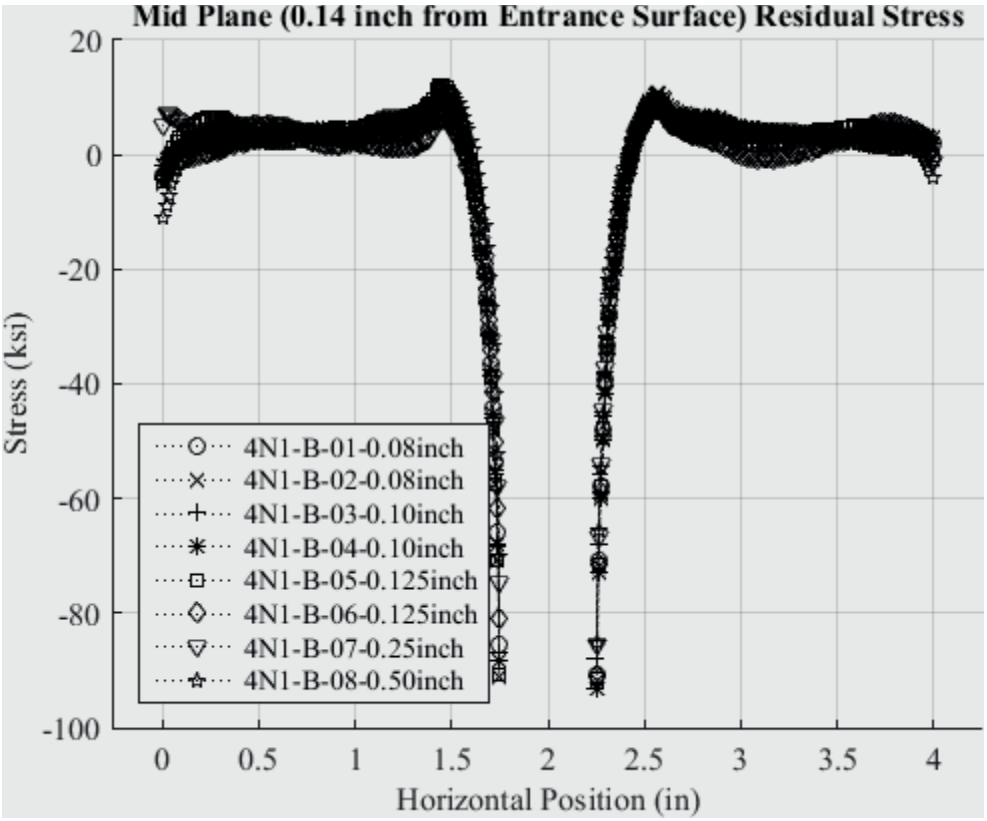

Fig. 374 Residual Stress Line Plot of All Cx4N1-B (2024-T351) Coupons at a Distance of 0.140 inch (Mid Plane Surface) from the Entrance Surface.

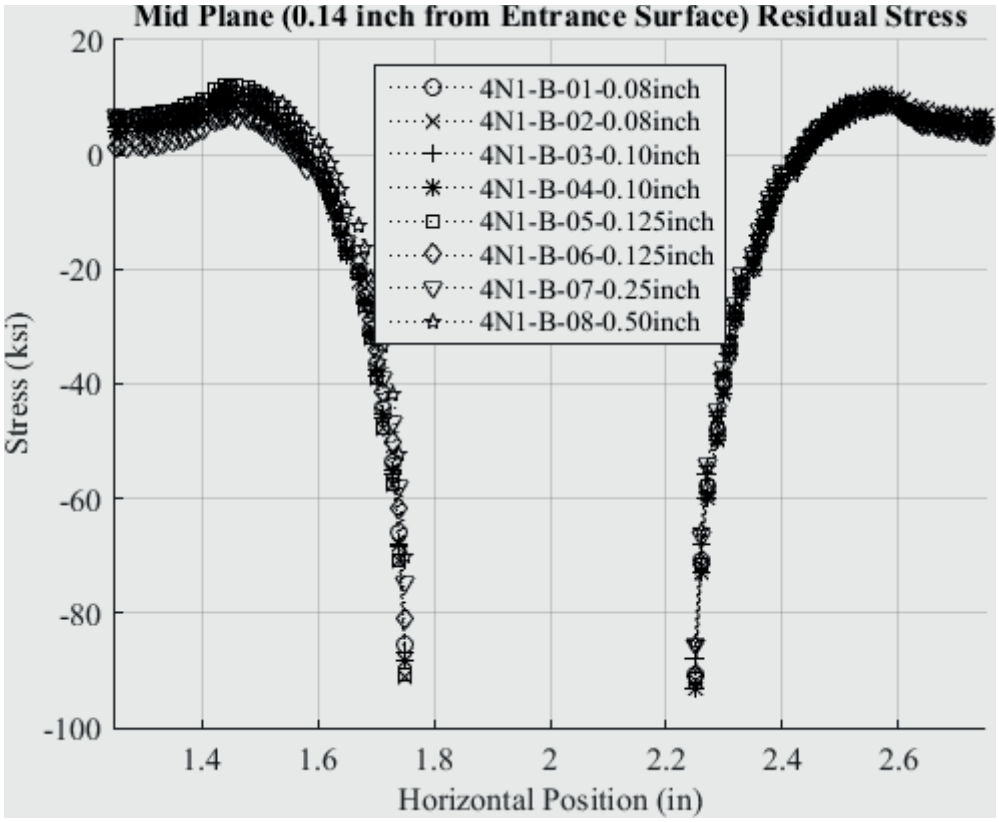

Fig. 375 Residual Stress Line Plot of All Cx4N1-B (2024-T351) Coupons at a Distance of 0.140 inch (Mid Plane Surface) from the Entrance Surface – Zoomed in Next to Hole.

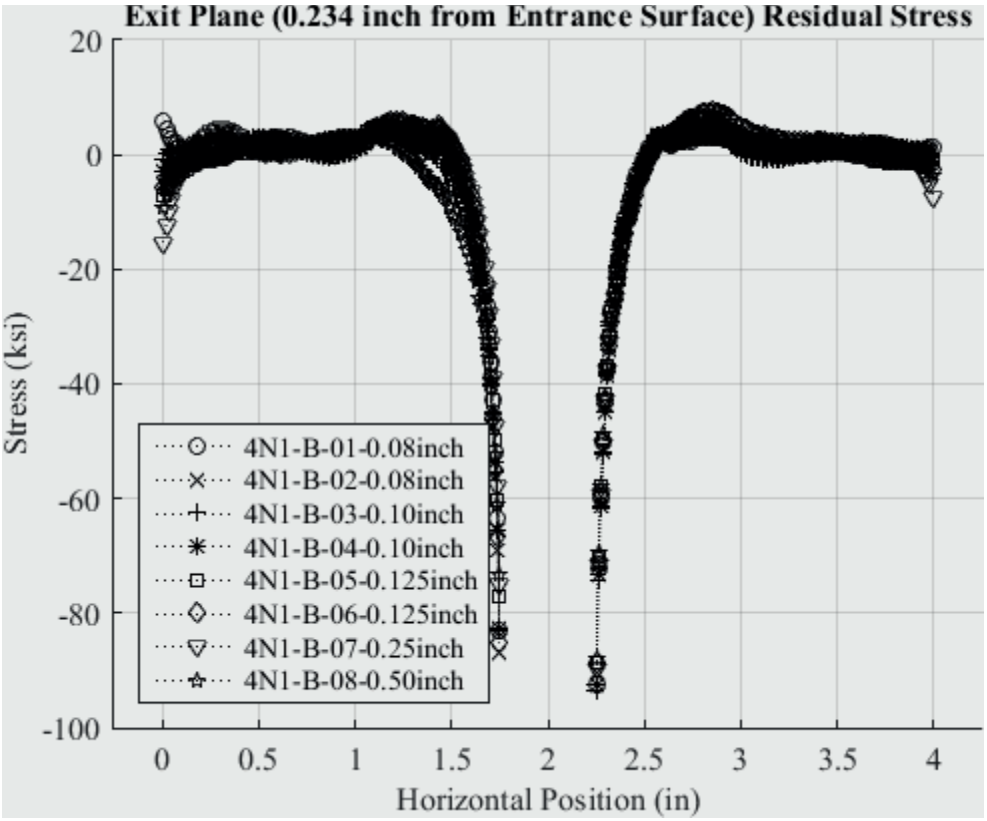

Fig. 376 Residual Stress Line Plot of All Cx4N1-B (2024-T351) Coupons at a Distance of 0.234 inch (Exit Surface) from the Entrance Surface.

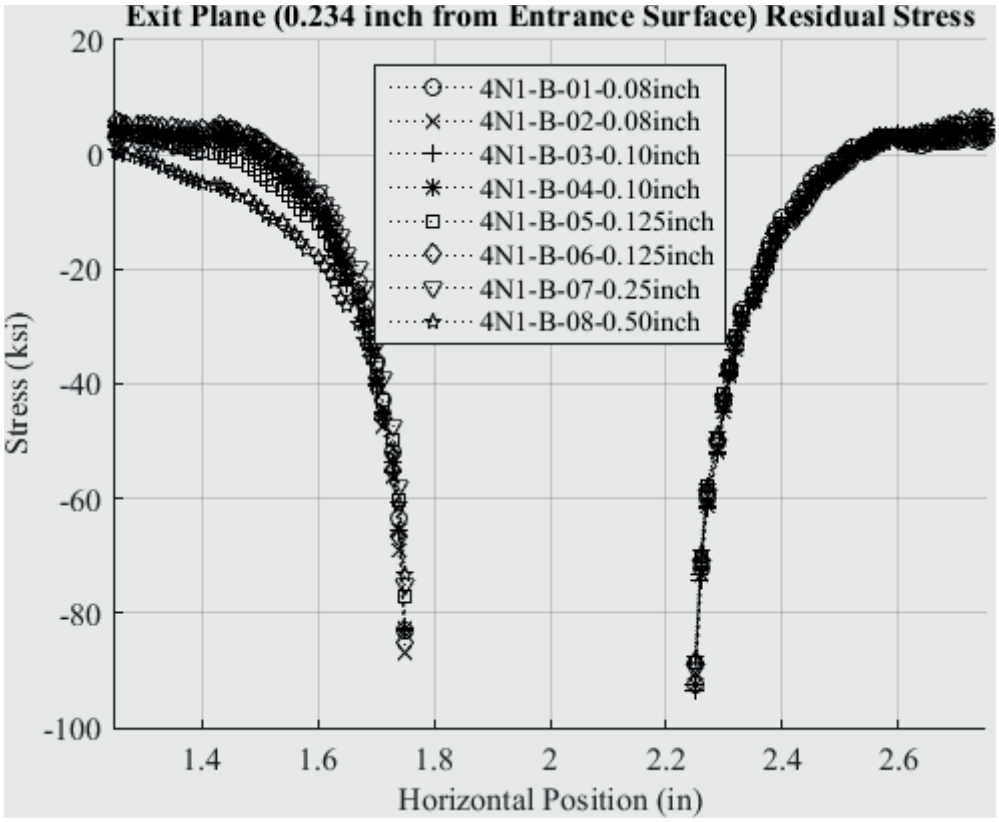

Fig. 377 Residual Stress Line Plot of All Cx4N1-B (2024-T351) Coupons at a Distance of 0.234 inch (Exit Surface) from the Entrance Surface – Zoomed in Next to Hole.

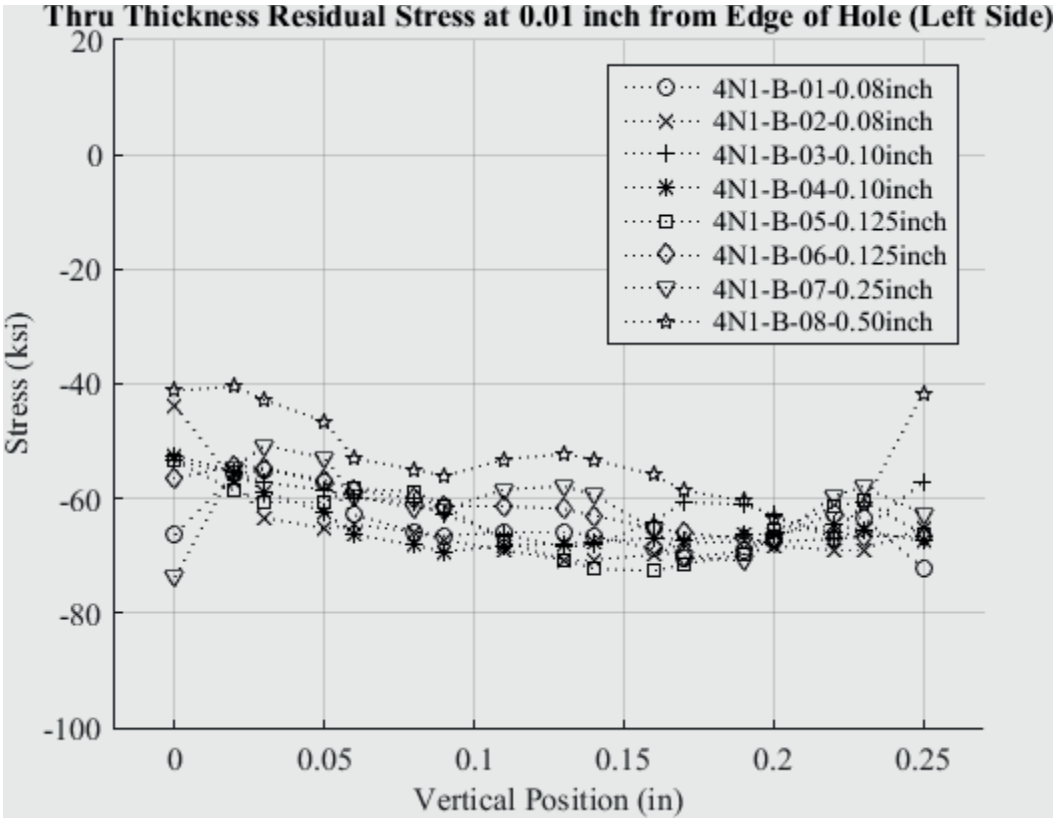

Fig. 378 Residual Stress Line Plot of all Cx4N1-B (2024-T351) Coupons Through the Thickness at 0.01 inch from Left Side of Hole.

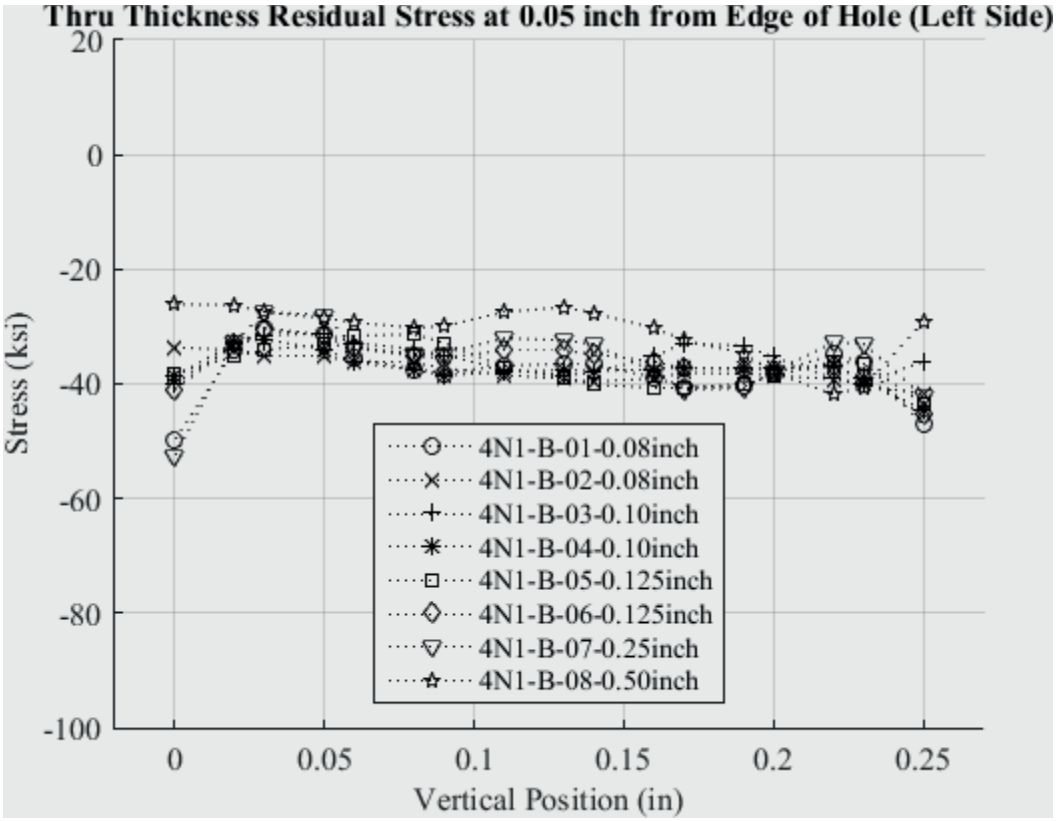

Fig. 379 Residual Stress Line Plot of all Cx4N1-B (2024-T351) Coupons Through the Thickness at 0.05 inch from Left Side of Hole.

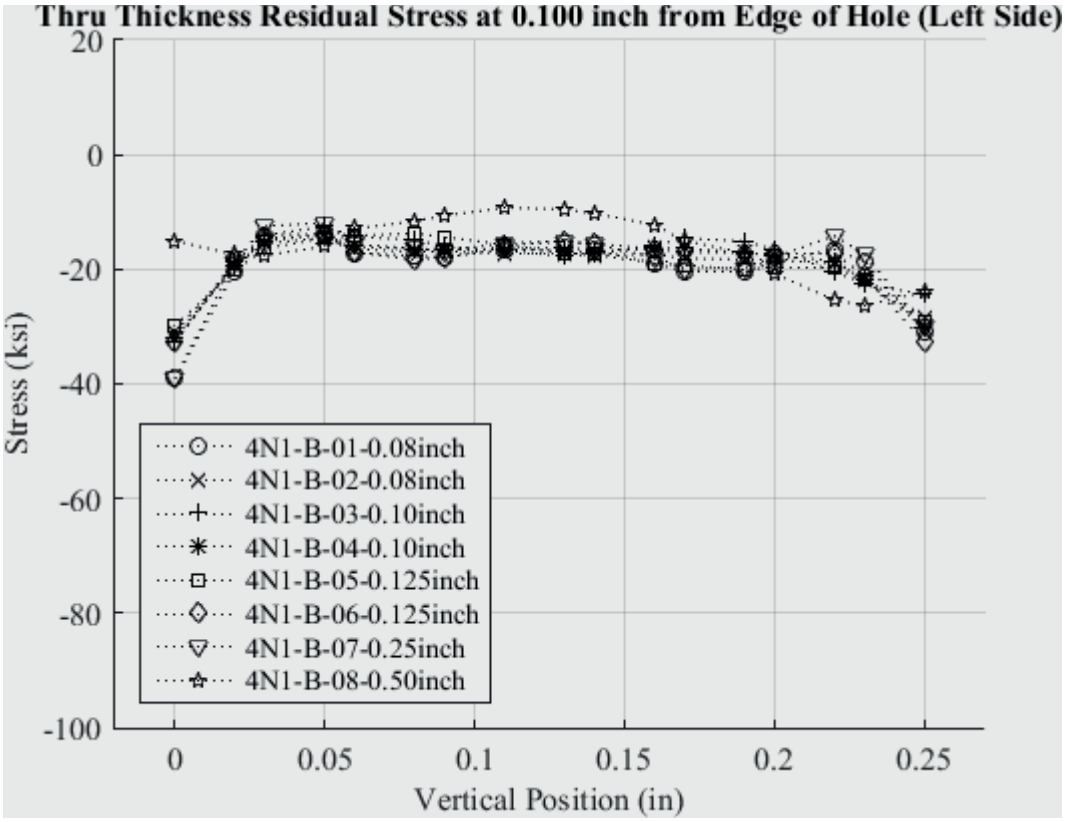

Fig. 380 Residual Stress Line Plot of all Cx4N1-B (2024-T351) Coupons Through the Thickness at 0.10 inch from Left Side of Hole.

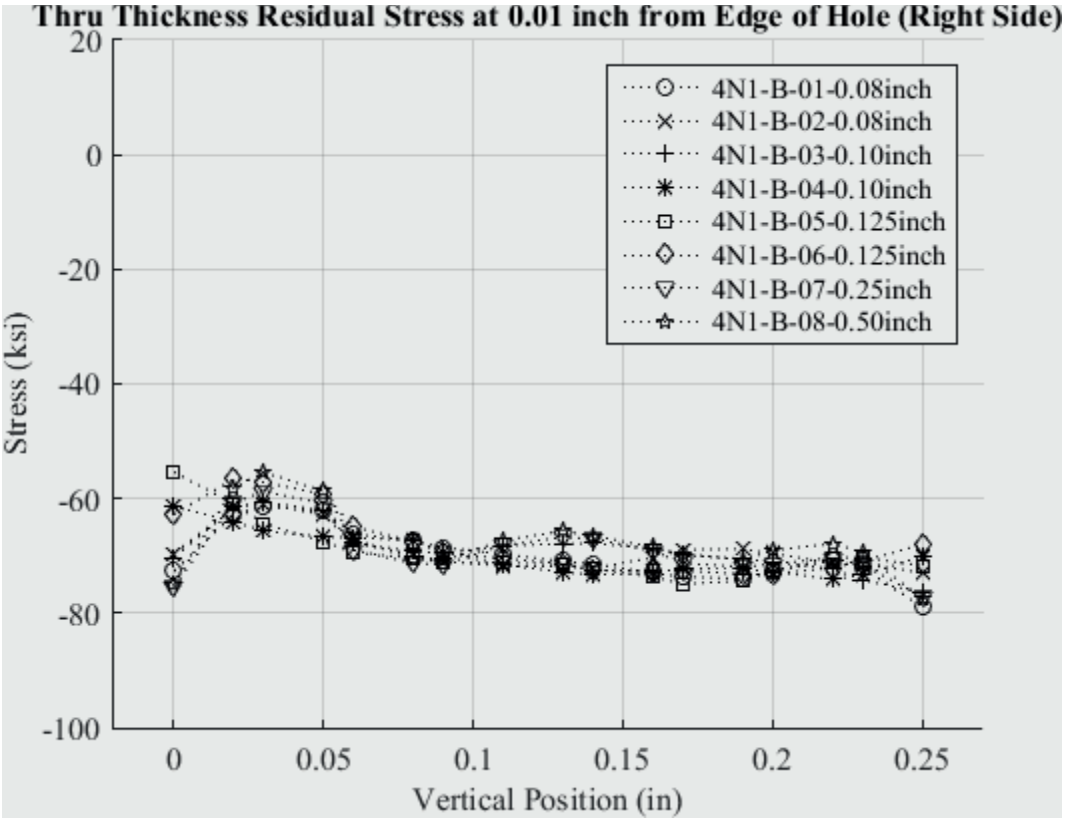

Fig. 381 Residual Stress Line Plot of all Cx4N1-B (2024-T351) Coupons Through the Thickness at 0.01 inch from Right Side of Hole.

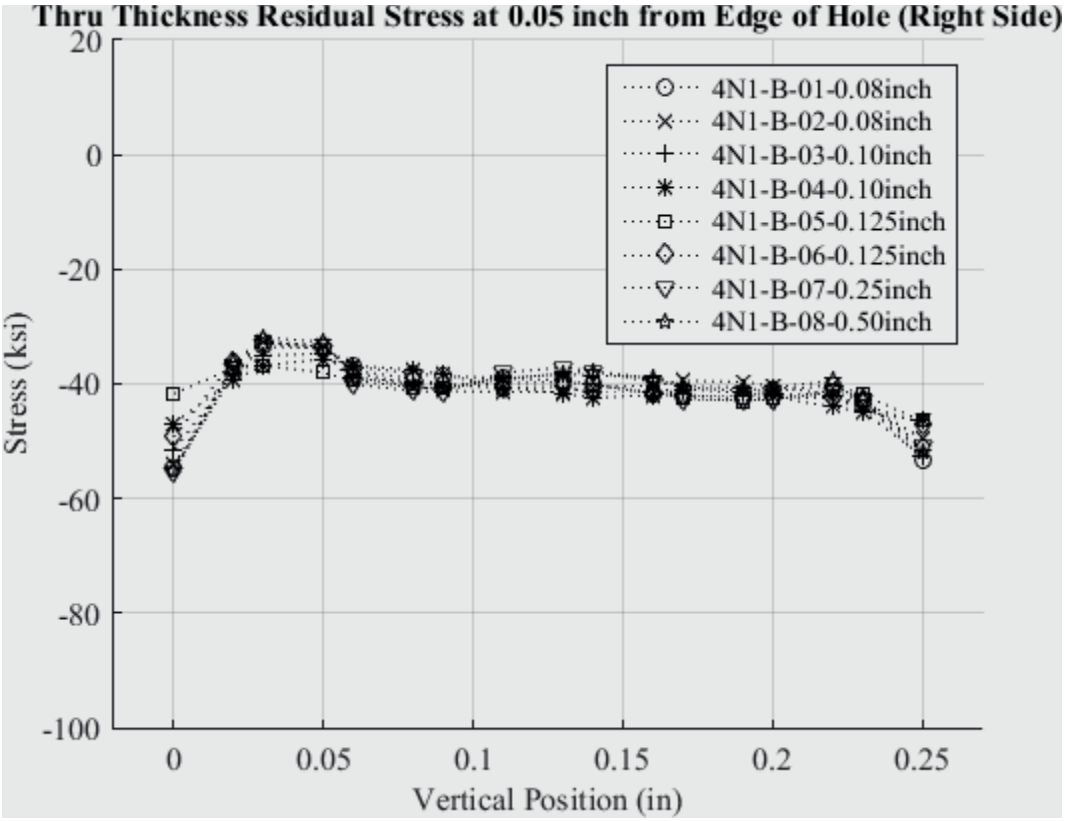

Fig. 382 Residual Stress Line Plot of all Cx4N1-B (2024-T351) Coupons Through the Thickness at 0.05 inch from Right Side of Hole.

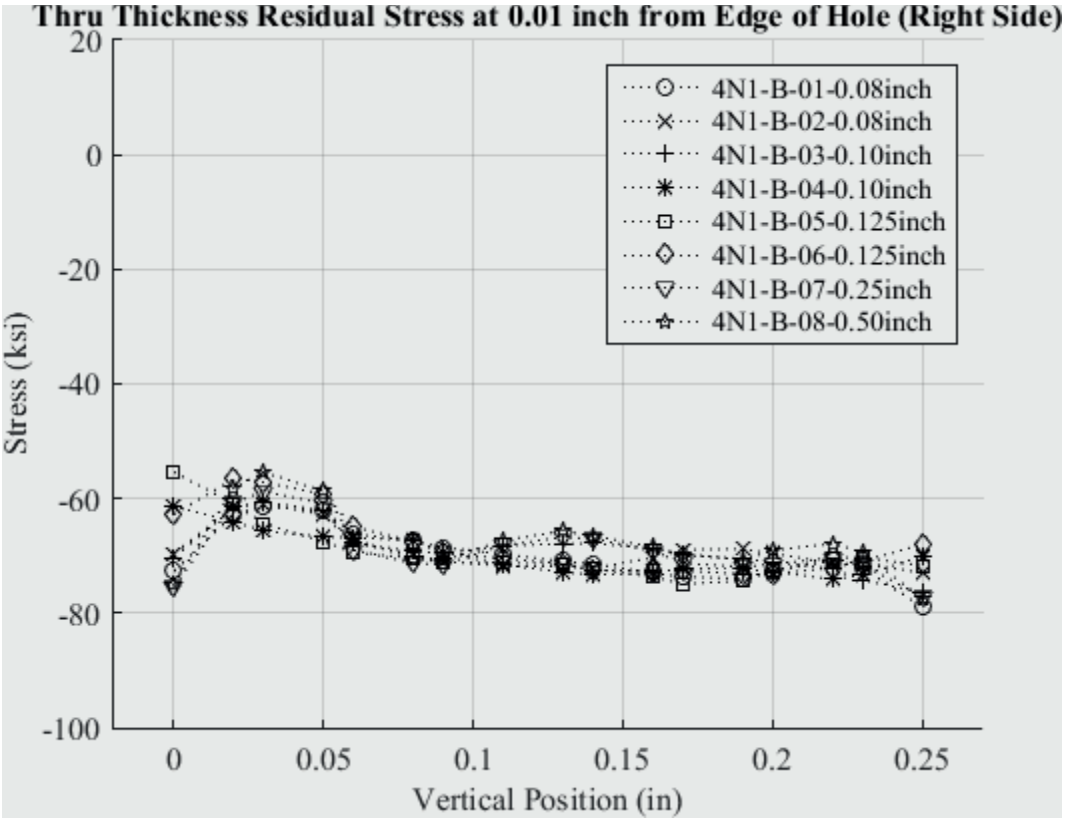

Fig. 383 Residual Stress Line Plot of all Cx4N1-B (2024-T351) Coupons Through the Thickness at 0.10 inch from Right Side of Hole.

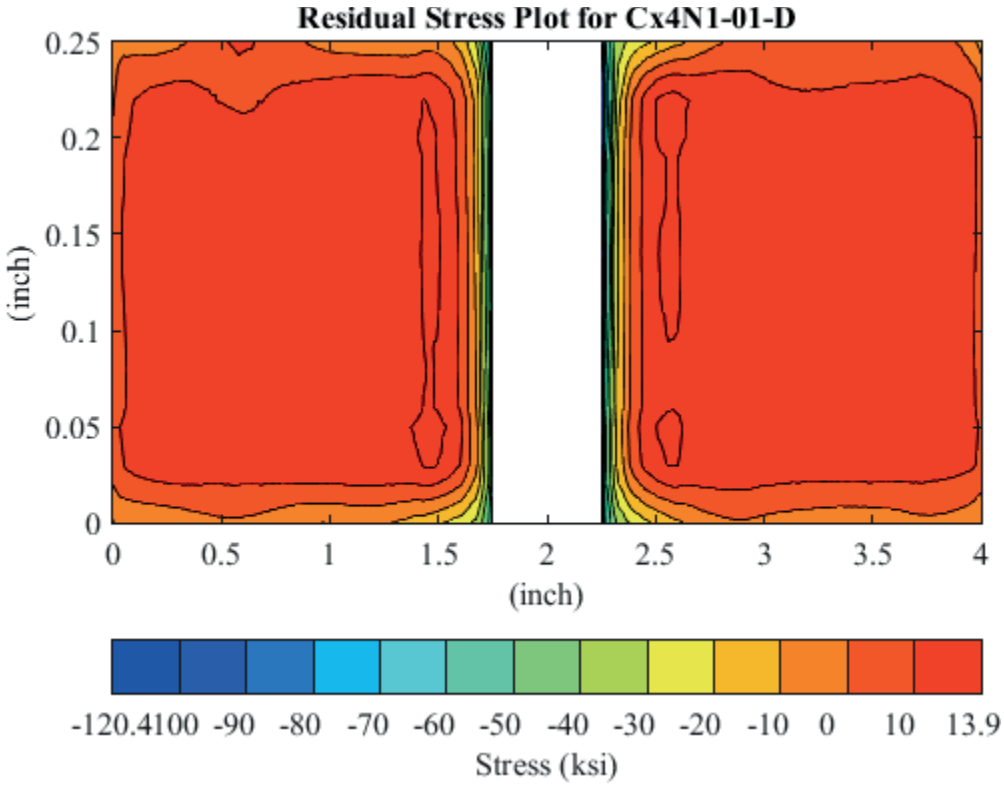

Fig. 384 Residual Stress Contour Plot of Coupon Cx4N1-01-D (7075-T651) – Mandrel Entrance Surface at Y=0, 0.0793 inch Fatigue Crack on Left Side of Hole on Mandrel Entrance Surface.

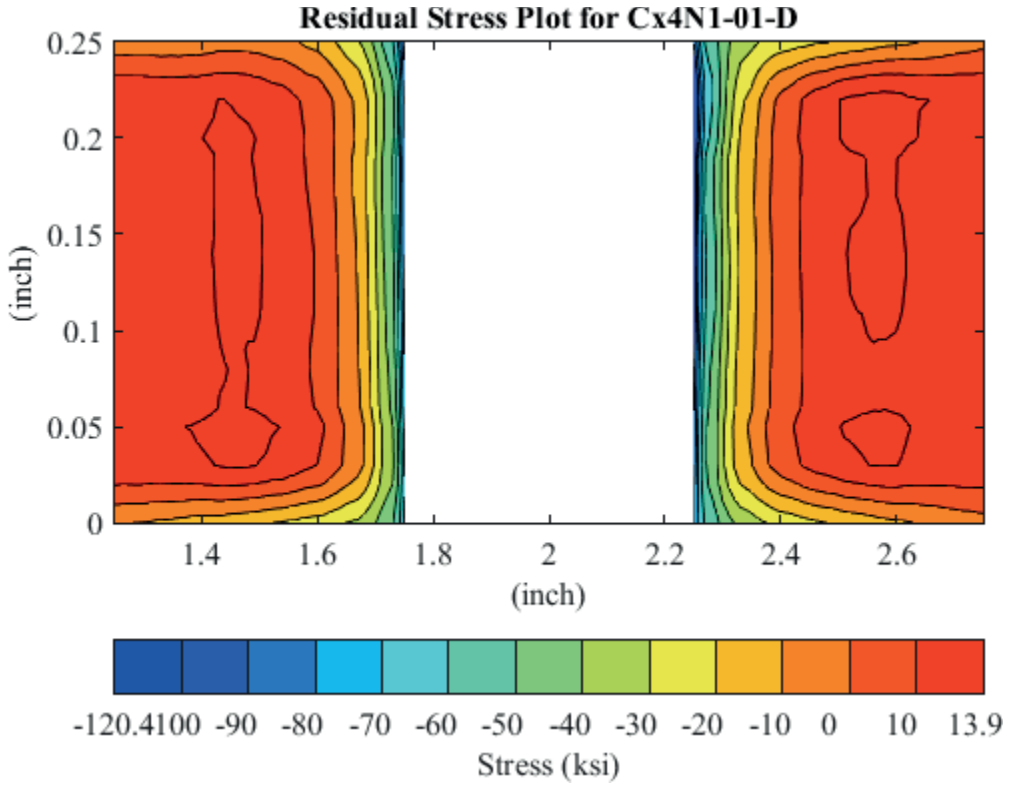

Fig. 385 Residual Stress Contour Plot of Coupon Cx4N1-01-D (7075-T651) – Mandrel Entrance Surface at Y=0, 0.0793 inch Fatigue Crack on Left Side of Hole on Mandrel Entrance Surface – Zoomed in Next to Hole.

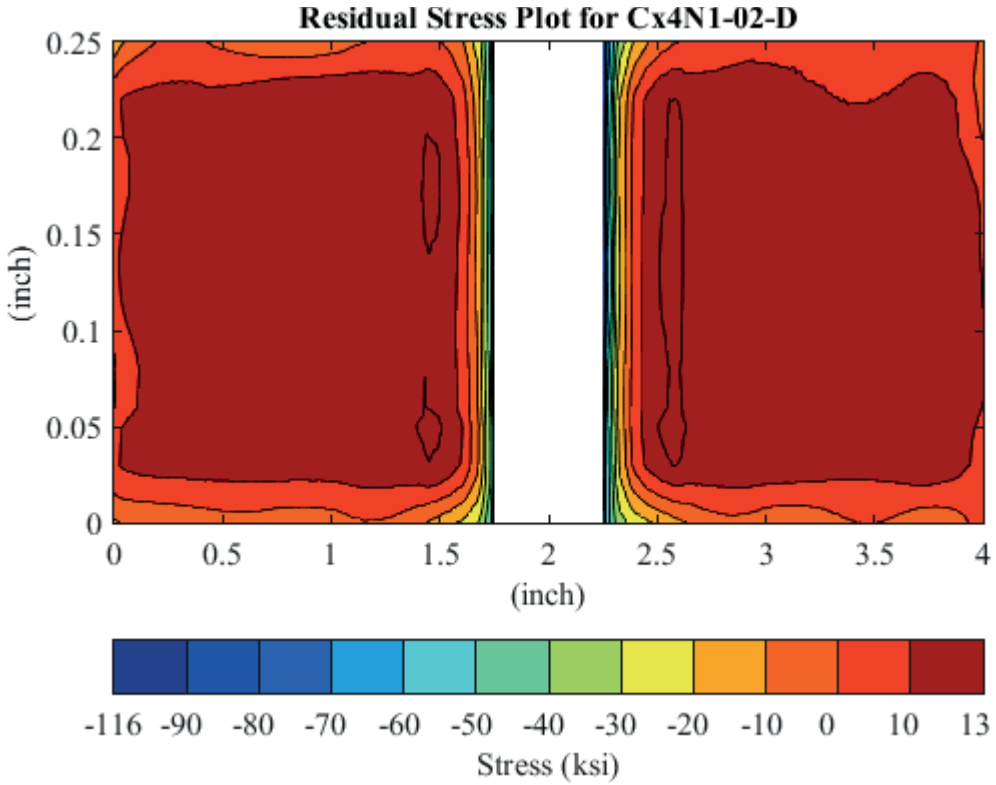

Fig. 386 Residual Stress Contour Plot of Coupon Cx4N1-02-D (7075-T651) – Mandrel Entrance Surface at Y=0, 0.0807 inch Fatigue Crack on Left Side of Hole on Mandrel Entrance Surface.

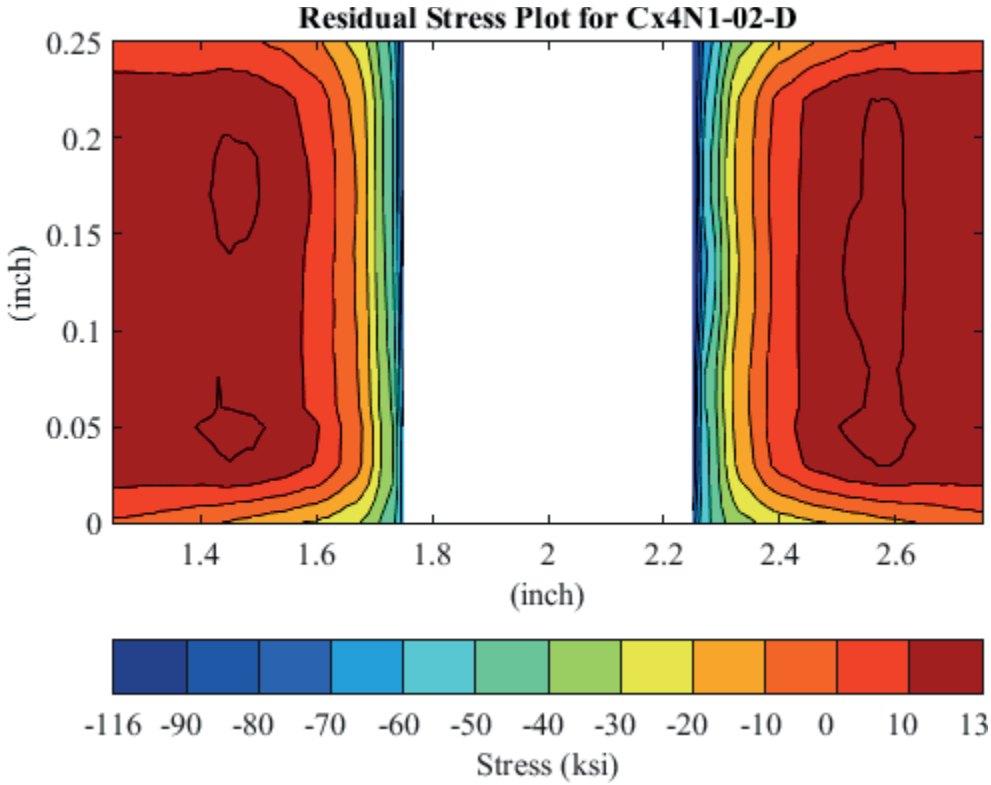

Fig. 387 Residual Stress Contour Plot of Coupon Cx4N1-02-D (7075-T651) – Mandrel Entrance Surface at Y=0, 0.0807 inch Fatigue Crack on Left Side of Hole on Mandrel Entrance Surface – Zoomed in Next to Hole.

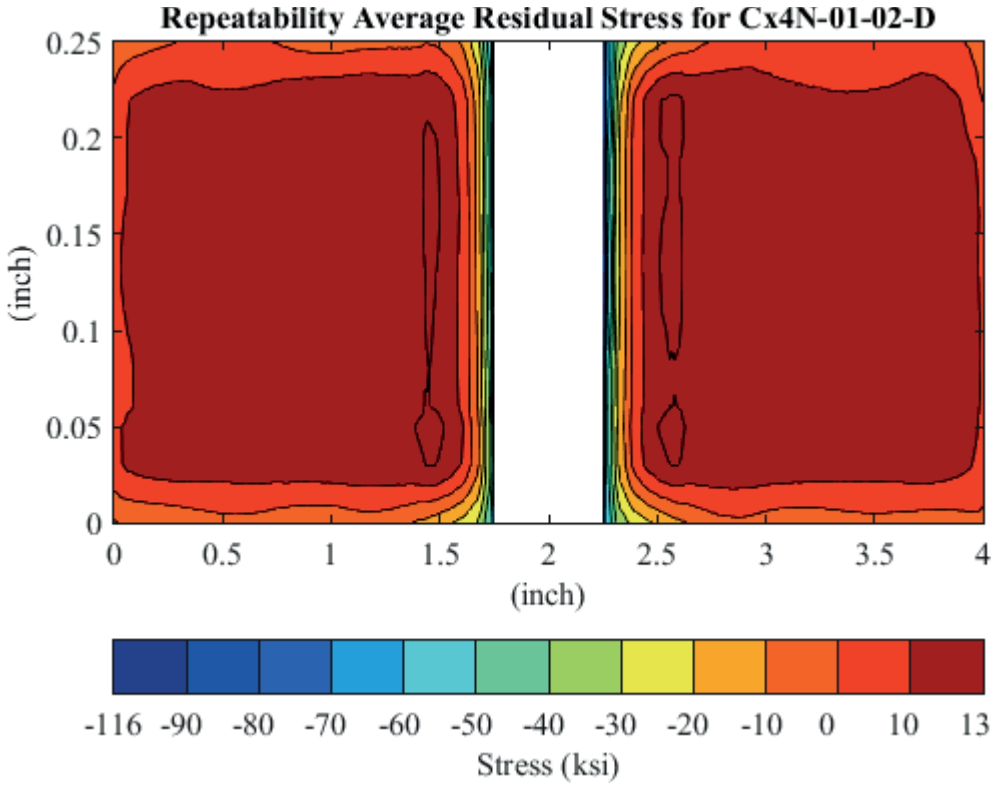

Fig. 388 Average Residual Stress Contour Plot of Coupons Cx4N1-01-D and Cx4N1-02-D (7075-T651) – Mandrel Entrance Surface at Y=0, 0.080 inch Fatigue Crack on Left Side of Hole on Mandrel Entrance Surface.

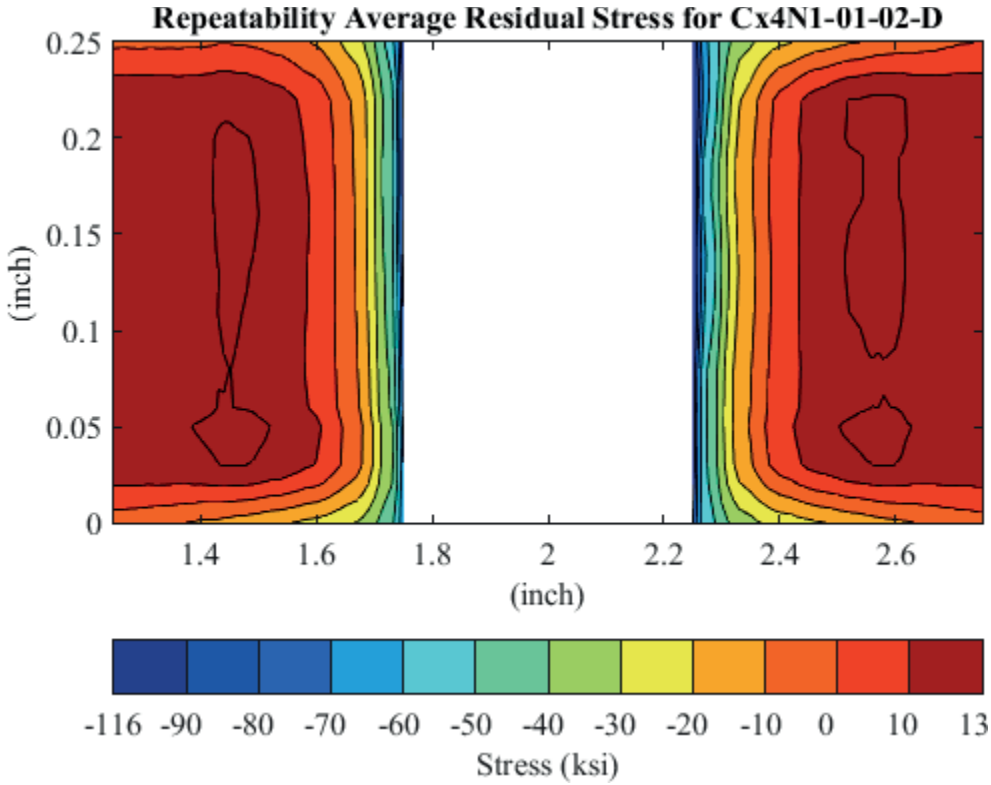

Fig. 389 Average Residual Stress Contour Plot of Coupons Cx4N1-01-D and Cx4N1-02-D (7075-T651) – Mandrel Entrance Surface at Y=0, 0.080 inch Fatigue Crack on Left Side of Hole on Mandrel Entrance Surface – Zoomed in Next to Hole.

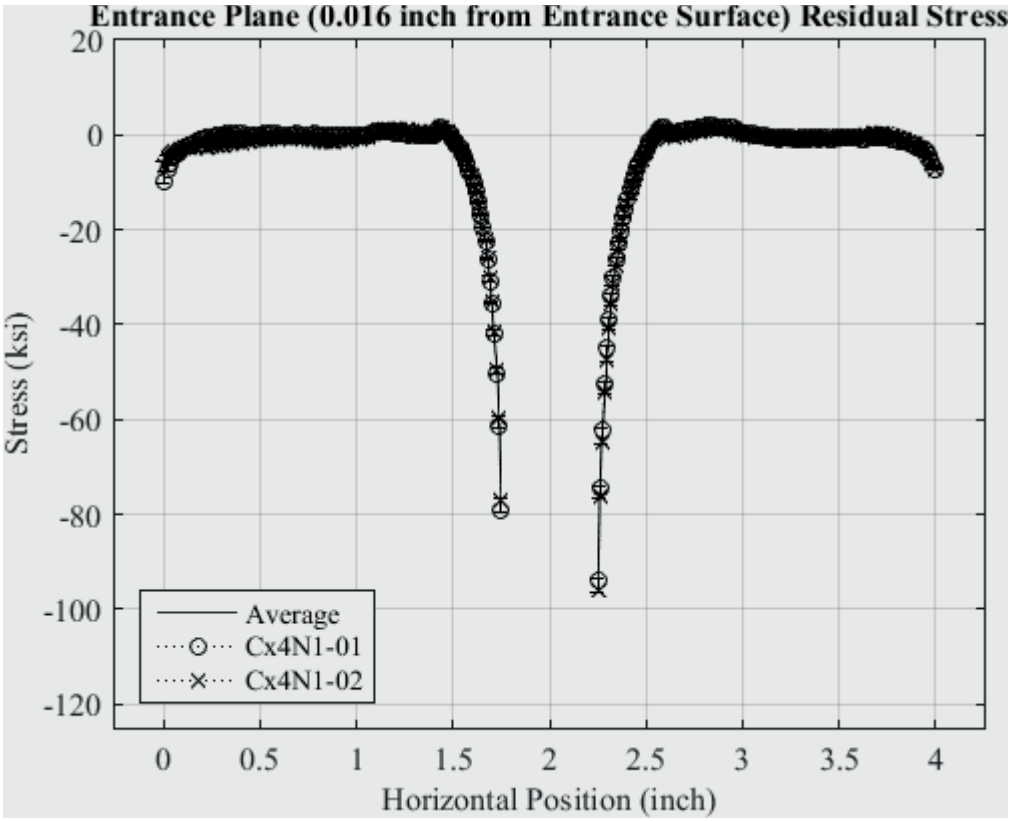

Fig. 390 Residual Stress Line Plot of Cx4N1-01-D and Cx4N1-02-D (7075-T651) at a Distance of 0.016 inch (Entrance Surface) from the Entrance Surface – Coupons had a 0.08 inch Fatigue Crack at the Left Entrance Surface.

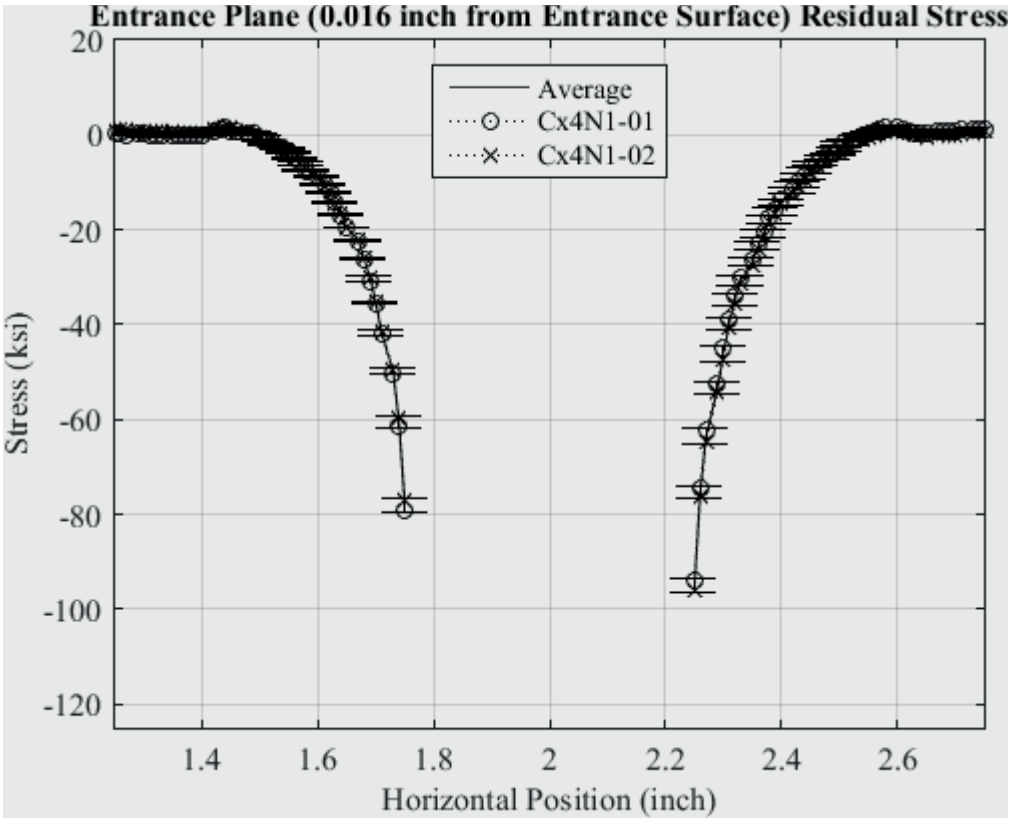

Fig. 391 Residual Stress Line Plot of Cx4N1-01-D and Cx4N1-02-D (7075-T651) at a Distance of 0.016 inch (Entrance Surface) from the Entrance Surface – Coupons had a 0.08 inch Fatigue Crack at the Left Entrance Surface – Zoomed in Next to Hole.

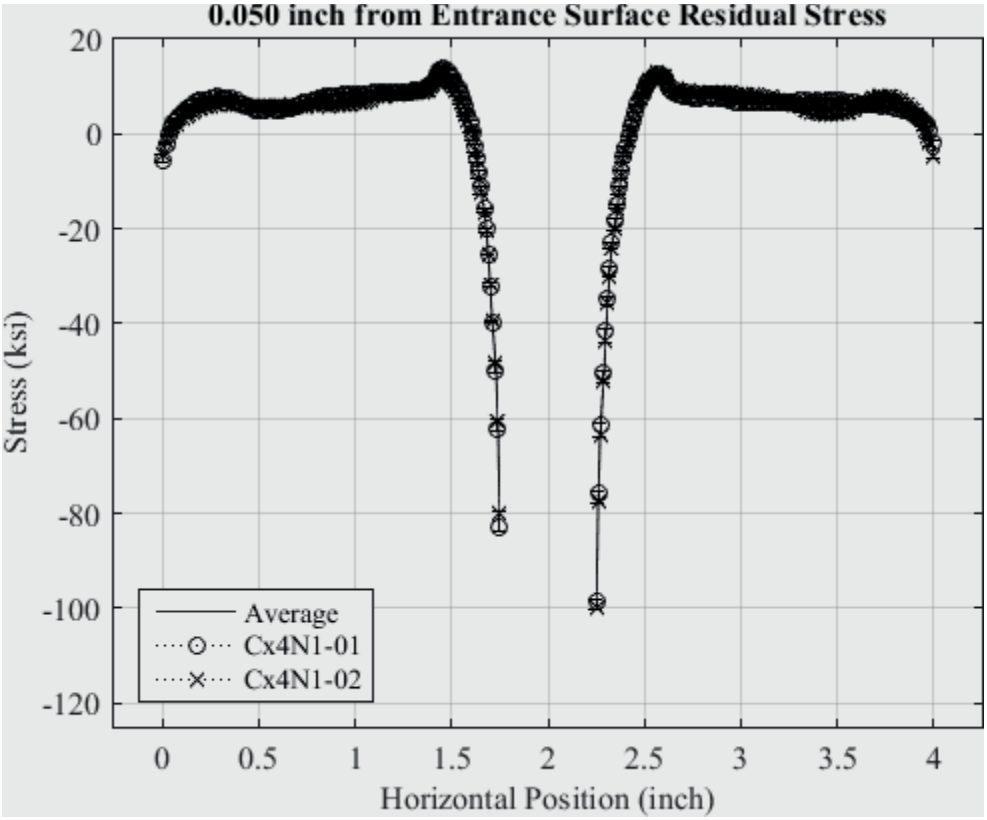

Fig. 392 Residual Stress Line Plot of Cx4N1-01-D and Cx4N1-02-D (7075-T651) at a Distance of 0.05 inch (Entrance Surface) from the Entrance Surface – Coupons had a 0.08 inch Fatigue Crack at the Left Entrance Surface.

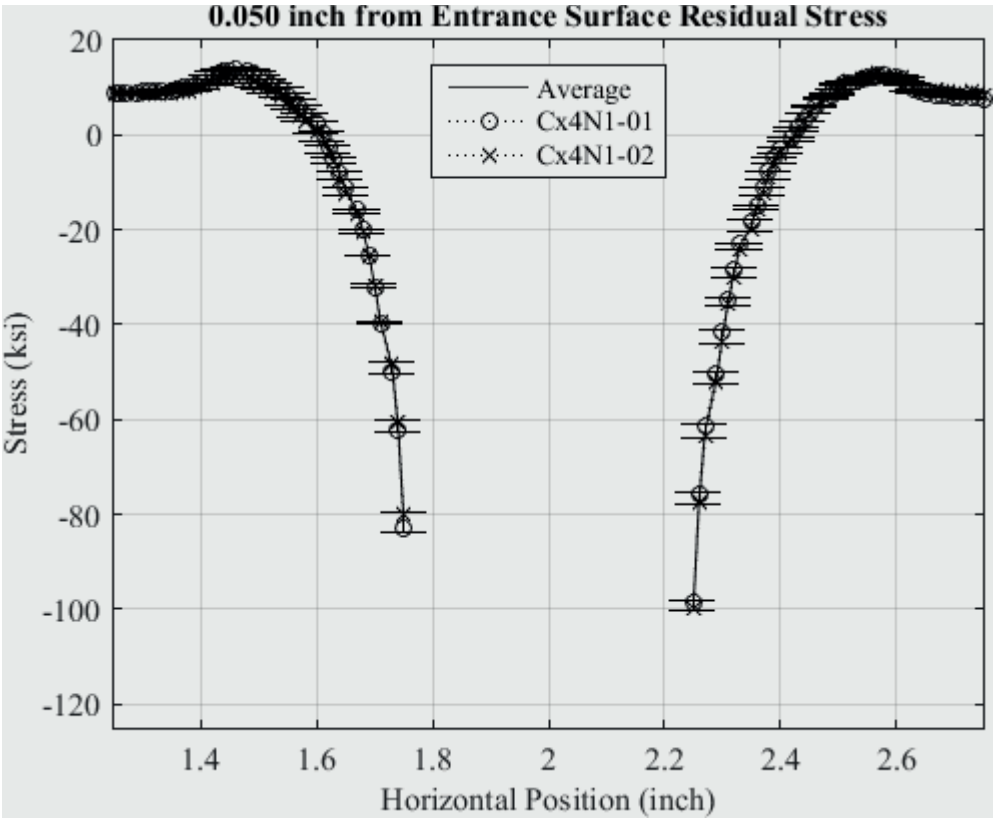

Fig. 393 Residual Stress Line Plot of Cx4N1-01-D and Cx4N1-02-D (7075-T651) at a Distance of 0.05 inch (Entrance Surface) from the Entrance Surface – Coupons had a 0.08 inch Fatigue Crack at the Left Entrance Surface – Zoomed in Next to Hole.

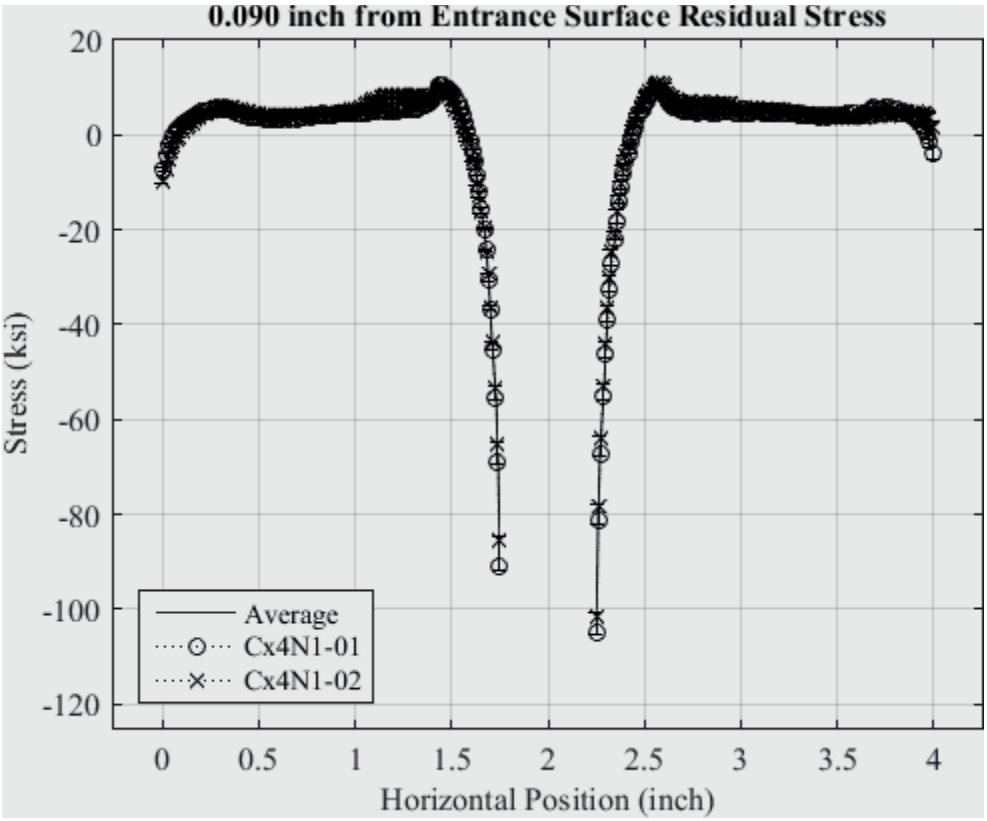

Fig. 394 Residual Stress Line Plot of Cx4N1-01-D and Cx4N1-02-D (7075-T651) at a Distance of 0.09 inch from the Entrance Surface – Coupons had a 0.08 inch Fatigue Crack at the Left Entrance Surface.

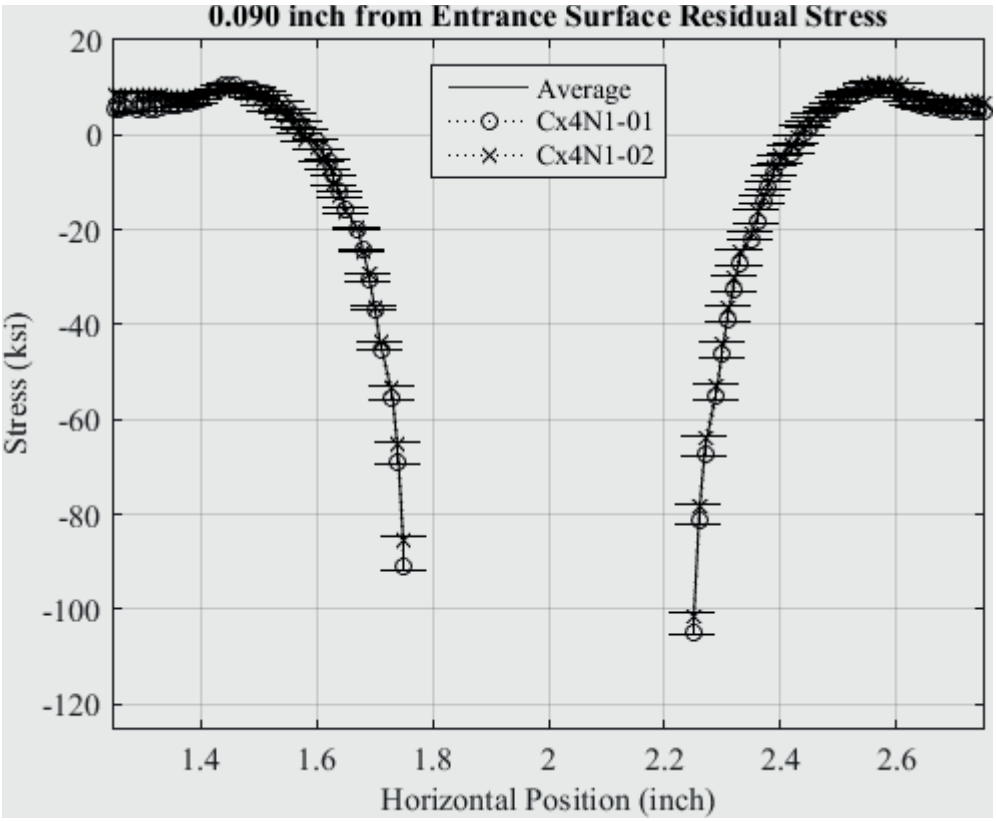

Fig. 395 Residual Stress Line Plot of Cx4N1-01-D and Cx4N1-02-D (7075-T651) at a Distance of 0.09 inch from the Entrance Surface – Coupons had a 0.08 inch Fatigue Crack at the Left Entrance Surface – Zoomed in Next to Hole.

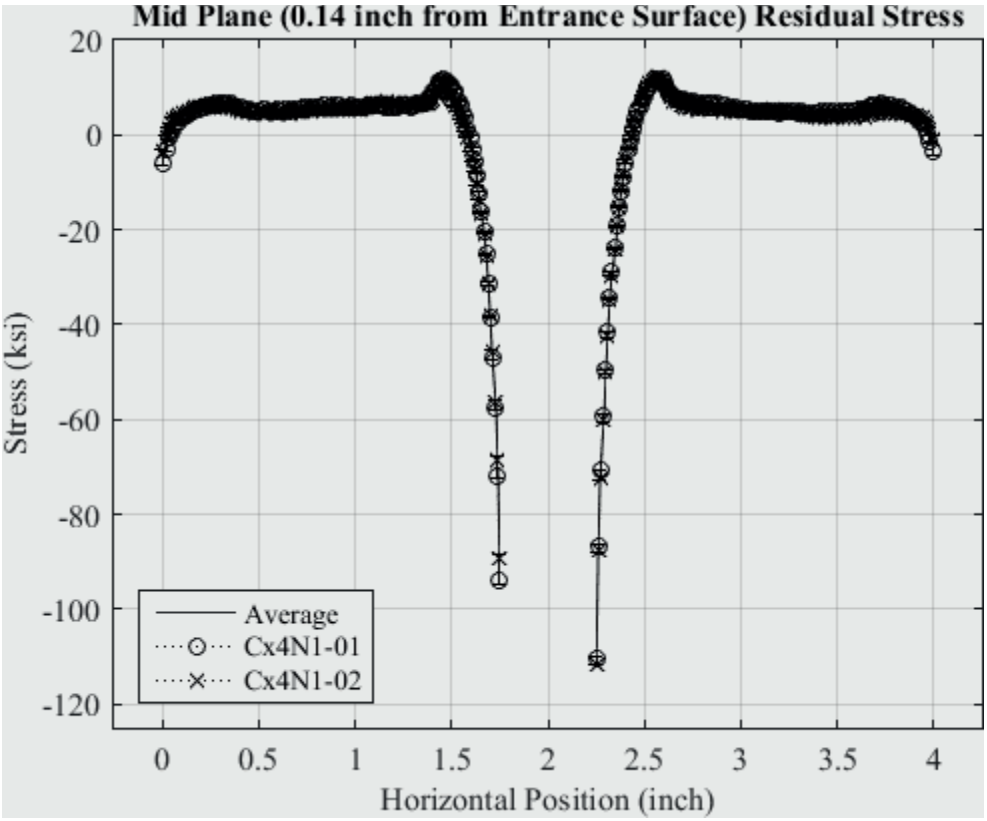

Fig. 396 Residual Stress Line Plot of Cx4N1-01-D and Cx4N1-02-D (7075-T651) at a Distance of 0.140 inch (Mid Plane Surface) from the Entrance Surface – Coupons had a 0.08 inch Fatigue Crack at the Left Entrance Surface

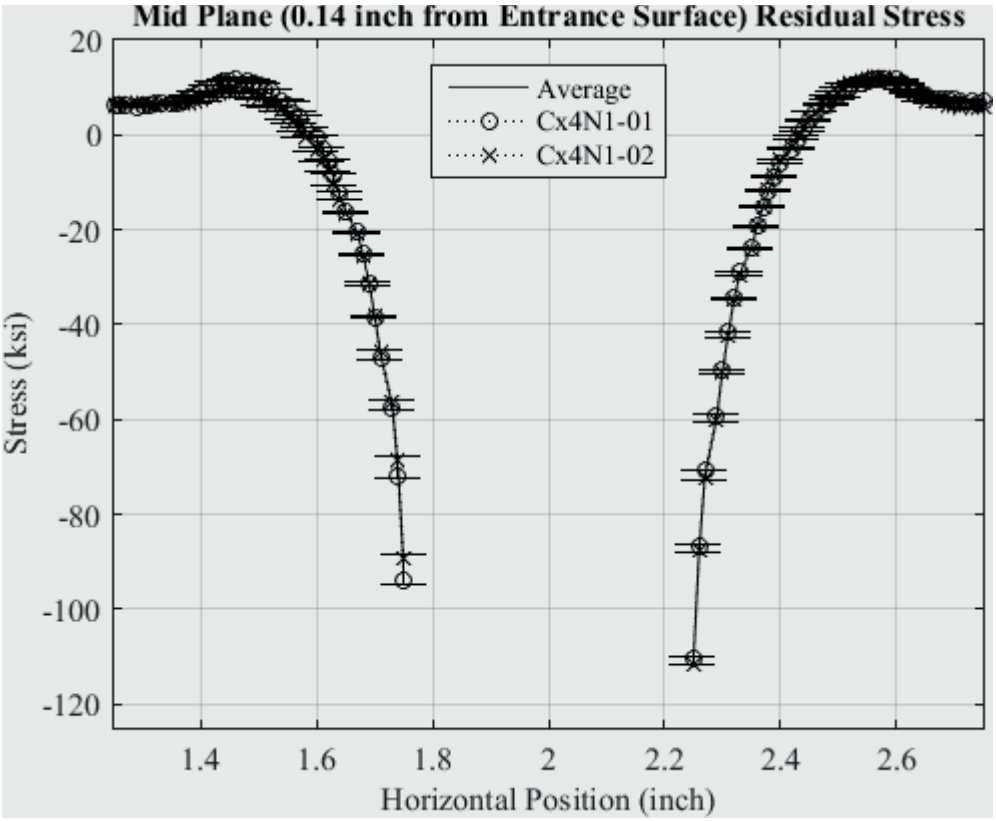

Fig. 397 Residual Stress Line Plot of Cx4N1-01-D and Cx4N1-02-D (7075-T651) at a Distance of 0.140 inch (Mid Plane Surface) from the Entrance Surface – Coupons had a 0.08 inch Fatigue Crack at the Left Entrance Surface – Zoomed in Next to Hole

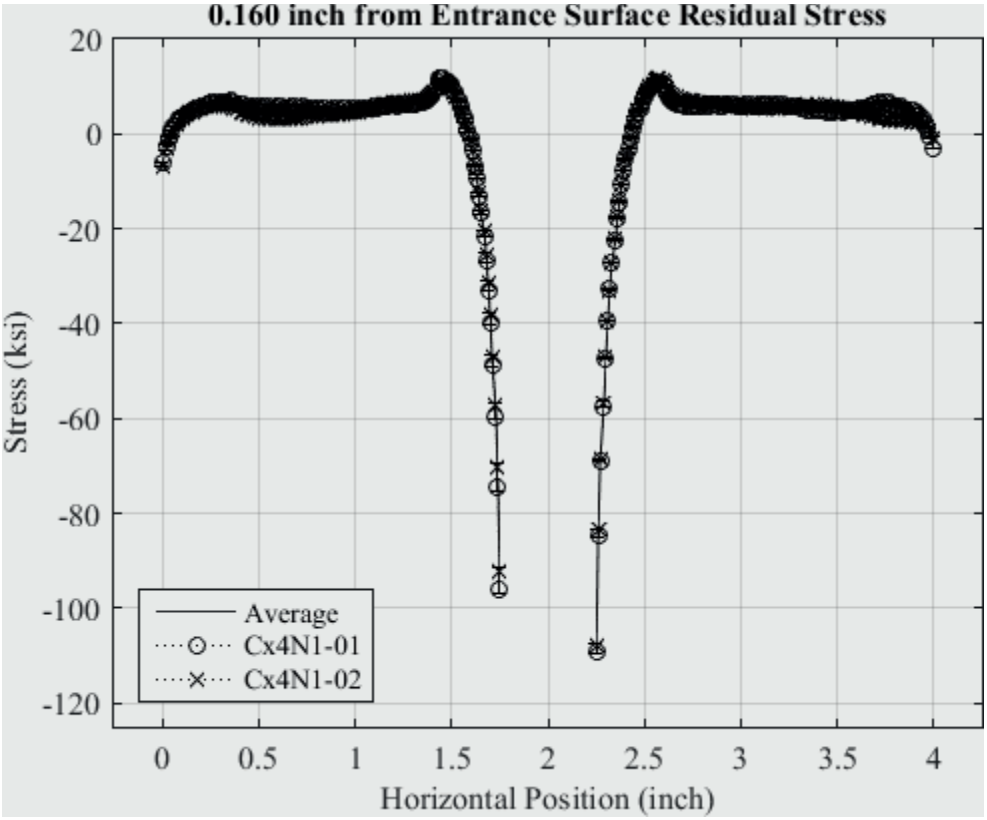

Fig. 398 Residual Stress Line Plot of Cx4N1-01-D and Cx4N1-02-D (7075-T651) at a Distance of 0.160 inch from the Entrance Surface – Coupons had a 0.08 inch Fatigue Crack at the Left Entrance Surface

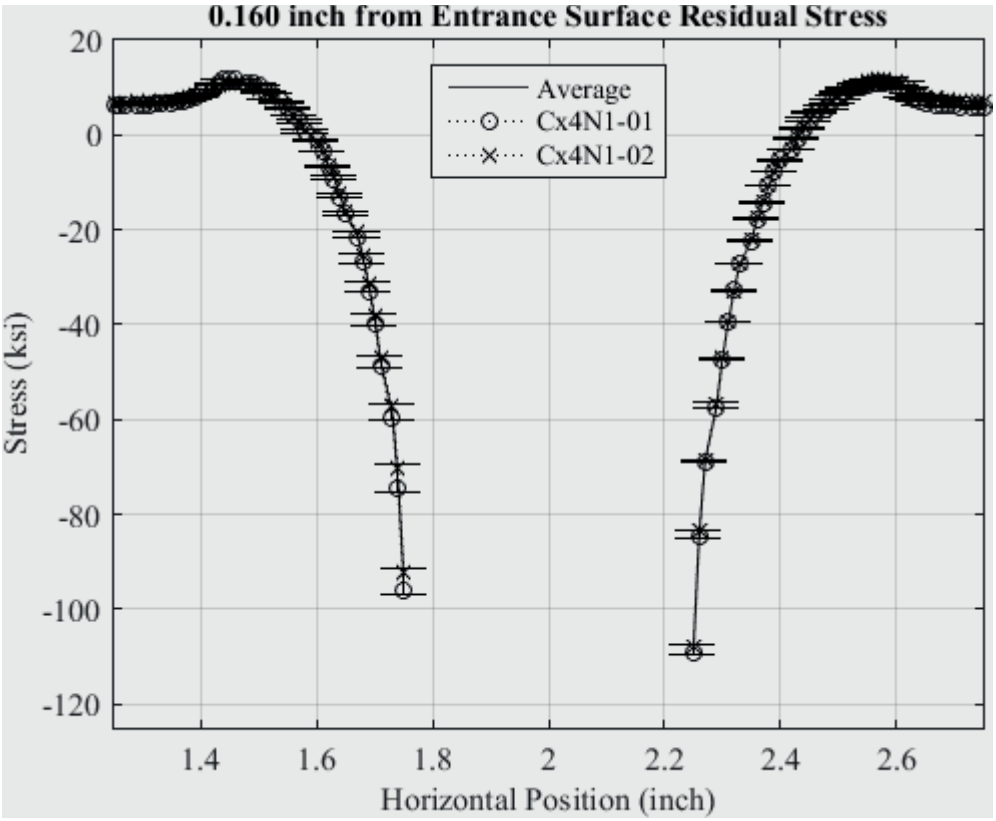

Fig. 399 Residual Stress Line Plot of Cx4N1-01-D and Cx4N1-02-D (7075-T651) at a Distance of 0.160 inch from the Entrance Surface – Coupons had a 0.08 inch Fatigue Crack at the Left Entrance Surface – Zoomed in Next to Hole.

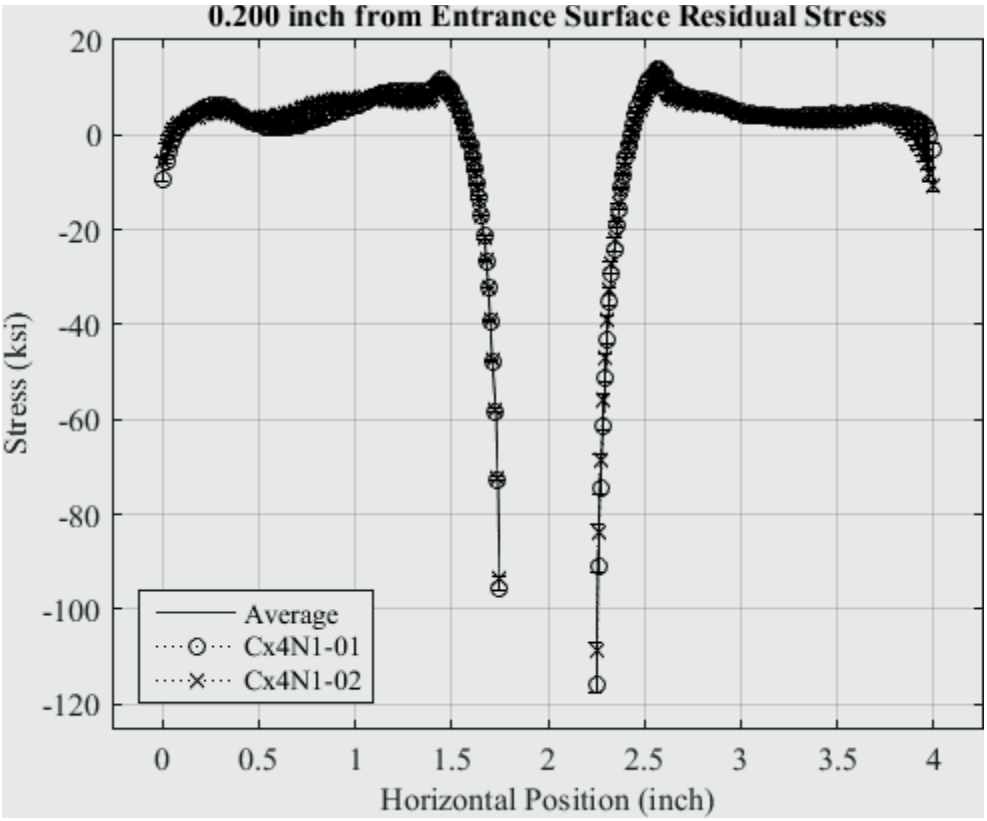

Fig. 400 Residual Stress Line Plot of Cx4N1-01-D and Cx4N1-02-D (7075-T651) at a Distance of 0.200 inch from the Entrance Surface – Coupons had a 0.08 inch Fatigue Crack at the Left Entrance Surface.

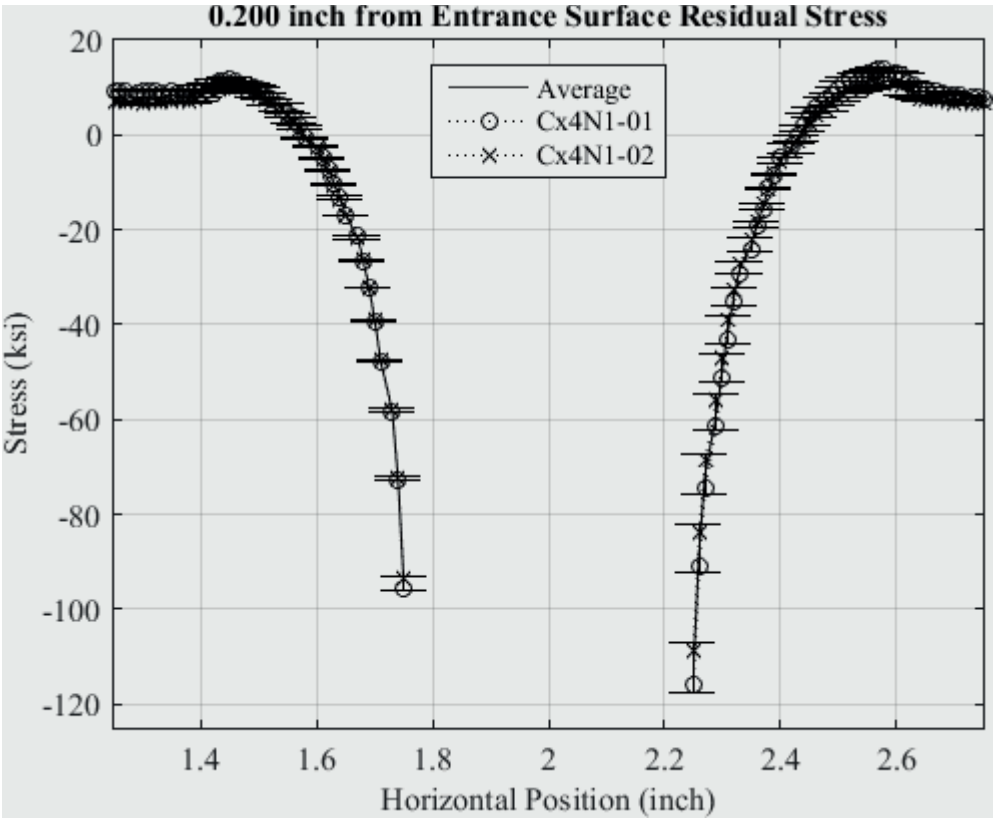

Fig. 401 Residual Stress Line Plot of Cx4N1-01-D and Cx4N1-02-D (7075-T651) at a Distance of 0.200 inch from the Entrance Surface – Coupons had a 0.08 inch Fatigue Crack at the Left Entrance Surface – Zoomed in Next to Hole.

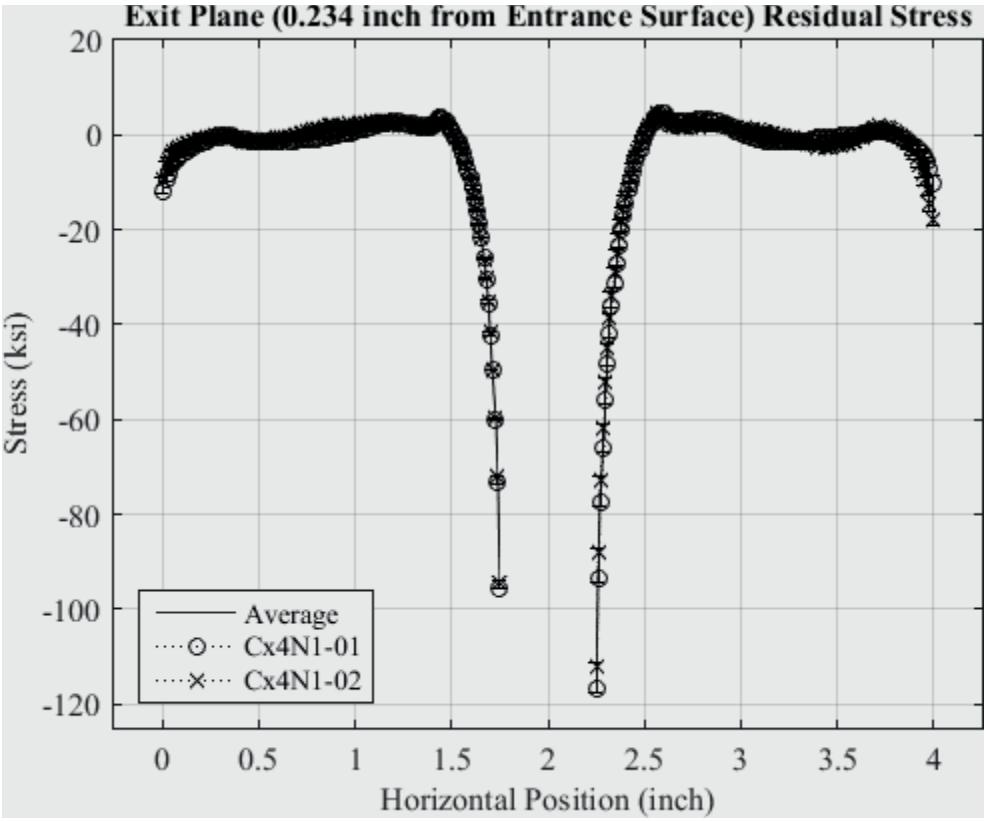

Fig. 402 Residual Stress Line Plot of Cx4N1-01-D and Cx4N1-02-D (7075-T651) at a Distance of 0.234 inch (Exit Surface) from the Entrance Surface – Coupons had a 0.08 inch Fatigue Crack at the Left Entrance Surface.

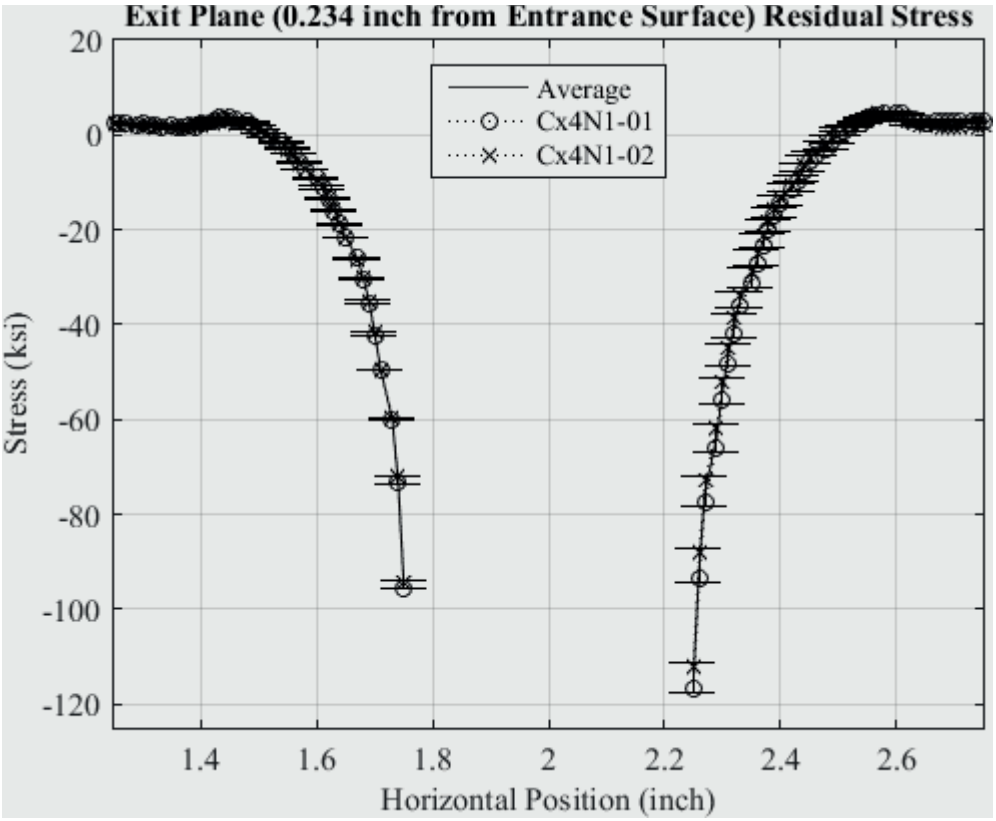

Fig. 403 Residual Stress Line Plot of Cx4N1-01-D and Cx4N1-02-D (7075-T651) at a Distance of 0.234 inch (Exit Surface) from the Entrance Surface – Coupons had a 0.08 inch Fatigue Crack at the Left Entrance Surface – Zoomed in Next to Hole.

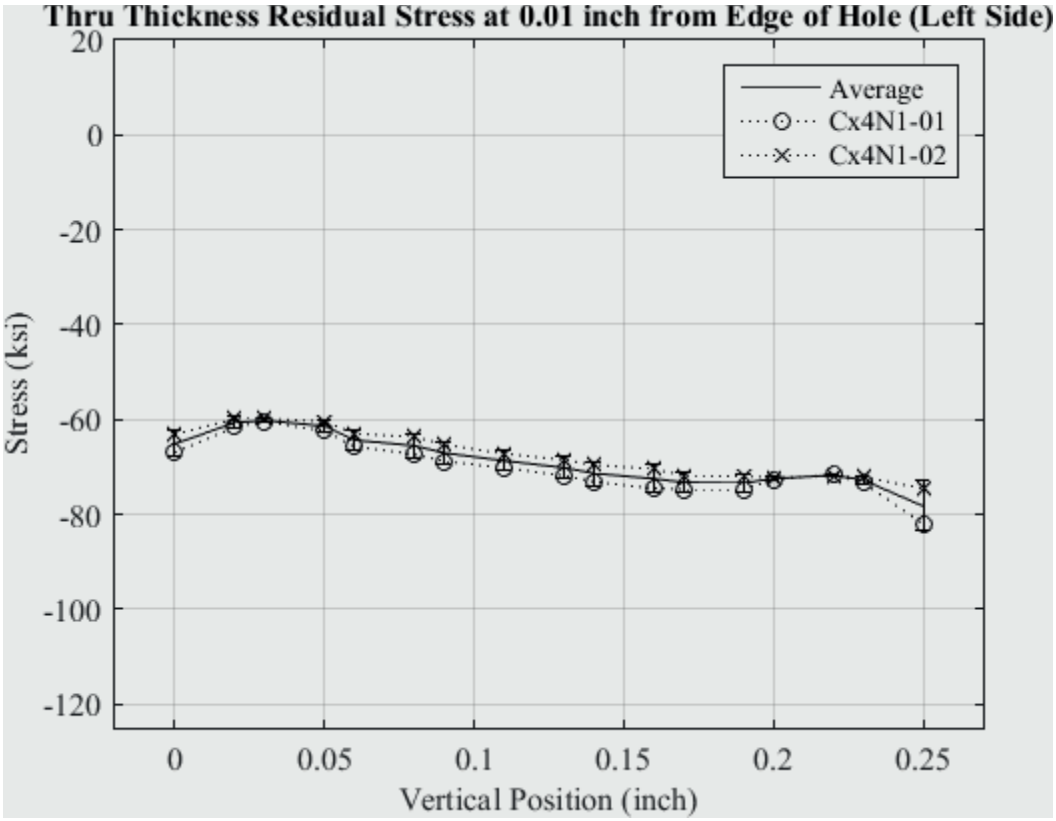

Fig. 404 Residual Stress Line Plot of Cx4N1-01-D and Cx4N1-02-D (7075-T651) Through the Thickness at 0.01 inch from Left Side of Hole – Coupons had a 0.08 inch Fatigue Crack at the Left Entrance Surface.

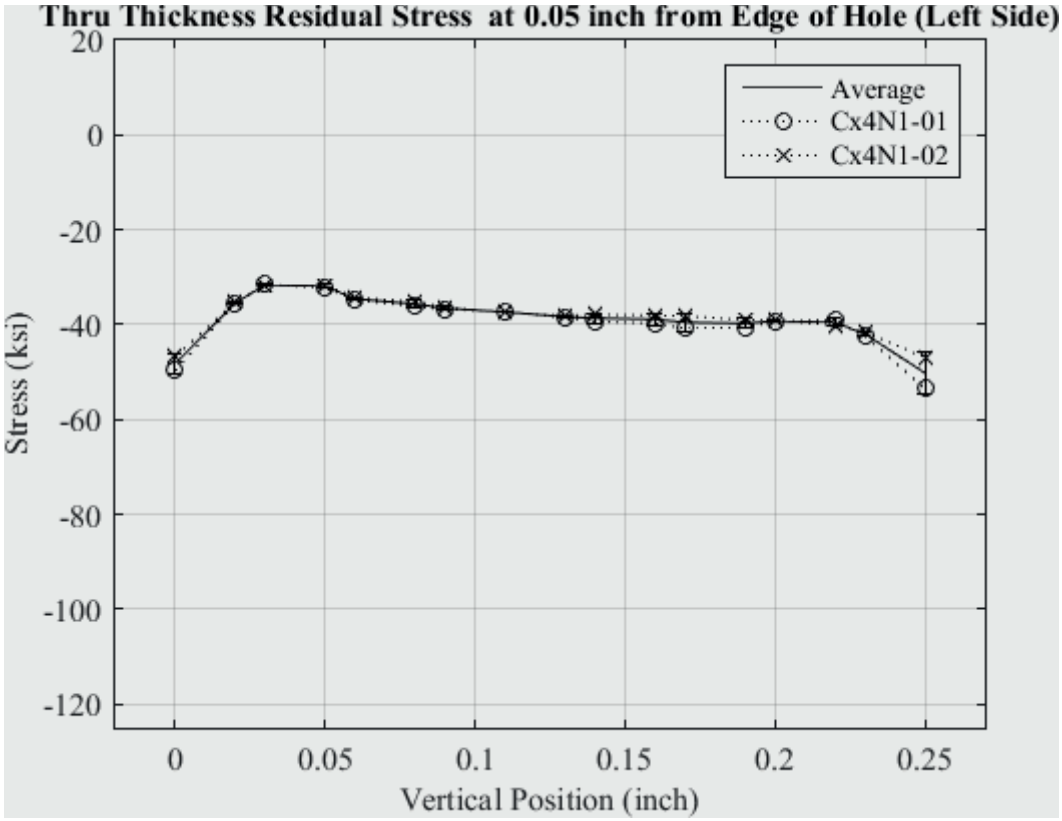

Fig. 405 Residual Stress Line Plot of Cx4N1-01-D and Cx4N1-02-D (7075-T651) Through the Thickness at 0.05 inch from Left Side of Hole – Coupons had a 0.08 inch Fatigue Crack at the Left Entrance Surface.

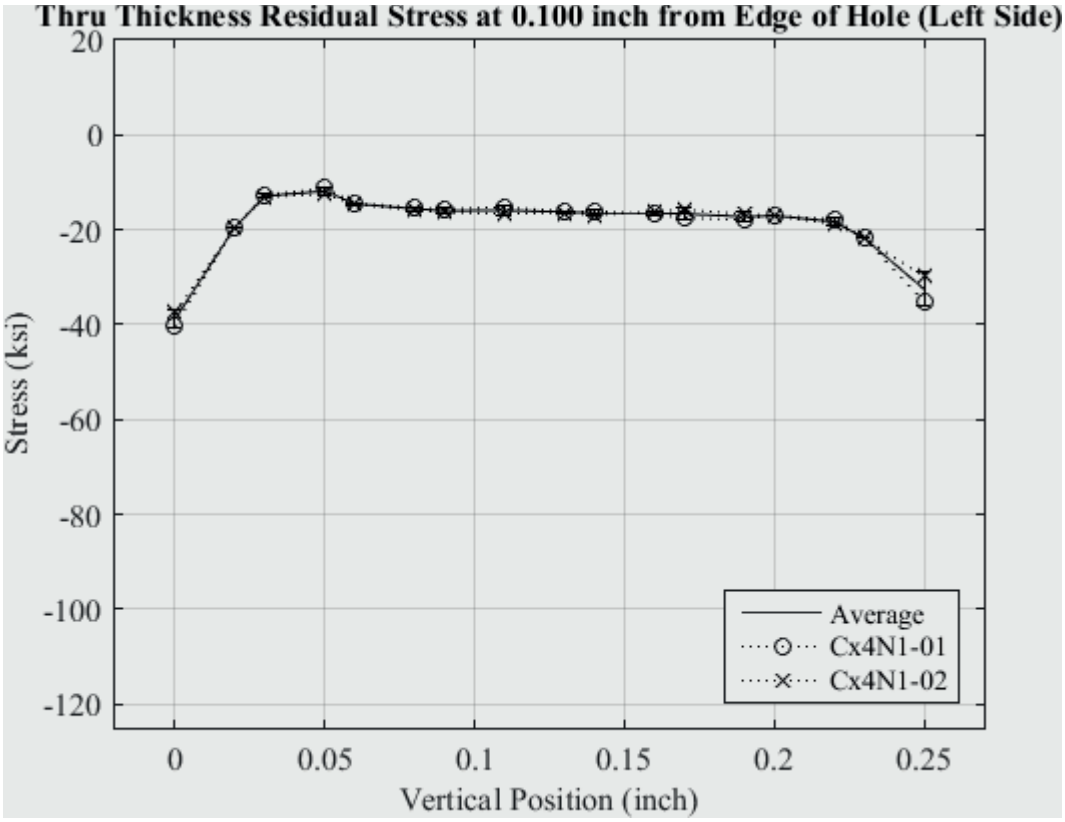

Fig. 406 Residual Stress Line Plot of Cx4N1-01-D and Cx4N1-02-D (7075-T651) Through the Thickness at 0.10 inch from Left Side of Hole – Coupons had a 0.08 inch Fatigue Crack at the Left Entrance Surface.

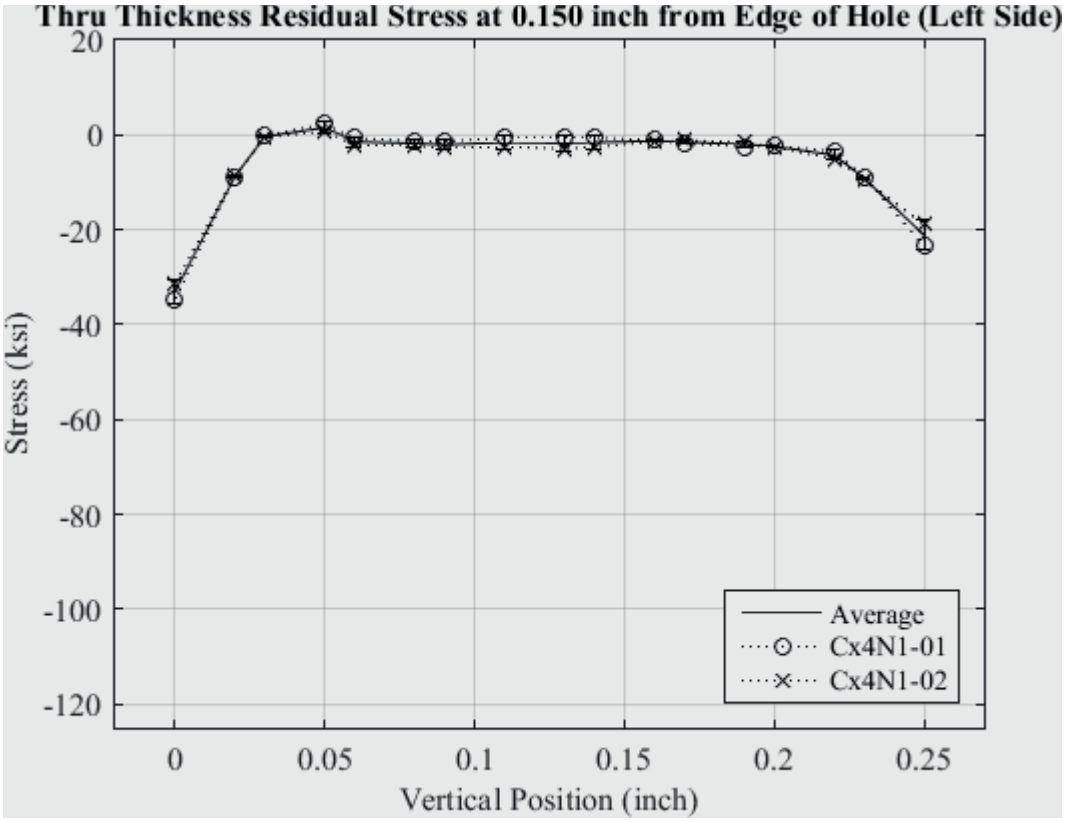

Fig. 407 Residual Stress Line Plot of Cx4N1-01-D and Cx4N1-02-D (7075-T651) Through the Thickness at 0.150 inch from Left Side of Hole – Coupons had a 0.08 inch Fatigue Crack at the Left Entrance Surface.

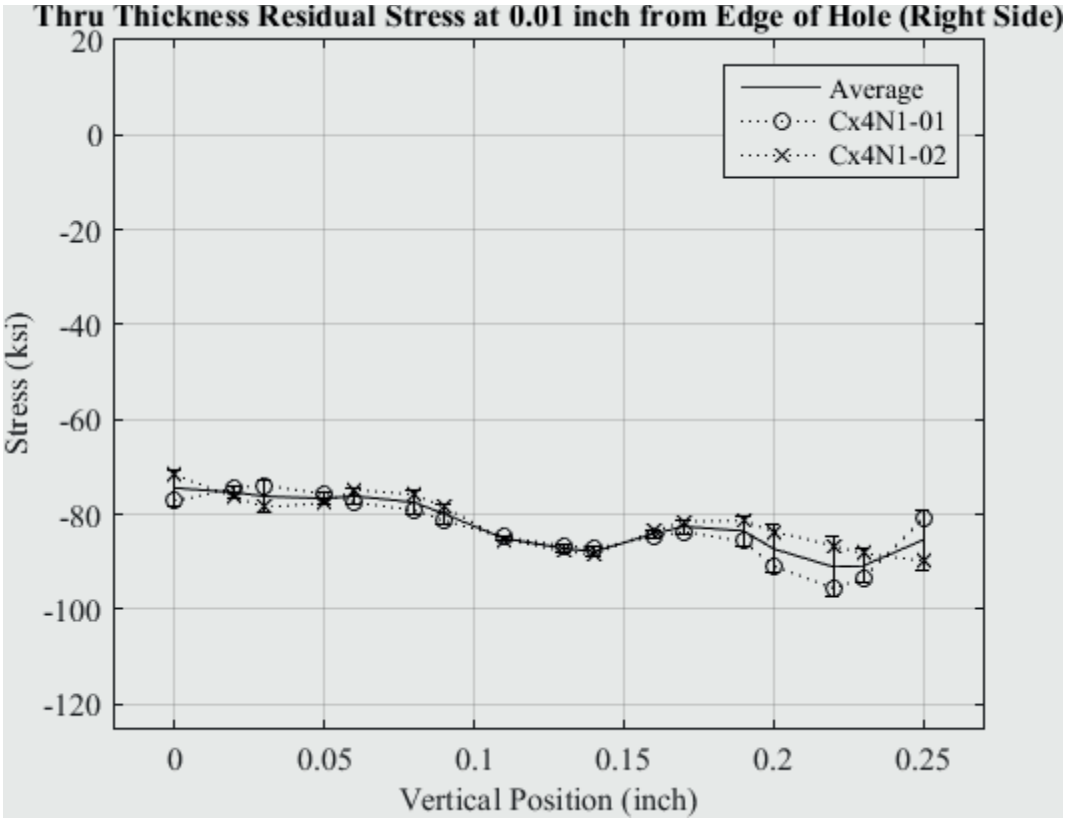

Fig. 408 Residual Stress Line Plot of Cx4N1-01-D and Cx4N1-02-D (7075-T651) Through the Thickness at 0.01 inch from Right Side of Hole – Coupons had a 0.08 inch Fatigue Crack at the Left Entrance Surface.

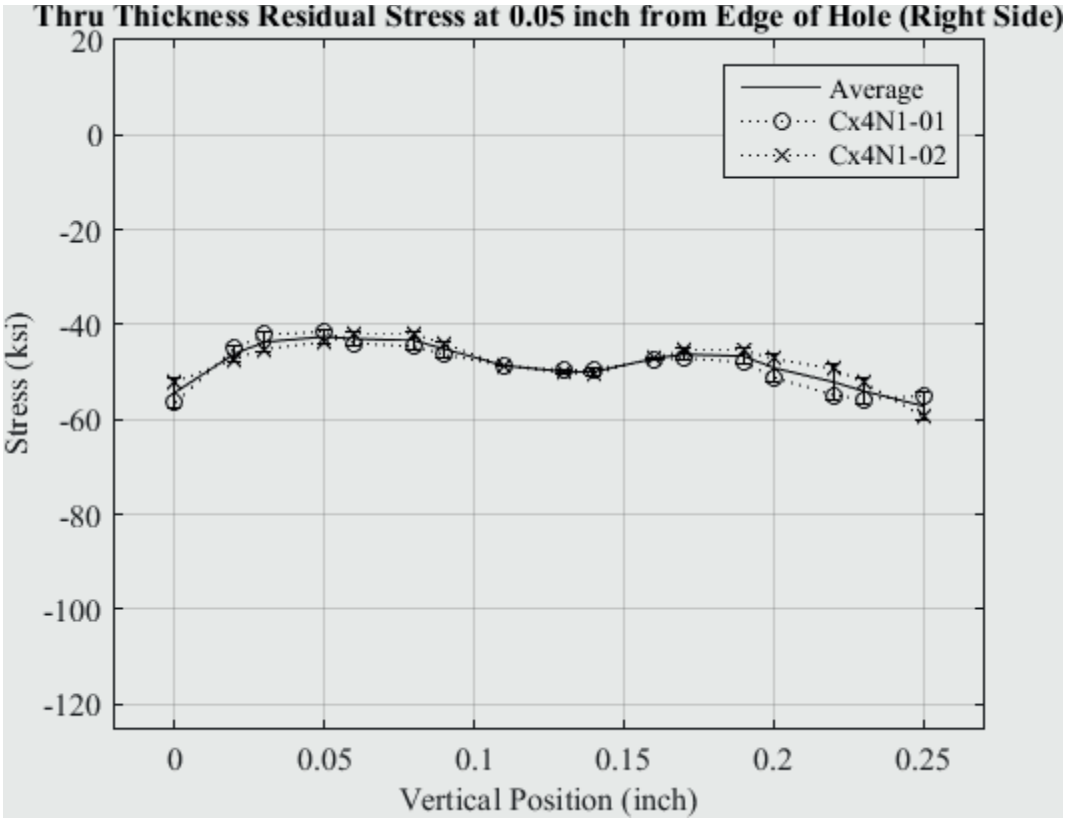

Fig. 409 Residual Stress Line Plot of Cx4N1-01-D and Cx4N1-02-D (7075-T651) Through the Thickness at 0.05 inch from Right Side of Hole – Coupons had a 0.08 inch Fatigue Crack at the Left Entrance Surface.

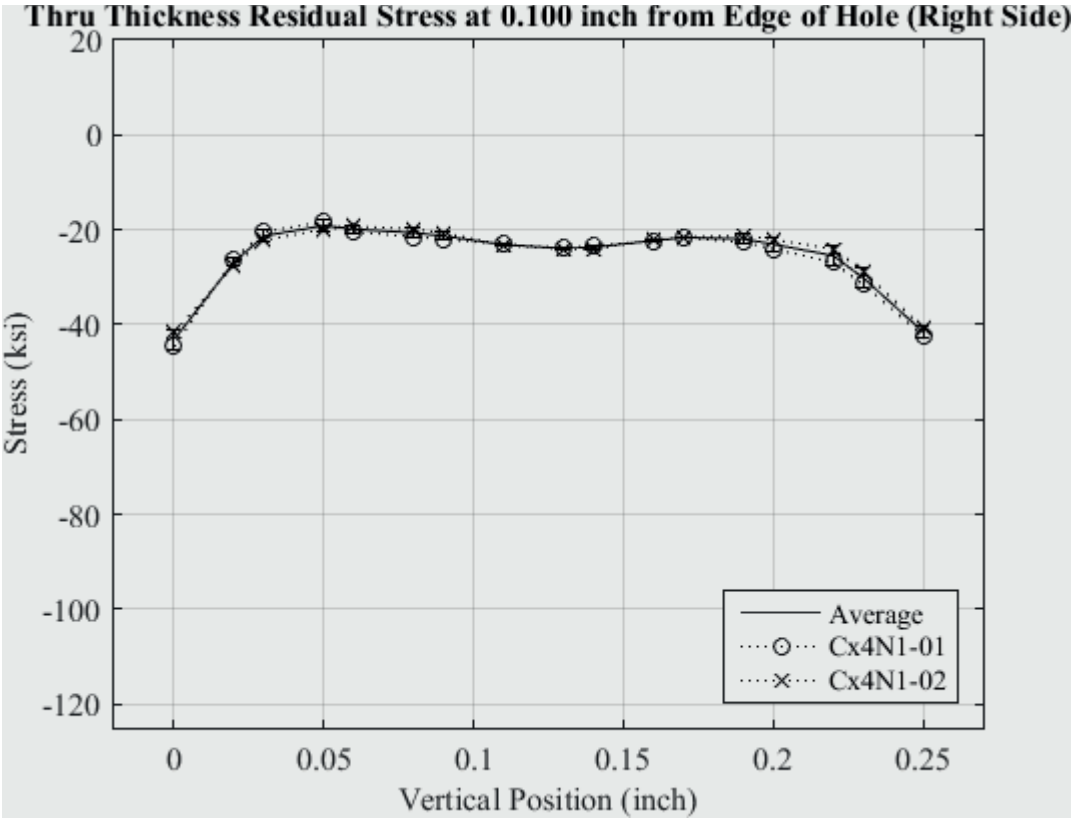

Fig. 410 Residual Stress Line Plot of Cx4N1-01-D and Cx4N1-02-D (7075-T651) Through the Thickness at 0.10 inch from Right Side of Hole – Coupons had a 0.08 inch Fatigue Crack at the Left Entrance Surface.

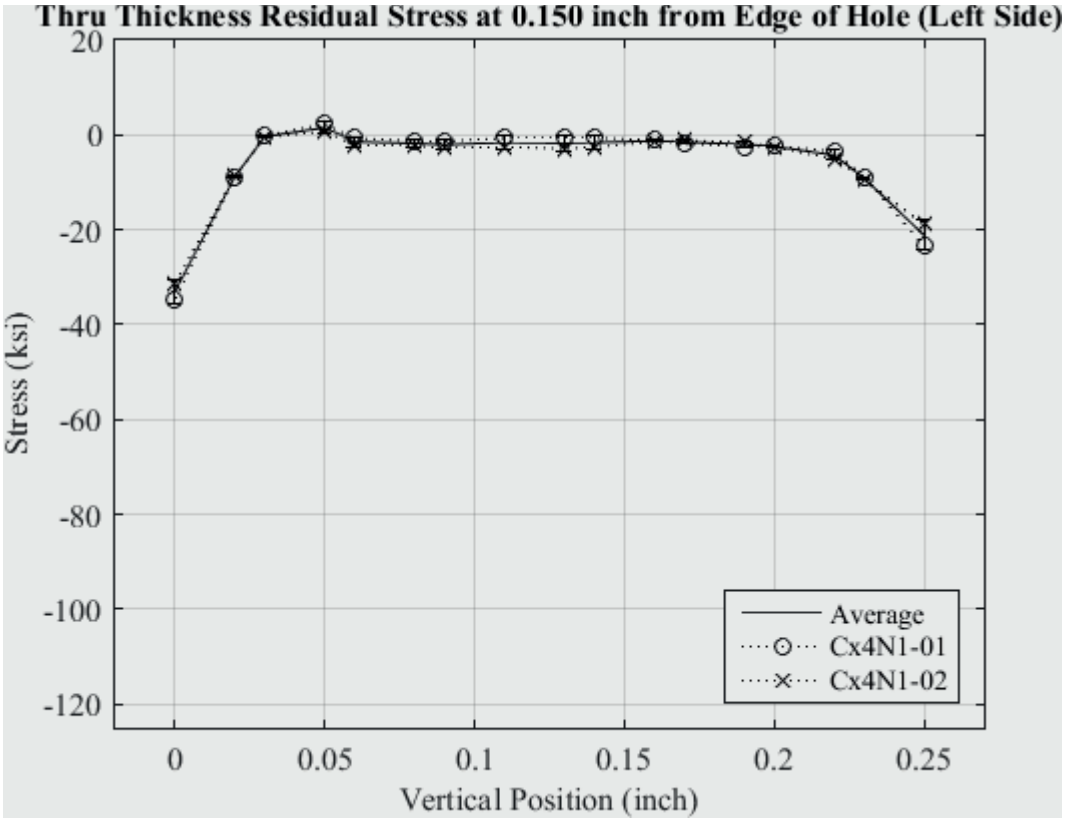

Fig. 411 Residual Stress Line Plot of Cx4N1-01-D and Cx4N1-02-D (7075-T651) Through the Thickness at 0.150 inch from Right Side of Hole – Coupons had a 0.08 inch Fatigue Crack at the Left Entrance Surface.

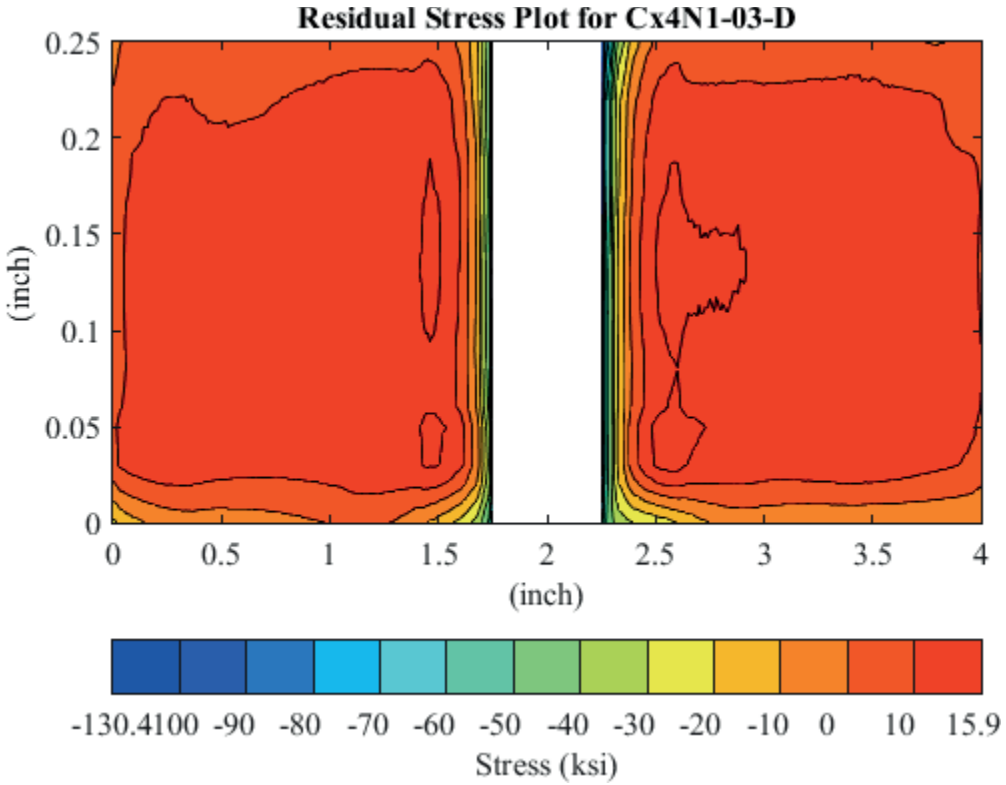

Fig. 412 Residual Stress Contour Plot of Coupon Cx4N1-03-D (7075-T651) – Mandrel Entrance Surface at Y=0, 0.0972 inch Fatigue Crack on Left Side of Hole on Mandrel Entrance Surface.

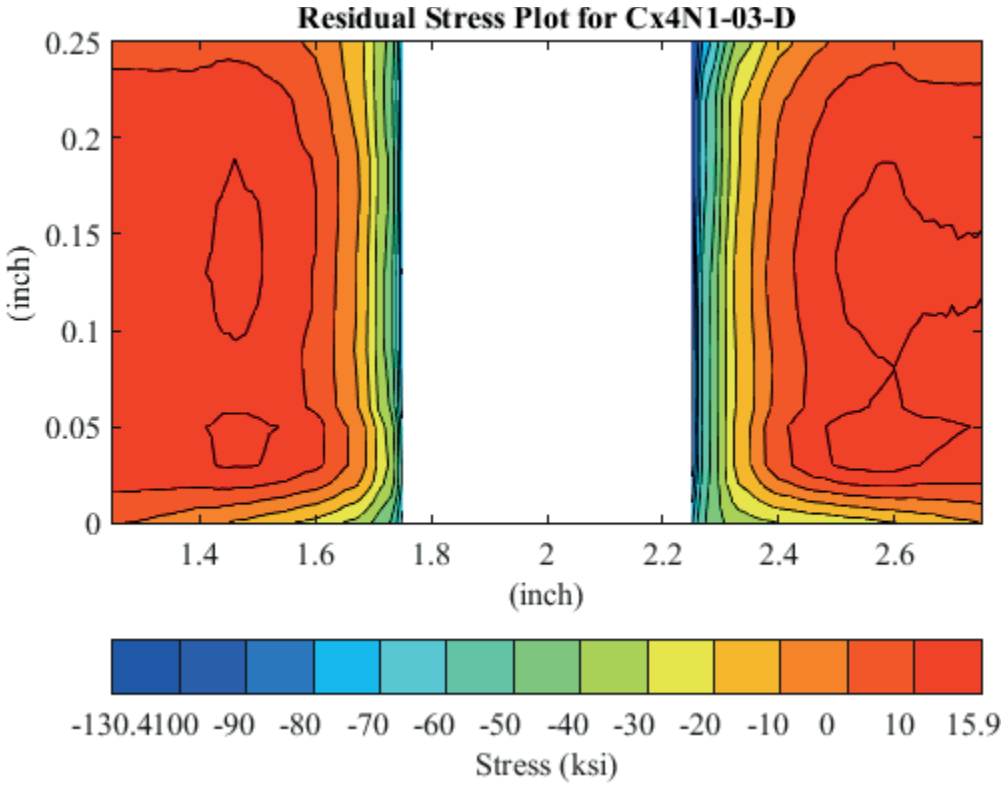

Fig. 413 Residual Stress Contour Plot of Coupon Cx4N1-03-D (7075-T651) – Mandrel Entrance Surface at Y=0, 0.0972 inch Fatigue Crack on Left Side of Hole on Mandrel Entrance Surface – Zoomed in Next to Hole.

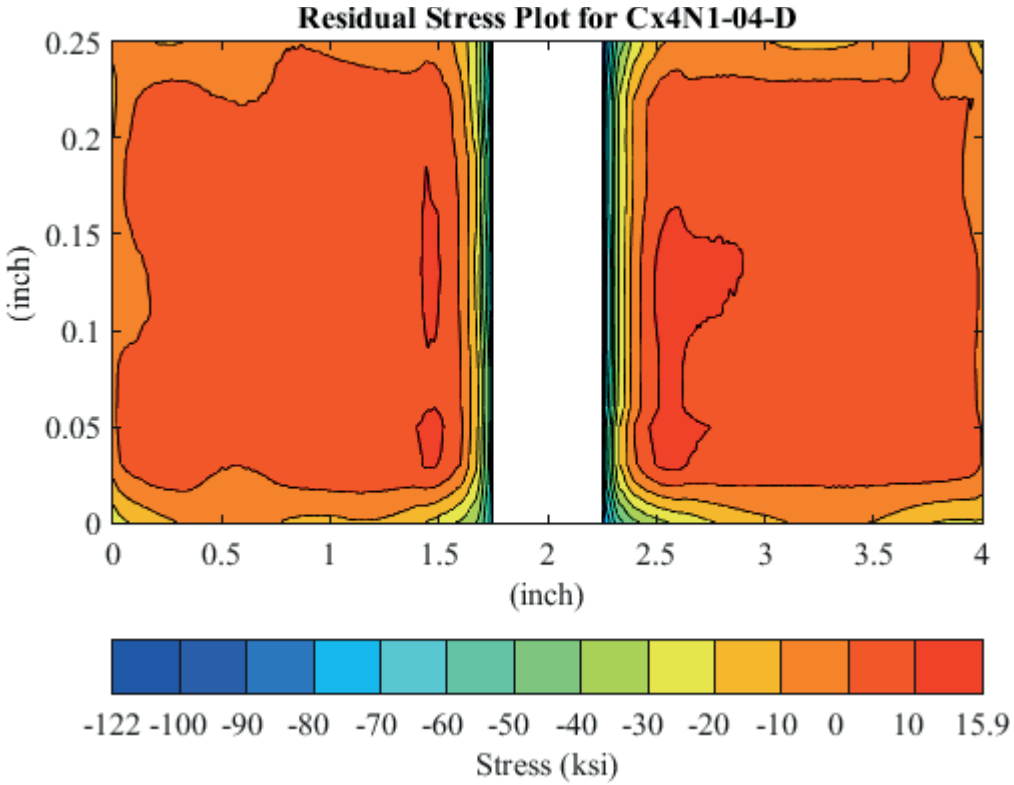

Fig. 414 Residual Stress Contour Plot of Coupon Cx4N1-04-D (7075-T651) – Mandrel Entrance Surface at Y=0, 0.1015 inch Fatigue Crack on Left Side of Hole on Mandrel Entrance Surface.

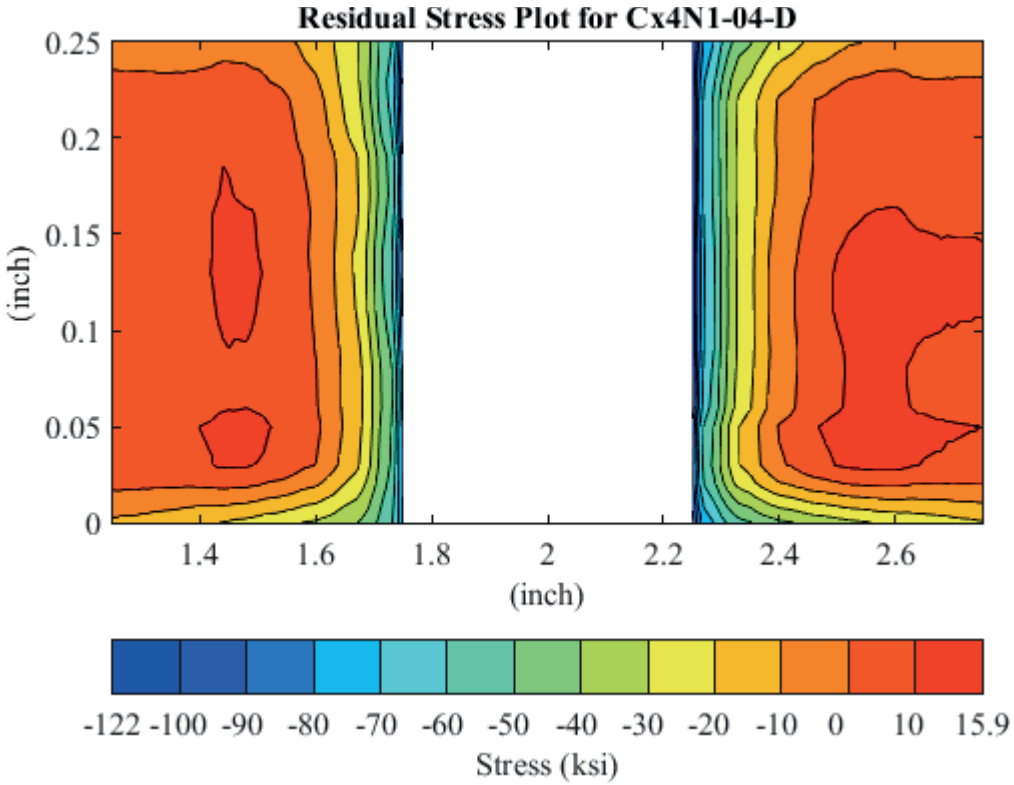

Fig. 415 Residual Stress Contour Plot of Coupon Cx4N1-04-D (7075-T651) – Mandrel Entrance Surface at Y=0, 0.1015 inch Fatigue Crack on Left Side of Hole on Mandrel Entrance Surface – Zoomed in Next to Hole.

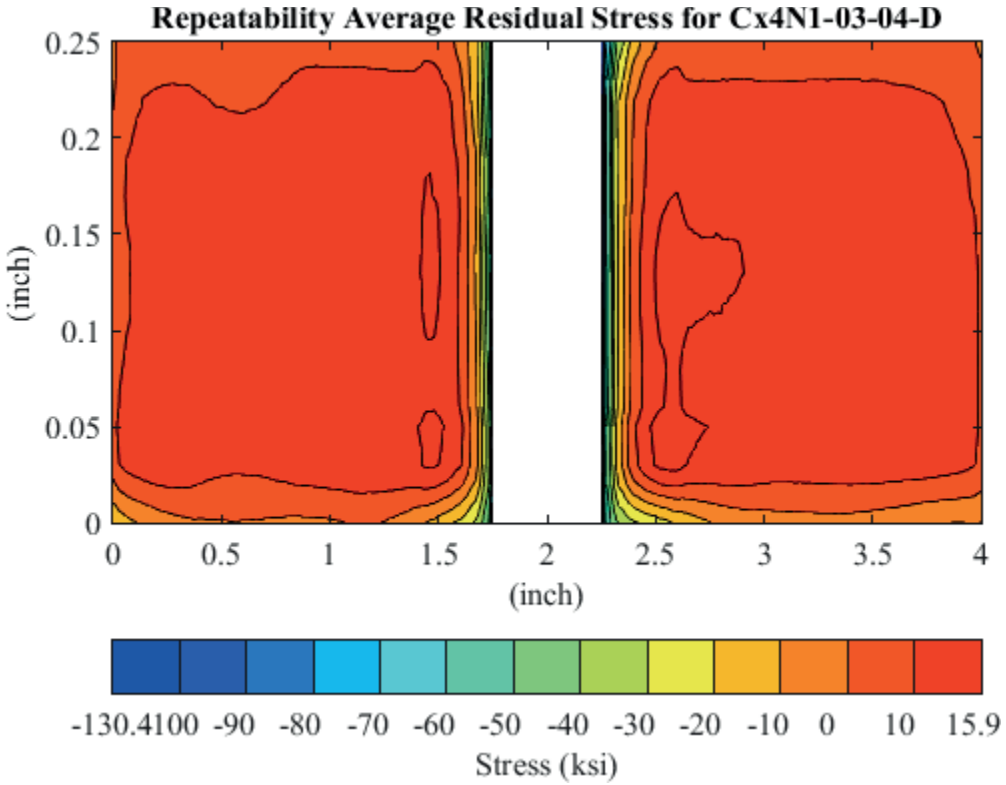

Fig. 416 Average Residual Stress Contour Plot of Coupons Cx4N1-03-D and Cx4N1-04-D (7075-T651) – Mandrel Entrance Surface at Y=0, 0.100 inch Fatigue Crack on Left Side of Hole on Mandrel Entrance Surface.

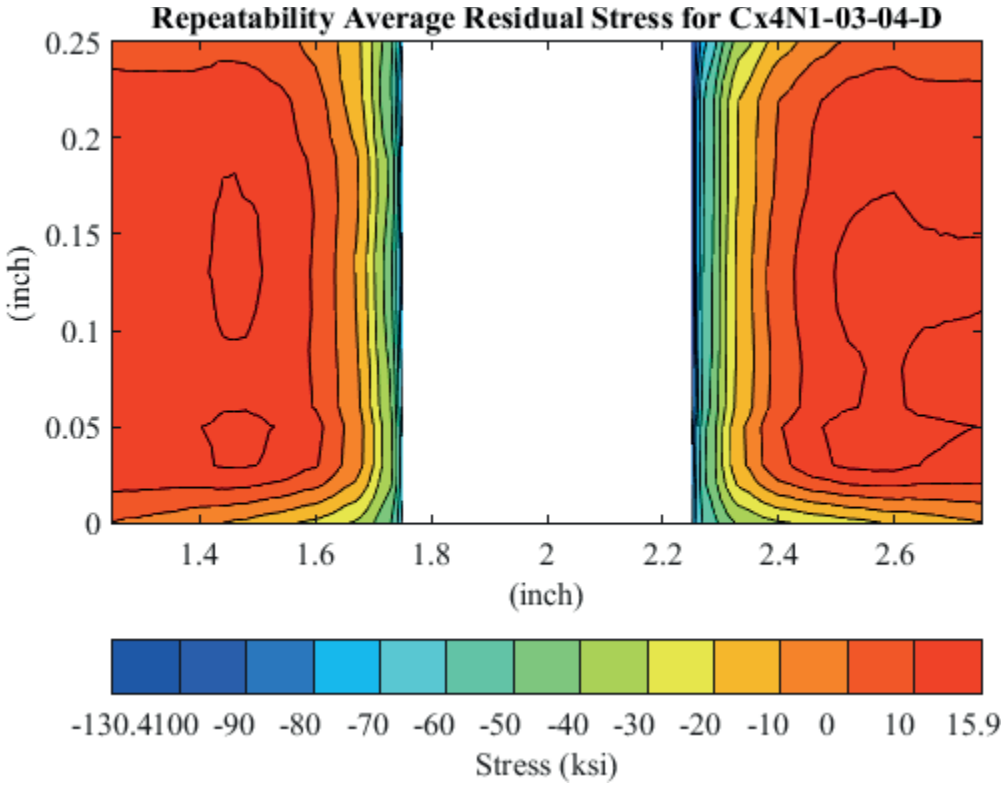

Fig. 417 Average Residual Stress Contour Plot of Coupons Cx4N1-03-D and Cx4N1-04-D (7075-T651) – Mandrel Entrance Surface at Y=0, 0.100 inch Fatigue Crack on Left Side of Hole on Mandrel Entrance Surface – Zoomed in Next to Hole.

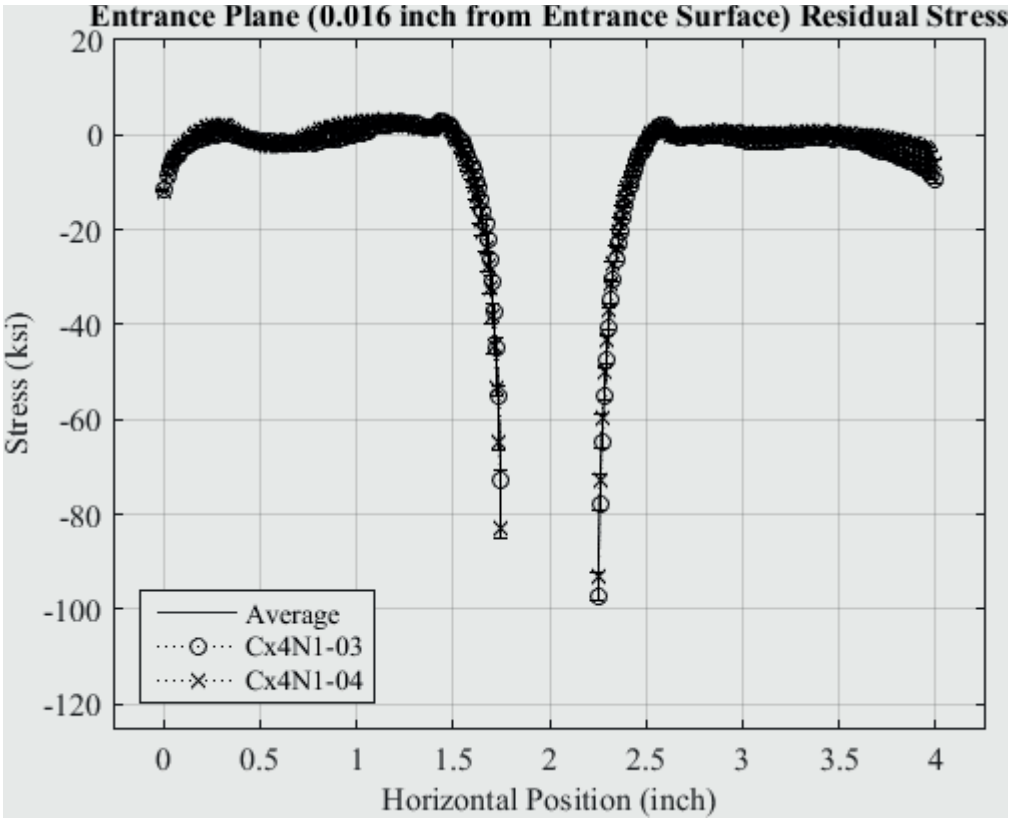

Fig. 418 Residual Stress Line Plot of Cx4N1-03-D and Cx4N1-04-D (7075-T651) at a Distance of 0.016 inch (Entrance Surface) from the Entrance Surface – Coupons had a 0.10 inch Fatigue Crack at the Left Entrance Surface.

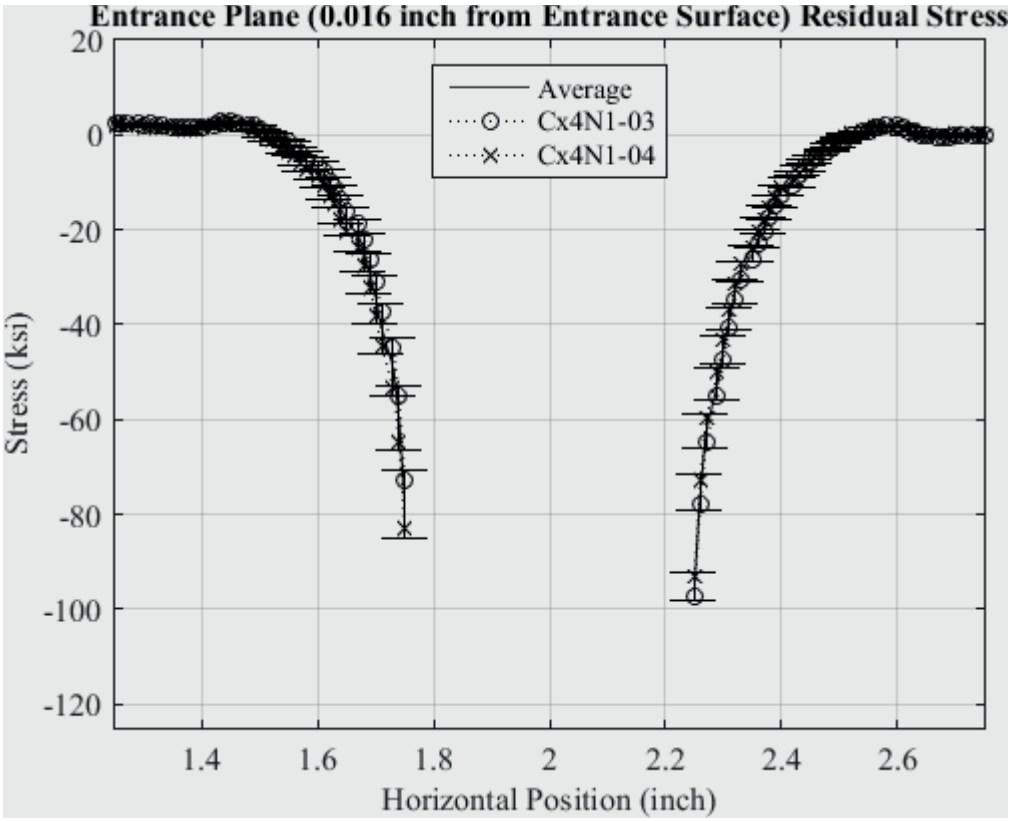

Fig. 419 Residual Stress Line Plot of Cx4N1-03-D and Cx4N1-04-D (7075-T651) at a Distance of 0.016 inch (Entrance Surface) from the Entrance Surface – Coupons had a 0.10 inch Fatigue Crack at the Left Entrance Surface – Zoomed in Next to Hole.

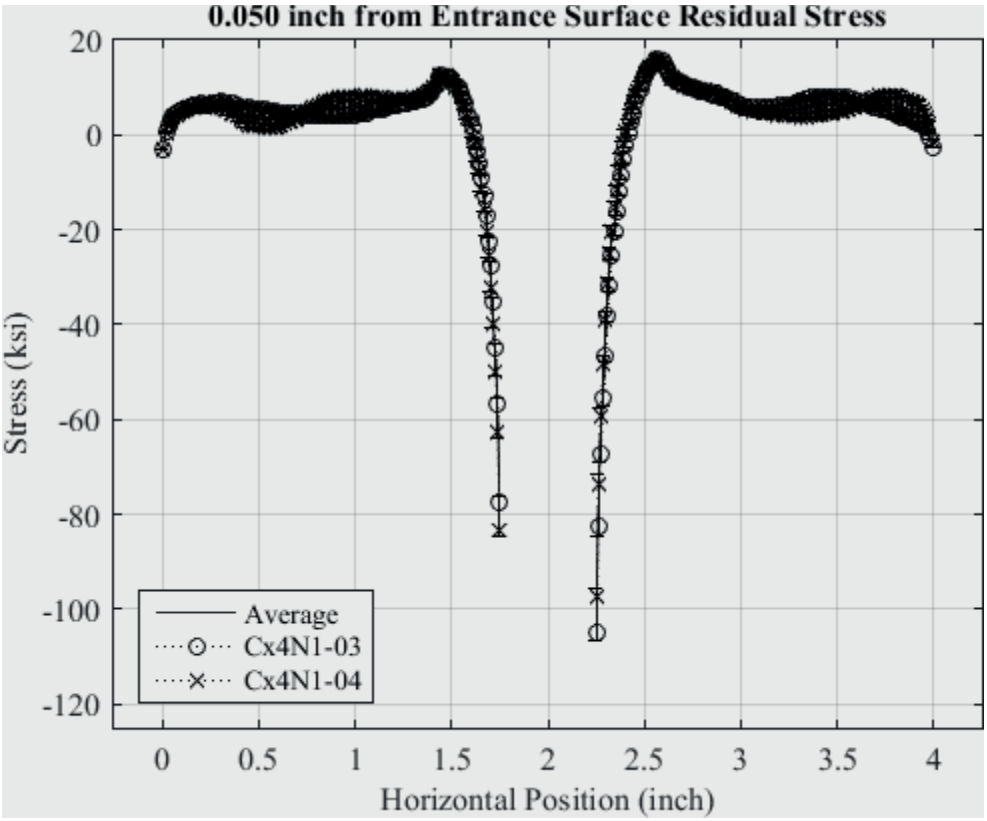

Fig. 420 Residual Stress Line Plot of Cx4N1-03-D and Cx4N1-04-D (7075-T651) at a Distance of 0.05 inch from the Entrance Surface – Coupons had a 0.10 inch Fatigue Crack at the Left Entrance Surface.

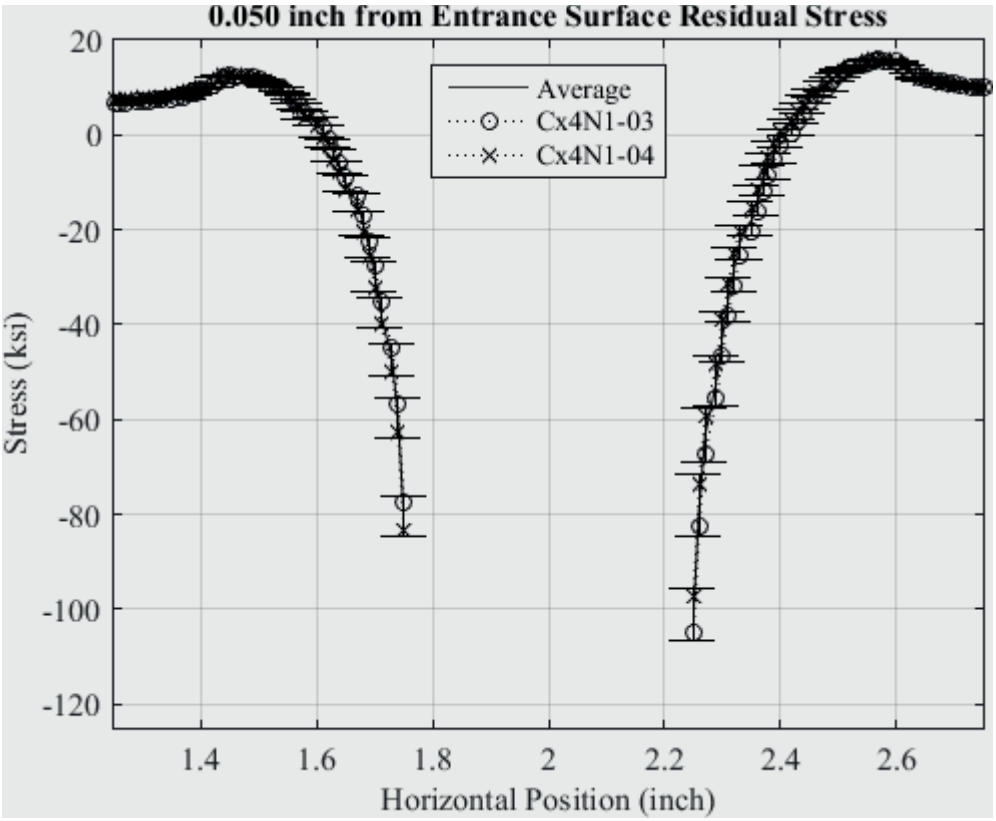

Fig. 421 Residual Stress Line Plot of Cx4N1-03-D and Cx4N1-04-D (7075-T651) at a Distance of 0.05 inch from the Entrance Surface – Coupons had a 0.10 inch Fatigue Crack at the Left Entrance Surface – Zoomed in Next to Hole.

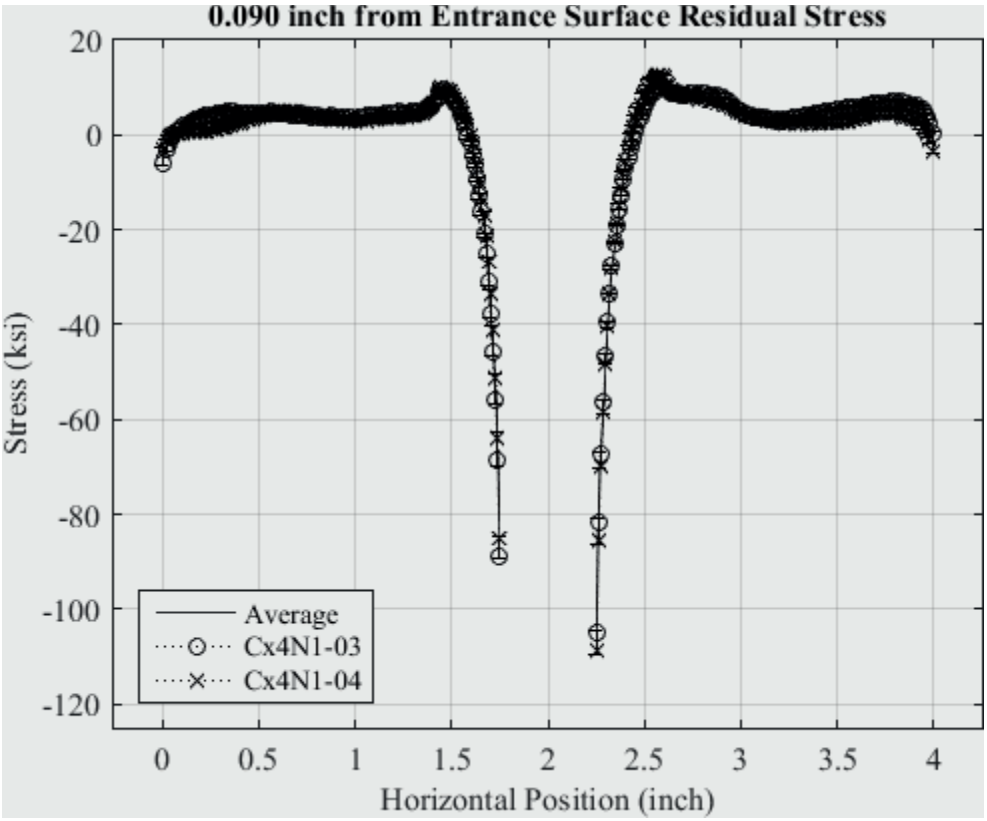

Fig. 422 Residual Stress Line Plot of Cx4N1-03-D and Cx4N1-04-D (7075-T651) at a Distance of 0.09 inch from the Entrance Surface – Coupons had a 0.10 inch Fatigue Crack at the Left Entrance Surface.

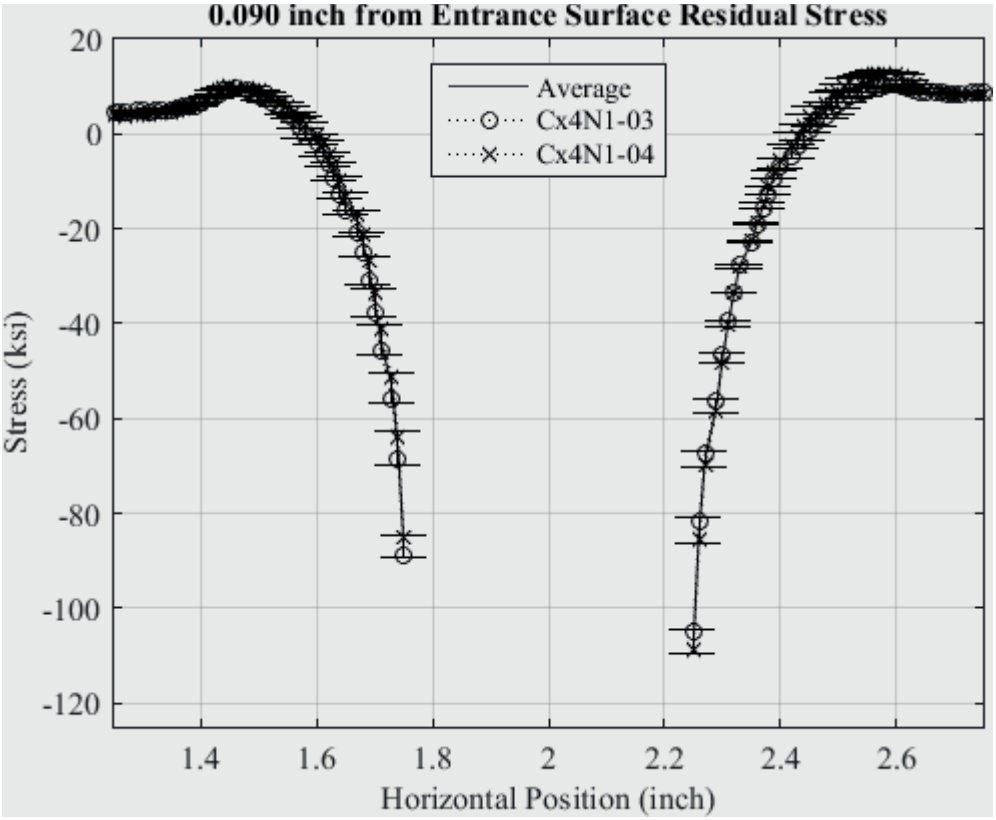

Fig. 423 Residual Stress Line Plot of Cx4N1-03-D and Cx4N1-04-D (7075-T651) at a Distance of 0.09 inch from the Entrance Surface – Coupons had a 0.10 inch Fatigue Crack at the Left Entrance Surface – Zoomed in Next to Hole.

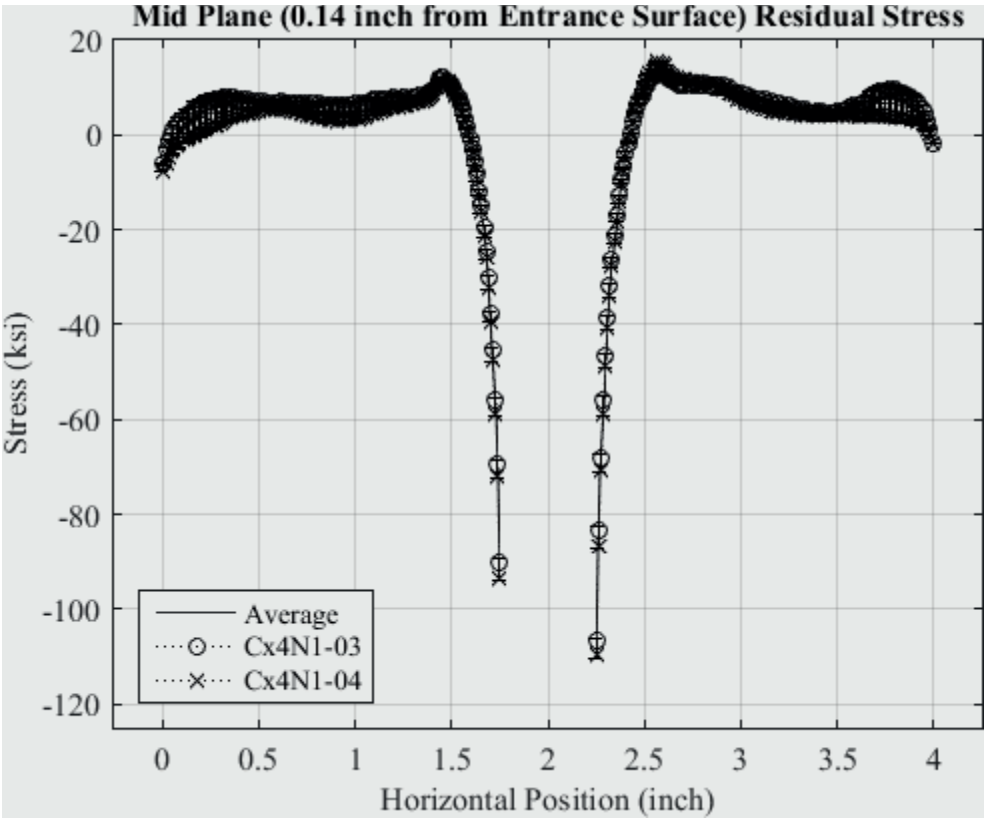

Fig. 424 Residual Stress Line Plot of Cx4N1-03-D and Cx4N1-04-D (7075-T651) at a Distance of 0.140 inch (Mid Plane Surface) from the Entrance Surface – Coupons had a 0.10 inch Fatigue Crack at the Left Entrance Surface.

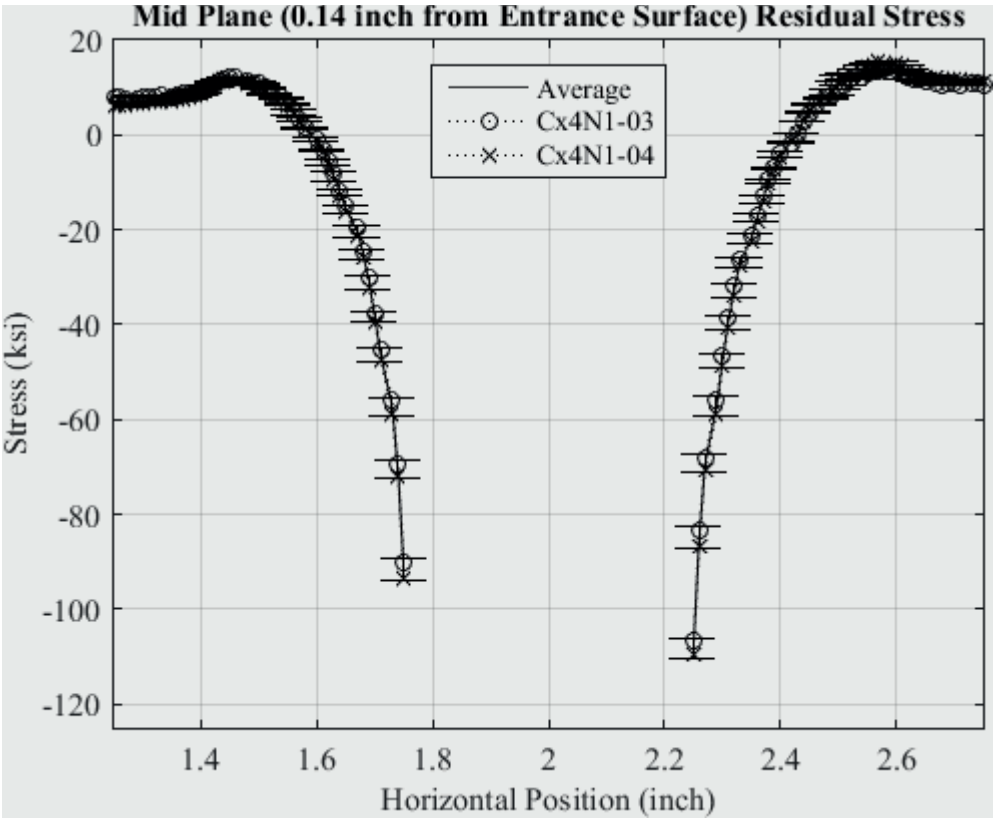

Fig. 425 Residual Stress Line Plot of Cx4N1-03-D and Cx4N1-04-D (7075-T651) at a Distance of 0.140 inch (Mid Plane Surface) from the Entrance Surface – Coupons had a 0.10 inch Fatigue Crack at the Left Entrance Surface – Zoomed in Next to Hole.

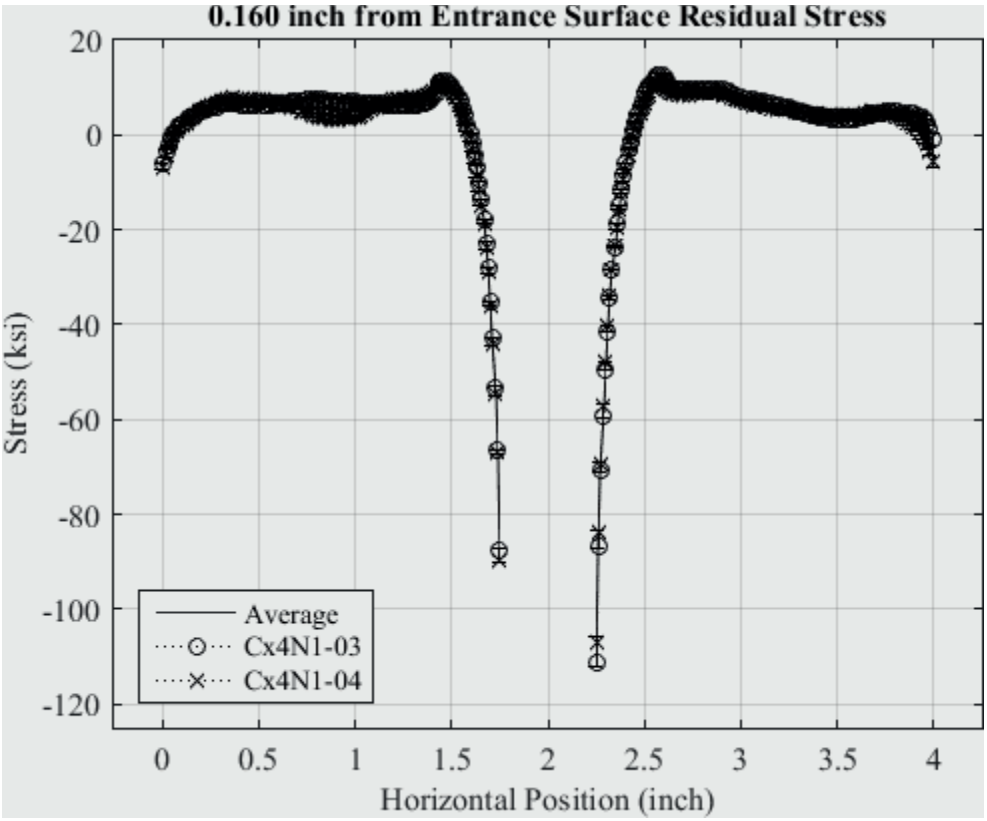

Fig. 426 Residual Stress Line Plot of Cx4N1-03-D and Cx4N1-04-D (7075-T651) at a Distance of 0.160 inch from the Entrance Surface – Coupons had a 0.10 inch Fatigue Crack at the Left Entrance Surface.

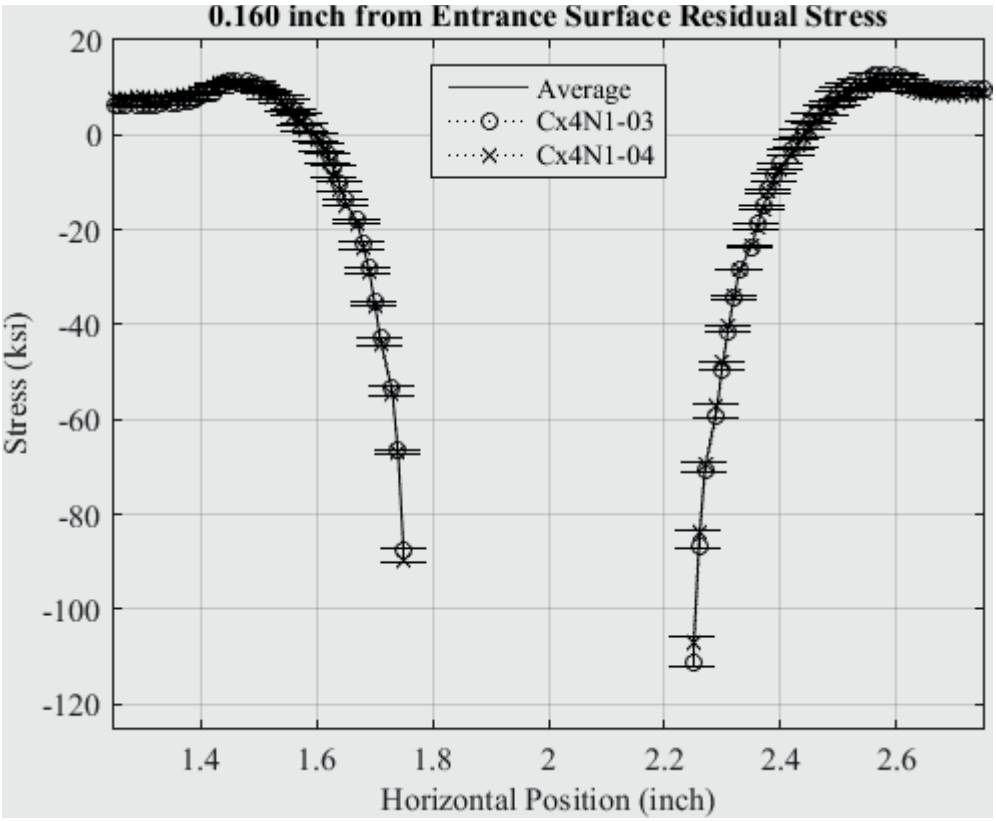

Fig. 427 Residual Stress Line Plot of Cx4N1-03-D and Cx4N1-04-D (7075-T651) at a Distance of 0.160 inch from the Entrance Surface – Coupons had a 0.10 inch Fatigue Crack at the Left Entrance Surface – Zoomed in Next to Hole.

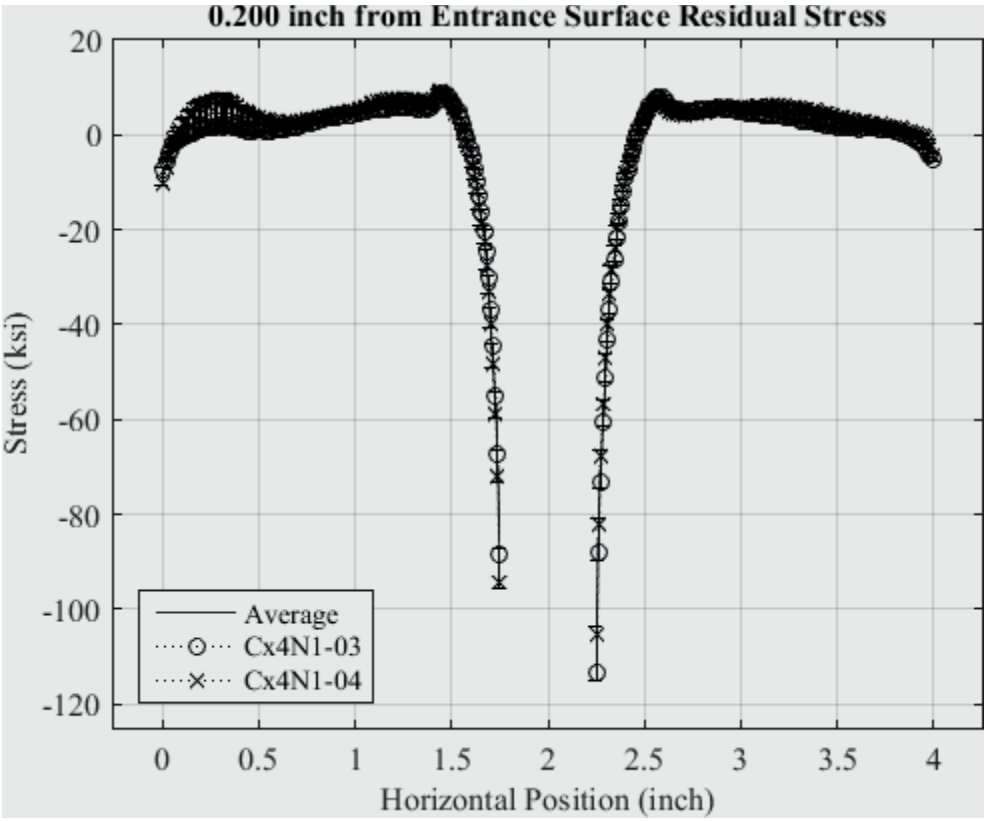

Fig. 428 Residual Stress Line Plot of Cx4N1-03-D and Cx4N1-04-D (7075-T651) at a Distance of 0.20 inch from the Entrance Surface – Coupons had a 0.10 inch Fatigue Crack at the Left Entrance Surface.

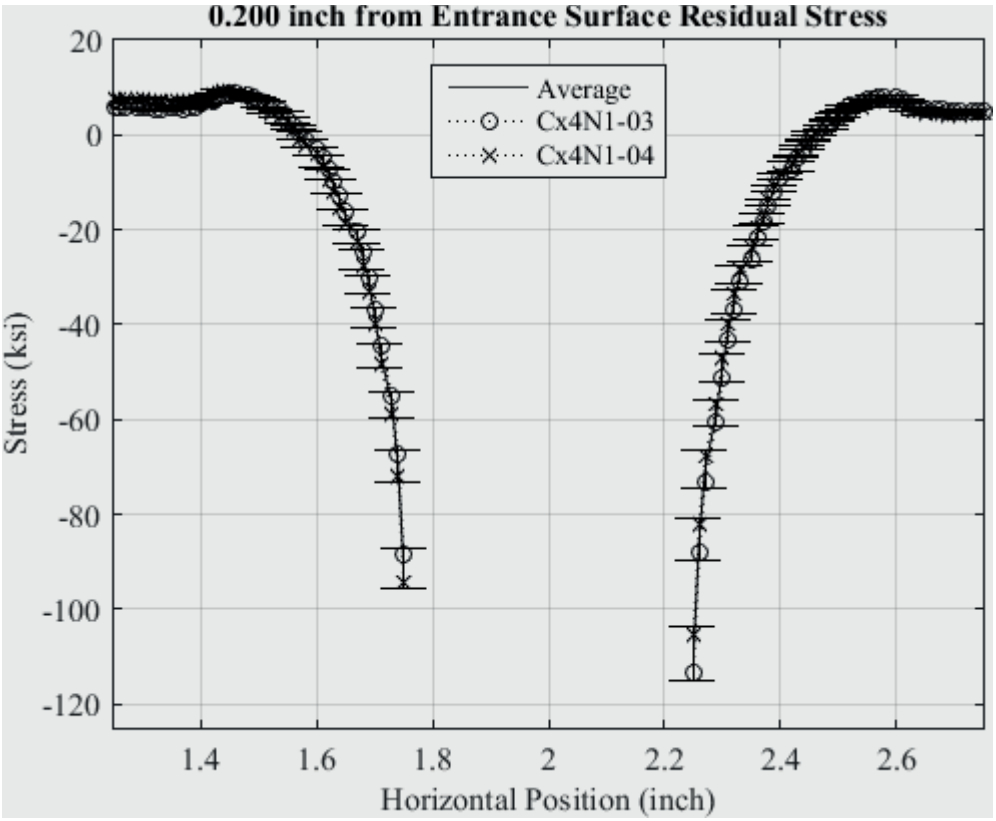

Fig. 429 Residual Stress Line Plot of Cx4N1-03-D and Cx4N1-04-D (7075-T651) at a Distance of 0.20 inch from the Entrance Surface – Coupons had a 0.10 inch Fatigue Crack at the Left Entrance Surface – Zoomed in Next to Hole.

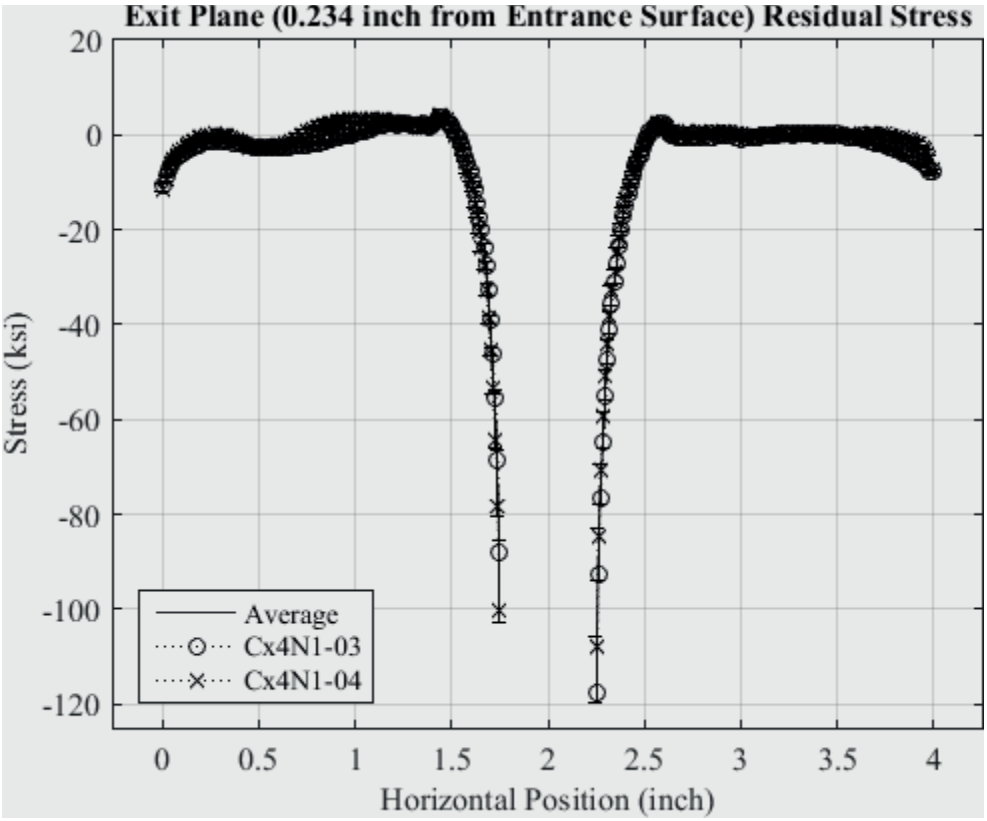

Fig. 430 Residual Stress Line Plot of Cx4N1-03-D and Cx4N1-04-D (7075-T651) at a Distance of 0.234 inch (Exit Surface) from the Entrance Surface – Coupons had a 0.10 inch Fatigue Crack at the Left Entrance Surface – Zoomed in Next to Hole.

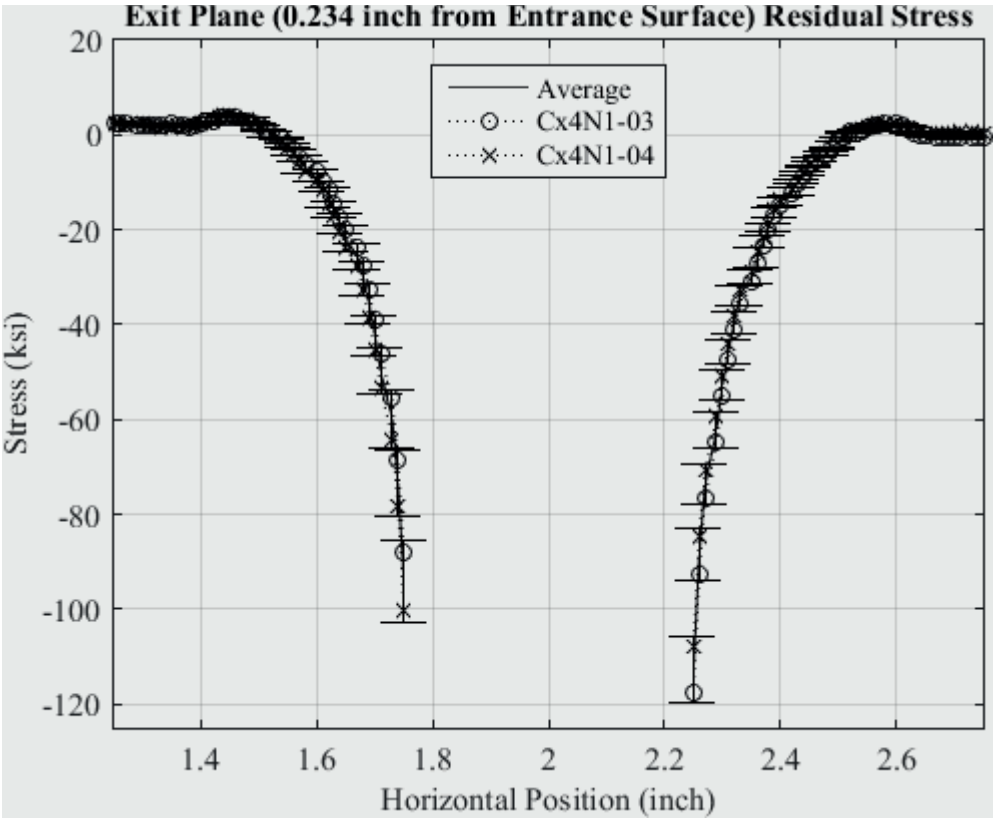

Fig. 431 Residual Stress Line Plot of Cx4N1-03-D and Cx4N1-04-D (7075-T651) at a Distance of 0.234 inch (Exit Surface) from the Entrance Surface – Coupons had a 0.10 inch Fatigue Crack at the Left Entrance Surface – Zoomed in Next to Hole.

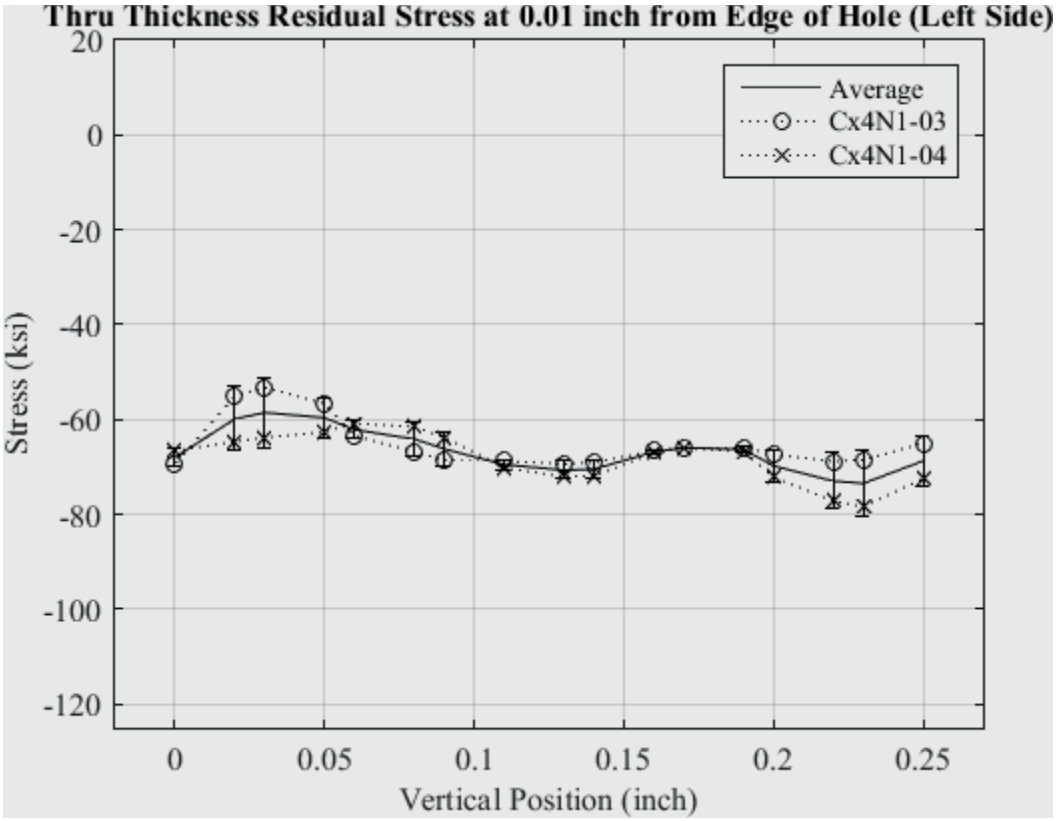

Fig. 432 Residual Stress Line Plot of Cx4N1-03-D and Cx4N1-04-D (7075-T651) Through the Thickness at 0.01 inch from Left Side of Hole – Coupons had a 0.10 inch Fatigue Crack at the Left Entrance Surface.

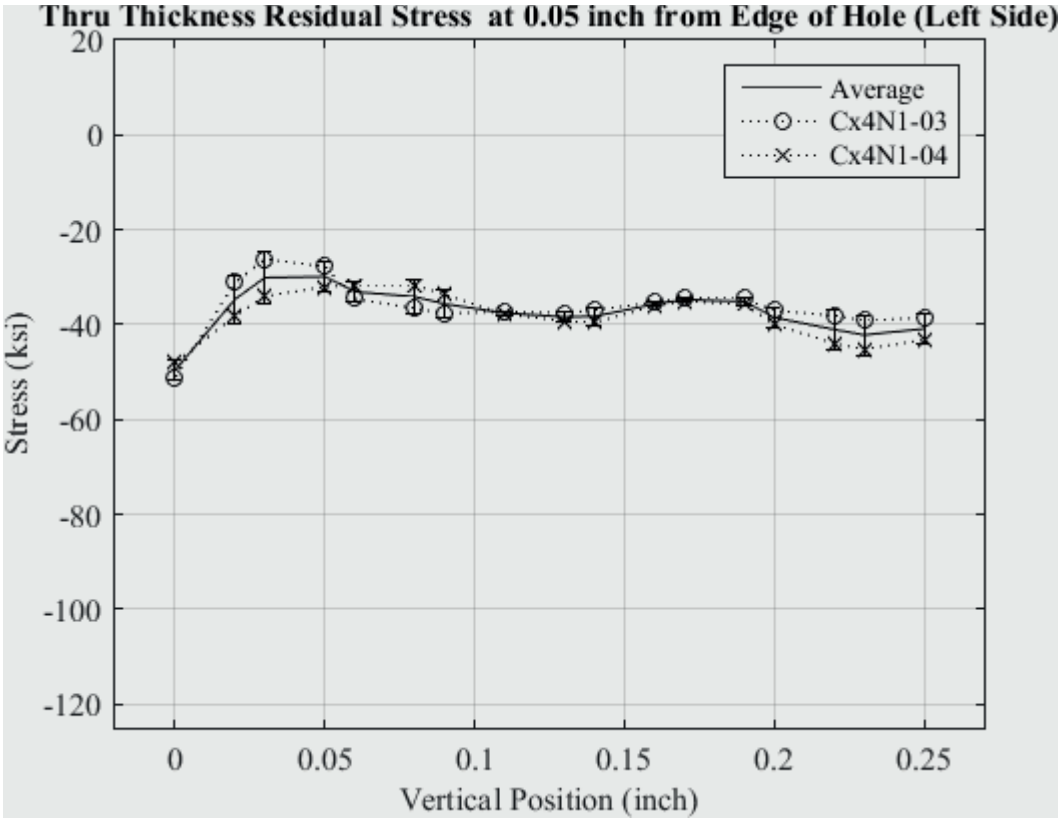

Fig. 433 Residual Stress Line Plot of Cx4N1-03-D and Cx4N1-04-D (7075-T651) Through the Thickness at 0.05 inch from Left Side of Hole – Coupons had a 0.10 inch Fatigue Crack at the Left Entrance Surface.

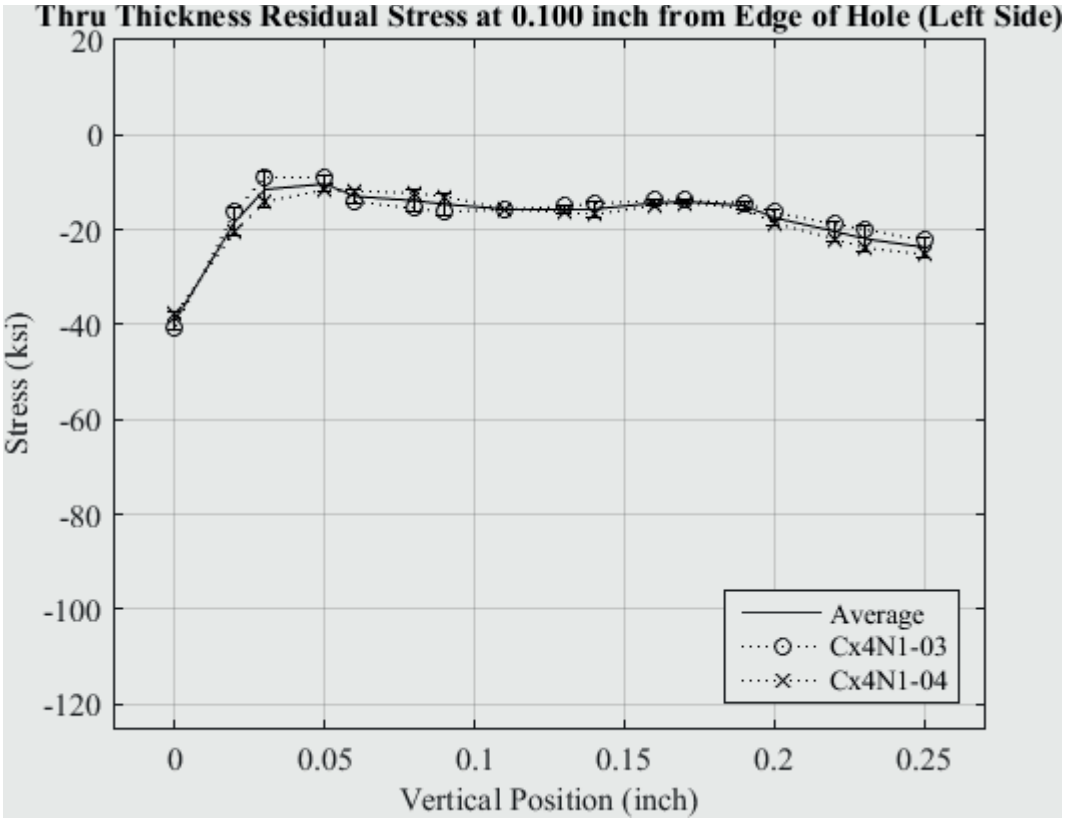

Fig. 434 Residual Stress Line Plot of Cx4N1-03-D and Cx4N1-04-D (7075-T651) Through the Thickness at 0.10 inch from Left Side of Hole – Coupons had a 0.10 inch Fatigue Crack at the Left Entrance Surface.

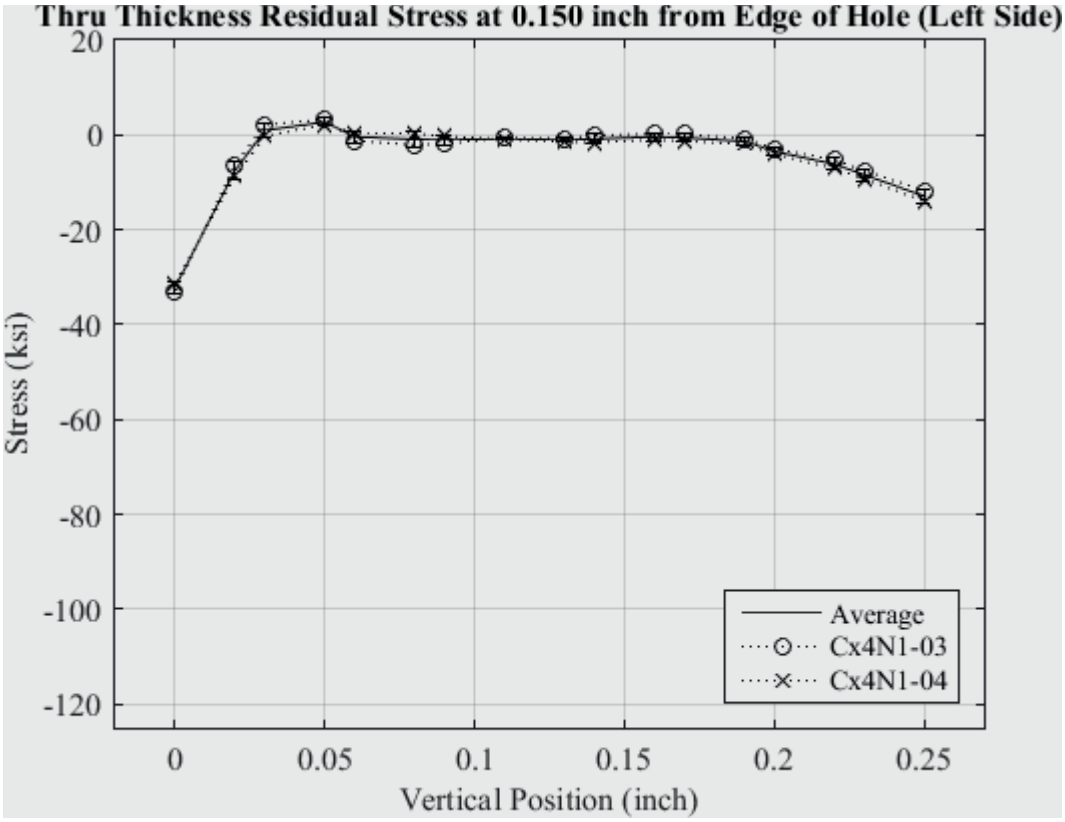

Fig. 435 Residual Stress Line Plot of Cx4N1-03-D and Cx4N1-04-D (7075-T651) Through the Thickness at 0.150 inch from Left Side of Hole – Coupons had a 0.10 inch Fatigue Crack at the Left Entrance Surface.

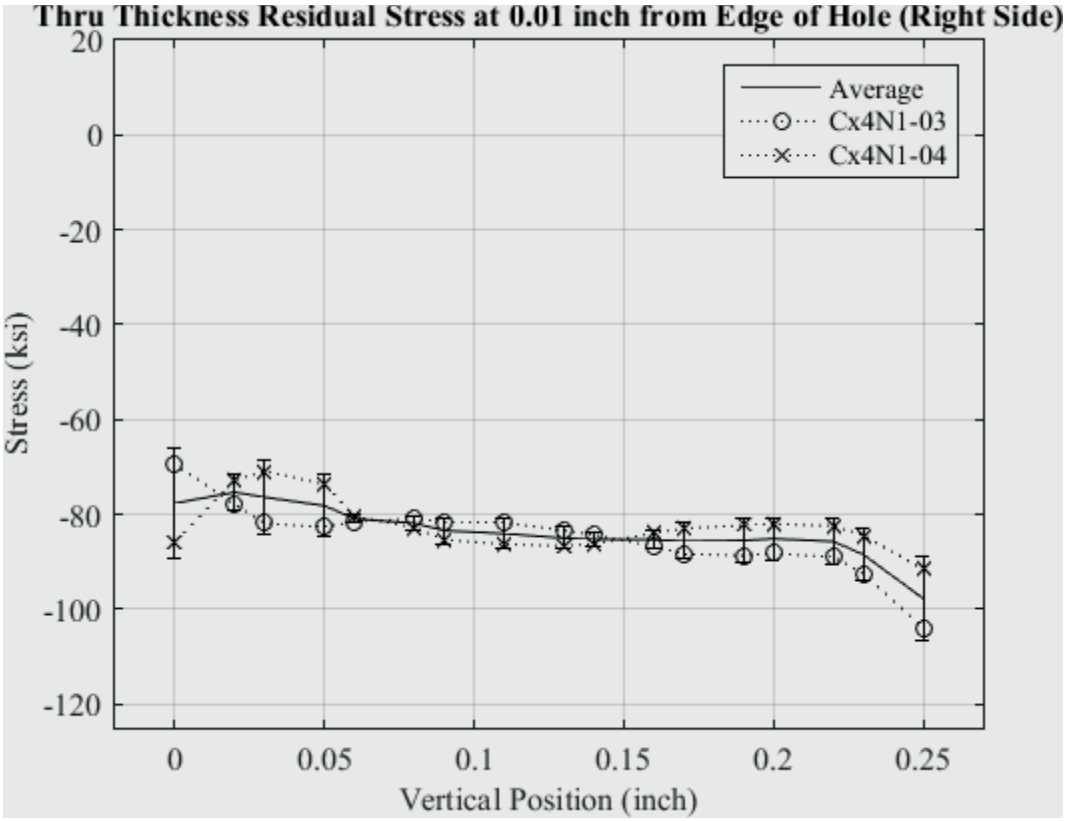

Fig. 436 Residual Stress Line Plot of Cx4N1-03-D and Cx4N1-04-D (7075-T651) Through the Thickness at 0.01 inch from Right Side of Hole – Coupons had a 0.10 inch Fatigue Crack at the Left Entrance Surface.

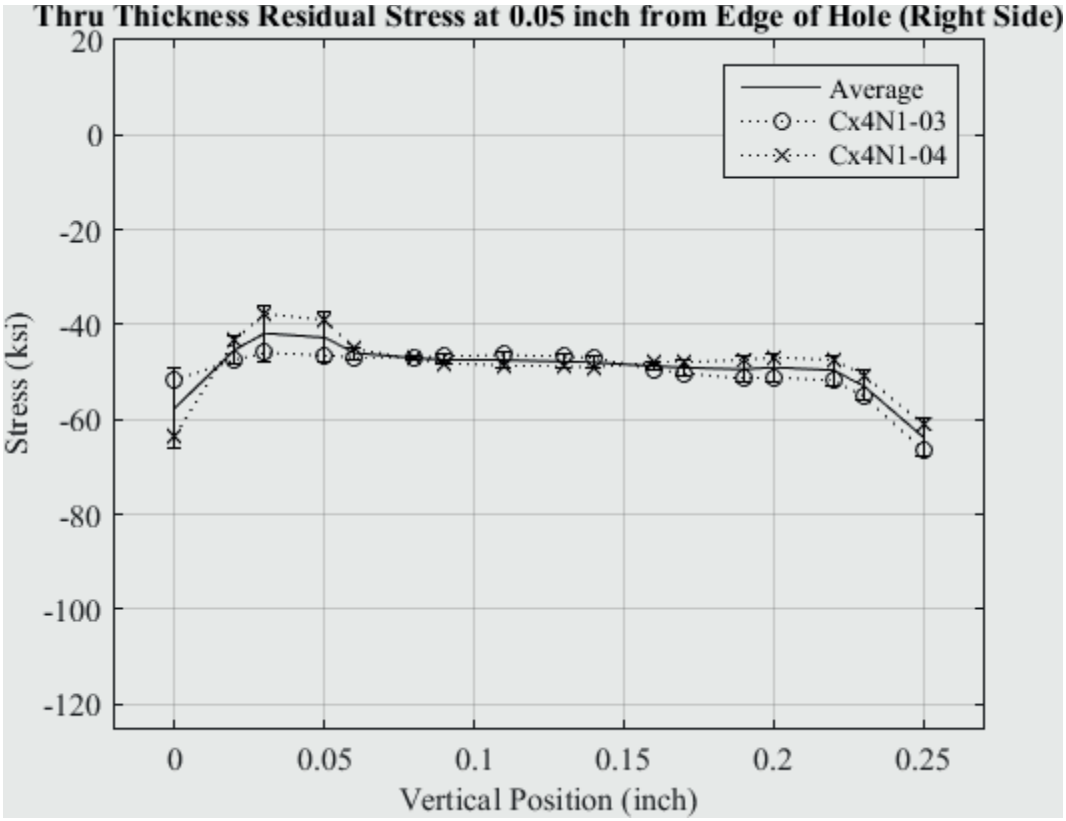

Fig. 437 Residual Stress Line Plot of Cx4N1-03-D and Cx4N1-04-D (7075-T651) Through the Thickness at 0.05 inch from Right Side of Hole – Coupons had a 0.10 inch Fatigue Crack at the Left Entrance Surface.

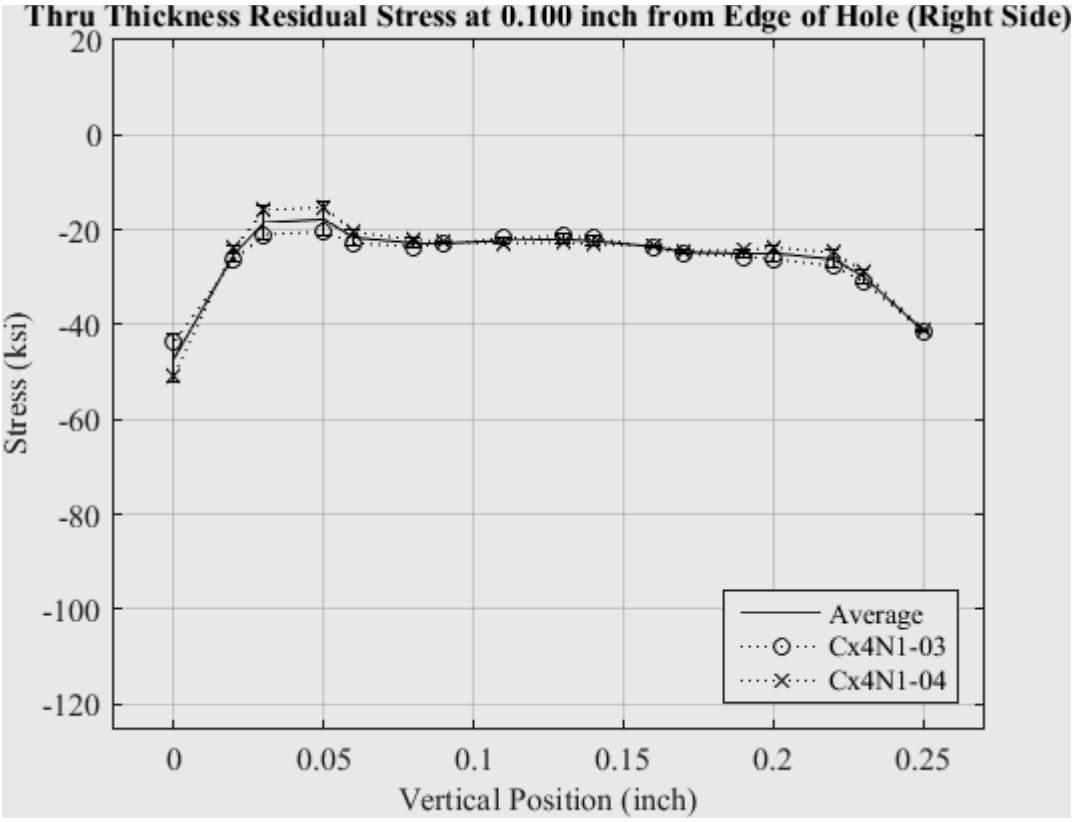

Fig. 438 Residual Stress Line Plot of Cx4N1-03-D and Cx4N1-04-D (7075-T651) Through the Thickness at 0.10 inch from Right Side of Hole – Coupons had a 0.10 inch Fatigue Crack at the Left Entrance Surface.

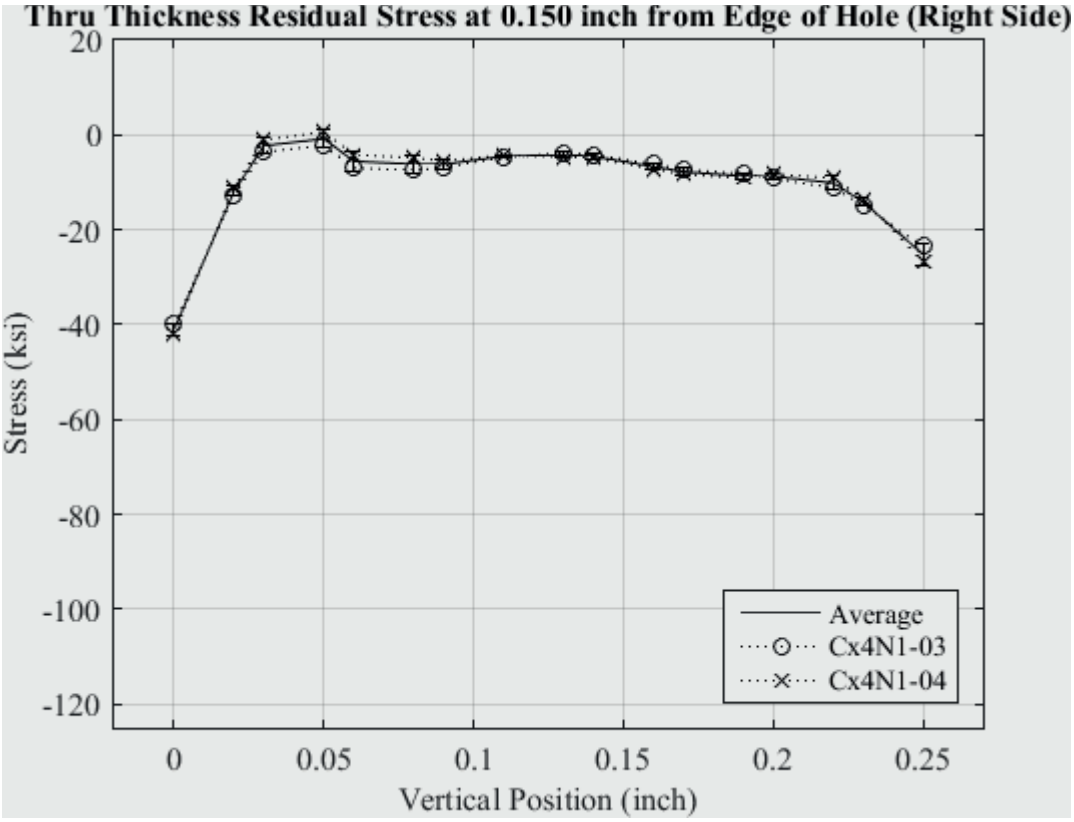

Fig. 439 Residual Stress Line Plot of Cx4N1-03-D and Cx4N1-04-D (7075-T651) Through the Thickness at 0.150 inch from Right Side of Hole – Coupons had a 0.10 inch Fatigue Crack at the Left Entrance Surface.

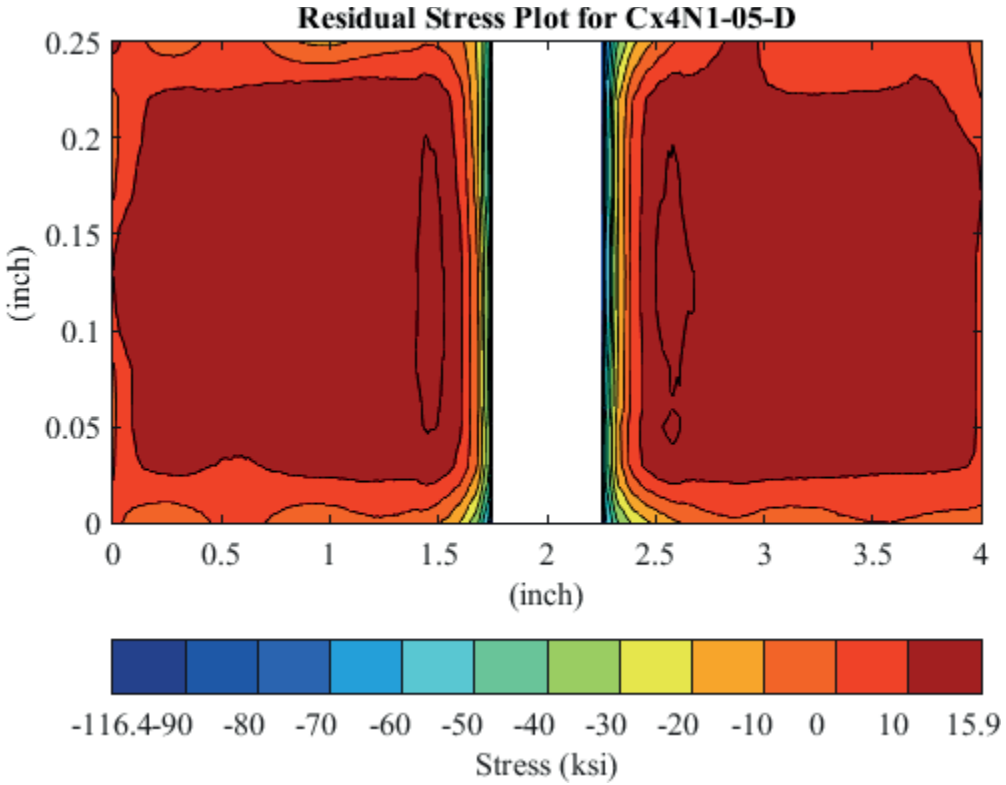

Fig. 440 Residual Stress Contour Plot of Coupon Cx4N1-05-D (7075-T651) – Mandrel Entrance Surface at Y=0, 0.1259 inch Fatigue Crack on Left Side of Hole on Mandrel Entrance Surface.

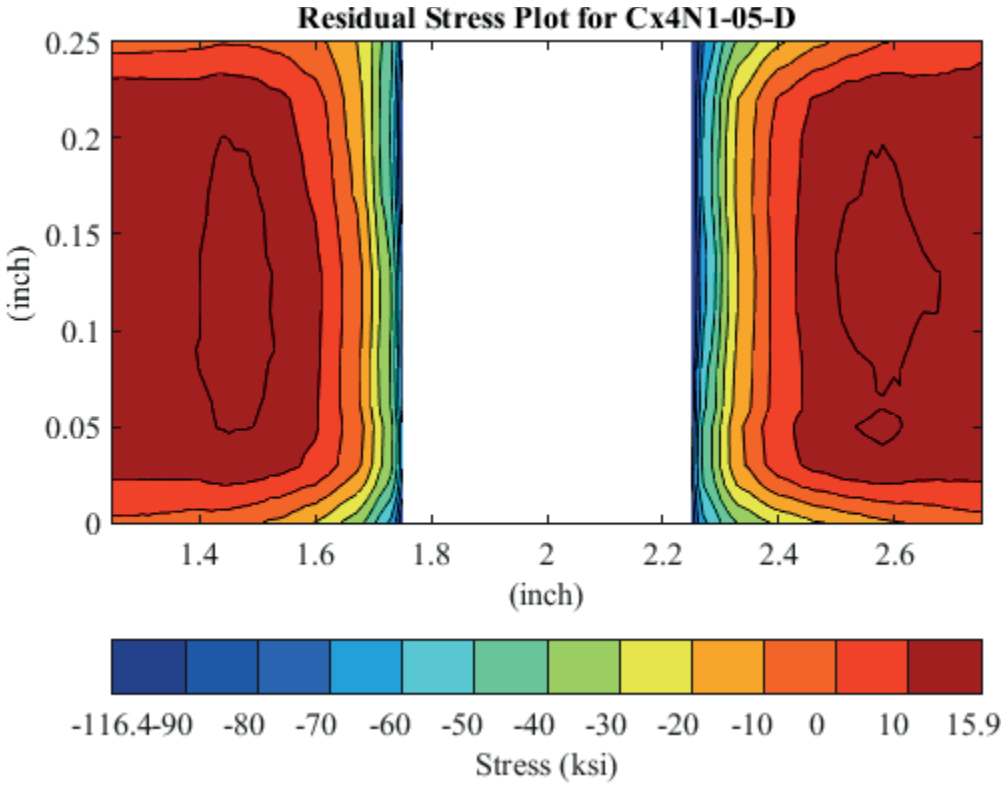

Fig. 441 Residual Stress Contour Plot of Coupon Cx4N1-05-D (7075-T651) – Mandrel Entrance Surface at Y=0, 0.1259 inch Fatigue Crack on Left Side of Hole on Mandrel Entrance Surface – Zoomed in Next to Hole.

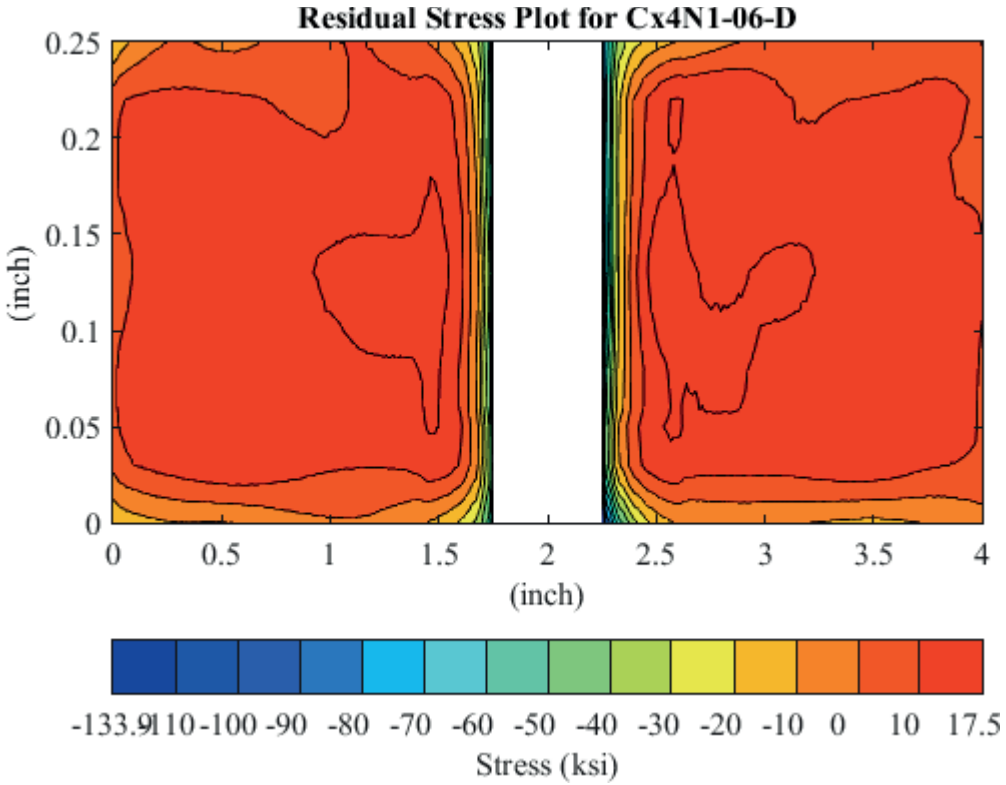

Fig. 442 Residual Stress Contour Plot of Coupon Cx4N1-06-D (7075-T651) – Mandrel Entrance Surface at Y=0, 0.1214 inch Fatigue Crack on Left Side of Hole on Mandrel Entrance Surface.

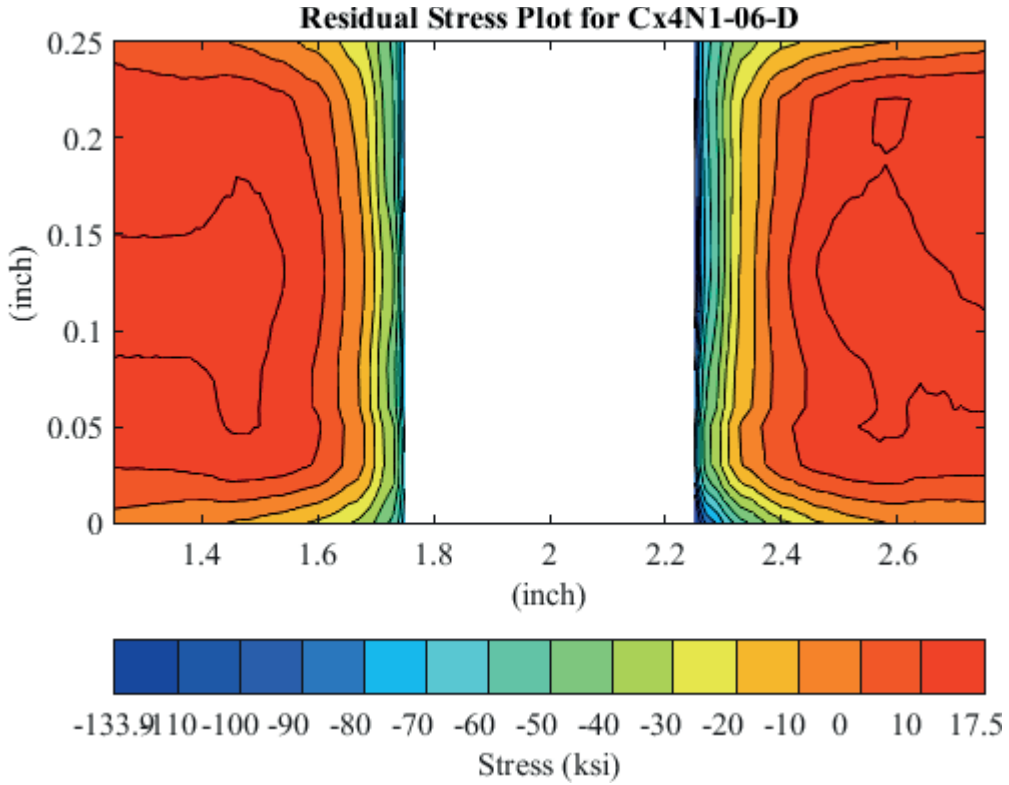

Fig. 443 Residual Stress Contour Plot of Coupon Cx4N1-06-D (7075-T651) – Mandrel Entrance Surface at Y=0, 0.1214 inch Fatigue Crack on Left Side of Hole on Mandrel Entrance Surface – Zoomed in Next to Hole.

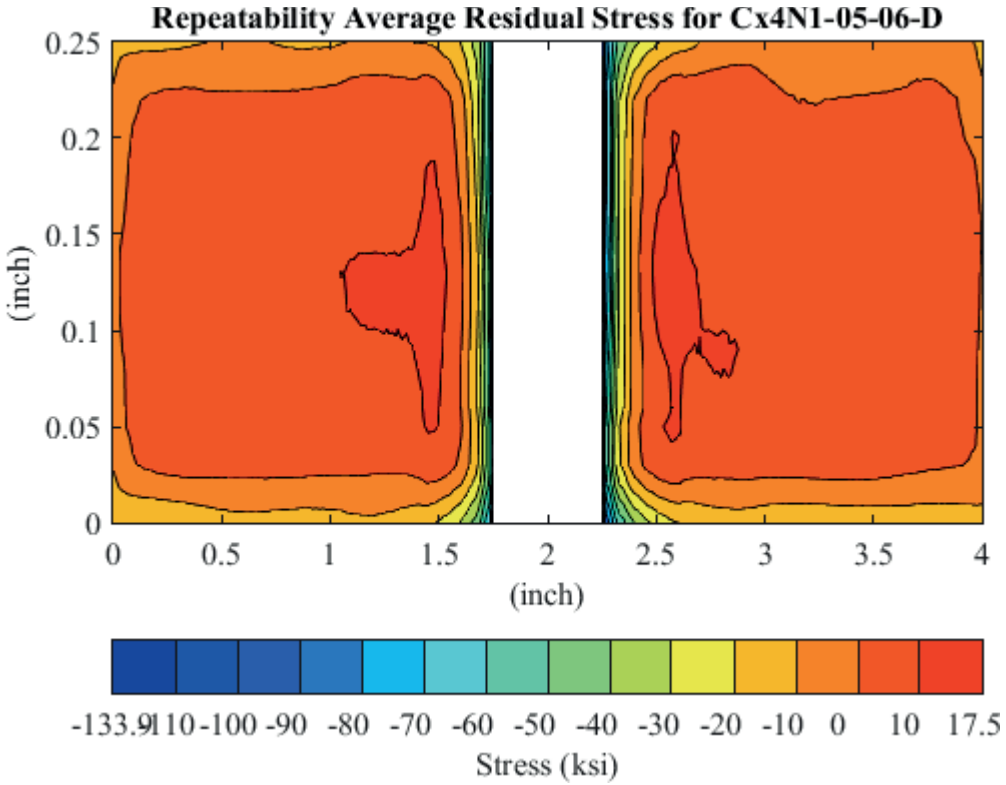

Fig. 444 Average Residual Stress Contour Plot of Coupons Cx4N1-05-D and Cx4N1-06-D (7075-T651) – Mandrel Entrance Surface at Y=0, 0.125 inch Fatigue Crack on Left Side of Hole on Mandrel Entrance Surface.

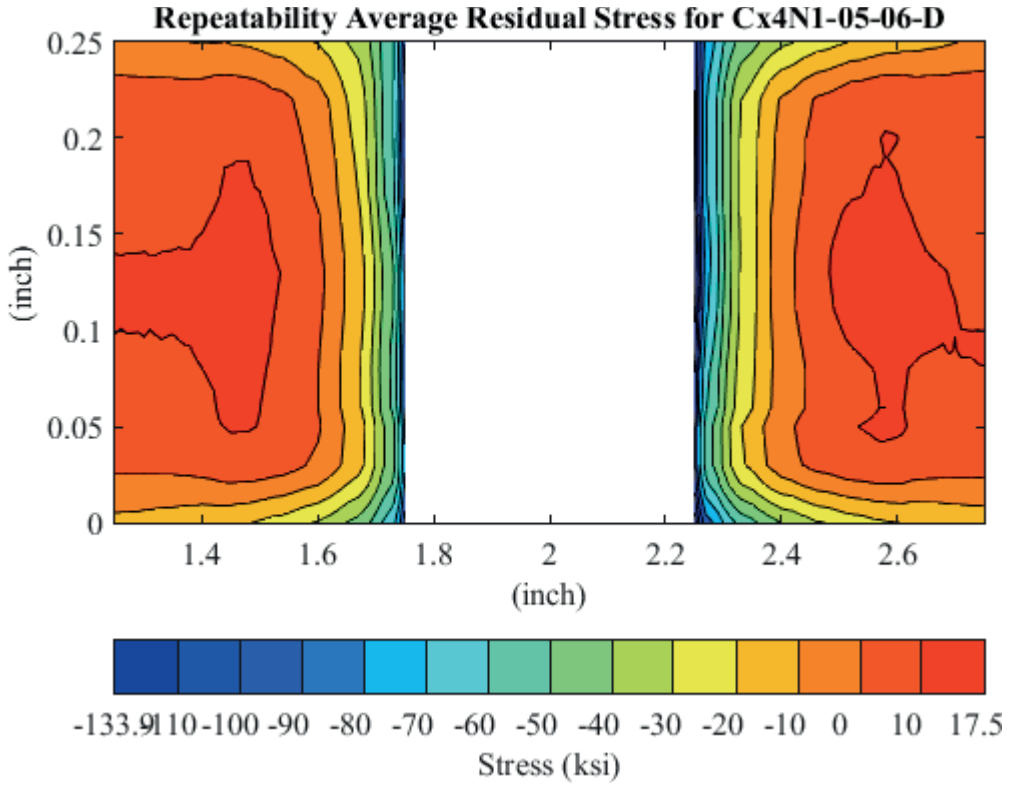

Fig. 445 Average Residual Stress Contour Plot of Coupons Cx4N1-05-D and Cx4N1-06-D (7075-T651) – Mandrel Entrance Surface at Y=0, 0.125 inch Fatigue Crack on Left Side of Hole on Mandrel Entrance Surface – Zoomed in Next to Hole.

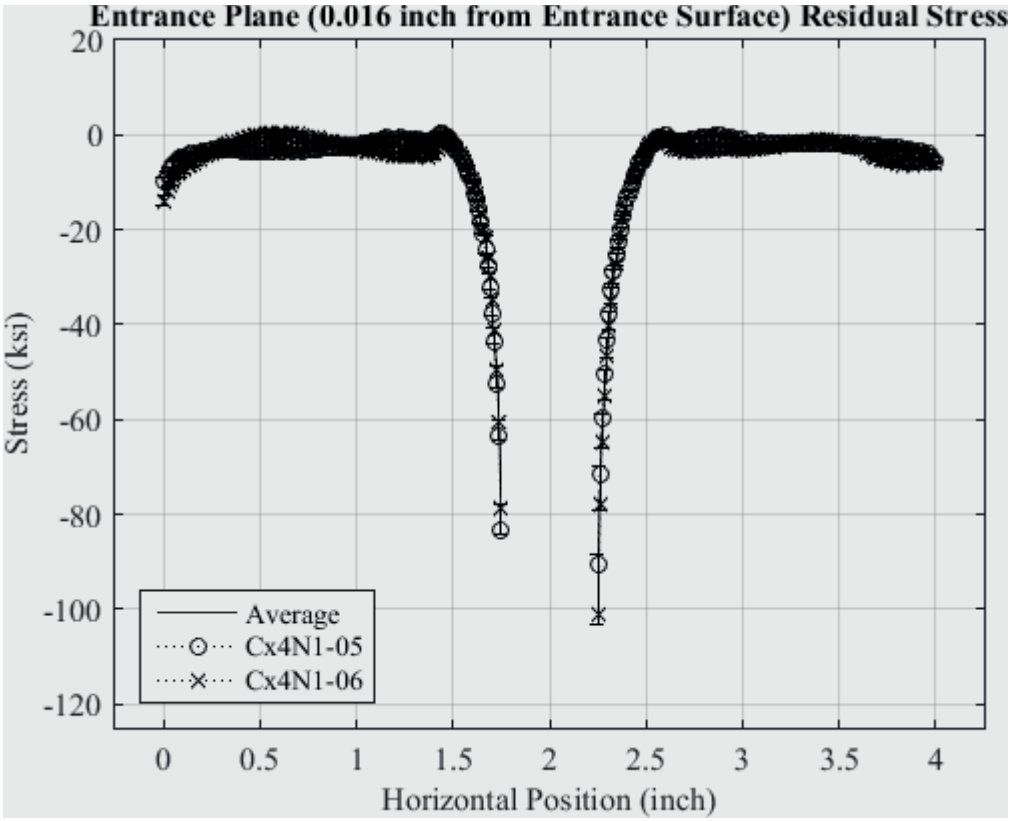

Fig. 446 Residual Stress Line Plot of Cx4N1-05-D and Cx4N1-06-D (7075-T651) at a Distance of 0.016 inch (Entrance Surface) from the Entrance Surface – Coupons had a 0.125 inch Fatigue Crack at the Left Entrance Surface.

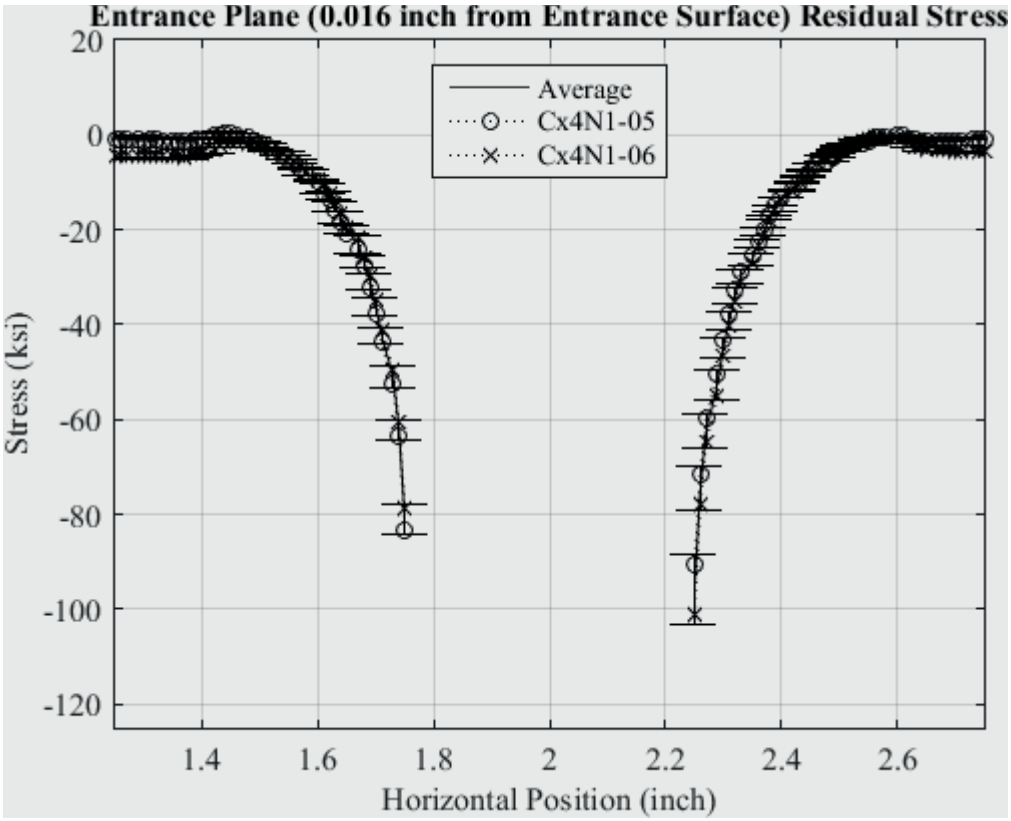

Fig. 447 Residual Stress Line Plot of Cx4N1-05-D and Cx4N1-06-D (7075-T651) at a Distance of 0.016 inch (Entrance Surface) from the Entrance Surface – Coupons had a 0.125 inch Fatigue Crack at the Left Entrance Surface – Zoomed in Next to Hole.

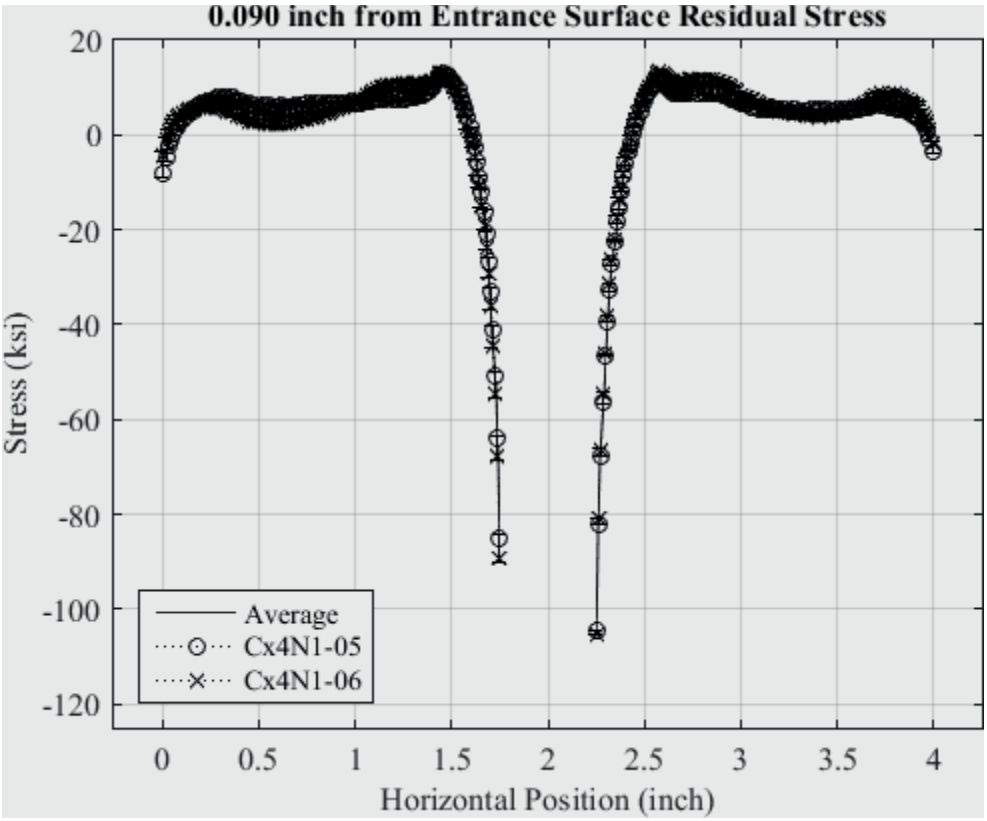

Fig. 448 Residual Stress Line Plot of Cx4N1-05-D and Cx4N1-06-D (7075-T651) at a Distance of 0.09 inch from the Entrance Surface – Coupons had a 0.125 inch Fatigue Crack at the Left Entrance Surface – Zoomed in Next to Hole.

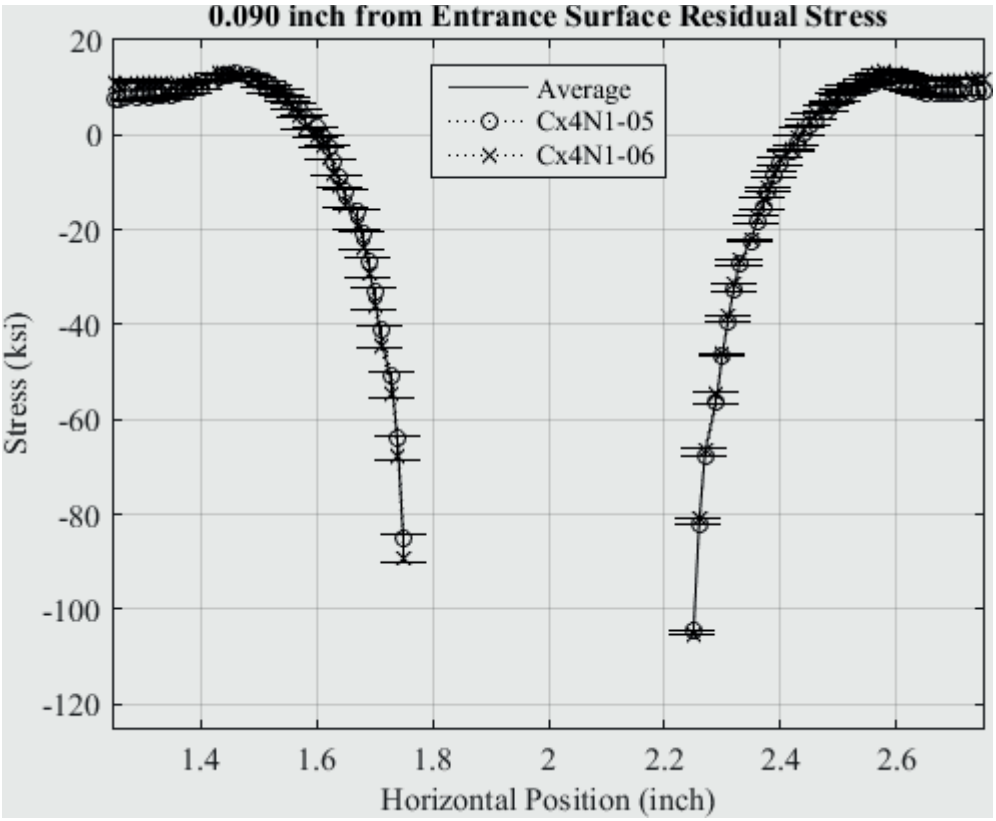

Fig. 449 Residual Stress Line Plot of Cx4N1-05-D and Cx4N1-06-D (7075-T651) at a Distance of 0.09 inch from the Entrance Surface – Coupons had a 0.125 inch Fatigue Crack at the Left Entrance Surface – Zoomed in Next to Hole.

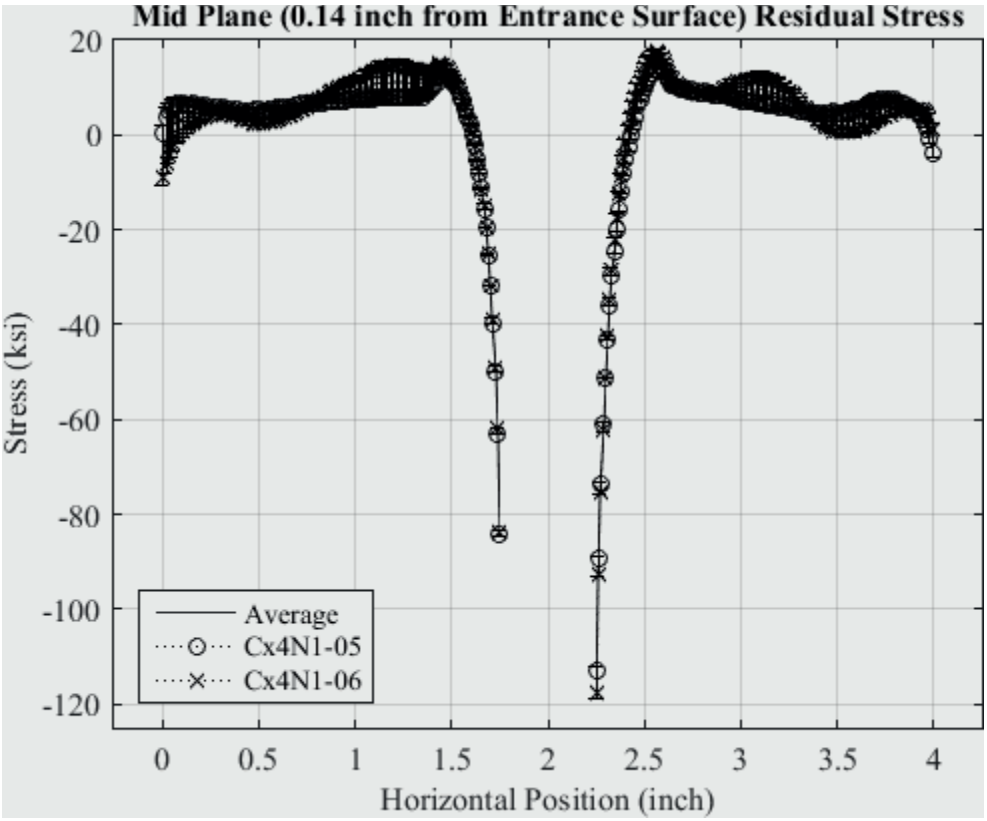

Fig. 450 Residual Stress Line Plot of Cx4N1-05-D and Cx4N1-06-D (7075-T651) at a Distance of 0.140 inch (Mid Plane Surface) from the Entrance Surface – Coupons had a 0.125 inch Fatigue Crack at the Left Entrance Surface.

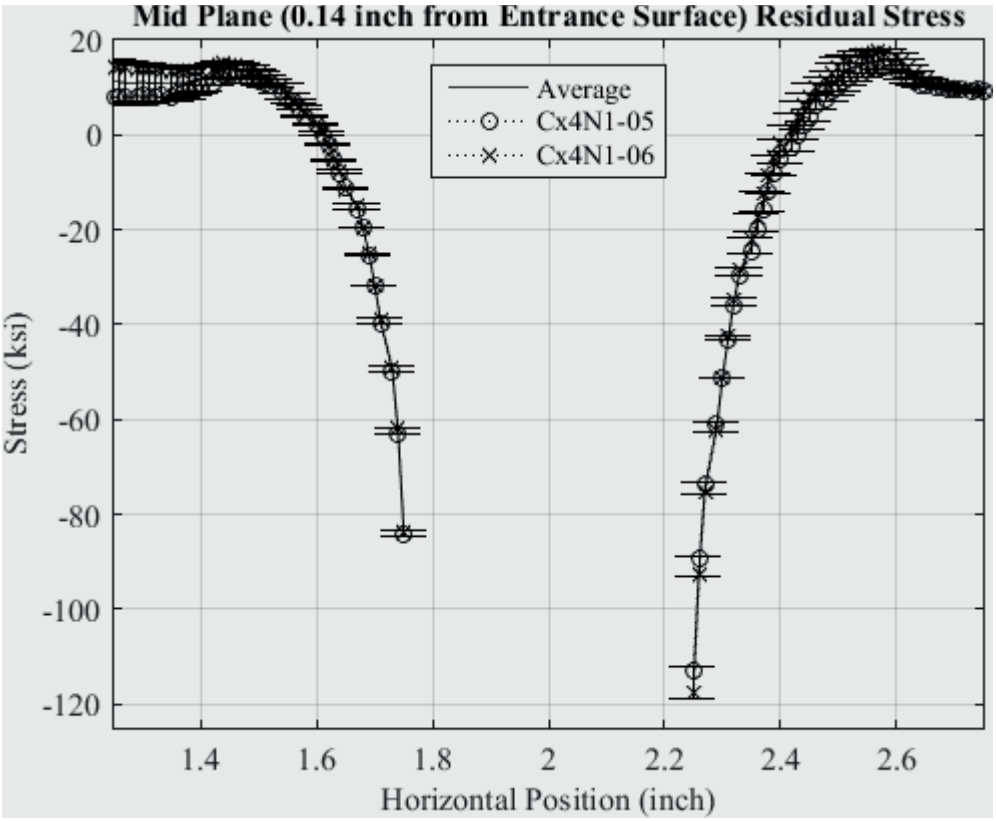

Fig. 451 Residual Stress Line Plot of Cx4N1-05-D and Cx4N1-06-D (7075-T651) at a Distance of 0.140 inch (Mid Plane Surface) from the Entrance Surface – Coupons had a 0.125 inch Fatigue Crack at the Left Entrance Surface – Zoomed in Next to Hole.

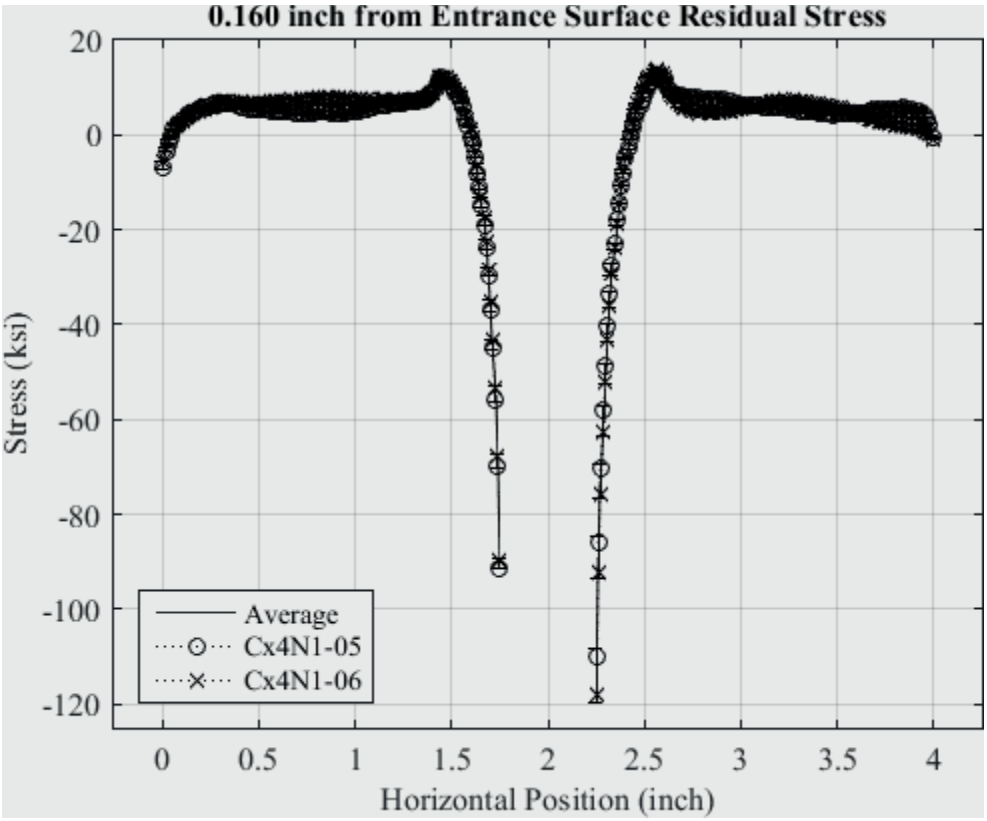

Fig. 452 Residual Stress Line Plot of Cx4N1-05-D and Cx4N1-06-D (7075-T651) at a Distance of 0.160 inch from the Entrance Surface – Coupons had a 0.125 inch Fatigue Crack at the Left Entrance Surface.

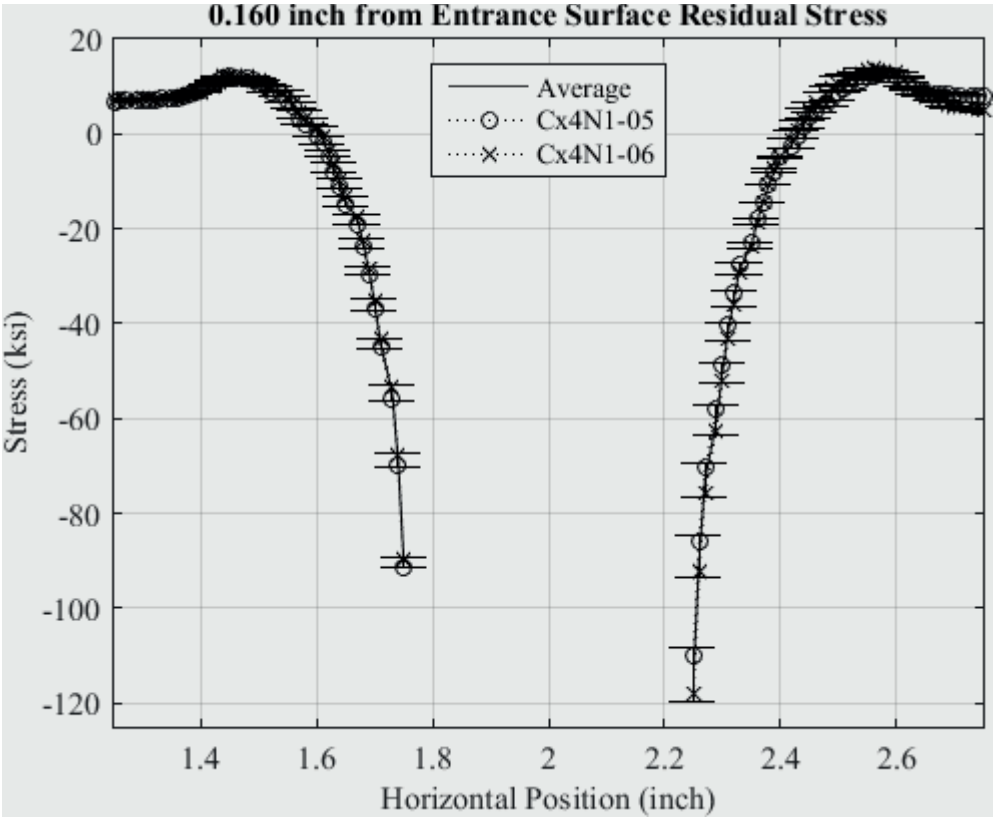

Fig. 453 Residual Stress Line Plot of Cx4N1-05-D and Cx4N1-06-D (7075-T651) at a Distance of 0.160 inch from the Entrance Surface – Coupons had a 0.125 inch Fatigue Crack at the Left Entrance Surface – Zoomed in Next to Hole.

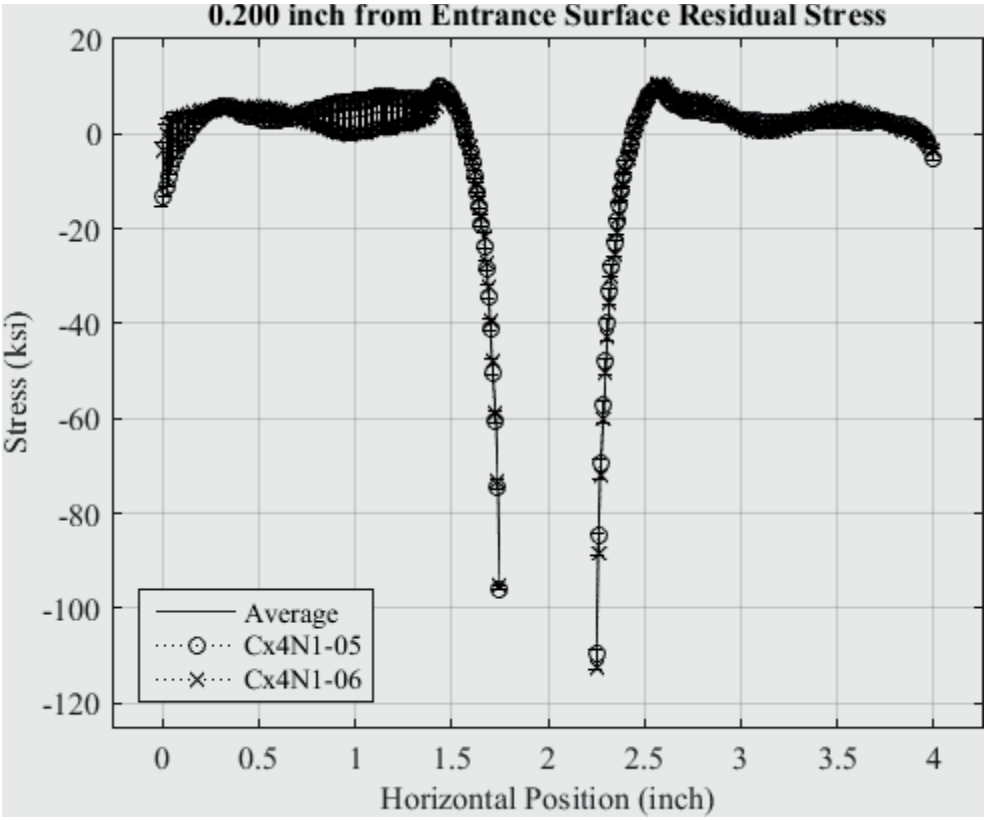

Fig. 454 Residual Stress Line Plot of Cx4N1-05-D and Cx4N1-06-D (7075-T651) at a Distance of 0.200 inch from the Entrance Surface – Coupons had a 0.125 inch Fatigue Crack at the Left Entrance Surface.

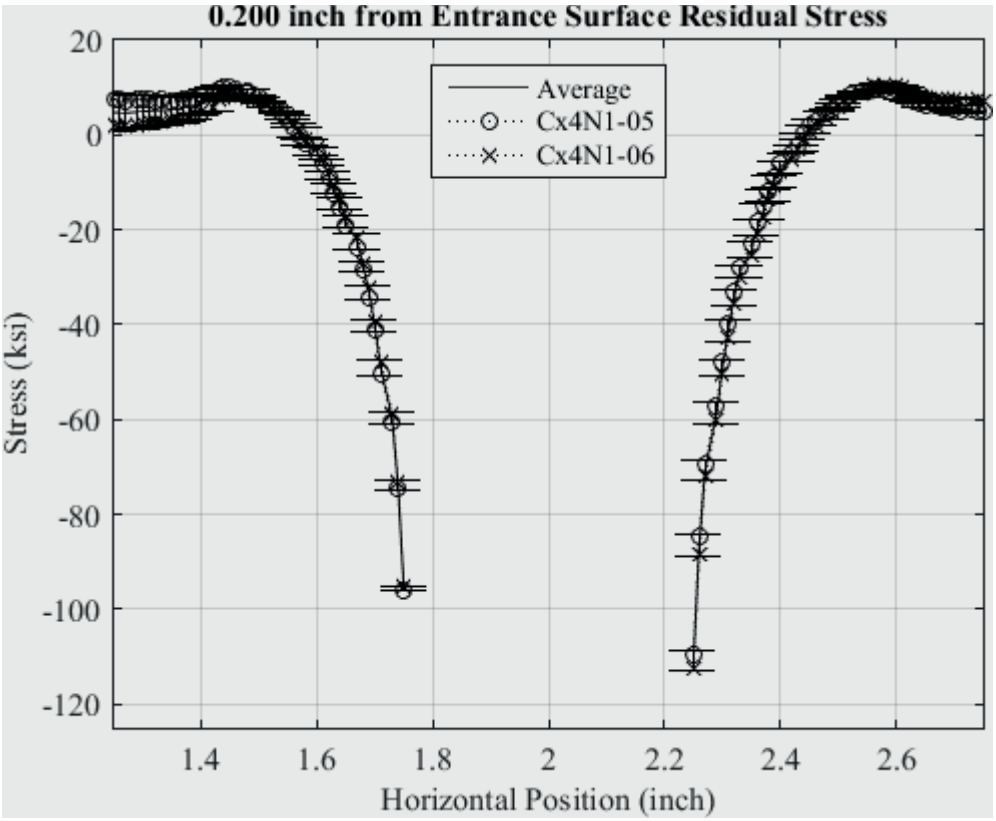

Fig. 455 Residual Stress Line Plot of Cx4N1-05-D and Cx4N1-06-D (7075-T651) at a Distance of 0.200 inch from the Entrance Surface – Coupons had a 0.125 inch Fatigue Crack at the Left Entrance Surface – Zoomed in Next to Hole.

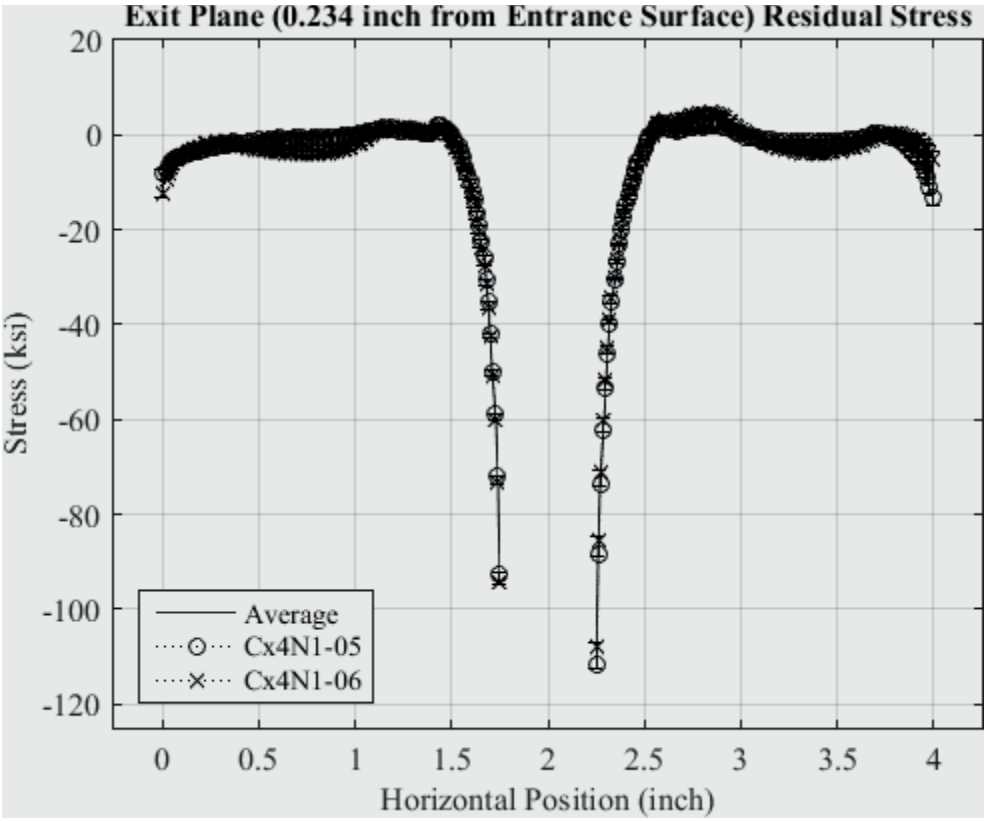

Fig. 456 Residual Stress Line Plot of Cx4N1-05-D and Cx4N1-06-D (7075-T651) at a Distance of 0.234 inch (Exit Surface) from the Entrance Surface – Coupons had a 0.125 inch Fatigue Crack at the Left Entrance Surface.

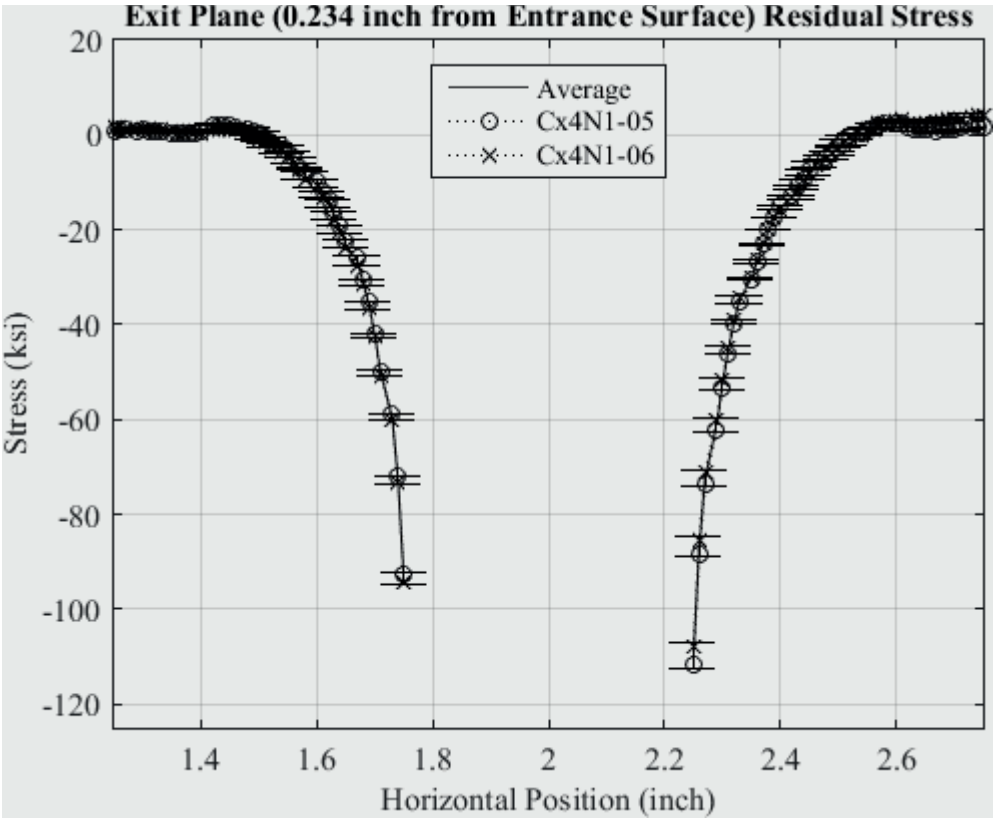

Fig. 457 Residual Stress Line Plot of Cx4N1-05-D and Cx4N1-06-D (7075-T651) at a Distance of 0.234 inch (Exit Surface) from the Entrance Surface – Coupons had a 0.125 inch Fatigue Crack at the Left Entrance Surface – Zoomed in Next to Hole.

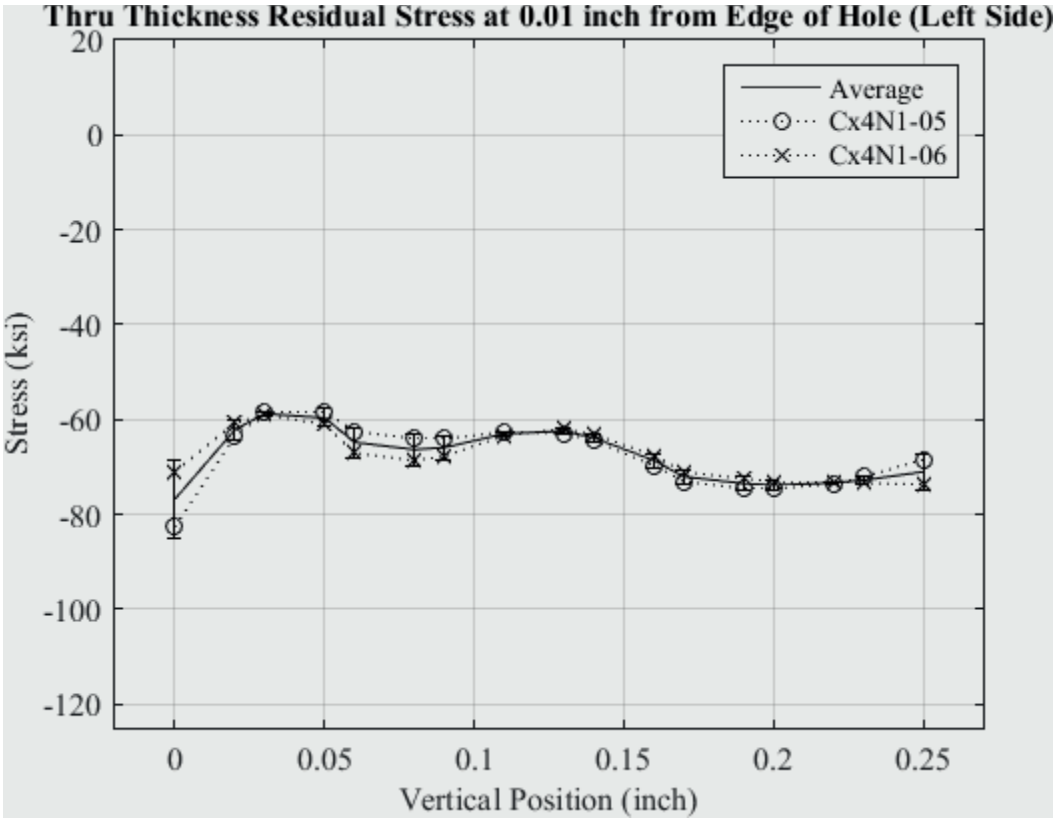

Fig. 458 Residual Stress Line Plot of Cx4N1-05-D and Cx4N1-06-D (7075-T651) Through the Thickness at 0.01 inch from Left Side of Hole – Coupons had a 0.125 inch Fatigue Crack at the Left Entrance Surface.

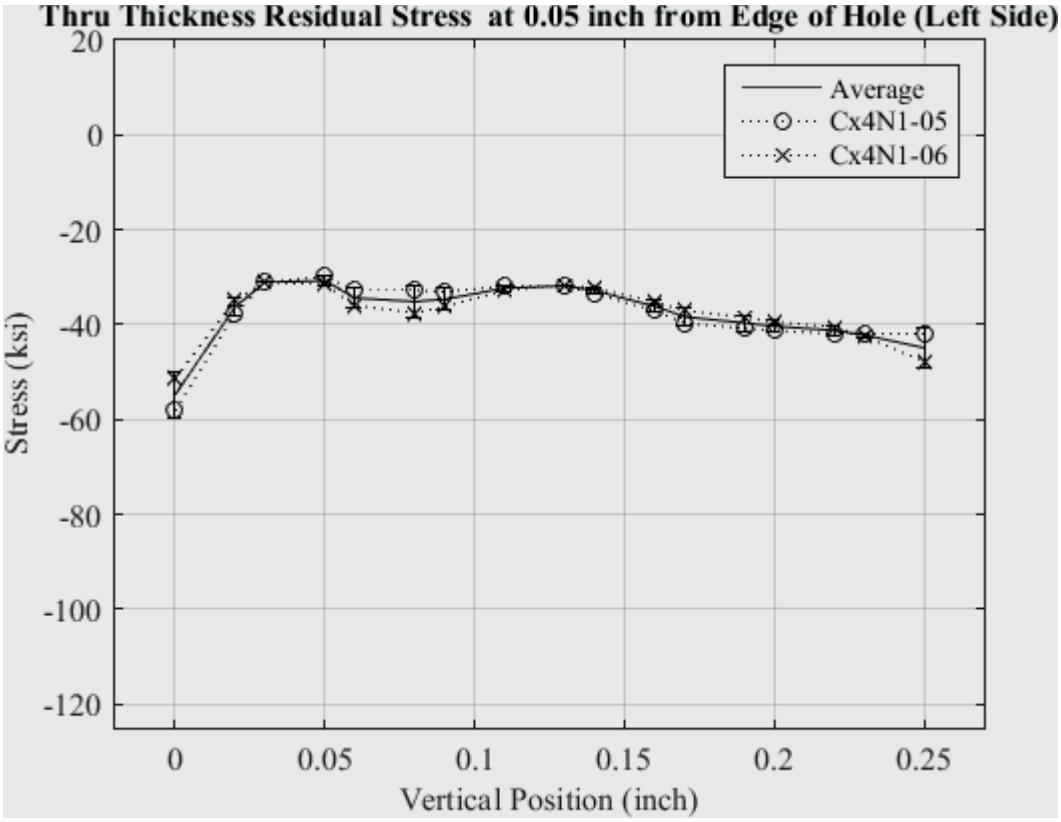

Fig. 459 Residual Stress Line Plot of Cx4N1-05-D and Cx4N1-06-D (7075-T651) Through the Thickness at 0.05 inch from Left Side of Hole – Coupons had a 0.125 inch Fatigue Crack at the Left Entrance Surface.

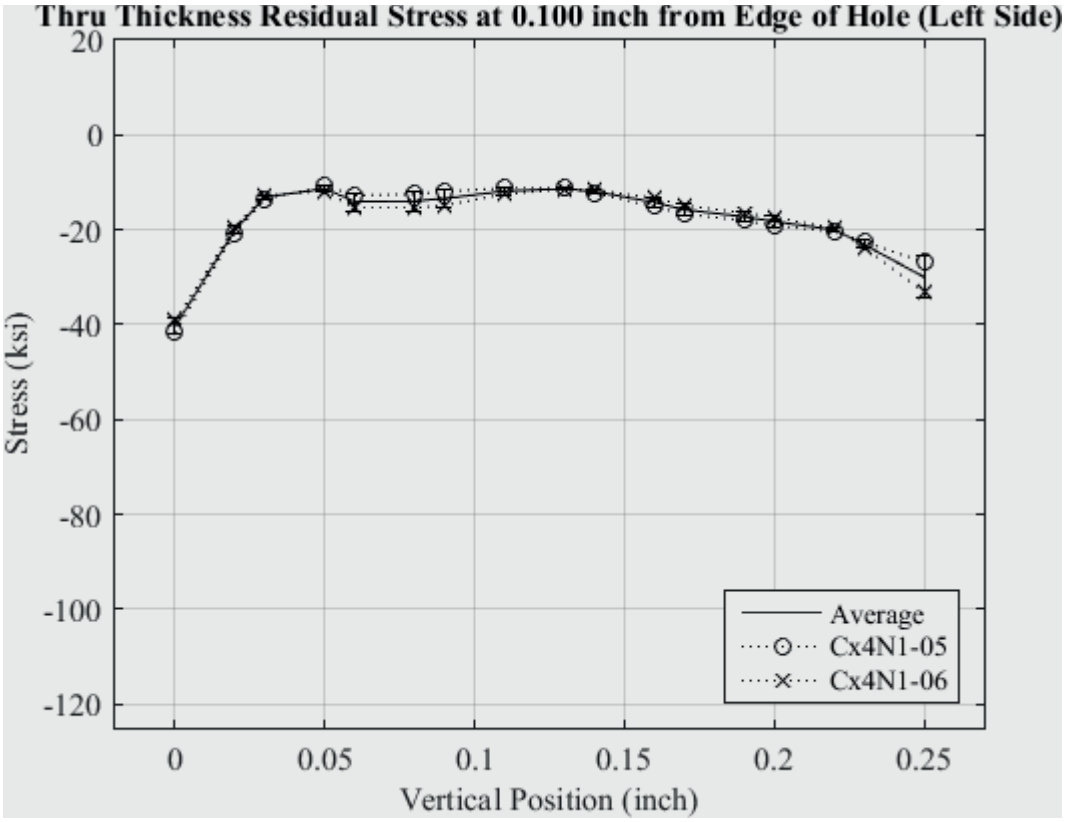

Fig. 460 Residual Stress Line Plot of Cx4N1-05-D and Cx4N1-06-D (7075-T651) Through the Thickness at 0.10 inch from Left Side of Hole – Coupons had a 0.125 inch Fatigue Crack at the Left Entrance Surface.

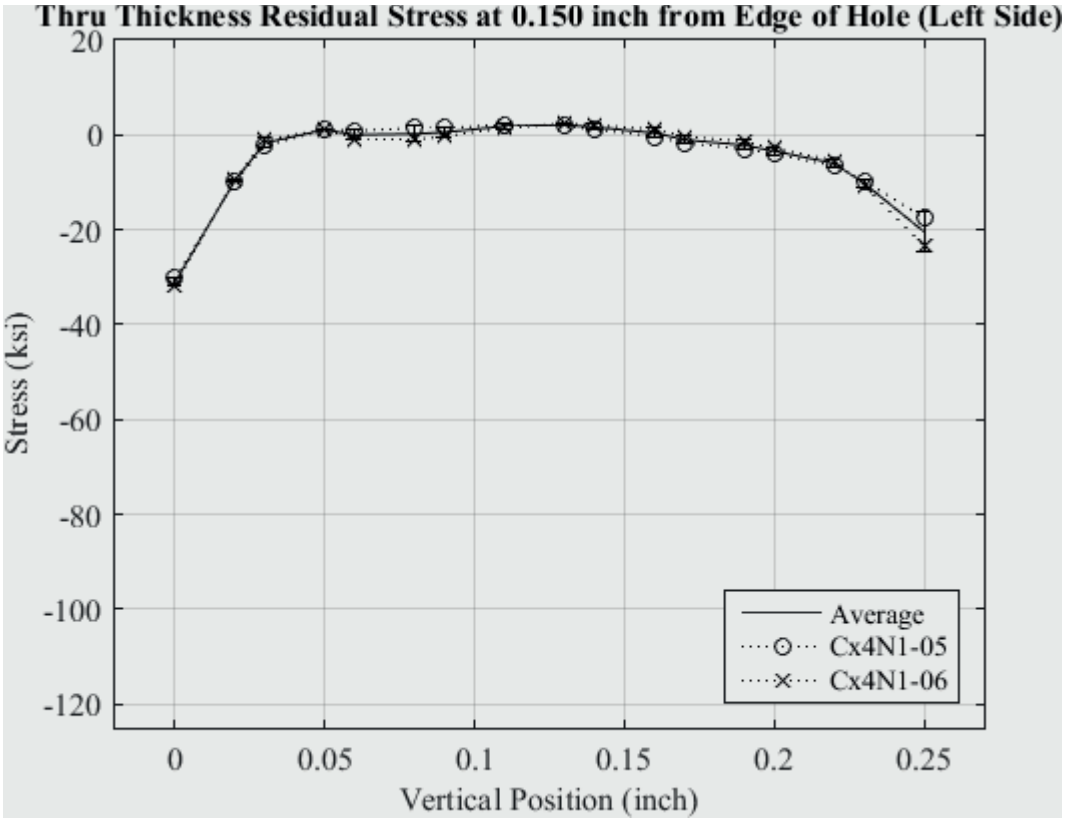

Fig. 461 Residual Stress Line Plot of Cx4N1-05-D and Cx4N1-06-D (7075-T651) Through the Thickness at 0.150 inch from Left Side of Hole – Coupons had a 0.125 inch Fatigue Crack at the Left Entrance Surface.

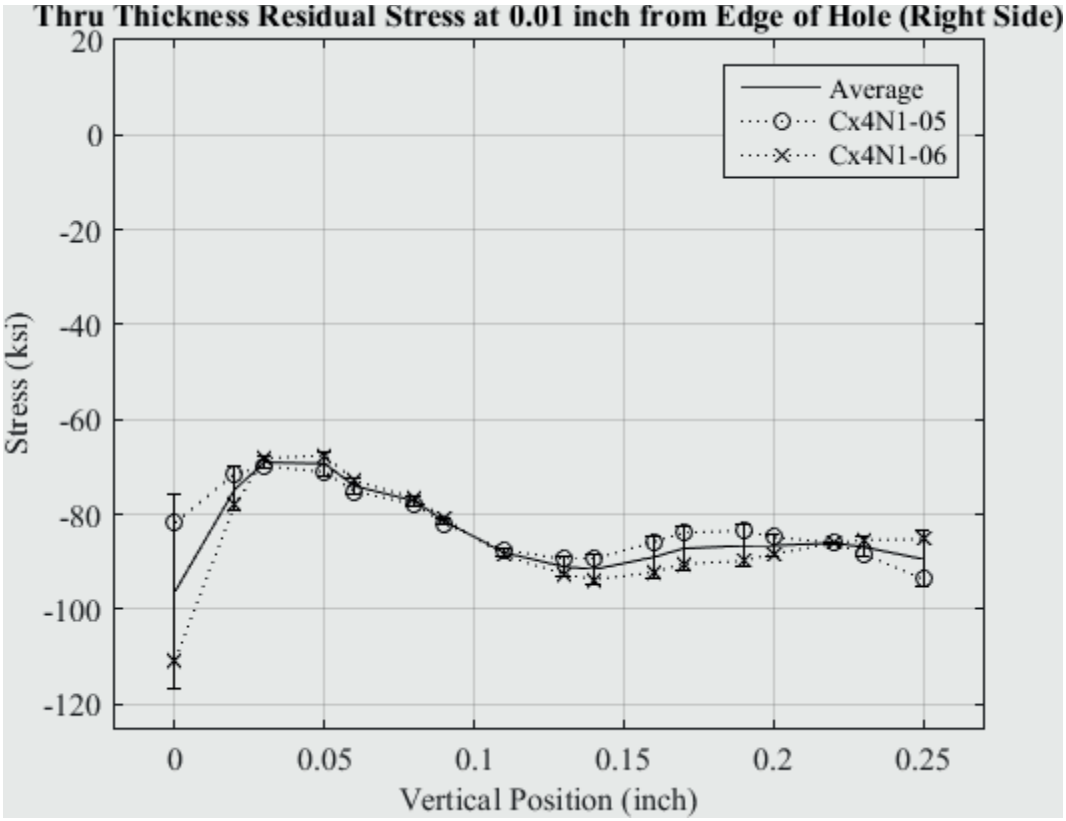

Fig. 462 Residual Stress Line Plot of Cx4N1-05-D and Cx4N1-06-D (7075-T651) Through the Thickness at 0.01 inch from Right Side of Hole – Coupons had a 0.125 inch Fatigue Crack at the Left Entrance Surface.

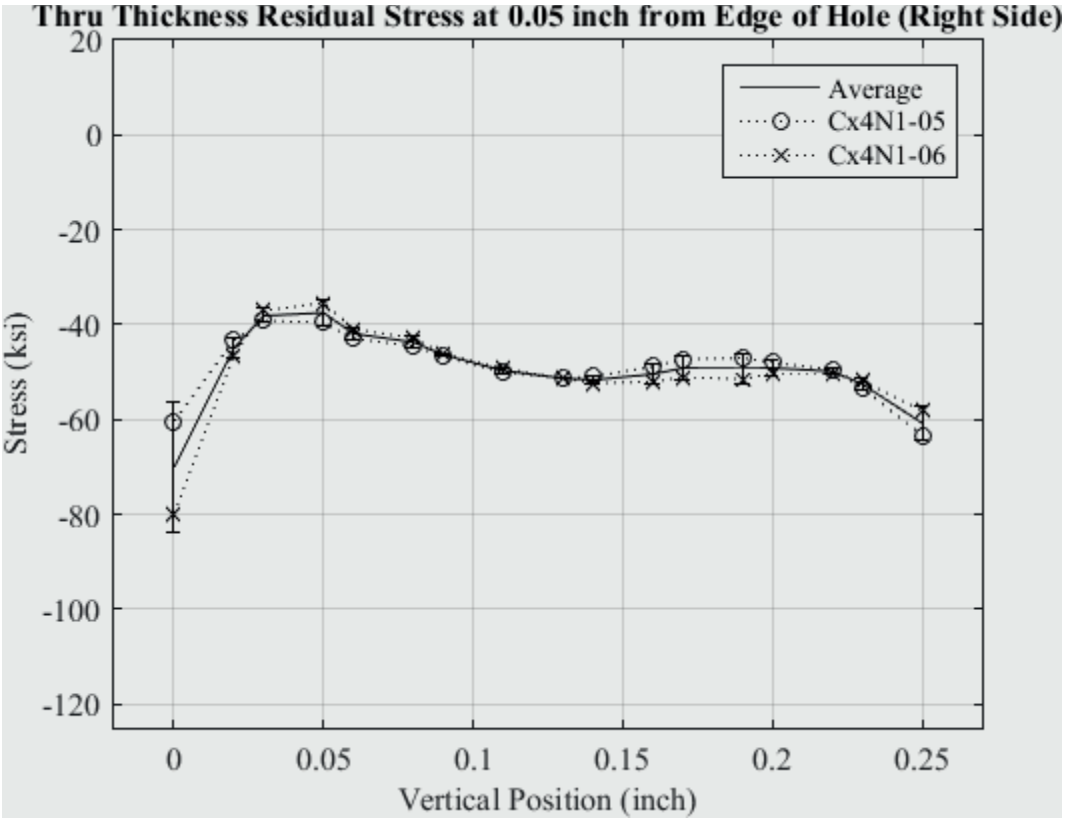

Fig. 463 Residual Stress Line Plot of Cx4N1-05-D and Cx4N1-06-D (7075-T651) Through the Thickness at 0.05 inch from Right Side of Hole – Coupons had a 0.125 inch Fatigue Crack at the Left Entrance Surface.

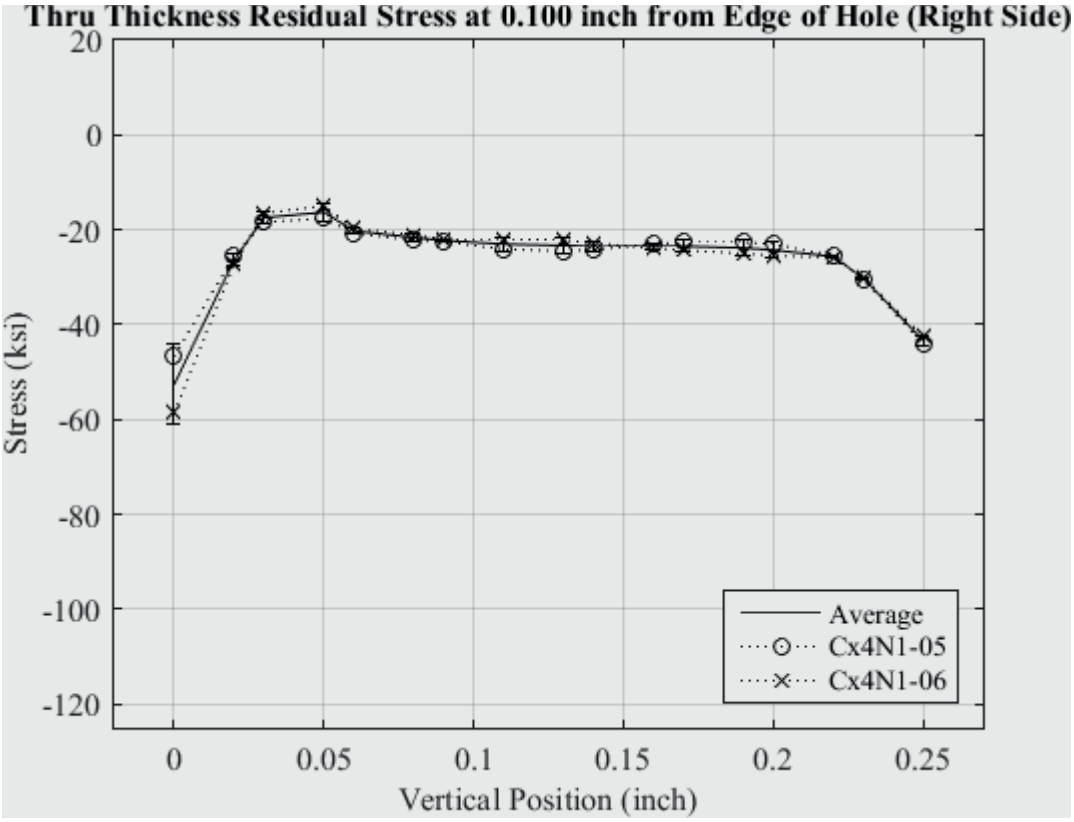

Fig. 464 Residual Stress Line Plot of Cx4N1-05-D and Cx4N1-06-D (7075-T651) Through the Thickness at 0.10 inch from Right Side of Hole – Coupons had a 0.125 inch Fatigue Crack at the Left Entrance Surface.

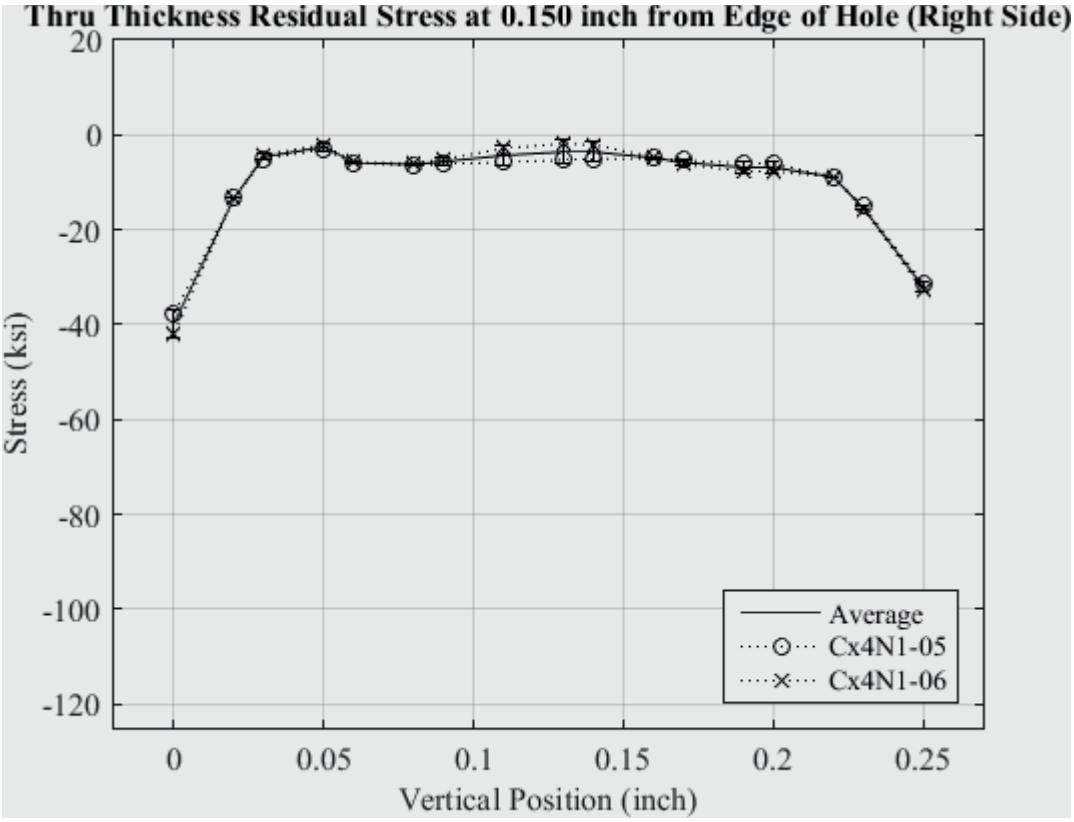

Fig. 465 Residual Stress Line Plot of Cx4N1-05-D and Cx4N1-06-D (7075-T651) Through the Thickness at 0.150 inch from Right Side of Hole – Coupons had a 0.125 inch Fatigue Crack at the Left Entrance Surface.

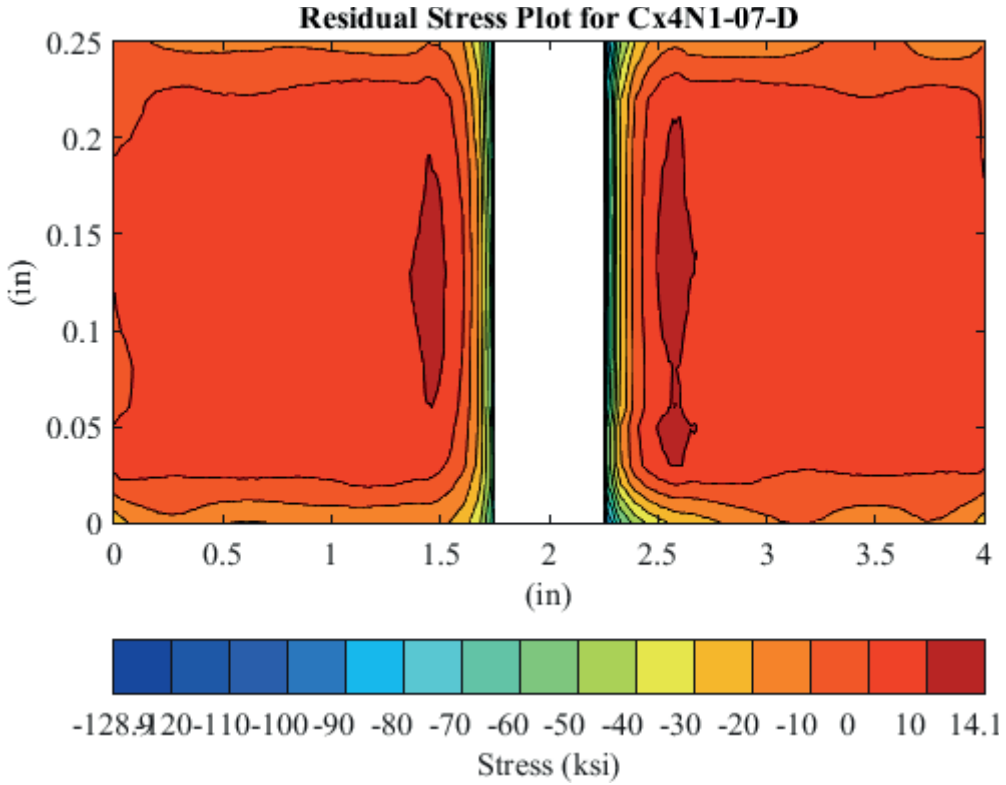

Fig. 466 Residual Stress Contour Plot of Coupon Cx4N1-07-D (7075-T651) – Mandrel Entrance Surface at Y=0, 0.2505 inch Fatigue Crack on Left Side of the Hole on Mandrel Entrance Surface.

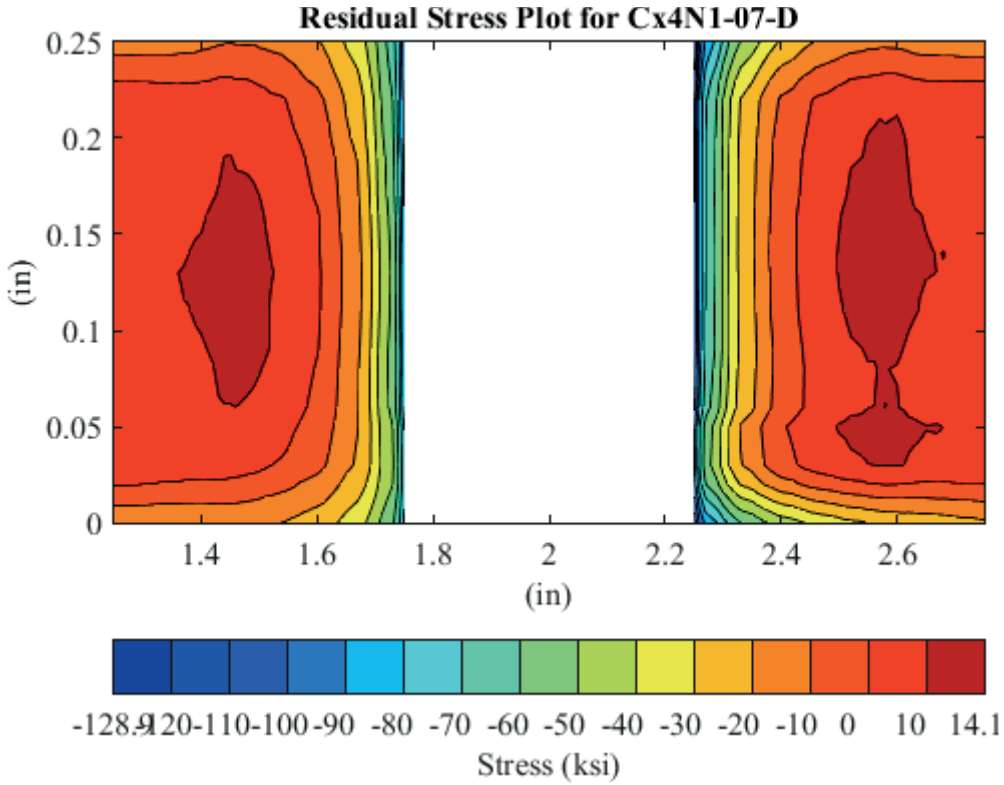

Fig. 467 Residual Stress Contour Plot of Coupon Cx4N1-07-D (7075-T651) – Mandrel Entrance Surface at Y=0, 0.2505 inch Fatigue Crack on Left Side of the Hole on Mandrel Entrance Surface – Zoomed in Next to Hole.

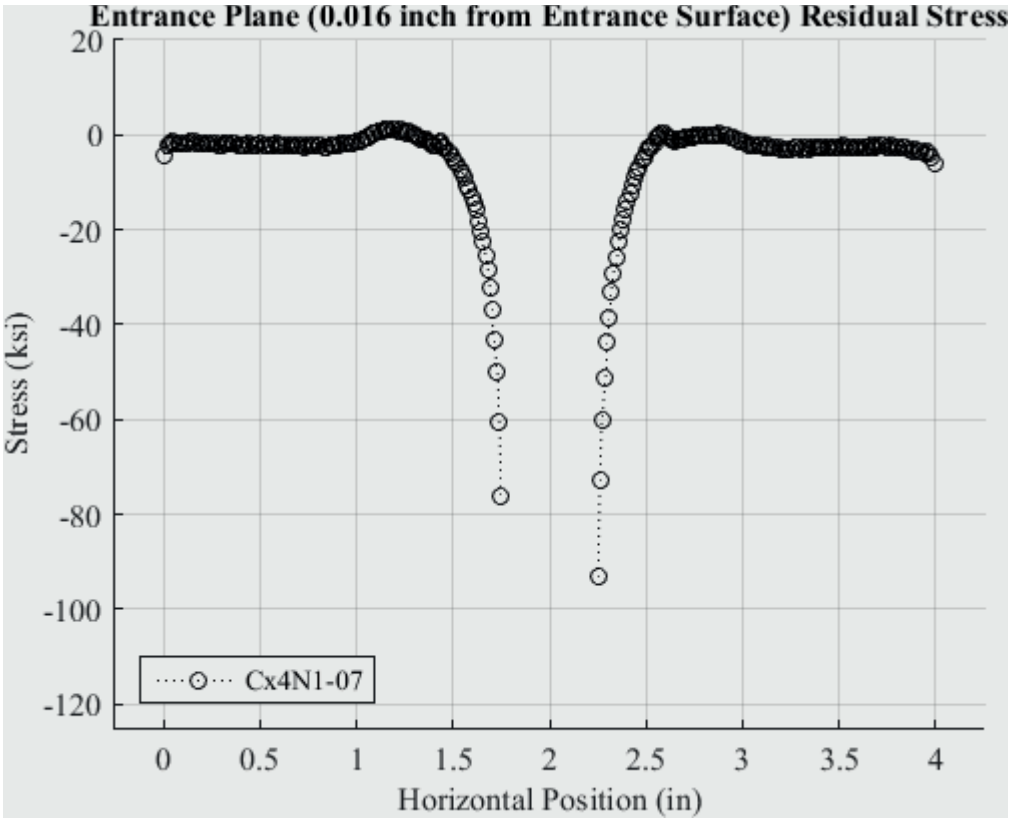

Fig. 468 Residual Stress Line Plot of Cx4N1-07-D (7075-T651) at a Distance of 0.016 inch (Entrance Surface) from the Entrance Surface – Coupons had a 0.2505 inch Fatigue Crack at the Left Entrance Surface.

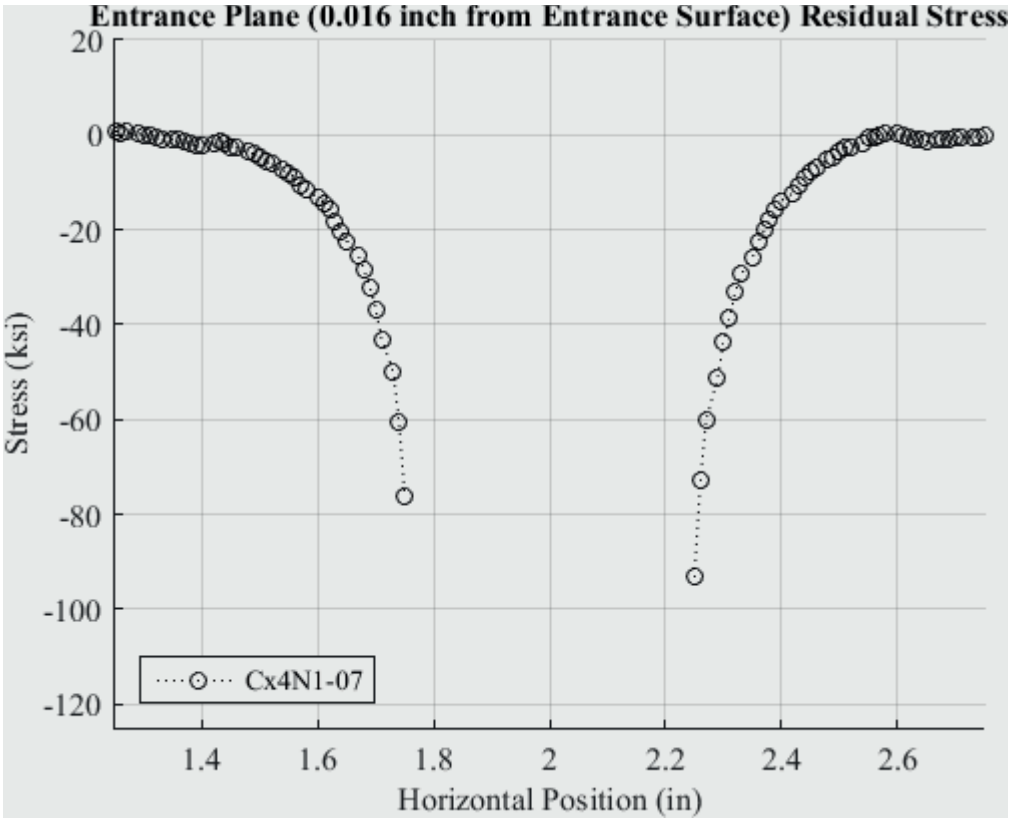

Fig. 469 Residual Stress Line Plot of Cx4N1-07-D (7075-T651) at a Distance of 0.016 inch (Entrance Surface) from the Entrance Surface – Coupons had a 0.2505 inch Fatigue Crack at the Left Entrance Surface – Zoomed in Next to Hole.

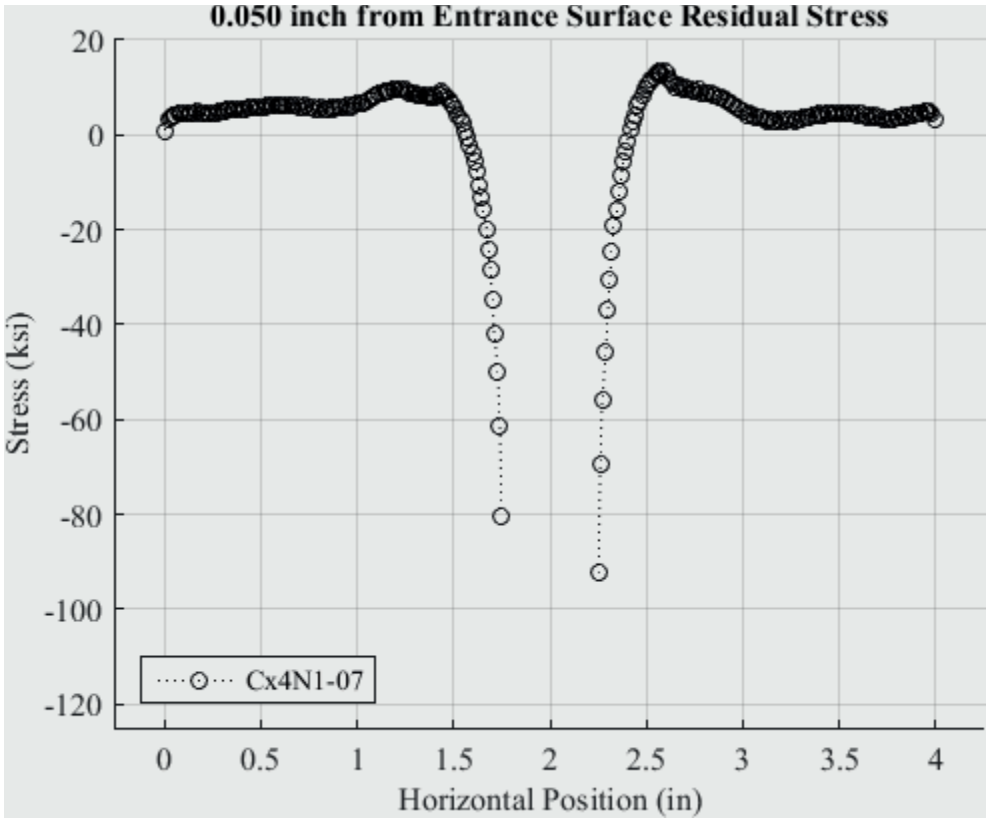

Fig. 470 Residual Stress Line Plot of Cx4N1-07-D (7075-T651) at a Distance of 0.05 inch from the Entrance Surface – Coupons had a 0.2505 inch Fatigue Crack at the Left Entrance Surface.

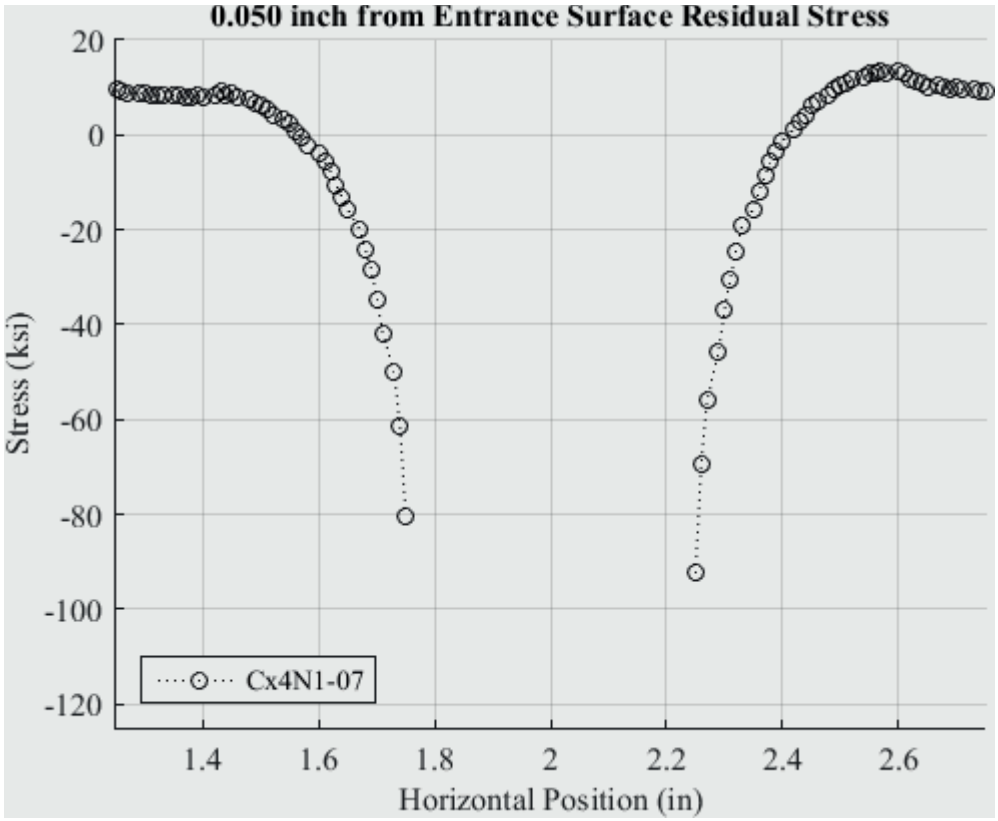

Fig. 471 Residual Stress Line Plot of Cx4N1-07-D (7075-T651) at a Distance of 0.05 inch from the Entrance Surface – Coupons had a 0.2505 inch Fatigue Crack at the Left Entrance Surface – Zoomed in Next to Hole.

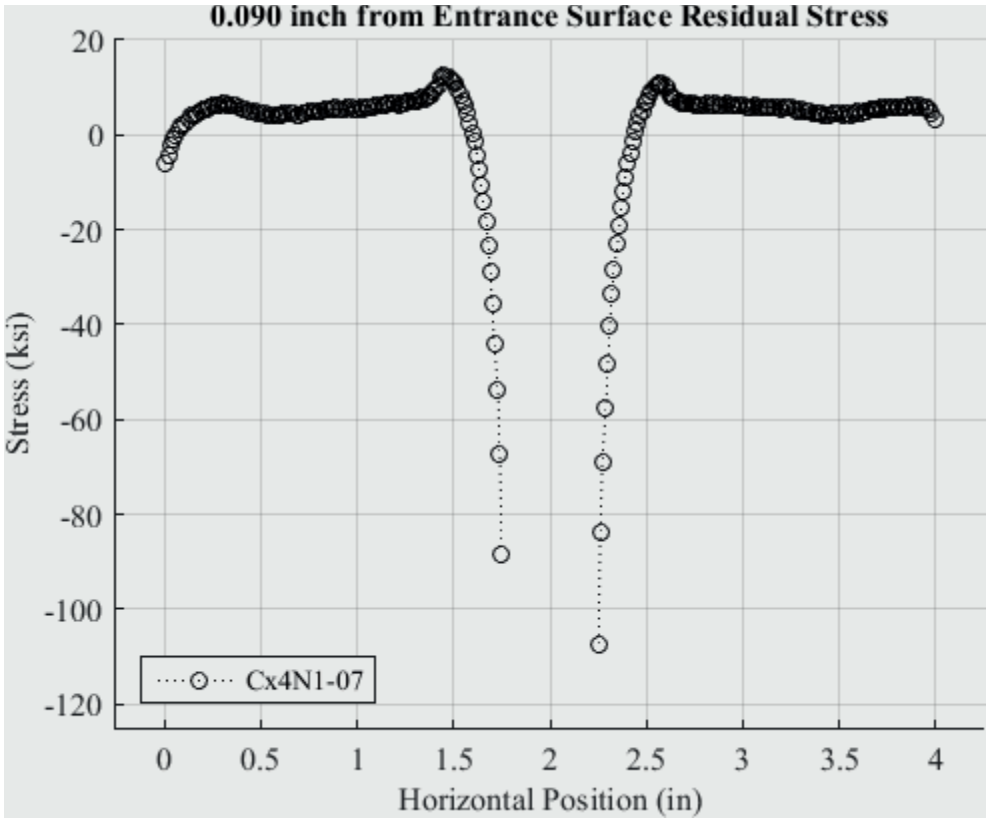

Fig. 472 Residual Stress Line Plot of Cx4N1-07-D (7075-T651) at a Distance of 0.09 inch from the Entrance Surface – Coupons had a 0.2505 inch Fatigue Crack at the Left Entrance Surface.

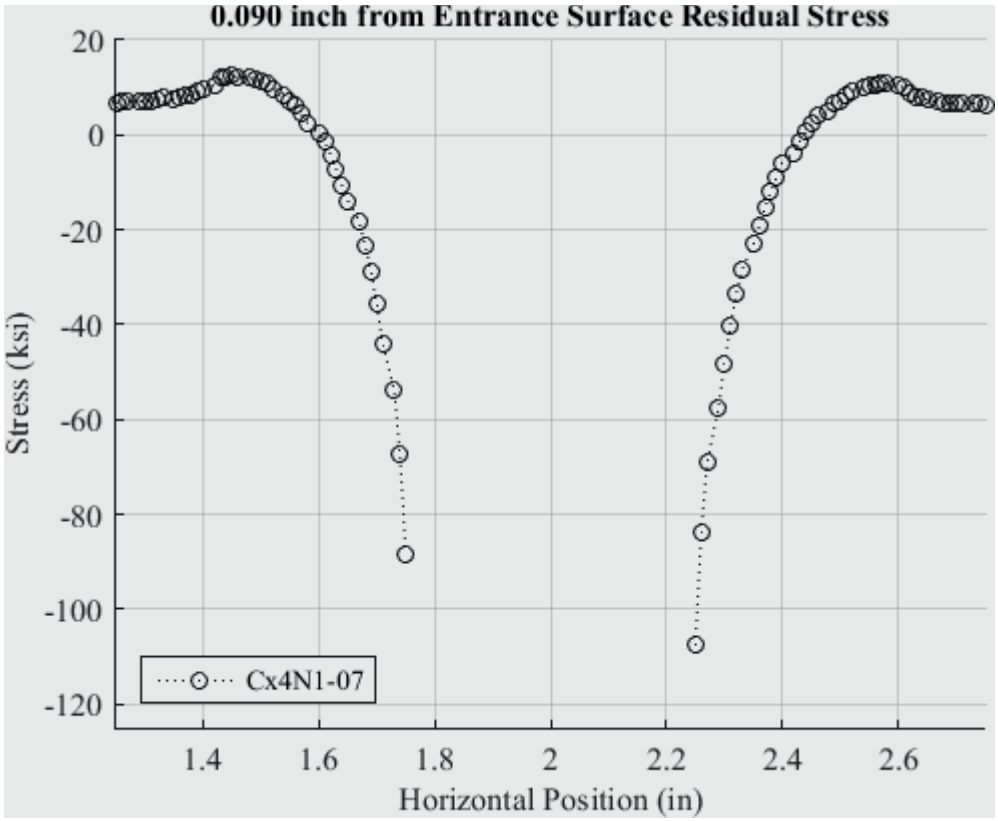

Fig. 473 Residual Stress Line Plot of Cx4N1-07-D (7075-T651) at a Distance of 0.09 inch from the Entrance Surface – Coupons had a 0.2505 inch Fatigue Crack at the Left Entrance Surface – Zoomed in Next to Hole.

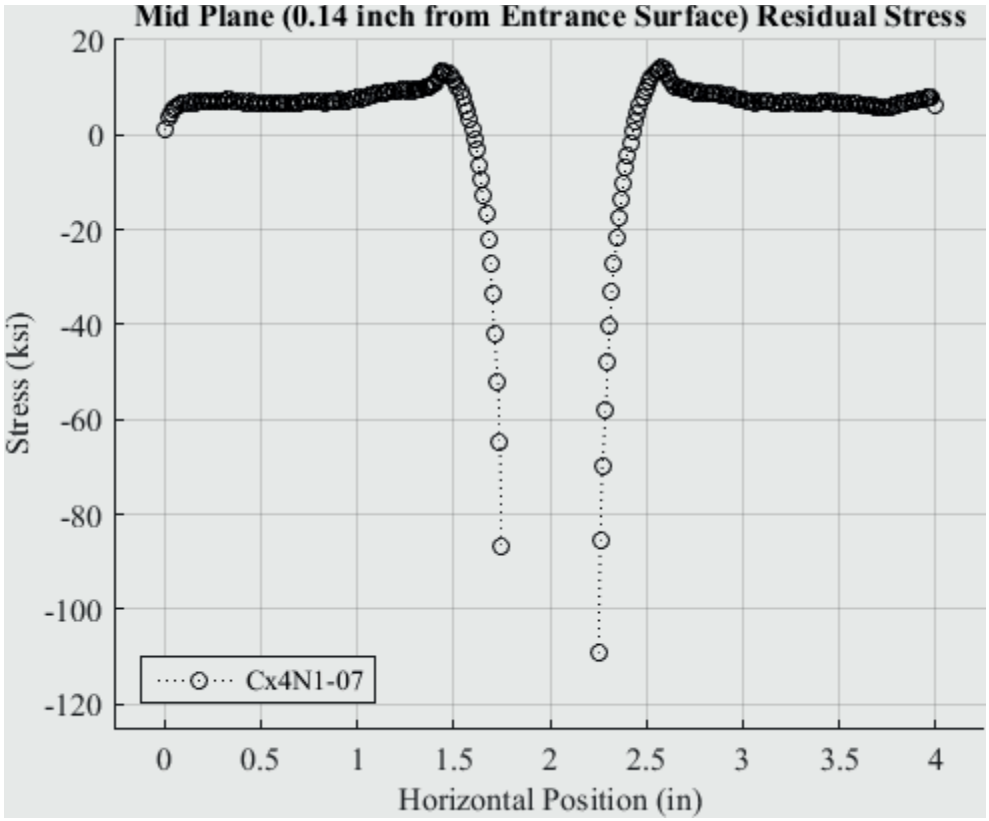

Fig. 474 Residual Stress Line Plot of Cx4N1-07-D (7075-T651) at a Distance of 0.140 inch (Mid Plane Surface) from the Entrance Surface – Coupons had a 0.2505 inch Fatigue Crack at the Left Entrance Surface.

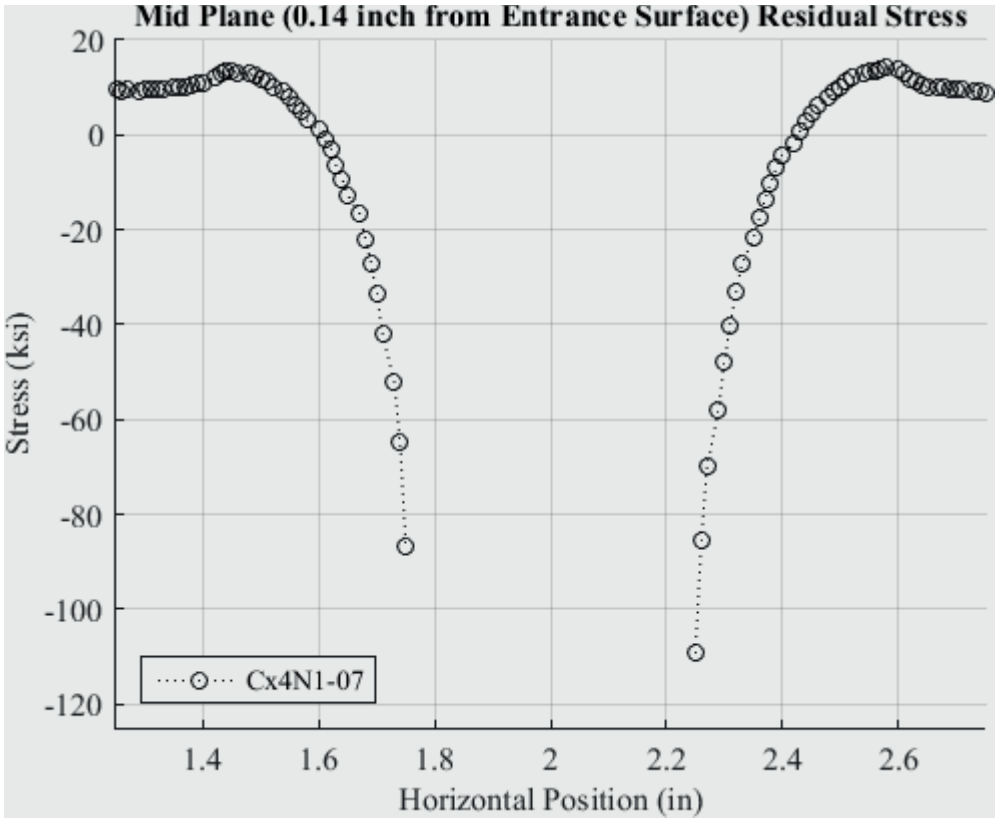

Fig. 475 Residual Stress Line Plot of Cx4N1-07-D (7075-T651) at a Distance of 0.140 inch (Mid Plane Surface) from the Entrance Surface – Coupons had a 0.2505 inch Fatigue Crack at the Left Entrance Surface – Zoomed in Next to Hole.

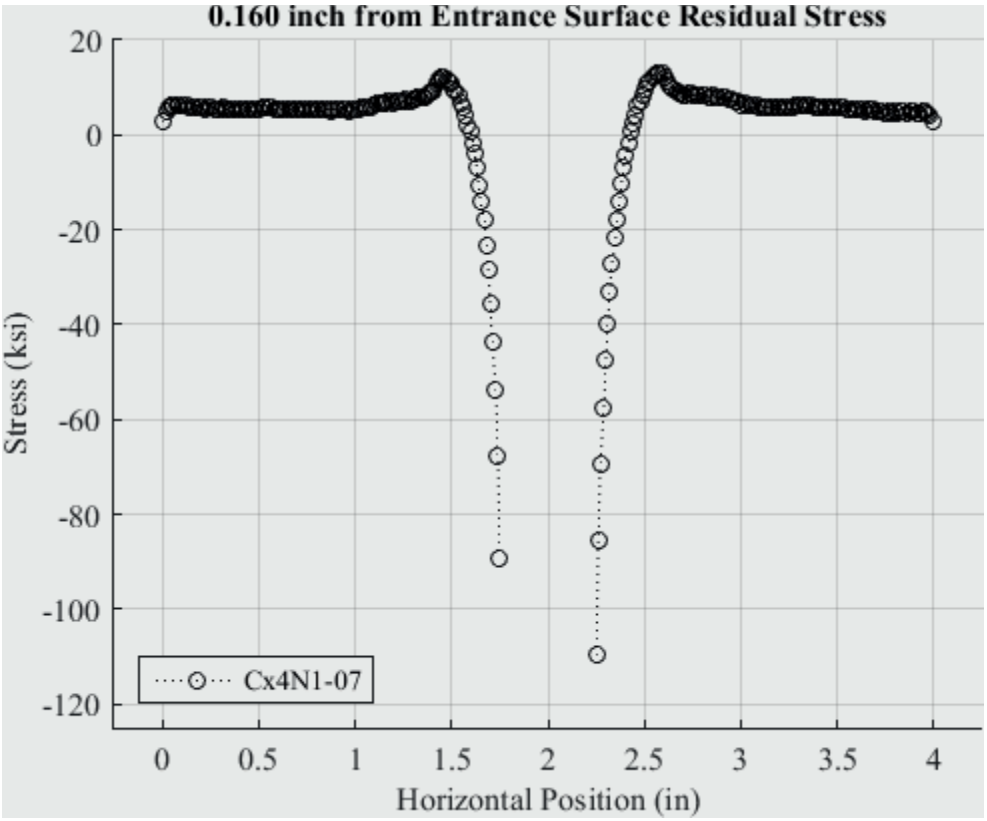

Fig. 476 Residual Stress Line Plot of Cx4N1-07-D (7075-T651) at a Distance of 0.160 inch from the Entrance Surface – Coupons had a 0.2505 inch Fatigue Crack at the Left Entrance Surface.

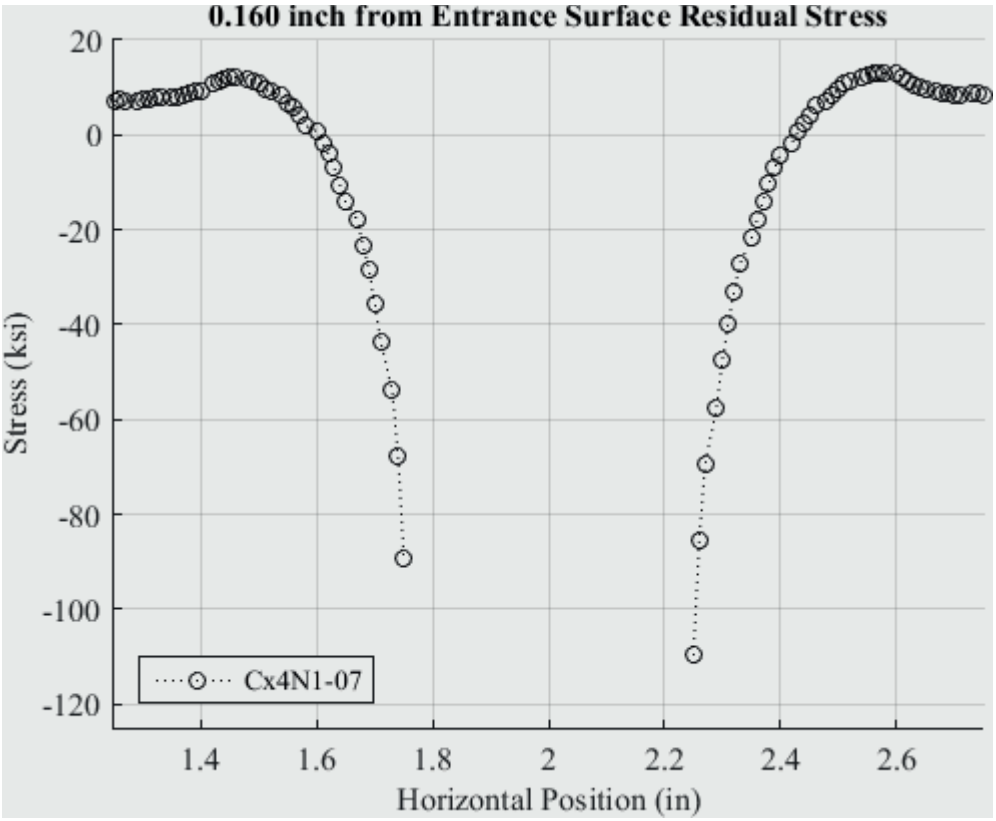

Fig. 477 Residual Stress Line Plot of Cx4N1-07-D (7075-T651) at a Distance of 0.160 inch from the Entrance Surface – Coupons had a 0.2505 inch Fatigue Crack at the Left Entrance Surface – Zoomed in Next to Hole.

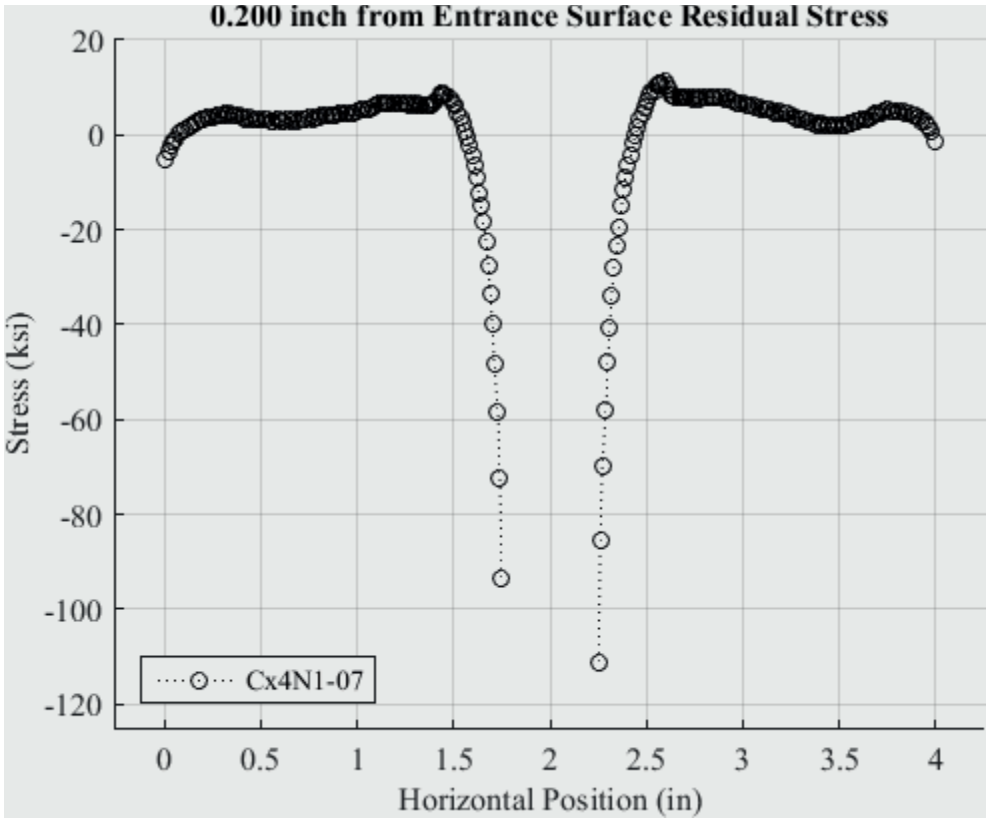

Fig. 478 Residual Stress Line Plot of Cx4N1-07-D (7075-T651) at a Distance of 0.200 inch from the Entrance Surface – Coupons had a 0.2505 inch Fatigue Crack at the Left Entrance Surface – Zoomed in Next to Hole.

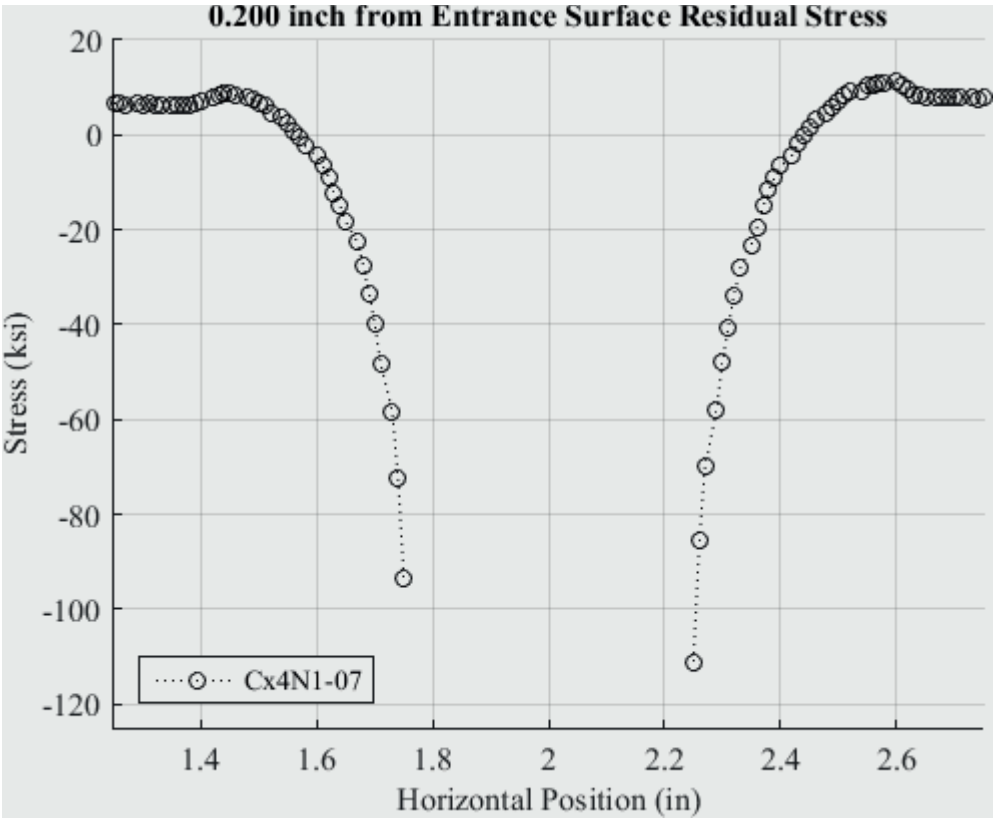

Fig. 479 Residual Stress Line Plot of Cx4N1-07-D (7075-T651) at a Distance of 0.200 inch from the Entrance Surface – Coupons had a 0.2505 inch Fatigue Crack at the Left Entrance Surface – Zoomed in Next to Hole.

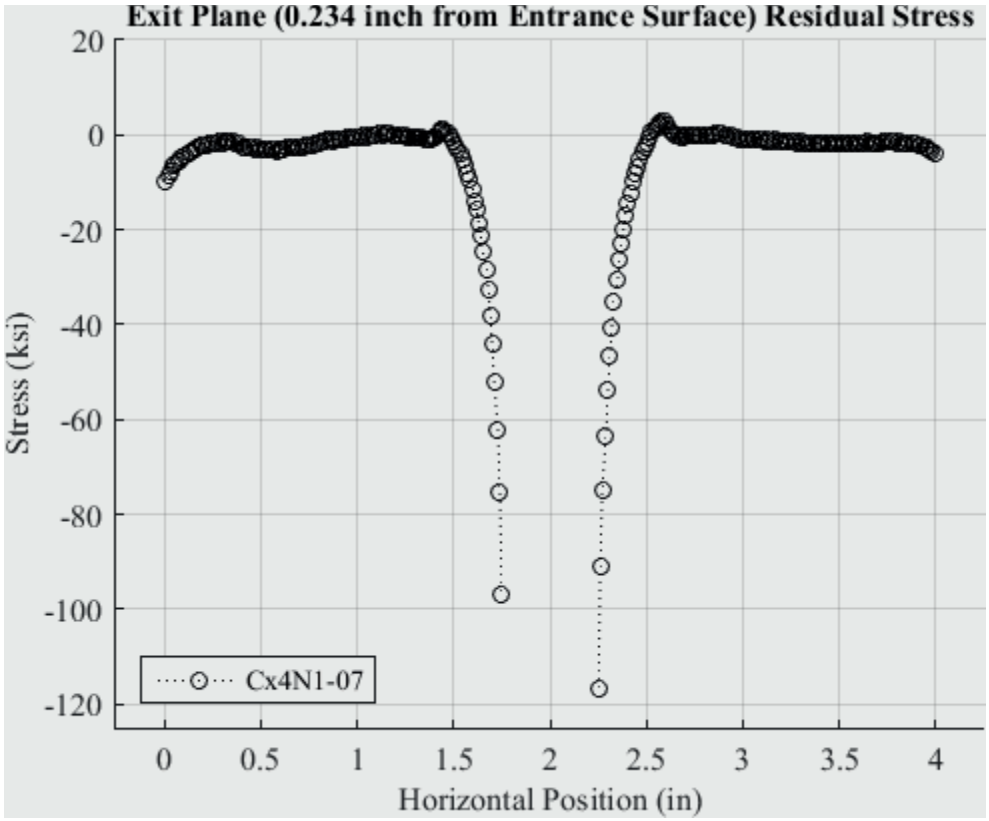

Fig. 480 Residual Stress Line Plot of Cx4N1-07-D (7075-T651) at a Distance of 0.234 inch (Exit Surface) from the Entrance Surface – Coupons had a 0.2505 inch Fatigue Crack at the Left Entrance Surface – Zoomed in Next to Hole.

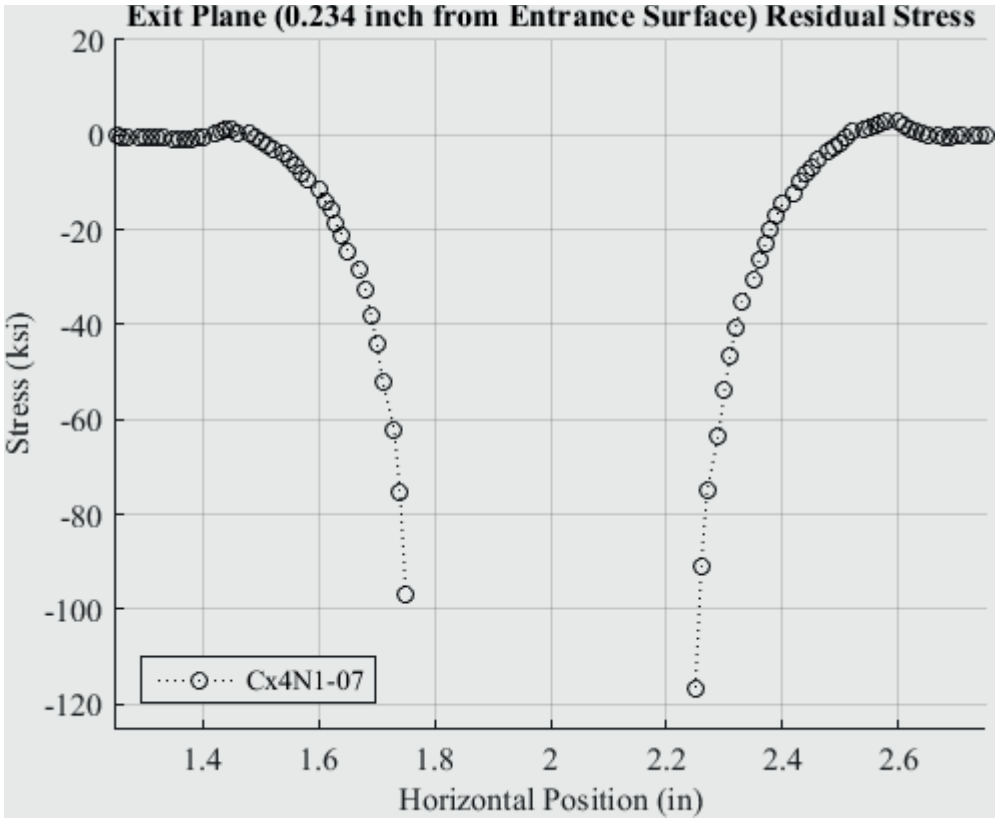

Fig. 481 Residual Stress Line Plot of Cx4N1-07-D (7075-T651) at a Distance of 0.234 inch (Exit Surface) from the Entrance Surface – Coupons had a 0.2505 inch Fatigue Crack at the Left Entrance Surface – Zoomed in Next to Hole.

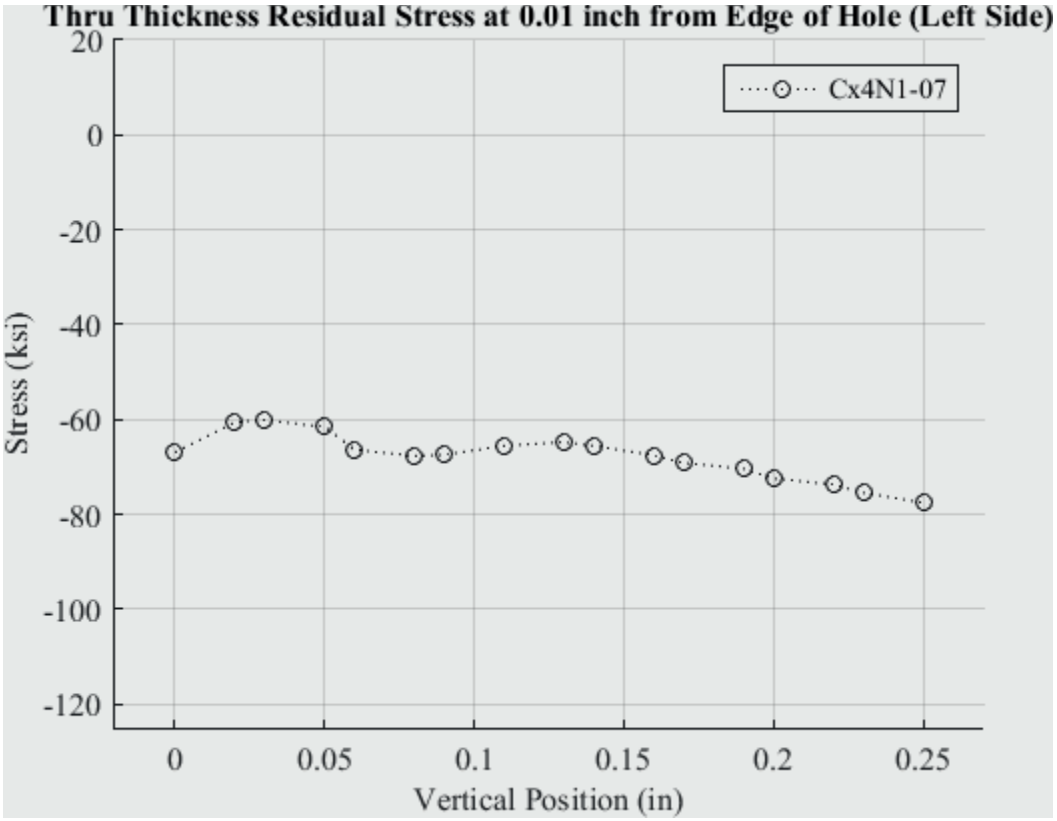

Fig. 482 Residual Stress Line Plot of Cx4N1-07-D (7075-T651) Through the Thickness at 0.01 inch from Left Side of Hole – Coupons had a 0.2505 inch Fatigue Crack at the Left Entrance Surface.

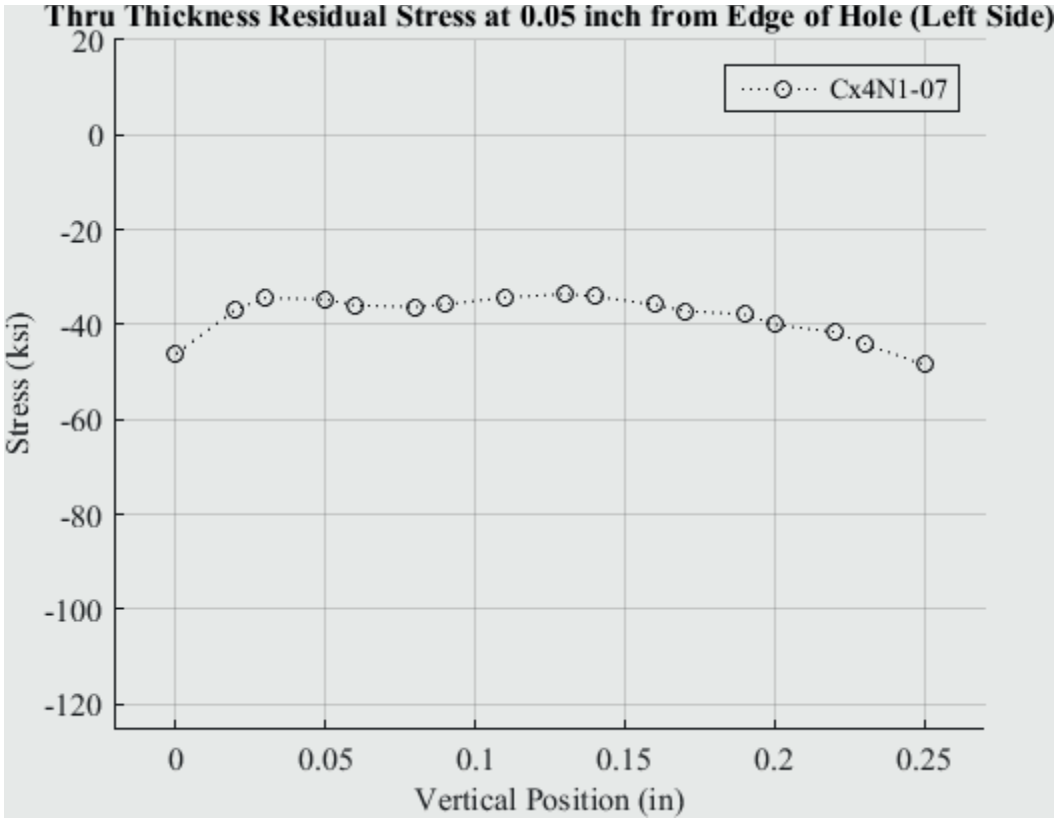

Fig. 483 Residual Stress Line Plot of Cx4N1-07-D (7075-T651) Through the Thickness at 0.05 inch from Left Side of Hole – Coupons had a 0.2505 inch Fatigue Crack at the Left Entrance Surface.

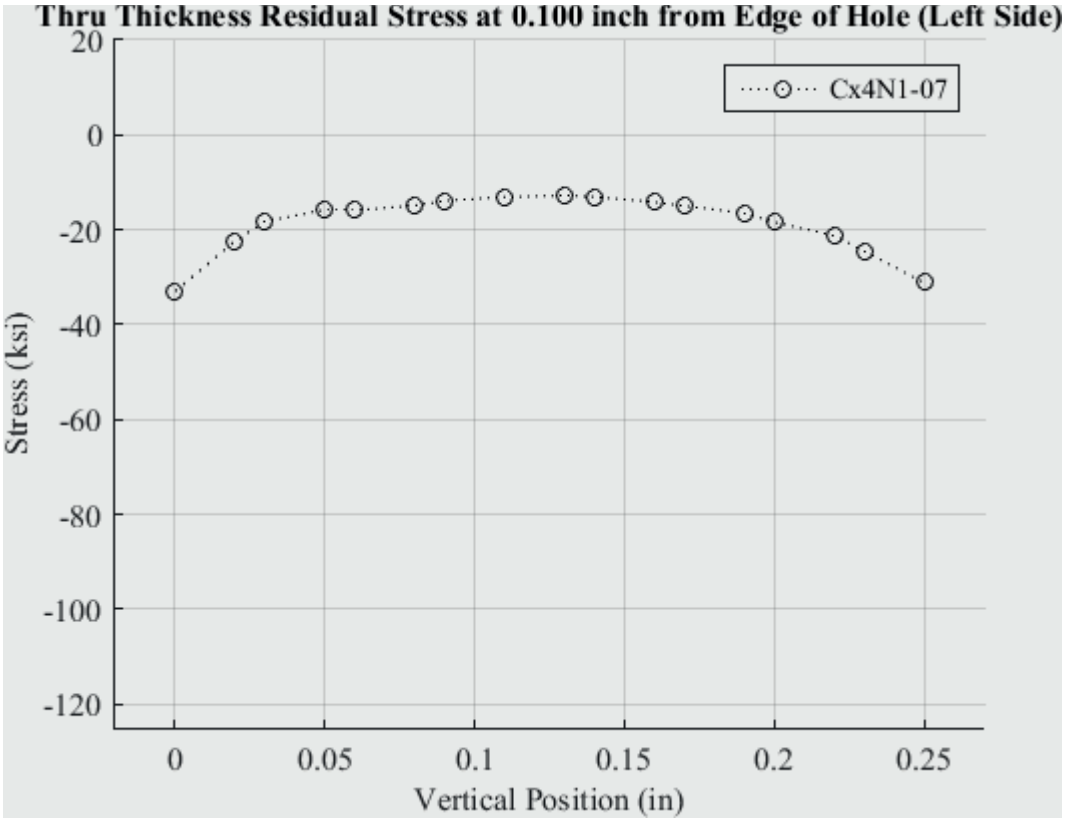

Fig. 484 Residual Stress Line Plot of Cx4N1-07-D (7075-T651) Through the Thickness at 0.10 inch from Left Side of Hole – Coupons had a 0.2505 inch Fatigue Crack at the Left Entrance Surface.

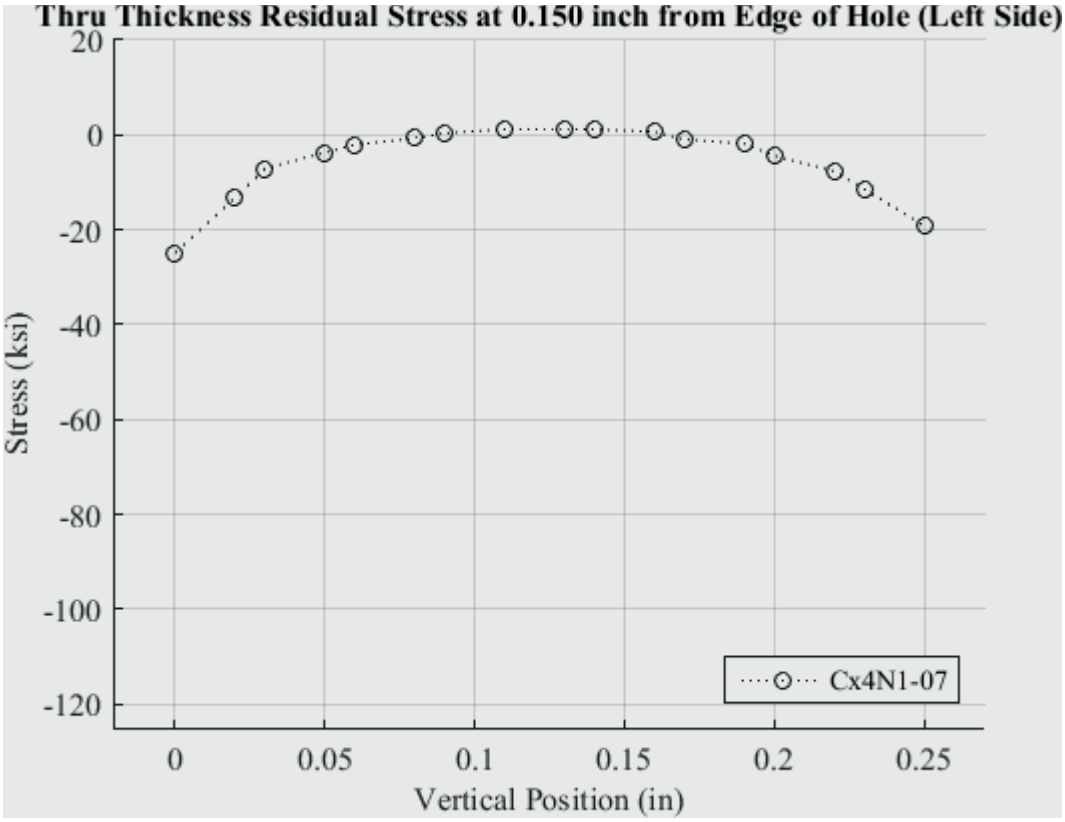

Fig. 485 Residual Stress Line Plot of Cx4N1-07-D (7075-T651) Through the Thickness at 0.150 inch from Left Side of Hole – Coupons had a 0.2505 inch Fatigue Crack at the Left Entrance Surface.

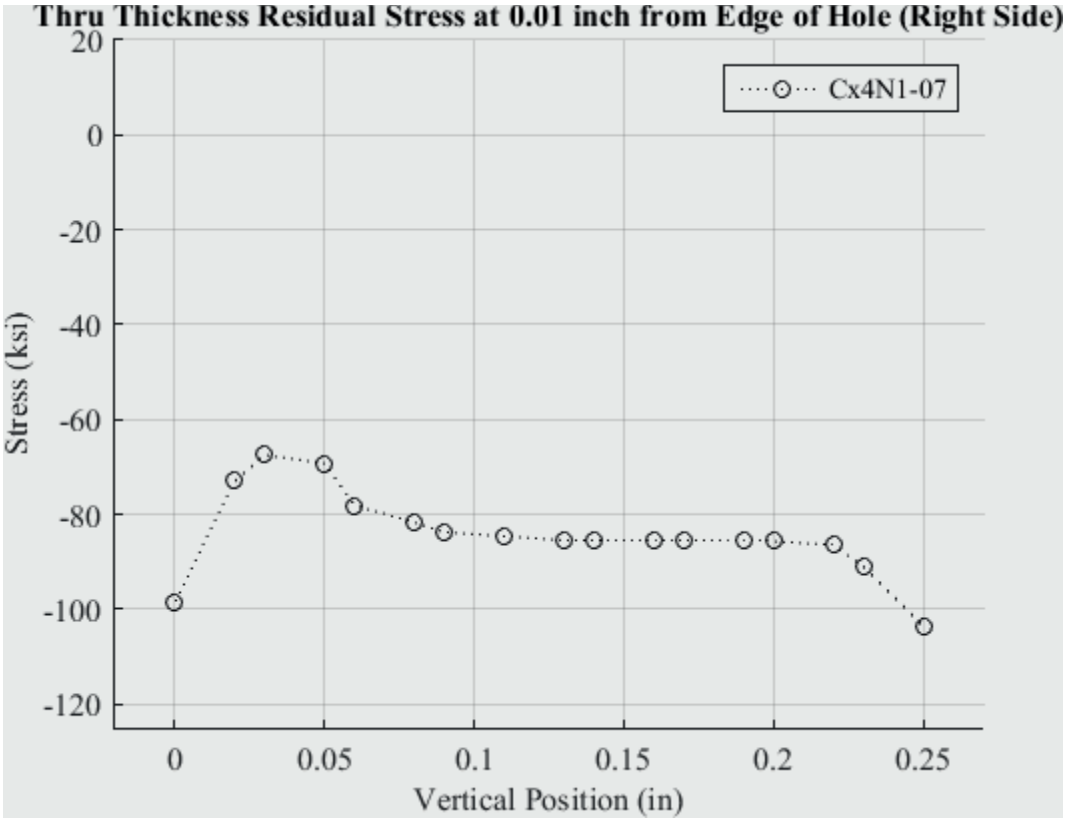

Fig. 486 Residual Stress Line Plot of Cx4N1-07-D (7075-T651) Through the Thickness at 0.01 inch from Right Side of Hole – Coupons had a 0.2505 inch Fatigue Crack at the Left Entrance Surface.

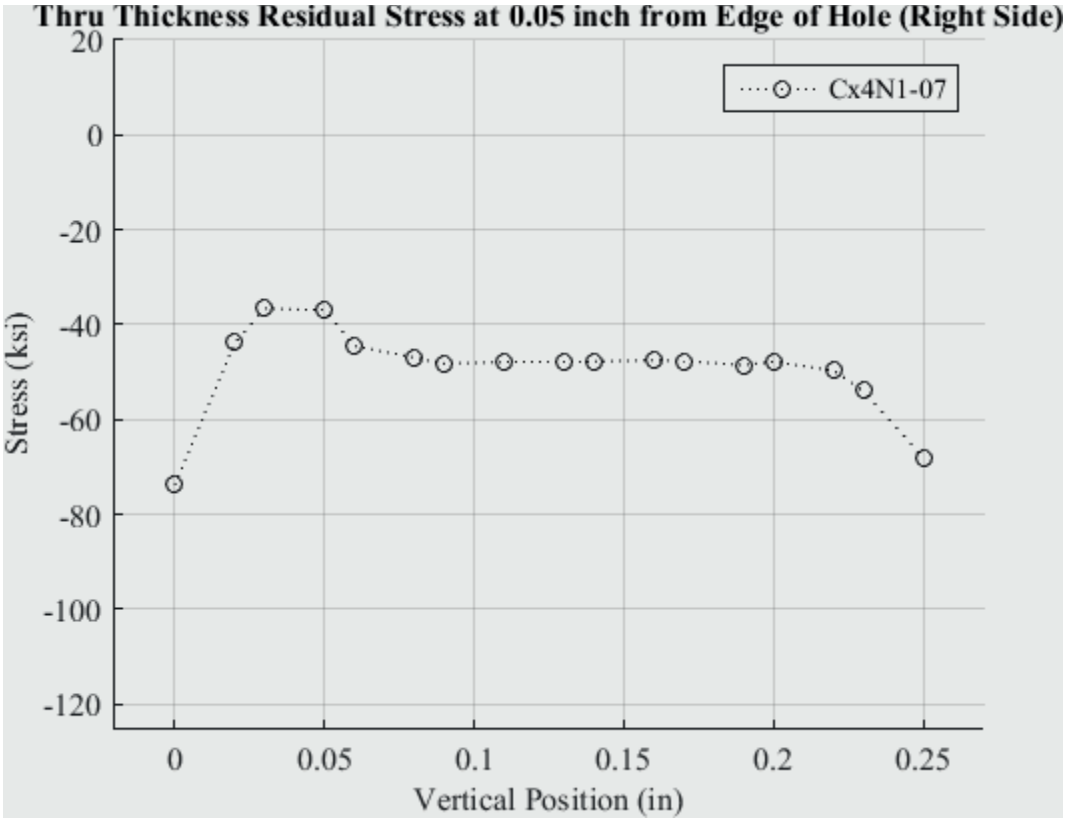

Fig. 487 Residual Stress Line Plot of Cx4N1-07-D (7075-T651) Through the Thickness at 0.05 inch from Right Side of Hole – Coupons had a 0.2505 inch Fatigue Crack at the Left Entrance Surface.

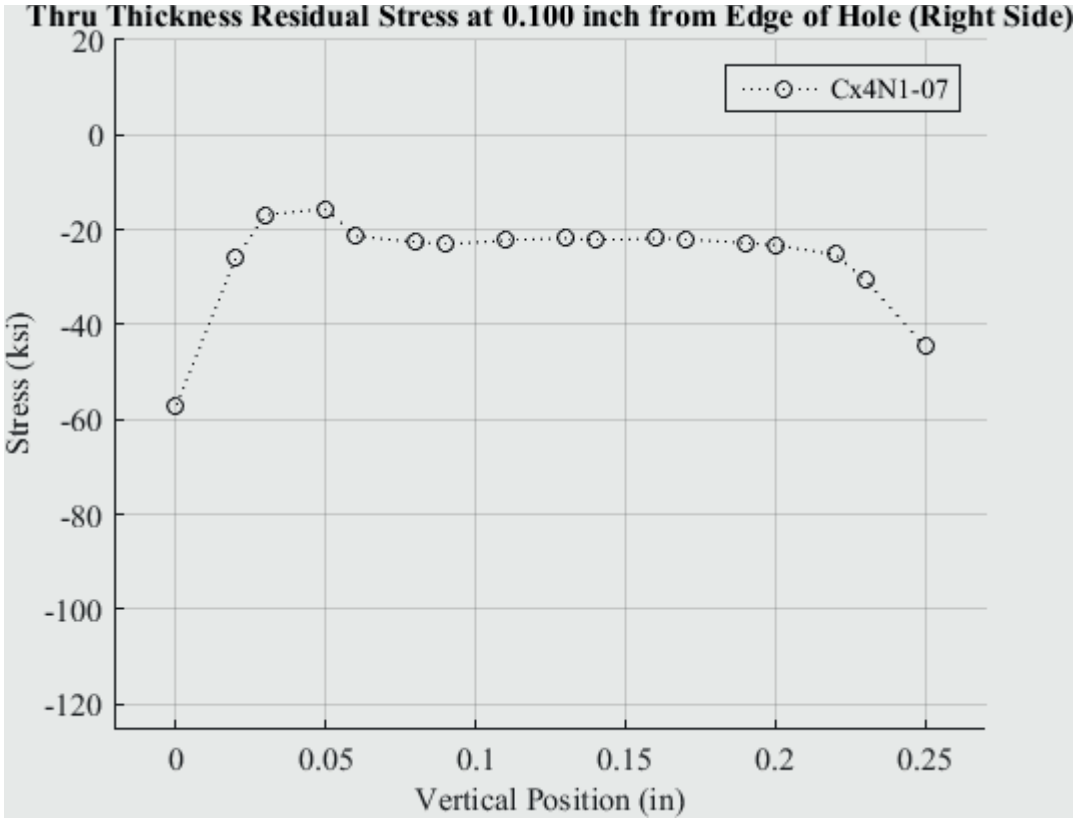

Fig. 488 Residual Stress Line Plot of Cx4N1-07-D (7075-T651) Through the Thickness at 0.10 inch from Right Side of Hole – Coupons had a 0.2505 inch Fatigue Crack at the Left Entrance Surface.

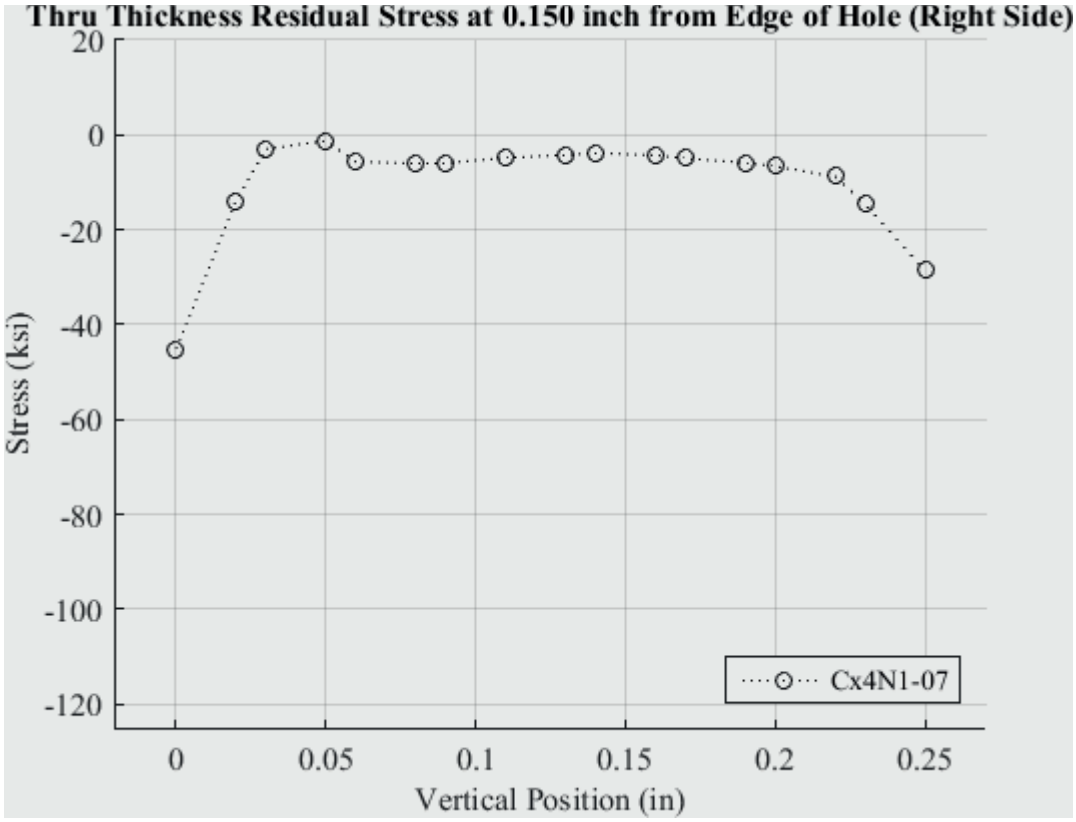

Fig. 489 Residual Stress Line Plot of Cx4N1-07-D (7075-T651) Through the Thickness at 0.150 inch from Right Side of Hole – Coupons had a 0.2505 inch Fatigue Crack at the Left Entrance Surface.

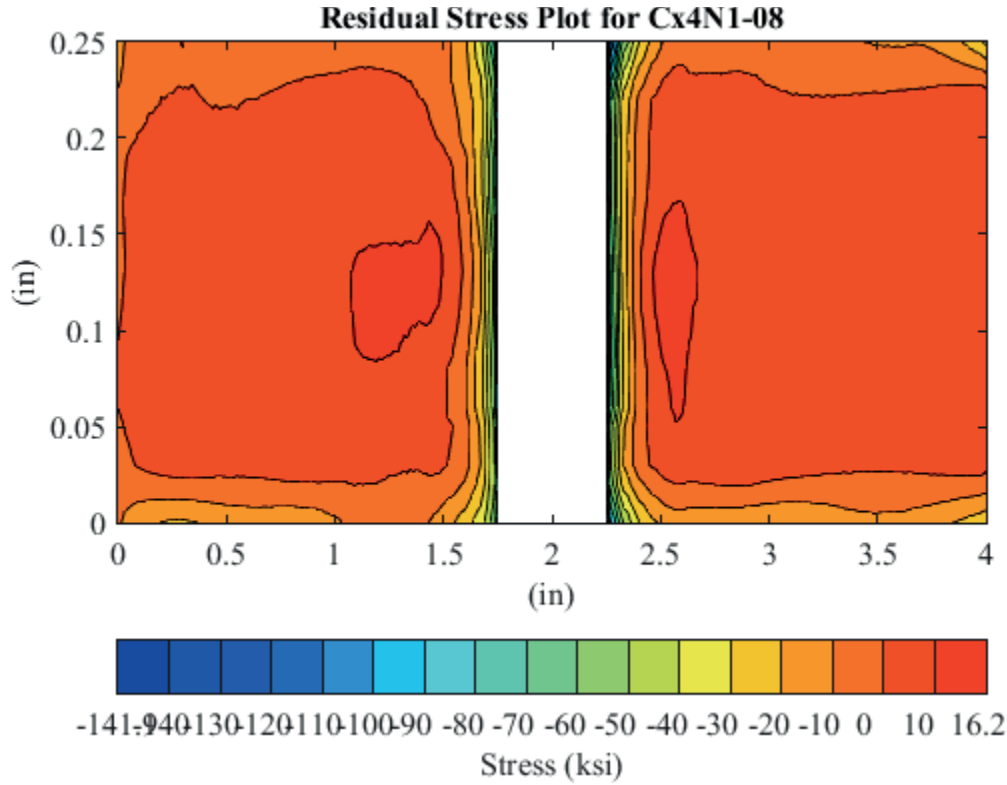

Fig. 490 Residual Stress Contour Plot of Coupon Cx4N1-08-D (7075-T651) – Mandrel Entrance Surface at Y=0, 0.5017 inch Fatigue Crack on Left Side of Hole on Mandrel Entrance Surface a Small Fatigue Crack was also on the Right Side of the Hole.

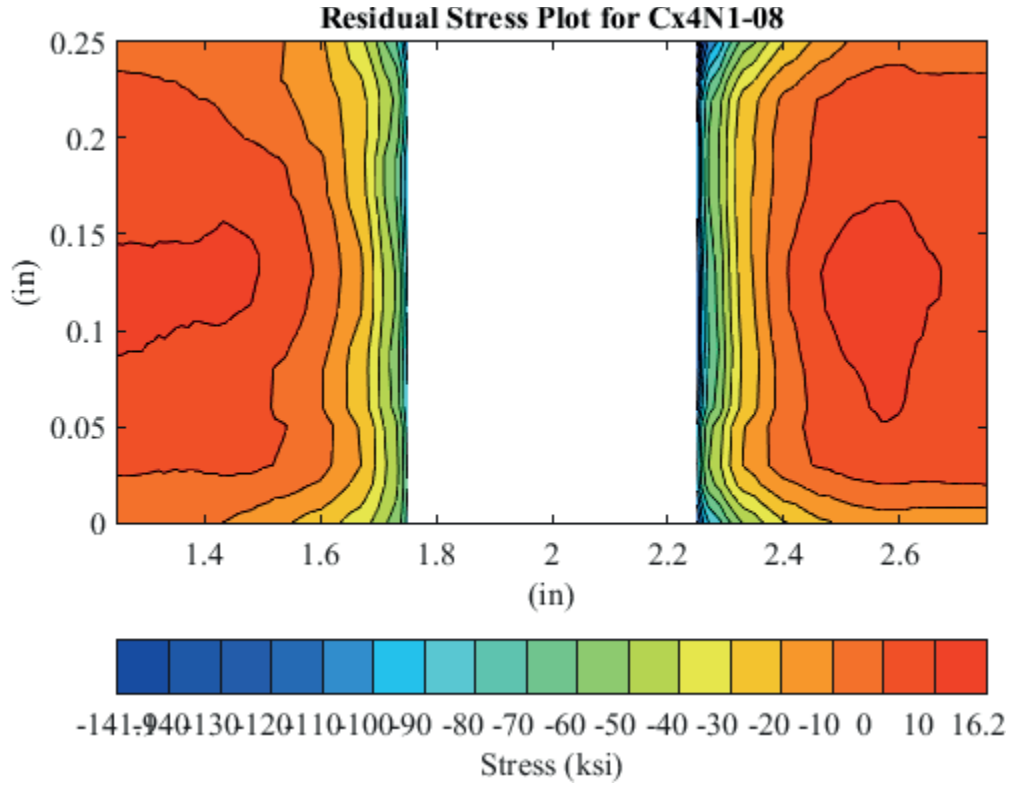

Fig. 491 Residual Stress Contour Plot of Coupon Cx4N1-08-D (7075-T651) – Mandrel Entrance Surface at Y=0, 0.5017 inch Fatigue Crack on Left Side of Hole on Mandrel Entrance Surface a Small Fatigue Crack was also on the Right Side of the Hole – Zoomed in Next to Hole.

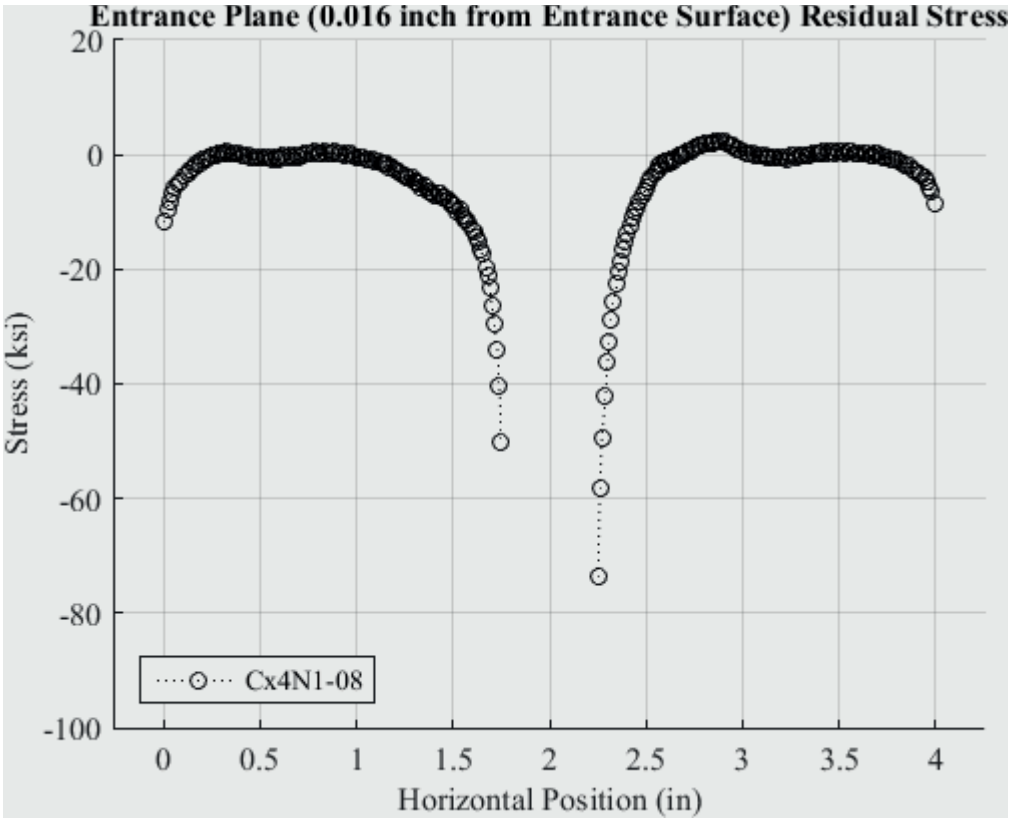

Fig. 492 Residual Stress Line Plot of Cx4N1-08-D (7075-T651) at a Distance of 0.016 inch (Entrance Surface) from the Entrance Surface – Coupons had a 0.5017 inch Fatigue Crack at the Left Entrance Surface a Small Fatigue Crack was also on the Right Side of the Hole.

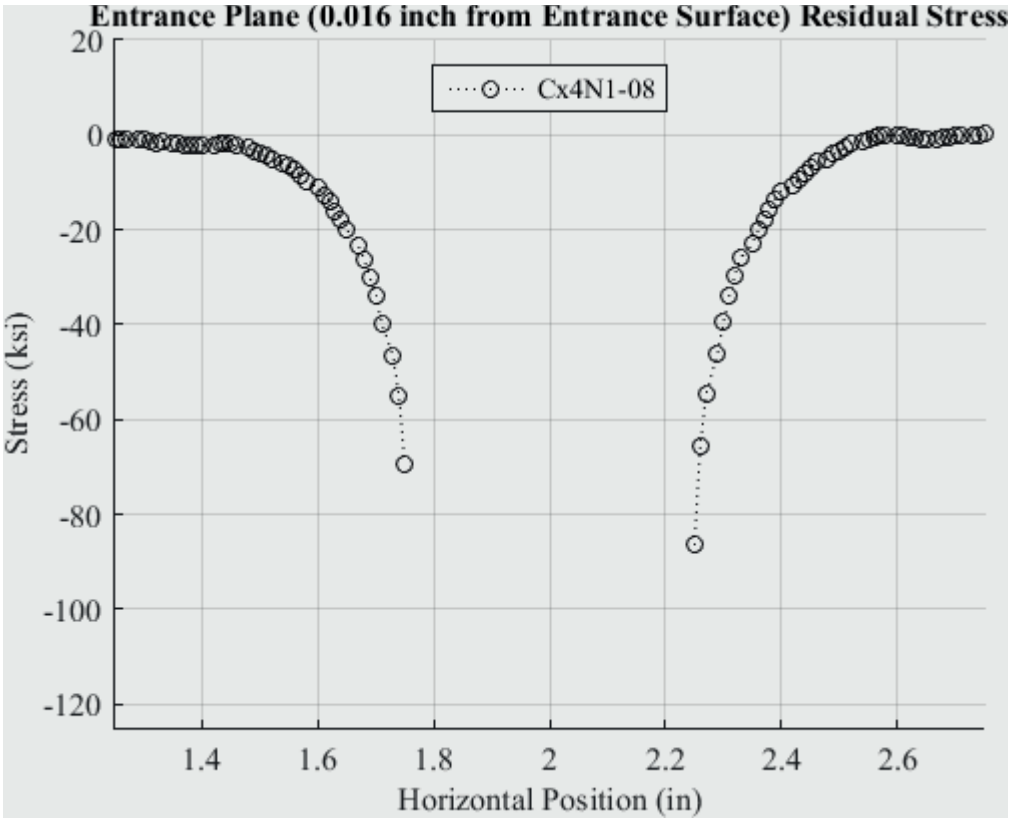

Fig. 493 Residual Stress Line Plot of Cx4N1-08-D (7075-T651) at a Distance of 0.016 inch (Entrance Surface) from the Entrance Surface – Coupons had a 0.5017 inch Fatigue Crack at the Left Entrance Surface a Small Fatigue Crack was also on the Right Side of the Hole – Zoomed in Next to Hole.

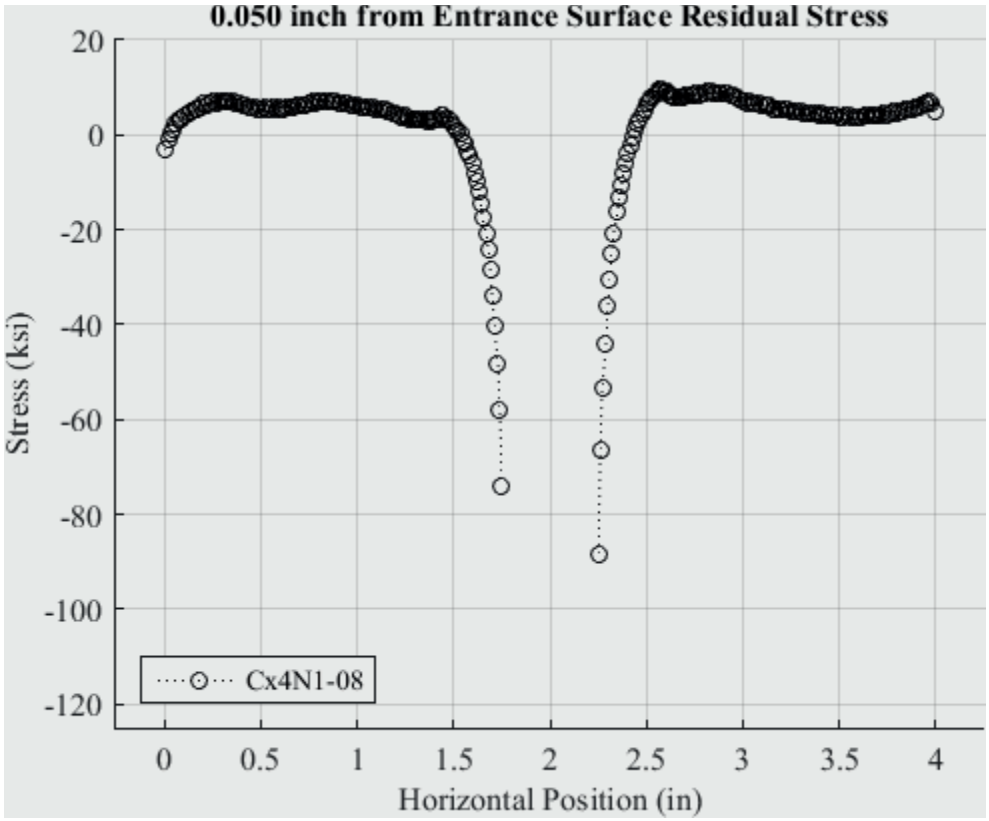

Fig. 494 Residual Stress Line Plot of Cx4N1-08-D (7075-T651) at a Distance of 0.05 inch from the Entrance Surface – Coupons had a 0.5017 inch Fatigue Crack at the Left Entrance Surface a Small Fatigue Crack was also on the Right Side of the Hole.

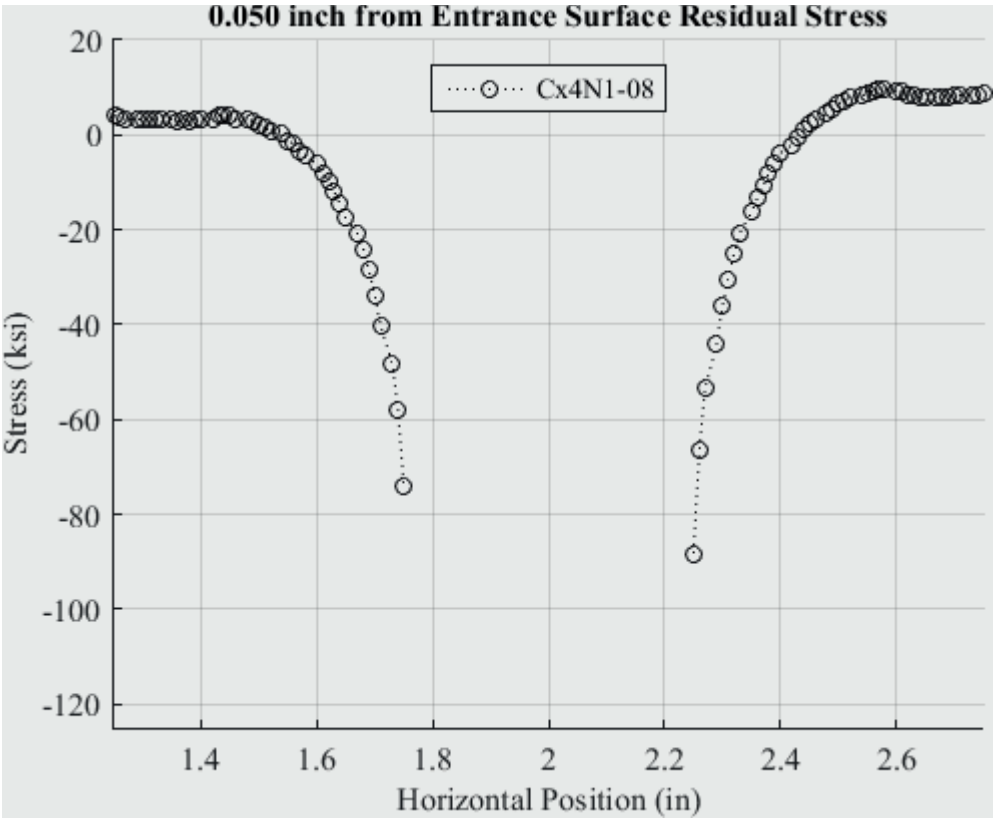

Fig. 495 Residual Stress Line Plot of Cx4N1-08-D (7075-T651) at a Distance of 0.05 inch from the Entrance Surface – Coupons had a 0.5017 inch Fatigue Crack at the Left Entrance Surface a Small Fatigue Crack was also on the Right Side of the Hole – Zoomed in Next to Hole.

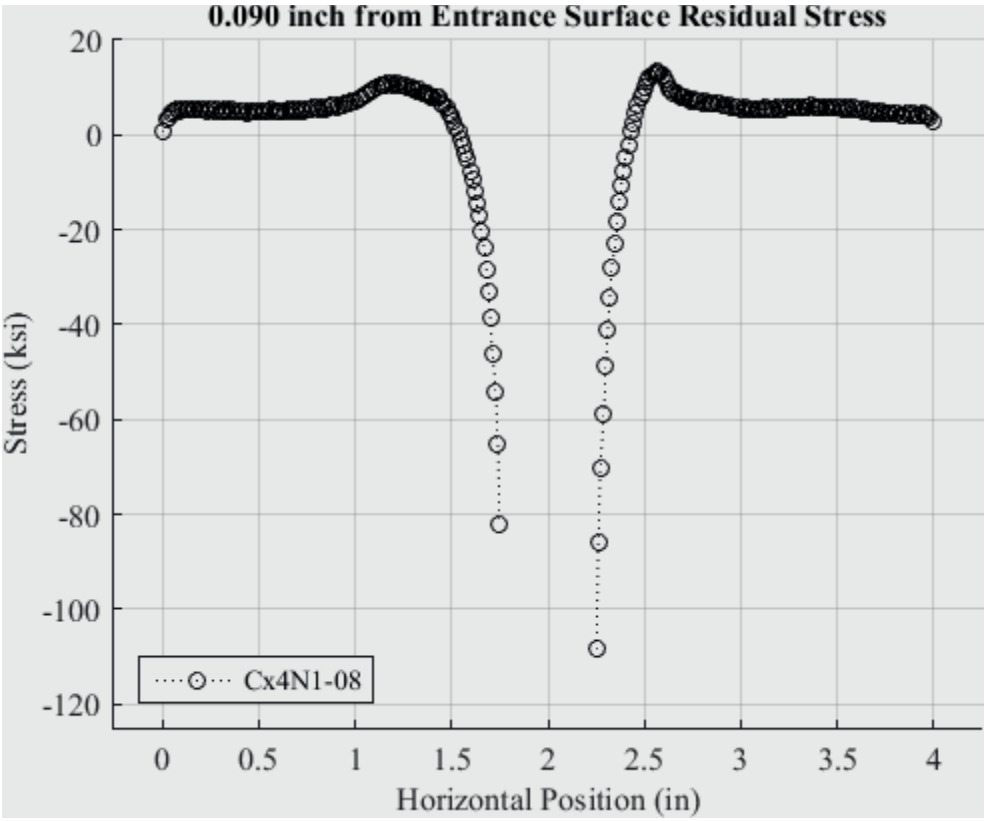

Fig. 496 Residual Stress Line Plot of Cx4N1-08-D (7075-T651) at a Distance of 0.09 inch from the Entrance Surface – Coupons had a 0.5017 inch Fatigue Crack at the Left Entrance Surface a Small Fatigue Crack was also on the Right Side of the Hole.

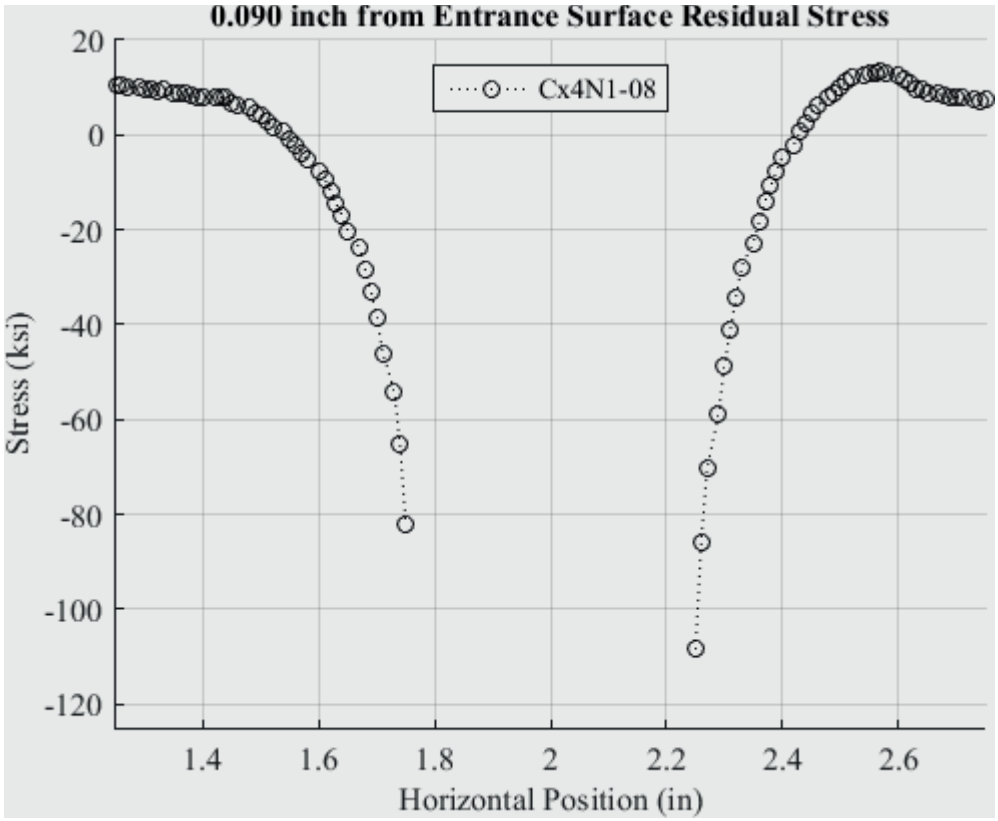

Fig. 497 Residual Stress Line Plot of Cx4N1-08-D (7075-T651) at a Distance of 0.09 inch from the Entrance Surface – Coupons had a 0.5017 inch Fatigue Crack at the Left Entrance Surface a Small Fatigue Crack was also on the Right Side of the Hole – Zoomed in Next to Hole.

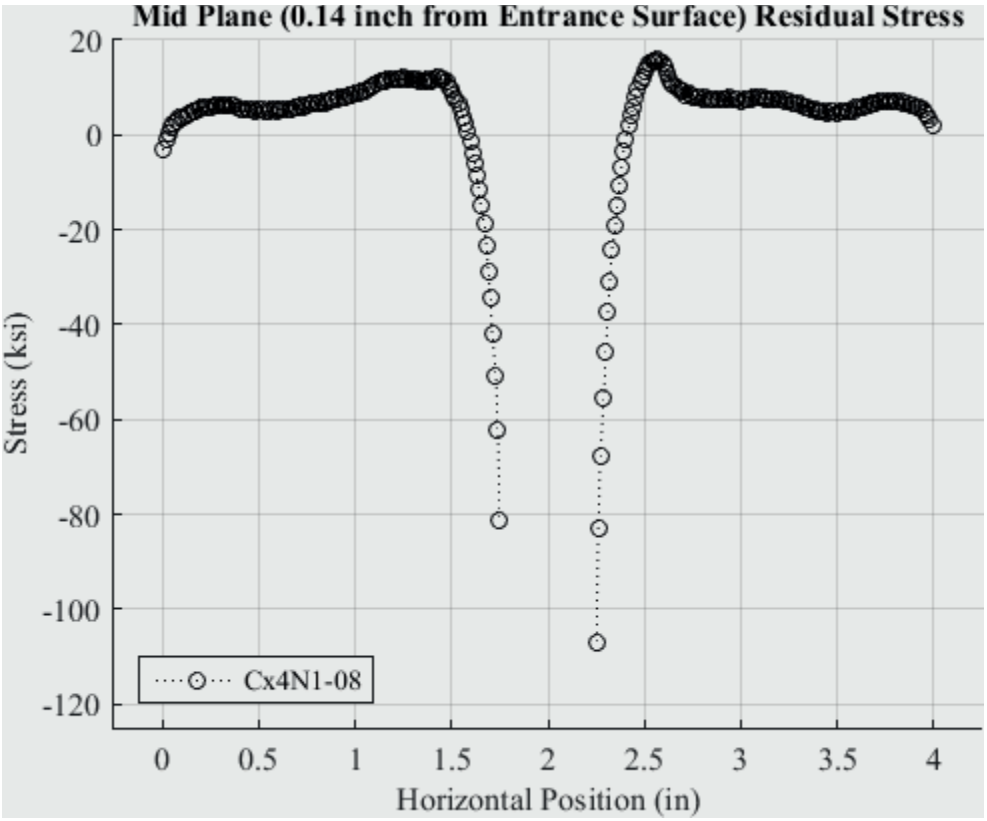

Fig. 498 Residual Stress Line Plot of Cx4N1-08-D (7075-T651) at a Distance of 0.140 inch (Mid Plane Surface) from the Entrance Surface – Coupons had a 0.5017 inch Fatigue Crack at the Left Entrance Surface a Small Fatigue Crack was also on the Right Side of the Hole.

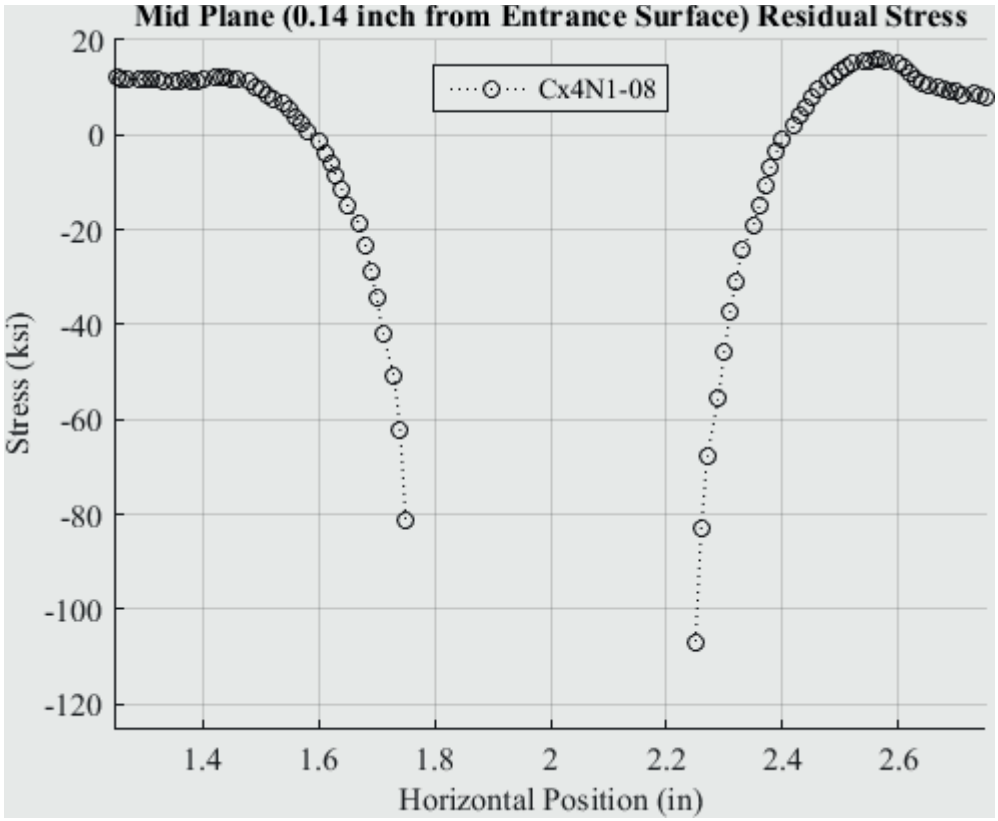

Fig. 499 Residual Stress Line Plot of Cx4N1-08-D (7075-T651) at a Distance of 0.140 inch (Mid Plane Surface) from the Entrance Surface – Coupons had a 0.5017 inch Fatigue Crack at the Left Entrance Surface a Small Fatigue Crack was also on the Right Side of the Hole – Zoomed in Next to Hole.

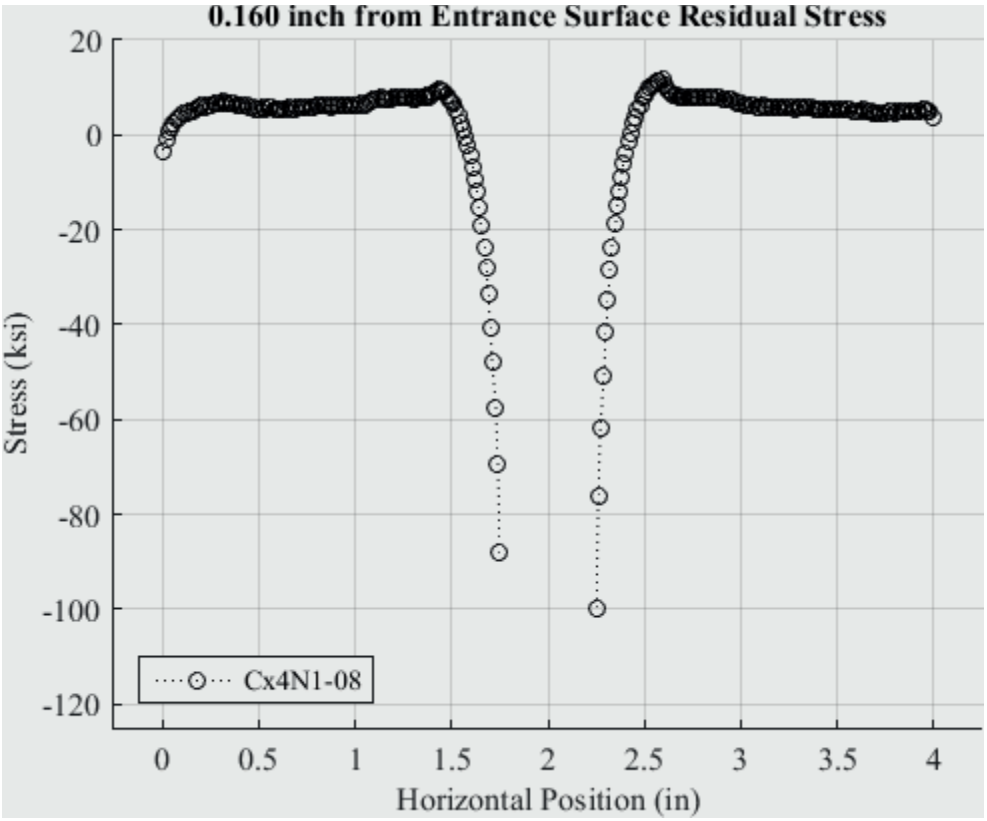

Fig. 500 Residual Stress Line Plot of Cx4N1-08-D (7075-T651) at a Distance of 0.160 inch from the Entrance Surface – Coupons had a 0.5017 inch Fatigue Crack at the Left Entrance Surface a Small Fatigue Crack was also on the Right Side of the Hole.

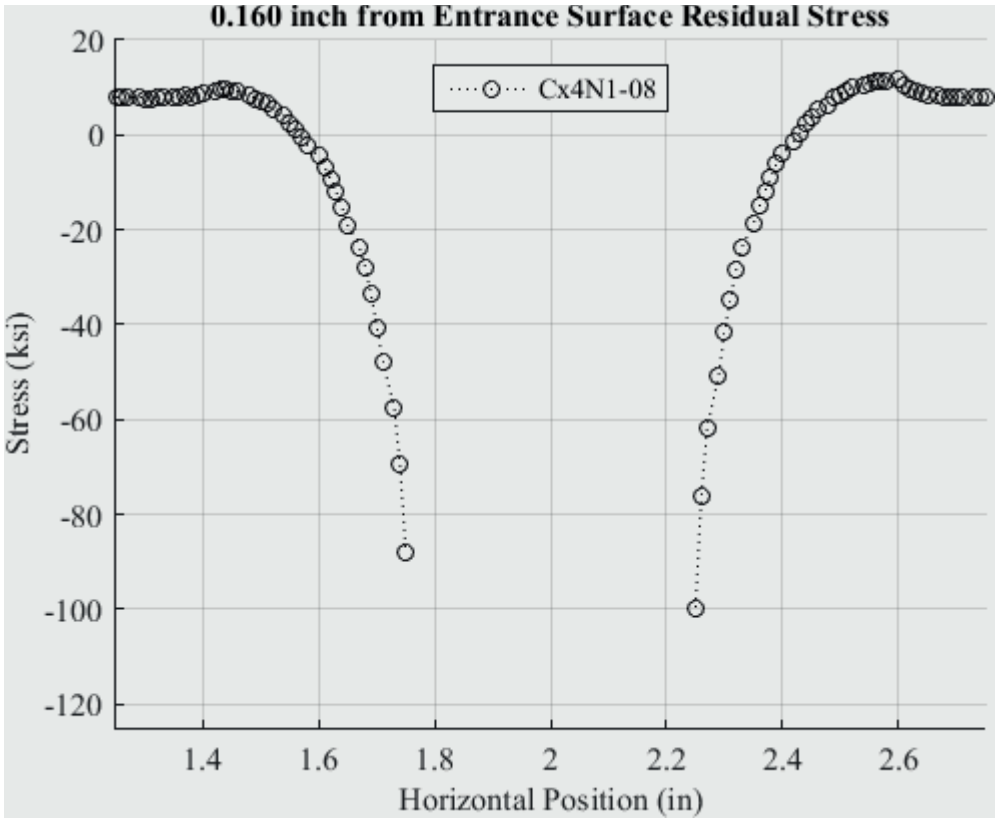

Fig. 501 Residual Stress Line Plot of Cx4N1-08-D (7075-T651) at a Distance of 0.160 inch from the Entrance Surface – Coupons had a 0.5017 inch Fatigue Crack at the Left Entrance Surface a Small Fatigue Crack was also on the Right Side of the Hole – Zoomed in Next to Hole.

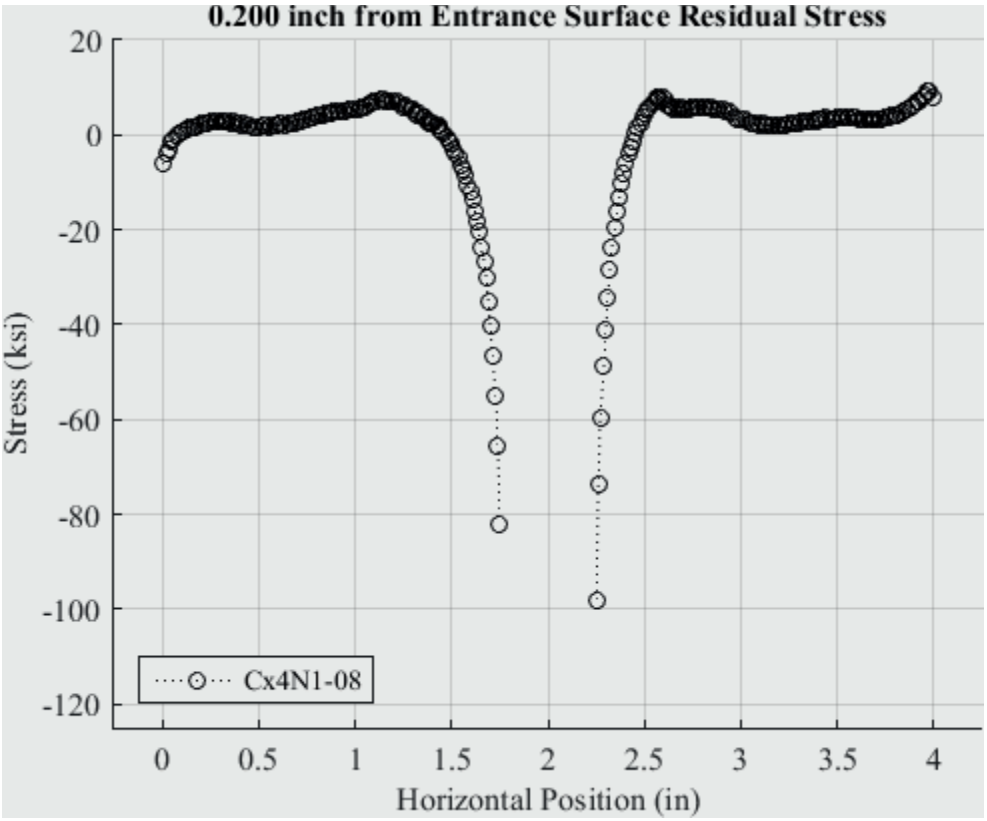

Fig. 502 Residual Stress Line Plot of Cx4N1-08-D (7075-T651) at a Distance of 0.200 inch from the Entrance Surface – Coupons had a 0.5017 inch Fatigue Crack at the Left Entrance Surface a Small Fatigue Crack was also on the Right Side of the Hole.

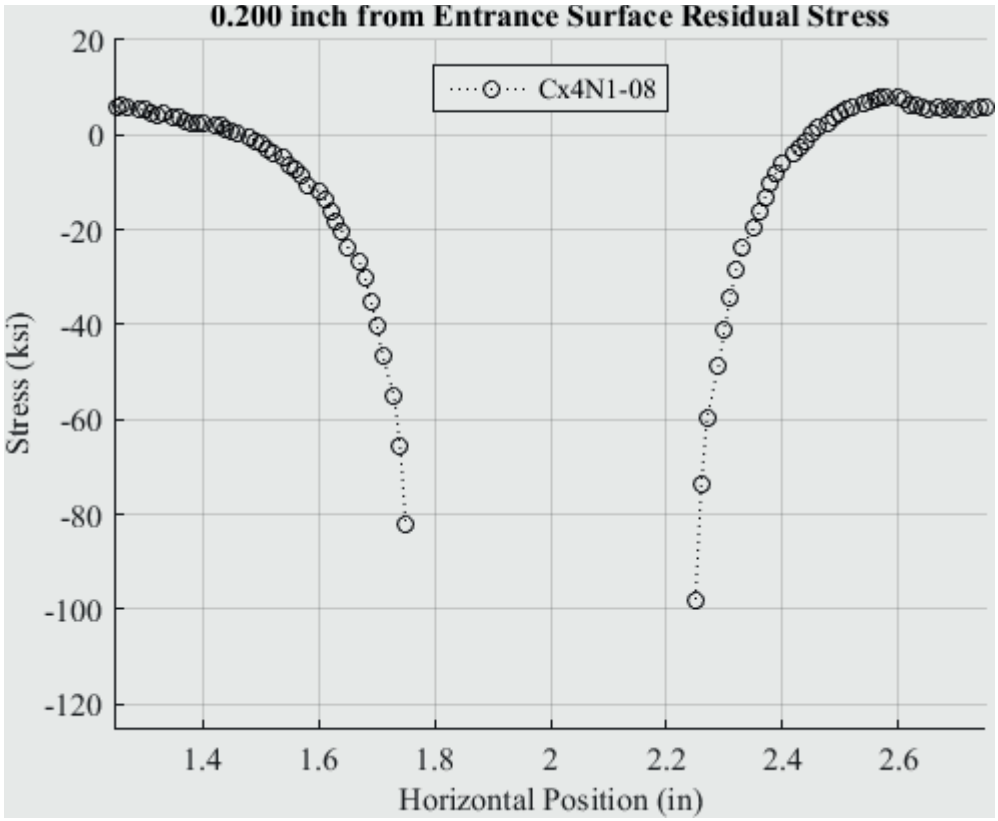

Fig. 503 Residual Stress Line Plot of Cx4N1-08-D (7075-T651) at a Distance of 0.200 inch from the Entrance Surface – Coupons had a 0.5017 inch Fatigue Crack at the Left Entrance Surface a Small Fatigue Crack was also on the Right Side of the Hole – Zoomed in Next to Hole.

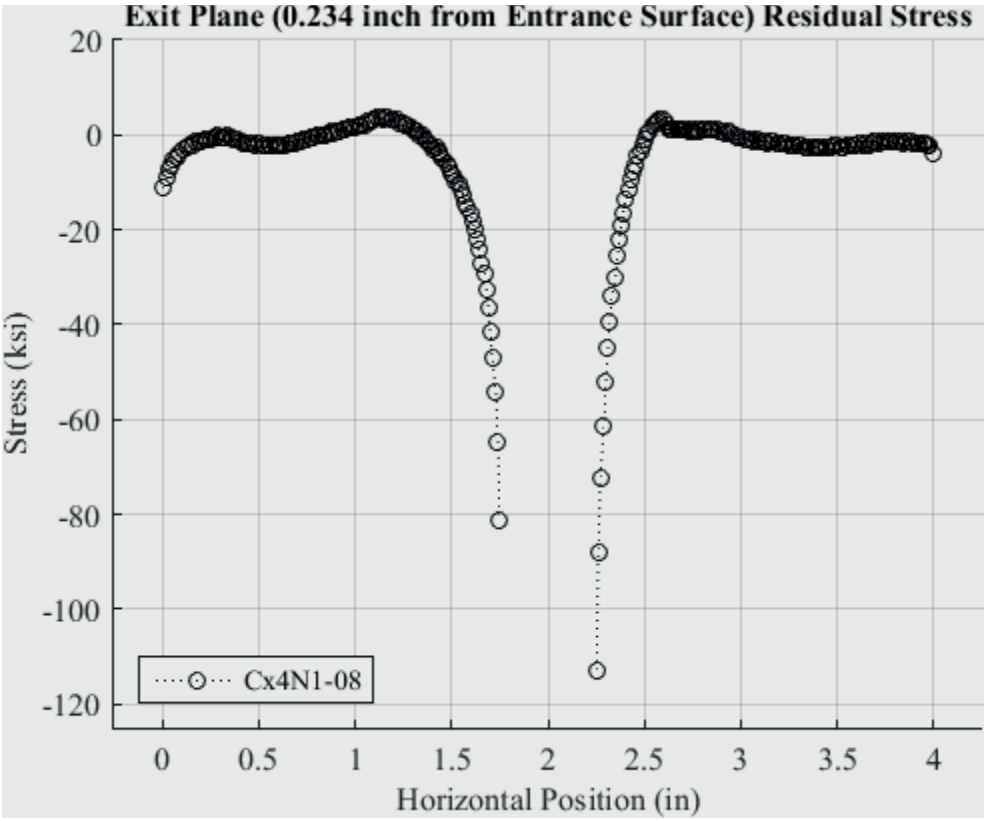

Fig. 504 Residual Stress Line Plot of Cx4N1-08-D (7075-T651) at a Distance of 0.234 inch (Exit Surface) from the Entrance Surface – Coupons had a 0.5017 inch Fatigue Crack at the Left Entrance Surface a Small Fatigue Crack was also on the Right Side of the Hole.

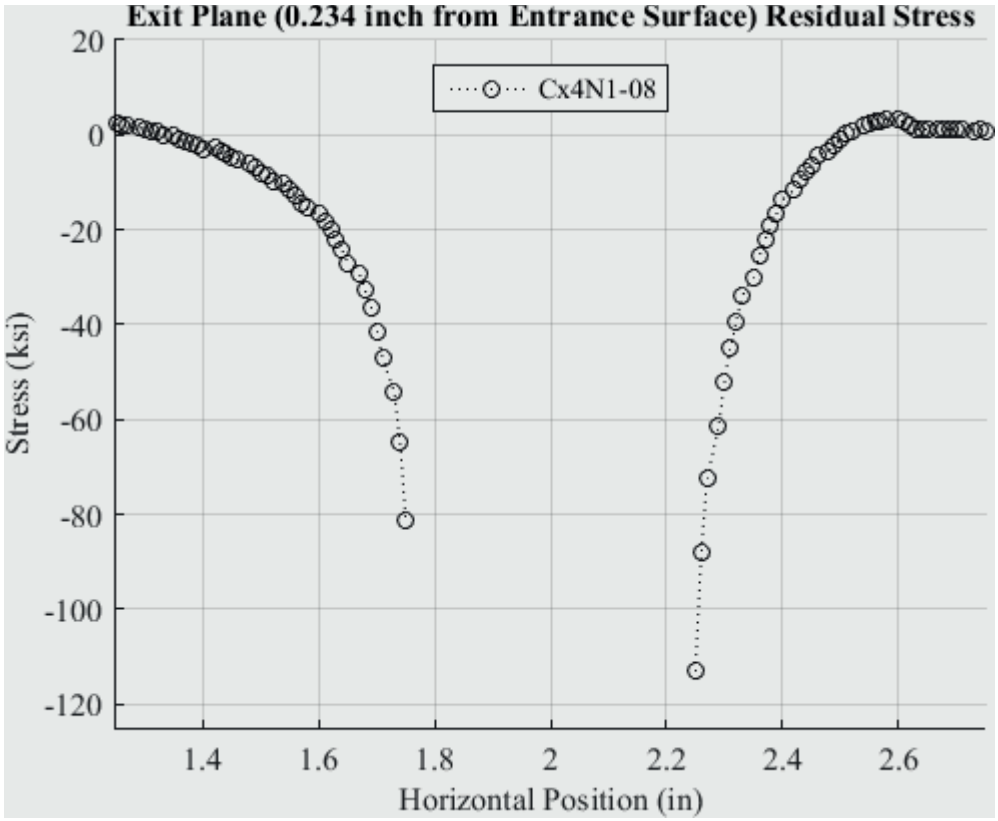

Fig. 505 Residual Stress Line Plot of Cx4N1-08-D (7075-T651) at a Distance of 0.234 inch (Exit Surface) from the Entrance Surface – Coupons had a 0.5017 inch Fatigue Crack at the Left Entrance Surface a Small Fatigue Crack was also on the Right Side of the Hole – Zoomed in Next to Hole.

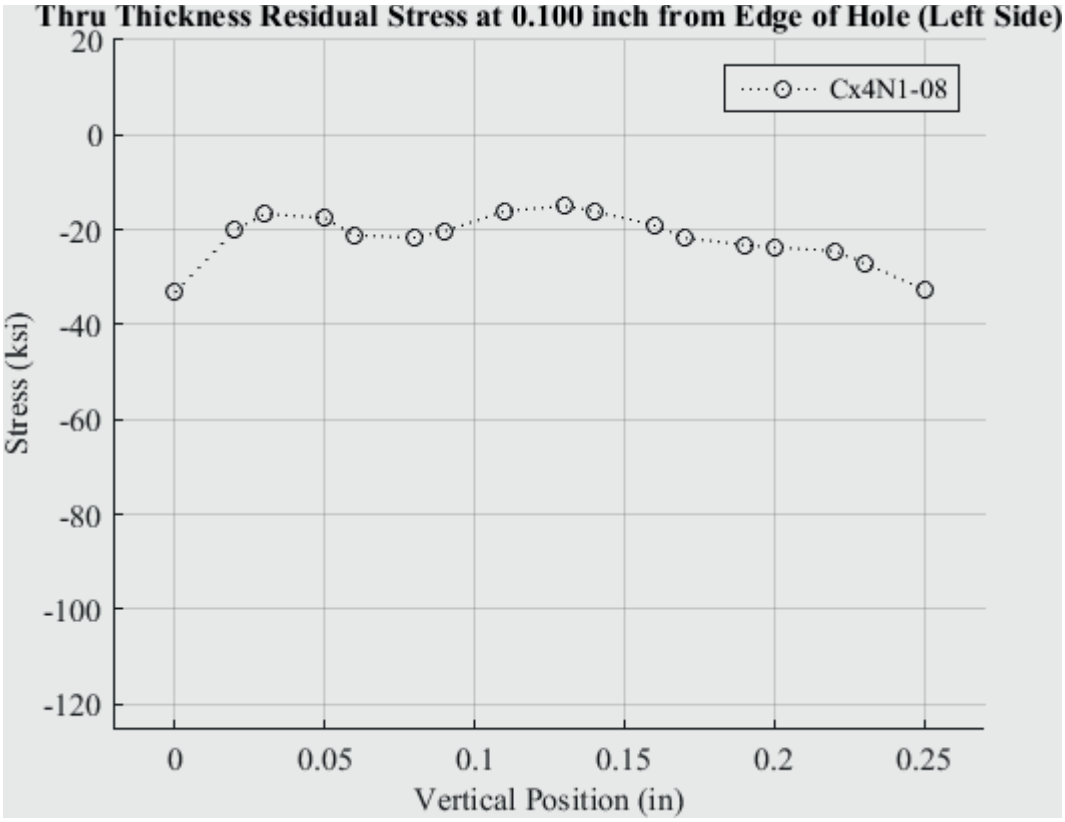

Fig. 506 Residual Stress Line Plot of Cx4N1-08-D (7075-T651) Through the Thickness at 0.01 inch from Left Side of Hole – Coupons had a 0.5017 inch Fatigue Crack at the Left Entrance Surface a Small Fatigue Crack was also on the Right Side of the Hole.

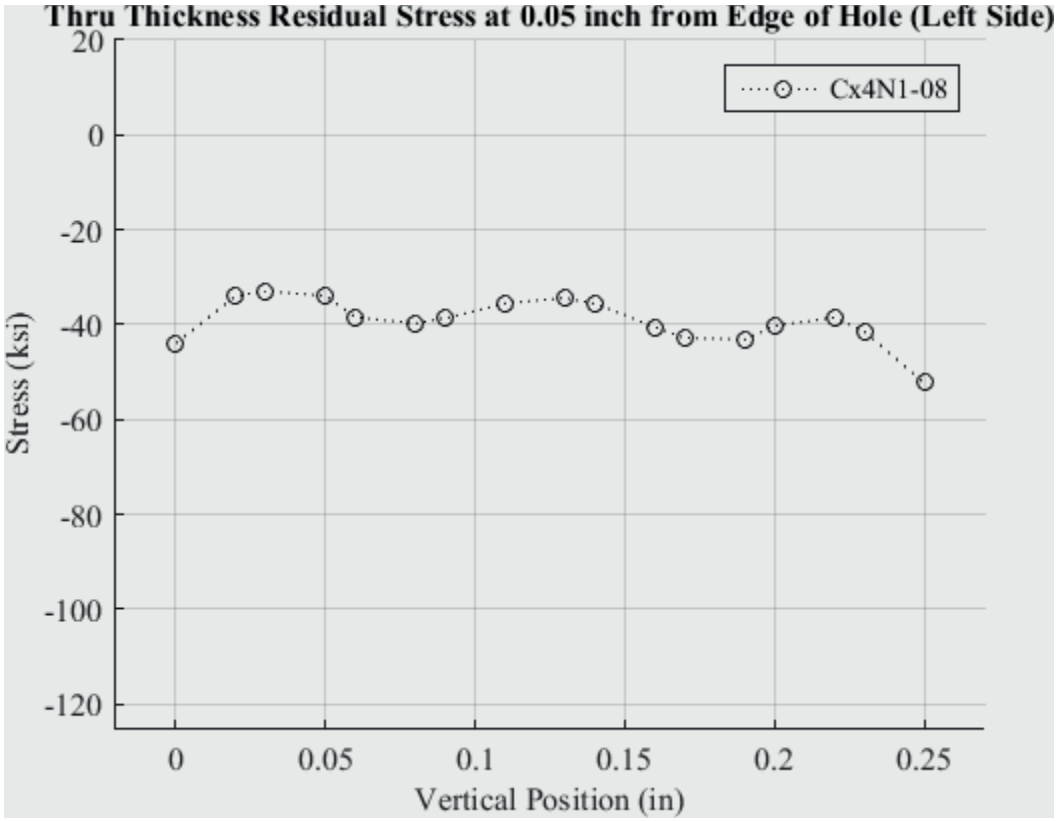

Fig. 507 Residual Stress Line Plot of Cx4N1-08-D (7075-T651) Through the Thickness at 0.05 inch from Left Side of Hole – Coupons had a 0.5017 inch Fatigue Crack at the Left Entrance Surface a Small Fatigue Crack was also on the Right Side of the Hole.

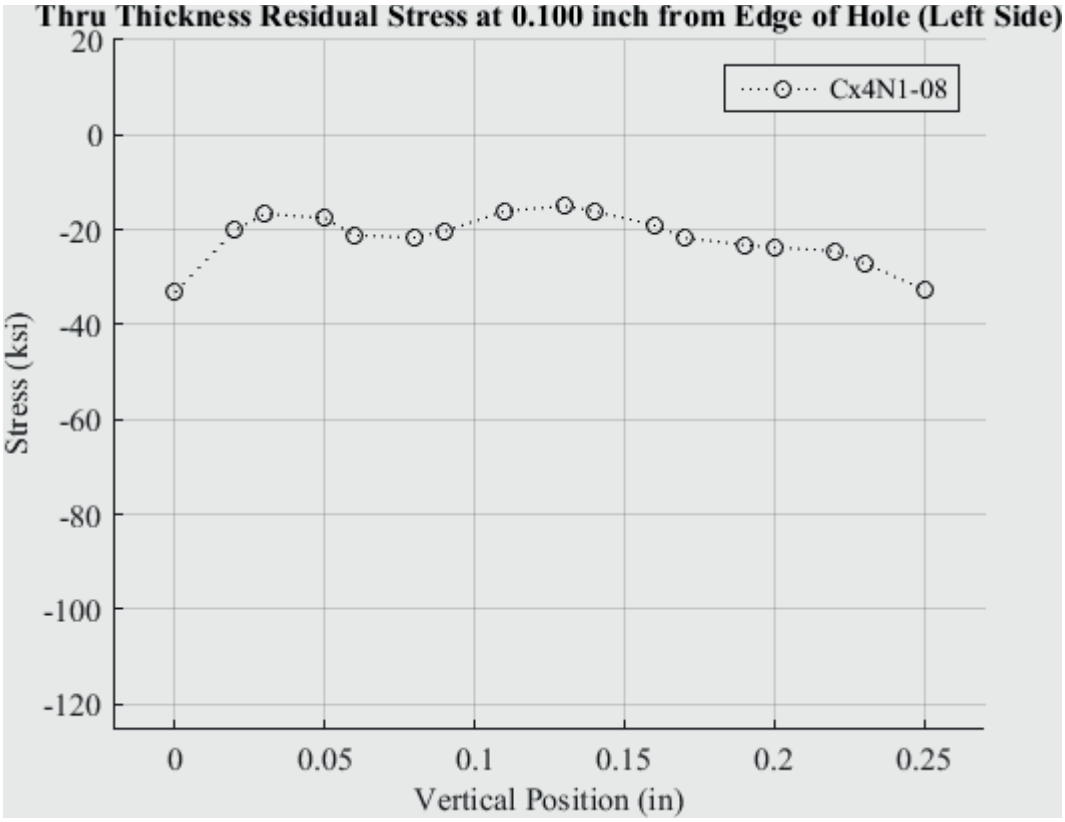

Fig. 508 Residual Stress Line Plot of Cx4N1-08-D (7075-T651) Through the Thickness at 0.10 inch from Left Side of Hole – Coupons had a 0.5017 inch Fatigue Crack at the Left Entrance Surface a Small Fatigue Crack was also on the Right Side of the Hole.

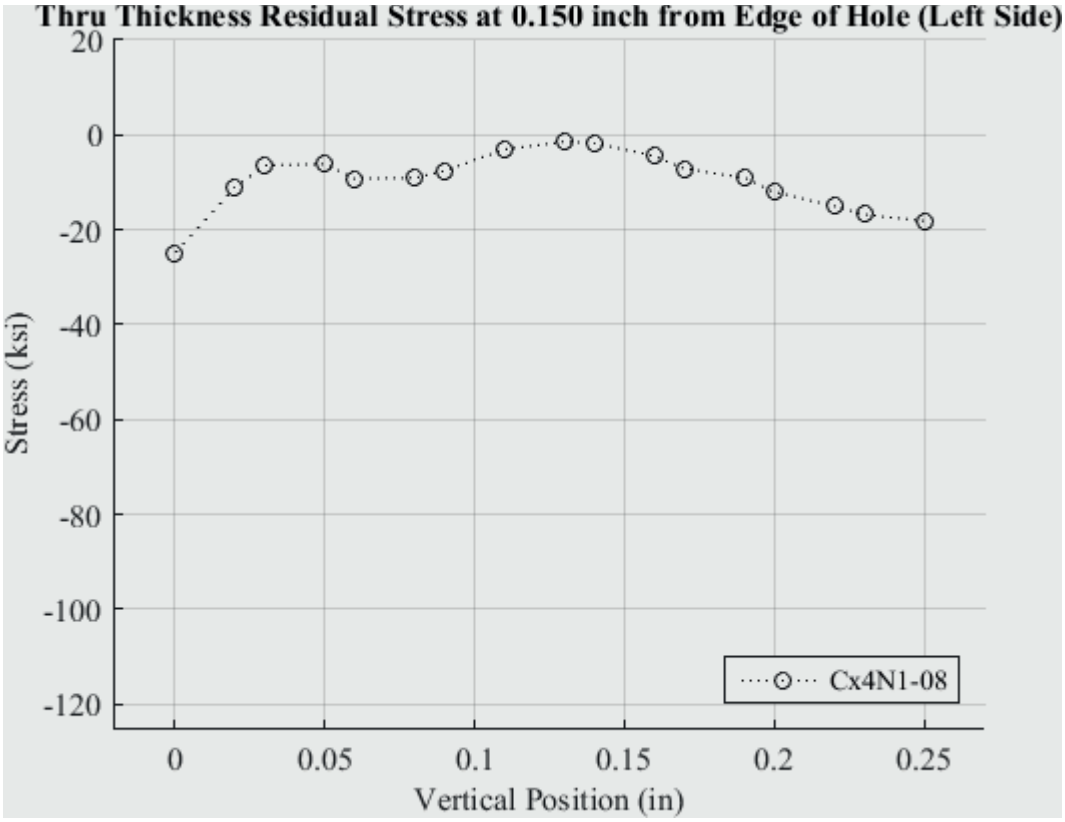

Fig. 509 Residual Stress Line Plot of Cx4N1-08-D (7075-T651) Through the Thickness at 0.150 inch from Left Side of Hole – Coupons had a 0.5017 inch Fatigue Crack at the Left Entrance Surface a Small Fatigue Crack was also on the Right Side of the Hole.

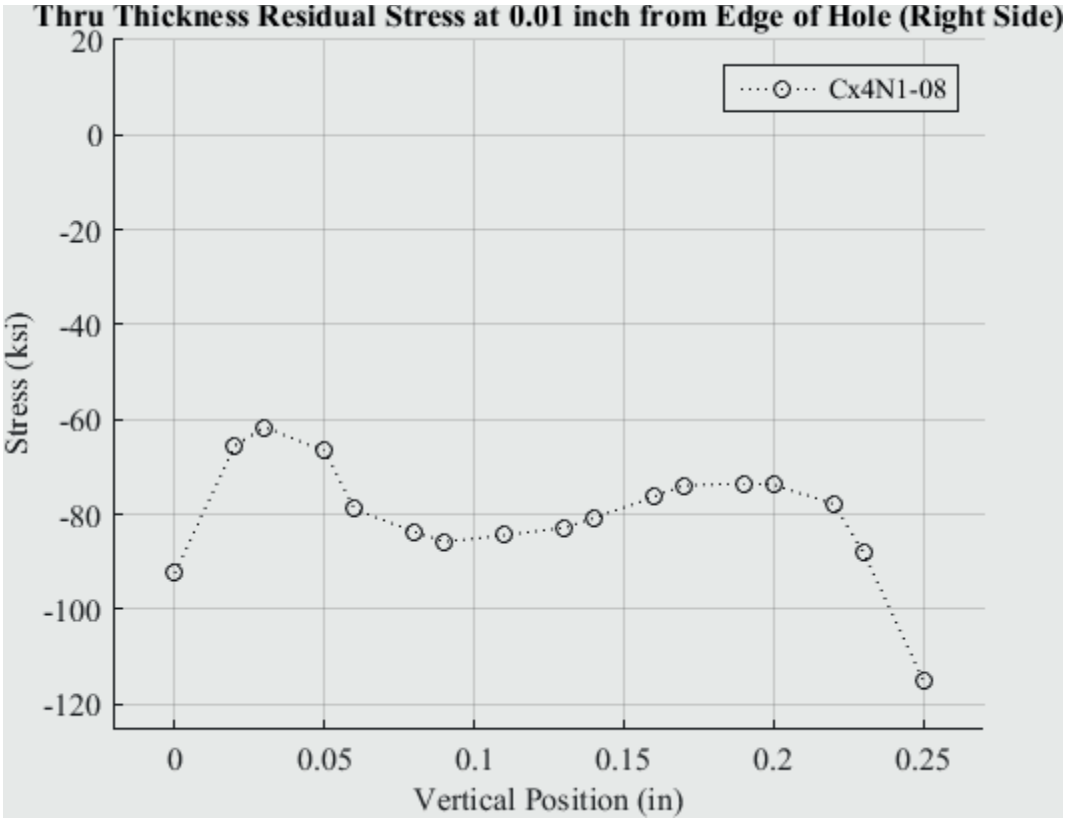

Fig. 510 Residual Stress Line Plot of Cx4N1-08-D (7075-T651) Through the Thickness at 0.01 inch from Right Side of Hole – Coupons had a 0.5017 inch Fatigue Crack at the Left Entrance Surface a Small Fatigue Crack was also on the Right Side of the Hole.

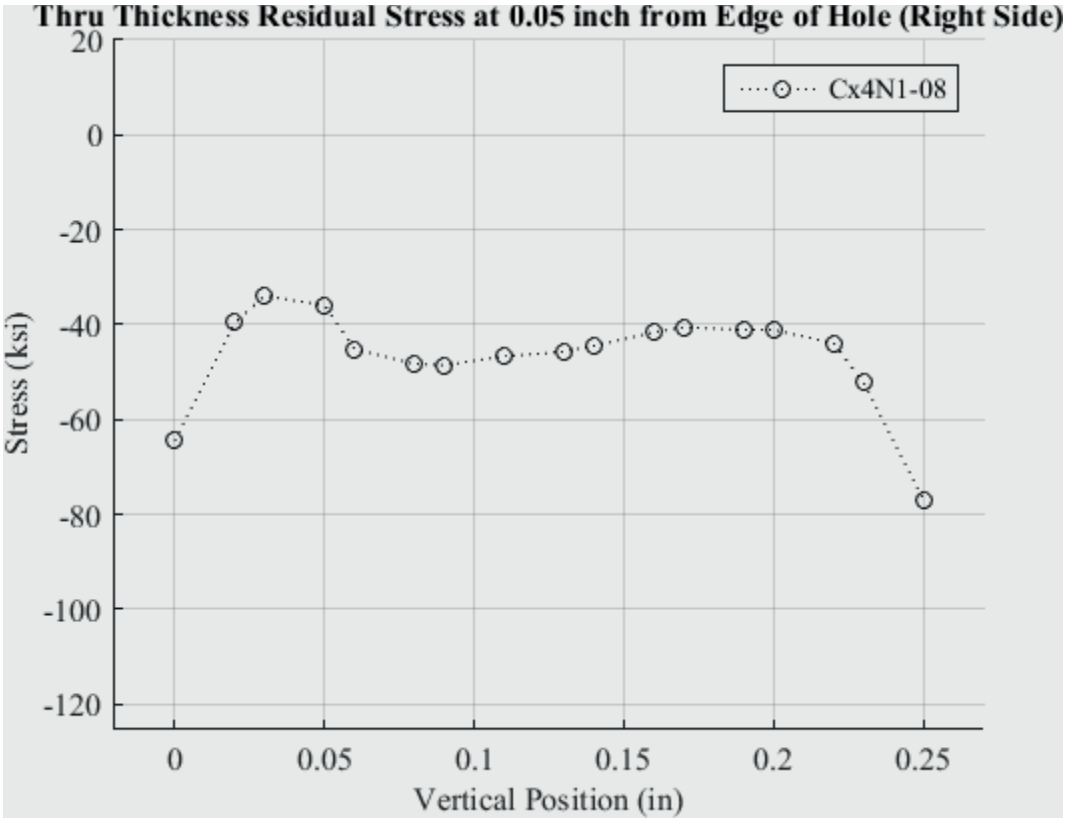

Fig. 511 Residual Stress Line Plot of Cx4N1-08-D (7075-T651) Through the Thickness at 0.05 inch from Right Side of Hole – Coupons had a 0.5017 inch Fatigue Crack at the Left Entrance Surface a Small Fatigue Crack was also on the Right Side of the Hole.

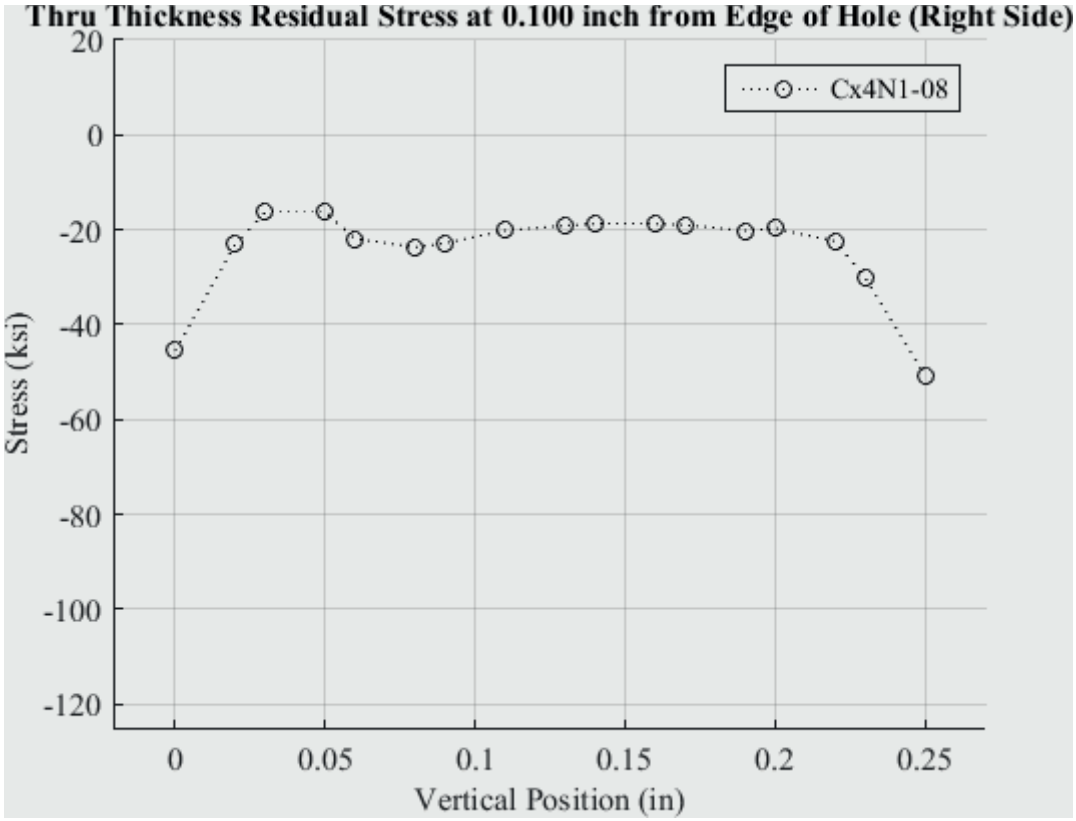

Fig. 512 Residual Stress Line Plot of Cx4N1-08-D (7075-T651) Through the Thickness at 0.10 inch from Right Side of Hole – Coupons had a 0.5017 inch Fatigue Crack at the Left Entrance Surface a Small Fatigue Crack was also on the Right Side of the Hole.

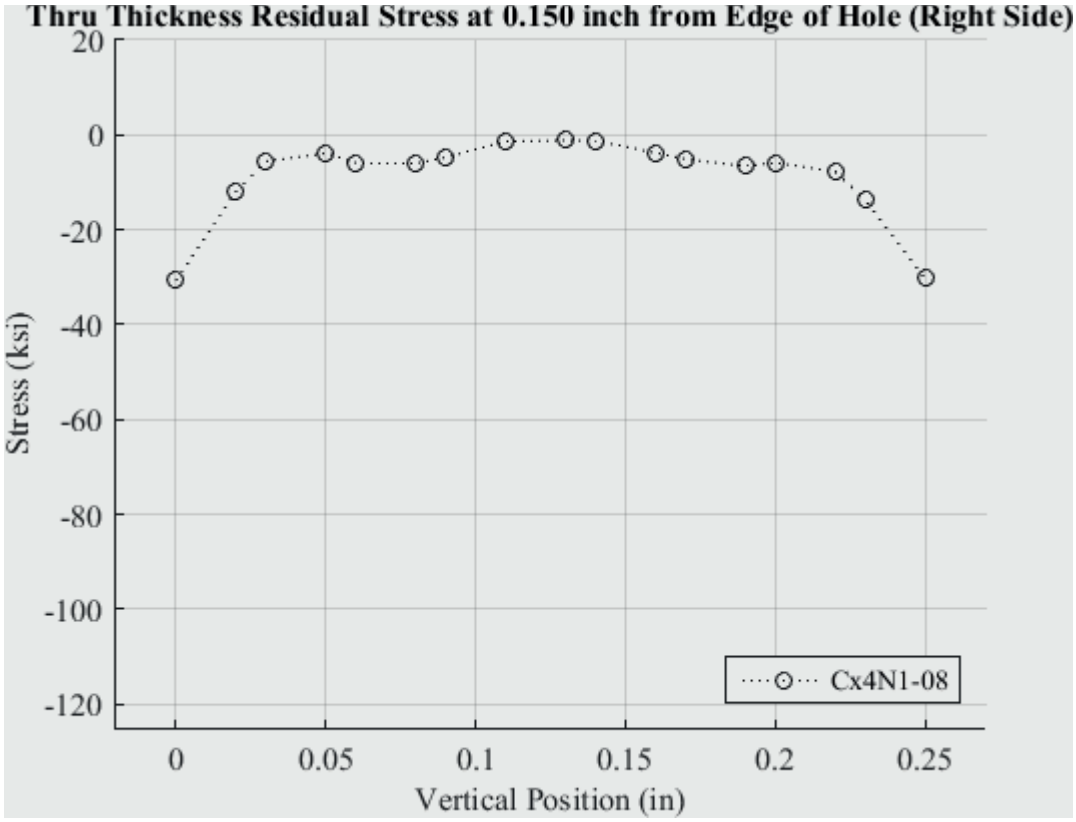

Fig. 513 Residual Stress Line Plot of Cx4N1-08-D (7075-T651) Through the Thickness at 0.150 inch from Right Side of Hole – Coupons had a 0.5017 inch Fatigue Crack at the Left Entrance Surface a Small Fatigue Crack was also on the Right Side of the Hole.

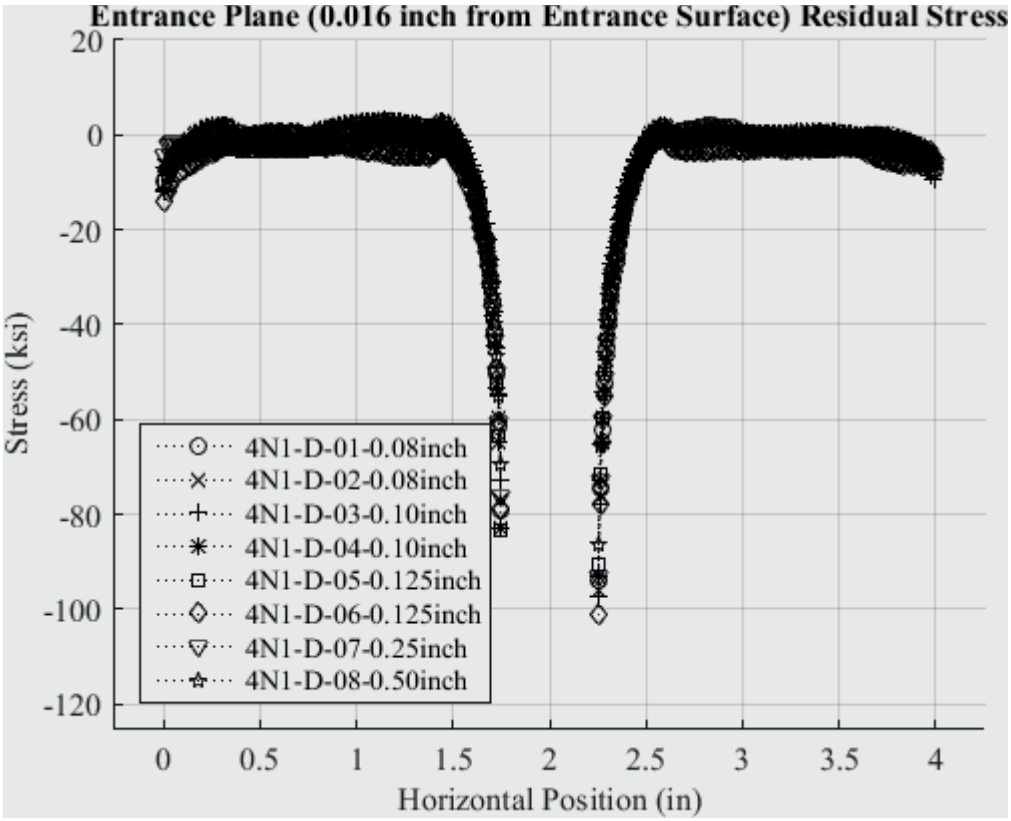

Fig. 514 Residual Stress Line Plot of All Cx4N1-D (7075-T651) Coupons at a Distance of 0.016 inch (Entrance Surface) from the Entrance Surface.

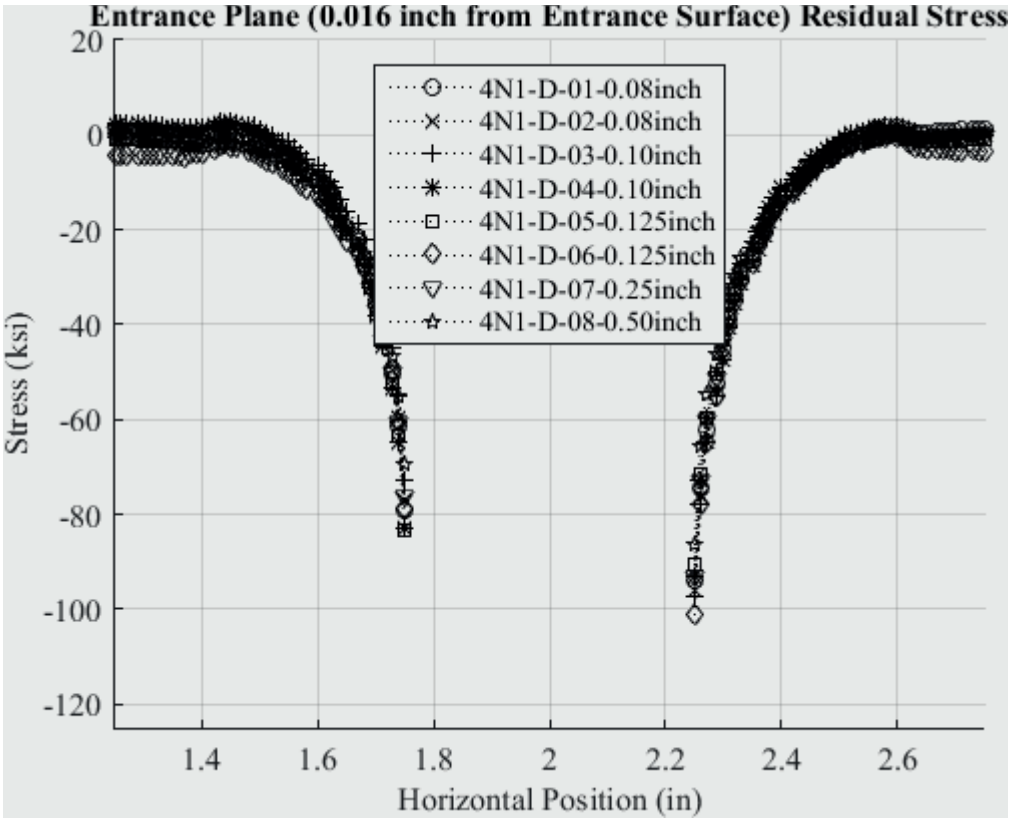

Fig. 515 Residual Stress Line Plot of All Cx4N1-D (7075-T651) Coupons at a Distance of 0.016 inch (Entrance Surface) from the Entrance Surface – Zoomed in Next to Hole.

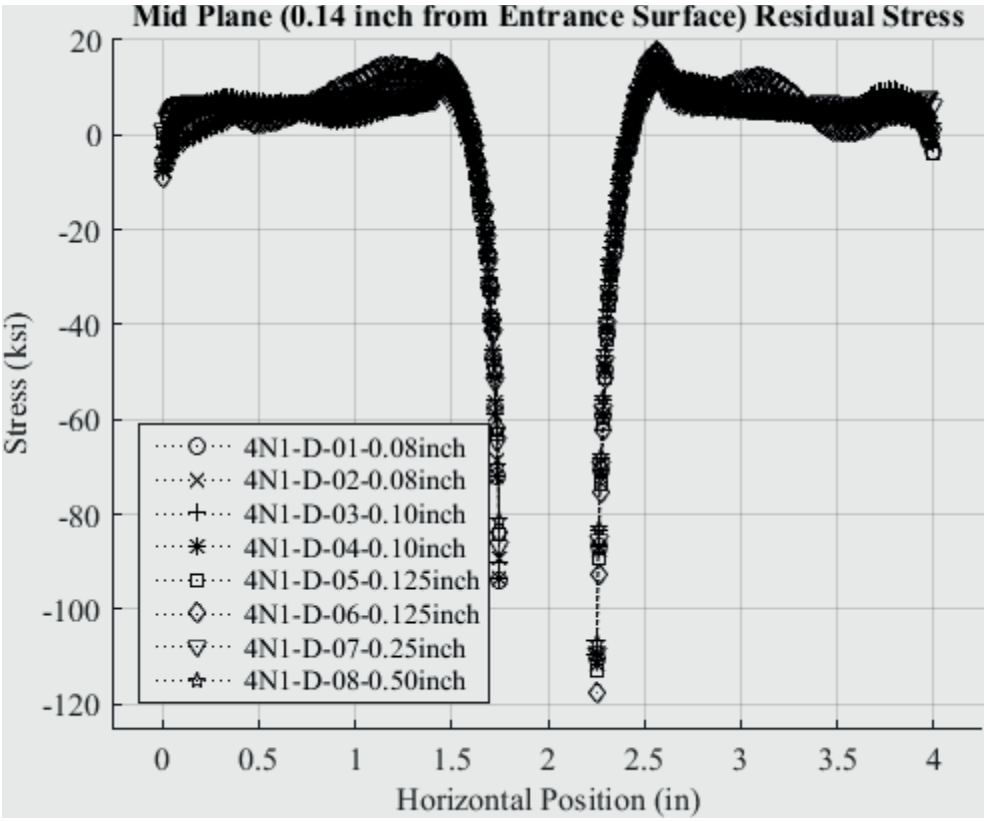

Fig. 516 Residual Stress Line Plot of All Cx4N1-D (7075-T651) Coupons at a Distance of 0.0140 inch (Mid Plane Surface) from the Entrance Surface.

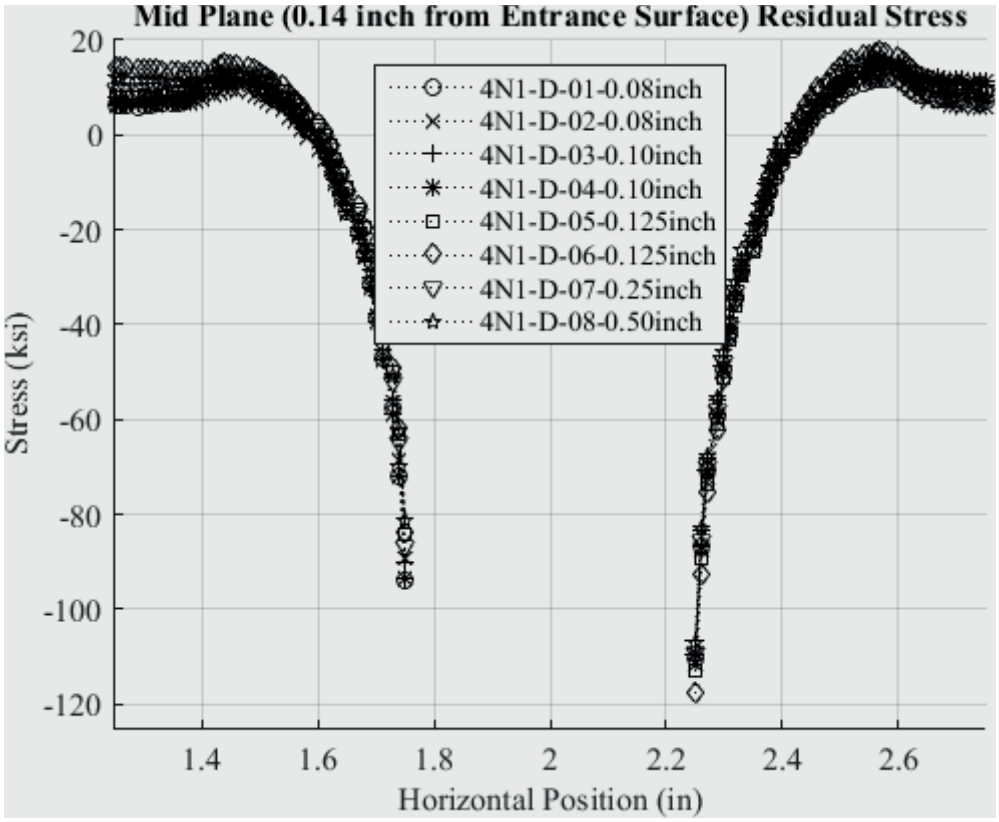

Fig. 517 Residual Stress Line Plot of All Cx4N1-D (7075-T651) Coupons at a Distance of 0.0140 inch (Mid Plane Surface) from the Entrance Surface – Zoomed in Next to Hole.

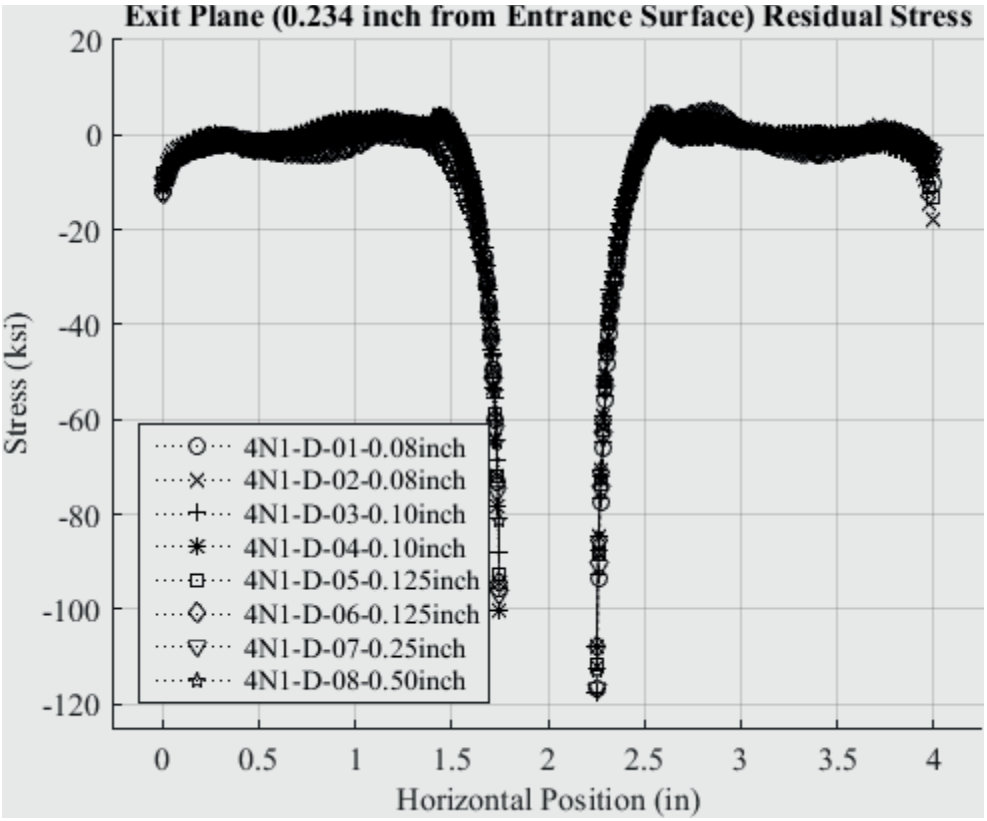

Fig. 518 Residual Stress Line Plot of All Cx4N1-D (7075-T651) Coupons at a Distance of 0.0234 inch (Exit Surface) from the Entrance Surface.

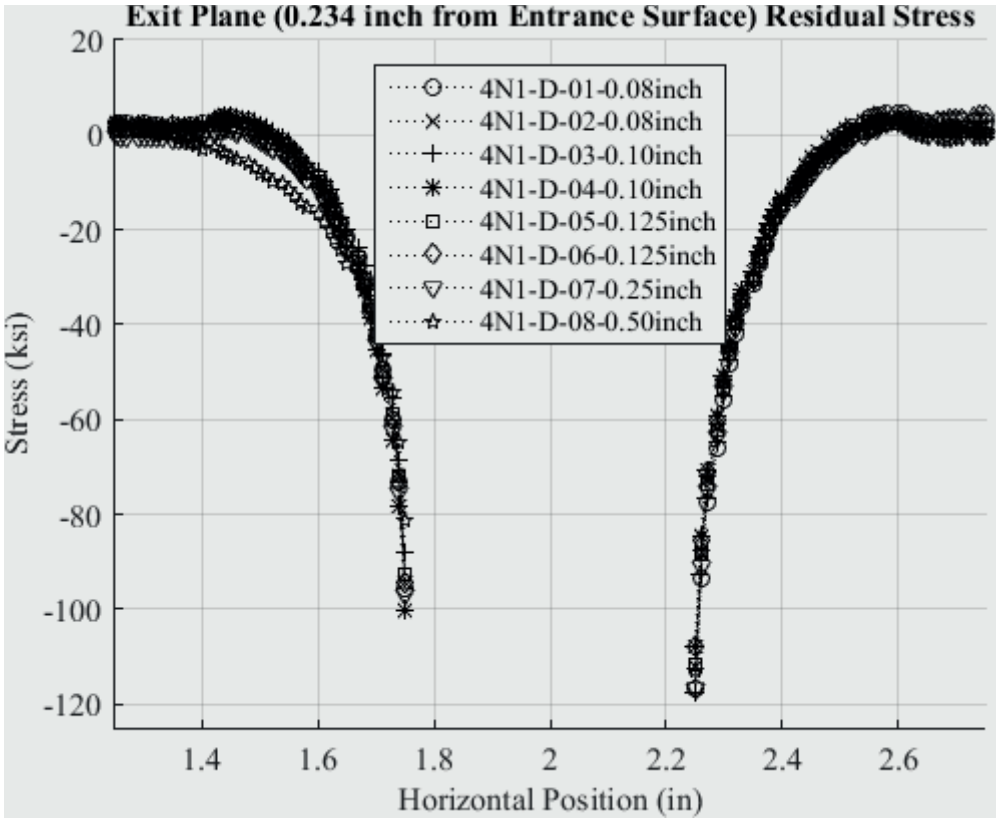

Fig. 519 Residual Stress Line Plot of All Cx4N1-D (7075-T651) Coupons at a Distance of 0.0234 inch (Exit Surface) from the Entrance Surface – Zoomed in Next to Hole.

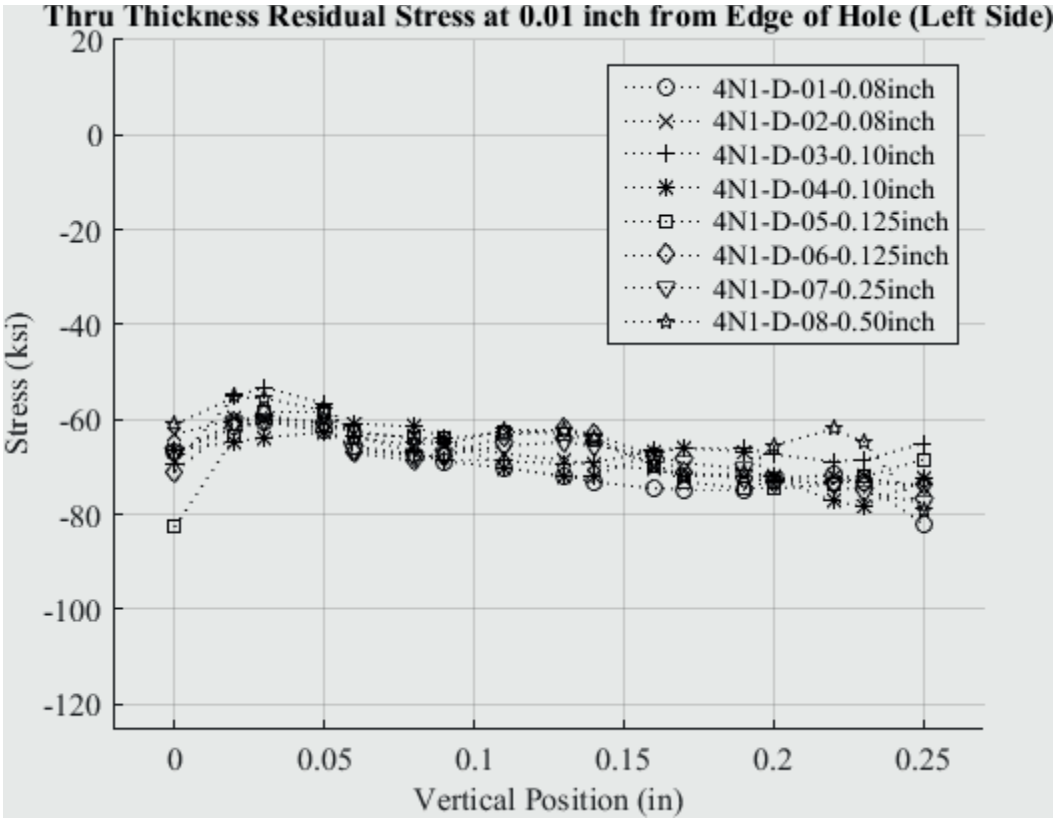

Fig. 520 Residual Stress Line Plot of all Cx4N1-D (7075-T651) Coupons Through the Thickness at 0.01 inch from Left Side of Hole.

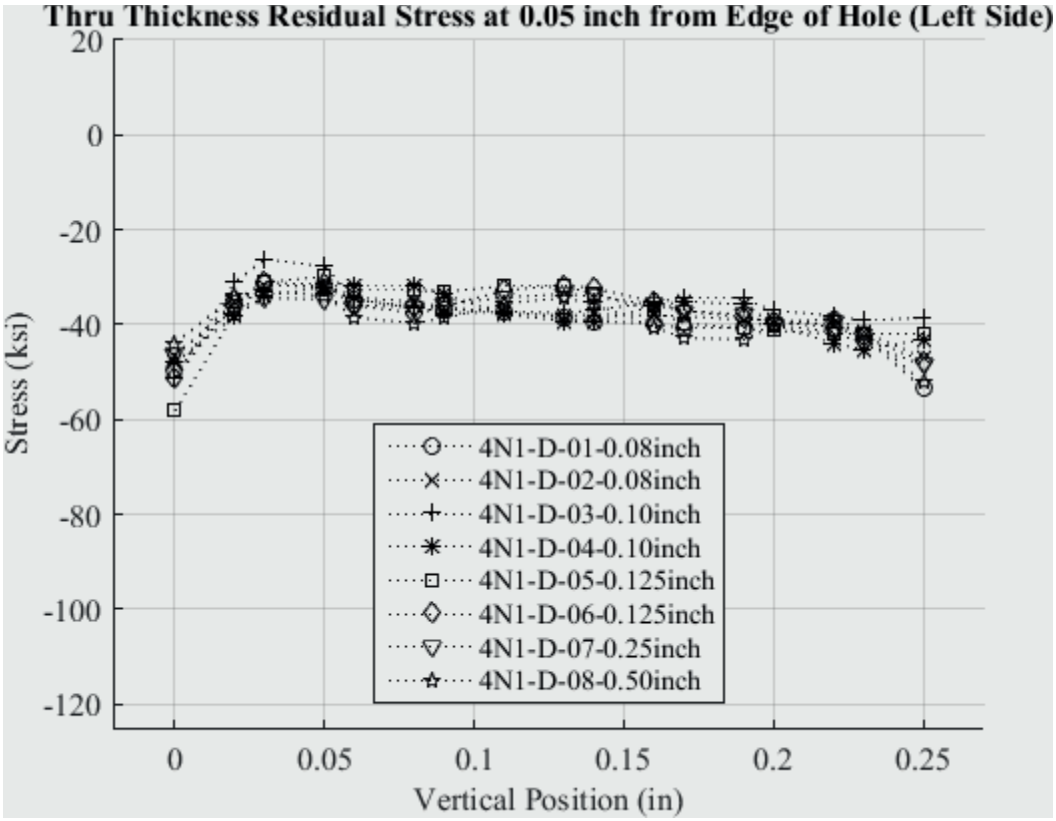

Fig. 521 Residual Stress Line Plot of all Cx4N1-D (7075-T651) Coupons Through the Thickness at 0.05 inch from Left Side of Hole.

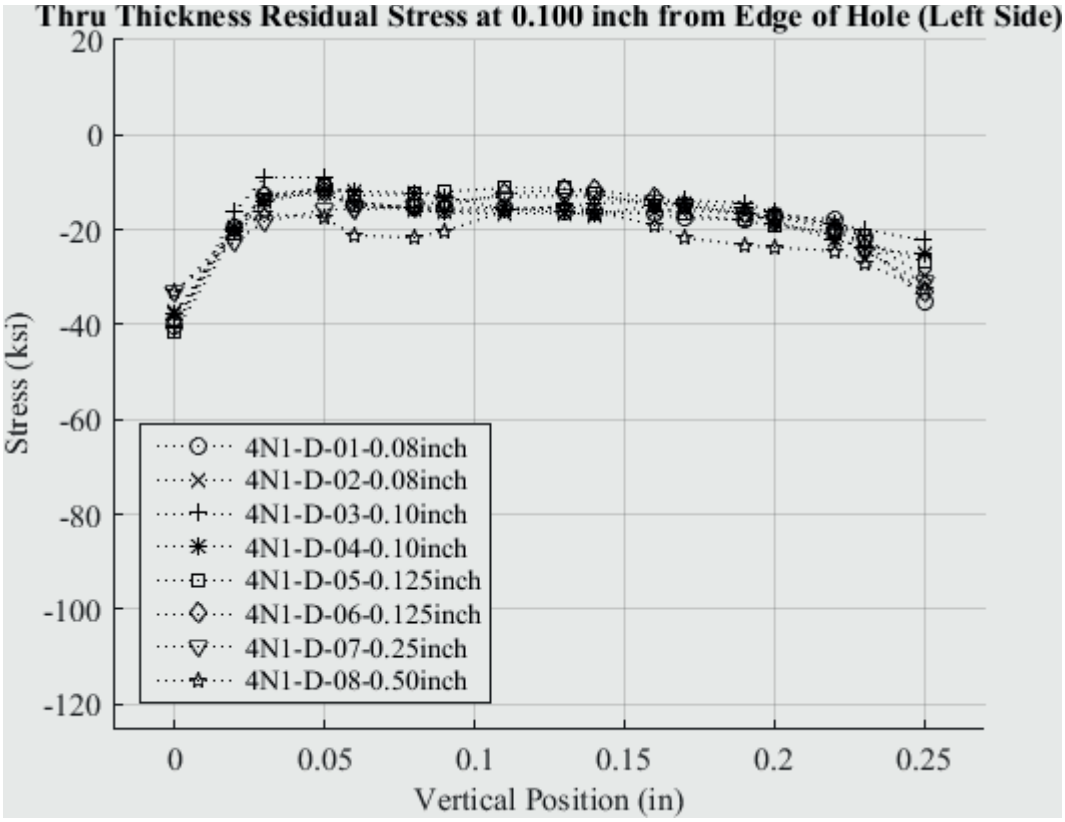

Fig. 522 Residual Stress Line Plot of all Cx4N1-D (7075-T651) Coupons Through the Thickness at 0.10 inch from Left Side of Hole.

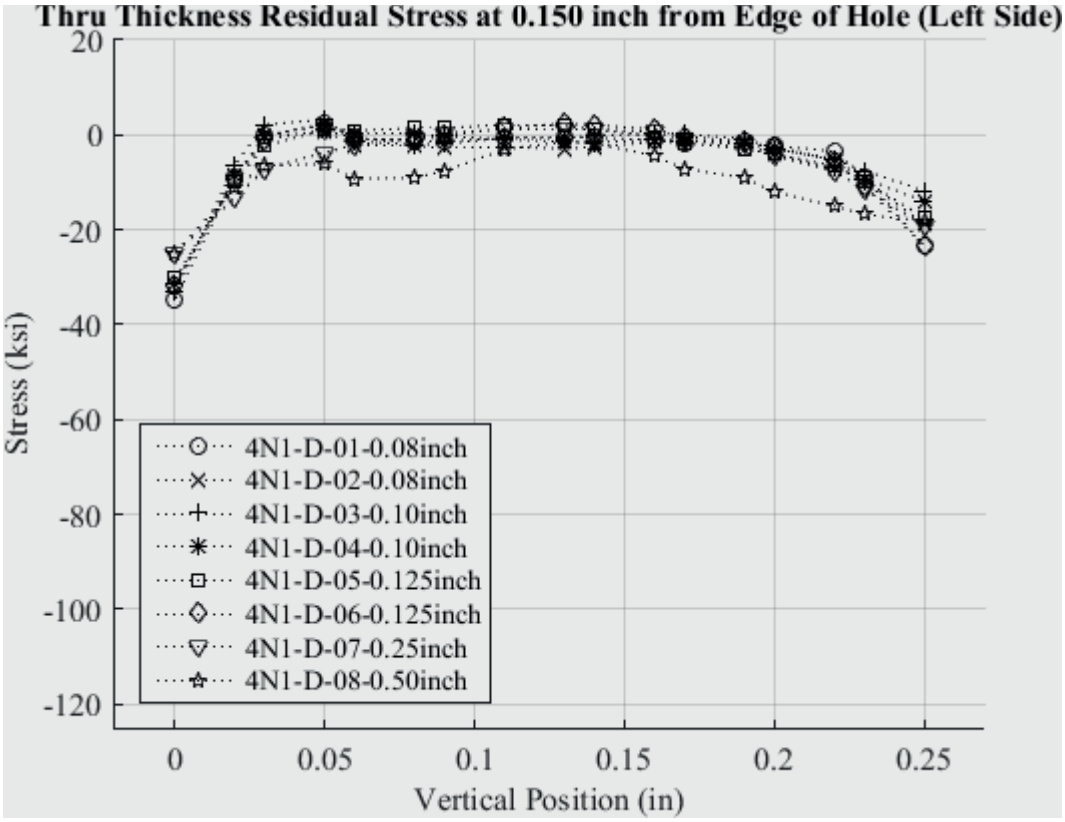

Fig. 523 Residual Stress Line Plot of all Cx4N1-D (7075-T651) Coupons Through the Thickness at 0.150 inch from Left Side of Hole.

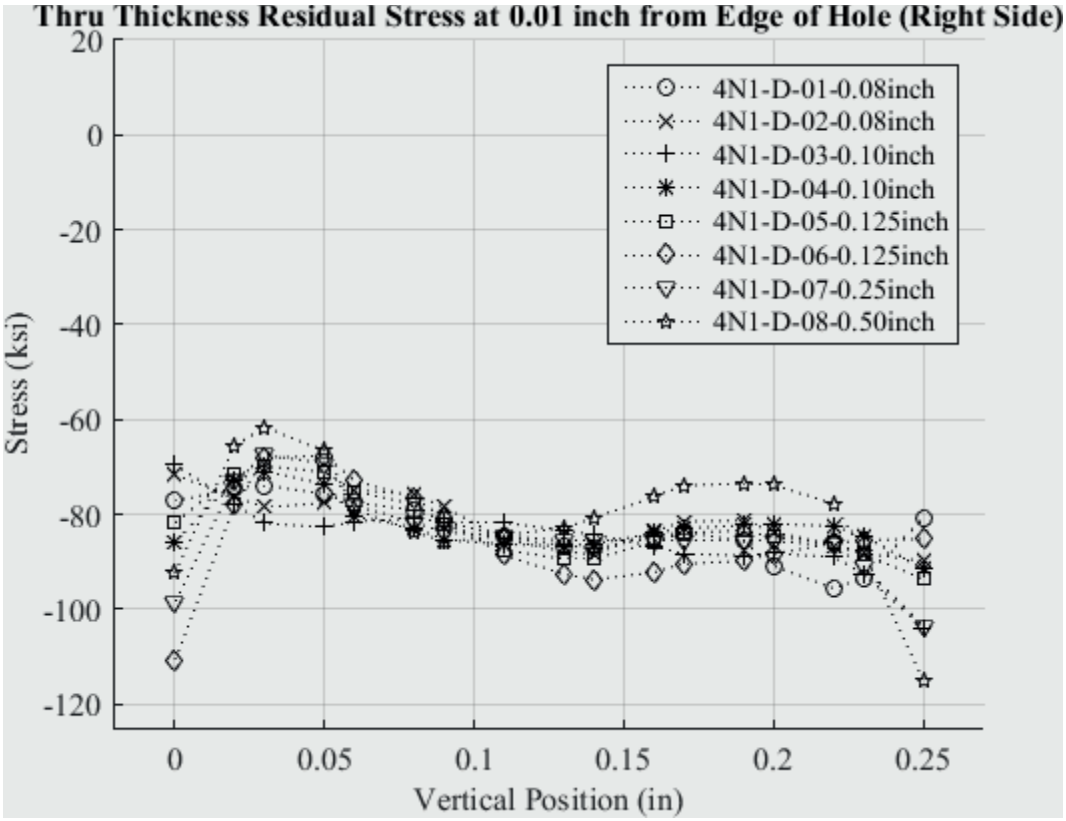

Fig. 524 Residual Stress Line Plot of all Cx4N1-D (7075-T651) Coupons Through the Thickness at 0.01 inch from Right Side of Hole.

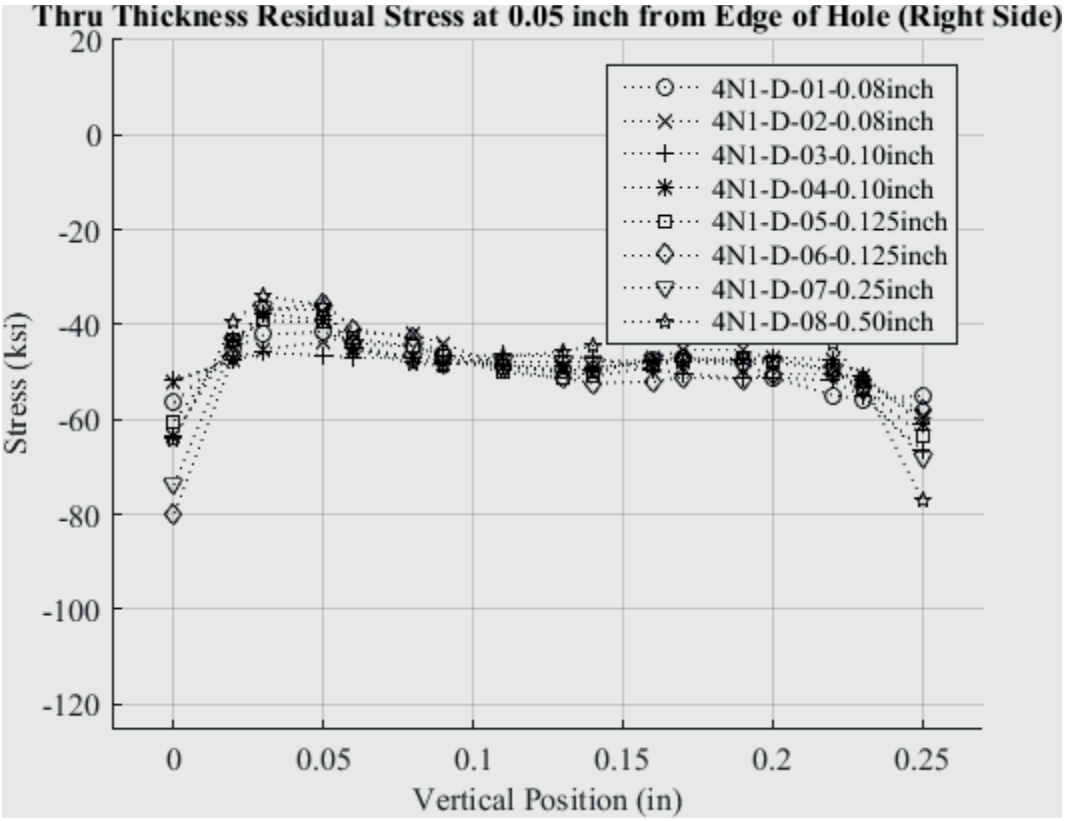

Fig. 525 Residual Stress Line Plot of all Cx4N1-D (7075-T651) Coupons Through the Thickness at 0.05 inch from Right Side of Hole.

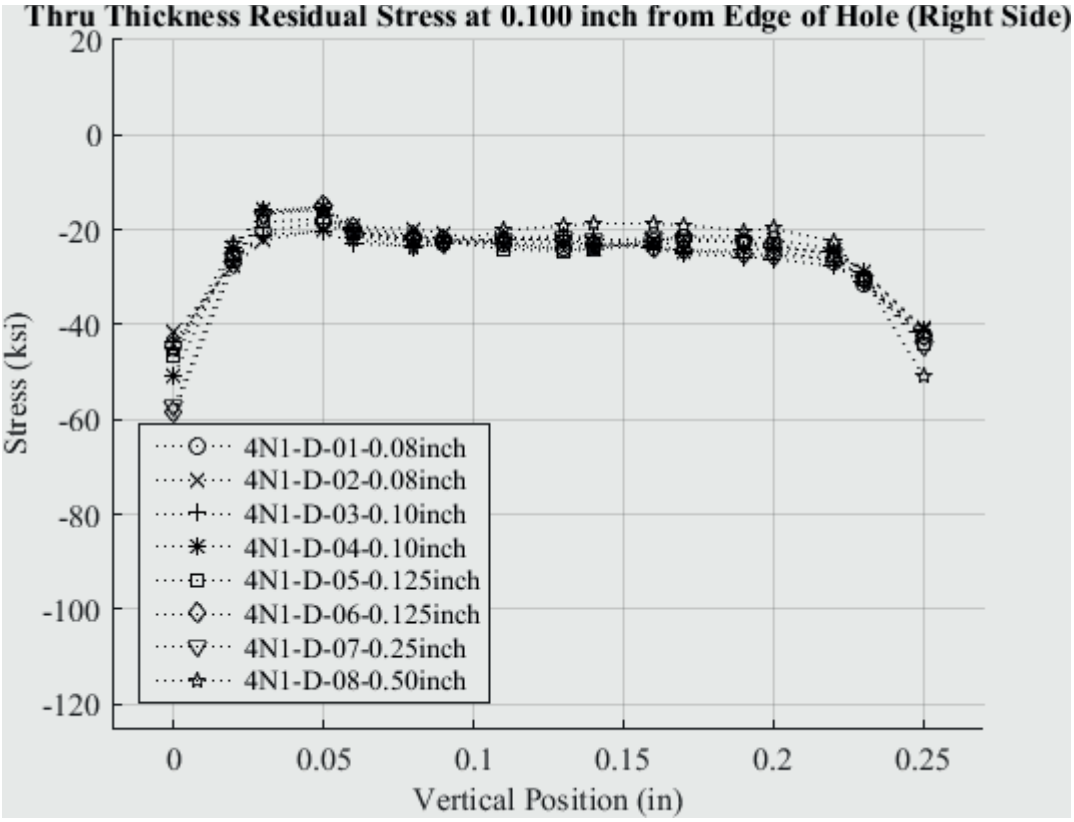

Fig. 526 Residual Stress Line Plot of all Cx4N1-D (7075-T651) Coupons Through the Thickness at 0.10 inch from Right Side of Hole.

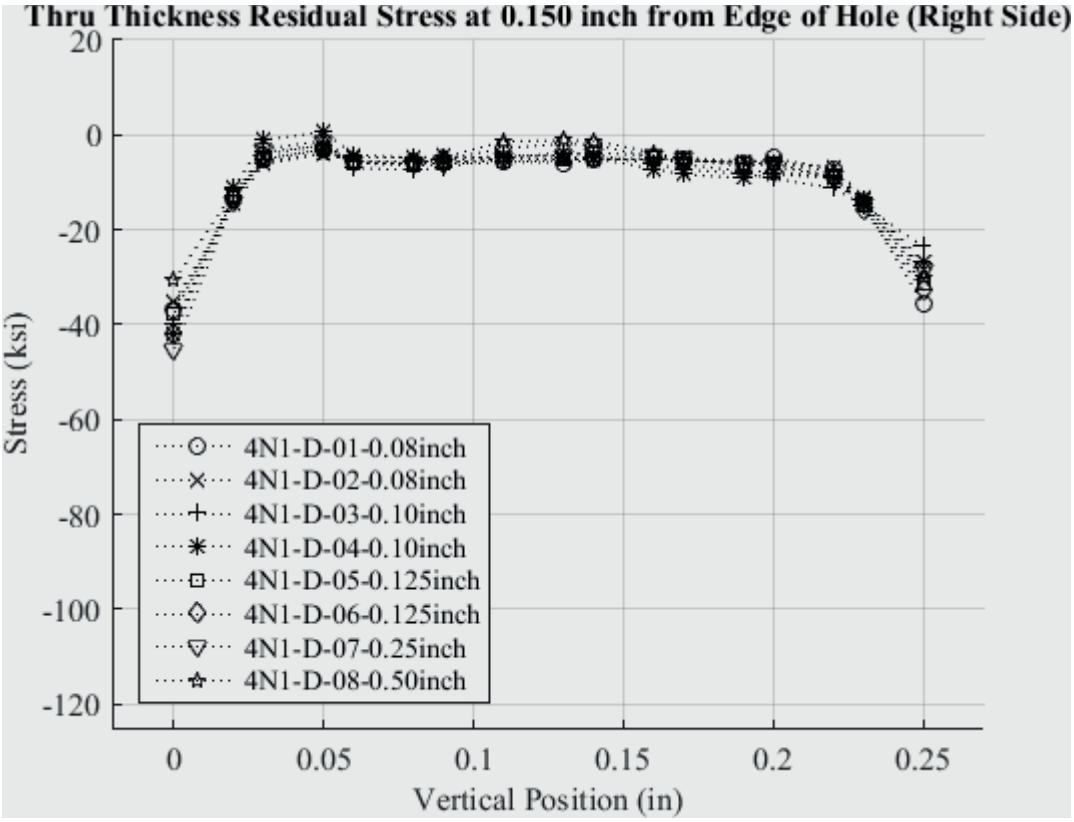

Fig. 527 Residual Stress Line Plot of all Cx4N1-D (7075-T651) Coupons Through the Thickness at 0.150 inch from Right Side of Hole.

7 COMPARISON OF RESIDUAL STRESSES BETWEEN BASELINE AND FATIGUE-CRACKED COUPONS

7.1 Development and Comparison of Single Measurement Uncertainty for Cx4N1-XX-B and Cx4N1-XX-D Cracked Coupons to Repeatability Uncertainty for CxA2 and CxD2 Baseline Uncracked Coupons

7.1.1 Development of Single Measurement Uncertainty for Cx4N1-XX-B (2024-T351) and Cx4N1-XX-D (7075-T651) Coupons

For each of the fatigue-cracked coupons the single measurement uncertainty was determined following the process outlined within section 4.3.2. This required that for each coupon five different knot density permutations were developed to produce the "model/fit error" and a series of Monte Carlo simulations were performed to determine the "displacement error".[132] The goal of performing this work was to provide a single measurement confidence bound that could be compared to the repeatability uncertainty of the replicates for a given fatigue-cracked condition. For all of the plots provided, the red line represents the CxA2 (baseline uncracked) condition with error bars that represent the repeatability uncertainty associated with those five coupons. The black line represents the individual coupon with the error bars representing the single measurement uncertainty associated with that individual measurement.

7.1.1.1 Radial Line Plots of Residual Stress Comparing Single Measurement Uncertainty Cx4N1-01-B (2024-T351) to Repeatability Uncertainty for CxA2 (2024-T351)

In order to gain a greater understanding of the difference in the calculated uncertainties between the single measurement method and the repeatability method, line plots were developed for the stresses through the thickness, radially away from the hole that provide the single measurement uncertainty for the Cx4N1-01-B (2024-T351), which had a fatigue crack on the left side of the hole of surface length 0.0797 inch. This single measurement and the uncertainty would allow for a comparison to the repeatability uncertainty as produced by the multiple replicates from the uncracked condition. If the residual stress and its associated standard deviation overlap then it would be possible to say that, for that area of the residual stress distributions, the two residual stress distributions are statistically similar within the bounds associated with a single standard deviation. Line plots for this comparison will be provided at only three of the five radial planes and only for two of the through-thickness planes. The radial line plot comparisons are provided in Fig. 528 through Fig. 533.

7.1.1.2 Line Plots of Through-Thickness Residual Stress Comparing Single Measurement Uncertainty Cx4N1-01-B (2024-T351) to Repeatability Uncertainty for CxA2 (2024-T351) for Left and Right Side of Hole

Residual stress line plots of the residual stress through the thickness of the material for both the left and right sides of the hole are provided, but only the first two planes of interest will be provided, at 0.01 inch and 0.05 inch from the edge of the hole. These line plots are provided in Fig. 534 through Fig. 537.

From these line plots it is possible to determine that when a 0.0797 inch fatigue

crack is developed within the residual stress field introduced by the Cx process the residual stress, as plotted through the thickness has been influenced. This influence is demonstrated by the shift in the residual stress in the area from the edge of the hole to around 0.10 inch. This region of difference is where the fatigue crack was present in the body and there is a statistical difference between the two residual stress lines evident by not only the shift of the line but also because the error bars in this area do not overlap.

As the fatigue crack was propagated to a larger size this difference between the single measurement and its associated uncertainty becomes ever greater from the CxA2 (2024-T351) baseline, uncracked coupon set.

7.1.2 Comparison of Single Measurement Uncertainty of Cx4N1-03-B (2024-T351) to the Repeatability Uncertainty of CxA2 (2024-T351)

7.1.2.1 Radial Line Plots of Residual Stress Comparing Single Measurement Uncertainty Cx4N1-03-B (2024-T351) to Repeatability Uncertainty for CxA2 (2024-T351)

The Cx4N1-03-B (2024-T351) coupon configuration had a fatigue crack of length 0.0974 inch along the Cx mandrel entrance surface. Residual stress line plots of the radial stress away from the hole are provided comparing the single measurement uncertainty to the repeatability uncertainty of the CxA2 (2024-T351) baseline coupon dataset. The single measurement data is in black and the CxA2 average is in red. Each has their associated uncertainty expressed by the double-sided error bars. Radial residual stress line plots are provided for the entrance, mid plane, and exit surfaces. These are provided in Fig. 538 through Fig. 543.

7.1.2.2 Line Plots of Through-Thickness Residual Stress Comparing Single Measurement Uncertainty Cx4N1-03-B (2024-T351) to Repeatability Uncertainty for CxA2 (2024-T351) for Left and Right Side of Hole

Residual stress through-thickness line plots for the left and right side of the Cx hole are provided in Fig. 544 through Fig. 547. Residual stress plots are provided for only two of the available through-thickness planes. The region of interest for the Cx4N1-03-B (2024-T351) condition is provided within these two planes.

For this fatigue-cracked coupon condition it is also possible to demonstrate that there is a statistical effect of the fatigue crack on the left side of the hole. This justified by the difference in the residual stress and the separation of the error bars between the baseline CxA2 average and the Cx4N1-03-B (2024-T351) residual stress field.[133]

7.1.3 Comparison of Single Measurement Uncertainty of Cx4N1-05-B (2024-T351) to the Repeatability Uncertainty of CxA2 (2024-T351)

7.1.3.1 Radial Line Plots of Residual Stress Comparing Single Measurement Uncertainty Cx4N1-05-B (2024-T351) to Repeatability Uncertainty for CxA2 (2024-T351)

The Cx4N1-05-B (2024-T351) coupon configuration had a fatigue crack length of 0.1259 inch along the Cx mandrel entrance surface. Residual stress line plots of the radial stress away from the hole are provided comparing the single measurement uncertainty to the repeatability uncertainty of the CxA2 (2024-T351) baseline coupon dataset. The single measurement data is in black and the CxA2 average is in red. Each has their associated uncertainty expressed by the double-sided error bars. Radial residual stress line plots are provided for the entrance, mid plane, and exit surfaces. These are provided in Fig. 548 through Fig. 553.

7.1.3.2 Line Plots of Through-Thickness Residual Stress Comparing Single Measurement Uncertainty Cx4N1-05-B (2024-T351) to Repeatability Uncertainty for CxA2 (2024-T351) for Left and Right Side of Hole

Residual stress through-thickness line plots for the left and right side of the Cx hole are provided in Fig. 554 through Fig. 557. Residual stress plots are provided for only two of the available through-thickness planes. The region of interest for the Cx4N1-05-B (2024-T351) condition is provided within these two planes.

7.1.4 Comparison of Single Measurement Uncertainty of Cx4N1-07-B (2024-T351) to the Repeatability Uncertainty of CxA2 (2024-T351)

7.1.4.1 Radial Line Plots of Residual Stress Comparing Single Measurement Uncertainty Cx4N1-07-B (2024-T351) to Repeatability Uncertainty for CxA2 (2024-T351)

The Cx4N1-07-B (2024-T351) coupon configuration had a 0.2515 inch surface crack on the Cx mandrel entrance face, the left side of the hole for these coupons. Residual stress line plots are provided along the same three radial planes through the thickness of the part. No secondary crack was present on the right side of the hole for this coupon. The radial residual stress line plots are provided in Fig. 558 through Fig. 563.

7.1.4.2 Line Plots of Through-Thickness Residual Stress Comparing Single Measurement Uncertainty Cx4N1-07-B (2024-T351) to Repeatability Uncertainty for CxA2 (2024-T351) for Left and Right Side of Hole

Through-thickness residual stress line plots are provided for this condition as well, as seen in Fig. 564 through Fig. 567. An additional line plot is provided for this coupon configuration at 0.10 inch away from the edge of the hole.

It can be seen from the through-thickness plots that the effect of the fatigue crack

on the left side of the hole had an influence on the residual stress at a greater distance from the edge of the hole, as shown in Fig. 566.

7.1.5 Comparison of Single Measurement Uncertainty of Cx4N1-08-B (2024-T351) to the Repeatability Uncertainty of CxA2 (2024-T351)

7.1.5.1 Radial Line Plots of Residual Stress Comparing Single Measurement Uncertainty Cx4N1-08-B (2024-T351) to Repeatability Uncertainty for CxA2 (2024-T351)

Residual stress line plots of the radial stress away from the edge of the hole for the Cx4N1-08-B (2024-T351) are compared to the baseline CxA2 condition for the entrance, mid plane, and exit surfaces in Fig. 568 through Fig. 573. The Cx4N1-08-B (2024-T351) coupon had a 0.4974 inch surface length crack on the Cx mandrel entrance surface. This crack had developed and propagated to a through-thickness crack and had developed a fatigue crack of approximate size of 0.05 inch surface length on the right side of the hole.

7.1.5.1 Line Plots of Through-Thickness Residual Stress Comparing Single Measurement Uncertainty Cx4N1-08-B (2024-T351) to Repeatability Uncertainty for CxA2 (2024-T351) for Left and Right Side of Hole

Residual stress line plots through the thickness of the Cx4N1-08-B (2024-T351) coupon are provided in Fig. 574 through Fig. 577. Additional through-thickness line plots are provided for this configuration because of the size of the crack that was present in the body.

As can be seen in Fig. 574 through Fig. 577 that the residual stress field was dramatically affected by the presence of the fatigue crack that was developed and propagated through the residual stress field introduced by the Cx process. The influence

of the fatigue crack can be seen though the thickness of the part, except for a region near 0.20 inch from the Cx mandrel entrance surface where the baseline CxA2 (2024-T351) average and standard deviation overlap the single measurement uncertainty associated with the residual stress for this coupon. For the right side of the hole it can be seen that there is no reduction in the residual stress field due to the cyclical loading of the coupon. For these coupons it actually shows an increase in the level of compressive residual stress, as compared to the baseline.

7.1.6 Comparison of Single Measurement Uncertainty of Cx4N1-01-D (7075-T651) to the Repeatability Uncertainty of CxD2 (7075-T651)

7.1.6.1 Radial Line Plots of Residual Stress Comparing Single Measurement Uncertainty Cx4N1-01-D (7075-T651) to Repeatability Uncertainty for CxD2 (7075-T651)

Residual stress line plots were developed for three of the standard planes of interest for these coupons. For this Cx4N1-01-D (7075-T651) coupon the left side of the hole had a 0.793 inch fatigue crack on the left side of the hole, along the Cx mandrel entrance surface. Residual stress line plots of these three planes are provided in Fig. 578 through Fig. 583.

7.1.6.2 Line Plots of Through-Thickness Residual Stress Comparing Single Measurement Uncertainty Cx4N1-01-D (7075-T651) to Repeatability Uncertainty for CxD2 (7075-T651) for Left and Right Side of Hole

Residual stress through-thickness line plots of the residual stress for both the left and right side of the Cxed hole are provided. The left side of the hole had a 0.0793 inch fatigue crack in it. These line plots are provided in Fig. 584 through Fig. 587.

It can be seen in Fig. 584 and Fig. 585 that the fatigue crack effects the residual

stress field through the thickness. This effect shifts the residual stress in a more positive direction, less compressive, as compared to the right side of the hole, where there was no fatigue crack and the residual stress is more compressive than the baseline coupon configuration.

7.1.7 Comparison of Single Measurement Uncertainty of Cx4N1-03-D (7075-T651) to the Repeatability Uncertainty of CxD2 (7075-T651)

7.1.7.1 Radial Line Plots of Residual Stress Comparing Single Measurement Uncertainty Cx4N1-03-D (7075-T651) to Repeatability Uncertainty for CxD2 (7075-T651)

Residual stress line plots of the stress radially away from the hole for the Cx4N1-03-D (7075-T651) coupon are provided in Fig. 588 through Fig. 593. The Cx4N1-03-D (7075-T651) coupon had a fatigue crack that had a surface length of 0.0972 inch along the mandrel entrance surface.

7.1.7.2 Line Plots of Through-Thickness Residual Stress Comparing Single Measurement Uncertainty Cx4N1-03-D (7075-T651) to Repeatability Uncertainty for CxD2 (7075-T651) for Left and Right Side of Hole

Residual stress line plots through the thickness were developed for both the left and right side of the Cxed hole. These are provided in Fig. 594 through Fig. 597.

The Cx4N1-03-D (7075-T651) coupon also shows a statistical difference between the baseline CxD2 (7075-T651) uncracked coupon configuration. From Fig. 594 and Fig. 595 there can be seen a shift in the residual stress field through the thickness. The right side of the hole shows a shift in the more compressive direction.

7.1.8 Comparison of Single Measurement Uncertainty of Cx4N1-05-D (7075-T651) to the Repeatability Uncertainty of CxD2 (7075-T651)

7.1.8.1 Radial Line Plots of Residual Stress Comparing Single Measurement Uncertainty Cx4N1-05-D (7075-T651) to Repeatability Uncertainty for CxD2 (7075-T651)

The Cx4N1-05-D (7075-T651) coupon configuration had a 0.1253 inch long surface crack along the Cx mandrel entrance surface, the left side of the hole for these residual stress plots. Residual stress line plots for the radial stress away from the hole are provided in Fig. 598 through Fig. 603.

7.1.8.2 Line Plots of Through-Thickness Residual Stress Comparing Single Measurement Uncertainty Cx4N1-05-D (7075-T651) to Repeatability Uncertainty for CxD2 (7075-T651) for Left and Right Side of Hole

Residual stress line plots through the thickness of the coupon, for both the left and the right side of the hole, are provided in Fig. 604 through Fig. 607.

The Cx4N1-05-D (7075-T651) coupons also showed an effect of the 0.1253 inch fatigue crack that was present on the left side of the hole, as shown in Fig. 604 and Fig. 605. The residual stress shifts towards the positive due to the presence of the crack. The right side of the hole does not experience this same shift relative to the baseline (CxD2) coupons.

7.1.9 Comparison of Single Measurement Uncertainty of Cx4N1-07-D (7075-T651) to the Repeatability Uncertainty of CxD2 (7075-T651)

7.1.9.1 Radial Line Plots of Residual Stress Comparing Single Measurement Uncertainty Cx4N1-07-D (7075-T651) to Repeatability Uncertainty for CxD2 (7075-T651)

The residual stress line plots for the single measurement uncertainty for the Cx4N1-07-D (7075-T651) coupon configuration, compared to the CxD2 (7075-T651) repeatability average, is plotted in radial line plots in Fig. 608 through Fig. 613.

7.1.9.2 Line Plots of Through-Thickness Residual Stress Comparing Single Measurement Uncertainty Cx4N1-07-D (7075-T651) to Repeatability Uncertainty for CxD2 (7075-T651) for Left and Right Side of Hole

Residual stress line plots through the thickness of the coupon are provided at all four through-thickness planes, for both the left and right sides of the hole. These residual stress line plots are provided in Fig. 614 through Fig. 617.

7.1.10 Comparison of Single Measurement Uncertainty of Cx4N1-08-D (7075-T651) to the Repeatability Uncertainty of CxD2 (7075-T651)

7.1.10.1 Radial Line Plots of Residual Stress Comparing Single Measurement Uncertainty Cx4N1-08-D (7075-T651) to Repeatability Uncertainty for CxD2 (7075-T651)

Residual stress line plots for the largest crack size developed in the 7075-T651 aluminum alloy coupons, 0.5017 inch along the mandrel entrance surface, are provided in Fig. 618 through Fig. 623. The fatigue crack that was developed in this coupon was a through crack on the left side and there was also a fatigue crack that was formed on the opposite side of the hole.

7.1.10.2 Line Plots of Through-Thickness Residual Stress Comparing Single Measurement Uncertainty Cx4N1-08-D (7075-T651) to Repeatability Uncertainty for CxD2 (7075-T651) for Left and Right Side of Hole

Through-thickness residual stress line plots were developed at all four through-thickness planes. They are provided in Fig. 624 through Fig. 627.

7.2 Comparison of Residual Stresses from CxA2 (2024-T351) Baseline Coupons to Cx4N1-XX-B (2024-T351) Fatigue-Cracked Coupons

These plots will provide information on each of the individual coupons, along with the average residual stress of the two coupons. Error bars will be provided for the average of the two coupons, when applicable, and the average of the CxA2 (2024-T351) baseline condition with error bars on that average which represents the repeatability uncertainty calculated previously.

7.2.1 Line Plots of Residual Stress for Cx4N1-01-B and Cx4N1-02-B Coupons Compared to the CxA2 Baseline Condition

An additional perspective that can be shown is a comparison of the combined cracked condition for the Cx4N1-01-02-B (2024-T351) as compared to the baseline CxA2 (2024-T351). Through this it is possible to gain an understanding of the effect of the fatigue crack at discrete lengths.

7.2.1.1 Line Plots of the Residual Stress Radially away from the Cx Hole for Cx4N1-01-B and Cx4N1-02-B Coupons Compared to the CxA2 Baseline Condition

Residual stress line plots at the entrance, mid plane, and exit surfaces are provided for this comparison. For each cross-section two plots are provided, one that gives the

residual stresses for the entire cross-section and the other is focused in at the first 0.25 inch away from the edge of the hole. These line plots are provided in Fig. 628 through Fig. 633.

7.2.1.2 Line Plots of the Through-Thickness Stress on the Left and the Right Side of the Cx Hole for Cx4N1-01-B and Cx4N1-02-B Coupons Compared to the CxA2 Baseline Condition

Residual stress line plots of the through-thickness residual stress for both the left and right side of the Cx hole are provided. Line plots at 0.01 inch, 0.05 inch, and 0.10 inch from the edge of the hole are provided in Fig. 634 through Fig. 639.

7.2.2 Line Plots of Residual Stress for Cx4N1-03-B and Cx4N1-04-B Coupons Compared to the CxA2 Baseline Condition

7.2.2.1 Line Plots of the Residual Stress Radially away from the Cx Hole for Cx4N1-03-B and Cx4N1-04-B Coupons Compared to the CxA2 Baseline Condition

Radial line plots of the residual stress for the Cx4N1-03 and -04-B (2024-T351) condition are provided in Fig. 640 through Fig. 645. These coupons had a fatigue crack length of 0.10 inch on the left side of the hole on the Cx mandrel entrance surface.

7.2.2.2 Line Plots of the Through-Thickness Stress on the Left and the Right Side of the Cx Hole for Cx4N1-03-B and Cx4N1-04-B Coupons Compared to the CxA2 Baseline Condition

Through-thickness line plots are provided at 0.01 inch, 0.05 inch, 0.10 inch, and 0.15 inch for both the left and right sides of the hole. These are provided in Fig. 646 through Fig. 653.

7.2.3 Line Plots of Residual Stress for Cx4N1-05-B and Cx4N1-06-B Coupons Compared to the CxA2 Baseline Condition

7.2.3.1 Line Plots of the Residual Stress Radially away from the Cx Hole for Cx4N1-05-B and Cx4N1-06-B Coupons Compared to the CxA2 Baseline Condition

Radial residual stress line plots for the Cx4N1-05-B and Cx4N1-6-B (2024-T351) are provided in Fig. 654 through Fig. 667. These coupons had a fatigue crack length of 0.125 inch along the left side of the Cx mandrel entrance surface.

7.2.3.2 Line Plots of the Through-Thickness Stress on the Left and the Right Side of the Cx Hole for Cx4N1-05-B and Cx4N1-06-B Coupons Compared to the CxA2 Baseline Condition

Through-thickness residual stress line plots for the left and right side of the Cx hole are provided in Fig. 660 through Fig. 667.

7.2.4 Line Plots of Residual Stress for Cx4N1-07-B Coupon Compared to the CxA2 Baseline Condition

For the Cx4N1-07-B configuration there was only one coupon produced. Therefore, there will only be the one residual stress line for the given condition, with no additional statistical analysis.

7.2.4.1 Line Plots of the Residual Stress Radially away from the Cx Hole for Cx4N1-07-B Coupon Compared to the CxA2 Baseline Condition

Residual stress line plots, showing the radial residual stress for coupon Cx4N1-07-B, are provided in Fig. 668 through Fig. 676. This coupon had a fatigue crack of surface length 0.2515 inch.

7.2.4.2 Line Plots of the Through-Thickness Stress on the Left and the Right Side of the Cx Hole for Cx4N1-07-B Coupon Compared to the CxA2 Baseline Condition

Through-thickness residual stress line plots are provided for this condition in Fig. 674 through Fig. 681.

7.2.5 Line Plots of Residual Stress for Cx4N1-08-B Coupon Compared to the CxA2 Baseline Condition

7.2.5.1 Line Plots of the Residual Stress Radially away from the Cx Hole for Cx4N1-08-B Coupon Compared to the CxA2 Baseline Condition

The Cx4N1-08-B (2024-T351) coupon had a fatigue crack length of 0.4974 inch on the left side of the hole, at the Cx mandrel entrance surface. This coupon also had a less than 0.05 inch fatigue crack on the right side of the coupon. Radial residual stress line plots are provided at the entrance, mid plane, and exit planes within the coupon in Fig. 682 through Fig. 687.

7.2.5.2 Line Plots of the Through-Thickness Stress on the Left and the Right Side of the Cx Hole for Cx4N1-08-B Coupon Compared to the CxA2 Baseline Condition

Through-thickness residual stress line plots for coupon Cx4N1-08-B are provided for both the left and right sides of the Cxed hole in Fig. 688 through Fig. 695.

7.2.6 General Comments Regarding Comparison of Individual Cx4N1-B (2024-T351) Coupons to CxA2 Average

It can be seen from the comparisons of each of the individual groups of fatigue-cracked coupons to the CxA2 (2024-T351) uncracked, baseline that for the fatigue-cracked side of the hole, there shows a shift in the residual stress, which correlates in the

depth, through the thickness, to the fatigue crack size. This can be determined because for each of the fatigue-cracked conditions an average is shown along with the standard deviation of that average residual stress. It is understood that with a maximum of only two replicates for three of the five conditions, there is little statistical power associated with these confidence bounds, however, this was the stated requirement per this work to determine difference in the residual stress fields.

The through-thickness residual stress line plots provide the most useful means to investigate the effect of the fatigue crack on the residual stress field. At a distance away from the edge of the hole of 0.01 inch to 0.10 inch it can be seen that even for the smallest sized fatigue cracks of approximately 0.08 inch there is a sift in the residual stress between the edge of the hole and 0.10 inch from the entrance surface. This shift continues to increase in magnitude and distance from the Cx mandrel entrance edge of the hole as the fatigue crack size became larger.

For the right side of the hole there seemed to be a general increase in the compressive magnitude of the residual stress field. It is unknown why this occurred, however if one was to assume that the left side of the hole had a similar magnitude of residual stress in it prior to the development and propagation of the fatigue crack then there is an even greater shift in the residual stress field due to the presence of the fatigue crack.

7.3 Comparison of Residual Stresses from CxD2 (7075-T651) Baseline Coupons to Cx4N1-XX-D (7075-T651) Fatigue-Cracked Coupons

Comparisons of the residual stress between the baseline CxD2 (7075-T651) and all of the Cx4N1-XX-D (7075-T651) coupons is provided by grouping of fatigue crack

sizes.

7.3.1 Line Plots of Residual Stress for Cx4N1-01-D and Cx4N1-02-D Coupon Compared to the CxD2 Baseline Condition

Residual stress line plots for both the radial and through-thickness directions are provided for the Cx4N1-01-D and Cx4N1-02-D (7075-T651) coupon configuration. These coupons had a fatigue crack that was developed and propagated to a surface length of 0.08 inch along the Cx mandrel entrance surface.

7.3.1.1 Line Plots of the Residual Stress Radially away from the Cx Hole for Cx4N1-01-D and Cx4N1-02-D Coupons Compared to the CxD2 Baseline Condition

Radial line plots of the residual stress are provided in Fig. 696 through Fig. 701. Plots are provided both the entire cross-section and for the first 0.25 inch away from the edge of the Cxed hole.

7.3.1.2 Line Plots of the Through-Thickness Stress on the Left and the Right Side of the Cx Hole for Cx4N1-01-D and Cx4N1-02-D Coupons Compared to the CxD2 Baseline Condition

Through-thickness residual stress line plots for the left and right side of the Cxed hole are provided in Fig. 702 through Fig. 707.

7.3.2 Line Plots of Residual Stress for Cx4N1-03-D and Cx4N1-04-D Coupon Compared to the CxD2 Baseline Condition

The Cx4N1-03-D and Cx4N1-04-D (7075-T651) coupon configuration had a fatigue crack that had propagated to a length of 0.10 inch on the left side of the hole, at

the Cx mandrel entrance surface.

7.3.2.1 Line Plots of the Residual Stress Radially away from the Cx Hole for Cx4N1-03-D and Cx4N1-04-D Coupons Compared to the CxD2 Baseline Condition

Radial line plots of the residual stress are provided at the entrance, mid plane, and exit planes for these coupons. The residual stress line plots are provided in Fig. 708 through Fig. 713.

7.3.2.2 Line Plots of the Through-Thickness Stress on the Left and the Right Side of the Cx Hole for Cx4N1-03-D and Cx4N1-04-D Coupons Compared to the CxD2 Baseline Condition

Line plots of the through-thickness residual stress are plotted in Fig. 714 through Fig. 721.

7.3.3 Line Plots of Residual Stress for Cx4N1-05-D and Cx4N1-06-D Coupon Compared to the CxD2 Baseline Condition

The Cx4N1-05-D and Cx4N1-06-D (7075-T651) coupon configuration had a fatigue crack on the left side of the Cxed hole which had an average surface length of 0.125 inch.

7.3.3.1 Line Plots of the Residual Stress Radially away from the Cx Hole for Cx4N1-05-D and Cx4N1-06-D Coupons Compared to the CxD2 Baseline Condition

Radial residual stress line plots are provided at the entrance, mid plane, and exit surfaces, and can be seen in Fig. 722 through Fig. 727.

7.3.3.2 Line Plots of the Through-Thickness Stress on the Left and the Right Side of the Cx Hole for Cx4N1-05-D and Cx4N1-06-D Coupons Compared to the CxD2 Baseline Condition

Through-thickness line plots of the residual stress for both the left and right side of the Cxed hole are provided in Fig. 728 through Fig. 735.

7.3.4 Line Plots of Residual Stress for Cx4N1-07-D Coupon Compared to the CxD2 Baseline Condition

The Cx4N1-07-D (7075-T651) coupon condition only had one replicate made and had a 0.2505 inch-long fatigue crack on the Cx mandrel entrance surface, on the left side of the hole.

7.3.4.1 Line Plots of the Residual Stress Radially away from the Cx Hole for Cx4N1-07-D Coupon Compared to the CxD2 Baseline Condition

The radial residual stress for the Cx4N1-07-D (7075-T651) coupon at the entrance, mid plane, and exit planes are provided in Fig. 736 through Fig. 741.

7.3.4.2 Line Plots of the Through-Thickness Stress on the Left and the Right Side of the Cx Hole for Cx4N1-07-D Coupon Compared to the CxD2 Baseline Condition

Through-thickness line plots of the residual stress on the left and right sides of the Cx hole are provide in Fig. 742 through Fig. 749.

7.3.5 Line Plots of Residual Stress for Cx4N1-08-D Coupon Compared to the CxD2 Baseline Condition

The Cx4N1-08-D coupon had a fatigue crack that had propagated through the thickness of the part on the left side of the hole. The surface length of that fatigue crack

along the Cx mandrel entrance surface was 0.5017 inch. This coupon also had nucleated and propagated a fatigue crack on the right side of the hole as well. This crack had a surface length that was less than 0.05 inch.

7.3.5.1 Line Plots of the Residual Stress Radially away from the Cx Hole for Cx4N1-08-D Coupon Compared to the CxD2 Baseline Condition

Residual stress line plots are provided for the three main surfaces for this condition and can be seen in Fig. 750 through Fig. 755.

7.3.5.2 Line Plots of the Through-Thickness Stress on the Left and the Right Side of the Cx Hole for Cx4N1-08-D Coupon Compared to the CxD2 Baseline Condition

Residual stress through-thickness line plots for the left and right side of the Cxed hole are provided in Fig. 756 through Fig. 763.

7.4 Comparison of Baseline CxA2 (2024-T351) and CxD2 (7075-T651) Coupons to the Fatigue-Cracked Cx4N1-XX-B (2024-T351) and Cx4N1-XX-D (7075-T651) Coupons

The hypothesis of this work is that a fatigue crack changes the residual stress field introduced by the Cx process in two aerospace aluminum alloys, 2024-T351 and 7075-T651. In order to determine if this hypothesis is true or not, a series of baseline, uncracked coupons were produced that had been Cxed to the "low" end of the applied expansion range, within the FTI specification.[3]

The contour method was used to quantify the 2D residual stress field along the plane of interest. A statistical method was used to determine the single measurement uncertainty and the repeatability uncertainty for the five replicate coupons that were

produced in the baseline condition. The residual stress distribution was then plotted via contour plots, and a series of line plots, both radially away from the hole and in through-thickness, at specific distances away from the left and right side of the Cxed hole. These coupons provided the baseline condition for comparison purposes to a series of identical coupons that were produced using the same machining tolerances and Cxed to the same applied expansion.

This next series of coupons had a fatigue crack propagated to a specific length on one side of the coupon. These fatigue cracks were propagated to lengths ranging from approximately 0.08 inch to 0.50 inch. For three of the conditions, two coupons were produced and served as a replicate. Thus an average and standard deviation was produced for those three conditions. However, the statistical power of these distributions is very low, due to the limited number of replicates produced. For the coupons that had 0.25 inch and 0.50 inch fatigue cracks, only one coupon was produced.

The coupons were then processed via the exact same contour method to determine the residual stress along the exact same plane of interest. Contour and line plots were produced for each of the individual coupons and for the groups of similar fatigue crack lengths. Line plots were provided for each of these crack length groups comparing the residual stress of the fatigue-cracked coupon to the baseline, uncracked condition. Statistical bounds were produced for the baseline condition by determining the average residual stress for the five replicates and applying the repeatability standard deviation as a double-sided error bar. For the cracked conditions the average residual stress was calculated for the two replicates and the repeatability standard deviation was applied to that average residual stress.

One of the key questions of this work was what defines "change" in the residual stress field by the presence of the fatigue crack. For this work "change" is defined as effecting the residual stress field so that the two error bars are statistically different, thus they do not overlap. This would demonstrate that each distribution of residual stresses is outside of the 68.2% confidence bounds on the residual stress. Thus, if the line plot's error bars do not overlap, there was a change in the residual stress field by the presence of the fatigue crack.

7.4.1 Comparison of Combined Residual Stresses from CxA2 (2024-T351) Baseline Coupons to Cx4N1-XX-B (2024-T351) Fatigue-Cracked Coupons

Residual stress line plots comparing the baseline CxA2 (2024-T351) Cxed condition to coupons that have had fatigue cracks developed in them are provided below. An additional set of plots, which focus on the region that is 0.50 inch away from the edge of the hole, are provided within the radial section. This area of residual stress can have the most dramatic influence on fatigue crack growth and is also the most difficult to determine via the contour method.[134] The critical aspect of this region of residual stress will be demonstrated later when predictions are made using the residual stress fields produced through this documented process.

7.4.1.1 Comparison of Radial Line Plots of Stress from Combined Cx4N1-XX-B (2024-T351) Coupons to the CxA2 Baseline Residual Stress Field

Radial residual stress line plots are provided at seven specific planes, as provided above. In addition to these standard full-length residual stress line plots, plots were produced that limit the range of the X coordinate to only 0.50 inch away from the hole.

These plots are provided for the left and right side of the Cxed hole. The standard line plots are provided in Fig. 764 through Fig. 770. These plots do not provide the residual stresses for each individual coupon, instead, for those that have replicates only, one of them is provided. From the previous section of this report it is possible to determine that the repeatability of these coupons is quite high. In addition to this when all of the coupons are plotted together it is difficult to see any features within the plot.

Additional line plots for the left side of the hole, which focus on the residual stress radially away from the hole, from the edge of the hole to 0.50 inch away, are provided in Fig. 771 through Fig. 777.

Similar line plots for the right side of the hole are shown in Fig. 778 through Fig. 784.

From the provided plots above it is possible to make some general comments regarding the effect of the fatigue crack on the residual stress field. The residual stress field shows a greater influence on from the presence of the fatigue crack near the Cx mandrel entrance surface. This is reasonable given that the fatigue cracks were propagated on this surface. As the fatigue crack grew to a larger size there is an ability to see the effect of the crack through the thickness of the part. There seems to be a trend where in the baseline, uncracked condition the residual stresses along the 0.200 inch from the Cx mandrel entrance face, is at a much higher level of tension than the cracked coupons. This is for all conditions, and for both the left and the right sides of the hole. This trend seems to be related to the fit at that cross-section and does not continue through the thickness of the part.

In addition to this there is a trend within the data that shows a decrease in the

level of compression which is directly related to the fatigue crack size that was within the body. Thus near the edge of the hole, for the first 0.10 inch it is possible to show that the 0.08 inch crack has less of an impact on the residual stress field than does the larger 0.125 inch through 0.50 inch crack. Through these plots it is possible to state that there is a direct effect of the fatigue crack on the residual stress field imposed by the Cx process. The right side of the hole shows no decrease in the residual stress due to the cyclical loading that it experienced. In order to gain a greater understanding of this effect through-thickness residual stress line plots are needed and will be discussed further.

7.4.1.2 Comparison of Through-Thickness Line Plots of Stress from Combined Cx4N1-XX-B (2024-T351) Coupons to the CxA2 Baseline Residual Stress Field

Through thickness residual stress line plots comparing the baseline CxA2 to all of the Cx4N1-XX-B (2024-T351) coupons are provided in Fig. 785 through Fig. 792.

Significant information can be determined from these through-thickness residual stress line plots. First it is possible to determine from the through-thickness line plots at 0.01 and 0.05 inch that there is a direct relationship between crack size and the reduction in the residual stress along that through-thickness line. As the cracks get larger, to 0.25 and 0.50 inch, this effect can be seen in the the 0.10 inch through-thickness line plots as well. For these plots the 0.50 inch fatigue-cracked coupon clearly stands out from the group. For the right side of the hole, the story is quite different. There does not seem to be any decrease in the residual stress field due to the cyclical loading that these coupons experienced. These through-thickness line plots help to clearly show that there is a direct effect of the presence of the fatigue crack. In addition, this effect is correlated to the

specific crack size. This is new information that has not been provided to the community.

7.4.2 Comparison of Combined Residual Stresses from CxD2 (7075-T651) Baseline Coupons to Cx4N1-XX-D (7075-T651) Fatigue-Cracked Coupons

7.4.2.1 Comparison of Radial Line Plots of Stress from Combined Cx4N1-XX-D (7075-T651) Coupons to the CxA2 Baseline Residual Stress Field

Radial residual stress line plots are provided at seven specific planes, as provided above. In addition to these standard full-length residual stress line plots, plots were produced that limit the range of the X coordinate frame to only 0.50 inch away from the hole. These plots are provided for the left and right side of the Cxed hole. The standard line plots are provided in Fig. 793 through Fig. 799.

In addition to those seven over view line plots additional plots were produced that limit the range in the X coordinate to focus on the region within 0.50 inch from the edge of the hole. Radial, residual stress line plots are provided for the left and right side of the hole in Fig. 800 through Fig. 813.

From these radial residual stress line plots it's possible to see that for the left side of the hole there was a significant shift in the residual stress field for all crack sizes, and this shift was able to be detected through the thickness of the part. The effect on the cracked side of the hole came back to within the range of the CxD2 (7075-T651) baseline coupons at approximately 0.25 inch away from the edge of the hole, one radius.

A shift in the residual stress field of similar magnitude for all of the crack sizes is very different from that demonstrated from the Cx4N1-B (2024-T351) coupons. The 2024 coupons showed a correlated effect of the shift in the residual stress field as a

function of crack size. From the residual stress fields determined through this research, this effect is not the same for the 7075-T651 material. For the uncracked side of the hole there is no evidence of the loading causing any decrease in the magnitude of the compressive residual stress field.

7.4.2.2 Comparison of Through-Thickness Line Plots of Stress from Combined Cx4N1-XX-D (7075-T651) Coupons to the CxD2 Baseline Residual Stress Field

In addition to the radial line plots of the residual stress through-thickness line plots were produced to enable a more thorough understanding of the residual stress field. These through-thickness line plots are provided in Fig. 814 through Fig. 821.

These through-thickness plots help to provide a much clearer view of the effect of the fatigue crack on the residual stress field. From Fig. 814 through Fig. 817 it is possible to see that for all of the fatigue crack sizes there is a shift in the residual stress field in the tensile direction. Unlike the Cx4N1-B (2024-T351) material this shift does not tend to correlate to crack size. In this material the shift in the residual stress field extends out to 0.15 inch away from the edge of the hole. Like the 2024-T351 material there is no evidence of a decrease in the compressive residual stress on the right side of the hole.

7.5 Conclusions of Comparison of Baseline CxA2 (2024-T351) and CxD2 (7075-T651) to Fatigue-Cracked Cx4N1-XX-B (2024-T351) and Cx4N1-XX-D (7075-T651)

7.5.1 Conclusion from Comparing Single Measurement Uncertainty Cx4N1-01-08-B (2024-T351) to Repeatability Uncertainty for CxA2 (2024-T351)

It can be seen in the through-thickness plots of the left side of the hole that there is a general trend of the residual stress magnitude decreasing as a function of the fatigue crack size developed within the coupon. This can be seen clearly at a distance of 0.01 inch and 0.05 inch away from the edge of the hole, as shown in Fig. 785 and Fig. 786. As the residual stress line plots move farther away from the edge of the hole the lines begin to converge and there is less ability to determine a statistical difference between them and the CxA2 (2024-T351) baseline, uncracked condition. However, it should be noted that for the Cx4N1-08-B (2024-T351) coupon the effect of the fatigue crack can be seen all the way to 0.150 inch away from the edge of the hole. This crack had a Cx mandrel entrance surface length of approximately 0.50 inch and was propagated all the way through the thickness of the coupon.

The right side of the hole showed no noticeable effect due to the presence of the crack on the other side of the hole and also no statistically definable effect due to the cyclic loading that the coupon experienced. It should be remembered that this effect is currently only related to constant amplitude loading in which the far-field, gross stress is well below yield. With this applied loading, for crack propagation, the local net stress at the hole was well above yield for the 2024 alloy, and just above yield for the 7075 material.

7.5.2 Conclusion from Comparing Single Measurement Uncertainty Cx4N1-01-08-D (7075-T651) to Repeatability Uncertainty for CxD2 (7075-T651)

Unlike the Cx4N1-XX-B (2024-T351) coupons these 7075-T651 coupons showed a shift in the residual stress due to the presence of the fatigue crack, regardless of the size of the fatigue crack. The shift in the residual stress was significant when compared to the baseline, CxD2 (7075-T651) coupons, however this shift was not dependent on the size of the fatigue crack developed in the coupon. This effect is quite different from that determined in the Cx4N1-B (2024-T351) coupons, in which there was a correlated effect in the residual stress field to fatigue crack size. Currently it is not known why this difference is demonstrated in these two aluminum alloys. One potential cause for this difference is the difference in the size of the plastic zone that would be developed during fatigue crack growth in the two alloys. This plastic zone size is related to the yield strength of the material.

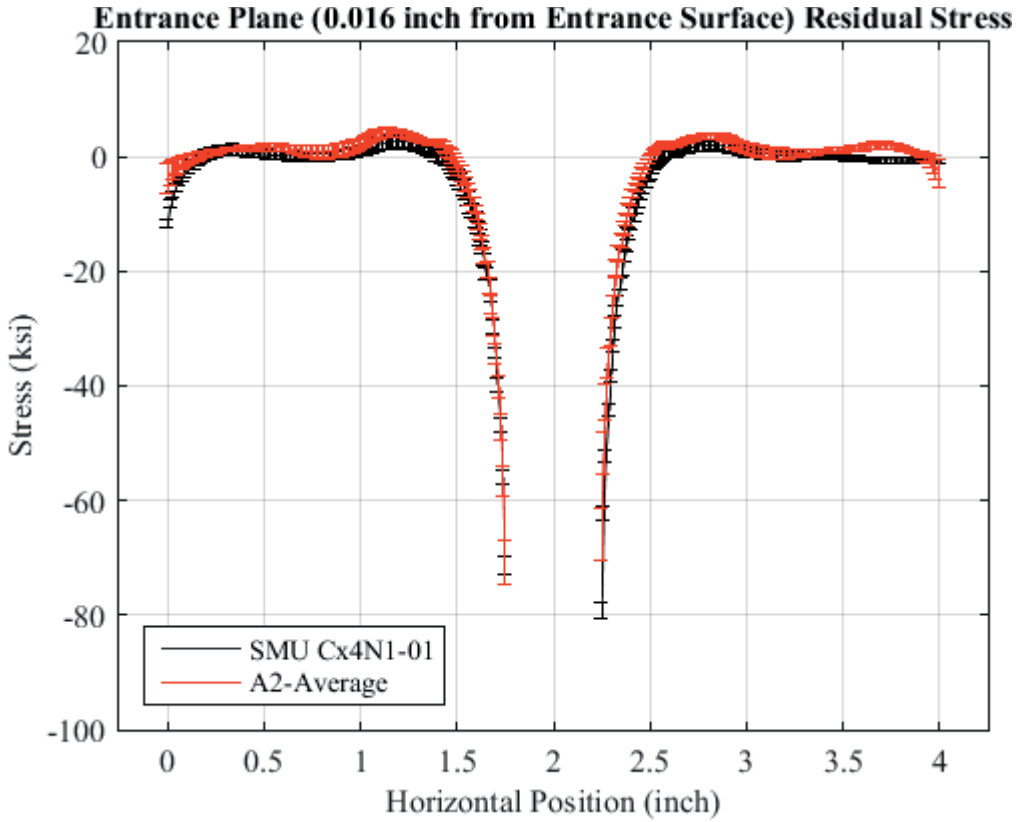

Fig. 528 Residual Stress Line Plot Comparing the Single Measurement Uncertainty of Cx4N1-01-B to the CxA2 (2024-T351) Average Residual Stress at a Distance of 0.016 inch (Entrance Surface) from the Entrance Surface – Cx4N1-01-B Coupon had a 0.0797 inch Fatigue Crack at the Left Entrance Surface.

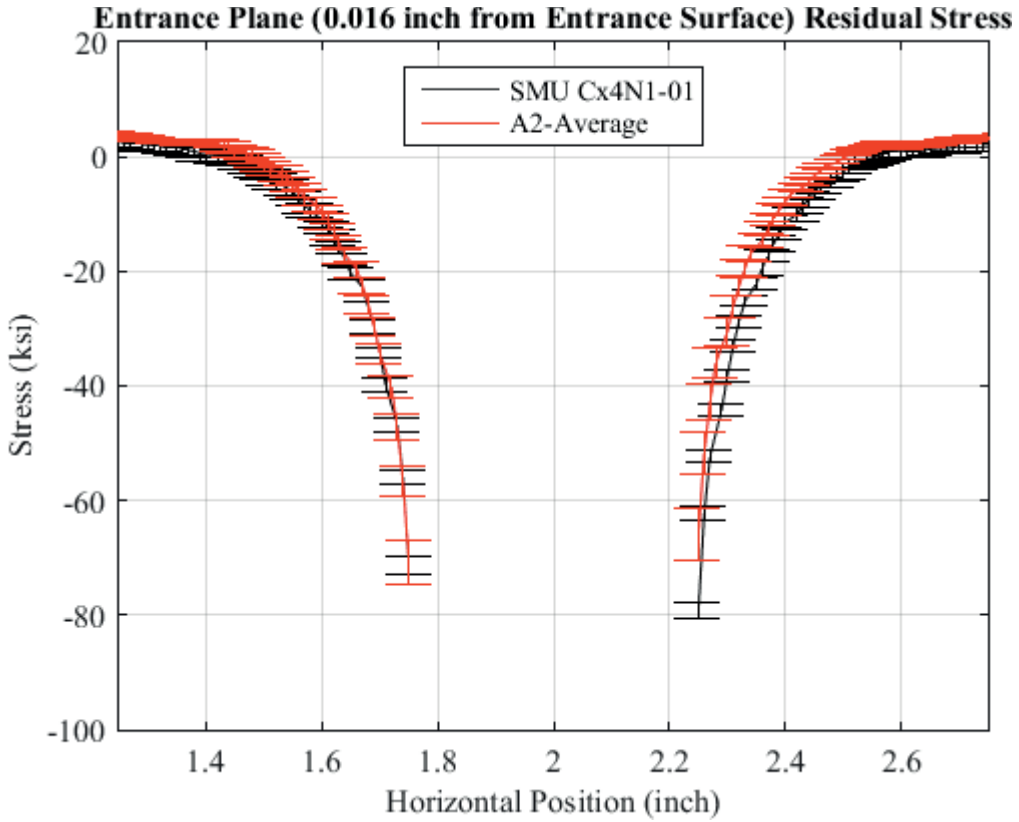

Fig. 529 Residual Stress Line Plot Comparing the Single Measurement Uncertainty of Cx4N1-01-B to the CxA2 (2024-T351) Average Residual Stress at a Distance of 0.016 inch (Entrance Surface) from the Entrance Surface – Cx4N1-01-B Coupon had a 0.0797 inch Fatigue Crack at the Left Entrance Surface – Zoomed in Next to Hole.

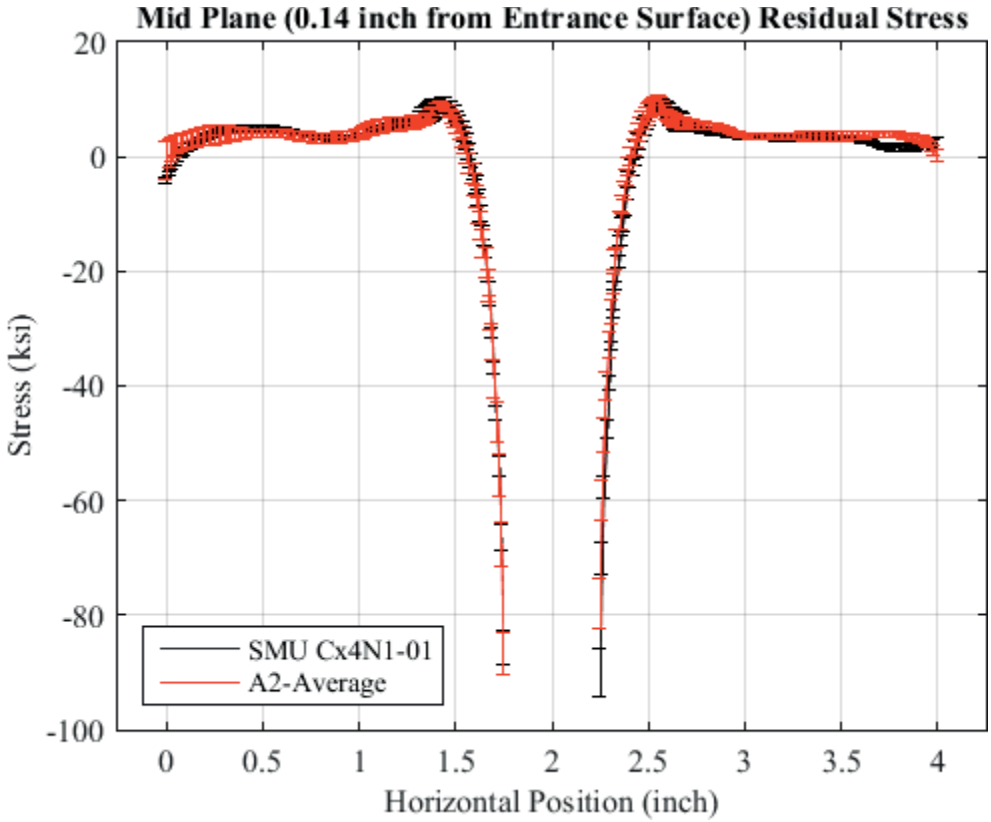

Fig. 530 Residual Stress Line Plot Comparing the Single Measurement Uncertainty of Cx4N1-01-B to the CxA2 (2024-T351) Average Residual Stress at a Distance of 0.140 inch (Mid Plane Surface) from the Entrance Surface – Cx4N1-01-B Coupon had a 0.0797 inch Fatigue Crack at the Left Entrance Surface.

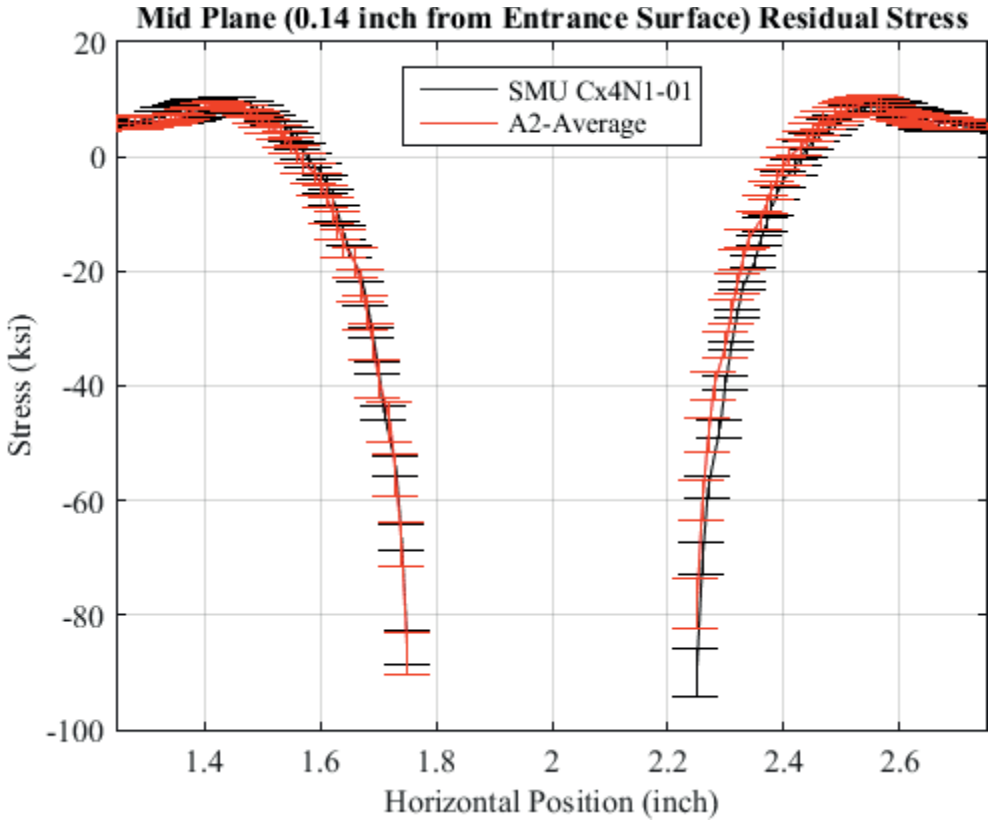

Fig. 531 Residual Stress Line Plot Comparing the Single Measurement Uncertainty of Cx4N1-01-B to the CxA2 (2024-T351) Average Residual Stress at a Distance of 0.140 inch (Mid Plane Surface) from the Entrance Surface – Cx4N1-01-B Coupon had a 0.0797 inch Fatigue Crack at the Left Entrance Surface – Zoomed in Next to Hole.

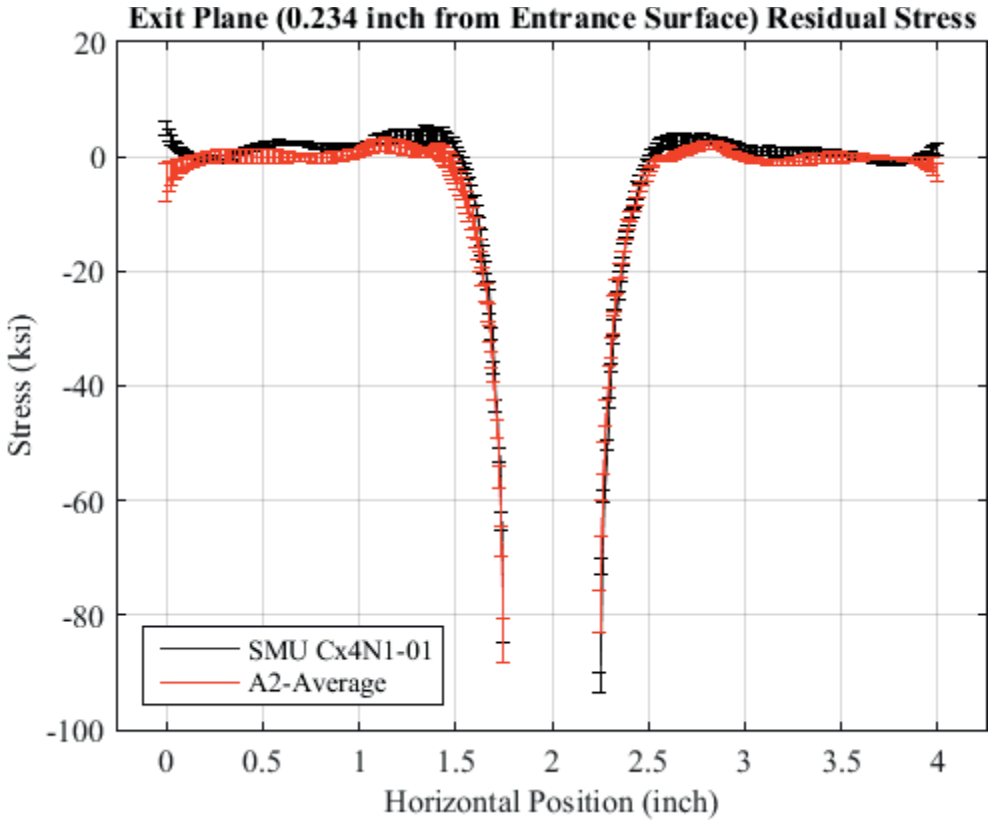

Fig. 532 Residual Stress Line Plot Comparing the Single Measurement Uncertainty of Cx4N1-01-B to the CxA2 (2024-T351) Average Residual Stress at a Distance of 0.234 inch (Exit Surface) from the Entrance Surface – Cx4N1-01-B Coupon had a 0.0797 inch Fatigue Crack at the Left Entrance Surface – Zoomed in Next to Hole.

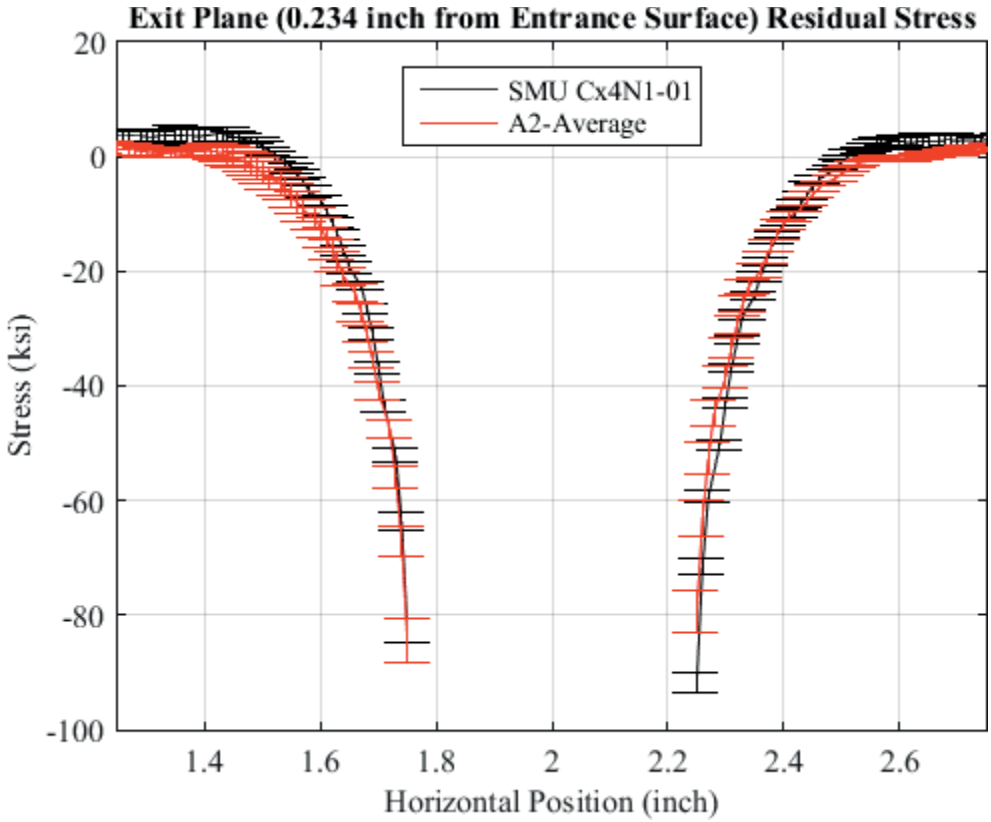

Fig. 533 Residual Stress Line Plot Comparing the Single Measurement Uncertainty of Cx4N1-01-B to the CxA2 (2024-T351) Average Residual Stress at a Distance of 0.234 inch (Exit Surface) from the Entrance Surface – Cx4N1-01-B Coupon had a 0.0797 inch Fatigue Crack at the Left Entrance Surface – Zoomed in Next to Hole.

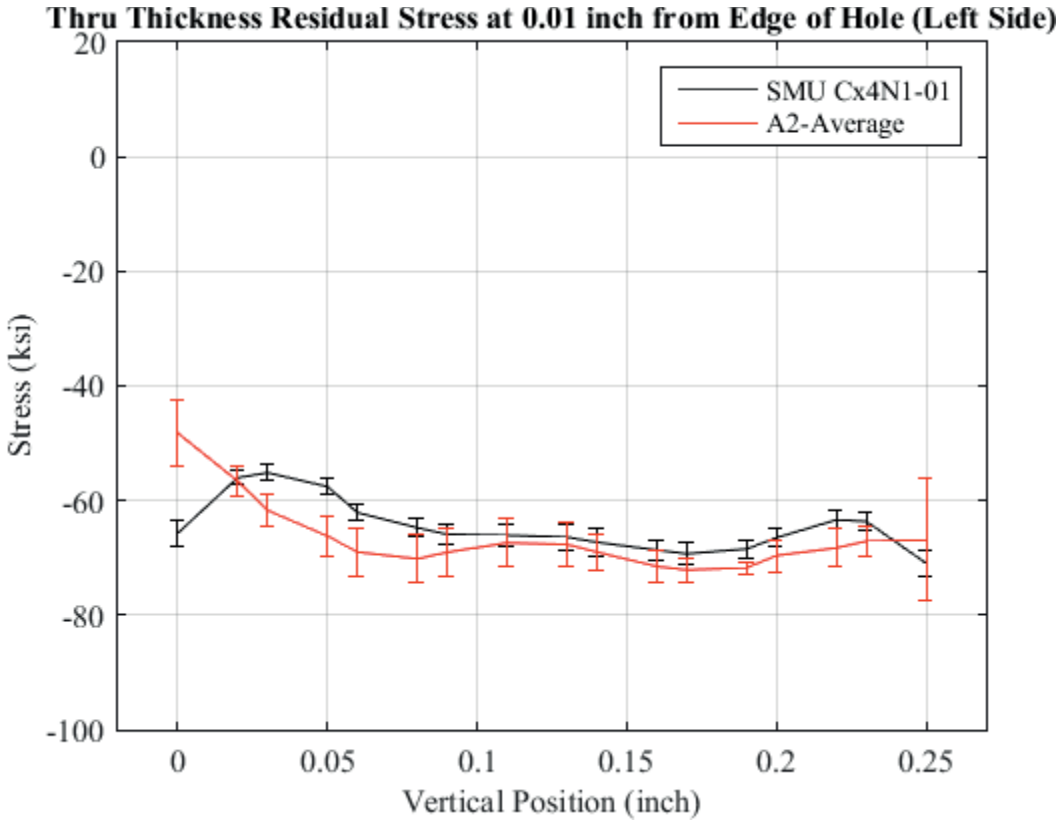

Fig. 534 Residual Stress Through Thickness Line Plot Comparing the Single Measurement Uncertainty of Cx4N1-01-B to the CxA2 (2024-T351) Average Residual Stress at a Distance 0.01 inch from Left Side of Hole – Coupon had a 0.0797 inch Fatigue Crack at the Left Entrance Surface.

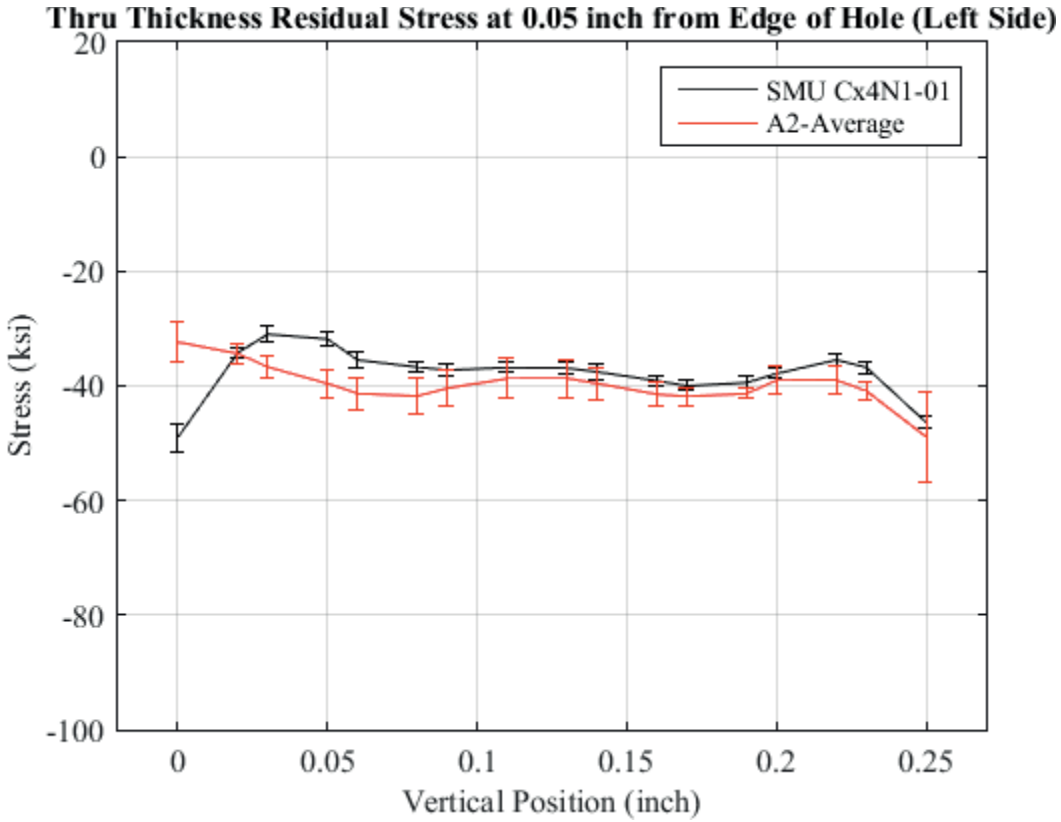

Fig. 535 Residual Stress Through Thickness Line Plot Comparing the Single Measurement Uncertainty of Cx4N1-01-B to the CxA2 (2024-T351) Average Residual Stress at a Distance 0.05 inch from Left Side of Hole – Coupon had a 0.0797 inch Fatigue Crack at the Left Entrance Surface.

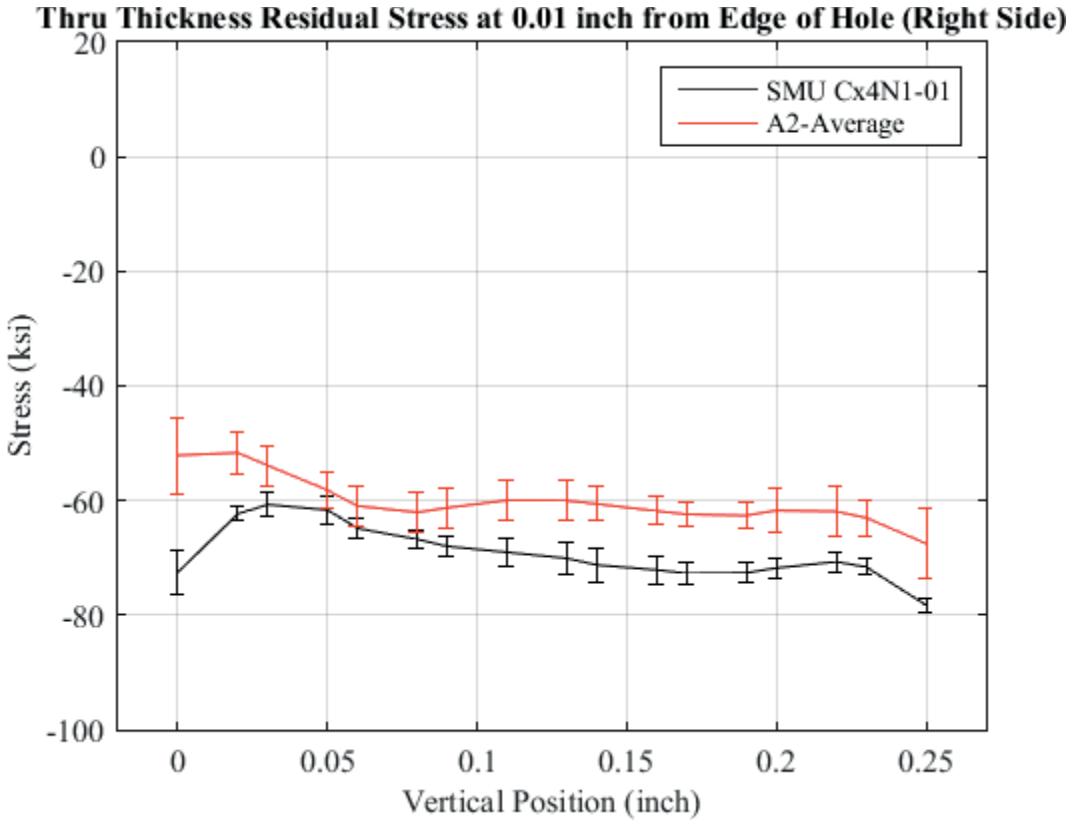

Fig. 536 Residual Stress Through Thickness Line Plot Comparing the Single Measurement Uncertainty of Cx4N1-01-B to the CxA2 (2024-T351) Average Residual Stress at a Distance 0.01 inch from Right Side of Hole – Coupon had a 0.0797 inch Fatigue Crack at the Left Entrance Surface.

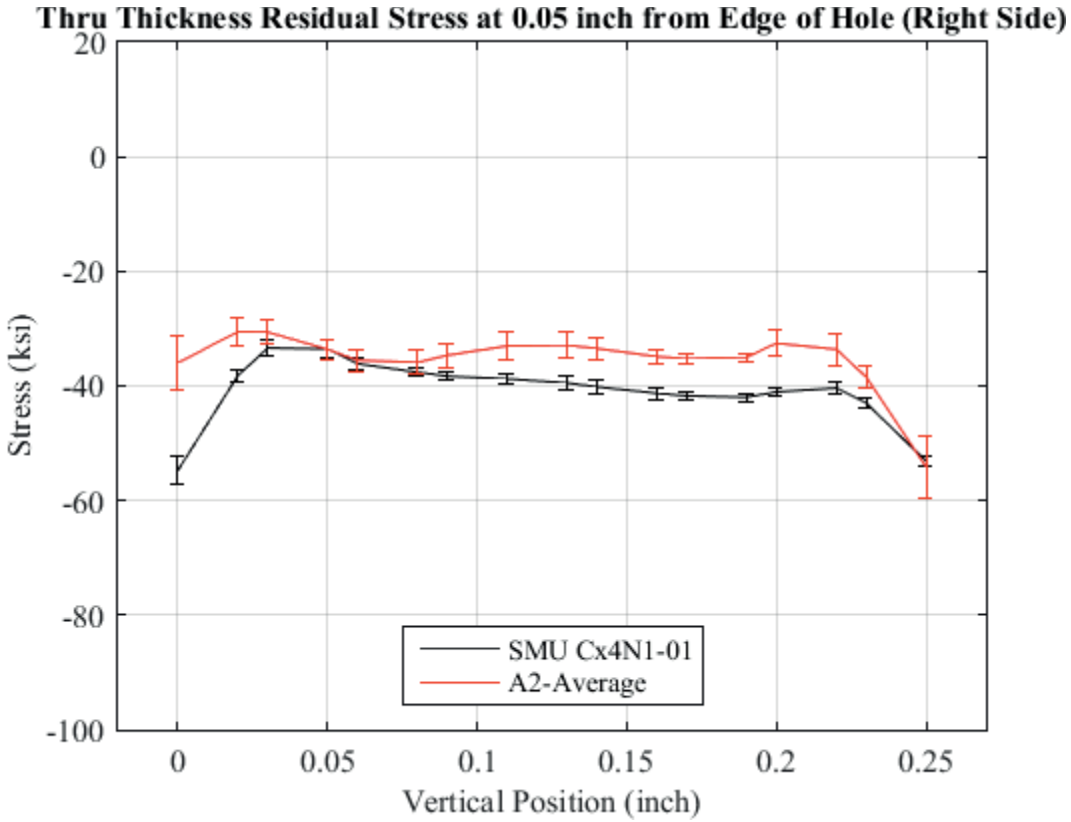

Fig. 537 Residual Stress Through Thickness Line Plot Comparing the Single Measurement Uncertainty of Cx4N1-01-B to the CxA2 (2024-T351) Average Residual Stress at a Distance 0.05 inch from Right Side of Hole – Coupon had a 0.0797 inch Fatigue Crack at the Left Entrance Surface.

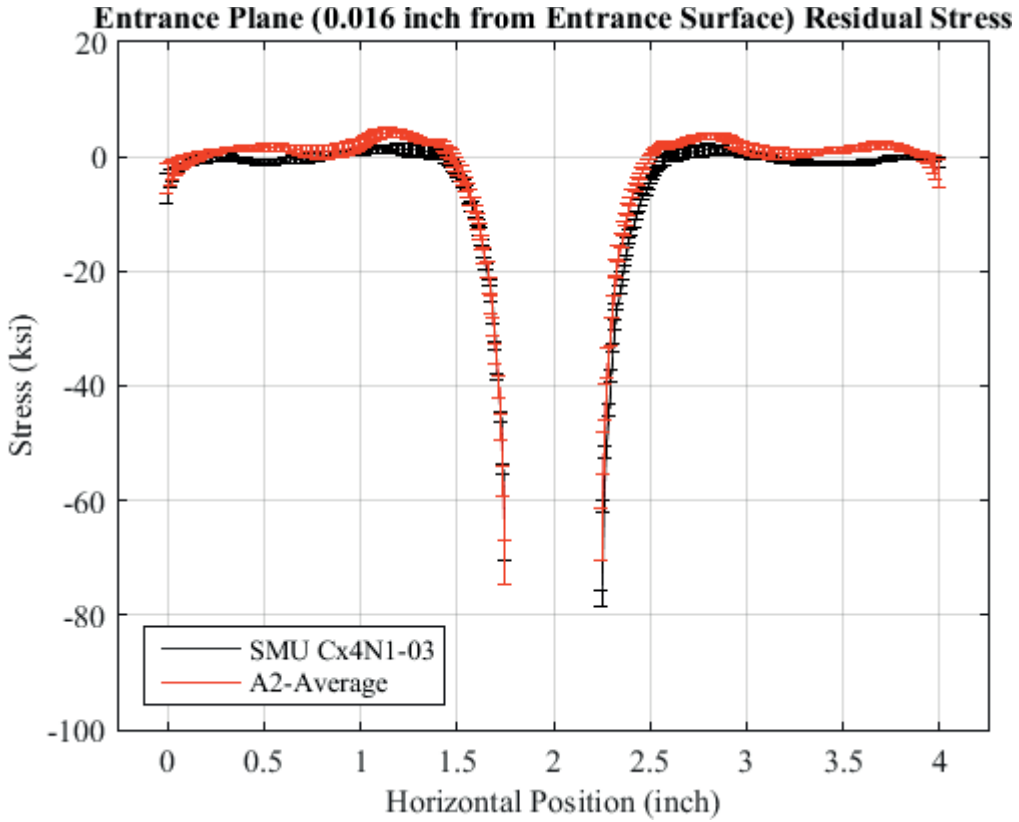

Fig. 538 Residual Stress Line Plot Comparing the Single Measurement Uncertainty of Cx4N1-03-B to the CxA2 (2024-T351) Average Residual Stress at a Distance of 0.016 inch (Entrance Surface) from the Entrance Surface – Cx4N1-03-B Coupon had a 0.0947 inch Fatigue Crack at the Left Entrance Surface.

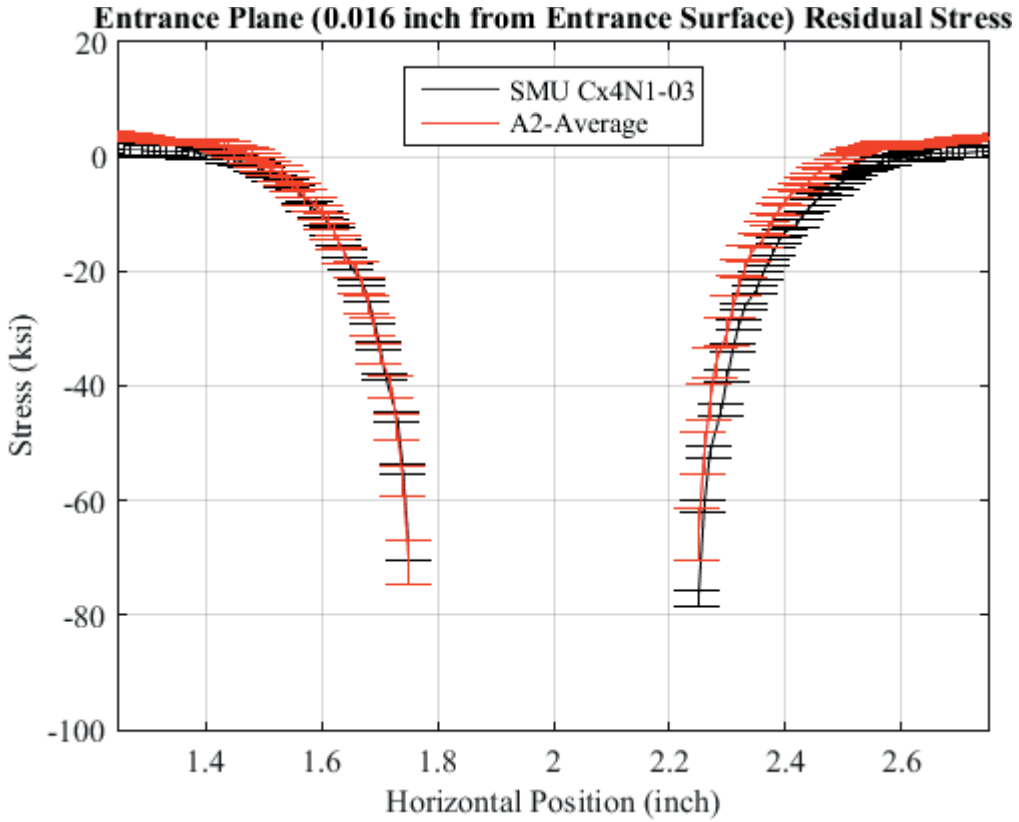

Fig. 539 Residual Stress Line Plot Comparing the Single Measurement Uncertainty of Cx4N1-03-B to the CxA2 (2024-T351) Average Residual Stress at a Distance of 0.016 inch (Entrance Surface) from the Entrance Surface – Cx4N1-03-B Coupon had a 0.0947 inch Fatigue Crack at the Left Entrance Surface – Zoomed in Next to Hole.

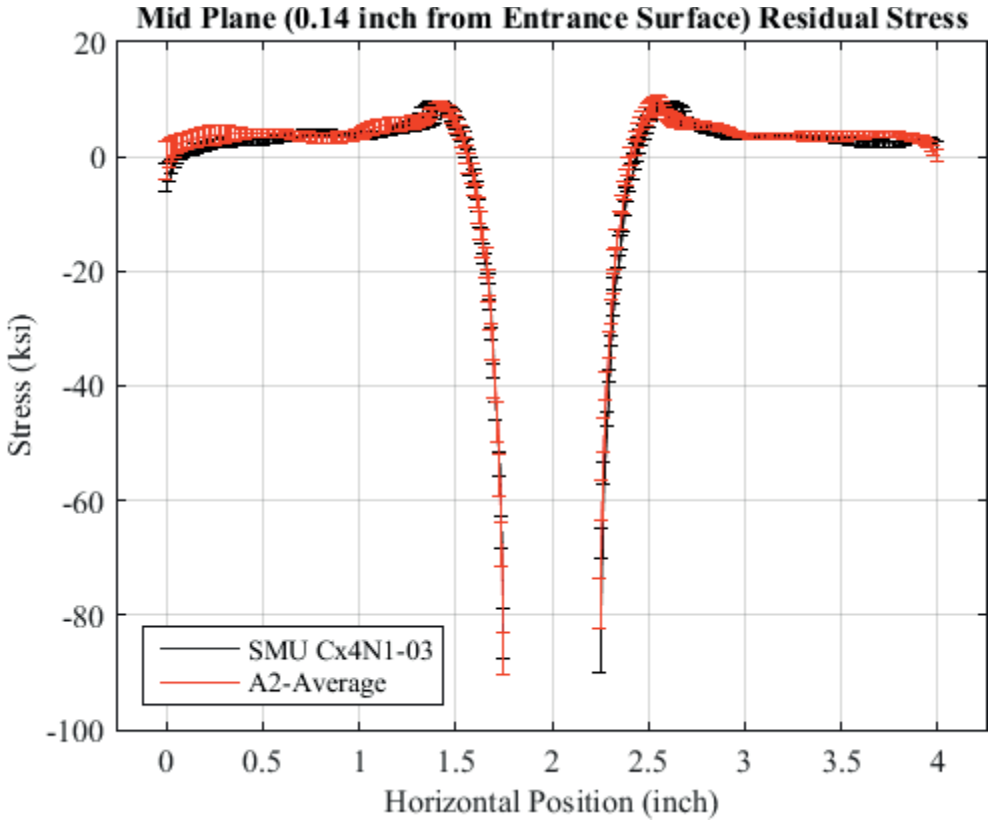

Fig. 540 Residual Stress Line Plot Comparing the Single Measurement Uncertainty of Cx4N1-03-B to the CxA2 (2024-T351) Average Residual Stress at a Distance of 0.140 inch (Mid Plane Surface) from the Entrance Surface – Cx4N1-03-B Coupon had a 0.0947 inch Fatigue Crack at the Left Entrance Surface.

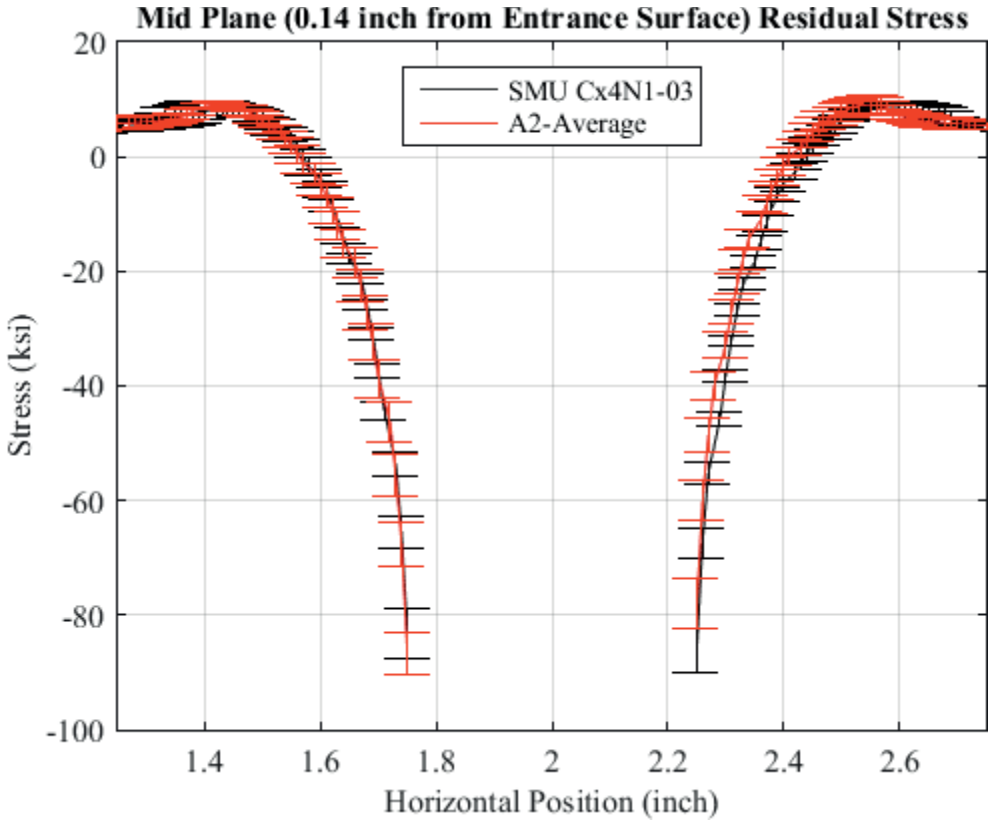

Fig. 541 Residual Stress Line Plot Comparing the Single Measurement Uncertainty of Cx4N1-03-B to the CxA2 (2024-T351) Average Residual Stress at a Distance of 0.140 inch (Mid Plane Surface) from the Entrance Surface – Cx4N1-03-B Coupon had a 0.0947 inch Fatigue Crack at the Left Entrance Surface – Zoomed in Next to Hole.

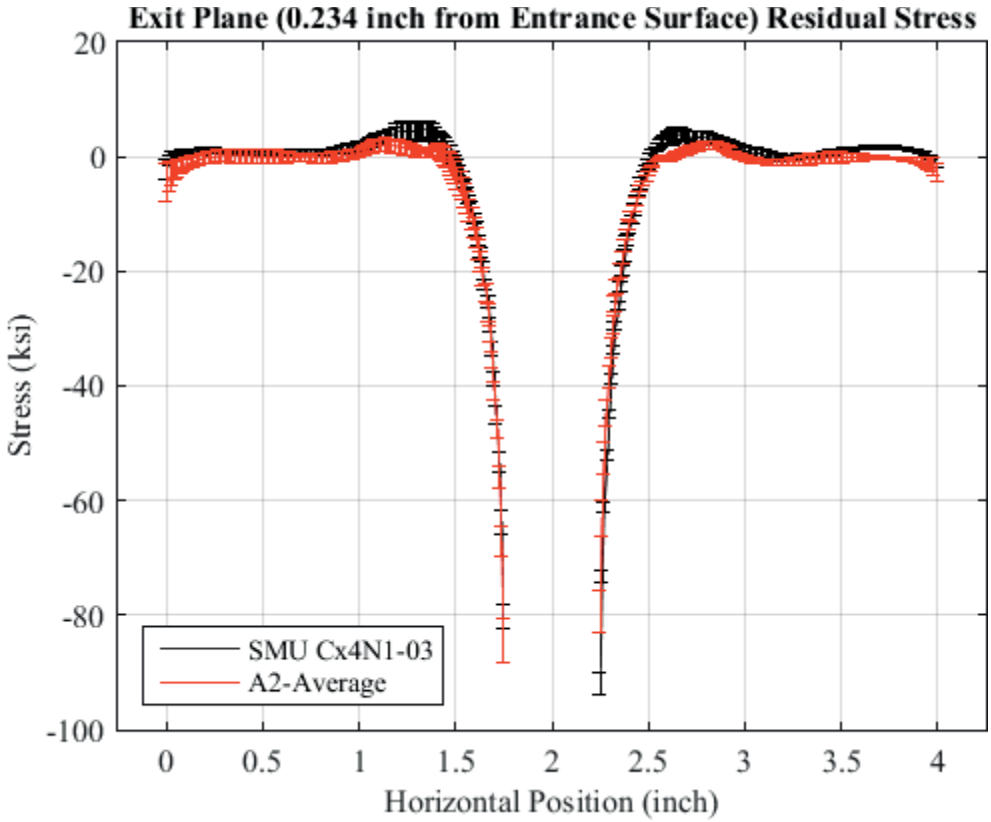

Fig. 542 Residual Stress Line Plot Comparing the Single Measurement Uncertainty of Cx4N1-03-B to the CxA2 (2024-T351) Average Residual Stress at a Distance of 0.234 inch (Exit Surface) from the Entrance Surface – Cx4N1-03-B Coupon had a 0.0947 inch Fatigue Crack at the Left Entrance Surface.

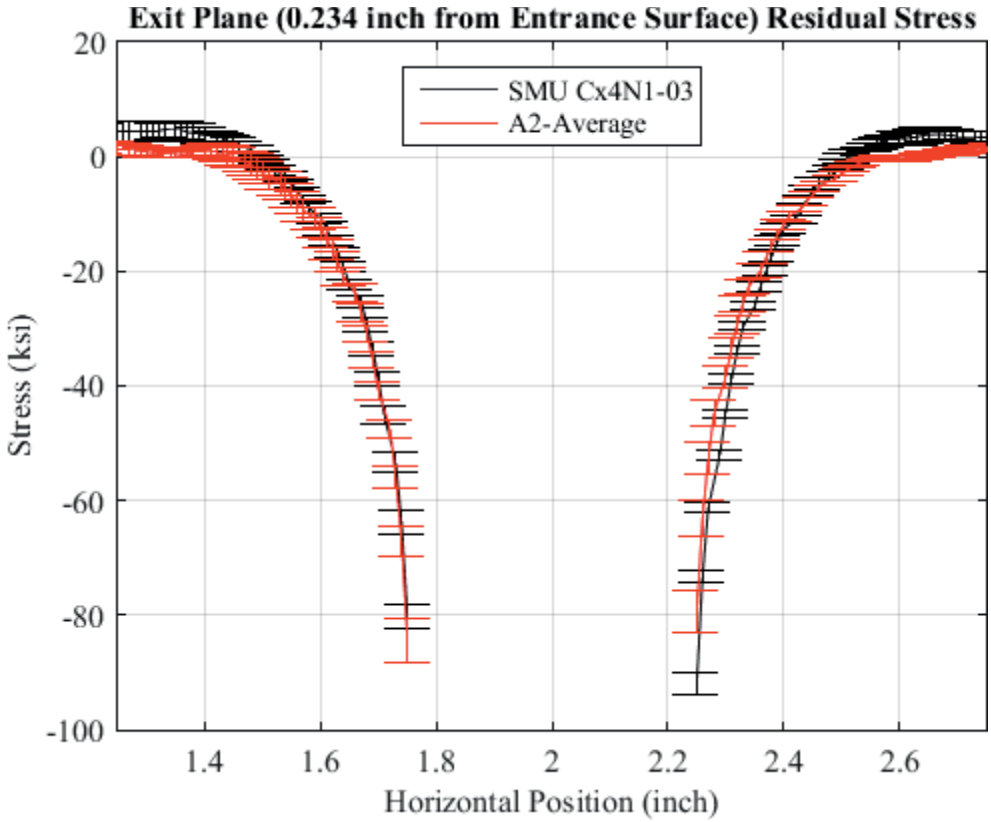

Fig. 543 Residual Stress Line Plot Comparing the Single Measurement Uncertainty of Cx4N1-03-B to the CxA2 (2024-T351) Average Residual Stress at a Distance of 0.234 inch (Exit Surface) from the Entrance Surface – Cx4N1-03-B Coupon had a 0.0947 inch Fatigue Crack at the Left Entrance Surface – Zoomed in Next to Hole.

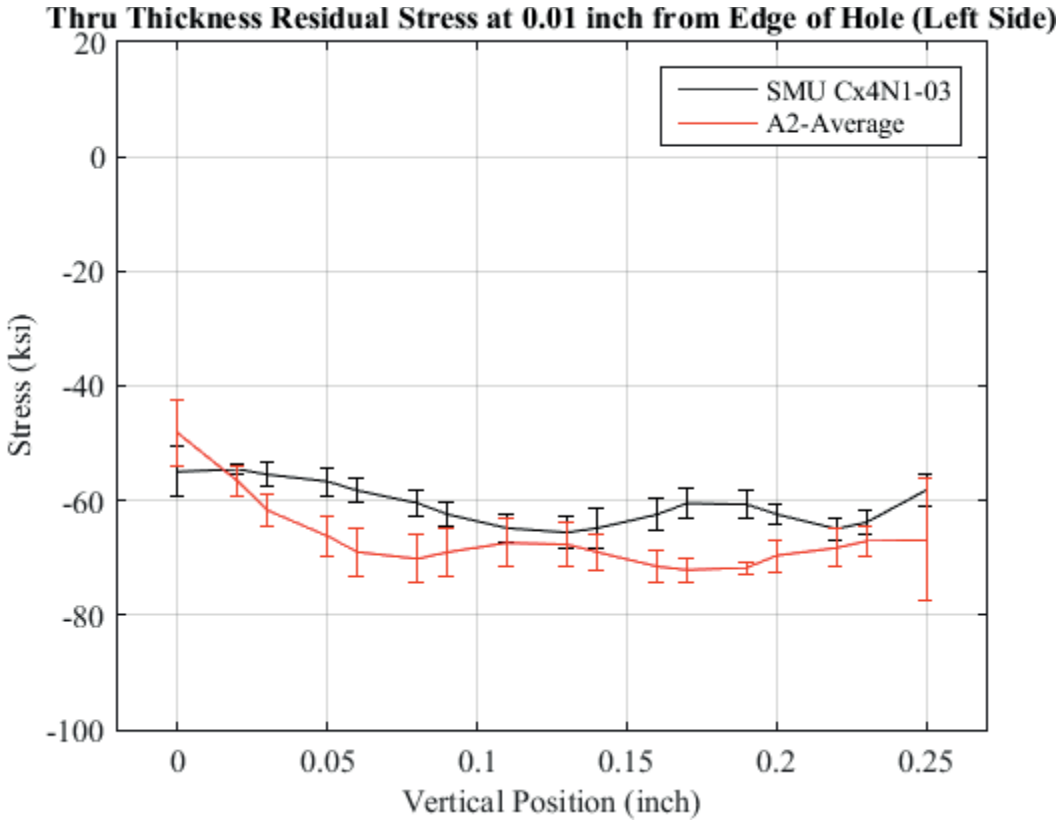

Fig. 544 Residual Stress Through Thickness Line Plot Comparing the Single Measurement Uncertainty of Cx4N1-03-B to the CxA2 (2024-T351) Average Residual Stress at a Distance 0.01 inch from Left Side of Hole – Coupon had a 0.0947 inch Fatigue Crack at the Left Entrance Surface.

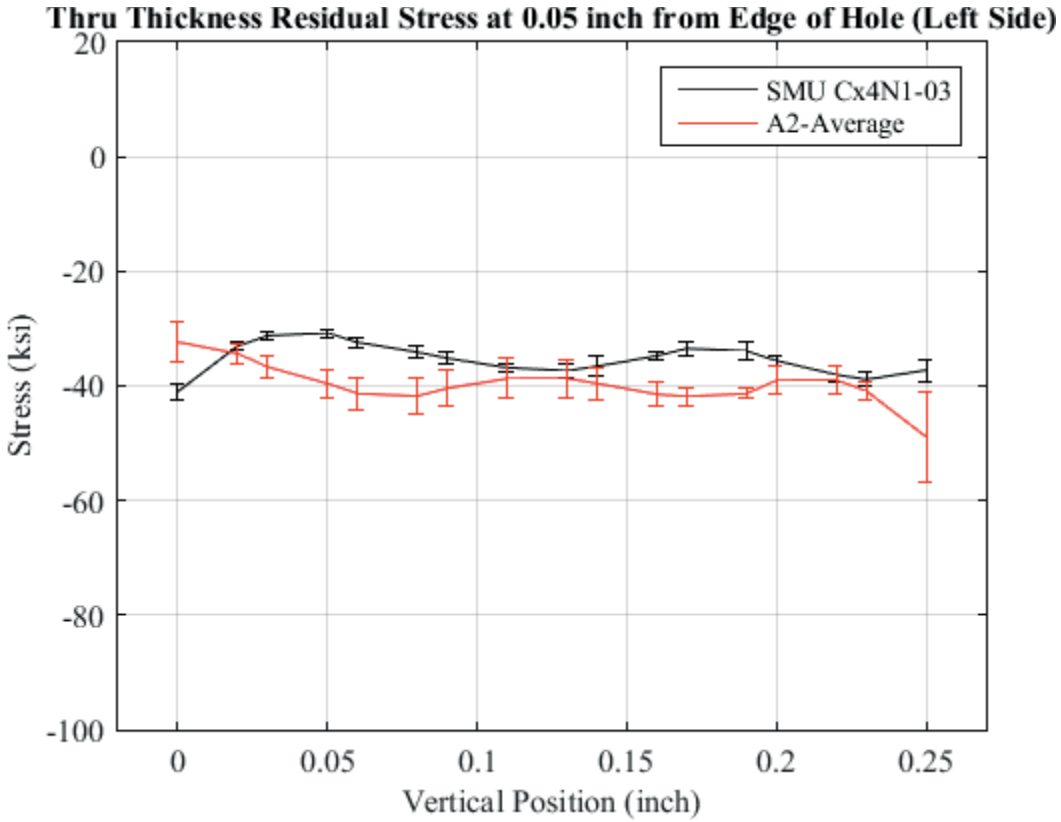

Fig. 545 Residual Stress Through Thickness Line Plot Comparing the Single Measurement Uncertainty of Cx4N1-03-B to the CxA2 (2024-T351) Average Residual Stress at a Distance 0.05 inch from Left Side of Hole – Coupon had a 0.0947 inch Fatigue Crack at the Left Entrance Surface.

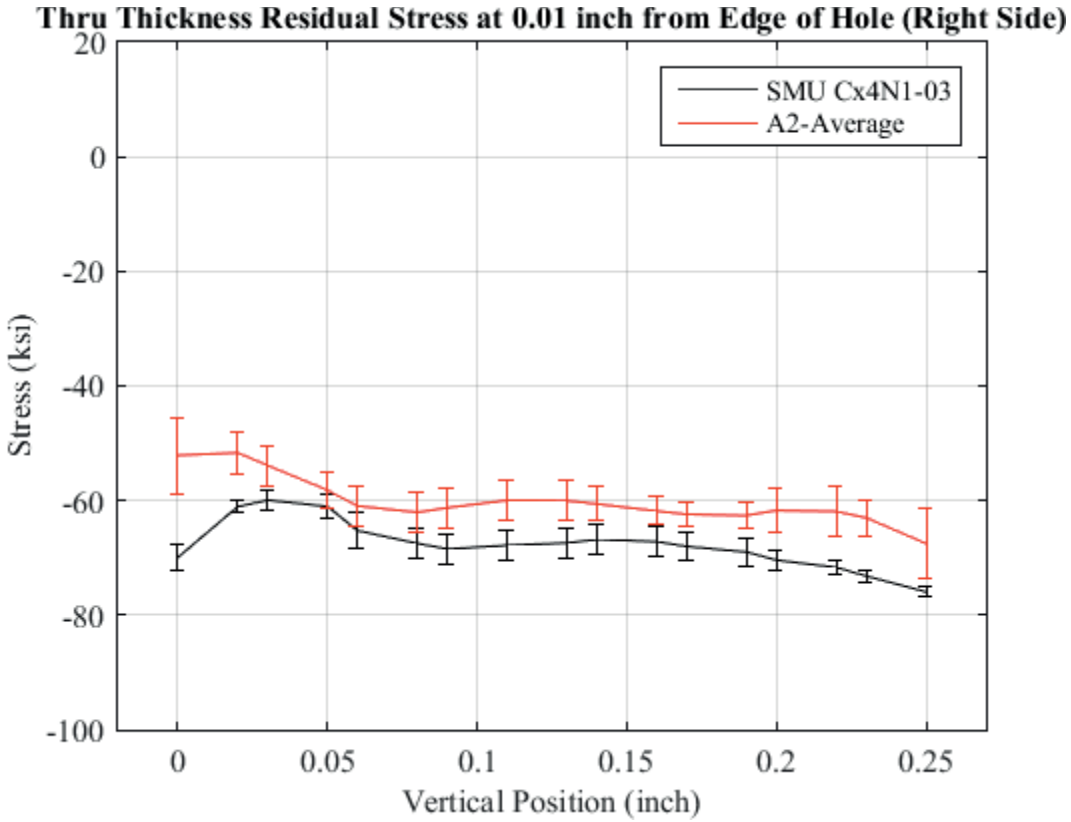

Fig. 546 Residual Stress Through Thickness Line Plot Comparing the Single Measurement Uncertainty of Cx4N1-03-B to the CxA2 (2024-T351) Average Residual Stress at a Distance 0.01 inch from Right Side of Hole – Coupon had a 0.0947 inch Fatigue Crack at the Left Entrance Surface.

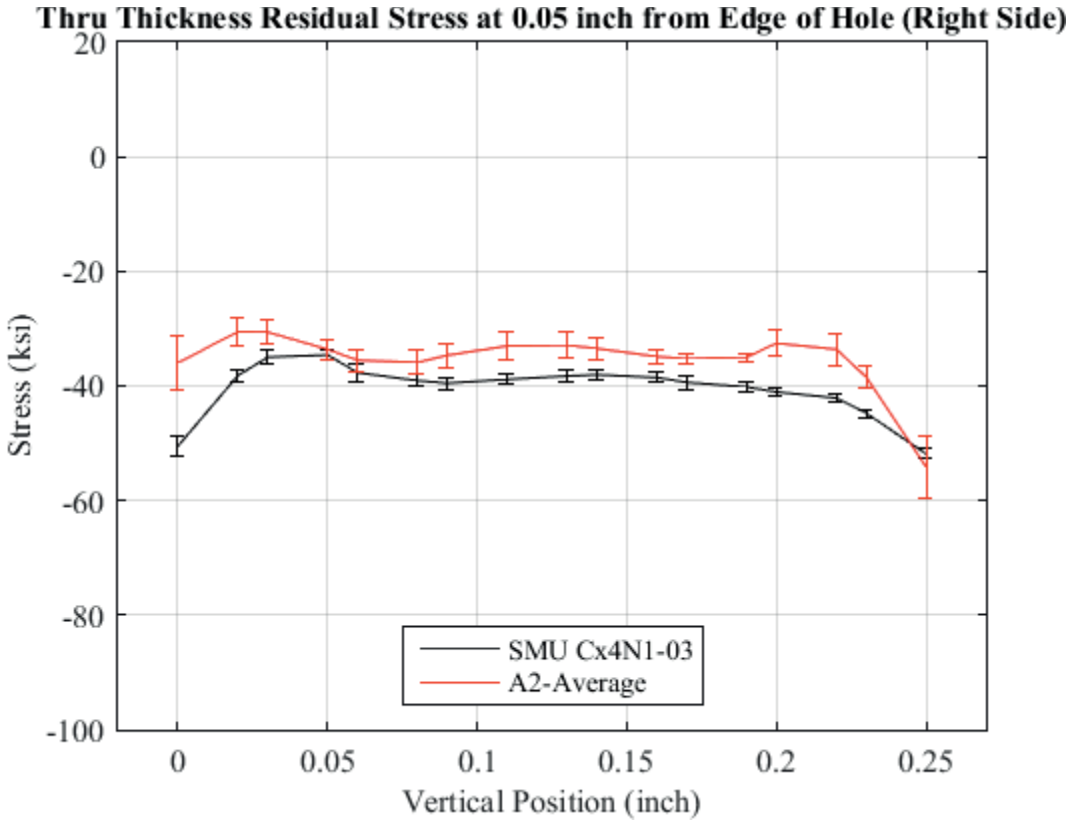

Fig. 547 Residual Stress Through Thickness Line Plot Comparing the Single Measurement Uncertainty of Cx4N1-03-B to the CxA2 (2024-T351) Average Residual Stress at a Distance 0.05 inch from Right Side of Hole – Coupon had a 0.0947 inch Fatigue Crack at the Left Entrance Surface.

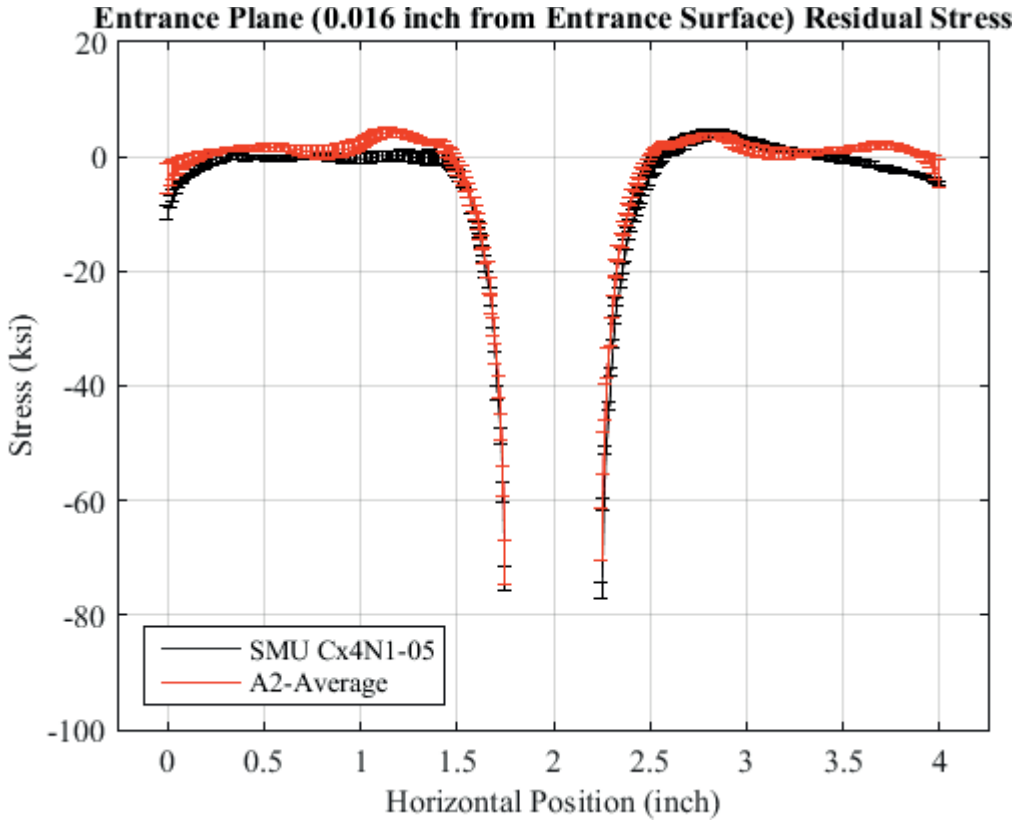

Fig. 548 Residual Stress Line Plot Comparing the Single Measurement Uncertainty of Cx4N1-05-B to the CxA2 (2024-T351) Average Residual Stress at a Distance of 0.016 inch (Entrance Surface) from the Entrance Surface – Cx4N1-05-B Coupon had a 0.1259 inch Fatigue Crack at the Left Entrance Surface.

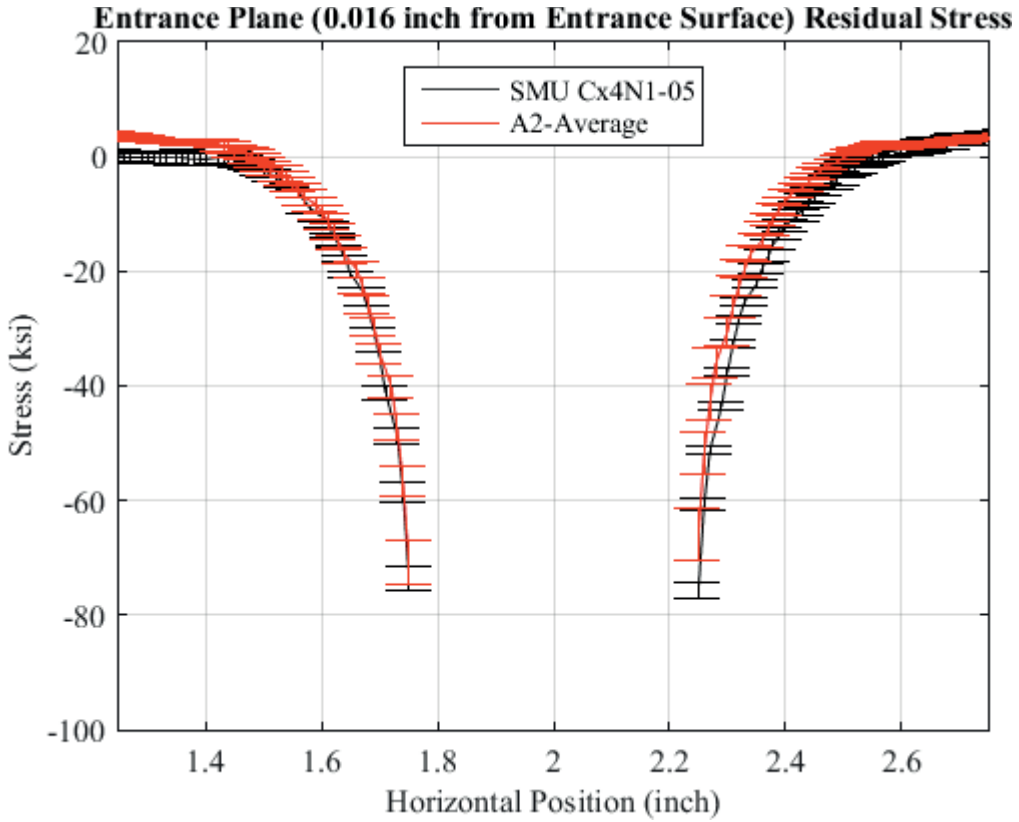

Fig. 549 Residual Stress Line Plot Comparing the Single Measurement Uncertainty of Cx4N1-05-B to the CxA2 (2024-T351) Average Residual Stress at a Distance of 0.016 inch (Entrance Surface) from the Entrance Surface – Cx4N1-05-B Coupon had a 0.1259 inch Fatigue Crack at the Left Entrance Surface – Zoomed in Next to Hole.

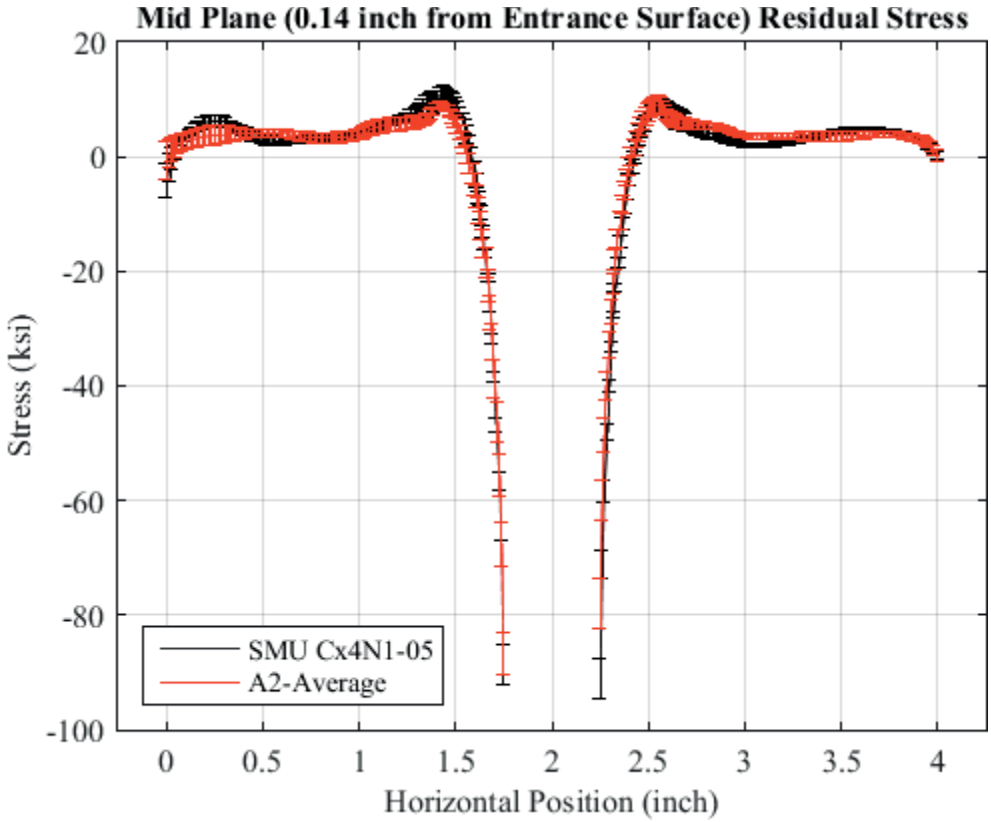

Fig. 550 Residual Stress Line Plot Comparing the Single Measurement Uncertainty of Cx4N1-05-B to the CxA2 (2024-T351) Average Residual Stress at a Distance of 0.140 inch (Mid Plane Surface) from the Entrance Surface – Cx4N1-05-B Coupon had a 0.1259 inch Fatigue Crack at the Left Entrance Surface.

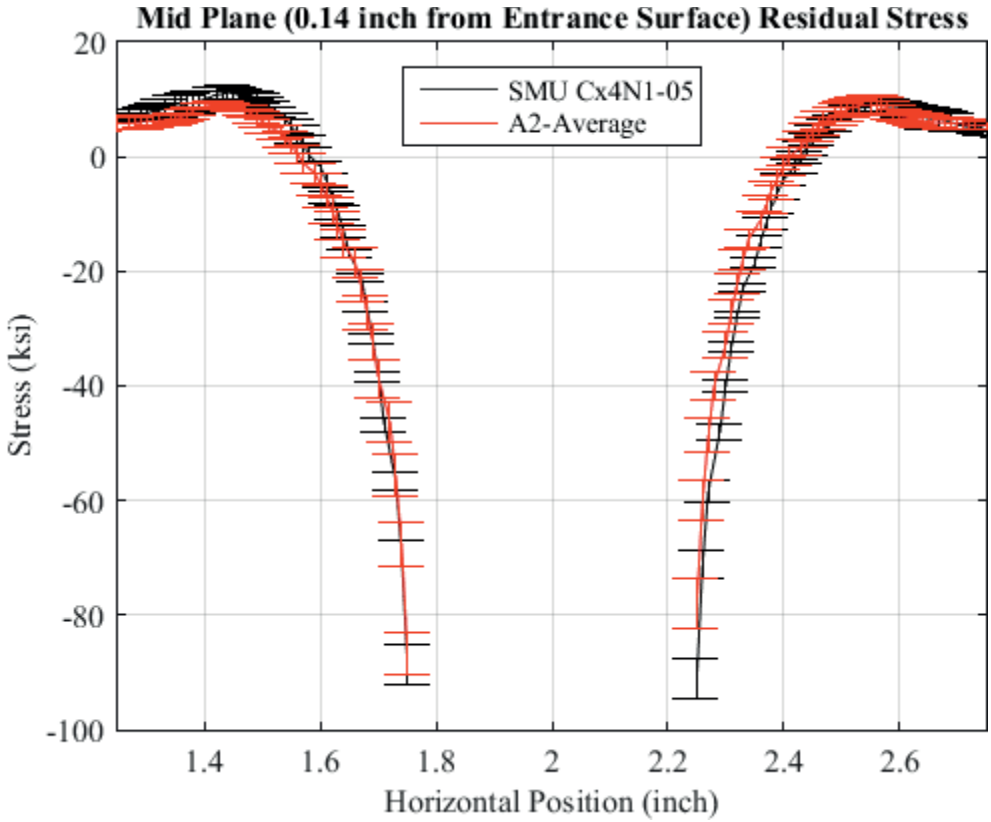

Fig. 551 Residual Stress Line Plot Comparing the Single Measurement Uncertainty of Cx4N1-05-B to the CxA2 (2024-T351) Average Residual Stress at a Distance of 0.140 inch (Mid Plane Surface) from the Entrance Surface – Cx4N1-05-B Coupon had a 0.1259 inch Fatigue Crack at the Left Entrance Surface – Zoomed in Next to Hole.

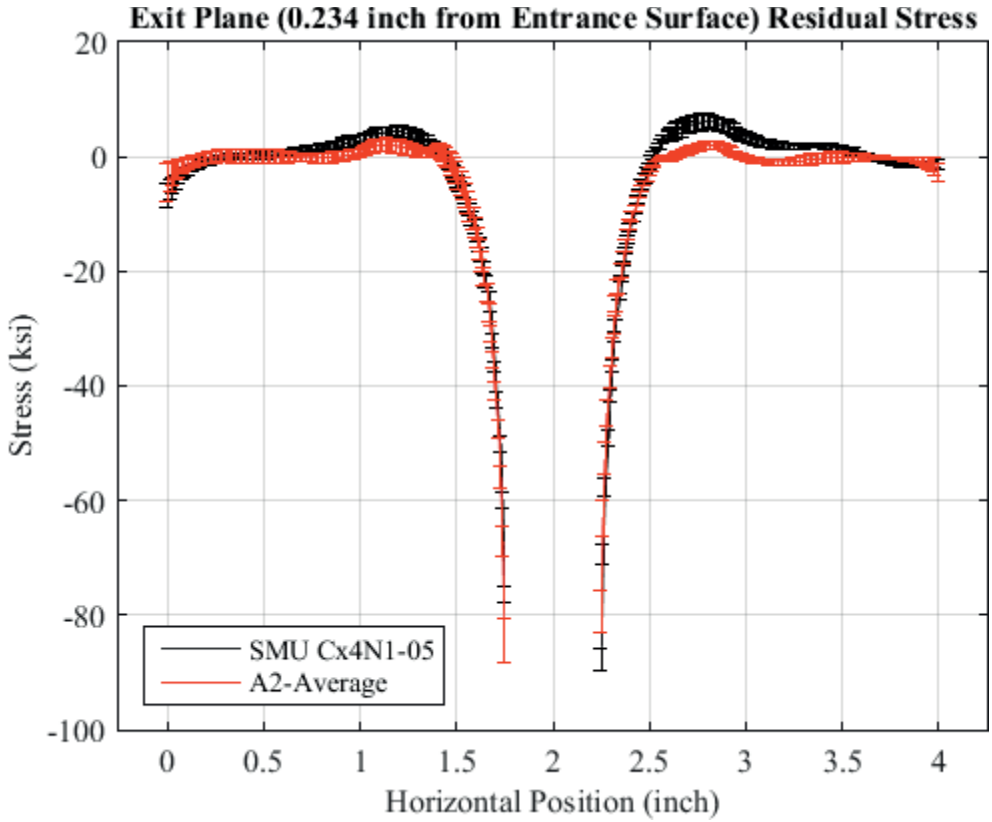

Fig. 552 Residual Stress Line Plot Comparing the Single Measurement Uncertainty of Cx4N1-05-B to the CxA2 (2024-T351) Average Residual Stress at a Distance of 0.234 inch (Exit Surface) from the Entrance Surface – Cx4N1-05-B Coupon had a 0.1259 inch Fatigue Crack at the Left Entrance Surface.

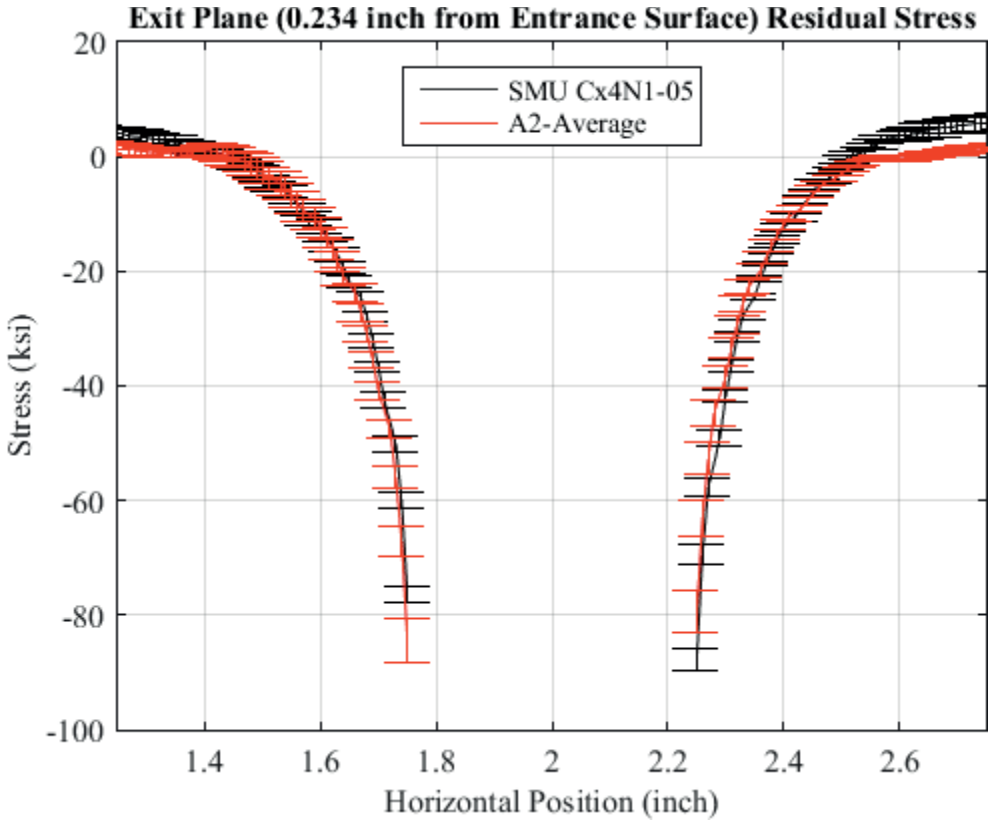

Fig. 553 Residual Stress Line Plot Comparing the Single Measurement Uncertainty of Cx4N1-05-B to the CxA2 (2024-T351) Average Residual Stress at a Distance of 0.234 inch (Exit Surface) from the Entrance Surface – Cx4N1-05-B Coupon had a 0.1259 inch Fatigue Crack at the Left Entrance Surface – Zoomed in Next to Hole.

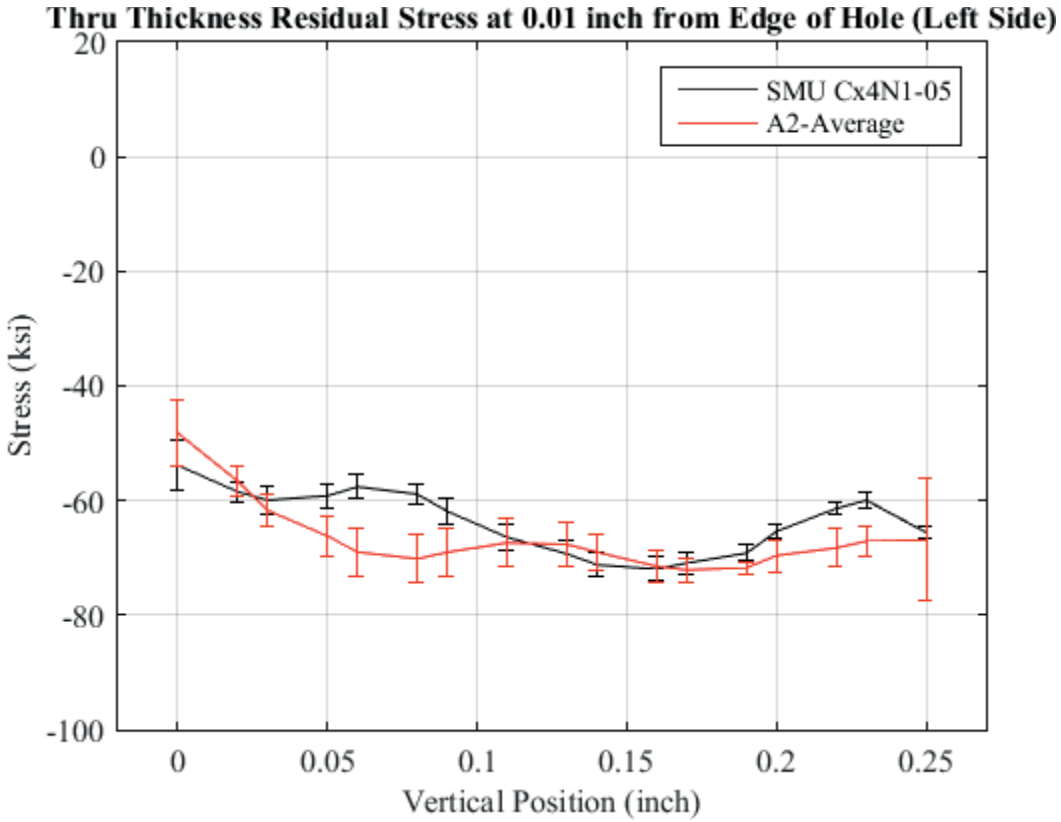

Fig. 554 Residual Stress Through Thickness Line Plot Comparing the Single Measurement Uncertainty of Cx4N1-05-B to the CxA2 (2024-T351) Average Residual Stress at a Distance 0.01 inch from Left Side of Hole – Coupon had a 0.1259 inch Fatigue Crack at the Left Entrance Surface.

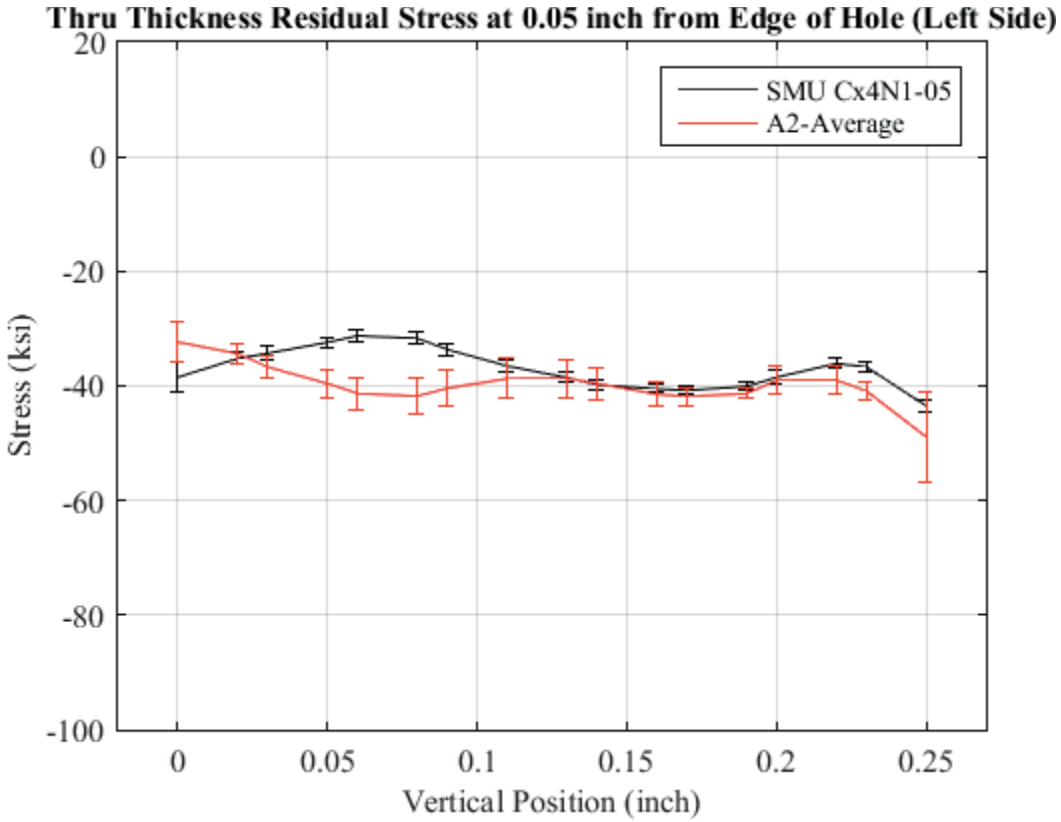

Fig. 555 Residual Stress Through Thickness Line Plot Comparing the Single Measurement Uncertainty of Cx4N1-05-B to the CxA2 (2024-T351) Average Residual Stress at a Distance 0.05 inch from Left Side of Hole – Coupon had a 0.1259 inch Fatigue Crack at the Left Entrance Surface.

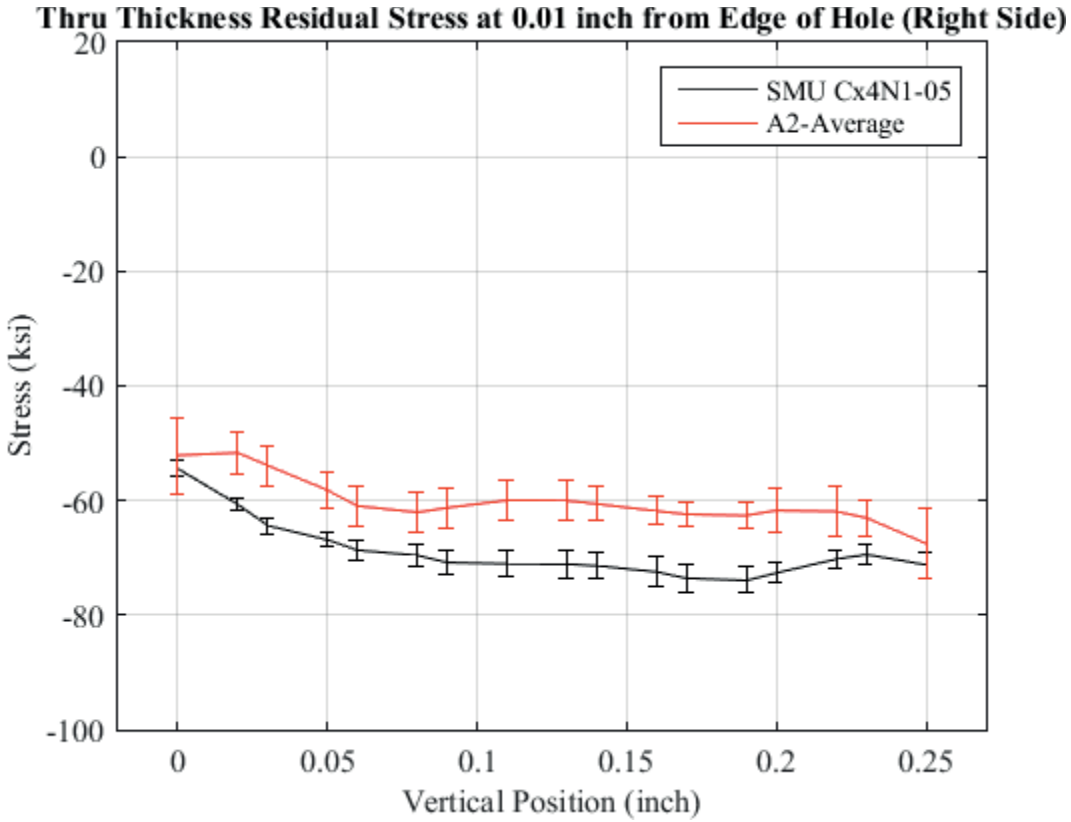

Fig. 556 Residual Stress Through Thickness Line Plot Comparing the Single Measurement Uncertainty of Cx4N1-05-B to the CxA2 (2024-T351) Average Residual Stress at a Distance 0.01 inch from Right Side of Hole – Coupon had a 0.1259 inch Fatigue Crack at the Left Entrance Surface.

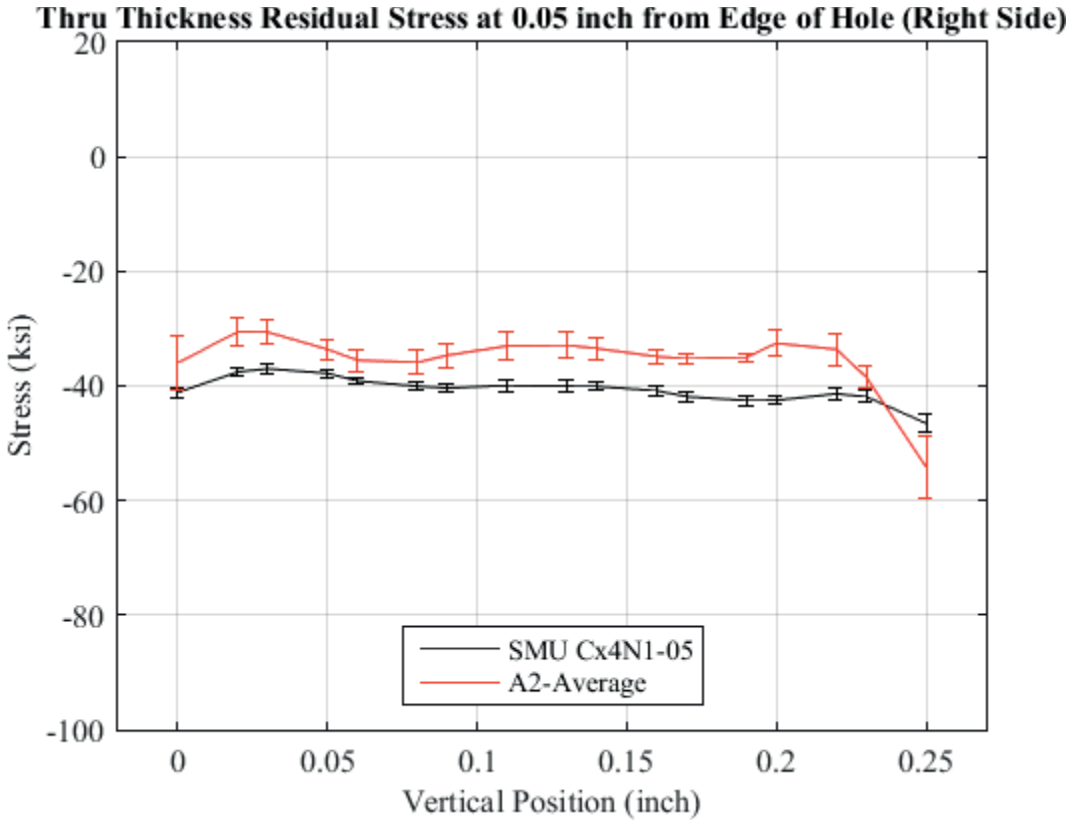

Fig. 557 Residual Stress Through Thickness Line Plot Comparing the Single Measurement Uncertainty of Cx4N1-05-B to the CxA2 (2024-T351) Average Residual Stress at a Distance 0.05 inch from Right Side of Hole – Coupon had a 0.1259 inch Fatigue Crack at the Left Entrance Surface.

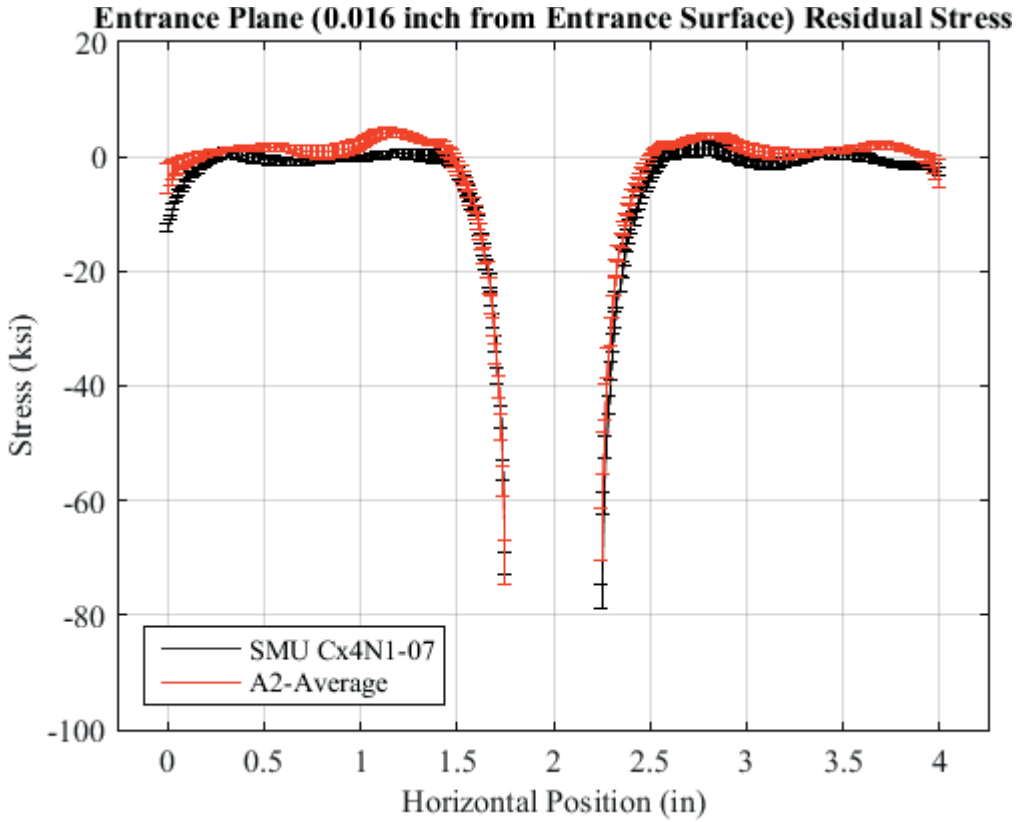

Fig. 558 Residual Stress Line Plot Comparing the Single Measurement Uncertainty of Cx4N1-07-B to the CxA2 (2024-T351) Average Residual Stress at a Distance of 0.016 inch (Entrance Surface) from the Entrance Surface – Cx4N1-07-B Coupon had a 0.2515 inch Fatigue Crack at the Left Entrance Surface.

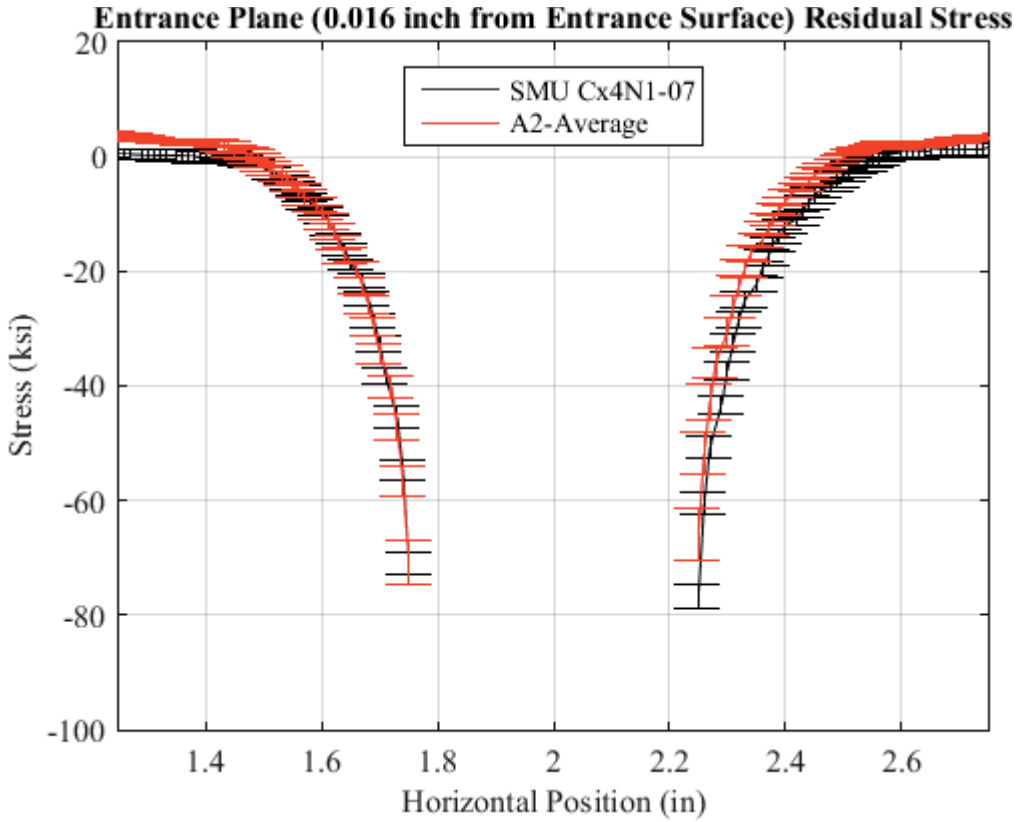

Fig. 559 Residual Stress Line Plot Comparing the Single Measurement Uncertainty of Cx4N1-07-B to the CxA2 (2024-T351) Average Residual Stress at a Distance of 0.016 inch (Entrance Surface) from the Entrance Surface – Cx4N1-07-B Coupon had a 0.2515 inch Fatigue Crack at the Left Entrance Surface – Zoomed in Next to Hole.

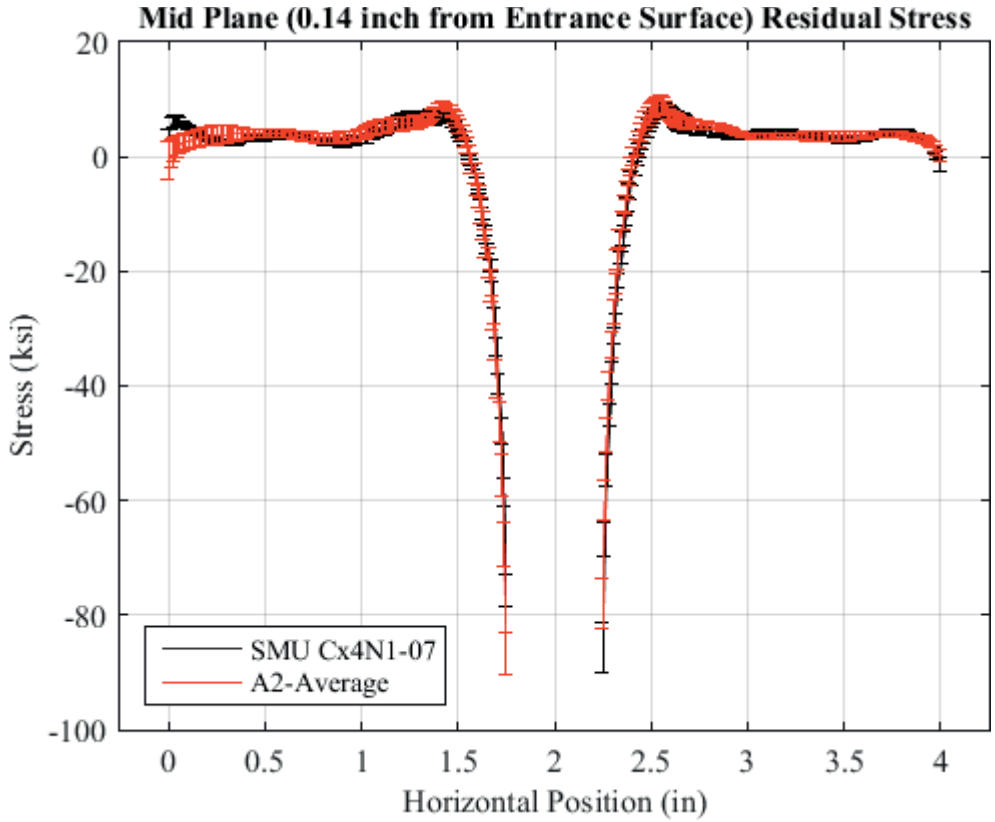

Fig. 560 Residual Stress Line Plot Comparing the Single Measurement Uncertainty of Cx4N1-07-B to the CxA2 (2024-T351) Average Residual Stress at a Distance of 0.140 inch (Mid Plane Surface) from the Entrance Surface – Cx4N1-07-B Coupon had a 0.2515 inch Fatigue Crack at the Left Entrance Surface.

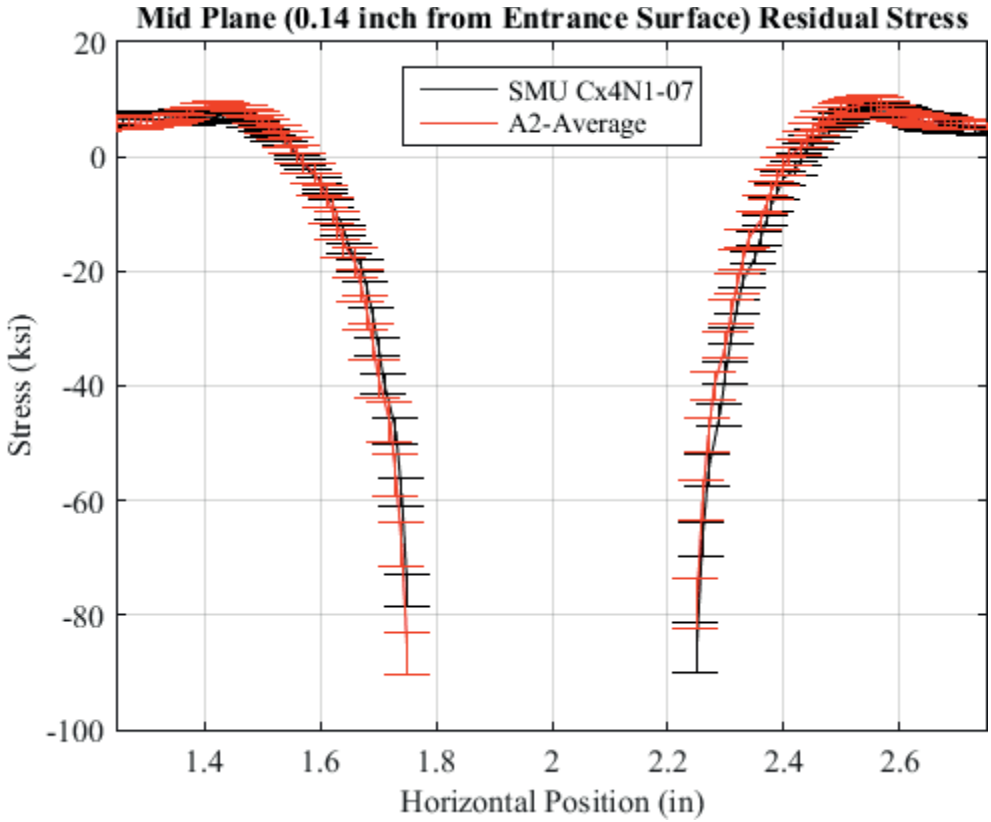

Fig. 561 Residual Stress Line Plot Comparing the Single Measurement Uncertainty of Cx4N1-07-B to the CxA2 (2024-T351) Average Residual Stress at a Distance of 0.140 inch (Mid Plane Surface) from the Entrance Surface – Cx4N1-07-B Coupon had a 0.2515 inch Fatigue Crack at the Left Entrance Surface – Zoomed in Next to Hole.

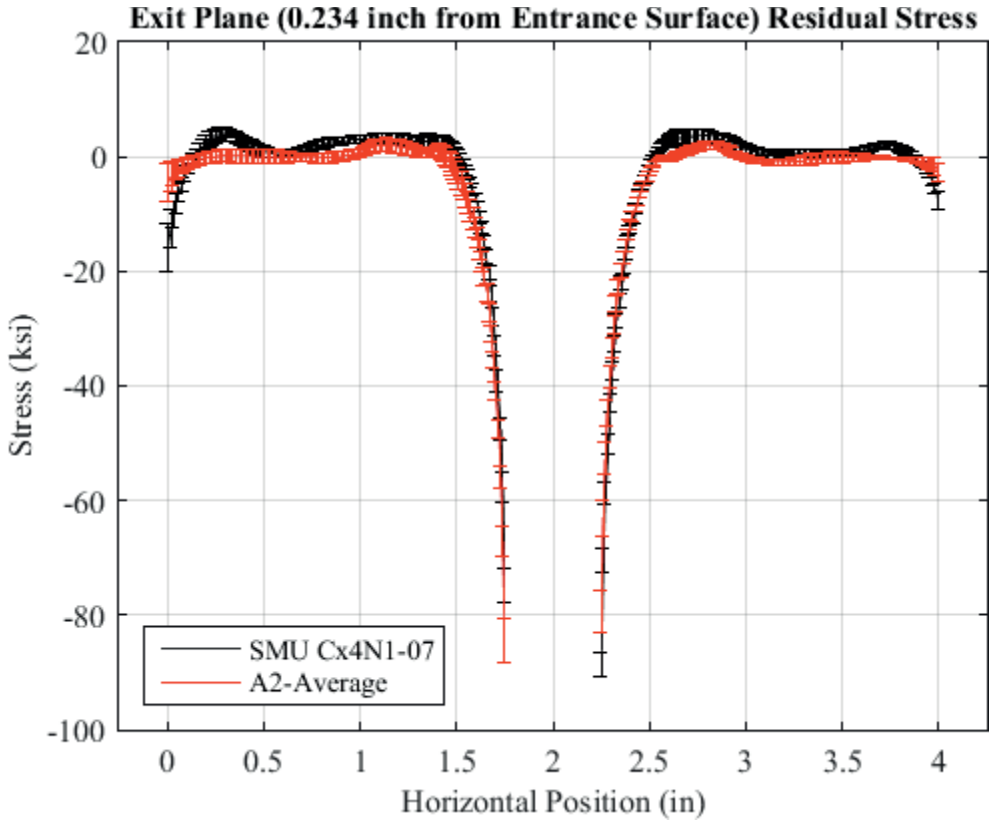

Fig. 562 Residual Stress Line Plot Comparing the Single Measurement Uncertainty of Cx4N1-07-B to the CxA2 (2024-T351) Average Residual Stress at a Distance of 0.234 inch (Exit Surface) from the Entrance Surface – Cx4N1-07-B Coupon had a 0.2515 inch Fatigue Crack at the Left Entrance Surface.

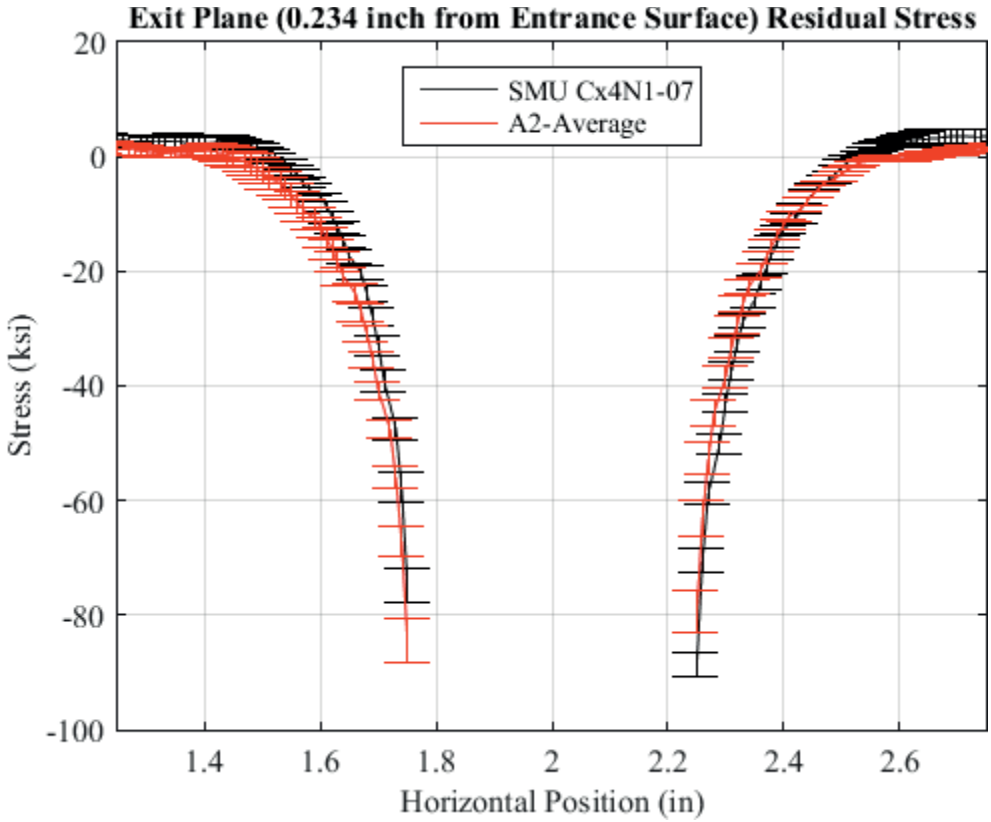

Fig. 563 Residual Stress Line Plot Comparing the Single Measurement Uncertainty of Cx4N1-07-B to the CxA2 (2024-T351) Average Residual Stress at a Distance of 0.234 inch (Exit Surface) from the Entrance Surface – Cx4N1-07-B Coupon had a 0.2515 inch Fatigue Crack at the Left Entrance Surface – Zoomed in Next to Hole.

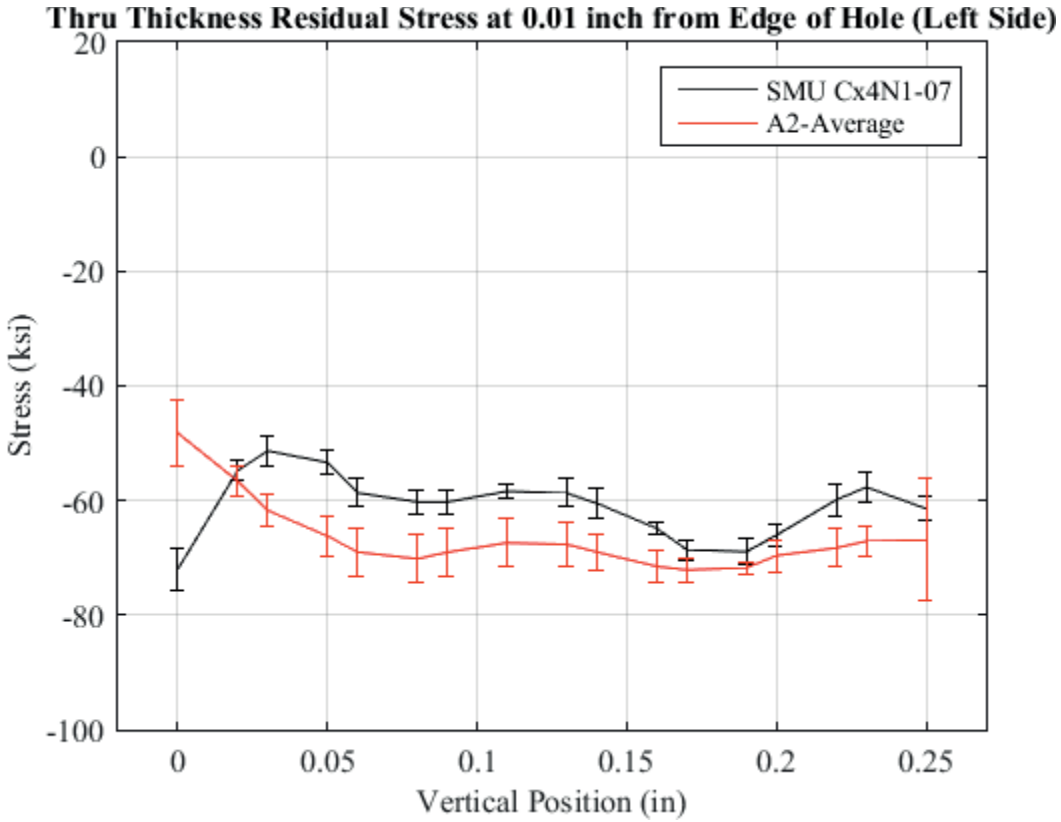

Fig. 564 Residual Stress Through Thickness Line Plot Comparing the Single Measurement Uncertainty of Cx4N1-07-B to the CxA2 (2024-T351) Average Residual Stress at a Distance 0.01 inch from Left Side of Hole – Coupon had a 0.2515 inch Fatigue Crack at the Left Entrance Surface.

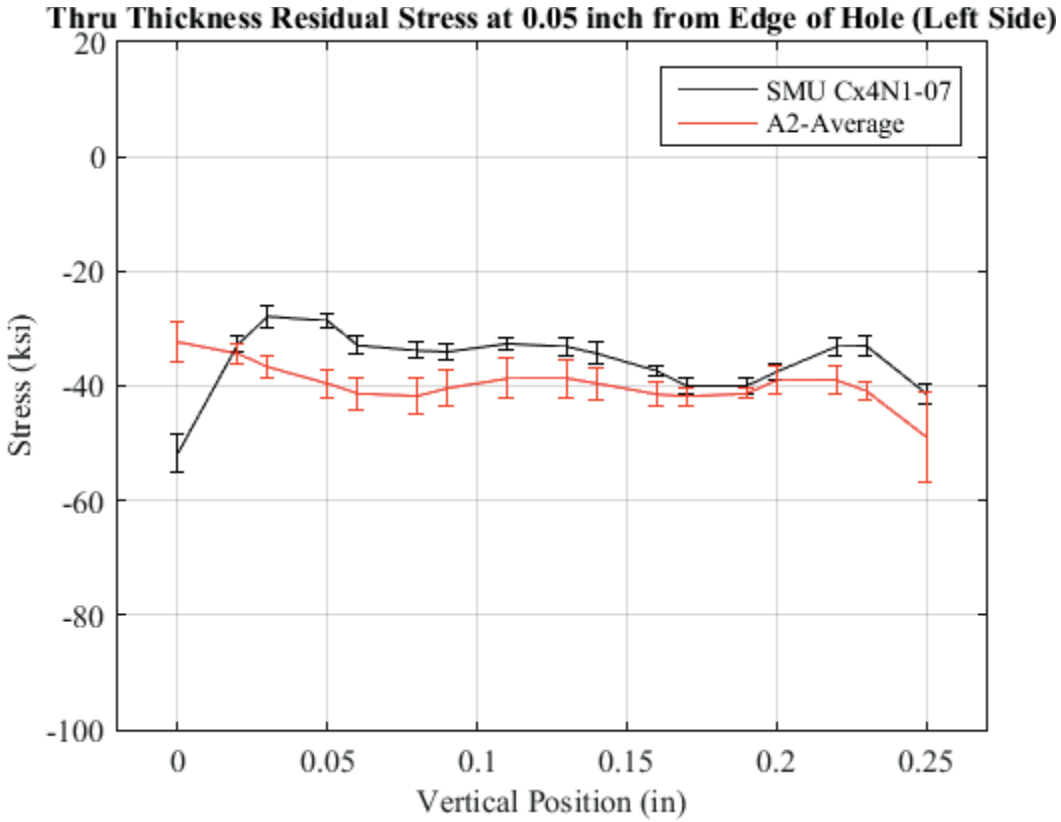

Fig. 565 Residual Stress Through Thickness Line Plot Comparing the Single Measurement Uncertainty of Cx4N1-07-B to the CxA2 (2024-T351) Average Residual Stress at a Distance 0.05 inch from Left Side of Hole – Coupon had a 0.2515 inch Fatigue Crack at the Left Entrance Surface.

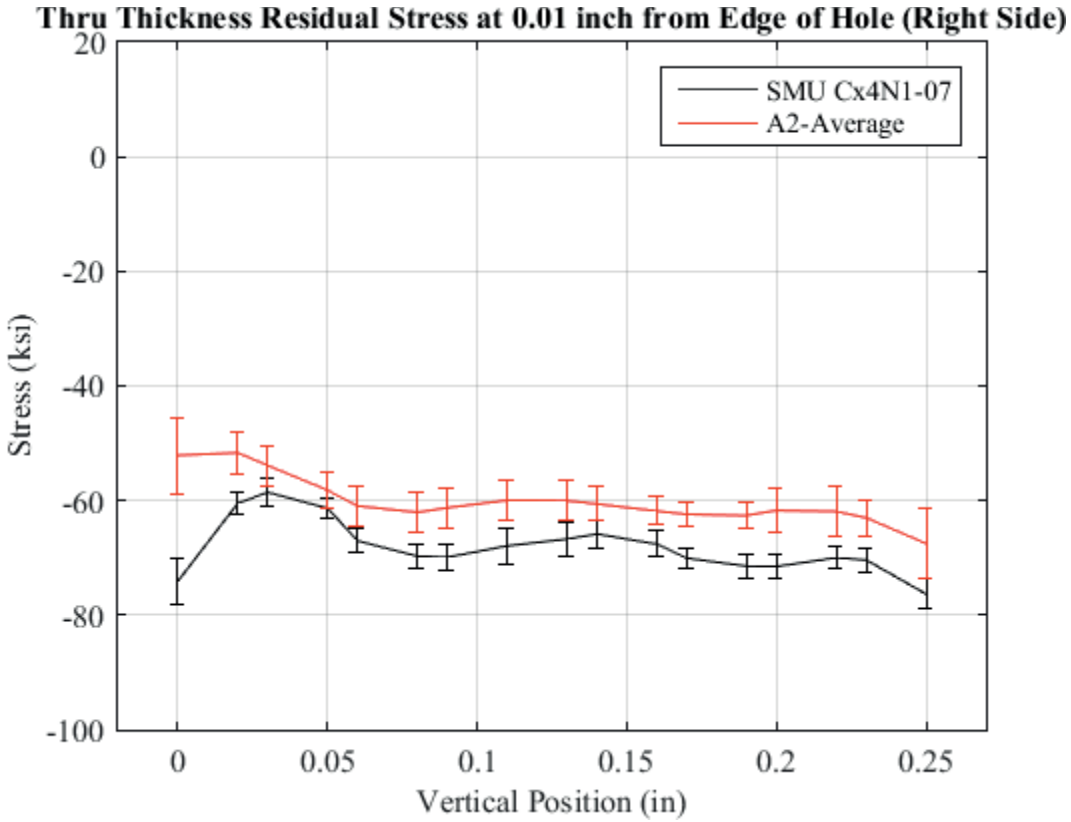

Fig. 566 Residual Stress Through Thickness Line Plot Comparing the Single Measurement Uncertainty of Cx4N1-07-B to the CxA2 (2024-T351) Average Residual Stress at a Distance 0.01 inch from Right Side of Hole – Coupon had a 0.2515 inch Fatigue Crack at the Left Entrance Surface.

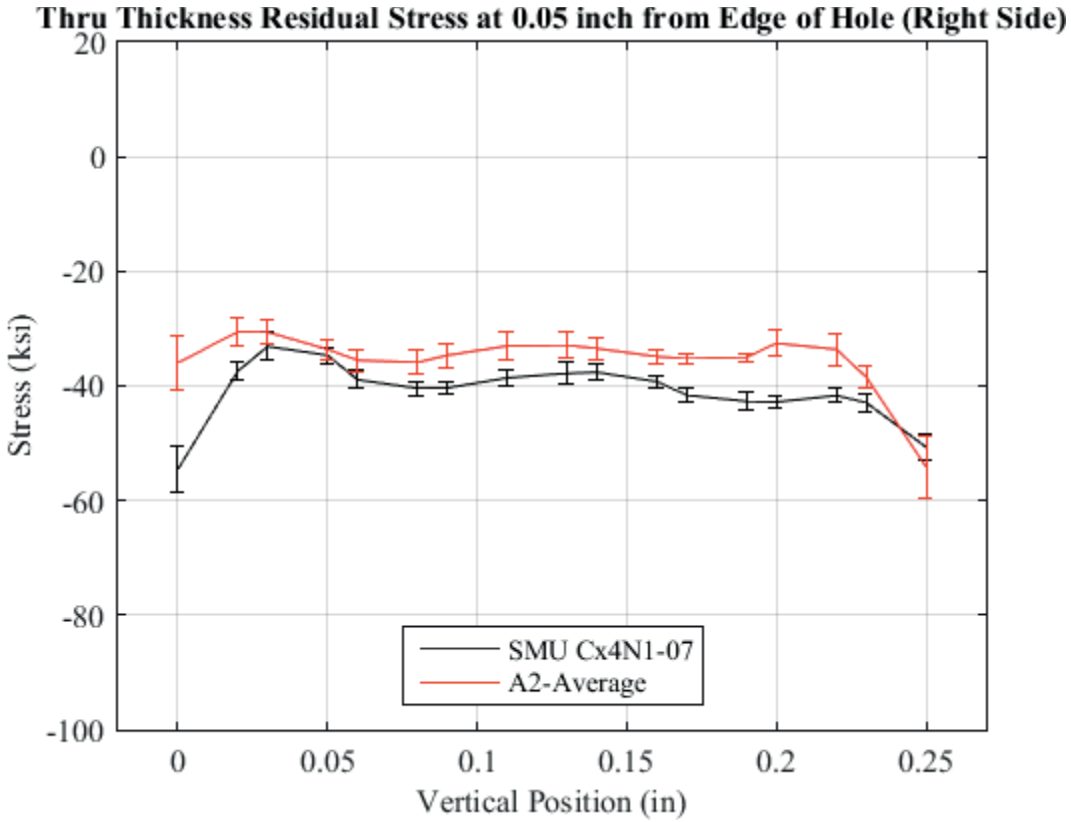

Fig. 567 Residual Stress Through Thickness Line Plot Comparing the Single Measurement Uncertainty of Cx4N1-07-B to the CxA2 (2024-T351) Average Residual Stress at a Distance 0.05 inch from Right Side of Hole – Coupon had a 0.2515 inch Fatigue Crack at the Left Entrance Surface.

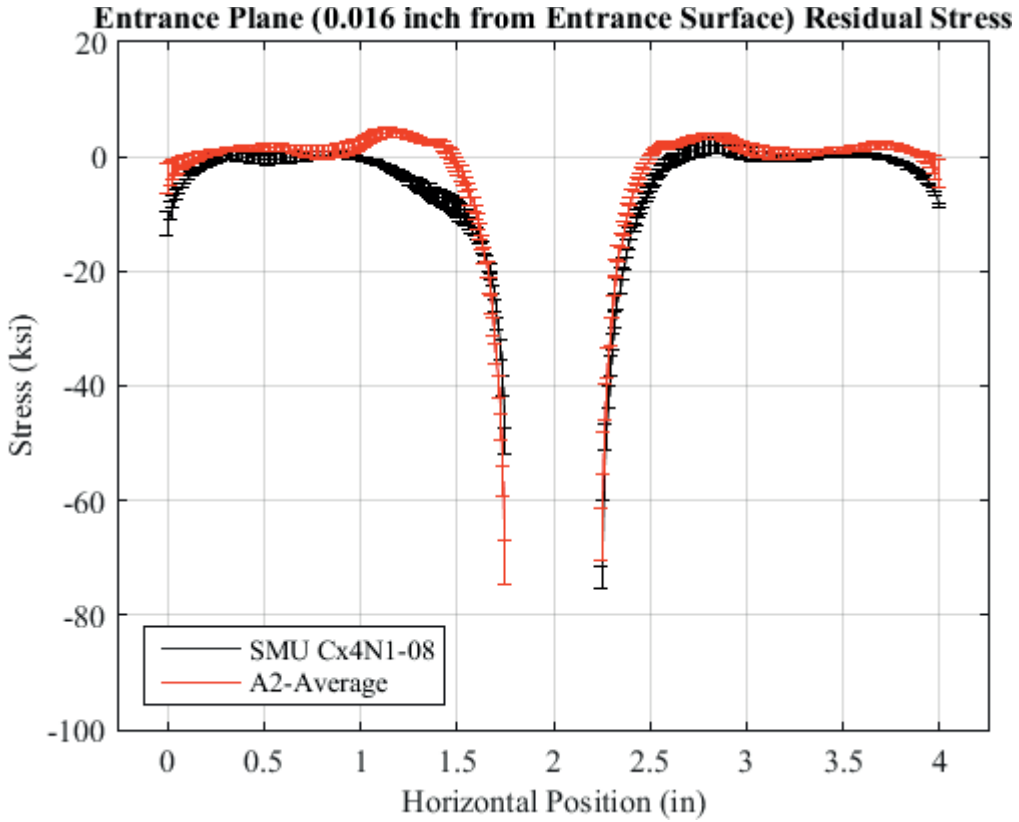

Fig. 568 Residual Stress Line Plot Comparing the Single Measurement Uncertainty of Cx4N1-08-B to the CxA2 (2024-T351) Average Residual Stress at a Distance of 0.016 inch (Entrance Surface) from the Entrance Surface – Cx4N1-08-B Coupon had a 0.4974 inch Fatigue Crack at the Left Entrance Surface.

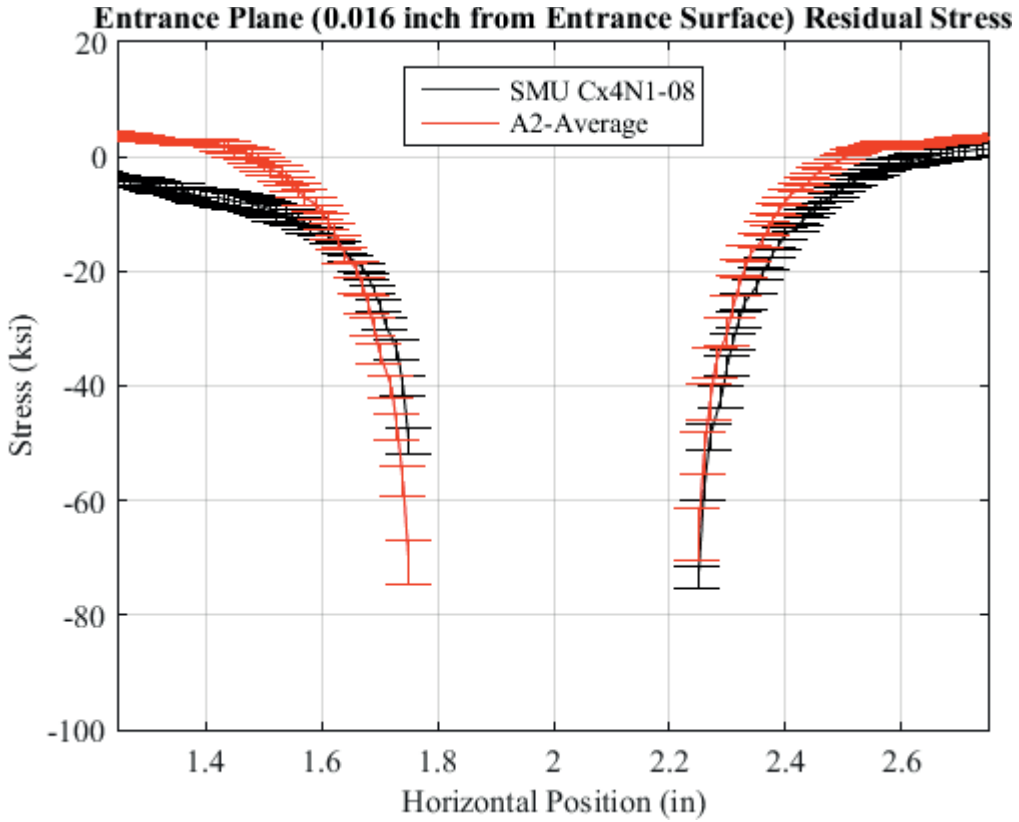

Fig. 569 Residual Stress Line Plot Comparing the Single Measurement Uncertainty of Cx4N1-08-B to the CxA2 (2024-T351) Average Residual Stress at a Distance of 0.016 inch (Entrance Surface) from the Entrance Surface – Cx4N1-08-B Coupon had a 0.4974 inch Fatigue Crack at the Left Entrance Surface – Zoomed in Next to Hole.

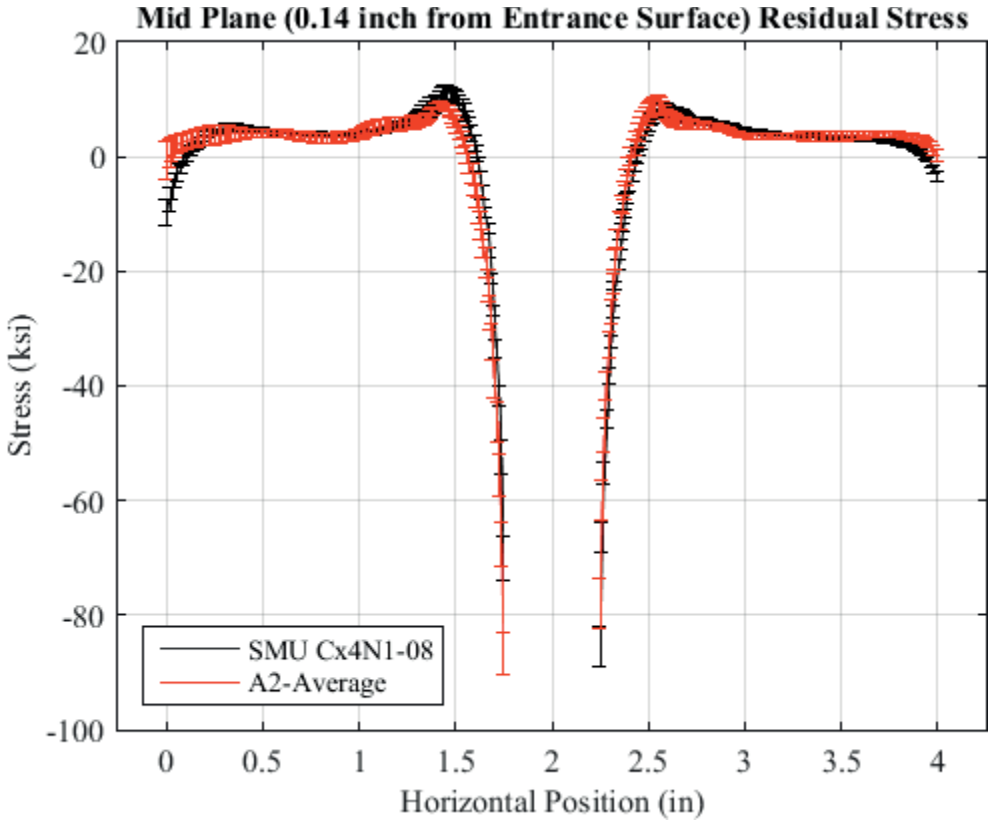

Fig. 570 Residual Stress Line Plot Comparing the Single Measurement Uncertainty of Cx4N1-08-B to the CxA2 (2024-T351) Average Residual Stress at a Distance of 0.140 inch (Mid Plane Surface) from the Entrance Surface – Cx4N1-08-B Coupon had a 0.4974 inch Fatigue Crack at the Left Entrance Surface.

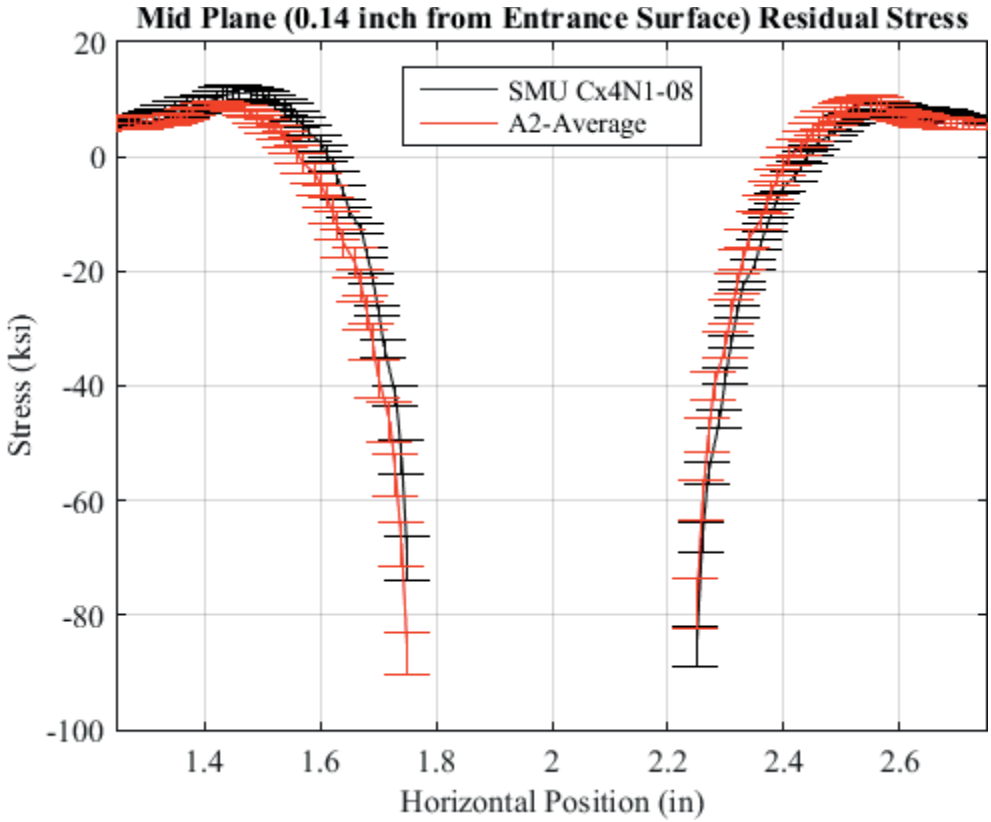

Fig. 571 Residual Stress Line Plot Comparing the Single Measurement Uncertainty of Cx4N1-08-B to the CxA2 (2024-T351) Average Residual Stress at a Distance of 0.140 inch (Mid Plane Surface) from the Entrance Surface – Cx4N1-08-B Coupon had a 0.4974 inch Fatigue Crack at the Left Entrance Surface – Zoomed in Next to Hole.

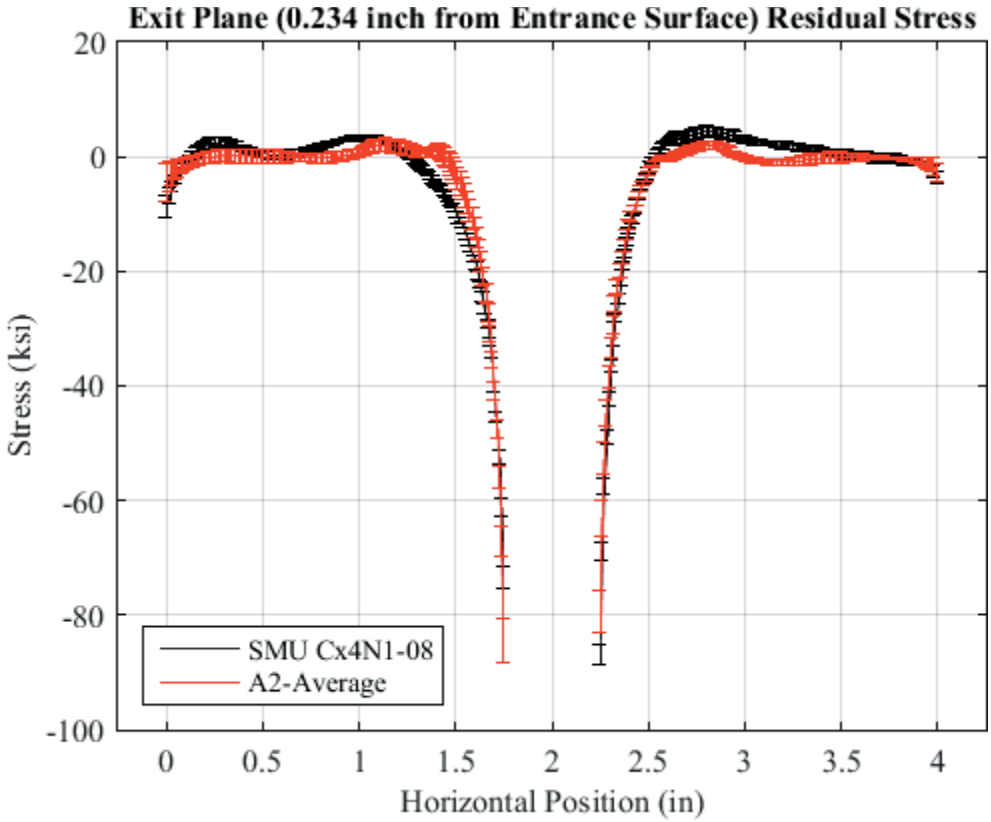

Fig. 572 Residual Stress Line Plot Comparing the Single Measurement Uncertainty of Cx4N1-08-B to the CxA2 (2024-T351) Average Residual Stress at a Distance of 0.234 inch (Exit Surface) from the Entrance Surface – Cx4N1-08-B Coupon had a 0.4974 inch Fatigue Crack at the Left Entrance Surface.

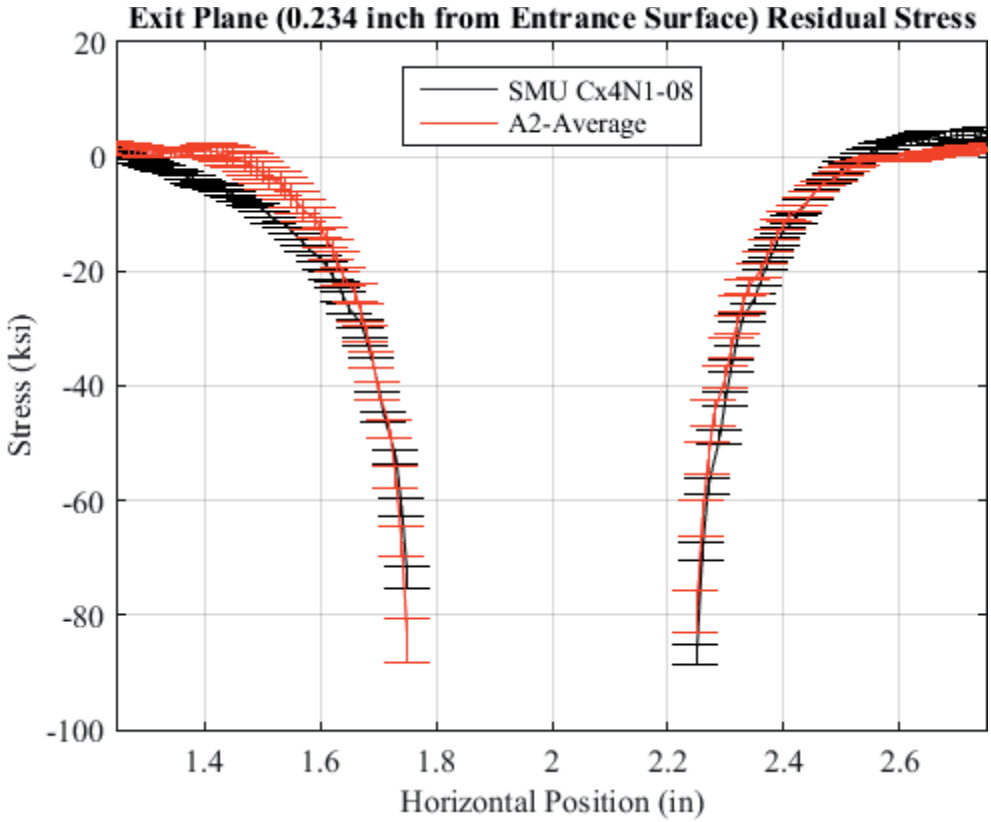

Fig. 573 Residual Stress Line Plot Comparing the Single Measurement Uncertainty of Cx4N1-08-B to the CxA2 (2024-T351) Average Residual Stress at a Distance of 0.234 inch (Exit Surface) from the Entrance Surface – Cx4N1-08-B Coupon had a 0.4974 inch Fatigue Crack at the Left Entrance Surface – Zoomed in Next to Hole.

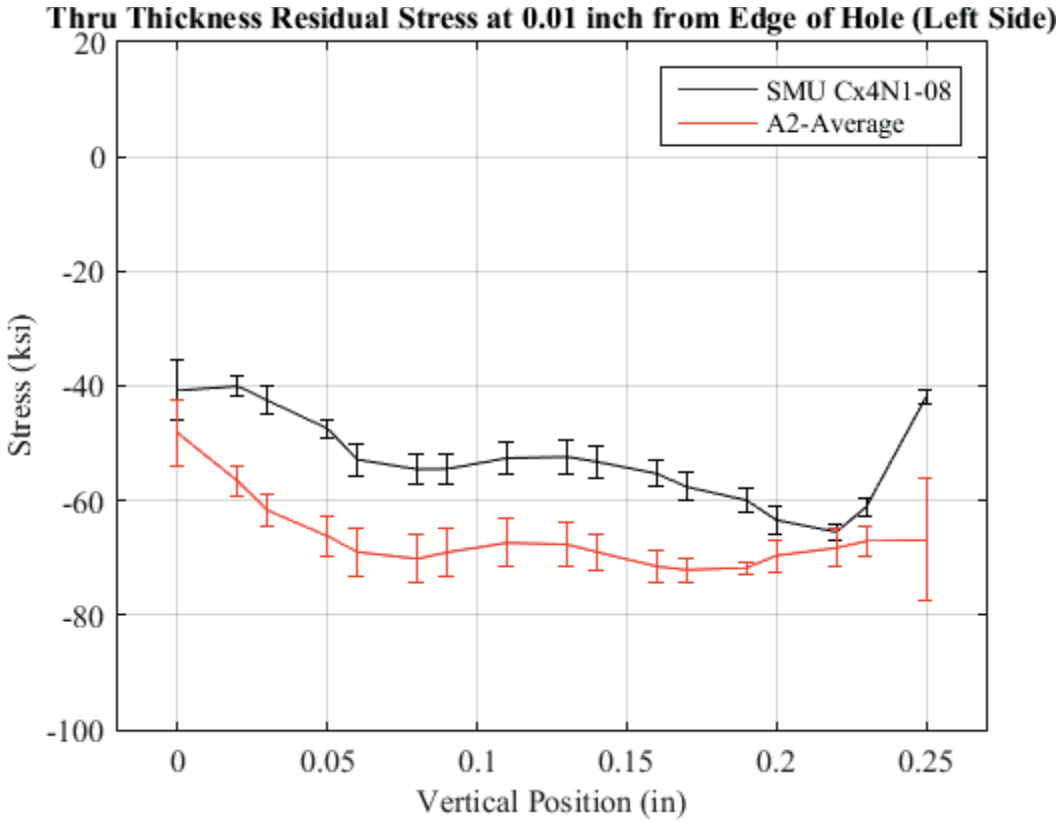

Fig. 574 Residual Stress Through Thickness Line Plot Comparing the Single Measurement Uncertainty of Cx4N1-08-B to the CxA2 (2024-T351) Average Residual Stress at a Distance 0.01 inch from Left Side of Hole – Coupon had a 0.4974 inch Fatigue Crack at the Left Entrance Surface.

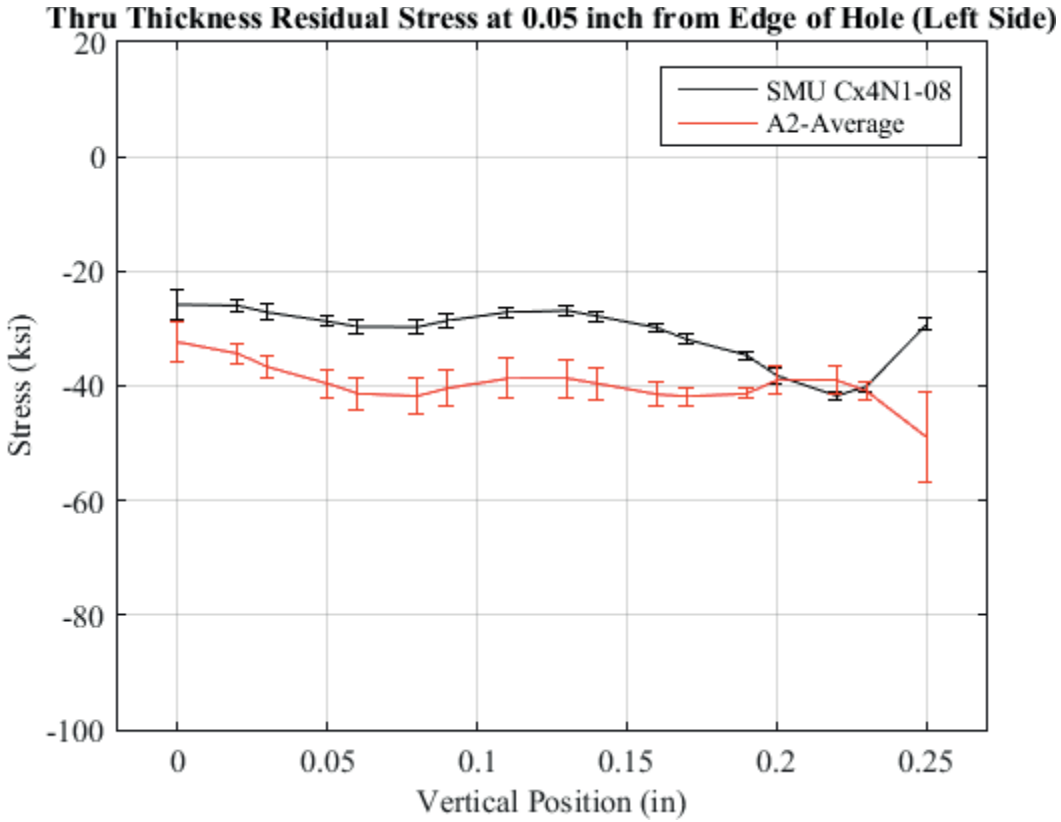

Fig. 575 Residual Stress Through Thickness Line Plot Comparing the Single Measurement Uncertainty of Cx4N1-08-B to the CxA2 (2024-T351) Average Residual Stress at a Distance 0.05 inch from Left Side of Hole – Coupon had a 0.4974 inch Fatigue Crack at the Left Entrance Surface.

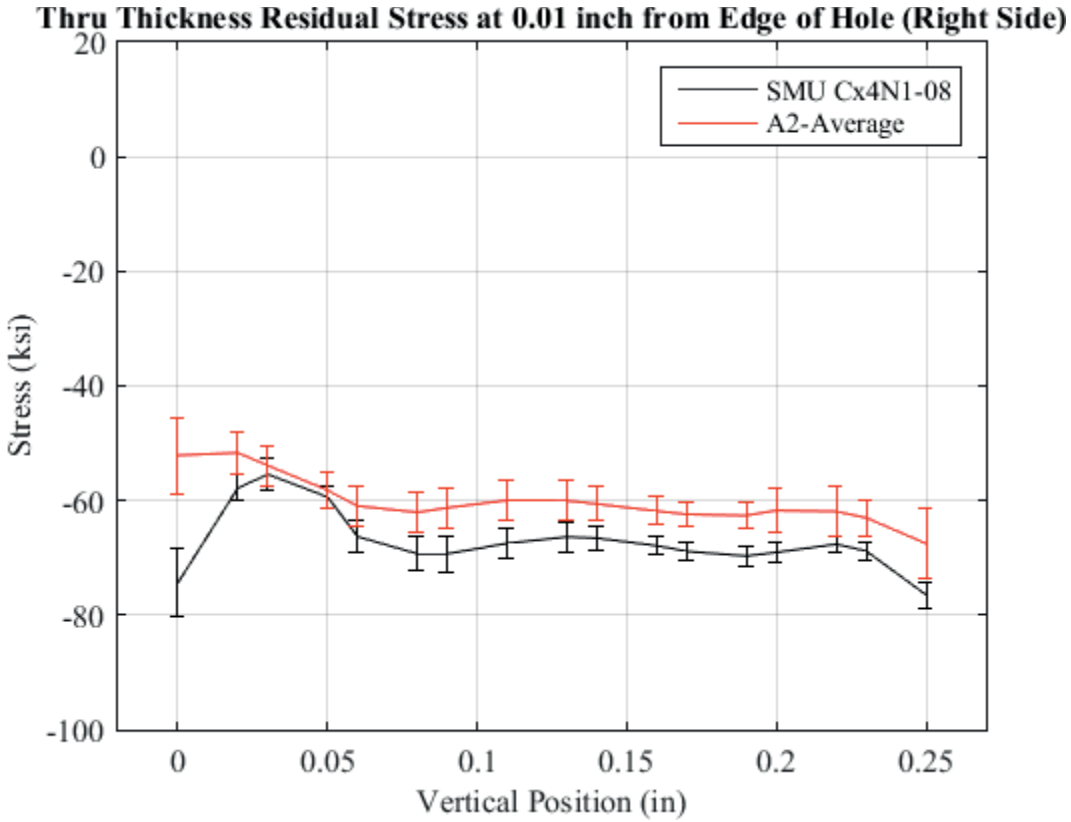

Fig. 576 Residual Stress Through Thickness Line Plot Comparing the Single Measurement Uncertainty of Cx4N1-08-B to the CxA2 (2024-T351) Average Residual Stress at a Distance 0.01 inch from Left Side of Hole – Coupon had a 0.4974 inch Fatigue Crack at the Left Entrance Surface.

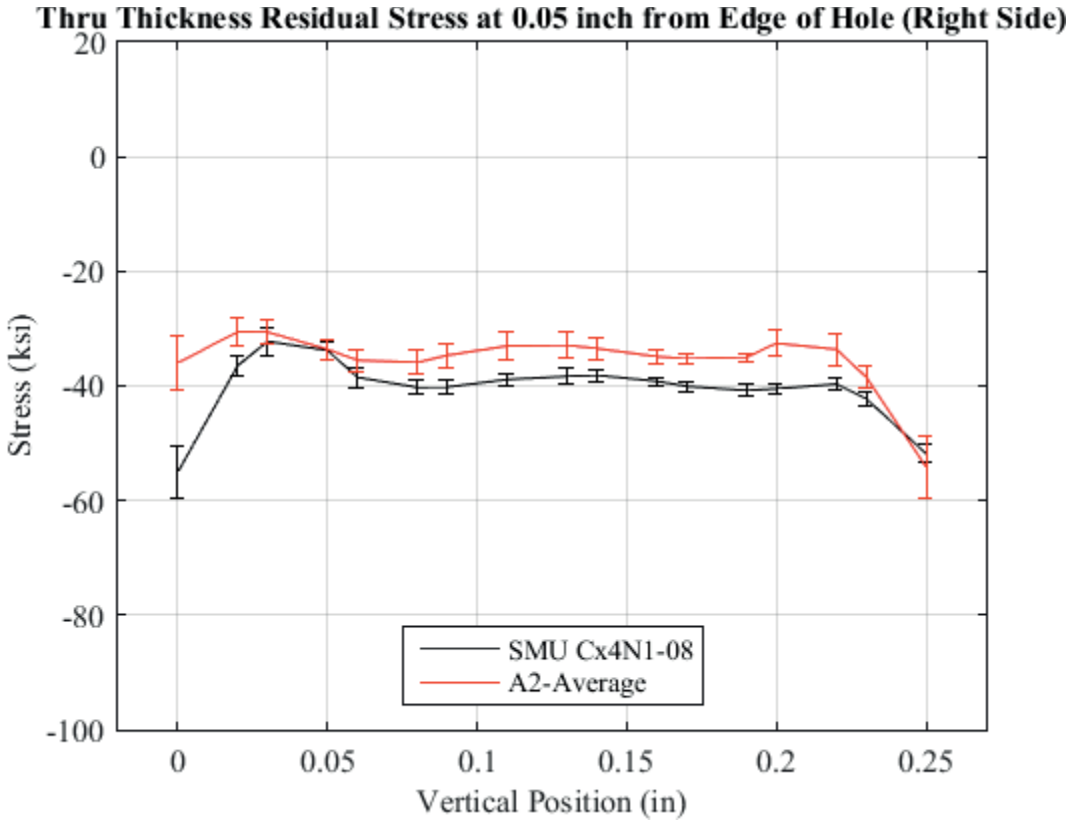

Fig. 577 Residual Stress Through Thickness Line Plot Comparing the Single Measurement Uncertainty of Cx4N1-08-B to the CxA2 (2024-T351) Average Residual Stress at a Distance 0.05 inch from Right Side of Hole – Coupon had a 0.4974 inch Fatigue Crack at the Left Entrance Surface.

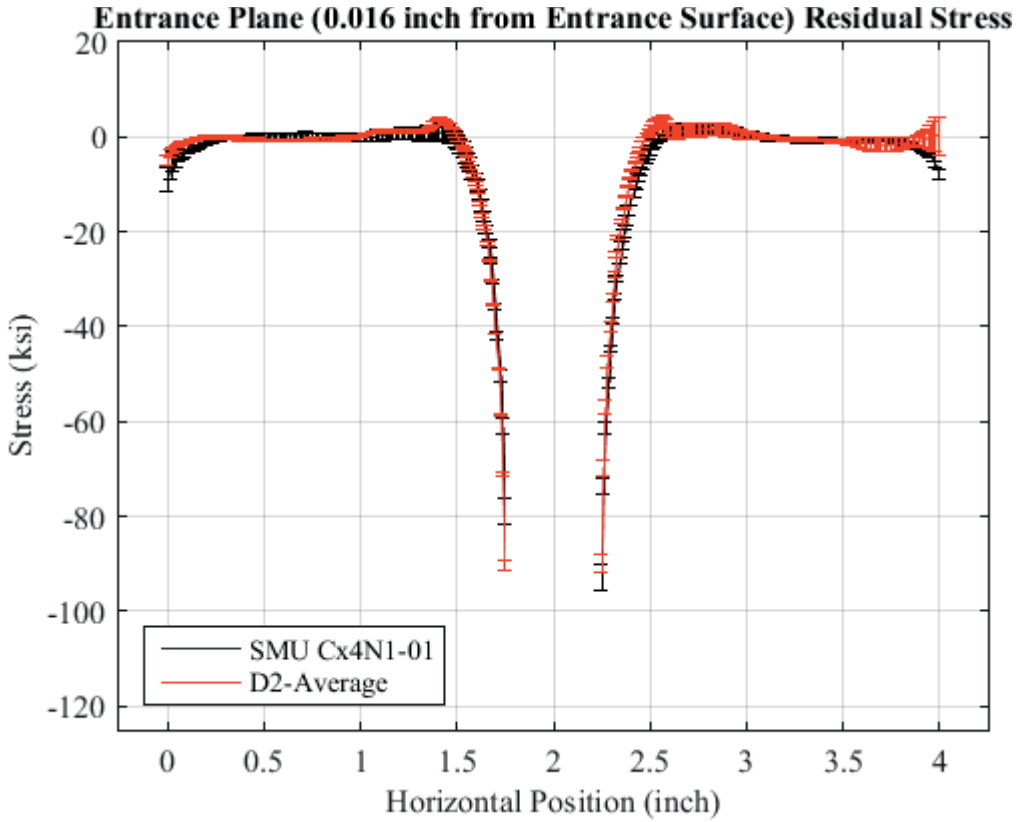

Fig. 578 Residual Stress Line Plot Comparing the Single Measurement Uncertainty of Cx4N1-01-D to the CxD2 (7075-T651) Average Residual Stress at a Distance of 0.016 inch (Entrance Surface) from the Entrance Surface – Cx4N1-01-D Coupon had a 0.0793 inch Fatigue Crack at the Left Entrance Surface.

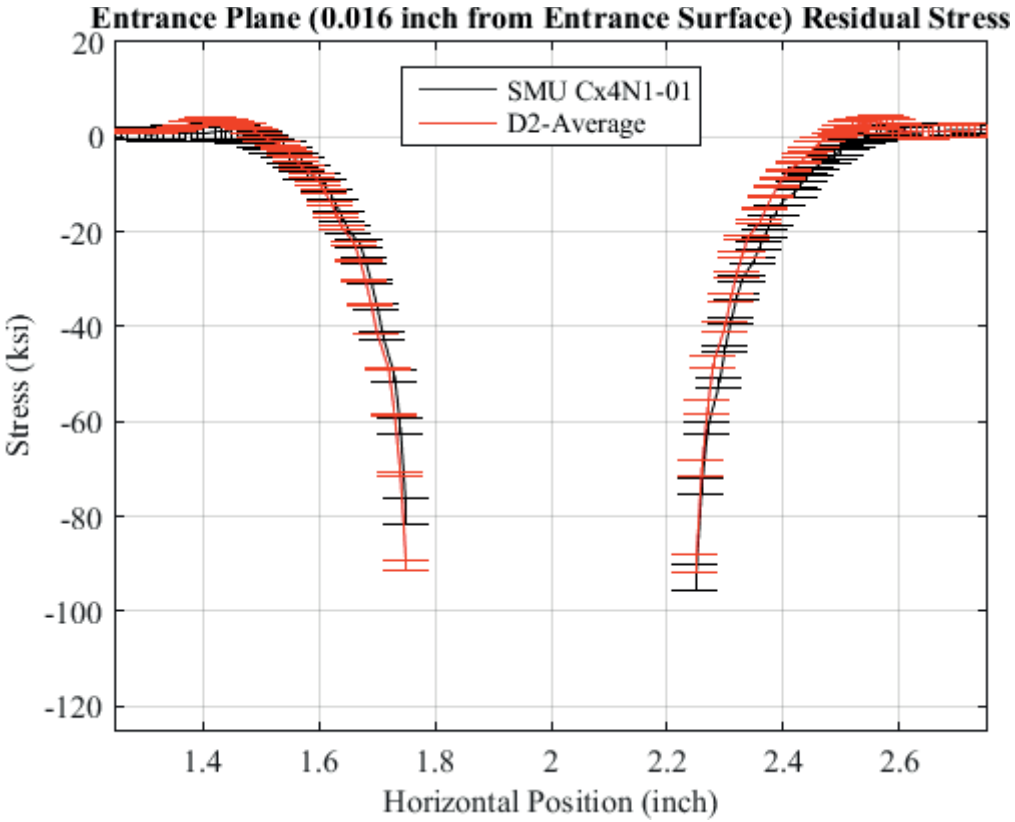

Fig. 579 Residual Stress Line Plot Comparing the Single Measurement Uncertainty of Cx4N1-01-D to the CxD2 (7075-T651) Average Residual Stress at a Distance of 0.016 inch (Entrance Surface) from the Entrance Surface – Cx4N1-01-D Coupon had a 0.0793 inch Fatigue Crack at the Left Entrance Surface – Zoomed in Next to Hole.

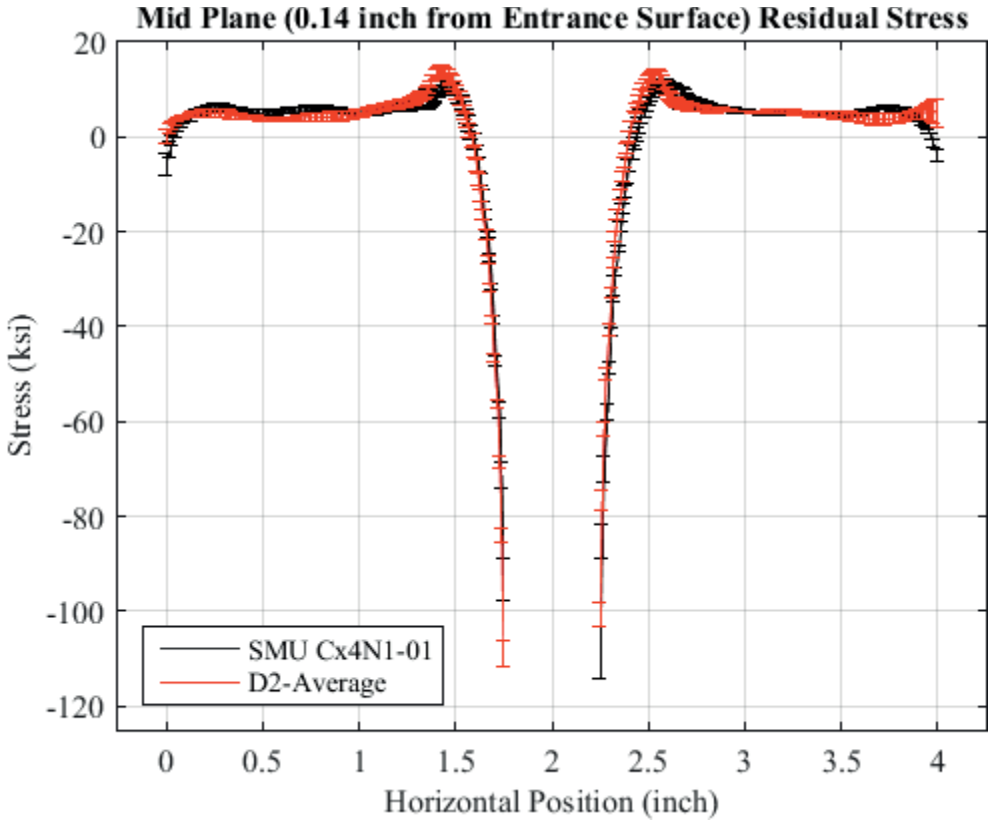

Fig. 580 Residual Stress Line Plot Comparing the Single Measurement Uncertainty of Cx4N1-01-D to the CxD2 (7075-T651) Average Residual Stress at a Distance of 0.140 inch (Mid Plane Surface) from the Entrance Surface – Cx4N1-01-D Coupon had a 0.0793 inch Fatigue Crack at the Left Entrance Surface.

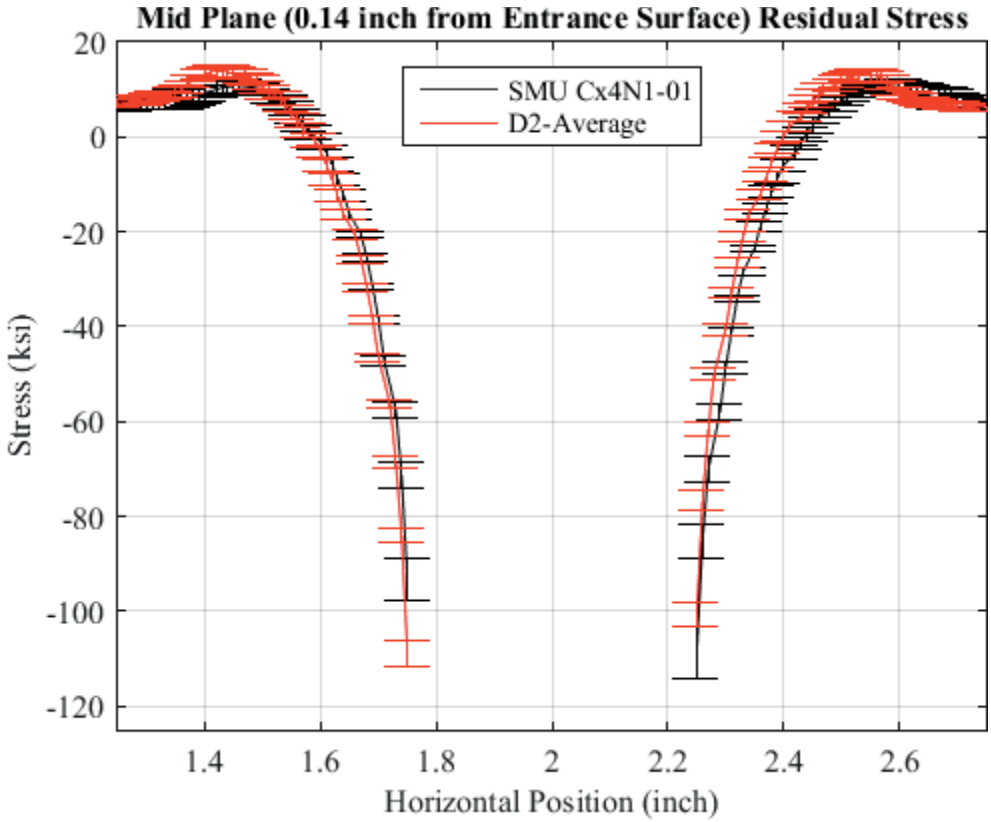

Fig. 581 Residual Stress Line Plot Comparing the Single Measurement Uncertainty of Cx4N1-01-D to the CxD2 (7075-T651) Average Residual Stress at a Distance of 0.140 inch (Mid Plane Surface) from the Entrance Surface – Cx4N1-01-D Coupon had a 0.0793 inch Fatigue Crack at the Left Entrance Surface – Zoomed in Next to Hole.

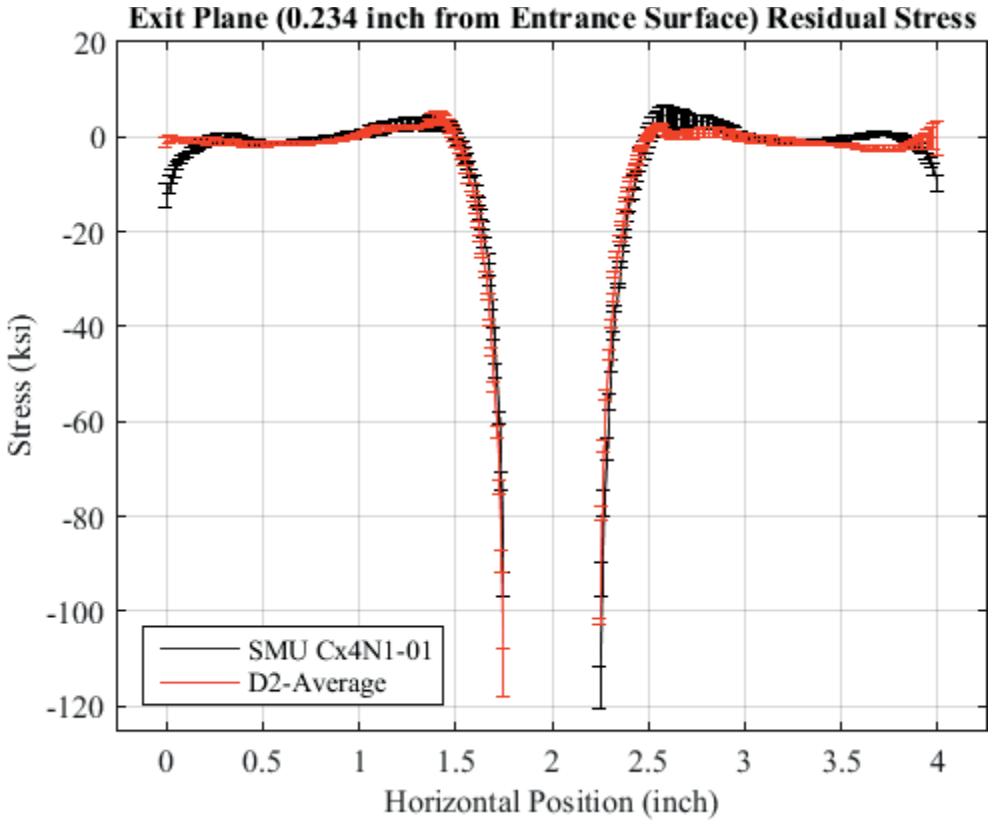

Fig. 582 Residual Stress Line Plot Comparing the Single Measurement Uncertainty of Cx4N1-01-D to the CxD2 (7075-T651) Average Residual Stress at a Distance of 0.234 inch (Exit Surface) from the Entrance Surface – Cx4N1-01-D Coupon had a 0.0793 inch Fatigue Crack at the Left Entrance Surface – Zoomed in Next to Hole.

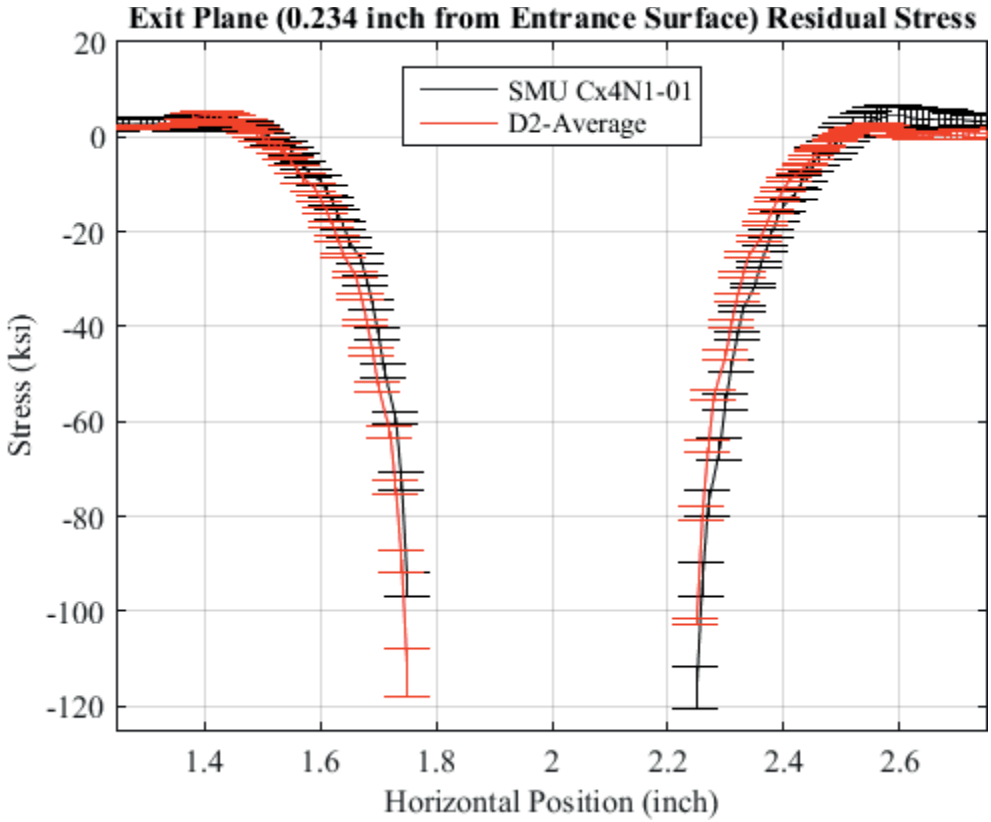

Fig. 583 Residual Stress Line Plot Comparing the Single Measurement Uncertainty of Cx4N1-01-D to the CxD2 (7075-T651) Average Residual Stress at a Distance of 0.234 inch (Exit Surface) from the Entrance Surface – Cx4N1-01-D Coupon had a 0.0793 inch Fatigue Crack at the Left Entrance Surface – Zoomed in Next to Hole.

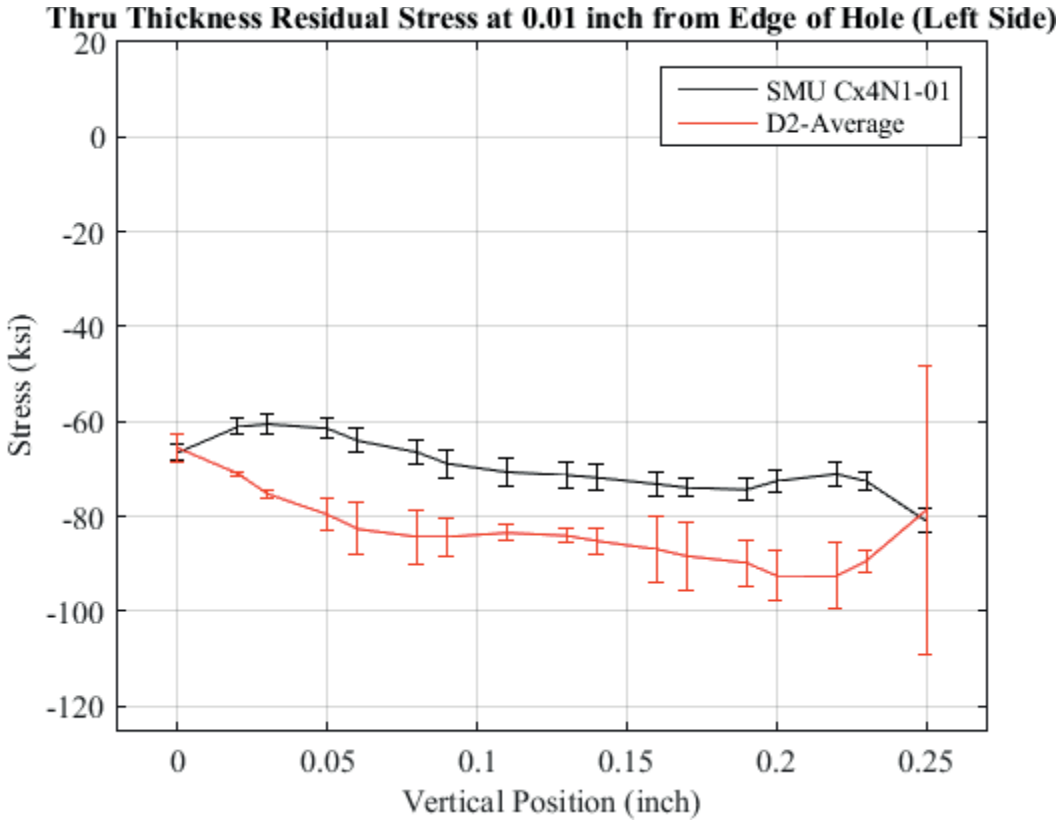

Fig. 584 Residual Stress Through Thickness Line Plot Comparing the Single Measurement Uncertainty of Cx4N1-01-D to the CxD2 (7075-T651) Average Residual Stress at a Distance 0.01 inch from Left Side of Hole – Coupon had a 0.0793 inch Fatigue Crack at the Left Entrance Surface.

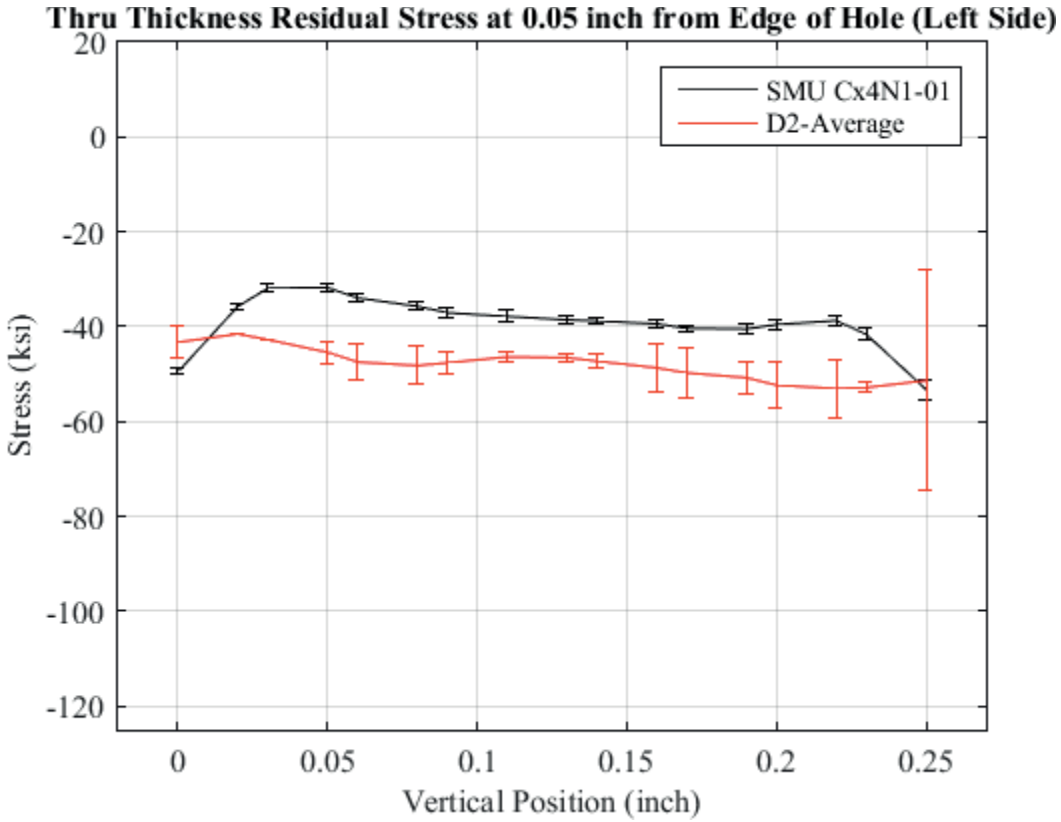

Fig. 585 Residual Stress Through Thickness Line Plot Comparing the Single Measurement Uncertainty of Cx4N1-01-D to the CxD2 (7075-T651) Average Residual Stress at a Distance 0.05 inch from Left Side of Hole – Coupon had a 0.0793 inch Fatigue Crack at the Left Entrance Surface.

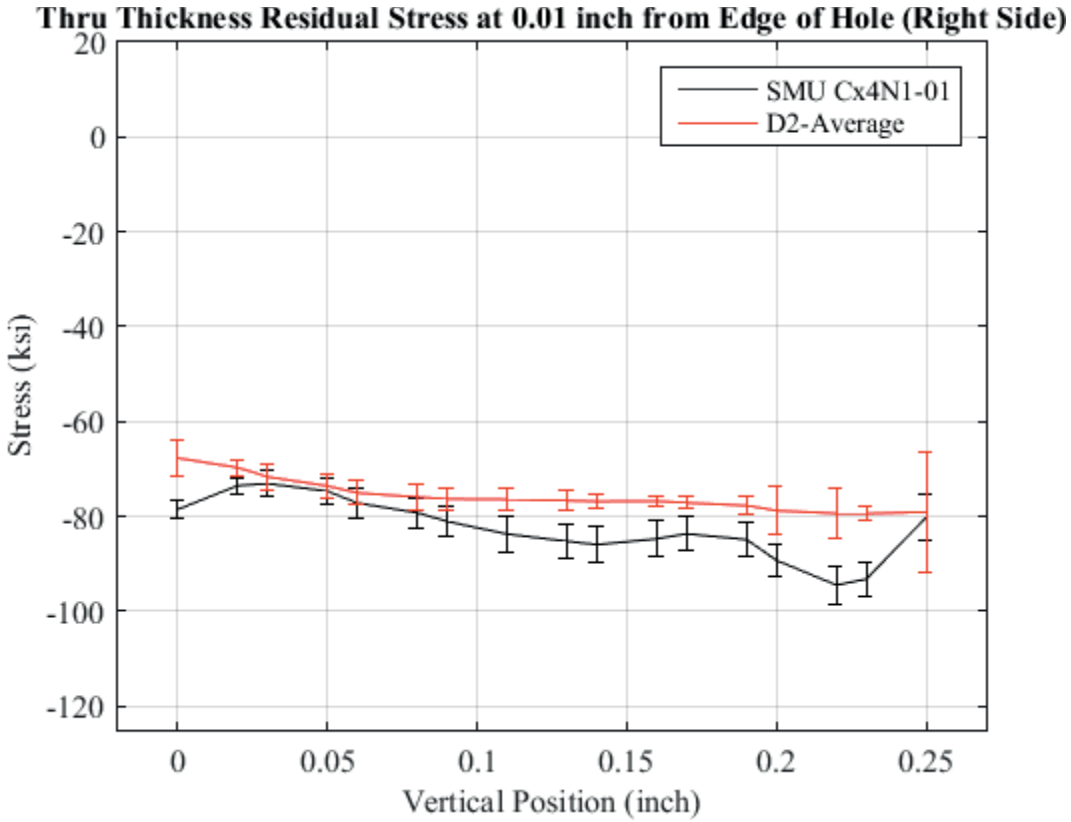

Fig. 586 Residual Stress Through Thickness Line Plot Comparing the Single Measurement Uncertainty of Cx4N1-01-D to the CxD2 (7075-T651) Average Residual Stress at a Distance 0.01 inch from Right Side of Hole – Coupon had a 0.0793 inch Fatigue Crack at the Left Entrance Surface.

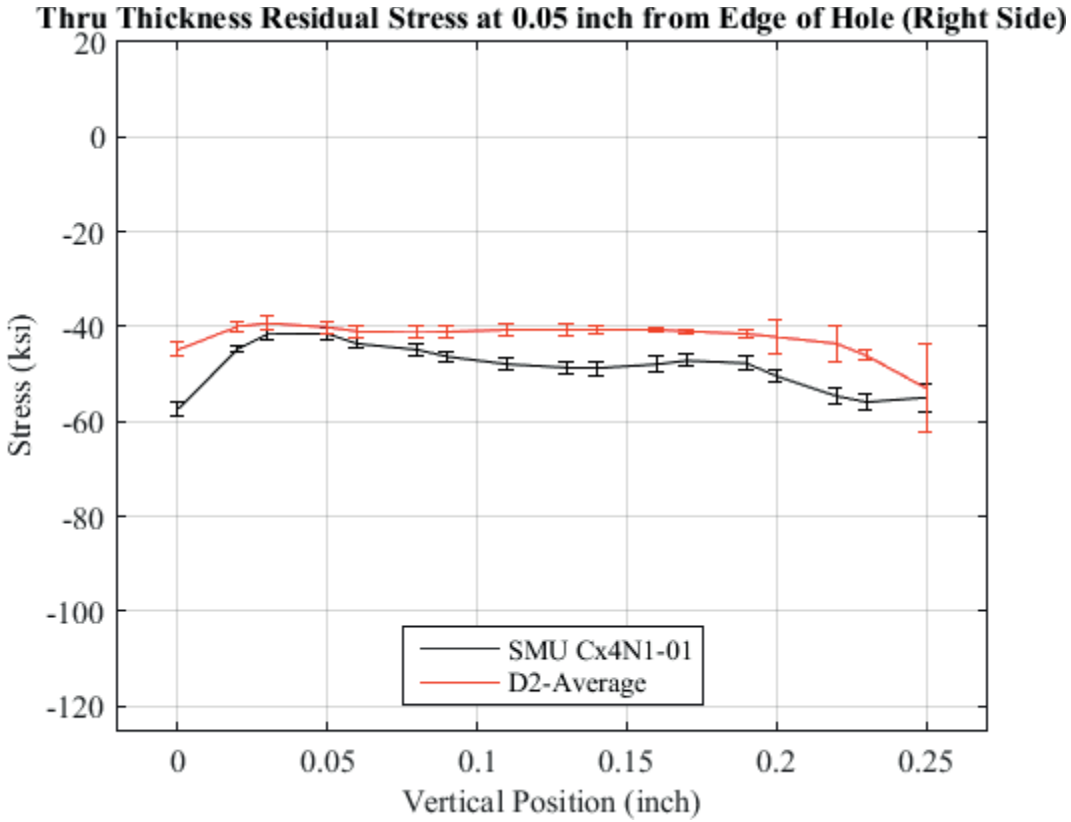

Fig. 587 Residual Stress Through Thickness Line Plot Comparing the Single Measurement Uncertainty of Cx4N1-01-D to the CxD2 (7075-T651) Average Residual Stress at a Distance 0.05 inch from Right Side of Hole – Coupon had a 0.0793 inch Fatigue Crack at the Left Entrance Surface.

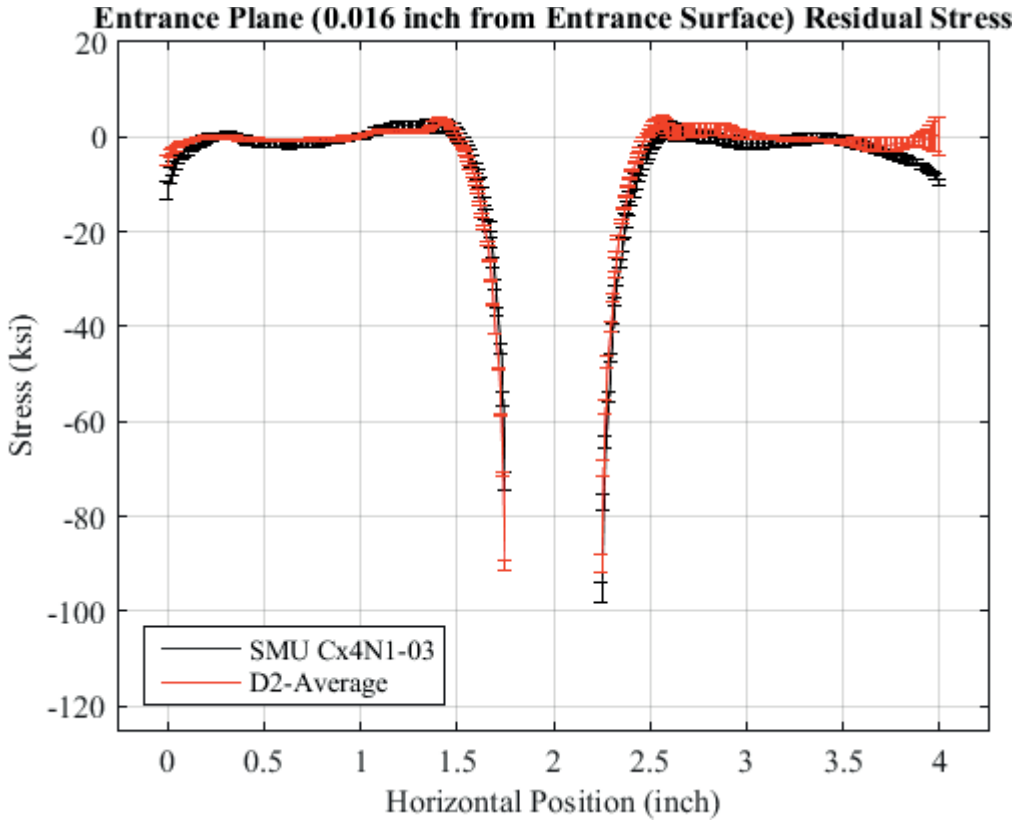

Fig. 588 Residual Stress Line Plot Comparing the Single Measurement Uncertainty of Cx4N1-03-D to the CxD2 (7075-T651) Average Residual Stress at a Distance of 0.016 inch (Entrance Surface) from the Entrance Surface – Cx4N1-03-D Coupon had a 0.0972 inch Fatigue Crack at the Left Entrance Surface.

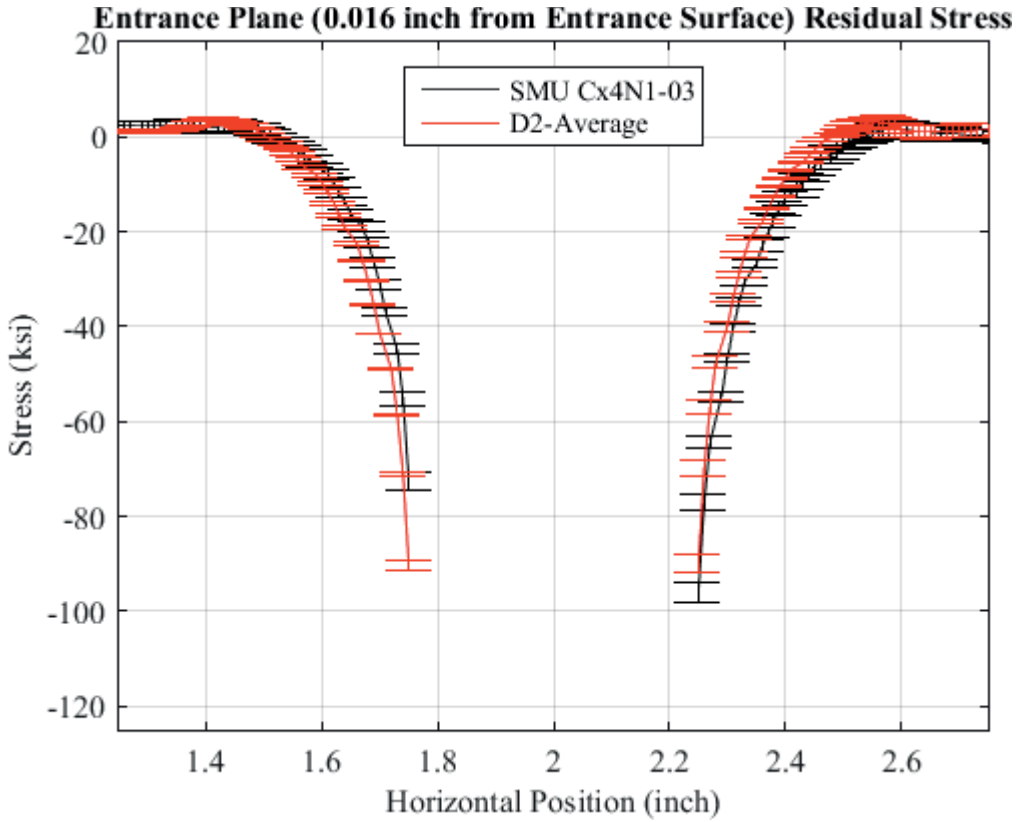

Fig. 589 Residual Stress Line Plot Comparing the Single Measurement Uncertainty of Cx4N1-03-D to the CxD2 (7075-T651) Average Residual Stress at a Distance of 0.016 inch (Entrance Surface) from the Entrance Surface – Cx4N1-03-D Coupon had a 0.0972 inch Fatigue Crack at the Left Entrance Surface – Zoomed in Next to Hole.

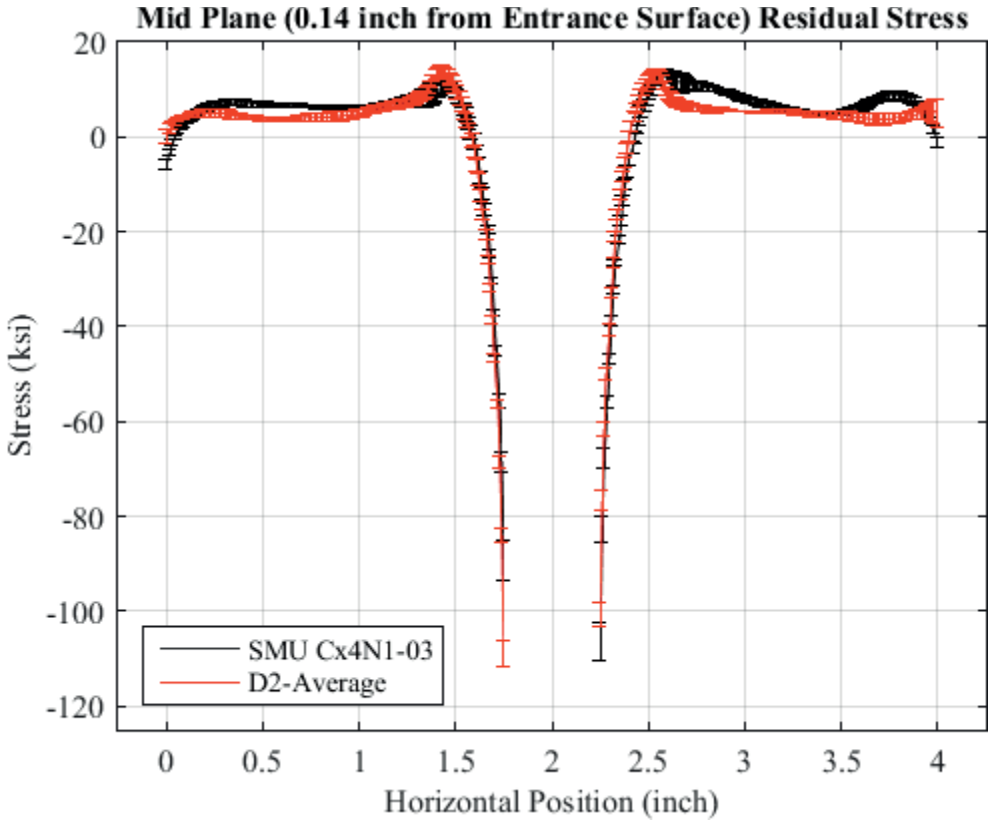

Fig. 590 Residual Stress Line Plot Comparing the Single Measurement Uncertainty of Cx4N1-03-D to the CxD2 (7075-T651) Average Residual Stress at a Distance of 0.140 inch (Mid Plane Surface) from the Entrance Surface – Cx4N1-03-D Coupon had a 0.0972 inch Fatigue Crack at the Left Entrance Surface.

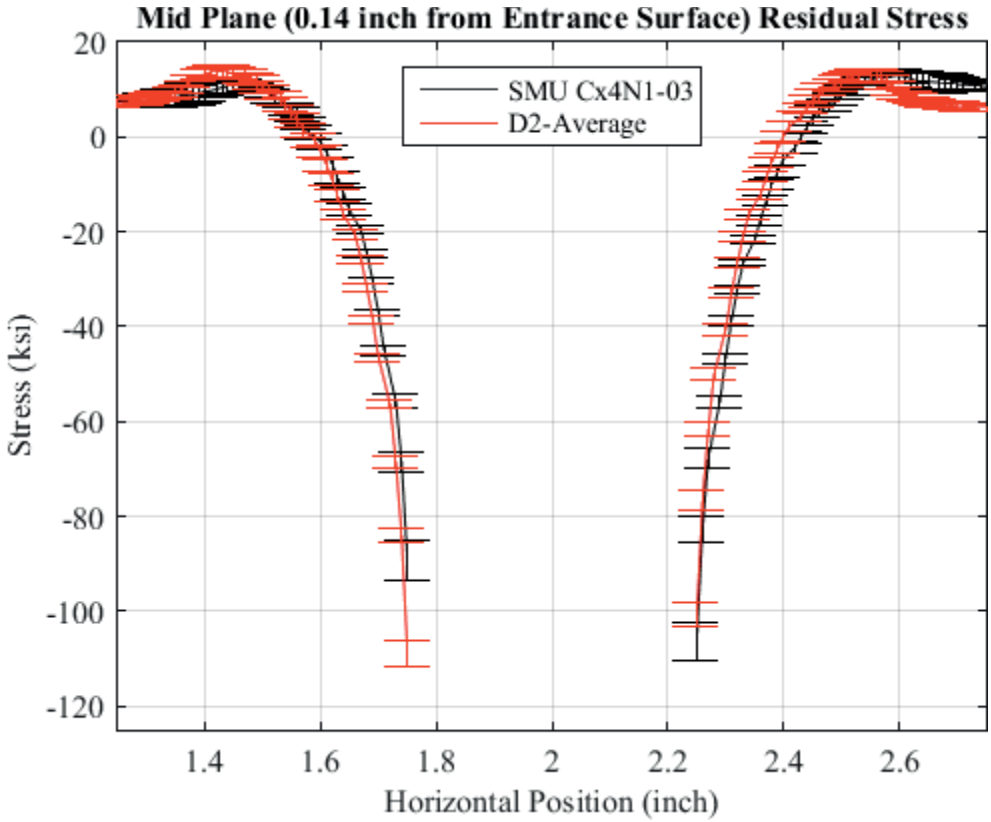

Fig. 591 Residual Stress Line Plot Comparing the Single Measurement Uncertainty of Cx4N1-03-D to the CxD2 (7075-T651) Average Residual Stress at a Distance of 0.140 inch (Mid Plane Surface) from the Entrance Surface – Cx4N1-03-D Coupon had a 0.0972 inch Fatigue Crack at the Left Entrance Surface – Zoomed in Next to Hole.

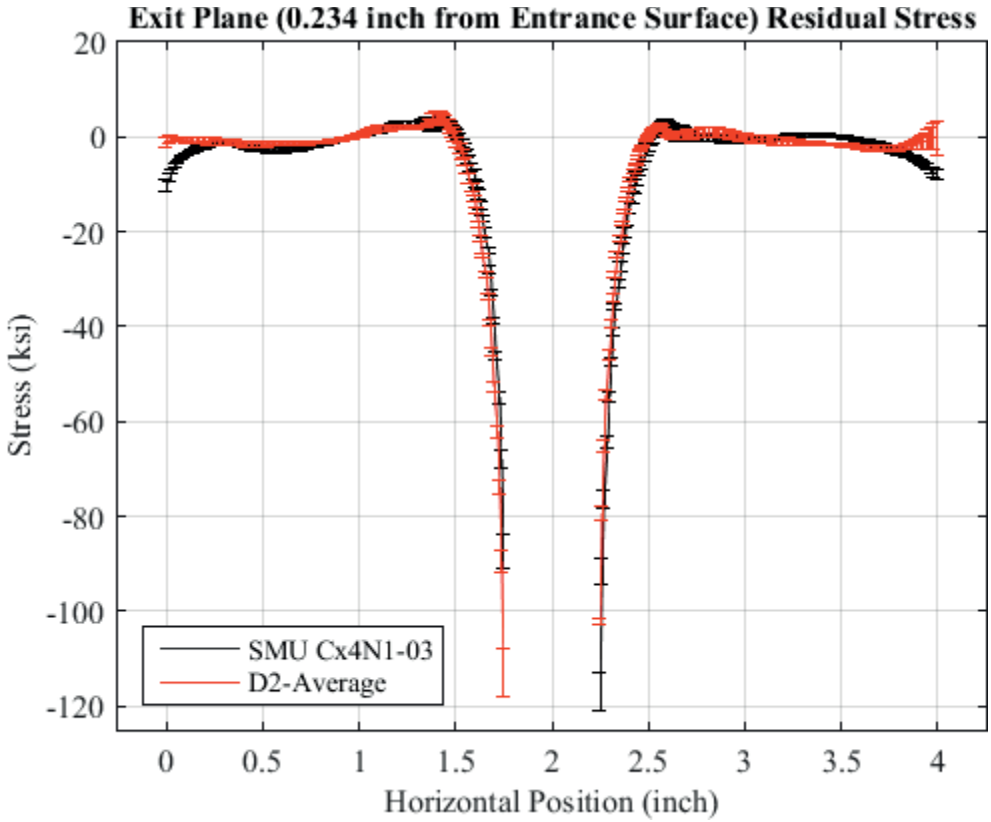

Fig. 592 Residual Stress Line Plot Comparing the Single Measurement Uncertainty of Cx4N1-03-D to the CxD2 (7075-T651) Average Residual Stress at a Distance of 0.234 inch (Exit Surface) from the Entrance Surface – Cx4N1-03-D Coupon had a 0.0972 inch Fatigue Crack at the Left Entrance Surface.

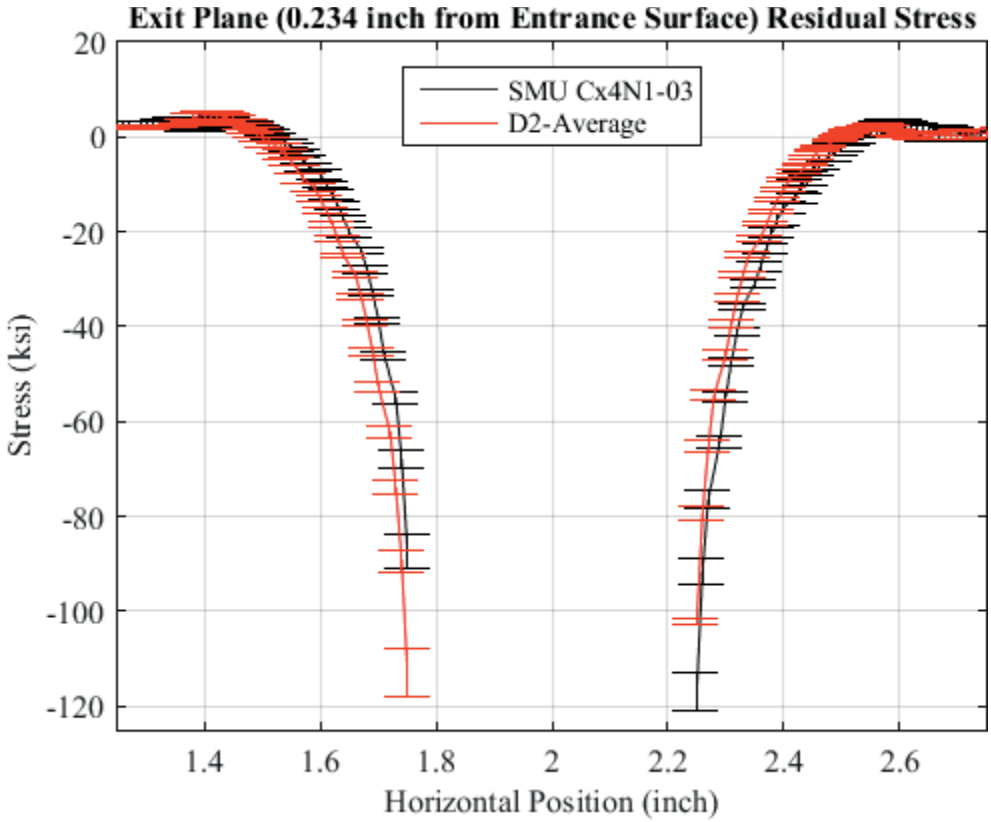

Fig. 593 Residual Stress Line Plot Comparing the Single Measurement Uncertainty of Cx4N1-03-D to the CxD2 (7075-T651) Average Residual Stress at a Distance of 0.234 inch (Exit Surface) from the Entrance Surface – Cx4N1-03-D Coupon had a 0.0972 inch Fatigue Crack at the Left Entrance Surface.

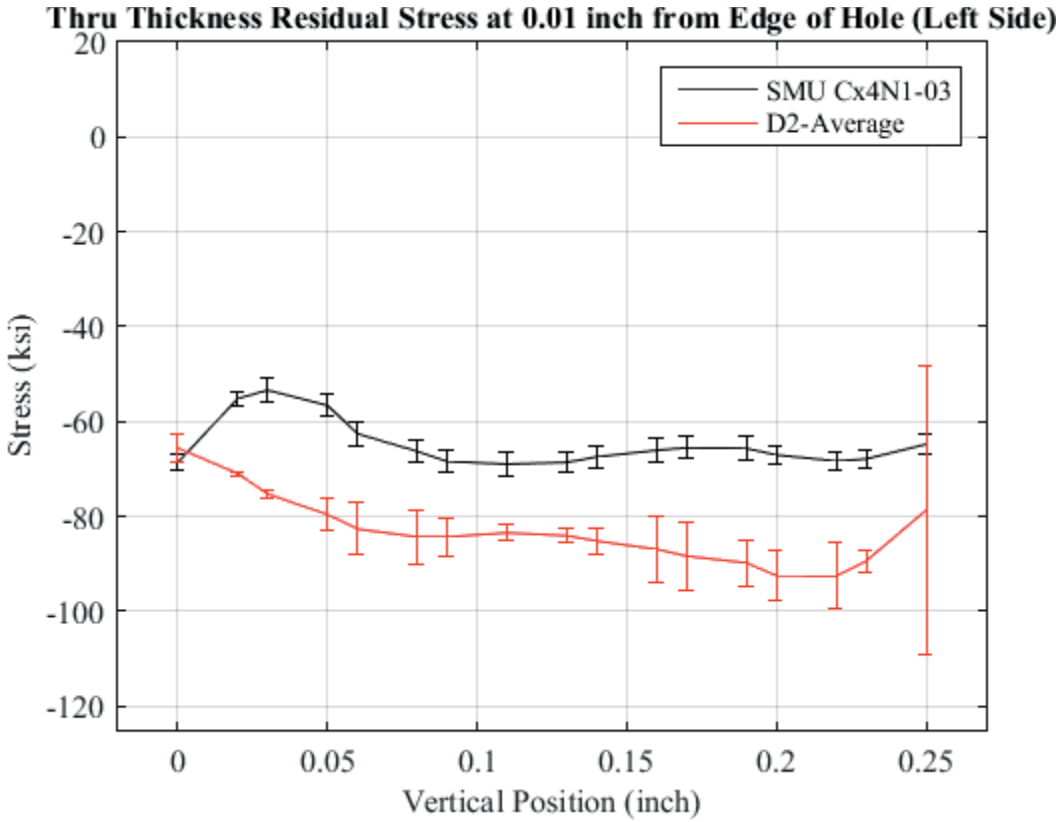

Fig. 594 Residual Stress Through Thickness Line Plot Comparing the Single Measurement Uncertainty of Cx4N1-03-D to the CxD2 (7075-T651) Average Residual Stress at a Distance 0.01 inch from Left Side of Hole – Coupon had a 0.0972 inch Fatigue Crack at the Left Entrance Surface.

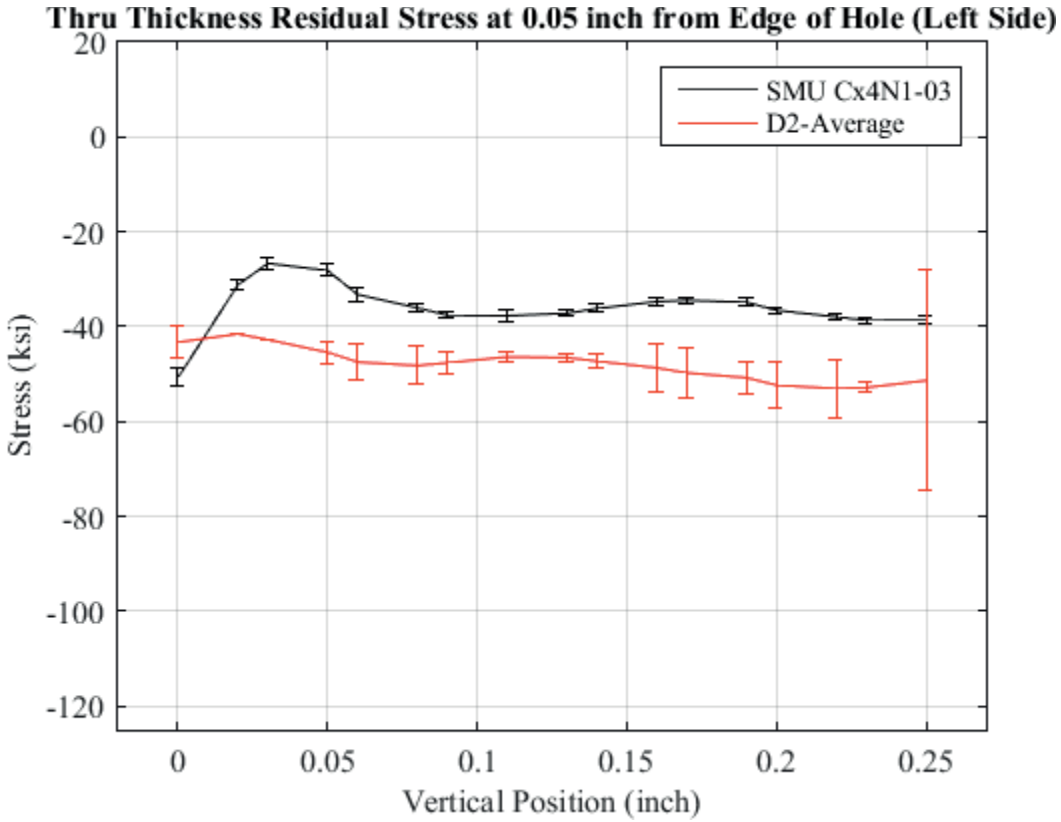

Fig. 595 Residual Stress Through Thickness Line Plot Comparing the Single Measurement Uncertainty of Cx4N1-03-D to the CxD2 (7075-T651) Average Residual Stress at a Distance 0.05 inch from Left Side of Hole – Coupon had a 0.0972 inch Fatigue Crack at the Left Entrance Surface.

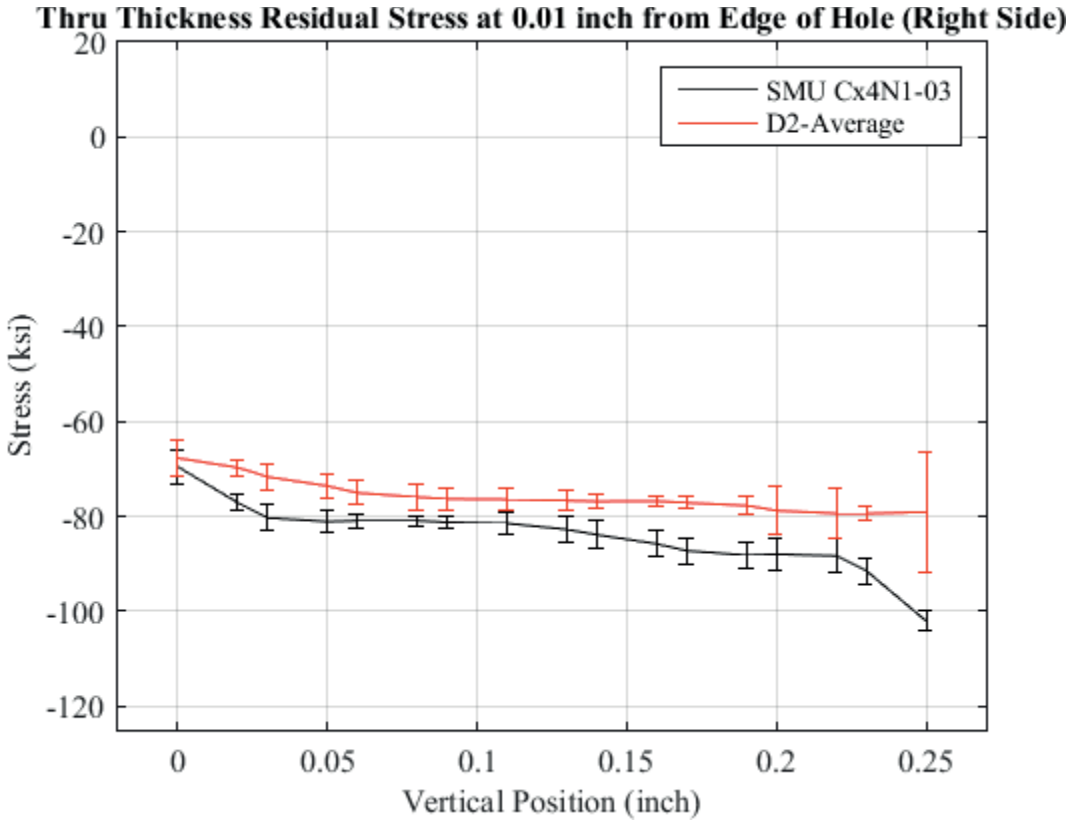

Fig. 596 Residual Stress Through Thickness Line Plot Comparing the Single Measurement Uncertainty of Cx4N1-03-D to the CxD2 (7075-T651) Average Residual Stress at a Distance 0.01 inch from Right Side of Hole – Coupon had a 0.0972 inch Fatigue Crack at the Left Entrance Surface.

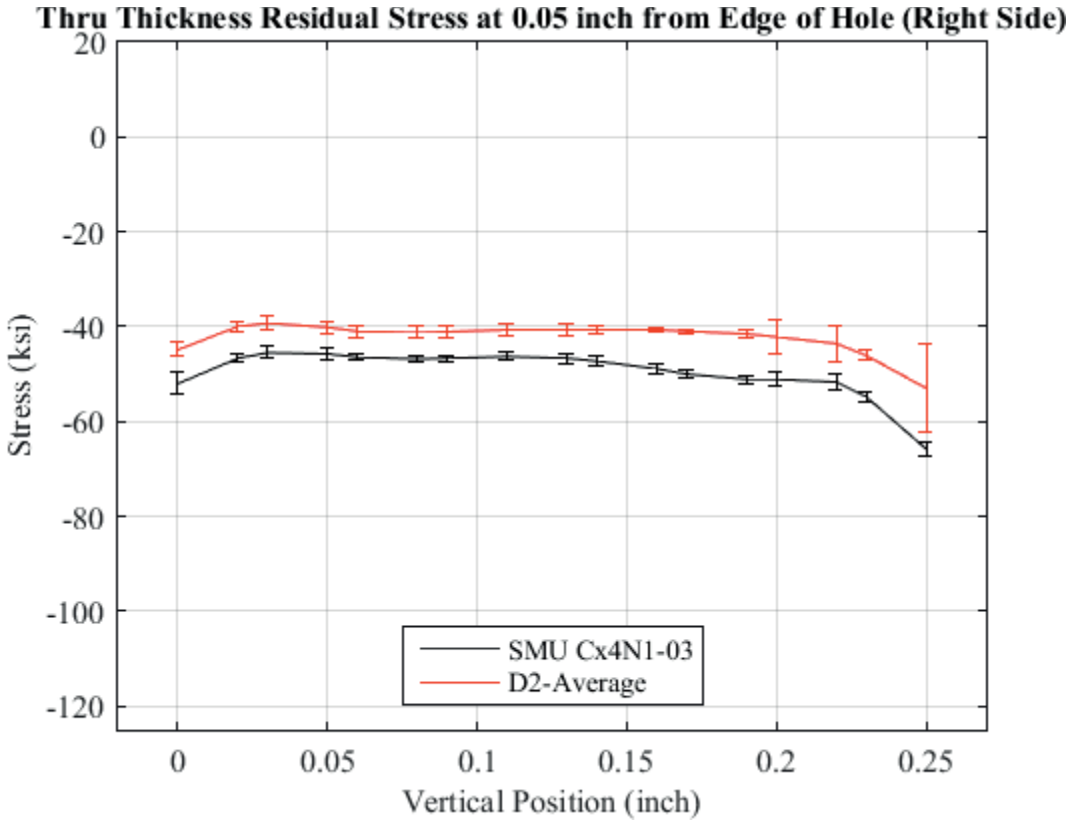

Fig. 597 Residual Stress Through Thickness Line Plot Comparing the Single Measurement Uncertainty of Cx4N1-03-D to the CxD2 (7075-T651) Average Residual Stress at a Distance 0.05 inch from Right Side of Hole – Coupon had a 0.0972 inch Fatigue Crack at the Left Entrance Surface.

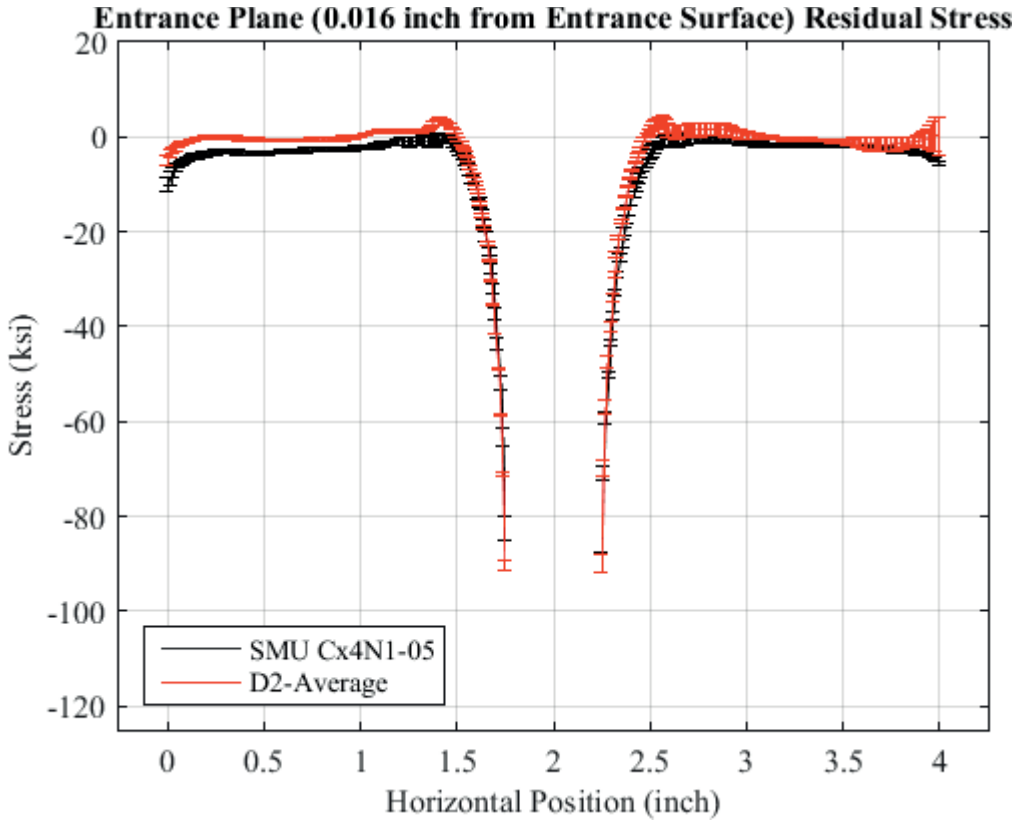

Fig. 598 Residual Stress Line Plot Comparing the Single Measurement Uncertainty of Cx4N1-05-D to the CxD2 (7075-T651) Average Residual Stress at a Distance of 0.016 inch (Entrance Surface) from the Entrance Surface – Cx4N1-05-D Coupon had a 0.1253 inch Fatigue Crack at the Left Entrance Surface.

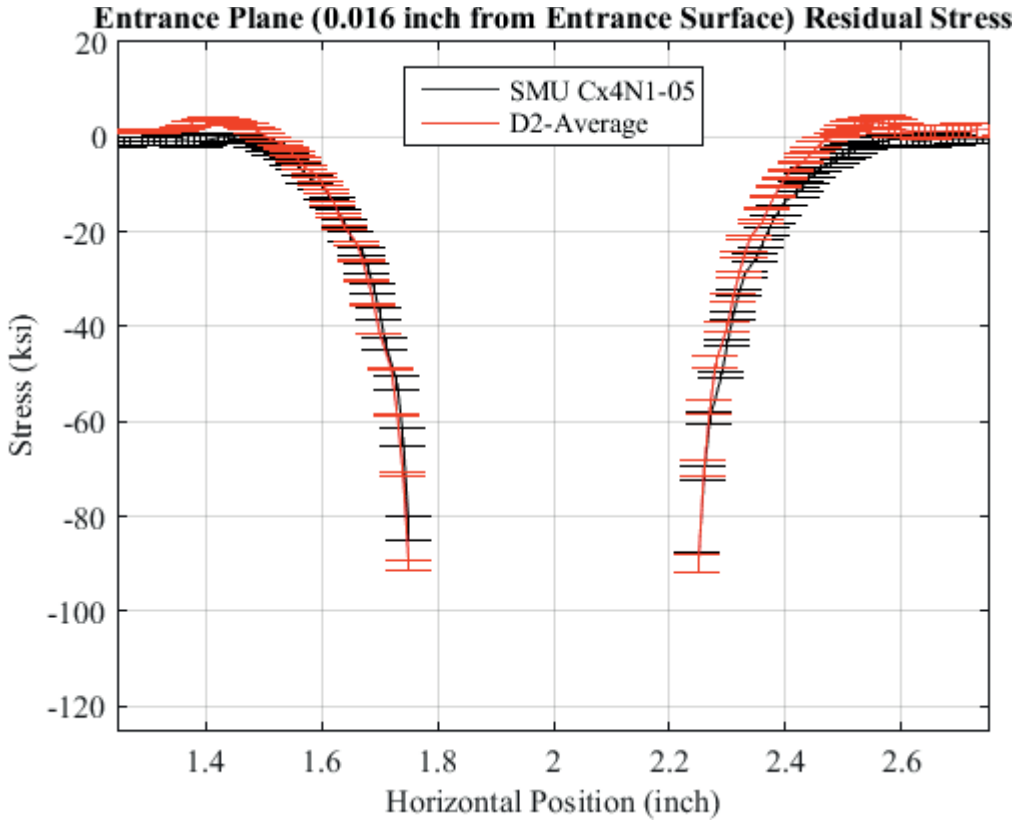

Fig. 599 Residual Stress Line Plot Comparing the Single Measurement Uncertainty of Cx4N1-05-D to the CxD2 (7075-T651) Average Residual Stress at a Distance of 0.016 inch (Entrance Surface) from the Entrance Surface – Cx4N1-05-D Coupon had a 0.1253 inch Fatigue Crack at the Left Entrance Surface – Zoomed in Next to Hole.

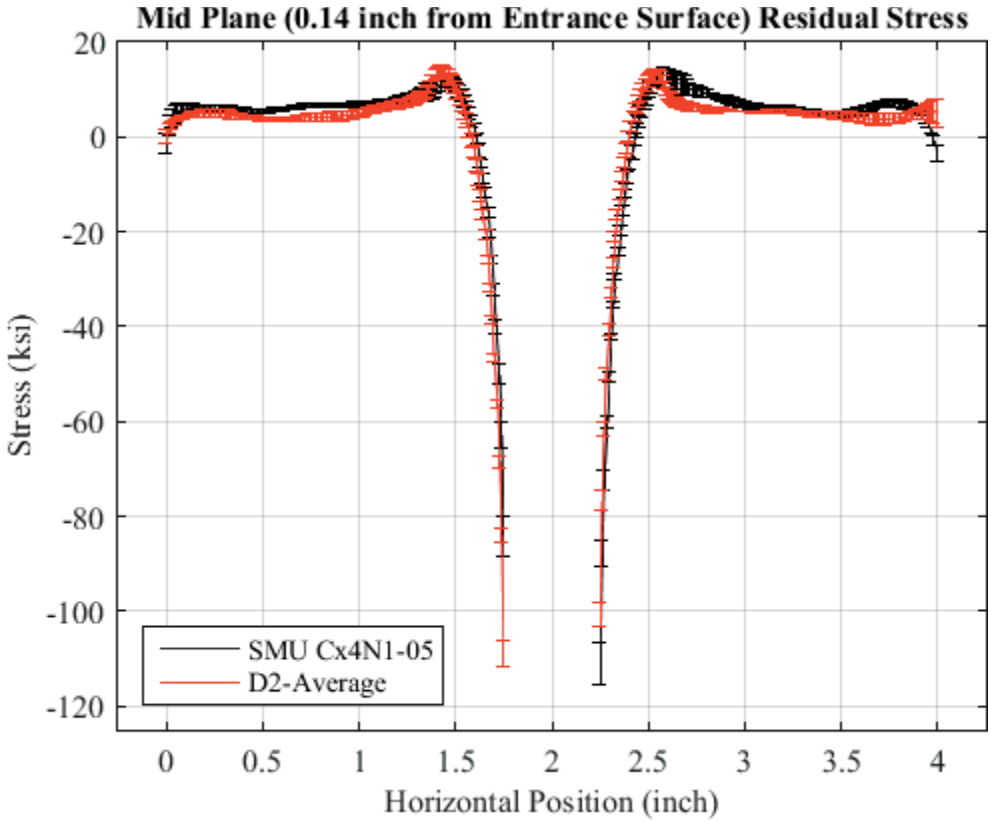

Fig. 600 Residual Stress Line Plot Comparing the Single Measurement Uncertainty of Cx4N1-05-D to the CxD2 (7075-T651) Average Residual Stress at a Distance of 0.140 inch (Mid Plane Surface) from the Entrance Surface – Cx4N1-05-D Coupon had a 0.1253 inch Fatigue Crack at the Left Entrance Surface.

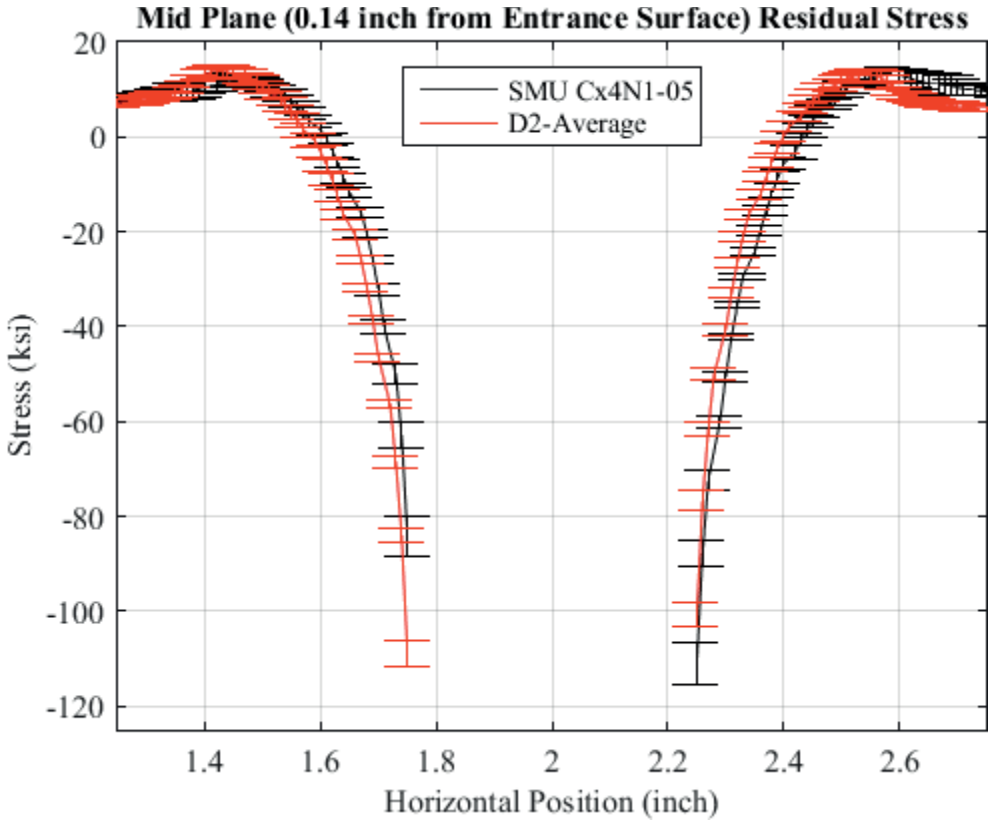

Fig. 601 Residual Stress Line Plot Comparing the Single Measurement Uncertainty of Cx4N1-05-D to the CxD2 (7075-T651) Average Residual Stress at a Distance of 0.140 inch (Mid Plane Surface) from the Entrance Surface – Cx4N1-05-D Coupon had a 0.1253 inch Fatigue Crack at the Left Entrance Surface – Zoomed in Next to Hole.

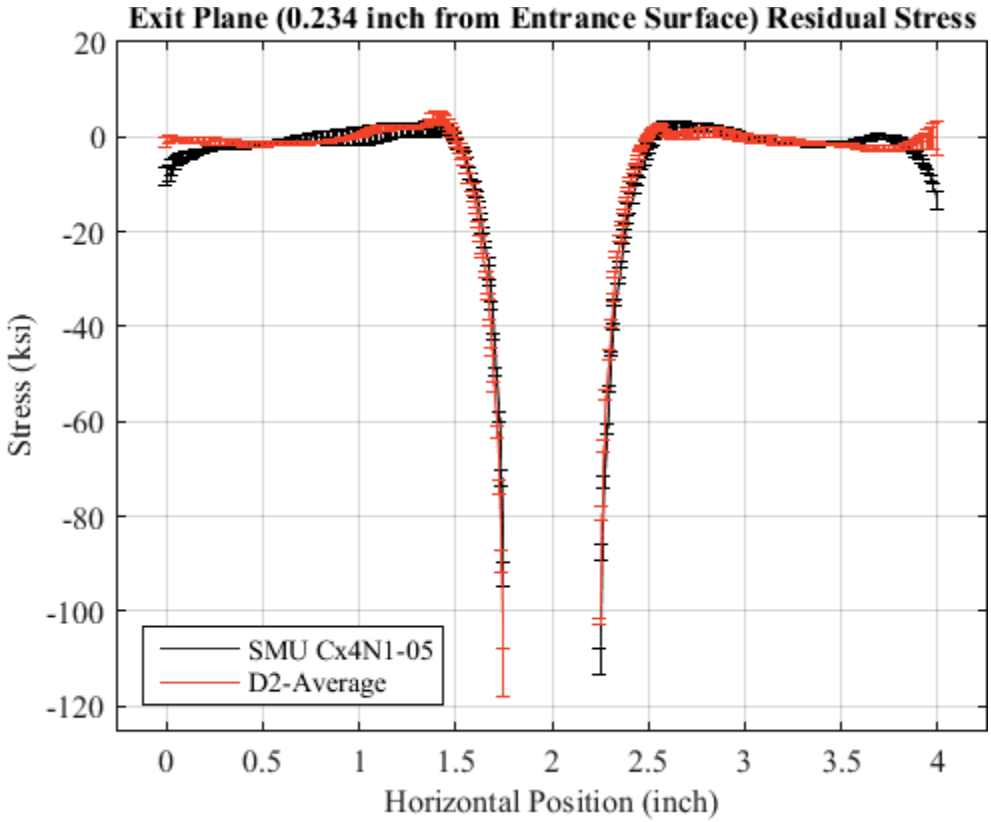

Fig. 602 Residual Stress Line Plot Comparing the Single Measurement Uncertainty of Cx4N1-05-D to the CxD2 (7075-T651) Average Residual Stress at a Distance of 0.234 inch (Exit Surface) from the Entrance Surface – Cx4N1-05-D Coupon had a 0.1253 inch Fatigue Crack at the Left Entrance Surface.

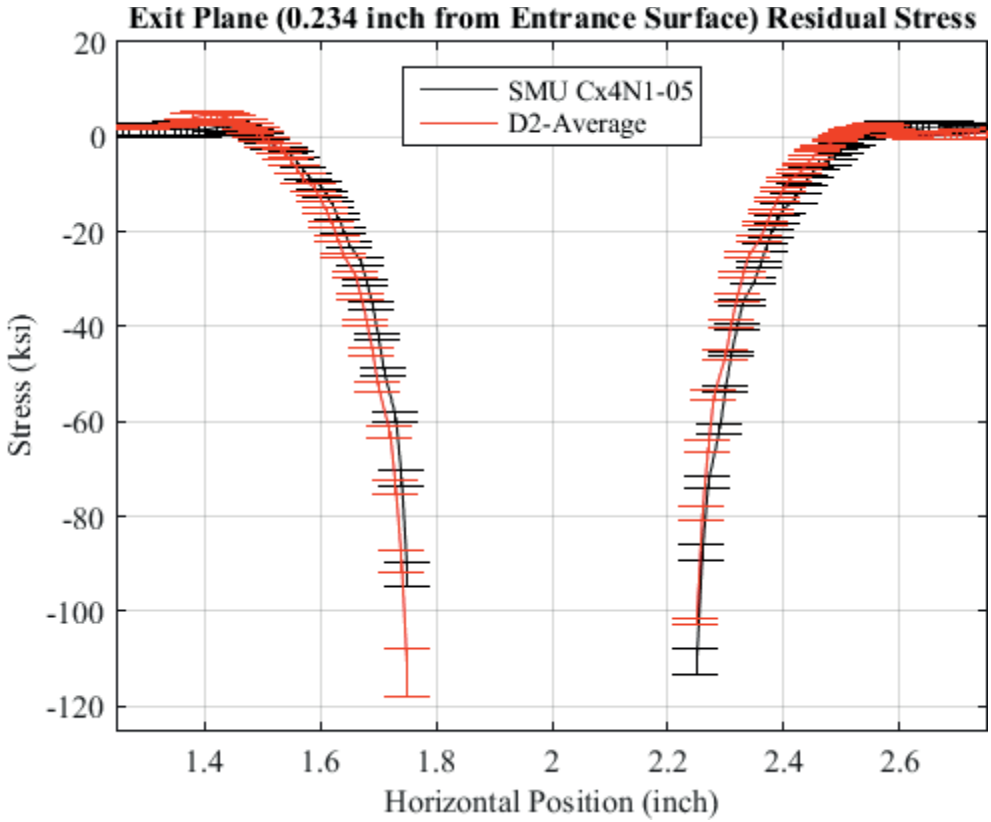

Fig. 603 Residual Stress Line Plot Comparing the Single Measurement Uncertainty of Cx4N1-05-D to the CxD2 (7075-T651) Average Residual Stress at a Distance of 0.234 inch (Exit Surface) from the Entrance Surface – Cx4N1-05-D Coupon had a 0.1253 inch Fatigue Crack at the Left Entrance Surface – Zoomed in Next to Hole.

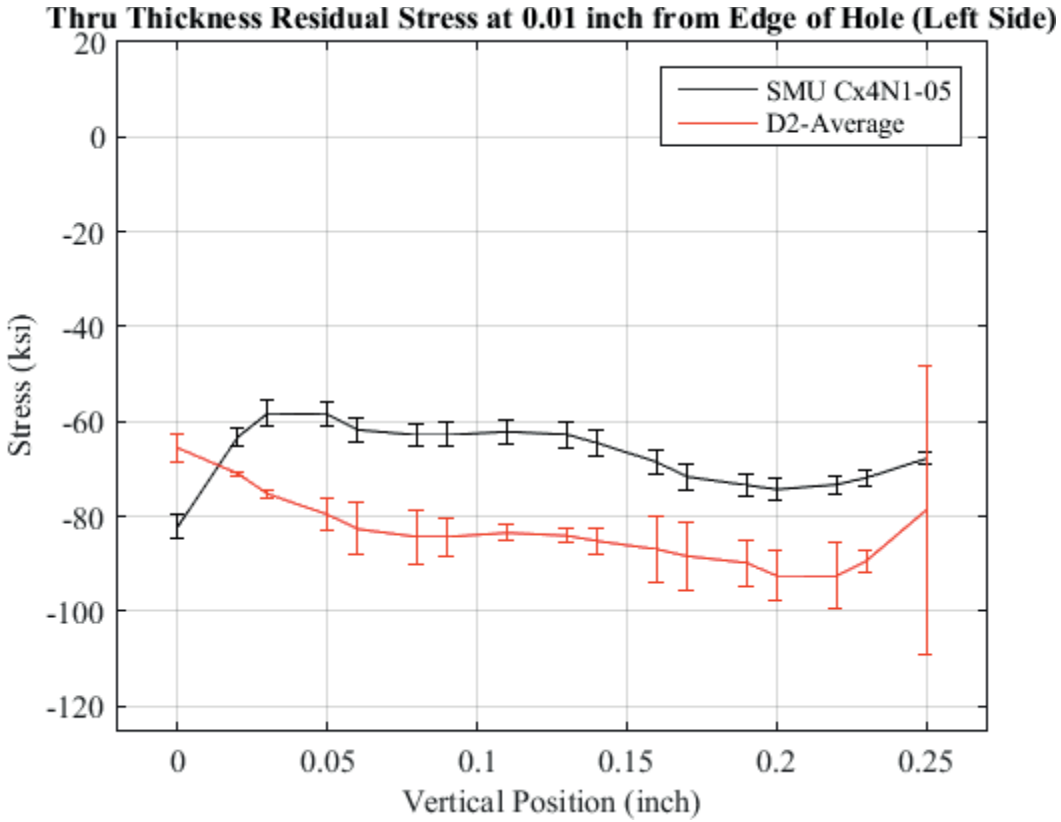

Fig. 604 Residual Stress Through Thickness Line Plot Comparing the Single Measurement Uncertainty of Cx4N1-05-D to the CxD2 (7075-T651) Average Residual Stress at a Distance 0.01 inch from Left Side of Hole – Coupon had a 0.1253 inch Fatigue Crack at the Left Entrance Surface.

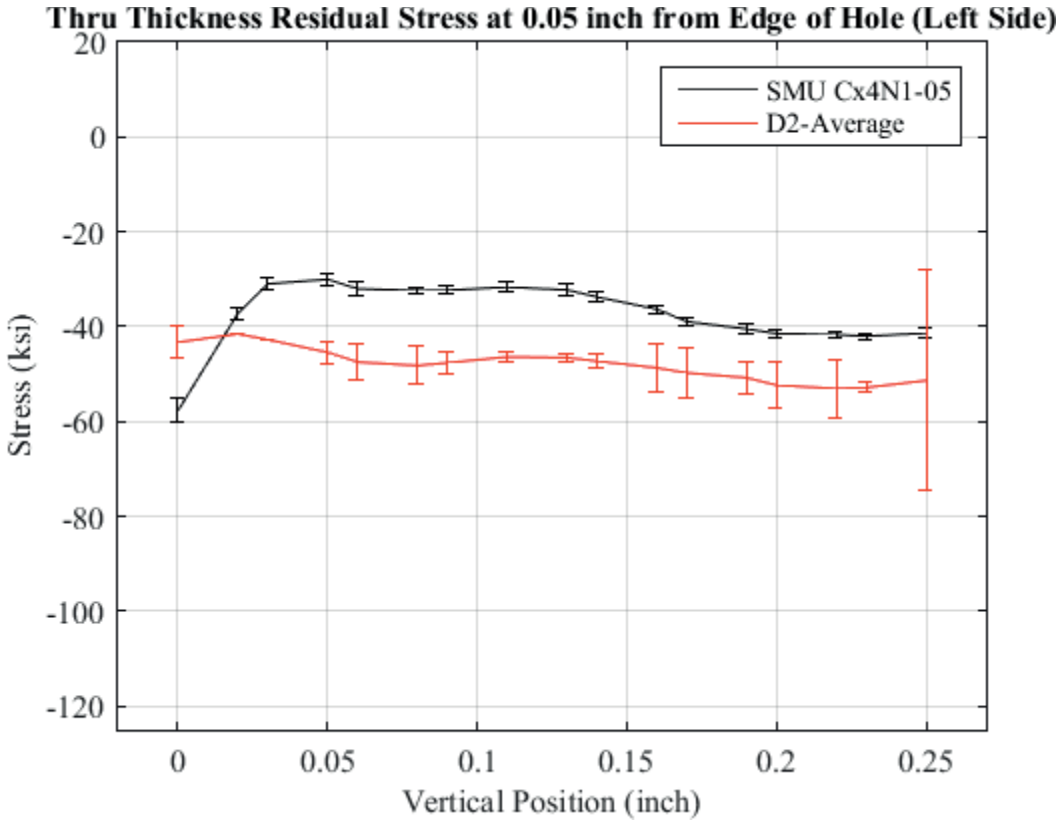

Fig. 605 Residual Stress Through Thickness Line Plot Comparing the Single Measurement Uncertainty of Cx4N1-05-D to the CxD2 (7075-T651) Average Residual Stress at a Distance 0.05 inch from Left Side of Hole – Coupon had a 0.1253 inch Fatigue Crack at the Left Entrance Surface.

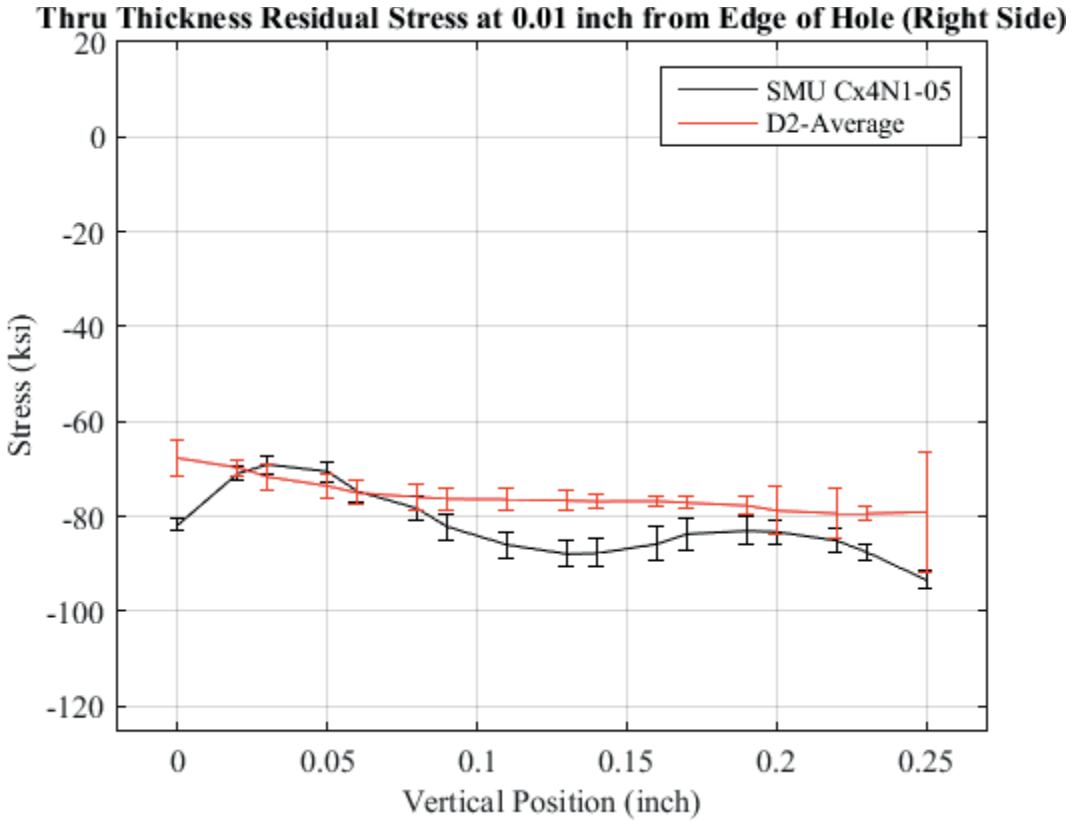

Fig. 606 Residual Stress Through Thickness Line Plot Comparing the Single Measurement Uncertainty of Cx4N1-05-D to the CxD2 (7075-T651) Average Residual Stress at a Distance 0.01 inch from Right Side of Hole – Coupon had a 0.1253 inch Fatigue Crack at the Left Entrance Surface.

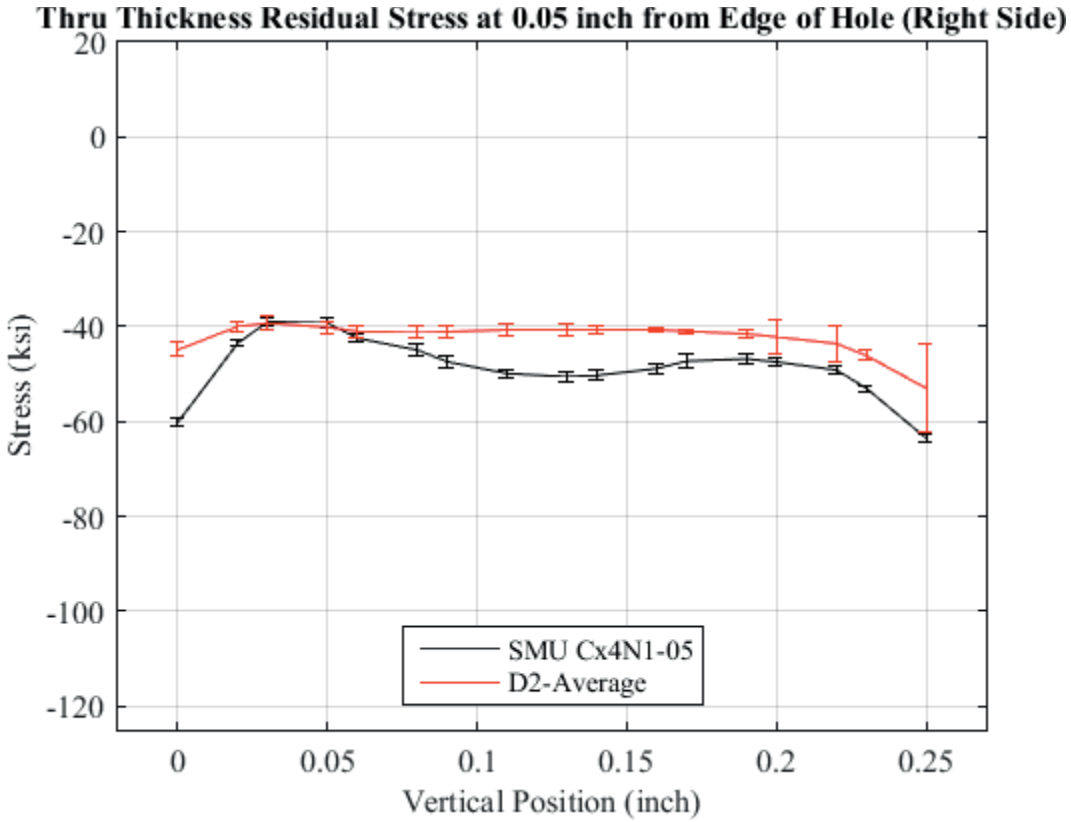

Fig. 607 Residual Stress Through Thickness Line Plot Comparing the Single Measurement Uncertainty of Cx4N1-05-D to the CxD2 (7075-T651) Average Residual Stress at a Distance 0.05 inch from Right Side of Hole – Coupon had a 0.1253 inch Fatigue Crack at the Left Entrance Surface.

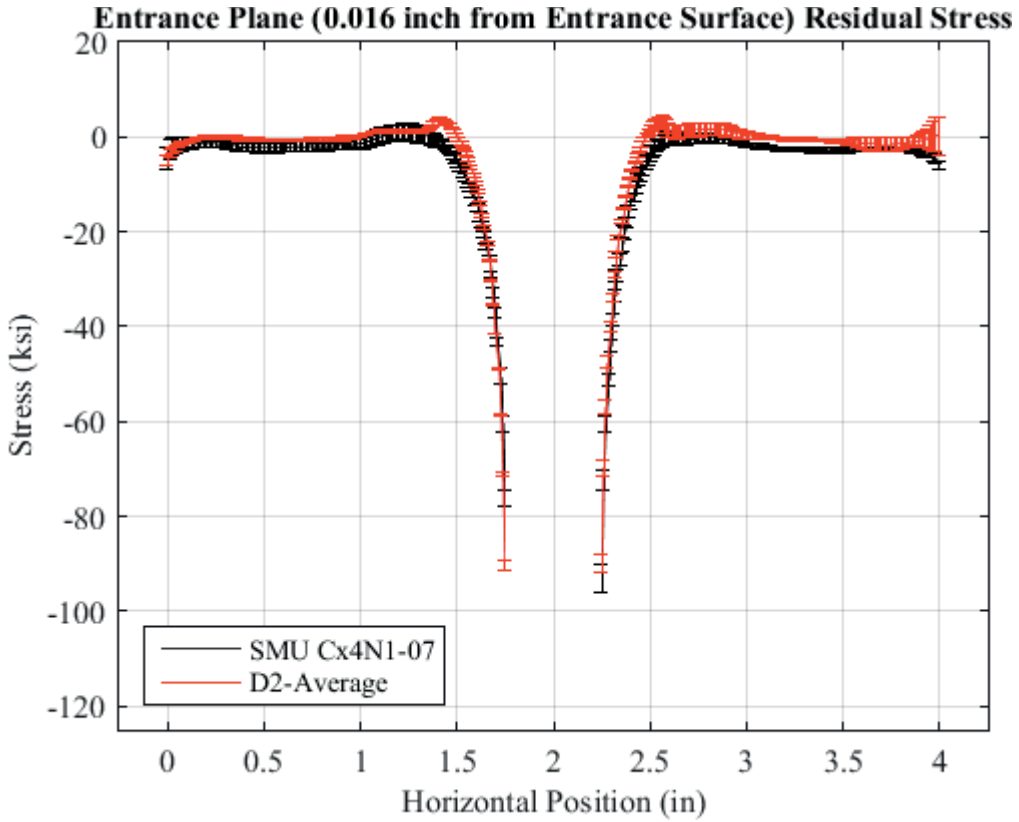

Fig. 608 Residual Stress Line Plot Comparing the Single Measurement Uncertainty of Cx4N1-07-D to the CxD2 (7075-T651) Average Residual Stress at a Distance of 0.016 inch (Entrance Surface) from the Entrance Surface – Cx4N1-07-D Coupon had a 0.2505 inch Fatigue Crack at the Left Entrance Surface.

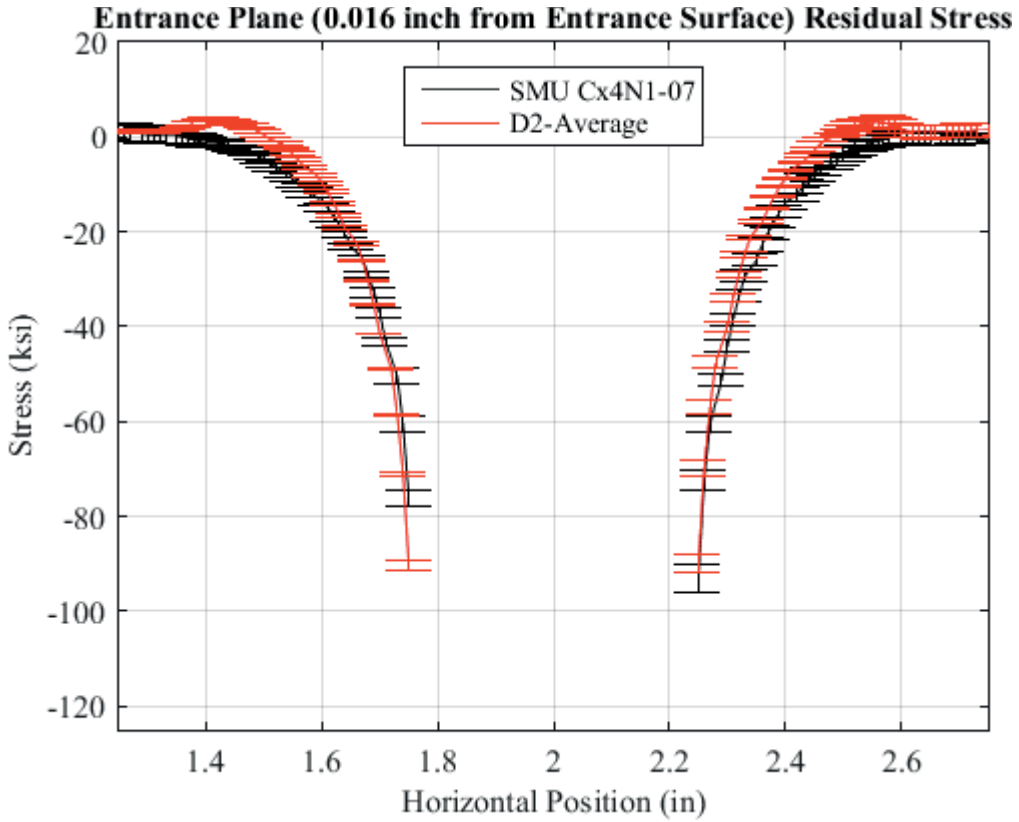

Fig. 609 Residual Stress Line Plot Comparing the Single Measurement Uncertainty of Cx4N1-07-D to the CxD2 (7075-T651) Average Residual Stress at a Distance of 0.016 inch (Entrance Surface) from the Entrance Surface – Cx4N1-07-D Coupon had a 0.2505 inch Fatigue Crack at the Left Entrance Surface – Zoomed in Next to Hole.

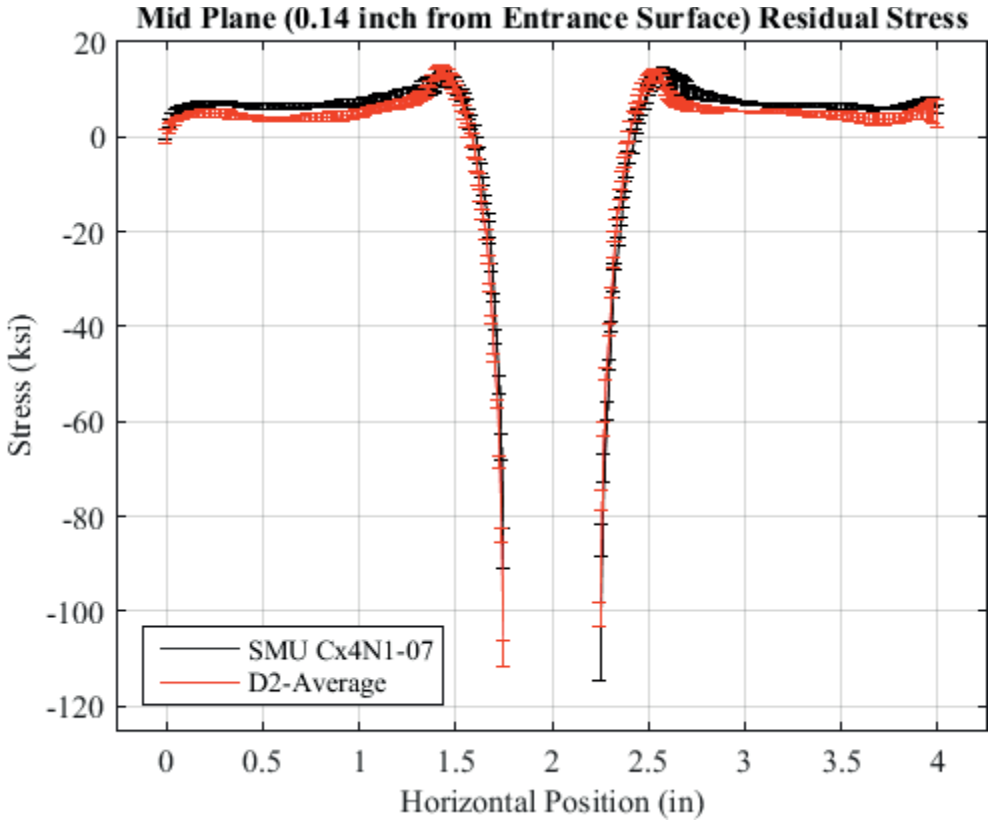

Fig. 610 Residual Stress Line Plot Comparing the Single Measurement Uncertainty of Cx4N1-07-D to the CxD2 (7075-T651) Average Residual Stress at a Distance of 0.140 inch (Mid Plane Surface) from the Entrance Surface – Cx4N1-07-D Coupon had a 0.2505 inch Fatigue Crack at the Left Entrance Surface.

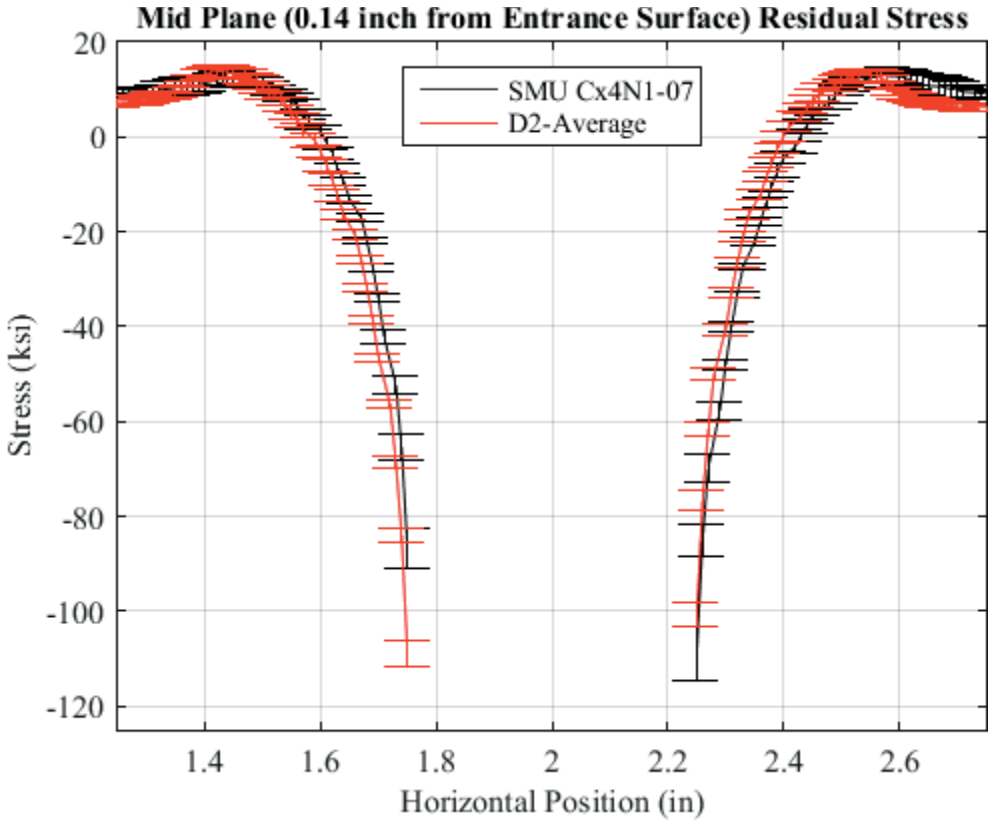

Fig. 611 Residual Stress Line Plot Comparing the Single Measurement Uncertainty of Cx4N1-07-D to the CxD2 (7075-T651) Average Residual Stress at a Distance of 0.140 inch (Mid Plane Surface) from the Entrance Surface – Cx4N1-07-D Coupon had a 0.2505 inch Fatigue Crack at the Left Entrance Surface – Zoomed in Next to Hole.

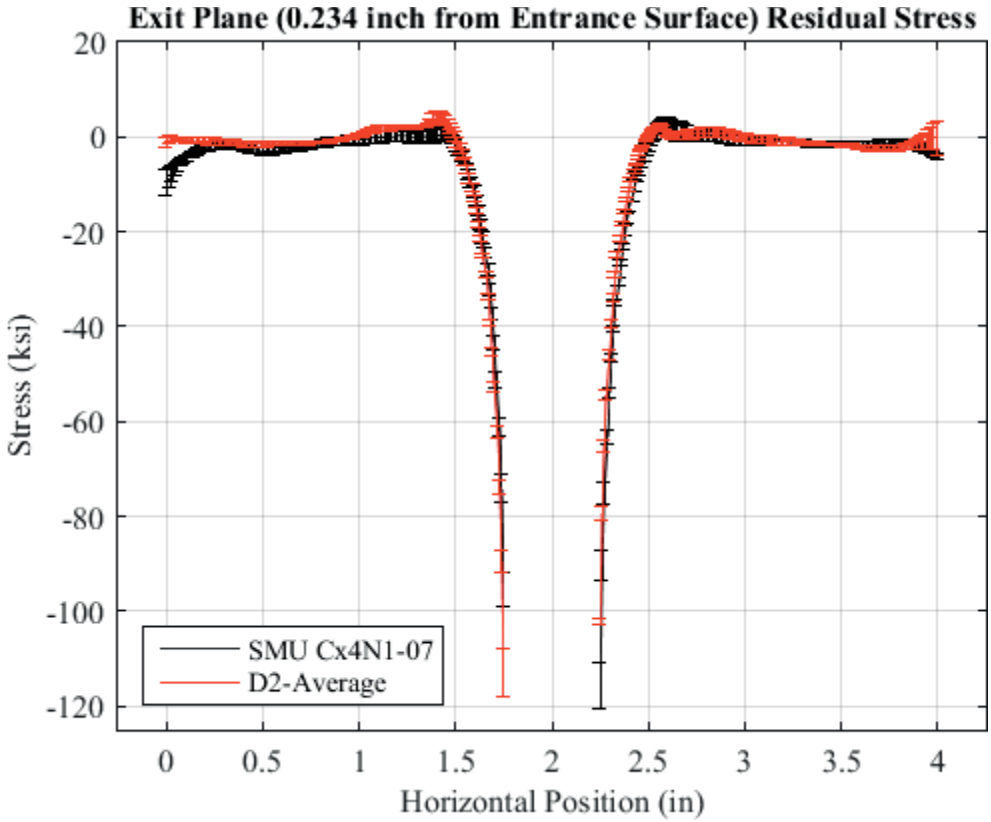

Fig. 612 Residual Stress Line Plot Comparing the Single Measurement Uncertainty of Cx4N1-07-D to the CxD2 (7075-T651) Average Residual Stress at a Distance of 0.234 inch (Exit Surface) from the Entrance Surface – Cx4N1-07-D Coupon had a 0.2505 inch Fatigue Crack at the Left Entrance Surface.

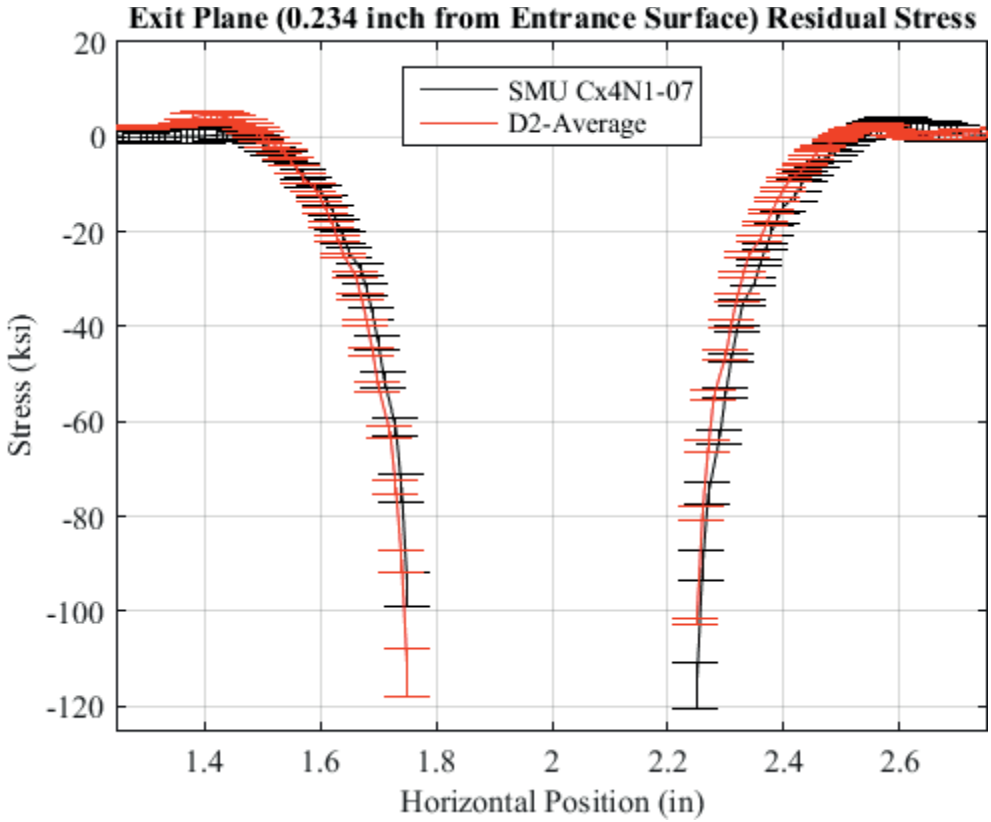

Fig. 613 Residual Stress Line Plot Comparing the Single Measurement Uncertainty of Cx4N1-07-D to the CxD2 (7075-T651) Average Residual Stress at a Distance of 0.234 inch (Exit Surface) from the Entrance Surface – Cx4N1-07-D Coupon had a 0.2505 inch Fatigue Crack at the Left Entrance Surface – Zoomed in Next to Hole.

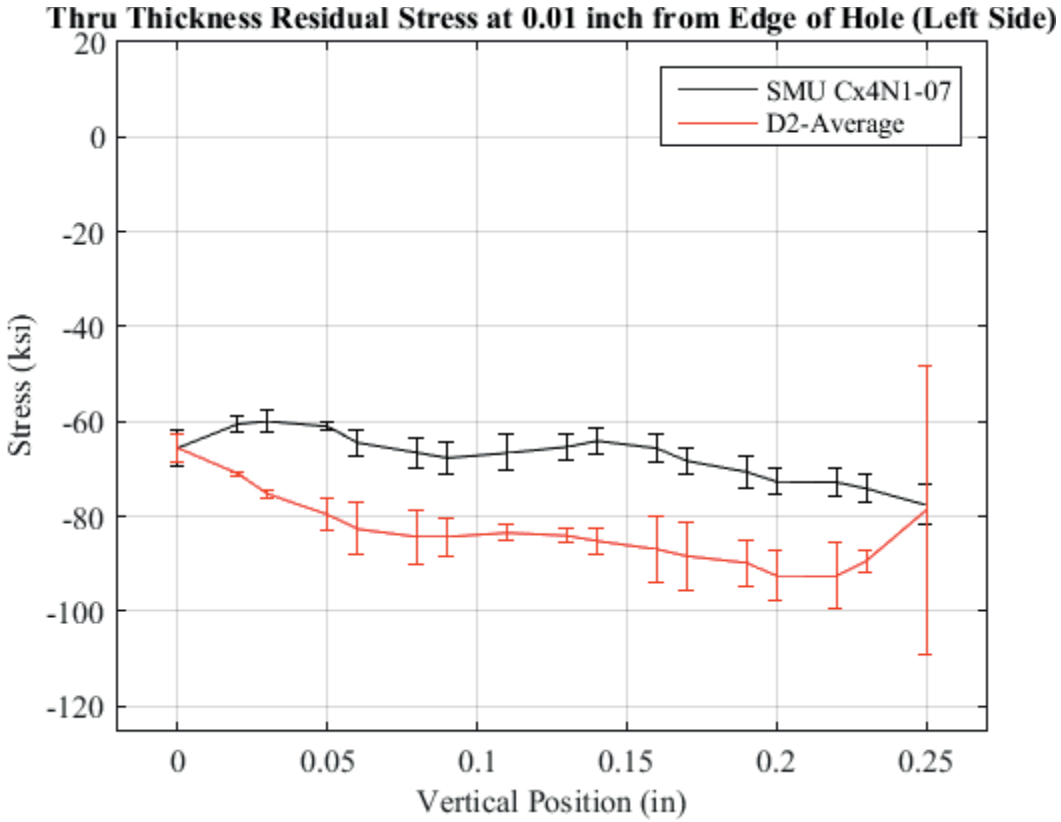

Fig. 614 Residual Stress Through Thickness Line Plot Comparing the Single Measurement Uncertainty of Cx4N1-07-D to the CxD2 (7075-T651) Average Residual Stress at a Distance 0.01 inch from Left Side of Hole – Coupon had a 0.2505 inch Fatigue Crack at the Left Entrance Surface.

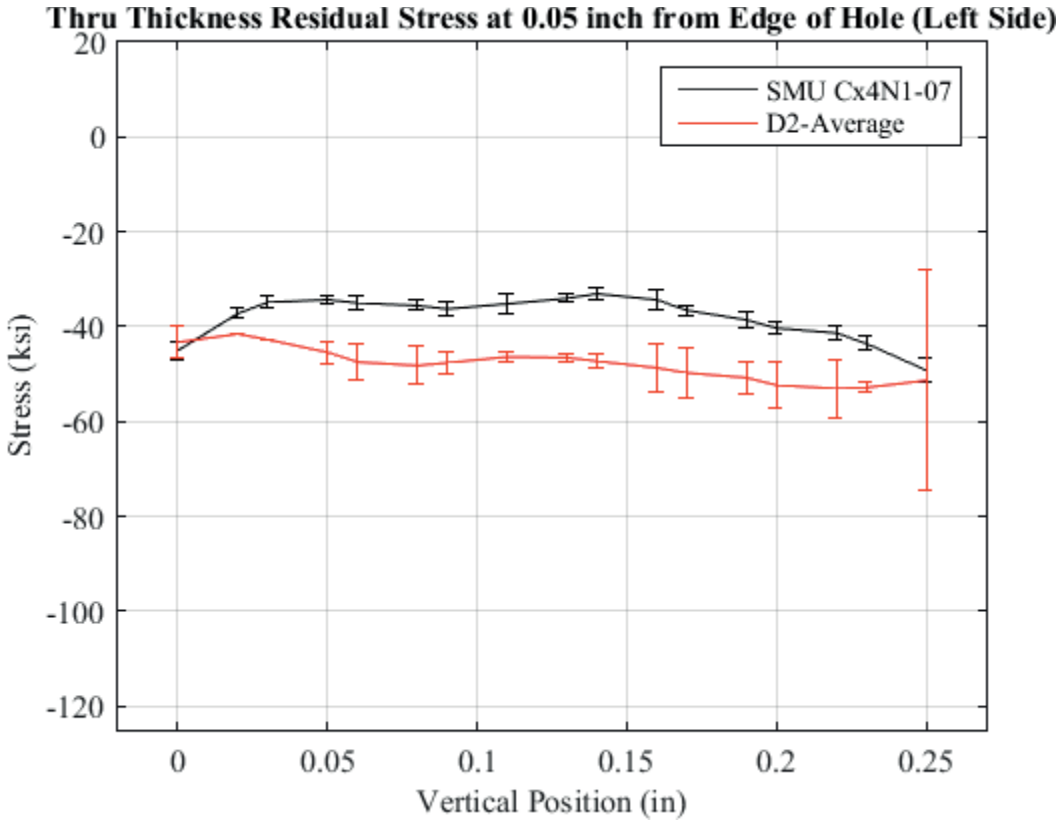

Fig. 615 Residual Stress Through Thickness Line Plot Comparing the Single Measurement Uncertainty of Cx4N1-07-D to the CxD2 (7075-T651) Average Residual Stress at a Distance 0.05 inch from Left Side of Hole – Coupon had a 0.2505 inch Fatigue Crack at the Left Entrance Surface.

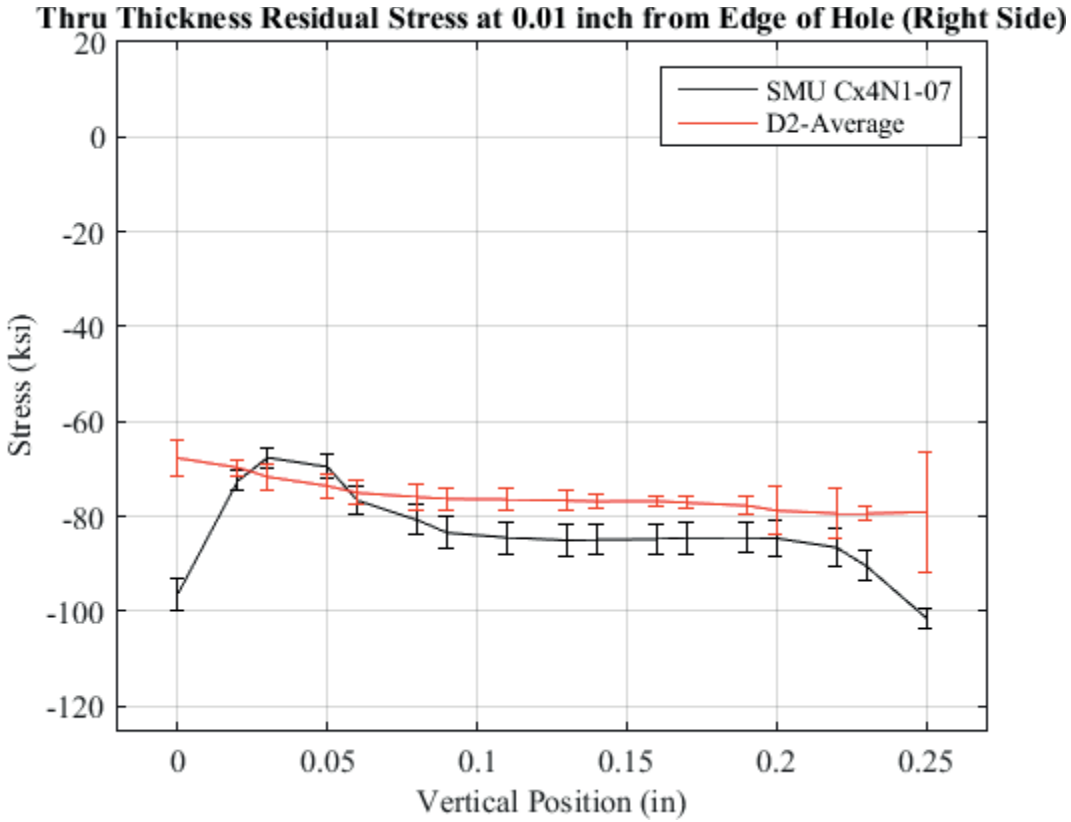

Fig. 616 Residual Stress Through Thickness Line Plot Comparing the Single Measurement Uncertainty of Cx4N1-07-D to the CxD2 (7075-T651) Average Residual Stress at a Distance 0.01 inch from Right Side of Hole – Coupon had a 0.2505 inch Fatigue Crack at the Left Entrance Surface.

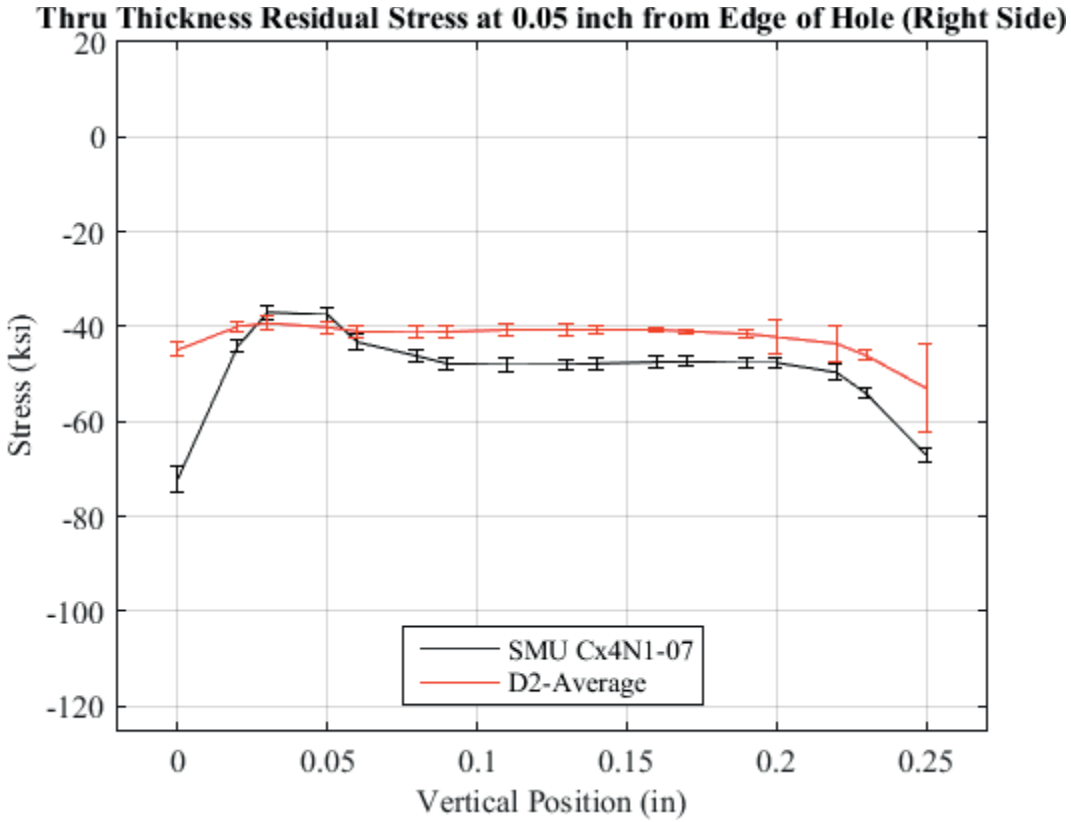

Fig. 617 Residual Stress Through Thickness Line Plot Comparing the Single Measurement Uncertainty of Cx4N1-07-D to the CxD2 (7075-T651) Average Residual Stress at a Distance 0.05 inch from Right Side of Hole – Coupon had a 0.2505 inch Fatigue Crack at the Left Entrance Surface.

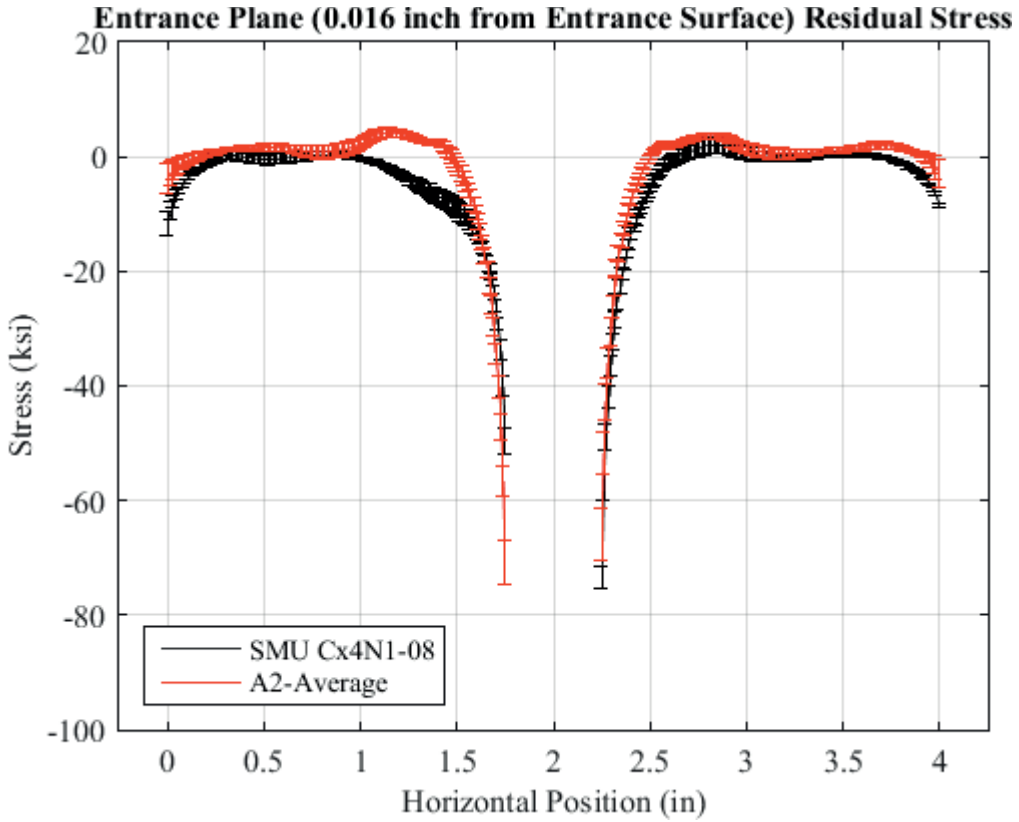

Fig. 618 Residual Stress Line Plot Comparing the Single Measurement Uncertainty of Cx4N1-08-D to the CxD2 (7075-T651) Average Residual Stress at a Distance of 0.016 inch (Entrance Surface) from the Entrance Surface – Cx4N1-08-D Coupon had a 0.2505 inch Fatigue Crack at the Left Entrance Surface, a Fatigue Crack was also Present on the Right Side of the Hole of a Surface Length Less that 0.05 inch.

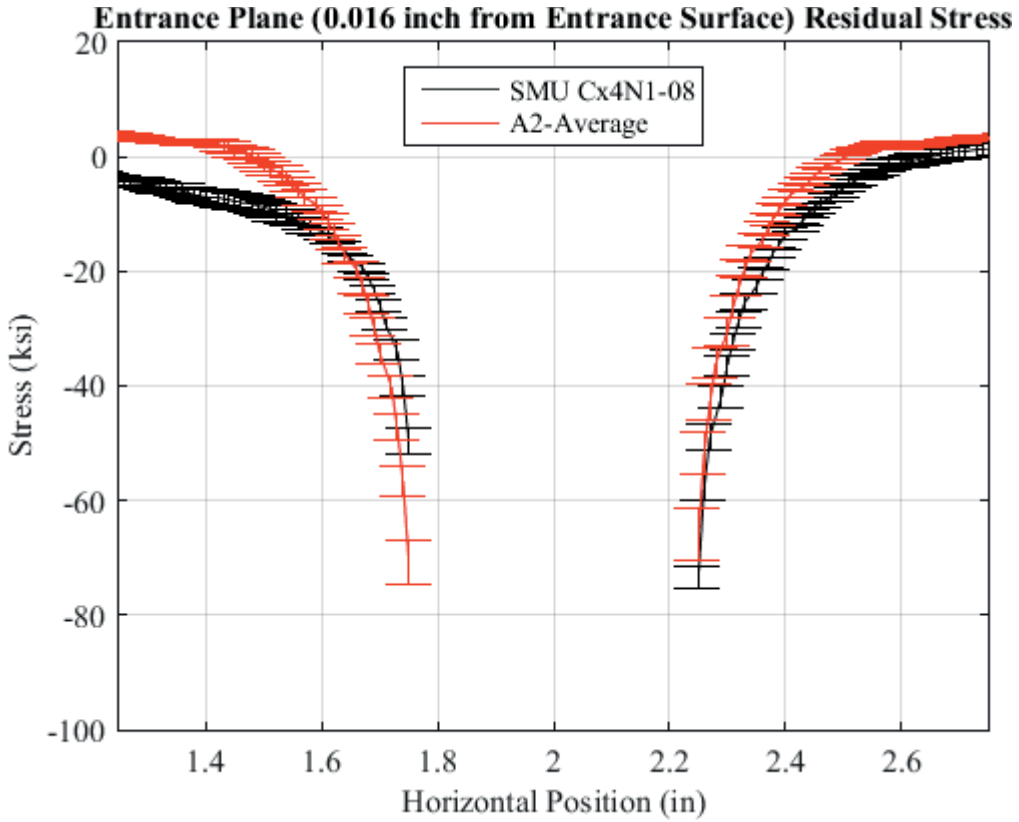

Fig. 619 Residual Stress Line Plot Comparing the Single Measurement Uncertainty of Cx4N1-08-D to the CxD2 (7075-T651) Average Residual Stress at a Distance of 0.016 inch (Entrance Surface) from the Entrance Surface – Cx4N1-08-D Coupon had a 0.2505 inch Fatigue Crack at the Left Entrance Surface, a Fatigue Crack was also Present on the Right Side of the Hole of a Surface Length Less that 0.05 inch – Zoomed in Next to Hole.

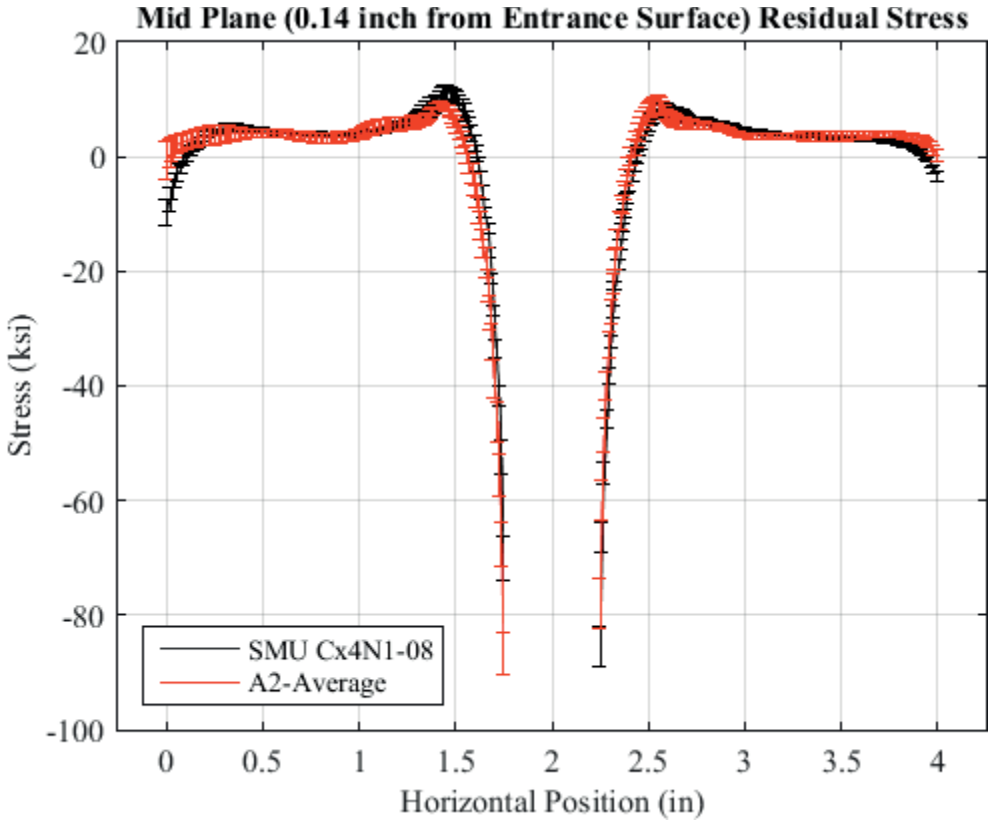

Fig. 620 Residual Stress Line Plot Comparing the Single Measurement Uncertainty of Cx4N1-08-D to the CxD2 (7075-T651) Average Residual Stress at a Distance of 0.140 inch (Mid Plane Surface) from the Entrance Surface – Cx4N1-08-D Coupon had a 0.2505 inch Fatigue Crack at the Left Entrance Surface, a Fatigue Crack was also Present on the Right Side of the Hole of a Surface Length Less that 0.05 inch.

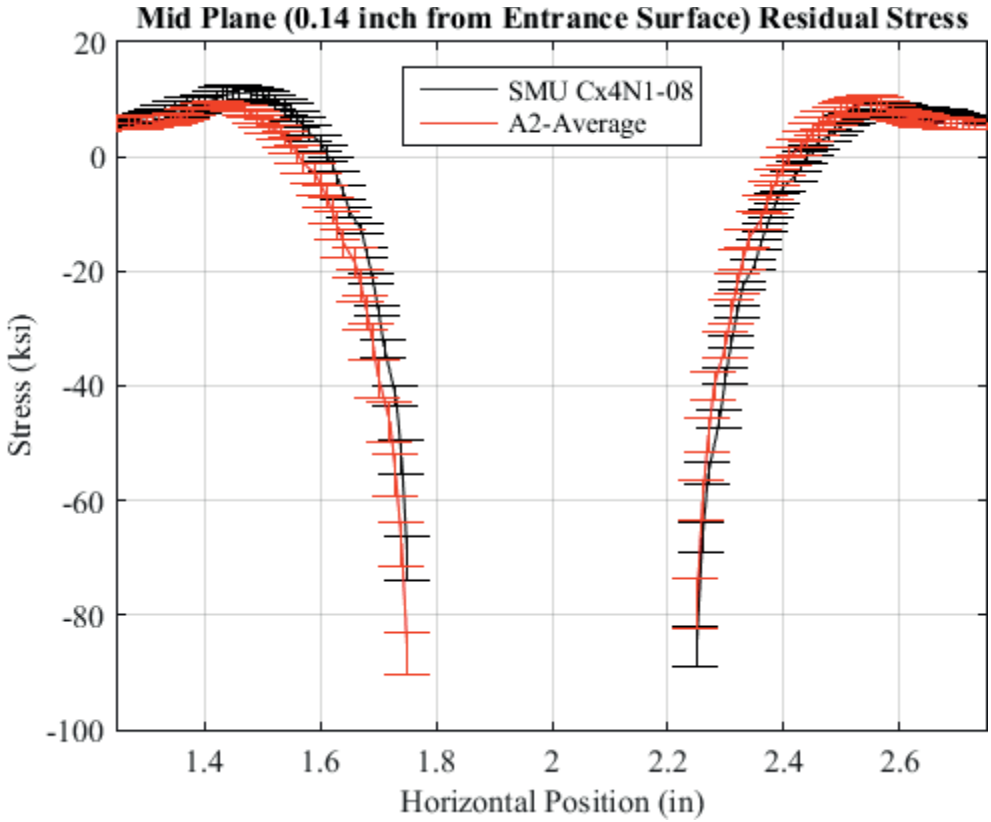

Fig. 621 Residual Stress Line Plot Comparing the Single Measurement Uncertainty of Cx4N1-08-D to the CxD2 (7075-T651) Average Residual Stress at a Distance of 0.140 inch (Mid Plane Surface) from the Entrance Surface – Cx4N1-08-D Coupon had a 0.2505 inch Fatigue Crack at the Left Entrance Surface, a Fatigue Crack was also Present on the Right Side of the Hole of a Surface Length Less that 0.05 inch – Zoomed in Next to Hole.

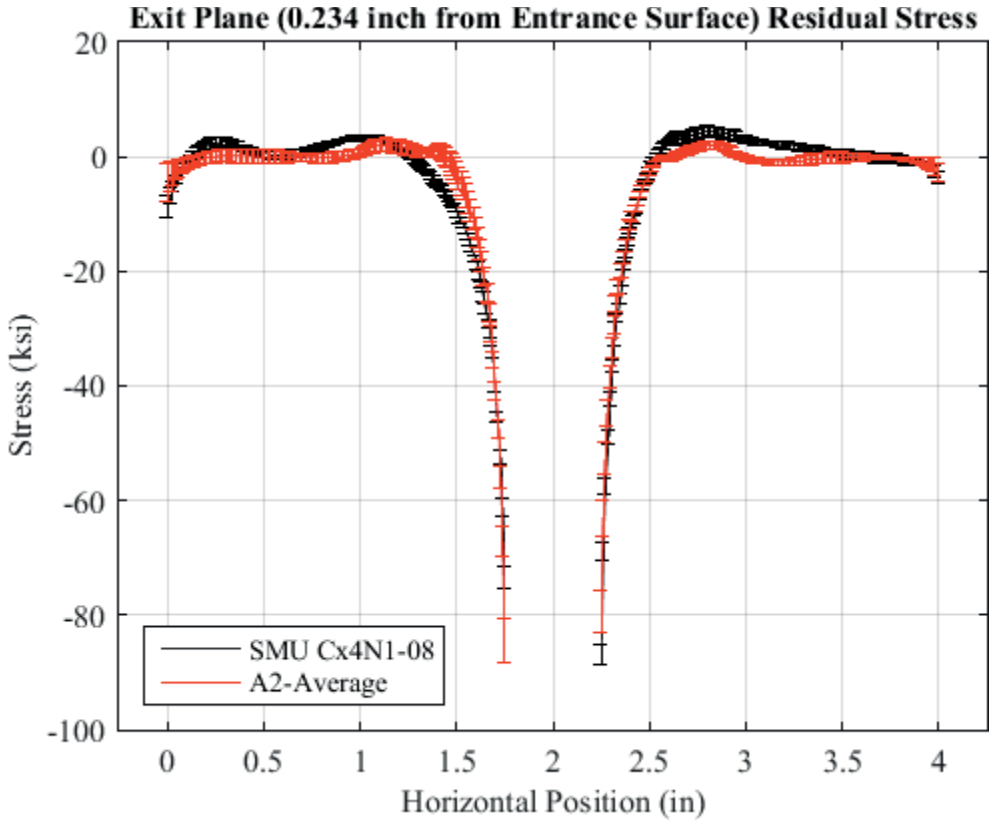

Fig. 622 Residual Stress Line Plot Comparing the Single Measurement Uncertainty of Cx4N1-08-D to the CxD2 (7075-T651) Average Residual Stress at a Distance of 0.234 inch (Exit Surface) from the Entrance Surface – Cx4N1-08-D Coupon had a 0.2505 inch Fatigue Crack at the Left Entrance Surface, a Fatigue Crack was also Present on the Right Side of the Hole of a Surface Length Less that 0.05 inch.

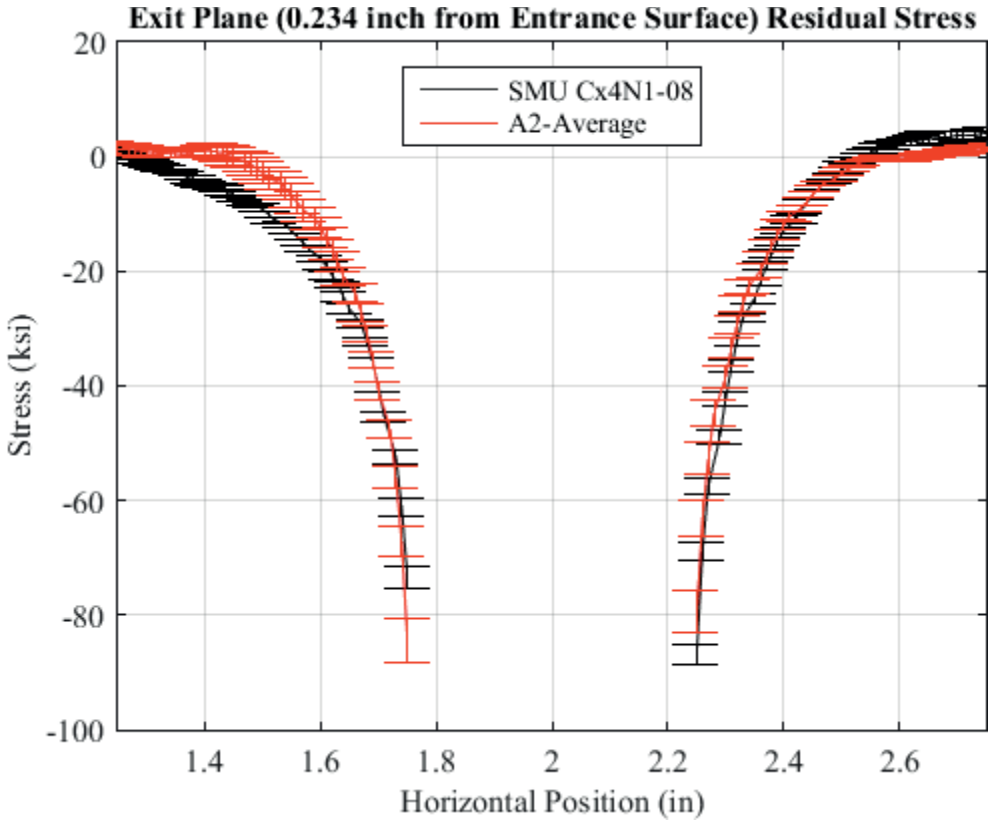

Fig. 623 Residual Stress Line Plot Comparing the Single Measurement Uncertainty of Cx4N1-08-D to the CxD2 (7075-T651) Average Residual Stress at a Distance of 0.234 inch (Exit Surface) from the Entrance Surface – Cx4N1-08-D Coupon had a 0.2505 inch Fatigue Crack at the Left Entrance Surface, a Fatigue Crack was also Present on the Right Side of the Hole of a Surface Length Less that 0.05 inch – Zoomed in Next to Hole.

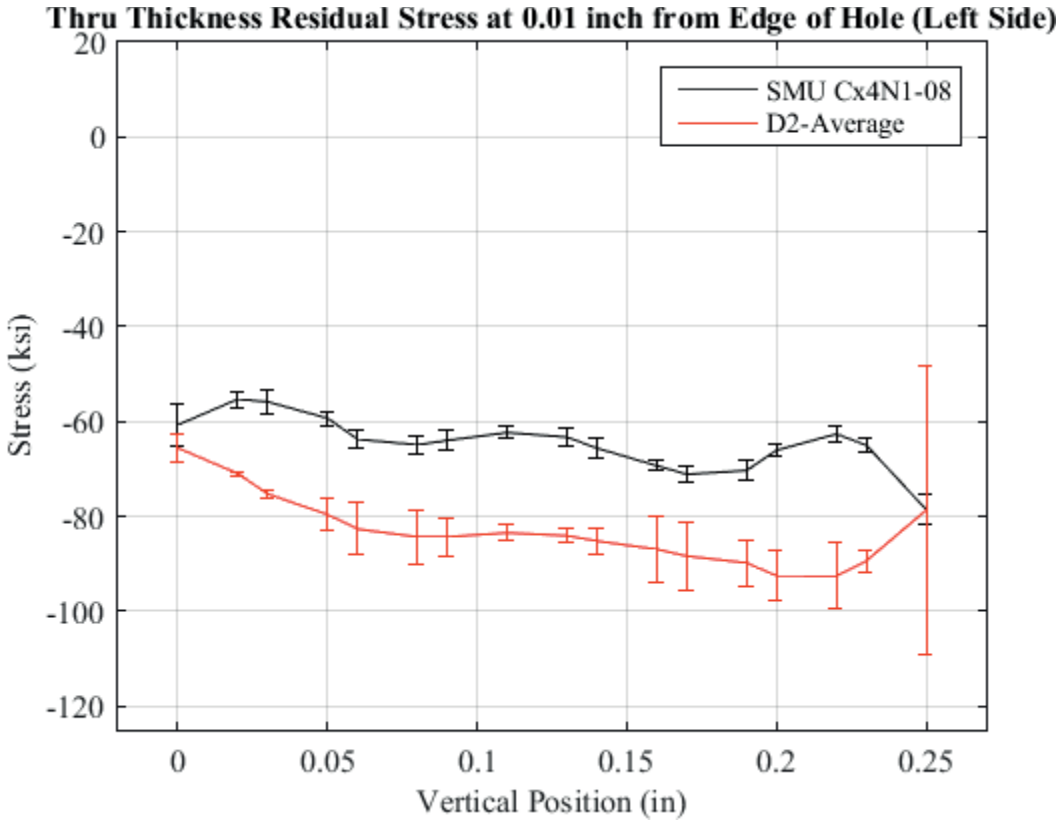

Fig. 624 Residual Stress Through Thickness Line Plot Comparing the Single Measurement Uncertainty of Cx4N1-07-D to the CxD2 (7075-T651) Average Residual Stress at a Distance 0.01 inch from Left Side of Hole – Coupon had a 0.2505 inch Fatigue Crack at the Left Entrance Surface, a Fatigue Crack was also Present on the Right Side of the Hole of a Surface Length Less that 0.05 inch.

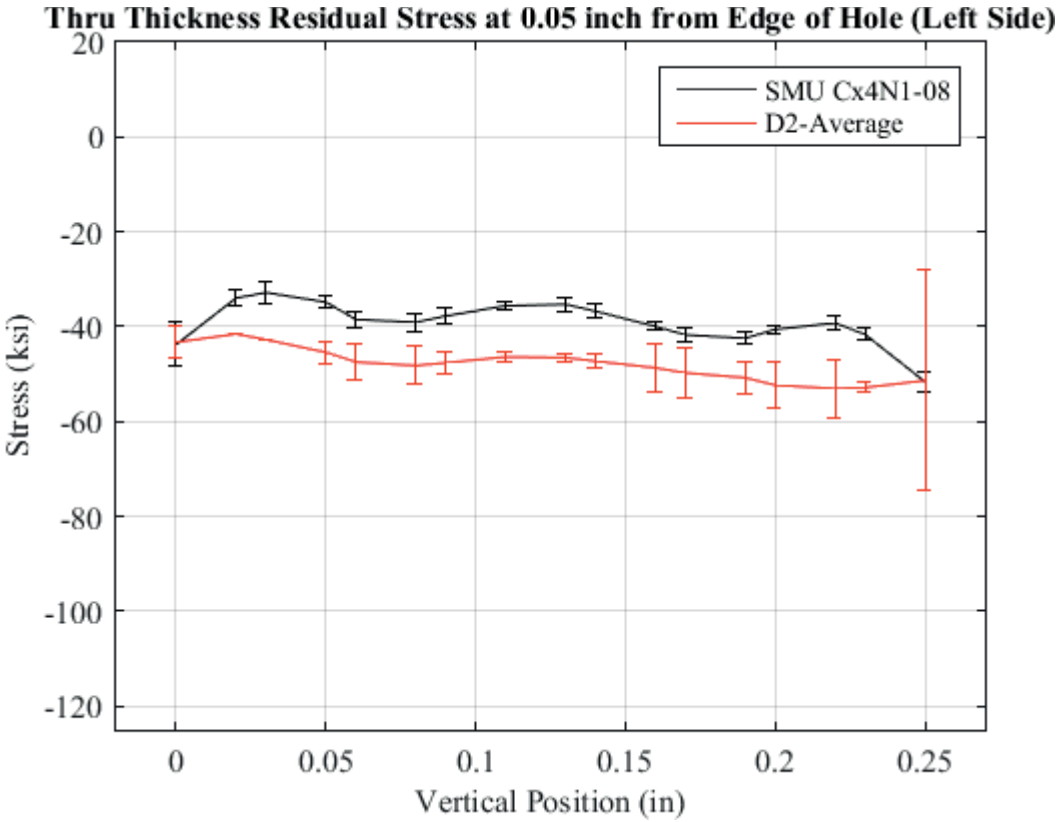

Fig. 625 Residual Stress Through Thickness Line Plot Comparing the Single Measurement Uncertainty of Cx4N1-07-D to the CxD2 (7075-T651) Average Residual Stress at a Distance 0.05 inch from Left Side of Hole – Coupon had a 0.2505 inch Fatigue Crack at the Left Entrance Surface, a Fatigue Crack was also Present on the Right Side of the Hole of a Surface Length Less that 0.05 inch.

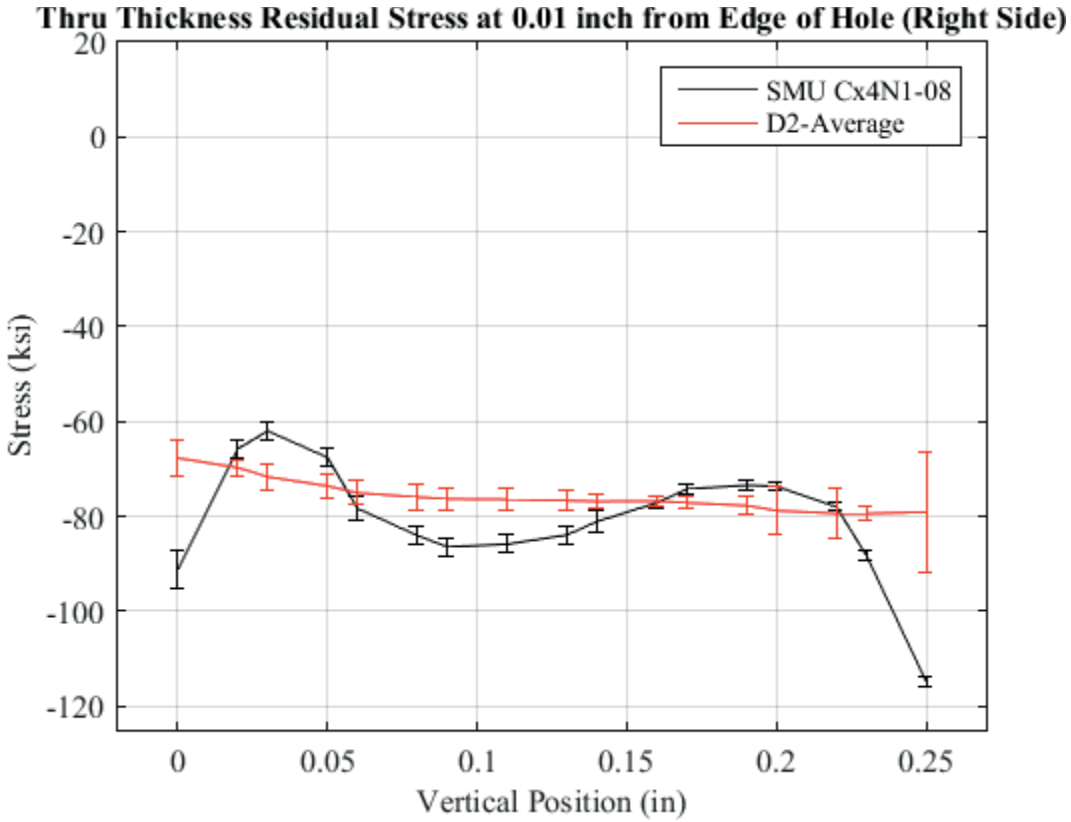

Fig. 626 Residual Stress Through Thickness Line Plot Comparing the Single Measurement Uncertainty of Cx4N1-07-D to the CxD2 (7075-T651) Average Residual Stress at a Distance 0.01 inch from Right Side of Hole – Coupon had a 0.2505 inch Fatigue Crack at the Left Entrance Surface, a Fatigue Crack was also Present on the Right Side of the Hole of a Surface Length Less that 0.05 inch.

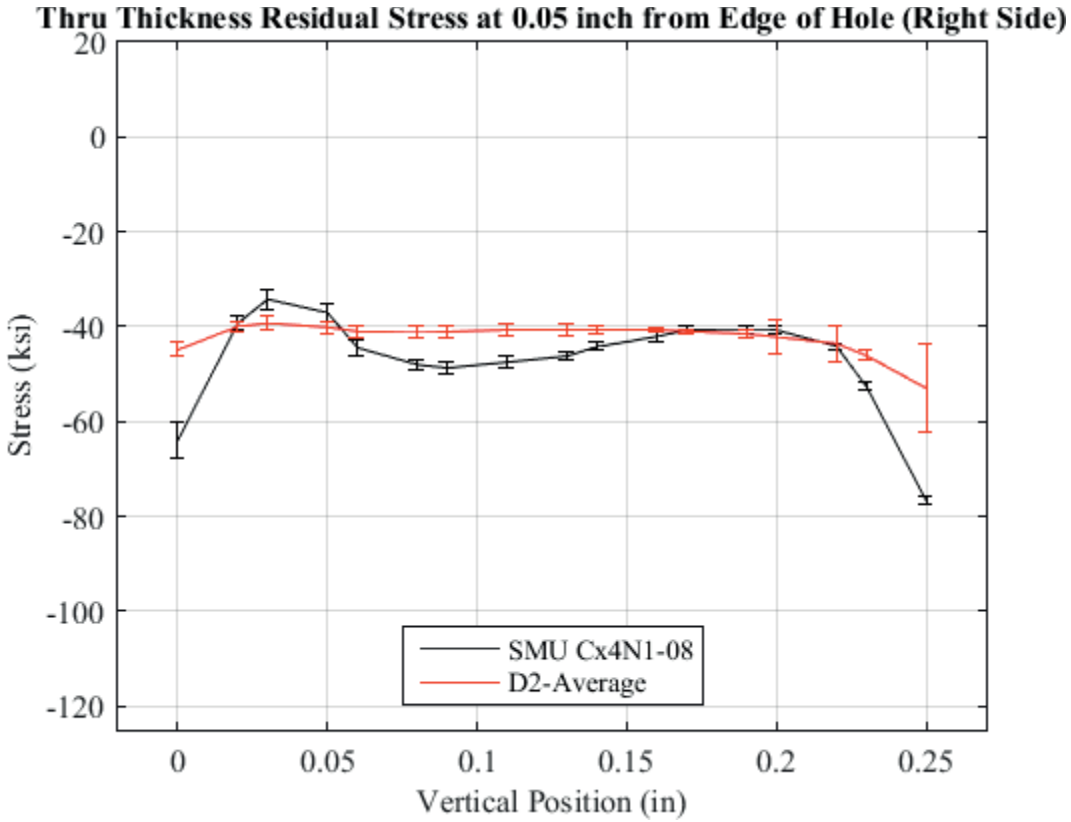

Fig. 627 Residual Stress Through Thickness Line Plot Comparing the Single Measurement Uncertainty of Cx4N1-07-D to the CxD2 (7075-T651) Average Residual Stress at a Distance 0.05 inch from Right Side of Hole – Coupon had a 0.2505 inch Fatigue Crack at the Left Entrance Surface, a Fatigue Crack was also Present on the Right Side of the Hole of a Surface Length Less that 0.05 inch.

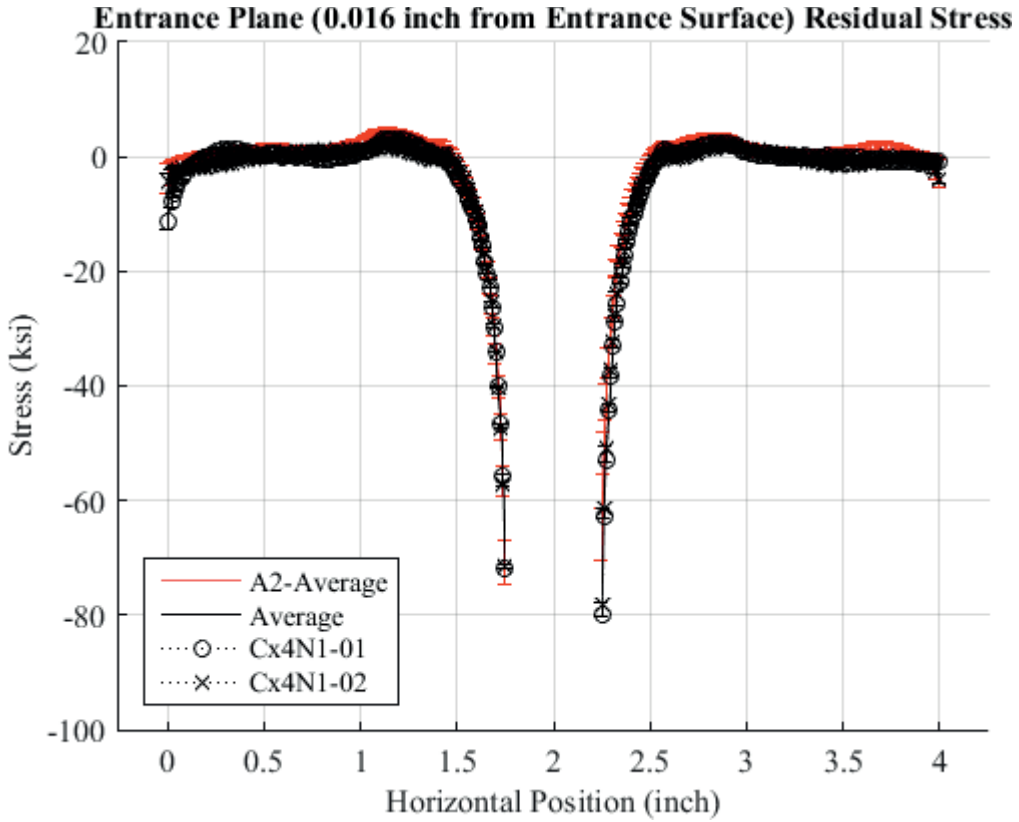

Fig. 628 Residual Stress Line Plot Comparing Cx4N1-01-B, Cx4N1-02-B, and the Average between the Two to the CxA2 (2024-T351) Average Residual Stress at a Distance of 0.016 inch (Entrance Surface) from the Entrance Surface – Cx4N1-01-B and Cx4N1-02-B Coupons had a 0.08 inch Fatigue Crack at the Left Entrance Surface.

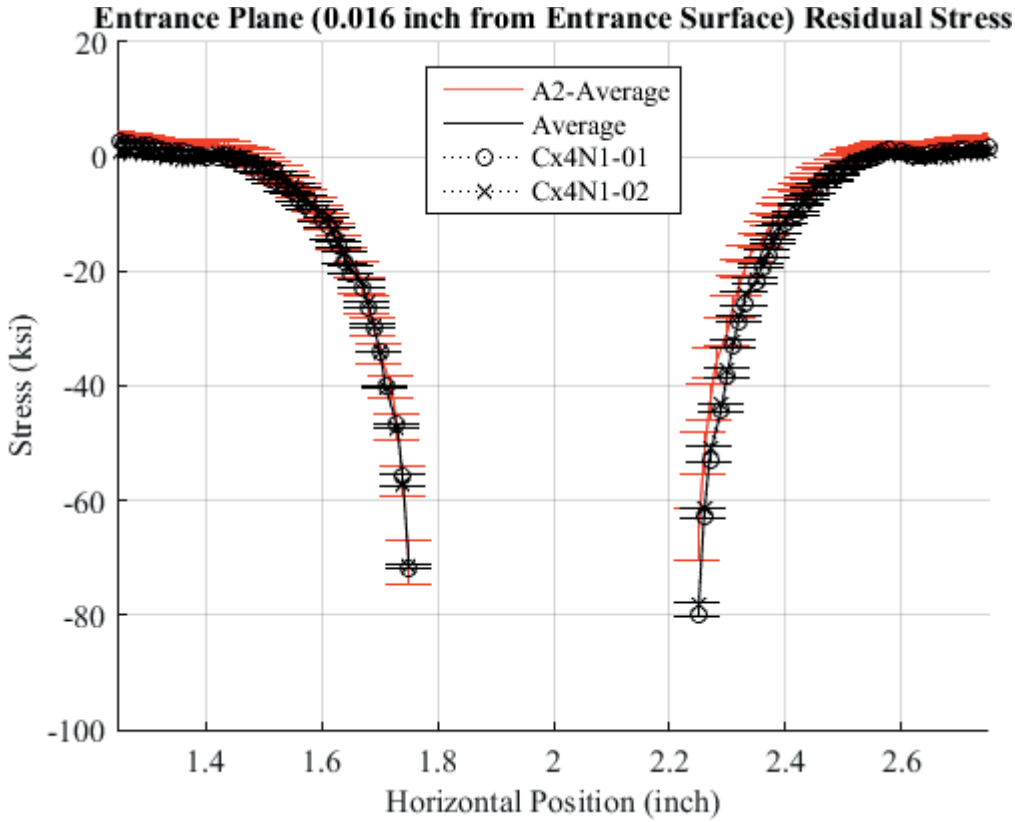

Fig. 629 Residual Stress Line Plot Comparing Cx4N1-01-B, Cx4N1-02-B, and the Average between the Two to the CxA2 (2024-T351) Average Residual Stress at a Distance of 0.016 inch (Entrance Surface) from the Entrance Surface – Cx4N1-01-B and Cx4N1-02-B Coupons had a 0.08 inch Fatigue Crack at the Left Entrance Surface – Zoomed in Next to Hole.

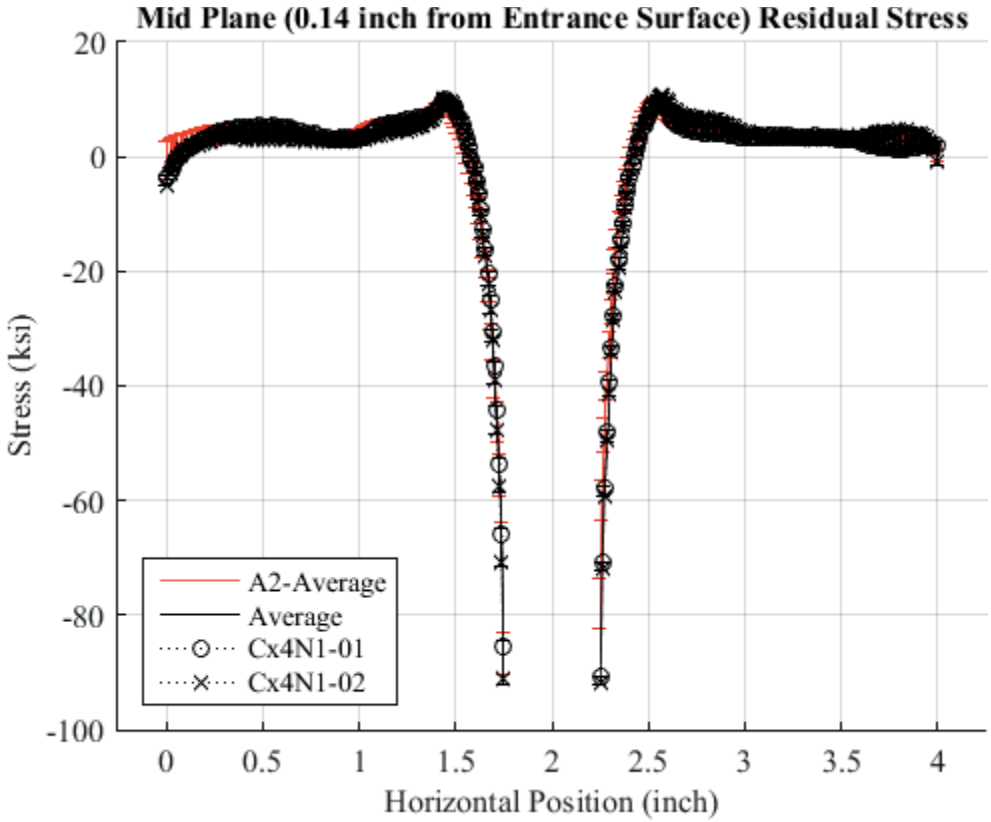

Fig. 630 Residual Stress Line Plot Comparing Cx4N1-01-B, Cx4N1-02-B, and the Average between the Two to the CxA2 (2024-T351) Average Residual Stress at a Distance of 0.140 inch (Mid Plane Surface) from the Entrance Surface – Cx4N1-01-B and Cx4N1-02-B Coupons had a 0.08 inch Fatigue Crack at the Left Entrance Surface.

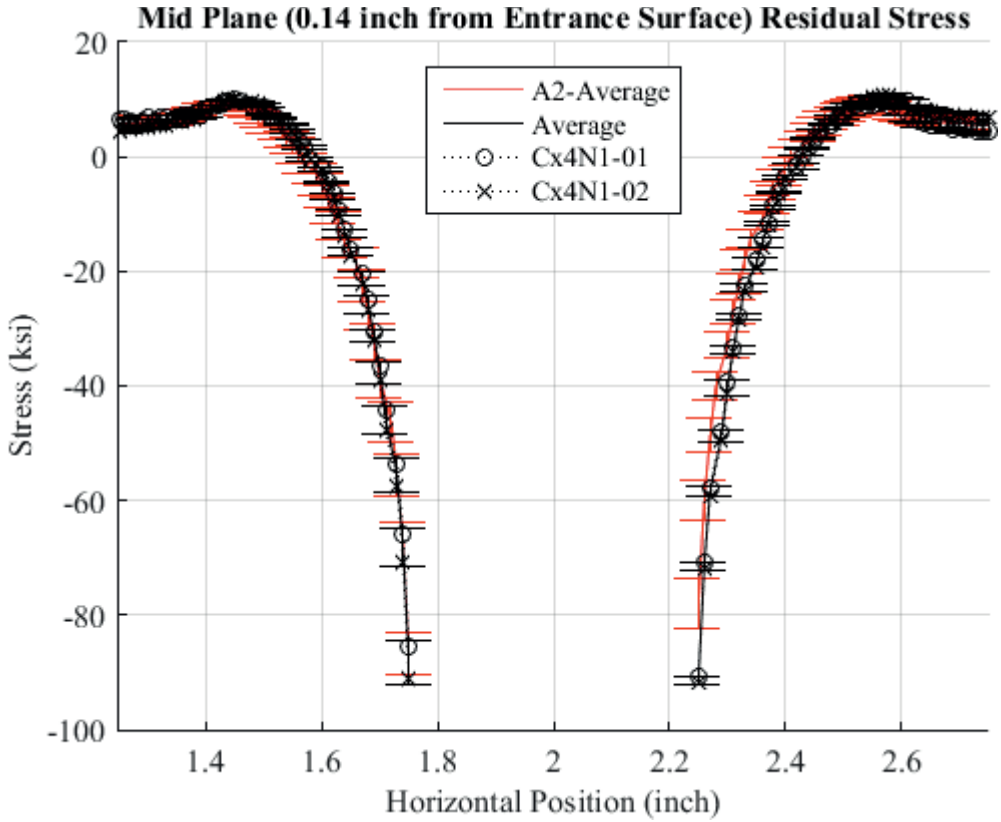

Fig. 631 Residual Stress Line Plot Comparing Cx4N1-01-B, Cx4N1-02-B, and the Average between the Two to the CxA2 (2024-T351) Average Residual Stress at a Distance of 0.140 inch (Mid Plane Surface) from the Entrance Surface – Cx4N1-01-B and Cx4N1-02-B Coupons had a 0.08 inch Fatigue Crack at the Left Entrance Surface – Zoomed in Next to Hole.

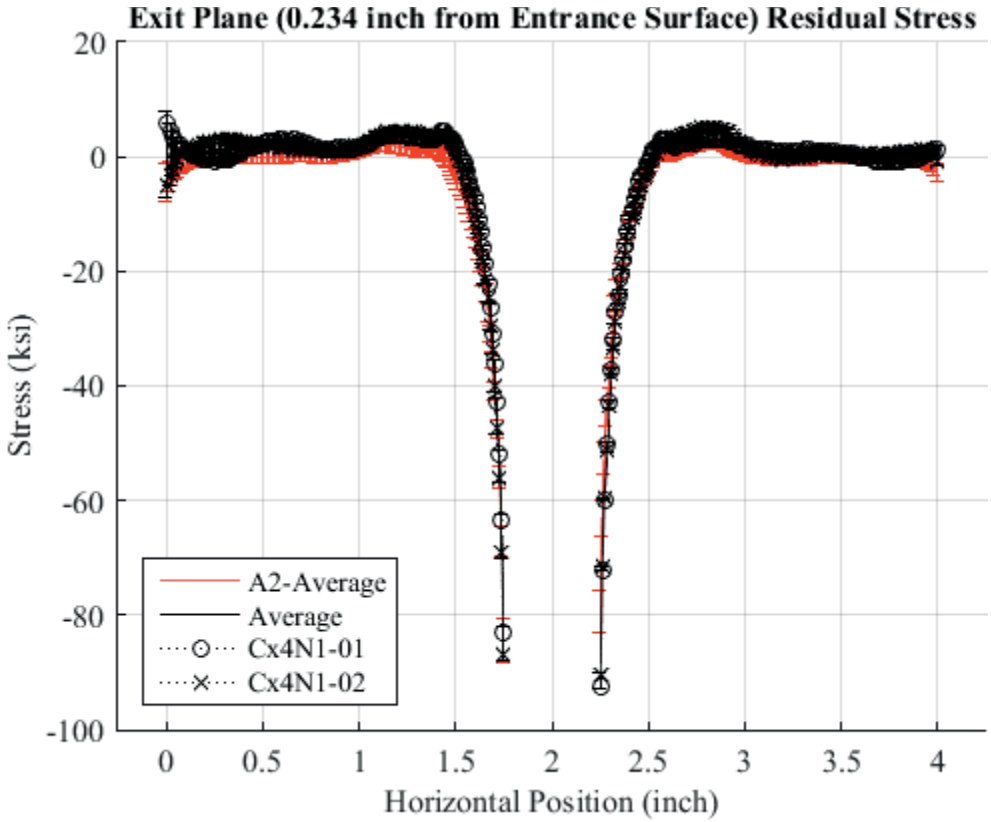

Fig. 632 Residual Stress Line Plot Comparing Cx4N1-01-B, Cx4N1-02-B, and the Average between the Two to the CxA2 (2024-T351) Average Residual Stress at a Distance of 0.234 inch (Exit Surface) from the Entrance Surface – Cx4N1-01-B and Cx4N1-02-B Coupons had a 0.08 inch Fatigue Crack at the Left Entrance Surface.

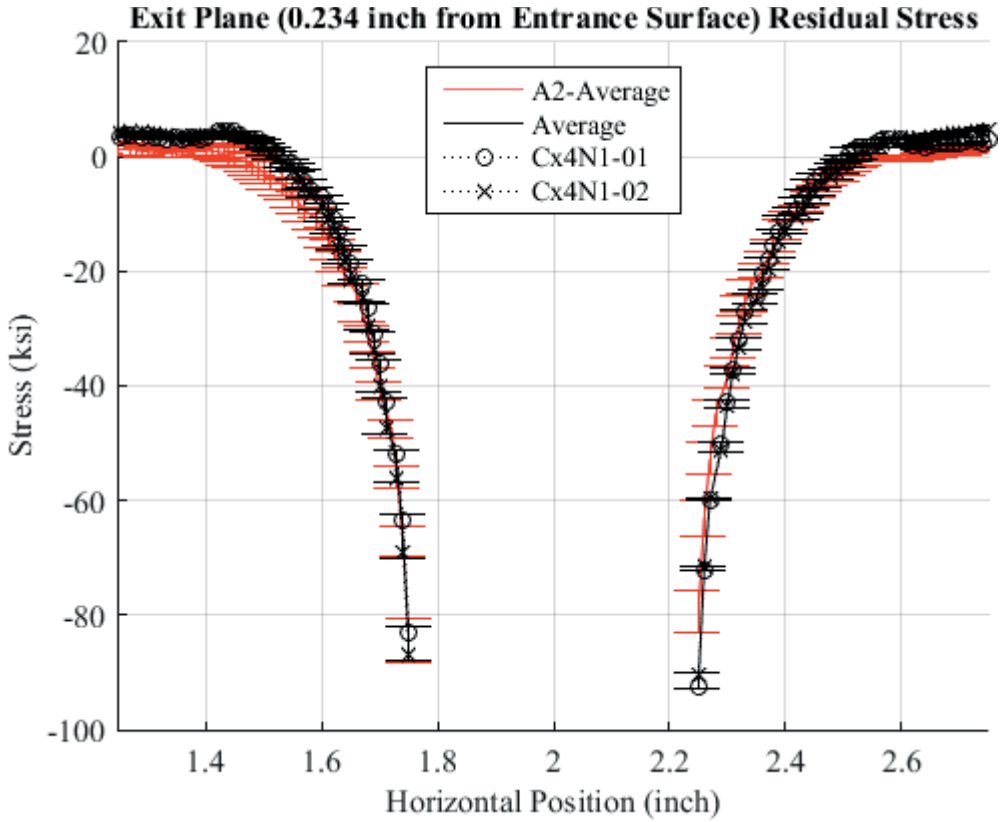

Fig. 633 Residual Stress Line Plot Comparing Cx4N1-01-B, Cx4N1-02-B, and the Average between the Two to the CxA2 (2024-T351) Average Residual Stress at a Distance of 0.234 inch (Exit Surface) from the Entrance Surface – Cx4N1-01-B and Cx4N1-02-B Coupons had a 0.08 inch Fatigue Crack at the Left Entrance Surface – Zoomed in Next to Hole.

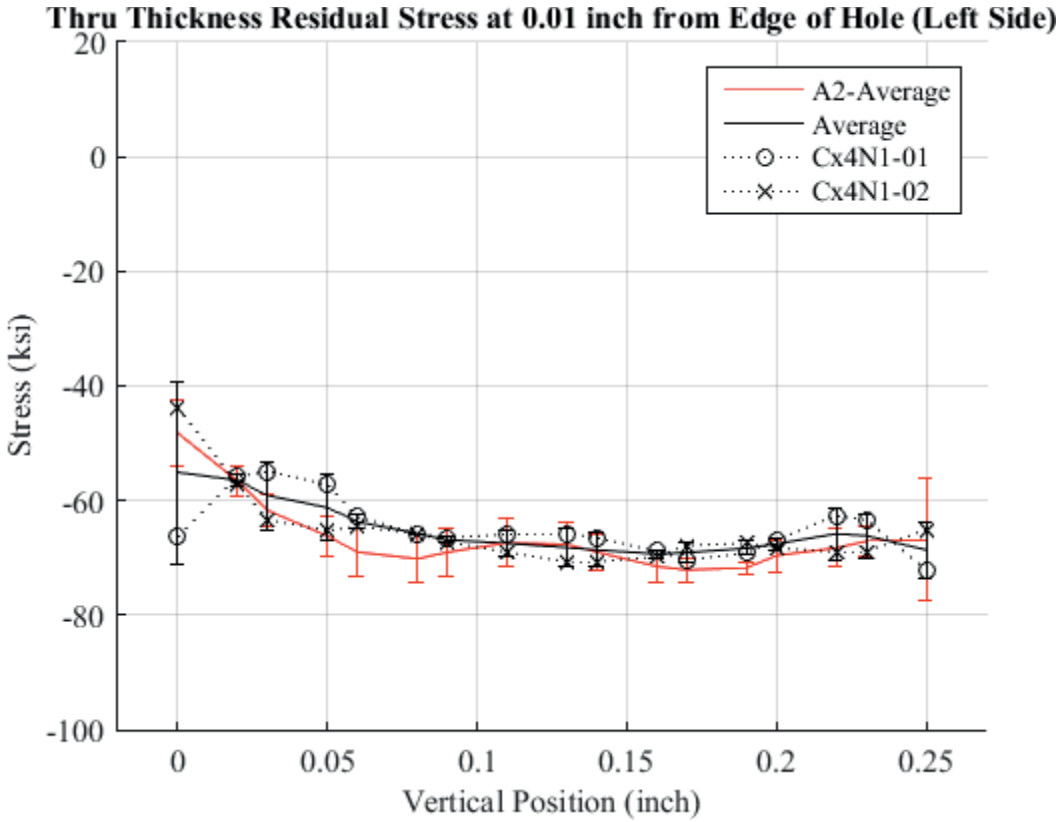

Fig. 634 Residual Stress Through-Thickness Line Plot Comparing Cx4N1-01-B, Cx4N1-02-B, and the Average between the Two to the CxA2 (2024-T351) Average Residual Stress at a Distance of 0.01 inch from the Left Side of the Hole – Cx4N1-01-B and Cx4N1-02-B Coupons had a 0.08 inch Fatigue Crack at the Left Entrance Surface.

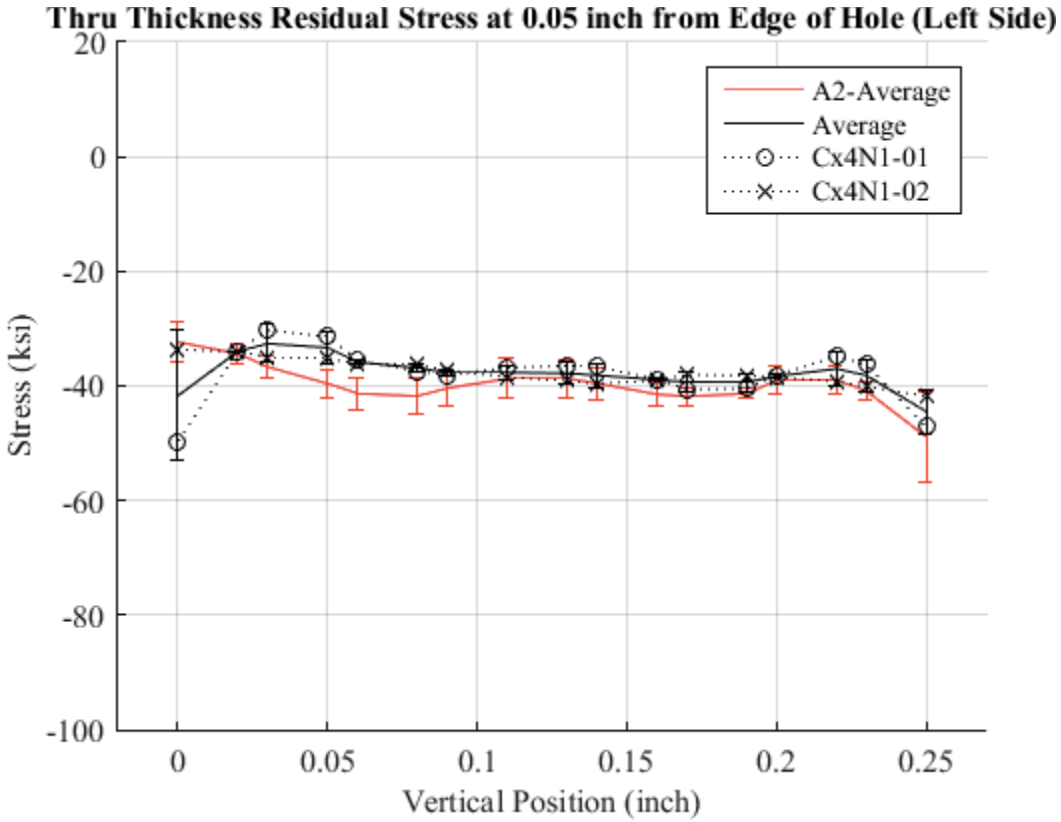

Fig. 635 Residual Stress Through-Thickness Line Plot Comparing Cx4N1-01-B, Cx4N1-02-B, and the Average between the Two to the CxA2 (2024-T351) Average Residual Stress at a Distance of 0.05 inch from the Left Side of the Hole – Cx4N1-01-B and Cx4N1-02-B Coupons had a 0.08 inch Fatigue Crack at the Left Entrance Surface.

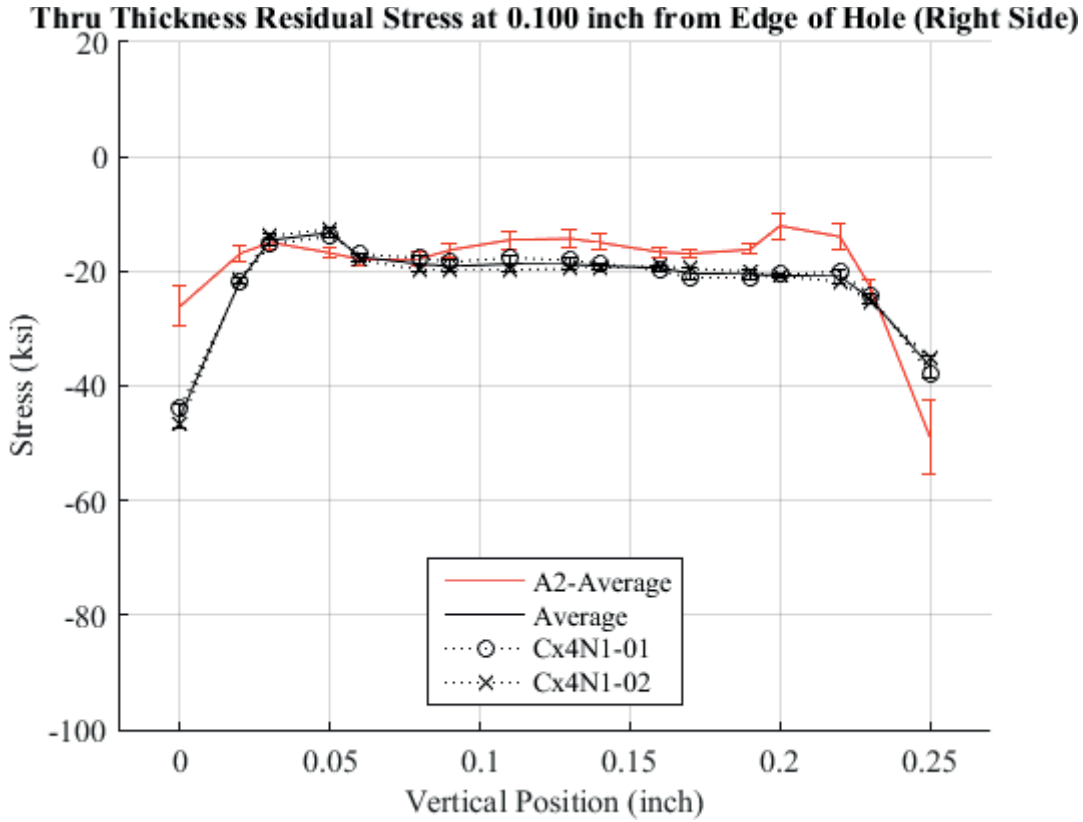

Fig. 636 Residual Stress Through-Thickness Line Plot Comparing Cx4N1-01-B, Cx4N1-02-B, and the Average between the Two to the CxA2 (2024-T351) Average Residual Stress at a Distance of 0.10 inch from the Left Side of the Hole – Cx4N1-01-B and Cx4N1-02-B Coupons had a 0.08 inch Fatigue Crack at the Left Entrance Surface.

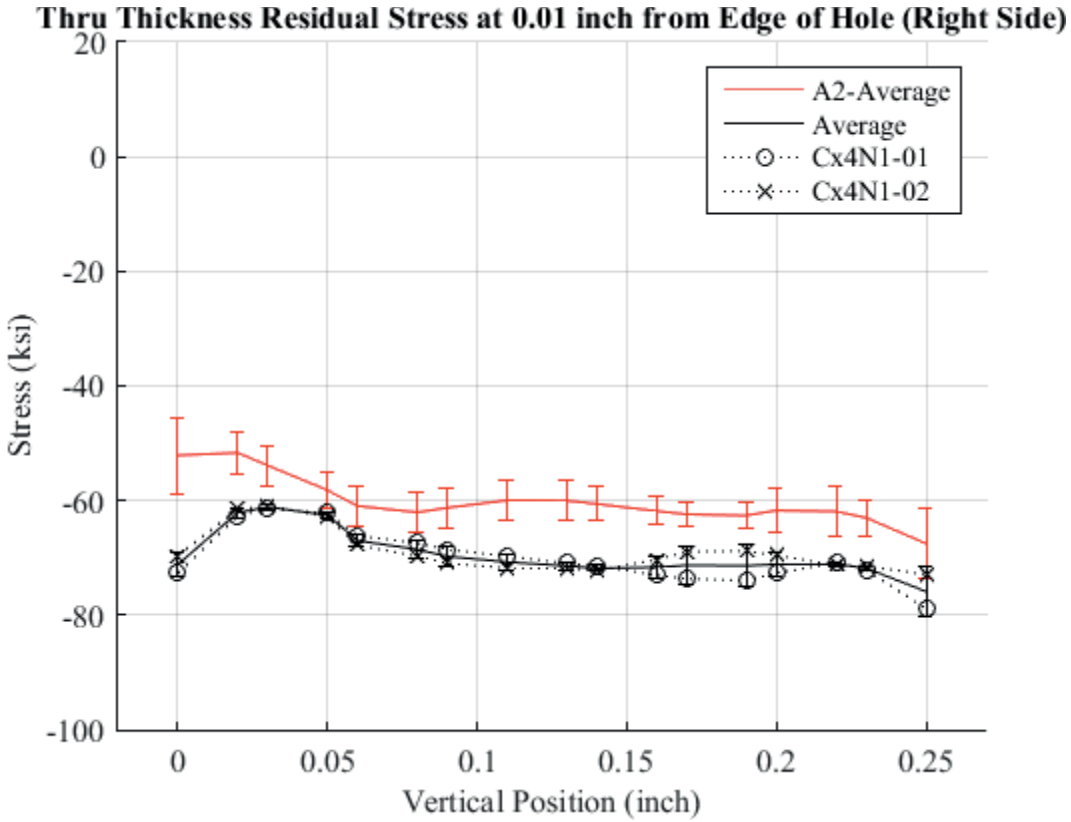

Fig. 637 Residual Stress Through-Thickness Line Plot Comparing Cx4N1-01-B, Cx4N1-02-B, and the Average between the Two to the CxA2 (2024-T351) Average Residual Stress at a Distance of 0.01 inch from the Right Side of the Hole – Cx4N1-01-B and Cx4N1-02-B Coupons had a 0.08 inch Fatigue Crack at the Left Entrance Surface.

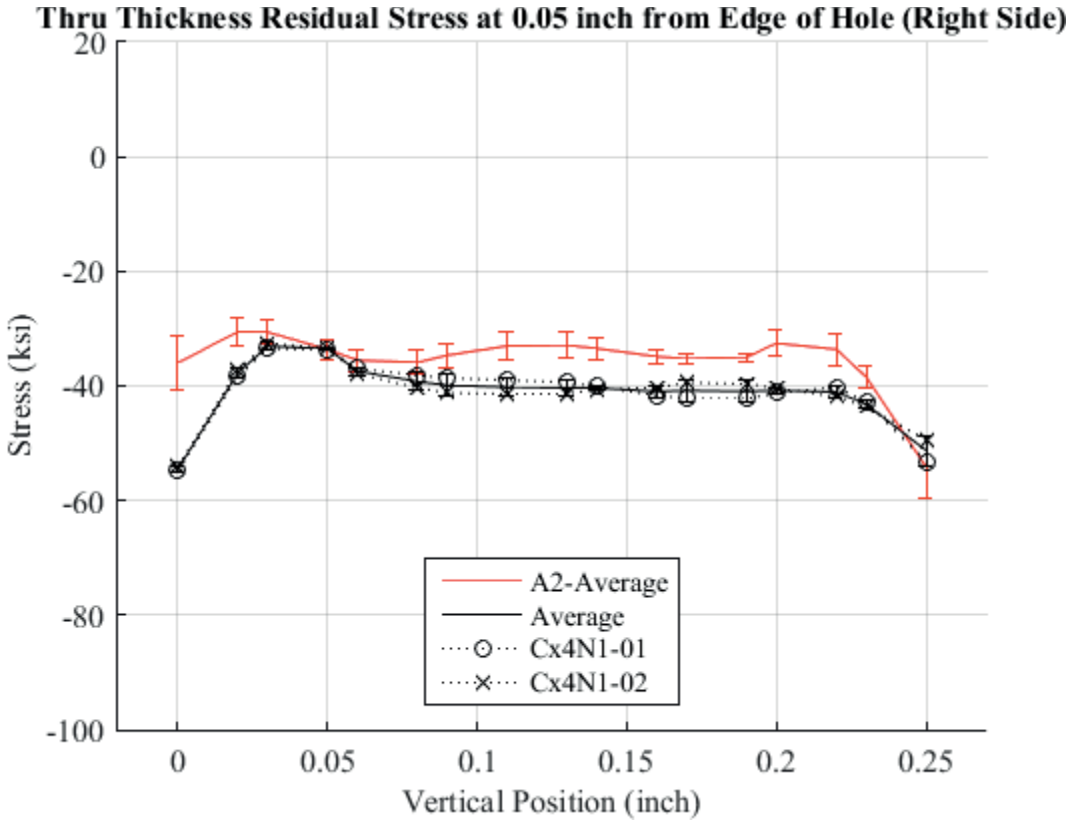

Fig. 638 Residual Stress Through-Thickness Line Plot Comparing Cx4N1-01-B, Cx4N1-02-B, and the Average between the Two to the CxA2 (2024-T351) Average Residual Stress at a Distance of 0.05 inch from the Right Side of the Hole – Cx4N1-01-B and Cx4N1-02-B Coupons had a 0.08 inch Fatigue Crack at the Left Entrance Surface.

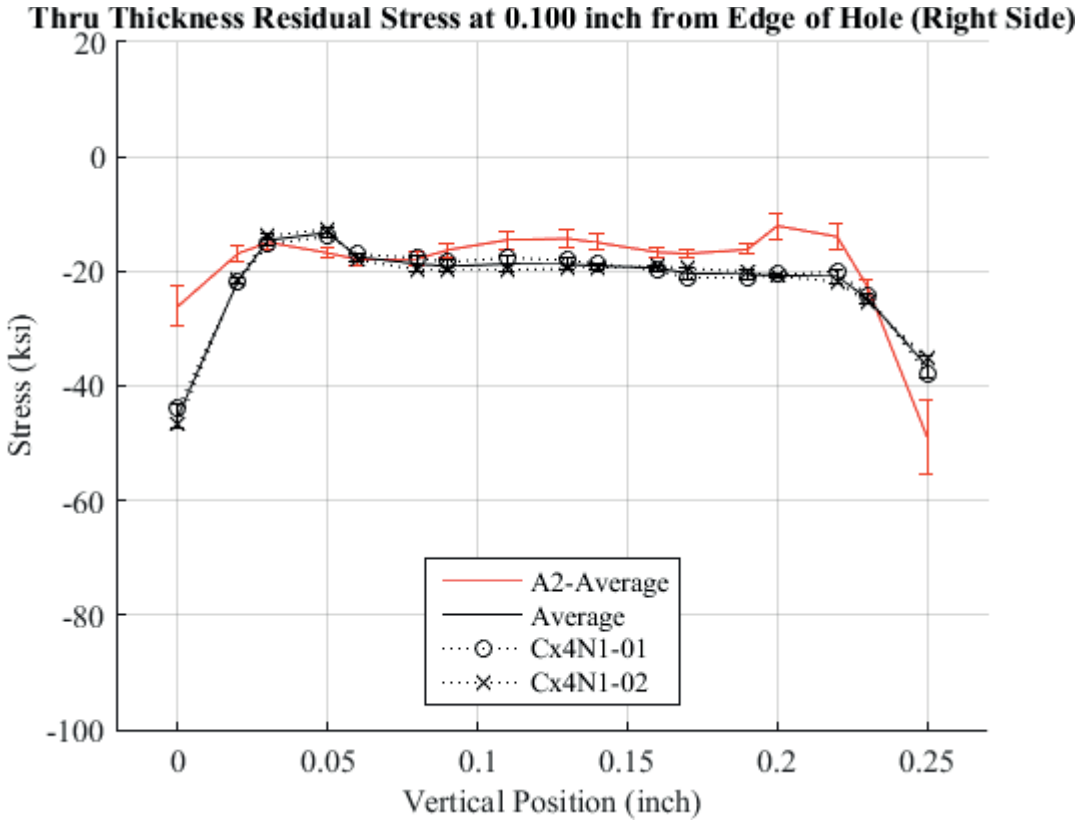

Fig. 639 Residual Stress Through-Thickness Line Plot Comparing Cx4N1-01-B, Cx4N1-02-B, and the Average between the Two to the CxA2 (2024-T351) Average Residual Stress at a Distance of 0.10 inch from the Right Side of the Hole – Cx4N1-01-B and Cx4N1-02-B Coupons had a 0.08 inch Fatigue Crack at the Left Entrance Surface.

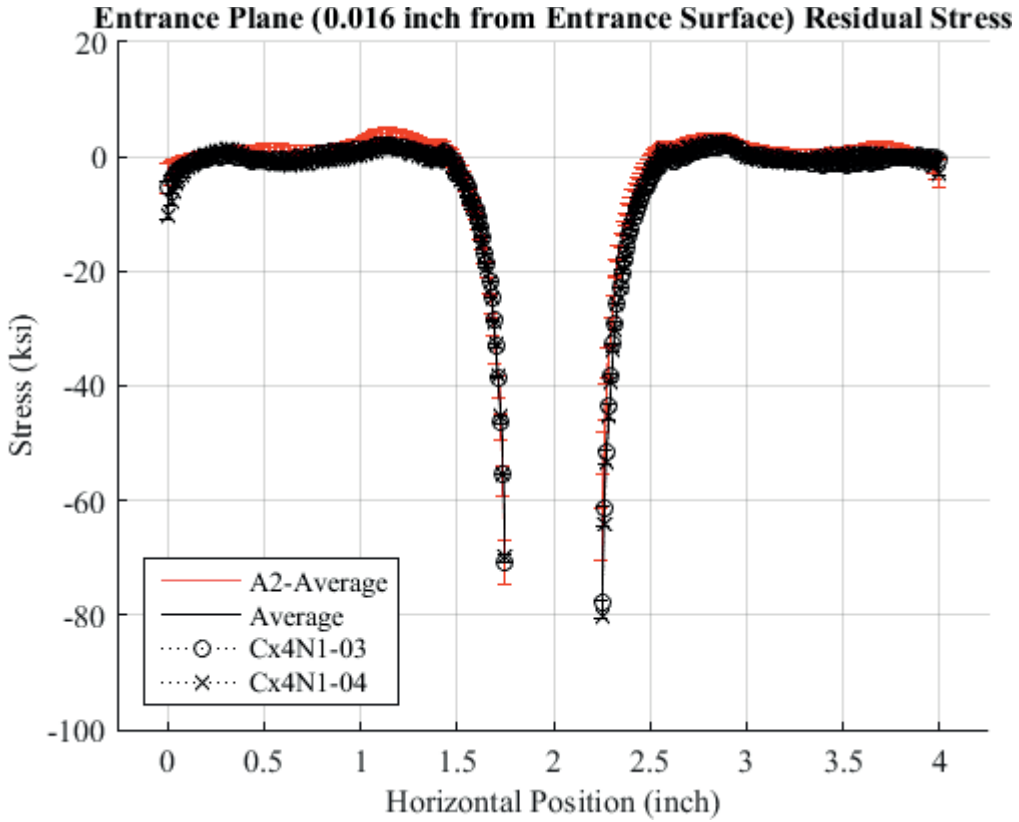

Fig. 640 Residual Stress Line Plot Comparing Cx4N1-03-B, Cx4N1-04-B, and the Average between the Two to the CxA2 (2024-T351) Average Residual Stress at a Distance of 0.016 inch (Entrance Surface) from the Entrance Surface – Cx4N1-03-B and Cx4N1-04-B Coupons had a 0.10 inch Fatigue Crack at the Left Entrance Surface.

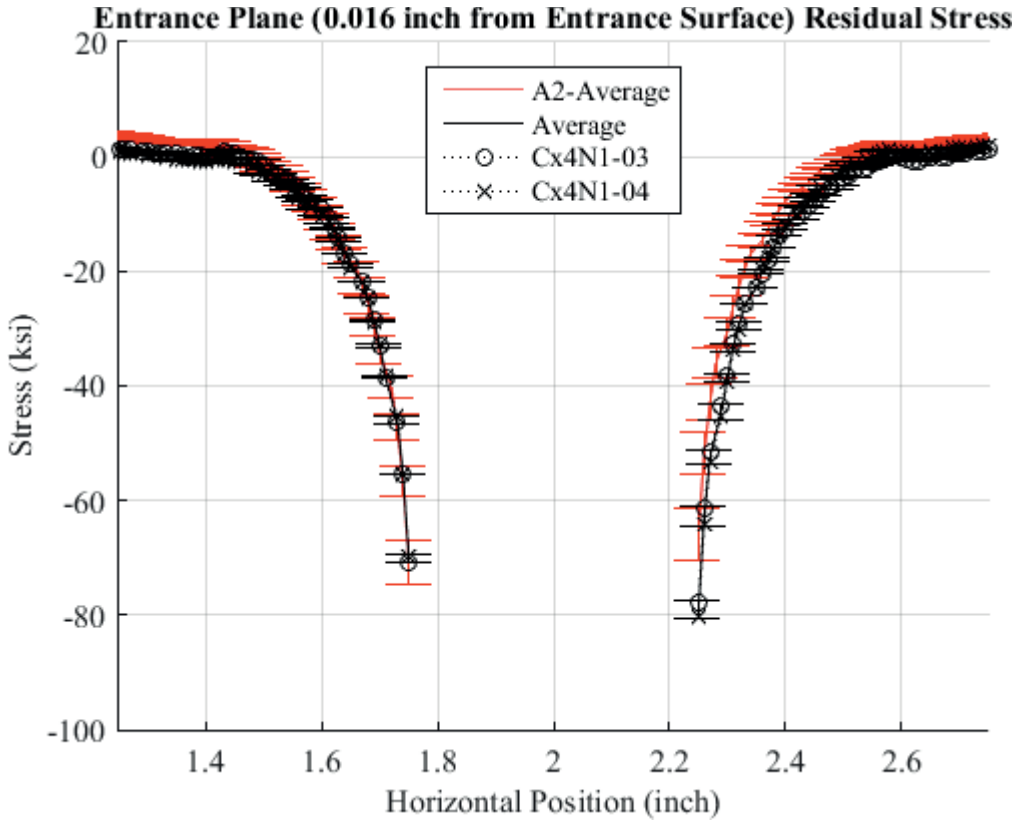

Fig. 641 Residual Stress Line Plot Comparing Cx4N1-03-B, Cx4N1-04-B, and the Average between the Two to the CxA2 (2024-T351) Average Residual Stress at a Distance of 0.016 inch (Entrance Surface) from the Entrance Surface – Cx4N1-03-B and Cx4N1-04-B Coupons had a 0.10 inch Fatigue Crack at the Left Entrance Surface – Zoomed in Next to Hole.

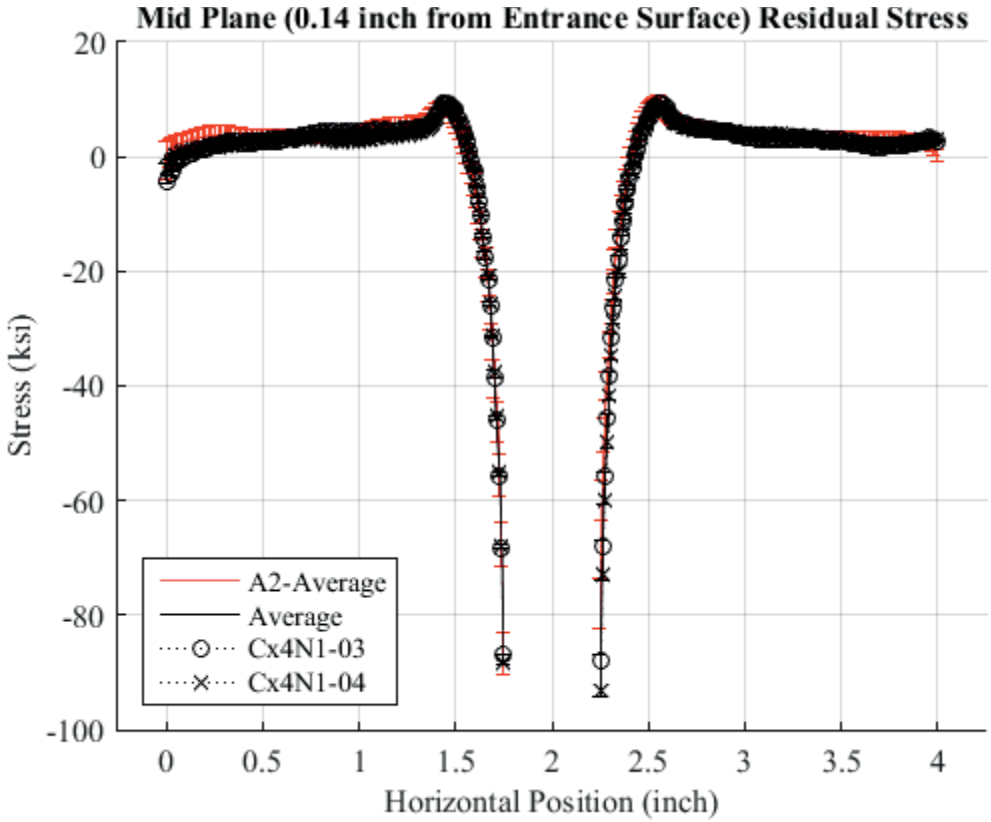

Fig. 642 Residual Stress Line Plot Comparing Cx4N1-03-B, Cx4N1-04-B, and the Average between the Two to the CxA2 (2024-T351) Average Residual Stress at a Distance of 0.140 inch (Mid-Surface Surface) from the Entrance Surface – Cx4N1-03-B and Cx4N1-04-B Coupons had a 0.10 inch Fatigue Crack at the Left Entrance Surface.

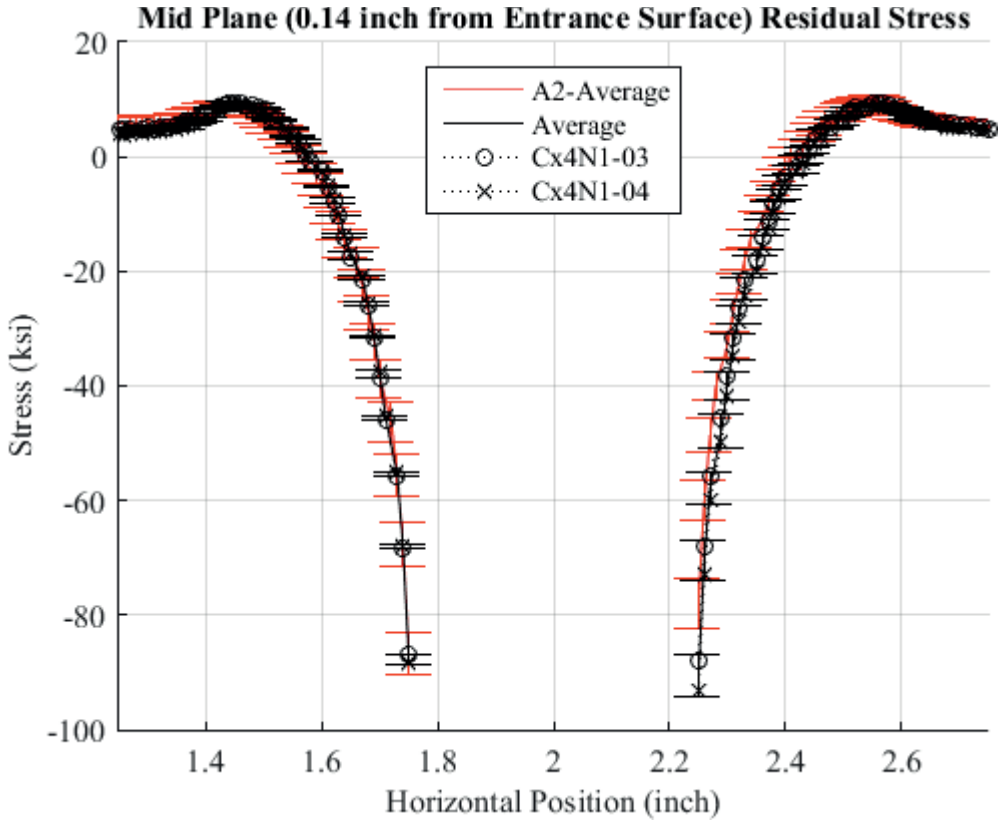

Fig. 643 Residual Stress Line Plot Comparing Cx4N1-03-B, Cx4N1-04-B, and the Average between the Two to the CxA2 (2024-T351) Average Residual Stress at a Distance of 0.140 inch (Mid-Surface Surface) from the Entrance Surface – Cx4N1-03-B and Cx4N1-04-B Coupons had a 0.10 inch Fatigue Crack at the Left Entrance Surface – Zoomed in Next to Hole.

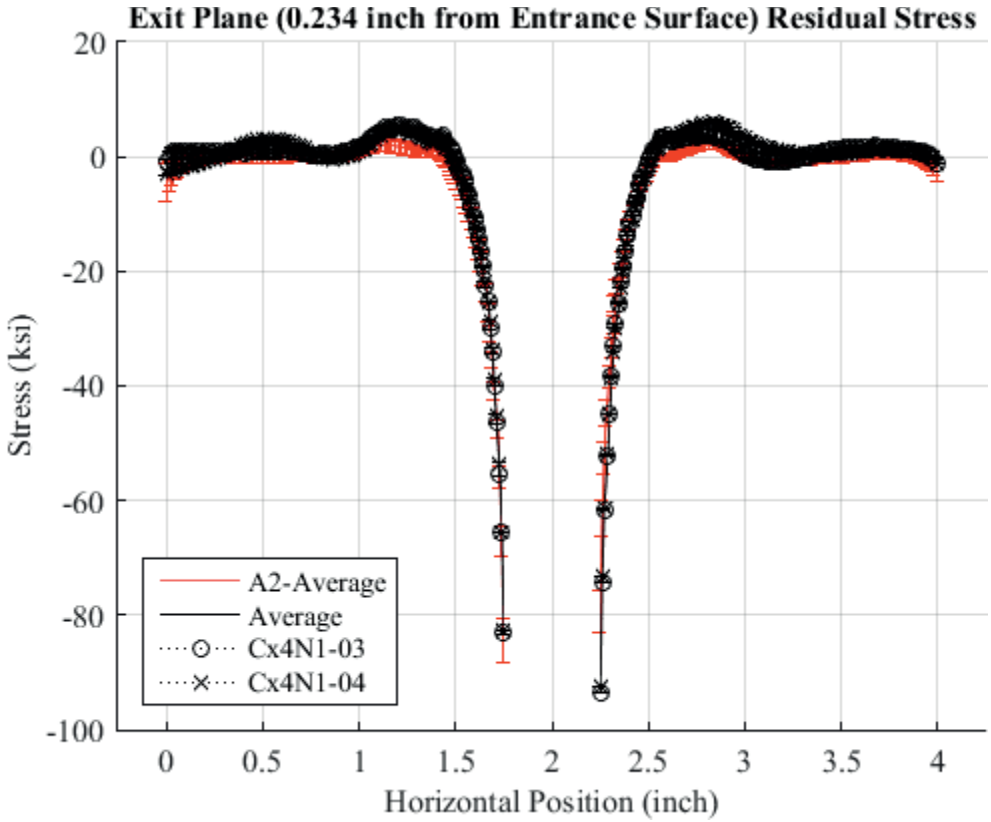

Fig. 644 Residual Stress Line Plot Comparing Cx4N1-03-B, Cx4N1-04-B, and the Average between the Two to the CxA2 (2024-T351) Average Residual Stress at a Distance of 0.234 inch (Exit Surface) from the Entrance Surface – Cx4N1-03-B and Cx4N1-04-B Coupons had a 0.10 inch Fatigue Crack at the Left Entrance Surface.

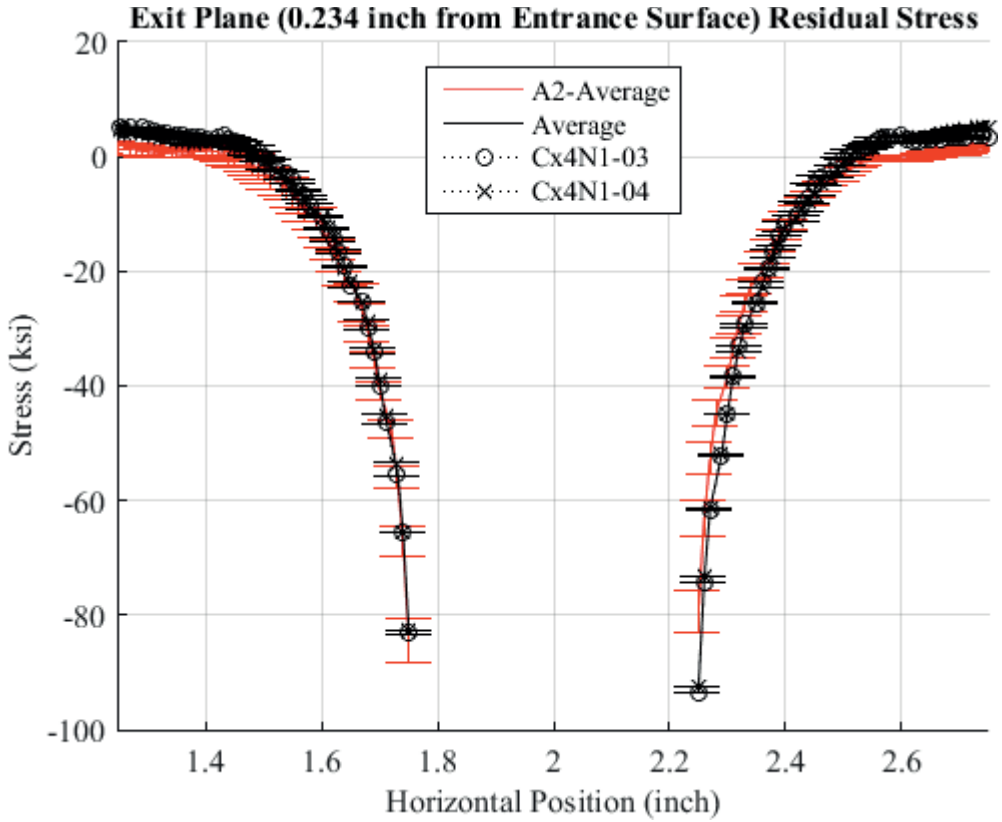

Fig. 645 Residual Stress Line Plot Comparing Cx4N1-03-B, Cx4N1-04-B, and the Average between the Two to the CxA2 (2024-T351) Average Residual Stress at a Distance of 0.234 inch (Exit Surface) from the Entrance Surface – Cx4N1-03-B and Cx4N1-04-B Coupons had a 0.10 inch Fatigue Crack at the Left Entrance Surface – Zoomed in Next to Hole.

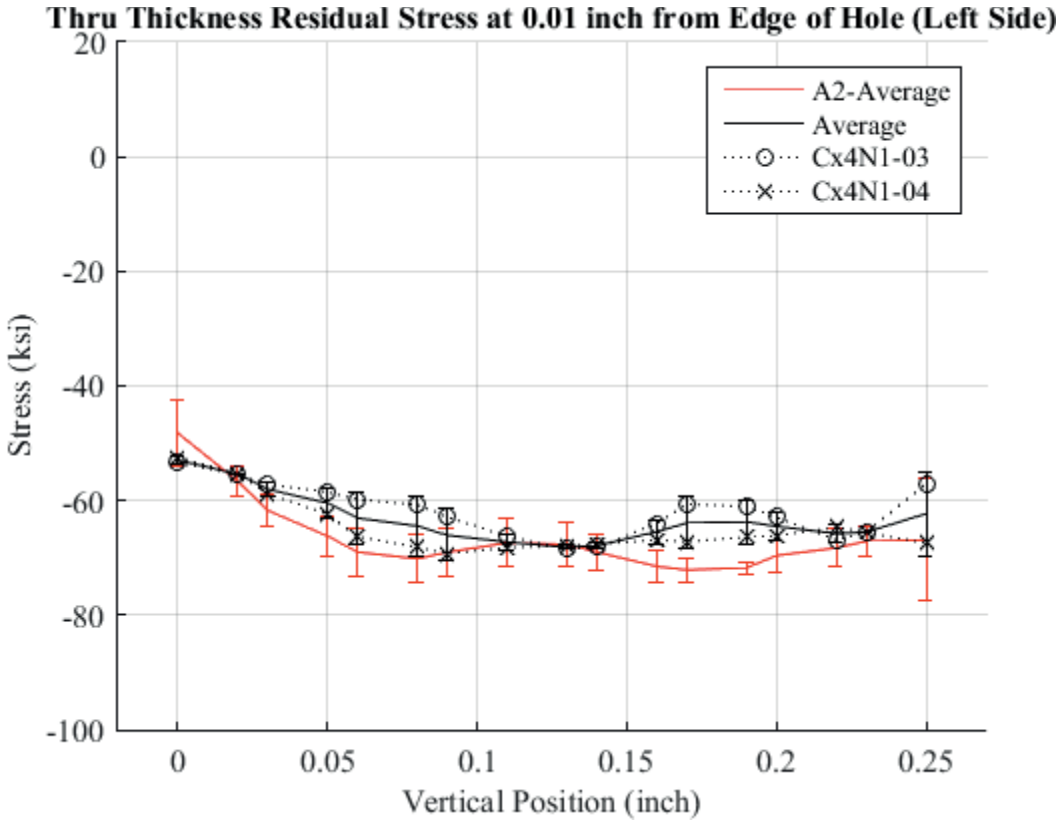

Fig. 646 Residual Stress Through-Thickness Line Plot Comparing Cx4N1-03-B, Cx4N1-04-B, and the Average between the Two to the CxA2 (2024-T351) Average Residual Stress at a Distance of 0.01 inch from the Left Side of the Hole – Cx4N1-03-B and Cx4N1-04-B Coupons had a 0.10 inch Fatigue Crack at the Left Entrance Surface.

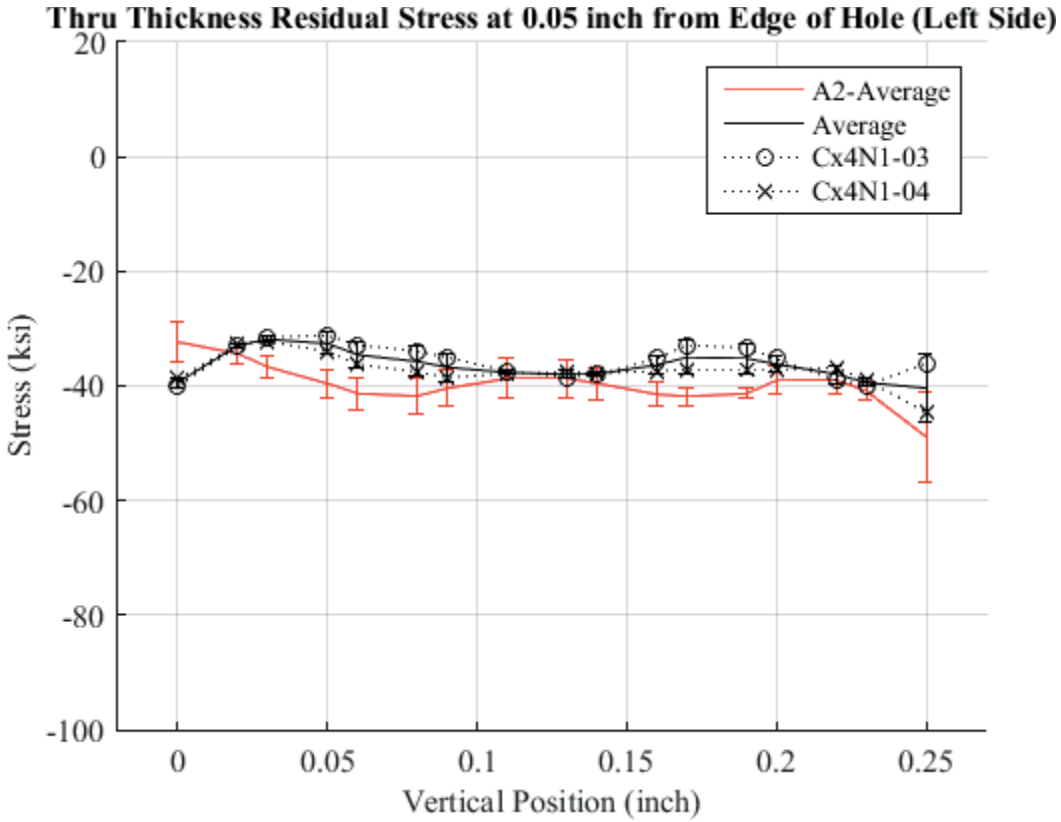

Fig. 647 Residual Stress Through-Thickness Line Plot Comparing Cx4N1-03-B, Cx4N1-04-B, and the Average between the Two to the CxA2 (2024-T351) Average Residual Stress at a Distance of 0.05 inch from the Left Side of the Hole – Cx4N1-03-B and Cx4N1-04-B Coupons had a 0.10 inch Fatigue Crack at the Left Entrance Surface.

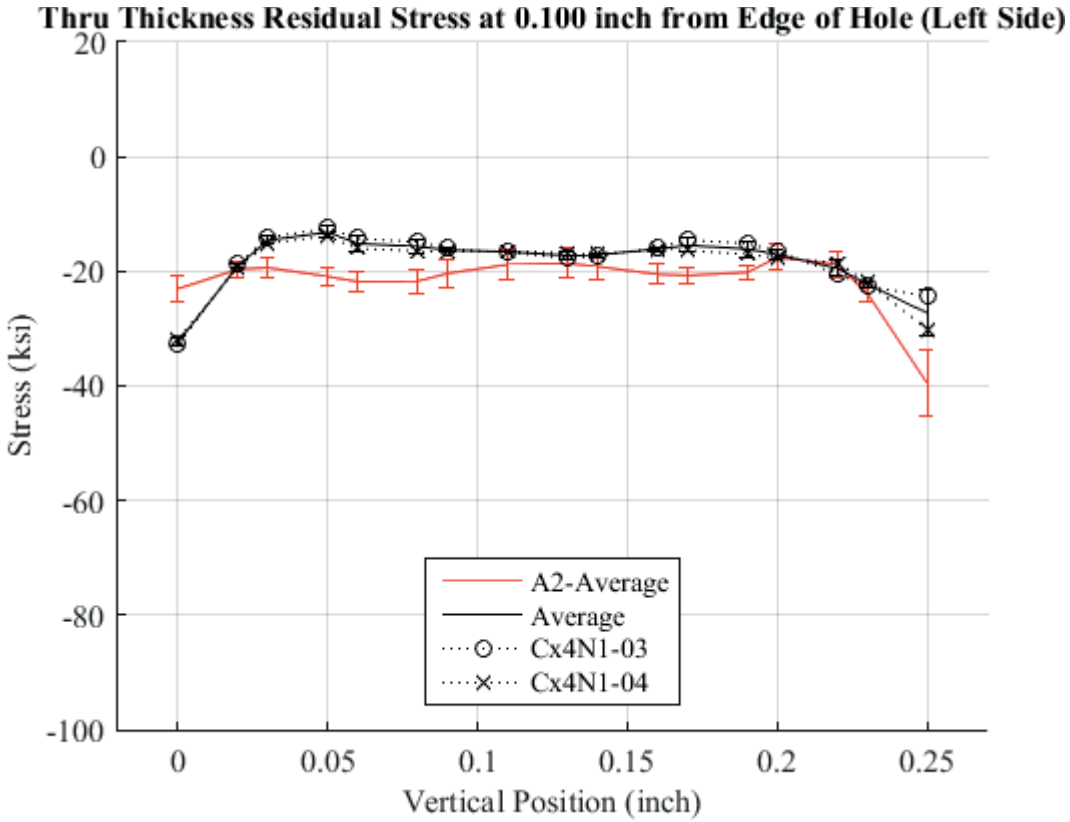

Fig. 648 Residual Stress Through-Thickness Line Plot Comparing Cx4N1-03-B, Cx4N1-04-B, and the Average between the Two to the CxA2 (2024-T351) Average Residual Stress at a Distance of 0.10 inch from the Left Side of the Hole – Cx4N1-03-B and Cx4N1-04-B Coupons had a 0.10 inch Fatigue Crack at the Left Entrance Surface.

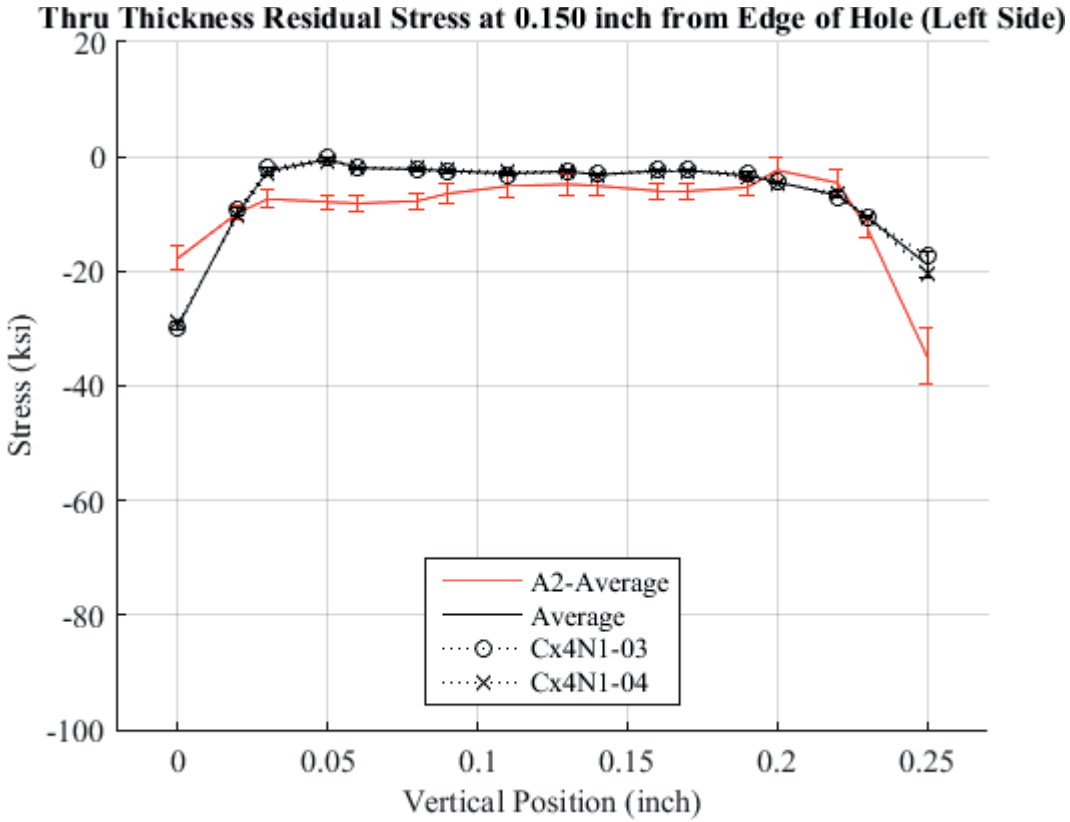

Fig. 649 Residual Stress Through-Thickness Line Plot Comparing Cx4N1-03-B, Cx4N1-04-B, and the Average between the Two to the CxA2 (2024-T351) Average Residual Stress at a Distance of 0.150 inch from the Left Side of the Hole – Cx4N1-03-B and Cx4N1-04-B Coupons had a 0.10 inch Fatigue Crack at the Left Entrance Surface.

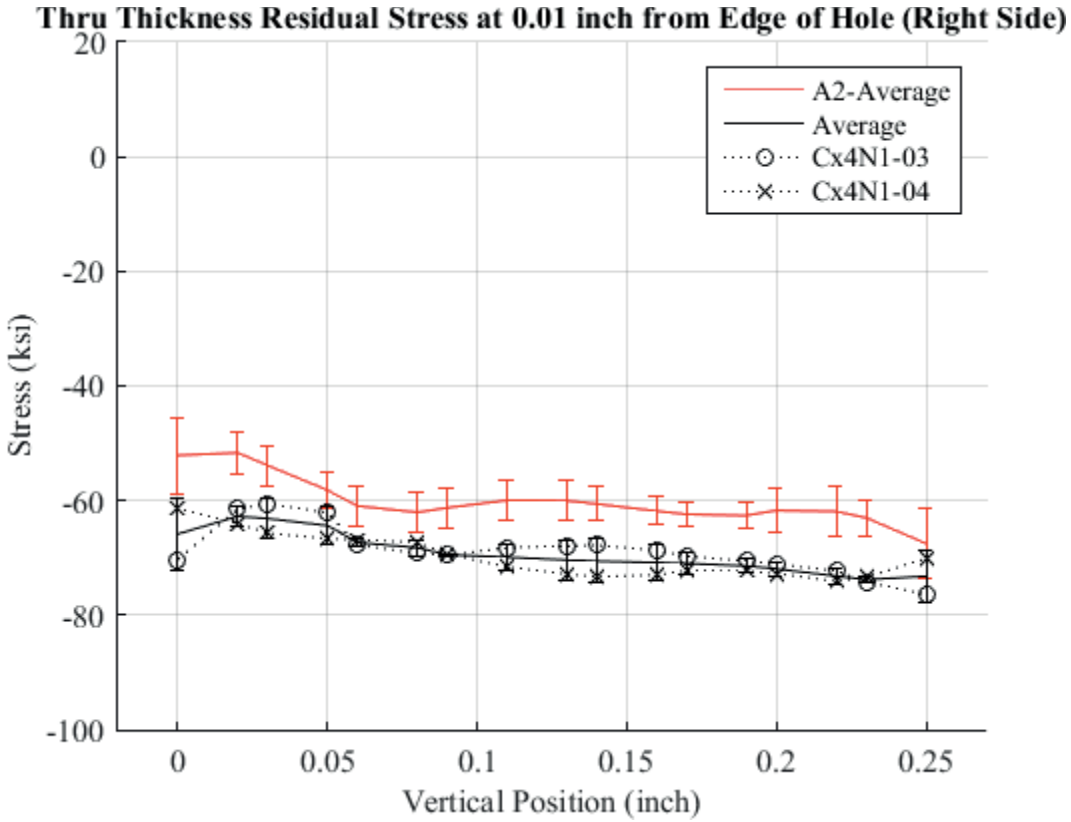

Fig. 650 Residual Stress Through-Thickness Line Plot Comparing Cx4N1-03-B, Cx4N1-04-B, and the Average between the Two to the CxA2 (2024-T351) Average Residual Stress at a Distance of 0.01 inch from the Right Side of the Hole – Cx4N1-03-B and Cx4N1-04-B Coupons had a 0.10 inch Fatigue Crack at the Left Entrance Surface.

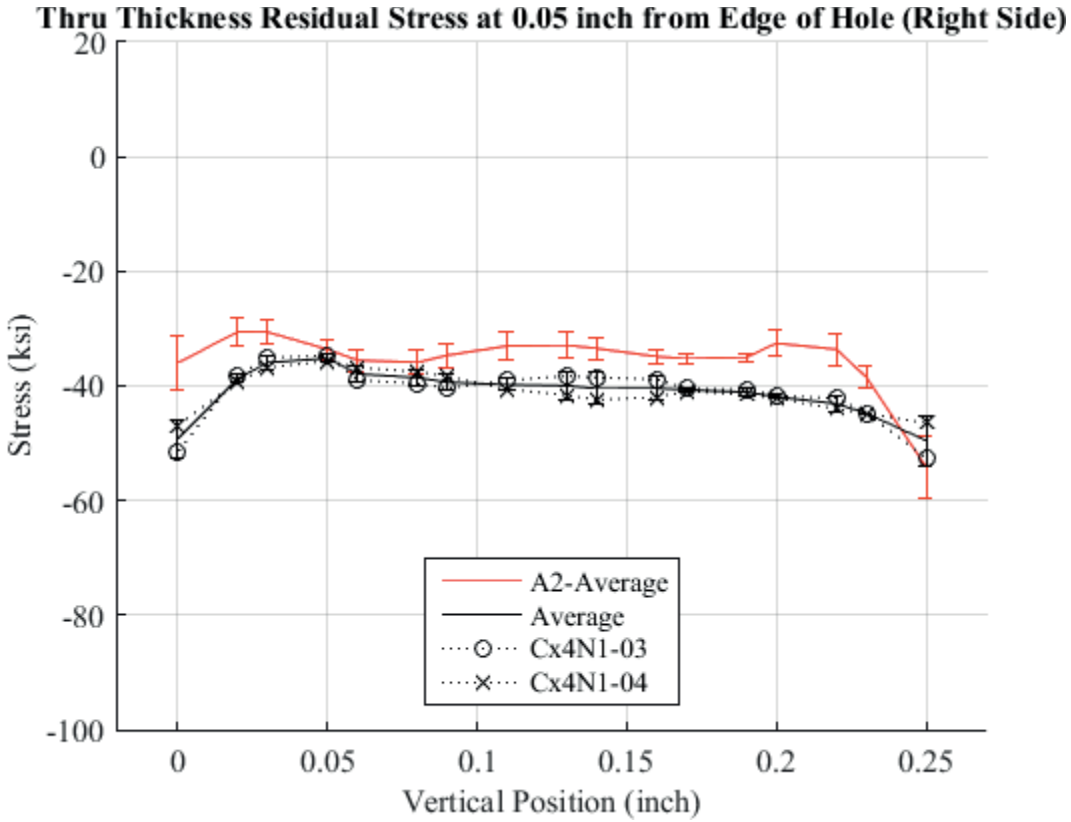

Fig. 651 Residual Stress Through-Thickness Line Plot Comparing Cx4N1-03-B, Cx4N1-04-B, and the Average between the Two to the CxA2 (2024-T351) Average Residual Stress at a Distance of 0.05 inch from the Right Side of the Hole – Cx4N1-03-B and Cx4N1-04-B Coupons had a 0.10 inch Fatigue Crack at the Left Entrance Surface.

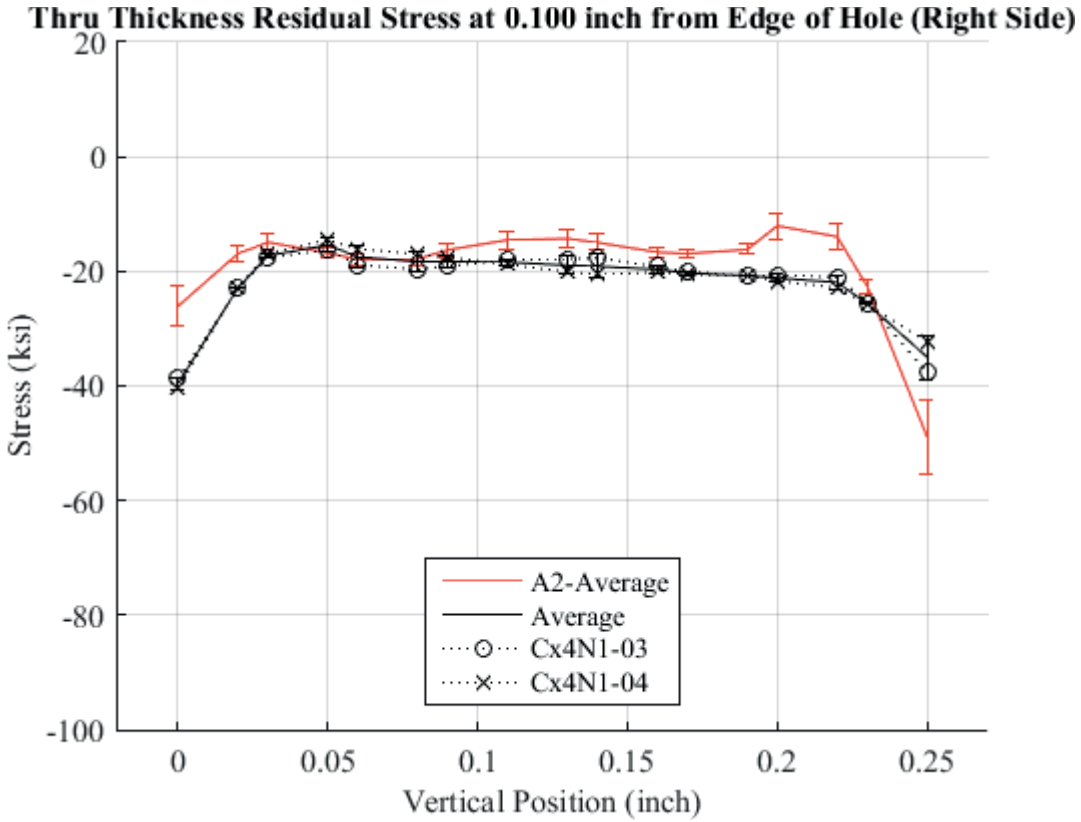

Fig. 652 Residual Stress Through-Thickness Line Plot Comparing Cx4N1-03-B, Cx4N1-04-B, and the Average between the Two to the CxA2 (2024-T351) Average Residual Stress at a Distance of 0.10 inch from the Right Side of the Hole – Cx4N1-03-B and Cx4N1-04-B Coupons had a 0.10 inch Fatigue Crack at the Left Entrance Surface.

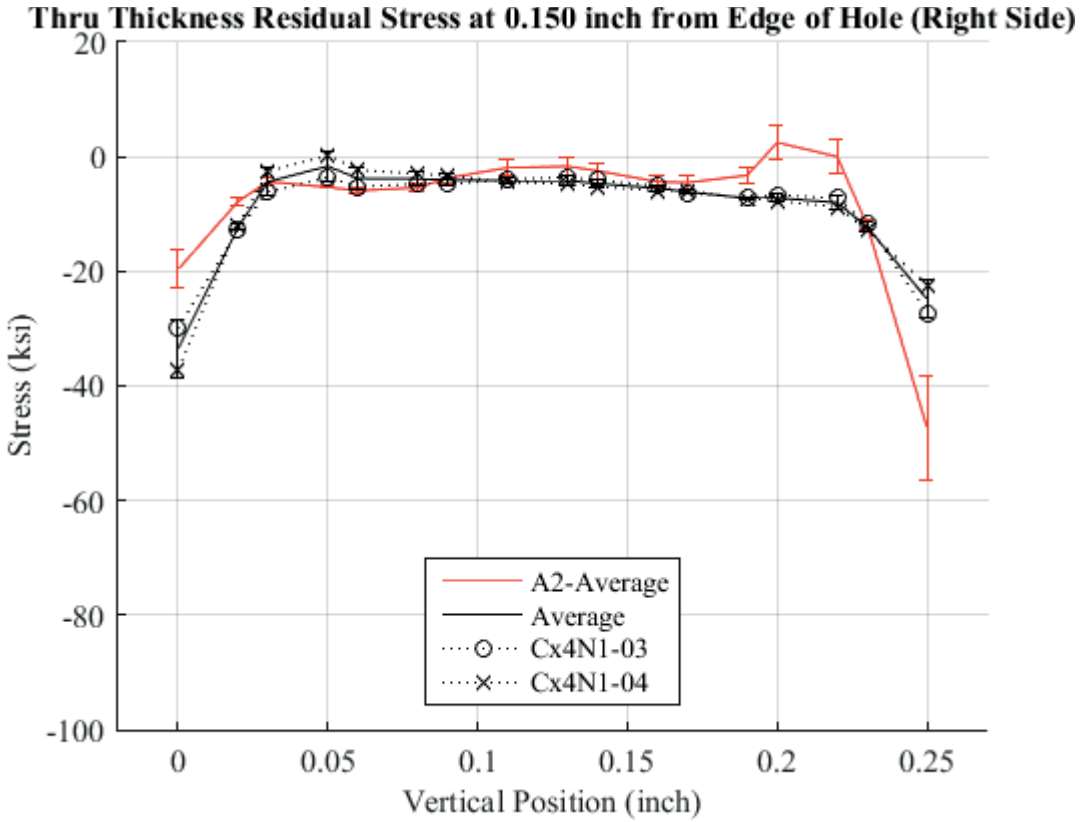

Fig. 653 Residual Stress Through-Thickness Line Plot Comparing Cx4N1-03-B, Cx4N1-04-B, and the Average between the Two to the CxA2 (2024-T351) Average Residual Stress at a Distance of 0.150 inch from the Right Side of the Hole – Cx4N1-03-B and Cx4N1-04-B Coupons had a 0.10 inch Fatigue Crack at the Left Entrance Surface.

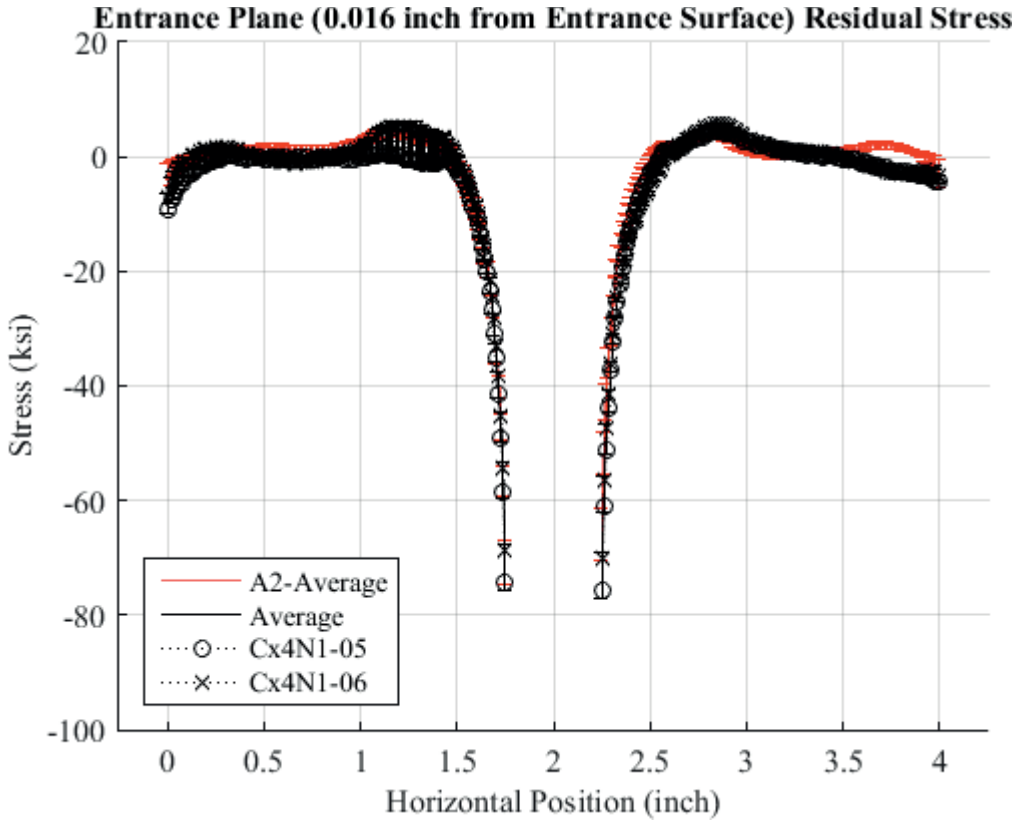

Fig. 654 Residual Stress Line Plot Comparing Cx4N1-05-B, Cx4N1-06-B, and the Average between the Two to the CxA2 (2024-T351) Average Residual Stress at a Distance of 0.016 inch (Entrance Surface) from the Entrance Surface – Cx4N1-05-B and Cx4N1-06-B Coupons had a 0.125 inch Fatigue Crack at the Left Entrance Surface.

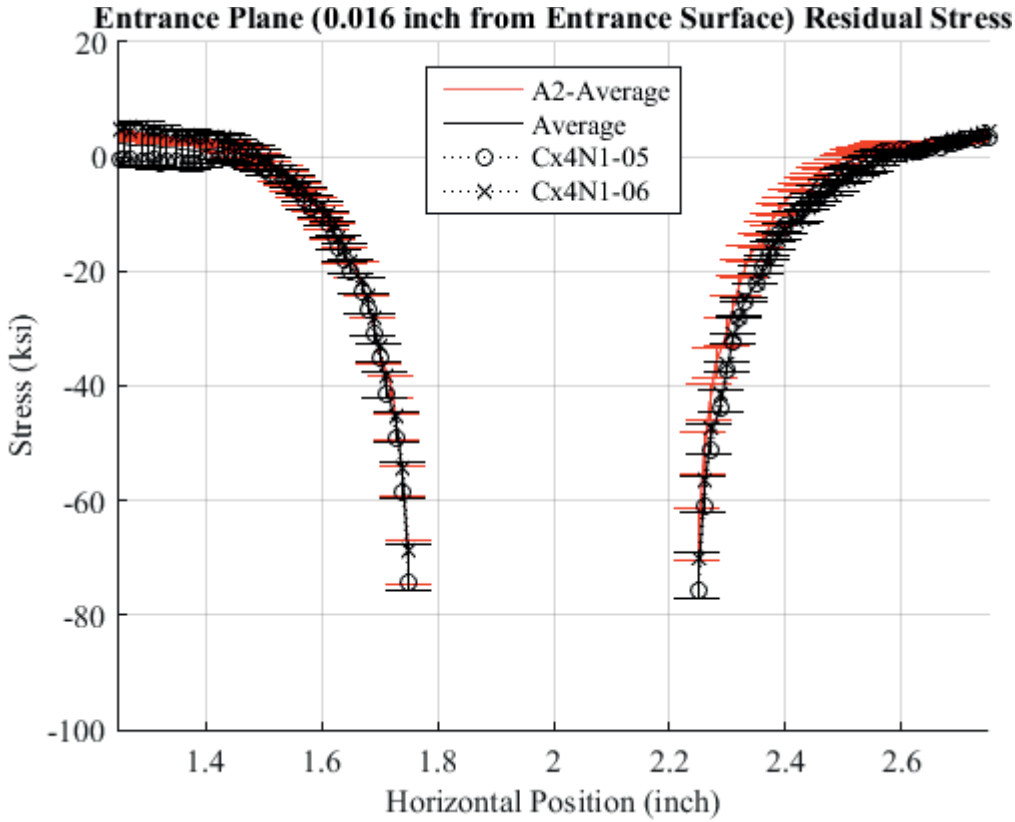

Fig. 655 Residual Stress Line Plot Comparing Cx4N1-05-B, Cx4N1-06-B, and the Average between the Two to the CxA2 (2024-T351) Average Residual Stress at a Distance of 0.016 inch (Entrance Surface) from the Entrance Surface – Cx4N1-05-B and Cx4N1-06-B Coupons had a 0.125 inch Fatigue Crack at the Left Entrance Surface – Zoomed in Next to Hole.

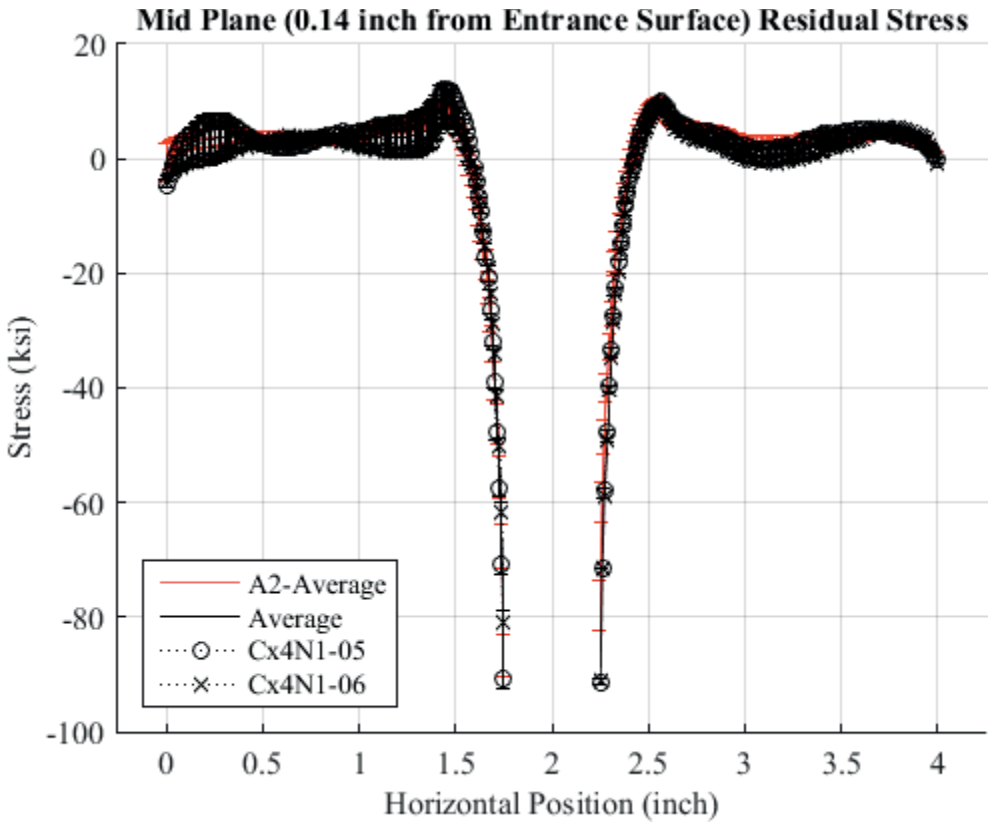

Fig. 656 Residual Stress Line Plot Comparing Cx4N1-05-B, Cx4N1-06-B, and the Average between the Two to the CxA2 (2024-T351) Average Residual Stress at a Distance of 0.140 inch (Mid Plane Surface) from the Entrance Surface – Cx4N1-05-B and Cx4N1-06-B Coupons had a 0.125 inch Fatigue Crack at the Left Entrance Surface.

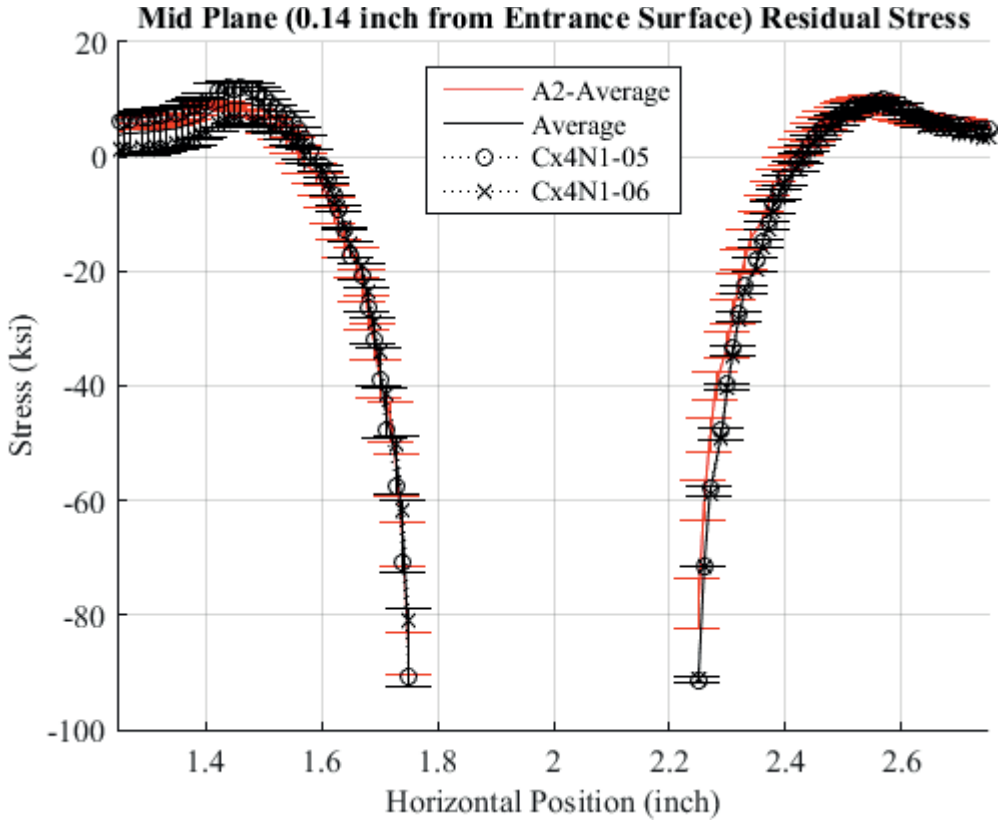

Fig. 657 Residual Stress Line Plot Comparing Cx4N1-05-B, Cx4N1-06-B, and the Average between the Two to the CxA2 (2024-T351) Average Residual Stress at a Distance of 0.140 inch (Mid Plane Surface) from the Entrance Surface – Cx4N1-05-B and Cx4N1-06-B Coupons had a 0.125 inch Fatigue Crack at the Left Entrance Surface – Zoomed in Next to Hole.

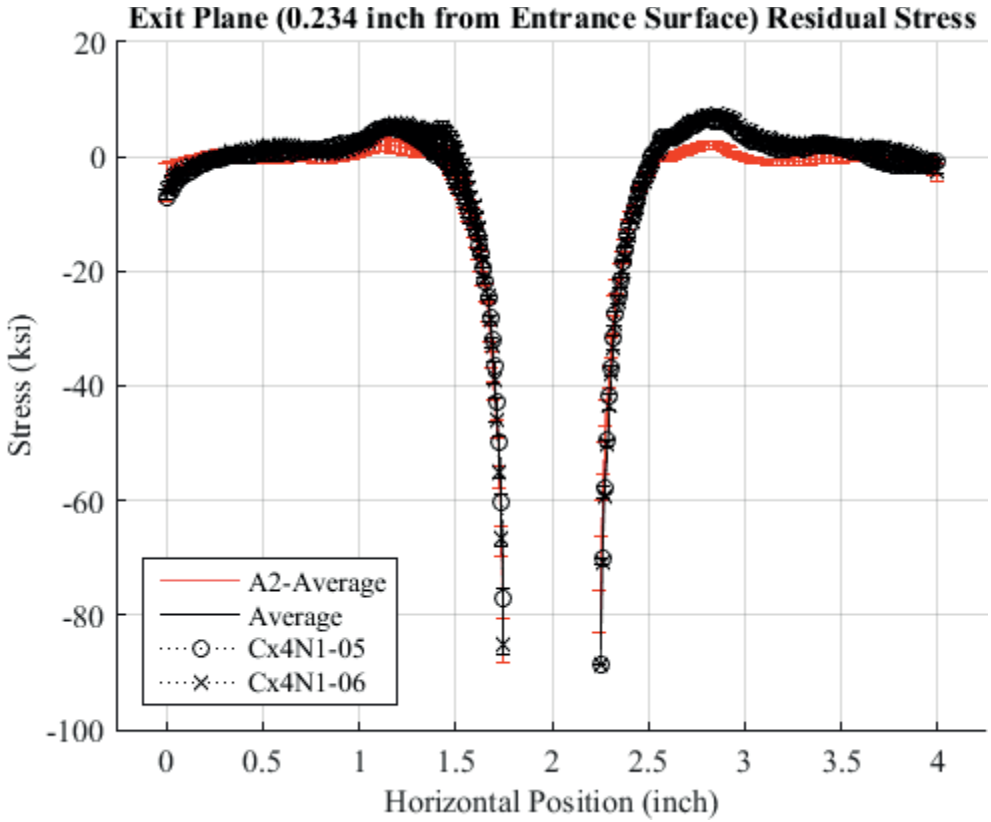

Fig. 658 Residual Stress Line Plot Comparing Cx4N1-05-B, Cx4N1-06-B, and the Average between the Two to the CxA2 (2024-T351) Average Residual Stress at a Distance of 0.234 inch (Exit Surface) from the Entrance Surface – Cx4N1-05-B and Cx4N1-06-B Coupons had a 0.125 inch Fatigue Crack at the Left Entrance Surface.

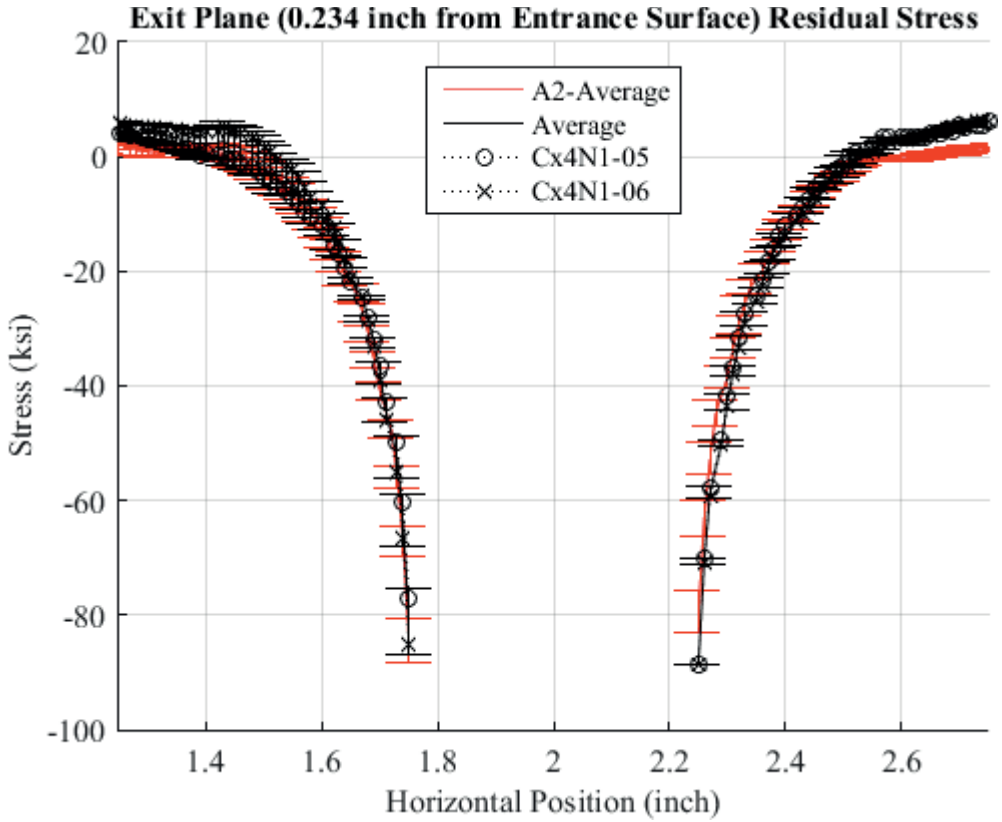

Fig. 659 Residual Stress Line Plot Comparing Cx4N1-05-B, Cx4N1-06-B, and the Average between the Two to the CxA2 (2024-T351) Average Residual Stress at a Distance of 0.234 inch (Exit Surface) from the Entrance Surface – Cx4N1-05-B and Cx4N1-06-B Coupons had a 0.125 inch Fatigue Crack at the Left Entrance Surface – Zoomed in Next to Hole.

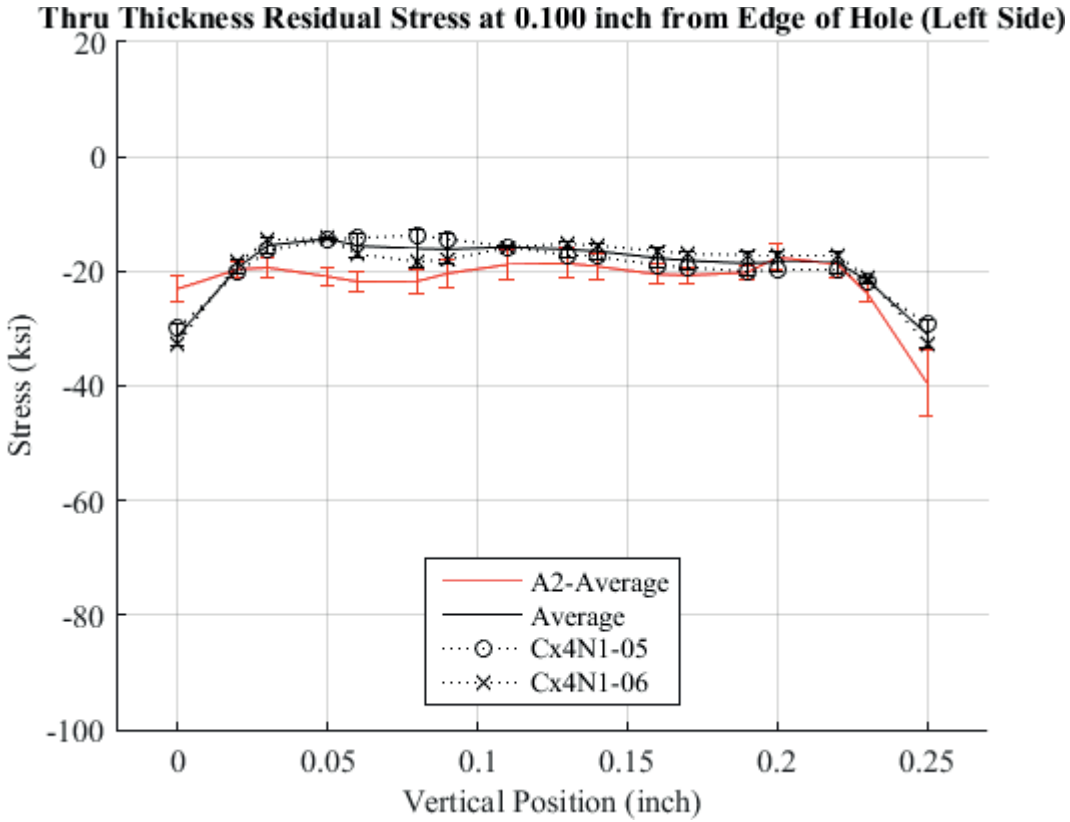

Fig. 660 Residual Stress Through-Thickness Line Plot Comparing Cx4N1-05-B, Cx4N1-06-B, and the Average between the Two to the CxA2 (2024-T351) Average Residual Stress at a Distance of 0.01 inch from the Left Side of the Hole – Cx4N1-05-B and Cx4N1-06-B Coupons had a 0.125 inch Fatigue Crack at the Left Entrance Surface.

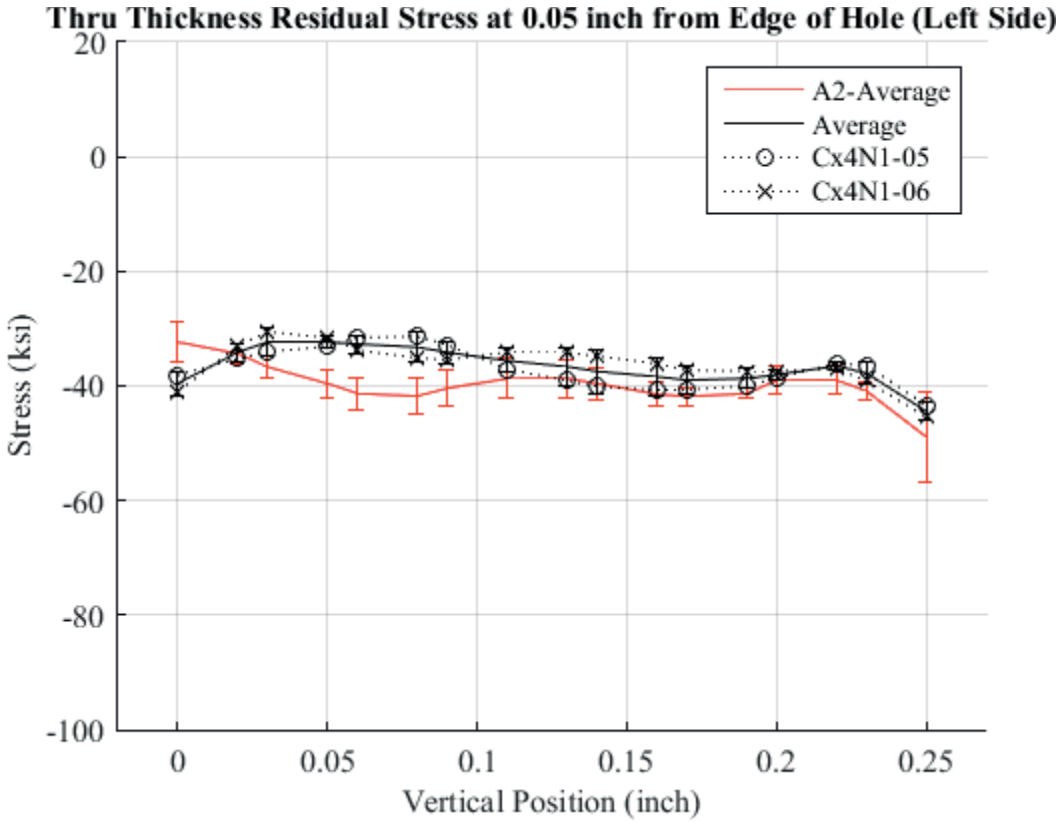

Fig. 661 Residual Stress Through-Thickness Line Plot Comparing Cx4N1-05-B, Cx4N1-06-B, and the Average between the Two to the CxA2 (2024-T351) Average Residual Stress at a Distance of 0.05 inch from the Left Side of the Hole – Cx4N1-05-B and Cx4N1-06-B Coupons had a 0.125 inch Fatigue Crack at the Left Entrance Surface.

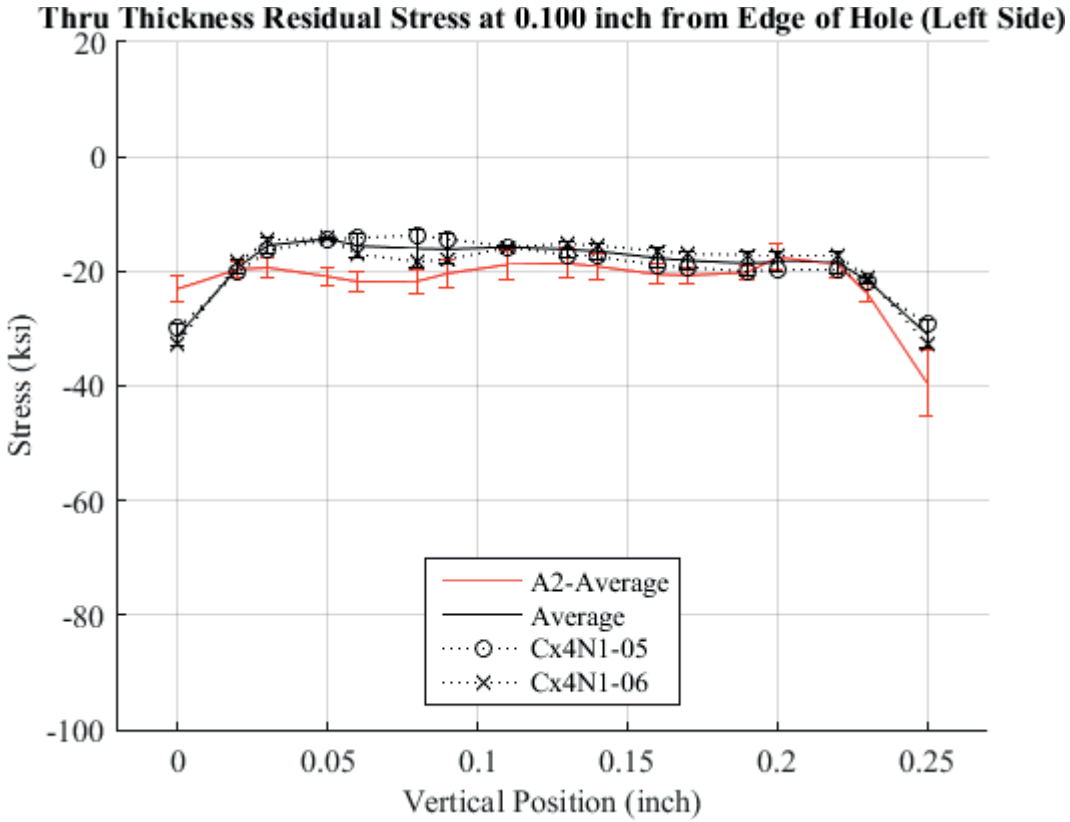

Fig. 662 Residual Stress Through-Thickness Line Plot Comparing Cx4N1-05-B, Cx4N1-06-B, and the Average between the Two to the CxA2 (2024-T351) Average Residual Stress at a Distance of 0.10 inch from the Left Side of the Hole – Cx4N1-05-B and Cx4N1-06-B Coupons had a 0.125 inch Fatigue Crack at the Left Entrance Surface.

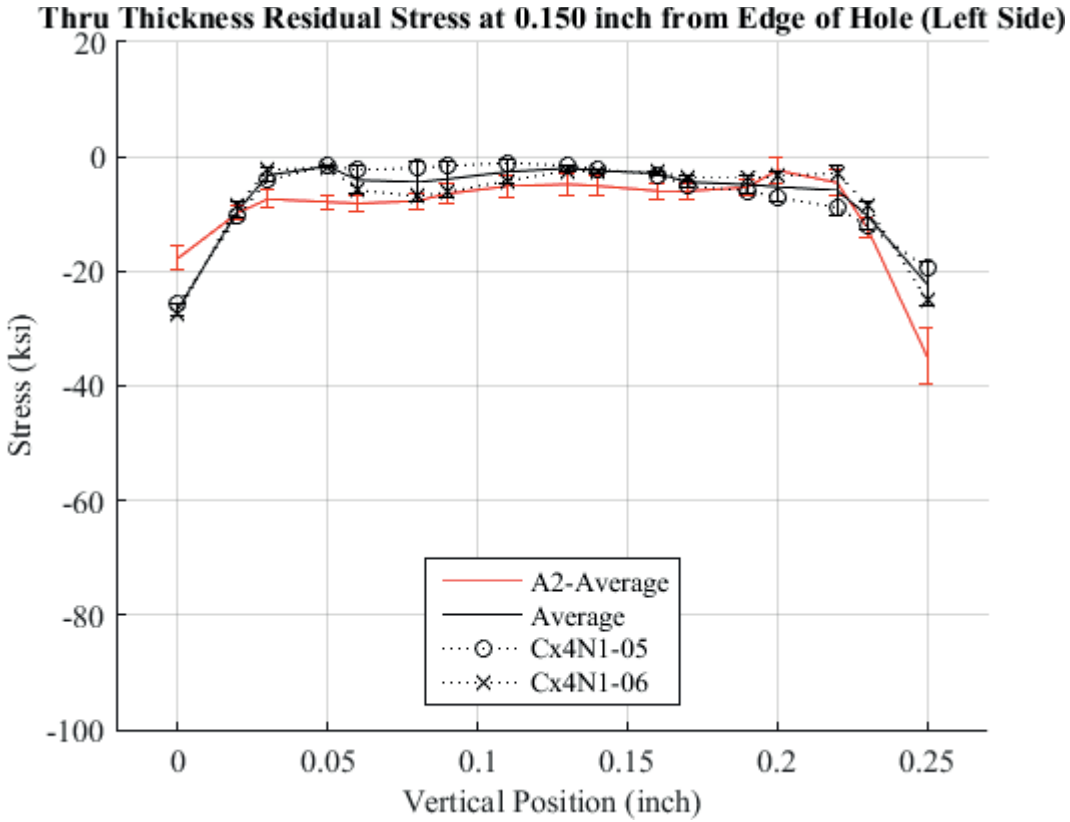

Fig. 663 Residual Stress Through-Thickness Line Plot Comparing Cx4N1-05-B, Cx4N1-06-B, and the Average between the Two to the CxA2 (2024-T351) Average Residual Stress at a Distance of 0.150 inch from the Left Side of the Hole – Cx4N1-05-B and Cx4N1-06-B Coupons had a 0.125 inch Fatigue Crack at the Left Entrance Surface.

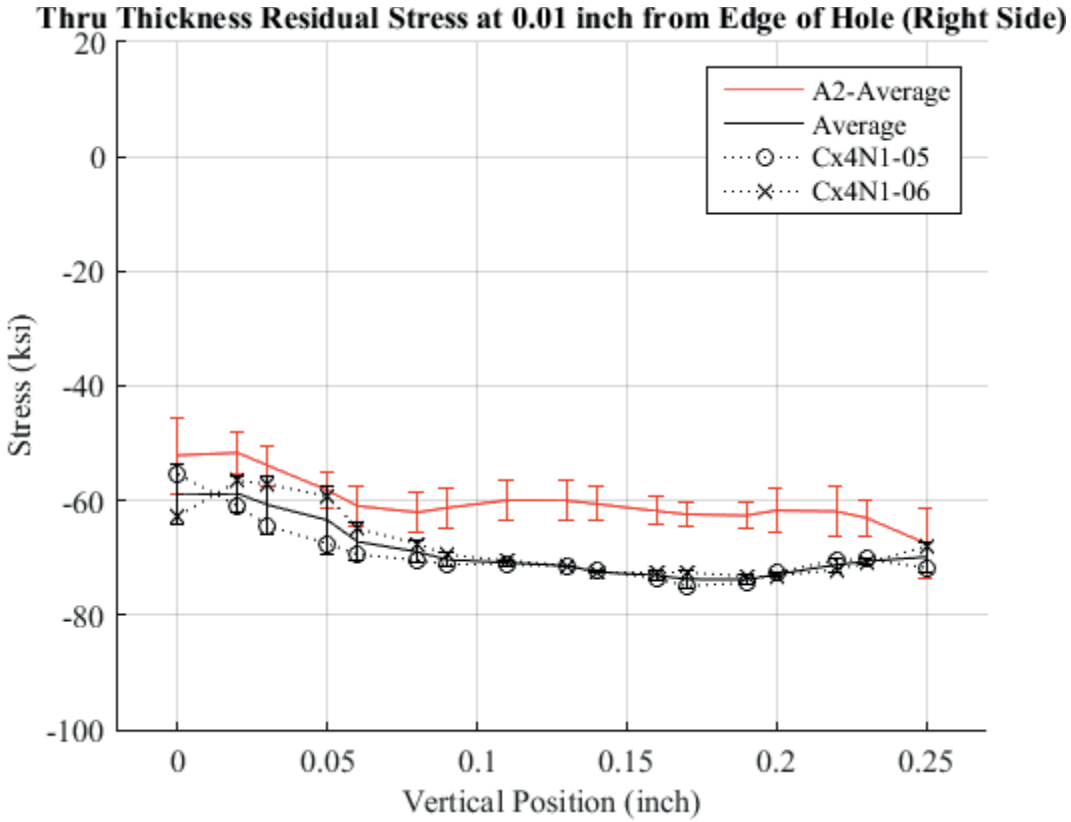

Fig. 664 Residual Stress Through-Thickness Line Plot Comparing Cx4N1-05-B, Cx4N1-06-B, and the Average between the Two to the CxA2 (2024-T351) Average Residual Stress at a Distance of 0.01 inch from the Right Side of the Hole – Cx4N1-05-B and Cx4N1-06-B Coupons had a 0.125 inch Fatigue Crack at the Left Entrance Surface.

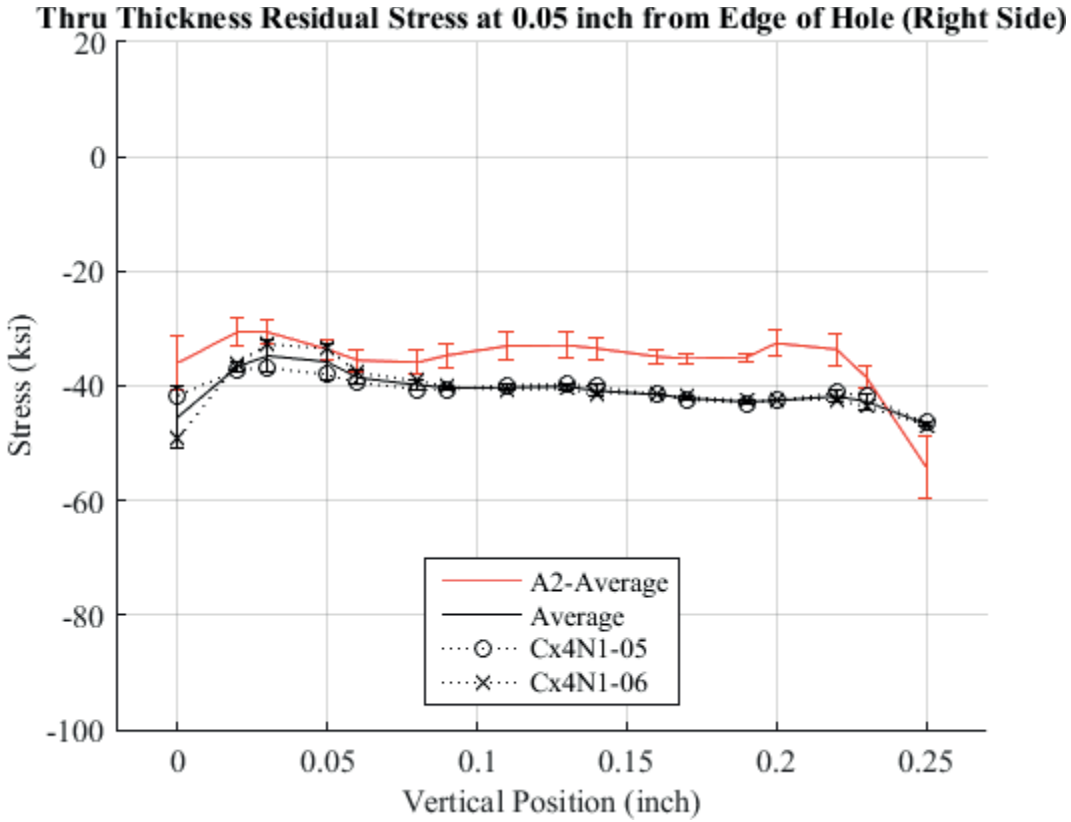

Fig. 665 Residual Stress Through-Thickness Line Plot Comparing Cx4N1-05-B, Cx4N1-06-B, and the Average between the Two to the CxA2 (2024-T351) Average Residual Stress at a Distance of 0.05 inch from the Right Side of the Hole – Cx4N1-05-B and Cx4N1-06-B Coupons had a 0.125 inch Fatigue Crack at the Left Entrance Surface.

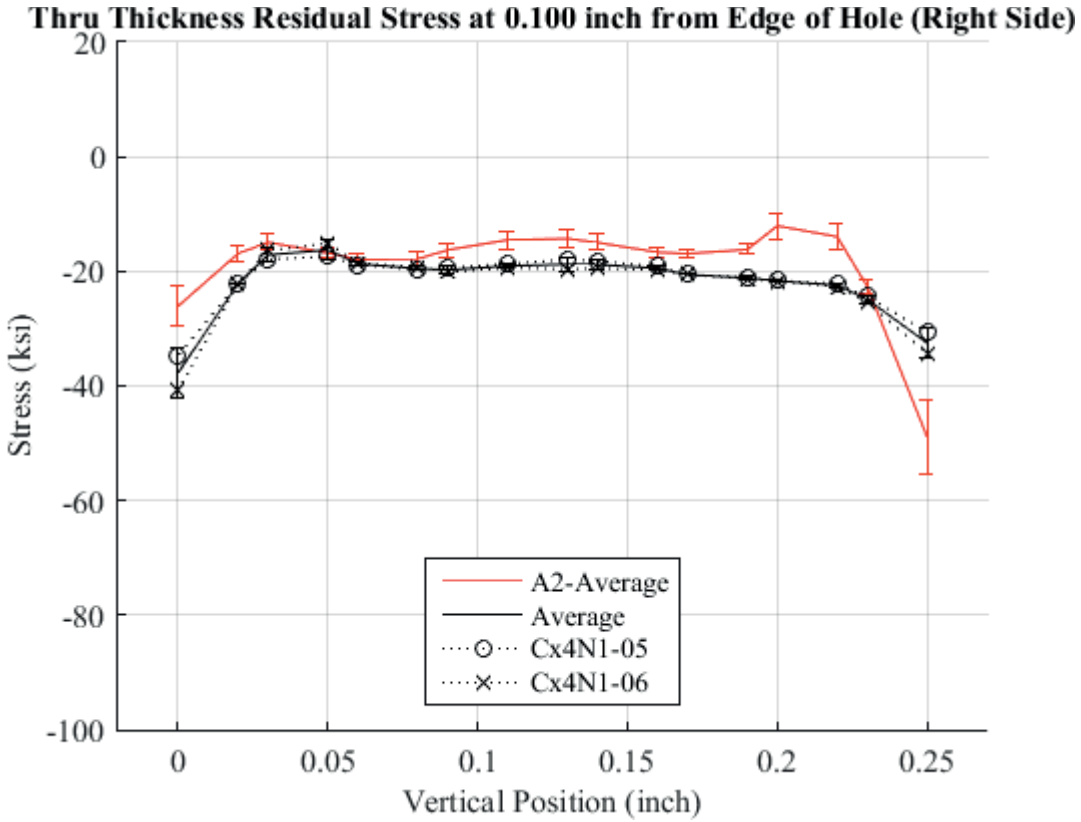

Fig. 666 Residual Stress Through-Thickness Line Plot Comparing Cx4N1-05-B, Cx4N1-06-B, and the Average between the Two to the CxA2 (2024-T351) Average Residual Stress at a Distance of 0.10 inch from the Right Side of the Hole – Cx4N1-05-B and Cx4N1-06-B Coupons had a 0.125 inch Fatigue Crack at the Left Entrance Surface.

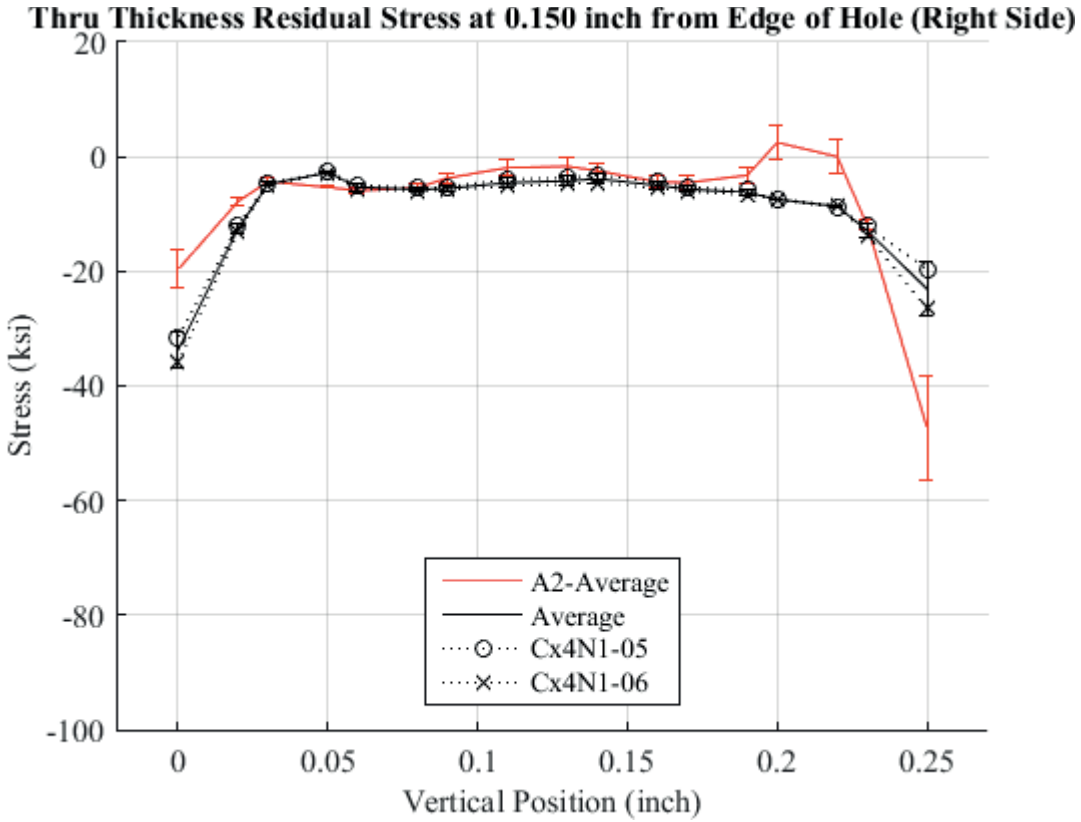

Fig. 667 Residual Stress Through-Thickness Line Plot Comparing Cx4N1-05-B, Cx4N1-06-B, and the Average between the Two to the CxA2 (2024-T351) Average Residual Stress at a Distance of 0.150 inch from the Right Side of the Hole – Cx4N1-05-B and Cx4N1-06-B Coupons had a 0.125 inch Fatigue Crack at the Left Entrance Surface.

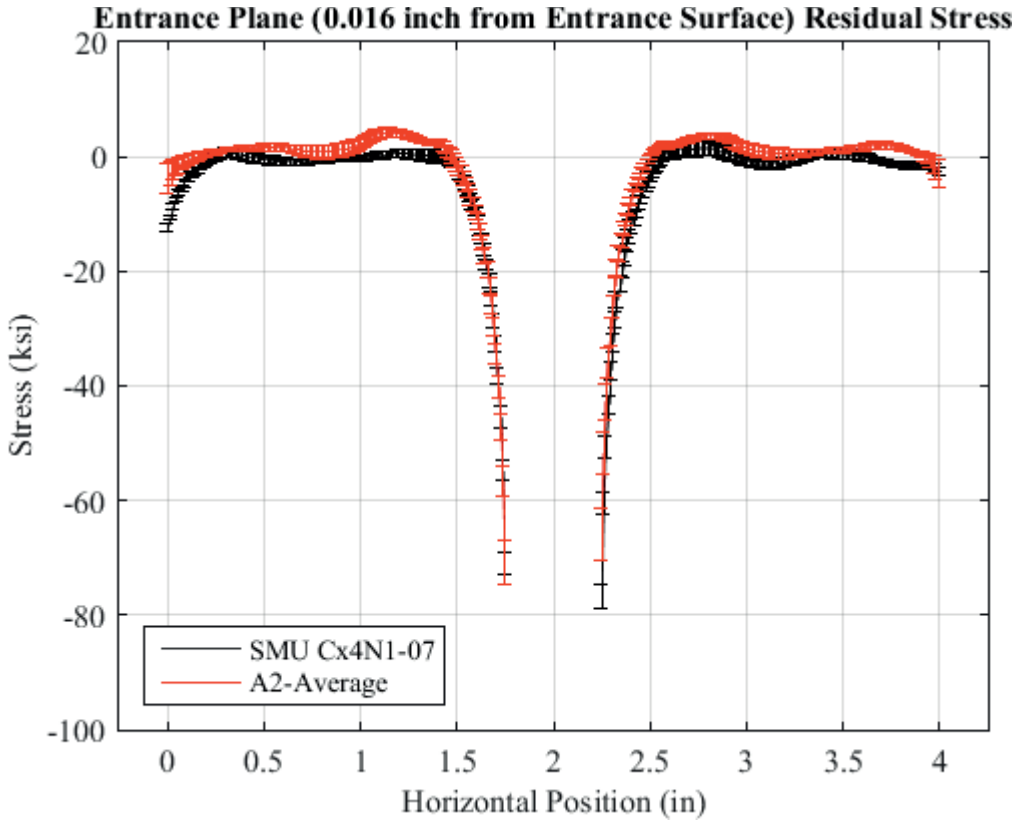

Fig. 668 Residual Stress Line Plot Comparing Cx4N1-07-B, and the Average between the Two to the CxA2 (2024-T351) Average Residual Stress at a Distance of 0.016 inch (Entrance Surface) from the Entrance Surface – Cx4N1-07-B Coupons had a 0.2515 inch Fatigue Crack at the Left Entrance Surface.

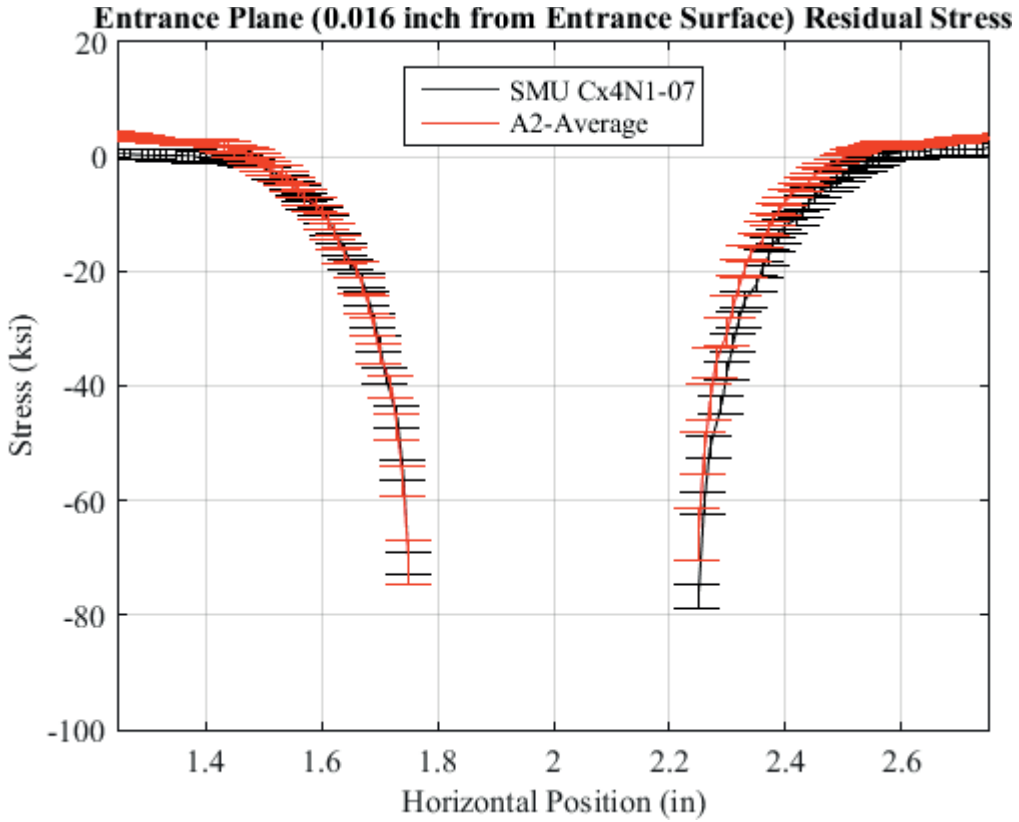

Fig. 669 Residual Stress Line Plot Comparing Cx4N1-07-B, and the Average between the Two to the CxA2 (2024-T351) Average Residual Stress at a Distance of 0.016 inch (Entrance Surface) from the Entrance Surface – Cx4N1-07-B Coupons had a 0.2515 inch Fatigue Crack at the Left Entrance Surface – Zoomed in Next to Hole.

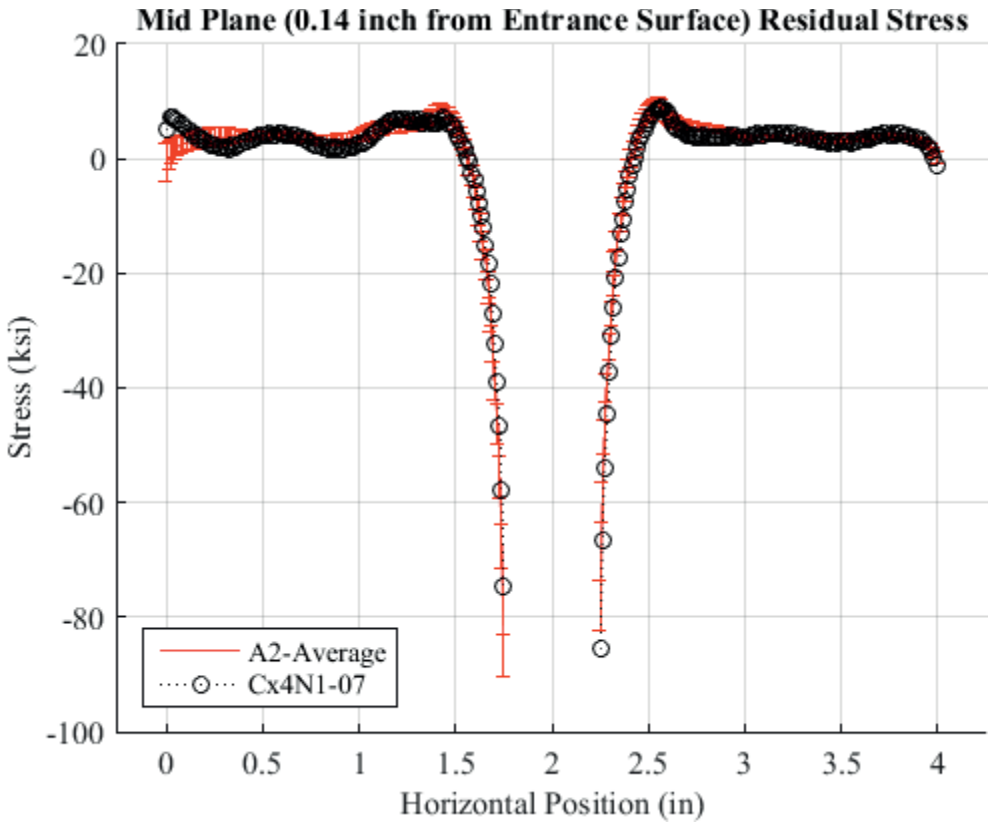

Fig. 670 Residual Stress Line Plot Comparing Cx4N1-07-B, and the Average between the Two to the CxA2 (2024-T351) Average Residual Stress at a Distance of 0.140 inch (Mid Plane Surface) from the Entrance Surface – Cx4N1-07-B Coupons had a 0.2515 inch Fatigue Crack at the Left Entrance Surface.

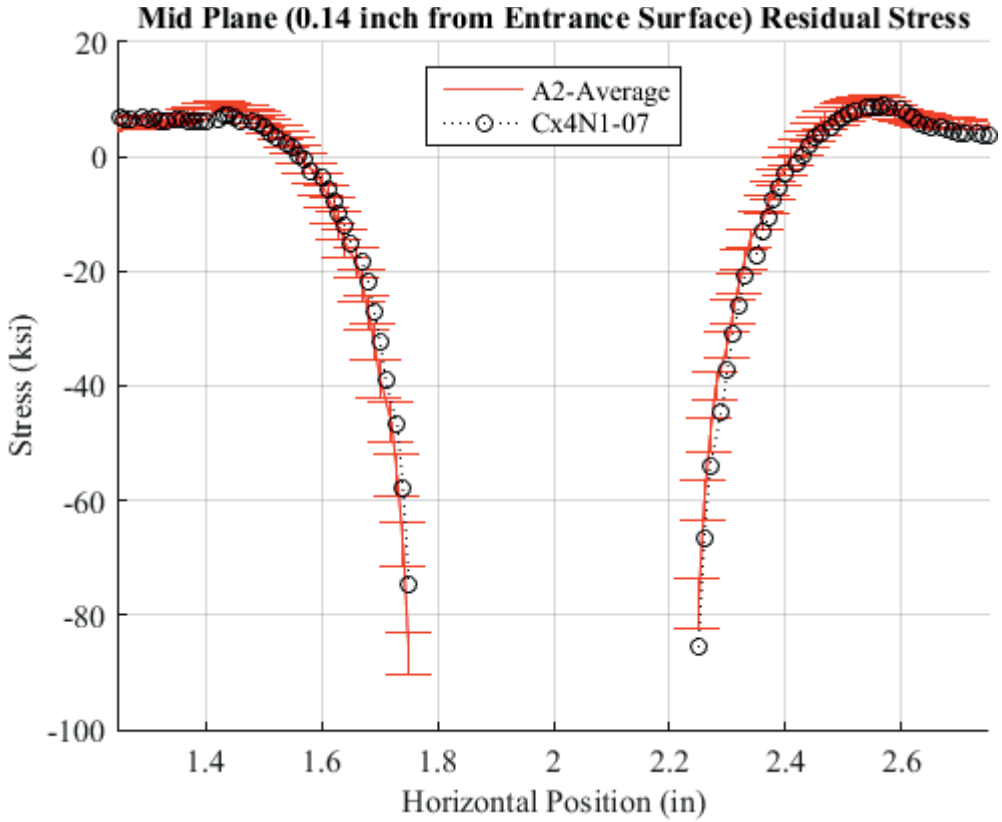

Fig. 671 Residual Stress Line Plot Comparing Cx4N1-07-B, and the Average between the Two to the CxA2 (2024-T351) Average Residual Stress at a Distance of 0.140 inch (Mid Plane Surface) from the Entrance Surface – Cx4N1-07-B Coupons had a 0.2515 inch Fatigue Crack at the Left Entrance Surface – Zoomed in Next to Hole.

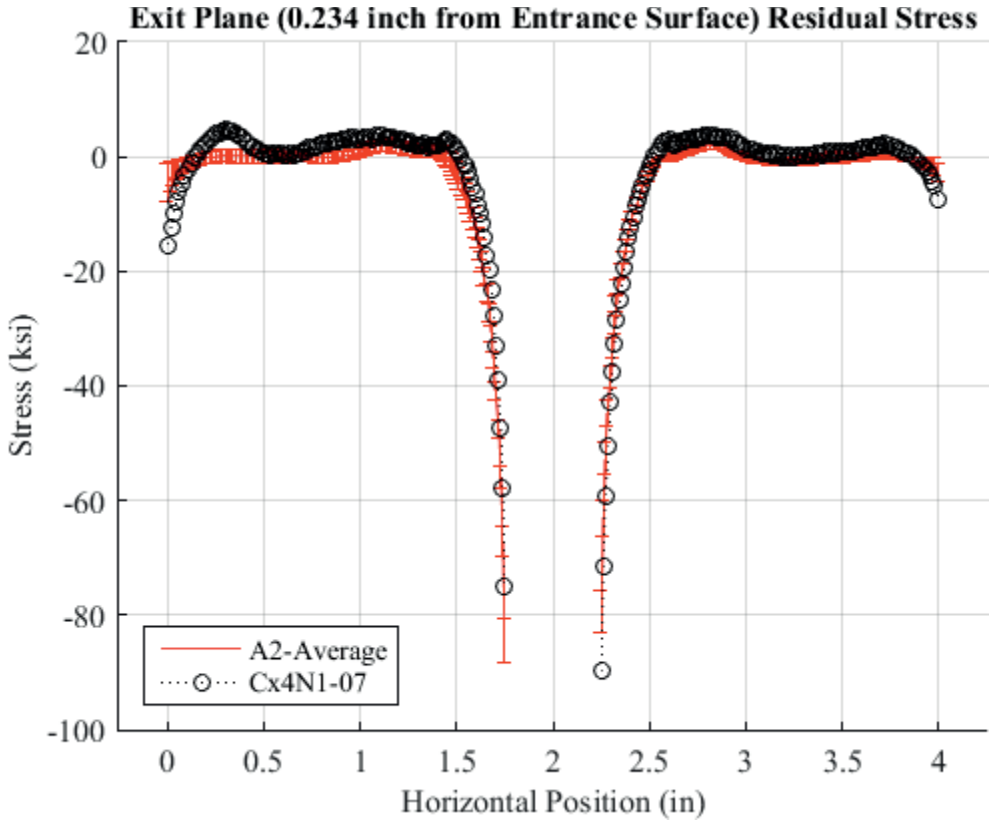

Fig. 672 Residual Stress Line Plot Comparing Cx4N1-07-B, and the Average between the Two to the CxA2 (2024-T351) Average Residual Stress at a Distance of 0234 inch (Exit Surface) from the Entrance Surface – Cx4N1-07-B Coupons had a 0.2515 inch Fatigue Crack at the Left Entrance Surface.

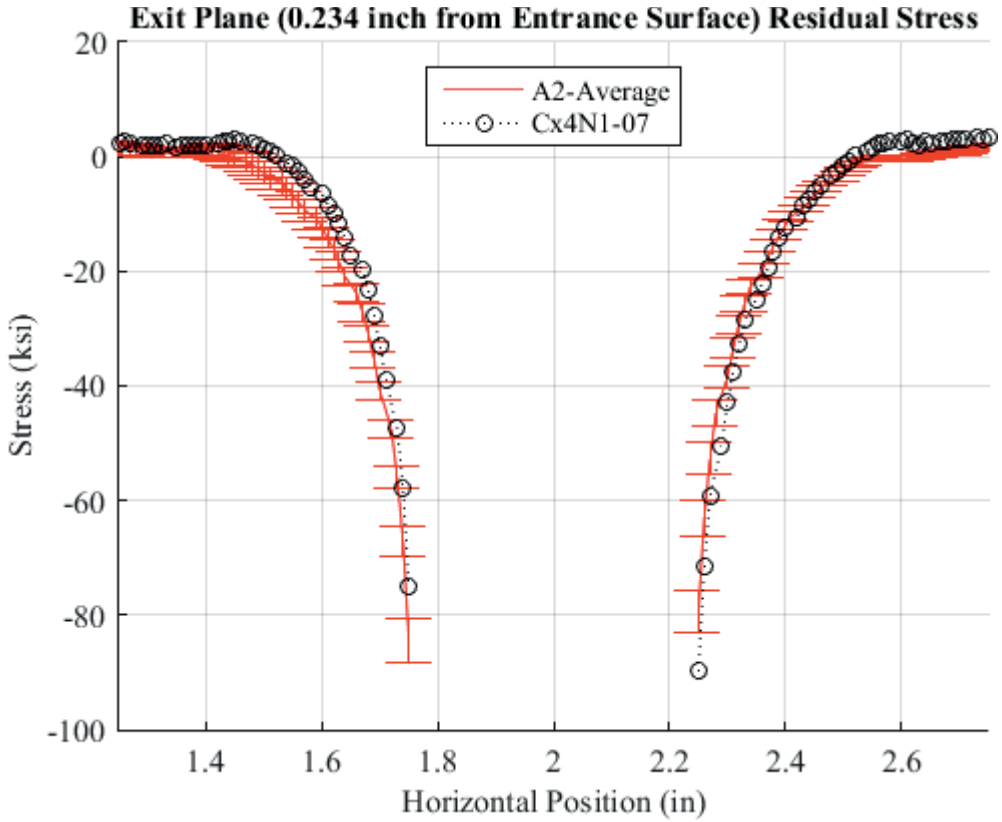

Fig. 673 Residual Stress Line Plot Comparing Cx4N1-07-B, and the Average between the Two to the CxA2 (2024-T351) Average Residual Stress at a Distance of 0234 inch (Exit Surface) from the Entrance Surface – Cx4N1-07-B Coupons had a 0.2515 inch Fatigue Crack at the Left Entrance Surface – Zoomed in Next to Hole.

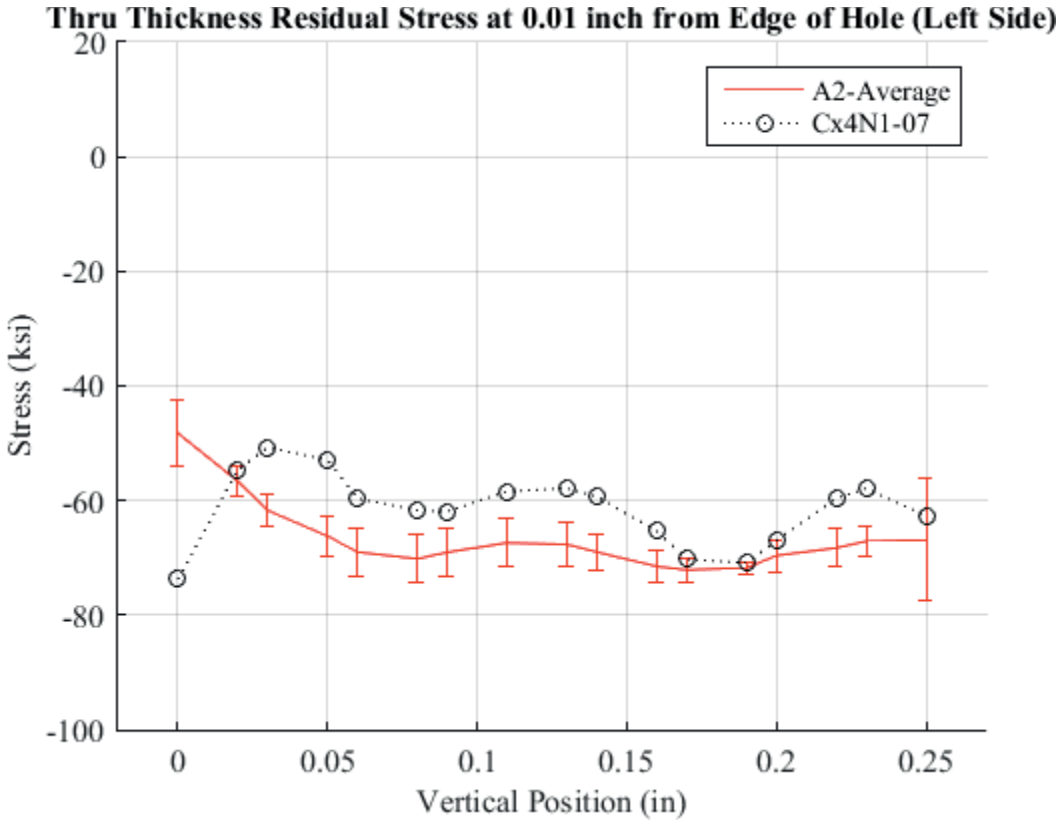

Fig. 674 Residual Stress Through-Thickness Line Plot Comparing Cx4N1-07-B, and the Average between the Two to the CxA2 (2024-T351) Average Residual Stress at a Distance of 0.01 inch from the Left Side of the Hole –Cx4N1-07-B Coupons had a 0.2515 inch Fatigue Crack at the Left Entrance Surface.

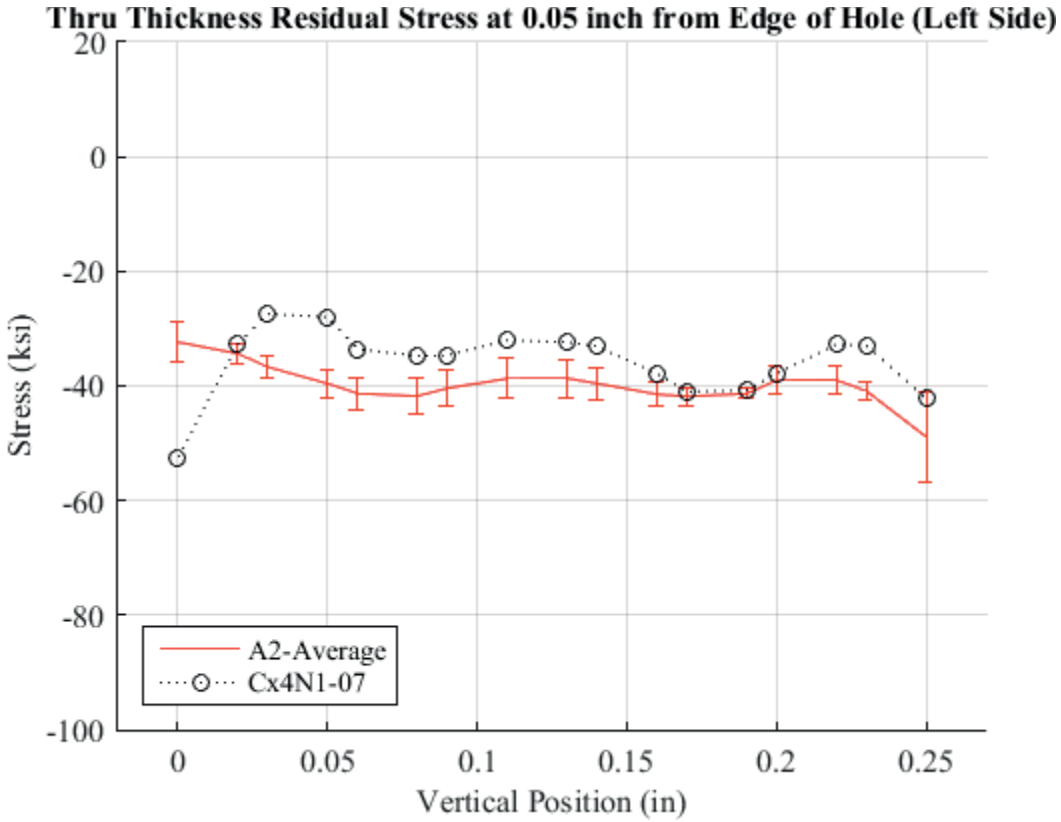

Fig. 675 Residual Stress Through-Thickness Line Plot Comparing Cx4N1-07-B, and the Average between the Two to the CxA2 (2024-T351) Average Residual Stress at a Distance of 0.05 inch from the Left Side of the Hole –Cx4N1-07-B Coupons had a 0.2515 inch Fatigue Crack at the Left Entrance Surface.

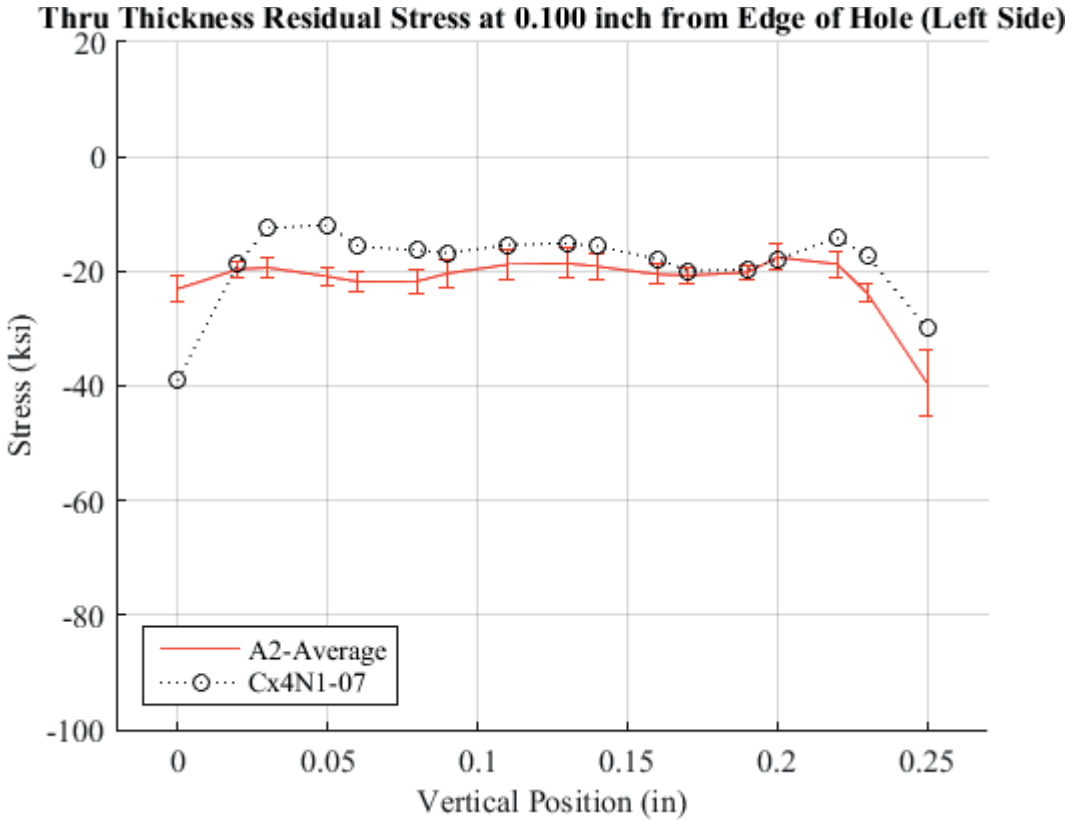

Fig. 676 Residual Stress Through-Thickness Line Plot Comparing Cx4N1-07-B, and the Average between the Two to the CxA2 (2024-T351) Average Residual Stress at a Distance of 0.10 inch from the Left Side of the Hole –Cx4N1-07-B Coupons had a 0.2515 inch Fatigue Crack at the Left Entrance Surface.

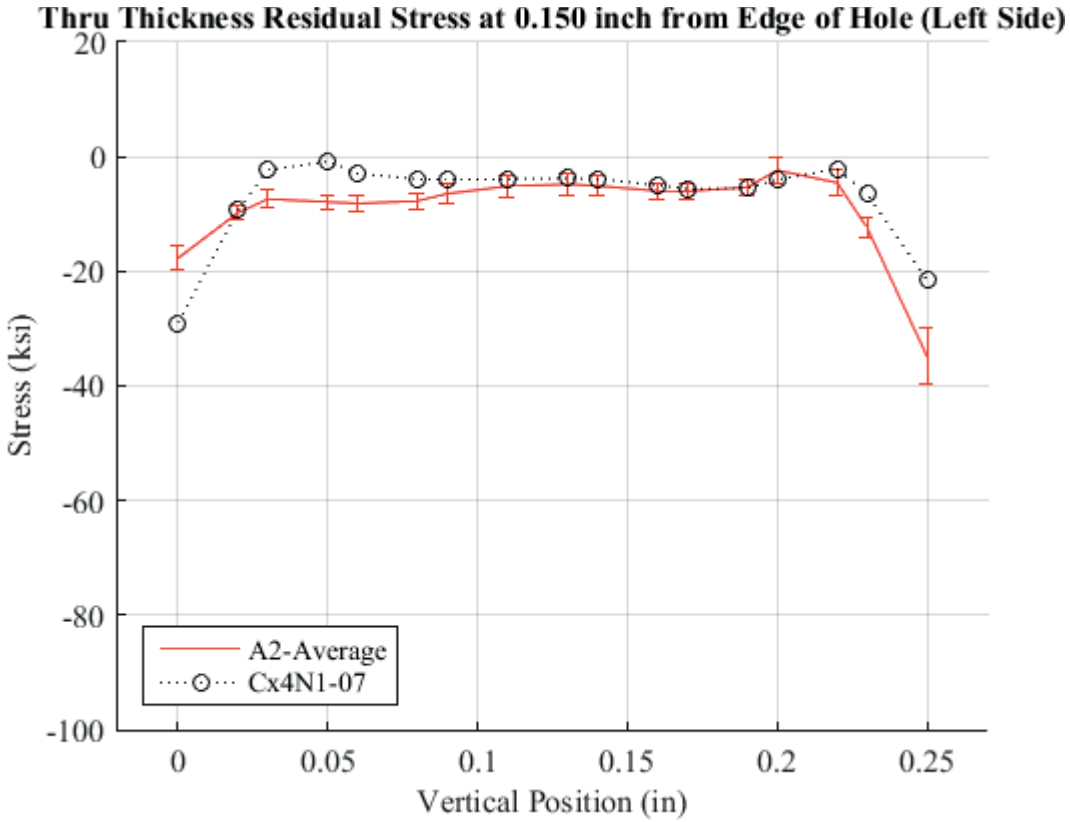

Fig. 677 Residual Stress Through-Thickness Line Plot Comparing Cx4N1-07-B, and the Average between the Two to the CxA2 (2024-T351) Average Residual Stress at a Distance of 0.125 inch from the Left Side of the Hole –Cx4N1-07-B Coupons had a 0.2515 inch Fatigue Crack at the Left Entrance Surface.

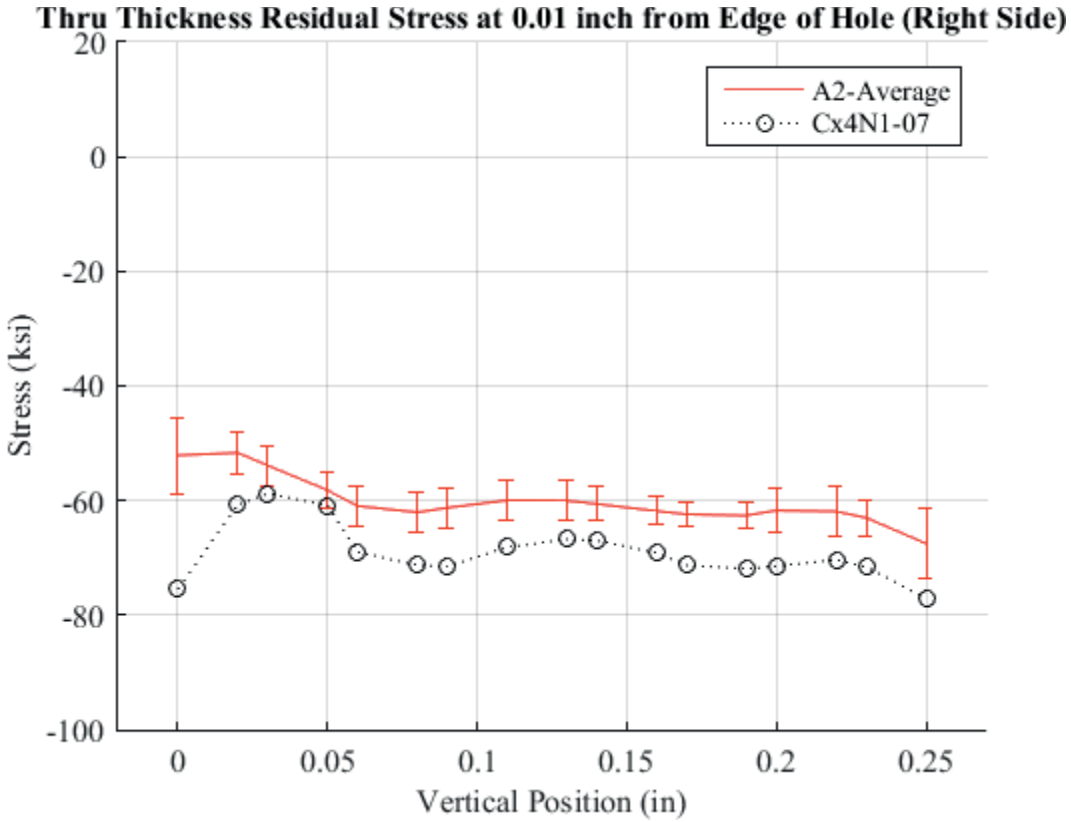

Fig. 678 Residual Stress Through-Thickness Line Plot Comparing Cx4N1-07-B, and the Average between the Two to the CxA2 (2024-T351) Average Residual Stress at a Distance of 0.01 inch from the Right Side of the Hole –Cx4N1-07-B Coupons had a 0.2515 inch Fatigue Crack at the Left Entrance Surface.

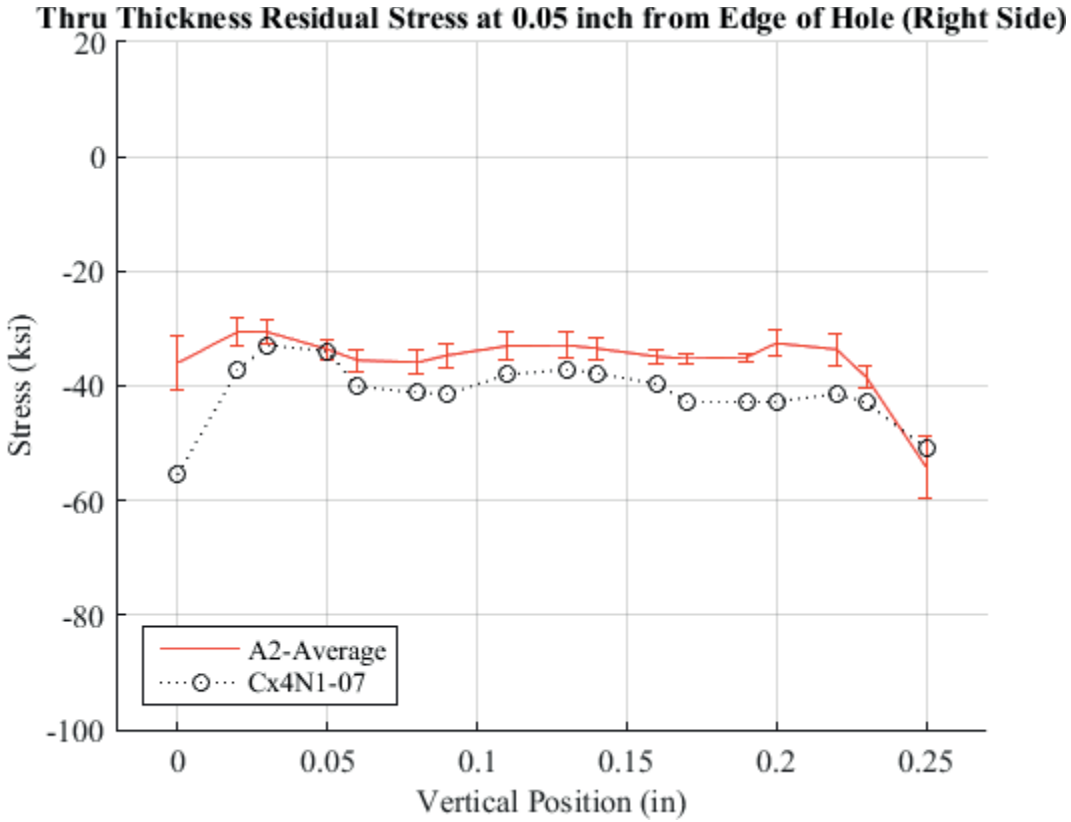

Fig. 679 Residual Stress Through-Thickness Line Plot Comparing Cx4N1-07-B, and the Average between the Two to the CxA2 (2024-T351) Average Residual Stress at a Distance of 0.05 inch from the Right Side of the Hole –Cx4N1-07-B Coupons had a 0.2515 inch Fatigue Crack at the Left Entrance Surface.

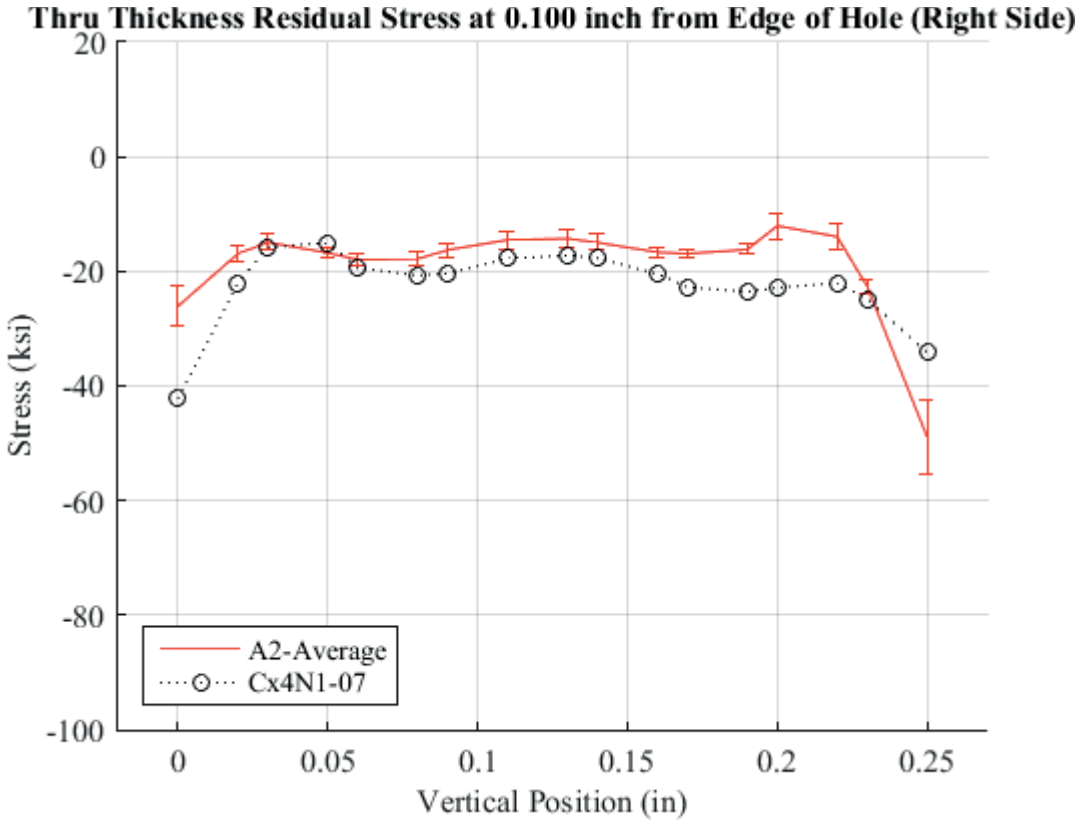

Fig. 680 Residual Stress Through-Thickness Line Plot Comparing Cx4N1-07-B, and the Average between the Two to the CxA2 (2024-T351) Average Residual Stress at a Distance of 0.10 inch from the Right Side of the Hole –Cx4N1-07-B Coupons had a 0.2515 inch Fatigue Crack at the Left Entrance Surface.

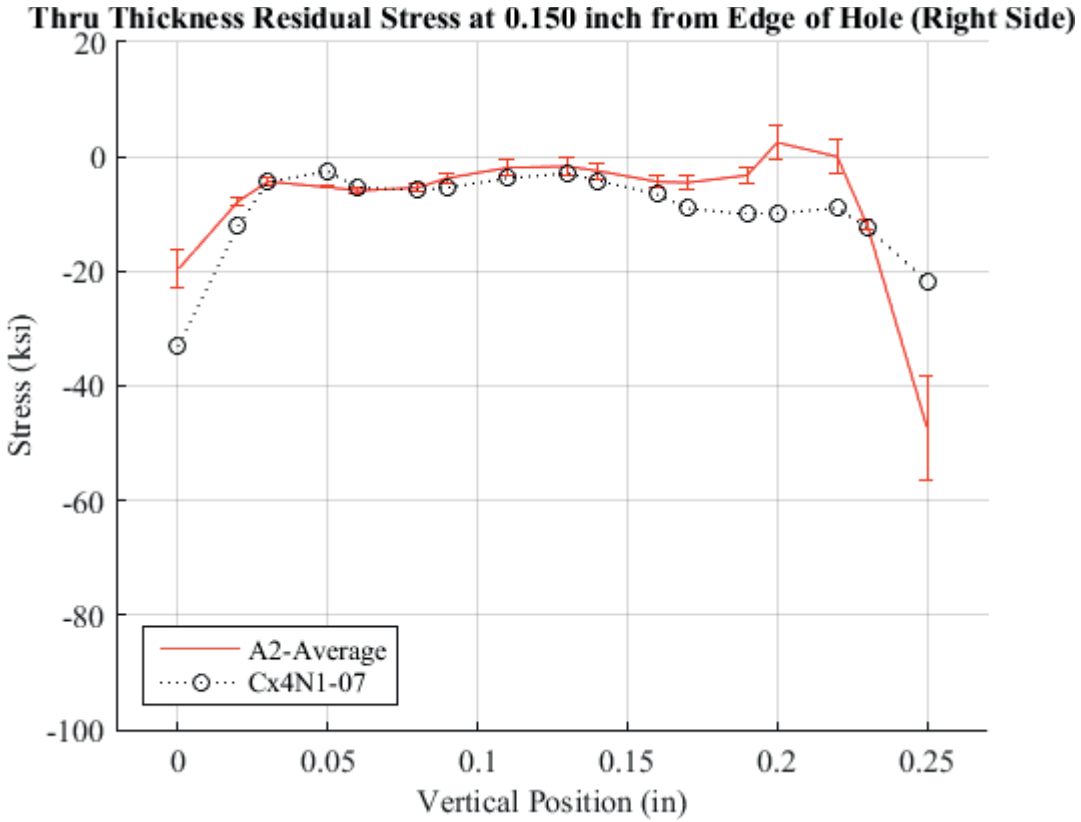

Fig. 681 Residual Stress Through-Thickness Line Plot Comparing Cx4N1-07-B, and the Average between the Two to the CxA2 (2024-T351) Average Residual Stress at a Distance of 0.150 inch from the Right Side of the Hole –Cx4N1-07-B Coupons had a 0.2515 inch Fatigue Crack at the Left Entrance Surface.

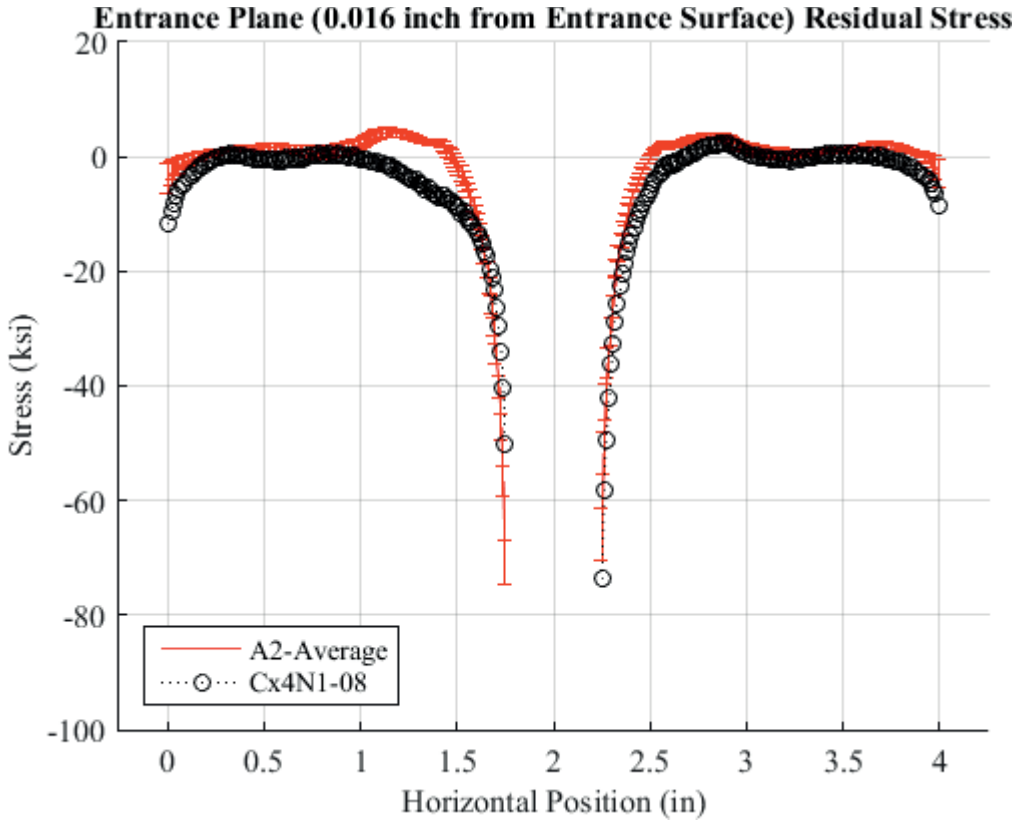

Fig. 682 Residual Stress Line Plot Comparing Cx4N1-08-B, and the Average between the Two to the CxA2 (2024-T351) Average Residual Stress at a Distance of 0.016 inch (Entrance Surface) from the Entrance Surface – Cx4N1-08-B Coupons had a 0.4974 inch Fatigue Crack at the Left Entrance Surface, There was also a Fatigue Crack on the Right Side of the Hole.

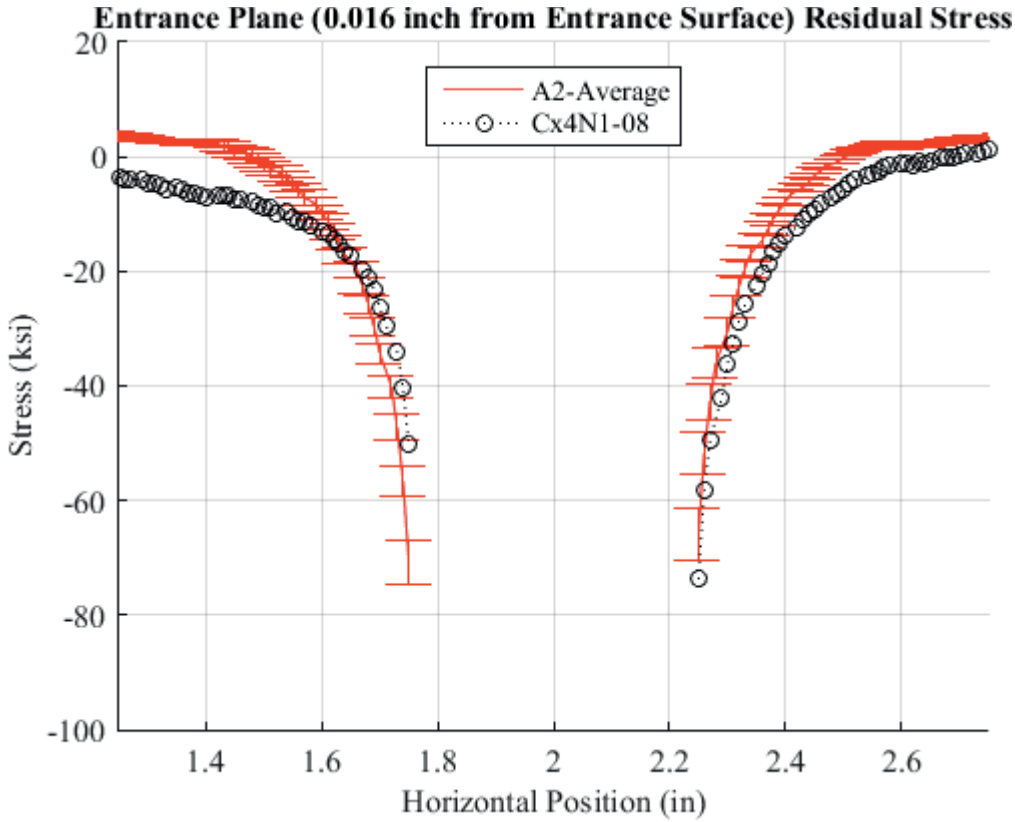

Fig. 683 Residual Stress Line Plot Comparing Cx4N1-08-B, and the Average between the Two to the CxA2 (2024-T351) Average Residual Stress at a Distance of 0.016 inch (Entrance Surface) from the Entrance Surface – Cx4N1-08-B Coupons had a 0.4974 inch Fatigue Crack at the Left Entrance Surface, There was also a Fatigue Crack on the Right Side of the Hole – Zoomed in Next to Hole.

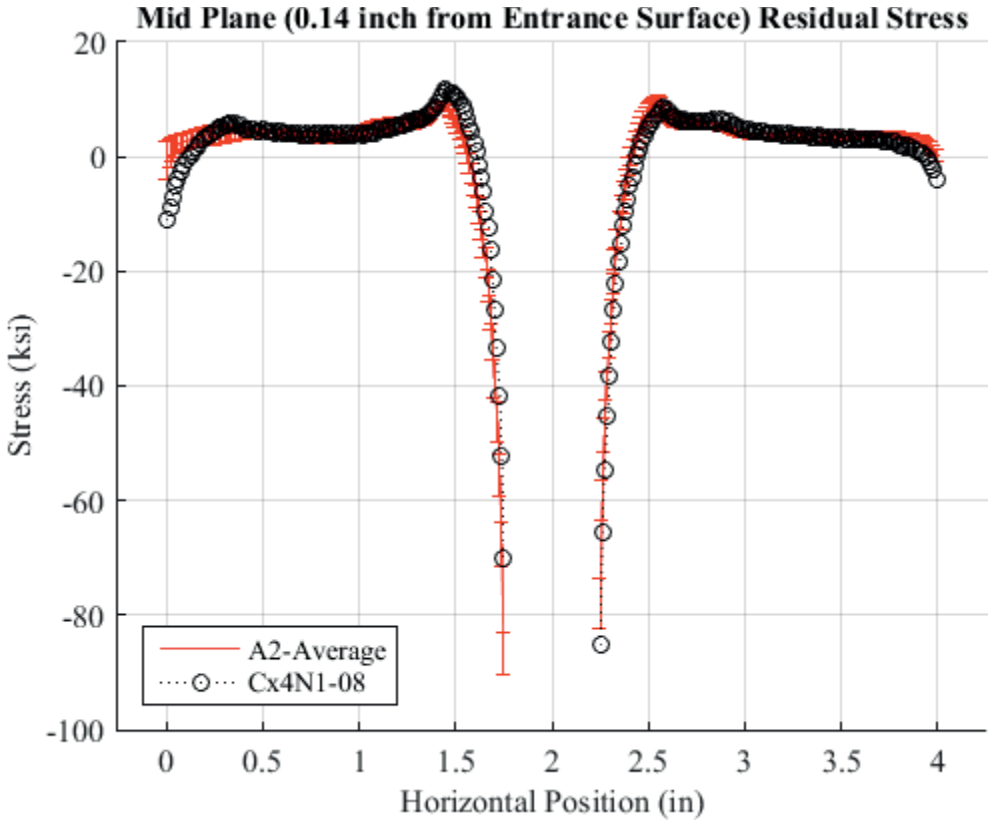

Fig. 684 Residual Stress Line Plot Comparing Cx4N1-08-B, and the Average between the Two to the CxA2 (2024-T351) Average Residual Stress at a Distance of 0.140 inch (Mid Plane Surface) from the Entrance Surface – Cx4N1-08-B Coupons had a 0.4974 inch Fatigue Crack at the Left Entrance Surface, There was also a Fatigue Crack on the Right Side of the Hole.

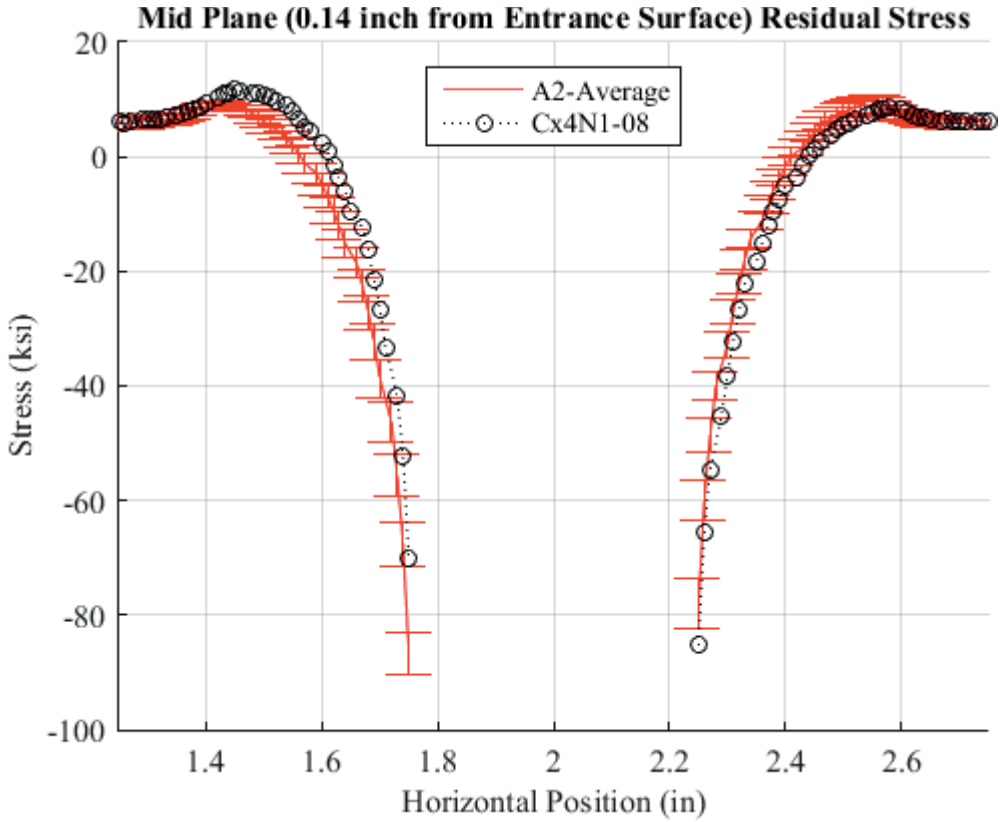

Fig. 685 Residual Stress Line Plot Comparing Cx4N1-08-B, and the Average between the Two to the CxA2 (2024-T351) Average Residual Stress at a Distance of 0.140 inch (Mid Plane Surface) from the Entrance Surface – Cx4N1-08-B Coupons had a 0.4974 inch Fatigue Crack at the Left Entrance Surface, There was also a Fatigue Crack on the Right Side of the Hole – Zoomed in Next to Hole.

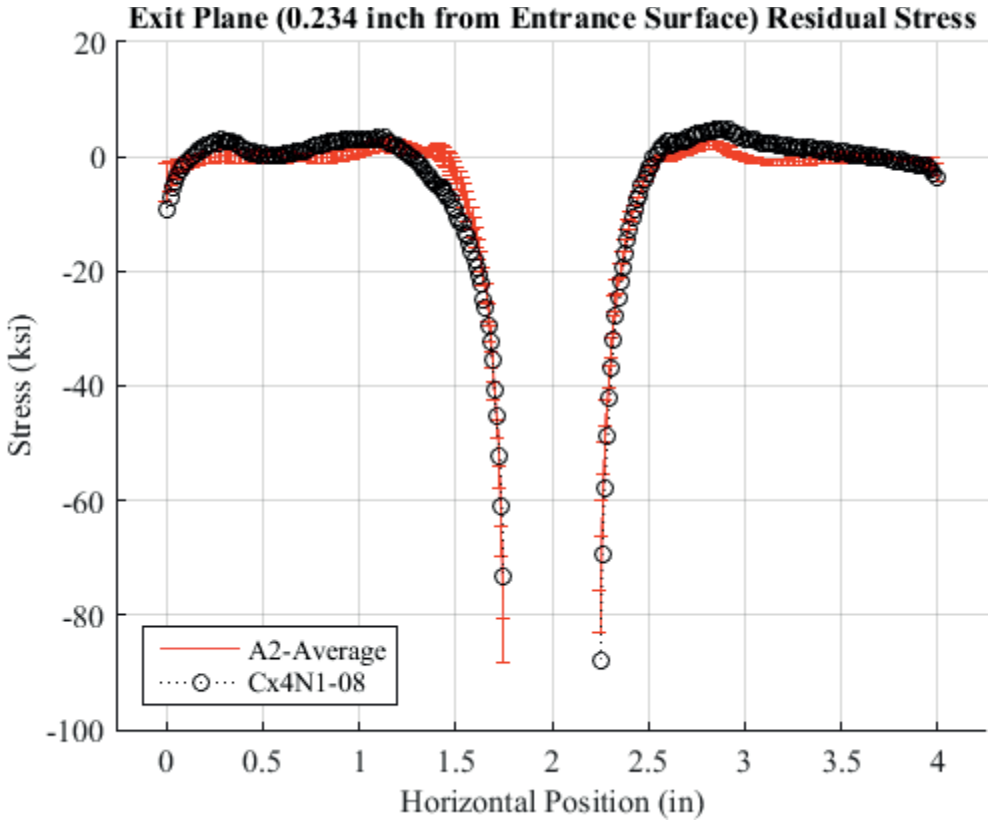

Fig. 686 Residual Stress Line Plot Comparing Cx4N1-08-B, and the Average between the Two to the CxA2 (2024-T351) Average Residual Stress at a Distance of 0.234 inch (Exit Surface) from the Entrance Surface – Cx4N1-08-B Coupons had a 0.4974 inch Fatigue Crack at the Left Entrance Surface, There was also a Fatigue Crack on the Right Side of the Hole.

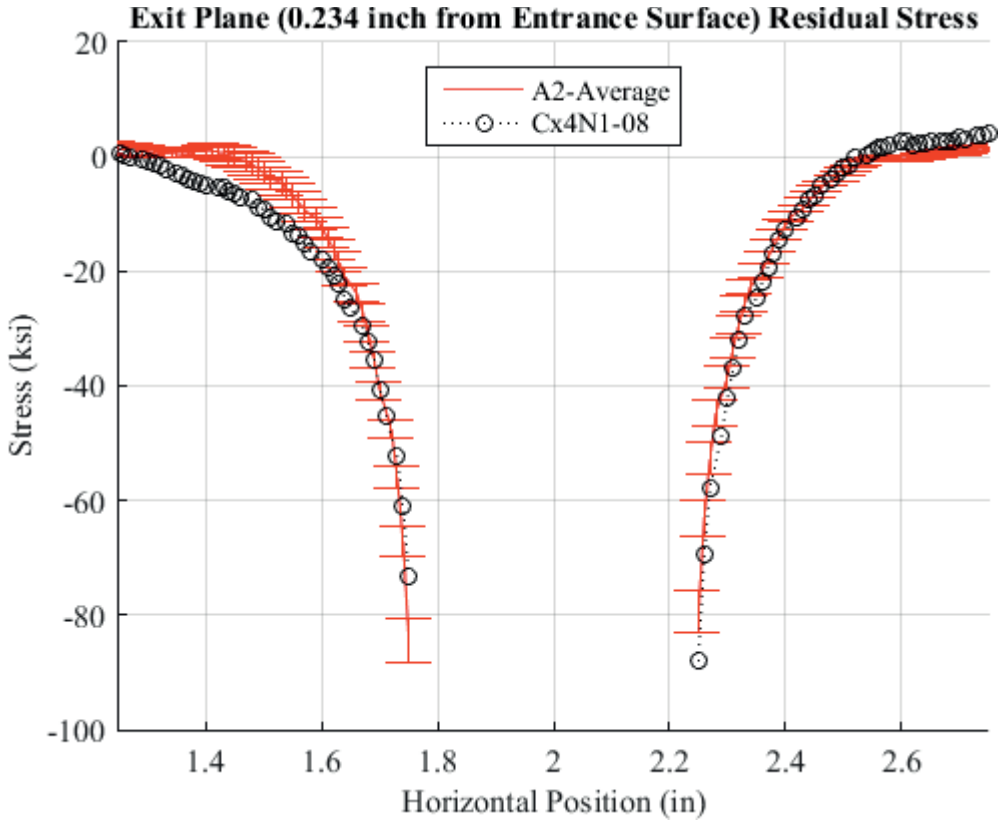

Fig. 687 Residual Stress Line Plot Comparing Cx4N1-08-B, and the Average between the Two to the CxA2 (2024-T351) Average Residual Stress at a Distance of 0.234 inch (Exit Surface) from the Entrance Surface – Cx4N1-08-B Coupons had a 0.4974 inch Fatigue Crack at the Left Entrance Surface, There was also a Fatigue Crack on the Right Side of the Hole – Zoomed in Next to Hole.

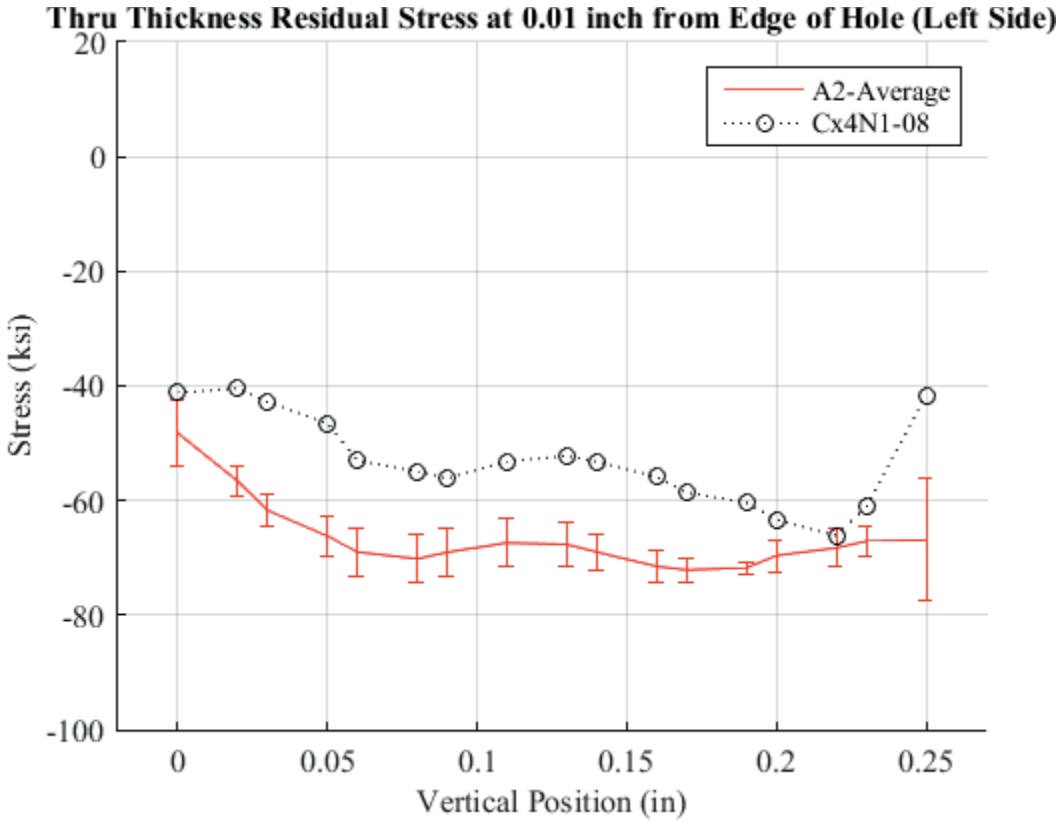

Fig. 688 Residual Stress Through-Thickness Line Plot Comparing Cx4N1-08-B, and the Average between the Two to the CxA2 (2024-T351) Average Residual Stress at a Distance of 0.01 inch from the Left Side of the Hole –Cx4N1-08-B Coupons had a 0.4974 inch Fatigue Crack at the Left Entrance Surface, There was also a Fatigue Crack on the Right Side of the Hole.

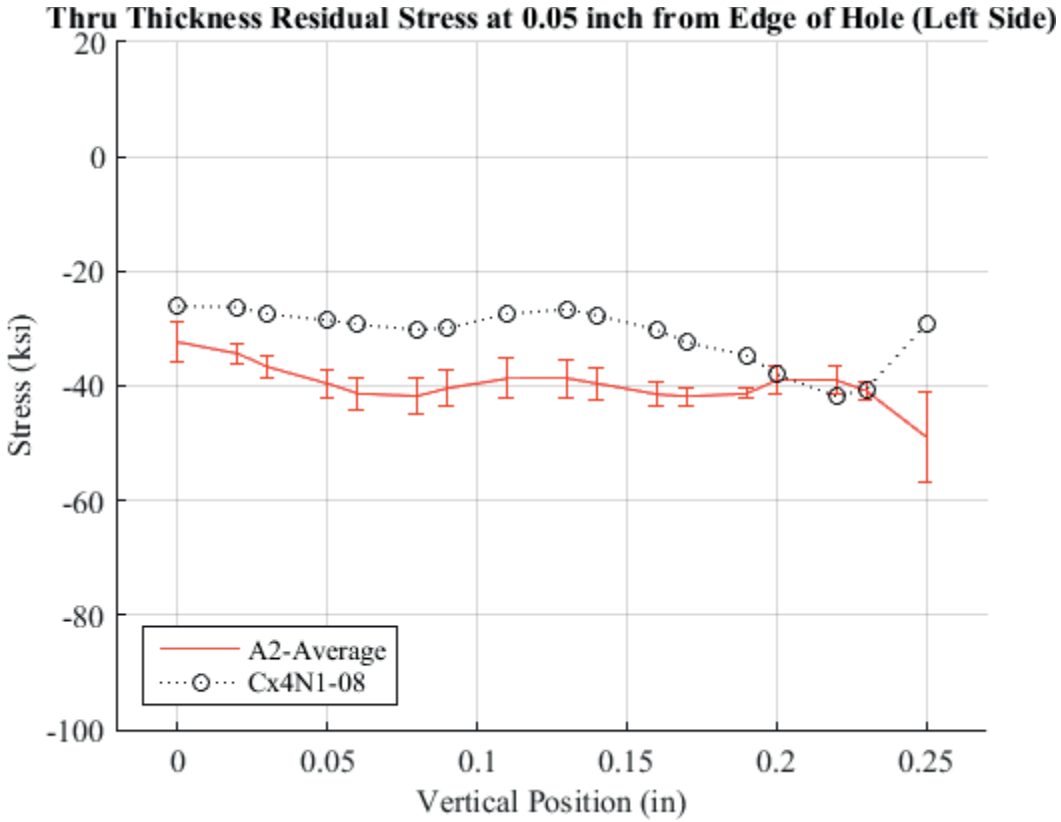

Fig. 689 Residual Stress Through-Thickness Line Plot Comparing Cx4N1-08-B, and the Average between the Two to the CxA2 (2024-T351) Average Residual Stress at a Distance of 0.05 inch from the Left Side of the Hole –Cx4N1-08-B Coupons had a 0.4974 inch Fatigue Crack at the Left Entrance Surface, There was also a Fatigue Crack on the Right Side of the Hole.

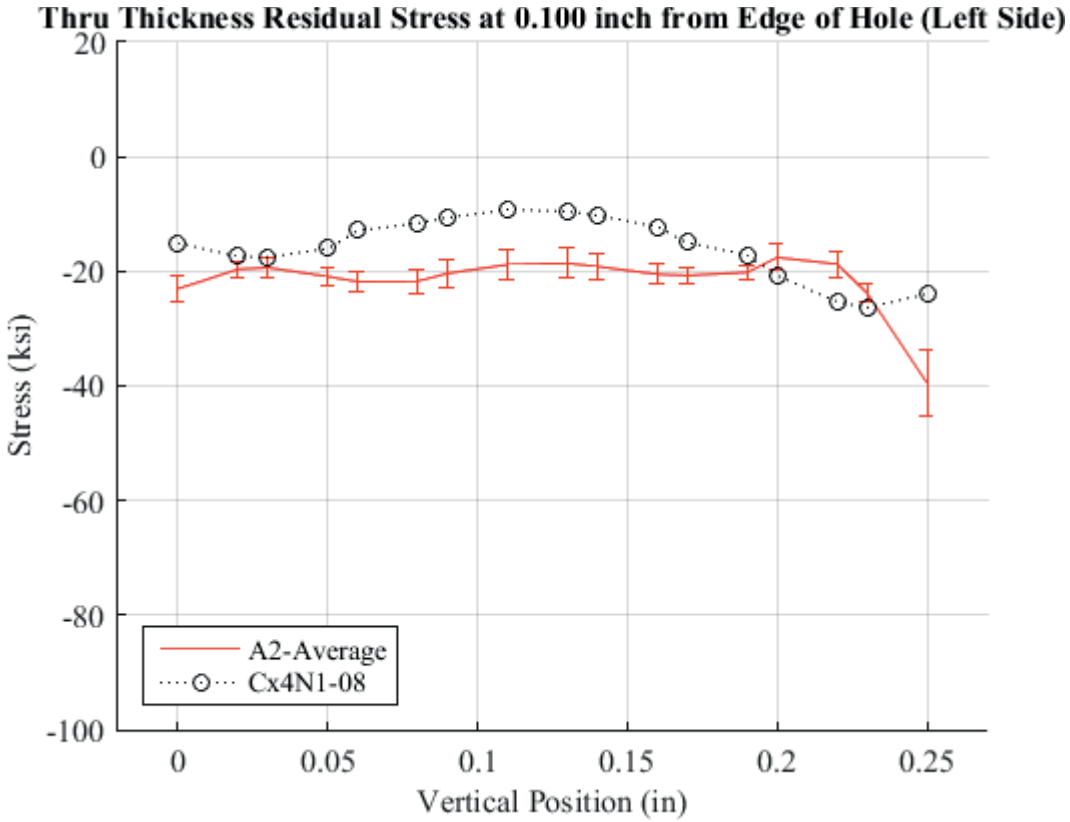

Fig. 690 Residual Stress Through-Thickness Line Plot Comparing Cx4N1-08-B, and the Average between the Two to the CxA2 (2024-T351) Average Residual Stress at a Distance of 0.10 inch from the Left Side of the Hole –Cx4N1-08-B Coupons had a 0.4974 inch Fatigue Crack at the Left Entrance Surface, There was also a Fatigue Crack on the Right Side of the Hole.

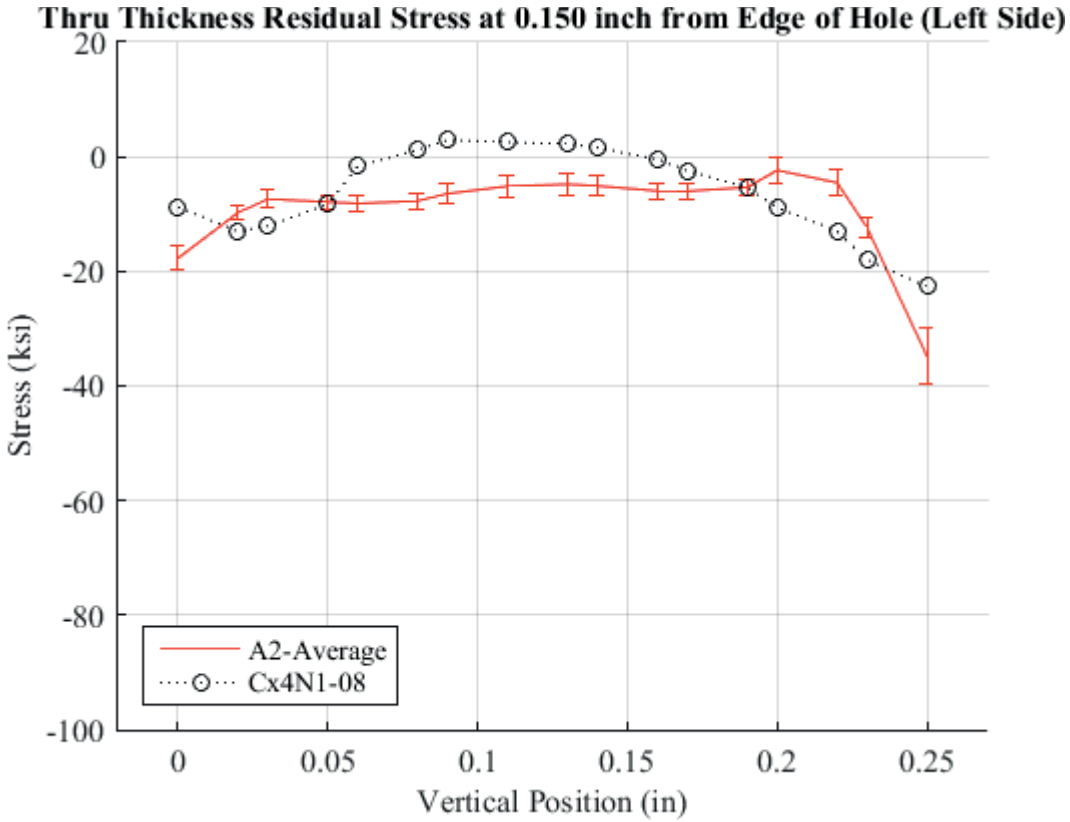

Fig. 691 Residual Stress Through-Thickness Line Plot Comparing Cx4N1-08-B, and the Average between the Two to the CxA2 (2024-T351) Average Residual Stress at a Distance of 0.150 inch from the Left Side of the Hole –Cx4N1-08-B Coupons had a 0.4974 inch Fatigue Crack at the Left Entrance Surface, There was also a Fatigue Crack on the Right Side of the Hole.

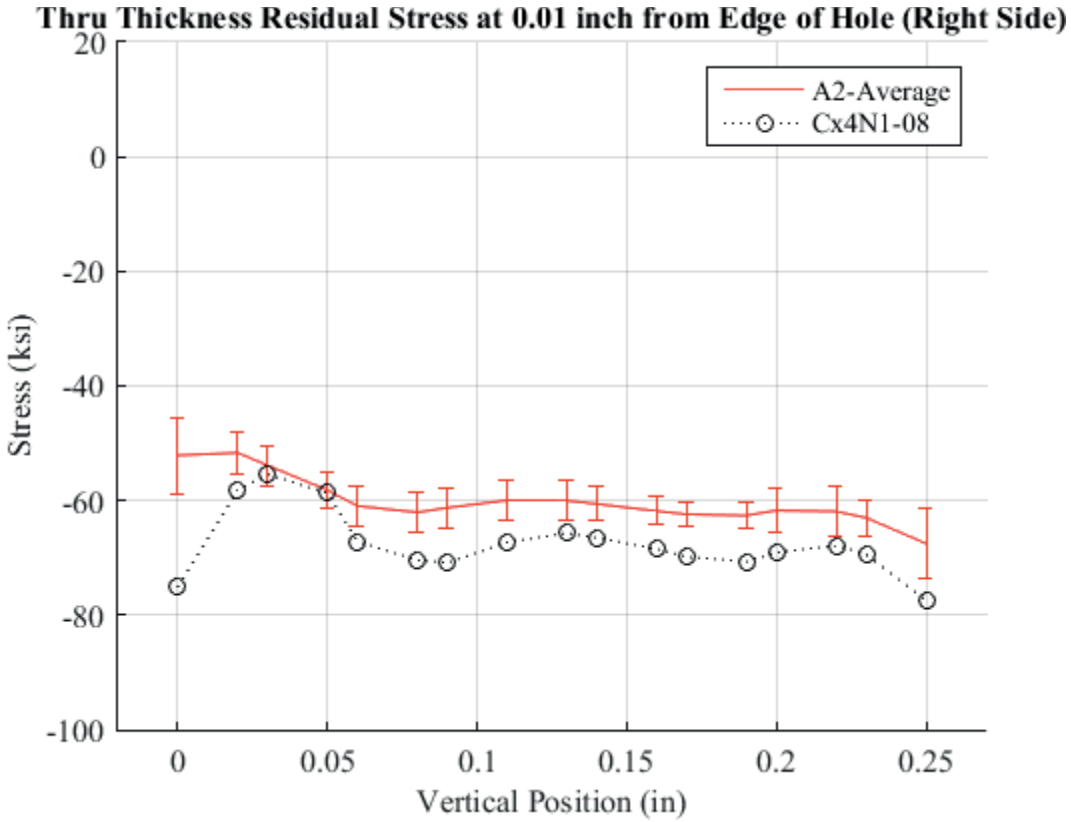

Fig. 692 Residual Stress Through-Thickness Line Plot Comparing Cx4N1-08-B, and the Average between the Two to the CxA2 (2024-T351) Average Residual Stress at a Distance of 0.01 inch from the Right Side of the Hole –Cx4N1-08-B Coupons had a 0.4974 inch Fatigue Crack at the Left Entrance Surface, There was also a Fatigue Crack on the Right Side of the Hole.

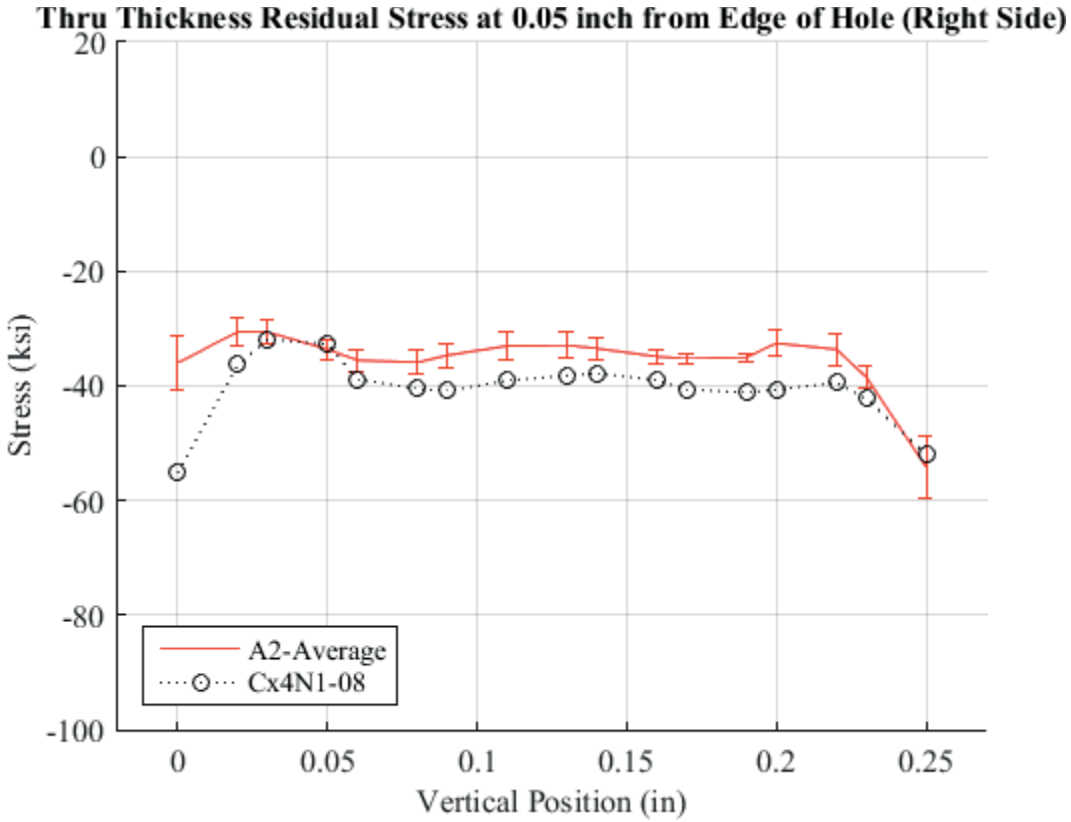

Fig. 693 Residual Stress Through-Thickness Line Plot Comparing Cx4N1-08-B, and the Average between the Two to the CxA2 (2024-T351) Average Residual Stress at a Distance of 0.05 inch from the Right Side of the Hole –Cx4N1-08-B Coupons had a 0.4974 inch Fatigue Crack at the Left Entrance Surface, There was also a Fatigue Crack on the Right Side of the Hole.

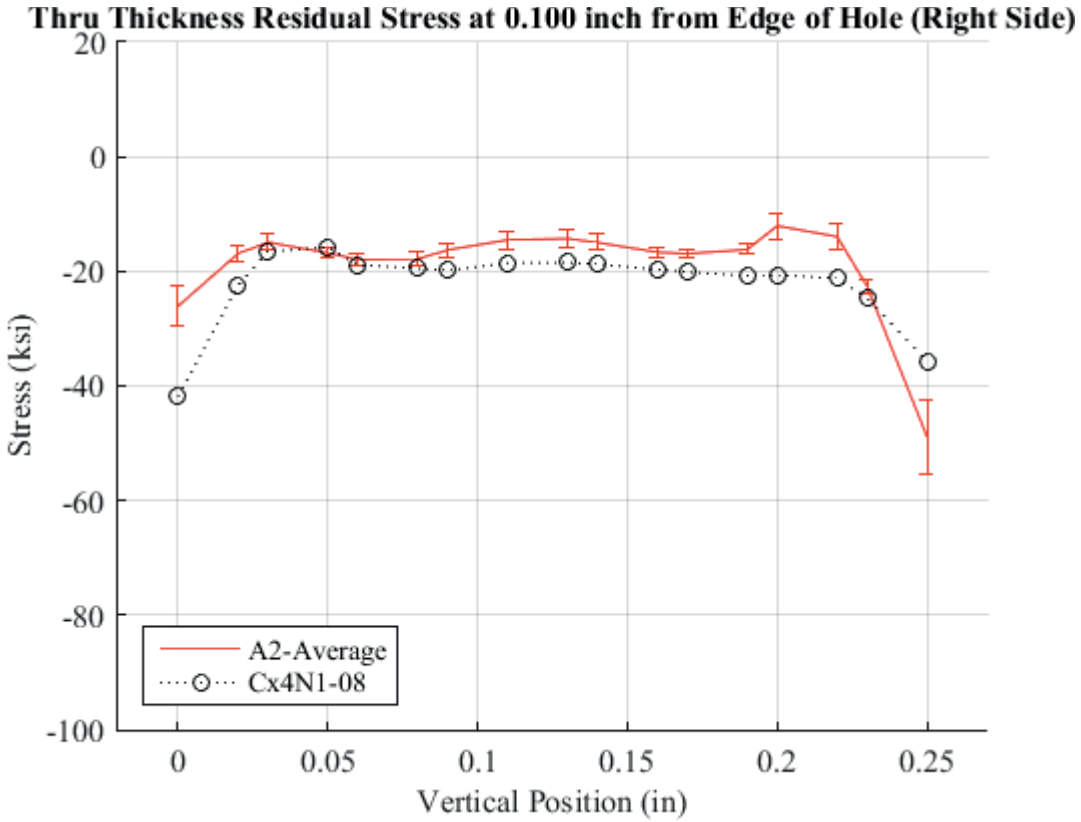

Fig. 694 Residual Stress Through-Thickness Line Plot Comparing Cx4N1-08-B, and the Average between the Two to the CxA2 (2024-T351) Average Residual Stress at a Distance of 0.10 inch from the Right Side of the Hole –Cx4N1-08-B Coupons had a 0.4974 inch Fatigue Crack at the Left Entrance Surface, There was also a Fatigue Crack on the Right Side of the Hole.

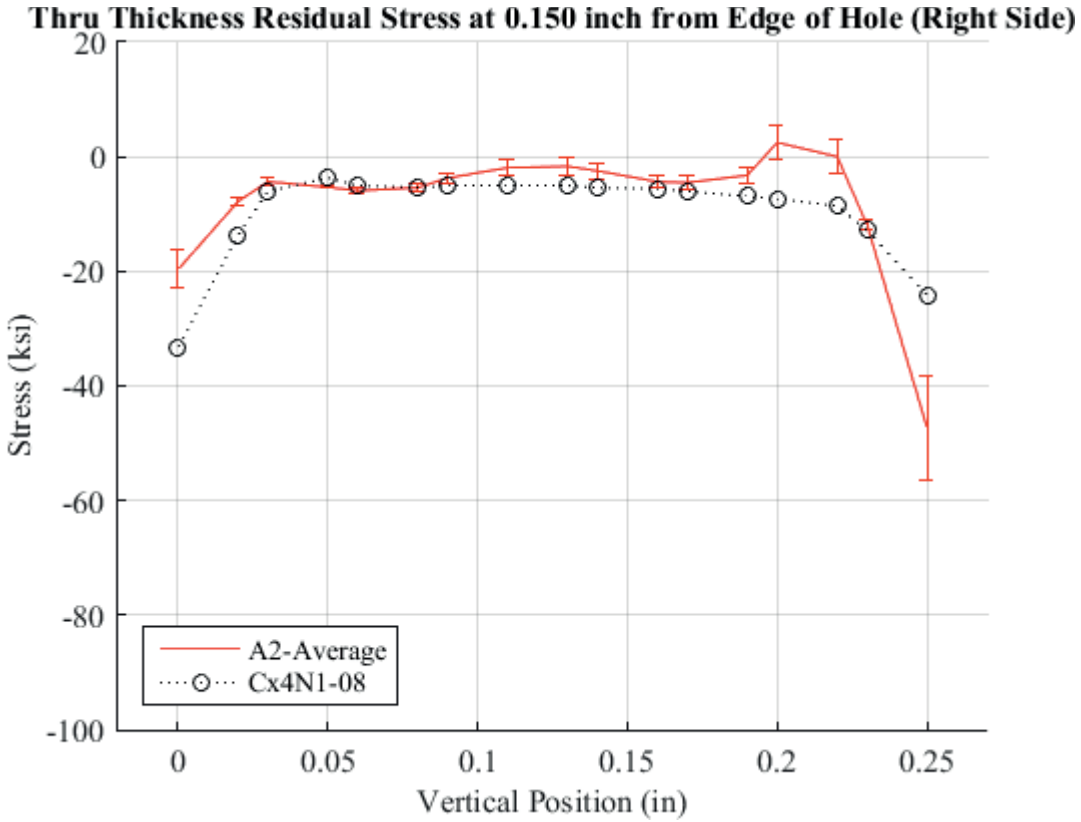

Fig. 695 Residual Stress Through-Thickness Line Plot Comparing Cx4N1-08-B, and the Average between the Two to the CxA2 (2024-T351) Average Residual Stress at a Distance of 0.150 inch from the Right Side of the Hole –Cx4N1-08-B Coupons had a 0.4974 inch Fatigue Crack at the Left Entrance Surface, There was also a Fatigue Crack on the Right Side of the Hole.

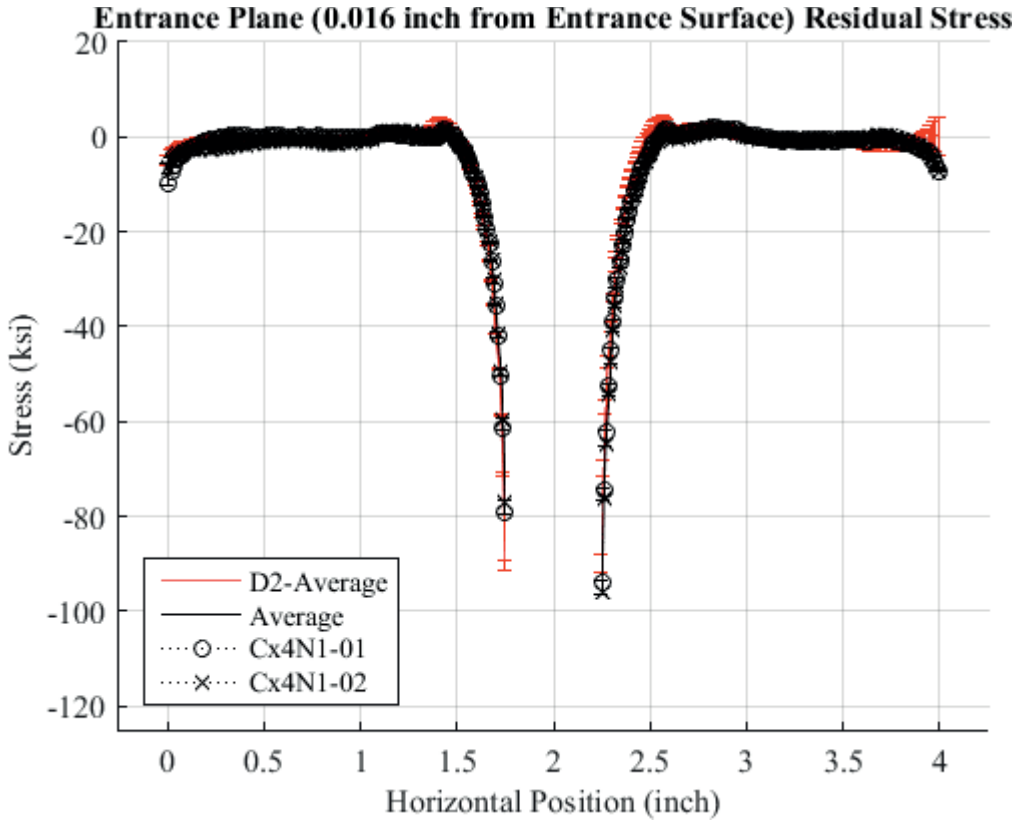

Fig. 696 Residual Stress Line Plot Comparing Cx4N1-01-D, Cx4N1-02-D, and the Average between the Two to the CxD2 (7075-T651) Average Residual Stress at a Distance of 0.016 inch (Entrance Surface) from the Entrance Surface – Cx4N1-01-D and Cx4N1-02-D Coupons had a 0.08 inch Fatigue Crack at the Left Entrance Surface.

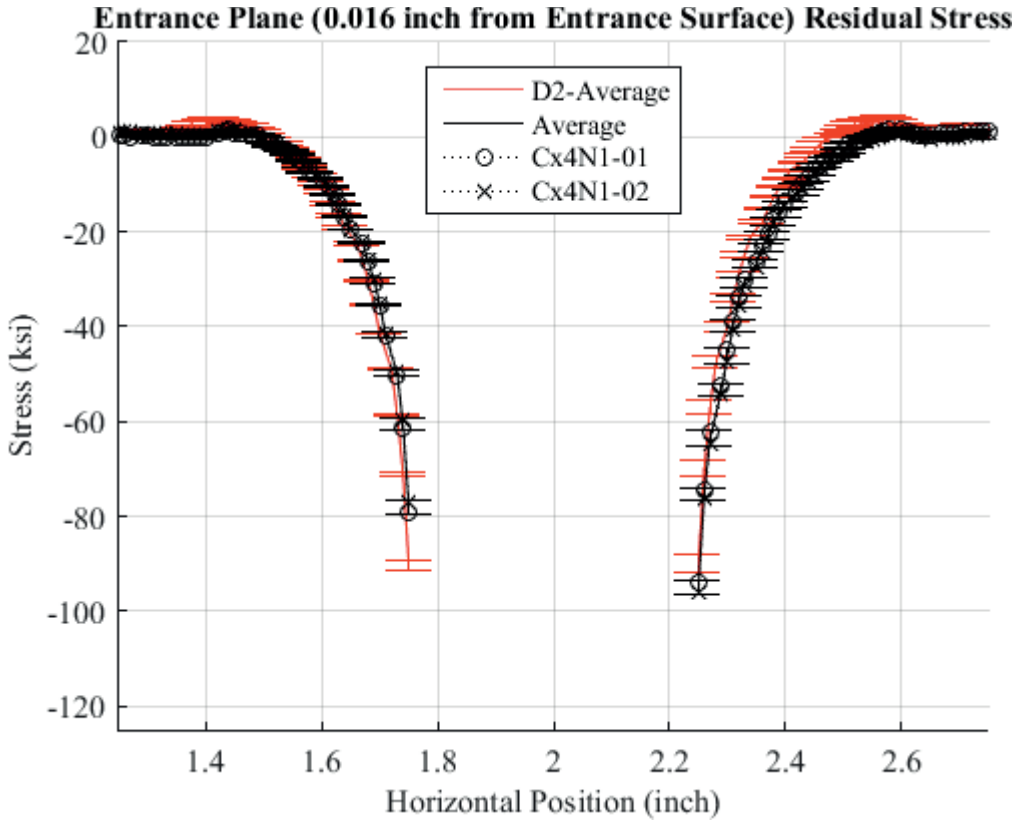

Fig. 697 Residual Stress Line Plot Comparing Cx4N1-01-D, Cx4N1-02-D, and the Average between the Two to the CxD2 (7075-T651) Average Residual Stress at a Distance of 0.016 inch (Entrance Surface) from the Entrance Surface – Cx4N1-01-D and Cx4N1-02-D Coupons had a 0.08 inch Fatigue Crack at the Left Entrance Surface – Zoomed in Next to Hole.

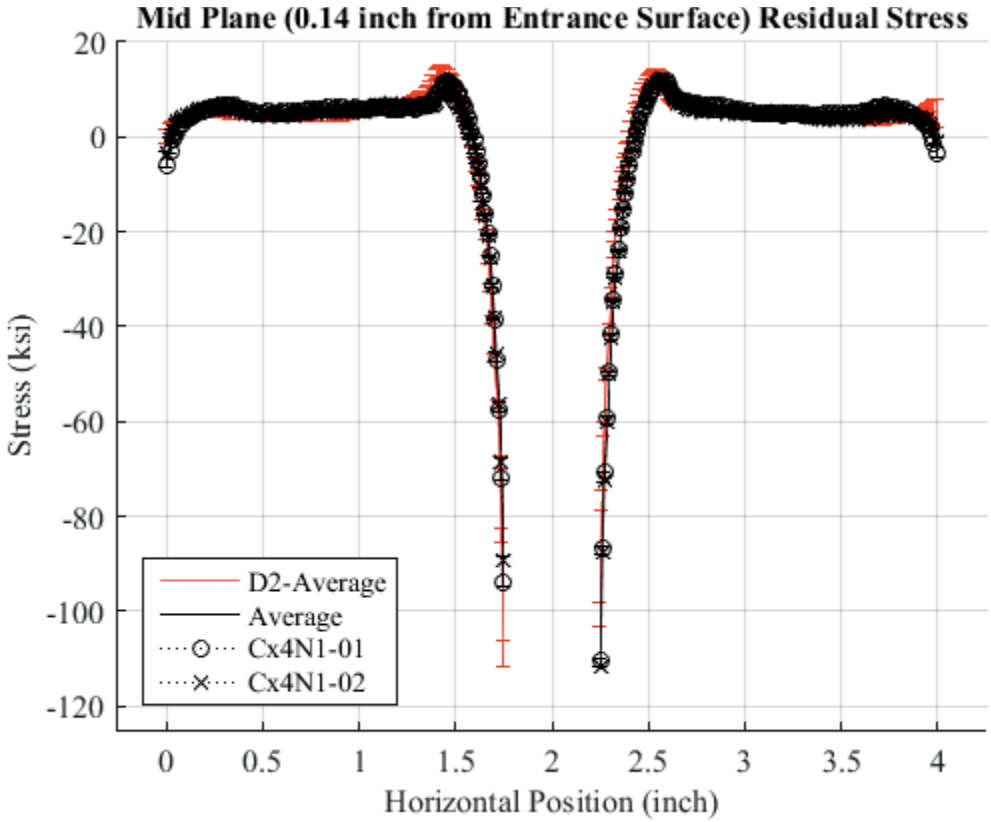

Fig. 698 Residual Stress Line Plot Comparing Cx4N1-01-D, Cx4N1-02-D, and the Average between the Two to the CxD2 (7075-T651) Average Residual Stress at a Distance of 0.140 inch (Mid Plane Surface) from the Entrance Surface – Cx4N1-01-D and Cx4N1-02-D Coupons had a 0.08 inch Fatigue Crack at the Left Entrance Surface.

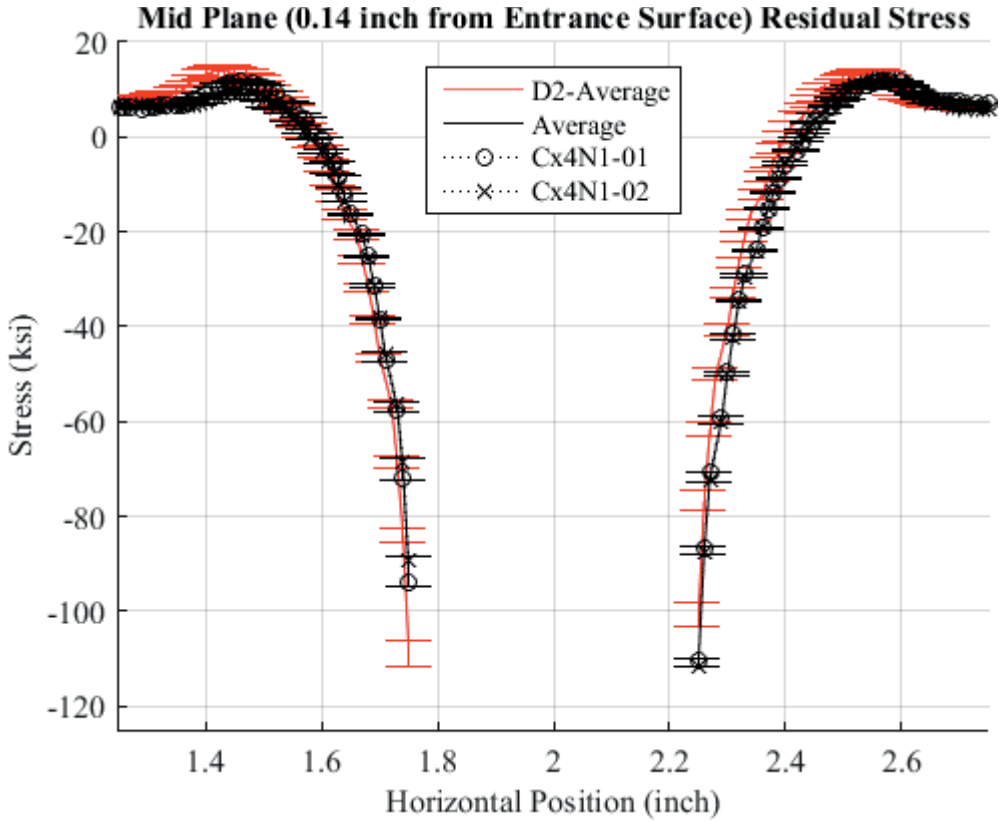

Fig. 699 Residual Stress Line Plot Comparing Cx4N1-01-D, Cx4N1-02-D, and the Average between the Two to the CxD2 (7075-T651) Average Residual Stress at a Distance of 0.140 inch (Mid Plane Surface) from the Entrance Surface – Cx4N1-01-D and Cx4N1-02-D Coupons had a 0.08 inch Fatigue Crack at the Left Entrance Surface – Zoomed in Next to Hole.

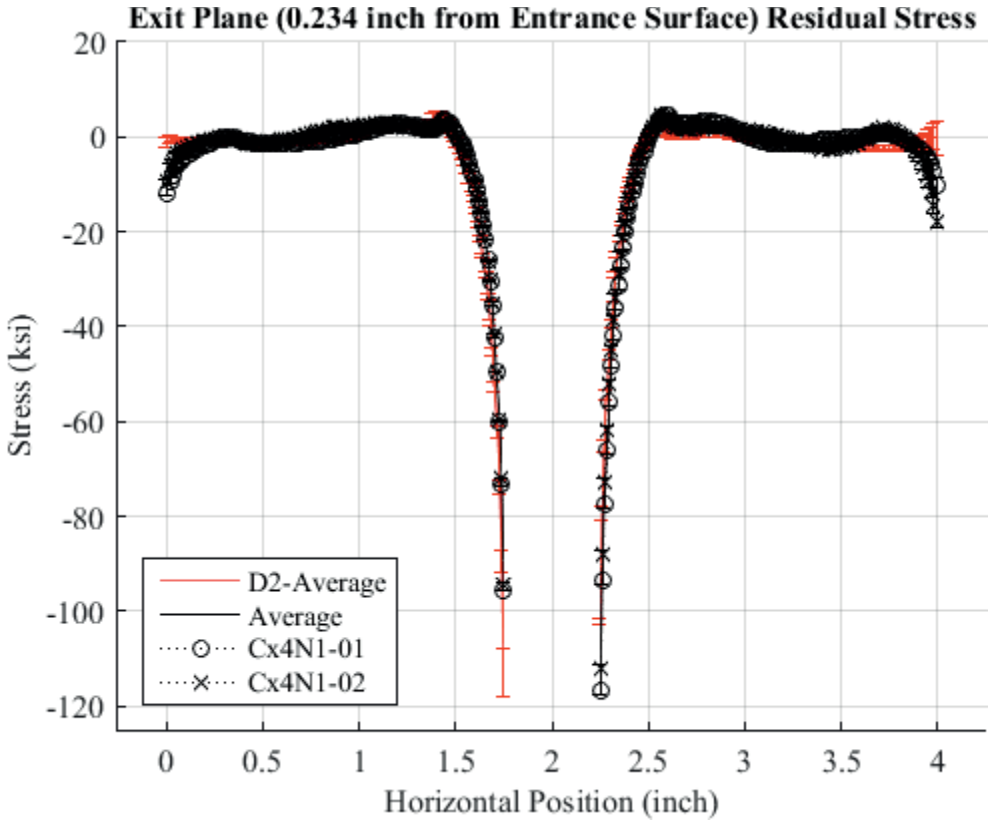

Fig. 700 Residual Stress Line Plot Comparing Cx4N1-01-D, Cx4N1-02-D, and the Average between the Two to the CxD2 (7075-T651) Average Residual Stress at a Distance of 0.234 inch (Exit Surface) from the Entrance Surface – Cx4N1-01-D and Cx4N1-02-D Coupons had a 0.08 inch Fatigue Crack at the Left Entrance Surface.

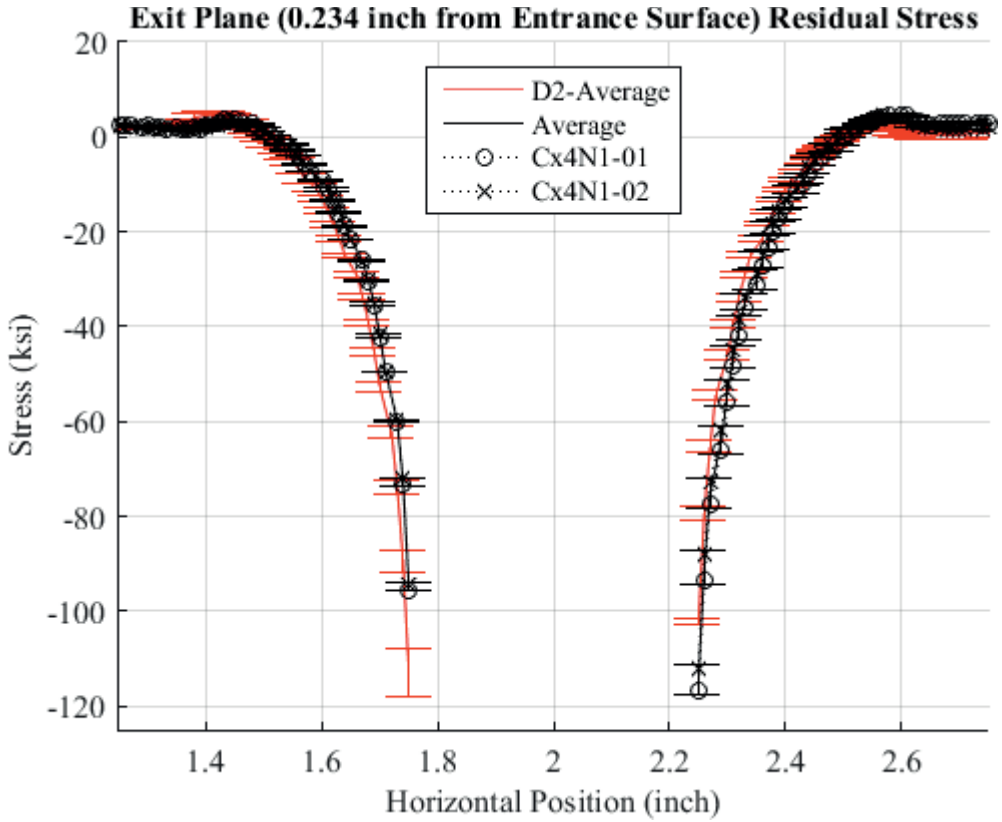

Fig. 701 Residual Stress Line Plot Comparing Cx4N1-01-D, Cx4N1-02-D, and the Average between the Two to the CxD2 (7075-T651) Average Residual Stress at a Distance of 0.234 inch (Exit Surface) from the Entrance Surface – Cx4N1-01-D and Cx4N1-02-D Coupons had a 0.08 inch Fatigue Crack at the Left Entrance Surface – Zoomed in Next to Hole.

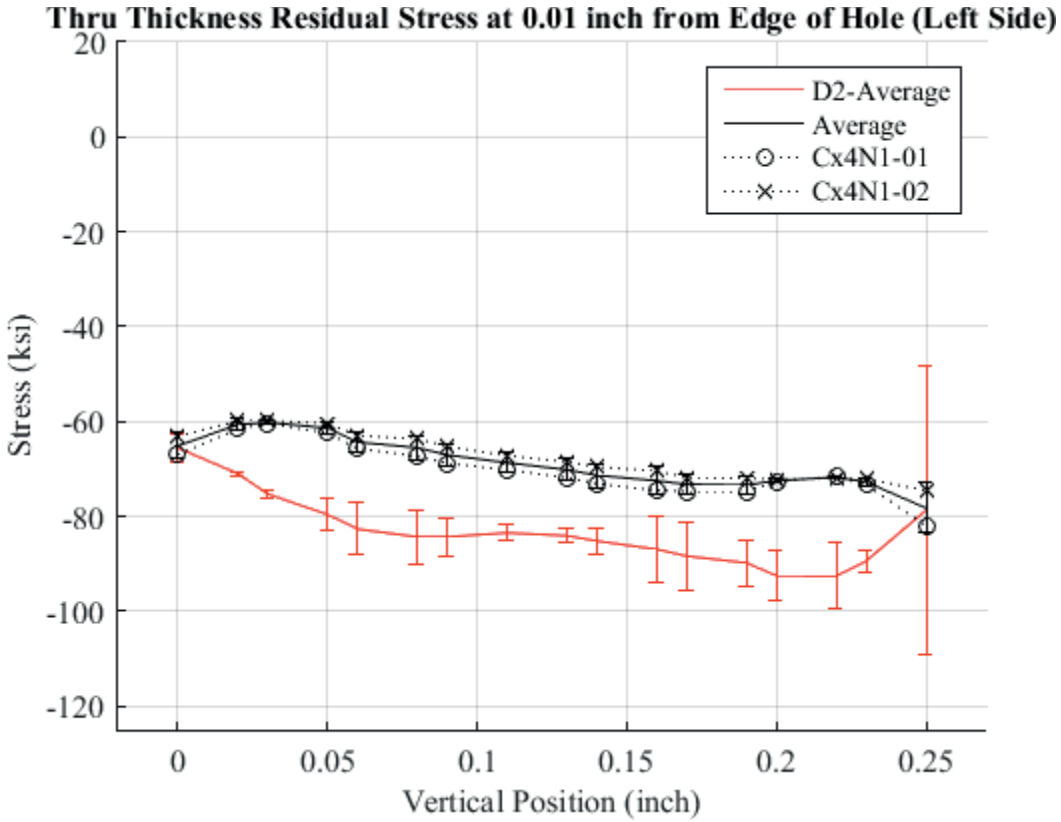

Fig. 702 Residual Stress Through-Thickness Line Plot Comparing Cx4N1-01-D, Cx4N1-02-D, and the Average between the Two to the CxD2 (7075-T651) Average Residual Stress at a Distance of 0.01 inch from the Left Side of the Hole – Cx4N1-01-D and Cx4N1-02-D Coupons had a 0.08 inch Fatigue Crack at the Left Entrance Surface.

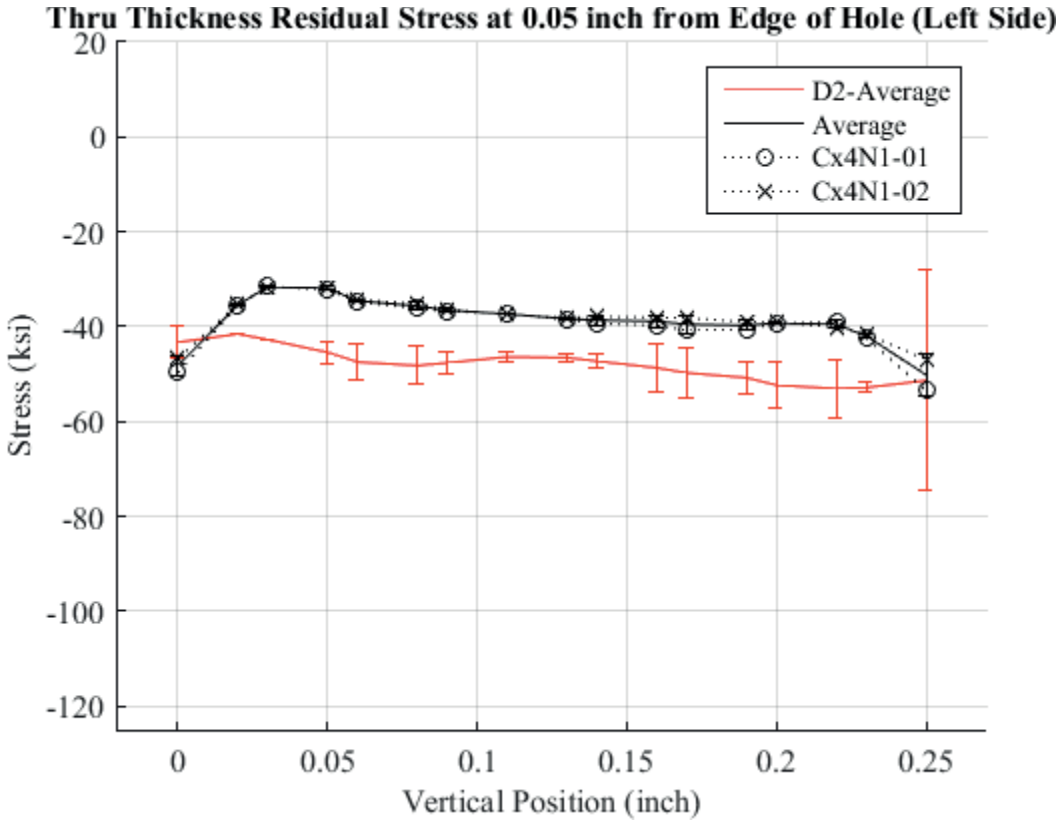

Fig. 703 Residual Stress Through-Thickness Line Plot Comparing Cx4N1-01-D, Cx4N1-02-D, and the Average between the Two to the CxD2 (7075-T651) Average Residual Stress at a Distance of 0.05 inch from the Left Side of the Hole – Cx4N1-01-D and Cx4N1-02-D Coupons had a 0.08 inch Fatigue Crack at the Left Entrance Surface.

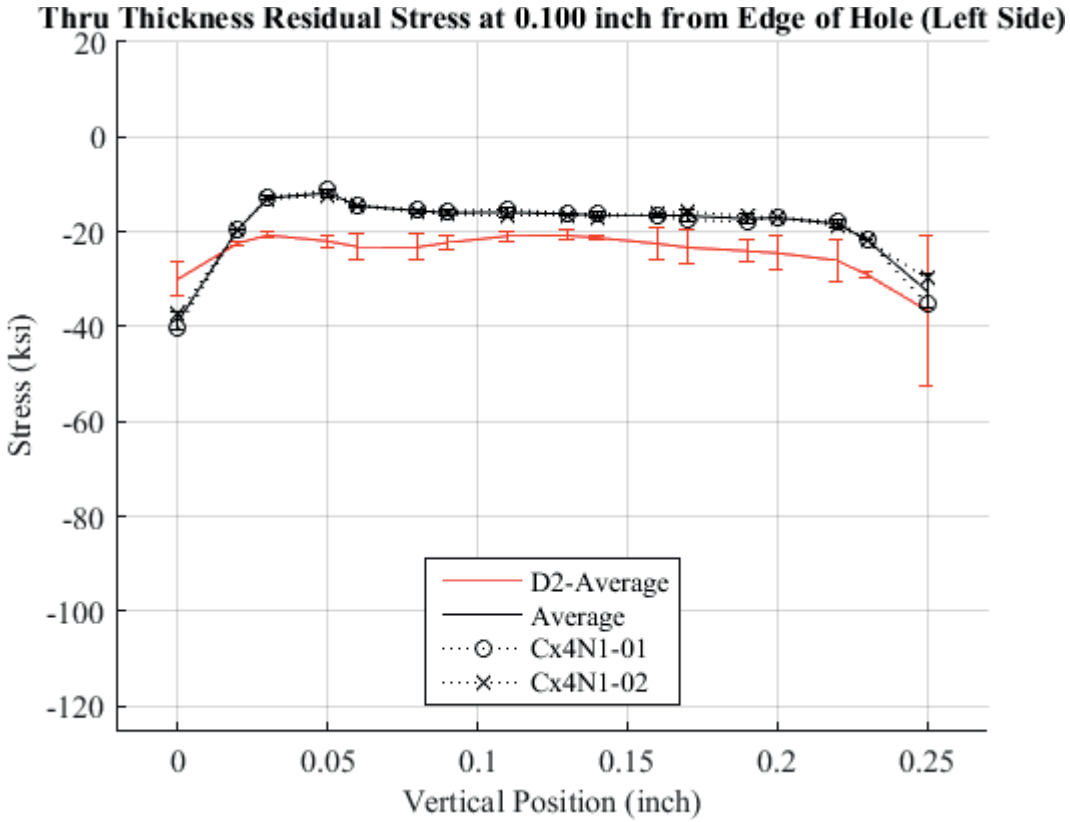

Fig. 704 Residual Stress Through-Thickness Line Plot Comparing Cx4N1-01-D, Cx4N1-02-D, and the Average between the Two to the CxD2 (7075-T651) Average Residual Stress at a Distance of 0.10 inch from the Left Side of the Hole – Cx4N1-01-D and Cx4N1-02-D Coupons had a 0.08 inch Fatigue Crack at the Left Entrance Surface.

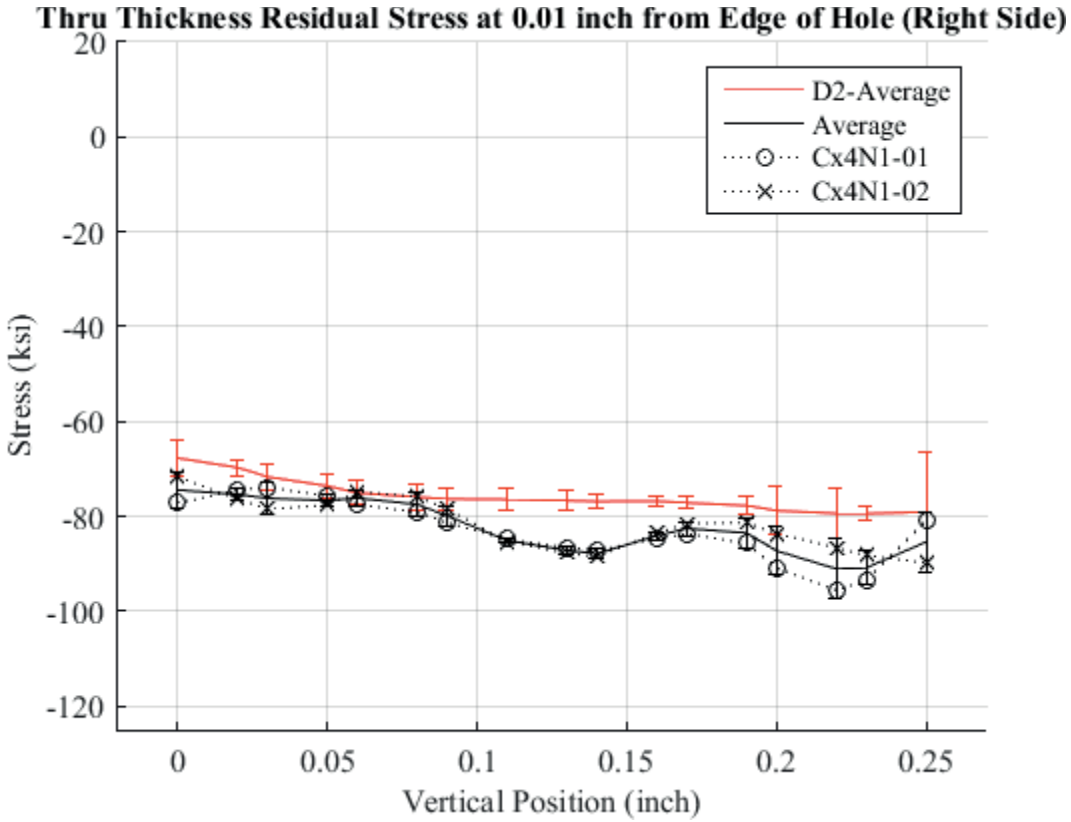

Fig. 705 Residual Stress Through-Thickness Line Plot Comparing Cx4N1-01-D, Cx4N1-02-D, and the Average between the Two to the CxD2 (7075-T651) Average Residual Stress at a Distance of 0.01 inch from the Right Side of the Hole – Cx4N1-01-D and Cx4N1-02-D Coupons had a 0.08 inch Fatigue Crack at the Left Entrance Surface.

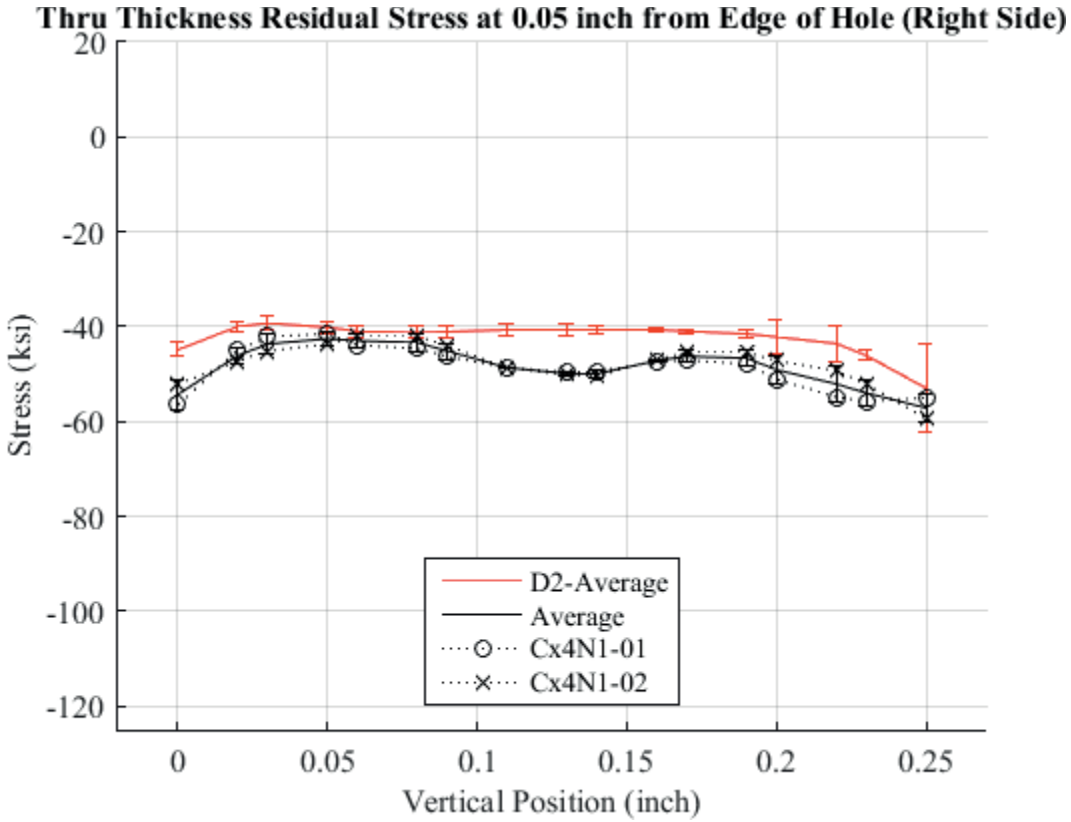

Fig. 706 Residual Stress Through-Thickness Line Plot Comparing Cx4N1-01-D, Cx4N1-02-D, and the Average between the Two to the CxD2 (7075-T651) Average Residual Stress at a Distance of 0.05 inch from the Right Side of the Hole – Cx4N1-01-D and Cx4N1-02-D Coupons had a 0.08 inch Fatigue Crack at the Left Entrance Surface.

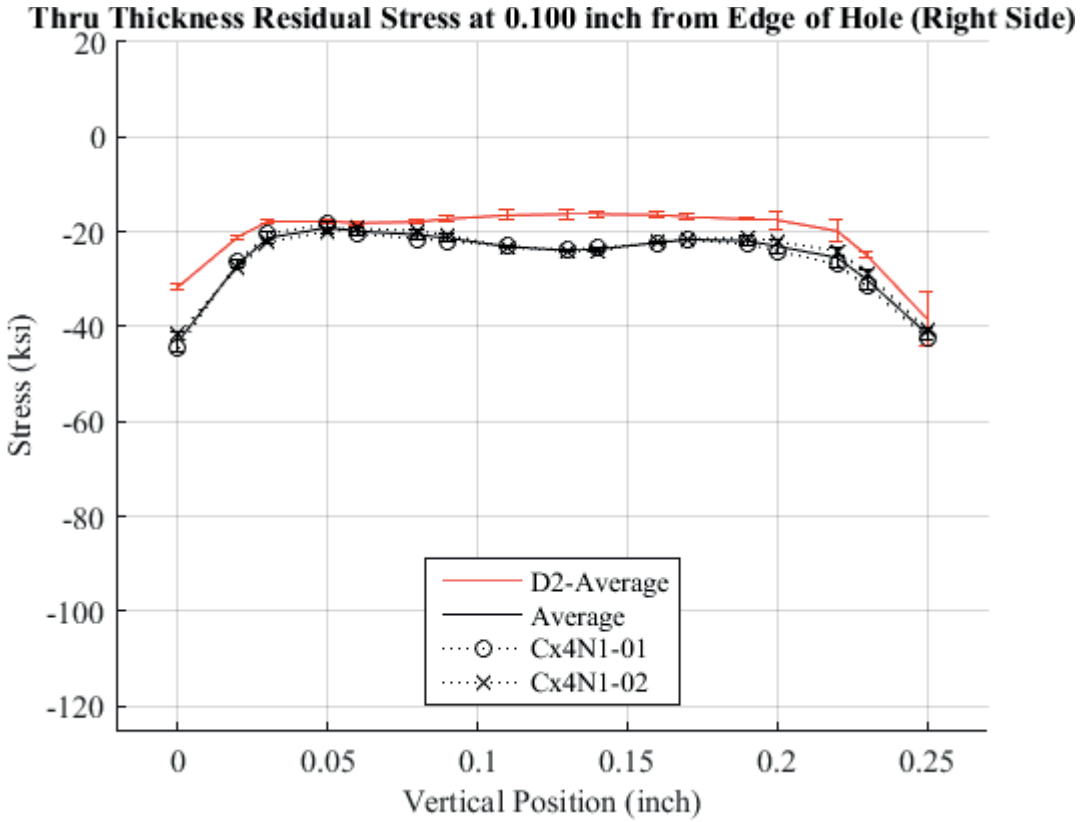

Fig. 707 Residual Stress Through-Thickness Line Plot Comparing Cx4N1-01-D, Cx4N1-02-D, and the Average between the Two to the CxD2 (7075-T651) Average Residual Stress at a Distance of 010 inch from the Right Side of the Hole – Cx4N1-01-D and Cx4N1-02-D Coupons had a 0.08 inch Fatigue Crack at the Left Entrance Surface.

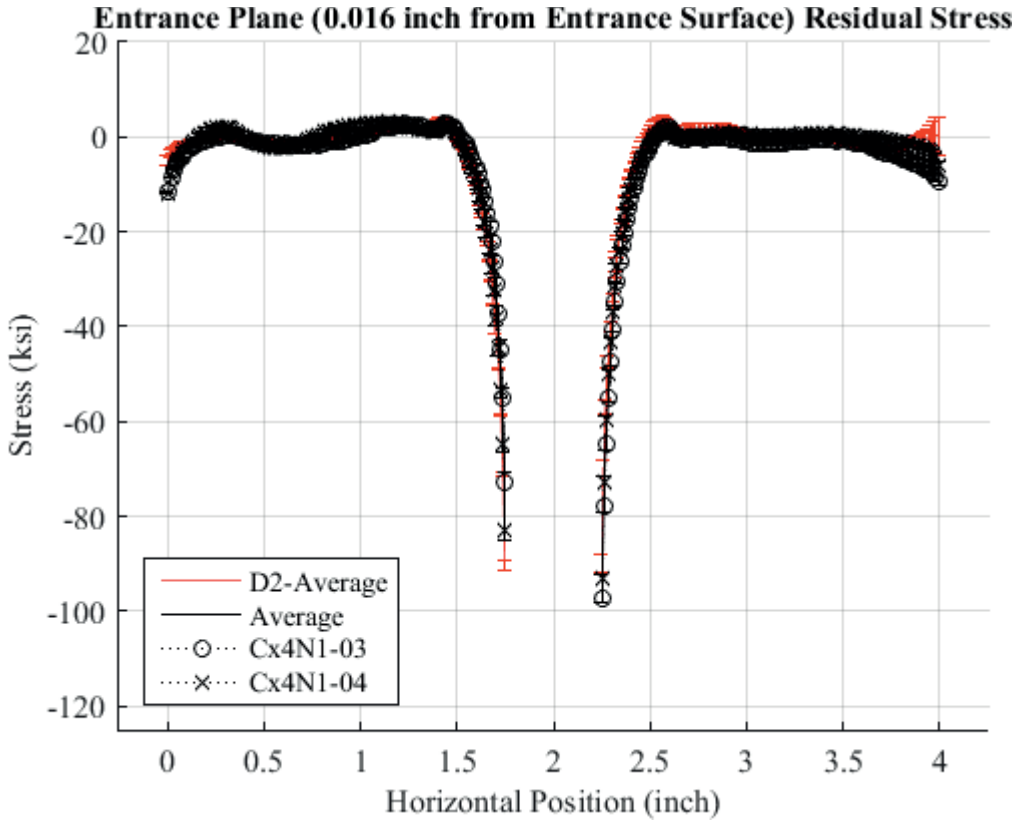

Fig. 708 Residual Stress Line Plot Comparing Cx4N1-03-D, Cx4N1-04-D, and the Average between the Two to the CxD2 (7075-T651) Average Residual Stress at a Distance of 0.016 inch (Entrance Surface) from the Entrance Surface – Cx4N1-03-D and Cx4N1-04-D Coupons had a 0.10 inch Fatigue Crack at the Left Entrance Surface.

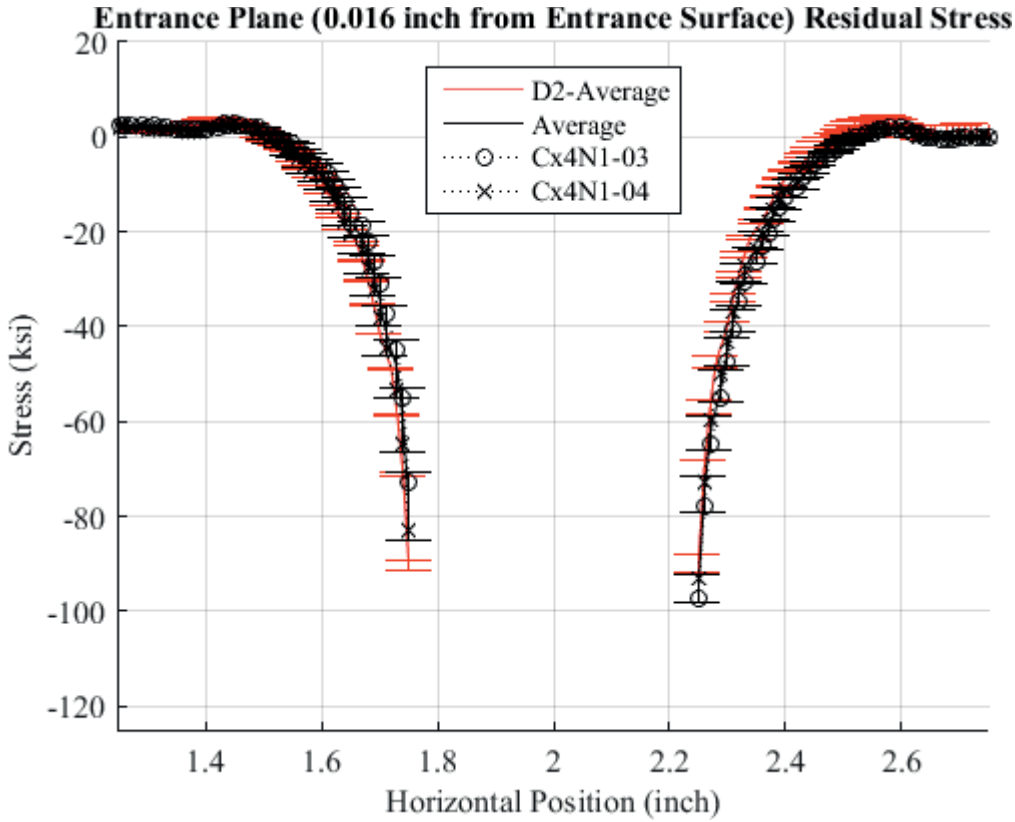

Fig. 709 Residual Stress Line Plot Comparing Cx4N1-03-D, Cx4N1-04-D, and the Average between the Two to the CxD2 (7075-T651) Average Residual Stress at a Distance of 0.016 inch (Entrance Surface) from the Entrance Surface – Cx4N1-03-D and Cx4N1-04-D Coupons had a 0.10 inch Fatigue Crack at the Left Entrance Surface – Zoomed in Next to Hole.

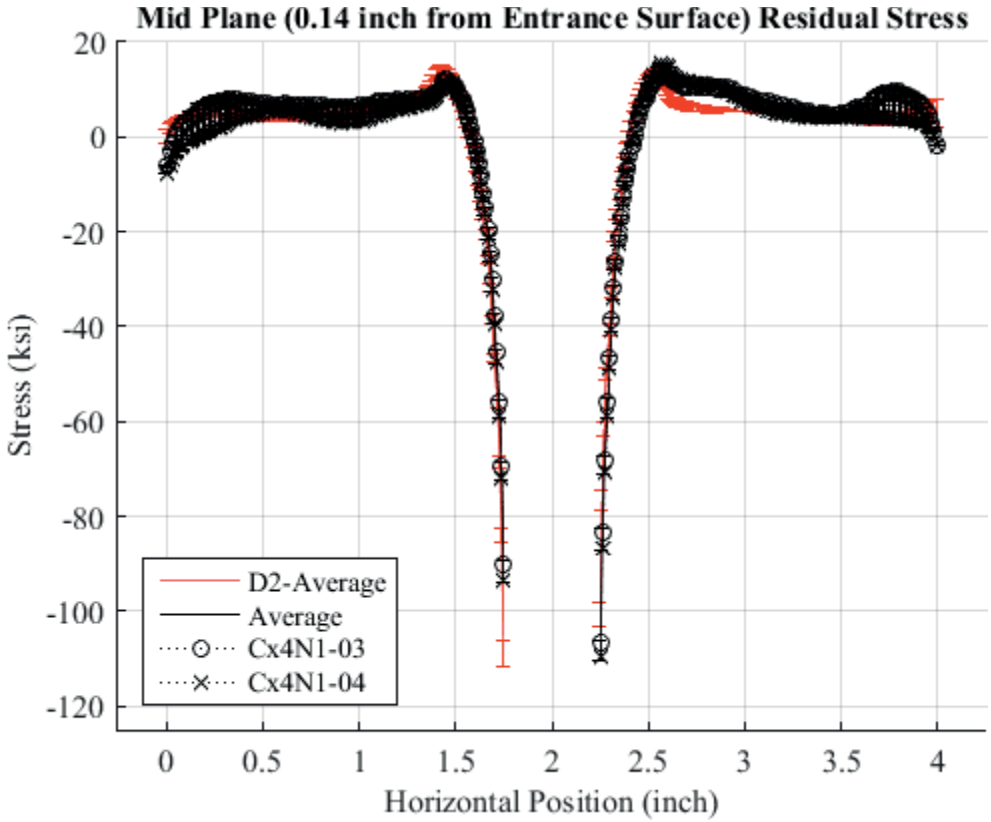

Fig. 710 Residual Stress Line Plot Comparing Cx4N1-03-D, Cx4N1-04-D, and the Average between the Two to the CxD2 (7075-T651) Average Residual Stress at a Distance of 0.140 inch (Mid Plane Surface) from the Entrance Surface – Cx4N1-03-D and Cx4N1-04-D Coupons had a 0.10 inch Fatigue Crack at the Left Entrance Surface.

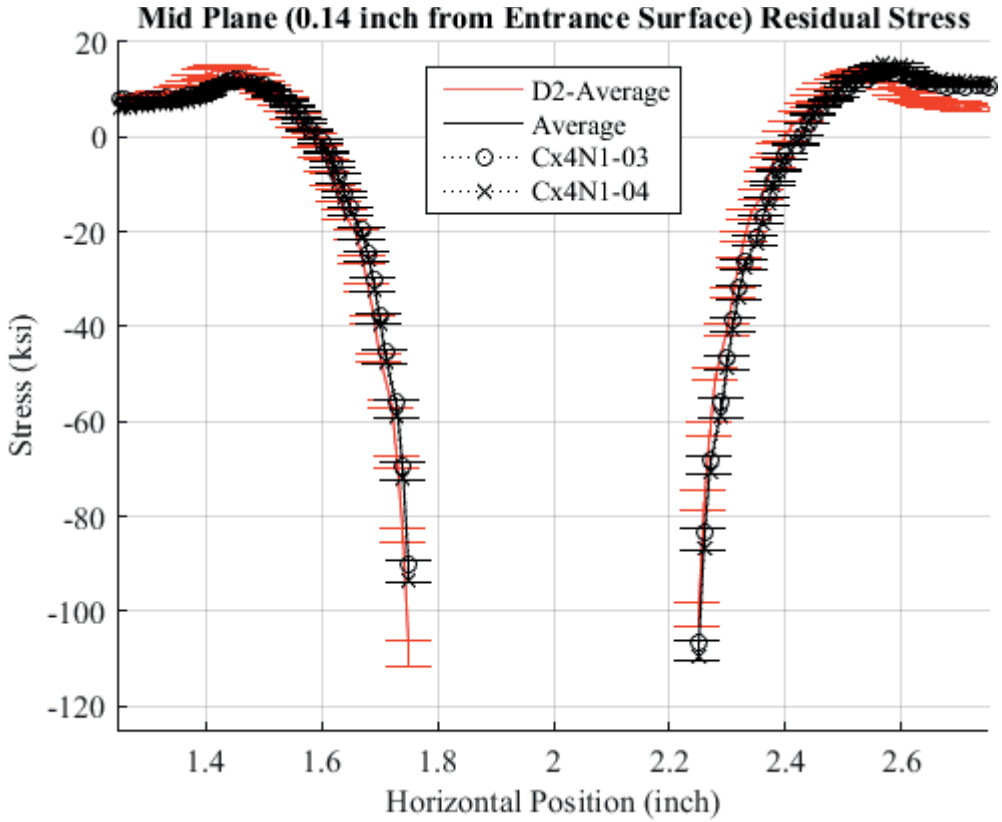

Fig. 711 Residual Stress Line Plot Comparing Cx4N1-03-D, Cx4N1-04-D, and the Average between the Two to the CxD2 (7075-T651) Average Residual Stress at a Distance of 0.140 inch (Mid Plane Surface) from the Entrance Surface – Cx4N1-03-D and Cx4N1-04-D Coupons had a 0.10 inch Fatigue Crack at the Left Entrance Surface – Zoomed in Next to Hole.

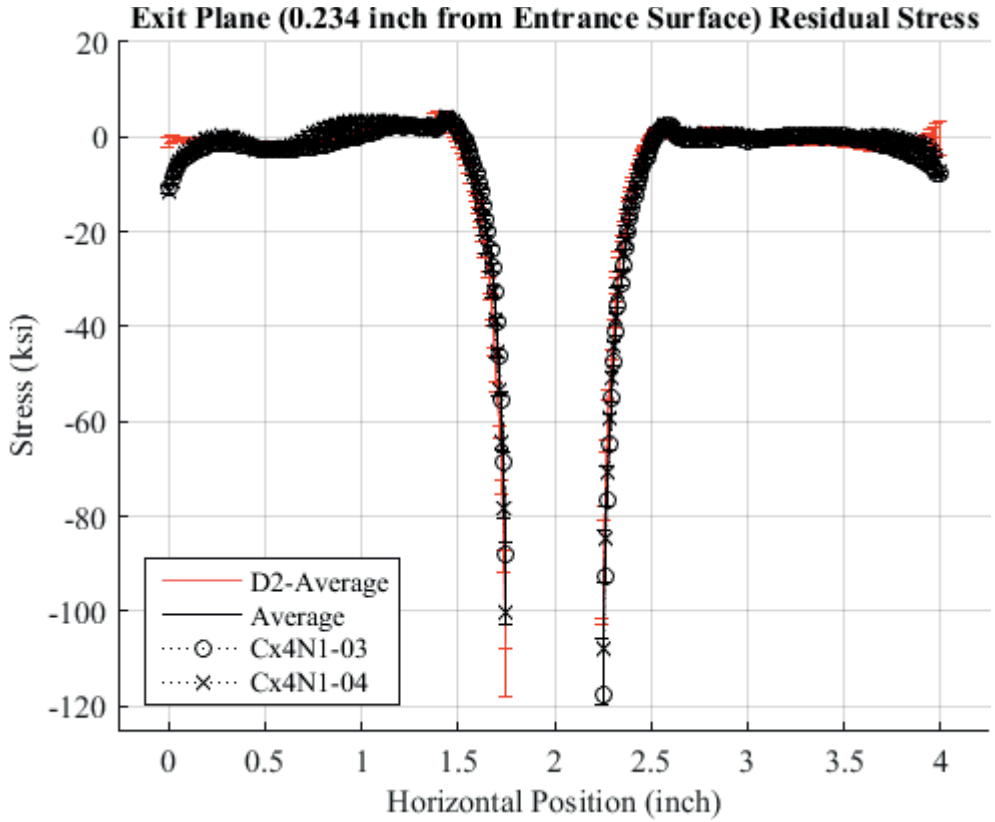

Fig. 712 Residual Stress Line Plot Comparing Cx4N1-03-D, Cx4N1-04-D, and the Average between the Two to the CxD2 (7075-T651) Average Residual Stress at a Distance of 0.234 inch (Exit Surface) from the Entrance Surface – Cx4N1-03-D and Cx4N1-04-D Coupons had a 0.10 inch Fatigue Crack at the Left Entrance Surface.

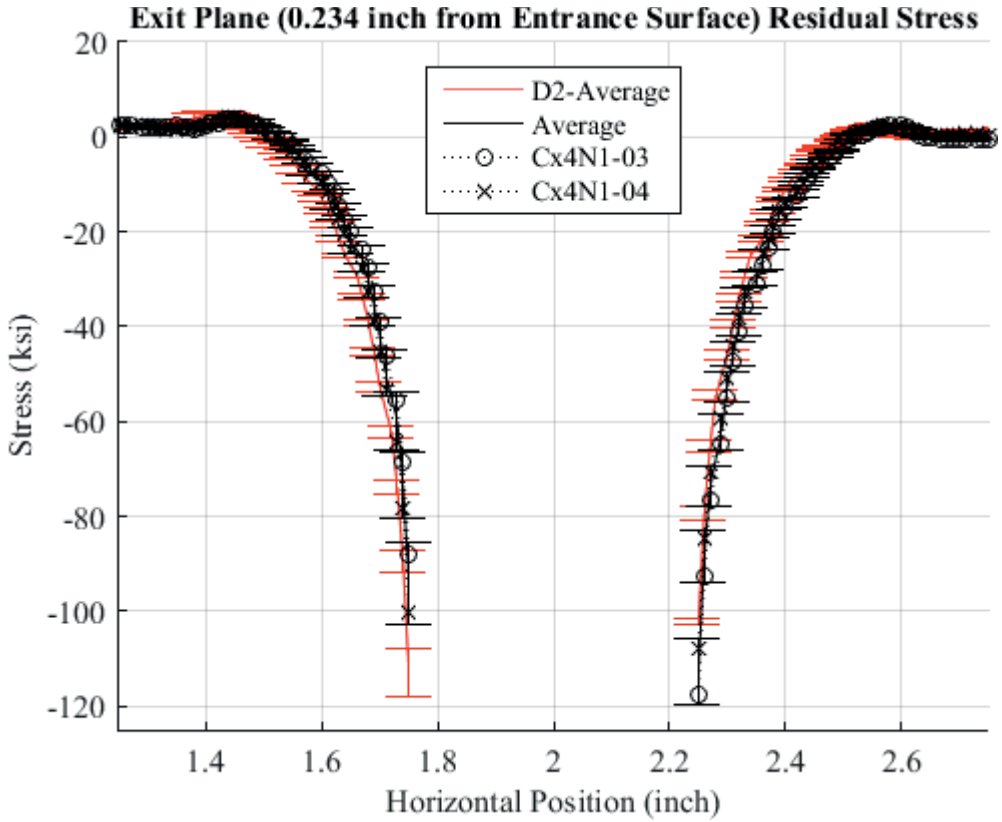

Fig. 713 Residual Stress Line Plot Comparing Cx4N1-03-D, Cx4N1-04-D, and the Average between the Two to the CxD2 (7075-T651) Average Residual Stress at a Distance of 0.234 inch (Exit Surface) from the Entrance Surface – Cx4N1-03-D and Cx4N1-04-D Coupons had a 0.10 inch Fatigue Crack at the Left Entrance Surface – Zoomed in Next to Hole.

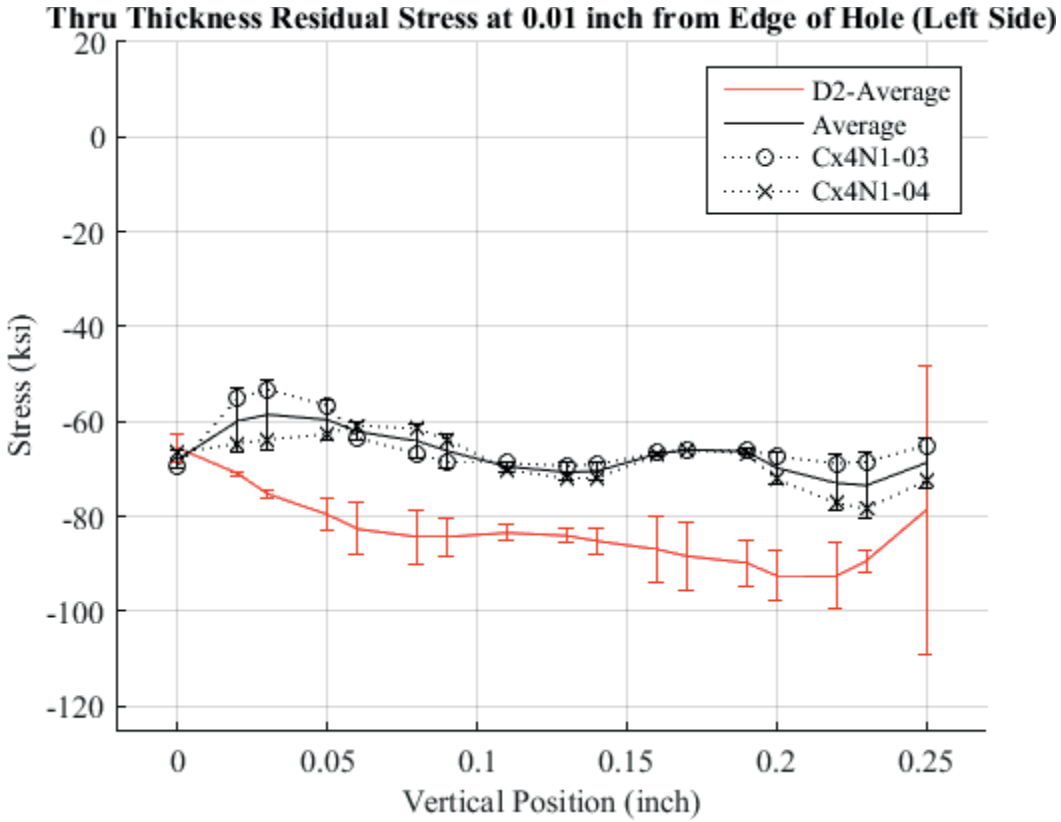

Fig. 714 Residual Stress Through-Thickness Line Plot Comparing Cx4N1-03-D, Cx4N1-04-D, and the Average between the Two to the CxD2 (7075-T651) Average Residual Stress at a Distance of 0.01 inch from the Left Side of the Hole – Cx4N1-03-D and Cx4N1-04-D Coupons had a 0.10 inch Fatigue Crack at the Left Entrance Surface.

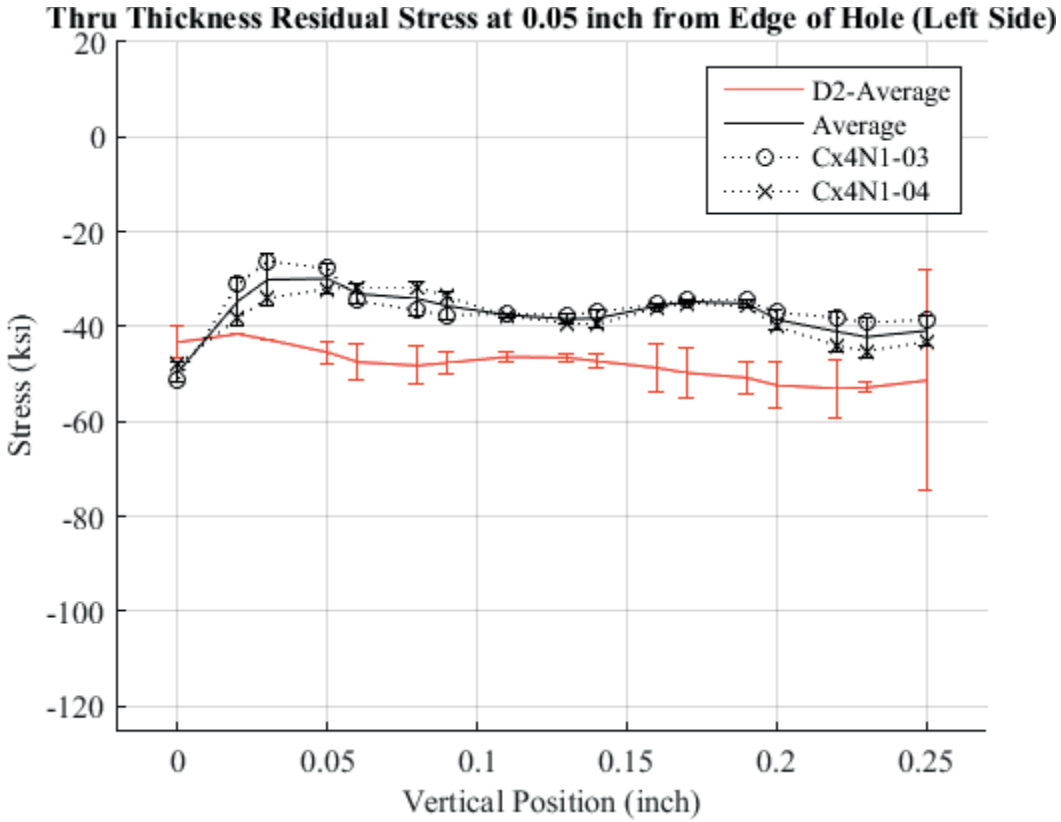

Fig. 715 Residual Stress Through-Thickness Line Plot Comparing Cx4N1-03-D, Cx4N1-04-D, and the Average between the Two to the CxD2 (7075-T651) Average Residual Stress at a Distance of 0.05 inch from the Left Side of the Hole – Cx4N1-03-D and Cx4N1-04-D Coupons had a 0.10 inch Fatigue Crack at the Left Entrance Surface.

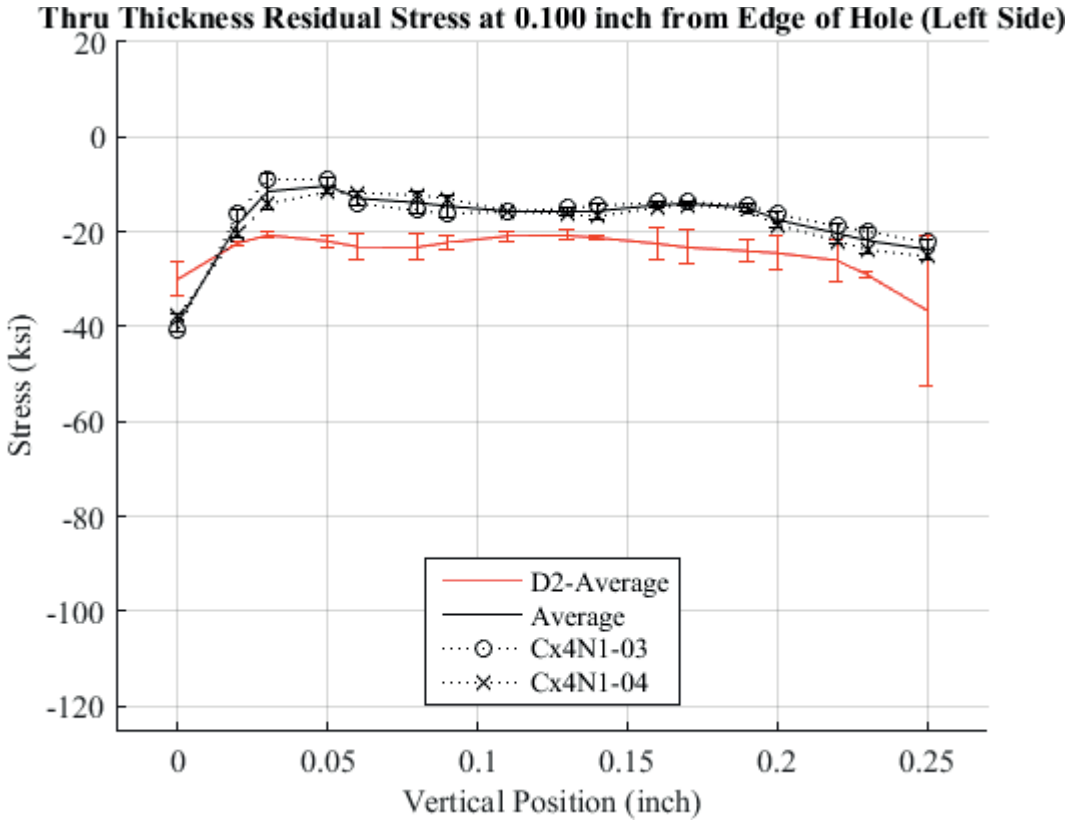

Fig. 716 Residual Stress Through-Thickness Line Plot Comparing Cx4N1-03-D, Cx4N1-04-D, and the Average between the Two to the CxD2 (7075-T651) Average Residual Stress at a Distance of 0.10 inch from the Left Side of the Hole – Cx4N1-03-D and Cx4N1-04-D Coupons had a 0.10 inch Fatigue Crack at the Left Entrance Surface.

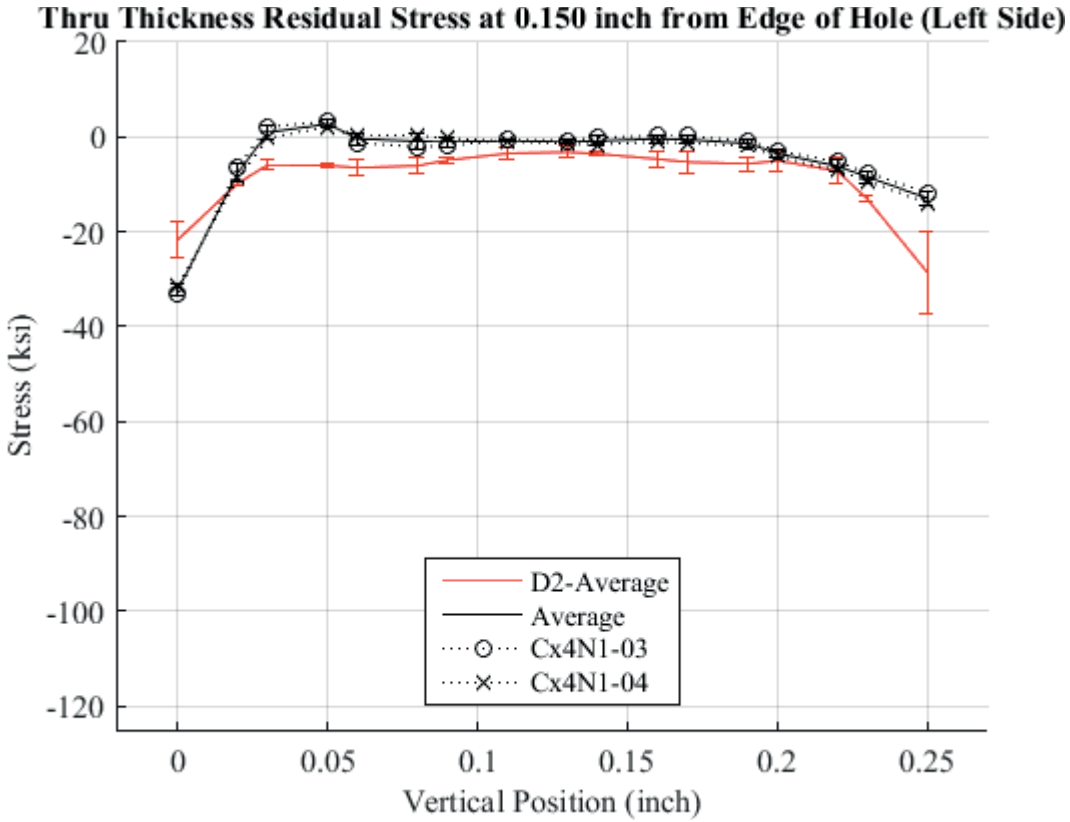

Fig. 717 Residual Stress Through-Thickness Line Plot Comparing Cx4N1-03-D, Cx4N1-04-D, and the Average between the Two to the CxD2 (7075-T651) Average Residual Stress at a Distance of 0.150 inch from the Left Side of the Hole – Cx4N1-03-D and Cx4N1-04-D Coupons had a 0.10 inch Fatigue Crack at the Left Entrance Surface.

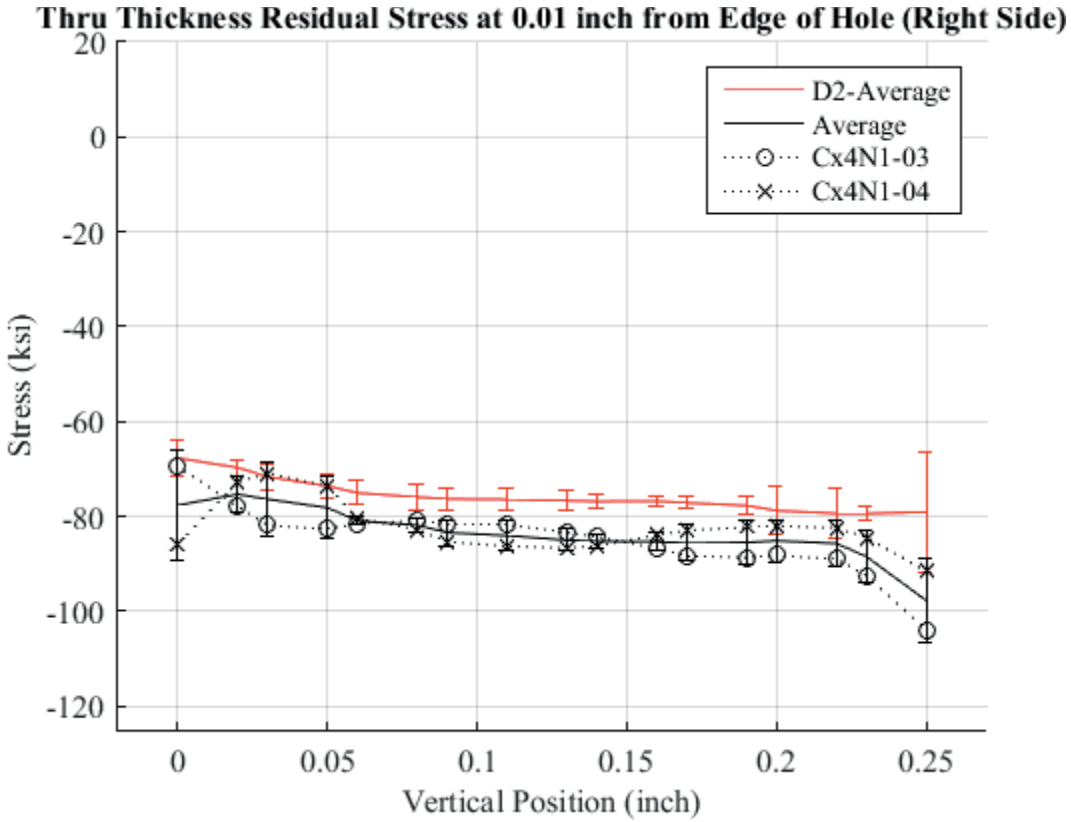

Fig. 718 Residual Stress Through-Thickness Line Plot Comparing Cx4N1-03-D, Cx4N1-04-D, and the Average between the Two to the CxD2 (7075-T651) Average Residual Stress at a Distance of 0.01 inch from the Right Side of the Hole – Cx4N1-03-D and Cx4N1-04-D Coupons had a 0.10 inch Fatigue Crack at the Left Entrance Surface.

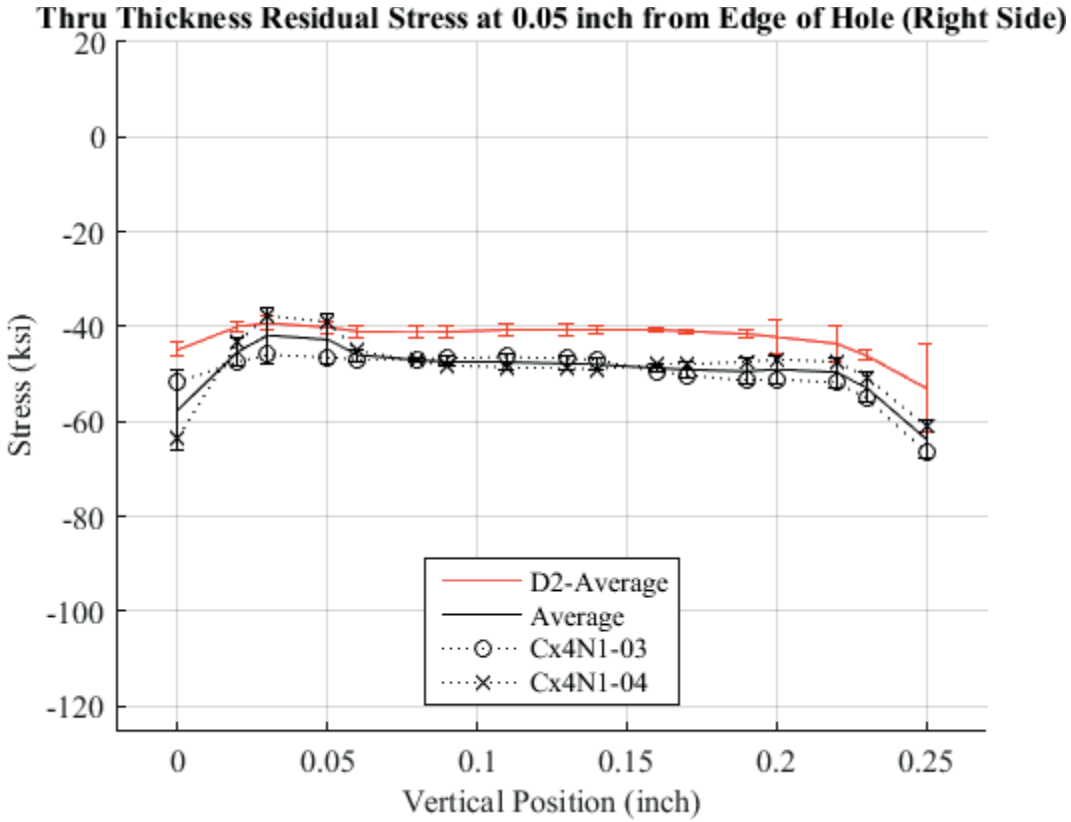

Fig. 719 Residual Stress Through-Thickness Line Plot Comparing Cx4N1-03-D, Cx4N1-04-D, and the Average between the Two to the CxD2 (7075-T651) Average Residual Stress at a Distance of 0.05 inch from the Right Side of the Hole – Cx4N1-03-D and Cx4N1-04-D Coupons had a 0.10 inch Fatigue Crack at the Left Entrance Surface.

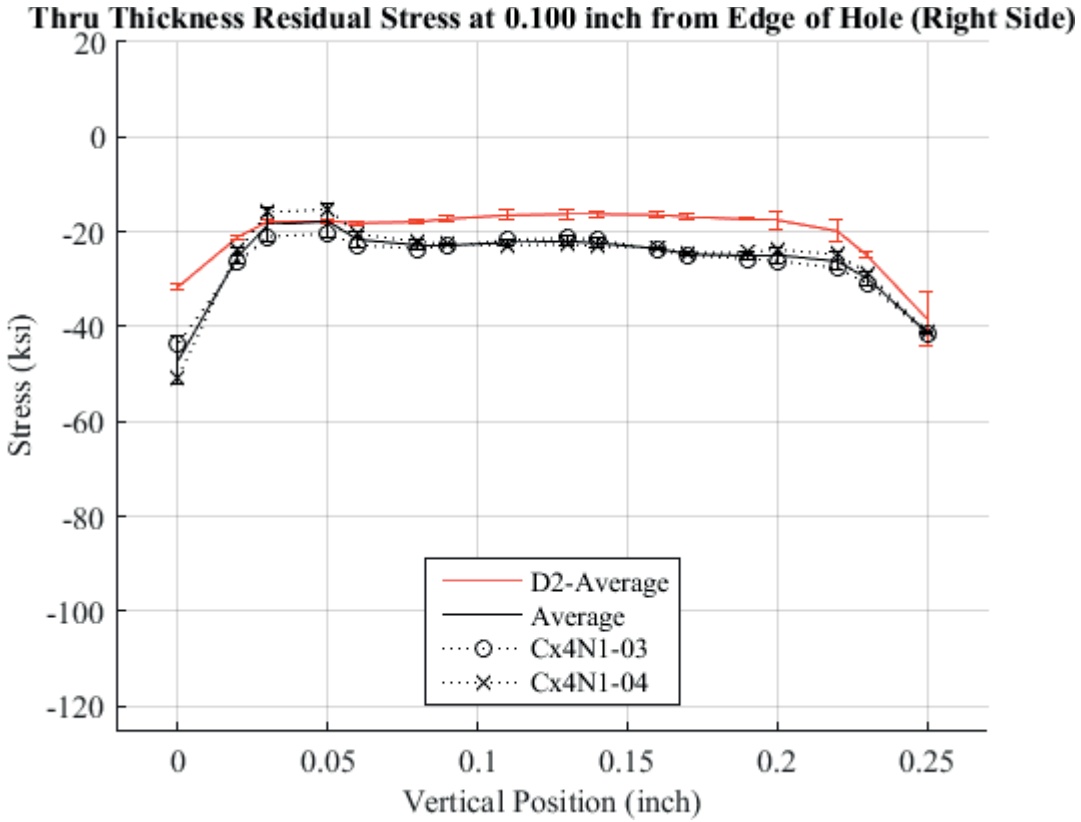

Fig. 720 Residual Stress Through-Thickness Line Plot Comparing Cx4N1-03-D, Cx4N1-04-D, and the Average between the Two to the CxD2 (7075-T651) Average Residual Stress at a Distance of 0.10 inch from the Right Side of the Hole – Cx4N1-03-D and Cx4N1-04-D Coupons had a 0.10 inch Fatigue Crack at the Left Entrance Surface.

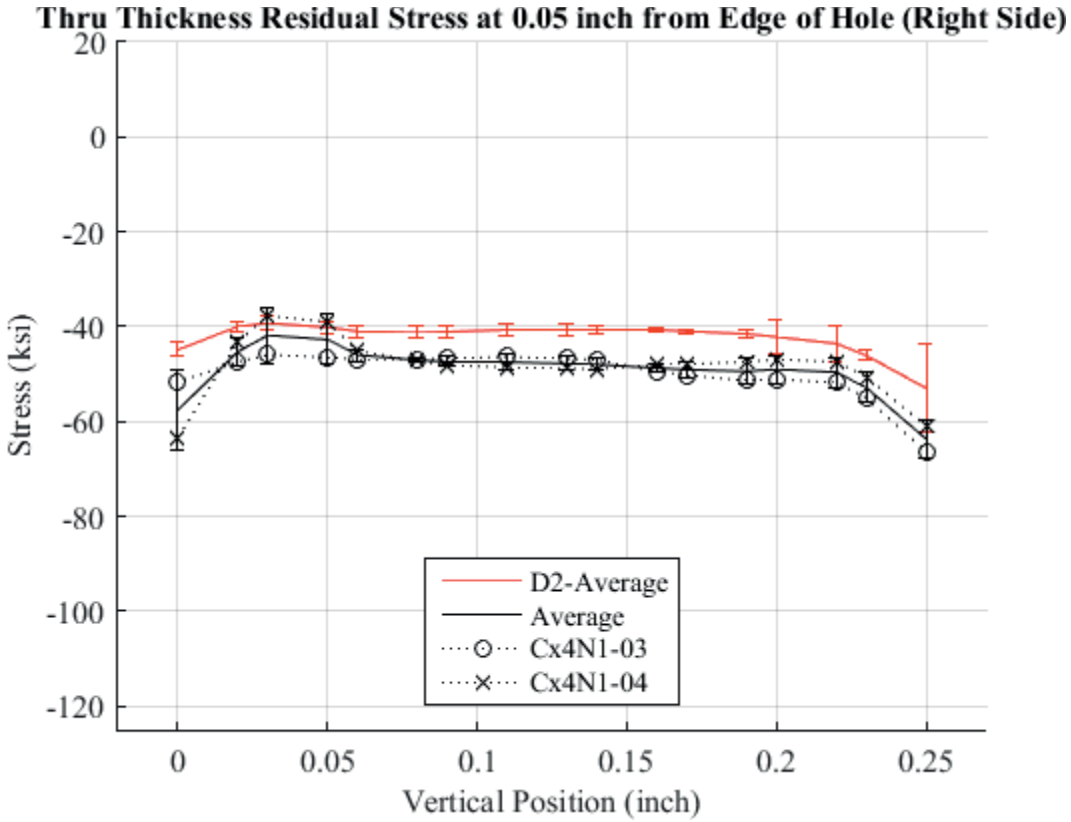

Fig. 721 Residual Stress Through-Thickness Line Plot Comparing Cx4N1-03-D, Cx4N1-04-D, and the Average between the Two to the CxD2 (7075-T651) Average Residual Stress at a Distance of 0.150 inch from the Right Side of the Hole – Cx4N1-03-D and Cx4N1-04-D Coupons had a 0.10 inch Fatigue Crack at the Left Entrance Surface.

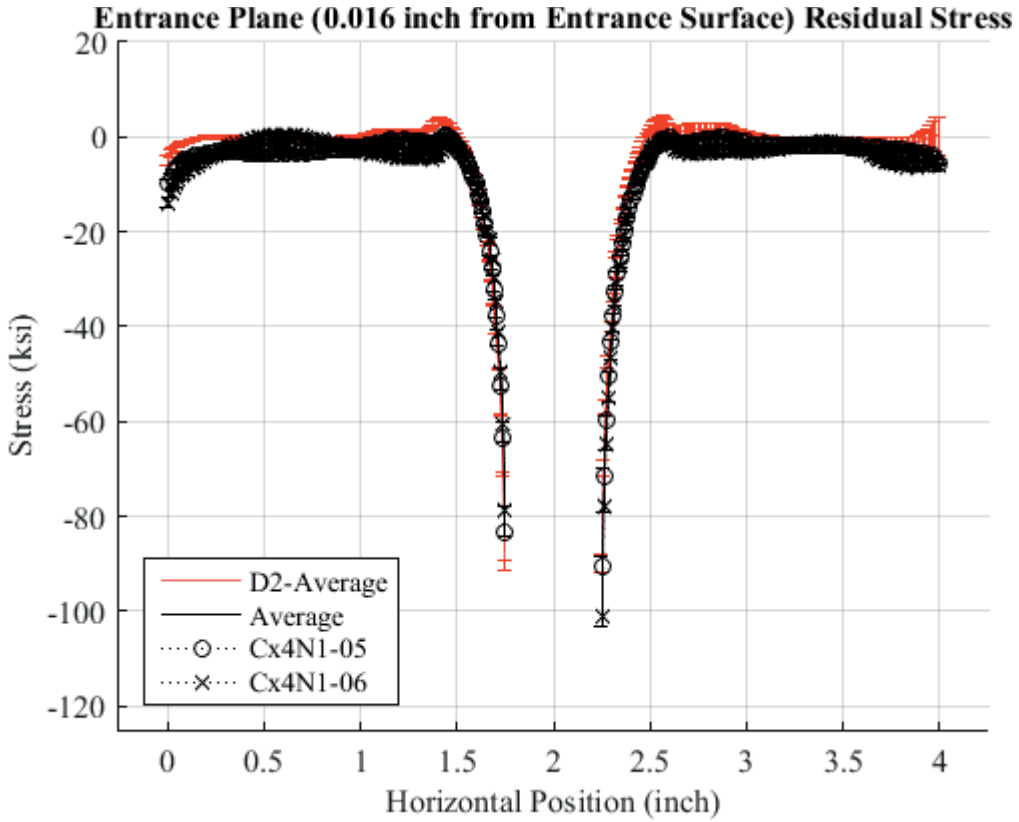

Fig. 722 Residual Stress Line Plot Comparing Cx4N1-05-D, Cx4N1-06-D, and the Average between the Two to the CxD2 (7075-T651) Average Residual Stress at a Distance of 0.016 inch (Entrance Surface) from the Entrance Surface – Cx4N1-05-D and Cx4N1-06-D Coupons had a 0.125 inch Fatigue Crack at the Left Entrance Surface.

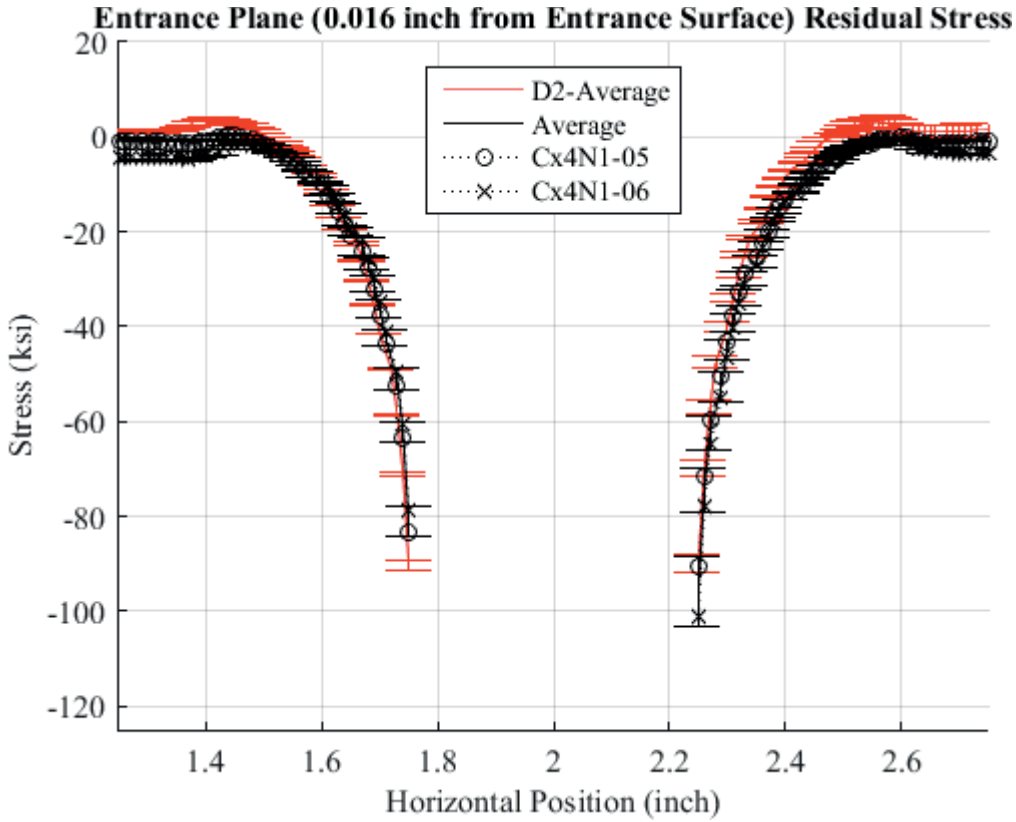

Fig. 723 Residual Stress Line Plot Comparing Cx4N1-05-D, Cx4N1-06-D, and the Average between the Two to the CxD2 (7075-T651) Average Residual Stress at a Distance of 0.016 inch (Entrance Surface) from the Entrance Surface – Cx4N1-05-D and Cx4N1-06-D Coupons had a 0.125 inch Fatigue Crack at the Left Entrance Surface – Zoomed in Next to Hole.

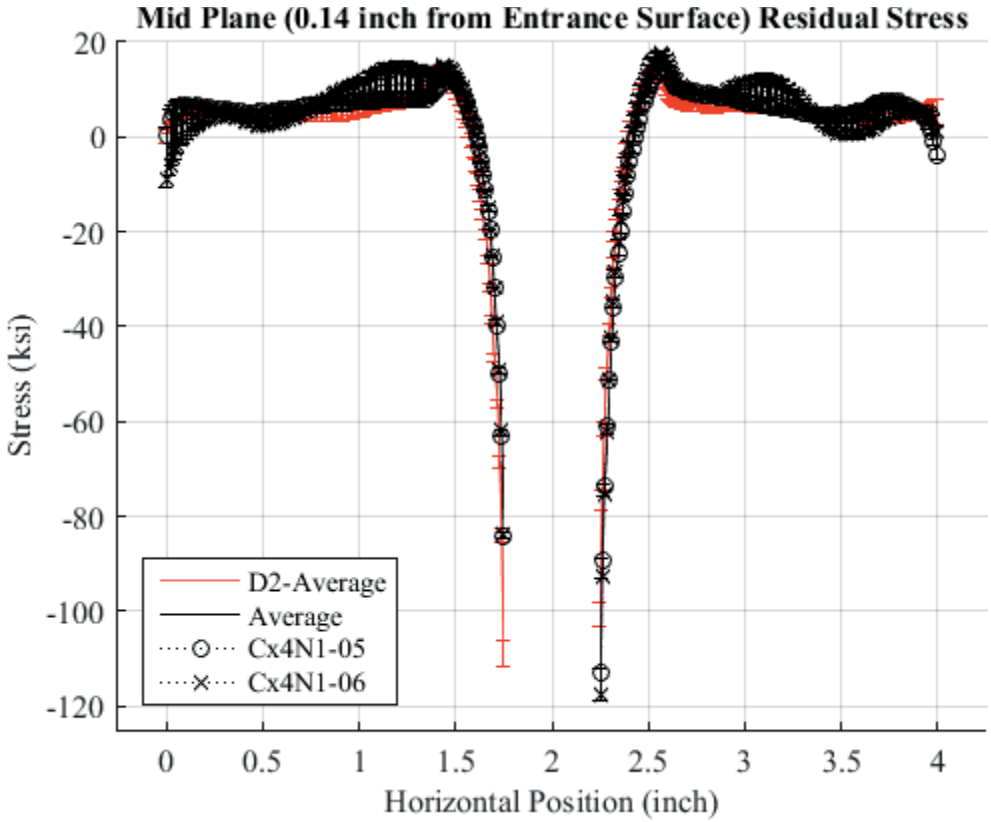

Fig. 724 Residual Stress Line Plot Comparing Cx4N1-05-D, Cx4N1-06-D, and the Average between the Two to the CxD2 (7075-T651) Average Residual Stress at a Distance of 0.140 inch (Mid Plane Surface) from the Entrance Surface – Cx4N1-05-D and Cx4N1-06-D Coupons had a 0.125 inch Fatigue Crack at the Left Entrance Surface.

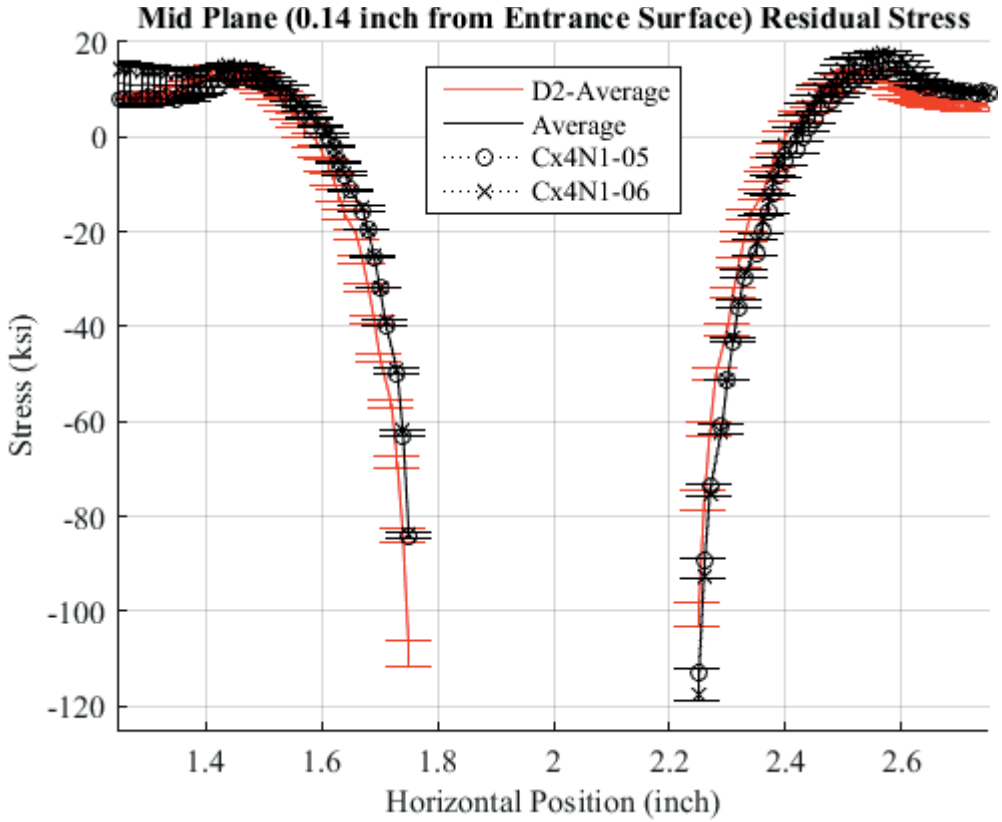

Fig. 725 Residual Stress Line Plot Comparing Cx4N1-05-D, Cx4N1-06-D, and the Average between the Two to the CxD2 (7075-T651) Average Residual Stress at a Distance of 0.140 inch (Mid Plane Surface) from the Entrance Surface – Cx4N1-05-D and Cx4N1-06-D Coupons had a 0.125 inch Fatigue Crack at the Left Entrance Surface – Zoomed in Next to Hole.

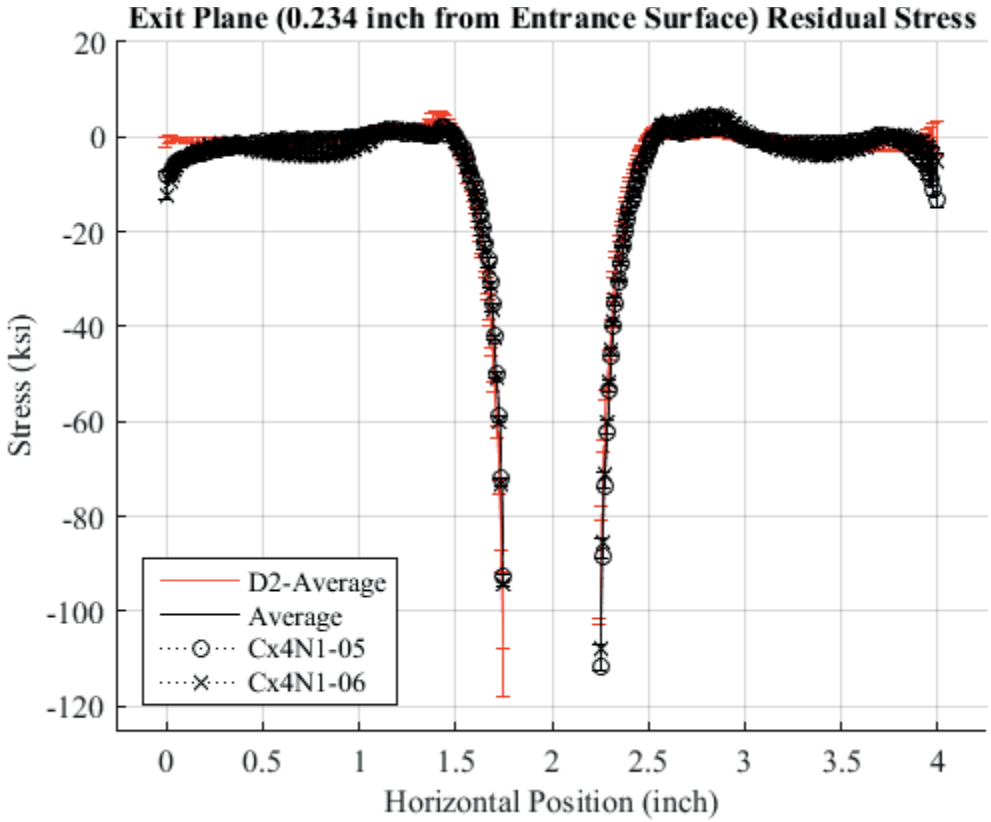

Fig. 726 Residual Stress Line Plot Comparing Cx4N1-05-D, Cx4N1-06-D, and the Average between the Two to the CxD2 (7075-T651) Average Residual Stress at a Distance of 0.234 inch (Exit Surface) from the Entrance Surface – Cx4N1-05-D and Cx4N1-06-D Coupons had a 0.125 inch Fatigue Crack at the Left Entrance Surface.

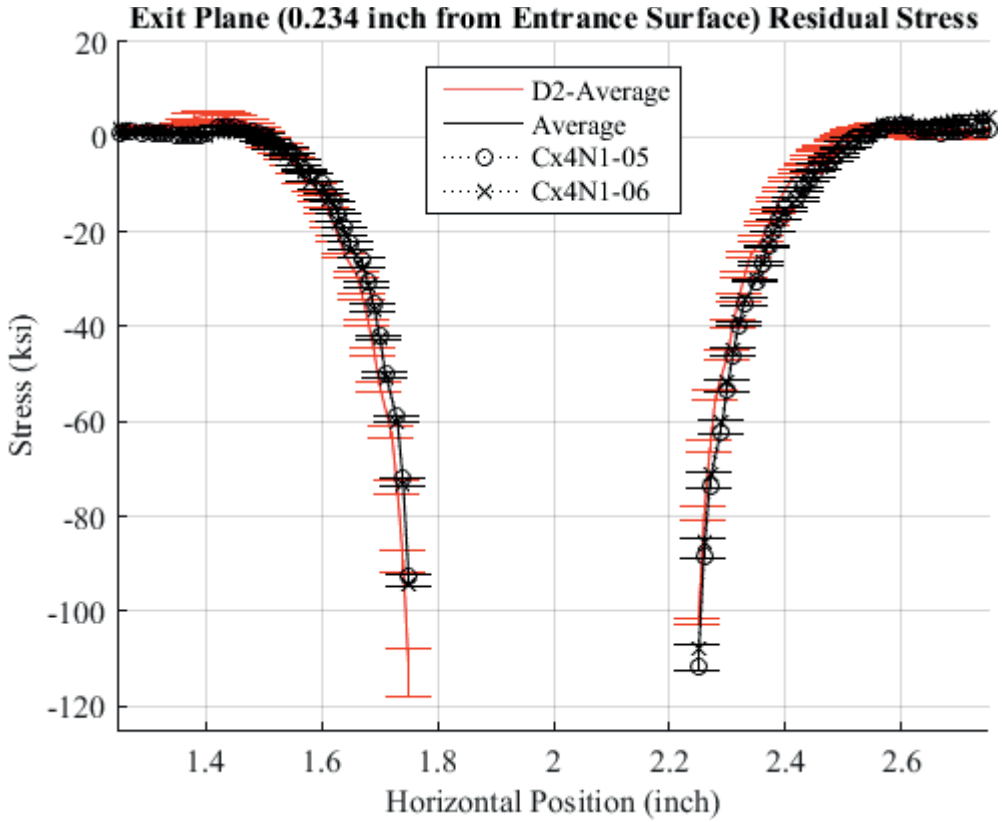

Fig. 727 Residual Stress Line Plot Comparing Cx4N1-05-D, Cx4N1-06-D, and the Average between the Two to the CxD2 (7075-T651) Average Residual Stress at a Distance of 0.234 inch (Exit Surface) from the Entrance Surface – Cx4N1-05-D and Cx4N1-06-D Coupons had a 0.125 inch Fatigue Crack at the Left Entrance Surface – Zoomed in Next to Hole.

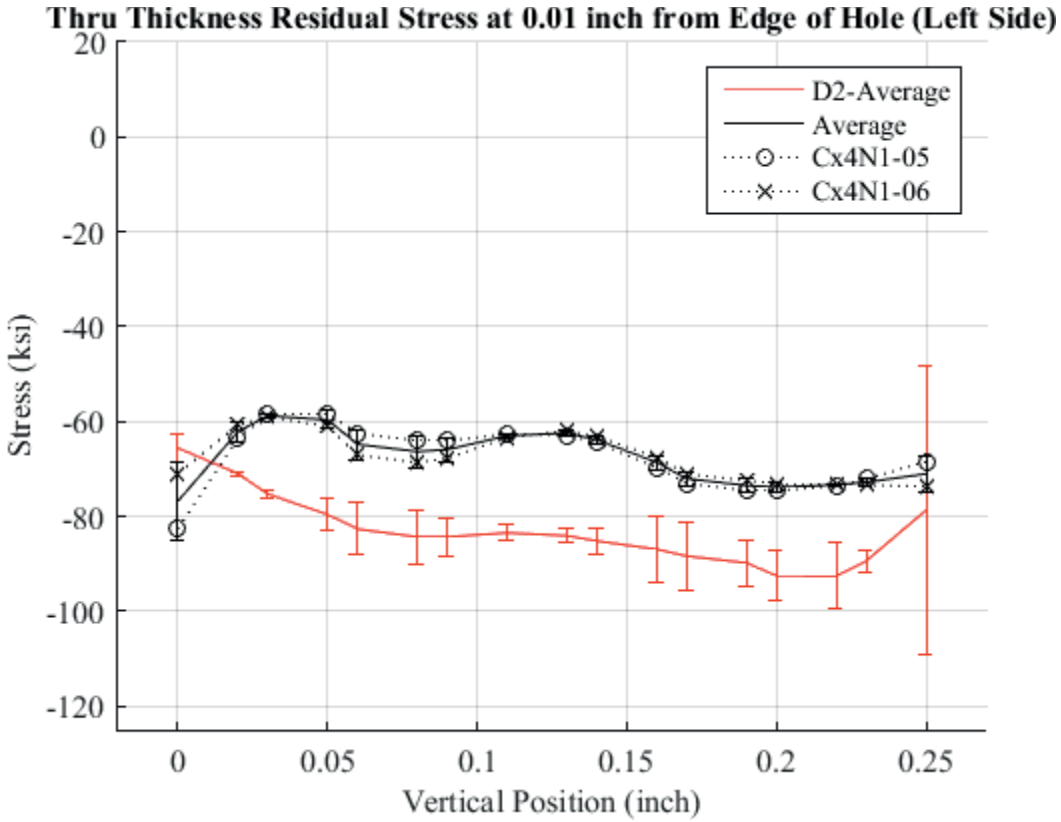

Fig. 728 Residual Stress Through-Thickness Line Plot Comparing Cx4N1-05-D, Cx4N1-06-D, and the Average between the Two to the CxD2 (7075-T651) Average Residual Stress at a Distance of 0.01 inch from the Left Side of the Hole – Cx4N1-05-D and Cx4N1-06-D Coupons had a 0.125 inch Fatigue Crack at the Left Entrance Surface.

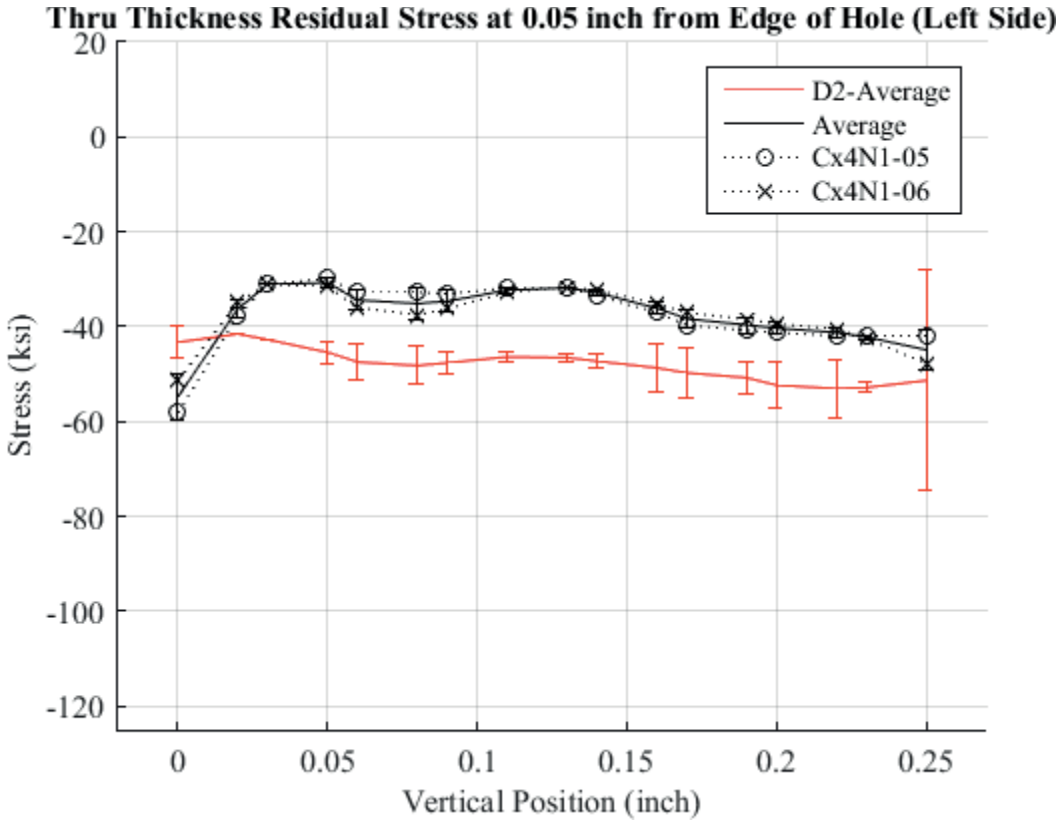

Fig. 729 Residual Stress Through-Thickness Line Plot Comparing Cx4N1-05-D, Cx4N1-06-D, and the Average between the Two to the CxD2 (7075-T651) Average Residual Stress at a Distance of 0.05 inch from the Left Side of the Hole – Cx4N1-05-D and Cx4N1-06-D Coupons had a 0.125 inch Fatigue Crack at the Left Entrance Surface.

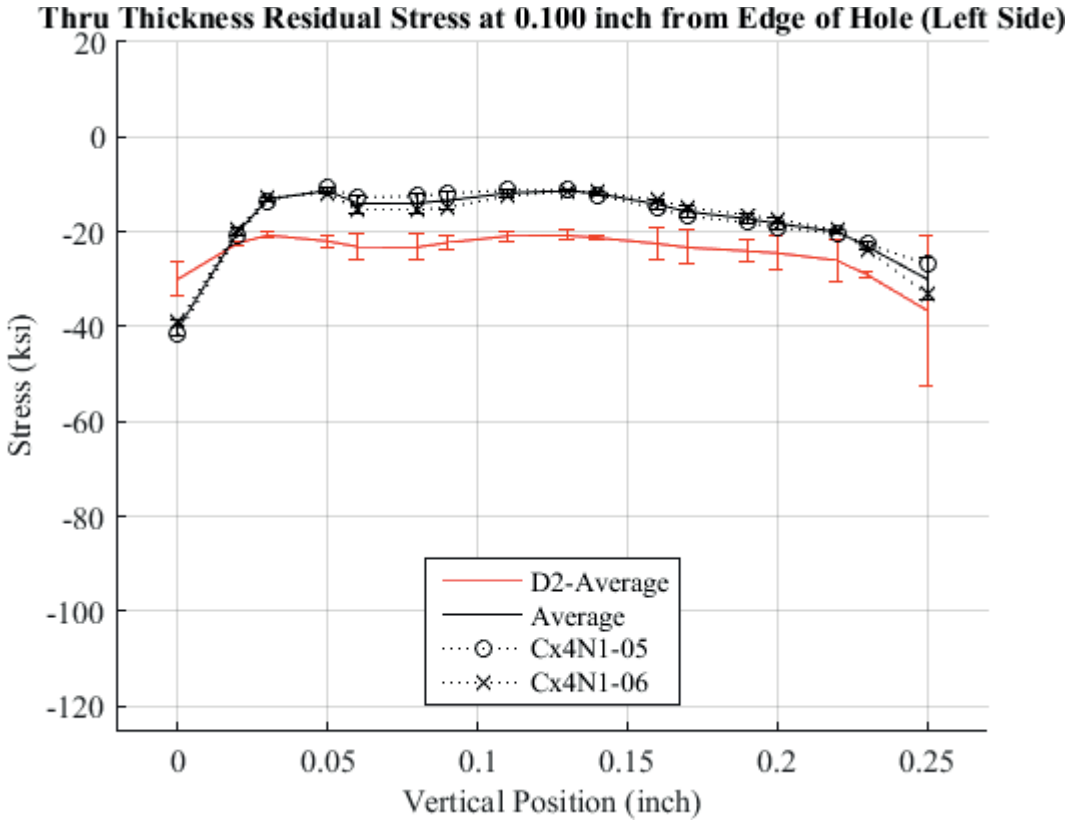

Fig. 730 Residual Stress Through-Thickness Line Plot Comparing Cx4N1-05-D, Cx4N1-06-D, and the Average between the Two to the CxD2 (7075-T651) Average Residual Stress at a Distance of 0.10 inch from the Left Side of the Hole – Cx4N1-05-D and Cx4N1-06-D Coupons had a 0.125 inch Fatigue Crack at the Left Entrance Surface.

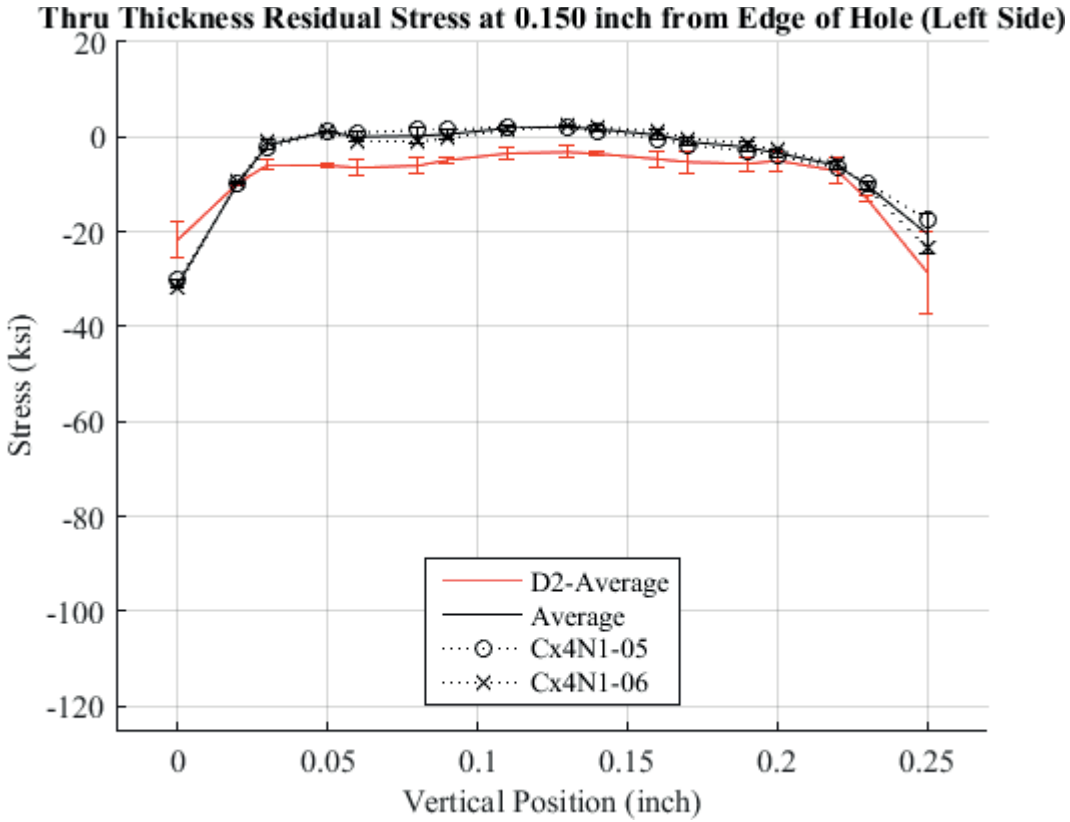

Fig. 731 Residual Stress Through-Thickness Line Plot Comparing Cx4N1-05-D, Cx4N1-06-D, and the Average between the Two to the CxD2 (7075-T651) Average Residual Stress at a Distance of 0.150 inch from the Left Side of the Hole – Cx4N1-05-D and Cx4N1-06-D Coupons had a 0.125 inch Fatigue Crack at the Left Entrance Surface.

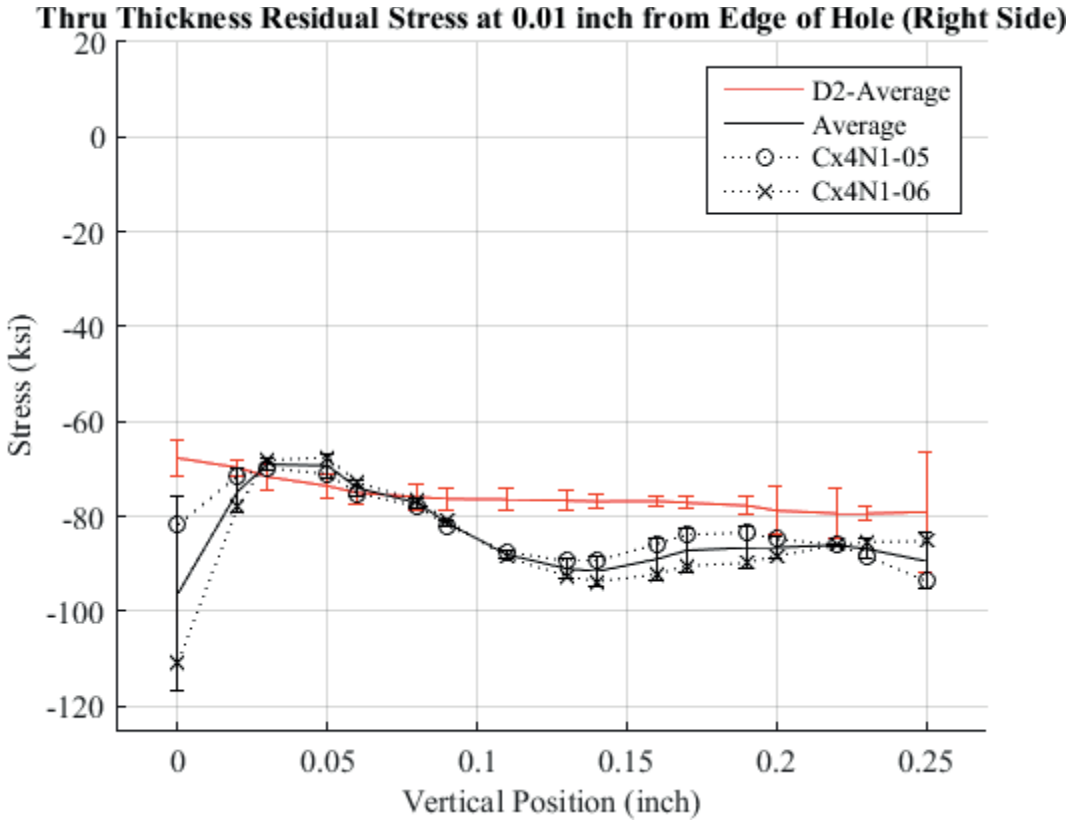

Fig. 732 Residual Stress Through-Thickness Line Plot Comparing Cx4N1-05-D, Cx4N1-06-D, and the Average between the Two to the CxD2 (7075-T651) Average Residual Stress at a Distance of 0.01 inch from the Right Side of the Hole – Cx4N1-05-D and Cx4N1-06-D Coupons had a 0.125 inch Fatigue Crack at the Left Entrance Surface.

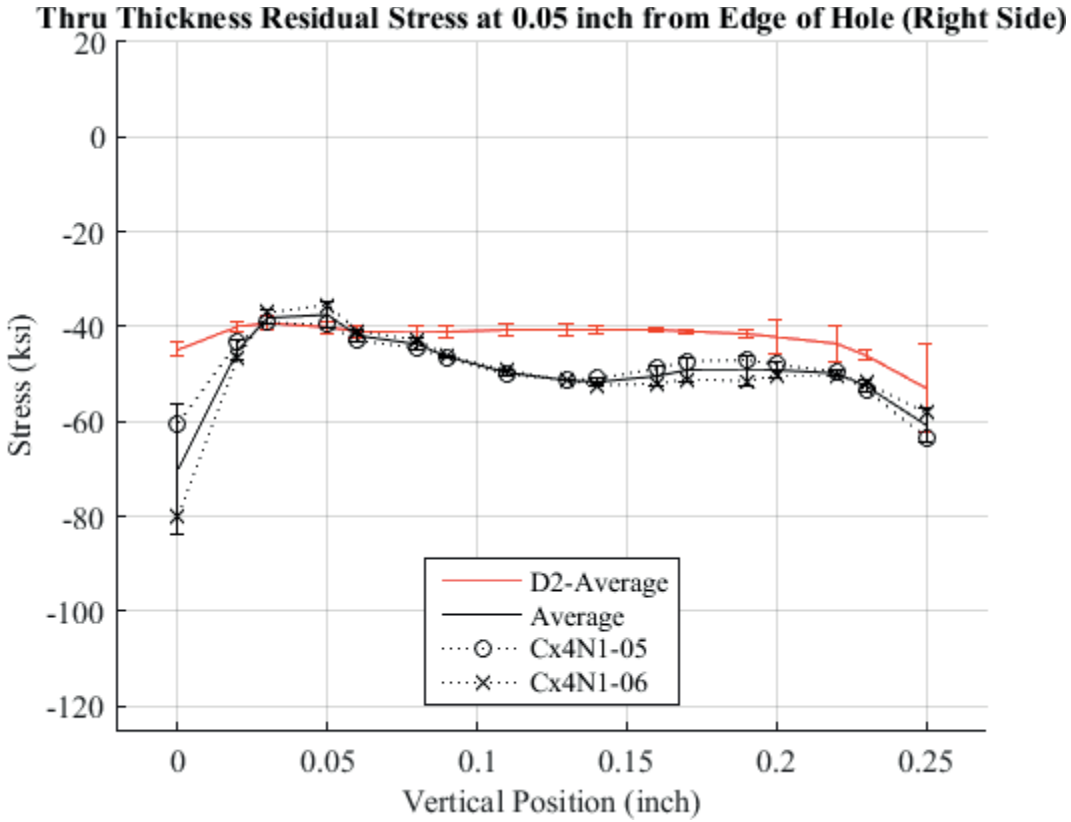

Fig. 733 Residual Stress Through-Thickness Line Plot Comparing Cx4N1-05-D, Cx4N1-06-D, and the Average between the Two to the CxD2 (7075-T651) Average Residual Stress at a Distance of 0.05 inch from the Right Side of the Hole – Cx4N1-05-D and Cx4N1-06-D Coupons had a 0.125 inch Fatigue Crack at the Left Entrance Surface.

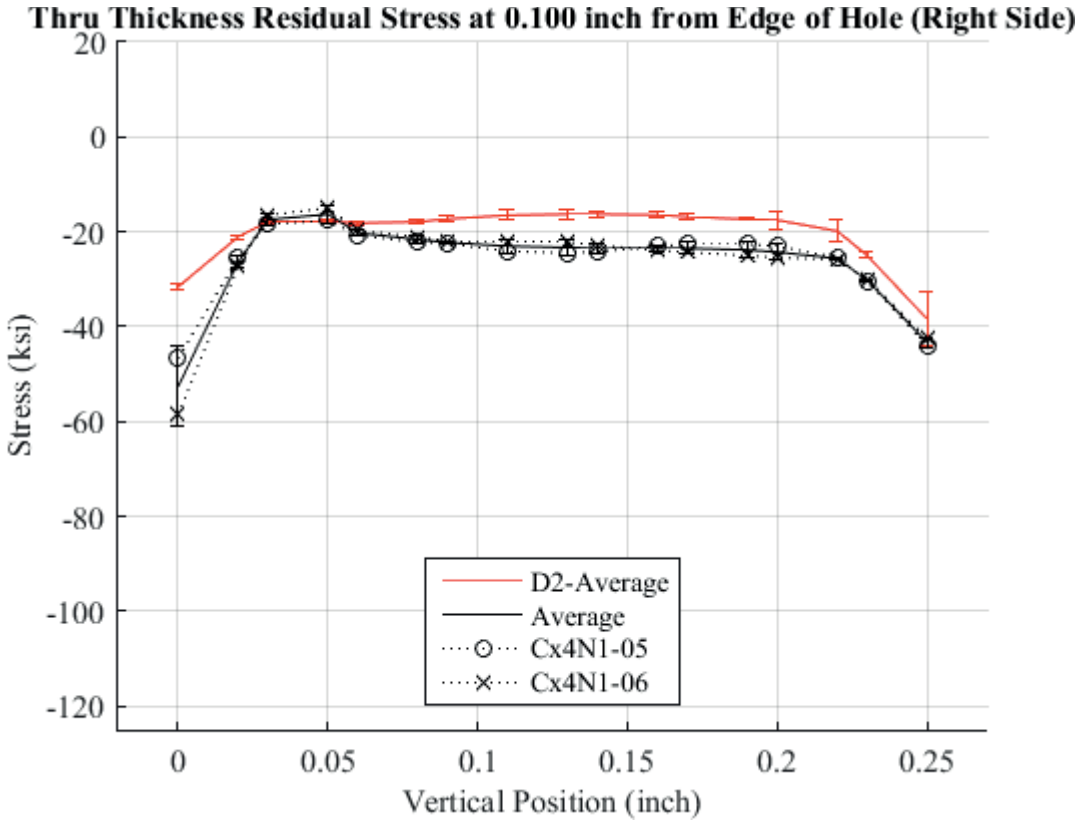

Fig. 734 Residual Stress Through-Thickness Line Plot Comparing Cx4N1-05-D, Cx4N1-06-D, and the Average between the Two to the CxD2 (7075-T651) Average Residual Stress at a Distance of 0.10 inch from the Right Side of the Hole – Cx4N1-05-D and Cx4N1-06-D Coupons had a 0.125 inch Fatigue Crack at the Left Entrance Surface.

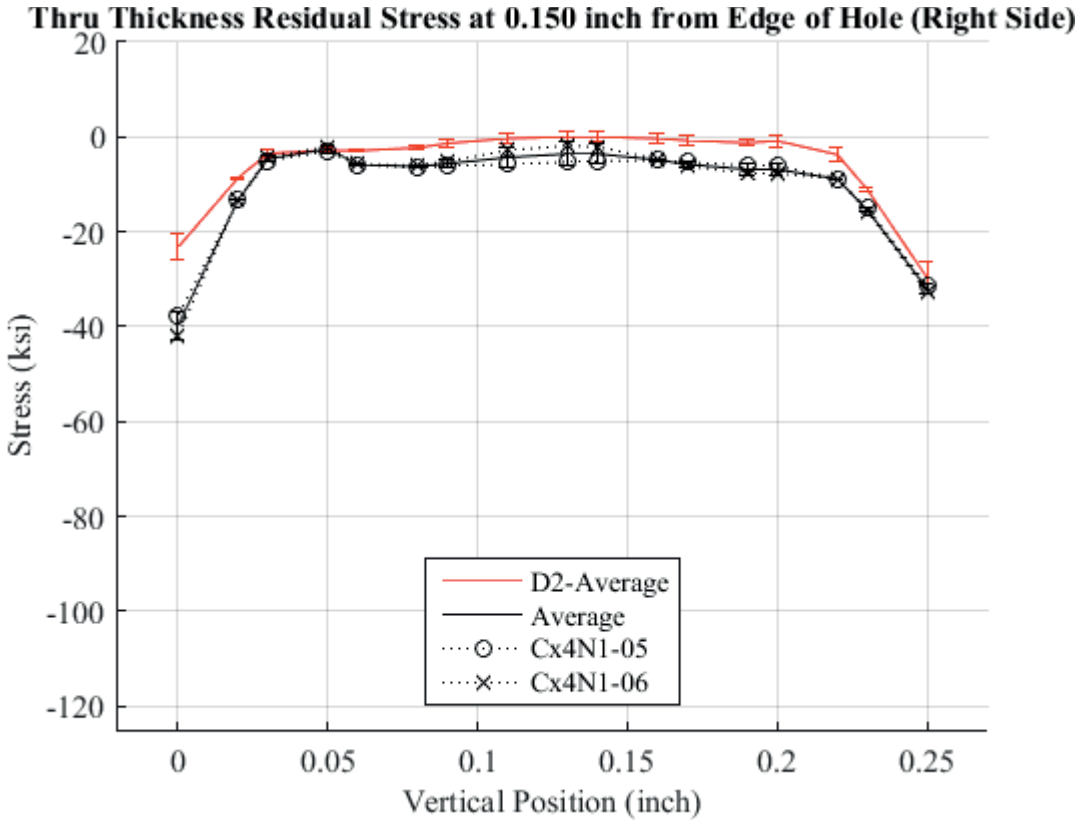

Fig. 735 Residual Stress Through-Thickness Line Plot Comparing Cx4N1-05-D, Cx4N1-06-D, and the Average between the Two to the CxD2 (7075-T651) Average Residual Stress at a Distance of 0.150 inch from the Right Side of the Hole – Cx4N1-05-D and Cx4N1-06-D Coupons had a 0.125 inch Fatigue Crack at the Left Entrance Surface.

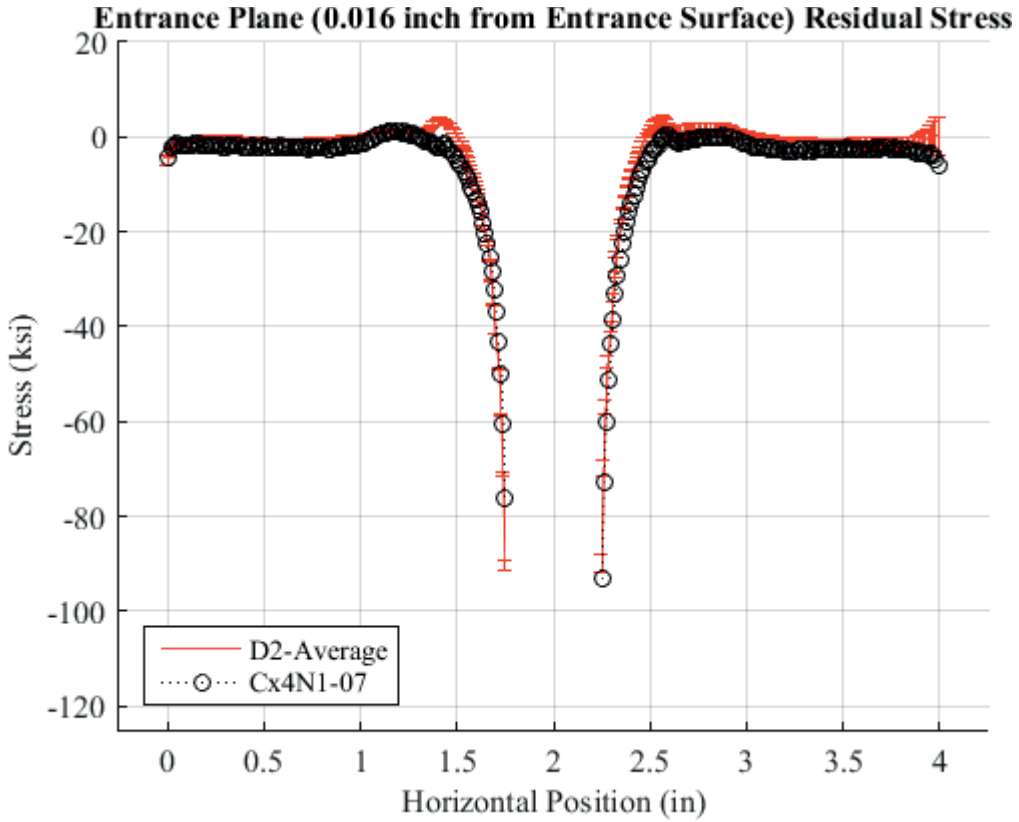

Fig. 736 Residual Stress Line Plot Comparing Cx4N1-07-D, and the Average between the Two to the CxD2 (7075-T651) Average Residual Stress at a Distance of 0.016 inch (Entrance Surface) from the Entrance Surface –Cx4N1-07-D Coupons had a 0.2505 inch Fatigue Crack at the Left Entrance Surface.

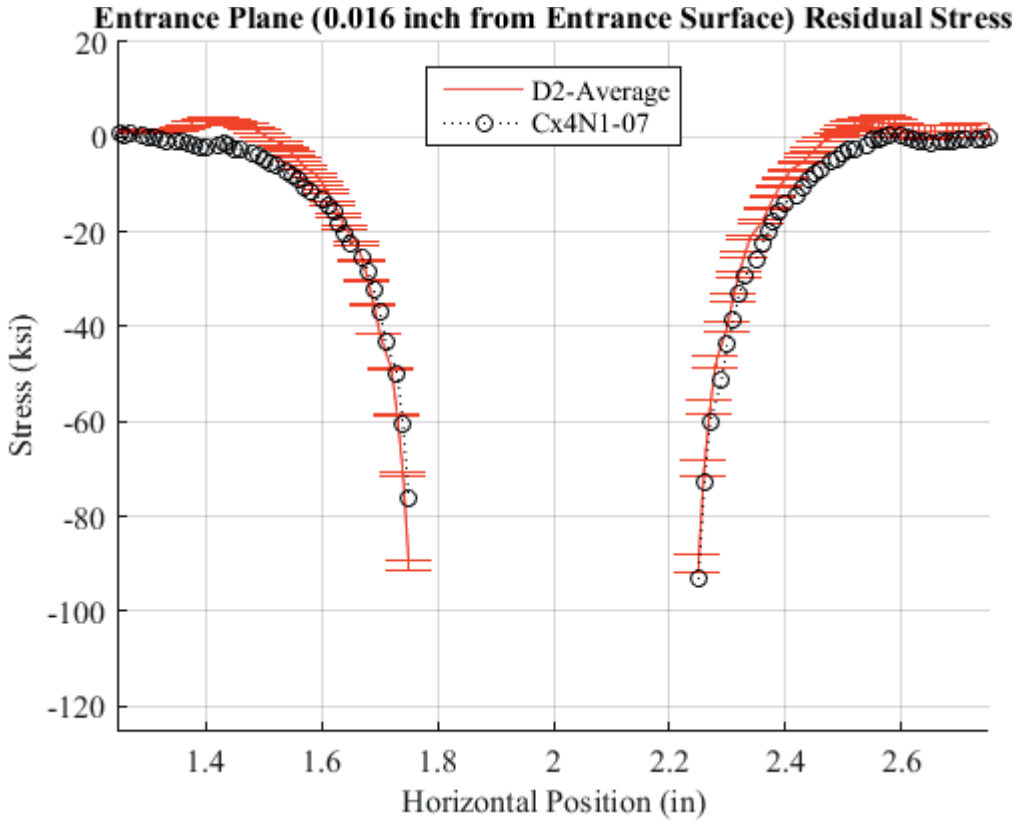

Fig. 737 Residual Stress Line Plot Comparing Cx4N1-07-D, and the Average between the Two to the CxD2 (7075-T651) Average Residual Stress at a Distance of 0.016 inch (Entrance Surface) from the Entrance Surface –Cx4N1-07-D Coupons had a 0.2505 inch Fatigue Crack at the Left Entrance Surface – Zoomed in Next to Hole.

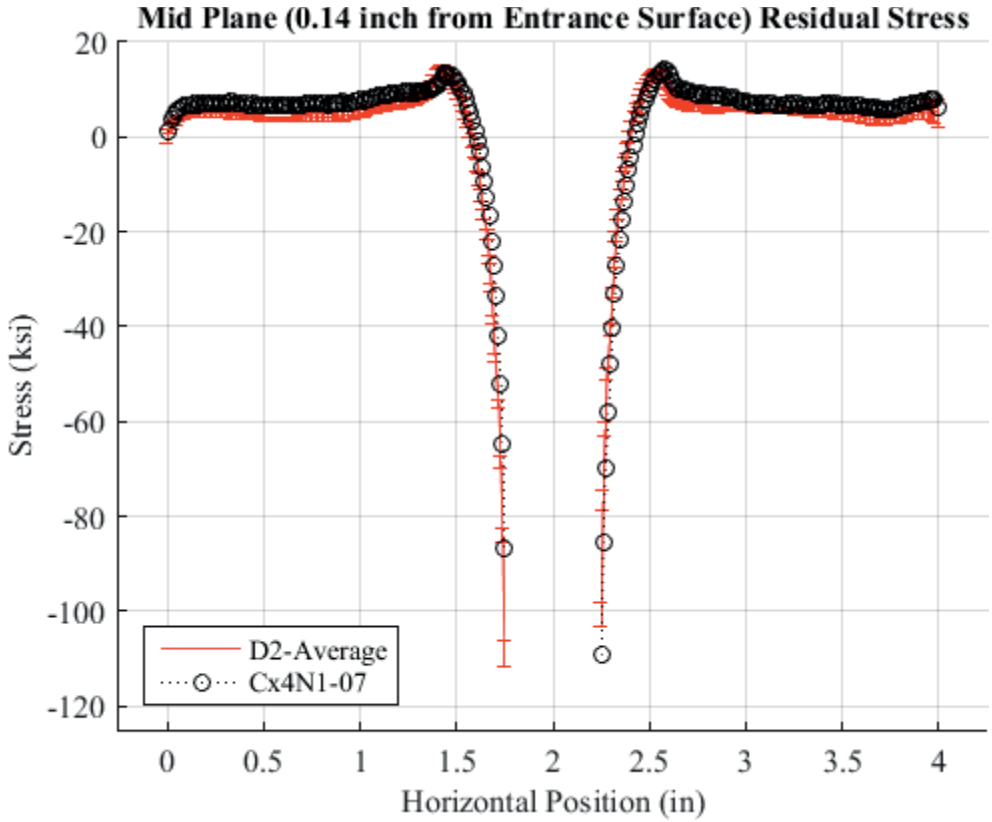

Fig. 738 Residual Stress Line Plot Comparing Cx4N1-07-D, and the Average between the Two to the CxD2 (7075-T651) Average Residual Stress at a Distance of 0.140 inch (Mid Plane Surface) from the Entrance Surface –Cx4N1-07-D Coupons had a 0.2505 inch Fatigue Crack at the Left Entrance Surface.

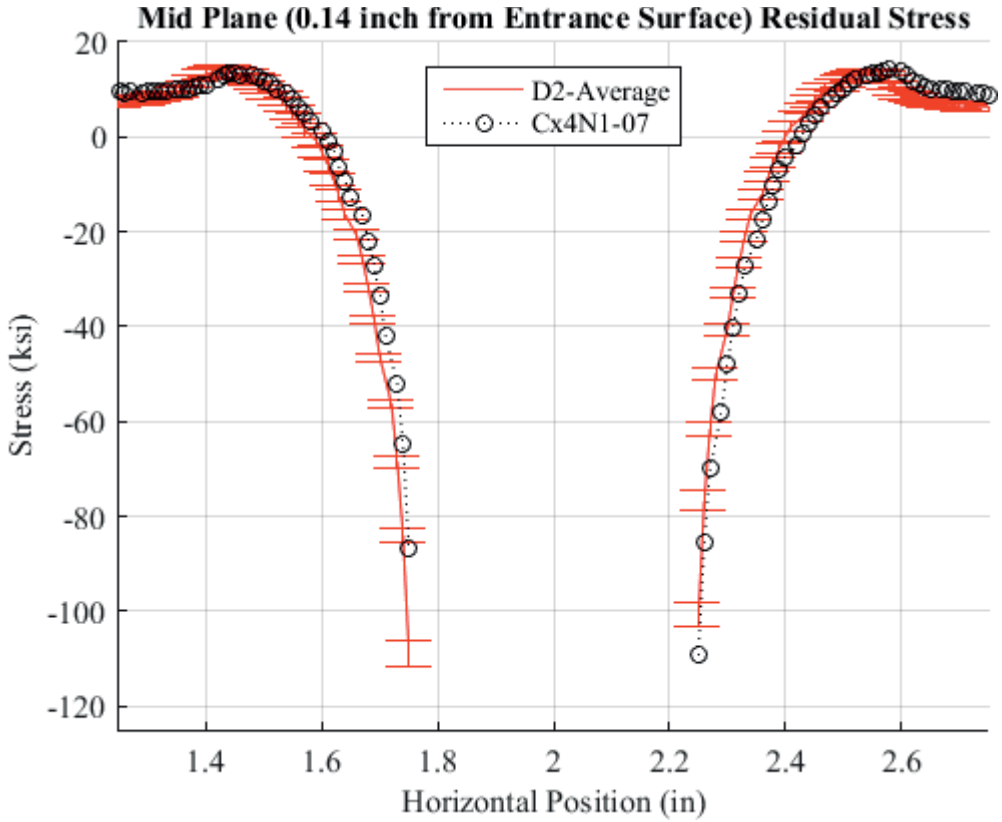

Fig. 739 Residual Stress Line Plot Comparing Cx4N1-07-D, and the Average between the Two to the CxD2 (7075-T651) Average Residual Stress at a Distance of 0.140 inch (Mid Plane Surface) from the Entrance Surface –Cx4N1-07-D Coupons had a 0.2505 inch Fatigue Crack at the Left Entrance Surface – Zoomed in Next to Hole.

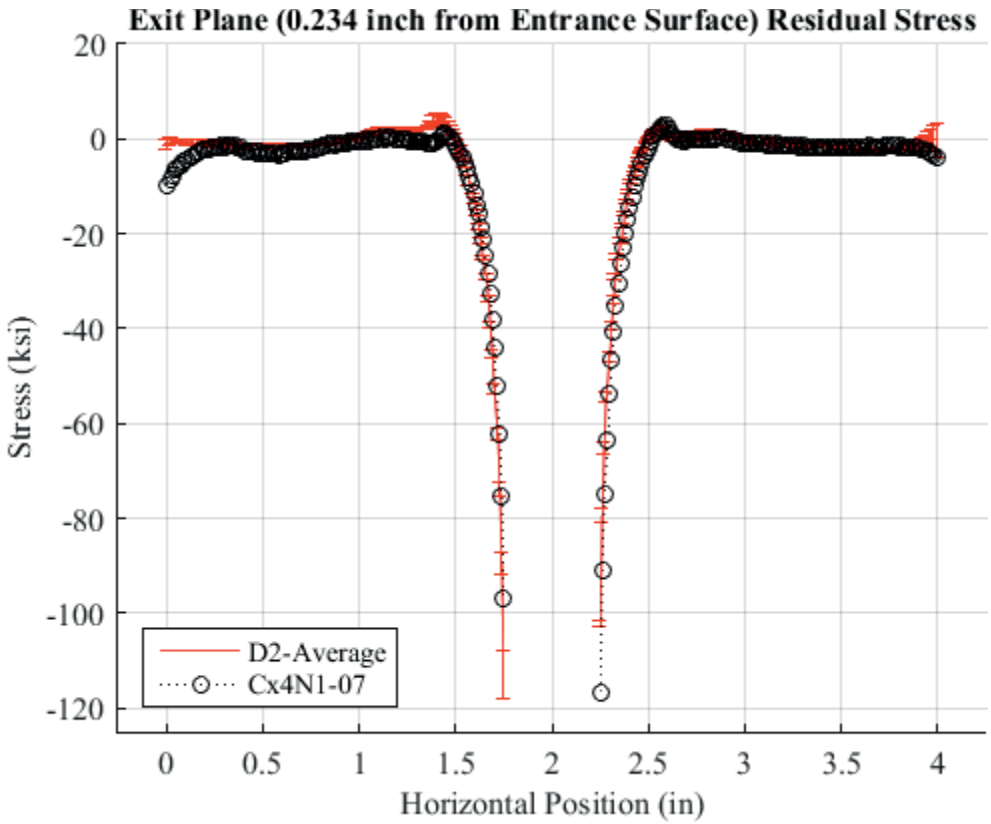

Fig. 740 Residual Stress Line Plot Comparing Cx4N1-07-D, and the Average between the Two to the CxD2 (7075-T651) Average Residual Stress at a Distance of 0.234 inch (Exit Surface) from the Entrance Surface –Cx4N1-07-D Coupons had a 0.2505 inch Fatigue Crack at the Left Entrance Surface.

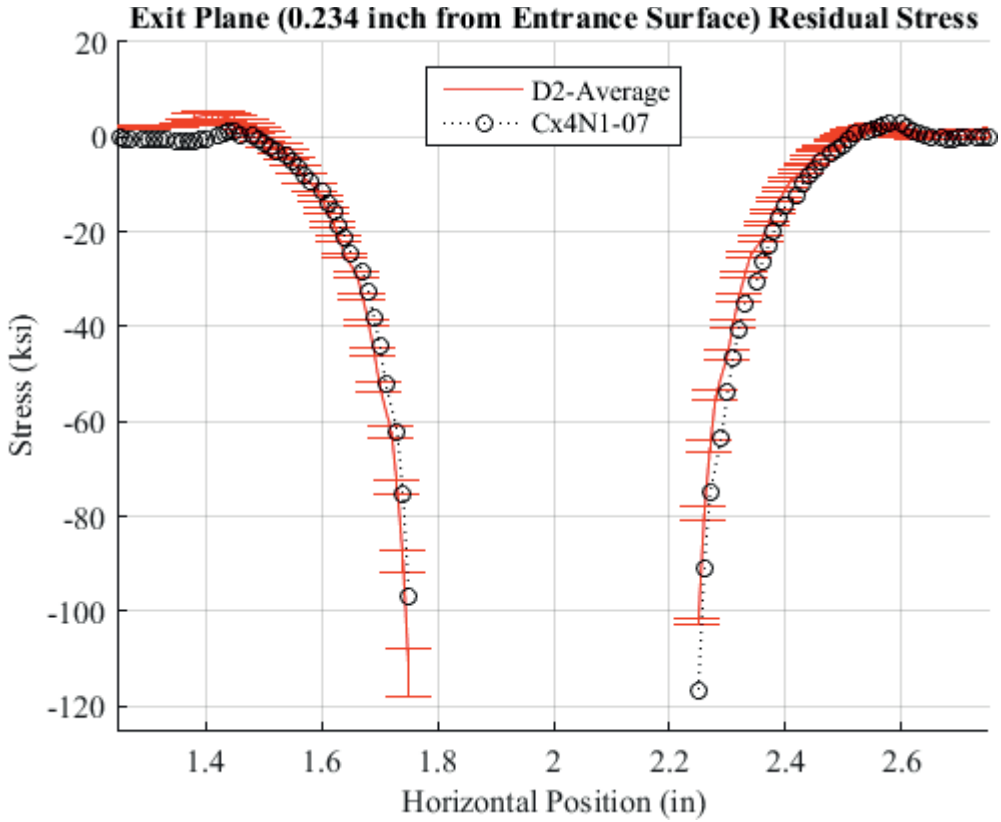

Fig. 741 Residual Stress Line Plot Comparing Cx4N1-07-D, and the Average between the Two to the CxD2 (7075-T651) Average Residual Stress at a Distance of 0.234 inch (Exit Surface) from the Entrance Surface –Cx4N1-07-D Coupons had a 0.2505 inch Fatigue Crack at the Left Entrance Surface – Zoomed in Next to Hole.

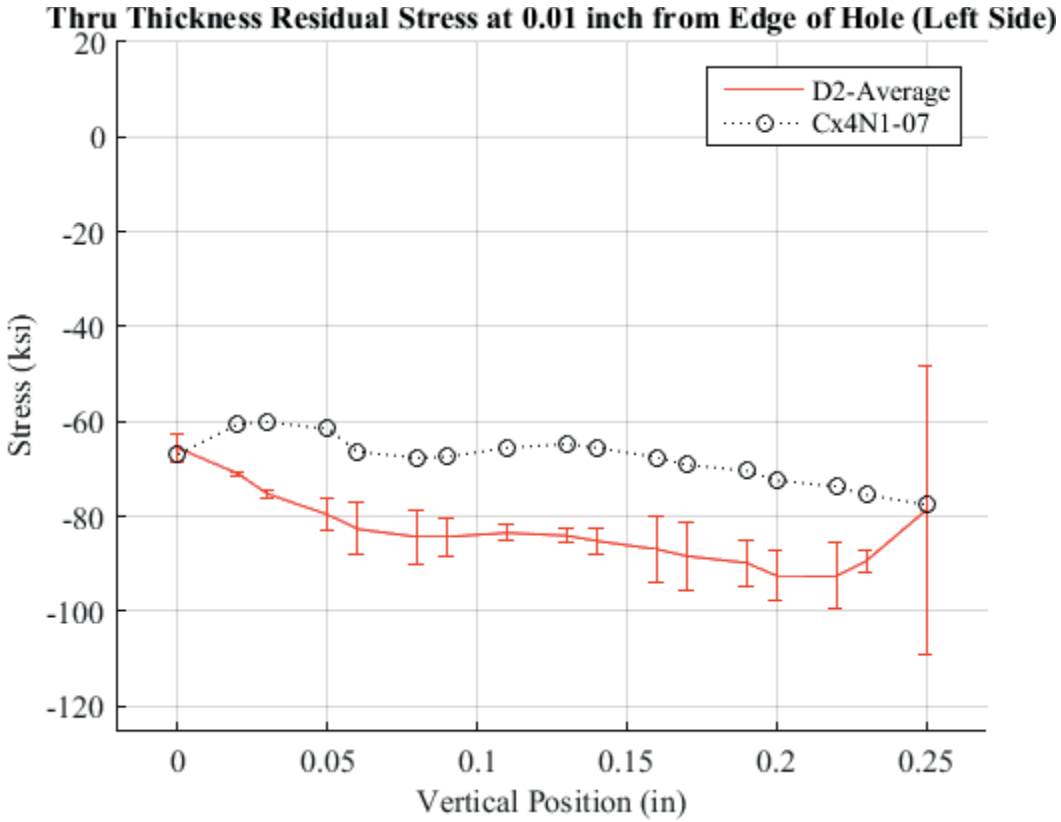

Fig. 742 Residual Stress Through-Thickness Line Plot Comparing Cx4N1-06-D, and the Average between the Two to the CxD2 (7075-T651) Average Residual Stress at a Distance of 0.01 inch from the Left Side of the Hole – Cx4N1-07-D Coupons had a 0.2505 inch Fatigue Crack at the Left Entrance Surface.

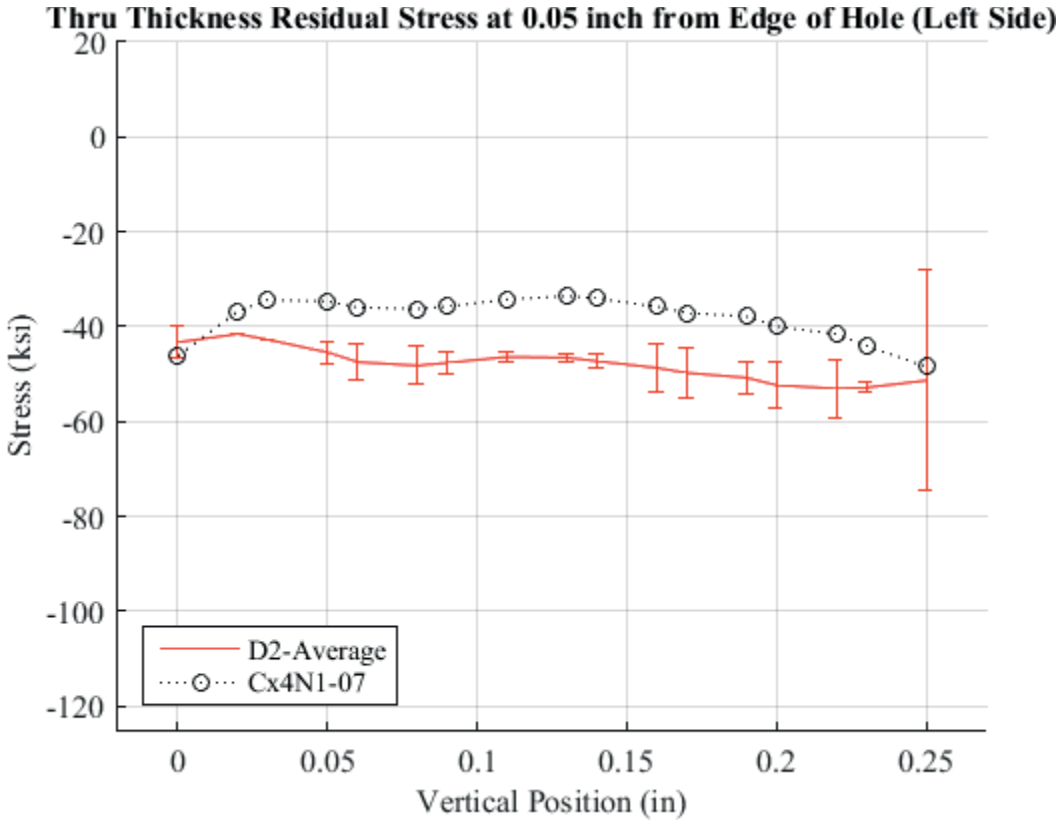

Fig. 743 Residual Stress Through-Thickness Line Plot Comparing Cx4N1-06-D, and the Average between the Two to the CxD2 (7075-T651) Average Residual Stress at a Distance of 0.05 inch from the Left Side of the Hole – Cx4N1-07-D Coupons had a 0.2505 inch Fatigue Crack at the Left Entrance Surface.

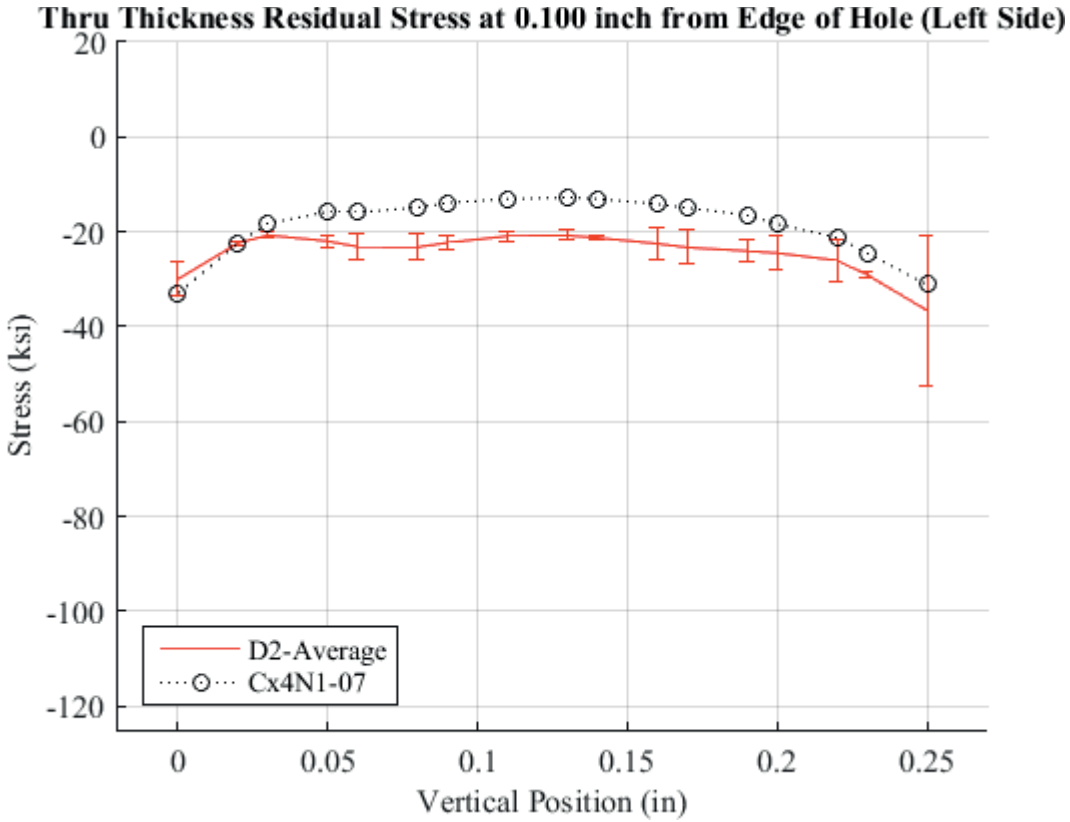

Fig. 744 Residual Stress Through-Thickness Line Plot Comparing Cx4N1-06-D, and the Average between the Two to the CxD2 (7075-T651) Average Residual Stress at a Distance of 0.10 inch from the Left Side of the Hole – Cx4N1-07-D Coupons had a 0.2505 inch Fatigue Crack at the Left Entrance Surface.

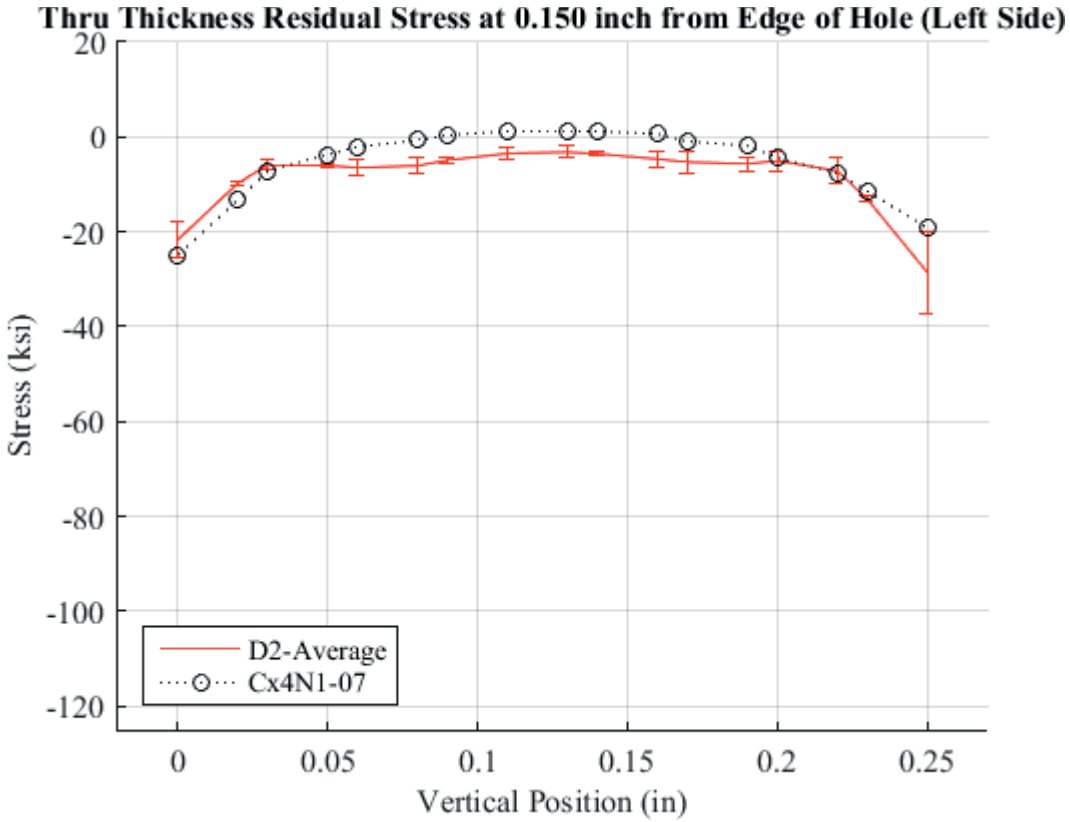

Fig. 745 Residual Stress Through-Thickness Line Plot Comparing Cx4N1-06-D, and the Average between the Two to the CxD2 (7075-T651) Average Residual Stress at a Distance of 0.150 inch from the Left Side of the Hole – Cx4N1-07-D Coupons had a 0.2505 inch Fatigue Crack at the Left Entrance Surface.

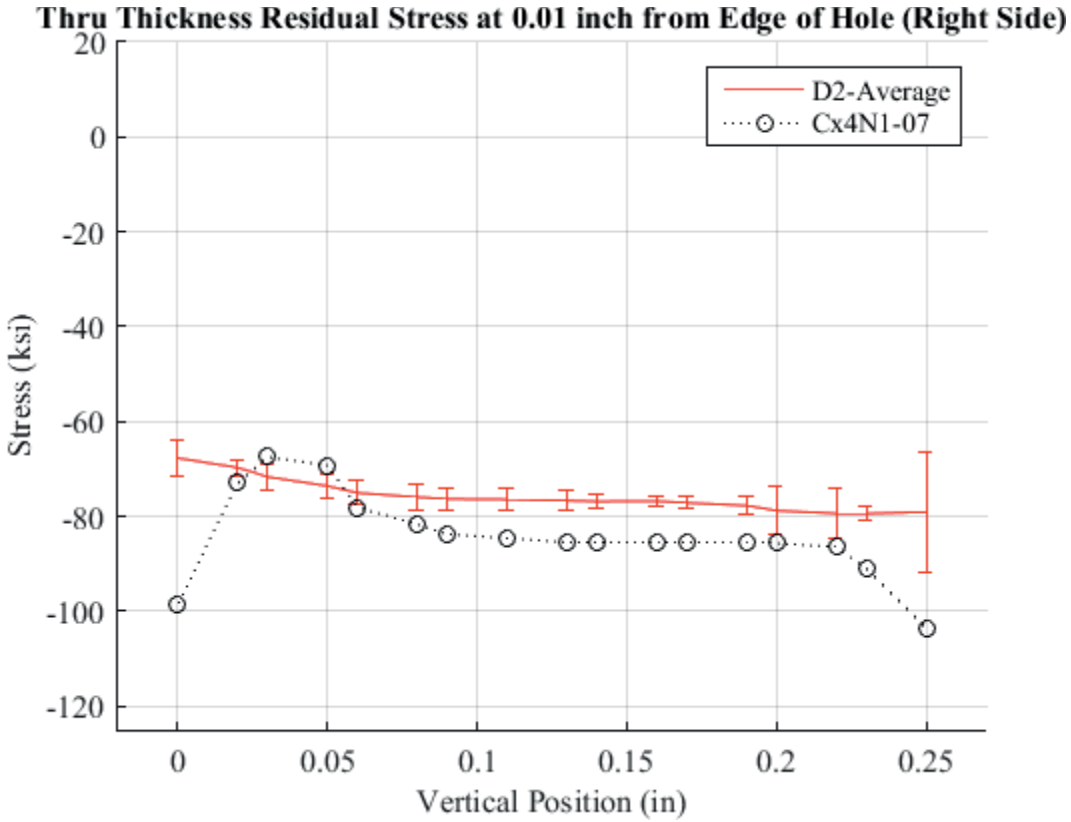

Fig. 746 Residual Stress Through-Thickness Line Plot Comparing Cx4N1-06-D, and the Average between the Two to the CxD2 (7075-T651) Average Residual Stress at a Distance of 0.01 inch from the Right Side of the Hole – Cx4N1-07-D Coupons had a 0.2505 inch Fatigue Crack at the Left Entrance Surface.

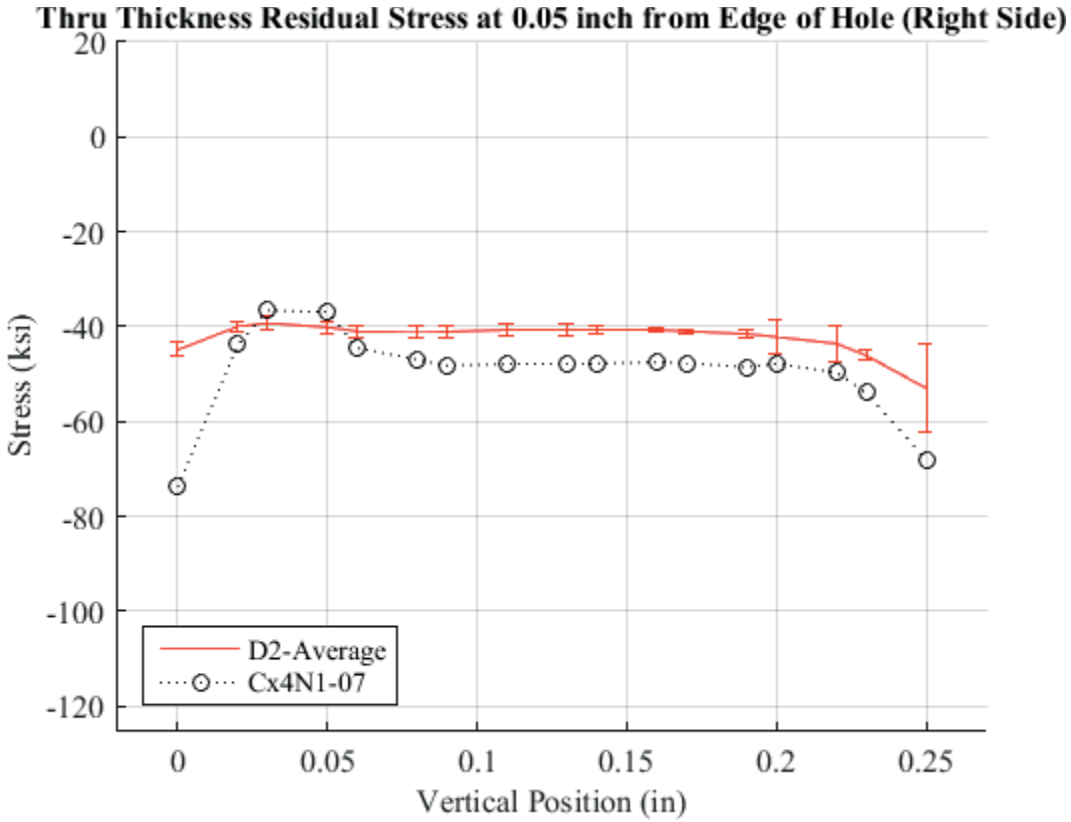

Fig. 747 Residual Stress Through-Thickness Line Plot Comparing Cx4N1-06-D, and the Average between the Two to the CxD2 (7075-T651) Average Residual Stress at a Distance of 0.05 inch from the Right Side of the Hole – Cx4N1-07-D Coupons had a 0.2505 inch Fatigue Crack at the Left Entrance Surface.

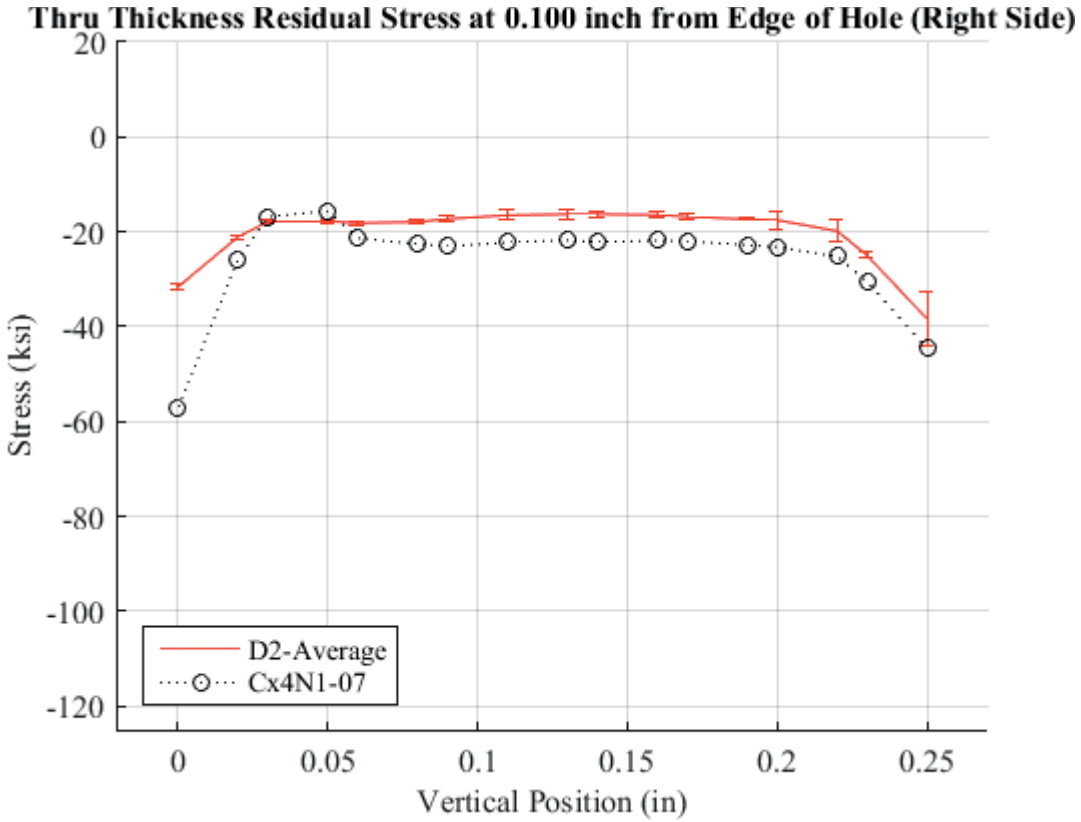

Fig. 748 Residual Stress Through-Thickness Line Plot Comparing Cx4N1-06-D, and the Average between the Two to the CxD2 (7075-T651) Average Residual Stress at a Distance of 0.10 inch from the Right Side of the Hole – Cx4N1-07-D Coupons had a 0.2505 inch Fatigue Crack at the Left Entrance Surface.

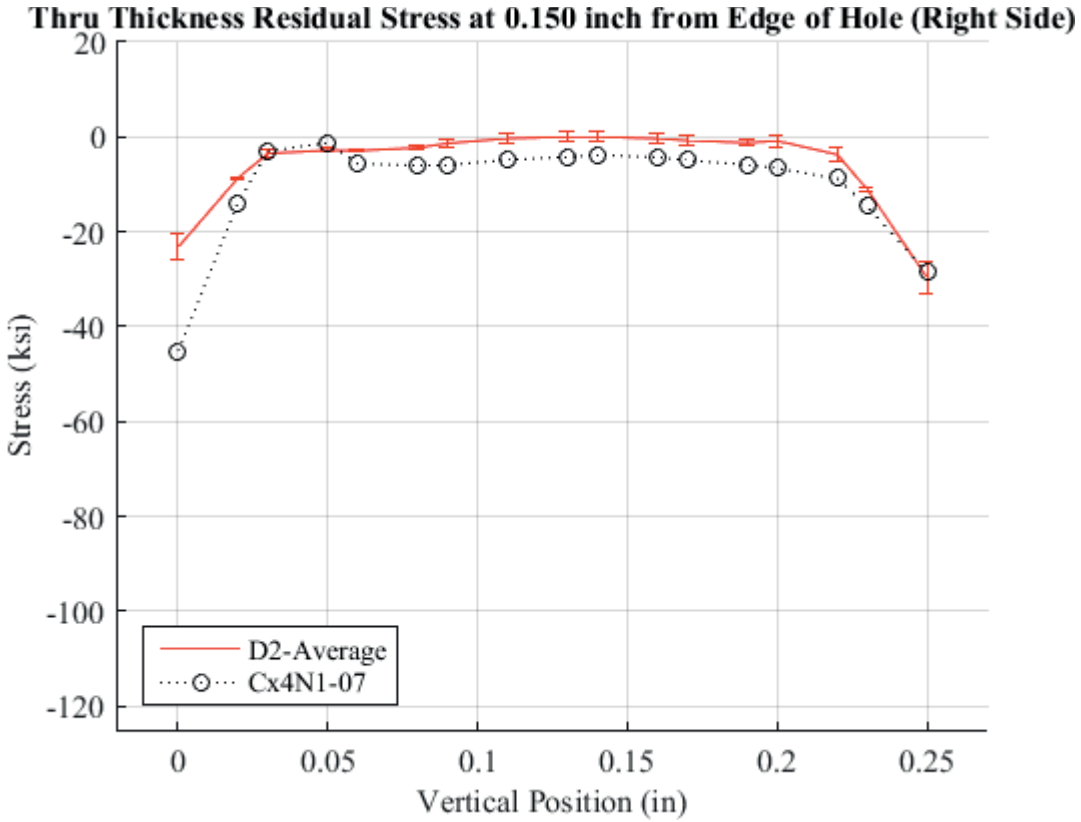

Fig. 749 Residual Stress Through-Thickness Line Plot Comparing Cx4N1-06-D, and the Average between the Two to the CxD2 (7075-T651) Average Residual Stress at a Distance of 0.150 inch from the Right Side of the Hole – Cx4N1-07-D Coupons had a 0.2505 inch Fatigue Crack at the Left Entrance Surface.

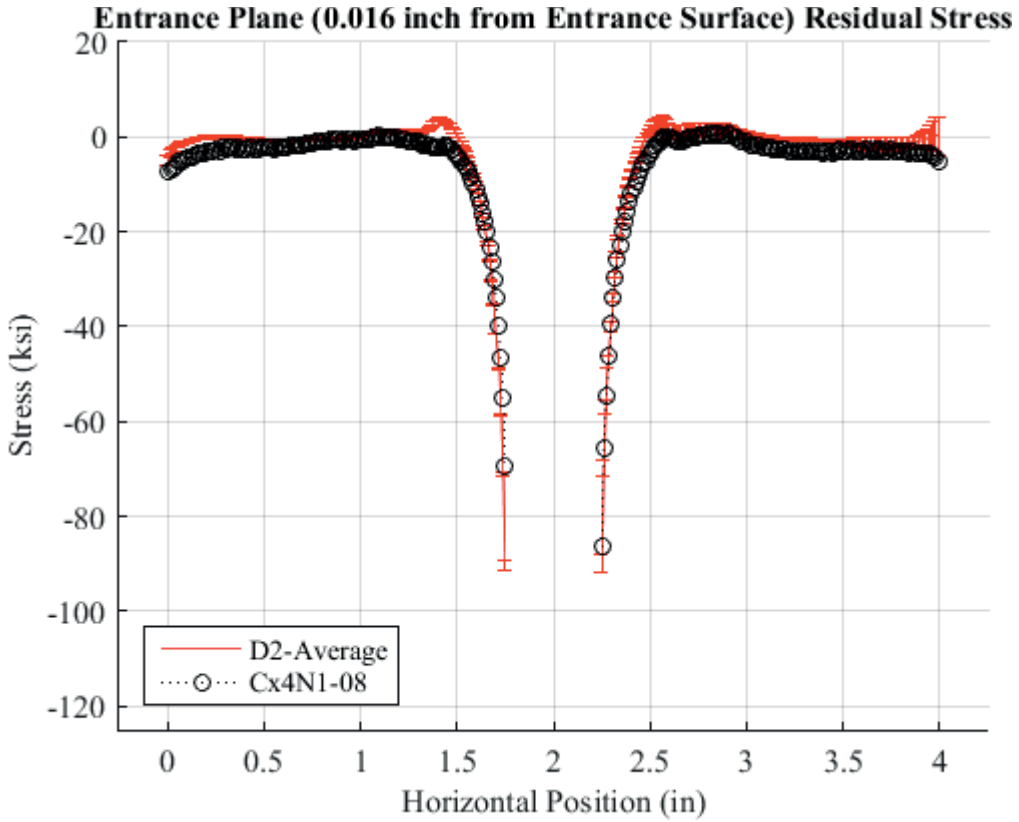

Fig. 750 Residual Stress Line Plot Comparing Cx4N1-08-D, and the Average between the Two to the CxD2 (7075-T651) Average Residual Stress at a Distance of 0.016 inch (Entrance Surface) from the Entrance Surface –Cx4N1-08-D Coupons had a 0.5017 inch Fatigue Crack at the Left Entrance Surface, There was also a Fatigue Crack on the Right Side of the Hole.

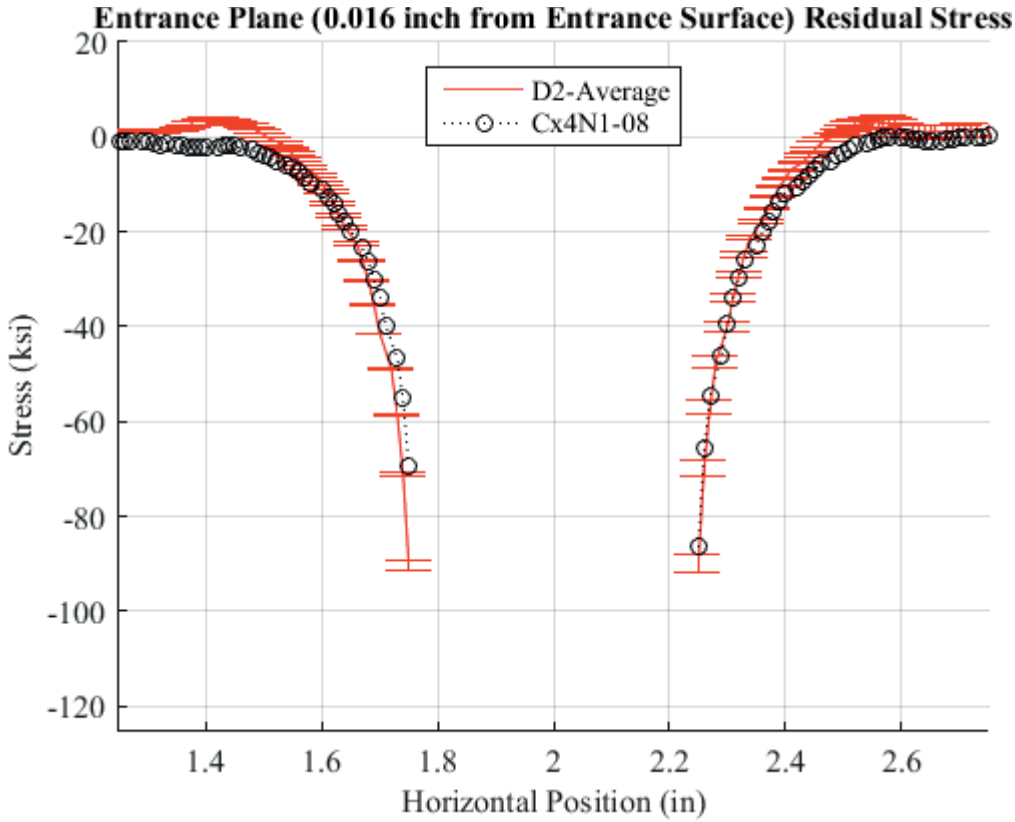

Fig. 751 Residual Stress Line Plot Comparing Cx4N1-08-D, and the Average between the Two to the CxD2 (7075-T651) Average Residual Stress at a Distance of 0.016 inch (Entrance Surface) from the Entrance Surface –Cx4N1-08-D Coupons had a 0.5017 inch Fatigue Crack at the Left Entrance Surface, There was also a Fatigue Crack on the Right Side of the Hole – Zoomed in Next to Hole.

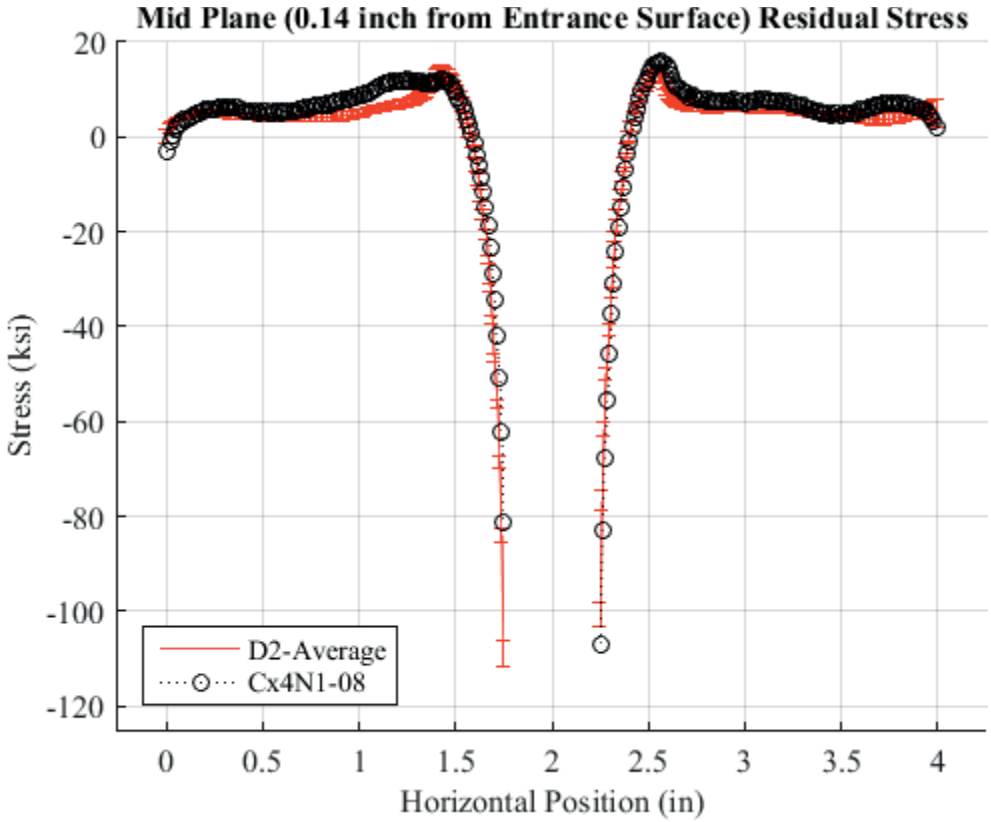

Fig. 752 Residual Stress Line Plot Comparing Cx4N1-08-D, and the Average between the Two to the CxD2 (7075-T651) Average Residual Stress at a Distance of 0.140 inch (Mid Plane Surface) from the Entrance Surface –Cx4N1-08-D Coupons had a 0.5017 inch Fatigue Crack at the Left Entrance Surface, There was also a Fatigue Crack on the Right Side of the Hole.

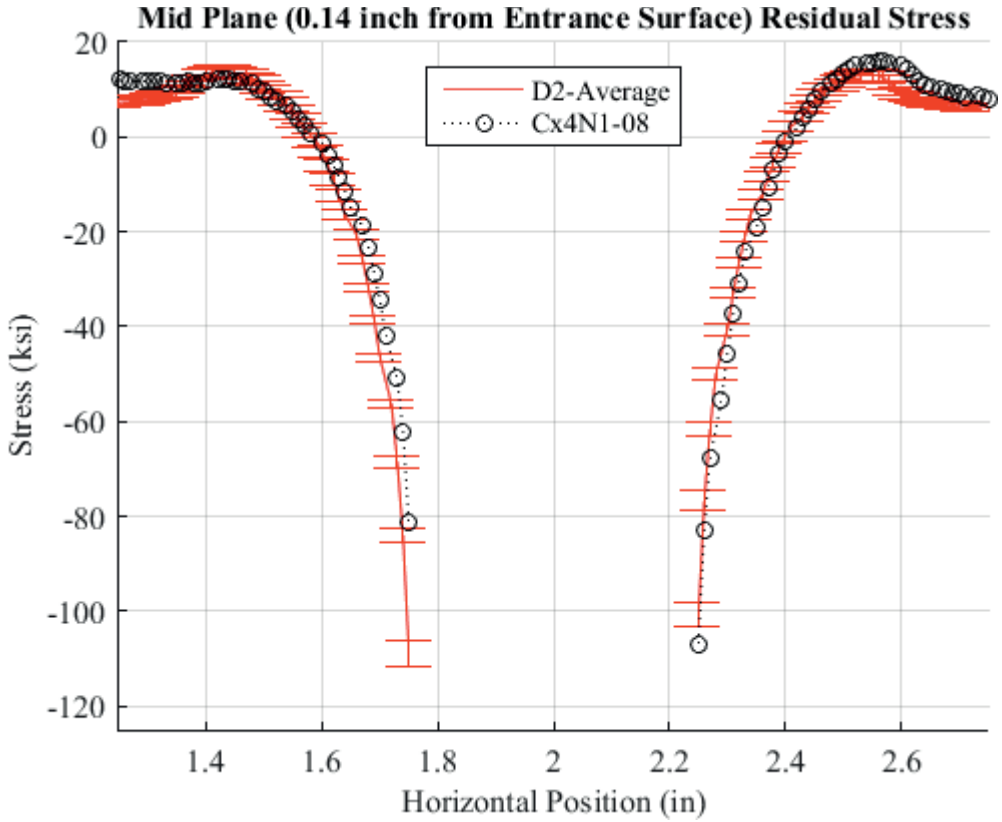

Fig. 753 Residual Stress Line Plot Comparing Cx4N1-08-D, and the Average between the Two to the CxD2 (7075-T651) Average Residual Stress at a Distance of 0.140 inch (Mid Plane Surface) from the Entrance Surface –Cx4N1-08-D Coupons had a 0.5017 inch Fatigue Crack at the Left Entrance Surface, There was also a Fatigue Crack on the Right Side of the Hole – Zoomed in Next to Hole.

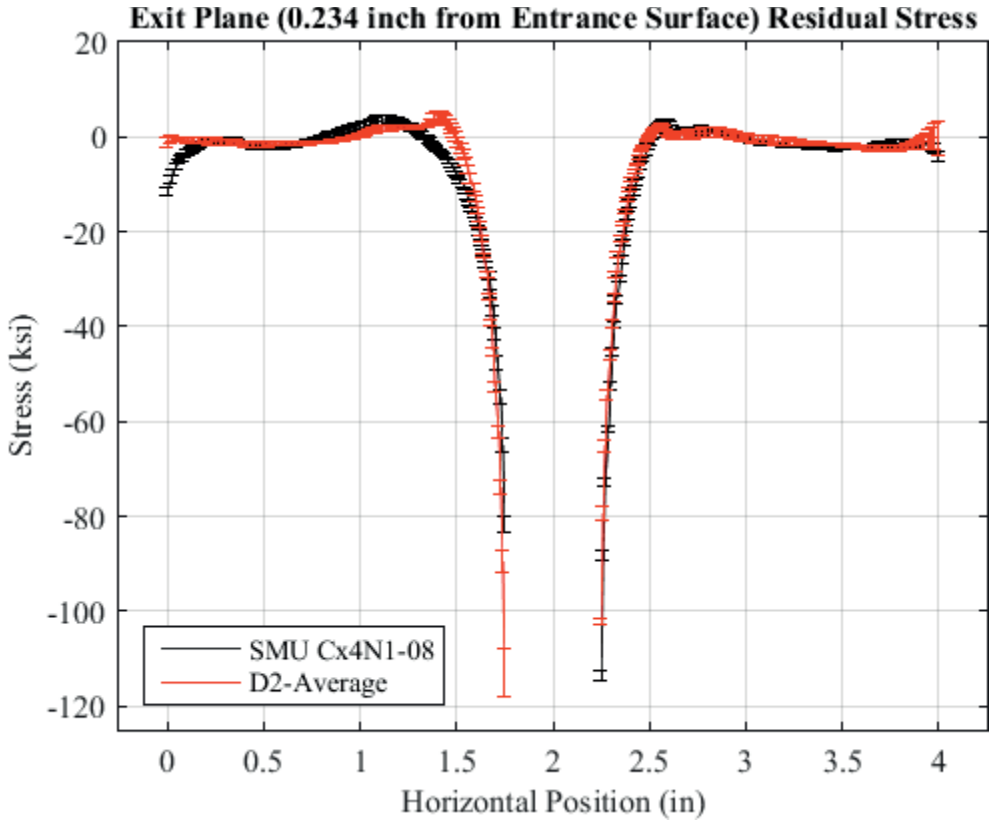

Fig. 754 Residual Stress Line Plot Comparing Cx4N1-08-D, and the Average between the Two to the CxD2 (7075-T651) Average Residual Stress at a Distance of 0.234 inch (Exit Surface) from the Entrance Surface –Cx4N1-08-D Coupons had a 0.5017 inch Fatigue Crack at the Left Entrance Surface, There was also a Fatigue Crack on the Right Side of the Hole.

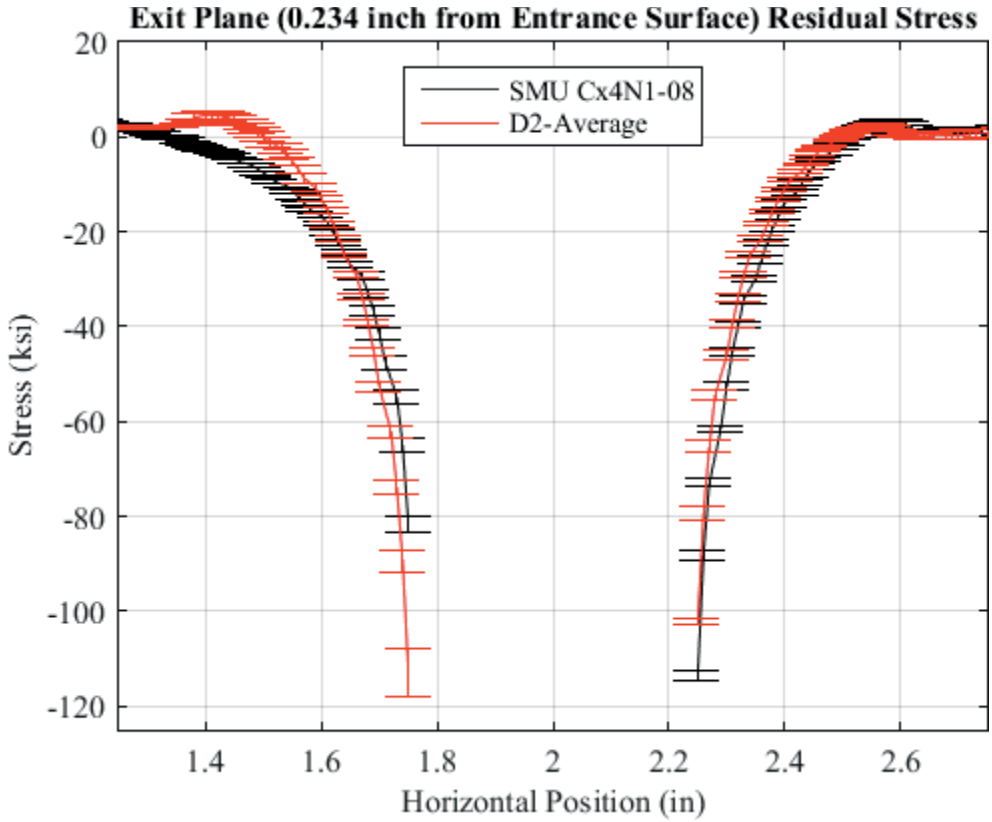

Fig. 755 Residual Stress Line Plot Comparing Cx4N1-08-D, and the Average between the Two to the CxD2 (7075-T651) Average Residual Stress at a Distance of 0.234 inch (Exit Surface) from the Entrance Surface –Cx4N1-08-D Coupons had a 0.5017 inch Fatigue Crack at the Left Entrance Surface, There was also a Fatigue Crack on the Right Side of the Hole – Zoomed in Next to Hole.

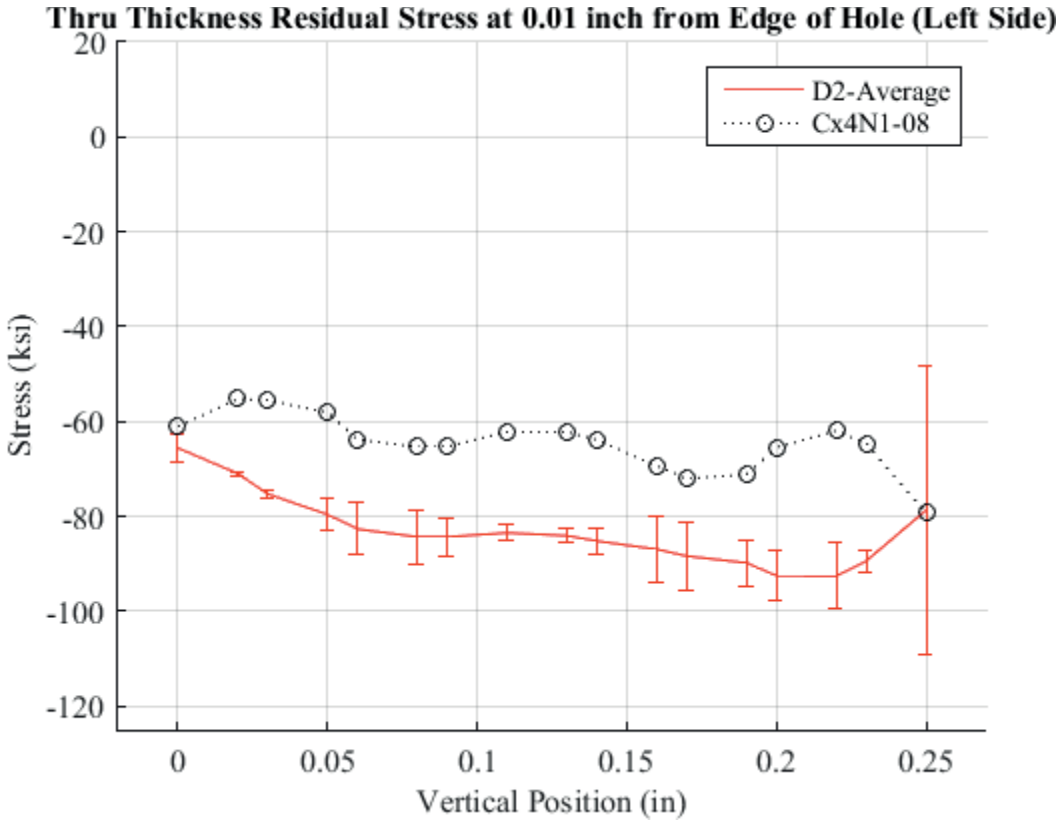

Fig. 756 Residual Stress Through-Thickness Line Plot Comparing Cx4N1-06-D, and the Average between the Two to the CxD2 (7075-T651) Average Residual Stress at a Distance of 0.01 inch from the Left Side of the Hole – Cx4N1-08-D Coupons had a 0.5017 inch Fatigue Crack at the Left Entrance Surface, There was also a Fatigue Crack on the Right Side of the Hole.

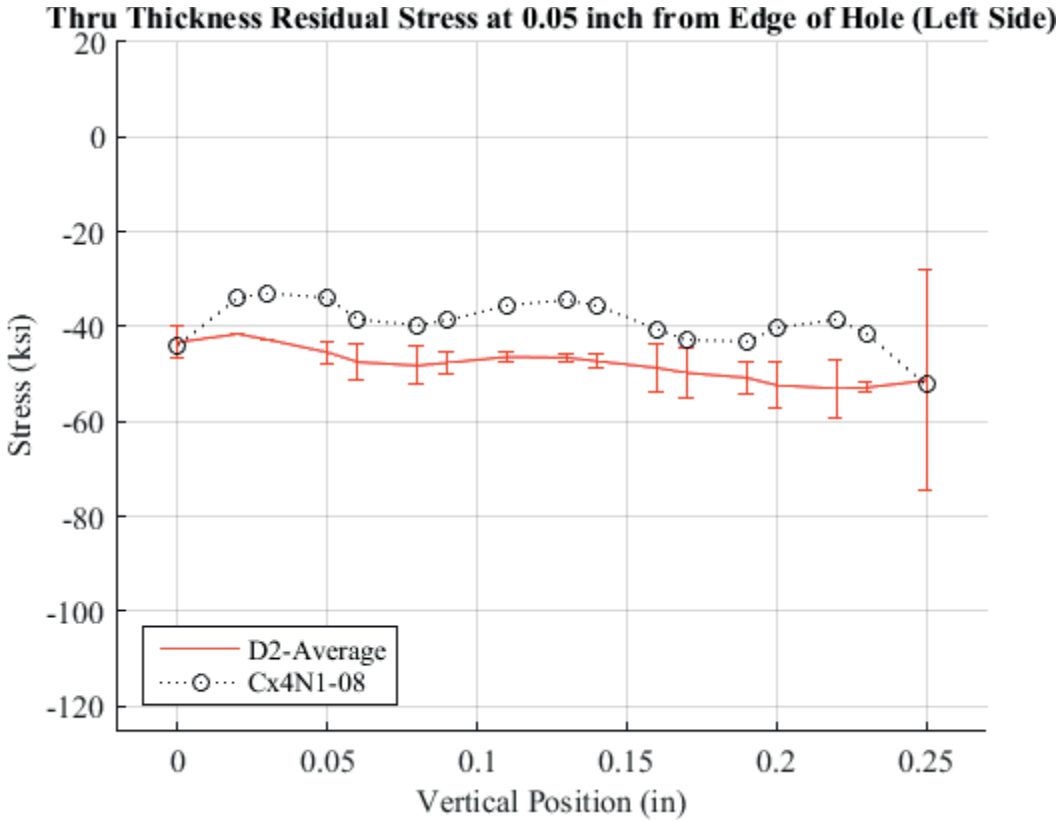

Fig. 757 Residual Stress Through-Thickness Line Plot Comparing Cx4N1-06-D, and the Average between the Two to the CxD2 (7075-T651) Average Residual Stress at a Distance of 0.05 inch from the Left Side of the Hole – Cx4N1-08-D Coupons had a 0.5017 inch Fatigue Crack at the Left Entrance Surface, There was also a Fatigue Crack on the Right Side of the Hole.

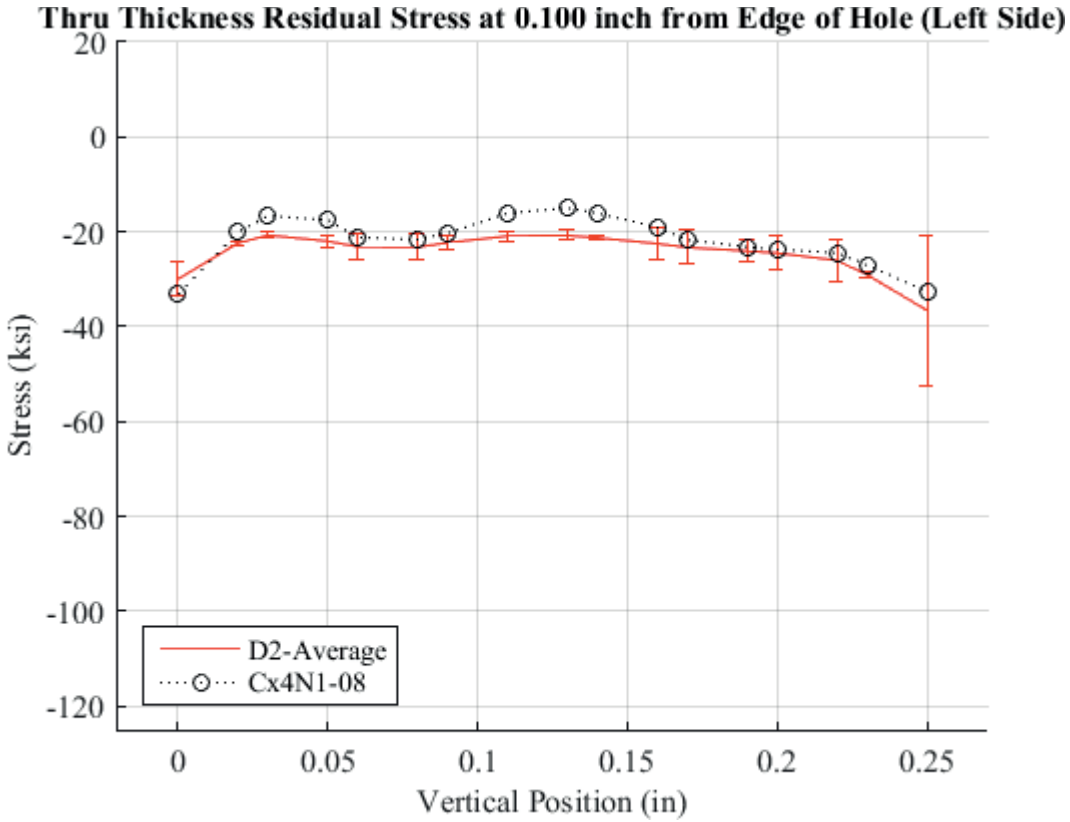

Fig. 758 Residual Stress Through-Thickness Line Plot Comparing Cx4N1-06-D, and the Average between the Two to the CxD2 (7075-T651) Average Residual Stress at a Distance of 0.10 inch from the Left Side of the Hole – Cx4N1-08-D Coupons had a 0.5017 inch Fatigue Crack at the Left Entrance Surface, There was also a Fatigue Crack on the Right Side of the Hole.

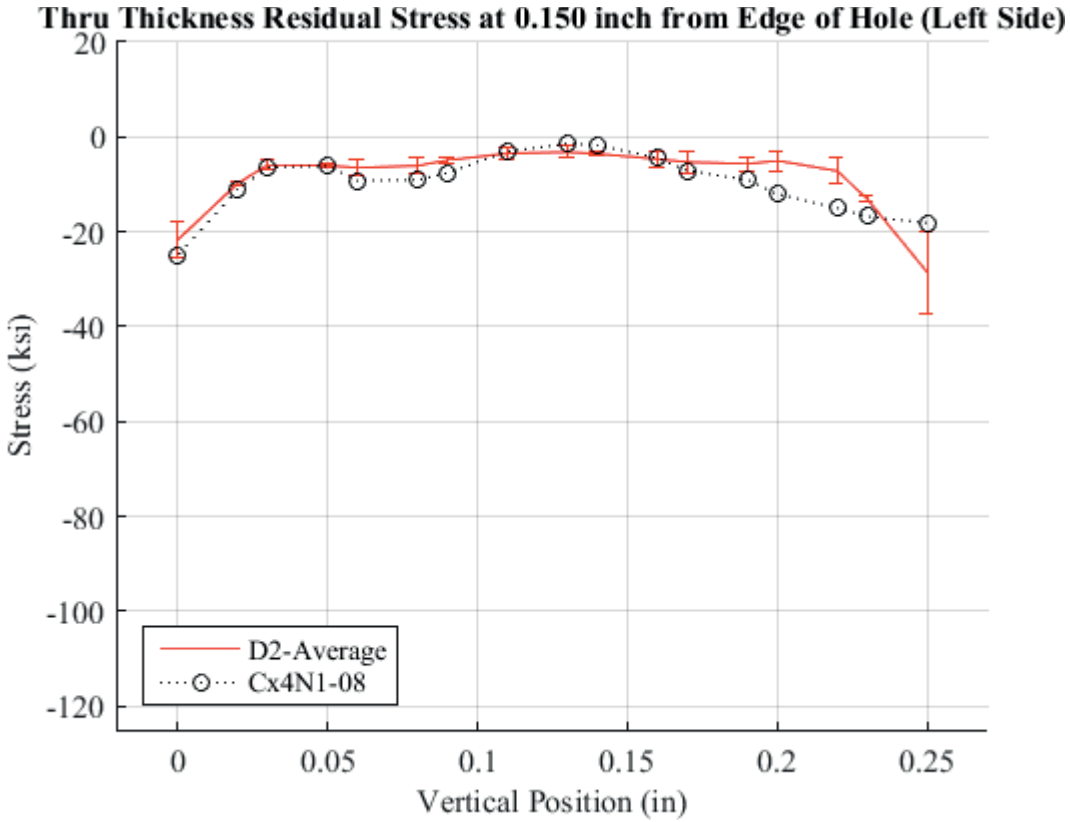

Fig. 759 Residual Stress Through-Thickness Line Plot Comparing Cx4N1-06-D, and the Average between the Two to the CxD2 (7075-T651) Average Residual Stress at a Distance of 0.150 inch from the Left Side of the Hole – Cx4N1-08-D Coupons had a 0.5017 inch Fatigue Crack at the Left Entrance Surface, There was also a Fatigue Crack on the Right Side of the Hole.

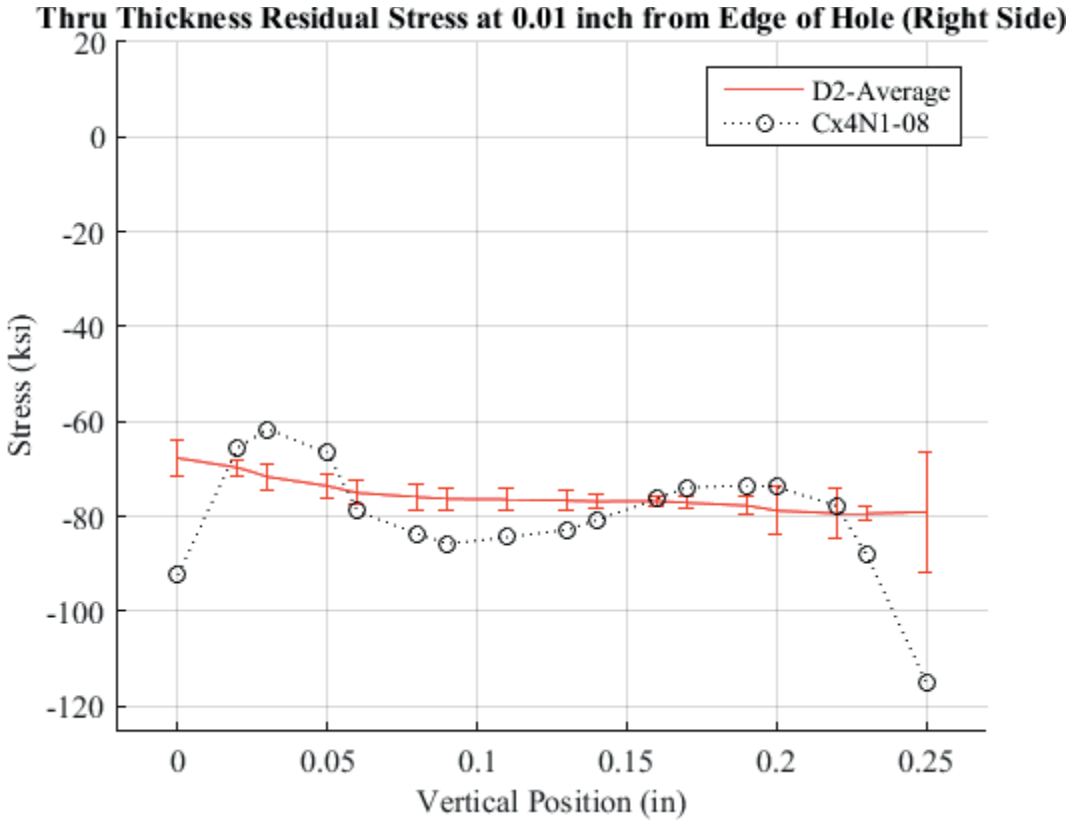

Fig. 760 Residual Stress Through-Thickness Line Plot Comparing Cx4N1-06-D, and the Average between the Two to the CxD2 (7075-T651) Average Residual Stress at a Distance of 0.01 inch from the Right Side of the Hole – Cx4N1-08-D Coupons had a 0.5017 inch Fatigue Crack at the Left Entrance Surface, There was also a Fatigue Crack on the Right Side of the Hole.

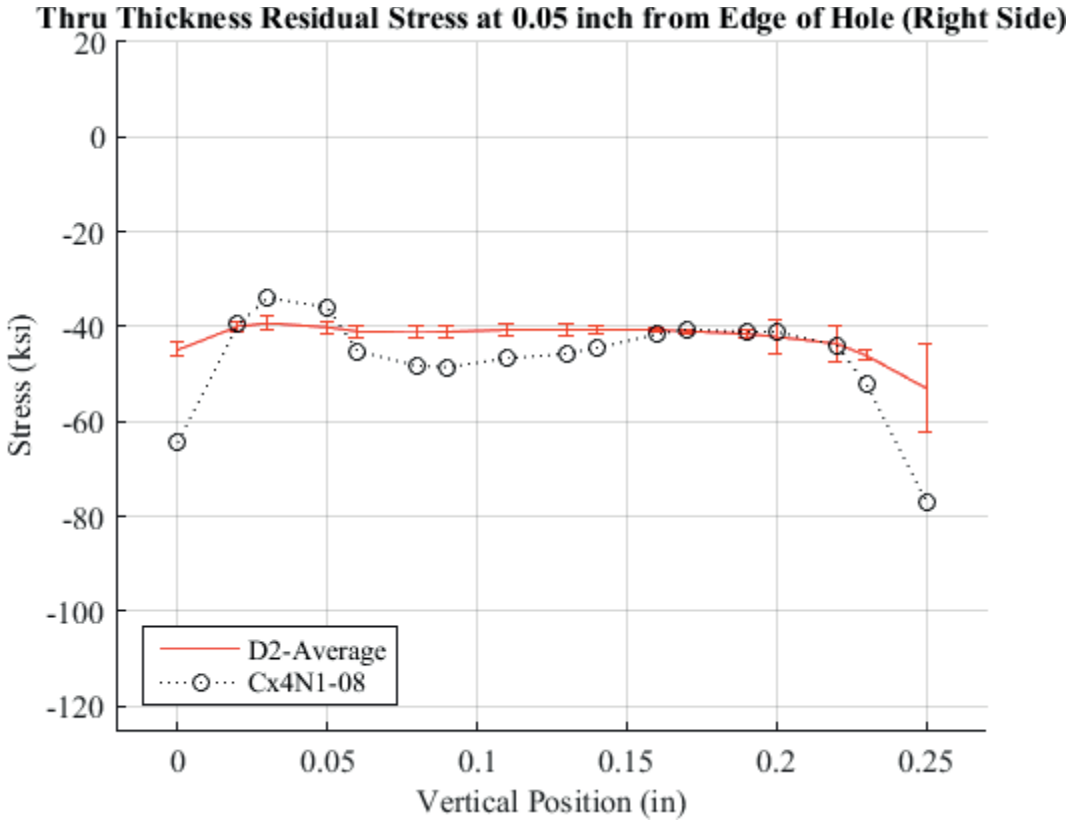

Fig. 761 Residual Stress Through-Thickness Line Plot Comparing Cx4N1-06-D, and the Average between the Two to the CxD2 (7075-T651) Average Residual Stress at a Distance of 0.05 inch from the Right Side of the Hole – Cx4N1-08-D Coupons had a 0.5017 inch Fatigue Crack at the Left Entrance Surface, There was also a Fatigue Crack on the Right Side of the Hole.

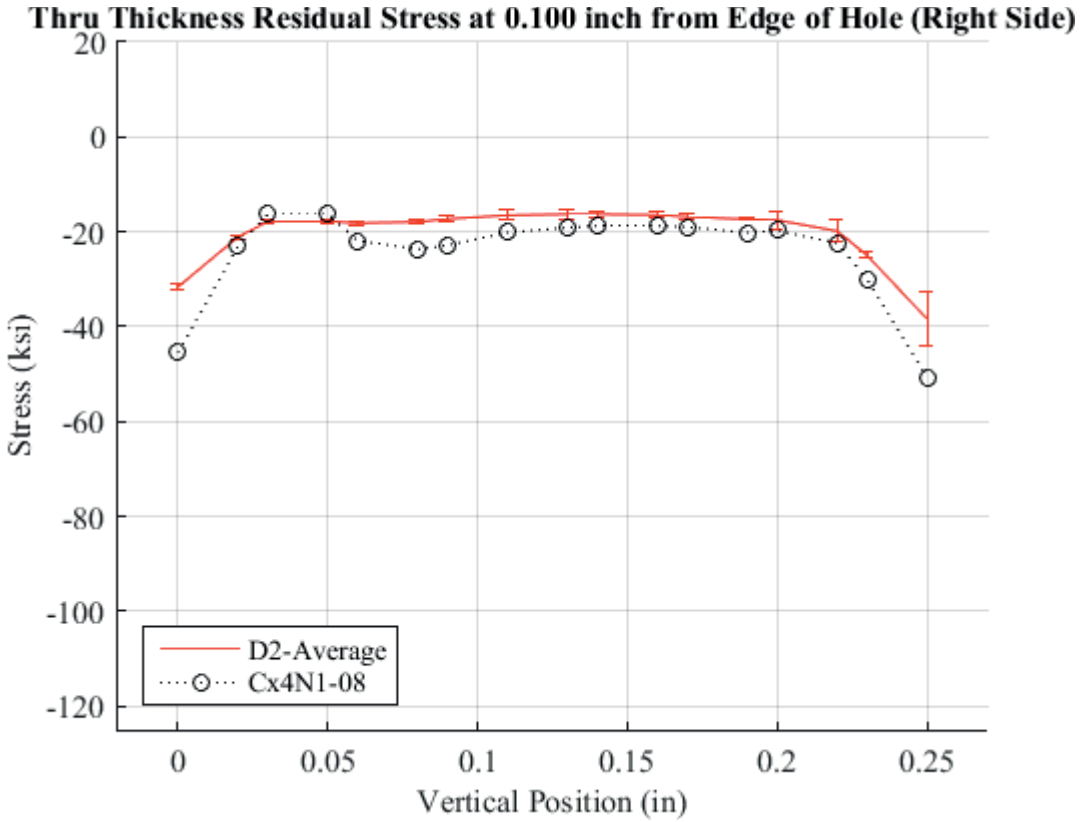

Fig. 762 Residual Stress Through-Thickness Line Plot Comparing Cx4N1-06-D, and the Average between the Two to the CxD2 (7075-T651) Average Residual Stress at a Distance of 0.10 inch from the Right Side of the Hole – Cx4N1-08-D Coupons had a 0.5017 inch Fatigue Crack at the Left Entrance Surface, There was also a Fatigue Crack on the Right Side of the Hole.

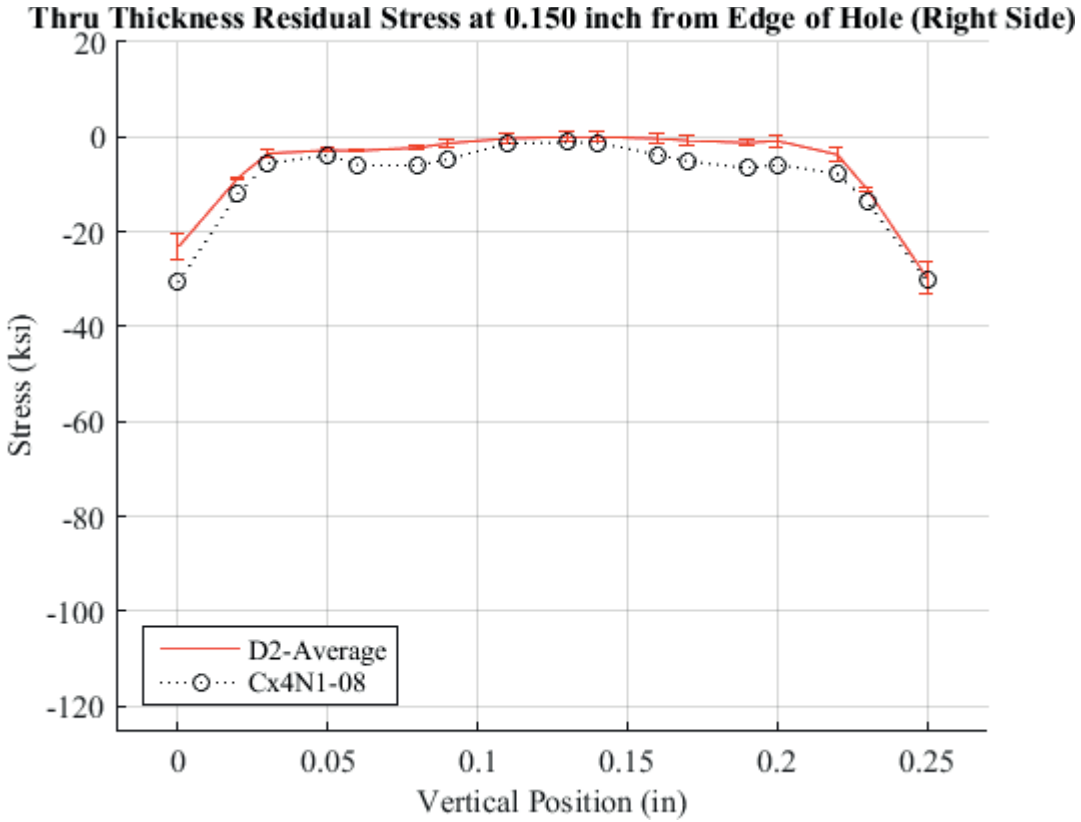

Fig. 763 Residual Stress Through-Thickness Line Plot Comparing Cx4N1-06-D, and the Average between the Two to the CxD2 (7075-T651) Average Residual Stress at a Distance of 0.150 inch from the Right Side of the Hole – Cx4N1-08-D Coupons had a 0.5017 inch Fatigue Crack at the Left Entrance Surface, There was also a Fatigue Crack on the Right Side of the Hole.

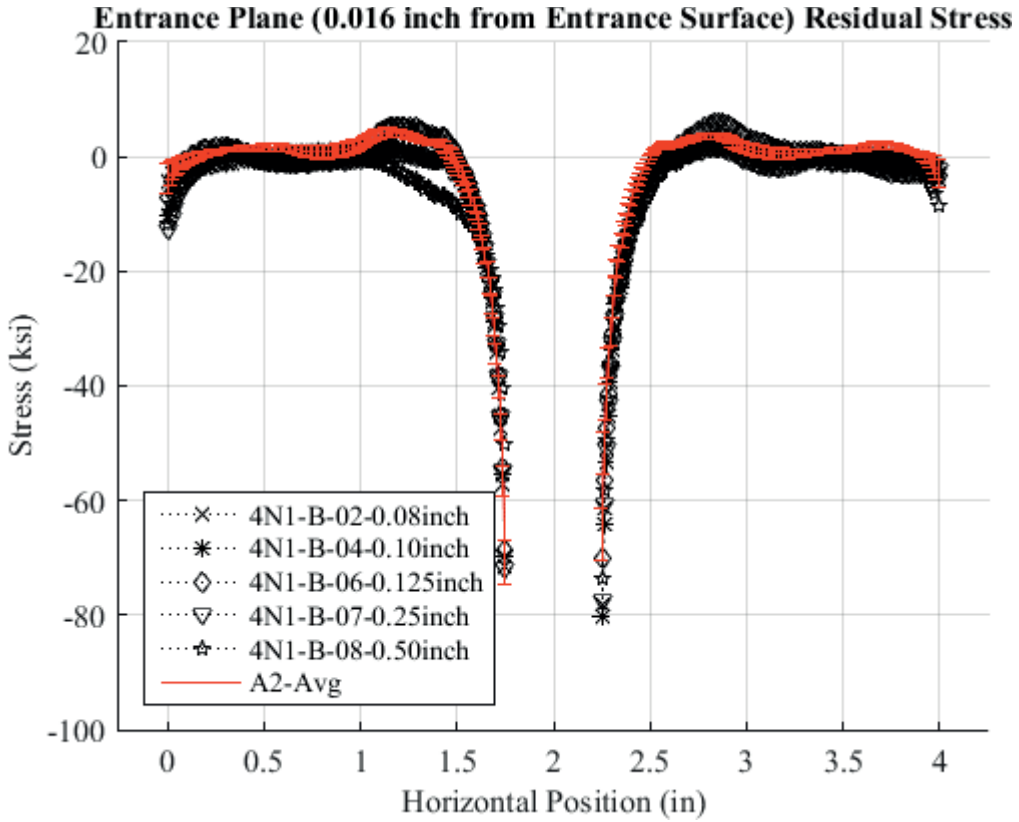

Fig. 764 Residual Stress Line Plot Comparing Cx4N1-02-B, Cx4N1-04-B, Cx4N1-06-B, CX4N1-07-B, Cx4N1-08-B, and the Average CxA2 (2024-T351) Average Residual Stress at a Distance of 0.016 inch (Entrance Surface) from the Entrance Surface. Error Bars are Provided on the CxA2 Average Residual Stress which Represent the Repeatability Uncertainty for the CxA2 Condition.

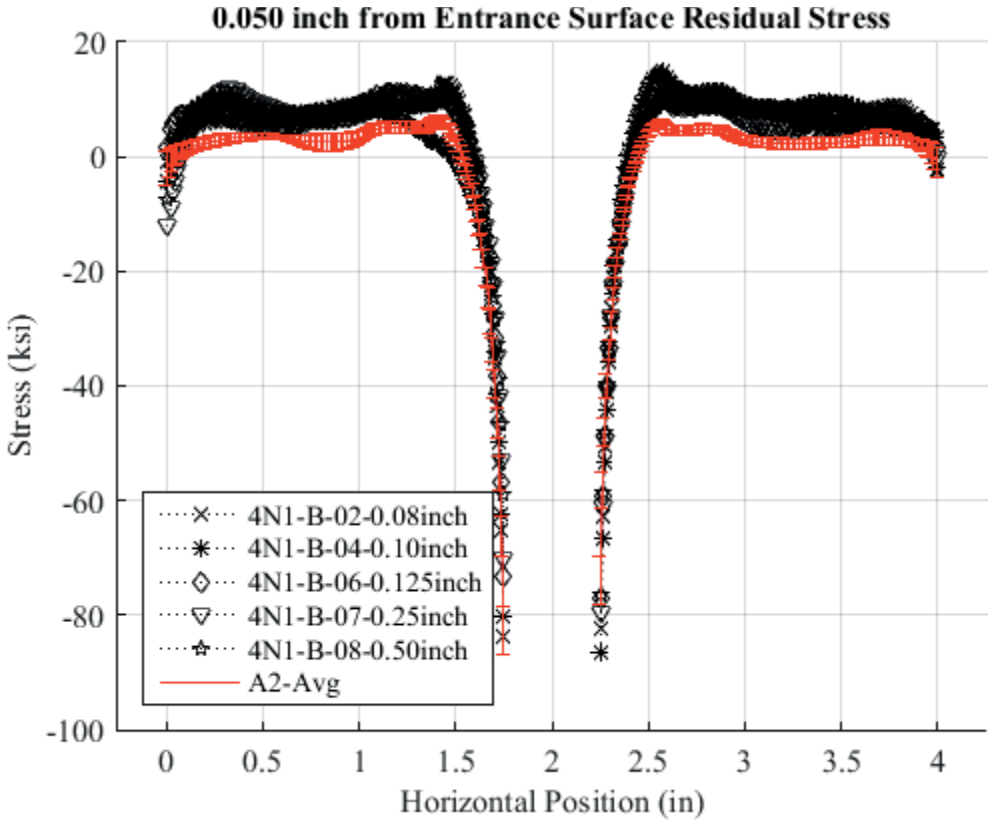

Fig. 765 Residual Stress Line Plot Comparing Cx4N1-02-B, Cx4N1-04-B, Cx4N1-06-B, CX4N1-07-B, Cx4N1-08-B, and the Average CxA2 (2024-T351) Average Residual Stress at a Distance of 0.05 inch from the Entrance Surface. Error Bars are Provided on the CxA2 Average Residual Stress which Represent the Repeatability Uncertainty for the CxA2 Condition.

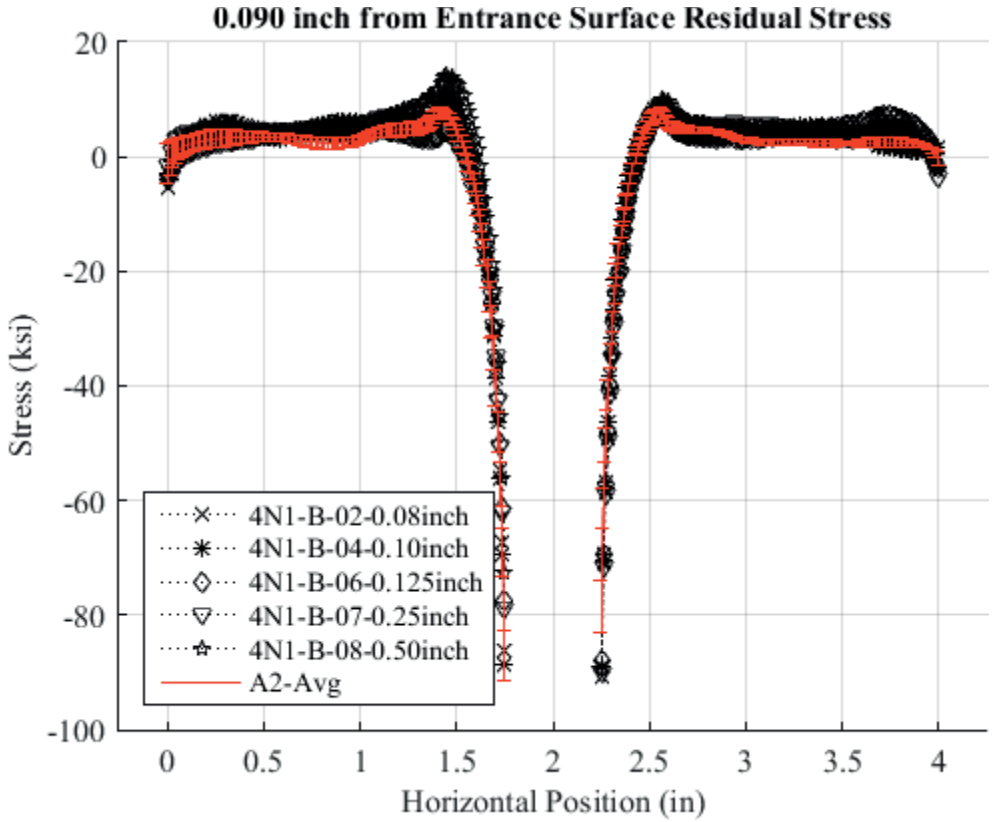

Fig. 766 Residual Stress Line Plot Comparing Cx4N1-02-B, Cx4N1-04-B, Cx4N1-06-B, CX4N1-07-B, Cx4N1-08-B, and the Average CxA2 (2024-T351) Average Residual Stress at a Distance of 0.09 inch from the Entrance Surface. Error Bars are Provided on the CxA2 Average Residual Stress which Represent the Repeatability Uncertainty for the CxA2 Condition.

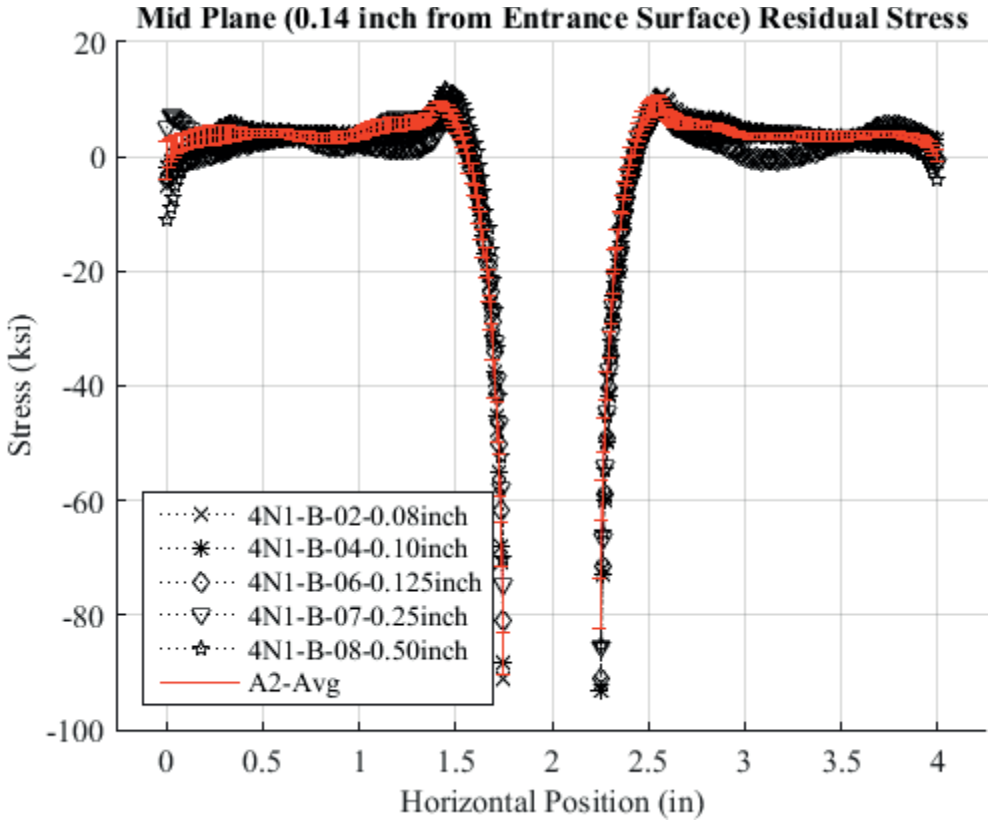

Fig. 767 Residual Stress Line Plot Comparing Cx4N1-02-B, Cx4N1-04-B, Cx4N1-06-B, CX4N1-07-B, Cx4N1-08-B, and the Average CxA2 (2024-T351) Average Residual Stress at a Distance of 0.140 inch (Mid Plane Surface) from the Entrance Surface. Error Bars are Provided on the CxA2 Average Residual Stress which Represent the Repeatability Uncertainty for the CxA2 Condition.

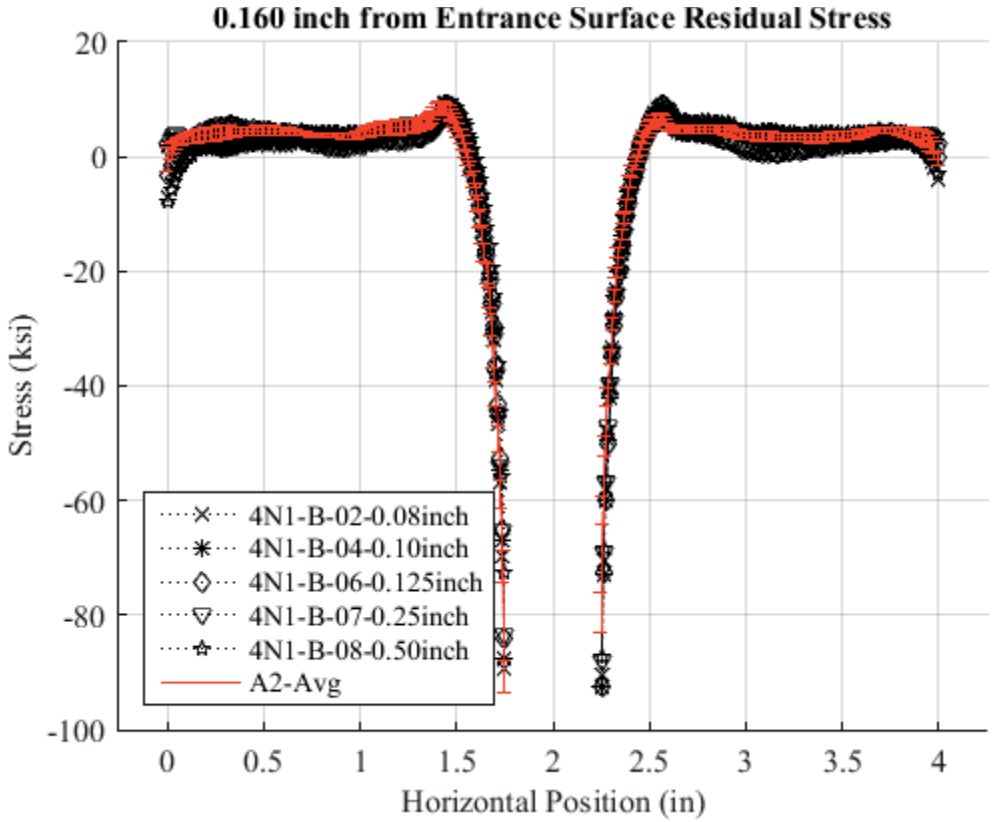

Fig. 768 Residual Stress Line Plot Comparing Cx4N1-02-B, Cx4N1-04-B, Cx4N1-06-B, CX4N1-07-B, Cx4N1-08-B, and the Average CxA2 (2024-T351) Average Residual Stress at a Distance of 0.160 inch from the Entrance Surface. Error Bars are Provided on the CxA2 Average Residual Stress which Represent the Repeatability Uncertainty for the CxA2 Condition.

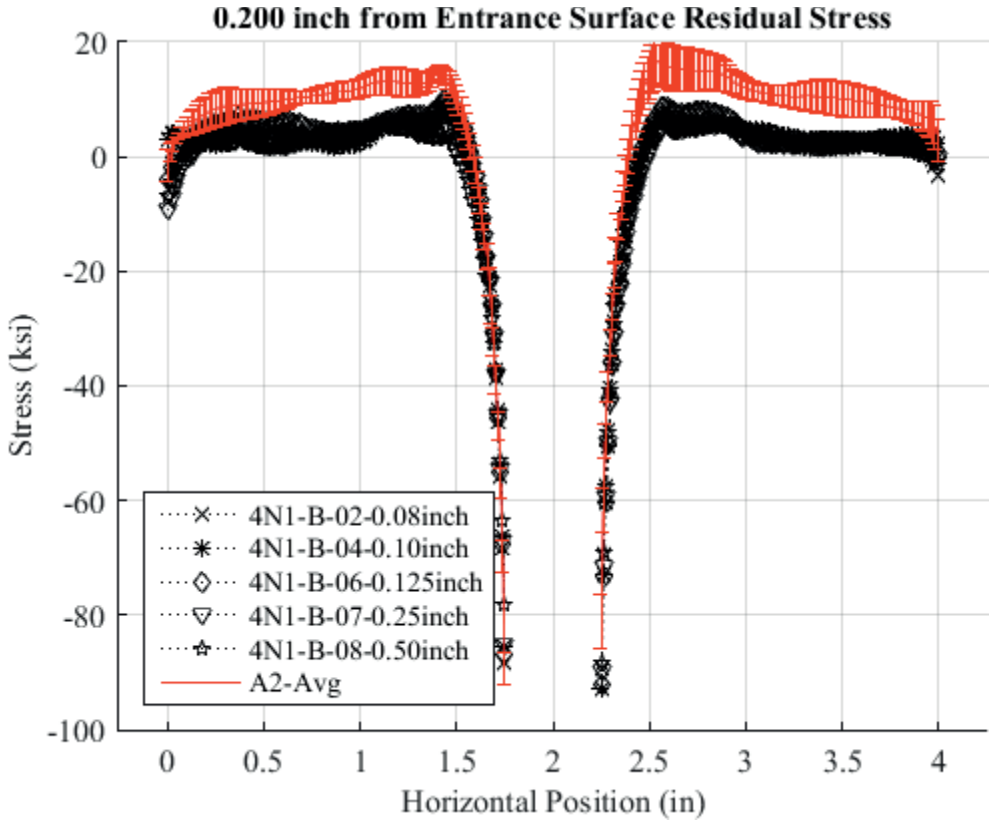

Fig. 769 Residual Stress Line Plot Comparing Cx4N1-02-B, Cx4N1-04-B, Cx4N1-06-B, CX4N1-07-B, Cx4N1-08-B, and the Average CxA2 (2024-T351) Average Residual Stress at a Distance of 0.200 inch from the Entrance Surface. Error Bars are Provided on the CxA2 Average Residual Stress which Represent the Repeatability Uncertainty for the CxA2 Condition.

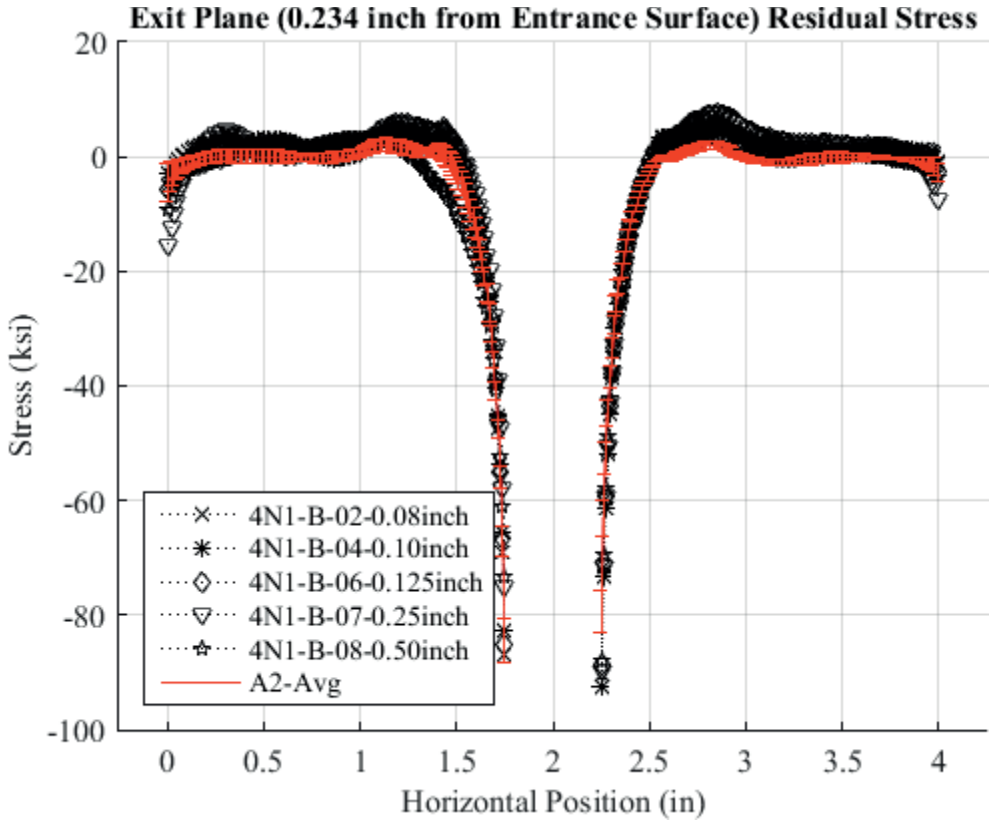

Fig. 770 Residual Stress Line Plot Comparing Cx4N1-02-B, Cx4N1-04-B, Cx4N1-06-B, CX4N1-07-B, Cx4N1-08-B, and the Average CxA2 (2024-T351) Average Residual Stress at a Distance of 0.234 inch (Exit Surface) from the Entrance Surface. Error Bars are Provided on the CxA2 Average Residual Stress which Represent the Repeatability Uncertainty for the CxA2 Condition.

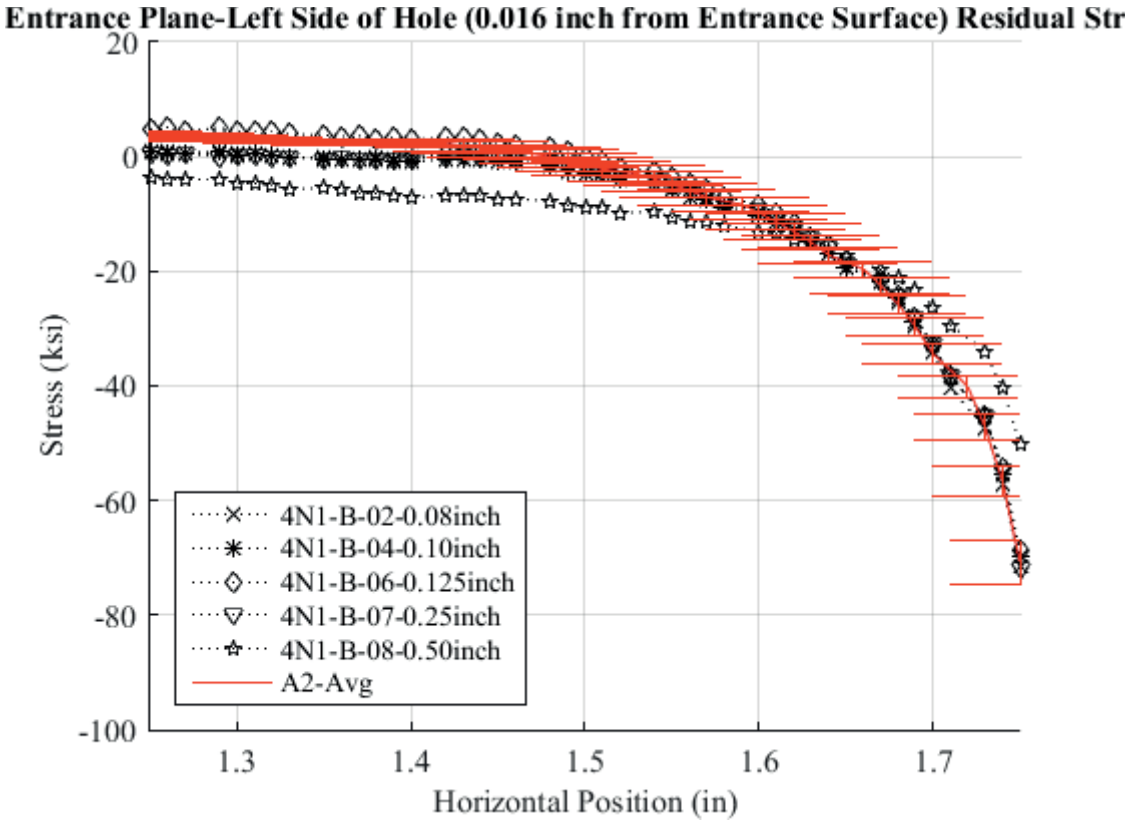

Fig. 771 Residual Stress Line Plot for First 0.50 inch away from Hole on Left Side of Hole Comparing Cx4N1-02-B, Cx4N1-04-B, Cx4N1-06-B, CX4N1-07-B, Cx4N1-08-B, and the Average CxA2 (2024-T351) Average Residual Stress at a Distance of 0.016 inch (Entrance Surface) from the Entrance Surface. Error Bars are Provided on the CxA2 Average Residual Stress which Represent the Repeatability Uncertainty for the CxA2 Condition.

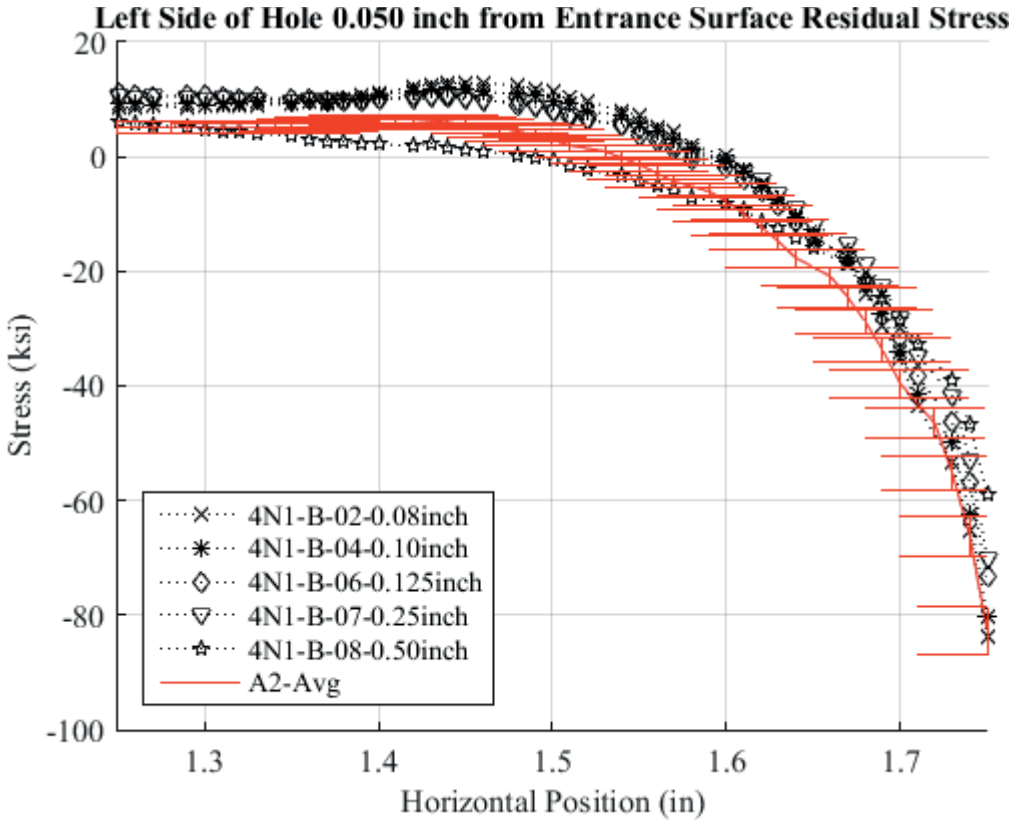

Fig. 772 Residual Stress Line Plot for First 0.50 inch away from Hole on Left Side of Hole Comparing Cx4N1-02-B, Cx4N1-04-B, Cx4N1-06-B, CX4N1-07-B, Cx4N1-08-B, and the Average CxA2 (2024-T351) Average Residual Stress at a Distance of 0.05 inch from the Entrance Surface. Error Bars are Provided on the CxA2 Average Residual Stress which Represent the Repeatability Uncertainty for the CxA2 Condition.

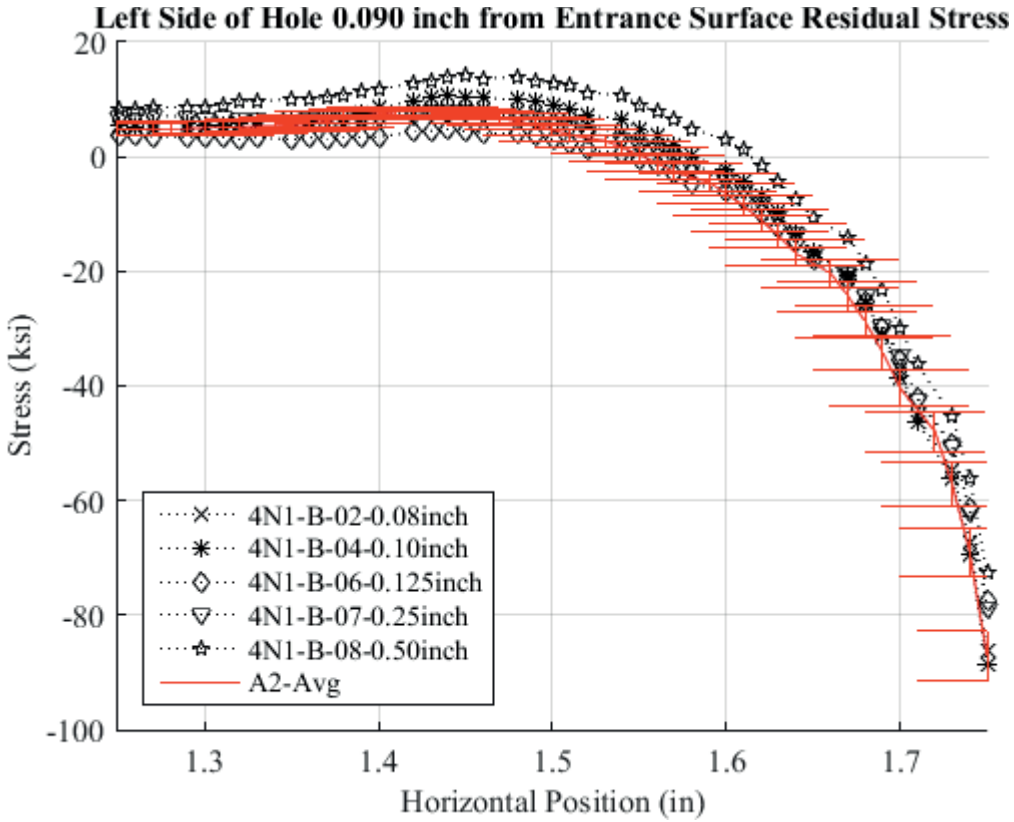

Fig. 773 Residual Stress Line Plot for First 0.50 inch away from Hole on Left Side of Hole Comparing Cx4N1-02-B, Cx4N1-04-B, Cx4N1-06-B, CX4N1-07-B, Cx4N1-08-B, and the Average CxA2 (2024-T351) Average Residual Stress at a Distance of 0.09 inch from the Entrance Surface. Error Bars are Provided on the CxA2 Average Residual Stress which Represent the Repeatability Uncertainty for the CxA2 Condition.

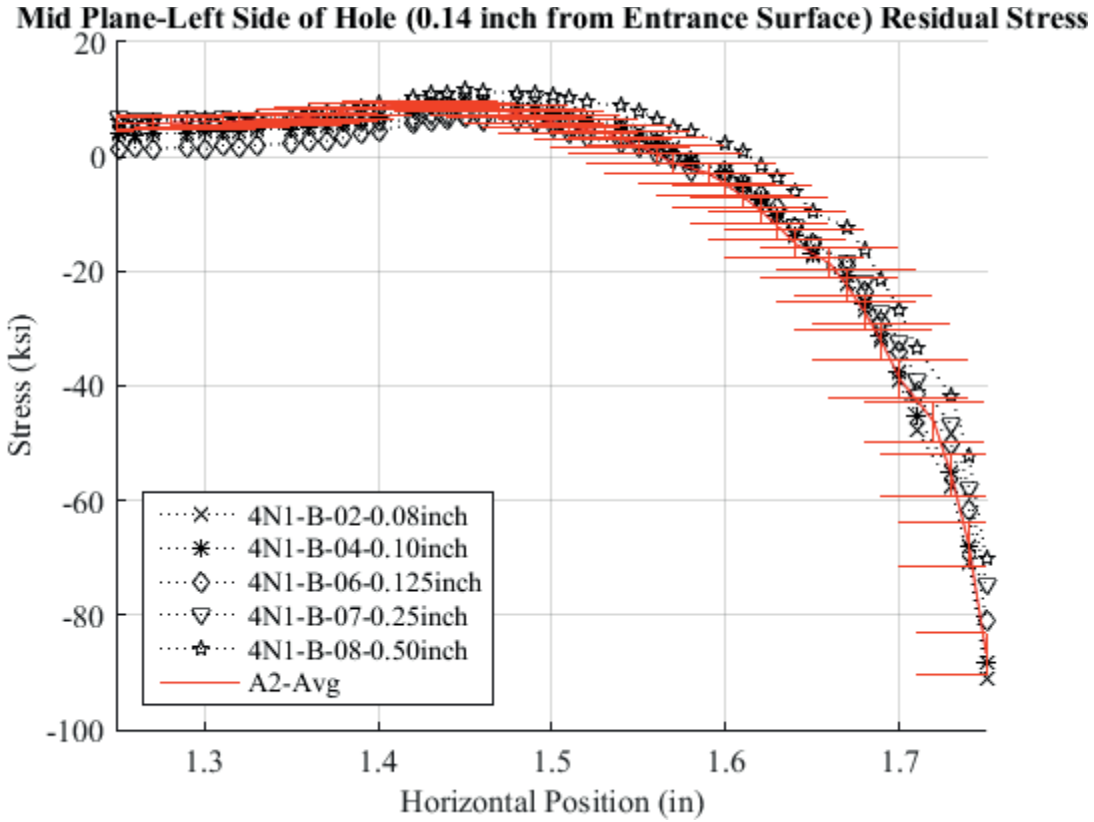

Fig. 774 Residual Stress Line Plot for First 0.50 inch away from Hole on Left Side of Hole Comparing Cx4N1-02-B, Cx4N1-04-B, Cx4N1-06-B, CX4N1-07-B, Cx4N1-08-B, and the Average CxA2 (2024-T351) Average Residual Stress at a Distance of 0.140 inch (Mid Plane Surface) from the Entrance Surface. Error Bars are Provided on the CxA2 Average Residual Stress which Represent the Repeatability Uncertainty for the CxA2 Condition.

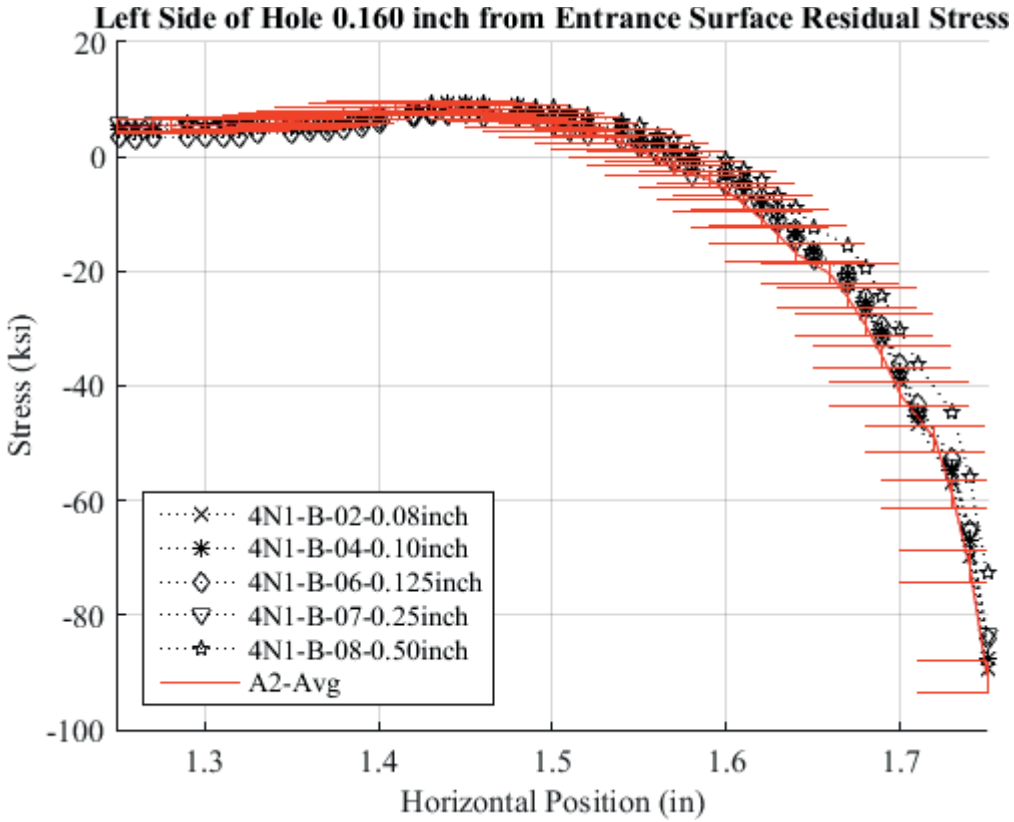

Fig. 775 Residual Stress Line Plot for First 0.50 inch away from Hole on Left Side of Hole Comparing Cx4N1-02-B, Cx4N1-04-B, Cx4N1-06-B, CX4N1-07-B, Cx4N1-08-B, and the Average CxA2 (2024-T351) Average Residual Stress at a Distance of 0.160 inch from the Entrance Surface. Error Bars are Provided on the CxA2 Average Residual Stress which Represent the Repeatability Uncertainty for the CxA2 Condition.

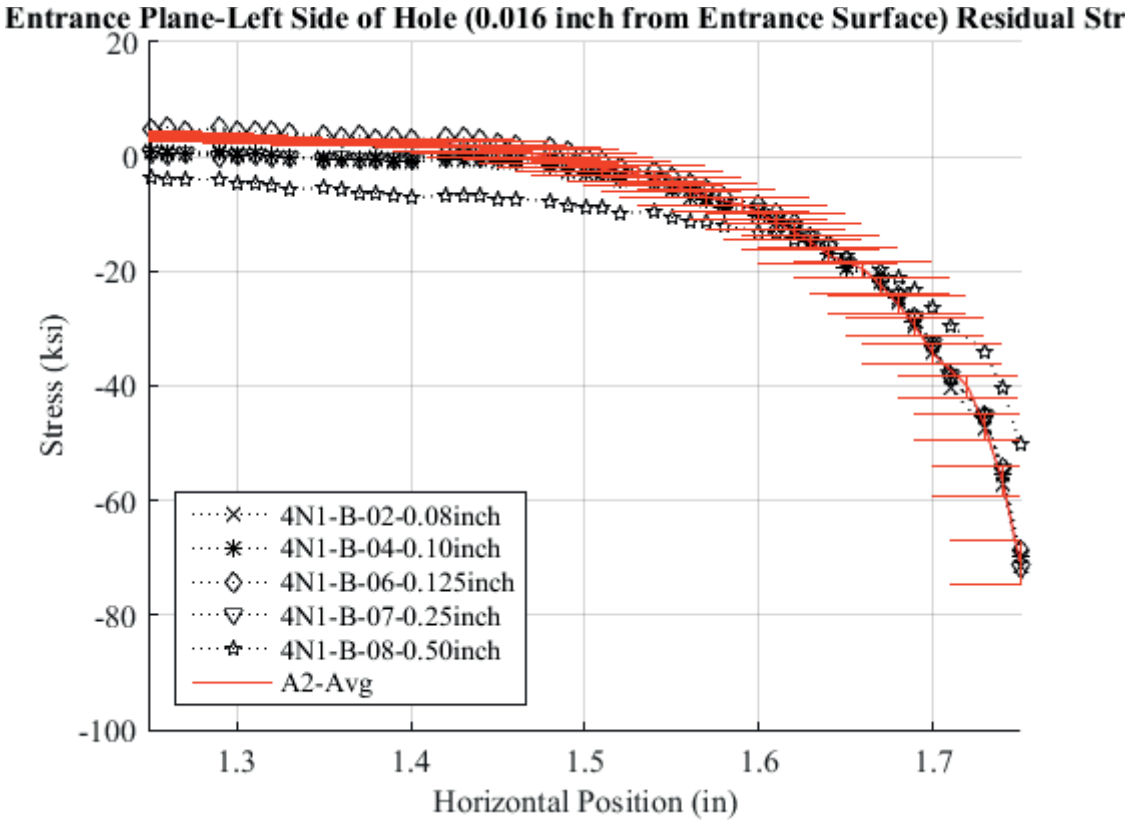

Fig. 776 Residual Stress Line Plot for First 0.50 inch away from Hole on Left Side of Hole Comparing Cx4N1-02-B, Cx4N1-04-B, Cx4N1-06-B, CX4N1-07-B, Cx4N1-08-B, and the Average CxA2 (2024-T351) Average Residual Stress at a Distance of 0.200 inch from the Entrance Surface. Error Bars are Provided on the CxA2 Average Residual Stress which Represent the Repeatability Uncertainty for the CxA2 Condition.

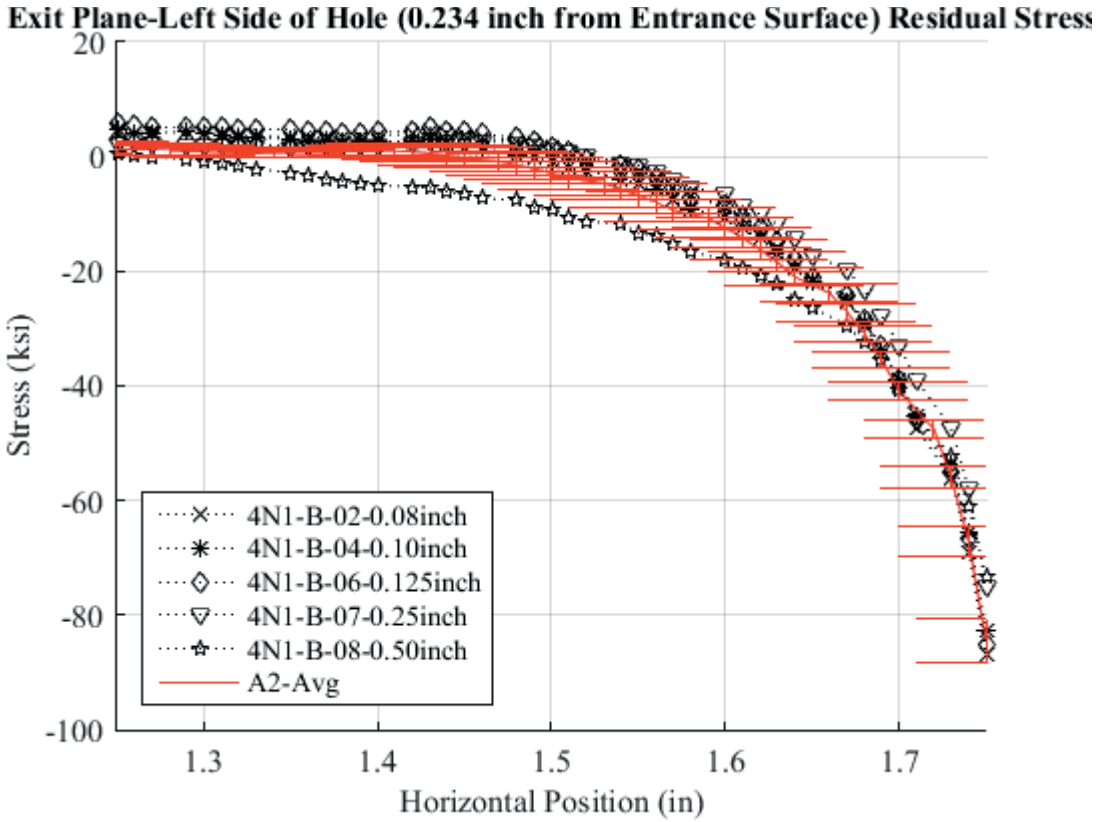

Fig. 777 Residual Stress Line Plot for First 0.50 inch away from Hole on Left Side of Hole Comparing Cx4N1-02-B, Cx4N1-04-B, Cx4N1-06-B, CX4N1-07-B, Cx4N1-08-B, and the Average CxA2 (2024-T351) Average Residual Stress at a Distance of 0.234 inch (Exit Surface) from the Entrance Surface. Error Bars are Provided on the CxA2 Average Residual Stress which Represent the Repeatability Uncertainty for the CxA2 Condition.

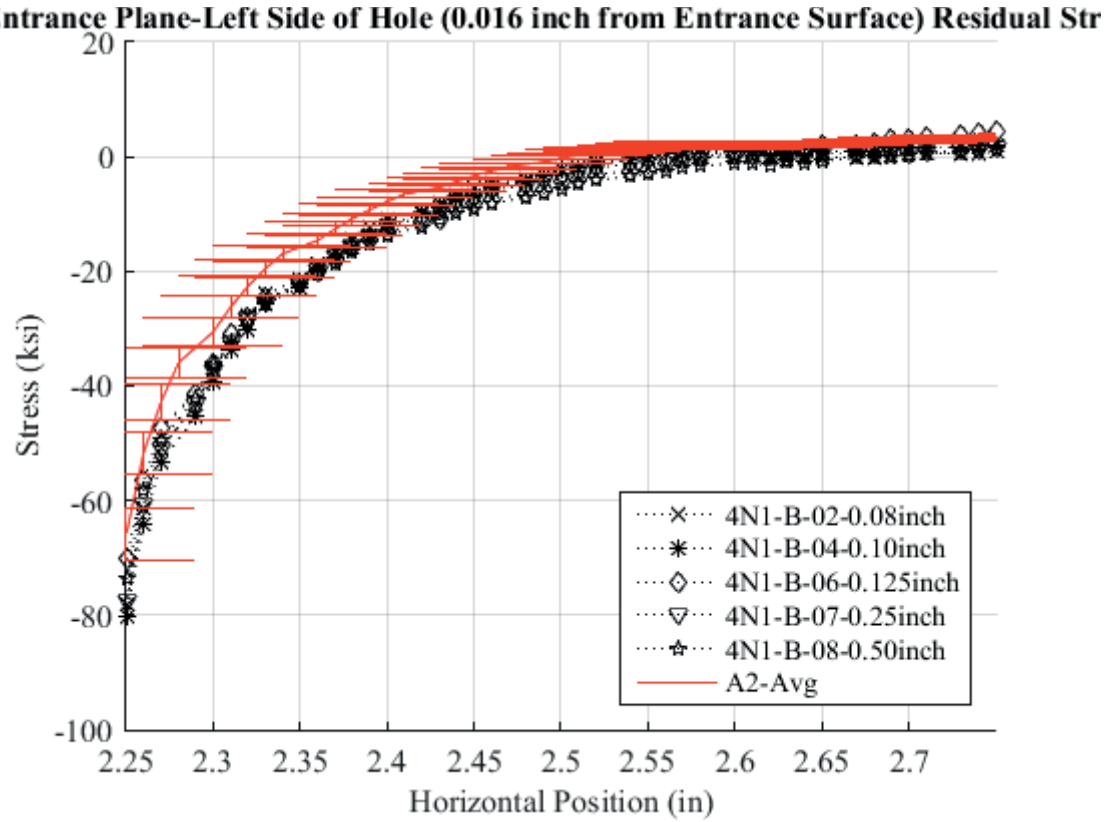

Fig. 778 Residual Stress Line Plot for First 0.50 inch away from Hole on Right Side of Hole Comparing Cx4N1-02-B, Cx4N1-04-B, Cx4N1-06-B, CX4N1-07-B, Cx4N1-08-B, and the Average CxA2 (2024-T351) Average Residual Stress at a Distance of 0.016 inch (Entrance Surface) from the Entrance Surface. Error Bars are Provided on the CxA2 Average Residual Stress which Represent the Repeatability Uncertainty for the CxA2 Condition.

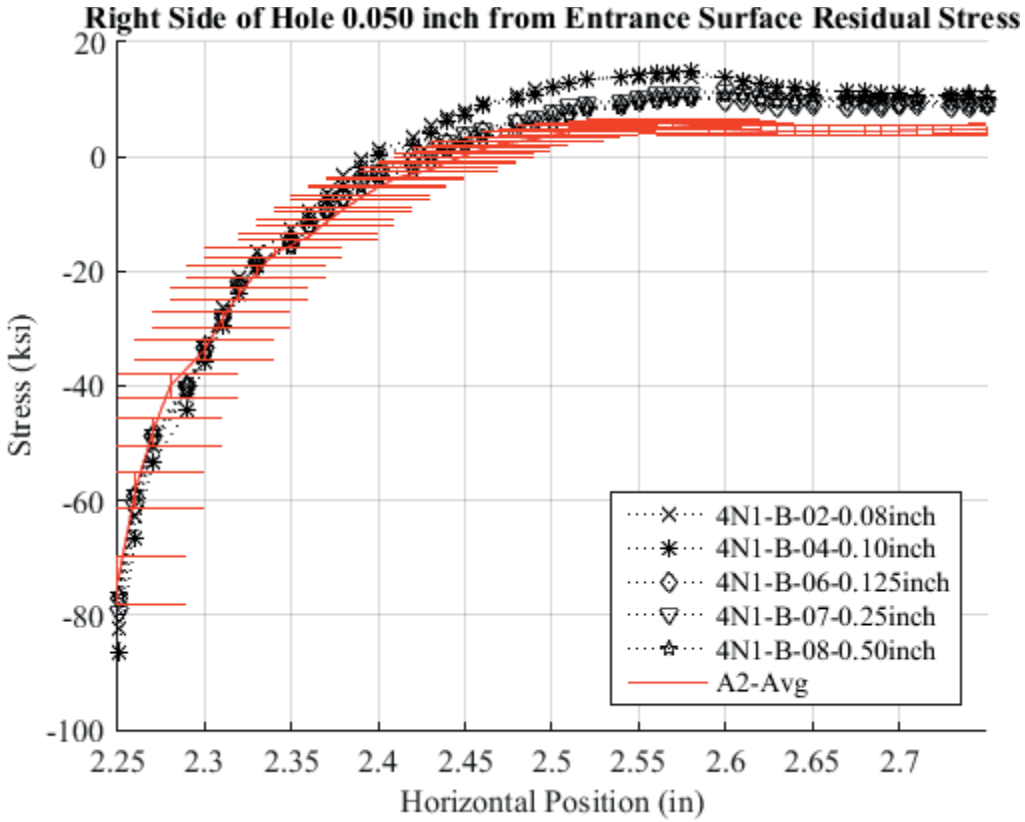

Fig. 779 Residual Stress Line Plot for First 0.50 inch away from Hole on Right Side of Hole Comparing Cx4N1-02-B, Cx4N1-04-B, Cx4N1-06-B, CX4N1-07-B, Cx4N1-08-B, and the Average CxA2 (2024-T351) Average Residual Stress at a Distance of 0.05 inch from the Entrance Surface. Error Bars are Provided on the CxA2 Average Residual Stress which Represent the Repeatability Uncertainty for the CxA2 Condition.

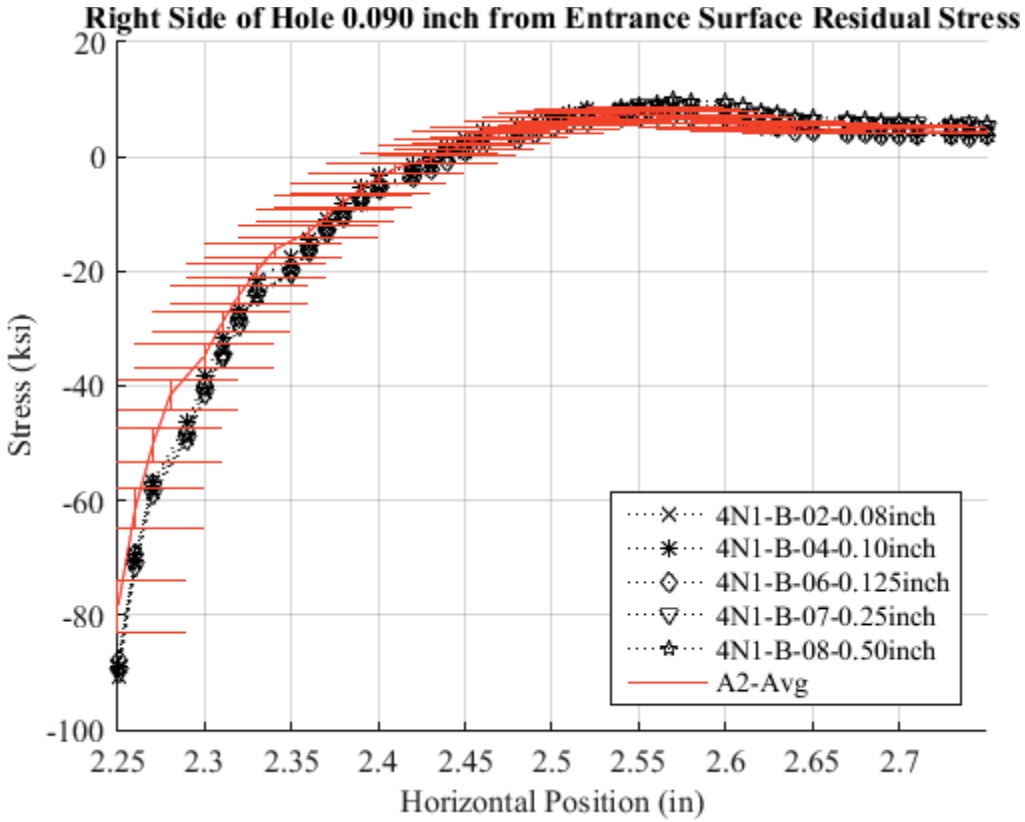

Fig. 780 Residual Stress Line Plot for First 0.50 inch away from Hole on Right Side of Hole Comparing Cx4N1-02-B, Cx4N1-04-B, Cx4N1-06-B, CX4N1-07-B, Cx4N1-08-B, and the Average CxA2 (2024-T351) Average Residual Stress at a Distance of 0.09 inch from the Entrance Surface. Error Bars are Provided on the CxA2 Average Residual Stress which Represent the Repeatability Uncertainty for the CxA2 Condition.

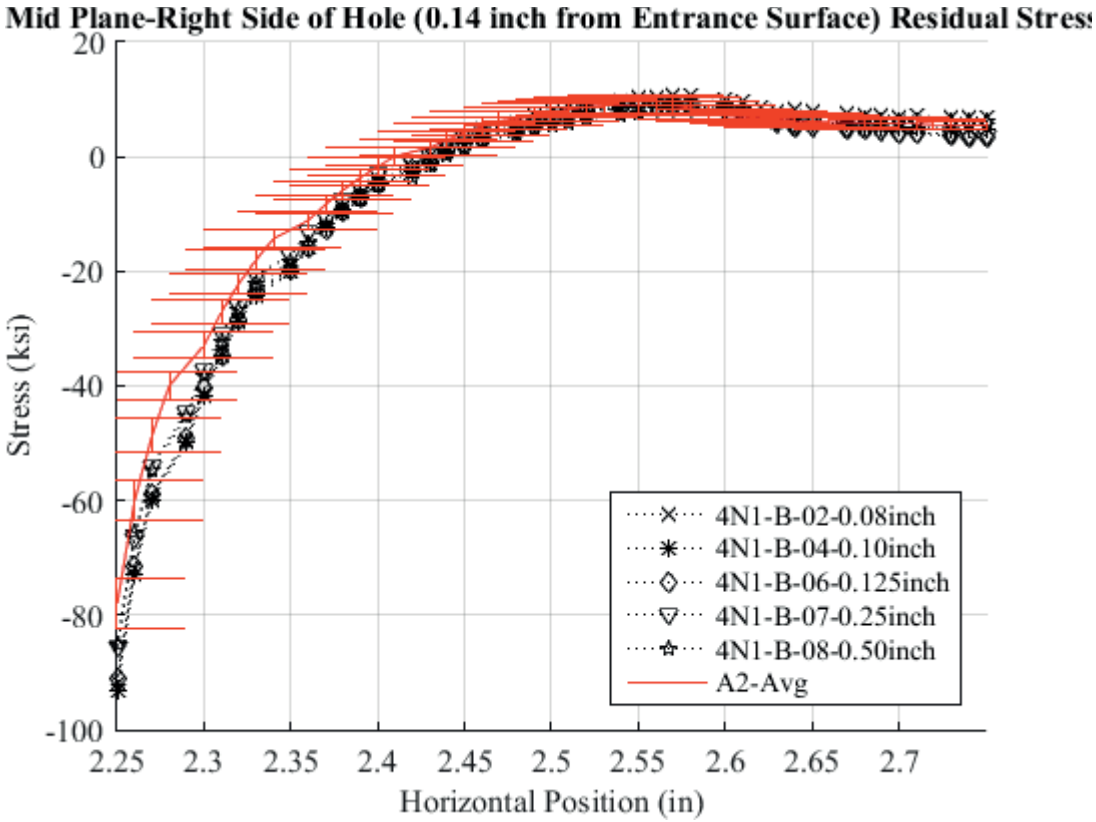

Fig. 781 Residual Stress Line Plot for First 0.50 inch away from Hole on Right Side of Hole Comparing Cx4N1-02-B, Cx4N1-04-B, Cx4N1-06-B, CX4N1-07-B, Cx4N1-08-B, and the Average CxA2 (2024-T351) Average Residual Stress at a Distance of 0.140 inch (Mid Plane Surface) from the Entrance Surface. Error Bars are Provided on the CxA2 Average Residual Stress which Represent the Repeatability Uncertainty for the CxA2 Condition.

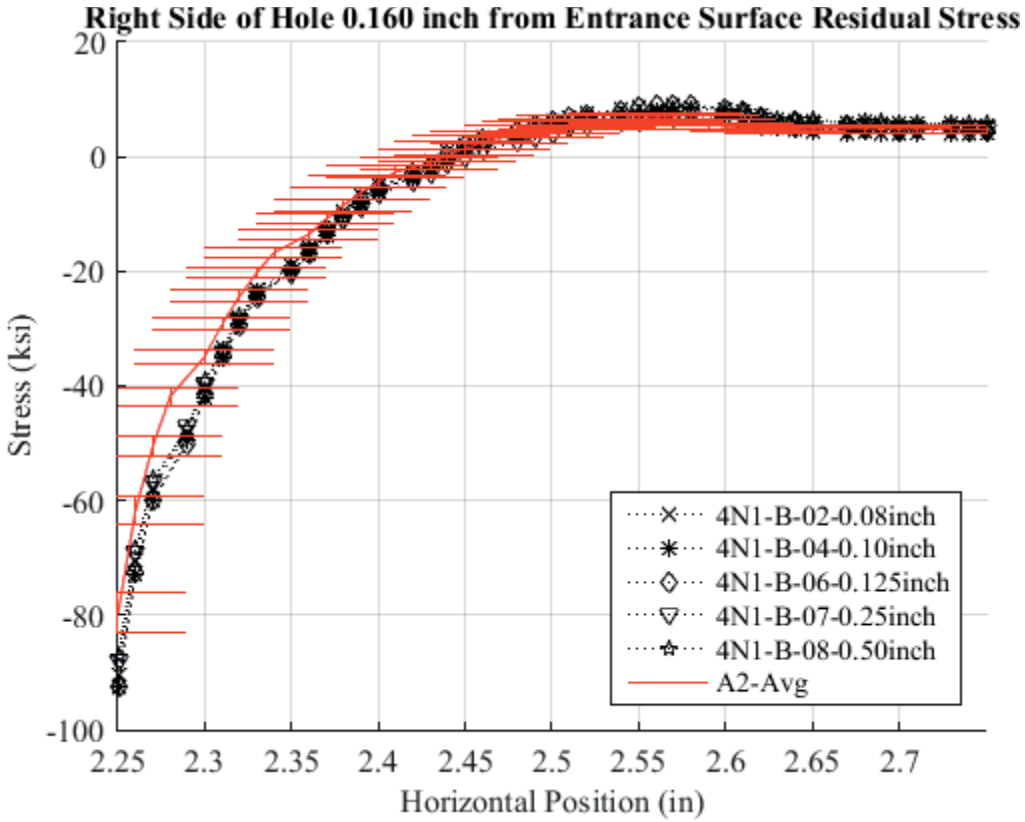

Fig. 782 Residual Stress Line Plot for First 0.50 inch away from Hole on Right Side of Hole Comparing Cx4N1-02-B, Cx4N1-04-B, Cx4N1-06-B, CX4N1-07-B, Cx4N1-08-B, and the Average CxA2 (2024-T351) Average Residual Stress at a Distance of 0.160 inch from the Entrance Surface. Error Bars are Provided on the CxA2 Average Residual Stress which Represent the Repeatability Uncertainty for the CxA2 Condition.

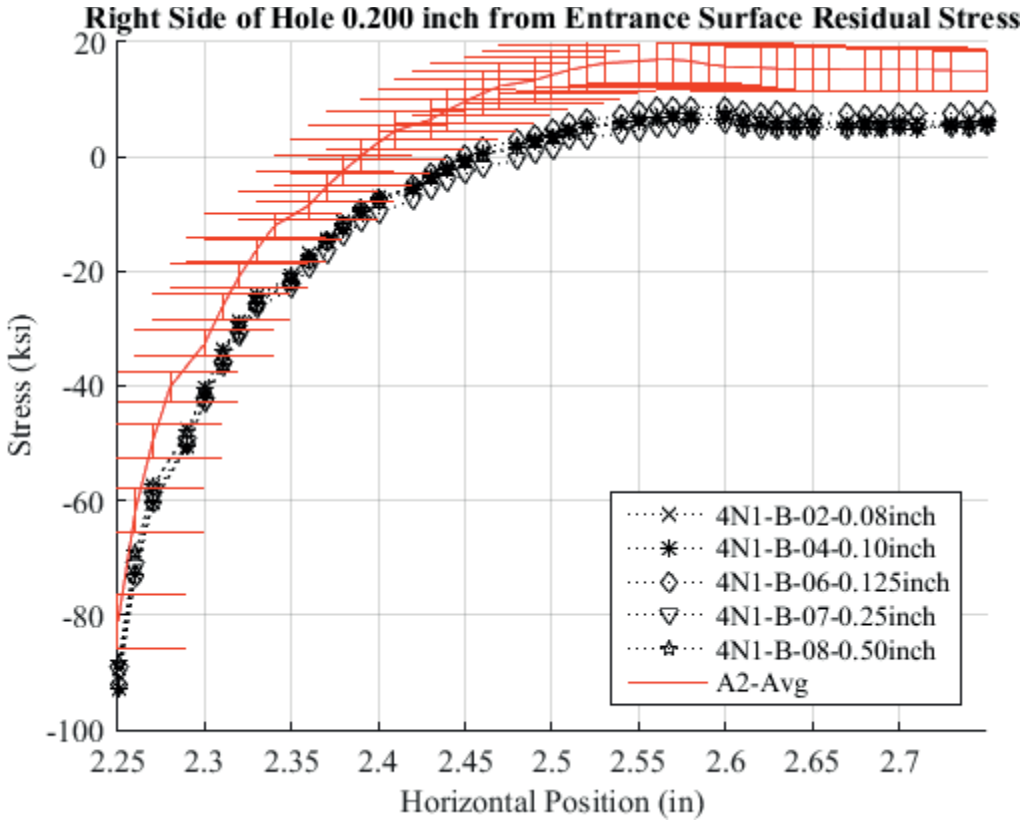

Fig. 783 Residual Stress Line Plot for First 0.50 inch away from Hole on Right Side of Hole Comparing Cx4N1-02-B, Cx4N1-04-B, Cx4N1-06-B, CX4N1-07-B, Cx4N1-08-B, and the Average CxA2 (2024-T351) Average Residual Stress at a Distance of 0.200 inch from the Entrance Surface. Error Bars are Provided on the CxA2 Average Residual Stress which Represent the Repeatability Uncertainty for the CxA2 Condition.

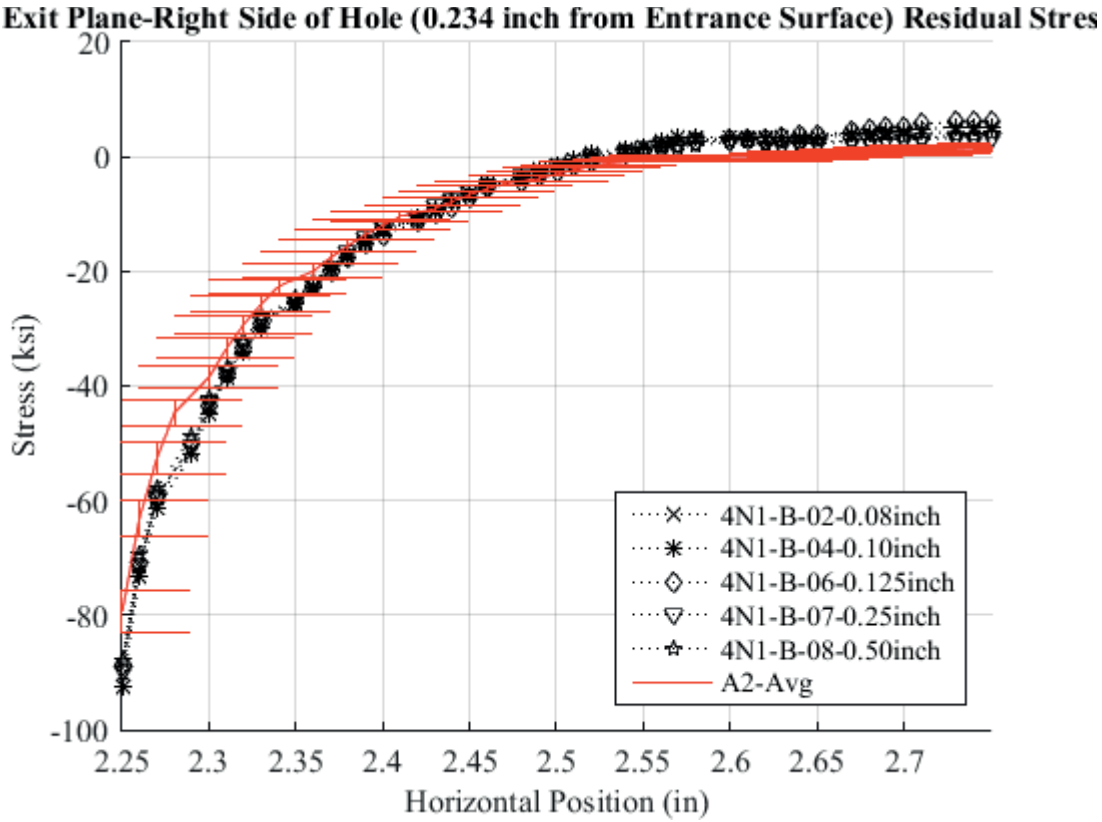

Fig. 784 Residual Stress Line Plot for First 0.50 inch away from Hole on Right Side of Hole Comparing Cx4N1-02-B, Cx4N1-04-B, Cx4N1-06-B, CX4N1-07-B, Cx4N1-08-B, and the Average CxA2 (2024-T351) Average Residual Stress at a Distance of 0.234 inch (Exit Surface) from the Entrance Surface. Error Bars are Provided on the CxA2 Average Residual Stress which Represent the Repeatability Uncertainty for the CxA2 Condition.

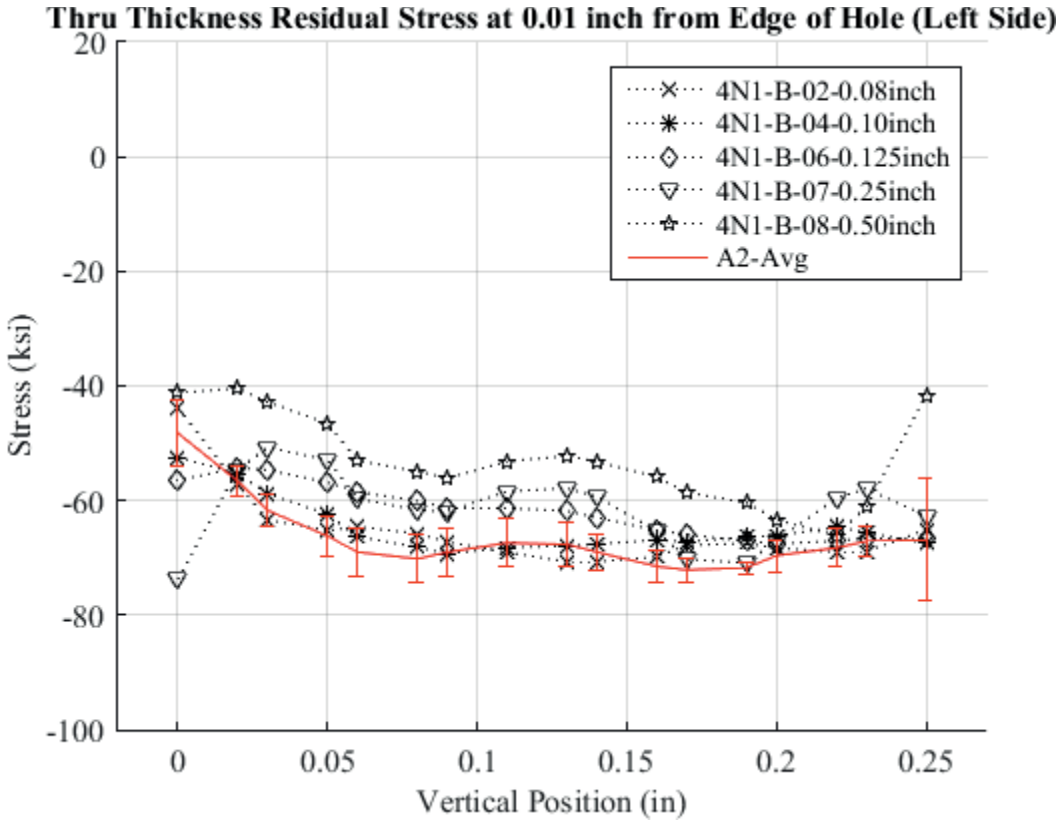

Fig. 785 Residual Stress Through-Thickness Line Plot Comparing Cx4N1-02-B, Cx4N1-04-B, Cx4N1-06-B, CX4N1-07-B, Cx4N1-08-B, and the Average CxA2 (2024-T351) Average Residual Stress at a Distance of 0.01 inch from the Left Side of the Hole. Error Bars are Provided on the CxA2 Average Residual Stress which Represent the Repeatability Uncertainty for the CxA2 Condition.

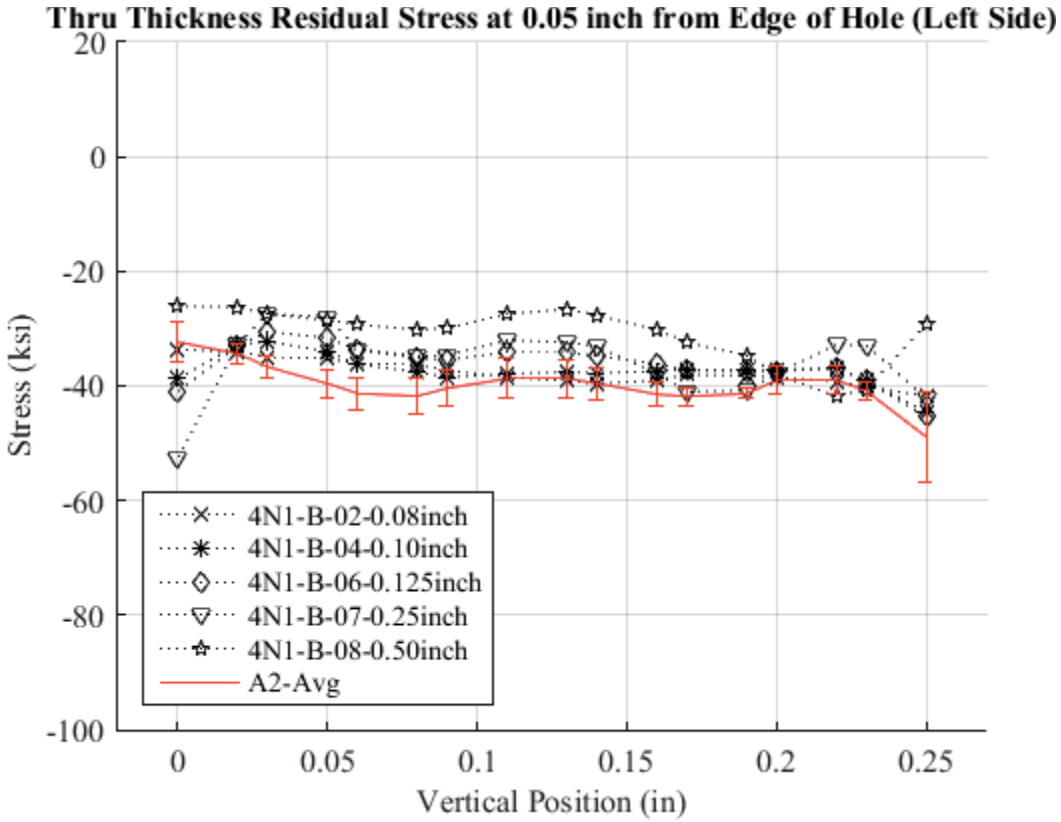

Fig. 786 Residual Stress Through-Thickness Line Plot Comparing Cx4N1-02-B, Cx4N1-04-B, Cx4N1-06-B, CX4N1-07-B, Cx4N1-08-B, and the Average CxA2 (2024-T351) Average Residual Stress at a Distance of 0.05 inch from the Left Side of the Hole. Error Bars are Provided on the CxA2 Average Residual Stress which Represent the Repeatability Uncertainty for the CxA2 Condition.

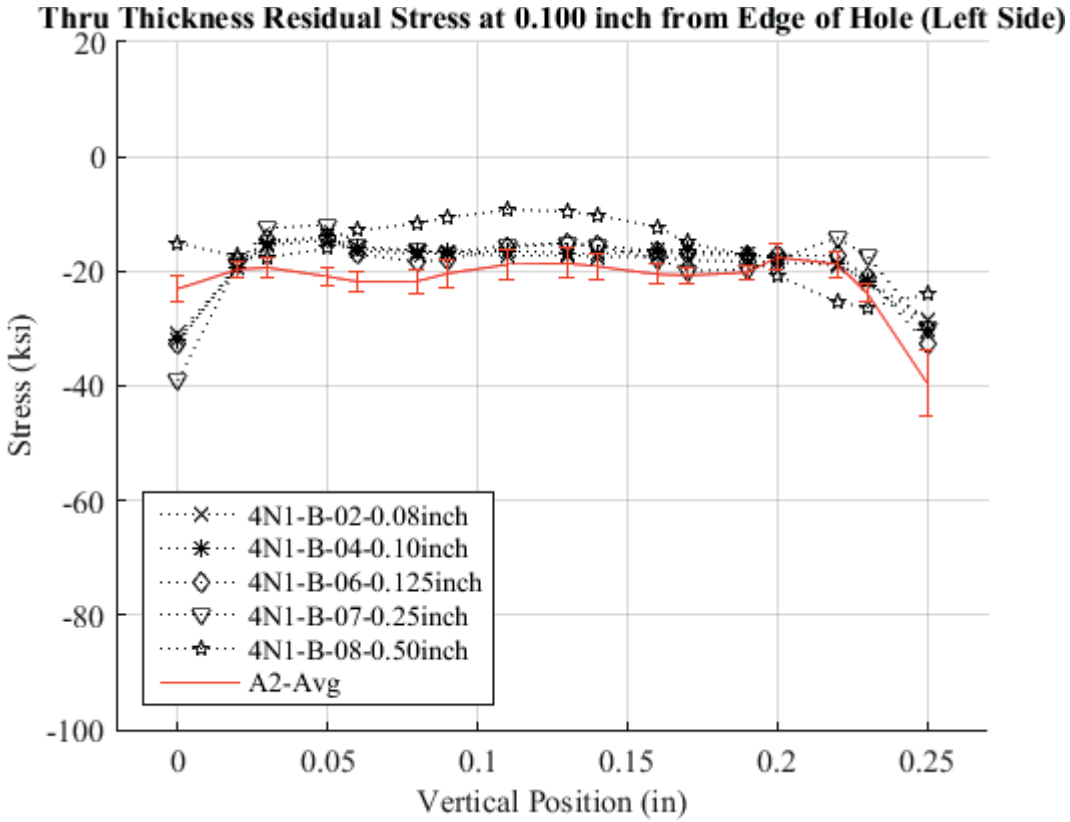

Fig. 787 Residual Stress Through-Thickness Line Plot Comparing Cx4N1-02-B, Cx4N1-04-B, Cx4N1-06-B, CX4N1-07-B, Cx4N1-08-B, and the Average CxA2 (2024-T351) Average Residual Stress at a Distance of 0.10 inch from the Left Side of the Hole. Error Bars are Provided on the CxA2 Average Residual Stress which Represent the Repeatability Uncertainty for the CxA2 Condition.

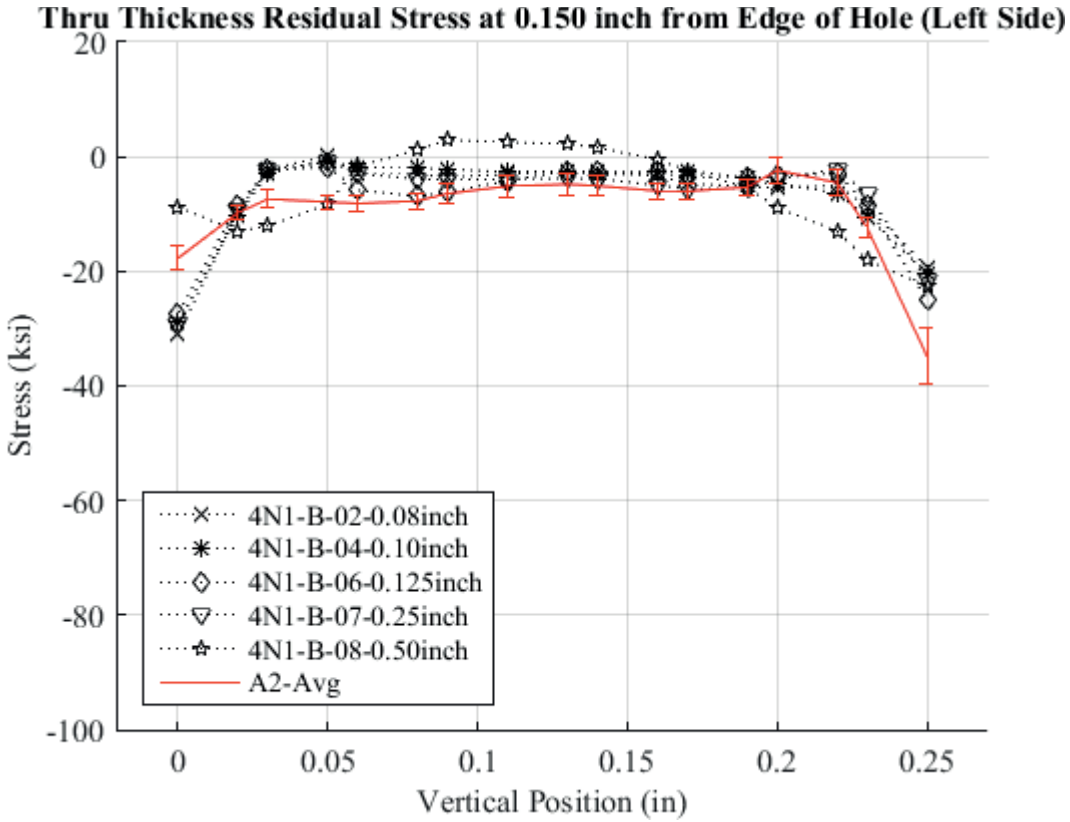

Fig. 788 Residual Stress Through-Thickness Line Plot Comparing Cx4N1-02-B, Cx4N1-04-B, Cx4N1-06-B, CX4N1-07-B, Cx4N1-08-B, and the Average CxA2 (2024-T351) Average Residual Stress at a Distance of 0.150 inch from the Left Side of the Hole. Error Bars are Provided on the CxA2 Average Residual Stress which Represent the Repeatability Uncertainty for the CxA2 Condition.

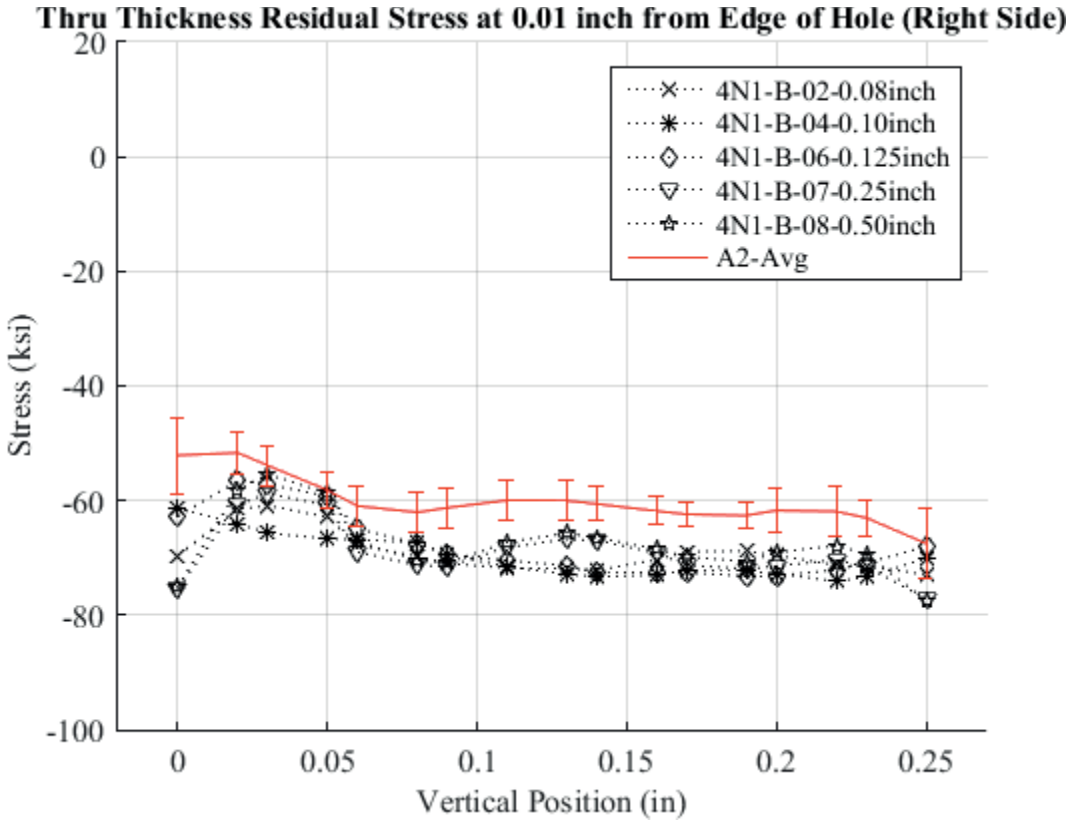

Fig. 789 Residual Stress Through-Thickness Line Plot Comparing Cx4N1-02-B, Cx4N1-04-B, Cx4N1-06-B, CX4N1-07-B, Cx4N1-08-B, and the Average CxA2 (2024-T351) Average Residual Stress at a Distance of 0.01 inch from the Right Side of the Hole. Error Bars are Provided on the CxA2 Average Residual Stress which Represent the Repeatability Uncertainty for the CxA2 Condition.

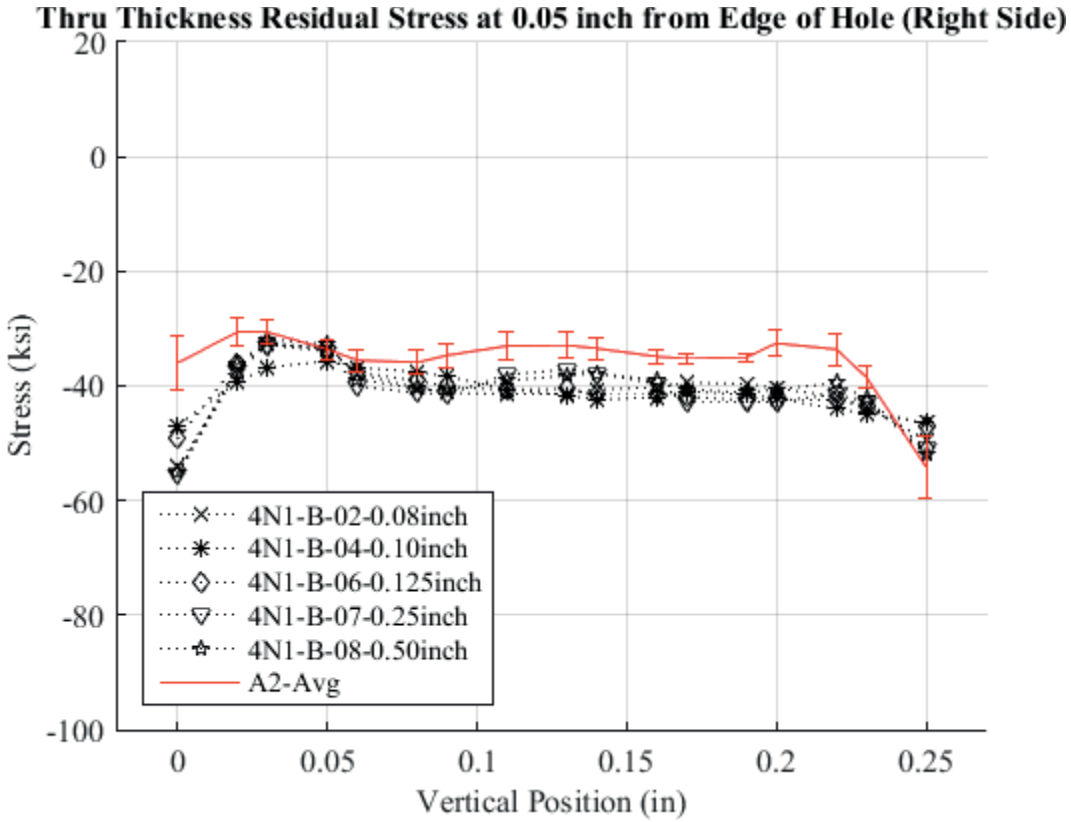

Fig. 790 Residual Stress Through-Thickness Line Plot Comparing Cx4N1-02-B, Cx4N1-04-B, Cx4N1-06-B, CX4N1-07-B, Cx4N1-08-B, and the Average CxA2 (2024-T351) Average Residual Stress at a Distance of 0.05 inch from the Right Side of the Hole. Error Bars are Provided on the CxA2 Average Residual Stress which Represent the Repeatability Uncertainty for the CxA2 Condition.

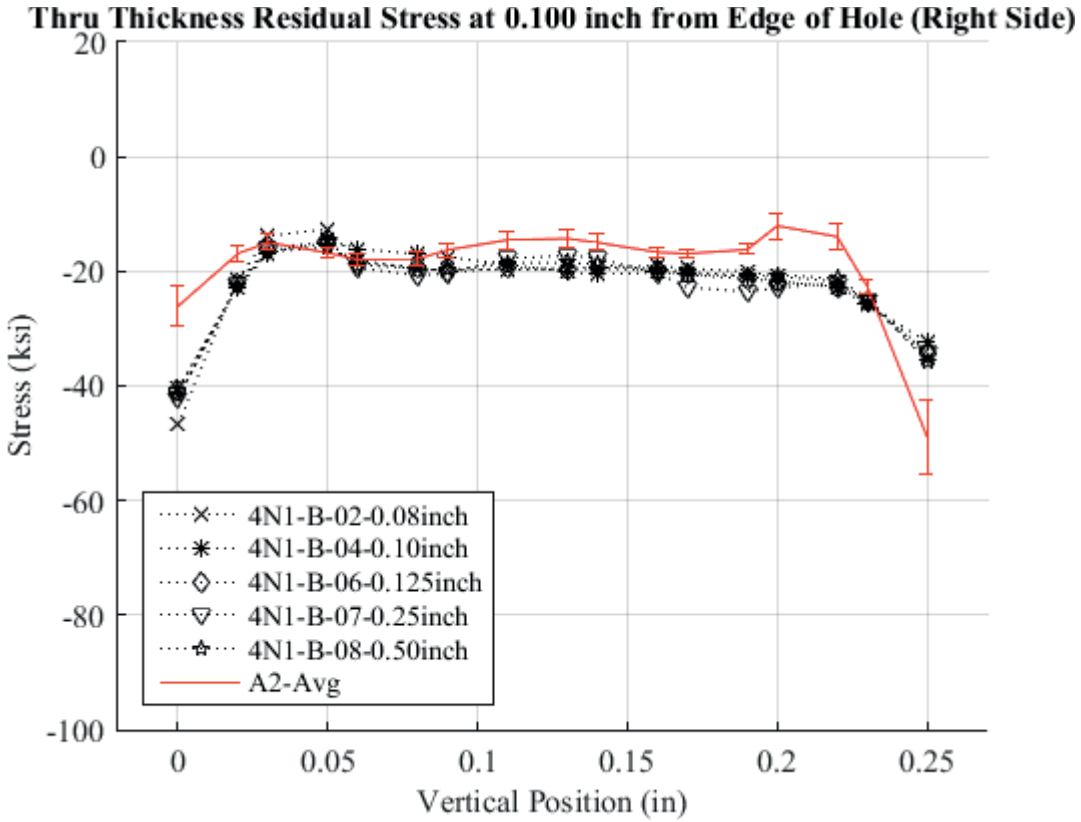

Fig. 791 Residual Stress Through-Thickness Line Plot Comparing Cx4N1-02-B, Cx4N1-04-B, Cx4N1-06-B, CX4N1-07-B, Cx4N1-08-B, and the Average CxA2 (2024-T351) Average Residual Stress at a Distance of 0.10 inch from the Right Side of the Hole. Error Bars are Provided on the CxA2 Average Residual Stress which Represent the Repeatability Uncertainty for the CxA2 Condition.

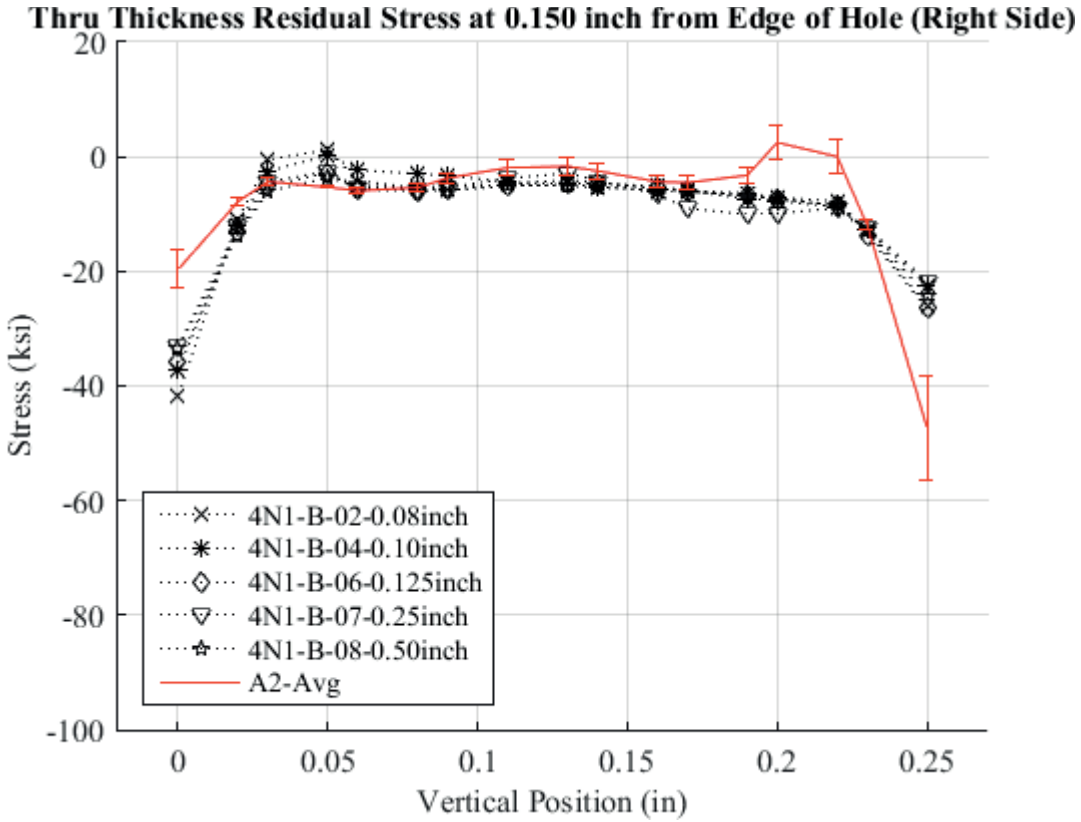

Fig. 792 Residual Stress Through-Thickness Line Plot Comparing Cx4N1-02-B, Cx4N1-04-B, Cx4N1-06-B, CX4N1-07-B, Cx4N1-08-B, and the Average CxA2 (2024-T351) Average Residual Stress at a Distance of 0.150 inch from the Right Side of the Hole. Error Bars are Provided on the CxA2 Average Residual Stress which Represent the Repeatability Uncertainty for the CxA2 Condition.

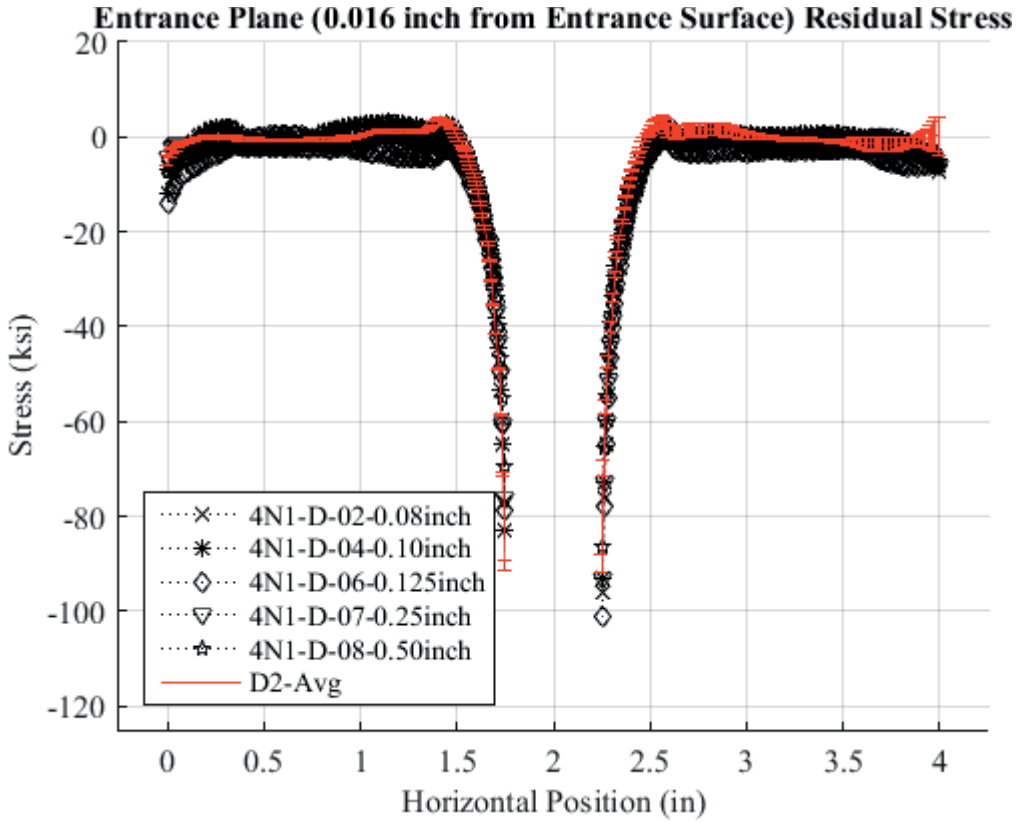

Fig. 793 Residual Stress Line Plot Comparing Cx4N1-02-D, Cx4N1-04-D, Cx4N1-06-D, CX4N1-07-D, Cx4N1-08-D, and the Average CxD2 (7075-T651) Average Residual Stress at a Distance of 0.016 inch (Entrance Surface) from the Entrance Surface. Error Bars are Provided on the CxD2 Average Residual Stress which Represent the Repeatability Uncertainty for the CxD2 Condition.

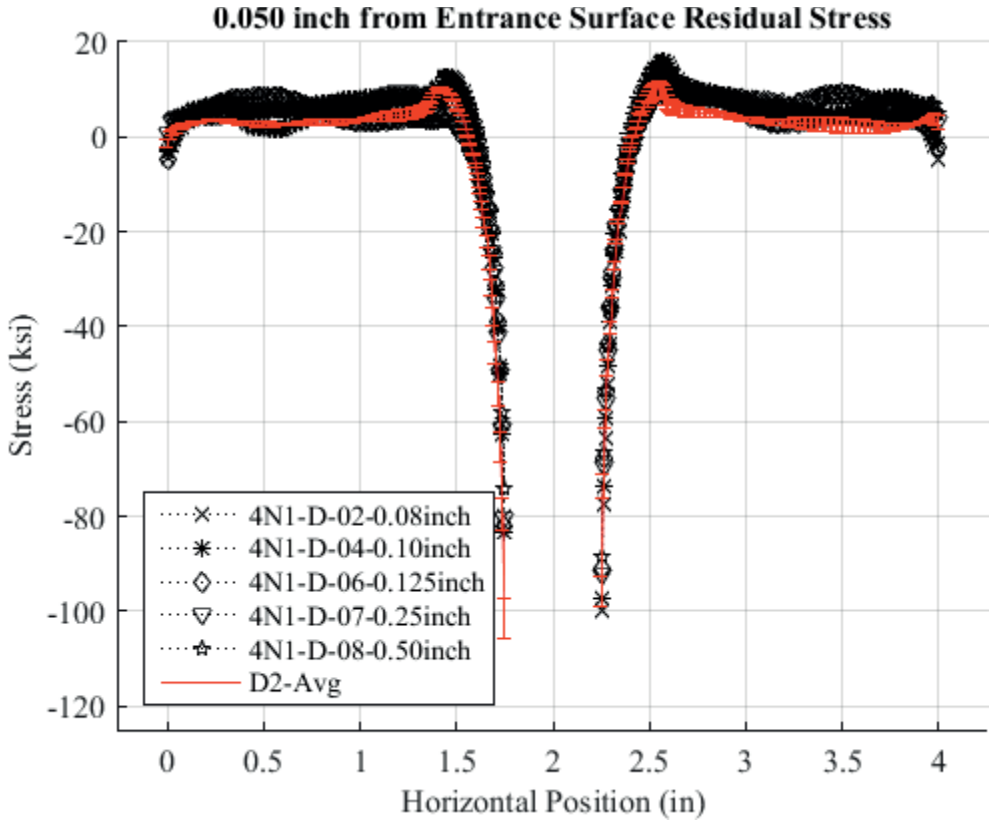

Fig. 794 Residual Stress Line Plot Comparing Cx4N1-02-D, Cx4N1-04-D, Cx4N1-06-D, CX4N1-07-D, Cx4N1-08-D, and the Average CxD2 (7075-T651) Average Residual Stress at a Distance of 0.05 inch from the Entrance Surface. Error Bars are Provided on the CxD2 Average Residual Stress which Represent the Repeatability Uncertainty for the CxD2 Condition.

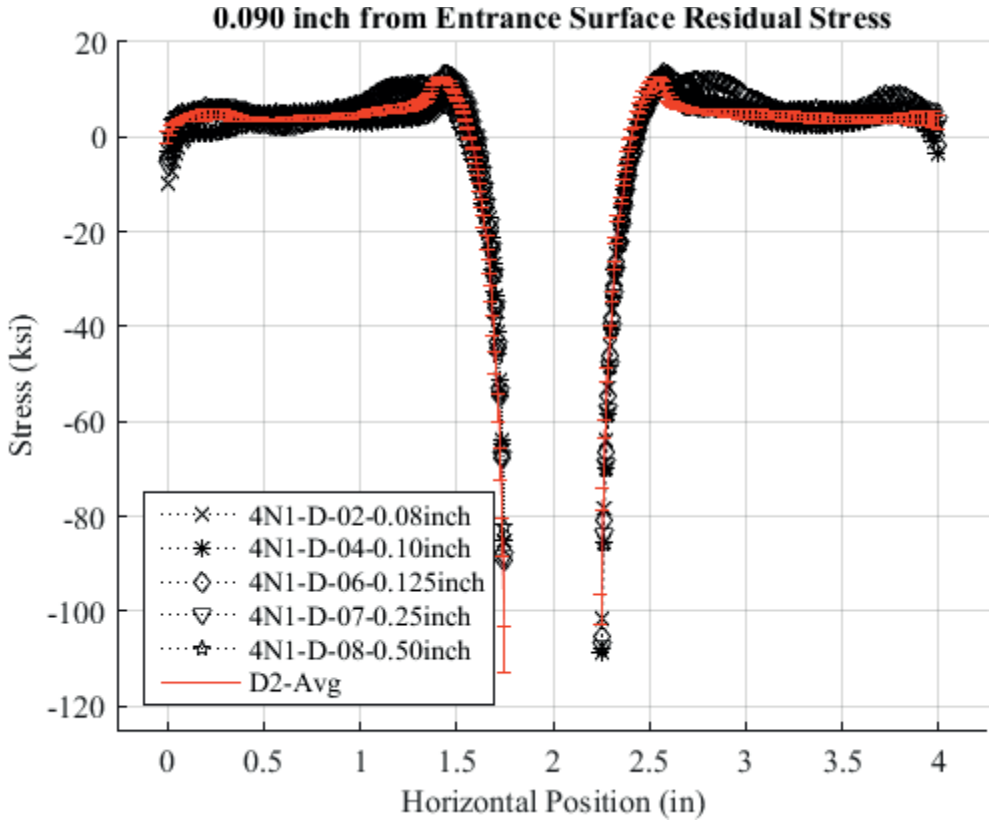

Fig. 795 Residual Stress Line Plot Comparing Cx4N1-02-D, Cx4N1-04-D, Cx4N1-06-D, CX4N1-07-D, Cx4N1-08-D, and the Average CxD2 (7075-T651) Average Residual Stress at a Distance of 0.09 inch from the Entrance Surface. Error Bars are Provided on the CxD2 Average Residual Stress which Represent the Repeatability Uncertainty for the CxD2 Condition.

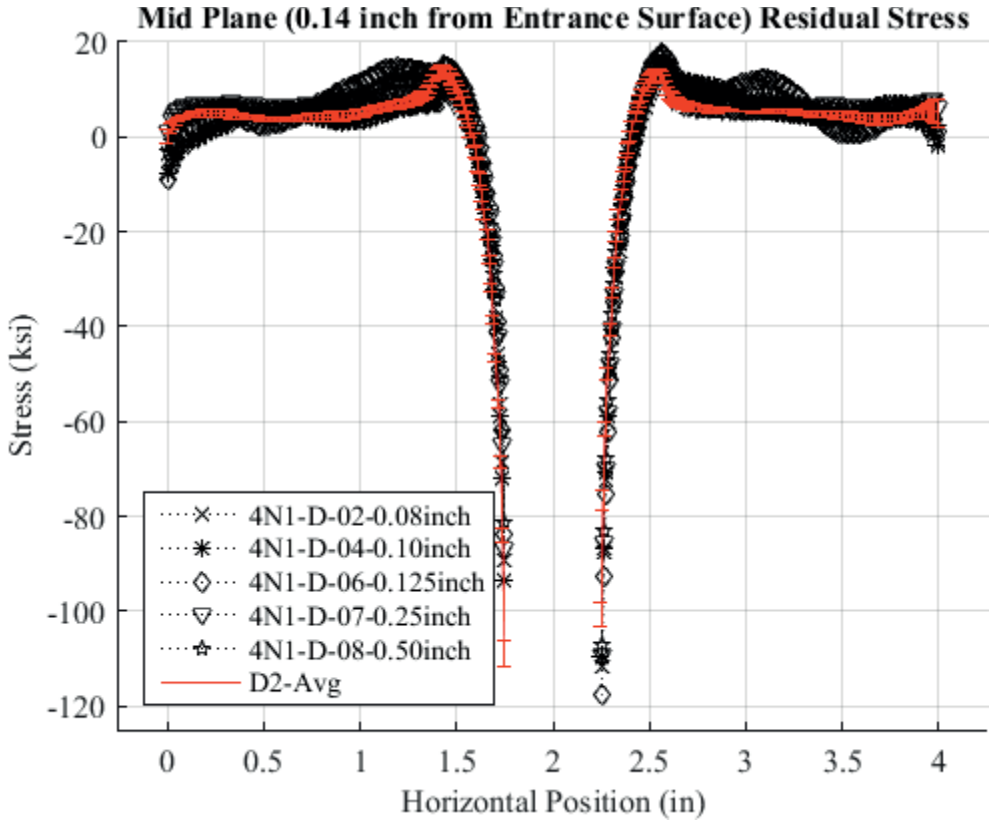

Fig. 796 Residual Stress Line Plot Comparing Cx4N1-02-D, Cx4N1-04-D, Cx4N1-06-D, CX4N1-07-D, Cx4N1-08-D, and the Average CxD2 (7075-T651) Average Residual Stress at a Distance of 0.140 inch (Mid Plane Surface) from the Entrance Surface. Error Bars are Provided on the CxD2 Average Residual Stress which Represent the Repeatability Uncertainty for the CxD2 Condition.

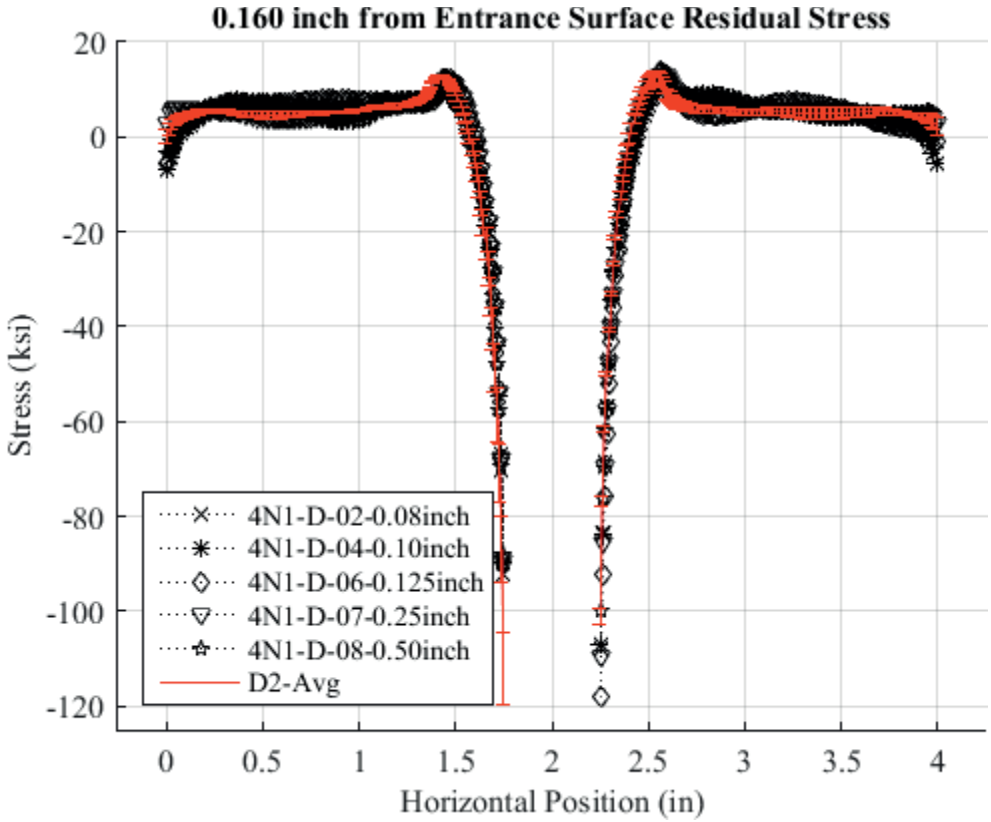

Fig. 797 Residual Stress Line Plot Comparing Cx4N1-02-D, Cx4N1-04-D, Cx4N1-06-D, CX4N1-07-D, Cx4N1-08-D, and the Average CxD2 (7075-T651) Average Residual Stress at a Distance of 0.160 inch from the Entrance Surface. Error Bars are Provided on the CxD2 Average Residual Stress which Represent the Repeatability Uncertainty for the CxD2 Condition.

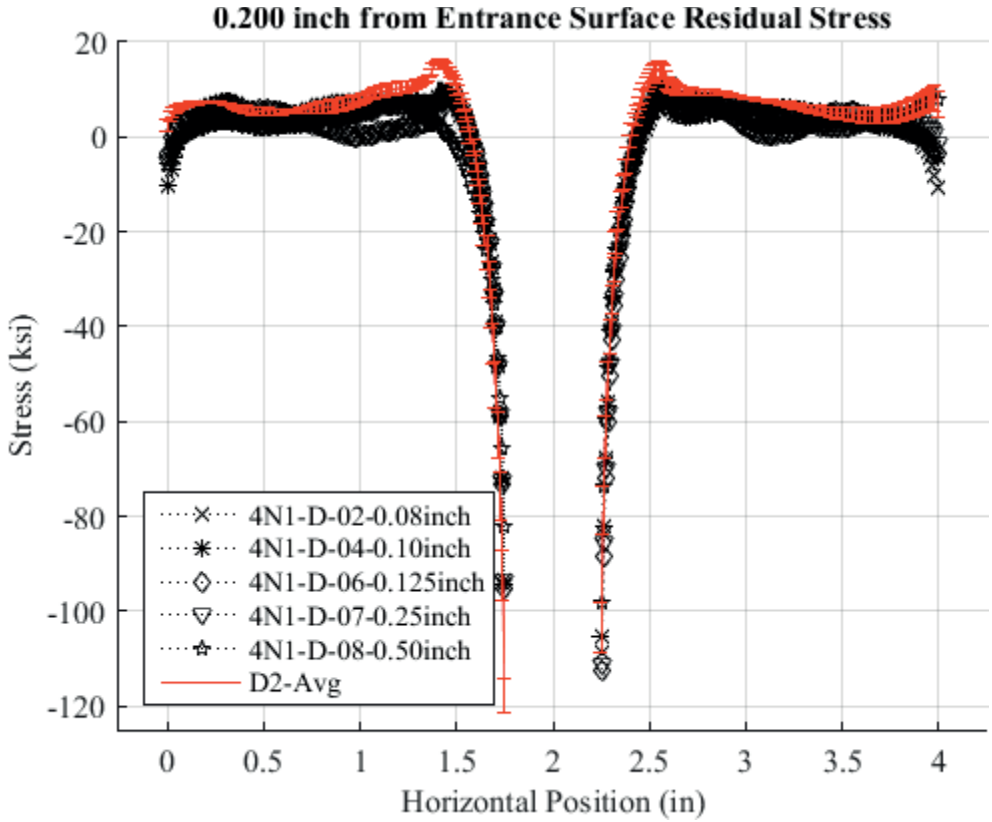

Fig. 798 Residual Stress Line Plot Comparing Cx4N1-02-D, Cx4N1-04-D, Cx4N1-06-D, CX4N1-07-D, Cx4N1-08-D, and the Average CxD2 (7075-T651) Average Residual Stress at a Distance of 0.200 inch from the Entrance Surface. Error Bars are Provided on the CxD2 Average Residual Stress which Represent the Repeatability Uncertainty for the CxD2 Condition.

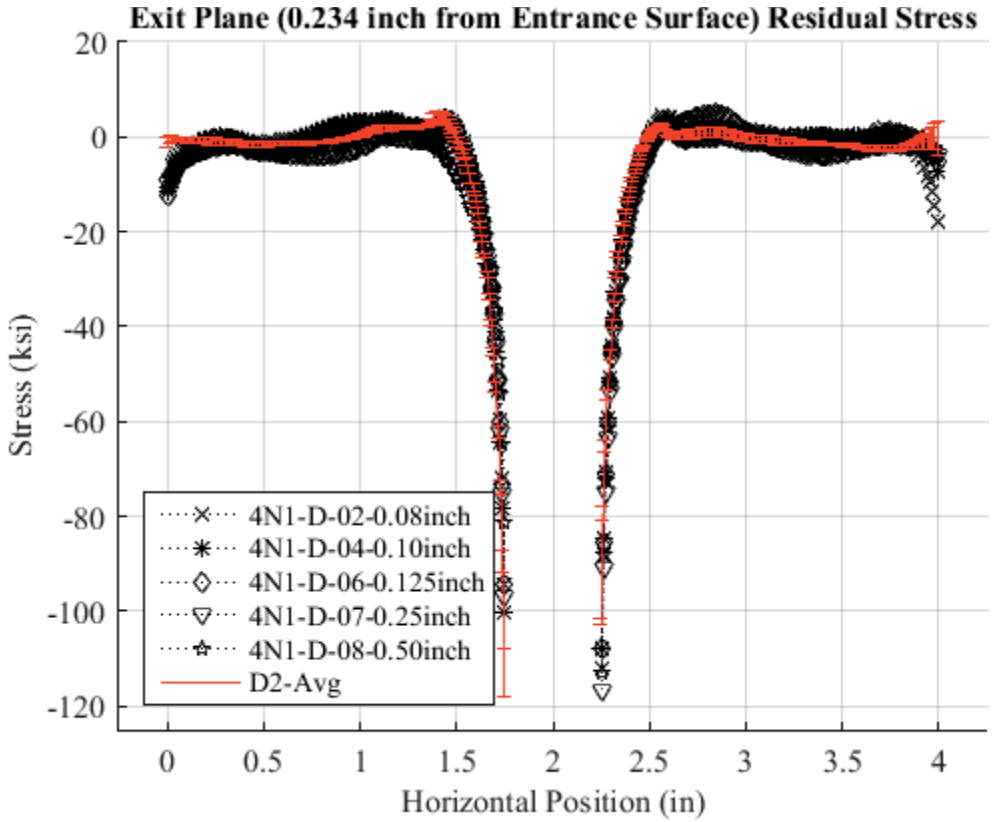

Fig. 799 Residual Stress Line Plot Comparing Cx4N1-02-D, Cx4N1-04-D, Cx4N1-06-D, CX4N1-07-D, Cx4N1-08-D, and the Average CxD2 (7075-T651) Average Residual Stress at a Distance of 0.234 inch (Exit Surface) from the Entrance Surface. Error Bars are Provided on the CxD2 Average Residual Stress which Represent the Repeatability Uncertainty for the CxD2 Condition.

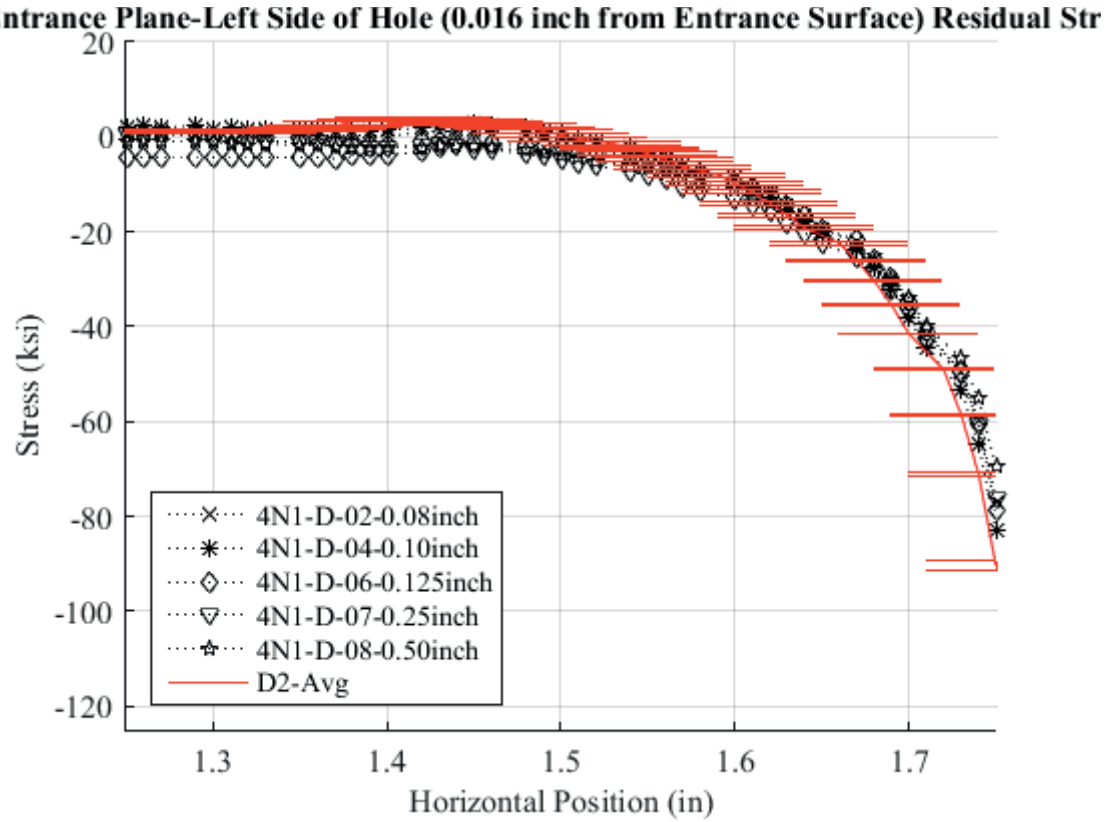

Fig. 800 Residual Stress Line Plot for First 0.50 inch away from Hole on Left Side of Hole Comparing Cx4N1-02-D, Cx4N1-04-D, Cx4N1-06-D, CX4N1-07-D, Cx4N1-08-D, and the Average CxD2 (7075-T651) Average Residual Stress at a Distance of 0.016 inch (Entrance Surface) from the Entrance Surface. Error Bars are Provided on the CxD2 Average Residual Stress which Represent the Repeatability Uncertainty for the CxD2 Condition.

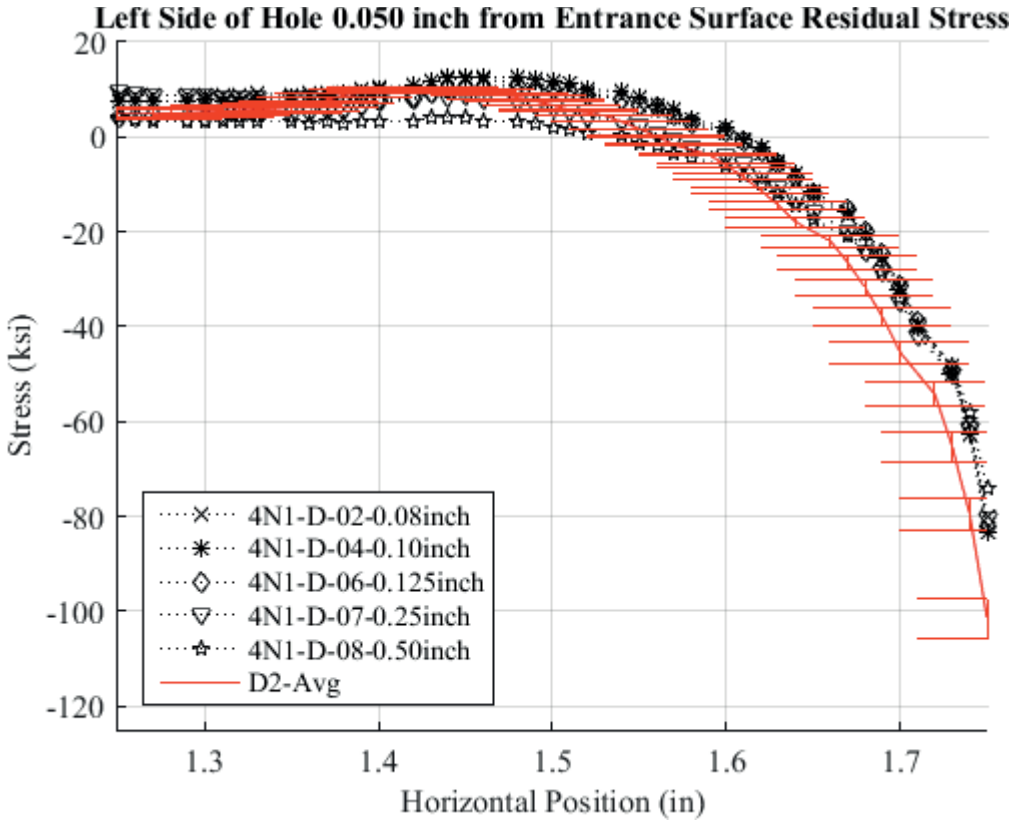

Fig. 801 Residual Stress Line Plot for First 0.50 inch away from Hole on Left Side of Hole Comparing Cx4N1-02-D, Cx4N1-04-D, Cx4N1-06-D, CX4N1-07-D, Cx4N1-08-D, and the Average CxD2 (7075-T651) Average Residual Stress at a Distance of 0.05 inch from the Entrance Surface. Error Bars are Provided on the CxD2 Average Residual Stress which Represent the Repeatability Uncertainty for the CxD2 Condition.

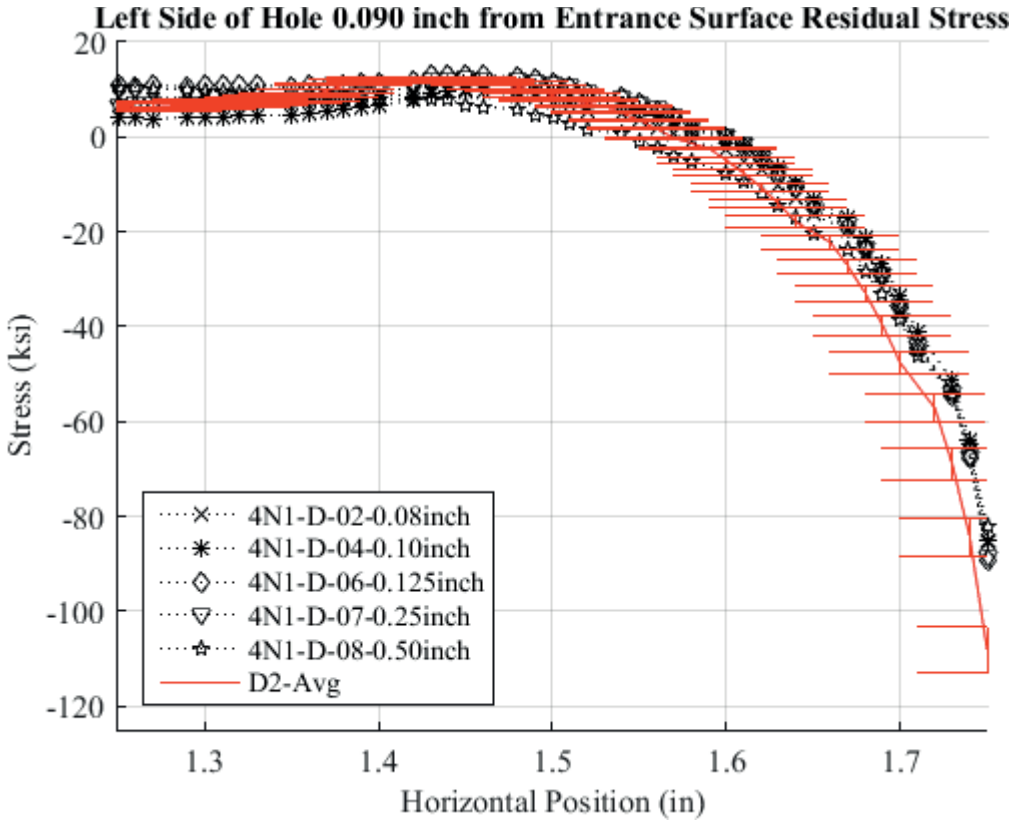

Fig. 802 Residual Stress Line Plot for First 0.50 inch away from Hole on Left Side of Hole Comparing Cx4N1-02-D, Cx4N1-04-D, Cx4N1-06-D, CX4N1-07-D, Cx4N1-08-D, and the Average CxD2 (7075-T651) Average Residual Stress at a Distance of 0.09 inch from the Entrance Surface. Error Bars are Provided on the CxD2 Average Residual Stress which Represent the Repeatability Uncertainty for the CxD2 Condition.

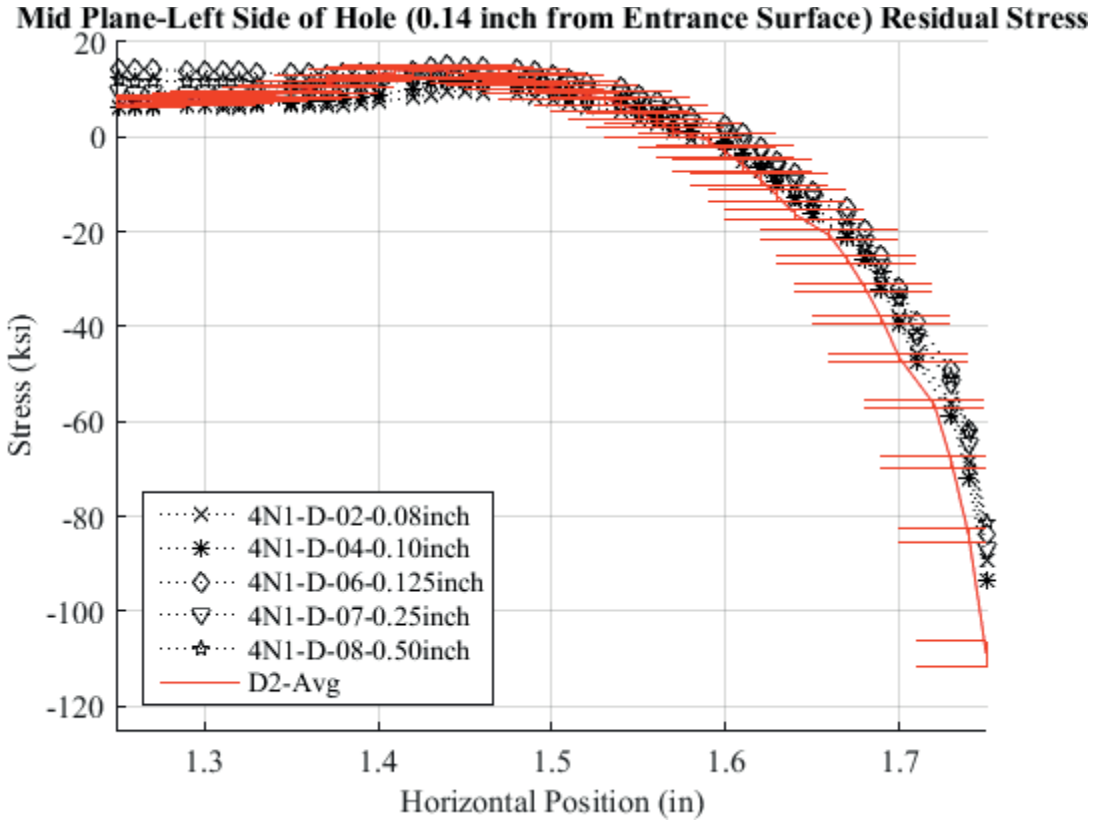

Fig. 803 Residual Stress Line Plot for First 0.50 inch away from Hole on Left Side of Hole Comparing Cx4N1-02-D, Cx4N1-04-D, Cx4N1-06-D, CX4N1-07-D, Cx4N1-08-D, and the Average CxD2 (7075-T651) Average Residual Stress at a Distance of 0.140 inch (Mid Plane Surface) from the Entrance Surface. Error Bars are Provided on the CxD2 Average Residual Stress which Represent the Repeatability Uncertainty for the CxD2 Condition.

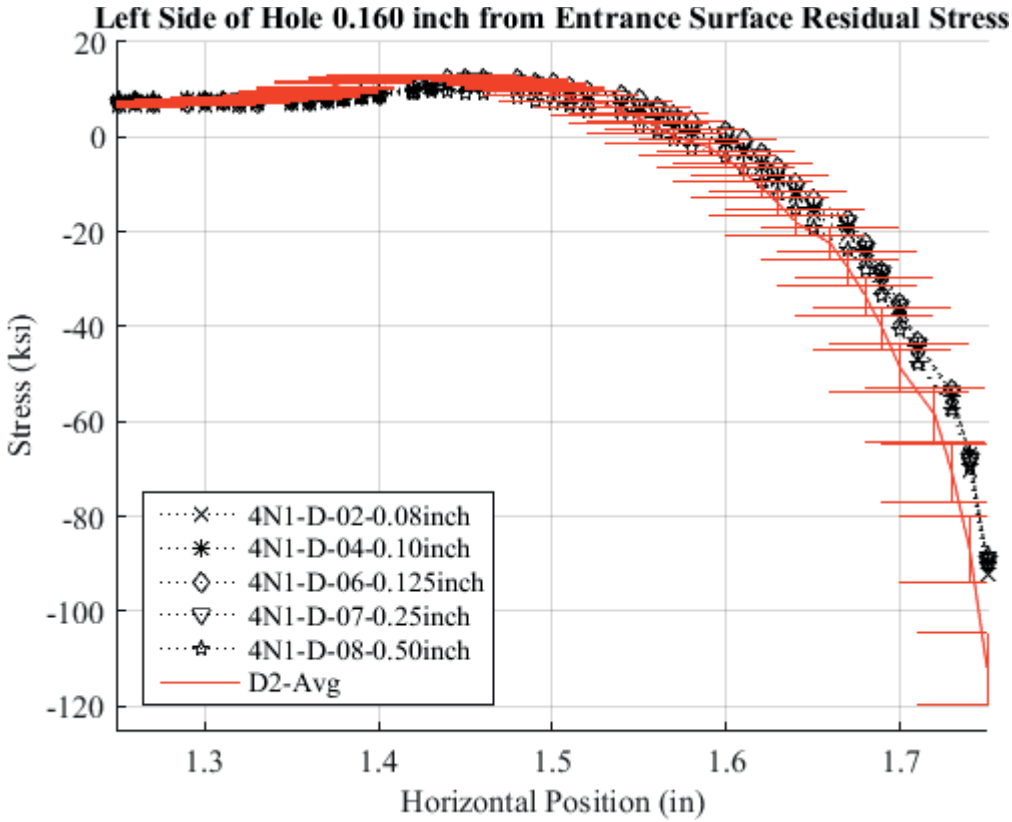

Fig. 804 Residual Stress Line Plot for First 0.50 inch away from Hole on Left Side of Hole Comparing Cx4N1-02-D, Cx4N1-04-D, Cx4N1-06-D, CX4N1-07-D, Cx4N1-08-D, and the Average CxD2 (7075-T651) Average Residual Stress at a Distance of 0.160 inch from the Entrance Surface. Error Bars are Provided on the CxD2 Average Residual Stress which Represent the Repeatability Uncertainty for the CxD2 Condition.

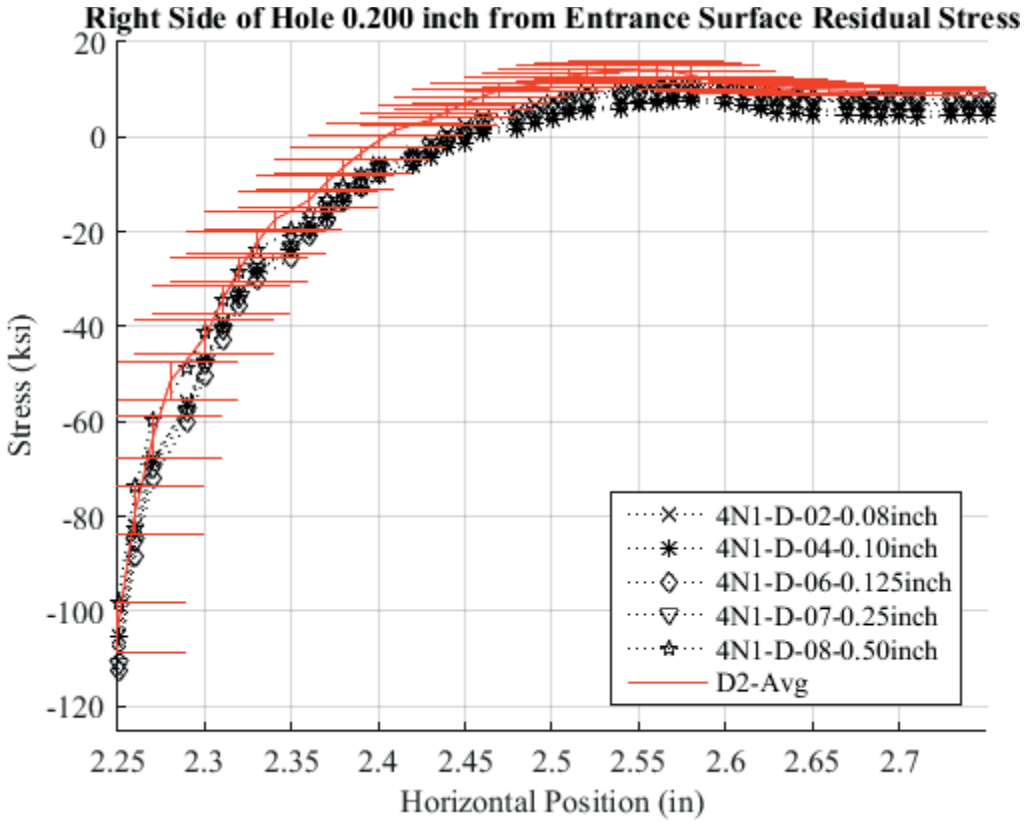

Fig. 805 Residual Stress Line Plot for First 0.50 inch away from Hole on Left Side of Hole Comparing Cx4N1-02-D, Cx4N1-04-D, Cx4N1-06-D, CX4N1-07-D, Cx4N1-08-D, and the Average CxD2 (7075-T651) Average Residual Stress at a Distance of 0.200 inch from the Entrance Surface. Error Bars are Provided on the CxD2 Average Residual Stress which Represent the Repeatability Uncertainty for the CxD2 Condition.

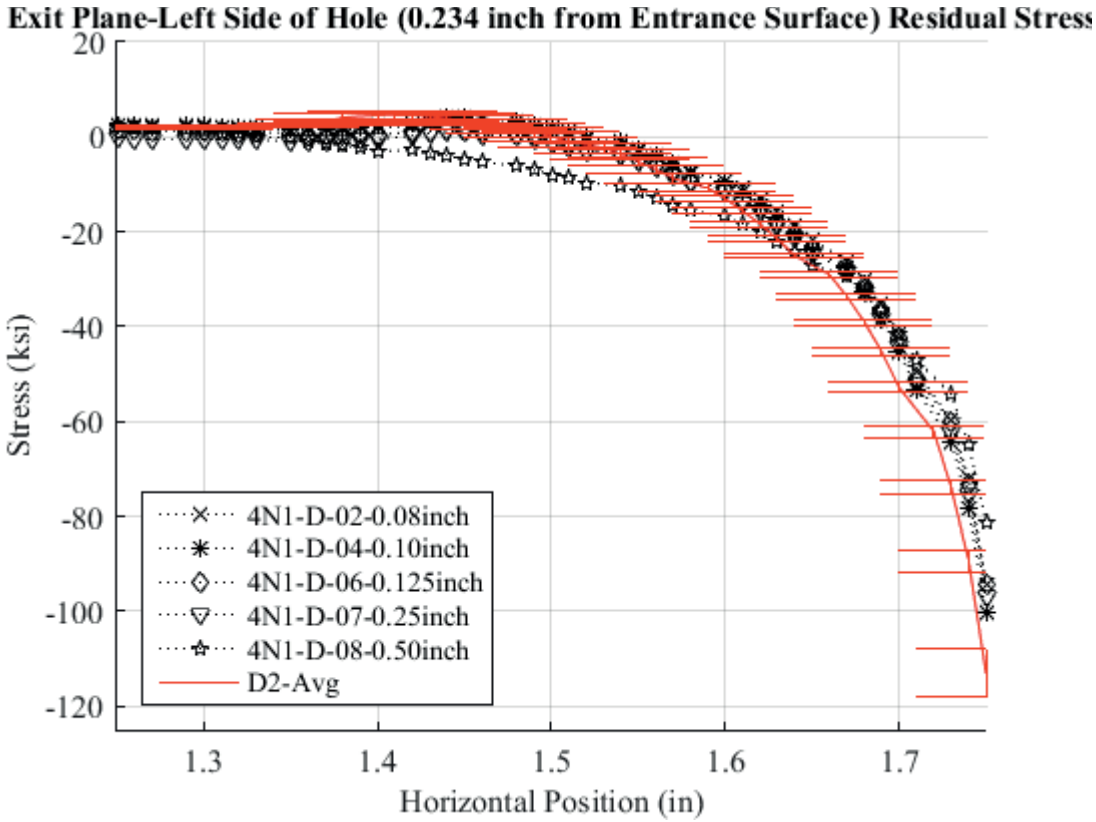

Fig. 806 Residual Stress Line Plot for First 0.50 inch away from Hole on Left Side of Hole Comparing Cx4N1-02-D, Cx4N1-04-D, Cx4N1-06-D, CX4N1-07-D, Cx4N1-08-D, and the Average CxD2 (7075-T651) Average Residual Stress at a Distance of 0.234 inch (Exit Surface) from the Entrance Surface. Error Bars are Provided on the CxD2 Average Residual Stress which Represent the Repeatability Uncertainty for the CxD2 Condition.

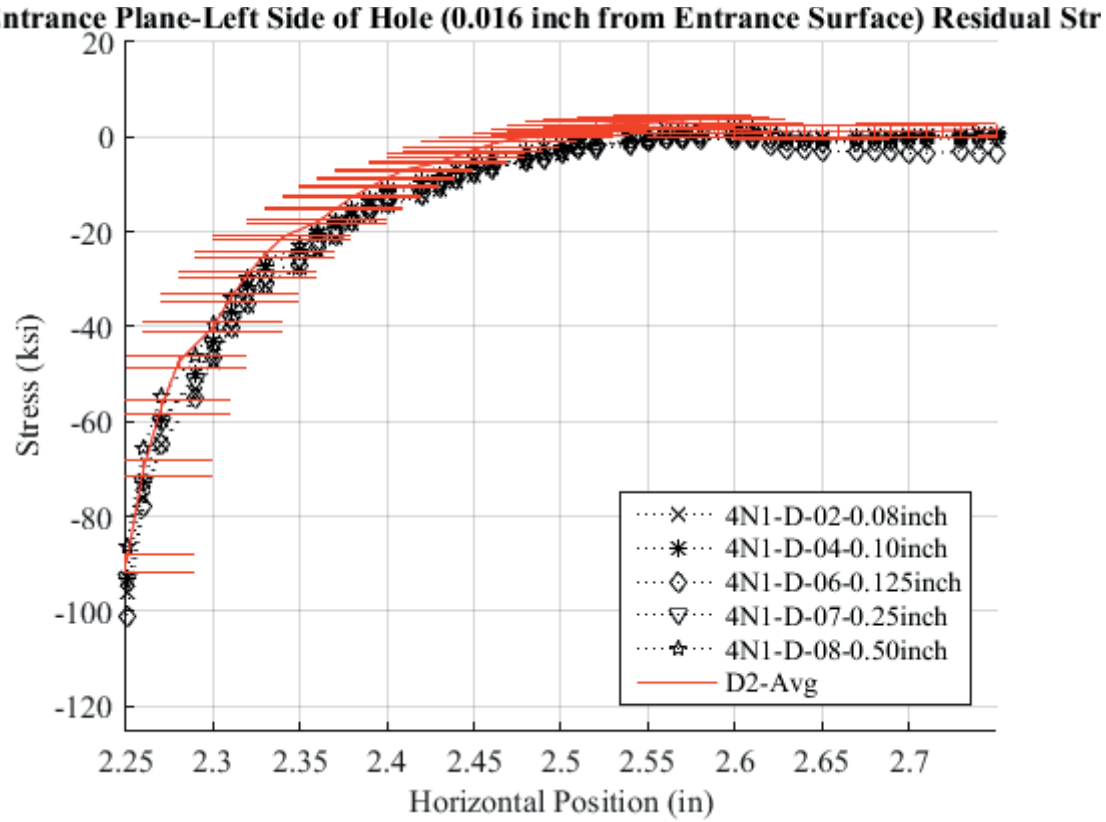

Fig. 807 Residual Stress Line Plot for First 0.50 inch away from Hole on Right Side of Hole Comparing Cx4N1-02-D, Cx4N1-04-D, Cx4N1-06-D, CX4N1-07-D, Cx4N1-08-D, and the Average CxD2 (7075-T651) Average Residual Stress at a Distance of 0.01 inch (Entrance Surface) from the Entrance Surface. Error Bars are Provided on the CxD2 Average Residual Stress which Represent the Repeatability Uncertainty for the CxD2 Condition.

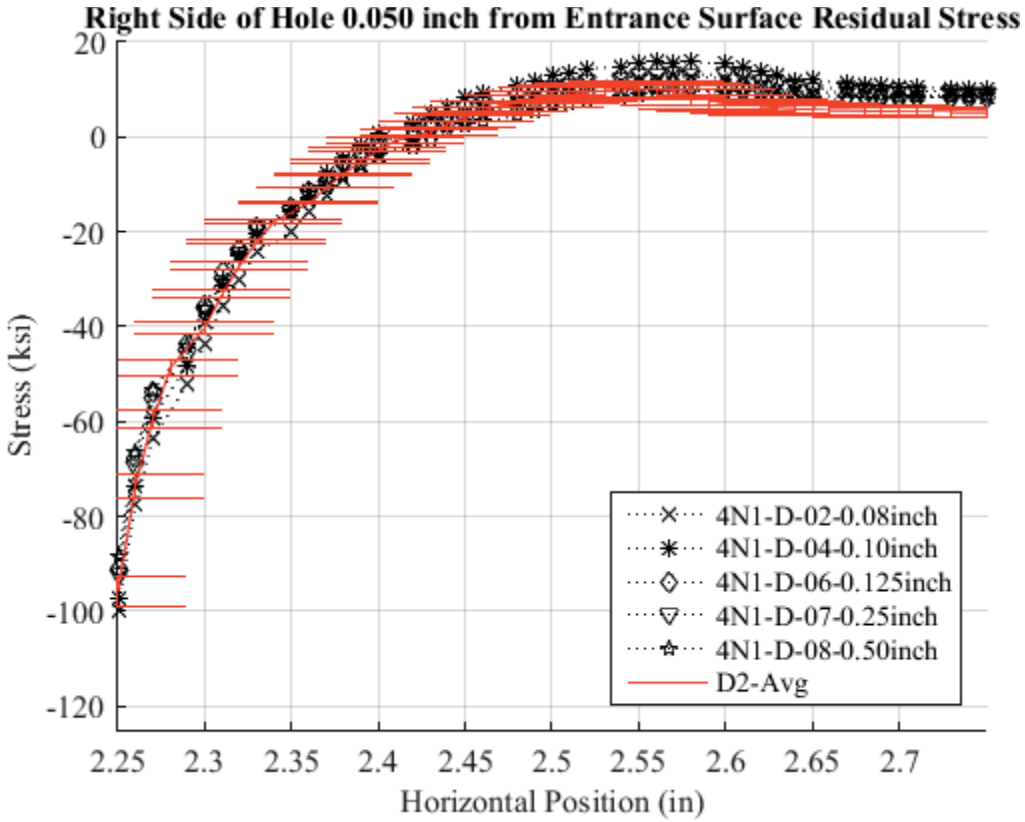

Fig. 808 Residual Stress Line Plot for First 0.50 inch away from Hole on Left Side of Hole Comparing Cx4N1-02-D, Cx4N1-04-D, Cx4N1-06-D, CX4N1-07-D, Cx4N1-08-D, and the Average CxD2 (7075-T651) Average Residual Stress at a Distance of 0.05 inch from the Entrance Surface. Error Bars are Provided on the CxD2 Average Residual Stress which Represent the Repeatability Uncertainty for the CxD2 Condition.

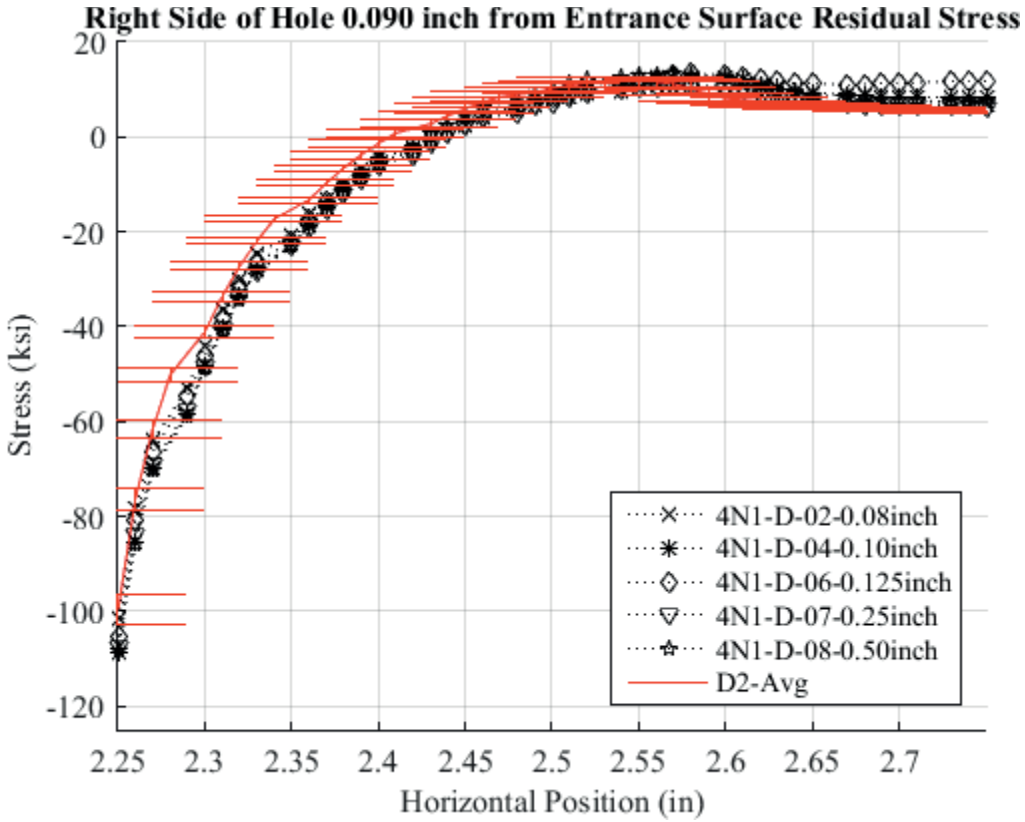

Fig. 809 Residual Stress Line Plot for First 0.50 inch away from Hole on Left Side of Hole Comparing Cx4N1-02-D, Cx4N1-04-D, Cx4N1-06-D, CX4N1-07-D, Cx4N1-08-D, and the Average CxD2 (7075-T651) Average Residual Stress at a Distance of 0.09 inch from the Entrance Surface. Error Bars are Provided on the CxD2 Average Residual Stress which Represent the Repeatability Uncertainty for the CxD2 Condition.

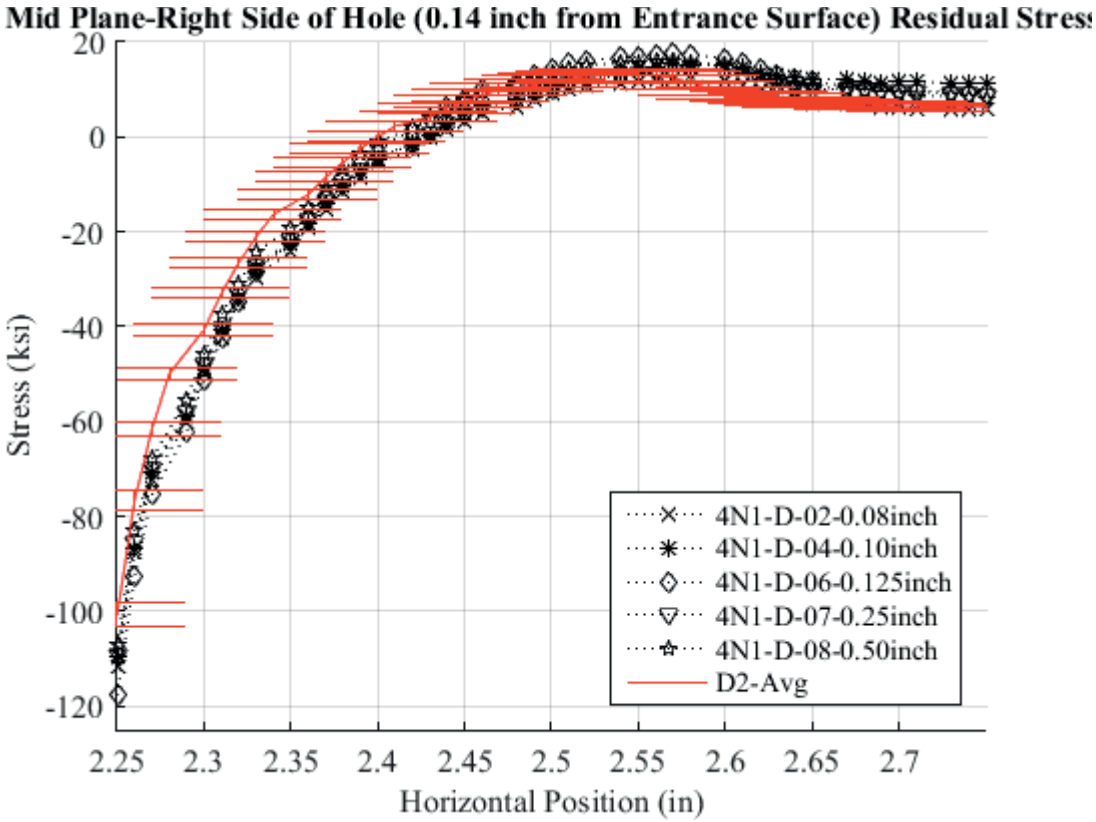

Fig. 810 Residual Stress Line Plot for First 0.50 inch away from Hole on Left Side of Hole Comparing Cx4N1-02-D, Cx4N1-04-D, Cx4N1-06-D, CX4N1-07-D, Cx4N1-08-D, and the Average CxD2 (7075-T651) Average Residual Stress at a Distance of 0.140 inch (Mid Plane Surface) from the Entrance Surface. Error Bars are Provided on the CxD2 Average Residual Stress which Represent the Repeatability Uncertainty for the CxD2 Condition.

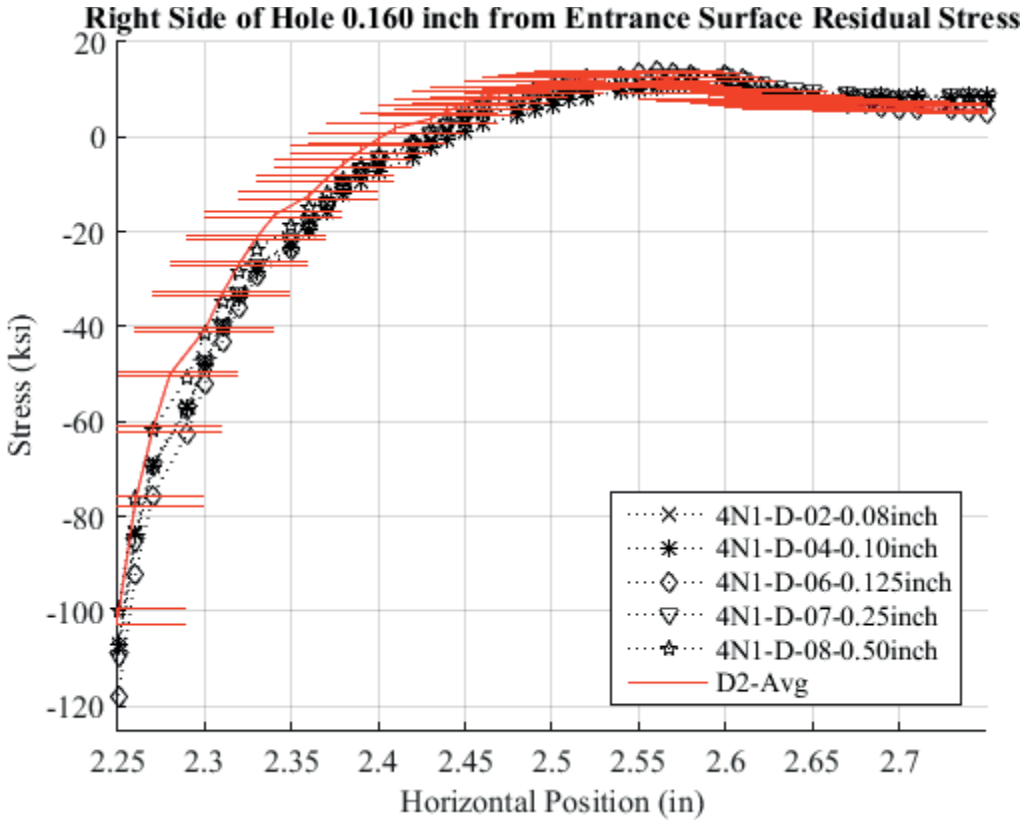

Fig. 811 Residual Stress Line Plot for First 0.50 inch away from Hole on Left Side of Hole Comparing Cx4N1-02-D, Cx4N1-04-D, Cx4N1-06-D, CX4N1-07-D, Cx4N1-08-D, and the Average CxD2 (7075-T651) Average Residual Stress at a Distance of 0.160 inch from the Entrance Surface. Error Bars are Provided on the CxD2 Average Residual Stress which Represent the Repeatability Uncertainty for the CxD2 Condition.

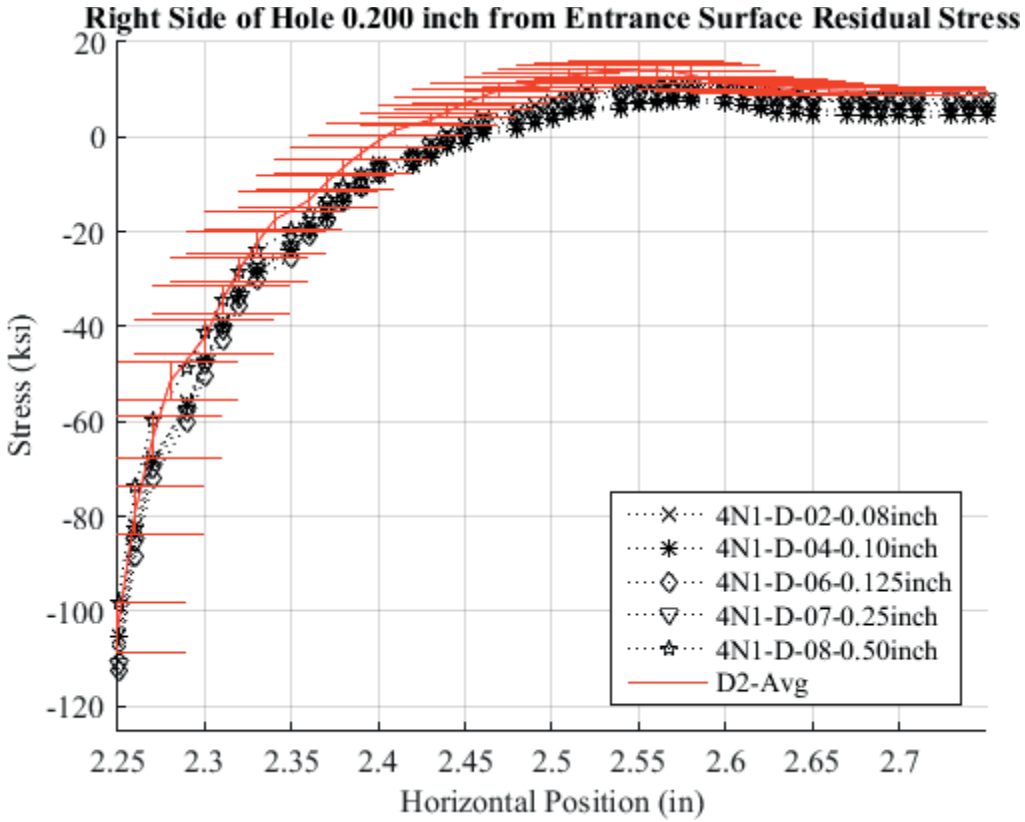

Fig. 812 Residual Stress Line Plot for First 0.50 inch away from Hole on Left Side of Hole Comparing Cx4N1-02-D, Cx4N1-04-D, Cx4N1-06-D, CX4N1-07-D, Cx4N1-08-D, and the Average CxD2 (7075-T651) Average Residual Stress at a Distance of 0.200 inch from the Entrance Surface. Error Bars are Provided on the CxD2 Average Residual Stress which Represent the Repeatability Uncertainty for the CxD2 Condition.

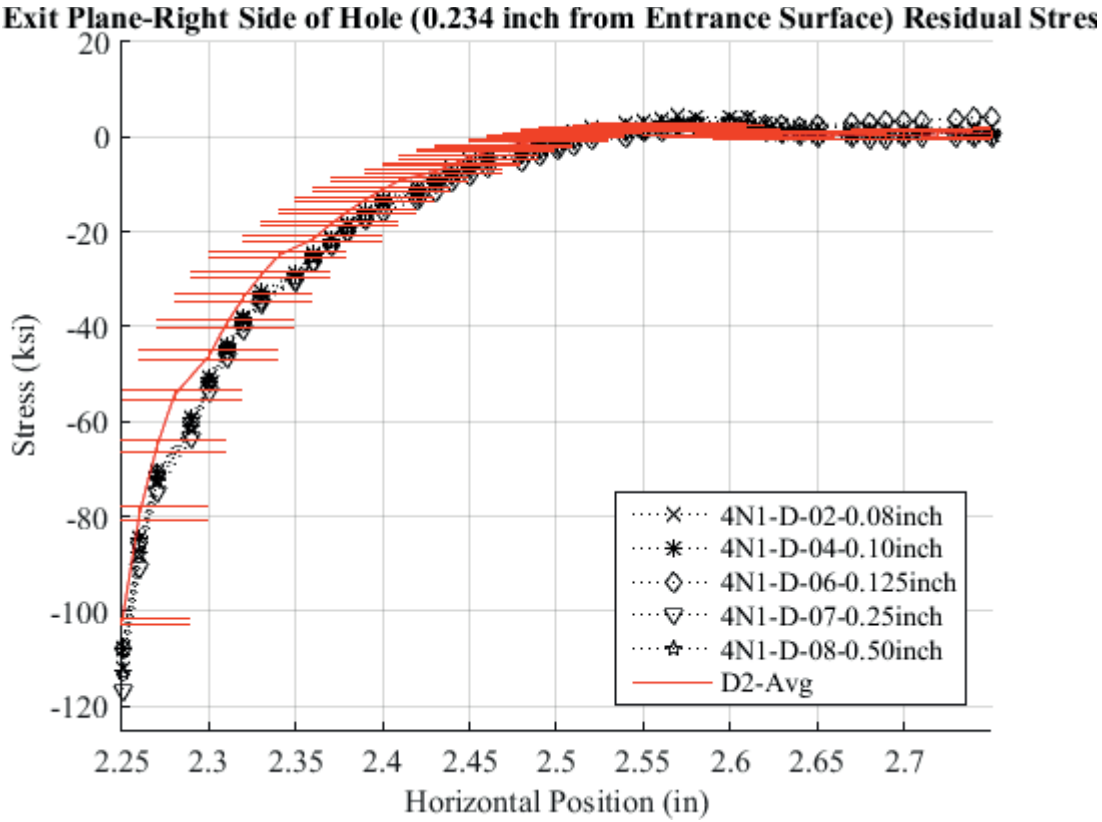

Fig. 813 Residual Stress Line Plot for First 0.50 inch away from Hole on Left Side of Hole Comparing Cx4N1-02-D, Cx4N1-04-D, Cx4N1-06-D, CX4N1-07-D, Cx4N1-08-D, and the Average CxD2 (7075-T651) Average Residual Stress at a Distance of 0.234 inch (Exit Surface) from the Entrance Surface. Error Bars are Provided on the CxD2 Average Residual Stress which Represent the Repeatability Uncertainty for the CxD2 Condition.

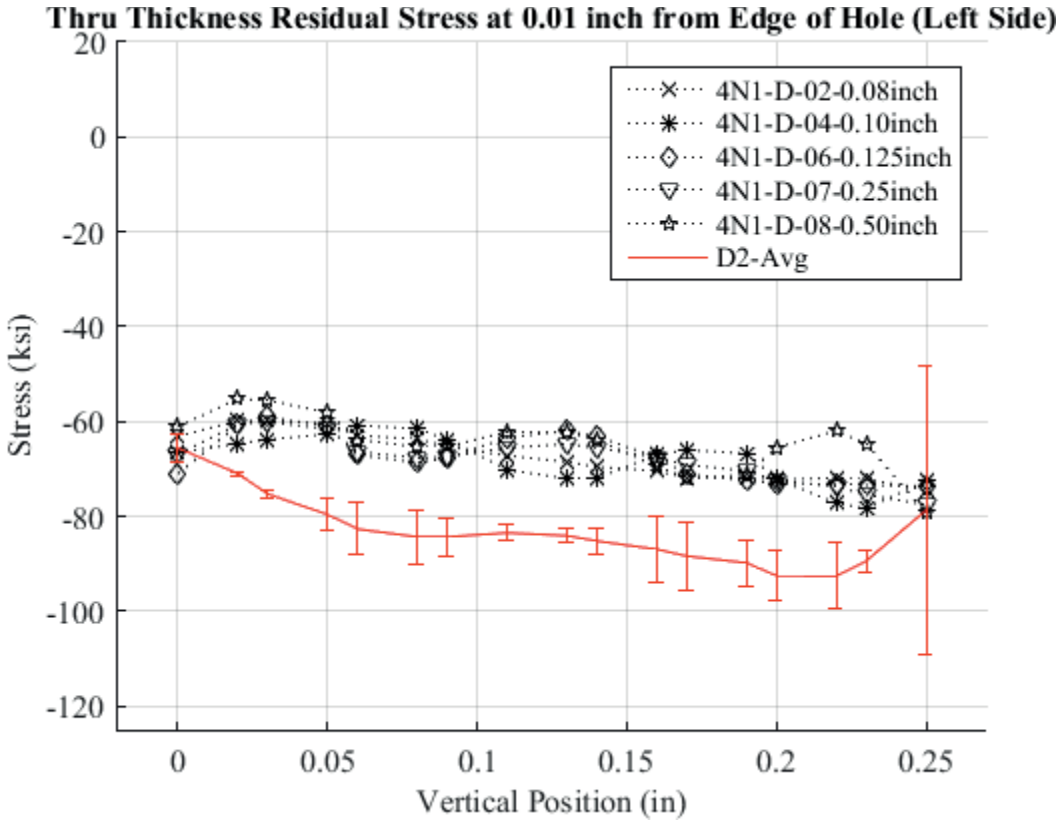

Fig. 814 Residual Stress Through-Thickness Line Plot Comparing Cx4N1-02-D, Cx4N1-04-D, Cx4N1-06-D, CX4N1-07-D, Cx4N1-08-D, and the Average CxD2 (7075-T651) Average Residual Stress at a Distance of 0.01 inch from the Left Side of the Hole. Error Bars are Provided on the CxD2 Average Residual Stress which Represent the Repeatability Uncertainty for the CxD2 Condition.

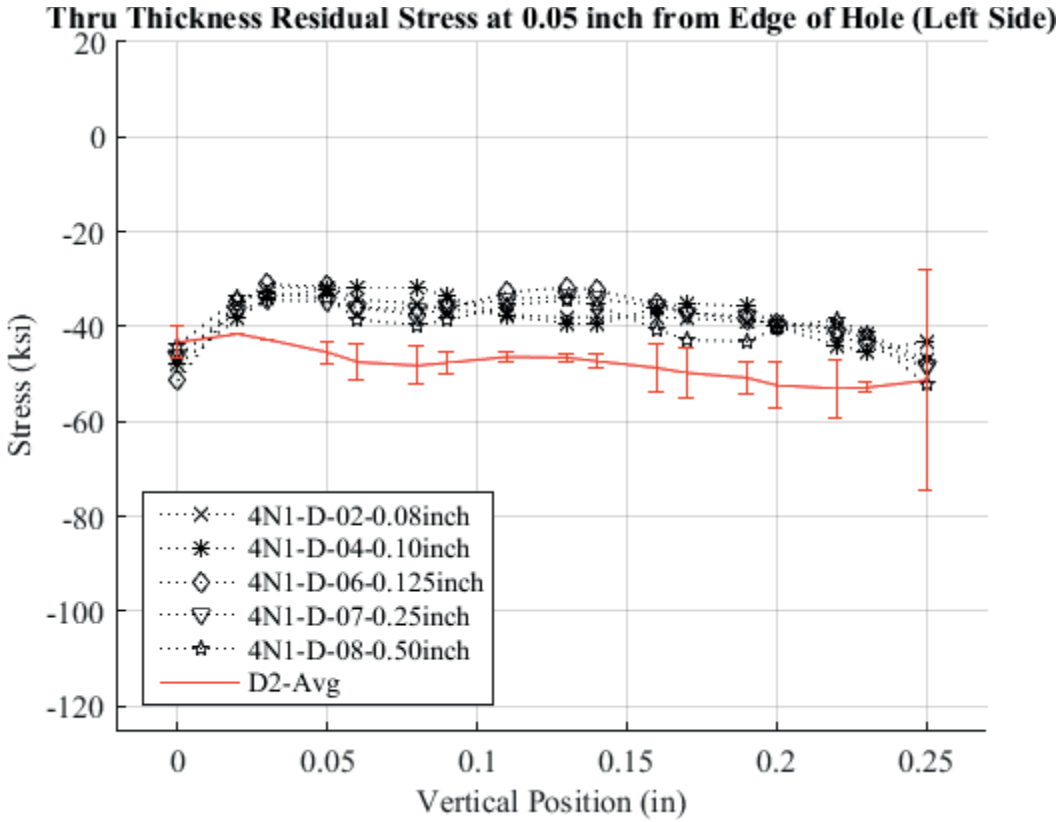

Fig. 815 Residual Stress Through-Thickness Line Plot Comparing Cx4N1-02-D, Cx4N1-04-D, Cx4N1-06-D, CX4N1-07-D, Cx4N1-08-D, and the Average CxD2 (7075-T651) Average Residual Stress at a Distance of 0.05 inch from the Left Side of the Hole. Error Bars are Provided on the CxD2 Average Residual Stress which Represent the Repeatability Uncertainty for the CxD2 Condition.

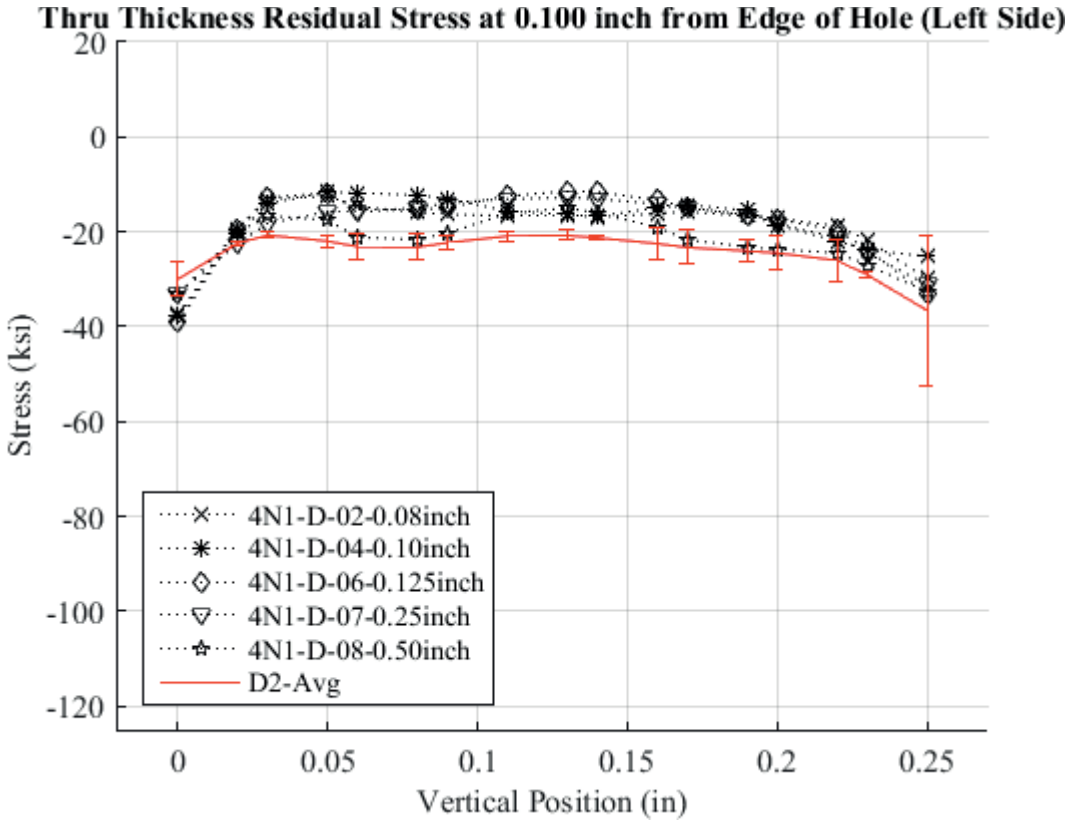

Fig. 816 Residual Stress Through-Thickness Line Plot Comparing Cx4N1-02-D, Cx4N1-04-D, Cx4N1-06-D, CX4N1-07-D, Cx4N1-08-D, and the Average CxD2 (7075-T651) Average Residual Stress at a Distance of 0.10 inch from the Left Side of the Hole. Error Bars are Provided on the CxD2 Average Residual Stress which Represent the Repeatability Uncertainty for the CxD2 Condition.

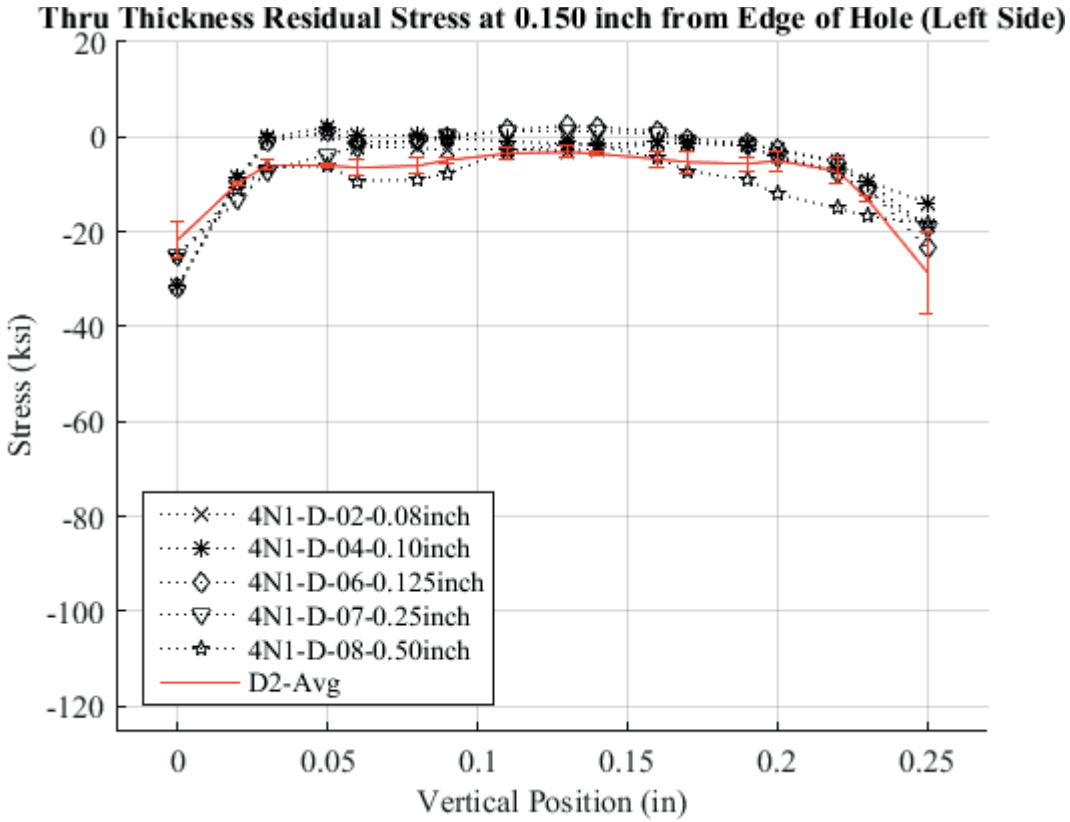

Fig. 817 Residual Stress Through-Thickness Line Plot Comparing Cx4N1-02-D, Cx4N1-04-D, Cx4N1-06-D, CX4N1-07-D, Cx4N1-08-D, and the Average CxD2 (7075-T651) Average Residual Stress at a Distance of 0.150 inch from the Left Side of the Hole. Error Bars are Provided on the CxD2 Average Residual Stress which Represent the Repeatability Uncertainty for the CxD2 Condition.

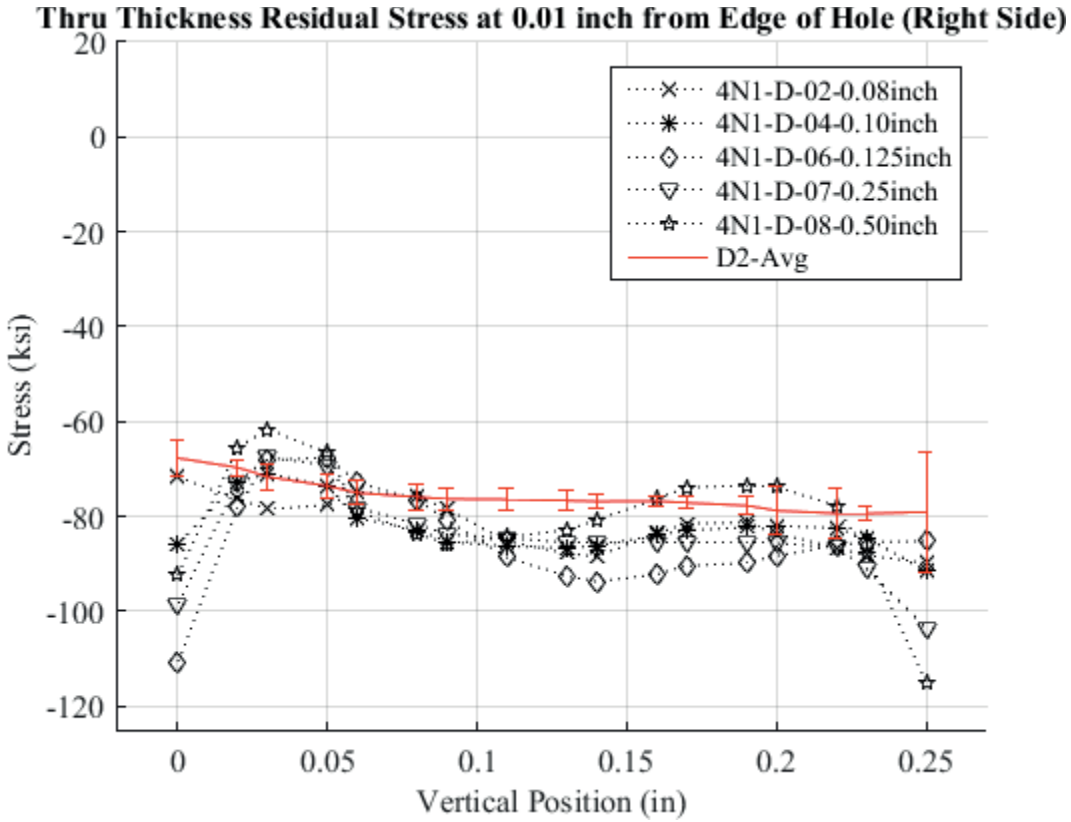

Fig. 818 Residual Stress Through-Thickness Line Plot Comparing Cx4N1-02-D, Cx4N1-04-D, Cx4N1-06-D, CX4N1-07-D, Cx4N1-08-D, and the Average CxD2 (7075-T651) Average Residual Stress at a Distance of 0.01 inch from the Right Side of the Hole. Error Bars are Provided on the CxD2 Average Residual Stress which Represent the Repeatability Uncertainty for the CxD2 Condition.

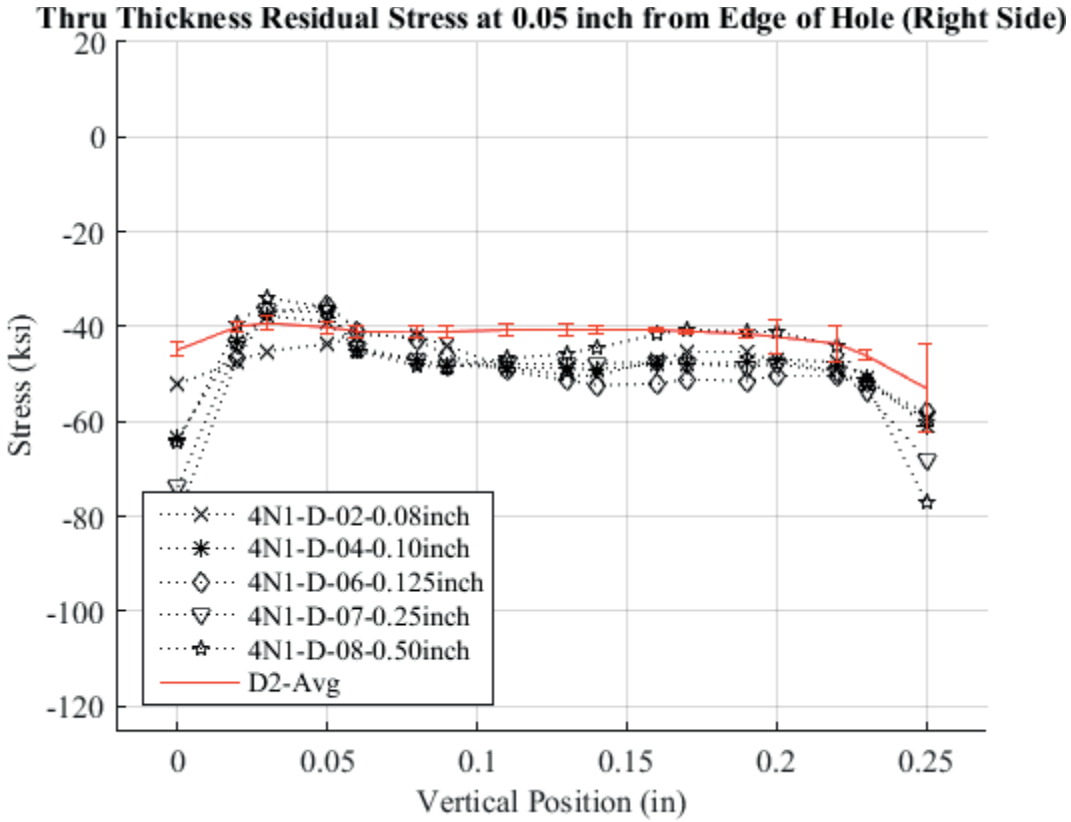

Fig. 819 Residual Stress Through-Thickness Line Plot Comparing Cx4N1-02-D, Cx4N1-04-D, Cx4N1-06-D, CX4N1-07-D, Cx4N1-08-D, and the Average CxD2 (7075-T651) Average Residual Stress at a Distance of 0.05 inch from the Right Side of the Hole. Error Bars are Provided on the CxD2 Average Residual Stress which Represent the Repeatability Uncertainty for the CxD2 Condition.

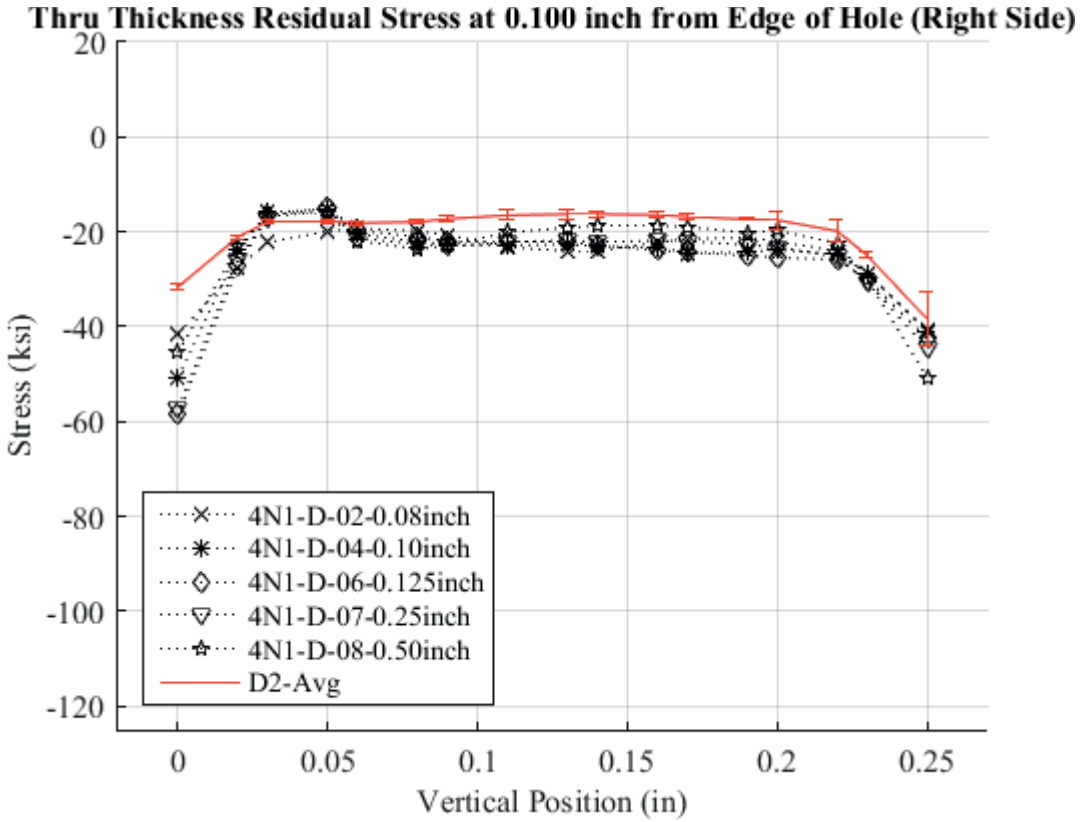

Fig. 820 Residual Stress Through-Thickness Line Plot Comparing Cx4N1-02-D, Cx4N1-04-D, Cx4N1-06-D, CX4N1-07-D, Cx4N1-08-D, and the Average CxD2 (7075-T651) Average Residual Stress at a Distance of 0.10 inch from the Right Side of the Hole. Error Bars are Provided on the CxD2 Average Residual Stress which Represent the Repeatability Uncertainty for the CxD2 Condition.

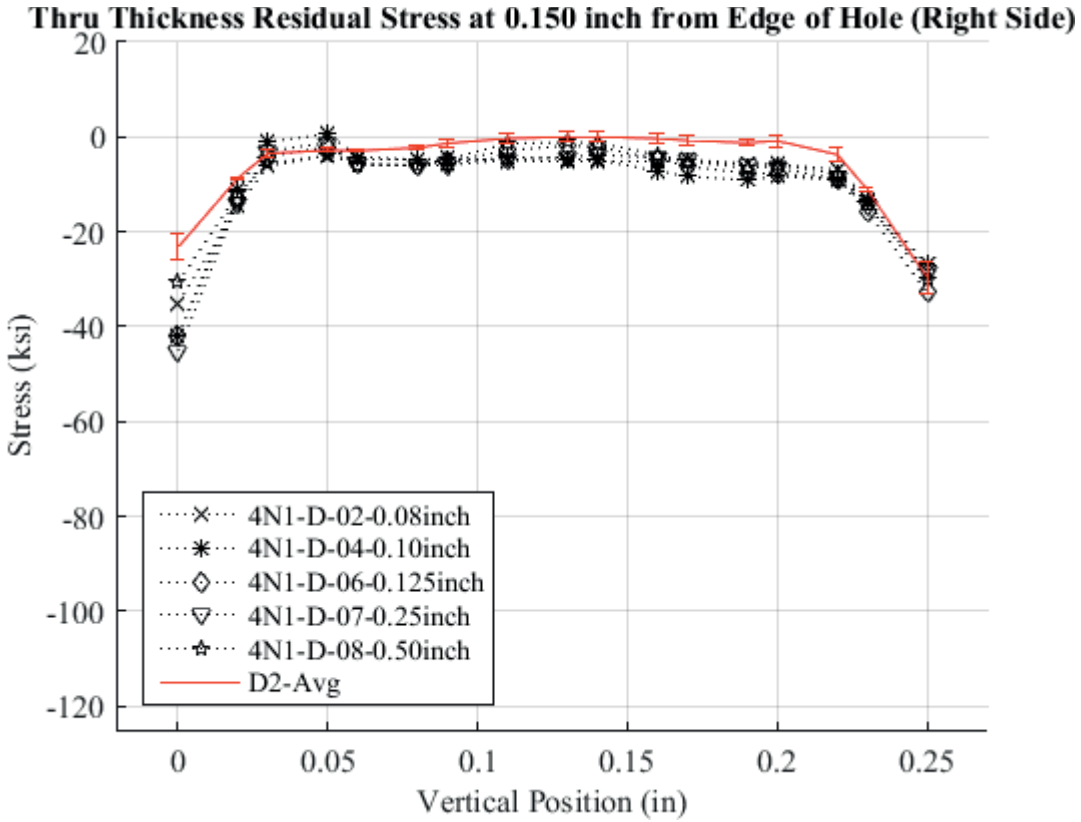

Fig. 821 Residual Stress Through-Thickness Line Plot Comparing Cx4N1-02-D, Cx4N1-04-D, Cx4N1-06-D, CX4N1-07-D, Cx4N1-08-D, and the Average CxD2 (7075-T651) Average Residual Stress at a Distance of 0.150 inch from the Right Side of the Hole. Error Bars are Provided on the CxD2 Average Residual Stress which Represent the Repeatability Uncertainty for the CxD2 Condition.

8 IMPLEMENTATION OF COLD EXPANSION RESIDUAL STRESSES FOR PREDICTION OF FATIGUE LIFE – UTILIZATION OF BASELINE CXA2 (2024-T351) AND CXD2 (7075-T651) RESIDUAL STRESS FIELDS

8.1 Development of Residual Stress Traction Functions for Implementation into StressCheck®

With residual stresses developed for all of the CxA2 (2024-T351) and CxD2 (7075-T651) coupons it was possible to then implement the residual stress distributions into a fatigue crack growth prediction. All of the fatigue crack growth predictions were performed using the BAMF framework.[135,136,137,138,139] BAMF is a Visual Basic plug-in that utilizes a FEA software, StressCheck® for the calculation of SIFs at the simulated crack front.

StressCheck® is a polynomial based, p-version FEA software that allows the user to impose onto the model a simulated crack front. As a p-version FEA software, StressCheck® uses a polynomial-based refinement method that increases the order of the basis function describing the geometry of the element edges. This type of finite element software differs from the standard h-version finite element program. Within h-version software mesh refinement is accomplished by increasing the number of elements in an area of interest, or across the model rather than increasing the basis function. For h-version FEA software codes, increasing the number of elements in the mesh provides a

greater degree of refinement of the calculated results. In addition to the level of refinement h-version software has multiple element types. These factors can have a significant influence on the final results.

StressCheck® allows for the polynomial order to range from one to eight that can increase the accuracy when modeling high strain gradients without increasing the number of elements in the model. This makes it possible to solve the model without refining the mesh, that is, increasing the element density. For all of the StressCheck® simulations a p-level of three was used. This polynomial order was determined by the convergence of the SIF as a function of p-level that had been performed previously.[72] The SIF is termed "super convergent" within StressCheck®, thus a lower order of polynomial is needed to reach a converged solution.[137] BAMF also then invokes the fatigue crack growth software, AFGROW, to determine the crack growth increment for each point along the crack front. Each nodal location along the crack front is then "propagated" this amount and the crack front then is re-meshed and the process of solving the model is performed again. Fig. 822 provides a graphical representation of the BAMF framework for a model that has no residual stress applied to it.

The α_{app} that is produced is then passed to AFGROW, where a K_{min} and K_{max} are calculated and used to determine the given Stress Ratio (R). The crack growth rate is then determined based on the material file used within AFGROW, and is directly related to the ΔK calculated. This process is performed for each node along the simulated crack front within StressCheck®. This individual nodal-crack-front growth is passed back to StressCheck® and each node along the crack front is "propagated" to a specific increment calculated from within AFGROW. This process is defined graphically within Fig. 823.

When a residual stress is added to the BAMF framework an additional step is required. Another model is built within StressCheck® for which only the residual stress is applied. This model is also solved and the SIF is extracted at each node along the crack front. This $K_{res.}$ then is passed to use to determine a new R and a crack growth rate (da/dN) is determined by a combined $K_{app.}$ and K_{res} at the total R. With a new crack growth rate (da/dN) determined through the material model used within AFGROW, the simulated crack is "propagated" this increment and the StressCheck® model is then remeshed and solved again for the updated crack front size and shape. This process is graphically represented within Fig. 824 and Fig. 825.

There have been many different methods for the implementation of the residual stress developed by the Cx process into a FEA simulation. These include the use of Eigenstrains, weight functions, and even the development and implementation of a Beta (β) correction which represented the effect of the residual stress from the Cx process on the fatigue crack growth rate.[140,141,72] An additional method has been developed and implemented within the StressCheck® software package. This allows for a crack face traction to be applied at the given coordinate system.[142,143,144,145] The contour integral method (CIM) allows for a traction stress to be applied as a "loaded crack" (LC) and thus through the BAMF framework a solution for the model can be solved in which the residual stress traction stress is applied and the K_{res} is extracted.

Within StressCheck® the LC is implemented through the development of a polynomial function that defines the residual stress field. Thus, for each of the residual stress fields that were developed via the contour method, a high order polynomial function had to be developed which would represent the residual stress field.

A MatLab script was developed to produce these fitting functions. A fifteenth order polynomial is the highest order that StressCheck® version 10.3 can accept, so an investigation was performed to determine the optimal fit function for the derived residual stress fields. Through this investigation, it was determined that the most appropriate metric for determining the optimal fit was to reduce the residual (the difference between the actual residual stress data and the fit of that data) to less than a maximum of 4 ksi at any individual location. Thus, for each residual stress function that was developed a plot of that function and the residual is produced to aid in the determination of this optimal fit.

The residual stress functions developed for the CxA2 (2024-T351) and CxD2 (7075-T651) were produced by placing only the left sides of the hole on the same grid, with the origin of the coordinate axis at the mandrel entrance surface, on the right side of the hole, and then averaging each nodal residual stress for each of the replicates within the given material. Thus, only the residual stresses determined for the left side of the hole were used to develop the residual stress functions. The reason that the coordinate system was placed on the right side of the hole was due to the defined nucleation coordinate system which was location within the FEM. This was on the right side of the hole, thus a simple translation of the location of the coordinate system was required. There were five replicates produced for the CxA2 (2024-T351) and three for the CxD2 (7075-T651) condition. Thus, for each material there was just one function that was produced for the average residual stress field for only the left side of the hole. This would allow for a future direct comparison of life to the cracked and uncracked conditions, since the fatigue crack was developed on only one side of the hole.

Prior to the develop of these residual stress traction functions the output residual

stress data was linearly interpolated to a spatial grid density of 0.005 inch by 0.005 inch. It was determined that in order to minimize the functional miss-fit between the residual stress data points the grid density had to be reduced down to this level. Prior to this research there had been no investigation into the required level of data spatial density. Through this work it was determined that the spacing is recommended to be on the order of the distance between the simulated crack front nodes. For this work the initial crack size was approximately 0.05 inch by 0.05 inch and thus if one were to calculate the arch spacing for eleven nodes across a quarter circle it would be shown that these nodes are spaced at approximately 0.005 inch internals along the arch. Because the residual stress fields that were developed are all linearly elastic, a linear interpolation scheme was used to increase the data density. It is understood that this has the potential to add another source of estimation, thus uncertainty into the analysis contained herein. The effects of this have not been investigated and it is recommended that in the future this be investigated.

The effect of the data density on the final residual stress function and its fit, has the potential to have a great impact on how residual stress fields are validated. If the spatial density of the validation method is not high enough it is possible to validate a measured strain field and calculated stress field that when imposed into a model with a simulated fatigue crack the data density is too low and thus the final predicted fatigue life is not accurate.

In addition to a function which represented the average residual stress field, a function was produced for the average residual stress shifted “down” by one repeatability standard deviation. The repeatability standard deviation for all of the coupons was

derived from the baseline coupon configuration for the representative material. This shift "down" represents a shift in the residual stress to a more compressive stress for all of the negative stress values and also a shift more compressive for the tension stresses. Another stress function was produced which was a shift "up" in the residual stress. This shifted all of the compressive and tension stresses up by one repeatability standard deviation.[146]

8.1.1 Residual Stress Traction Functions for CxA2 (2024-T351) Coupons

For each of the residual stress distributions for the CxA2 (2024-T351) coupons, average, "up" and "down" one standard deviation, a surface contour plot was developed and is provided along with a plot of the residuals. The residuals are the point-by-point differences between the fit and the actual residual stress data.

These residual stress functions were developed by averaging only the left side of each of the CxA2 (2024-T351) coupons. This resulting function would provide a direct comparison of stress between the baseline, uncracked condition, and the fatigue-cracked condition later developed in the Cx4N1-XX-B (2024-T351) coupons. The functions that were produced for each of these CxA2 (2024-T351) coupons is provided in the Appendix. These functions will not be provided within the body of this report, however plots of some of these functions will be provided below.

8.1.1.1 Residual Stress Function for Average CxA2 Residual Stress from Repeatability Distribution

The residual stress surface plot for the average CxA2 (2024-T351) condition is provided in Fig. 826. A plot of the residuals between the fit and the actual residual stress data is provided in Fig. 827. It can be seen from this that the largest residuals are closest

to the hole. This is the area of greatest importance and thus this is an area of concern when applying this method for implementing residual stresses into a FEA simulation. Thus great care is required when developing residual stress fit functions to optimize the function for locations of greatest interest. In addition, there are limitations within the application of LC method for StressCheck® and these all need to be considered when applying residual stresses within a finite element simulation.

8.1.1.2 Residual Stress Function for "Up" One Standard Deviation from the Average CxA2 Residual Stress from Repeatability Distribution

In addition to producing residual stress functions for the average residual stress condition, a function was produced for the residual stress field that represents one of the statistical bounds developed within this work. The residual stress surface plot for the "up" one standard deviation is provided in Fig. 828, and the plot of the residuals is provided in Fig. 829.

8.1.1.3 Residual Stress Function for "Down" One Standard Deviation from the Average CxA2 Residual Stress from Repeatability Distribution

The residual stress condition for the "down" one standard deviation would represent a greater magnitude of residual stress for all of the compression stresses. The function that represents this condition is plotted in Fig. 830. The residuals are plotted in Fig. 831.

8.1.2 Residual Stress Traction Functions for CxD2 (7075-T651) Coupons

Residual stress functions were produced for the CxD2 (7075-T651) condition as well. The same process was used and surface plots of the average, "up" and "down" one standard deviation will be provided. These residual stress functions were developed by averaging only the left side of each of the CxD2 (7075-T651) coupons. This would provide a direct comparison of stress between the baseline, uncracked condition, and the fatigue-cracked condition later developed in the Cx4N1-XX-D (7075-T651) coupons. These residual stress traction equations are provided in the Appendix.

8.1.2.1 Residual Stress Function for "Average" CxD2 (7075-T651) Residual Stress from Repeatability Distribution

The residual stress surface plot for the polynomial fit for the CxD2 (7075-T651) average residual stress field is provided in Fig. 832. The surface plot of the residuals are provided in Fig. 833.

8.1.2.2 Residual Stress Function for "Up" One Standard Deviation from the Average CxD2 Residual Stress from Repeatability Distribution

The surface plot for the "up" one standard deviation is provided in Fig. 834. The residuals between the fit and the actual data are provided in Fig. 835.

8.1.2.3 Residual Stress Function for "Down" One Standard Deviation from the Average CxD2 Residual Stress from Repeatability Distribution

The surface plot for the "down" one standard deviation condition on the residual stress is provided in Fig. 836. The residuals are plotted in Fig. 837.

8.2 Selection of Material Model for Fatigue Crack Growth Predictions for Both 2024-T351 and 7075-T651 Material

One of the key components to accurately predict the behavior of a material in the presence of a fatigue crack is the development of a material model. These models come in two main forms, an equation (fit), or a tabular look-up file.[147,148,149,150] For this work one material file was selected for each material (2024-T351 and 7075-T651) to perform all of the fatigue crack growth predictions.

The static properties for the 2024-T351 coupons can be seen in Fig. 838 and for the 7075-T651 material, that is shown in Fig. 839. It should be noted that these static properties may not match those that were used for the development of the FEA, in connection with the calculation of residual stresses.

8.2.1 Tabular Look-up Material File for 2024-T351

The material file that was used for all of the 2024-T351 life predictions was developed from a tabular look-up file which contained three Stress Ratios (Rs), which include -1, 0, and 0.5. The data have a lower da/dN of 1.00e-13 inch/cycle and an upper limit on da/dN at 0.1 inch/cycle. A plot of these three crack growth curves is provided in Fig. 840. As seen in Fig. 840, the data have no “threshold” regions in the lower ΔK range.

8.2.2 Tabular Look-up Material File for 7075-T651

This file was developed from three Stress Ratios (Rs), including -0.33, 0.1, and 0.5. These curves have a lower da/dN of 1.0e-15 inch/cycle and an upper bound of 0.01 inch/cycle. Fig. 841 show these three curves plotted together. The material data for

7075-T651 shows a more vertical drop as it approaches the lower bound of ΔK but no "threshold" value is imposed.

8.3 Fatigue Coupon Geometry for Fatigue Crack Growth Predictions

The modeled fatigue coupon matched the drawing dimensions, as shown in Fig. 204 and in Fig. 206. No statistical analysis was performed on the metrology performed on the coupons, so the nominal drawing dimensions were defined within the model as is common practice.

8.4 Loading Conditions for Fatigue Crack Growth Predictions for 2024-T351 and 7075-T651 with an Open Hole Processed to the "Low" End of the Applied Expansion Specification

For the predictions, two far-field applied stresses were selected. For the CxA2 (2024-T351) material a far-field stress of 25 ksi was applied and for the CxD2 (7075-T651) material a far-field stress of 26.5 ksi was used. For both of these predictions the Stress Ratio (R) was set to 0.1. The coupon was fixed with a "fixed" constraint at one end of the coupon, and the applied load was provided at the opposite end. This can be seen in Fig. 842.

8.5 Initial Flaw Size and Shape for All Fatigue Life Predictions

For all of the predictions the IFS was set to a semi-circular flaw which had a surface crack length of 0.04083 inch and a bore length of 0.0486 inch.[56] This IFS was applied based on fractographic work performed on Cx holes which were notched and then final reamed to remove any evidence of the wire EDM notch. The simulated crack

within StressCheck® had eleven points distributed about the arch length and for the IFS these points were not evenly distributed along that arch, as shown in Fig. 843. However, BAMF redistributes them evenly after the first simulated growth increment. An image of this IFS meshed within the StressCheck® model is provided in Fig. 844.

8.6 Application of Residual Stress Equation as a "Loaded Crack" Traction Stress

As shown in Fig. 842 a far-field stress was applied to each model, but in addition to this far-field traction stress, a local "Loaded Crack" traction stress was applied. This local stress was centered at the nucleation system for the simulated fatigue crack. This X,Y=0,0 location was referenced to the same coordinate axis as residual stress function that was developed, and outlined in section 8.1. The application of this local traction stress is visualized within StressCheck® as shown in Fig. 845 for a crack of approximate length 0.05 inch along the surface. Then in Fig. 846 a similar CIM-LC is applied for a crack that was much larger. Each of the functions developed to represent the residual stress field for the baseline, uncracked conditions as outlined previously.

8.6.1 Contour Stress Plots of Applied Residual Stress Traction Functions within StressCheck®

In an effort to ensure that the residual stress fields that were developed and applied to StressCheck® as a "Loaded Crack" each residual stress equation was visualized by a contour plot within StressCheck®. This was done for both of the material coupon configurations, CxA2 (2024-T351) and CxD2 (7075-T651) and also for the three residual stress distributions that were developed, average, one standard deviation "down" and one

standard deviation “Up”. Within the body of this report only the average residual stress contour plots are provided for each material. These can be seen in Fig. 847 for the CxA2 (2024-T351) average residual stress condition, and in Fig. 848 for the average condition in the CxD2 (7075-T651) material condition. All of the other baseline residual stress contour plots are provided in the Appendix.

8.7 Meshing Parameters for the Initial Condition within StressCheck® and BAMF

All of the StressCheck® models had the main part meshed using the “auto mesh” feature. The crack front then was meshed separately. The simulated crack is first defined within the “mesh” parameter as a “crack face” and then the spline that defines the front of the crack was meshed using a “boundary layer” mesh refinement. Within StressCheck® the mesh parameters are input within the StressCheck Input -> Mesh tab. Within that tab the “create” “mesh” “bndy. layer” drop-downs must be selected, and this is shown in Fig. 849. For models that are run through BAMF the crack front boundary layer mesh refinement is hard coded. The parameters for this mesh definition is provided are Table 9.

8.8 Fatigue Crack Growth Prediction Results for CxA2 (2024-T351) and CxD2 (7075-T651) Using BAMF

Fatigue crack growth predictions were produced for three residual stress conditions for both the CxA2 (2024-T351) and the CxD2 (7075-T651) coupon conditions. The residual stress functions used for these predictions represented the average residual stress on the left side of the Cxed hole. Table 10 provides a breakdown

of the fatigue life predictions that were performed for the baseline CxA2 (2024-T351) and CxD2 (7075-T651) residual stress conditions. The lives provided are to a fatigue crack length of 0.51 inch. This final crack size was selected due to the rate at which the fatigue crack is propagating at this size for this geometry. This crack length represents over 99.99 percent of the total life of the coupon. In addition to this there were fatigue cracks that were propagated to this size for the Cx4N1 conditions, for both materials, and so it was desired to include this residual stress field into future fatigue crack growth predictions.

8.8.1 Fatigue Crack Growth Predictions for the CxA2 (2024-T351) Coupon Configuration

As shown in Table 10, three fatigue life predictions were performed for the CxA2 (2024-T351) condition, in an effort to quantify the effect of residual stress distribution on the life predicted. The residual stress distribution that was applied to adjust the average residual stress field was the “repeatability” standard deviation, not the “single measurement” standard deviation or uncertainty. The life predictions for the CxA2 (2024-T351) condition are provided in Fig. 850. In addition to providing the life predictions for this condition, the average predicted life was produced by the three residual stress fields, and a standard deviation, or uncertainty was determined. This is shown in Fig. 851

In addition to the total number of cycles and the shape of the fatigue crack growth curve, a plot of the crack growth rate versus the Cx mandrel fatigue crack length (c) was plotted in Fig. 852. This plot provides additional insight into the range of crack growth rates that are calculated at the Cx mandrel surface across the range of crack sizes

produced in the BAMF run. The final plot that was produced for these life predictions is one that provides a look at the change SIF (ΔK) compared to the crack growth rate (dc/dN) at the Cx mandrel entrance surface. This plot is provided in Fig. 853. From these plots it is possible to understand not only the crack life, but the rates and crack driving force at the Cx mandrel entrance surface.

8.8.2 Fatigue Crack Shape Predictions for the CxA2 (2024-T351) Coupon Configuration

In addition to the Cx mandrel surface length versus cycles being provided by BAMF, it is also possible to develop a plot that shows the fatigue crack shape evolution from the IFS to the final fracture size. Three of these plots are provided to represent the predicted shape for the three residual stress distributions that were developed, average, "up" one standard deviation, and "down" one standard deviation. These fatigue crack growth shape curves are shown in Fig. 854 through Fig. 856.

8.8.3 Fatigue Crack Growth Predictions for the CxD2 (7075-T651) Coupon Configuration

In addition to the prediction made for the CxA2 (2024-T351) material condition, three fatigue crack growth predictions were developed for the CxD2 (7075-T651) material. As provided in Table 10 the far-field stress was 26.5 ksi, with a R = 0.1. Three residual stress distributions were used to develop the "Loaded Crack" face traction stress, the average, adjusted "down" one standard deviation, and also adjusted "up" one standard deviation. The residual stress functions for these are shown in Fig. 832 through Fig. 837. A crack growth prediction for this condition is provided in Fig. 857, showing the effect of

the residual stress distribution on the predicted fatigue life. In addition to providing the life predictions for this condition, the average predicted life was produced by the three residual stress fields, and a standard deviation, or uncertainty was determined. This is shown in Fig. 858.

In addition to the total number of cycles and the shape of the fatigue crack growth curve, a plot of the crack growth rate versus the Cx mandrel fatigue crack length (c) was plotted in Fig. 859. This plot provides additional insight into the range of crack growth rates that are calculated at the Cx mandrel surface across the range of crack sizes produced in the BAMF run. The final plot that was produced for these life predictions is one that provides a look at the change SIF (ΔK) compared to the crack growth rate (dc/dN) at the Cx mandrel entrance surface. This plot is provided in Fig. 860. From these plots it is possible to understand not only then crack life, but the rates and crack driving force at the Cx mandrel entrance surface.

8.8.4 Fatigue Crack Shape Predictions for the CxD2 (7075-T651) Coupon Configuration

A prediction of the crack shape evolution for this condition was developed and is provided in Fig. 861 through Fig. 863.

From these crack shape predictions, it is possible to see that due to the residual stress field that is imposed the fatigue crack no longer propagates in a semi-elliptical shape as it progresses away from the initial crack size. From these it shows that there should be some amount of “pinning” of the crack along the bore of the hole, between the 0.05 inch initial crack size and 0.1 inch away from the Cx mandrel entrance surface. This type of “pinning” is shown in the predictions for all three of the residual stress field

distributions and for both of the materials. The main difference is only the number of cycles that it takes to push through this location and propagate through the thickness of the part. This type of fatigue crack evolution has been demonstrated in the literature, as shown in Fig. 864. Thus the predictions of the crack shape were producing results that were matching those seen in other test. These predictions however needed to be compared to test results.

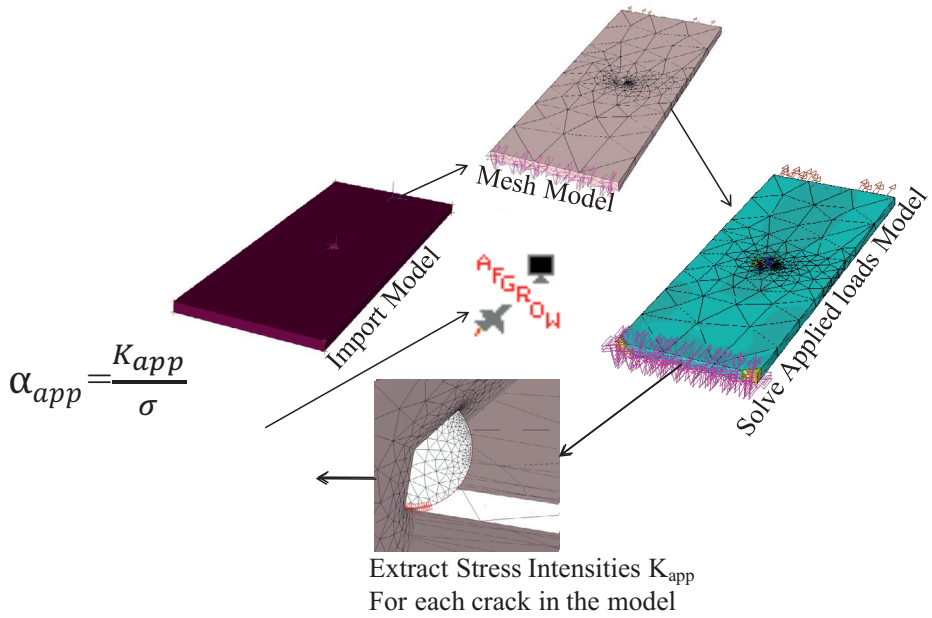

Fig. 822 Breakdown of Process within StressCheck® for Implementation of BAMF for a Model without Residual Stress.[139]

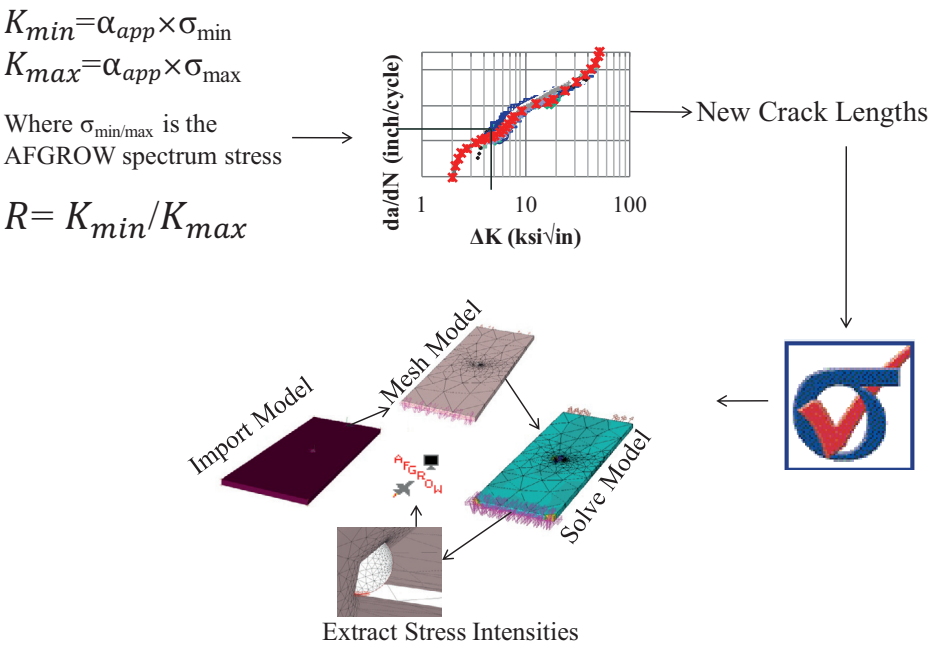

Fig. 823 Breakdown of Process for the Passing of Information to AFGROW for Development of da/dN and Crack "Propagation" within StressCheck® without a Residual Stress Applied to the FEA.[139]

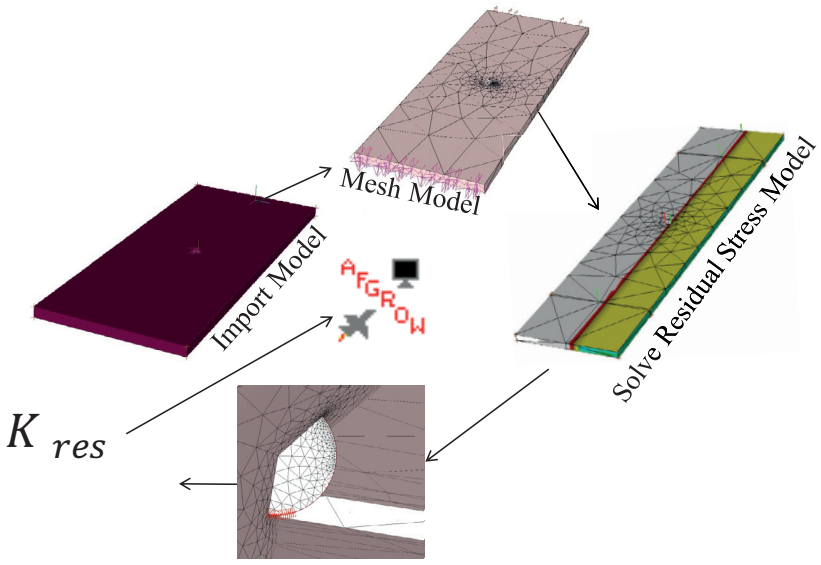

Fig. 824 Breakdown of Process within StressCheck® for Implementation of BAMF for Model with an Applied Residual Stress.[139]

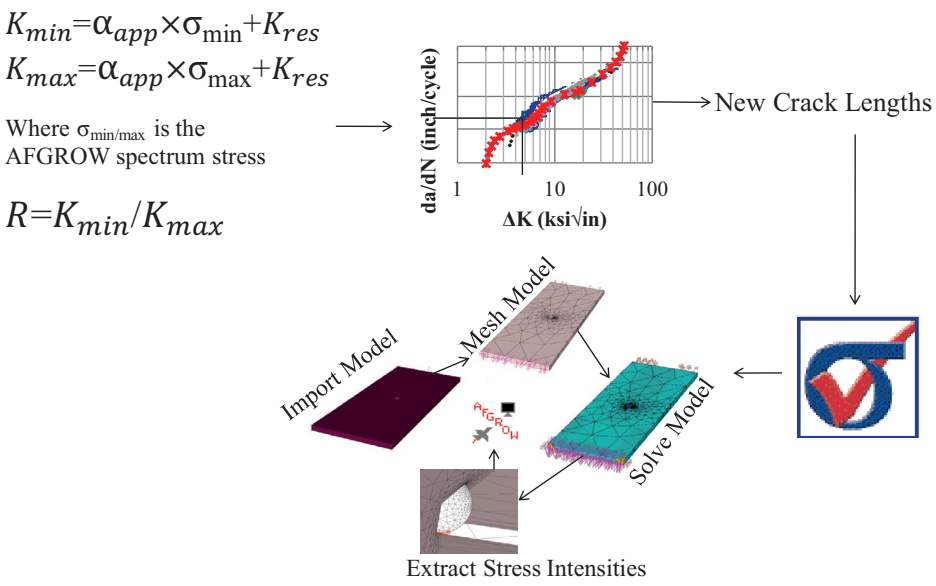

Fig. 825 Breakdown of Process for the Passing of Information to AFGROW for the Development of da/dN and Crack "Propagation" within StressCheck® with and a Residual Stress Applied to FEA.[139]

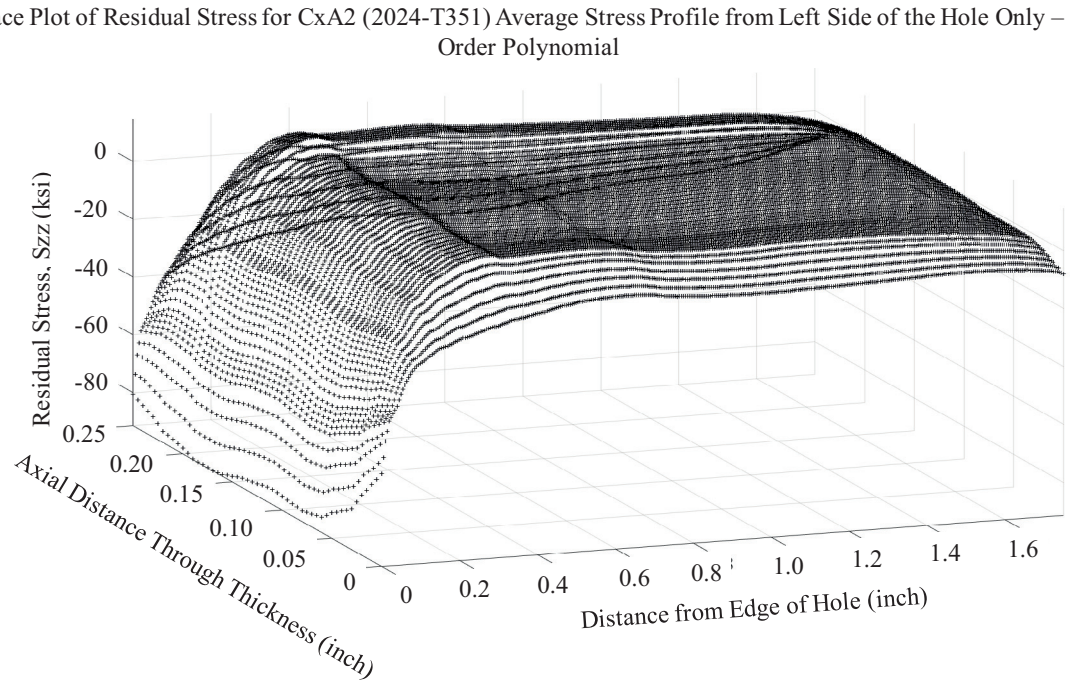

Fig. 826 Surface Plot of Residual Stress Traction Function Developed for the "Average" of the Left Side of the Hole for the Residual Stress Condition CxA2 (2024-T351).

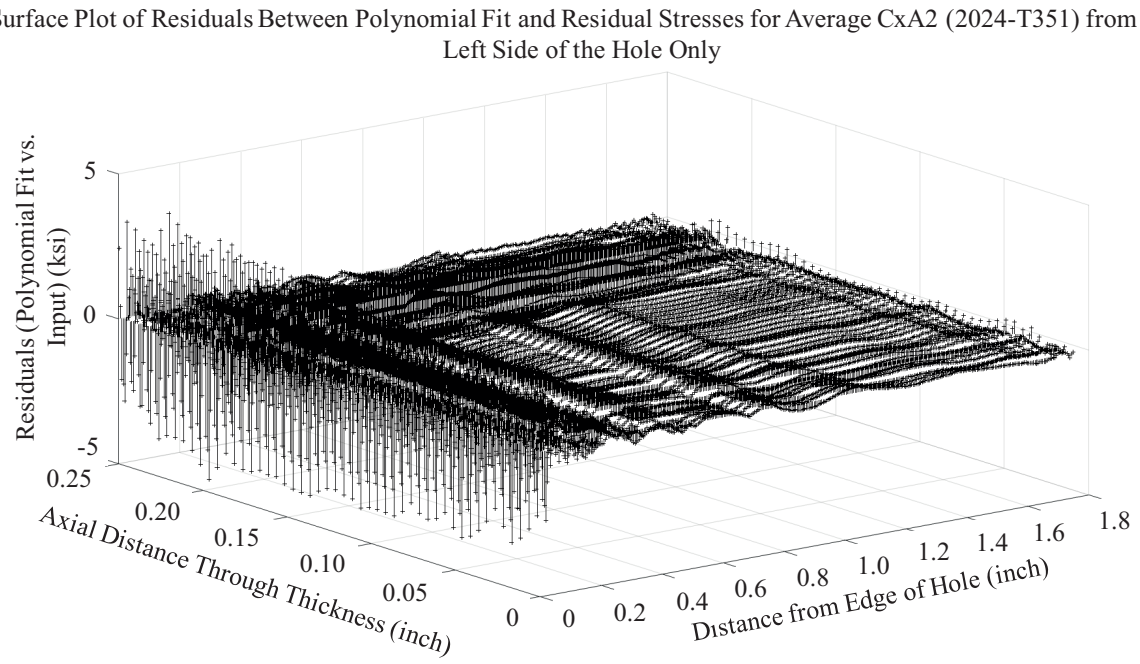

Fig. 827 Surface Plot of the Residual between the Polynomial Fit and the Actual Residual Stress Data for the “Average” of the Left Side of the Hole for the Residual Stress Condition CxA2 (2024-T351).

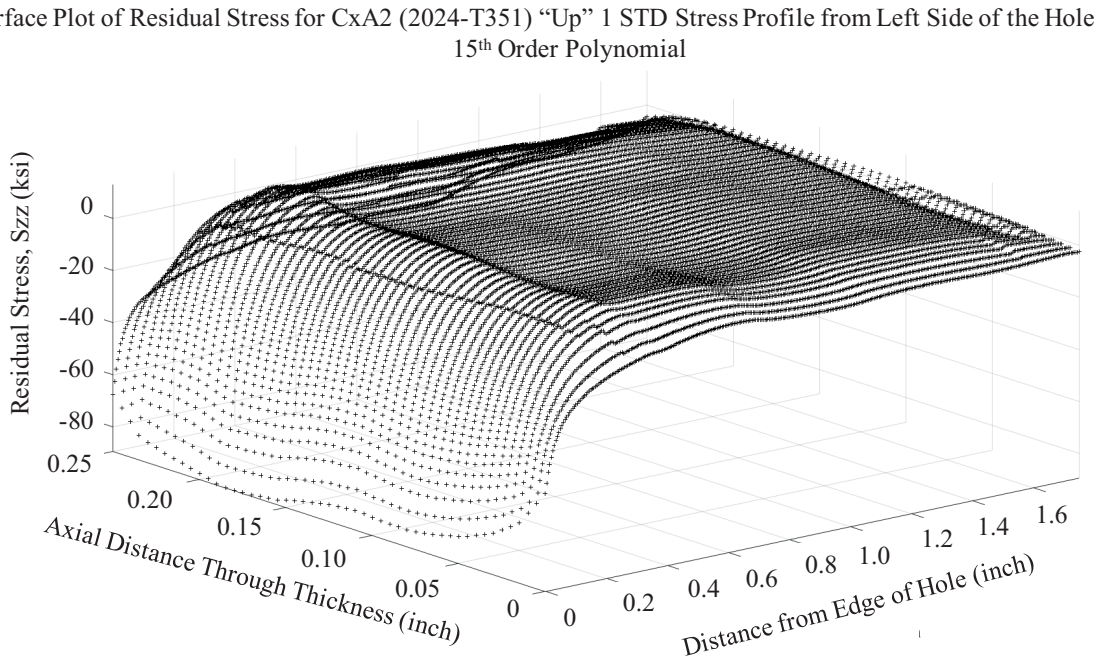

Fig. 828 Surface Plot of Residual Stress Traction Function Developed for the "Up" One Standard Deviation for the Left Side of the Hole for the Residual Stress Condition CxA2 (2024-T351).

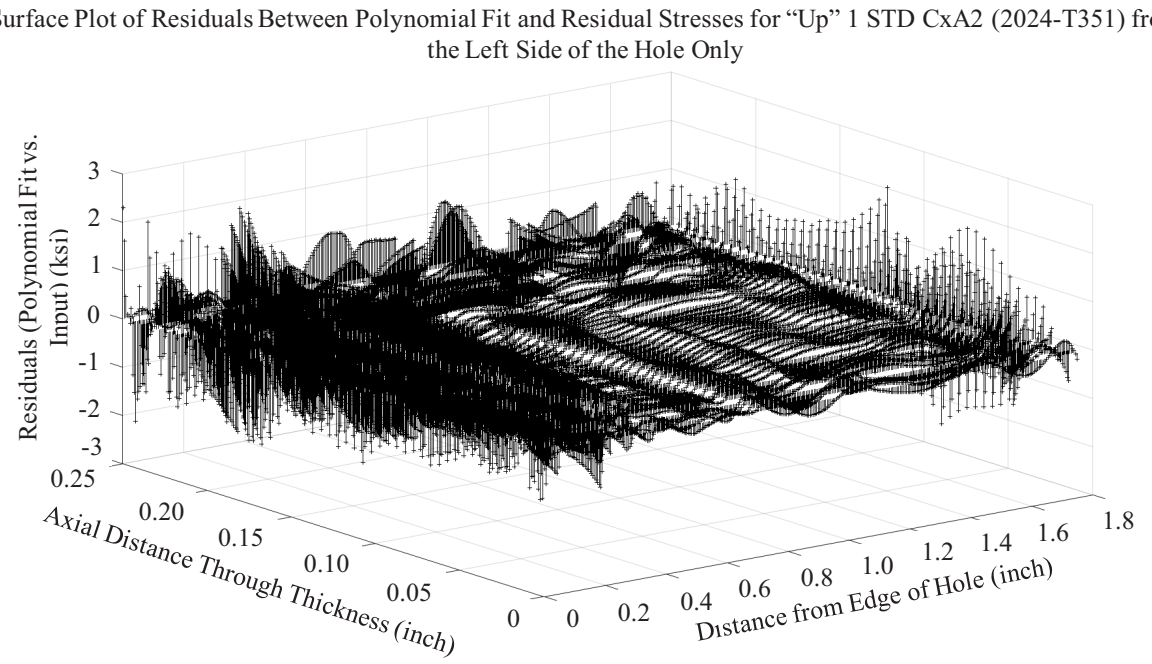

Fig. 829 Surface Plot of the Residual between the Polynomial Fit and the Actual Residual Stress Data for the "Up" One Standard Deviation for the Left Side of the Hole for the Residual Stress Condition CxA2 (2024-T351).

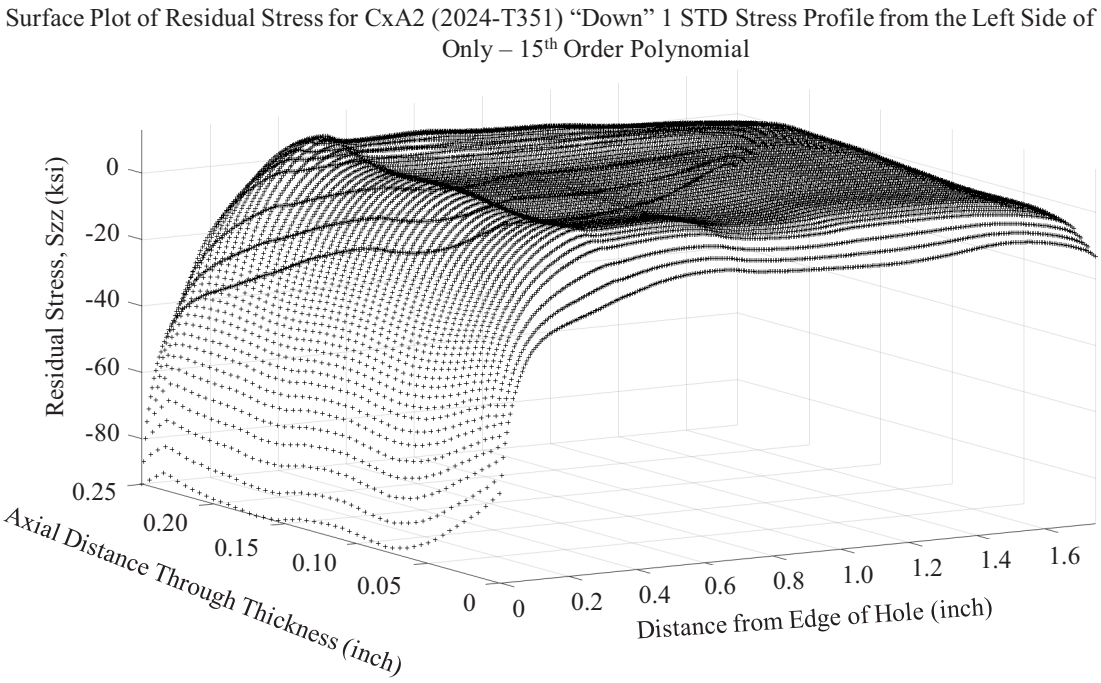

Fig. 830 Surface Plot of Residual Stress Traction Function Developed for the "Down" One Standard Deviation for the Left Side of the Hole for the Residual Stress Condition CxA2 (2024-T351).

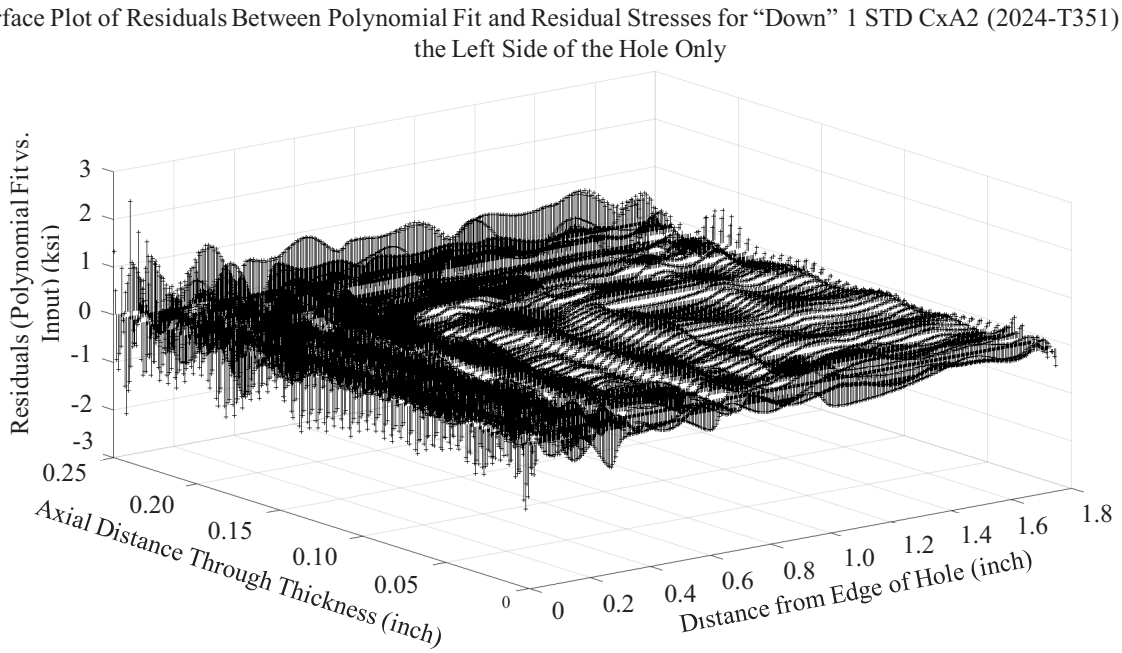

Fig. 831 Surface Plot of the Residual between the Polynomial Fit and the Actual Residual Stress Data for the "Down" One Standard Deviation for the Left Side of the Hole for the Residual Stress Condition CxA2 (2024-T351).

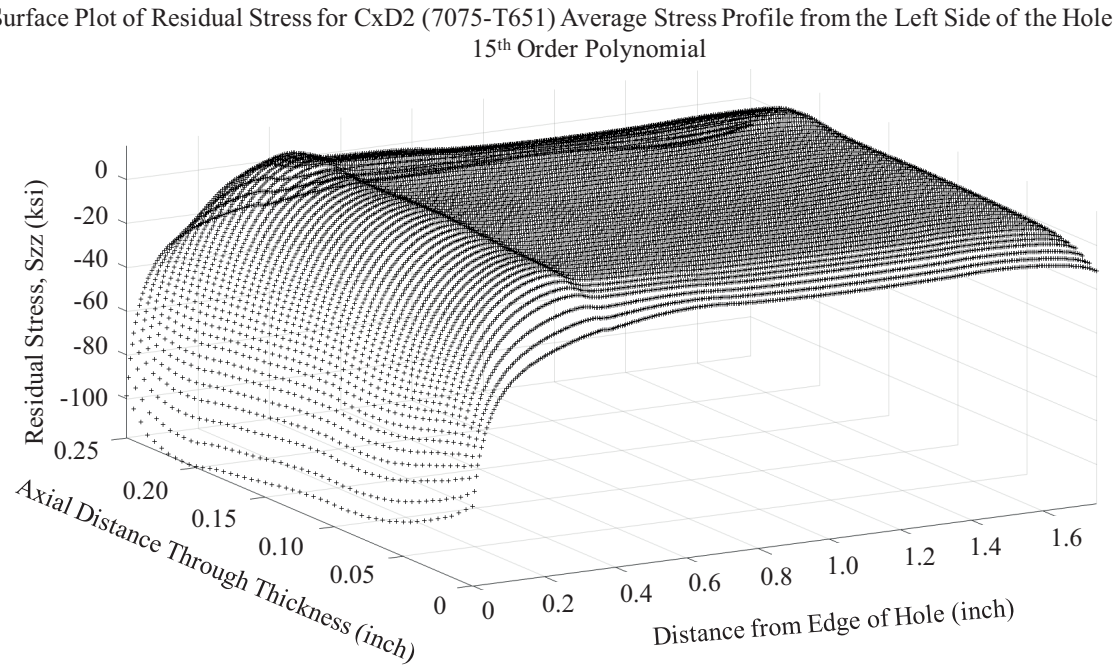

Fig. 832 Surface Plot of Residual Stress Traction Function Developed for the Left Side of the Hole for the "Average" Residual Stress Condition CxD2 (7075-T651).

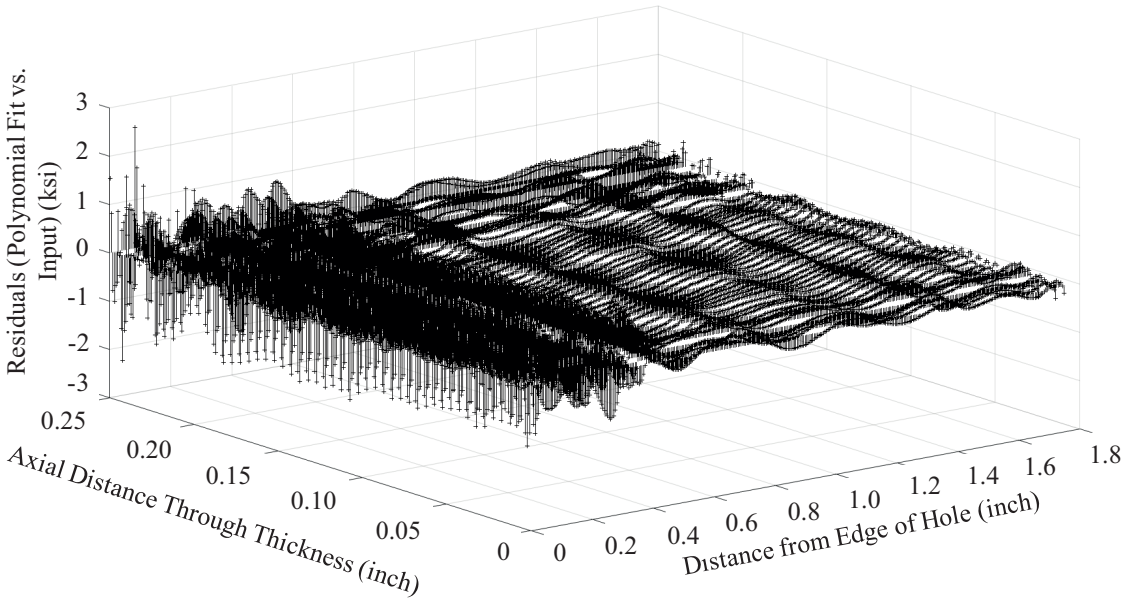

Fig. 833 Surface Plot of the Residual between the Polynomial Fit and the Actual Residual Stress Data for the Left Side of the Hole for the "Average" Residual Stress Condition CxD2 (7075-T651).

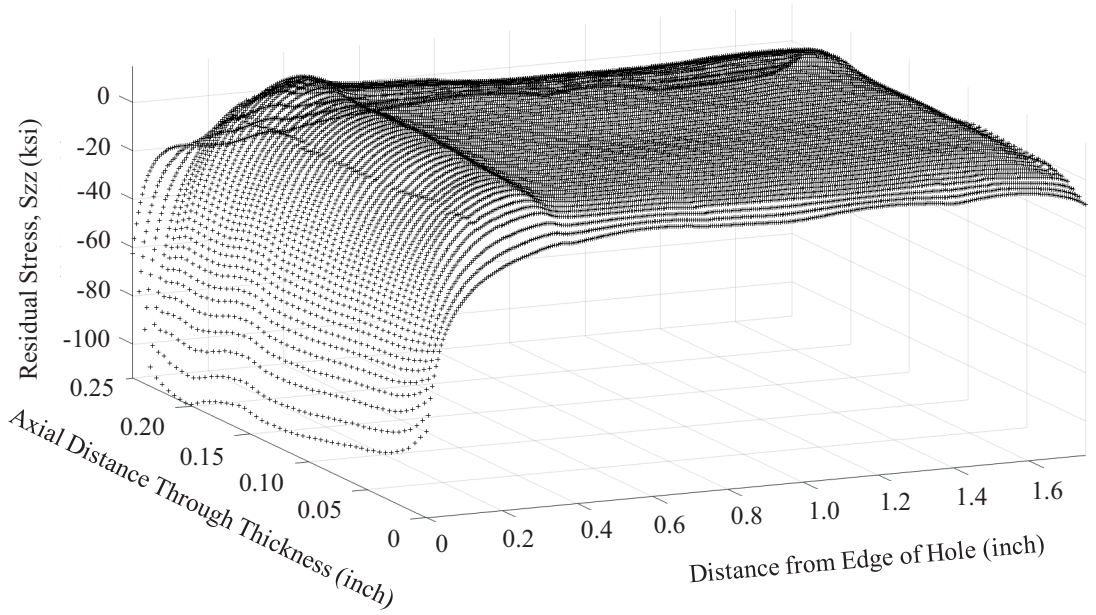

Fig. 834 Surface Plot of Residual Stress Traction Function Developed for the "Up" One Standard Deviation for the Left Side of the Hole for the Residual Stress Condition CxD2 (7075-T651).

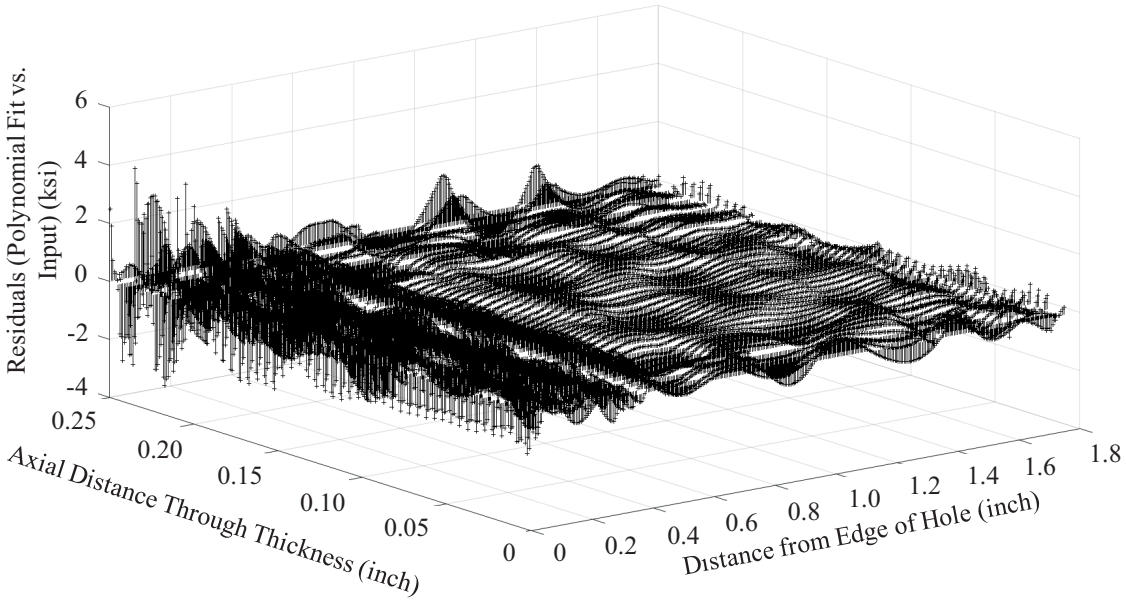

Fig. 835 Surface Plot of the Residual between the Polynomial Fit and the Actual Residual Stress Data for the "Up" One Standard Deviation for the Left Side of the Hole for the Residual Stress Condition CxD2 (7075-T651).

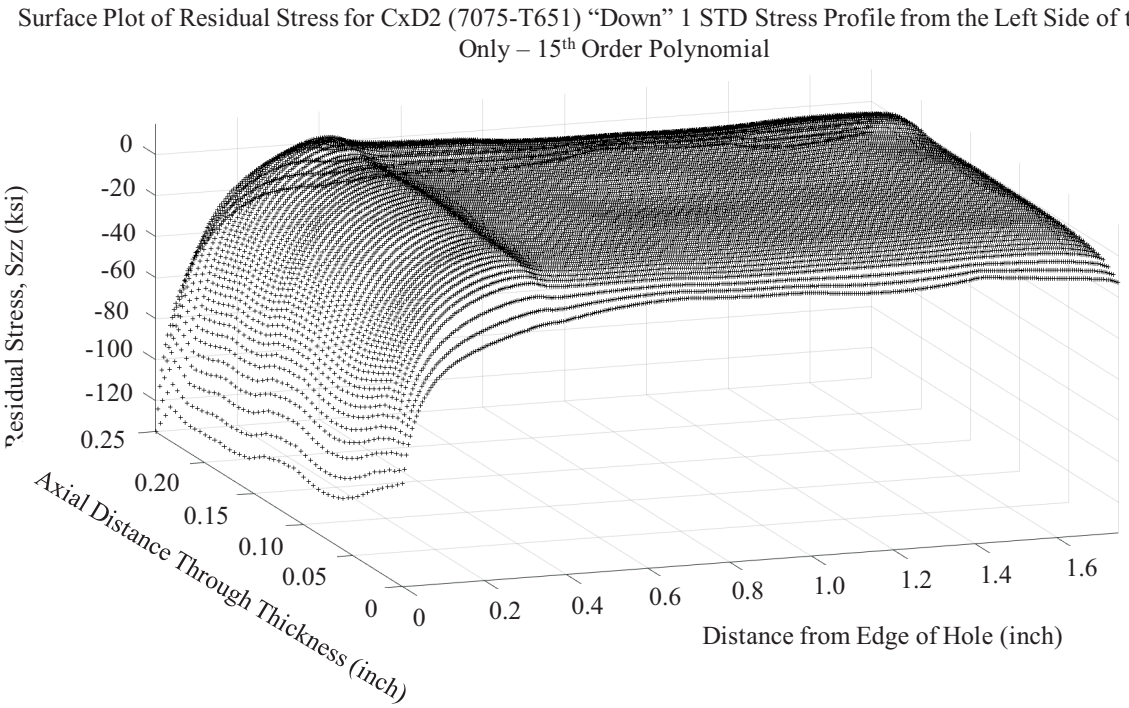

Fig. 836 Surface Plot of Residual Stress Traction Function Developed for the "Down" One Standard Deviation for the Left Side of the Hole for the Residual Stress Condition CxD2 (7075-T651).

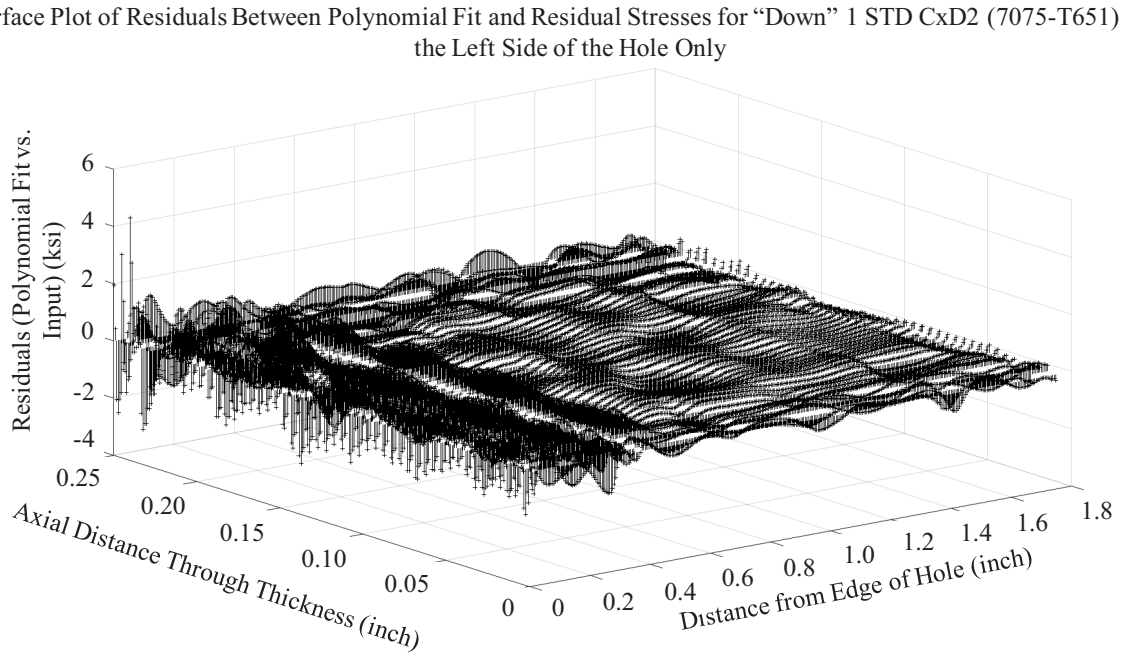

Fig. 837 Surface Plot of the Residual between the Polynomial Fit and the Actual Residual Stress Data for the "Down" One Standard Deviation for the Left Side of the Hole for Residual Stress Condition for CxD2 (7075-T651).

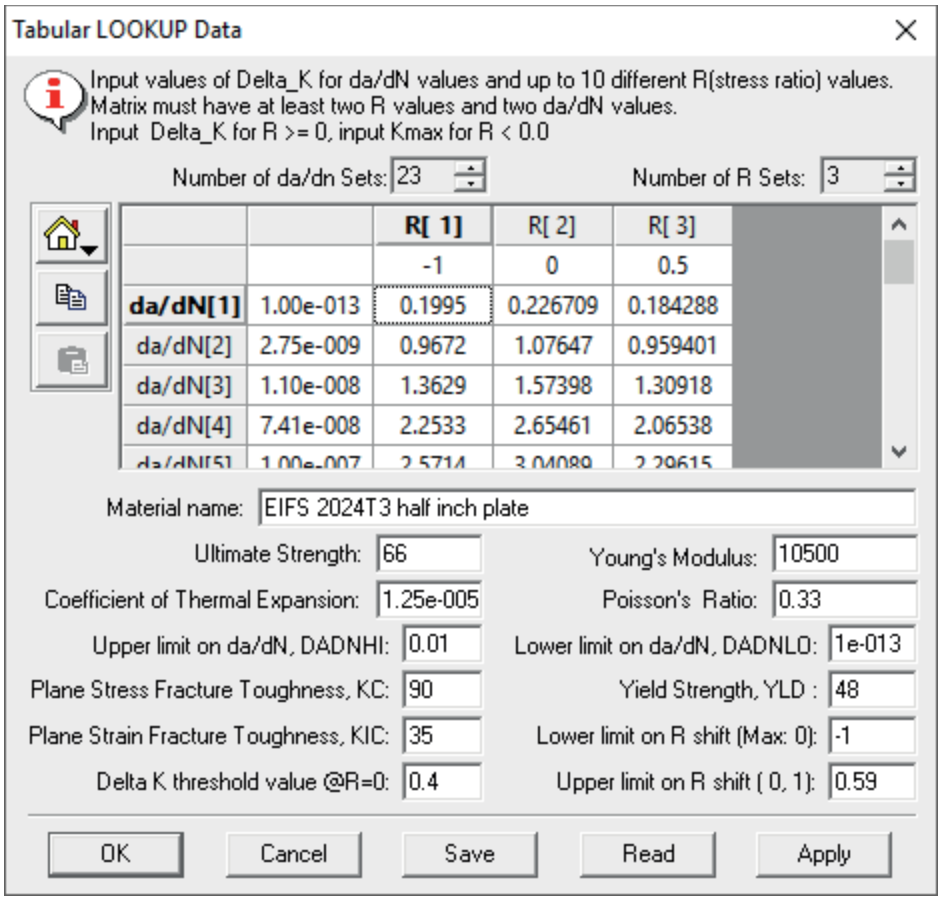

Fig. 838 Static Material Properties for the 2024-T351 Material Used for all Fatigue Crack Growth Predictions.

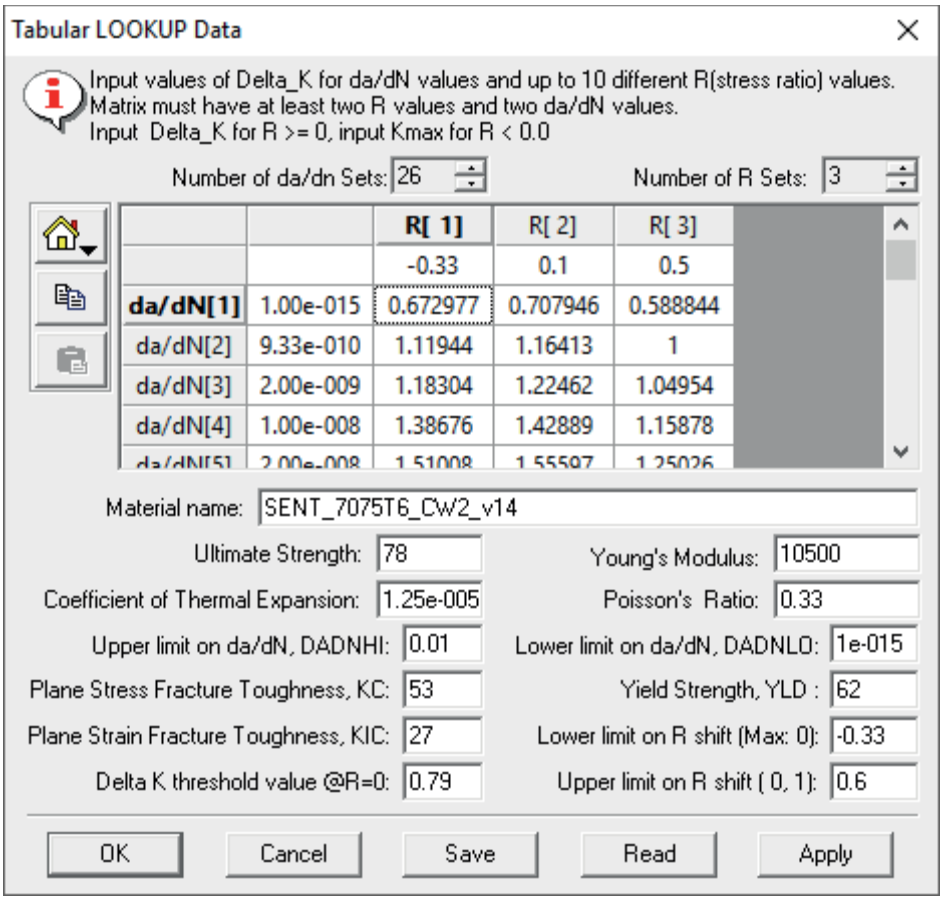

Fig. 839 Static Material Properties for the 7075-T651 Material Used for all Fatigue Crack Growth Predictions.

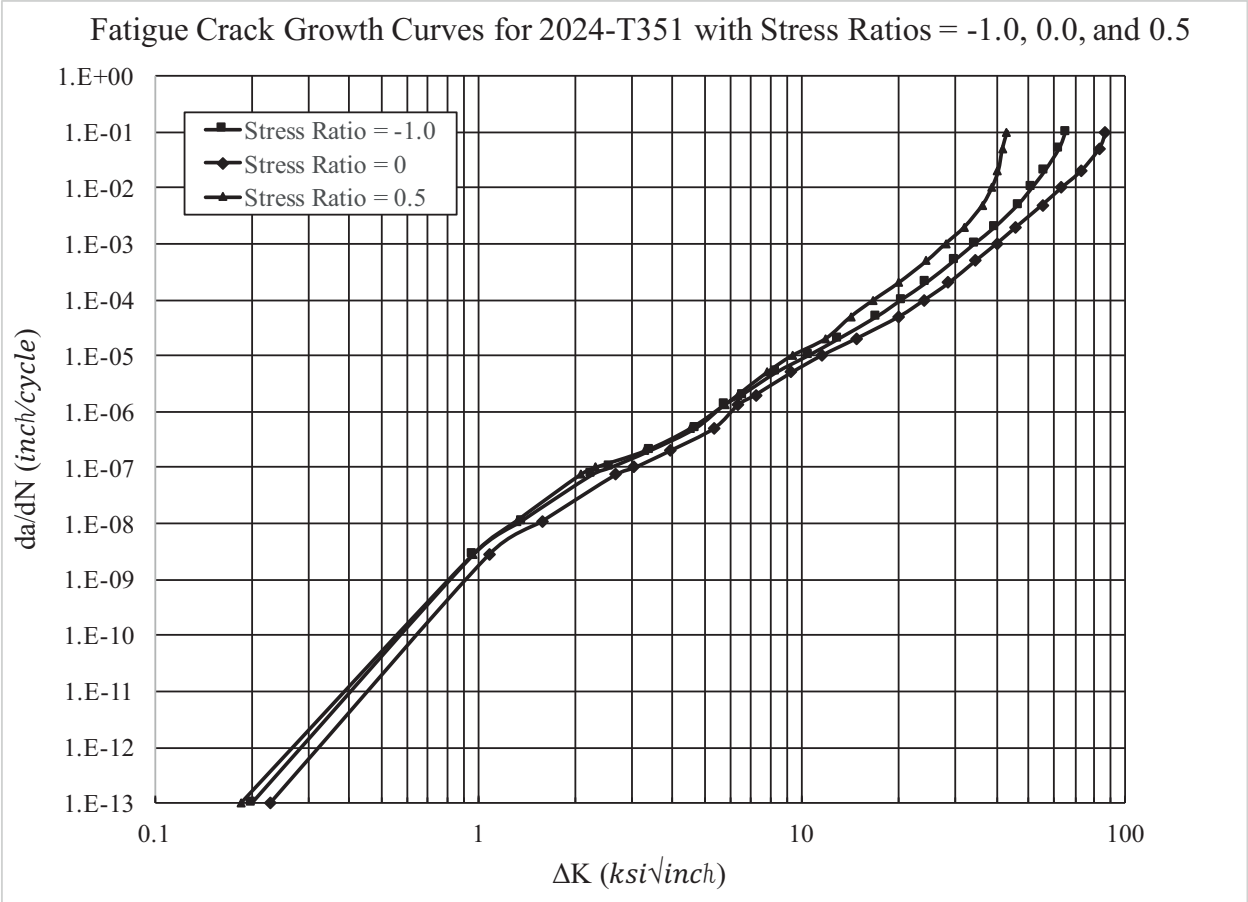

Fig. 840 Fatigue Crack Growth Curves Used for all 2024-T351 Fatigue Crack Growth Predictions.

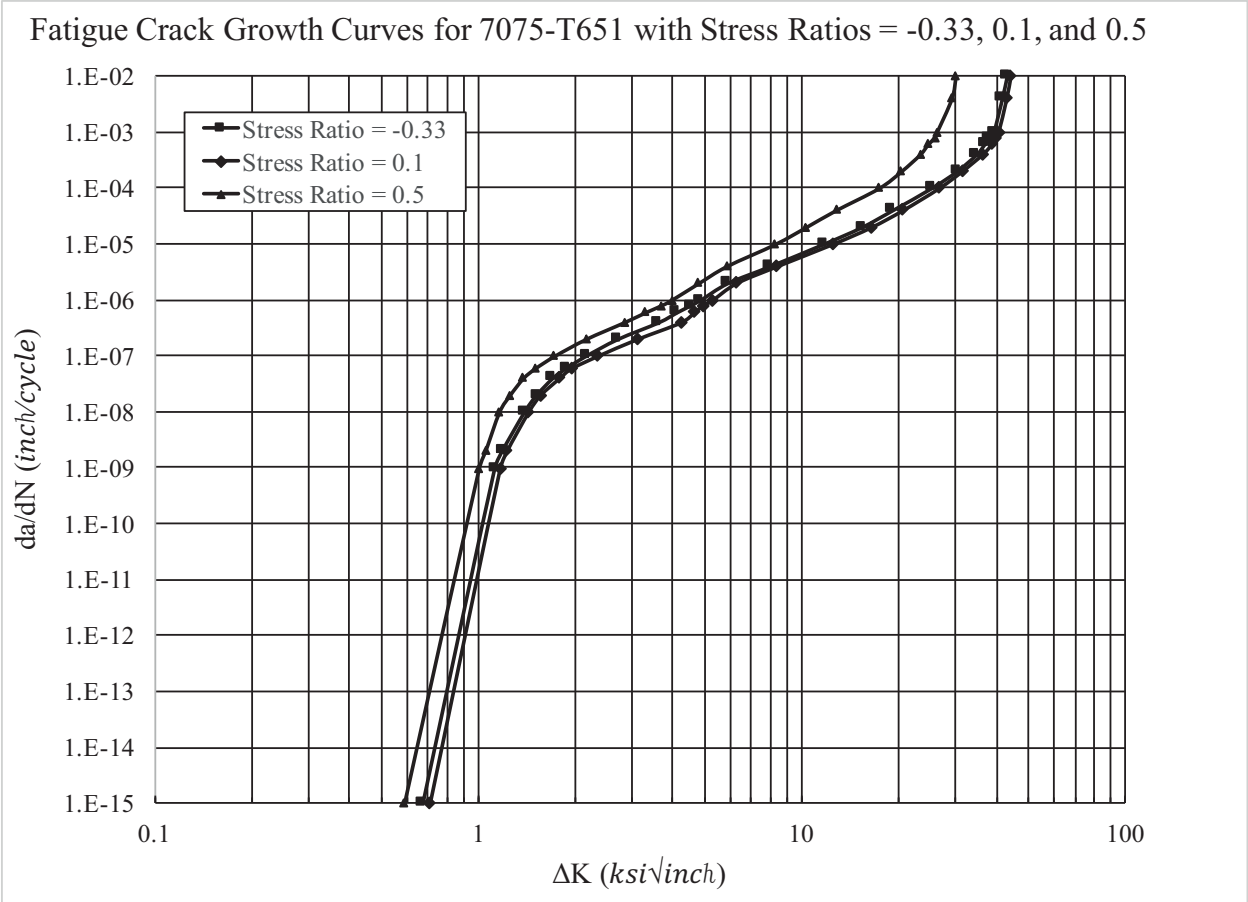

Fig. 841 Fatigue Crack Growth Curves Used for all 7075-T651 Fatigue Crack Growth Predictions.

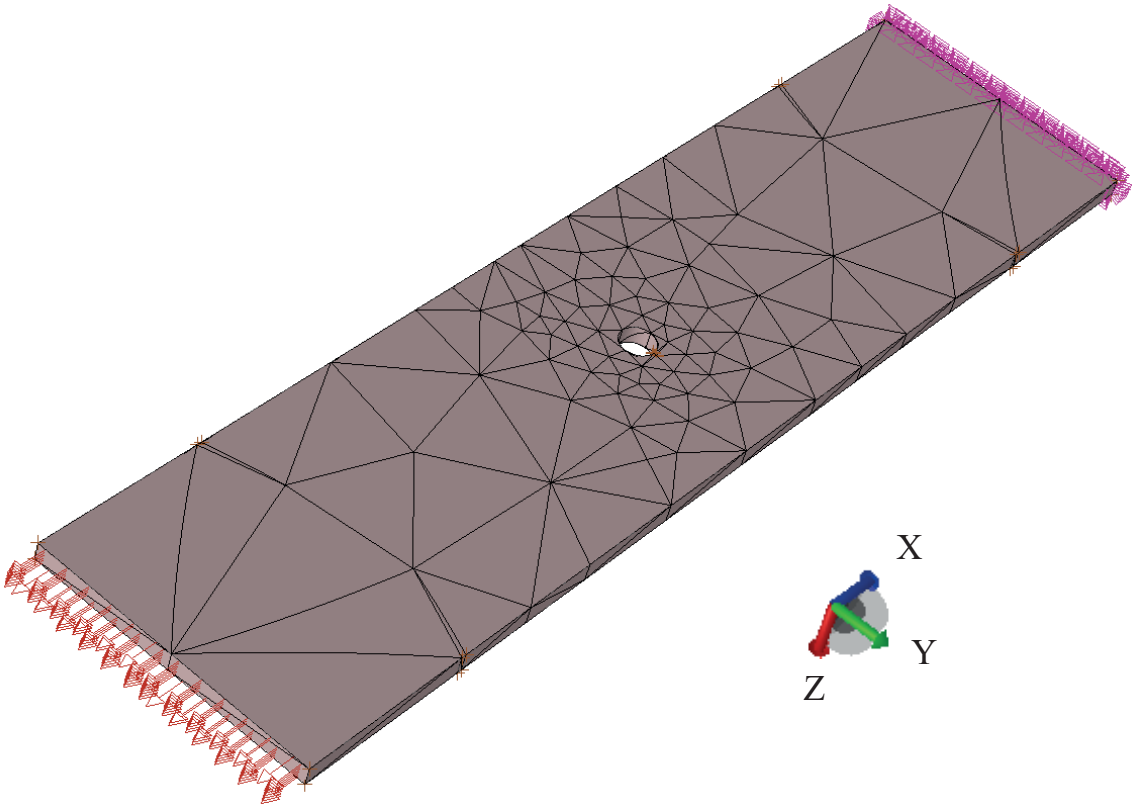

Fig. 842 Image of the Meshed Simulated Fatigue Coupon Showing the Body “Automesh” within StressCheck®.

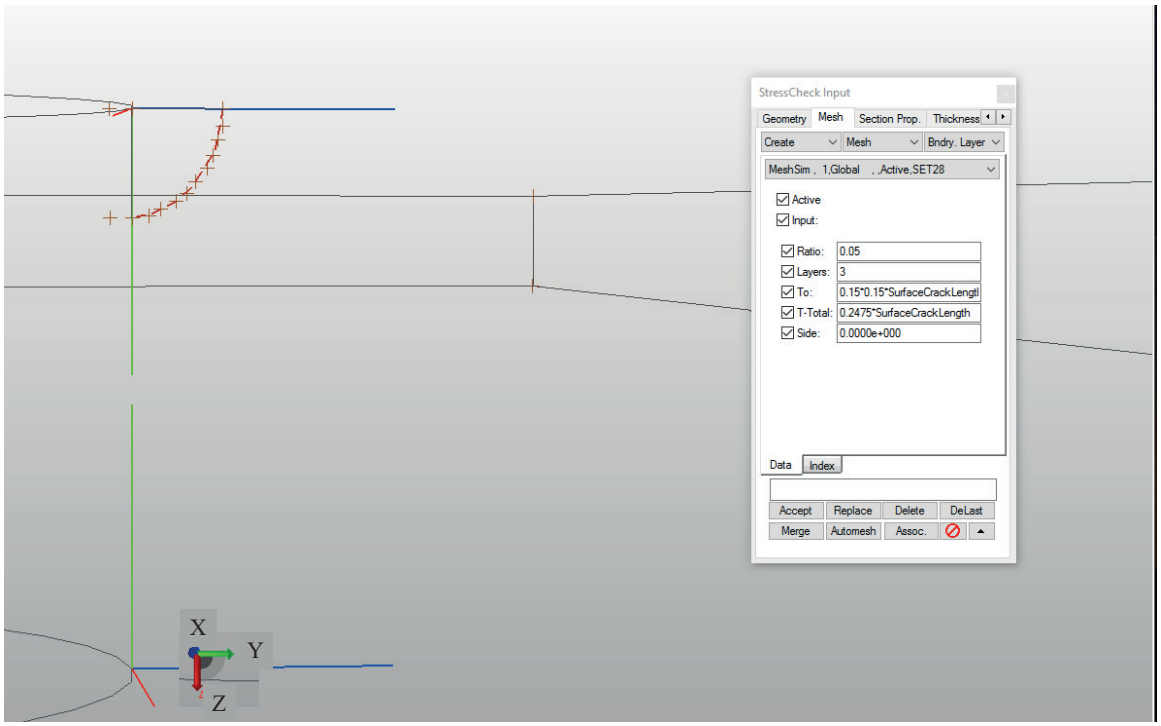

Fig. 843 Image of Simulated Cack Front within StressCheck®/BAMF Showing Location of Spatial Points Along Crack Front.

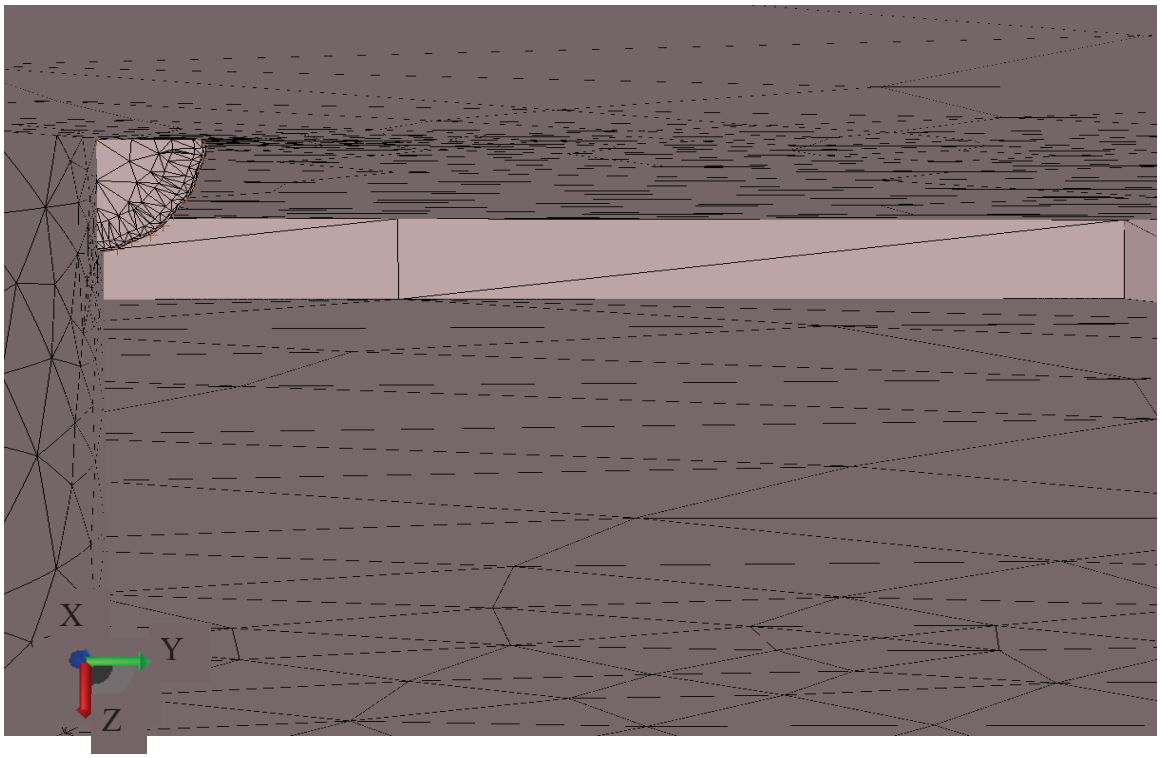

Fig. 844 Image of Simulated Crack Front within StressCheck®/BAMF Showing Mesh Density at the Crack Front.

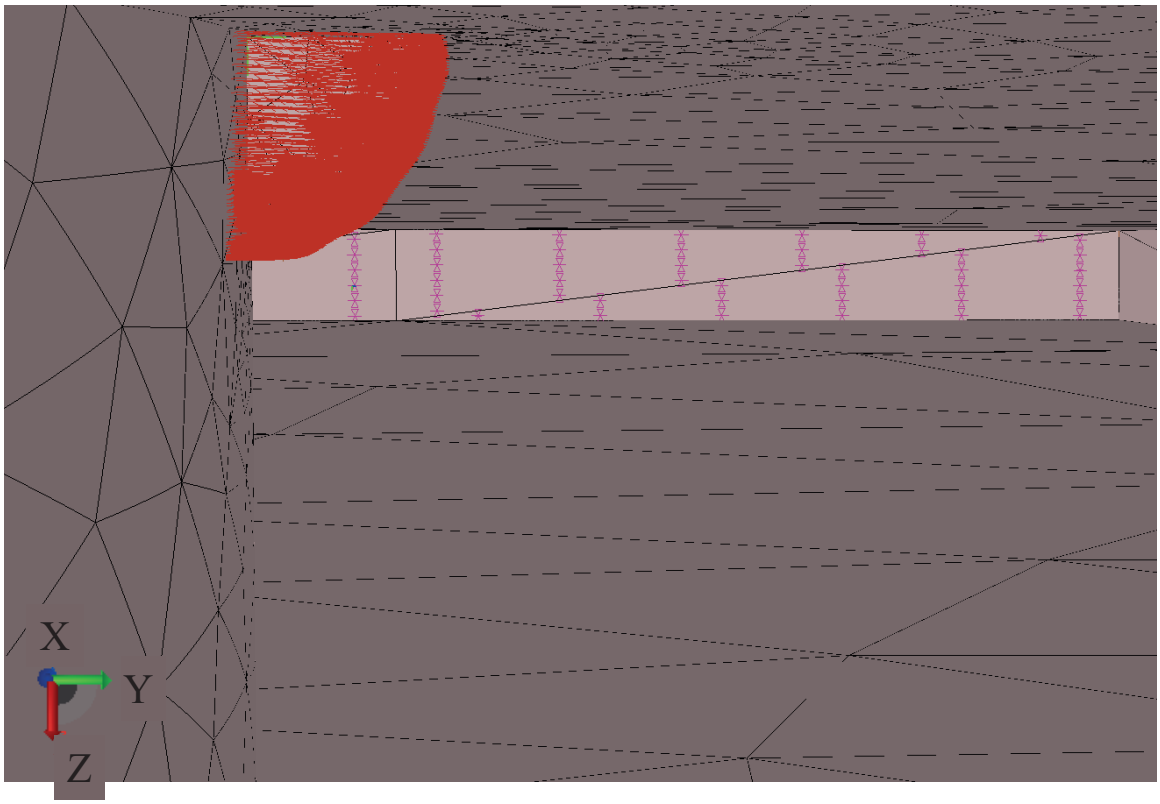

Fig. 845 Image of Simulated Fatigue Crack of Approximate Size 0.05 inch at the Cx Mandrel Entrance Surface with the Residual Stress Traction Applied as the “Loaded Crack” Front.

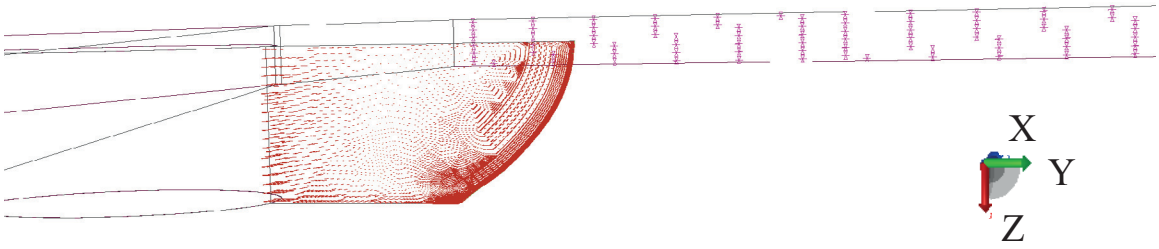

Fig. 846 Image of Simulated Fatigue Crack of Approximate size 0.50 inch on Cx Mandrel Entrance Surface and 0.30 inch on Cx Mandrel Exit Surface.

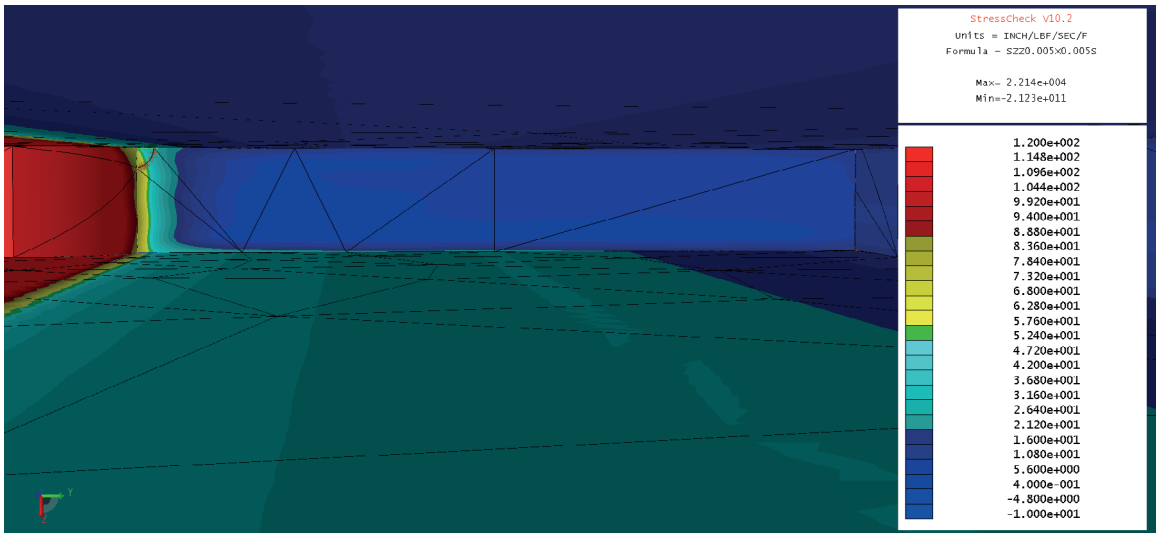

Fig. 847 Residual Stress Contour Plot of Applied Crack Face Traction as a “Loaded Crack” for the Average Residual Stress Condition in the CxA2 (2024-T351) Material.

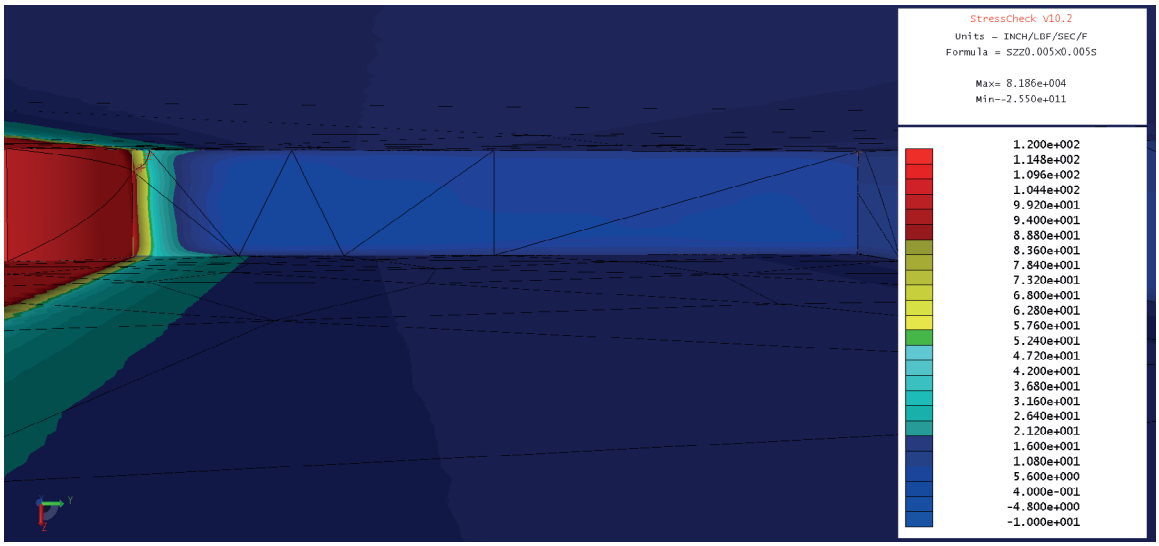

Fig. 848 Residual Stress Contour Plot of Applied Crack Face Traction as a “Loaded Crack” for the Average Residual Stress Condition in the CxD2 (7075-T651) Material.

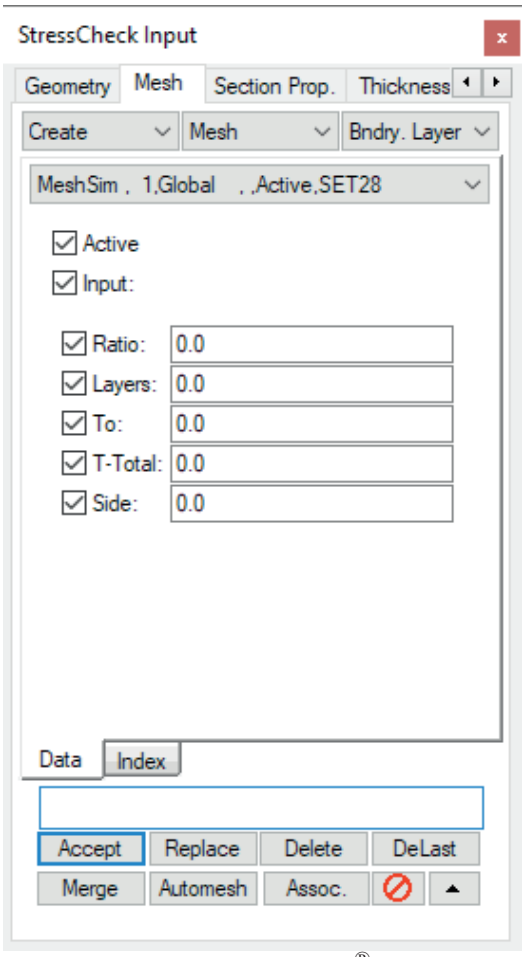

Fig. 849 Mesh Parameters Input within StressCheck® for Boundary Layer Refinement.

Table 9 Crack Front Boundary Layer Refinement Parameters for Defining Initial Mesh Density for BAMF/StressCheck®

	Number of Points Along Crack Front (NumPoints)	Minimum Crack Length Along Crack Front (inch) (MinCrackLength)	Number of Mesh Layers	To	T_Total	Ratio
Initial Crack Size	11	0.04083	2	0.15 x 0.15 x (MinCrackLength)	4 x To	1.25 x (NumPoints)

Table 10 Configuration of Fatigue Life Predictions for CxA2 (2024-T351) and CxD2 (7075-T651) Coupons – Residual Stress Function Defined by Left Side of Baseline, Uncracked Cxed Hole

Material	Initial Flaw Size (inch)	Residual Stress Distribution	Sides of Hole Averaged	Far Field Stress (ksi)	Stress Ratio	Predicted Life (cycles)
2024-T351	0.04083x0.0486	Average	Left Side Only	25	0.1	112,950
		Down				206,420
		Up				75,521
7075-T651		Average		26.5		338,408
		Down				1,247,000
		Up				213,479

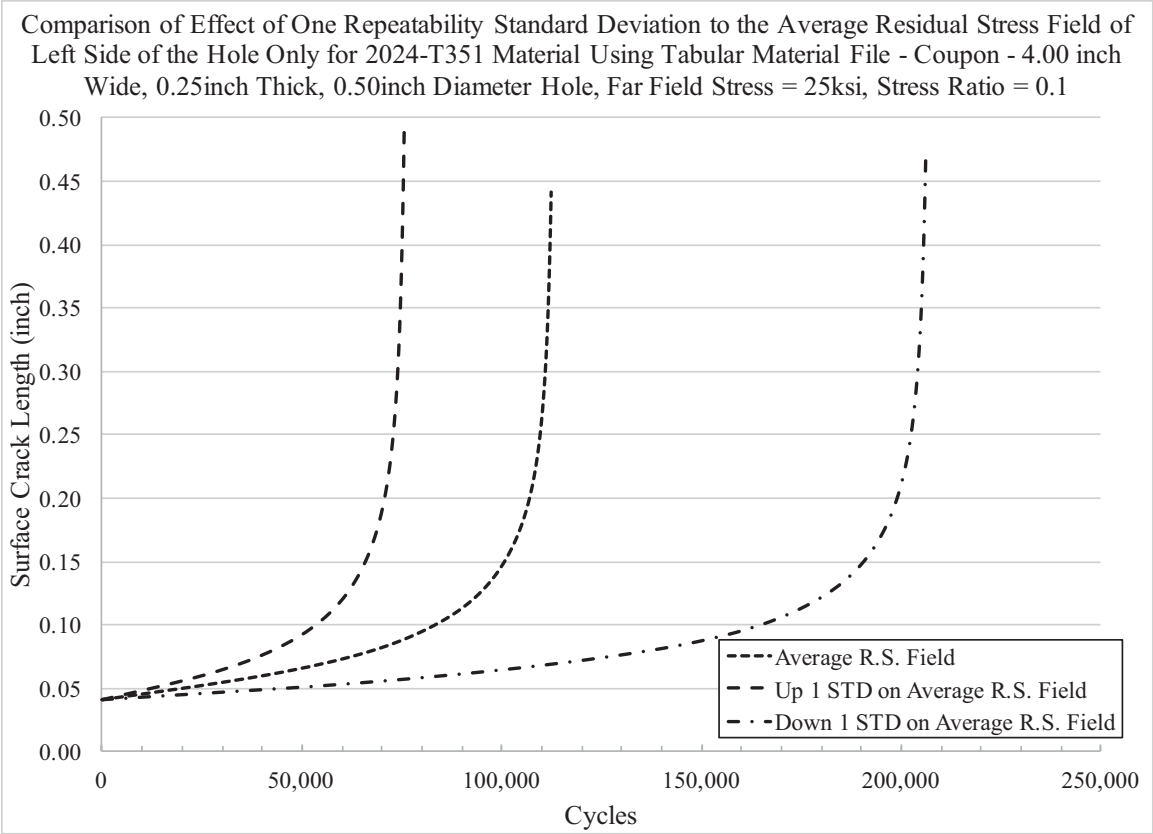

Fig. 850 Fatigue Life Prediction of CxA2 (2024-T351) Coupon Configuration, Cxed to the “Low” End of the Applied Expansion Specification, Using Three Residual Stress Distributions.

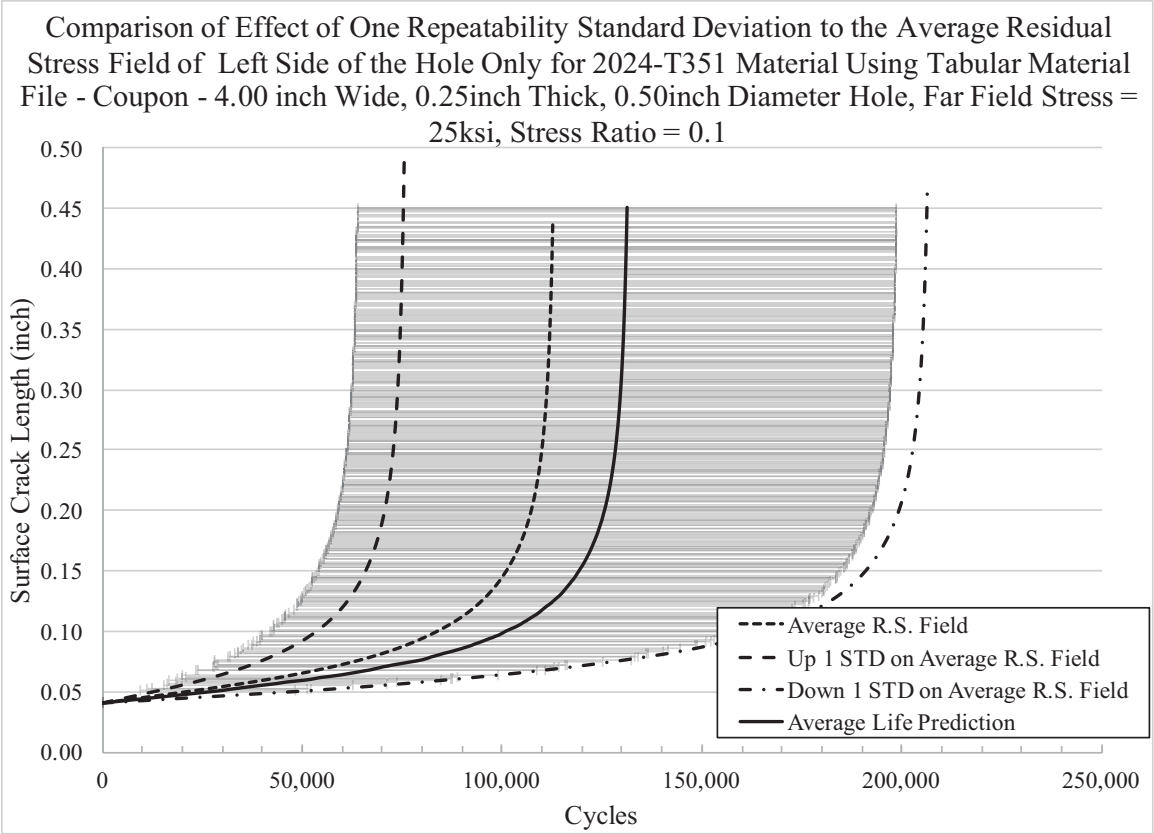

Fig. 851 Additional Statistics Provided for the Fatigue Life Predictions for the CxA2 (2024-T351) Coupon Configuration, Showing the Average Life Prediction Along with the Standard Deviation on the Average for the Life.

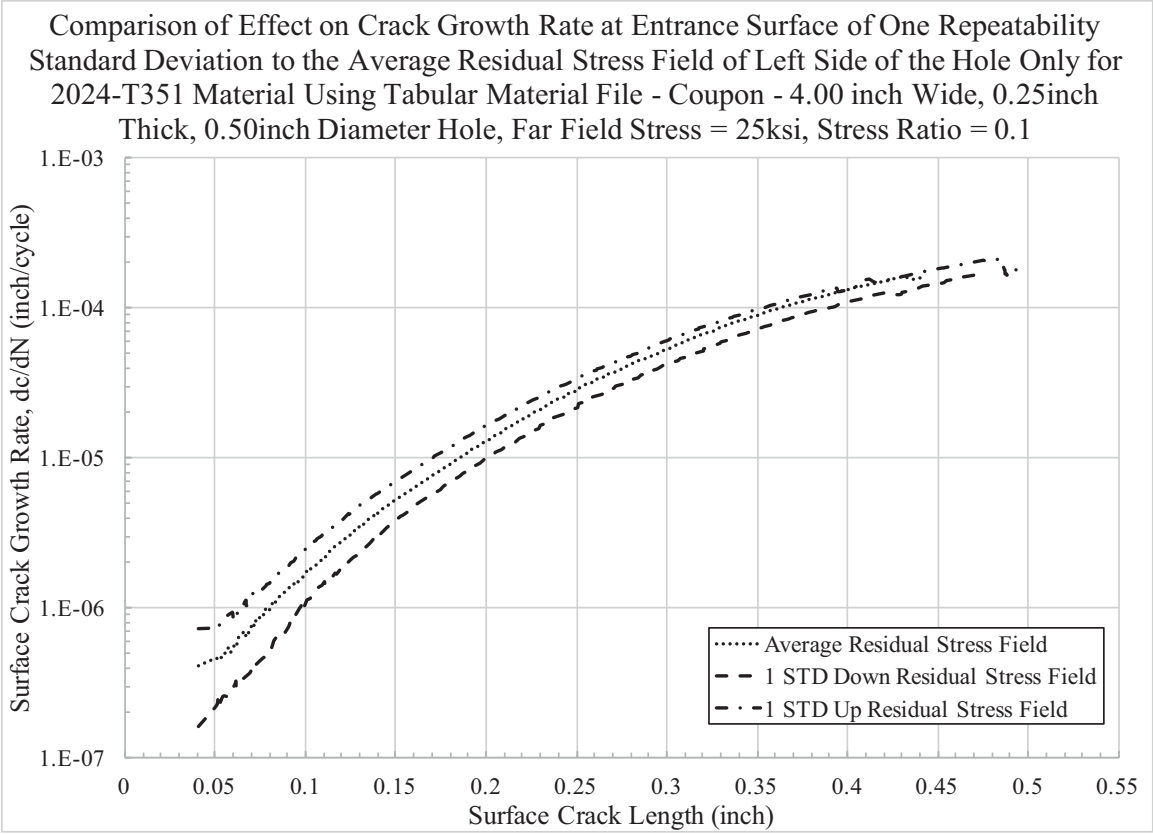

Fig. 852 Plot of Fatigue Crack Growth Rate at the Cx Mandrel Entrance Surface for all Three Residual Stress Distributions for the CxA2 (2024-T351) “Low” Applied Cx Condition.

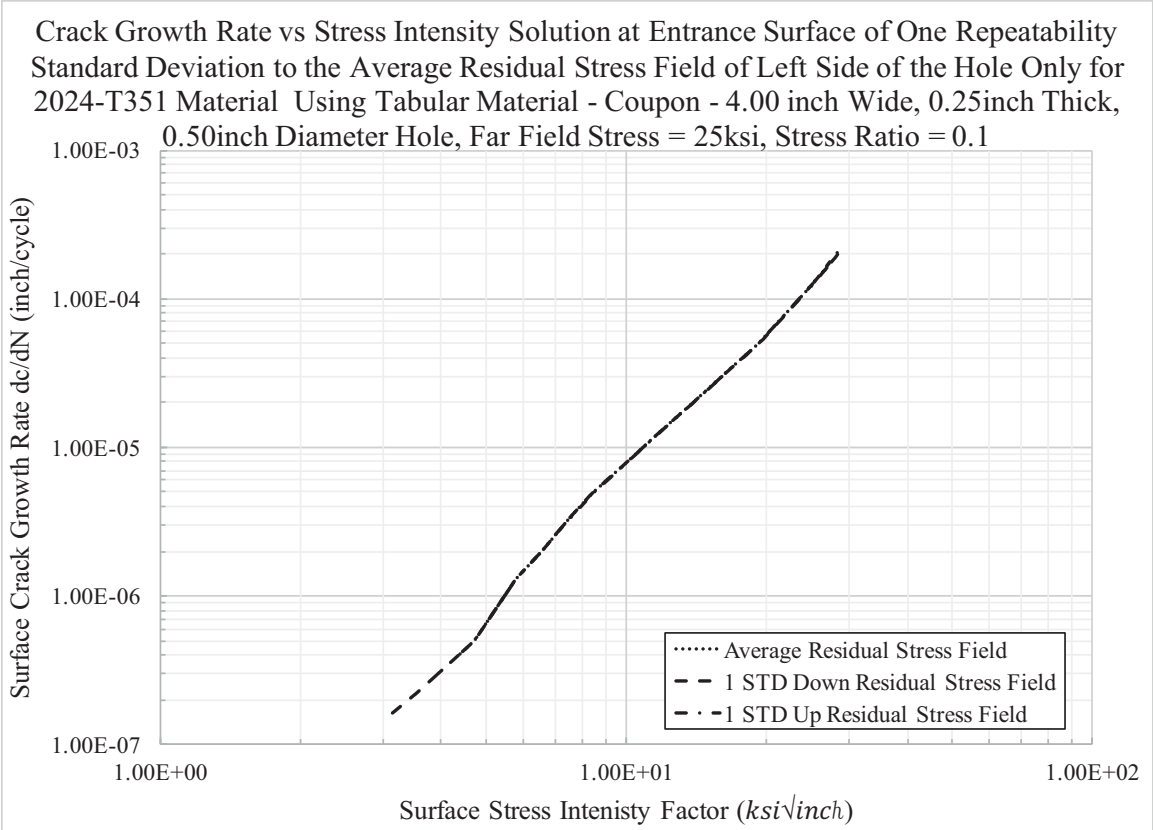

Fig. 853 Plot of Fatigue Crack Growth Rate at the Cx Mandrel Entrance Surface (dc/dN) Versus the SIF (ΔK) at the Cx Mandrel Entrance Surface for CxA2 (2024-T351).

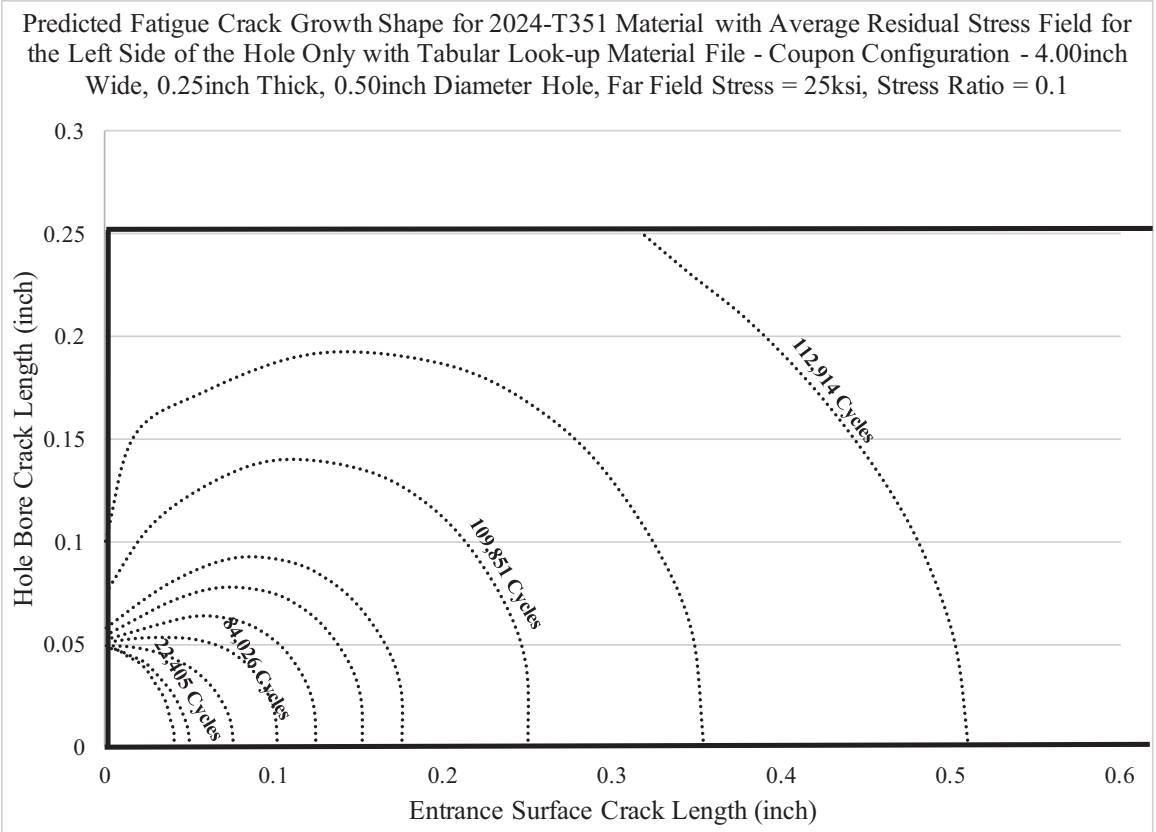

Fig. 854 Predicted Fatigue Crack Shape Evolution for CxA2 (2024-T351) with the Average Residual Stress Field for Only the Left Side of the Hole Used to Develop the Residual Stress Field.

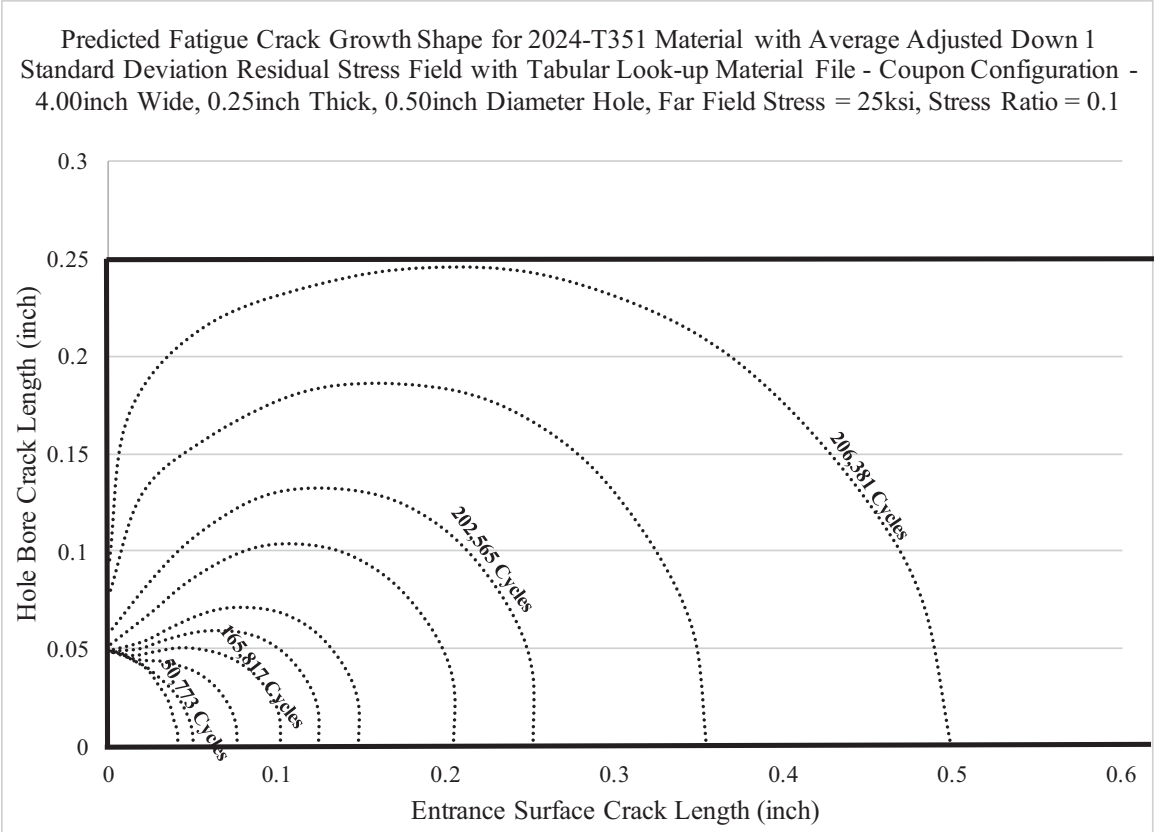

Fig. 855 Predicted Fatigue Crack Shape Evolution for CxA2 (2024-T351) with the Residual Stress Field Adjusted “Down” One Standard Deviation for Only the Left Side of the Hole Used to Develop the Residual Stress Field.

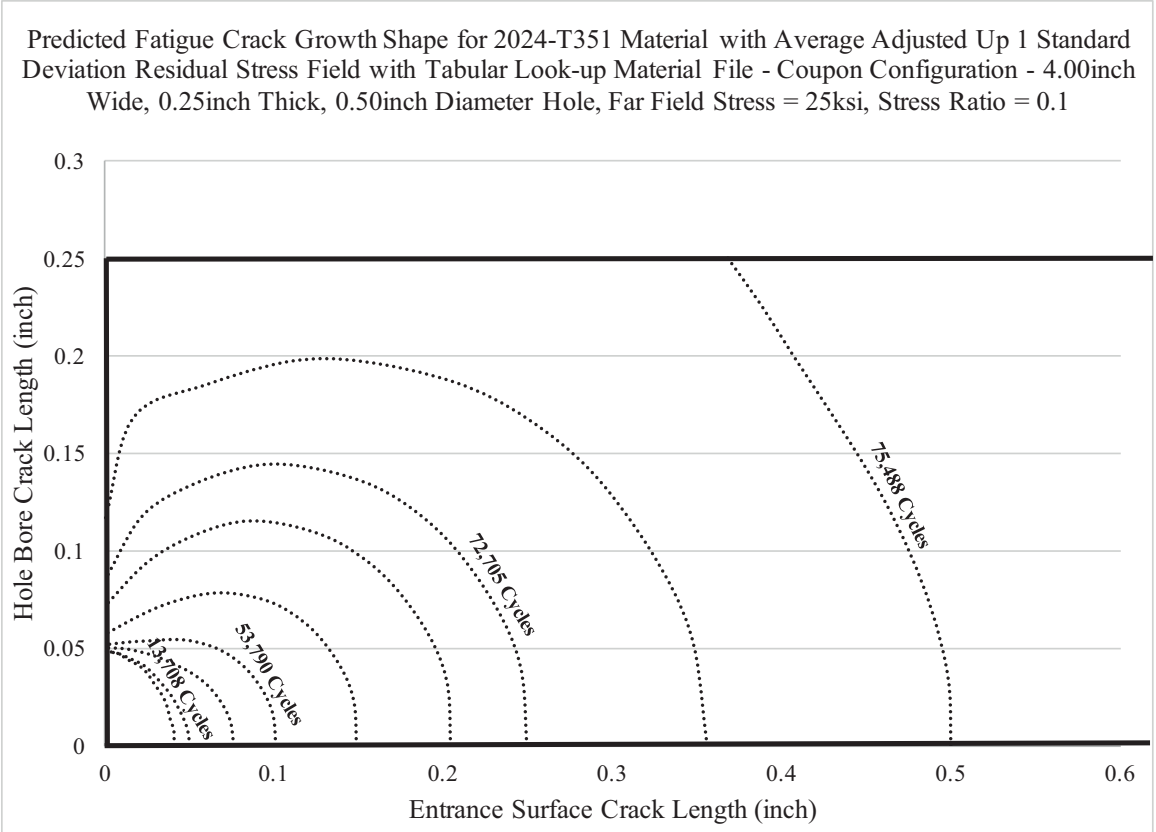

Fig. 856 Predicted Fatigue Crack Shape Evolution for CxA2 (2024-T351) with the Residual Stress Field Adjusted “Up” One Standard Deviation for Only the Left Side of the Hole Used to Develop the Residual Stress Field.

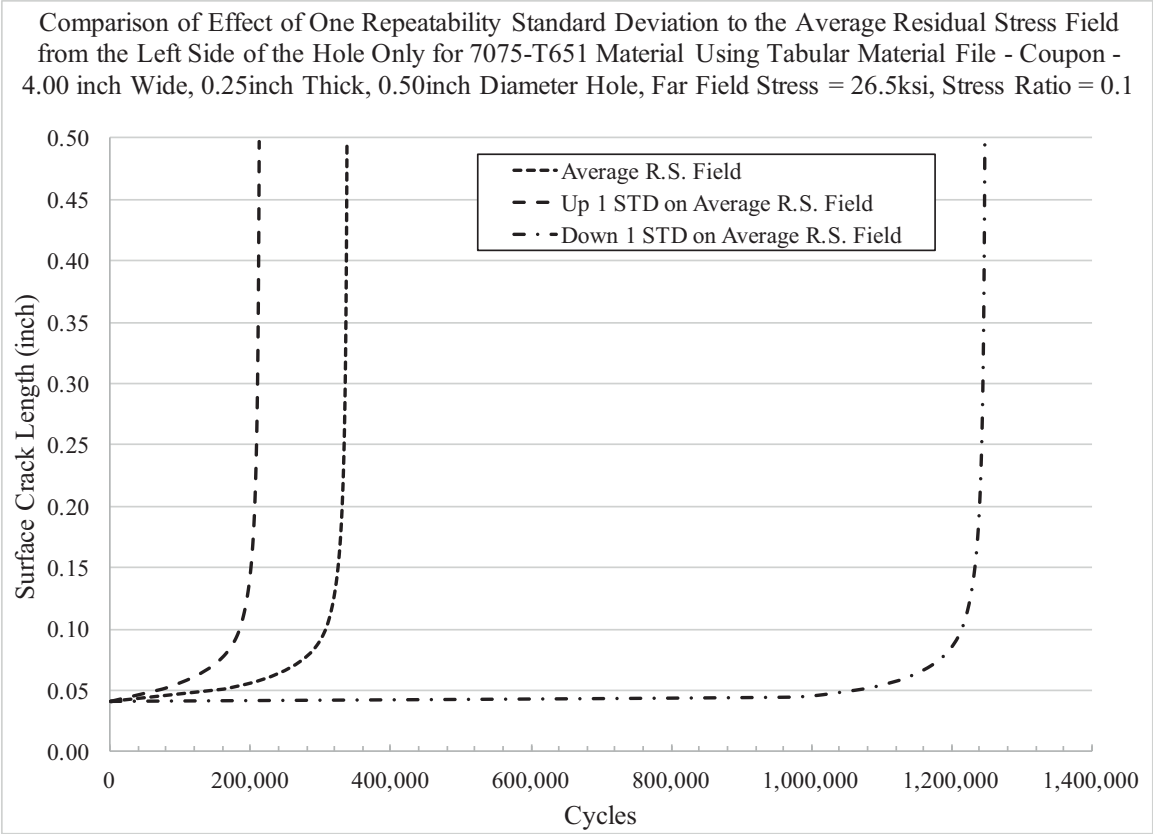

Fig. 857 Fatigue Life Prediction of CxD2 (7075-T651) Coupon Configuration, Cxed to the “Low” End of the Applied Expansion Specification, Using Three Residual Stress Distributions.

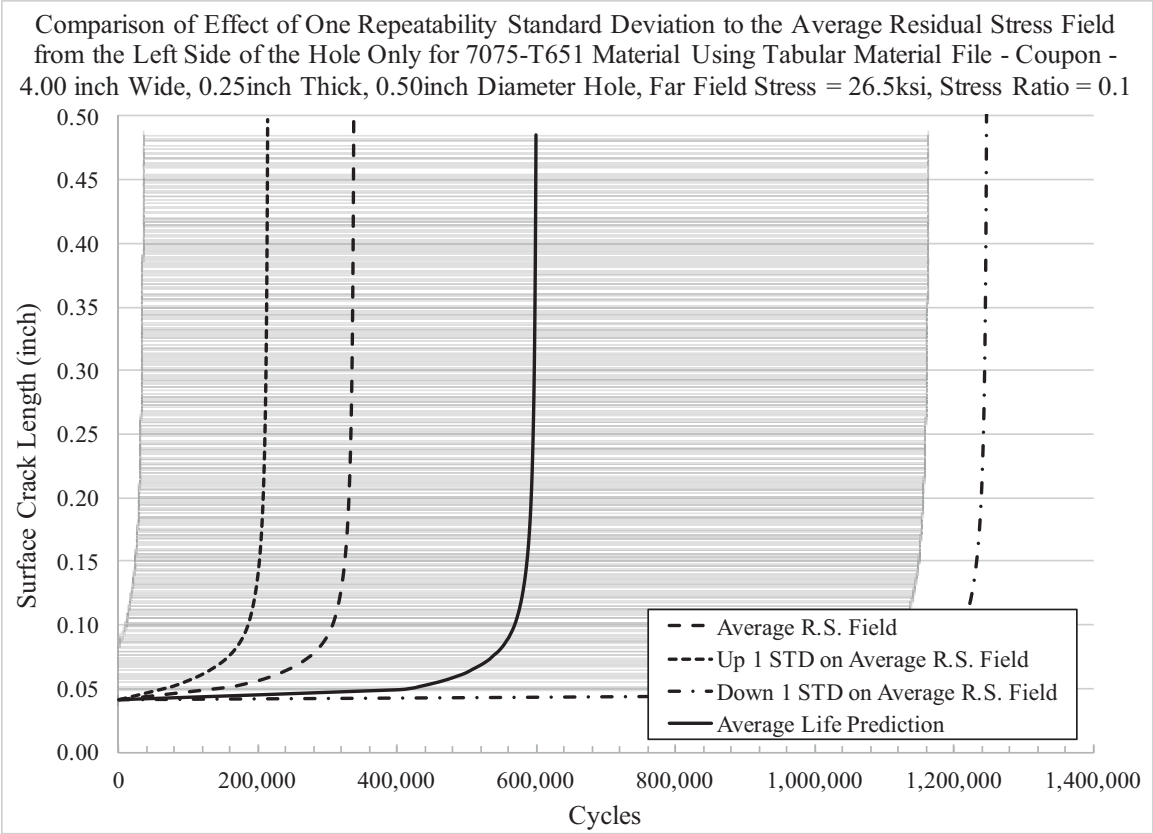

Fig. 858 Additional Statistics Provided for the Fatigue Life Predictions for the CxD2 (7075-T651) Coupon Configuration, Showing the Average Life Prediction Along with the Standard Deviation on the Average for the Life.

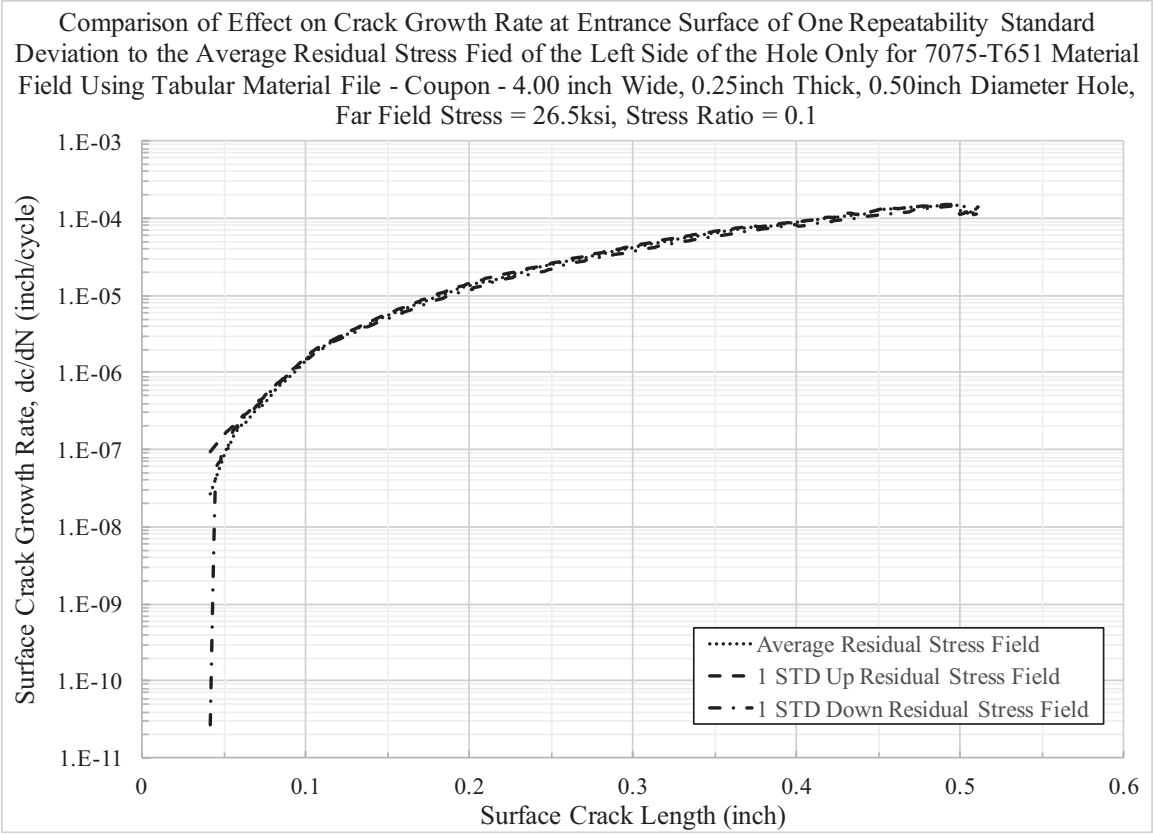

Fig. 859 Plot of Fatigue Crack Growth Rate at the Cx Mandrel Entrance Surface for all Three Residual Stress Distributions for the CxD2 (7075-T651) “Low” Applied Cx Condition.

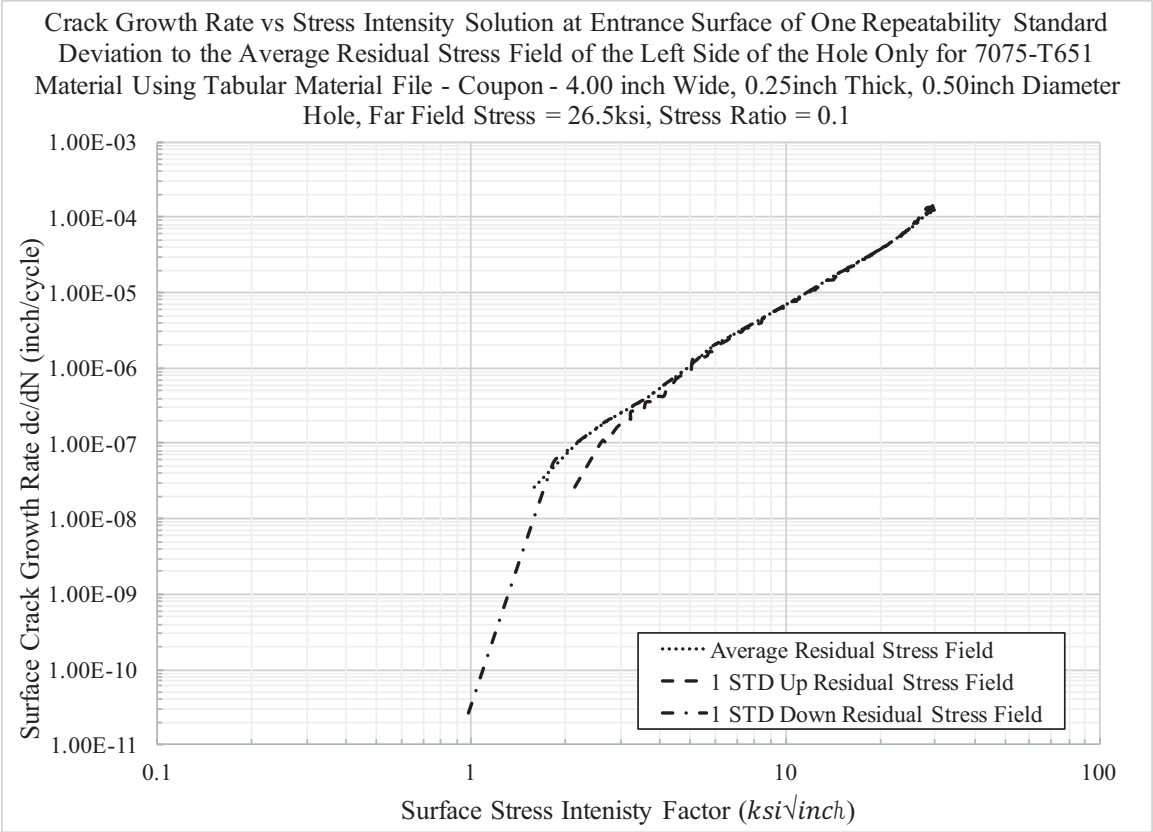

Fig. 860 Plot of Fatigue Crack Growth Rate at the Cx Mandrel Entrance Surface (dc/dN) Versus the SIF (ΔK) at the Cx Mandrel Entrance Surface for CxD2 (7075-T651).

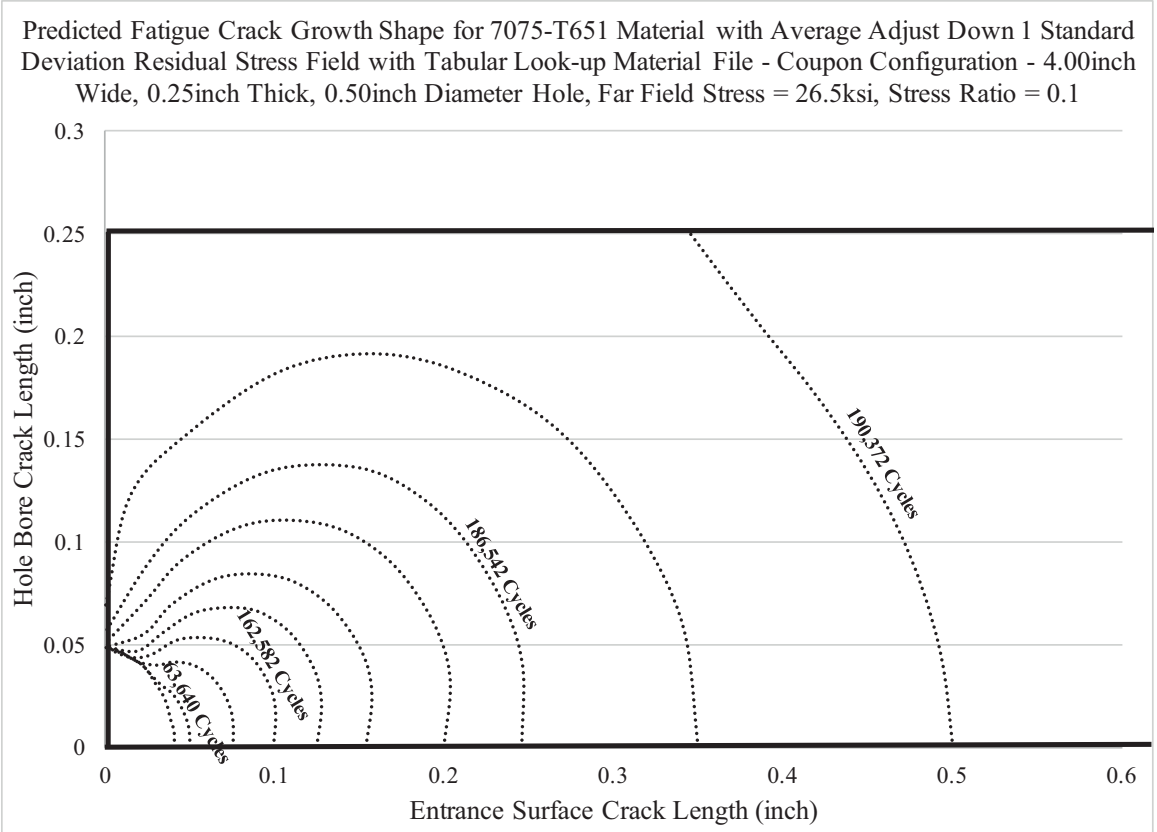

Fig. 861 Predicted Fatigue Crack Shape Evolution for CxD2 (7075-T651) with the Average Residual Stress Field for Only the Left Side of the Hole Used to Develop the Residual Stress Field.

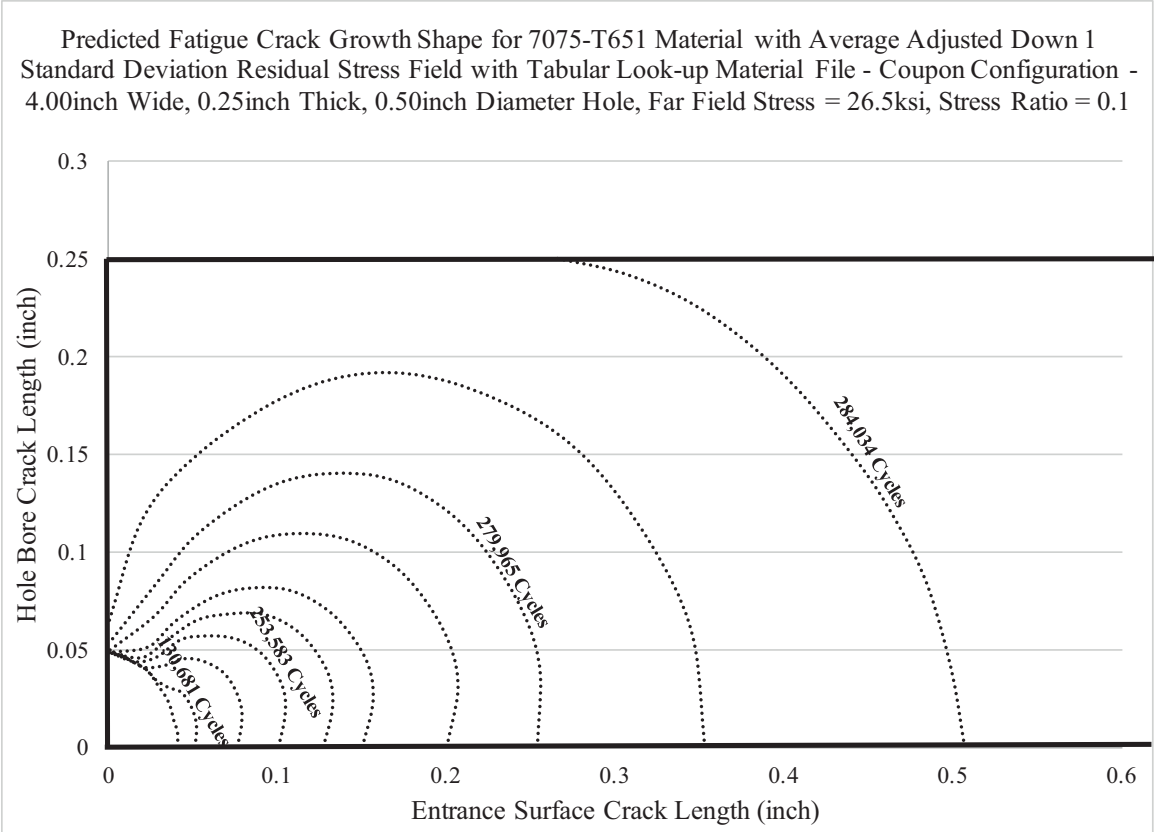

Fig. 862 Predicted Fatigue Crack Shape Evolution for CxD2 (7075-T651) with the Residual Stress Field Adjusted "Down" One Standard Deviation for Only the Left Side of the Hole Used to Develop the Residual Stress Field.

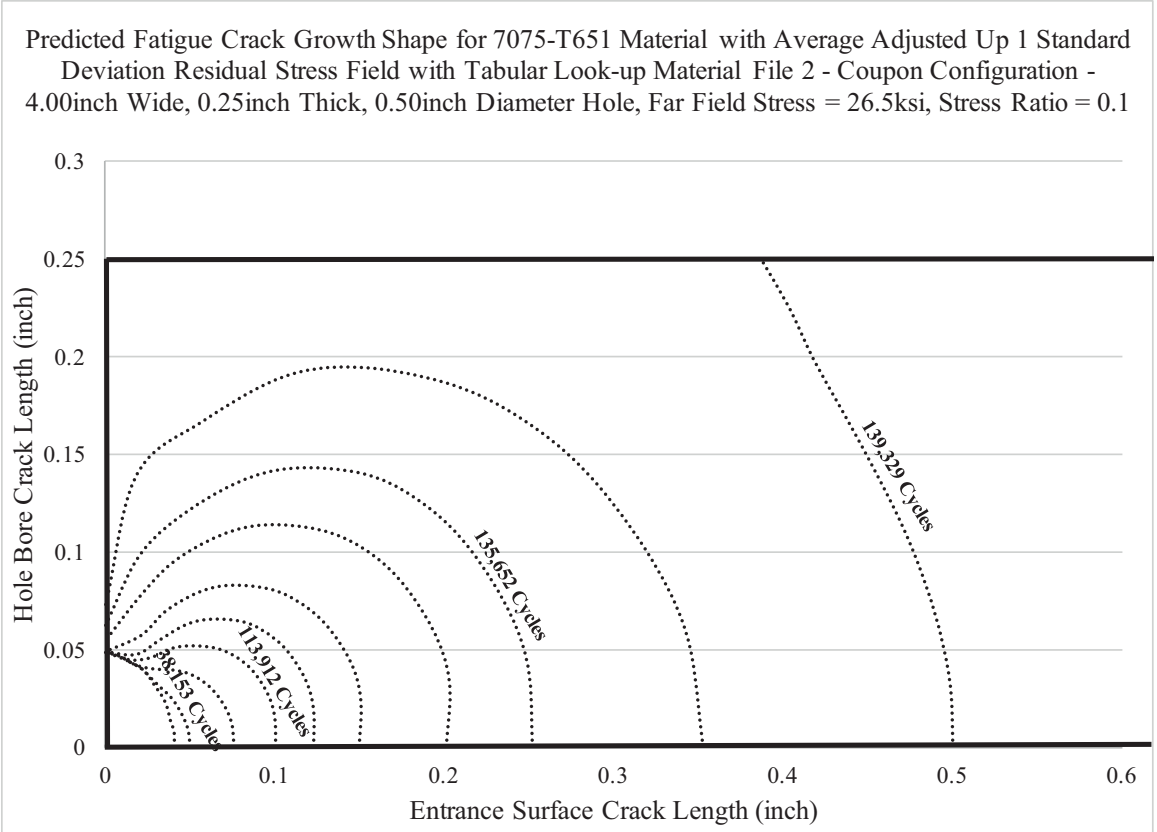

Fig. 863 Predicted Fatigue Crack Shape Evolution for CxD2 (7075-T651) with the Residual Stress Field Adjusted "Up" One Standard Deviation for Only the Left Side of the Hole Used to Develop the Residual Stress Field.

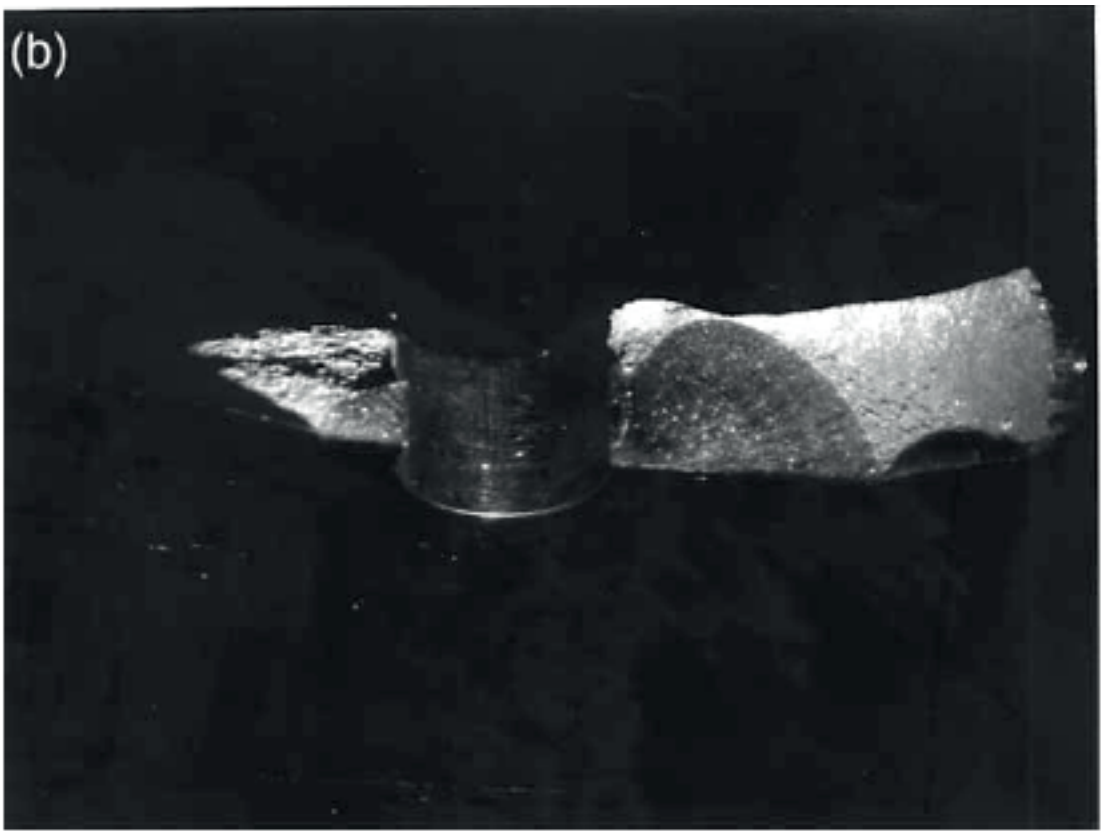

Fig. 864 Image of Fatigue Crack Growth at a Cxed Hole in 7050-T7451 Aluminum Showing the “Pinning” of the Crack Near the Center of the Bore of the Hole.[151]

9 IMPLEMENTATION OF COLD EXPANSION RESIDUAL STRESSES FOR PREDICTION OF FATIGUE LIFE – UTILIZATION OF CRACKED CX4N1-XX-B (2024-T351) AND CX4N1-XX-D (7075-T651) RESIDUAL STRESS FIELDS

9.1 Utilization of StressCheck® Finite Element Model within BAMF for Life Predictions and Fatigue Crack Growth Shapes of Cracked Cold Expanded Specimens

The same FEM was used within StressCheck® to predict the fatigue life and fatigue crack growth shape with the implementation of the residual stress fields developed for the cracked Cx4N1 coupons. The purpose of this was to minimize or eliminate any source of systematic error that could arise from the development of a new model or process used within BAMF. This meant that the same geometry was used, along with the same mesh parameters, and far-field loads and constraints, as was developed and implemented for the life predictions for the CxA2 (2024-T351) and CxD2 (7075-T651) material configurations.

9.2 Development of Residual Stress Functions for the Cx4N1-XX-B (2024-T351) and Cx4N1-XX-D (7075-T651) Cracked Residual Stress Conditions

Residual stresses were developed for a series of coupons which had a range of fatigue crack sizes developed in them, as discussed previously. The residual stress profiles developed for these cracked conditions were used to develop fifteenth (15^{th})

order bivariant polynomial function that represented the residual stress profile along that given surface. For most of the Cx4N1 coupons there were two replicates produced, except for the -07 (0.25 inch) and the -08 (0.50 inch) crack sizes. For these larger crack sizes, only one coupon was produced. In the case of the replicate conditions the two coupons residual stress fields were averaged at every point and a single residual stress profile was produced for the cracked side of the hole (the left side of the hole).

With the data now averaged and the standard deviations known for each point, the same process was used to develop the residual stress functions as was discussed for the baseline, uncracked coupons. However, for the cracked coupons a residual stress function was produced for each individual crack size, for the average residual stress, and the "up" and "down" single repeatability standard deviation. Thus, for both the Cx4N1-XX-B (2024-T351) and the Cx4N1-XX-D (7075-T651) coupon sets there was a total of fifteen functions developed for each. These functions then were grouped into their appropriate statistical characterization, "average", "up", and "down", each having five functions developed. All of the residual stress traction functions for the Cx4N1-XX-B (2024-T351) are provided in the Appendix.

9.2.1 Residual Stress Surface Plots for Cx4N1-01-08-B (2024-T351)

The "average" residual stress surface plots for all of the Cx4N1-XX-B (2024-T351) coupons, and the associated residuals surface plot, are provided in Fig. 865 through Fig. 874. The surface plots and the residual plots for the "up" and "down" conditions for all of the Cx4N1-XX-B coupons are provided in the Appendix.

9.2.2 Residual Stress Surface Plots for Cx4N1-01-08-D (7075-T651)

The average residual stress surface plots for the Cx4N1-XX-D (7075-T651) conditions are provided in Fig. 875 through Fig. 884. The surface plots and the residual plots for the "up" and "down" conditions are provided in the Appendix. The residual stress functions that were calculated to produce these surfaces all are provided within the Appendix.

9.3 Implementation of Residual Stress Functions into StressCheck® for Fatigue Life Predictions

With a series of residual stress profiles developed that capture the effect of a fatigue crack at different crack lengths, it was possible to now modify the residual stress fields within StressCheck® to include the effect of the fatigue crack. The purpose of this exercise was to determine if the effects of the fatigue crack, seen in the residual stresses determined via the contour method, have an effect on a fatigue life prediction, and if that prediction more accurately simulates what is observed in test, both from a fatigue life and fatigue crack shape evolution standpoint.

For each residual stress condition there were six residual stress equations developed, which represented a circular zone away from the edge of the hole, starting at the X, Y =0 location and moving radially out to 0.75 inch. These residual stress equations applied the specific residual stresses at each fatigue-cracked size in an attempt to replicate the residual stress field that was in the body at each crack size. Thus, a bivariant, piecewise function was developed for the residual stress field imposed in the StressCheck®, and had the form provided below:

$$f(X,Y) = \begin{cases} Szz0\_0.040, & (X,Y < 0.04)inch \\ Szz0.04\_0.09, & (X,Y \geq 0.04 < 0.09)inch \\ Szz0.09\_0.1125, & (X,Y \geq 0.09 < 0.1125)inch \\ Szz0.1125\_0.187, & (X,Y \geq 0.1125 < 0.1875)inch \\ Szz0.1875\_0.375, & (X,Y \geq 0.1875 < 0.375)inch \\ Szz0.375\_0.75, & (X,Y \geq 0.375 < 0.75)inch \end{cases}$$

with the individual functions being called, like Szz0_0.040, and expressed within the function call-out in StressCheck® as seen in Fig. 885. The functions that were used for the six steps represented the baseline, uncracked condition, and then the additional five cracked residual stress conditions determined from the Cx4N1 coupons. Each of these residual stress fields were applied for a specific distance away from the nucleation coordinate system, where the crack was centered, and was then pieced together by the Szz function shown in Fig. 885.

The individual steps for the application of the functions were chosen at the centers, between a pair of the residual stress determination locations. Thus, the first set of equations were built from the baseline, uncracked coupons, and was applied from 0.0 inch to 0.04 inch away from the edge of the hole. Then the first fatigue-cracked residual stress field, from coupons Cx4N1-01-02 was applied from 0.04 inch to 0.09 inch. The next function steps were as follows:

- Szz0.09_0.01125 – Cx4N1-03-04 (0.10 inch crack) applied from 0.09 inch to 0.1125 inch
- Szz0.01125_0.187 – Cx4N1-05-06 (0.125 inch crack) applied from 0.1125 inch to 0.1875 inch
- Szz0.1875_0.375 – Cx4N1-07 (0.25 inch crack) applied from 0.1875 inch to 0.375 inch

- Szz0.375_0.75 – Cx4N1-08 (0.50 inch crack) applied from 0.375 inch to 0.75 inch

A visualization of how these residual stress functions were applied is shown in Fig. 886, with the individual numbers representing the range and applied residual stress function from the Cx4N1-XX fatigue-cracked coupons. This information is further defined within Table 11.

9.3.1 Visualization of Residual Stress Equations within StressCheck® for the Cx4N1-XX-B (2024-T351) Coupon Configuration

In order to validate if the equations were applied consistently, a contour stress plot was developed for each residual stress equation, as applied to the model. The combined, bivariant function residual stress contour plots are provided in Fig. 887 through Fig. 892 for the average residual stress condition for the Cx4N1-XX-B (2024-T351) coupon configuration. Fig. 893 provides a residual stress contour plot of the combined, piecewise function, in which a the process outlined within Table 11 is applied.

9.3.2 Visualization of Residual Stress Equations within StressCheck® for the Cx4N1-XX-D (7075-T651) Coupon Configuration

The average residual stress statistical distribution for the Cx4N1-XX-D (7075-T651) coupon configuration is provide in Fig. 894 through Fig. 899. Fig. 900 provides a residual stress contour plot of the final piecewise function that was developed to represent the effect of the crack within the model, as outlined in Table 11. The residual stress contour plots, as applied within StressCheck® for the “up” and “down” statistical distribution for both the Cx4N1-XX-B (2024-T351) and Cx4N1-XX-D (7075-T651)

coupon configurations are provided in the Appendix.

9.4 Fatigue Life Predictions Using Residual Stresses Developed from Fatigue Cracked 2024-T351 and 7075-T651 Coupons

A series of fatigue life predictions were developed for the two material alloys that were fatigue-cracked with residual stresses. The predicted fatigue condition was identical to those performed using the baseline, uncracked residual stress fields developed and implemented with StressCheck® and BAMF. In addition to the predicted condition being the same, the same StressCheck® models and BAMF parameters were used. The only difference between the baseline fatigue predictions and these are the residual stress functions used to characterize the residual stress state in the body. For these predictions, a bivariant, piecewise residual stress function was developed and imposed on the material.

Table 12 provides a breakdown of the key parameters of the fatigue life predictions. All of the predictions performed using the fatigue-cracked residual stress fields used the same two tabular look-up material models as used in the baseline, uncracked life predictions. The IFS also was the same, as was the loading conditions for these predictions.

Provided for each prediction is a crack growth chart that shows all three life predictions, along with the crack growth rate at the Cx mandrel entrance surface (dc/dN vs. c) and also the crack growth rate vs. the Stress Intensity Factor for the node that is at the surface of the part, (dc/dN vs. ΔK).

9.4.1 Fatigue Life Prediction for the Cx4N1-XX-B (2024-T351) Material with a "Low" Applied Cx Expansion Configuration – Using the CxA2 (2024-T351) Residual Stress Condition from 0.0 – 0.04 inch

Three different residual stress distributions were developed to be used to predict the fatigue life of the coupons tested. The first residual stress, bivariant, piecewise function took the residual stress baseline, uncracked residual stress field for the first 0.04 inch of the residual stress field. From this point on the residual stress field was stitched together at the midpoints of the fatigue crack sizes which were developed and the coupons were processed via the contour method to determine residual stresses. The goal of this was to utilize a "Simpson's Rule" approach to breaking the function into midpoints.[152]

The first series of fatigue life curve for the Cx4N1-XX-B (2024-T351) prediction were developed using this initial function. The fatigue life prediction for this condition utilized the same AFGROW material model and StressCheck® model. The only change in the BAMF run was the inclusion of the bivariant, piecewise function to represent the combined residual stress field through the part, due to the effect of the fatigue crack.

The fatigue life prediction for this condition also utilized three different residual stress distributions, in an effort to quantify the effect of the Cx repeatability uncertainty on the fatigue crack growth prediction. Thus, like for the baseline predictions, these included the one "up" and one "down" residual stress distribution, along with the "average" residual stress condition. The life prediction for all of these three residual stress conditions is provided in Fig. 901. The other plots that are associated with this prediction are provided in Fig. 901 through Fig. 903.

9.4.2 Fatigue Life Prediction for the Cx4N1-XX-D (7075-T651) Material with a "Low" Applied Cx Expansion Configuration – Using the CxD2 (7075-T651) Residual Stress Condition from 0.0 – 0.04 inch

Like that which was performed for the Cx4N1-XX-B (2024-T351) condition, three life predictions were performed using the average, one "Up", and one "down" statistical residual stress distribution with the inclusion of the effect of a fatigue crack on the residual stress field, as determined via the contour method. Like the predictions provided within section 9.4.1. This series of predictions utilized the CxD2 (7075-T651) residual stress from 0.00 – 0.04 inch away from the edge of the hole, as shown in Table 11.

The fatigue life prediction for this condition is provided in Fig. 904. In addition to the life prediction, the crack growth rate at the Cx mandrel entrance surface versus the Cx mandrel entrance surface crack length is provided in Fig. 905 and Fig. 906.

It should be noted that for this series of predictions the one "up" residual stress distribution, which was developed to have less compression in those regions of the stress field that are under compression, shows a longer life than the "average" and the one "down" residual stress distribution. This will be discussed in detail within the conclusions and recommendations sections.

9.4.3 Fatigue Life Prediction for the Cx4N1-XX-B (2024-T351) Material with a "Low" Applied Cx Expansion Configuration – Using the Cx4N1-01-02-B (2024-T351) Residual Stress Condition from 0.0 – 0.09 inch

In an effort to do a sensitivity study on the effect of the adjustment of the depths of the modified bivariant residual stress function, another series of fatigue crack growth predictions were performed for both the 2024-T351 and 7075-T651 material conditions.

For this next series the Cx4N1-01-02 residual stress fields were applied from the edge of the hole out to 0.09 inch away from the edge. This would try to account for any change in the residual stress field do to the presence of the crack, close to the edge of the hole. Table 13 provides an overview of these six BAMF life predictions that were performed.

For all of these predictions the same StressCheck® model, and AFGROW settings were used, the only differences were that the residual stress, bivariant polynomial utilized the same function for Zone 1 and Zone 2, as shown in Table 14.

Life predictions using this modified bivariant function is provided in Fig. 907 along with the crack growth rate data and dc/dN vs. ΔK, in Fig. 908 and Fig. 909.

9.4.4 Fatigue Life Prediction for the Cx4N1-XX-D (7075-T651) Material with a "Low" Applied Cx Expansion Configuration – Using the CxD2 (7075-T651) Residual Stress Condition from 0.0 – 0.09 inch

The same process was used for the 7075-T651 material predictions, as shown in Table 13. It should be noted that the average predicted life for the previous condition, utilizing the baseline, uncracked, CxD2 residual stress field for the first 0.04 inch away from the edge of the hole, provided a life prediction of 183,226 cycles. With this change in the residual stress field, bivariant function the life prediction dropped to 100,988 cycles, almost half the life. While for the 2024-T351 material the change actually increased the average life prediction from 137,991 cycles to 154,693 cycles. The fatigue crack growth curve for this prediction, showing all three of the residual stress distributions, is shown in Fig. 910. The crack growth rate versus the Cx mandrel entrance surface is shown in Fig. 911 and the rate versus the Cx mandrel entrance surface SIF is provided in Fig. 912.

9.4.5 Conclusions from Fatigue Life Predictions when Applying a Statistical Distribution to the Bivariant, Piecewise Function Representing the Effect of the Fatigue Crack on the Residual Stress Field

From these plots it can be seen that when the statistical repeatability standard deviation is applied to the residual stress fields, this had a significant impact on the predicted fatigue life. This is true for both materials and was not dependent on depth of the applied residual stress function, per Table 11 and Table 14. The effect of this statistical distribution ranged from a shift in life from 3 to 5 times from the "up" to the "down" statistical distribution. This change in life due to the shift in the statistical distribution demonstrates that it is essential to understand and quantify the statistical uncertainty associated with the Cx residual stress field, if the benefits of this process are ever to be applied to the lifing of a critical component on an aircraft or any other structure.

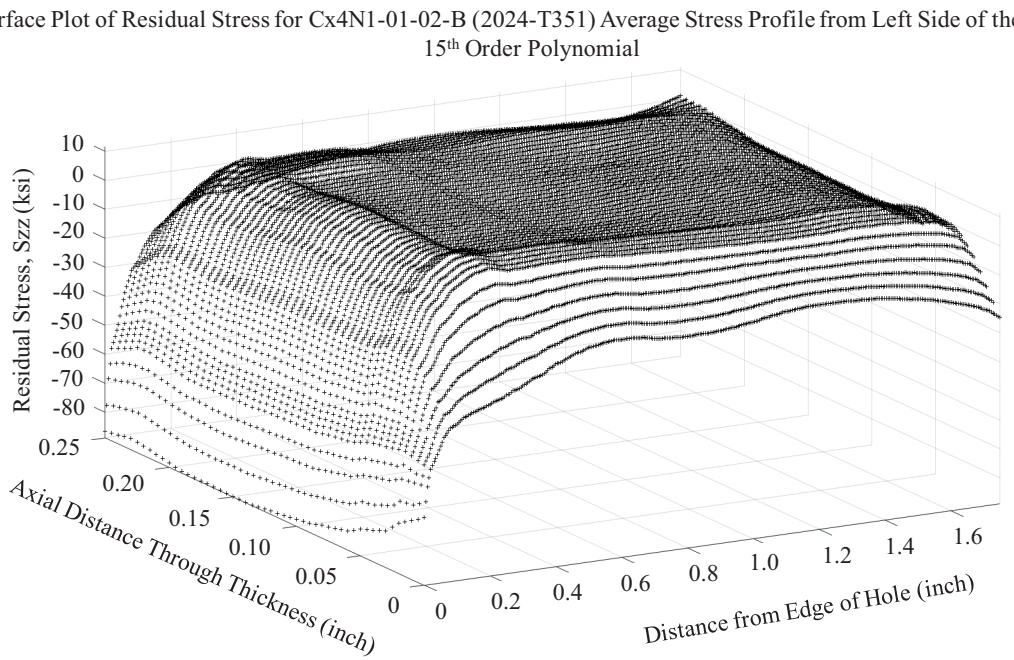

Fig. 865 Surface Plot of Residual Stress Traction Function Developed for the Average of the Cracked Side of the Hole for the Residual Stress Condition Cx4N1-01-02-B (2024-T351), these Coupons Had an Approximately 0.08 inch Surface Crack in the Cx Mandrel Entrance Surface.

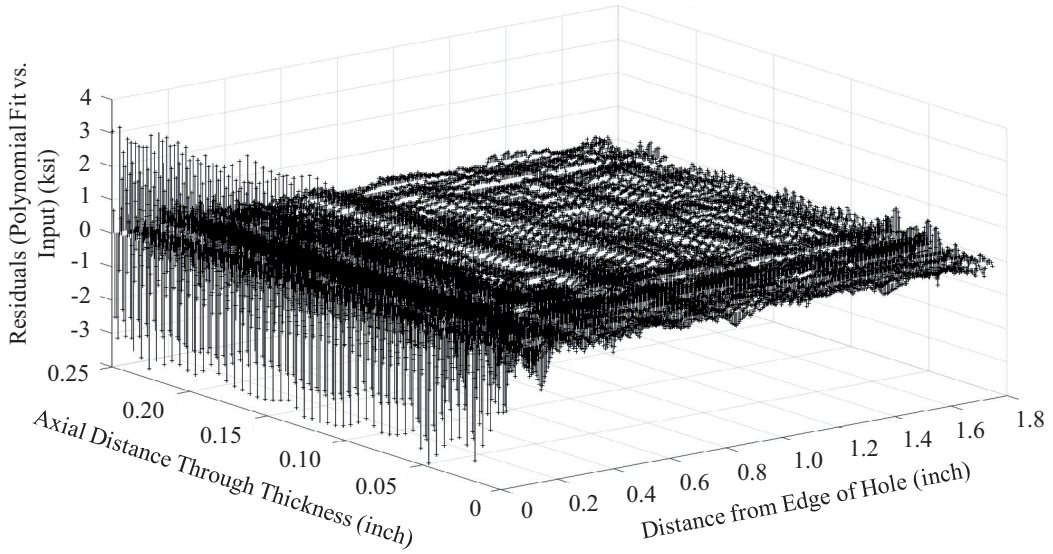

Fig. 866 Surface Plot of the Residual between the Polynomial Fit and the Actual Residual Stress Data for the Average of the Left Side of the Hole for the Residual Stress Condition Cx4N1-01-02-B (2024-T351), these Coupons Had an Approximately 0.08 inch Surface Crack in the Cx Mandrel Entrance Surface.

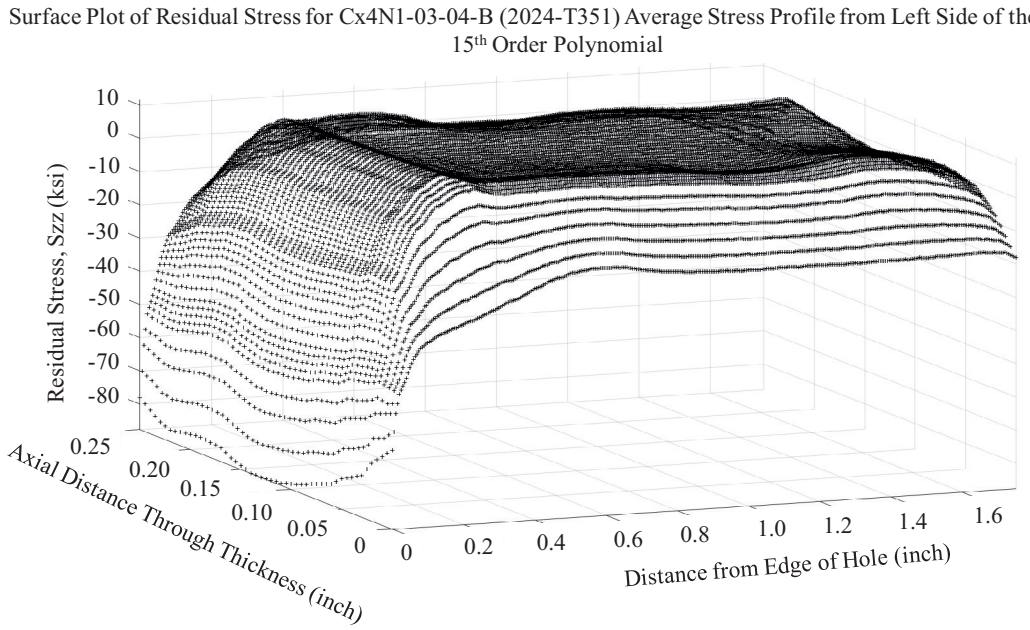

Fig. 867 Surface Plot of Residual Stress Traction Function Developed for the Average of the Cracked Side of the Hole for the Residual Stress Condition Cx4N1-03-04-B (2024-T351), these Coupons Had an Approximately 0.10 inch Surface Crack in the Cx Mandrel Entrance Surface.

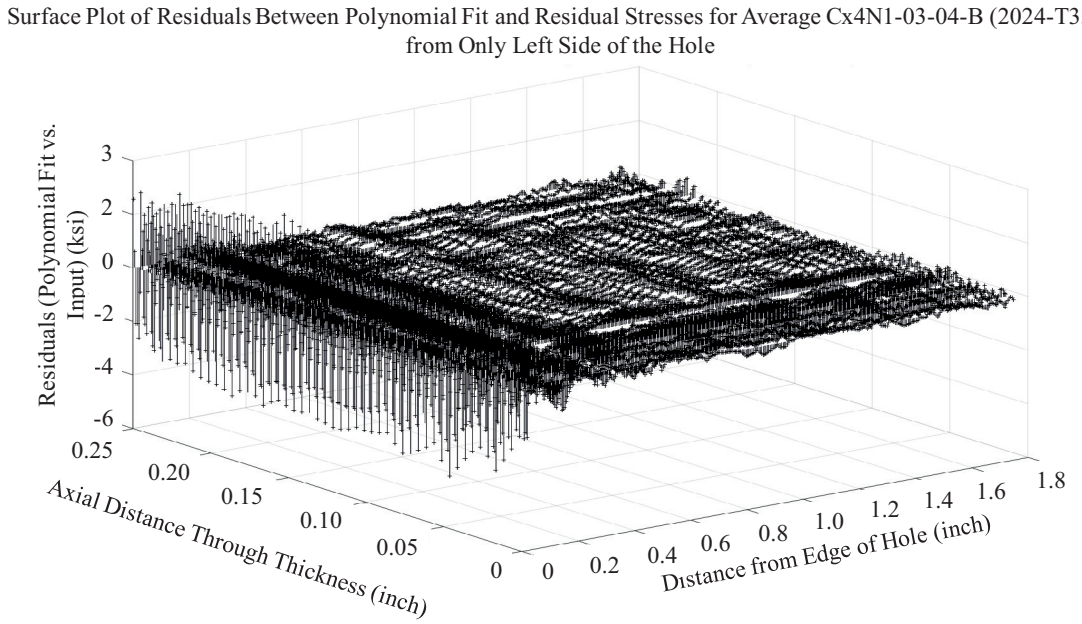

Fig. 868 Surface Plot of the Residual between the Polynomial Fit and the Actual Residual Stress data for the Average of the Left Side of the Hole for the Residual Stress Condition Cx4N1-03-04-B (2024-T351), these Coupons Had an Approximately 0.10 inch Surface Crack in the Cx Mandrel Entrance Surface.

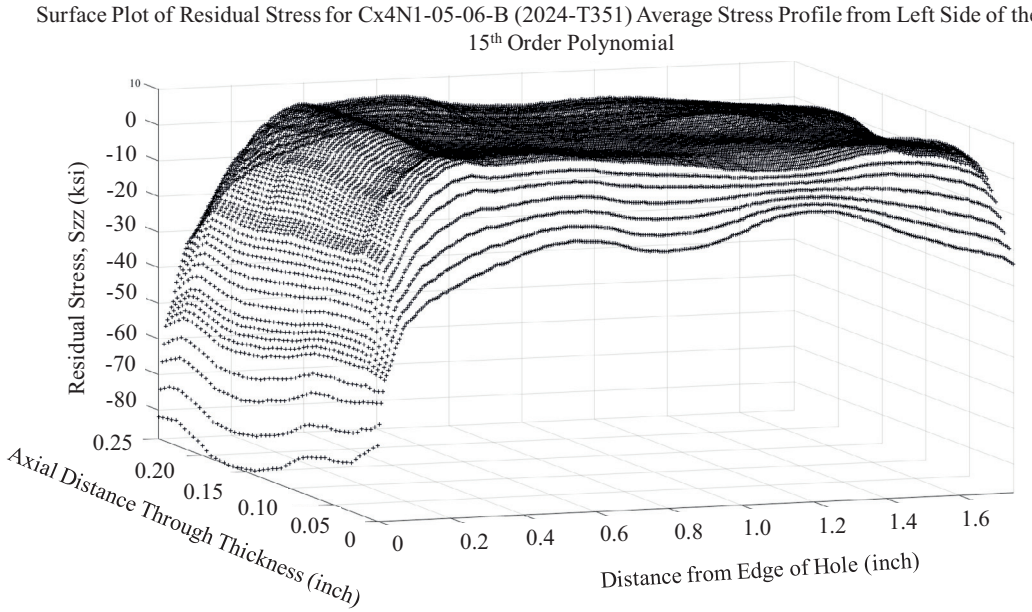

Fig. 869 Surface Plot of Residual Stress Traction Function Developed for the Average of the Cracked Side of the Hole for the Residual Stress Condition Cx4N1-05-06-B (2024-T351), these Coupons Had an Approximately 0.125 inch Surface Crack in the Cx Mandrel Entrance Surface.

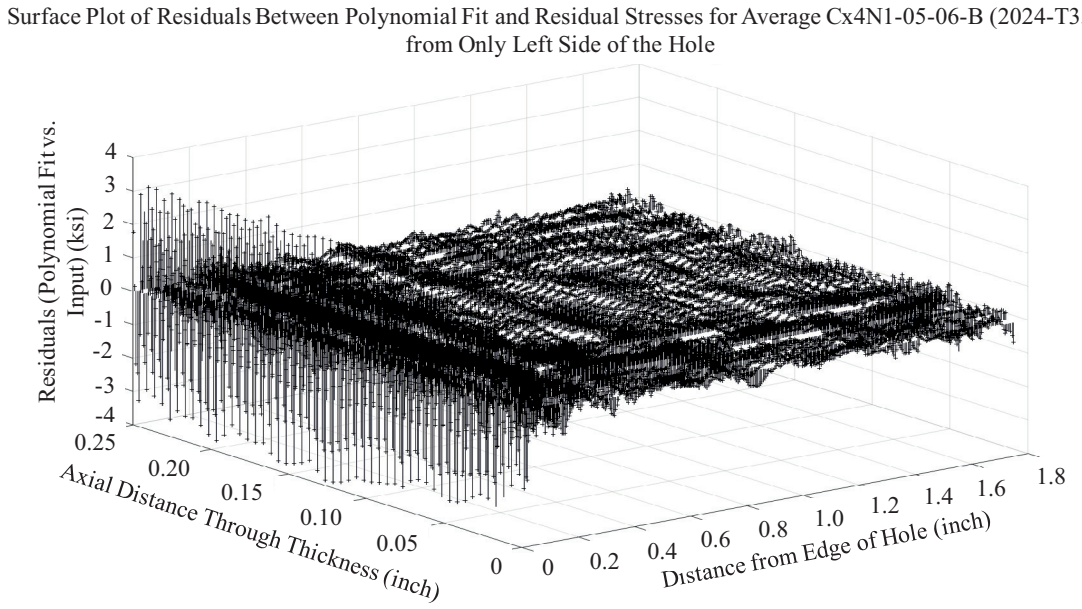

Fig. 870 Surface Plot of the Residual between the Polynomial Fit and the Actual Residual Stress Data for the Average of the Left Side of the Hole for the Residual Stress Condition Cx4N1-05-06-B (2024-T351), these Coupons Had an Approximately 0.125 inch Surface Crack in the Cx Mandrel Entrance Surface.

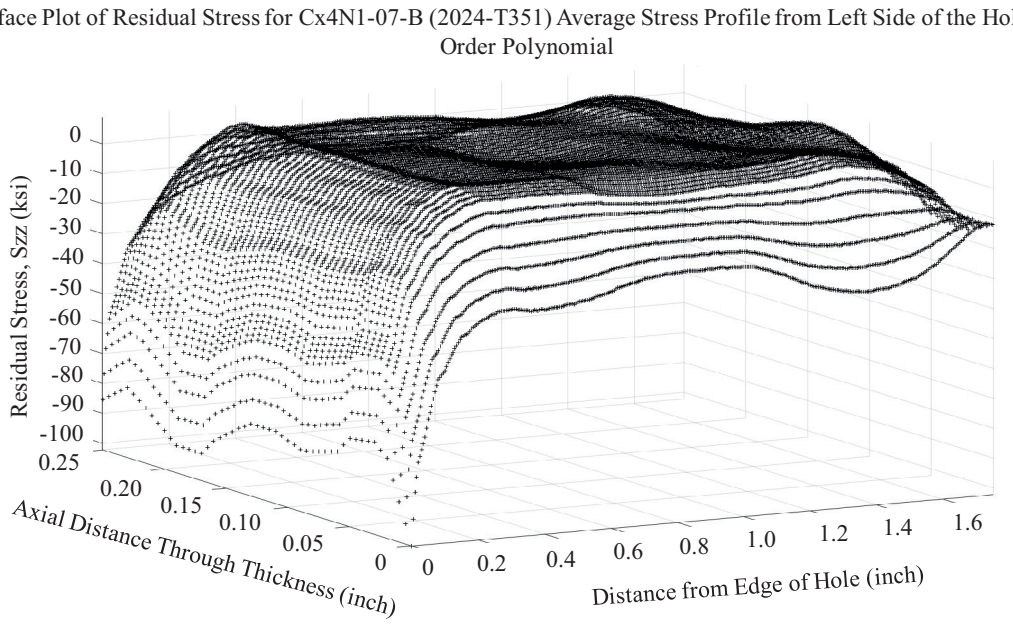

Fig. 871 Surface Plot of Residual Stress Traction Function Developed for the Average of the Cracked Side of the Hole for the Residual Stress Condition Cx4N1-07-B (2024-T351), this Coupon Had an Approximately 0.25 inch Surface Crack in the Cx Mandrel Entrance Surface.

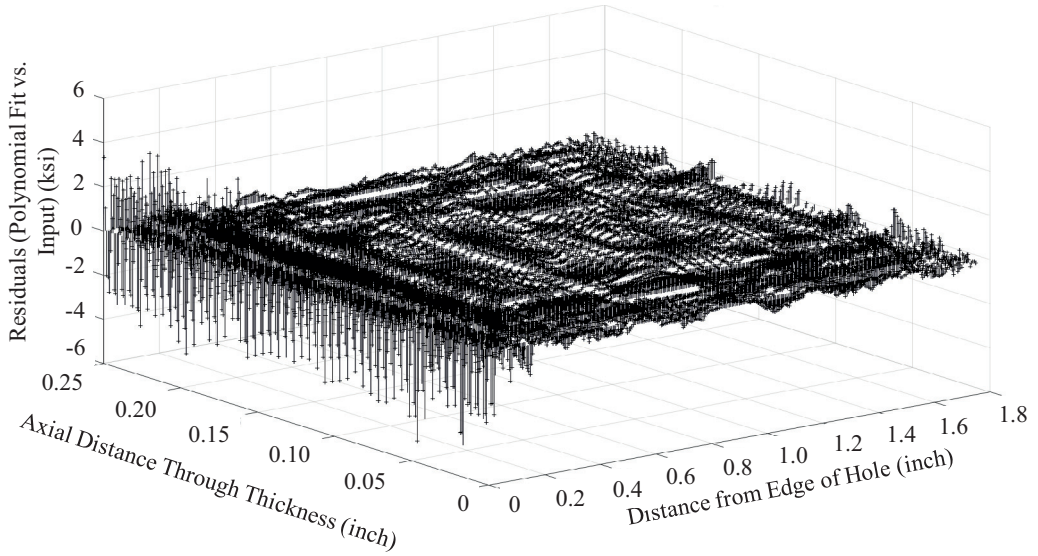

Fig. 872 Surface Plot of the Residual between the Polynomial Fit and the Actual Residual Stress Data for the Average of the Left Side of the Hole for the Residual Stress Condition Cx4N1-07-B (2024-T351), this Coupon Had an Approximately 0.25 inch Surface Crack in the Cx Mandrel Entrance Surface.

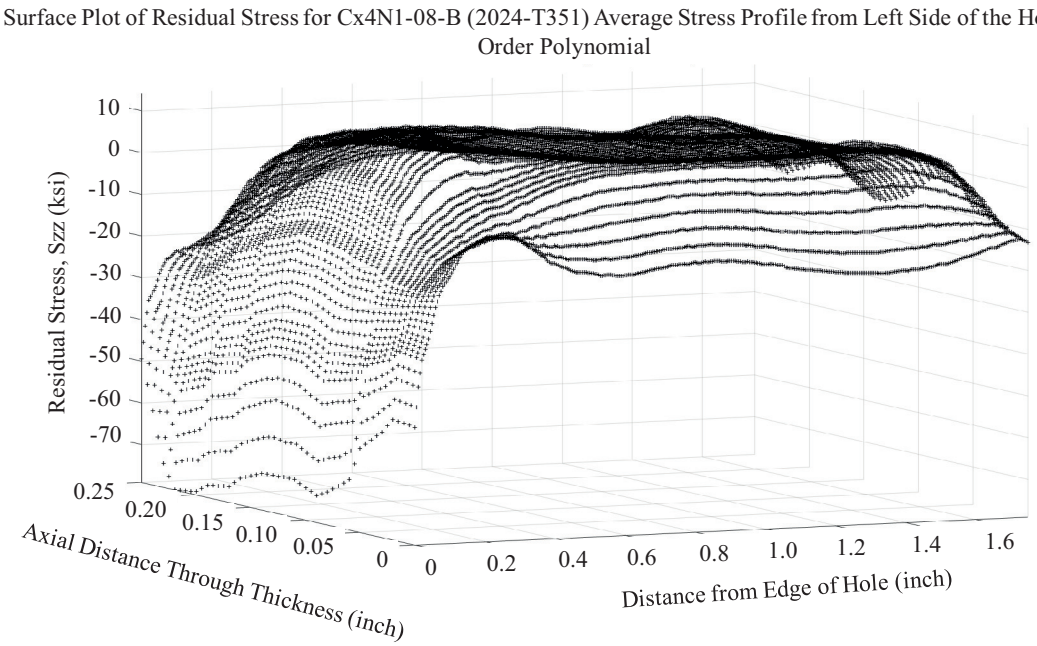

Fig. 873 Surface Plot of Residual Stress Traction Function Developed for the Average of the Cracked Side of the Hole for the Residual Stress Condition Cx4N1-08-B (2024-T351), this Coupon Had an Approximately 0.50 inch Surface Crack in the Cx Mandrel Entrance Surface.

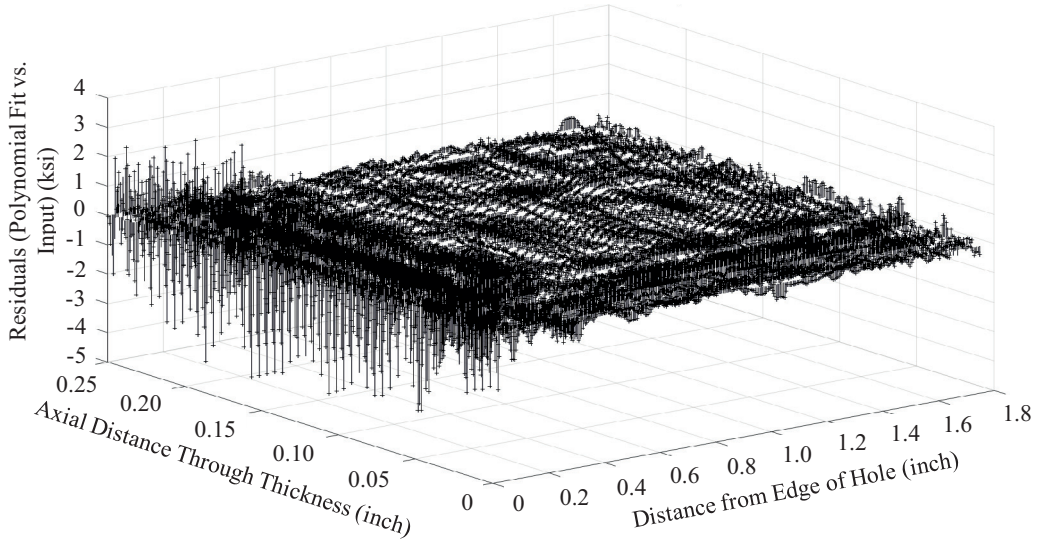

Fig. 874 Surface Plot of the Residual between the Polynomial Fit and the Actual Residual Stress Data for the Average of the Left Side of the Hole for the Residual Stress Condition Cx4N1-08-B (2024-T351), this Coupon Had an Approximately 0.50 inch Surface Crack in the Cx Mandrel Entrance Surface.

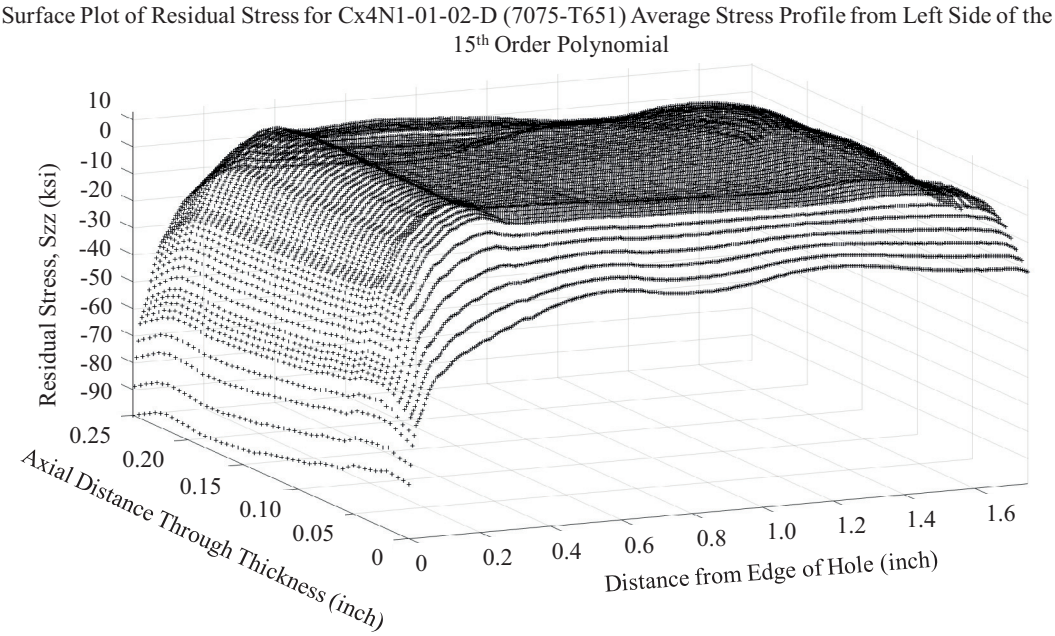

Fig. 875 Surface Plot of Residual Stress Traction Function Developed for the Average of the Cracked Side of the Hole for the Residual Stress Condition Cx4N1-01-02-D (7075-T651), these Coupons Had an Approximately 0.08 inch Surface Crack in the Cx Mandrel Entrance Surface.

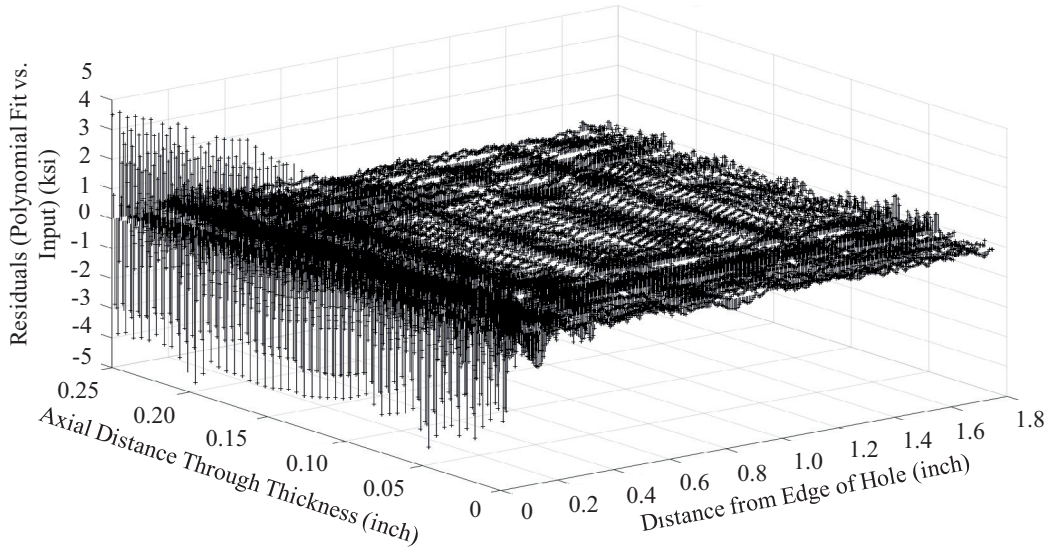

Fig. 876 Surface Plot of the Residual between the Polynomial Fit and the Actual Residual Stress Data for the Average of the Left Side of the Hole for the Residual Stress Condition Cx4N1-01-02-D (7075-T651), these Coupons Had an Approximately 0.08 inch Surface Crack in the Cx Mandrel Entrance Surface.

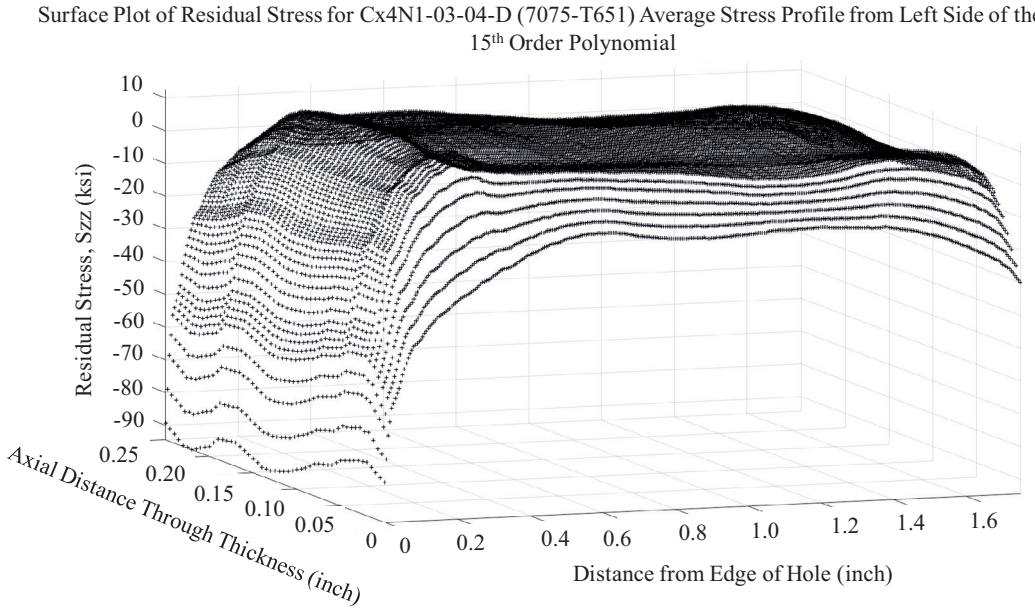

Fig. 877 Surface Plot of Residual Stress Traction Function Developed for the Average of the Cracked Side of the Hole for the Residual Stress Condition Cx4N1-03-04-D (7075-T651), these Coupons Had an Approximately 0.10 inch Surface Crack in the Cx Mandrel Entrance Surface.

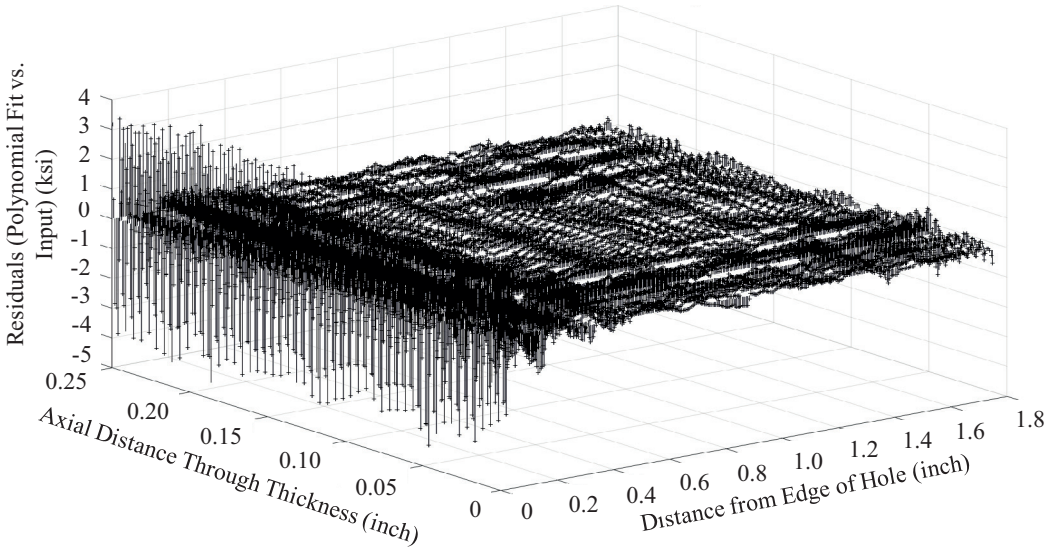

Fig. 878 Surface Plot of the Residual between the Polynomial Fit and the Actual Residual Stress Data for the Average of the Left Side of the Hole for the Residual Stress Condition Cx4N1-03-04-D (7075-T651), these Coupons Had an Approximately 0.10 inch Surface Crack in the Cx Mandrel Entrance Surface.

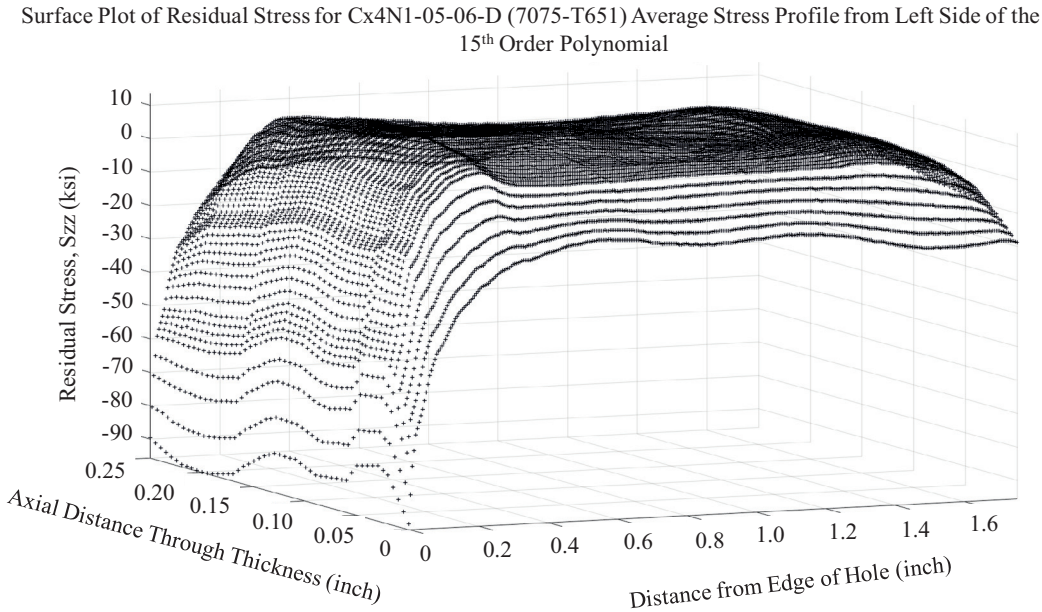

Fig. 879 Surface Plot of Residual Stress Traction Function Developed for the Average of the Cracked Side of the Hole for the Residual Stress Condition Cx4N1-05-06-D (7075-T651), these Coupons Had an Approximately 0.125 inch Surface Crack in the Cx Mandrel Entrance Surface.

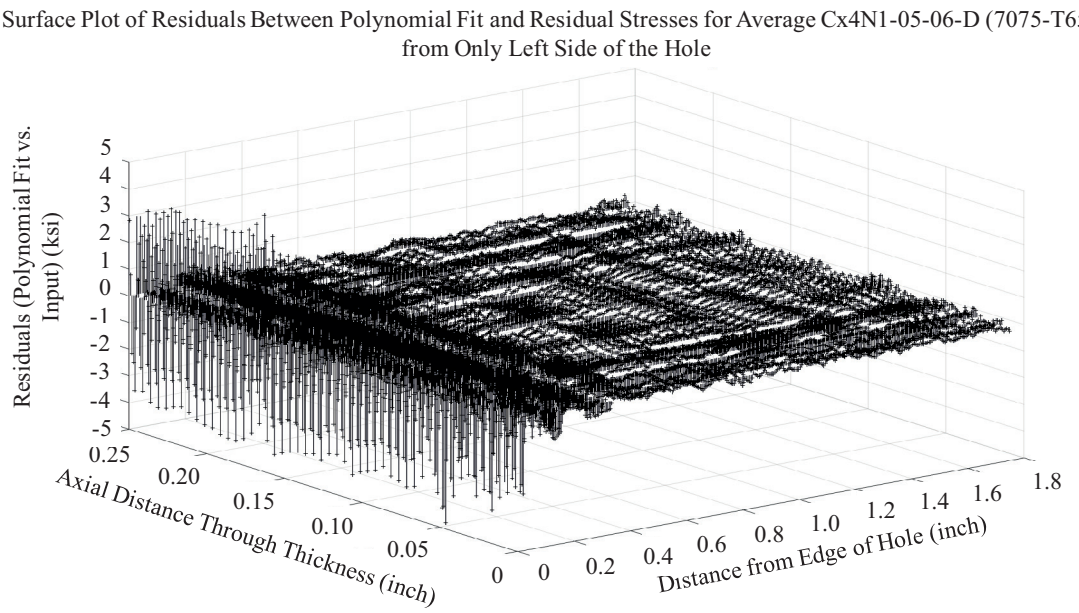

Fig. 880 Surface Plot of the Residual between the Polynomial Fit and the Actual Residual Stress Data for the Average of the Left Side of the Hole for the Residual Stress Condition Cx4N1-05-06-D (7075-T651), these Coupons Had an Approximately 0.125 inch Surface Crack in the Cx Mandrel Entrance Surface.

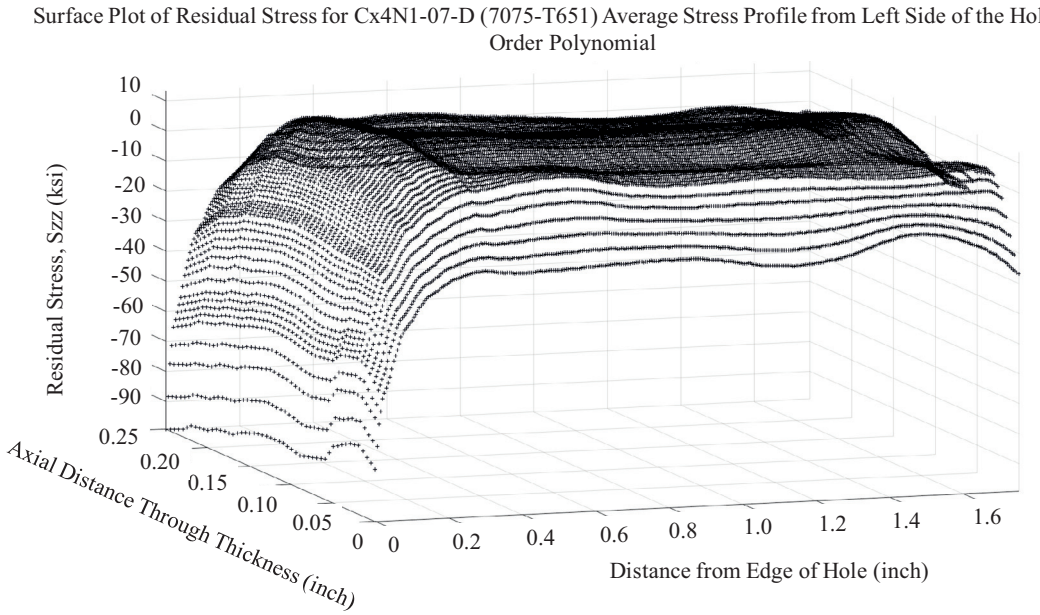

Fig. 881 Surface Plot of Residual Stress Traction Function Developed for the Average of the Cracked Side of the Hole for the Residual Stress Condition Cx4N1-07-D (7075-T651), these Coupons Had an Approximately 0.25 inch Surface Crack in the Cx Mandrel Entrance Surface.

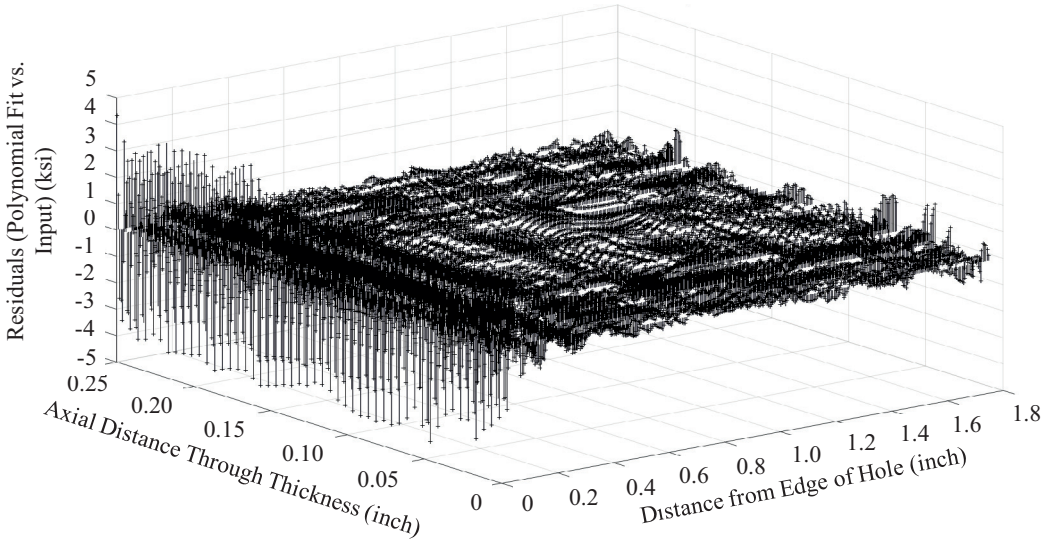

Fig. 882 Surface Plot of the Residual between the Polynomial Fit and the Actual Residual Stress Data for the Average of the Left Side of the Hole for the Residual Stress Condition Cx4N1-07-D (7075-T651), these Coupons Had an Approximately 0.25 inch Surface Crack in the Cx Mandrel Entrance Surface.

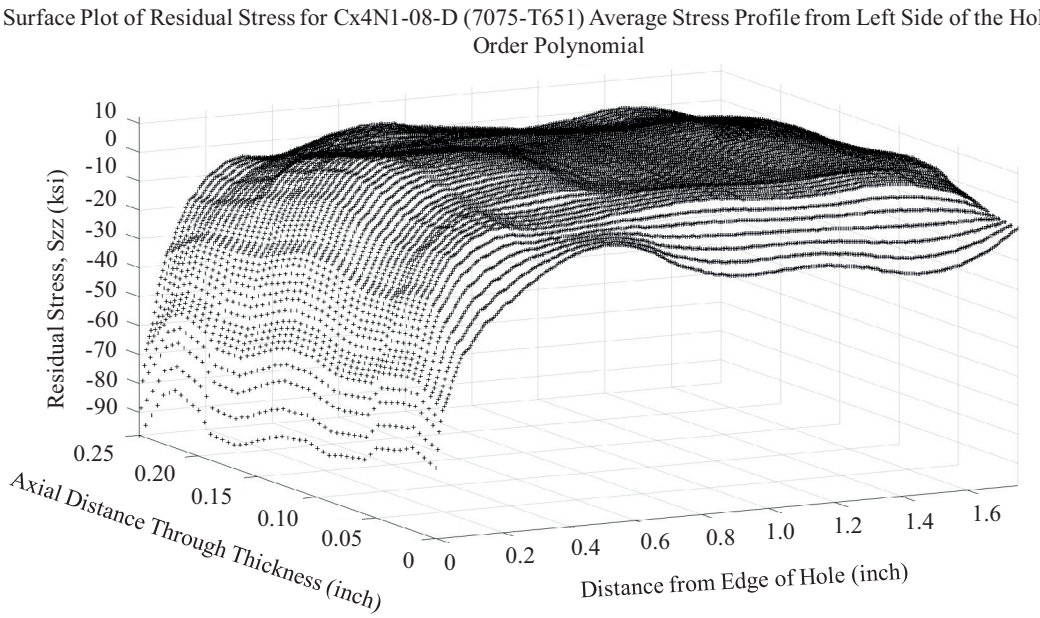

Fig. 883 Surface Plot of Residual Stress Traction Function Developed for the Average of the Cracked Side of the Hole for the Residual Stress Condition Cx4N1-08-D (7075-T651), these Coupons Had an Approximately 0.50 inch Surface Crack in the Cx Mandrel Entrance Surface.

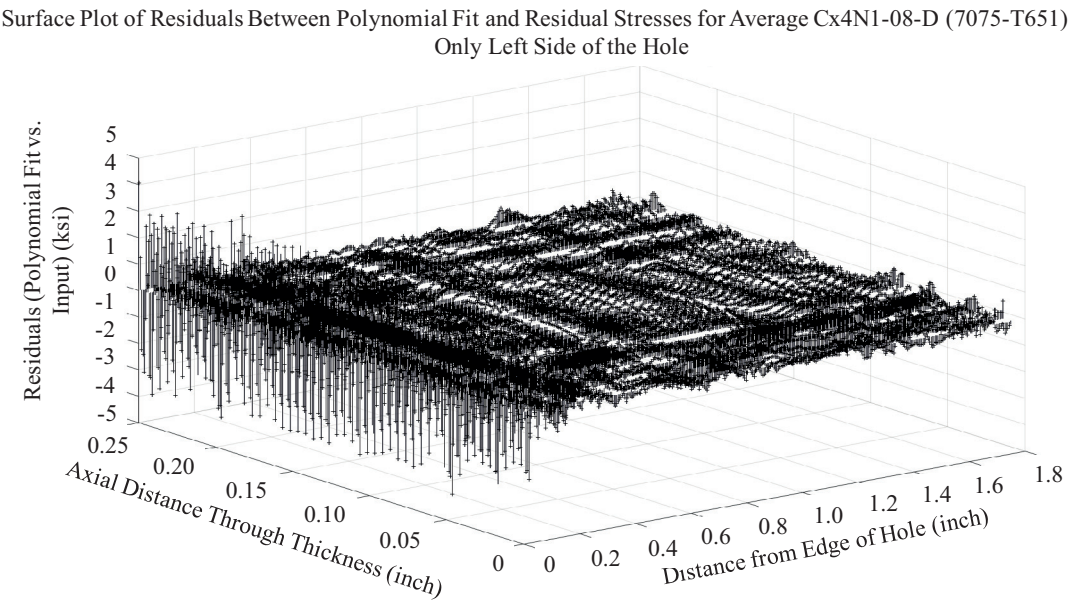

Fig. 884 Surface Plot of the Residual between the Polynomial Fit and the Actual Residual Stress Data for the Average of the Left Side of the Hole for the Residual Stress Condition Cx4N1-08-D (7075-T651), these Coupons Had an Approximately 0.50 inch Surface Crack in the Cx Mandrel Entrance Surface.

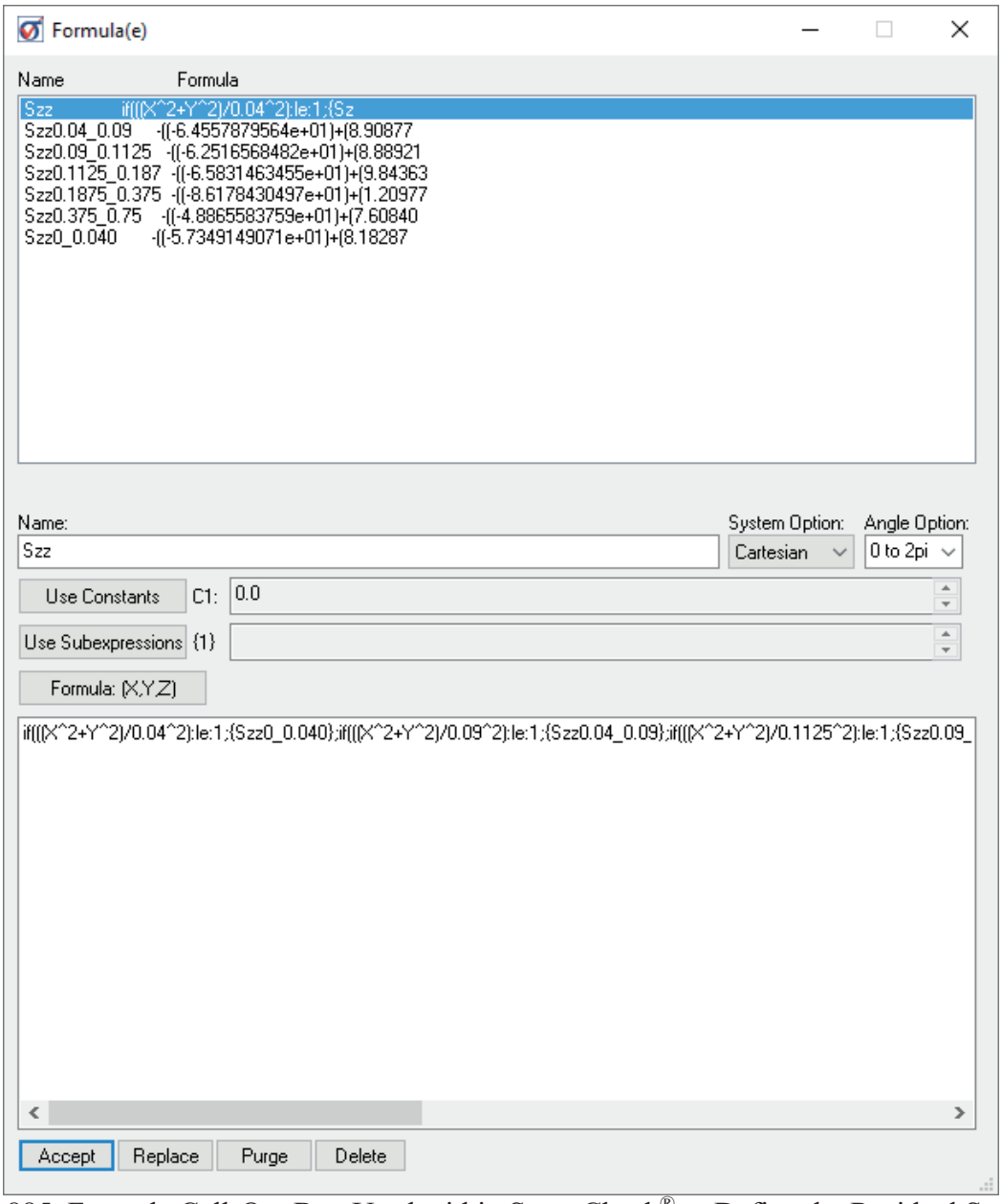

Fig. 885 Formula Call-Out Box Used within StressCheck® to Define the Residual Stress Functions for the Cx4N1-XX-B (2024-T351) Average Residual Stress.

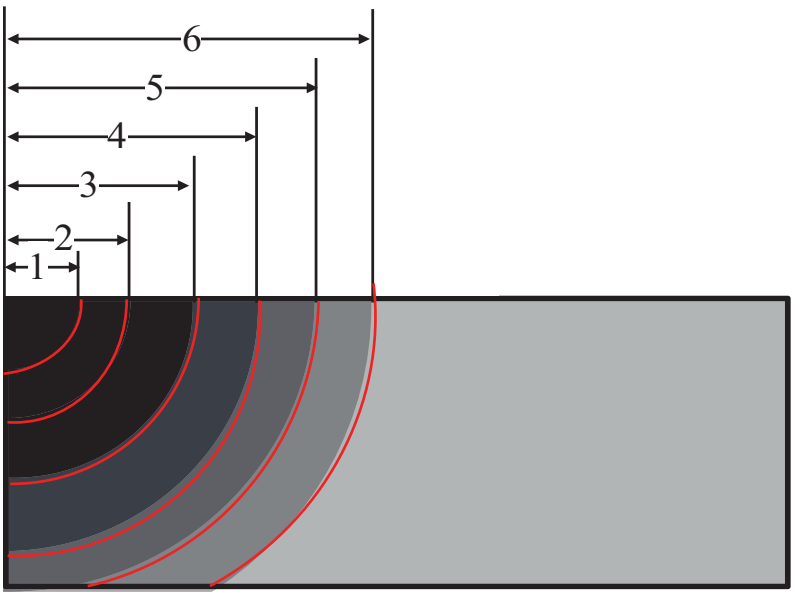

Fig. 886 Basic Diagram Showing the Breakdown of How the Cx4N1-XX Residual Stress "Loaded Crack" Traction Functions Were Applied at the Edge of the Hole.

Table 11 Breakdown of Residual Stress "Loaded Crack" Traction Function – Showing Coupons Names and Distances Applied

Plot Number	Residual Stress from Faituge Cracked Coupons	Distance Applied
1	Baseline Non-Cracked Residual Stress	0.00 - 0.04inch
2	Residual Stress for -01-02 (0.08inch) Crack Length	0.04 - 0.09inch
3	Residual Stress for -03-04 (0.10inch) Crack Length	0.09 - 0.1125inch
4	Residual Stress for -05-06 (0.125inc) Crack Length	0.1125 - 0.1875inch
5	Residual Stress for -07 (0.25inch) Crack Length	0.1875 - 0.375inch
6	Residual Stress for -08 (0.5inch) Crack Length	0.375 - 0.75inch

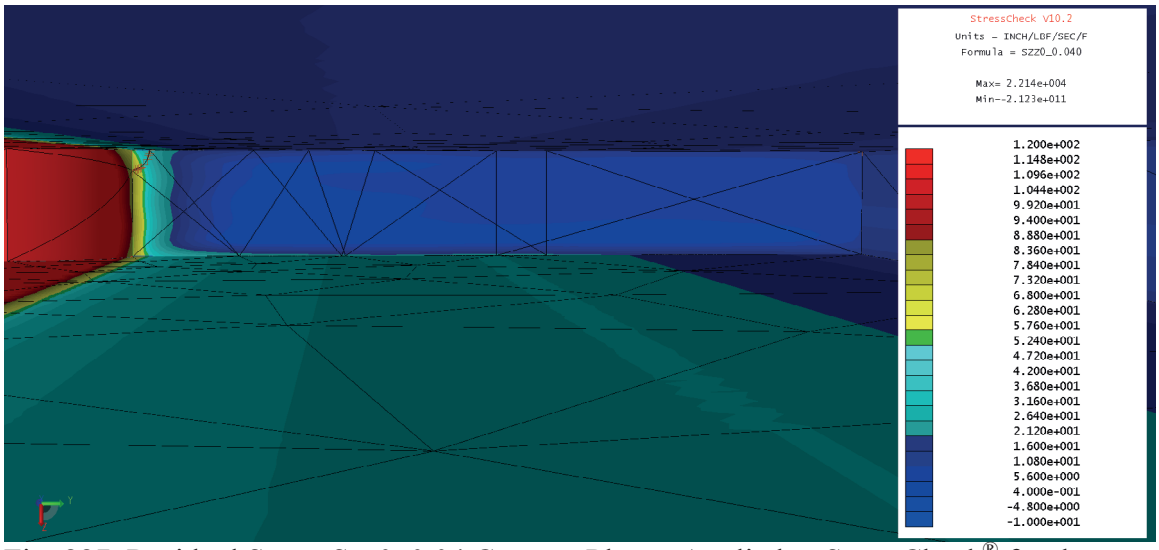

Fig. 887 Residual Stress Szz0_0.04 Contour Plot as Applied to StressCheck® for the Cx4N1-XX-B (2024-T351) Coupon Configuration.

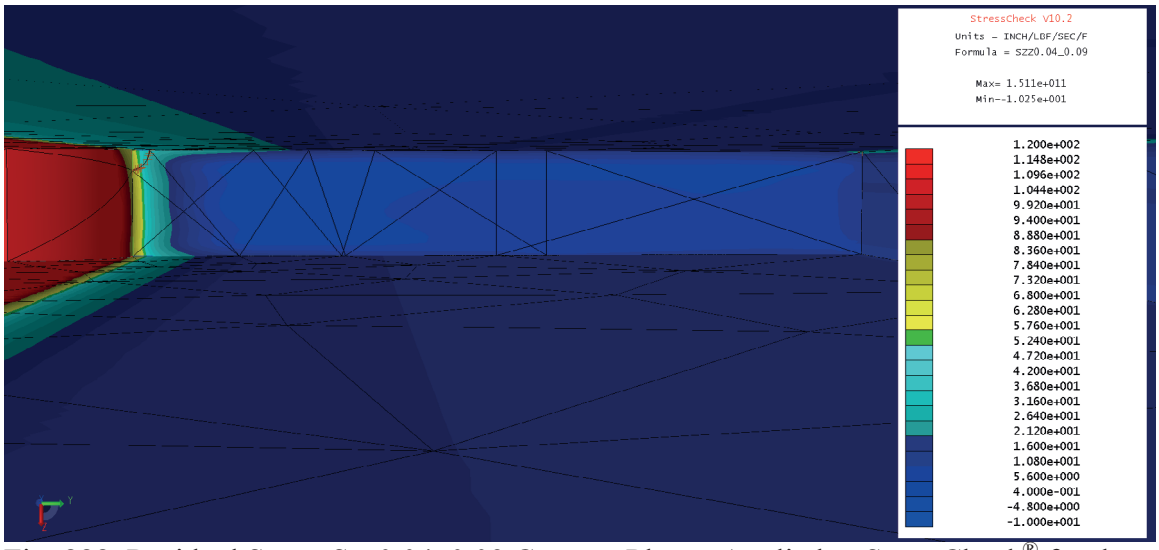

Fig. 888 Residual Stress Szz0.04_0.09 Contour Plot as Applied to StressCheck® for the Cx4N1-XX-B (2024-T351) Coupon Configuration.

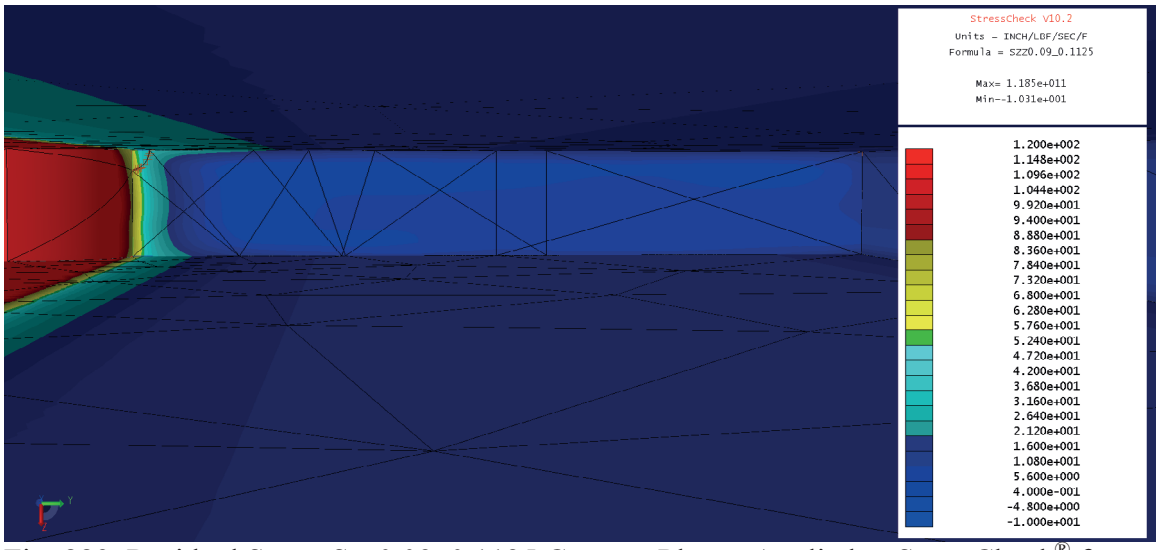

Fig. 889 Residual Stress Szz0.09_0.1125 Contour Plot as Applied to StressCheck® for the Cx4N1-XX-B (2024-T351) Coupon Configuration.

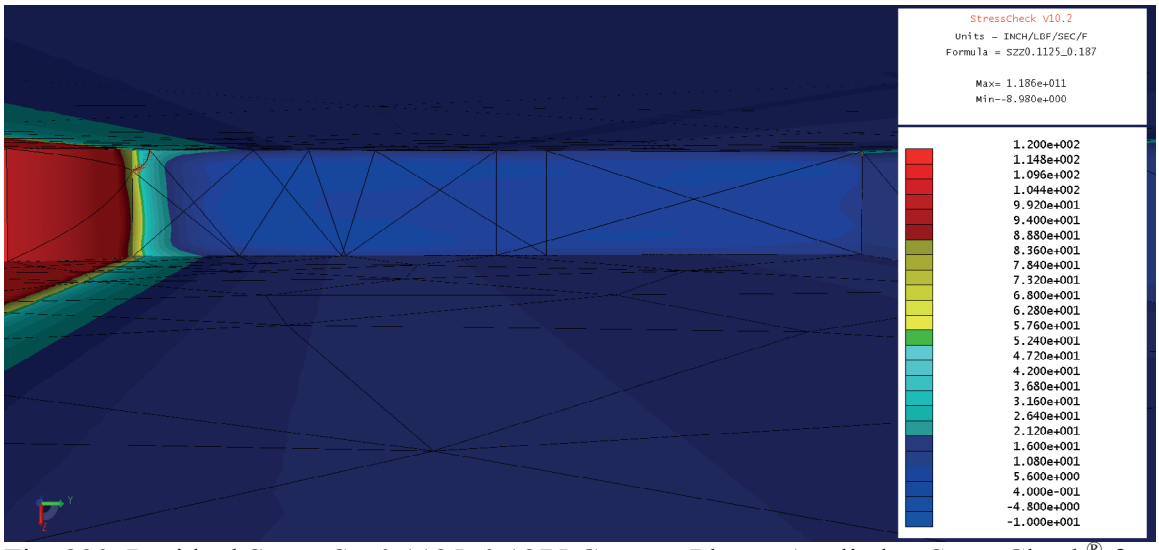

Fig. 890 Residual Stress Szz0.1125_0.1875 Contour Plot as Applied to StressCheck® for the Cx4N1-XX-B (2024-T351) Coupon Configuration.

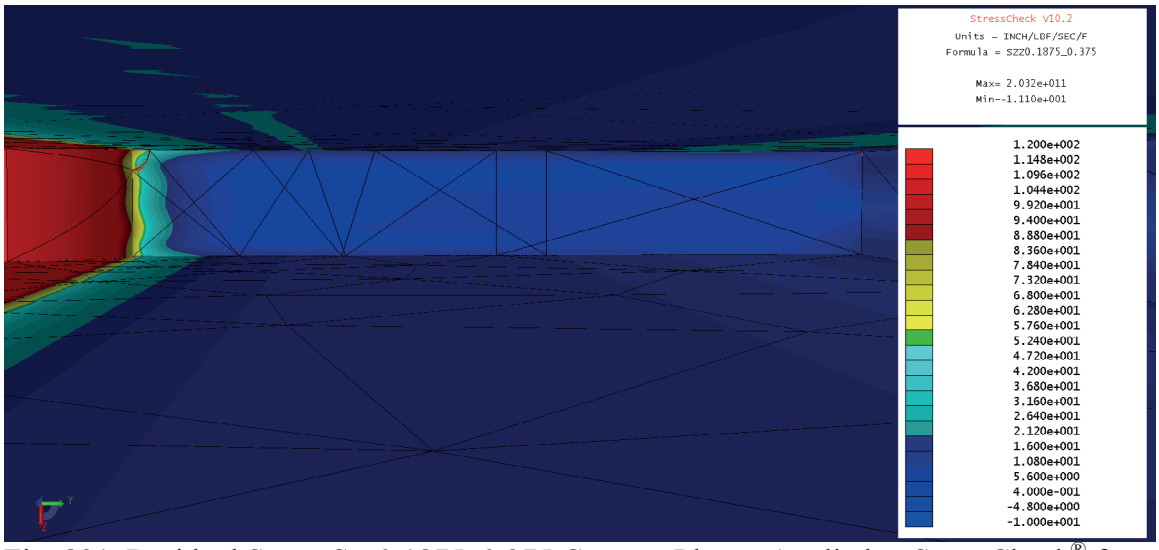

Fig. 891 Residual Stress Szz0.1875_0.375 Contour Plot as Applied to StressCheck® for the Cx4N1-XX-B (2024-T351) Coupon Configuration.

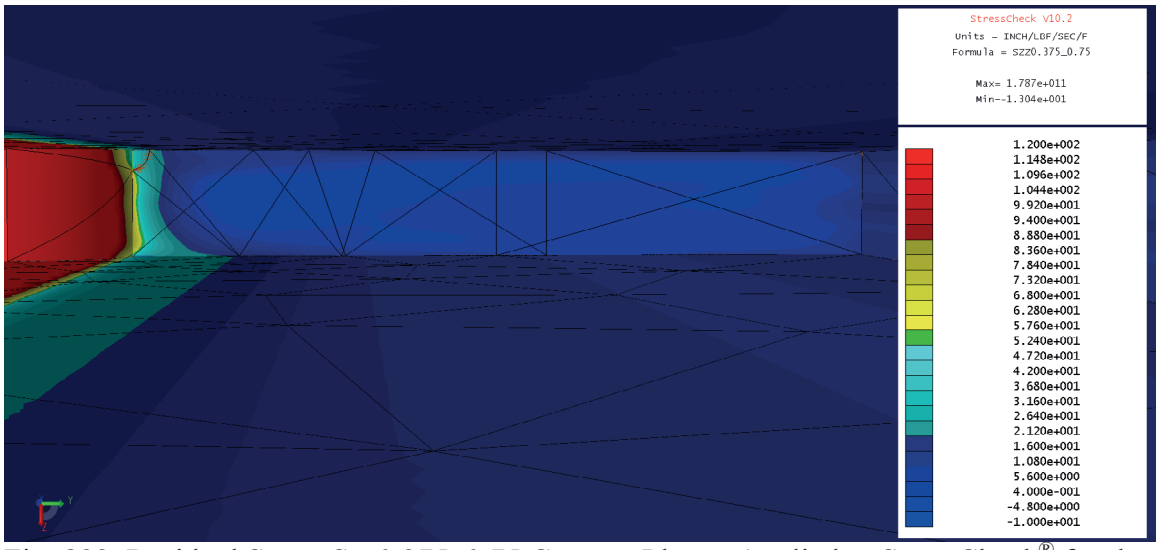

Fig. 892 Residual Stress Szz0.375_0.75 Contour Plot as Applied to StressCheck® for the Cx4N1-XX-B (2024-T351) Coupon Configuration.

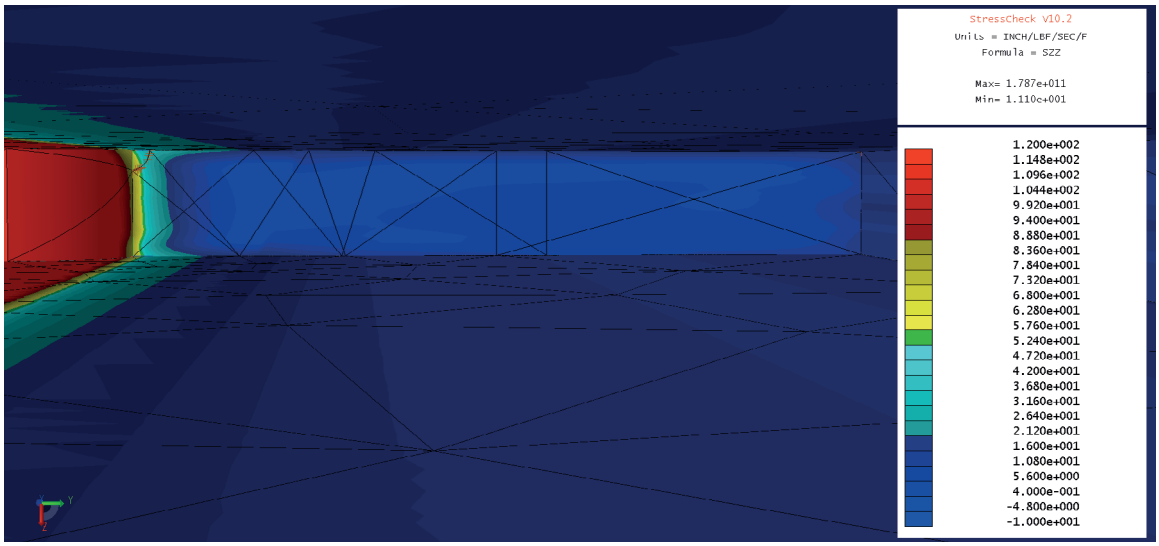

Fig. 893 Residual Stress Szz for the Combined Residual Stress Bivariant, Piecewise Contour Plot as Applied to StressCheck® for the Cx4N1-XX-B (2024-T351) Coupon Configuration.

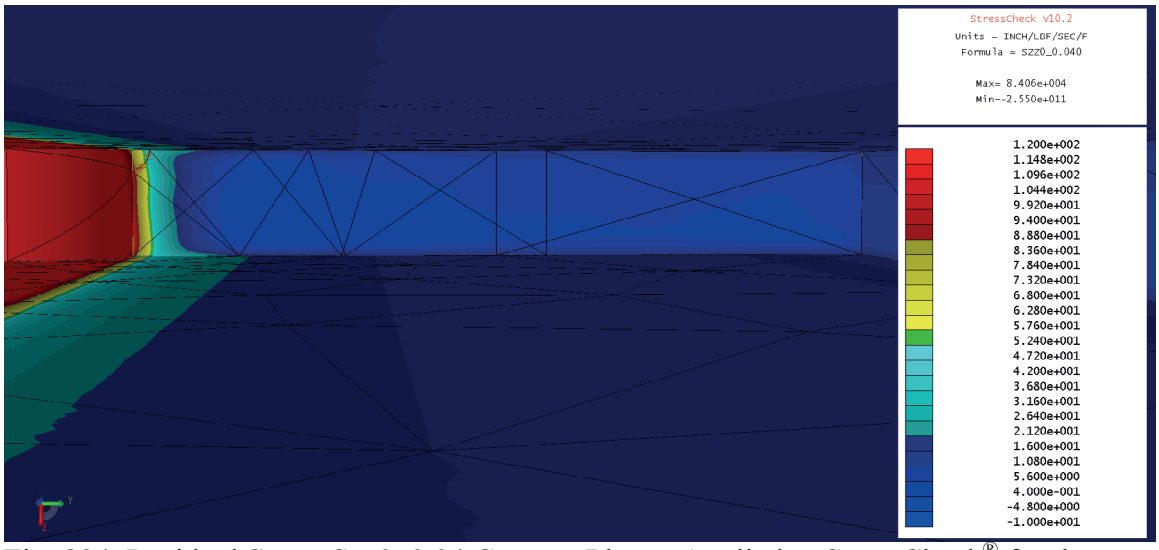

Fig. 894 Residual Stress Szz0_0.04 Contour Plot as Applied to StressCheck® for the Cx4N1-XX-D (7075-T651) Coupon Configuration.

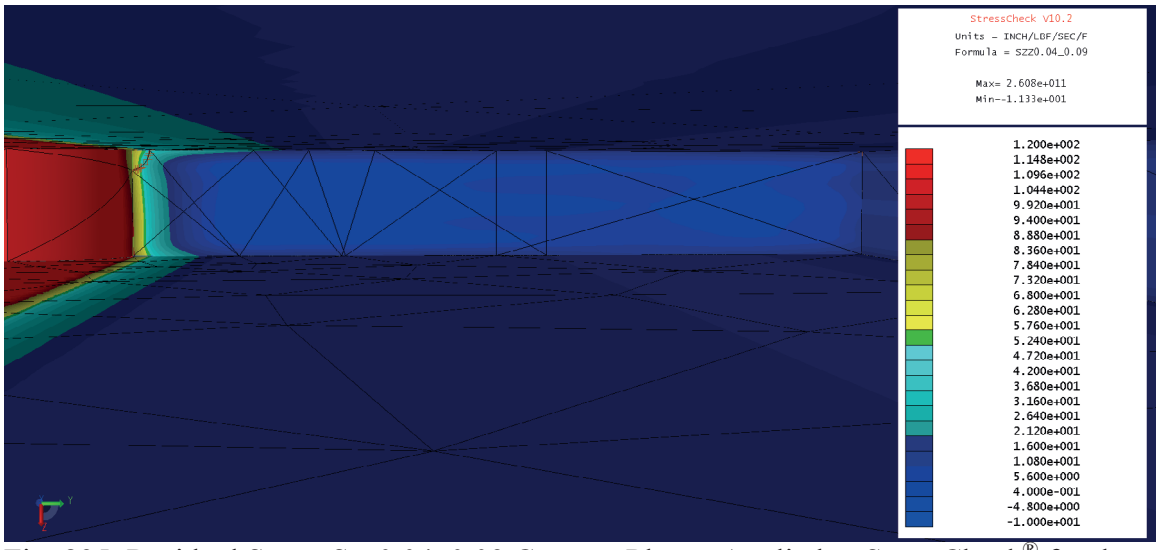

Fig. 895 Residual Stress Szz0.04_0.09 Contour Plot as Applied to StressCheck® for the Cx4N1-XX-D (7075-T651) Coupon Configuration.

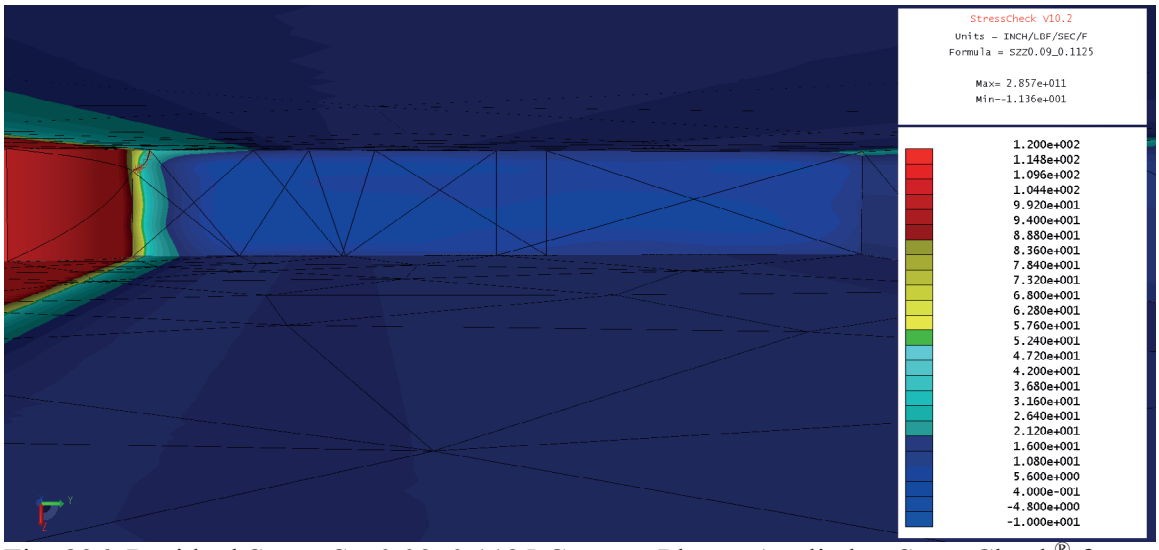

Fig. 896 Residual Stress Szz0.09_0.1125 Contour Plot as Applied to StressCheck® for the Cx4N1-XX-D (7075-T651) Coupon Configuration.

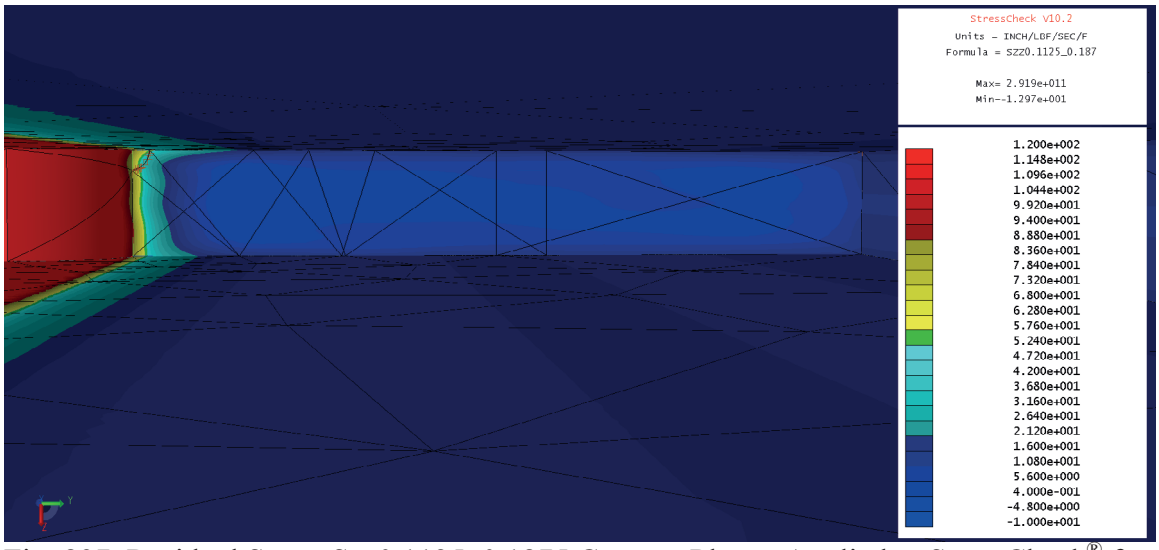

Fig. 897 Residual Stress Szz0.1125_0.1875 Contour Plot as Applied to StressCheck® for the Cx4N1-XX-D (7075-T651) Coupon Configuration.

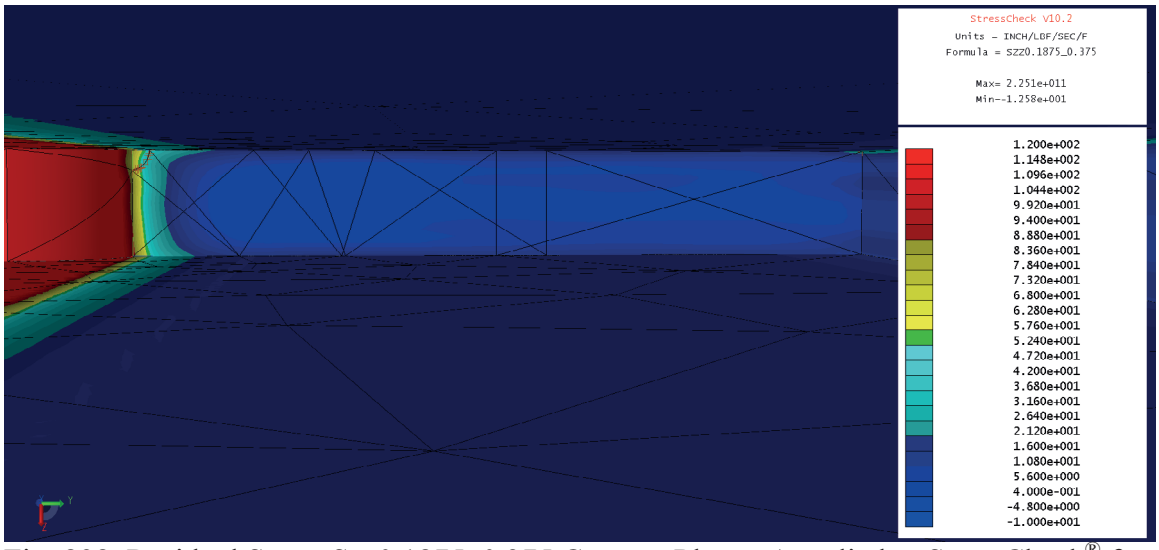

Fig. 898 Residual Stress Szz0.1875_0.375 Contour Plot as Aapplied to StressCheck® for the Cx4N1-XX-D (7075-T651) Coupon Configuration.

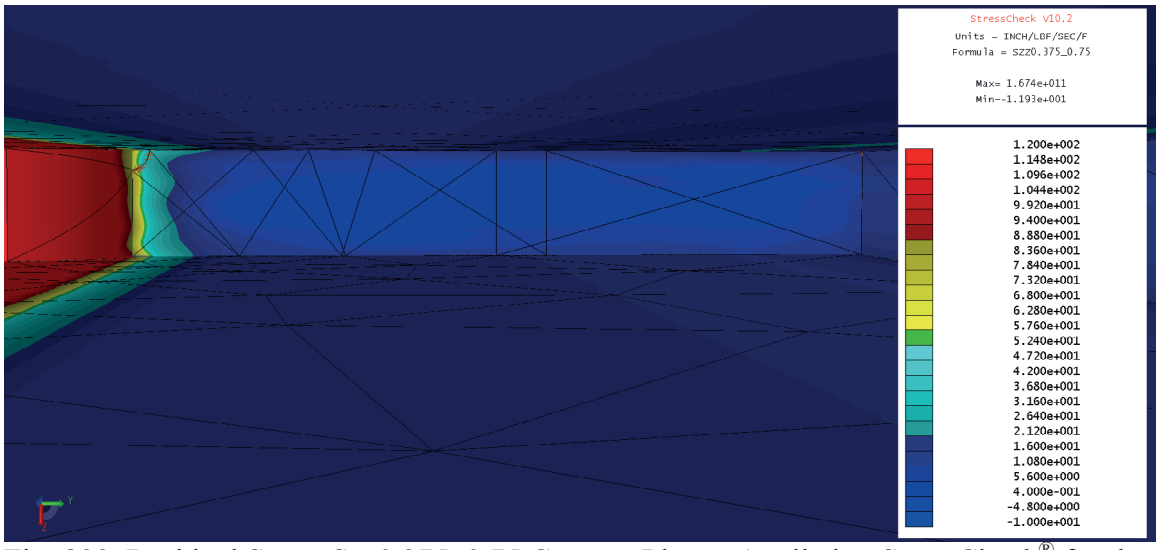

Fig. 899 Residual Stress Szz0.375_0.75 Contour Plot as Applied to StressCheck® for the Cx4N1-XX-D (7075-T651) Coupon Configuration.

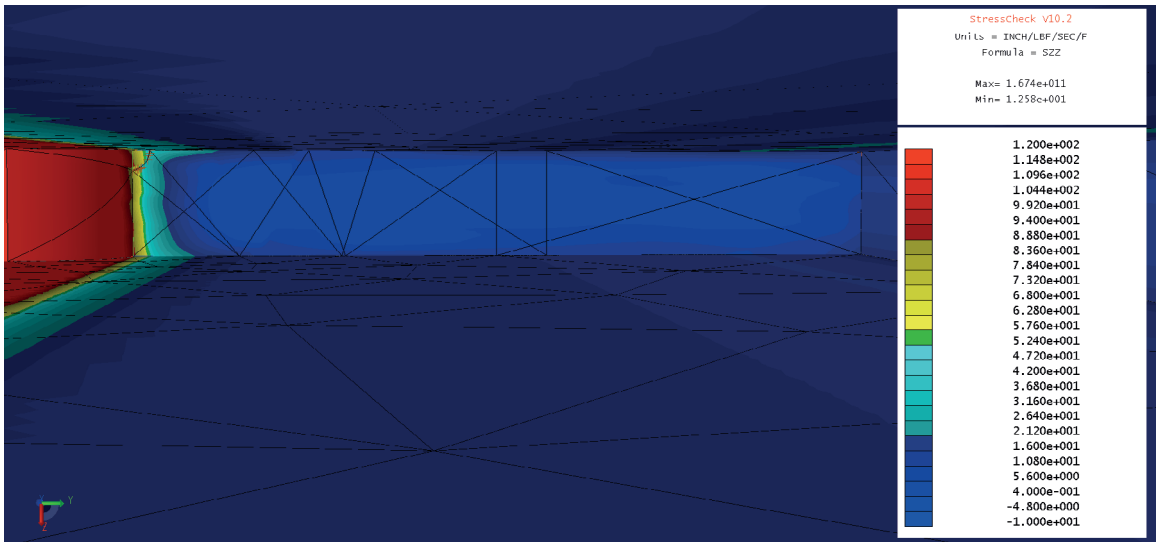

Fig. 900 Residual Stress Szz for the Combined Residual Stress Bivariant, Piecewise Contour Plot as Applied to StressCheck® for the Cx4N1-XX-D (7075-T651) Coupon Configuration.

Table 12 Configuration of Fatigue Life Predictions for Cx4N1-XX-B (2024-T351) and Cx4N1-XX-D (7075-T651) Coupons – Residual Stress Function Utilized the CxA2 and CxD2 Baseline Data for 0.0 – 0.04 inch away from the Hole

Preditions Made with 4N1 Functions and 0.00 - 0.04 as the Baseline CxA2 and CxD2 Functions					
Coupon Type	Material Model	Residual Stress Distribution	Time to Completion	Cycles	Average Predicted Life (cycles)
CxA2	APES	Average	7:12	112,156	137,991
		1STDDwn	9:26	231,899	
		1STDUp	6:21	69,919	
CxD2	APES	Average	9:33	125,738	183,226
		1STDDwn	10:19	171,256	
		1STDUp	8:41	252,684	

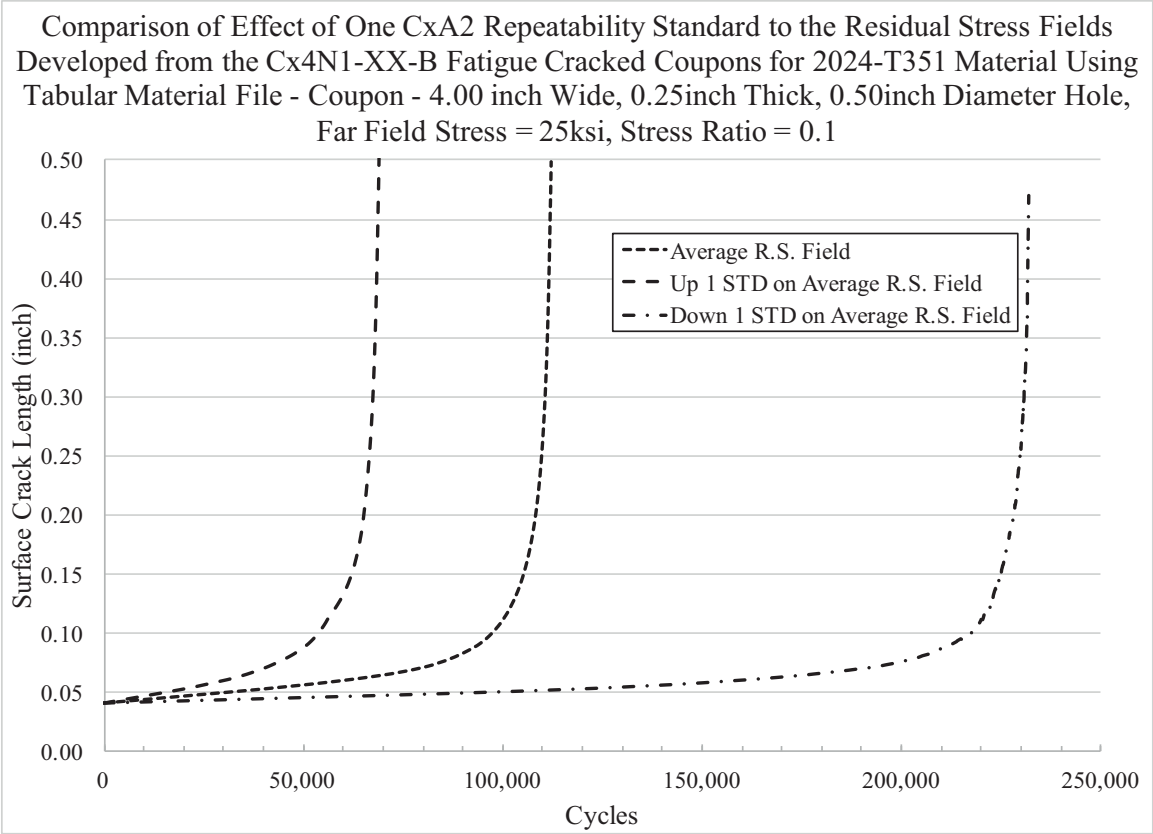

Fig. 901 Fatigue Life Prediction for the CxA2 (2024-T351) “Low” Applied Expansion Condition, with the Residual Stress Field Developed Using the CxA2 (2024-T351) Average Residual Stress from 0.0 inch – 0.04 inch, Showing the Effect of the Residual Stress Repeatability Standard Deviation on the Predicted Life.

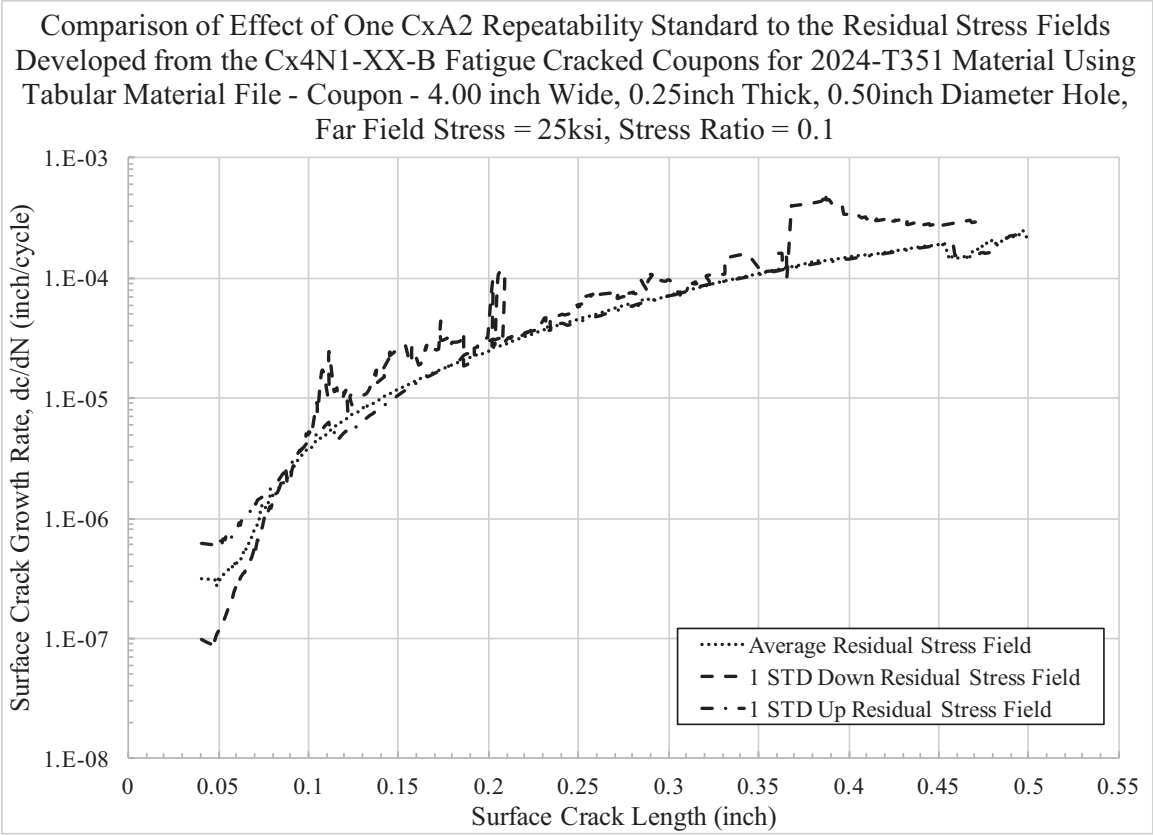

Fig. 902 Plot of Fatigue Crack Growth Rate (dc/dN) Compared to the Cx Mandrel Entrance Surface Crack Length (c), for the CxA2 (2024-T351) "Low" Applied Expansion Condition, with the Residual Stress Field Developed Using the CxA2 (2024-T351) Average Residual Stress from 0.0 inch – 0.04 inch, Showing the Effect of the Cx Repeatability Standard Deviation on the Predicted Cx Mandrel Entrance Surface Crack Growth Rate.

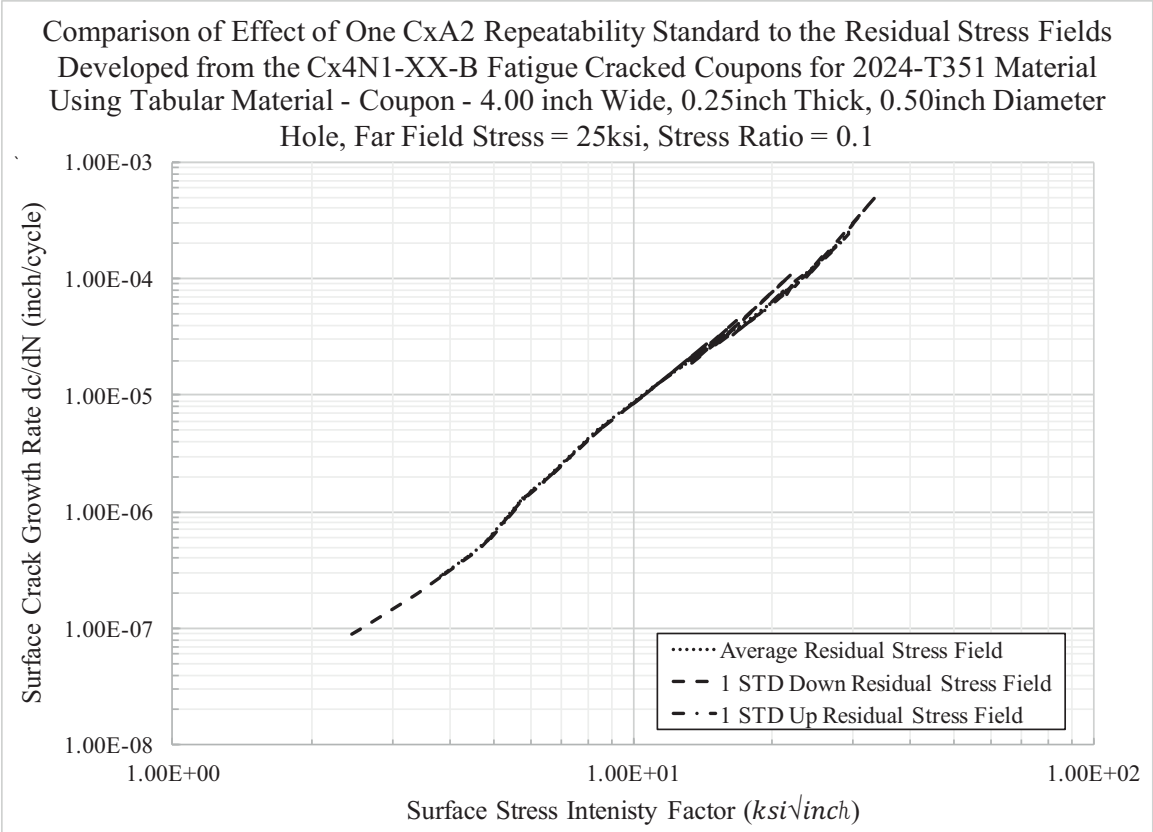

Fig. 903 Plot of Fatigue Crack Growth Rate (dc/dN) at the Cx Mandrel Entrance Versus the ΔK Developed via StressCheck® for the Cx Mandrel Entrance Surface for the CxA2 (2024-T351) "Low" Applied Expansion Condition, with the Residual Stress Field Developed using the CxA2 (2024-T351) Average Residual Stress from 0.0 inch – 0.04 inch.

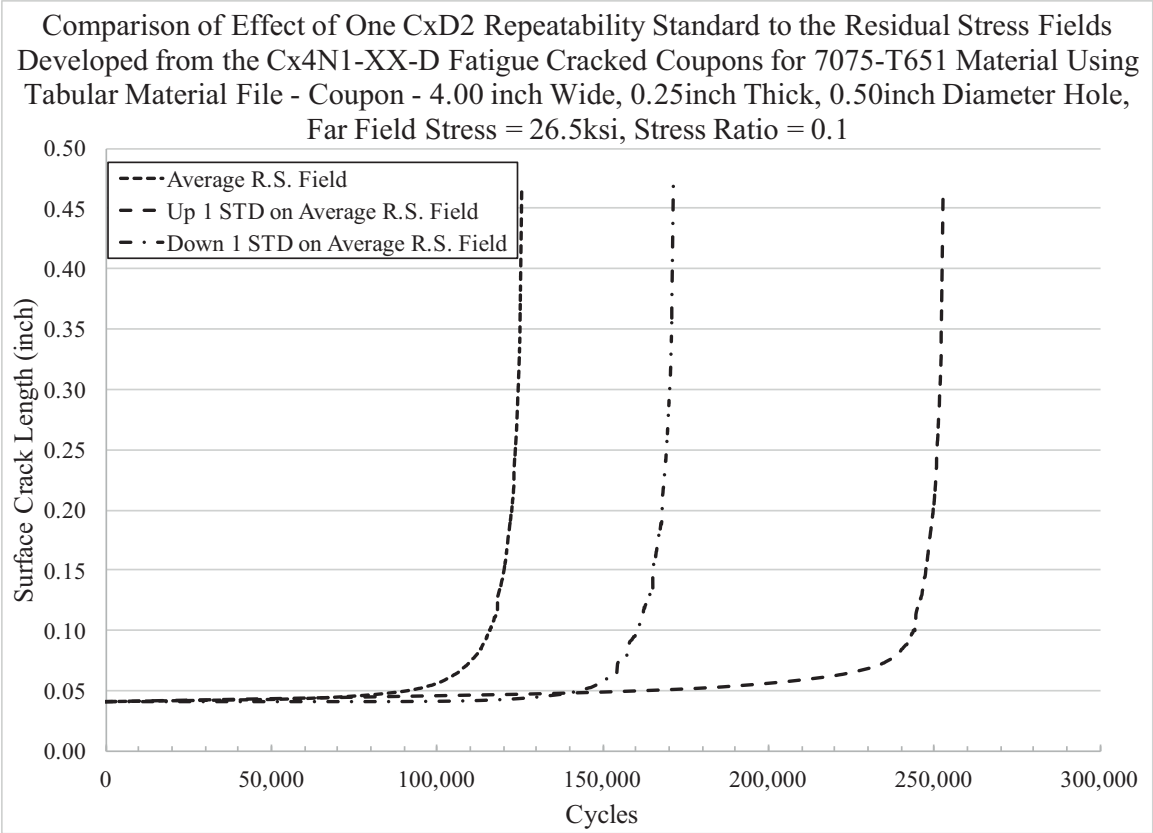

Fig. 904 Fatigue Life Prediction for the CxD2 (7075-T651) “Low” Applied Expansion Condition, with the Residual Stress Field Developed Using the CxD2 (7075-T651) Average Residual Stress from 0.0 inch – 0.04 inch, Showing the Effect of the Residual Stress Repeatability Standard Deviation on the Predicted Life.

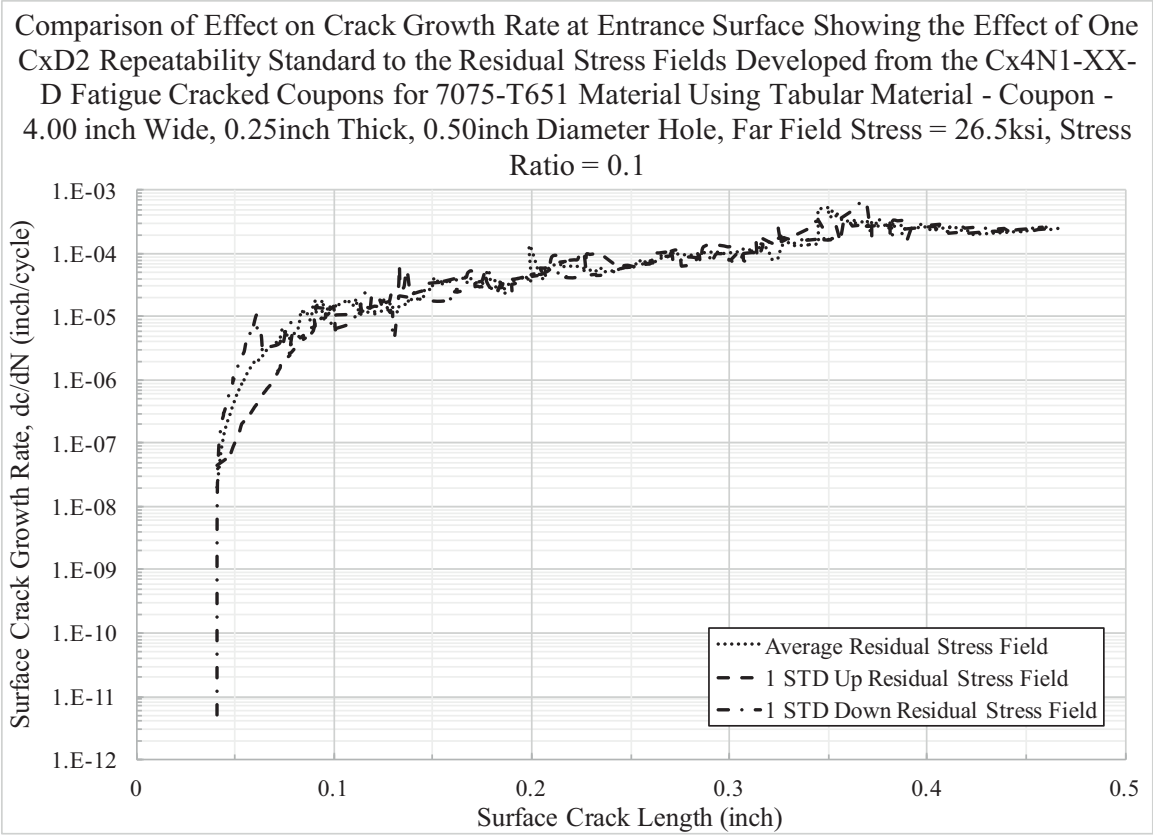

Fig. 905 Plot of Fatigue Crack Growth Rate (dc/dN) Compared to the Cx Mandrel Entrance Surface Crack Length (c), for the CxD2 (7075-T651) “Low” Applied Expansion Condition, with the Residual Stress Field Developed using the CxD2 (7075-T651) Average Residual Stress from 0.0 inch – 0.04 inch, Showing the Effect of the Cx Repeatability Standard Deviation on the Predicted Cx Mandrel Entrance Surface Crack Growth Rate.

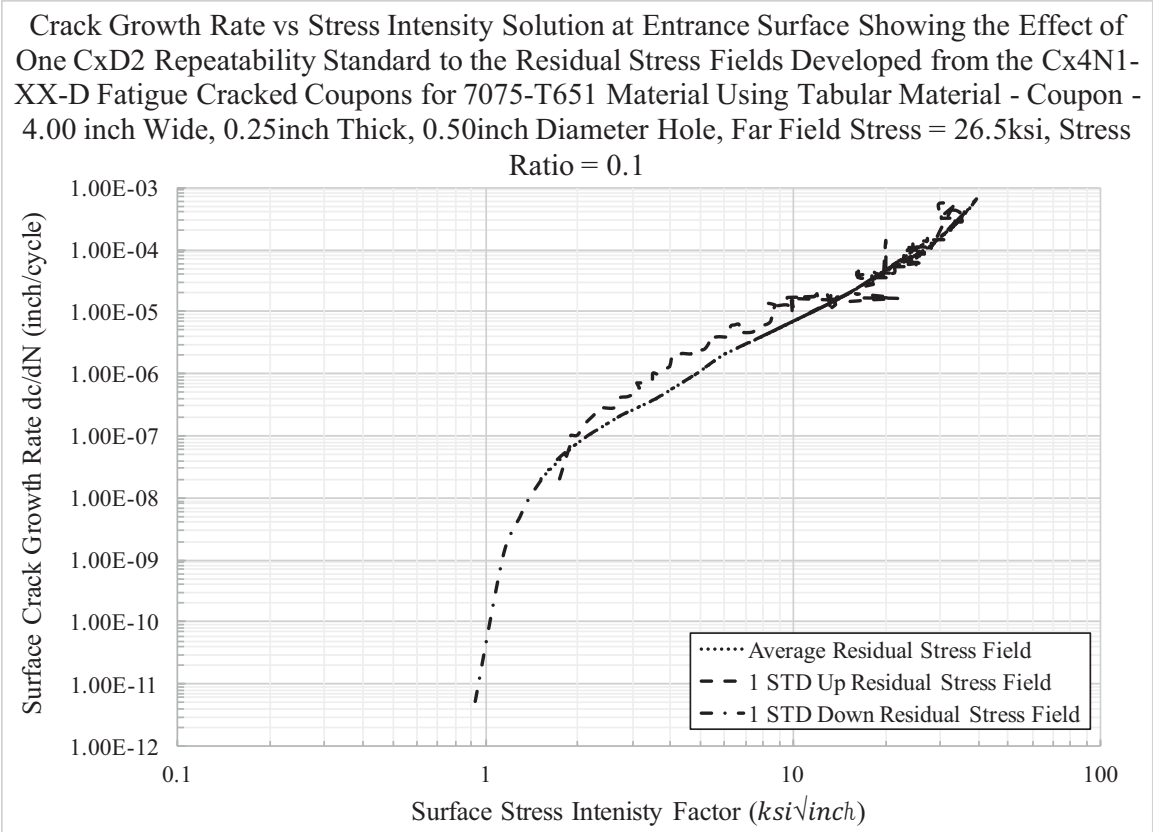

Fig. 906 Plot of Fatigue Crack Growth Rate (dc/dN) at the Cx Mandrel Entrance Versus the ΔK Developed via StressCheck® for the Cx Mandrel Entrance Surface for the CxD2 (7075-T651) "Low" Applied Expansion Condition, with the Residual Stress Field Developed using the CxD2 (7075-T651) Average Residual Stress from 0.0 inch – 0.04 inch.

Table 13 Configuration of Fatigue Life Predictions for Cx4N1-XX-B (2024-T351) and Cx4N1-XX-D (7075-T651) Coupons – Residual Stress Function Utilized the Cx4N1-01-02 Fatigue-Cracked Residual Stress Field Data for 0.0 – 0.09 inch away from the Hole

Preditions Made with 4N1 Functions and 0.00 - 0.09 as Cx4N1-01-02-XX (0.08inch Crack) Functions					
Coupon Type	Material Model	Residual Stress Distribution	Time to Completion	Cycles	Average Predicted Life (cycles)
CxA2	APES	Average	7:16	127,956	154,693
		1STDDwn	10:04	270,965	
		1STDUp	7:10	65,158	
CxD2	APES	Average	8:05	64,314	100,988
		1STDDwn	8:28	80,492	
		1STDUp	11:10	158,157	

Table 14 Breakdown of Residual Stress "Loaded Crack" Traction Function – Showing Coupons Names and Distances Applied for the Adjusted Bivariant "Loaded Crack" Traction Equation

Plot Number	Residual Stress from Faituge Cracked Coupons	Distance Applied
1	Residual Stress for -01-02 (0.08inch) Crack Length	0.00 - 0.09inch
2		
3	Residual Stress for -03-04 (0.10inch) Crack Length	0.09 - 0.1125inch
4	Residual Stress for -05-06 (0.125inc) Crack Length	0.1125 - 0.1875inch
5	Residual Stress for -07 (0.25inch) Crack Length	0.1875 - 0.375inch
6	Residual Stress for -08 (0.5inch) Crack Length	0.375 - 0.75inch

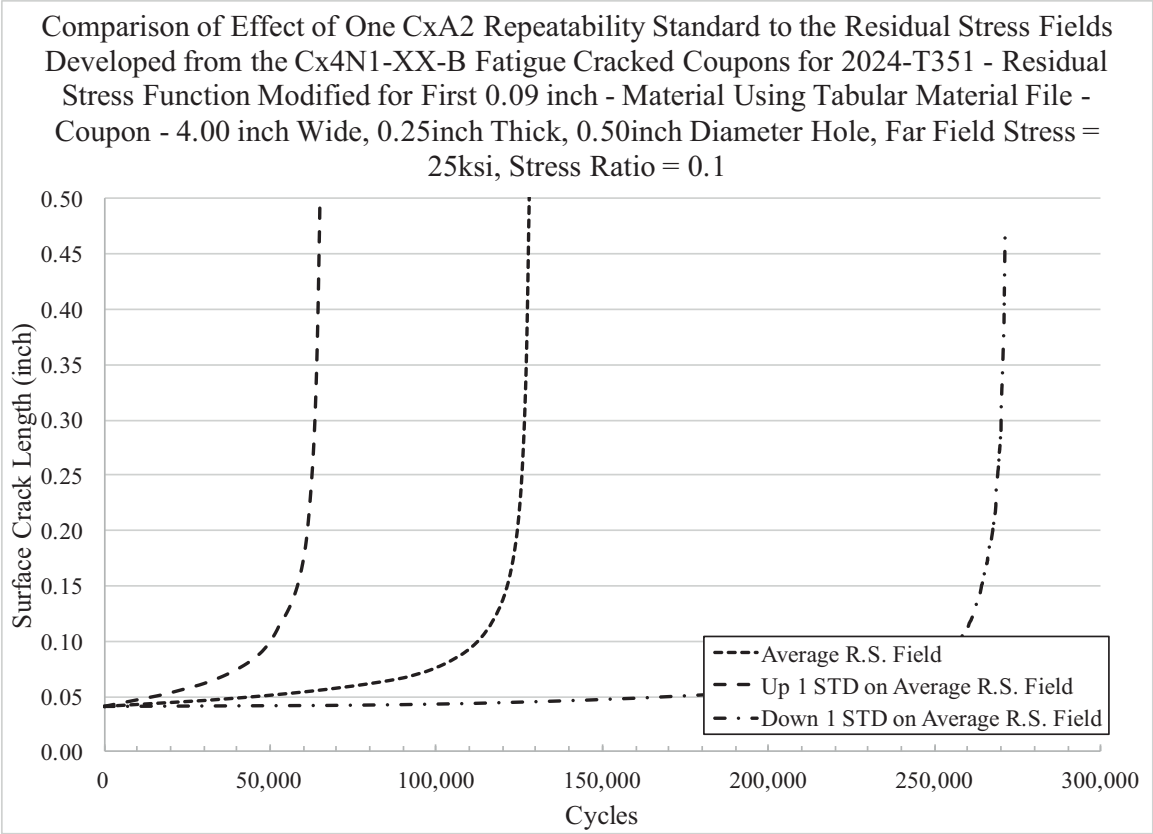

Fig. 907 Fatigue Life Prediction for the CxA2 (2024-T351) “Low” Applied Expansion Condition, with the Residual Stress Field Developed using the CxA2 (2024-T351) Average Residual Stress from 0.0 inch – 0.09 inch, Showing the Effect of the Residual Stress Repeatability Standard Deviation on the Predicted Life.

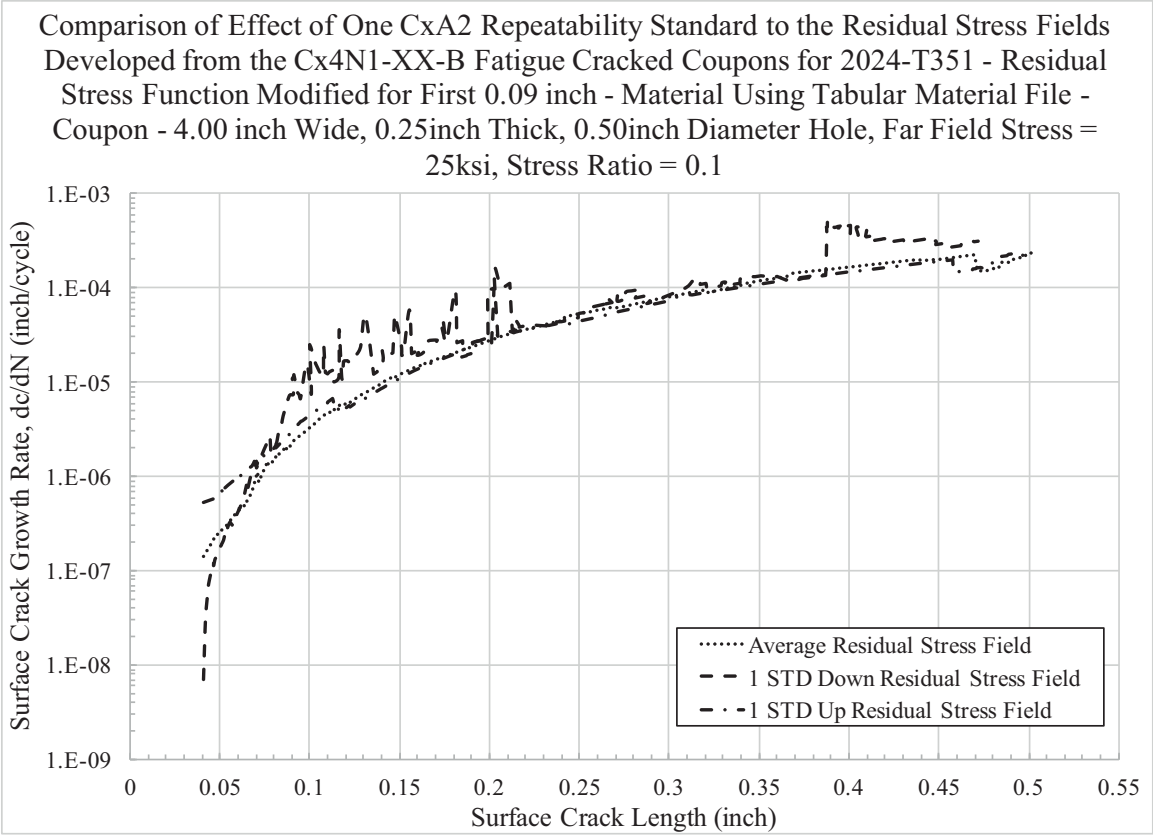

Fig. 908 Plot of Fatigue Crack Growth Rate (dc/dN) Compared to the Cx Mandrel Entrance Surface Crack Length (c), for the CxA2 (2024-T351) “Low” Applied Expansion Condition, with the Residual Stress Field Developed Using the CxA2 (2024-T351) Average Residual Stress from 0.0 inch – 0.09 inch, Showing the Effect of the Cx Repeatability Standard Deviation on the Predicted Cx Mandrel Entrance Surface Crack Growth Rate.

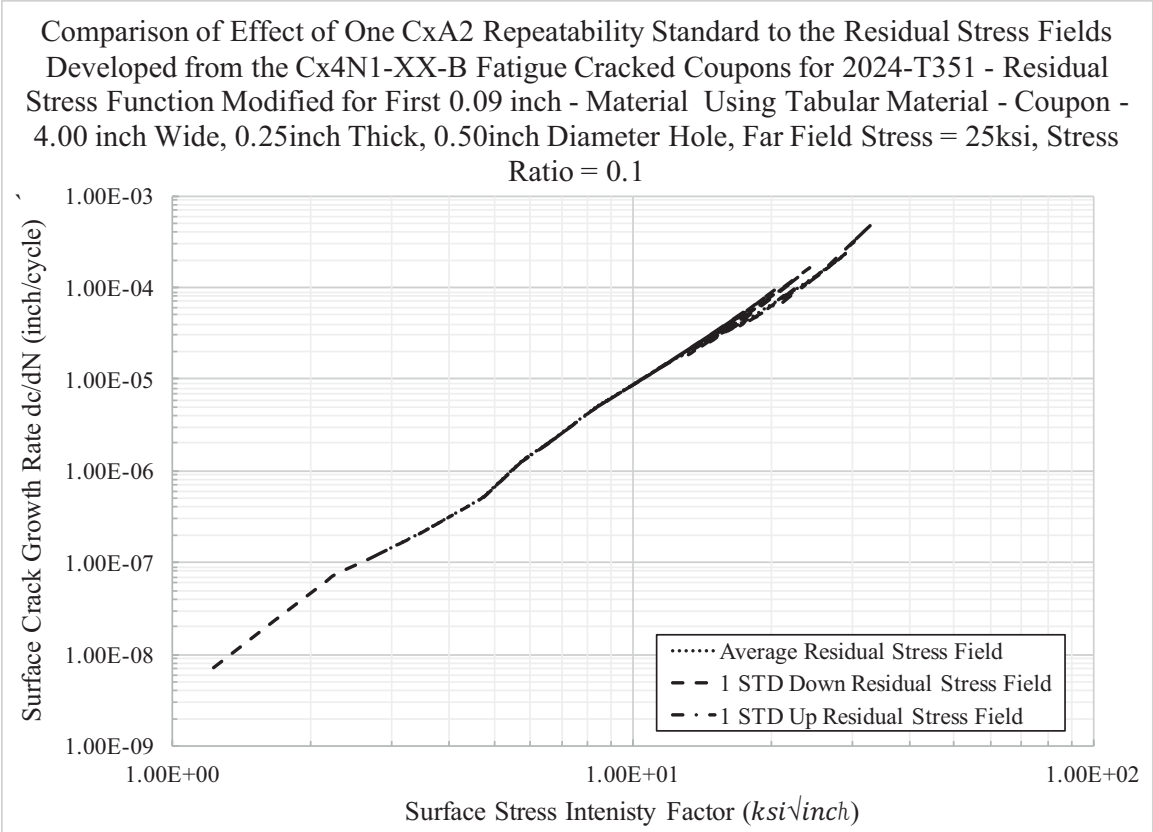

Fig. 909 Plot of Fatigue Crack Growth Rate (dc/dN) at the Cx Mandrel Entrance Versus the ΔK Developed via StressCheck® for the Cx Mandrel Entrance Surface for the CxA2 (2024-T351) "Low" Applied Expansion Condition, with the Residual Stress Field Developed Using the CxA2 (2024-T351) Average Residual Stress from 0.0 inch – 0.09 inch.

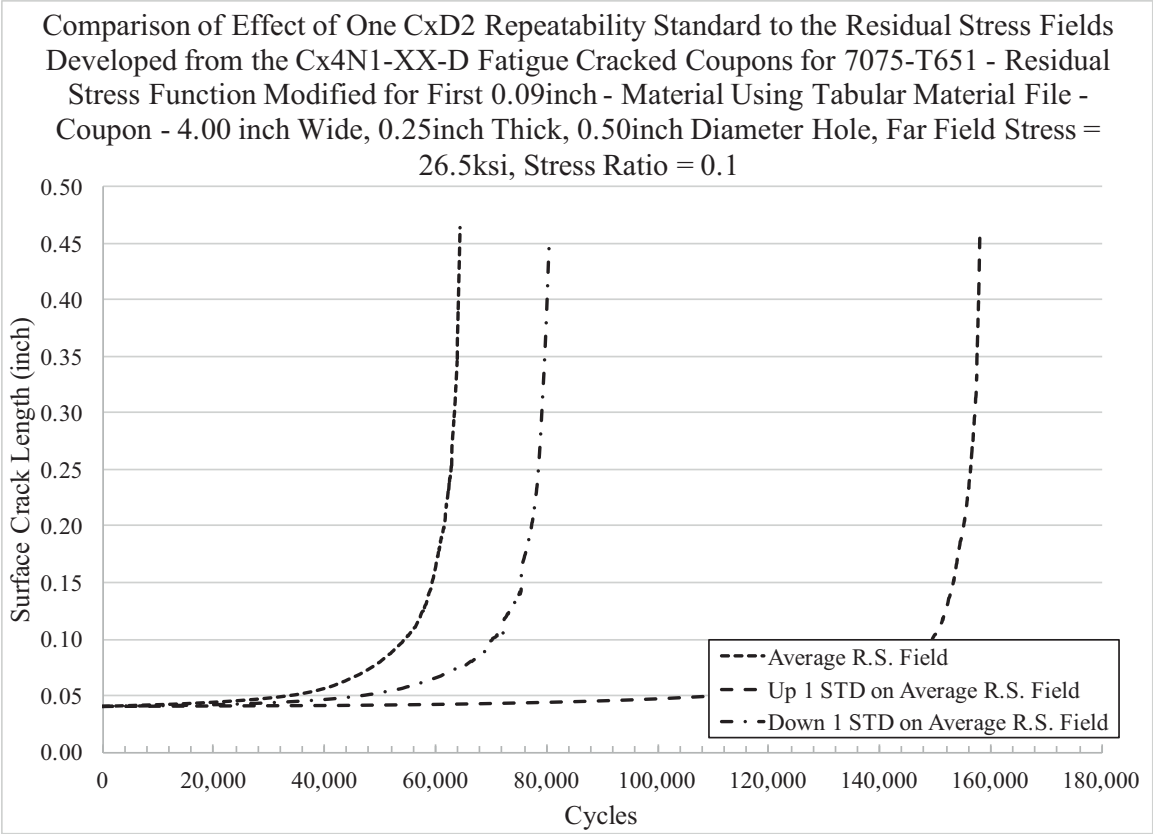

Fig. 910 Fatigue Life Prediction for the CxD2 (7075-T651) “Low” Applied Expansion Condition, with the Residual Stress Field Developed Using the CxD2 (7075-T651) Average Residual Stress from 0.0 inch – 0.09 inch, Showing the Effect of the Residual Stress Repeatability Standard Deviation on the Predicted Life.

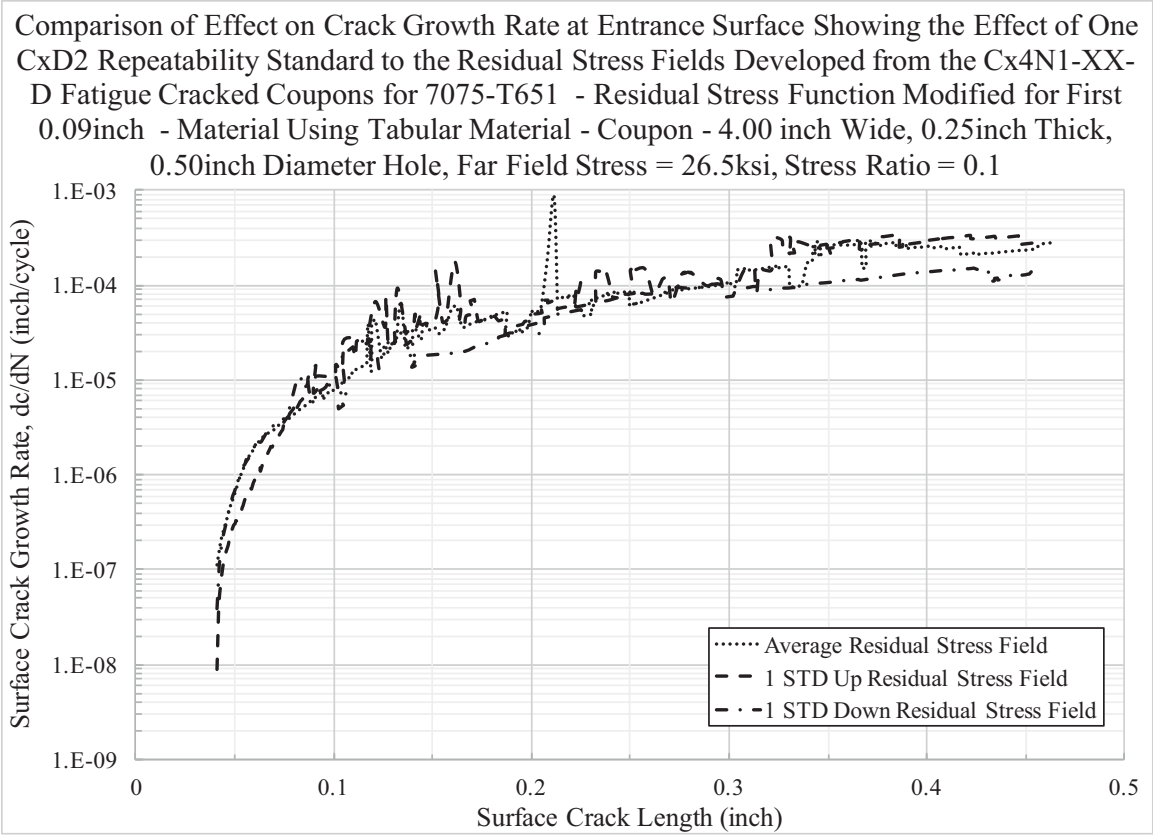

Fig. 911 Plot of Fatigue Crack Growth Rate (dc/dN) Compared to the Cx Mandrel Entrance Surface Crack Length (c), for the CxD2 (7075-T651) “Low” Applied Expansion Condition, with the Residual Stress Field Developed Using the CxD2 (7075-T651) Average Residual Stress from 0.0 inch – 0.09 inch, Showing the Effect of the Cx Repeatability Standard Deviation on the Predicted Cx Mandrel Entrance Surface Crack Growth Rate.

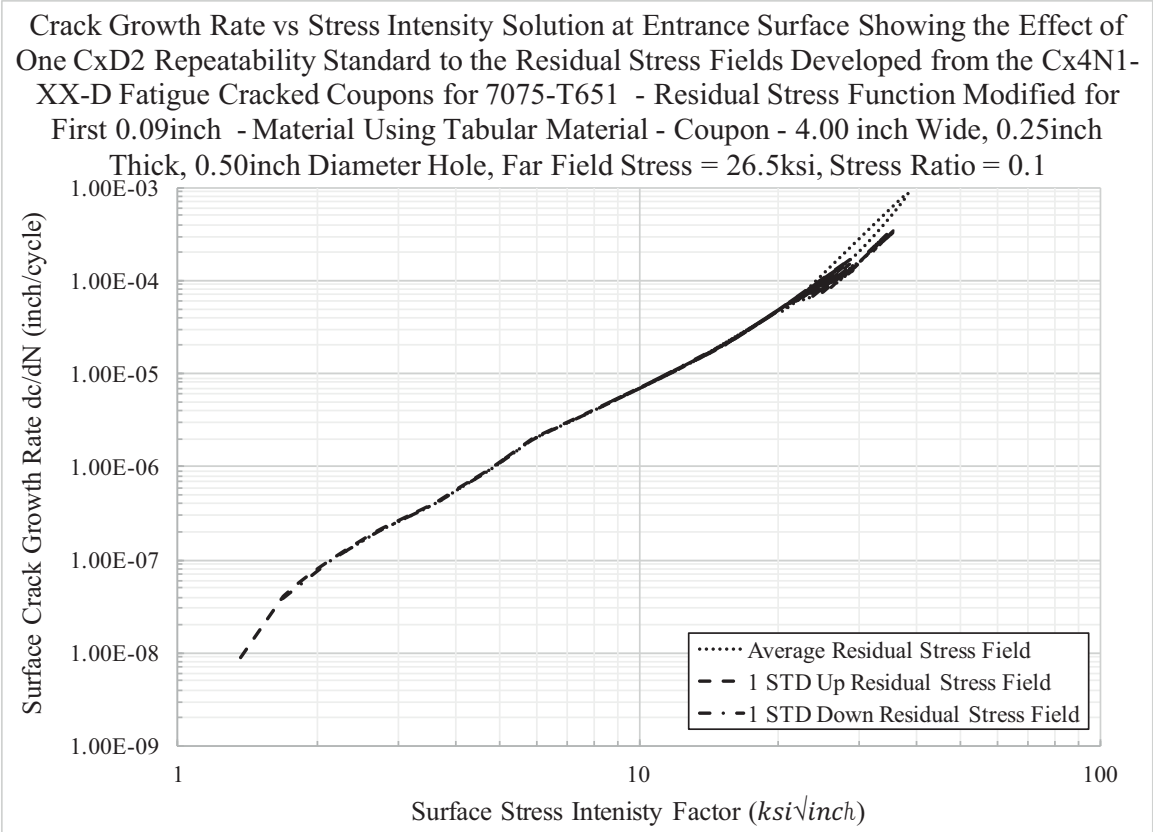

Fig. 912 Plot of Fatigue Crack Growth Rate (dc/dN) at the Cx Mandrel Entrance Versus the ΔK Developed via StressCheck® for the Cx Mandrel Entrance Surface for the CxD2 (7075-T651) "Low" Applied Expansion Condition, with the Residual Stress Field Developed Using the CxD2 (7075-T651) Average Residual Stress from 0.0 inch – 0.09 inch.

10 DEVELOPMENT AND EXECUTION OF FATIGUE TESTS FOR EVALUATION OF LIFE PREDICTIONS FOR "LOW" APPLIED EXPANSION LEVELS IN 2024-T351 AND 7075-T651 ALUMINUM ALLOYS

10.1 Development of Fatigue Coupons for Testing

At the beginning of the program four coupons were set aside to provide a blind validation of predictions made with the baseline, uncracked residual stress fields and those developed from the fatigue-cracked Cx4N1-XX-B-D coupons. These coupons were identical to those developed for the Cx4N1 program. They were precracked and final reamed to an initial flaw size of approximately 0.03 x 0.03 inch on the Cx mandrel entrance surface side. For both of the materials the Cx4N1-09 and -10 coupons were precracked and left in this condition. These coupons were in the final drawing condition as shown in Fig. 913 and Fig. 914. In addition to the drawing, an image of Cx4N1-09-D (7075-T651) is provide in Fig. 915, showing the condition of the coupon prior to testing. The fatigue crack was nucleated and propagated on the right side of the hole.

10.2 Development of Marker Banding Sequence for the Documentation of the Fatigue Crack Growth Shape Evolution from a Cold Expanded Hole

In addition to fatigue testing these coupons it was determined that it would be beneficial to apply a marker banding sequence to the constant amplitude loading that planned. Marker bands are utilized to produce either a visible to the naked eye, or under

magnification, marks on the fracture surface that document the fatigue crack shape and length at different stages of propagation.[153,154,155,156,157] It was determined that for all of the 2024-T351 coupons a far-field stress of 25 ksi would be applied at a R = 0.1. For the 7075-T651 coupons a far-field stress of 26.5 ksi was chosen, again at a R = 0.1. However, in order to perform the marker sequence a 15% overload, R of 0, would be introduced into the sequence for five cycles, followed by 790 cycles at a R of .73, followed by another five cycles at a 15% overload, R of 0. This sequence has been demonstrated to produce no statistically quantifiable influence on the fatigue life.[158,159] An image of this type of sequence can be viewed within the AFGROW Fatigue crack Growth software package and is provide in Fig. 916 and Fig. 917.

Through the use of these types of marker sequences it is possible to mark the fracture surface at a level that requires assisted visual instruments to find and document the marks. An example of these types of marks can be seen in Fig. 918. This marker was produced in 7075-T651 using the same marker sequence but with a lower far-field stress level of 23.5 ksi.

10.3 Fatigue Testing of Cx4N1-09-10-B (2024-T351) and –D (7075-T651) Coupons

Of the four coupons set aside for the blind prediction, three were tested correctly. One of the 7075-T651 coupons was tested at an incorrect test level and thus was not used for prediction validation. On each of the three coupons that were tested at the correct maximum stress and 15% overload, the total life and also the marker banding of the fracture face was collected. For all of the life curves the marker sequence cycles have been removed.

10.3.1 Fatigue crack Growth Curves (S-N) for the 2024-T351 “Low” Applied Cold Expansion Levels

For the two 2024-T351 coupons a constant amplitude, far-field stress level of 25 ksi, was used with a 15% overload (28.75 ksi) marker applied. Both of the 2024 coupons were tested at the correct stress level. The crack growth curve for these two coupons is provided in Fig. 919. As can be seen in Fig. 919 the fatigue tests for these two coupons was performed in a very repeatable manner, with minimal scatter in the fatigue lives.

10.3.2 Marker Banding of 2024-T351 Fatigue Coupons at “Low” Applied Expansion Levels

In addition to the fatigue life, each of the two fatigue coupons were marker banded to help document the fatigue crack shape evolution when the hole has been Cxed to the “low” applied expansion level. Fig. 920 provides documentation of both of the fatigue coupons marker banding and shape evolution. The fatigue crack growth evolution of these fatigue cracks is different from that documented in previous reports, as shown in Fig. 921.

10.3.3 Fatigue crack Growth Curves (S-N) for the 7075-T651 “Low” Applied Cold Expansion Levels

The remaining 7075 coupon was correctly tested at a far-field stress of 26.5 ksi, Stress Ratio (R) = 0.1, with a 15% overload marker sequence with a far-field stress of 30.5 ksi. The crack growth curve for coupon Cx4N1-09-D (7075-T651) is provided in Fig. 922. With only one fatigue coupon tested, two additional crack growth curves were added to provide a greater understanding of the fatigue crack growth characteristics of this material under the “low” applied expansion level.

For all of the Cx4N1-XX-D (7075-T651) coupons the fatigue cracks that were developed prior to having them cut at Hill Engineering, LLC., were developed under a constant amplitude, far-field stress of 26.5 ksi, R = 0.1. Thus, for the -07 and -08 conditions, cracks were propagated and tracked until they reached their required Cx mandrel surface length. The fatigue crack growth lives were added to that produced by coupon Cx4N1-09-D (7075-T651), and combined they are provided in Fig. 923.

When these two additional coupons fatigue lives are added into the overall view it can be seen that there is a much greater dispersion of fatigue lives within the 7075-T651 material than that which is seen in the 2024-T351 material. All three of these coupons were Cxed using the same tooling and methods. The loading sequence was the same as well.

10.3.4 Marker Banding of 7075-T651 Fatigue Coupons at "Low" Applied Expansion Levels

Only fatigue coupon Cx4N1-09-D (7075-T651) was marker banded appropriately. A map of the fatigue crack evolution for fatigue coupon Cx4N1-09-D (7075-T651) is provided in Fig. 924.

Like the 2024-T351 coupons this 7075-T651 coupon did not show the "P-shaped" crack for as long over the evolution as has been seen in the past for this material, in this thickness, as shown in Fig. 925. It is possible that the reason for the increased Cx mandrel exit side pinning of the fatigue crack is due to a higher level of applied expansion that was introduced into these coupons via the nominal tolerance stack-ups that were present during the Cx process.

10.4 Conclusions from the Fatigue Testing of Cx4N1-09-10-B (2024-T351) and –D (7075-T651) Coupons

Of the four "low" applied expansion coupons that were set aside for fatigue crack growth testing, only three of them were tested at the correct test level. Each of the three coupons that were tested had a series of marker bands that were introduced into them that were used to develop a fatigue crack growth evolutional map, from the initial flaw size, post ream, to the final fracture size. The marker sequence that was selected provided no statistically quantifiable influence on the fatigue crack growth characteristics of the coupons. Thus, these coupons represent a condition for both fatigue life and shape that could be compared to the previous predictions of the fatigue crack growth behavior of coupons that were Cxed to the "low" end of the applied expansion level for both 2024-T351 and 7075-T651 aluminum alloys.

The fatigue testing of the 2024-T351 aluminum alloy showed very consistent fatigue lives and fatigue crack growth shapes, as documented by the marker banding. With only one of the 7075-T651 coupons tested at the correct test level, two additional coupon fatigue lives were added for comparison. These two additional coupons were tested at the same stress level and Stress Ratio (R), but were tested to develop crack lengths and be cut and have their residual stress determined via the contour method. When Cx4N1-07-D and Cx4N1-08-D (7075-T651) coupons were added to the crack growth curve, it showed a dramatic variation in the fatigue lives of the two sets of coupons. It is currently not known why there is such a dramatic difference, however the predictions of this condition, using the repeatability standard deviation, show this type of spread in the fatigue lives. So it is possible that the lives represent the typical dispersion seen in fatigue crack growth lives of Cx coupons. As a check to see if these "crack

development" coupons were somehow tested differently than the final two fatigue coupons, Fig. 926 shows the addition of Cx4N1-08-B (2024-T351) which was used to develop a 0.50 inch fatigue crack, under the same constant amplitude loading as the fatigue tested coupons, for the same material. As can be seen in Fig. 926 the fatigue tested and the "crack development" coupons behaved very similarly within the 2024-T351 aluminum alloy. This builds confidence that even though the fatigue tested 7075-T651 coupon, Cx4N1-09-D had a significantly different fatigue life than the two that were used to develop cracks for residual stress determination, the difference that is seen in the life is due to the statistical spread of the lives, due to the Cx process.

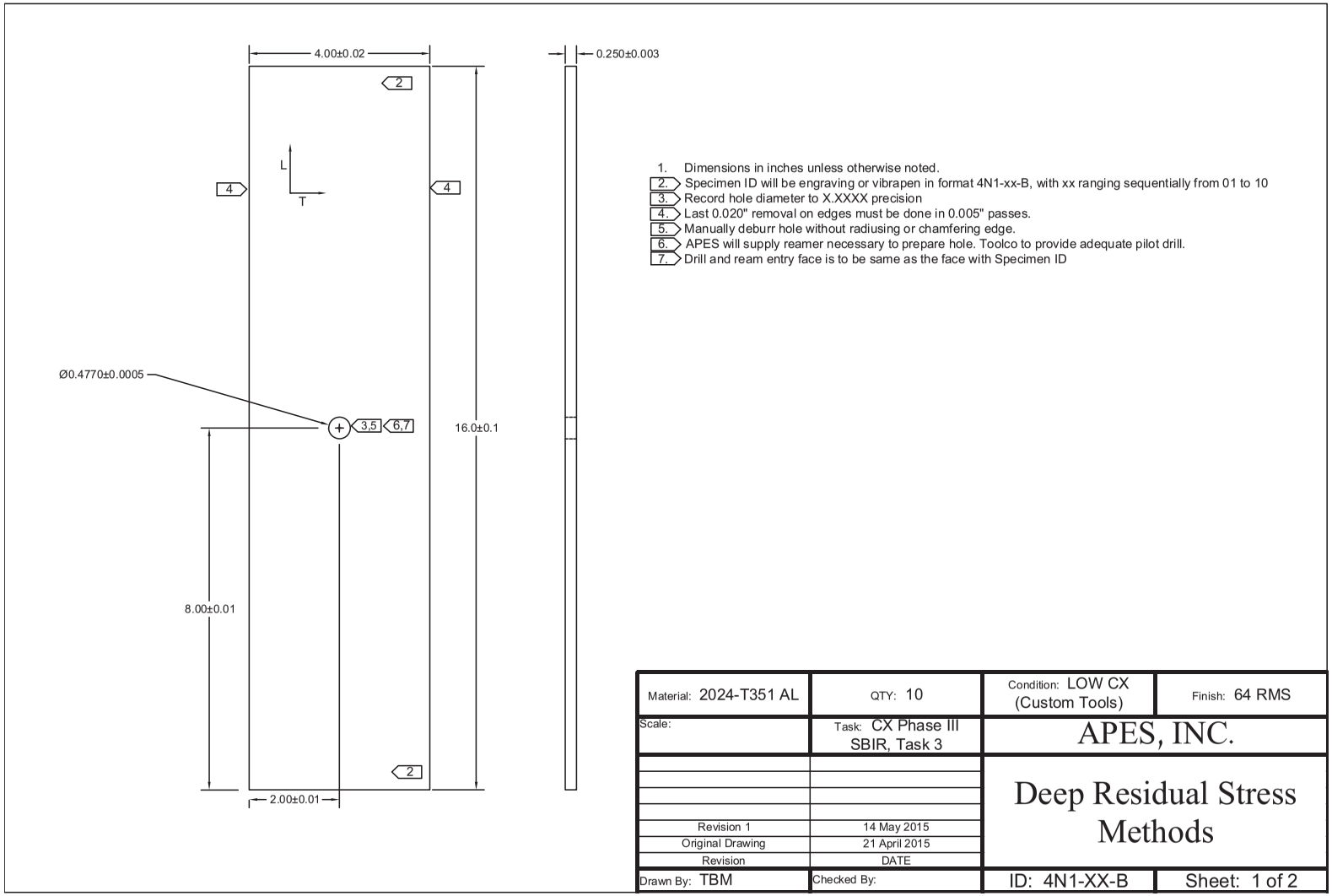

Fig. 913 Fatigue Coupon Drawing Showing Final Hole Size of 0.4770 for Cx4N1-XX-B (2024-T351) ”Low” Applied Cx Expansion Level.

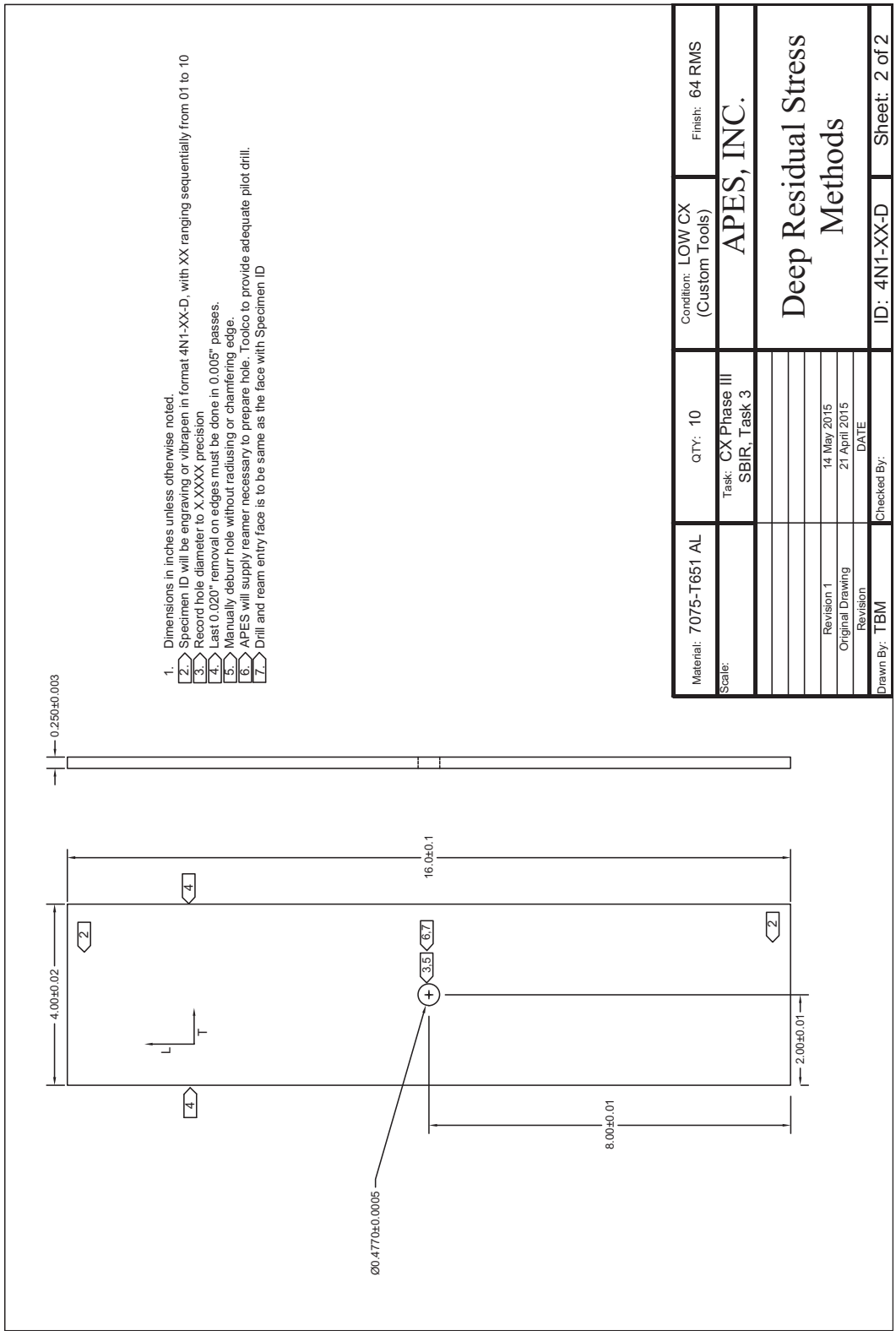

Fig. 914 Fatigue Coupon Drawing Showing Final Hole Size of 0.4770 for Cx4N1-XX-D (7075-T651) "Low" Applied Cx Expansion Level.

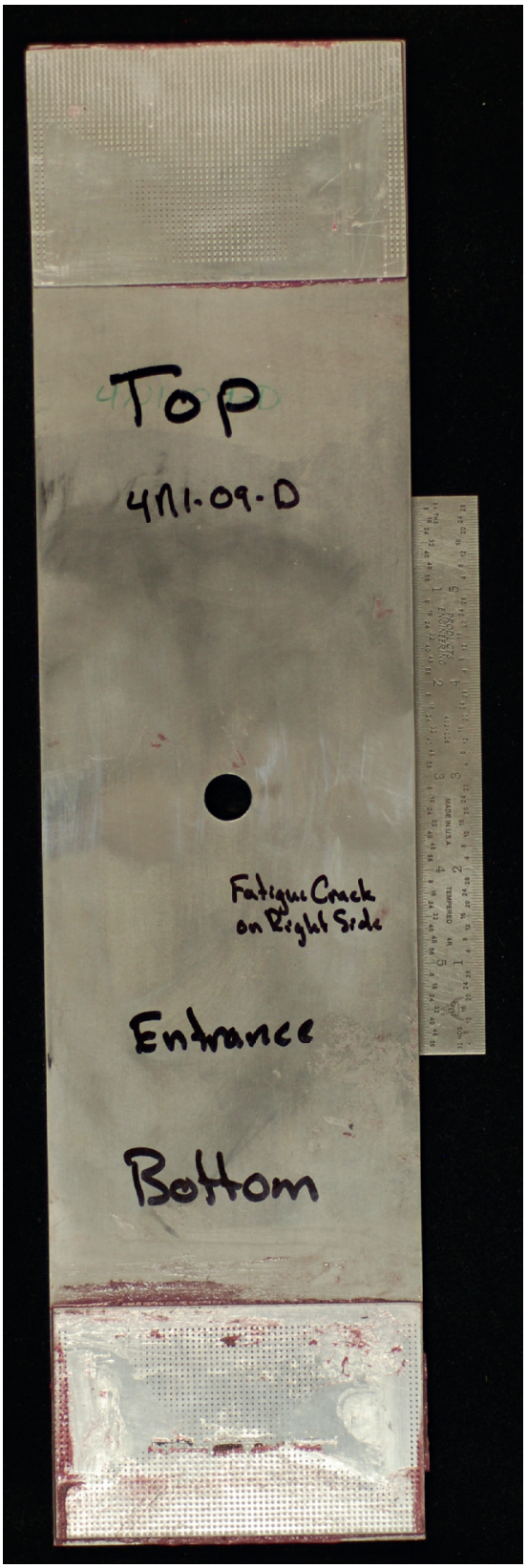

Fig. 915 Macro Image of Fatigue Coupon Cx4N1-09-D Prior to Fatigue Testing, Initial Crack is on the Right Side of the Cx Hole.

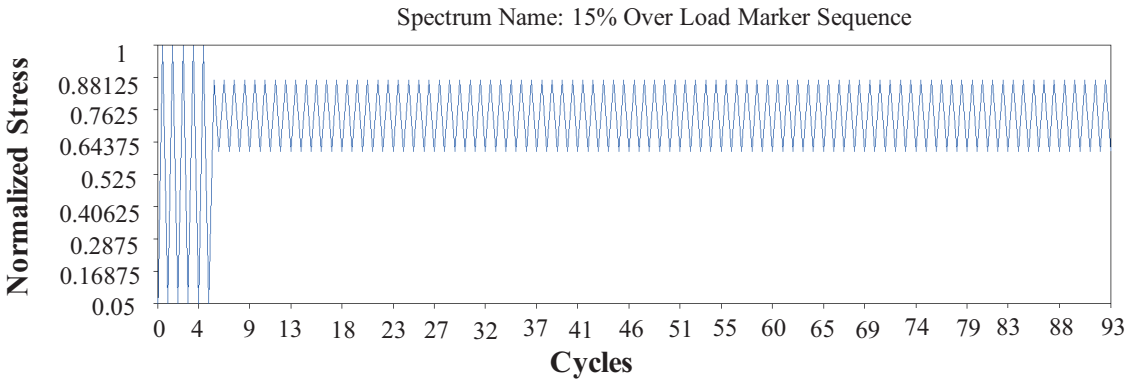

Fig. 916 Marker Banding Sequence Showing First Marker Sequence at 15% Overload at the Beginning of the Loading Sequence.

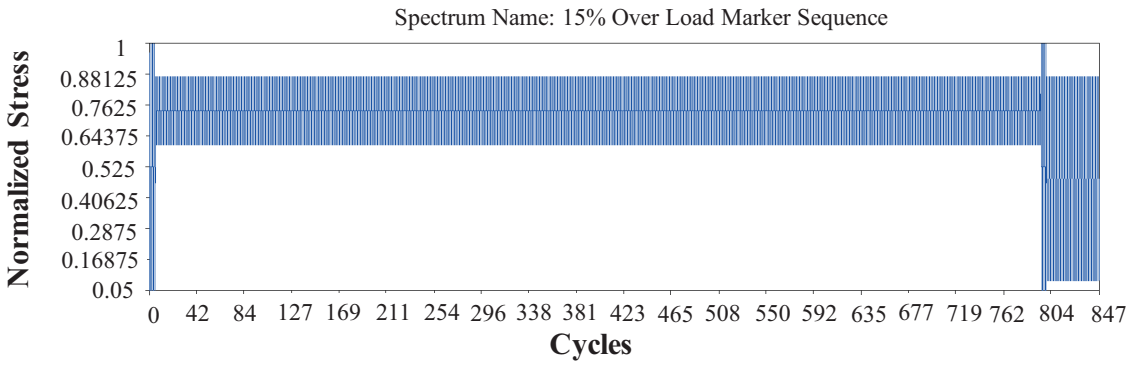

Fig. 917 Larger View of Marker Banding Sequence Showing Second 15% Overload Band at 790 Cycles.

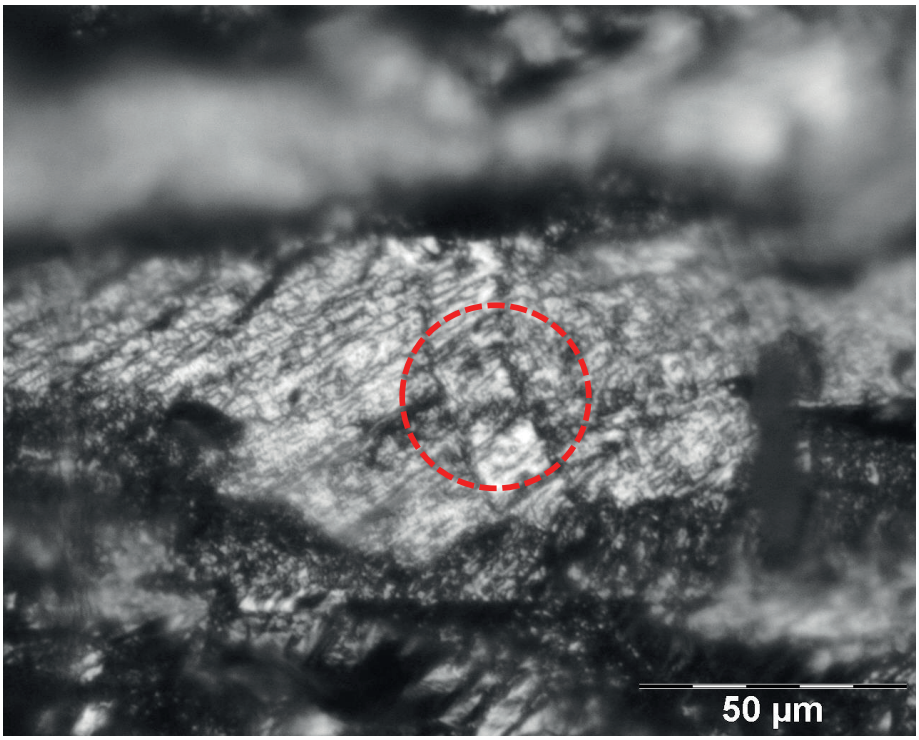

Fig. 918 Image of an Example of Typical Marker Banding on a Fracture Surface, as Viewed via an Optical Microscope [Image Courtesy of Dr. Tom Mills (APES Inc.)].

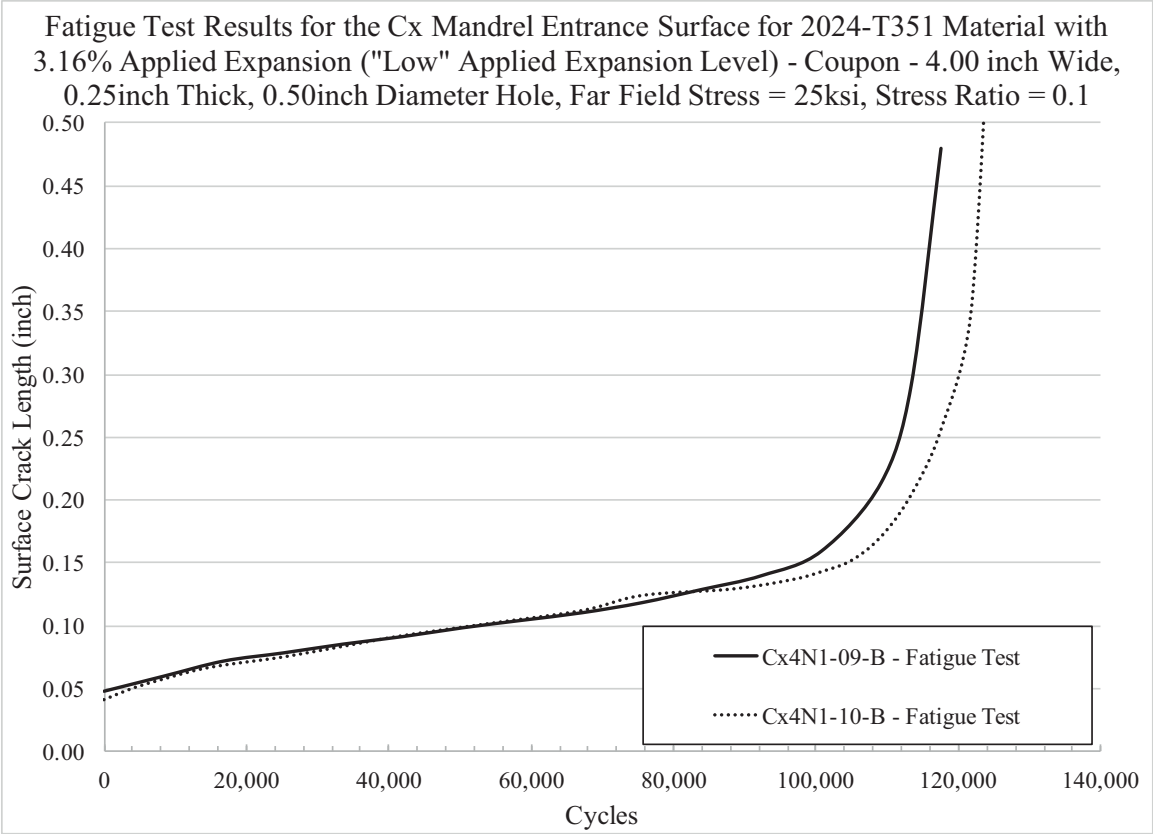

Fig. 919 Fatigue Crack Growth Curves for Fatigue Coupons Cx4N1-09-B and Cx4N1-10-B (2024-T351) Showing the Crack Length Versus Cycles for the Cx Mandrel Entrance Surface.

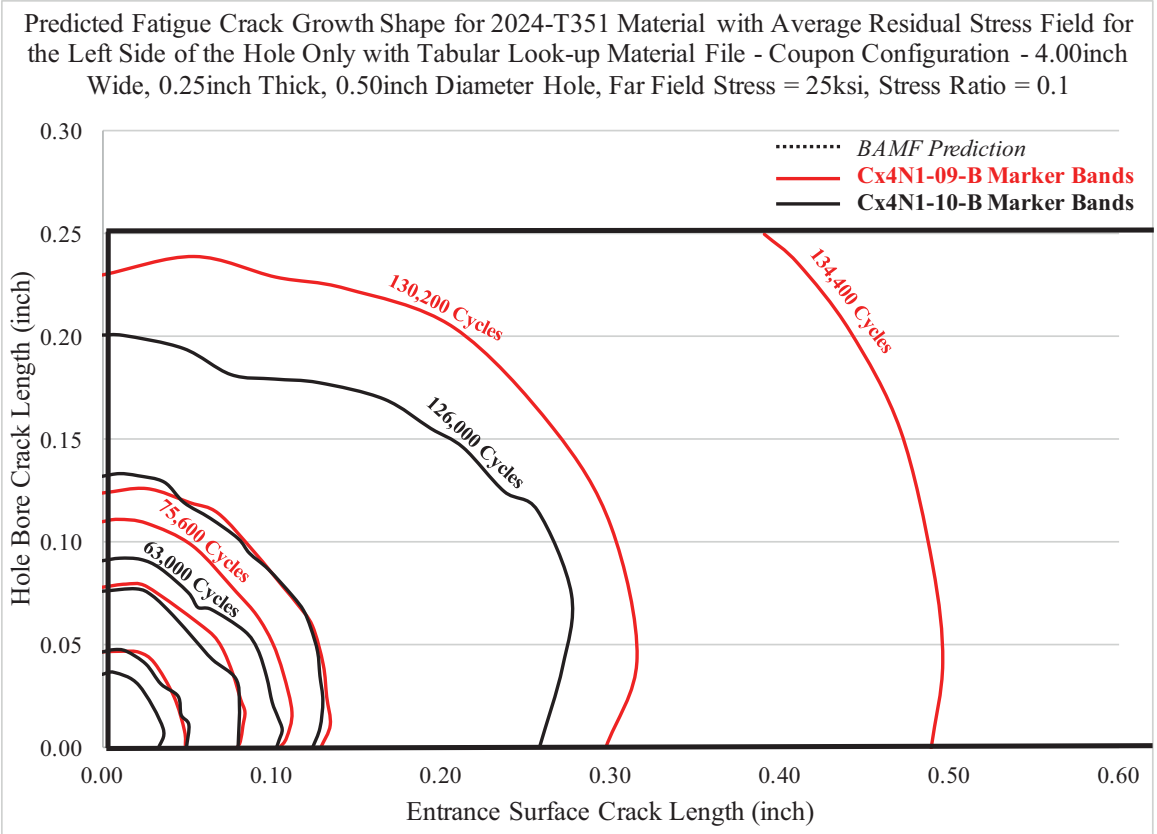

Fig. 920 Marker Banding Map of Fatigue Coupons Cx4N1-09-D and Cx4N1-10-B (2024-T351) Cxed to the “Low” Applied Expansion Level.

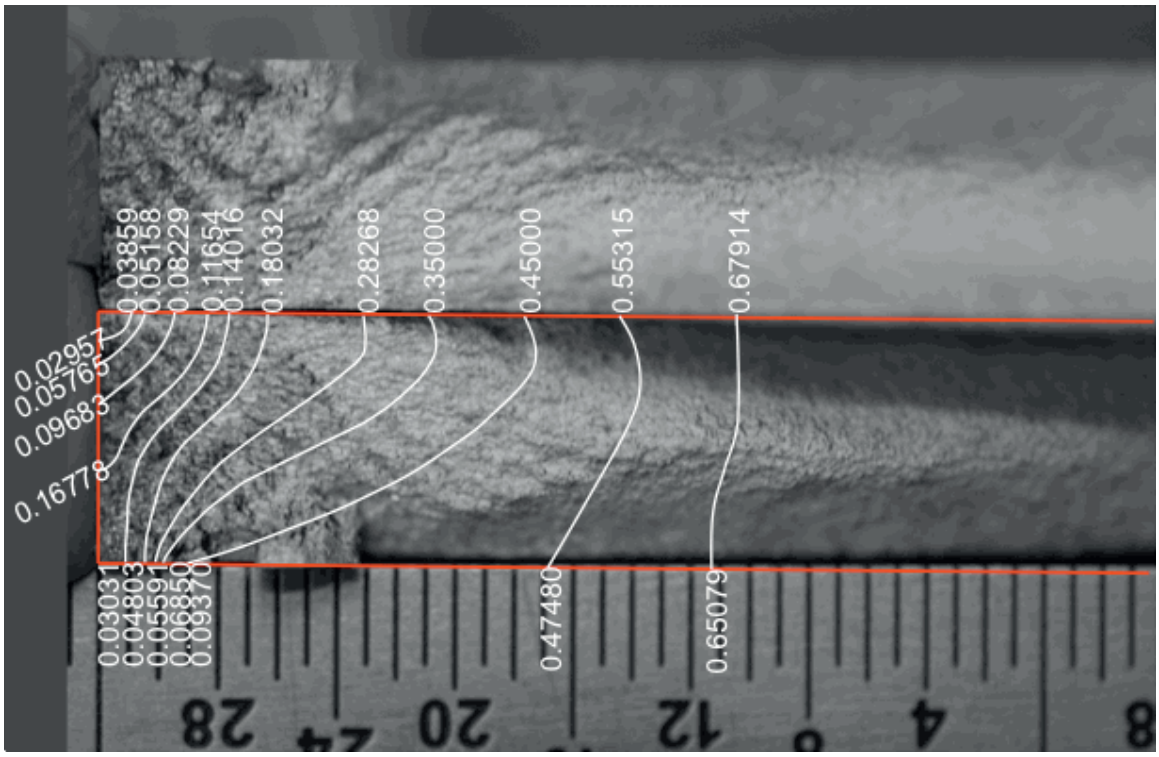

Fig. 921 Image of Fatigue Crack Growth Shape Evolution at a Cx Hole in 2024-T351, Cxed to Approximately 3.6% Applied Expansion.[54]

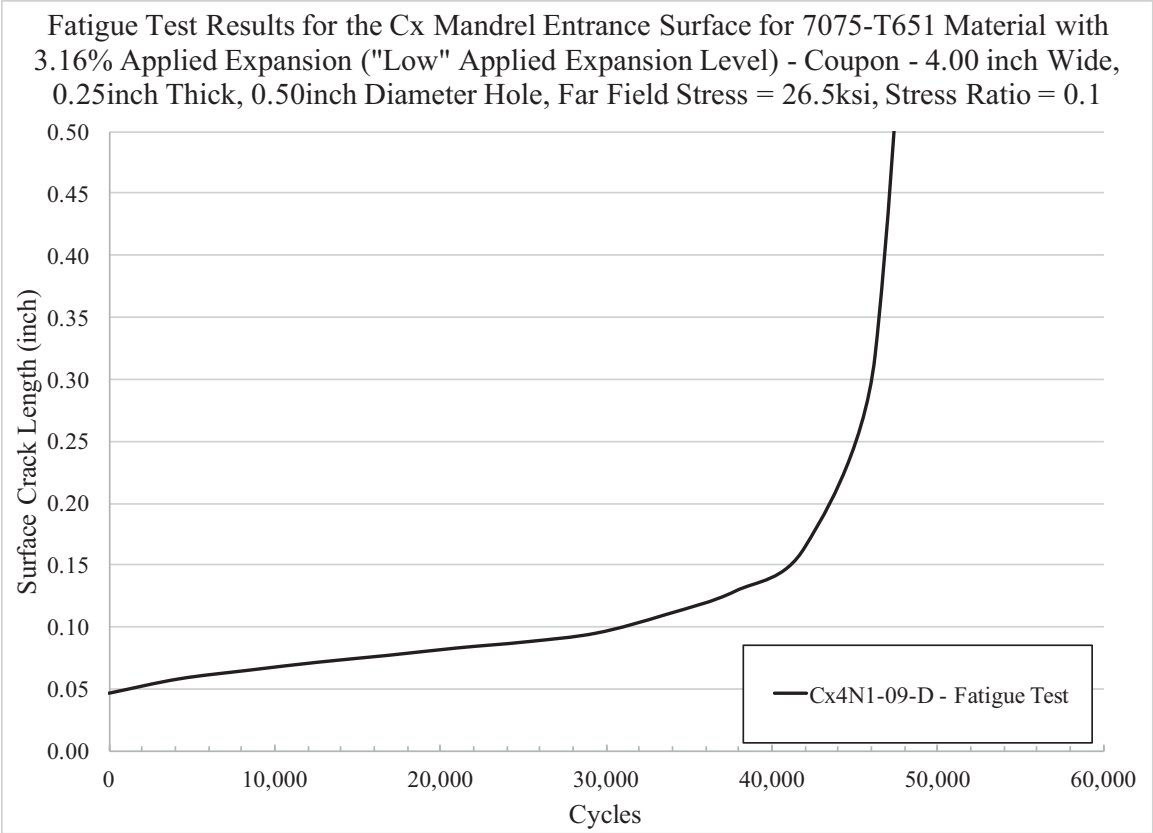

Fig. 922 Fatigue Crack Growth Curves for Fatigue Coupons Cx4N1-09-D (7075-T651) Showing the Crack Length Versus Cycles for the Cx Mandrel Entrance Surface.

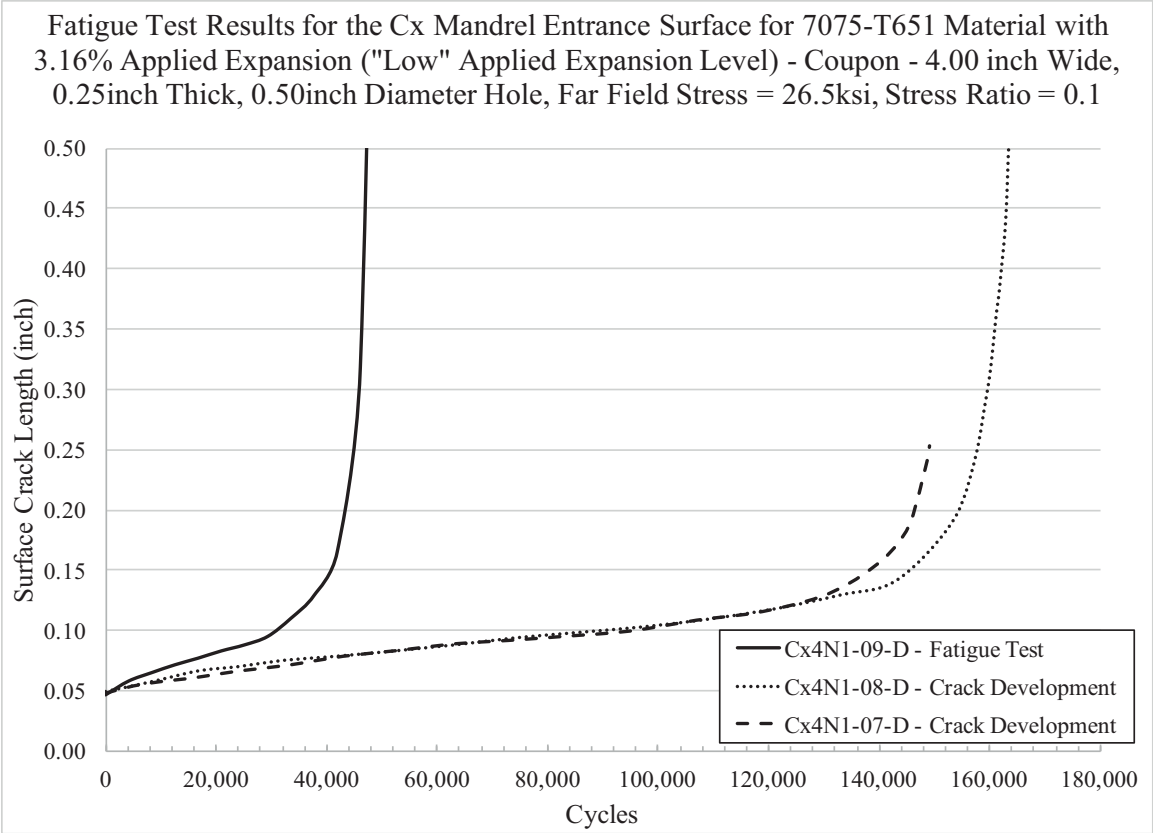

Fig. 923 Fatigue Crack Growth Curves for Fatigue Coupon Cx4N1-09-D (7075-T651) and also Crack Development Coupons Cx4N1-07-08-D (7075-T651).

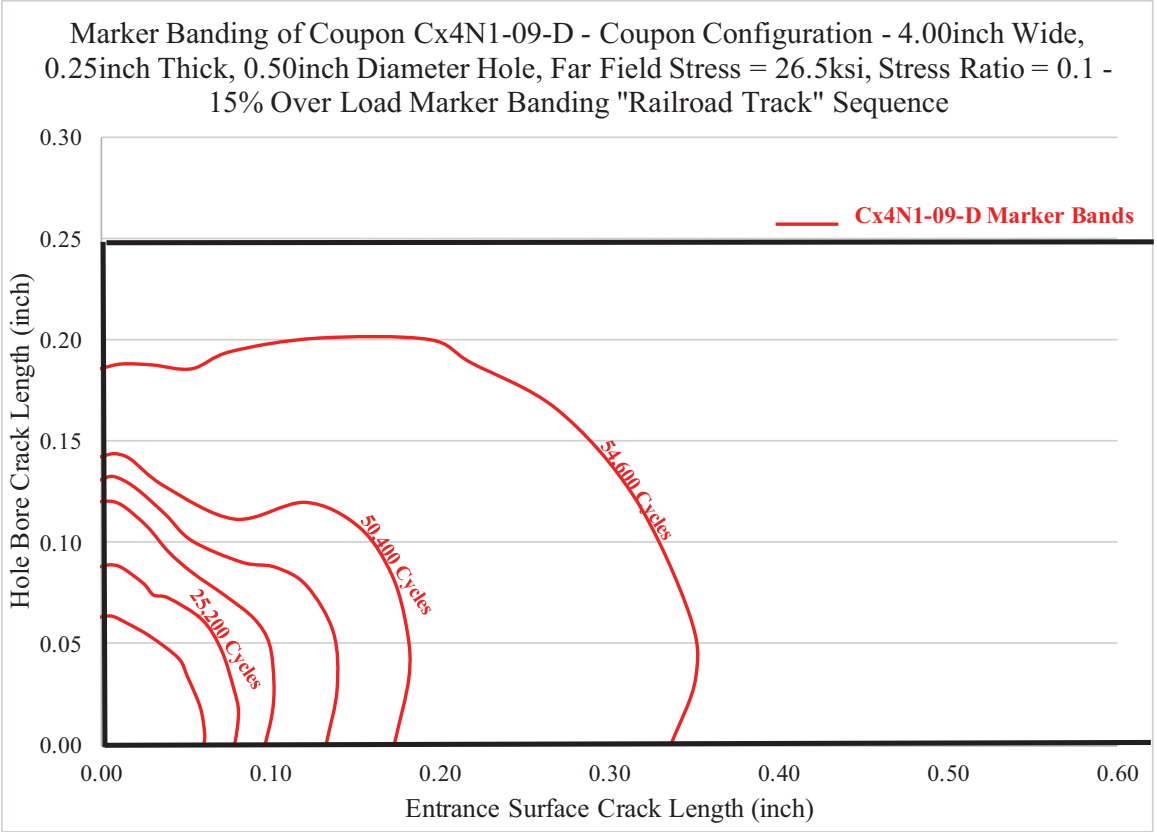

Fig. 924 Marker Banding Map of Fatigue Coupons Cx4N1-09-D (7075-T651) Cxed to the “Low” Applied Expansion Level.

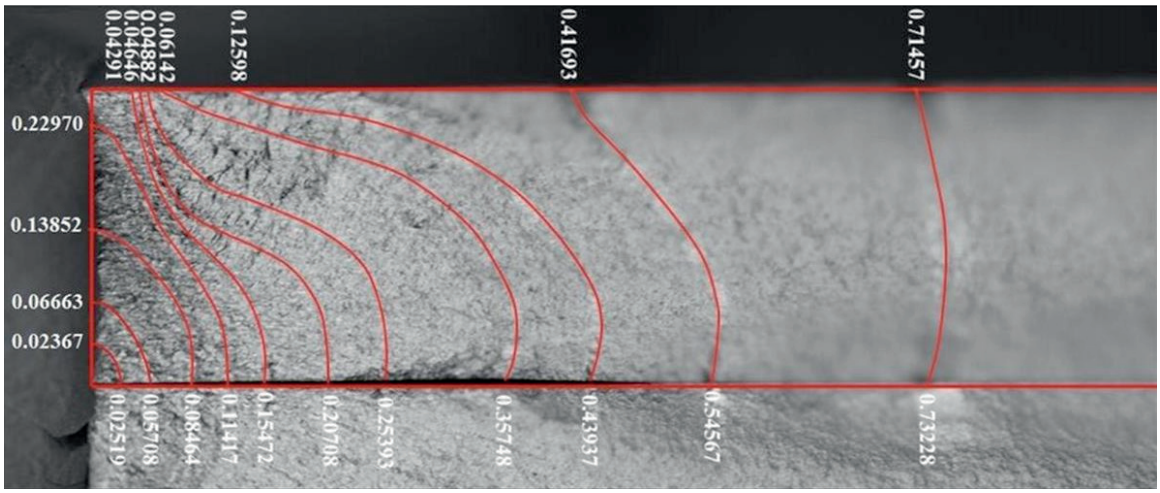

Fig. 925 Image of Fatigue Crack Growth Shape Evolution at a Cx hole in 7075-T651, Cxed to Approximately 3.6% Applied Expansion.[72]

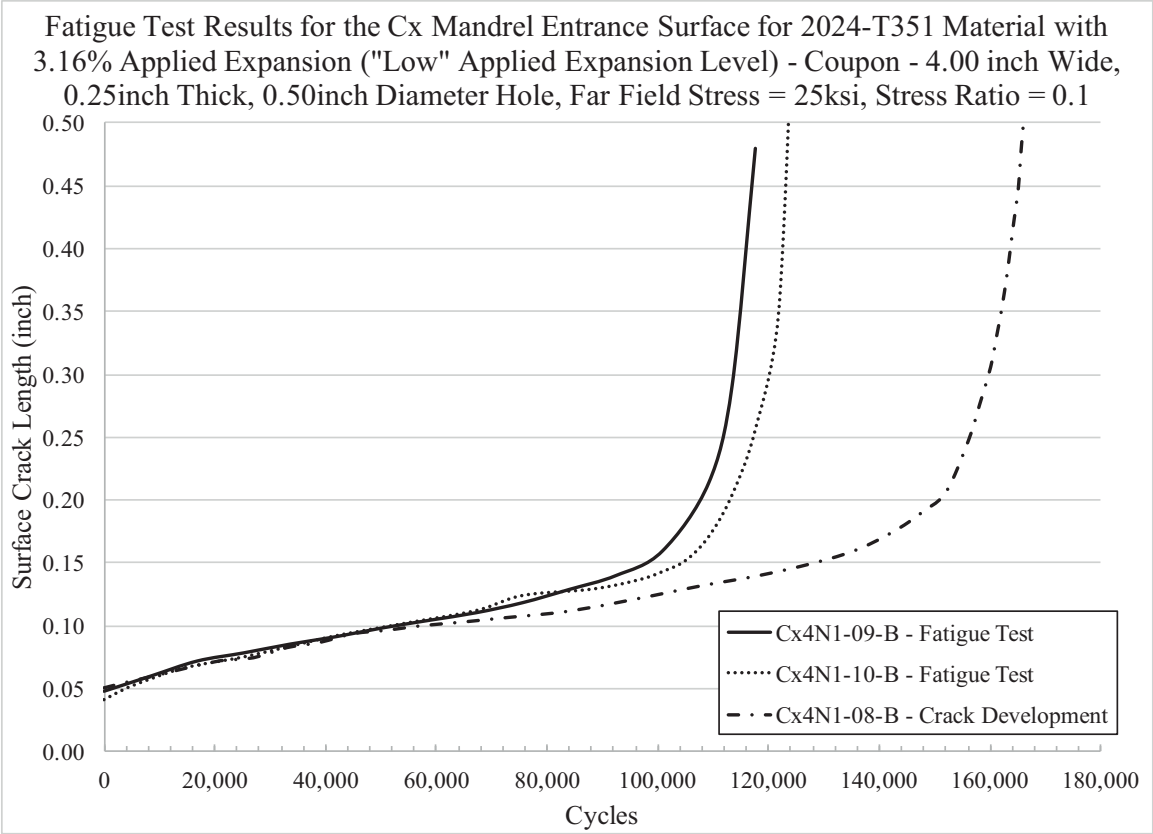

Fig. 926 Fatigue Life of Fatigue Test Coupons Cx4N1-09-B, Cx4N1-10-B (2024-T351) and the Fatigue Crack Development Coupon Cx4N1-08-B (2024-T351).

11 COMPARISONS OF FATIGUE LIFE AND CRACK SHAPE EVOLUTION TO FATIGUE TESTS FOR EVALUATION OF DEVELOPED LIFE PREDICTION METHODS FOR "LOW" APPLIED EXPANSION LEVELS IN 2024-T351 AND 7075-T651 ALUMINUM ALLOYS

11.1 Comparisons of Fatigue Life and Crack Shape Evolution Using the Baseline, Uncracked Residual Stress Distributions from the Average of the Left Side of the Hole for CxA2 (2024-T351) and CxD2 (7075-T651) to Fatigue Test Data

11.1.1 Comparison of Fatigue Life Predictions Using Baseline, Uncracked CxA2 (2024-T351) Residual Stress – Averaged on Left Side of the Hole to Fatigue Test Data

Fatigue crack growth calculations were developed within BAMF to predict the fatigue test condition of 25 ksi, Stress Ratio (R) = 0.1 using the baseline, uncracked CxA2 (2024-T351). For this condition three residual stress distributions were developed using only the residual stresses from the left side of the hole. For the CxA2 (2024-T351) there were five coupons that were developed and the residual stresses that were used for these fatigue crack growth prediction were an average of the left side of the hole of those five coupons. With five coupons available from the baseline, uncracked condition a statistical distribution was able to be developed. Using this statistical power, the repeatability standard deviation of the baseline, uncracked condition was applied to the cracked Cx4N1 coupons. From this it was possible to not only develop the average residual stress field but to also adjust the stress field "up" and "down" by one standard

deviation. Thus, these residual stress fields represent a plus or minus one statistical standard deviation on the mean residual stress distribution and would be able to capture the residual stress field that was introduced with a 68.4% confidence on that applied residual stress distribution. Table 15 provides an overview of the BAMF predictions using the CxA2 (2024-T351) baseline, uncracked residual stress distributions, and the average fatigue life demonstrated through test.

A crack growth plot of showing a comparison of the three residual stress distribution's predicted fatigue life as compared to the tested life of Cx4N1-09-B and Cx4N1-10-B (2024-T351) and also the crack develop life for Cx4N1-08-B is provided in Fig. 927. It should be noted that coupon Cx4N1-08-B was one of the coupons that was used during the fatigue testing and residual stress determination phase of this work. The -08 coupon configuration had a fatigue crack that was propagated to a length of approximately 0.50 inch. The propagation of this crack was done under the same loading conditions as these fatigue tests, thus it is possible to include this coupon in as one that can be used when comparing prediction versus test. As can be seen in Fig. 927, the BAMF prediction for this condition, using the three statistical distributions, bounds the fatigue test data very well, with the average residual stress distribution almost lying on top of two of the fatigue test data points. However, it should be noted that the prediction does not capture the initial growth period, from the initial precracked (0.04 inch x 0.048 inch) size to about 0.10 inch of growth. This is still an area of fatigue crack growth that is not well predicted. However, with additional work it could be understood and a more physics-based approached developed to allow for a more accurate prediction to be made, which would include this phase of fatigue crack growth development and propagation.

With three life predictions performed, it is possible to calculate the average life prediction and establish a statistical bound for that average life prediction. This is provided in Fig. 928. The error bars within Fig. 928 represent one standard deviation on the average fatigue life prediction. Thus it can be seen that the average prediction with the statistical bounds, captures all three of the tested fatigue crack growth lives. This provides a high level of confidence that using the residual stress distribution, and the material file within AFGROW/BAMF, will allow for an accurate life prediction, for this material and loading condition. If we have a different loading condition, like spectrum loading with either peak stresses near the material's yield strength, or if we have significant levels of compression in the spectrum, then the level of confidence in the prediction will decrease.

11.1.2 Comparison of Fatigue Crack Growth Evolution Using Baseline, Uncracked CxA2 (2024-T351) Residual Stress – Averaged on Left Side of the Hole to Fatigue Test Data

The two fatigue crack growth coupons (Cx4N1-09-B and Cx4N1-10-B) were tested using a marker banding sequence allowing a comparison of the the fatigue crack growth shape evolution for each of the three residual stress distributions. These comparisons are provided in Fig. 929 through Fig. 931. It can be seen from these figures that the predicted shape evolution matches well along the Cx mandrel entrance surface, but does not predict the evolution of the crack up down bore of the Cxed hole very accurately. The prediction shows that the crack will pin and hold close (approximately 0.10 inch) from the Cx mandrel entrance surface, but this is not the case with the test. The test shows a more semi-circular shape of the crack, until it almost breaks through the

Cx mandrel exit surface. Once it breaks through that Cx mandrel exit surface the predictions and the test again come back together. Also, there is little influence of the statistical distribution on the crack shape evolution. As has been demonstrated before, the majority of the predicted and tested fatigue life is consumed within the first 0.125 inch from the edge of the hole. One reason for this difference is that the residual stress profile that was developed via the contour method is not correct near the bore of the hole. Another reason for this difference between prediction and test could be that the fatigue crack growth material properties are different along the bore of the hole, as compared to the surface. For all of these models only one material file was used for both of the material orientations. In addition, the influence of crack closure was not taken into account, and this has the potential to dramatically influence the fatigue crack growth rates, and thus shapes.

It should also be noted that the majority of the difference between the three fatigue life predictions is found within the first 0.05 inch from the edge of the hole. On average it takes 22,000 cycles for the initial crack size of 0.040 inch x 0.048 inch (surface length x bore length) to get to a surface crack size of 0.05 inch, where as for the “down” one statistical distribution it takes almost 51,000 cycles and then for the “up” one it takes approximately 14,000 cycles. Thus, it can be concluded that the area of most impact on the fatigue life and shape is near the edge of the hole, from the edge to approximately 0.10 inch.

11.1.3 Comparison of Fatigue Life Predictions Using Baseline, Uncracked CxD2 (7075-T651) Residual Stress – Averaged on Left Side of the Hole to Fatigue Test Data

Like the CxA2 (2024-T351) life predictions using their residual stress distributions, this was also done for the CxD2 (7075-T651) coupon condition. Only three coupons were produced, however it was still possible to compute the average and standard deviation for the left side of the hole for this condition. Using these three statistical distributions, three life predictions were produced using BAMF. Table 16 provides an overview of the three life predictions that were performed for this condition. Only one fatigue test was performed, because of the two that were set aside, one was tested at the incorrect far-field stress level. In an effort to gain a greater understanding of the fatigue life, two additional fatigue lives were added to the average test life. The data for this came from Cx4N1-07-D and Cx4N1-08-D (7075-T651). These two coupons were used to develop fatigue cracks and were fatigue tested under the same stress levels as the single fatigue test, Cx4N1-09-D (7075-T651). Table 17 provides an updated average fatigue test life that the predictions can be compared to. It can be seen when comparing Table 16 to Table 17 that the fatigue life of Cx4N1-09-D (7075-T651) was significantly shorter than the two crack development coupons. This difference also is shown in the fatigue life prediction comparisons as provided in Fig. 932. Like the predictions for the 2024-T351 material condition, three residual stress distributions were used to provide a distribution of fatigue life predictions.

As seen in Fig. 932 there is a tremendous impact of the statistical distribution on the residual stress field when it then is integrated within a fatigue crack growth prediction. The one “down” statistical distribution increased the fatigue life by more than

4 times. Again, the major impact of this comes at the small crack sizes, from the IFS to approximately 0.075 inch away from the edge of the hole.

With three life predictions performed it was possible to provide an average predicted fatigue life and apply a confidence bound to that prediction. The error bars present in Fig. 933 represent one standard deviation on the average prediction. From these plots, it shows that the application of the residual stress fields from the average of the left side of the hole for coupons CxD2 (7075-T651) provides a predicted fatigue life that is much larger than that which was demonstrated via test. As shown in Fig. 933, if one standard deviation were applied to the lower end of the average life prediction it would cover the three fatigue test lives.

11.1.4 Comparison of Fatigue Crack Growth Evolution Using Baseline, Uncracked CxD2 (7075-T651) Residual Stress – Averaged on Left Side of the Hole to Fatigue Test Data

In addition to the fatigue life it was possible to marker band coupon Cx4N1-09-D (7075-T651) and thus a comparison of the fatigue crack shape evolution from test to the BAMF prediction was possible. This comparison was developed for all three residual stress distribution life predictions and are provided in Fig. 934 through Fig. 936. It can be seen in Fig. 934 through Fig. 936 that the BAMF life prediction does not match the fatigue life evolution up the bore of the Cx hole. The prediction shows significant pinning just down from the Cx mandrel entrance surface, but the fatigue test does not show that this will occur. The crack shape along the Cx mandrel entrance surface matches very well between the test and the prediction. Another major finding from these comparisons is that again, as seen in the 2024-T351 coupons, the major influence on the

life is demonstrated near the edge of the hole, from the IFS to about 0.075 inch away from the edge. This is demonstrated by the difference in the number of cycles the predictions show it will take to get from the final precrack size of 0.04 inch along the Cx mandrel entrance surface to a length of 0.05 inch. For the "average" residual stress distribution it took almost 162,000 cycles to propagate this 0.01 inch. For the one "down" residual stress distribution it took over 1,000,000 cycles and for the one "up" it took only 74,000 cycles. Compare these predictions to test it took only 25,000 cycles to propagate the fatigue crack from the final precrack size to approximately 0.075 inch.

From these comparisons to test it can be stated that the CxD2 (7075-T651) averaged residual stresses from the left side of the hole, when integrated into a BAMF life prediction, using the stated material file, produces a predicted fatigue life that is much greater than that which is demonstrated from test. This conclusion is much different from that shown by the CxA2 (2020-T351) material data.

11.2 Comparisons of Fatigue Life and Crack Shape Evolution Using Residual Stress Distributions Developed from the Fatigue-Cracked Cx4N1-XX Coupons Using the Residual Stress from the CxA2 (2024-T351) and CxD2 (7075-T651) Coupons from the Edge of the Hole to 0.04 inch away, and Compares to Fatigue Test Data

11.2.1 Comparison of Fatigue Life Predictions Using Residual Stress Fields from Cx4N1-XX-B, Fatigue-Cracked Coupons Using the Baseline, Uncracked CxA2 (2024-T351) Residual Stress from the Edge of the Hole to 0.04 inch

In an effort to understand if the presence of a fatigue crack within the residual stress field developed from the Cx process has an influence on the fatigue life, and validate that effect from test, the same comparisons of life were developed. Table 18 provides a breakdown of the different zones that were developed and their associated

residual stresses. This piecewise, bivariant residual stress function was imposed in the model in a semi-circular form, as shown in Fig. 937.

Again three life predictions were developed using a bivariant, high order polynomial fit to the residual stress data, as produced via the contour method. For these predictions the baseline, uncracked residual stress fields from the CxA2 (2024-T351) condition were used from the edge of the hole to 0.04 inch. Table 19 provides an overview of the life predicted using this function, as compared to the average fatigue test life from coupons Cx4N1-09-B and Cx4N1-10-B (2024-T351).

A comparison of the predicted fatigue life, using this residual stress field, is provided in Fig. 938 and Fig. 939. From Fig. 938 it can be seen that as compared to Fig. 927 when the addition of the effect of the fatigue crack is introduced to the residual stress field, used within BAMF/StressCheck®, there is little impact on the fatigue life prediction.

11.2.2 Comparison of Fatigue Crack Growth Evolution Using Fatigue-Cracked Cx4N1-XX-B (2024-T351) Residual Stress with the Baseline, Uncracked CxA2 (2024-T351) Residual Stress Imposed from the Edge of the Hole to 0.04 inch

The predicted fatigue crack growth shapes for the three residual stress statistical distributions were also developed for this residual stress function condition and are compared to that developed for the 2024 material via the marker banding tests in Fig. 940 through Fig. 942.

For the change in the function that was imposed to represent the residual stress there shows little change in the fatigue crack shape evolution, as compared to the use of the baseline, uncracked CxA2 (2024-T351) function. Like the predictions using that

baseline function the fatigue crack shape evolution matches favorably along the Cx mandrel entrance surface, but predicts a higher level of pinning along the bore of the hole, which is not seen in test.

11.2.3 Comparison of Fatigue Life Predictions Using Residual Stress Fields from Cx4N1-XX-D, Fatigue-Cracked Coupons Using the Baseline, Uncracked CxD2 (7075-T651) Residual Stress from the Edge of the Hole to 0.04 inch

Like that developed for the 2024-T351 material system, the same method was used on the 7075-T651 material. Table 20 provides an overview of the three BAMF life predictions that were performed using the adjusted residual stress function, which utilized the determined residual stress from the CxD2 (7075-T651) from the edge of the hole, 0.0 – 0.04 inch away from the edge of the hole. As can be seen from this there is a dramatic decrease in the average predicted fatigue life when the Cx4N1-XX-D (7075-T651) residual stress distributions are taken into account within the imposed bivariant "loaded crack" traction stress within StressCheck®.

The fatigue crack growth predictions, using these updated bivariant, piecewise functions are provided in Fig. 943. In order to determine an uncertainty estimate for the three fatigue crack growth predictions, an average of the three predictions was developed and error bars were calculated using one standard deviation from the mean. This is provided in Fig. 944. It should be noted that the inclusion of the residual stress fields determined from the Cx4N1-XX-D (7075-T651) coupons reduces the average predicted life from approximately 600,000 cycles to just over 180,000. This is a significant reduction in the predicted fatigue life and as shown in Fig. 944 the single standard deviation of the predicted life from the three residual stress field distributions covers two

of the three sets of fatigue test data developed for this condition.

In addition to this it should be noted that Table 20 shows that the fatigue life of the one "up" residual stress field has a longer predicted fatigue life than the "average" and the one "down" statistical distribution. This is not what was expected. For all of the other predictions the one "up" residual stress distribution had a shorter life. This will be discussed at the conclusion of this section and a potential cause of this will be outlined.

11.2.4 Comparison of Fatigue Crack Growth Evolution Using Fatigue-Cracked Cx4N1-XX-D (7075-T651) Residual Stress with the Baseline, Uncracked CxD2 (7075-T651) Residual Stress Imposed from the Edge of the Hole to 0.04 inch

The fatigue crack growth evolution was developed for all three of the residual stress distributions used for these fatigue life predictions. These predictions were compared to the single marker band coupon that was tested using the appropriate far-field stress level, Cx4N1-09-D (7075-T651). These comparisons are provided in Fig. 945 through Fig. 947. From these three fatigue crack growth shape evolution plots it can be seen that the predictions capture the Cx mandrel entrance face shape evolution but the shape of the crack as it progresses down the bore of the hole is not being predicted accurately. Again, the predictions show the fatigue crack "pinning" near the Cx entrance face and not allowing the crack to progress down the bore of the hole through to the Cx mandrel exit face. However, during this test the marker bands show that instead of pinning at the hole bore surface the fatigue crack pinned away from the edge of the hole, at about a distance of 0.125 inch up the bore, and at around 0.10 inch down the Cx mandrel entrance surface. Additional work would need to be performed to predict this shape evolution, as provided by this one test.

11.3 Comparisons of Fatigue Life and Crack Shape Evolution Using Residual Stress Distributions Developed from the Fatigue-Cracked Cx4N1-XX Coupons Using the Residual Stress from the Cx4N1-01-02-B (2024-T351) and Cx4N1-01-02-D (7075-T651)

11.3.1 Comparison of Fatigue Life Predictions Using Residual Stress Fields from Cx4N1-XX-B (2024-T351), Fatigue-Cracked Coupons Using the Cx4N1-01-02-B (2024-T351) Cracked Condition Residual Stress from the Edge of the Hole to 0.09 inch

In order to gain a greater understanding of the impact on the fatigue life prediction by the inclusion of the residual stresses from the fatigue-cracked coupons, the Cx4N1-XX-B (2024-T351) condition, the residual stress field developed from the Cx4N1-01-02-B (2024-T351) was imposed into the residual stress piecewise, bivariant polynomial function. The residual stresses from the Cx4N1-01-02-B (2024-T351) were imposed from the edge of the hole to 0.09 inch, as provided in Table 21. The same semi-circular shape was used for this function, as provided in Fig. 937.

Using this modified function, three fatigue life predictions were again made using the same statistical repeatability distribution to adjust the “average” residual stress field “up” or “down”. Table 22 provides a breakdown of the predicted life for these three residual stress statistical distributions. The fatigue life prediction, compared to test is provided in Fig. 948 and Fig. 949. It should be noted that with this shift in the residual stress field function the average life prediction was greater, as compared to the prediction utilizing the baseline, uncracked CxA2 (2024-T351) for the first 0.04 inch. The life was extended from 138,000 cycles to 155,000 cycles.

11.3.2 Comparison of Fatigue crack Growth Evolution Using Fatigue-Cracked Cx4N1-XX-B (2024-T351) Residual Stress using Cx4N1-01-02-B (2024-T351) for Residual Stress from Edge of Hole to 0.09 inch

In addition to the fatigue crack growth curves the fatigue crack shape evolution was determined and compared to the two marker banded coupons, as provided previously. The comparisons of the marker banded coupons to the prediction for the three residual stress statistical distributions are provided in Fig. 950 through Fig. 952.

11.3.3 Comparison of Fatigue Life Predictions Using Residual Stress Fields from Cx4N1-XX-D (7075-T651), Fatigue-Cracked Coupons Using the Cx4N1-01-02-D (7075-T651) Cracked Condition Residual Stress from the Edge of the Hole to 0.09 inch

The same method was used for the 7075-T651 material configuration. Table 23 outlines the fatigue life predictions and how they compare to the combined fatigue life of three of the Cx4N1-XX-D (7075-T651) coupon conditions. The fatigue life predictions, as compared to the fatigue test data are provided in Fig. 953 and Fig. 954.

11.3.4 Comparison of Fatigue Crack Growth Evolution Using Fatigue-Cracked Cx4N1-XX-D (7075-T651) Residual Stress using Cx4N1-01-02-D (7075-T651) for Residual Stress from Edge of Hole to 0.09 inch

The fatigue crack evolution prediction using this update residual stress function for the three residual stress statistical distributions are provided in Fig. 955 through Fig. 957.

11.4 Conclusions from the Inclusion of Residual Stresses from Fatigue-Cracked Coupons into the Development of the Residual Stress Function Imposed in the Fatigue Crack Growth Prediction

Through this work it was possible for three different high order, bivariant piecewise polynomial functions to capture the residual stress that is introduced into the material around the hole at the "low" applied expansion with and without the influence of a fatigue crack. Through imposing these functions into a fatigue crack growth software package it was possible to predict the fatigue crack growth life, the crack growth curve shape, and the crack front shape evolution, and compare all of these to test. Through this work it was determined that for the 2024-T351 material if one were to apply the one repeatability standard deviation to the residual stress field, and use it within BAMF for a life prediction, it would capture the scatter found within the fatigue test and thus provide a very accurate solution for the life of the part from the provided initial crack size to final fracture. However, this approach does not provide for an accurate prediction of the initial crack growth curve save, or the crack shape evolution from the initial crack size to final fracture. As the effect of the fatigue crack was introduced into the prediction via a change in the residual stress function, the change in the total life, the crack growth curve shape, and the crack shape evolution was influenced very little. This trend can be seen in Table 24 for the 2024-T351 coupon configuration, and in the provided crack growth curves, and comparisons to the marker banded coupons. One interesting finding is that even though the residual stress for this alloy shows a correlation between fatigue crack size and the decrease in the residual stress field, the effect of this decrease in the residual stress field is not translated into a decrease in the fatigue life. For the 2024-T351 material it shows the opposite trend, however it should be noted that this shift in the life

is very small, and potentially within the statistical noise of the major influencing factors relative to these predictions.

The same process for adjusting the residual stress function that would be used within StressCheck® for fatigue crack growth predictions of the 2024-T351 configuration was applied to the 7075-T651 fatigue test predictions. However, a very different trend was manifested. Table 25 provides a breakdown of this trend. As the effect of the fatigue crack was imposed closer to the hole the fatigue life prediction moves closer to the life that was demonstrated through fatigue testing. In addition to the prediction becoming closer to the tested fatigue life, the direction of that change is different than that demonstrated in the 2024-T351 alloy. In the 7075-T651 the life becomes significantly shorter while in the 2024-T351 it becomes slightly longer. For the 7075-T651 material there continues to be a lack of correlation between the tested fatigue crack growth curve shape and crack growth evolution, when compared to the prediction. The predictions continue to predict a crack growth rate near the edge of the hole that is much slower than what is demonstrated in test. This could be related to inaccuracies within the provided residual stress field, that are outside of the one repeatability standard deviation. This has the potential to also answer why the predicted crack shape evolution does not match up with that captured during test. For both materials the prediction shows that the crack should have a significant reduction in the crack growth rate at the edge of the hole, near the Cx mandrel entrance surface. However, during test this is not demonstrated. Quite the opposite, during fatigue testing of this condition it was documented that the cracks would propagate faster down the bore of the hole and then slow down and “pin” subsurface, closer to the Cx mandrel exit surface.

From the data presented it is concluded that a fatigue crack has an influence on the residual stress that is introduced into both the 2024-T351 and 7075-T651 aluminum alloys, and that as the effect of this fatigue crack is introduced into the residual stress function that will be used in a fatigue crack growth prediction, that prediction will more accurately predict the fatigue life, for a constant amplitude fatigue test, at a R of 0.1.

In addition to the predicted fatigue life for the given test conditions a prediction of the fatigue crack shape evolution was predicted through BAMF. These predictions do not match up, for either material, the location of the fatigue crack growth "pinning." For each material, and for each statistical distribution of the residual stress, the predictions always placed this fatigue crack "pinning" at the edge of the bore of the hole and occurred between 0.075 inch and 0.125 inch from the Cx mandrel entrance surface. From the marker banding it can be seen that the actual fatigue crack "pinning" occurs away from the edge of the hole trends towards the Cx mandrel exit surface and away from the hole. This is an area of prediction that needs additional research to match the physics of fatigue crack shape evolution at a Cxed hole.

11.4.1 Effect of Bivariant, High-Order Polynomial Fits with the Influence of Residuals between Fit and Actual Data near the Edge of the Hole

One of the findings of this work was determined from the fatigue life predictions for the 7075-T651 material. When the residual stress equations, from the fatigue-cracked conditions, were applied with the one "up" condition the fatigue life prediction showed a longer life than both the "average" and the "down" residual stress distribution. This demonstrates one of the limitations in the approach that was taken to apply the determined residual stresses within StressCheck®. This was demonstrated in Table 23.

This result was not expected because the residual stress was reduced spatially across the field, thus how can it be possible that the life could be longer?

The residual stress fields that were produced via the contour method were fit using a fifteenth order polynomial and plotted to show a surface plot of the fit and also the spatial residual between the fit and the actual. The order of polynomial was selected in an effort to reduce the spatial difference, or residual, to a specific maximum near the edge of the hole. For all of these fits the goal was to select an order of polynomial that produced a maximum residual no greater than 4 ksi.

The 7075-T651 coupons exhibited a lower level of repeatability uncertainty near the edge of the hole, than that determined for the 2024-T351 material. This uncertainty was on the order of 4-8 ksi. However, as shown in Fig. 958 the ability of the polynomial to fit that surface fluctuates on the order of ± 4ksi. Thus, it is possible that even though one might be using the "up" residual stress distribution from the contour method, when there are limitations to the ability to fit the data, and the repeatability uncertainty is low, one might have stresses that are near the nucleation site that are more compressive than the one "down" residual stress distribution, even though the one "up" distribution was used.

The effect of this uncertainty in the applied residual stress field is shown in Fig. 959 and Fig. 960. As can be seen when comparing these two plots the residual stress near the edge of the hole and at the first five of the eleven points along the crack is at a slightly deeper compression level for the one "up" residual stress condition than what is seen for the "average" condition. Near the edge of the hole as one moves down the bore it can be seen that the "average" residual stress distribution has a lower compression than

the one “up” condition. However, when using these residual stresses for the calculations of SIFs, ± 4 – 8 ksi can make a significant difference on the calculated SIF, changing it $\pm 2ksi\sqrt{inch}$. If the fatigue crack’s SIF is near the lower end of the da/dN vs. ΔK material property this small shift in ΔK can have a significant effect on the crack growth rate.

This effect is shown in Table 26 and Table 27. Due to the bounce in the calculated and then applied residual stress field the Total SIF for the first two points along the surface are higher in the “up” condition than they are in the “average” condition. This slight difference in the Total SIF is magnified by the location of these SIFs within the material model, and because of this, the predicted fatigue life of the “up” condition is longer than the “average” and the “down” condition.

Table 15 Life Predictions Using BAMF Showing Predicted and Average Test Life of Cx4N1-09-B and Cx4N1-10-B (2024-T351) for the “Low” Applied Cold Expansion Level in 2024-T351

Predictions Made with CxA2 (2024-T351) Average of Left Side of Hole					
Coupon Type	Material Model	Residual Stress Distribution	Cycles	Average Predicted Life (cycles)	Average Test Life (cycles)
CxA2	APES	Average	112,950	131,630	129,600
		1STDDwn	206,420		
		1STDUp	75,521		

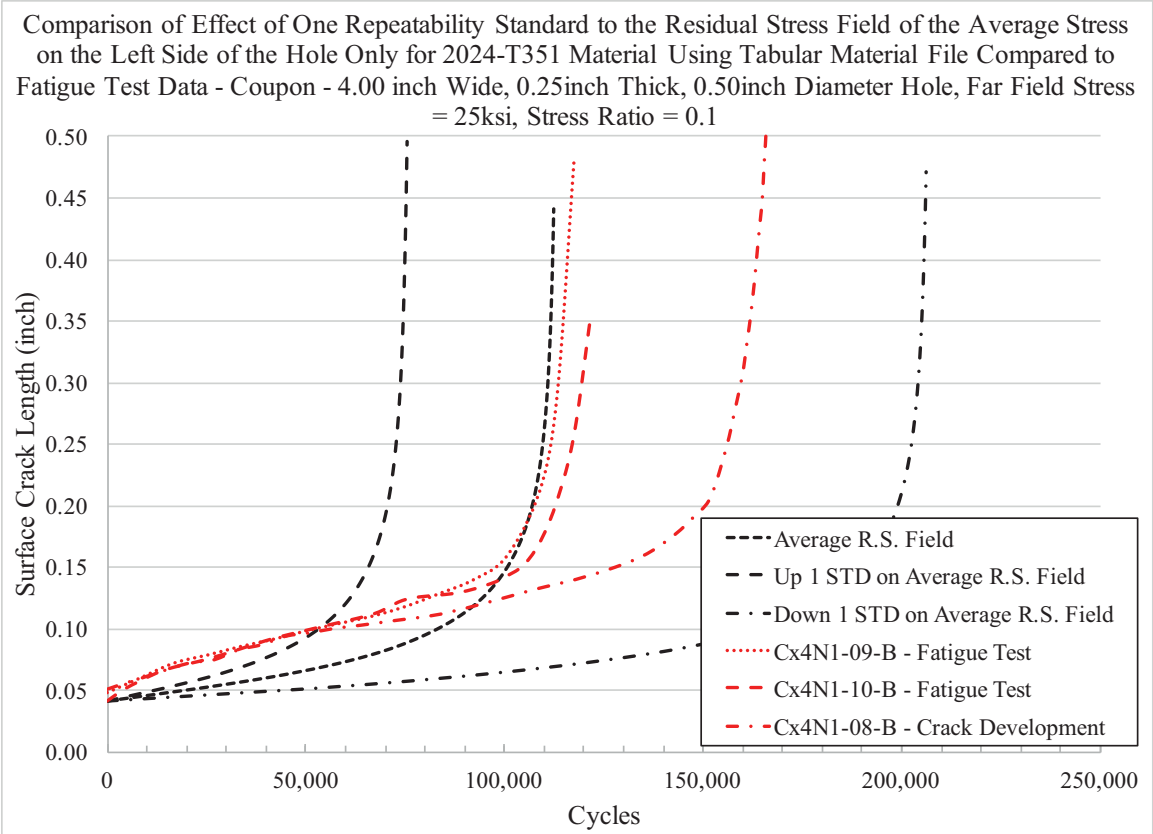

Fig. 927 Fatigue Crack Growth Curve Showing the Predicted Fatigue Life for the 2024-T351 “Low” Applied Expansion Using Three Statistical Distributions, and Compares These to Test Data from Cx4N1-09-B and CxN41-10-B, Along with “Crack Development” Coupon Cx4N1-08-B (2024-T351).

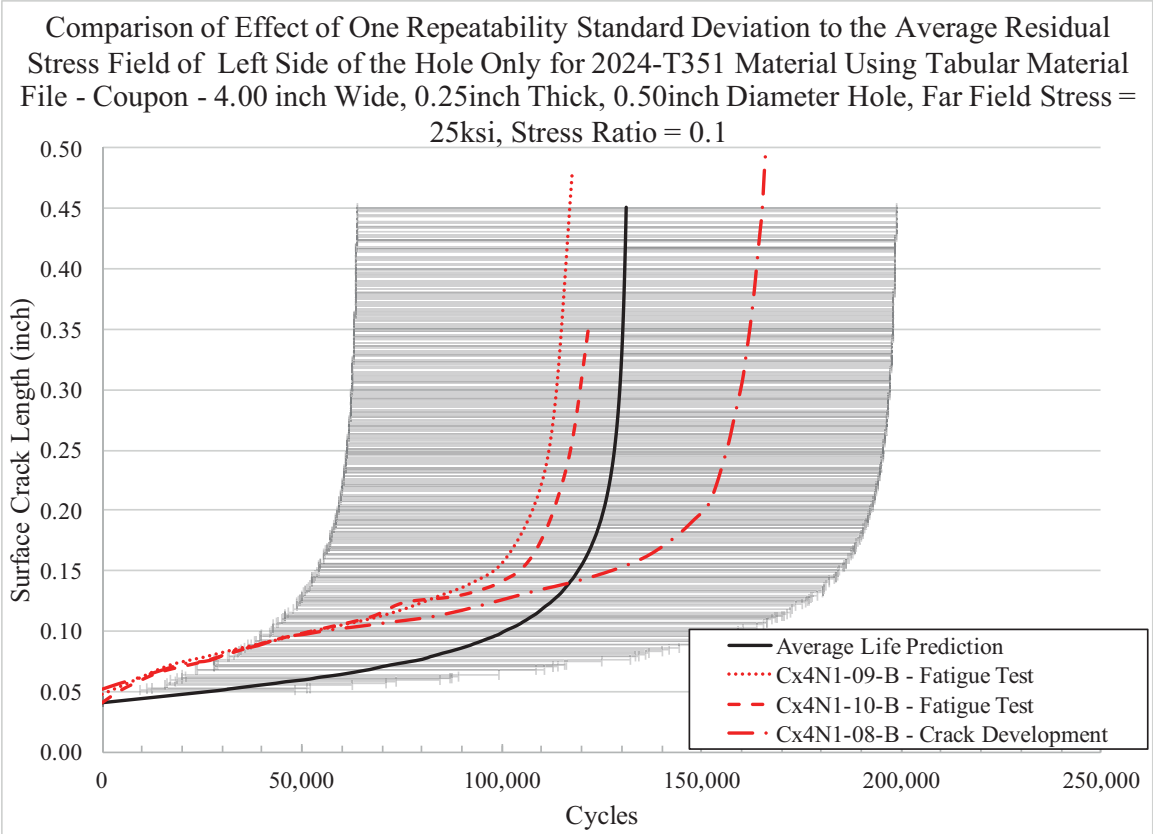

Fig. 928 Fatigue Crack Growth Curve Showing the Average of the Predicted Fatigue Life for the 2024-T351 “Low” Applied Expansion Using the Three Statistical Distributions, and Applies a Confidence Bound Using One Standard Deviation and Compares These to Test Data from Cx4N1-09-B and CxN41-10-B, Along with “Crack Development” Coupon Cx4N1-08-B (2024-T351).

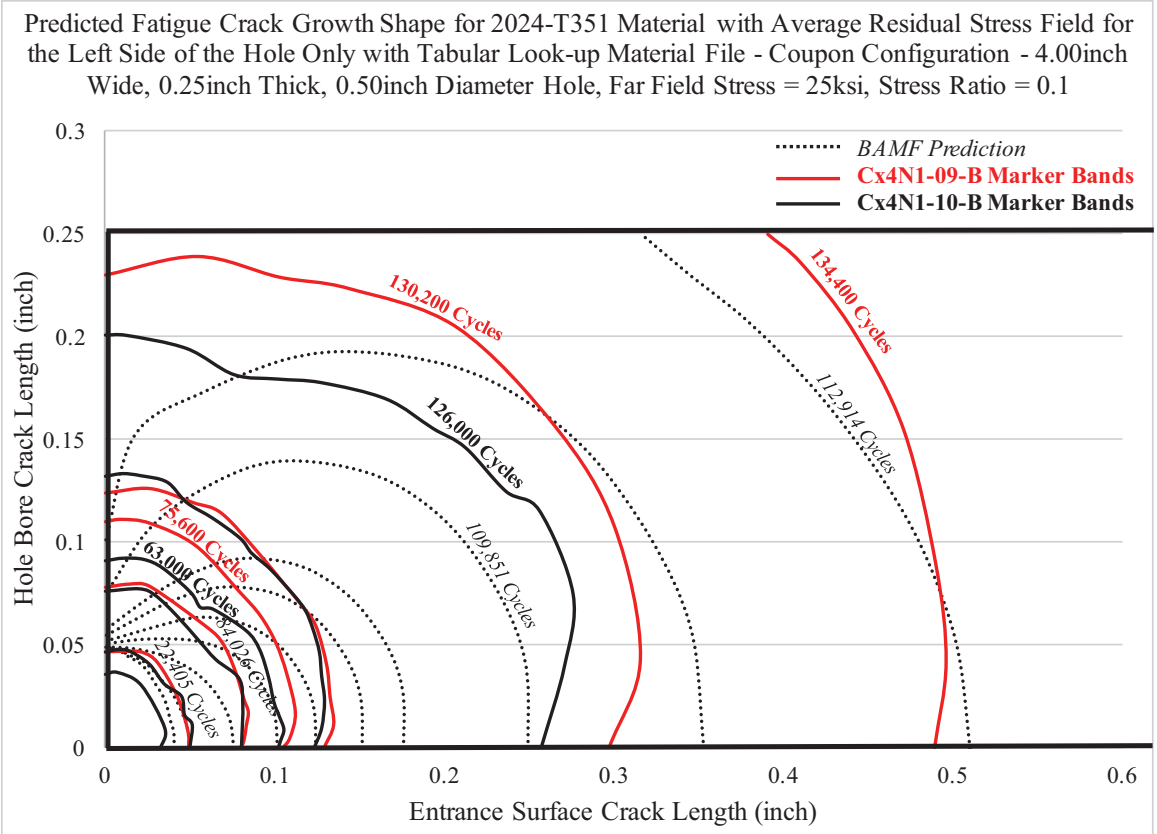

Fig. 929 Comparison of Fatigue Crack Growth Evolution, as Provided by Marker Banding and Through Prediction via BAMF for the “Average” Residual Stress Distribution for the Left Side of the Hole for the CxA2 (2024-T351) Condition.

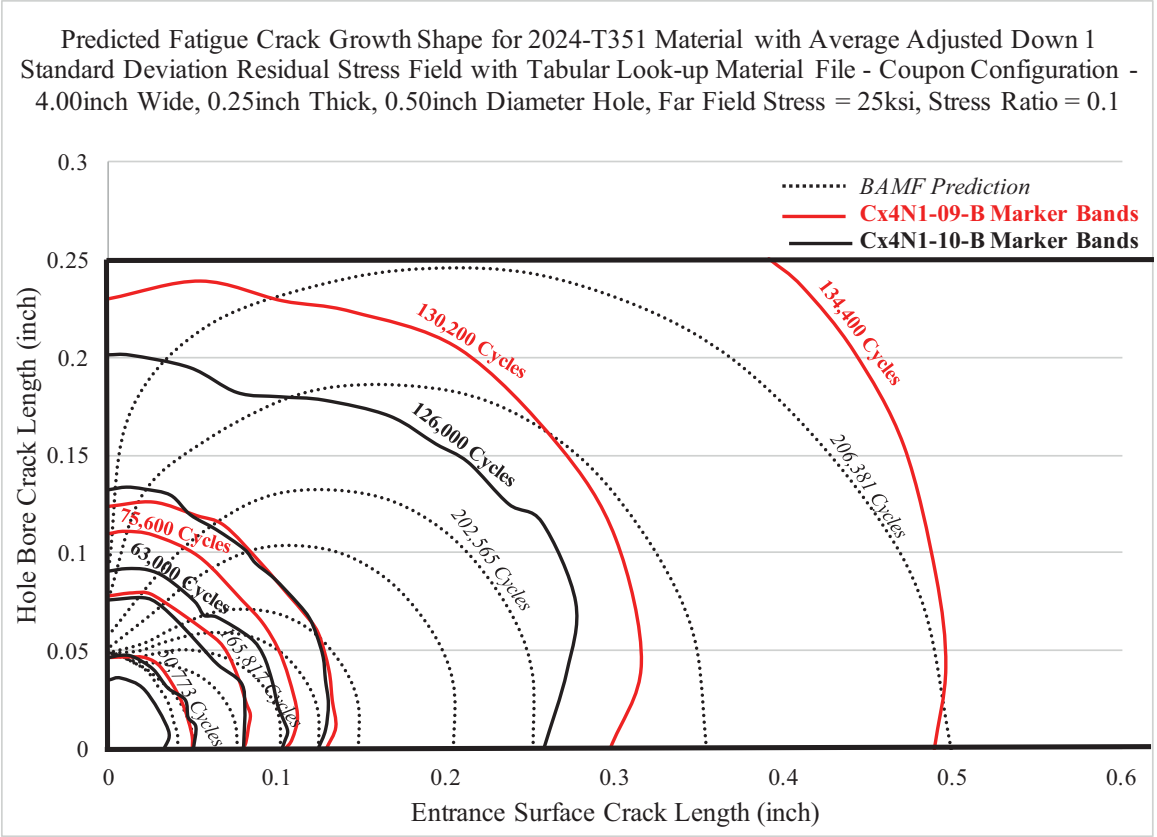

Fig. 930 Comparison of Fatigue Crack Growth Evolution, as Provided by Marker Banding and Through Prediction via BAMF for the "Down" One Statistical Distribution on Residual Stress Distribution for the Left Side of the Hole for the CxA2 (2024-T351) Condition.

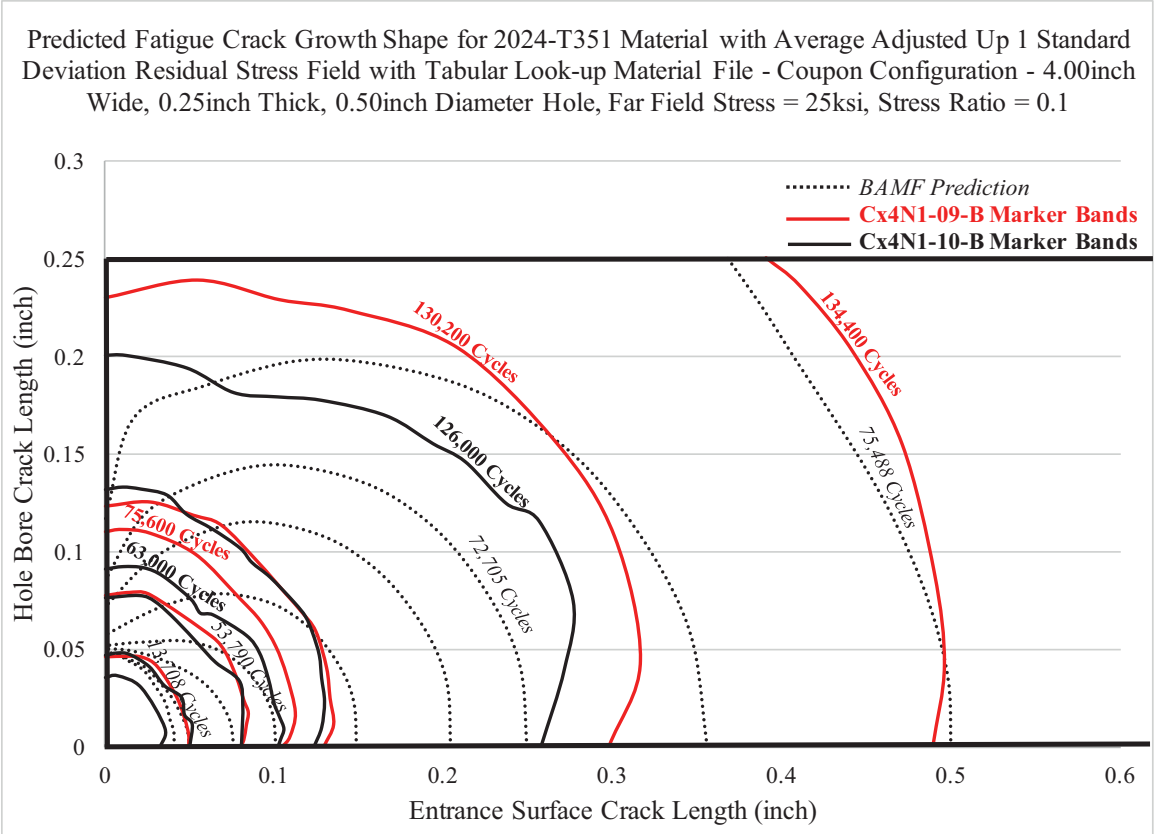

Fig. 931 Comparison of Fatigue Crack Growth Evolution, as Provided by Marker Banding and Through Prediction via BAMF for the “Up” One Statistical Distribution on Residual Stress Distribution for the Left Side of the Hole for the CxA2 (2024-T351) Condition.

Table 16 Life Predictions Using BAMF Showing Predicted and Test Life of Cx4N1-09-D (7075-T651) for the "Low" Applied Cold Expansion Level in 7075-T651

Predictions Made with CxD2 (7075-T651) Average of Left Side of Hole					
Coupon Type	Material Model	Residual Stress Distribution	Cycles	Average Predicted Life (cycles)	Test Life (cycles)
CxD2	APES	Average	338,408	599,629	58,800
		1STDDwn	1,247,000		
		1STDUp	213,479		

Table 17 Life Predictions Using BAMF Showing Predicted, Average of Fatigue Test Life and Cx4N1-08-D and Cx4N1-07-D (7075-T651 “Crack Development” Coupons) for the “Low” Applied Cold Expansion Level in 7075-T651

Predictions Made with CxD2 (7075-T651) Average of Left Side of Hole					
Coupon Type	Material Model	Residual Stress Distribution	Cycles	Average Predicted Life (cycles)	Average of Test Life and Crack Development Life (cycles)
CxD2	APES	Average	338,408	599,629	136,767
		1STDDwn	1,247,000		
		1STDUp	213,479		

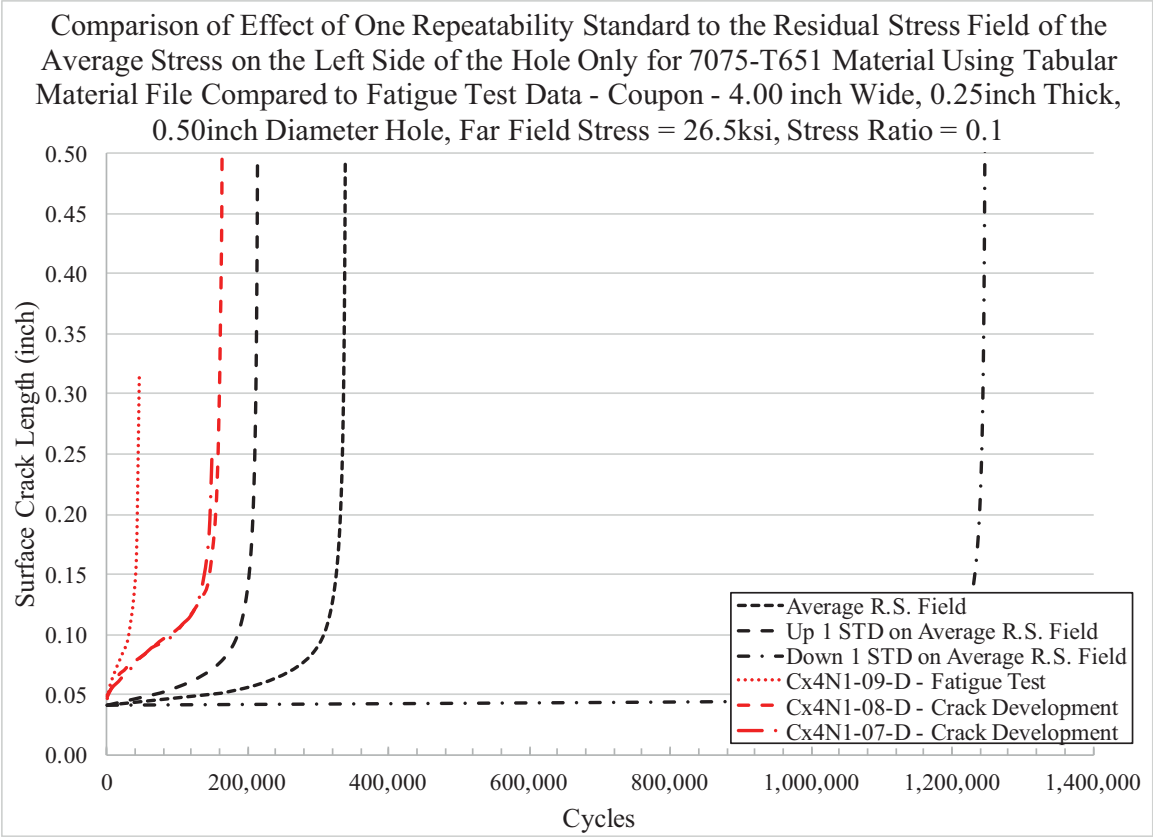

Fig. 932 Fatigue Crack Growth Curve Showing the Predicted Fatigue Life for the 7075-T651 “Low” Applied Expansion Using Three Statistical Distributions, and Compares to Test Data from Cx4N1-09-D and “Crack Development” Coupons Cx4N1-07-D and Cx4N1-08-D (7075-T651).

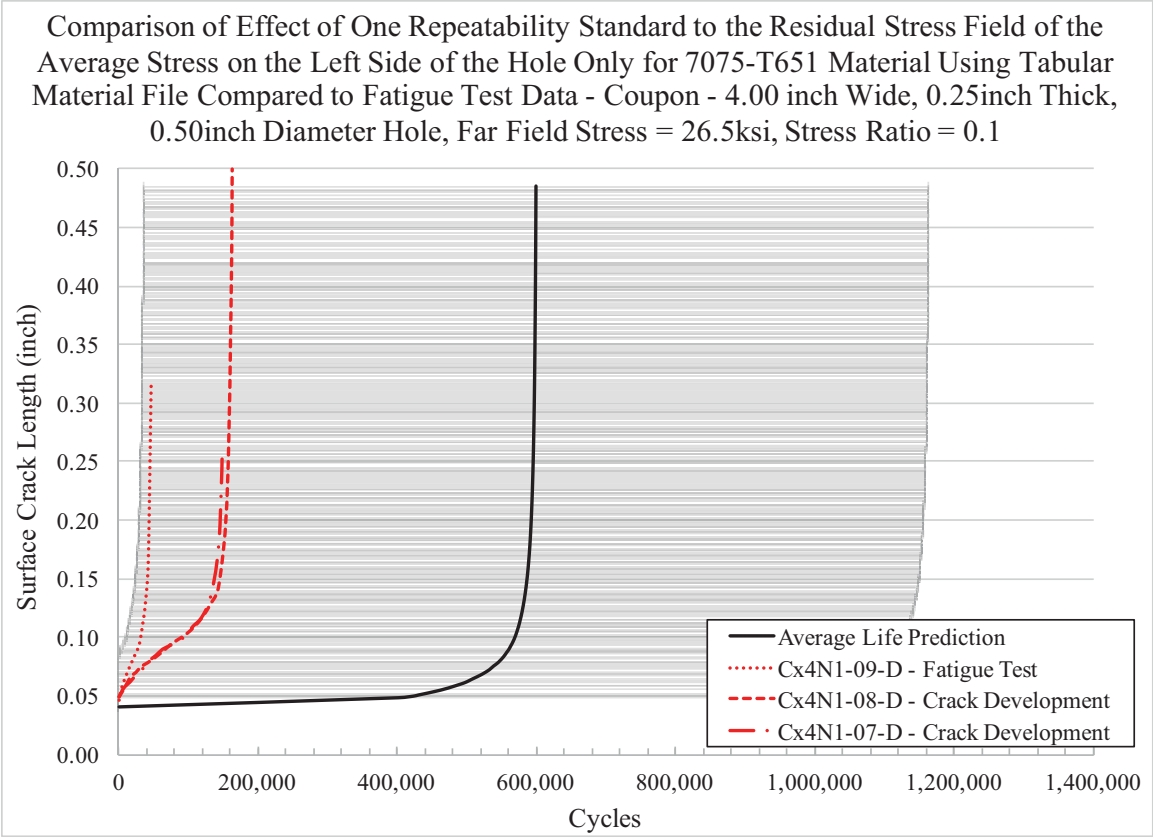

Fig. 933 Fatigue Crack Growth Curve Showing the Average of the Predicted Fatigue Life for the 7075-T651 “Low” Applied Expansion Using the Three Statistical Distributions, and Applies a Confidence Bound Using One Standard Deviation and Compares These to Test Data from Cx4N1-09-D, Along with “Crack Development” Coupon Cx4N1-08-B and Cx4N1-07-D (7075-T651).

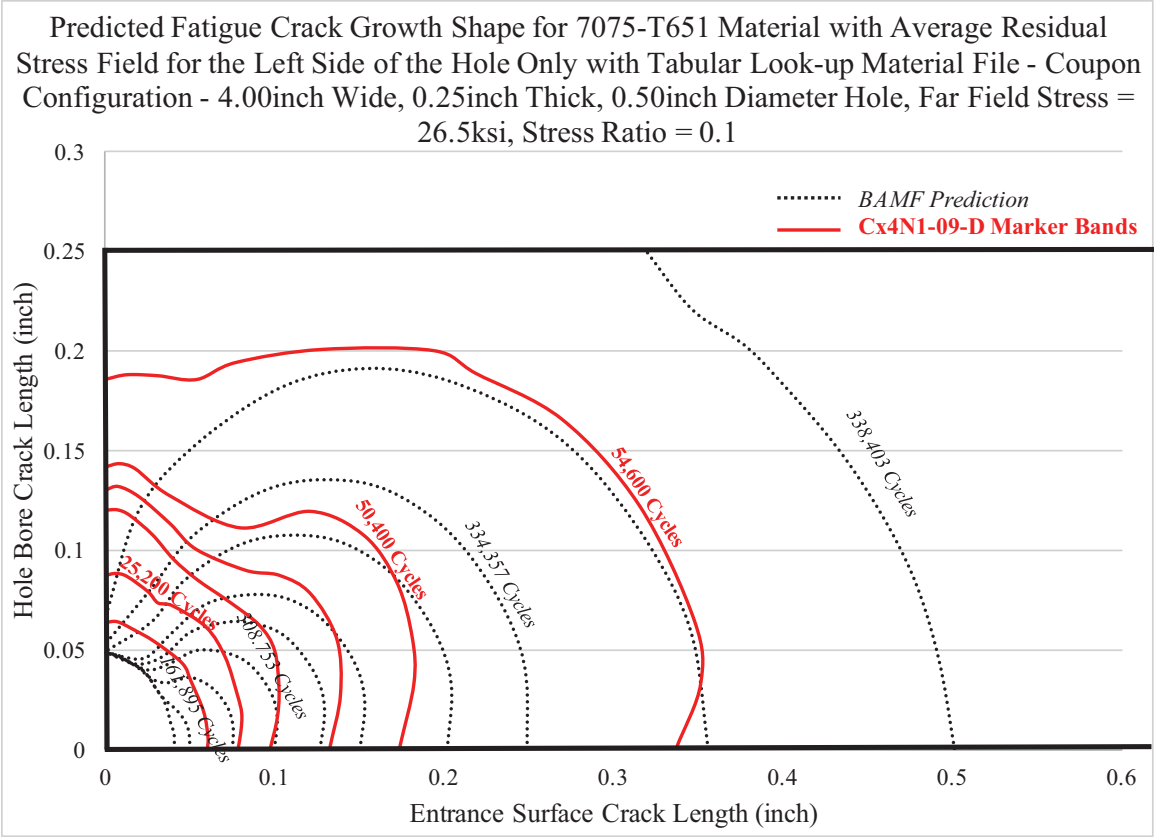

Fig. 934 Comparison of Fatigue Crack Growth Evolution, as Provided by Marker Banding and Through Prediction via BAMF for the “Average” Residual Stress Distribution for the Left Side of the Hole for the CxD2 (7075-T651) Condition.

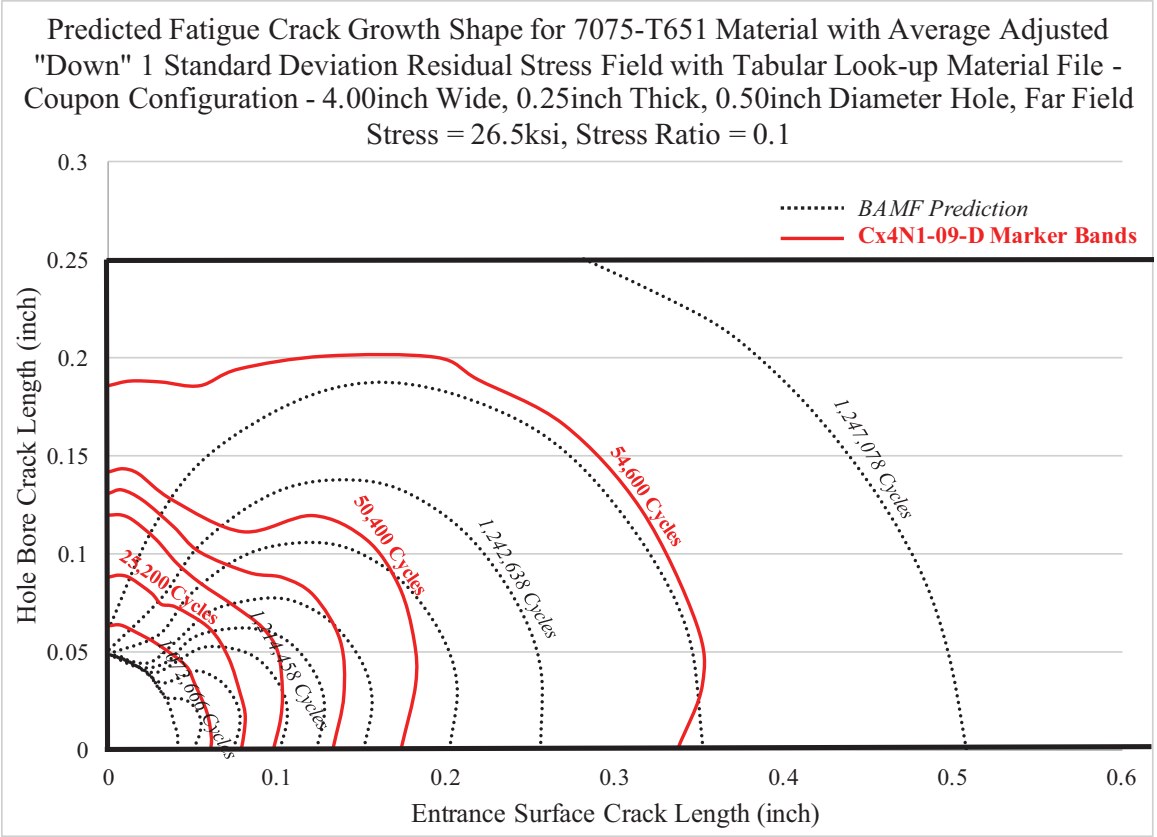

Fig. 935 Comparison of Fatigue Crack Growth Evolution, as Provided by Marker Banding and Through Prediction via BAMF for the “Down” One Statistical Distribution on Residual Stress Distribution for the Left Side of the Hole for the CxD2 (7075-T651) Condition.

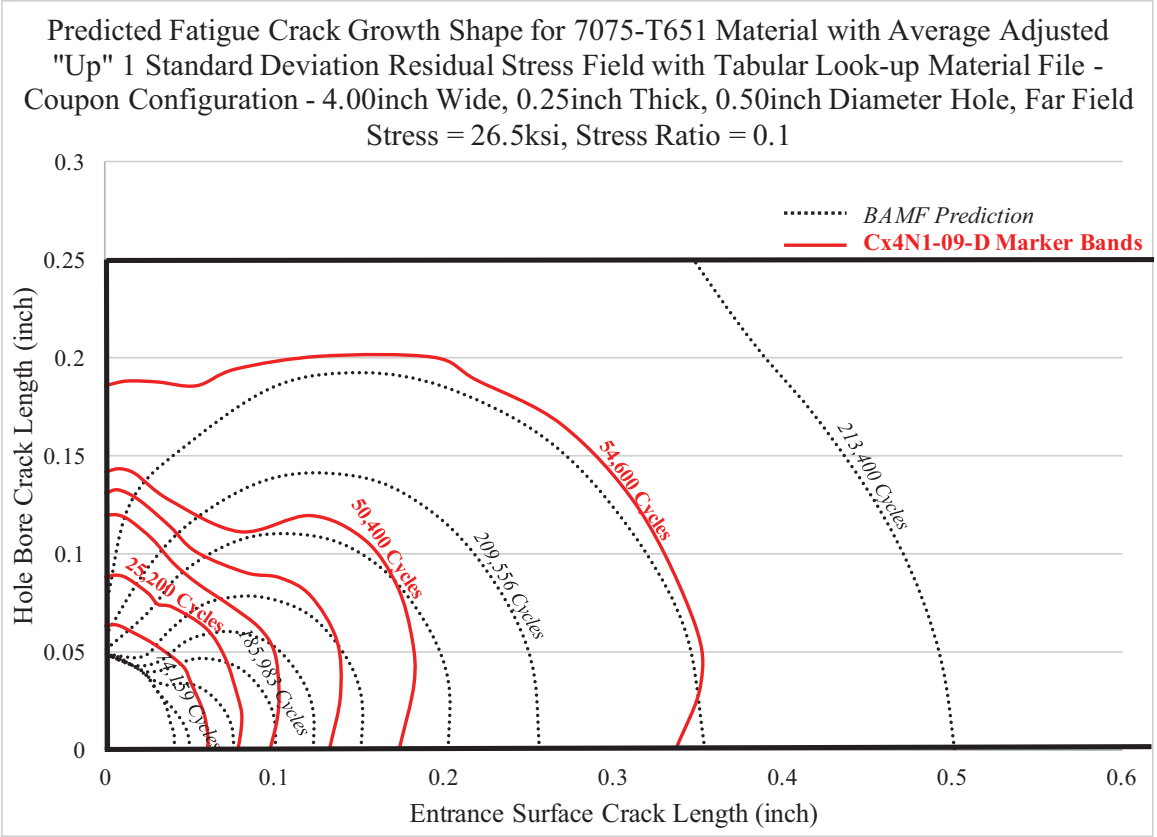

Fig. 936 Comparison of Fatigue Crack Growth Evolution, as Provided by Marker Banding and Through Prediction via BAMF for the “Up” One Statistical Distribution on Residual Stress Distribution for the Left Side of the Hole for the CxD2 (7075-T651) Condition.

Table 18 Breakdown of Residual Stress Functions Used in the Piecewise, Bivariant "Loaded Crack" Traction Stress Which was Imposed in StressCheck® with the Inclusion of the Baseline, Uncracked Condition

Plot Number	Residual Stress from Faituge Cracked Coupons	Distance Applied
1	Baseline Non-Cracked Residual Stress	0.00 - 0.04inch
2	Residual Stress for -01-02 (0.08inch) Crack Length	0.04 - 0.09inch
3	Residual Stress for -03-04 (0.10inch) Crack Length	0.09 - 0.1125inch
4	Residual Stress for -05-06 (0.125inc) Crack Length	0.1125 - 0.1875inch
5	Residual Stress for -07 (0.25inch) Crack Length	0.1875 - 0.375inch
6	Residual Stress for -08 (0.5inch) Crack Length	0.375 - 0.75inch

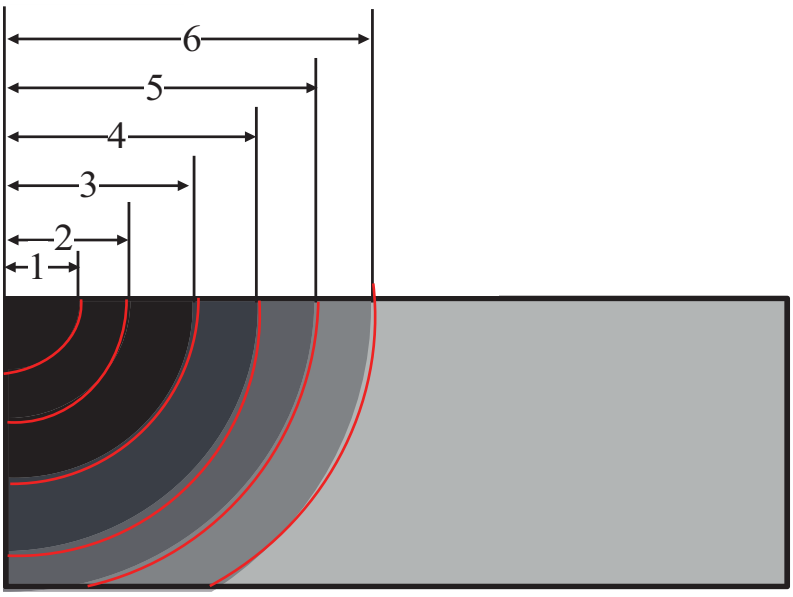

Fig. 937 Basic Figure Showing the General Shape of the Piecewise, Bivariant Polynomial Residual Stress “Loaded Crack” Traction Stress with Coordinating Zone Numbers from Table 18.

Table 19 Life Predictions Using BAMF Showing Predicted Life Using Cx4N1-XX-B (2024-T351) Cracked Coupons and CxA2 (2024-T351) and Average Test Life of Cx4N1-09-B and Cx4N1-10-B (2024-T351) for the “Low” Applied Cold Expansion Level in 2024-T351

Predictions Made with 4N1 Functions and 0.00 - 0.04 as the Baseline from CxA2 (2024-T351) Function					
Coupon Type	Material Model	Residual Stress Distribution	Cycles	Average Predicted Life (cycles)	Average Test Life (cycles)
CxA2	APES	Average	112,156	137,991	129,600
		1STDDwn	231,899		
		1STDUp	69,919		

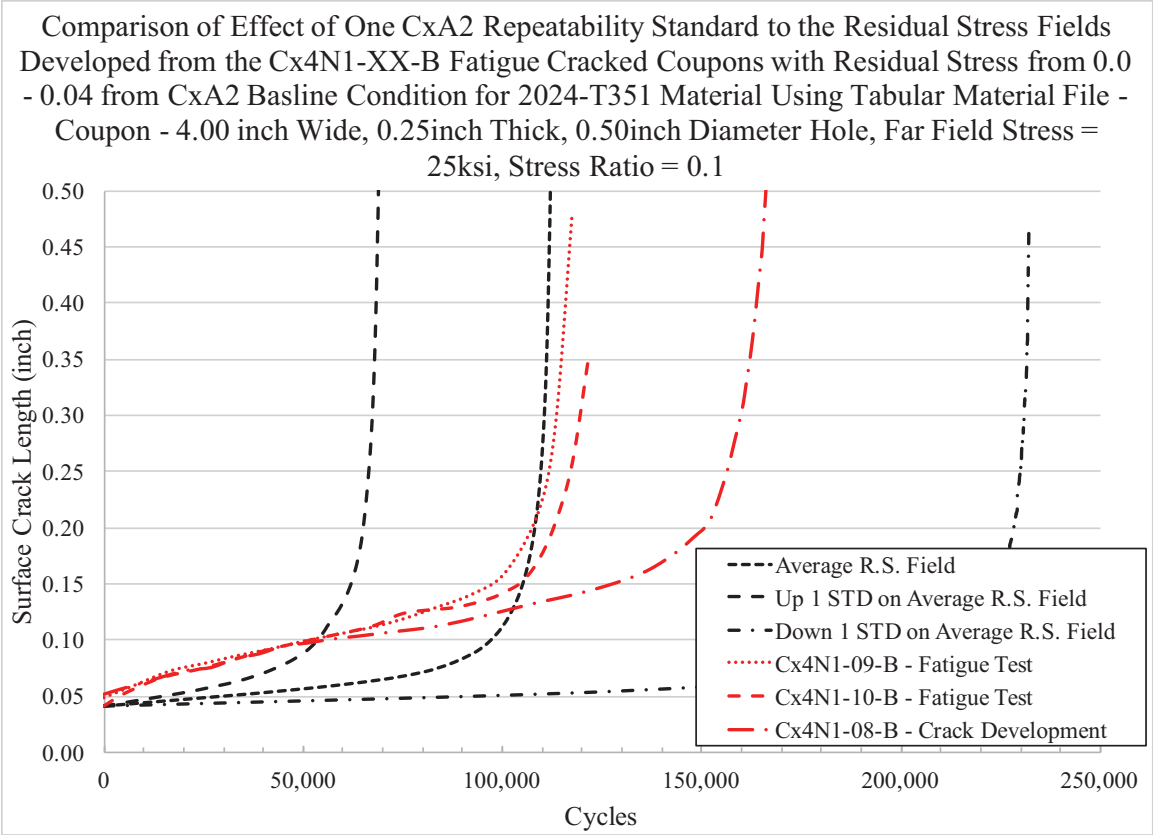

Fig. 938 Fatigue Crack Growth Curve Showing the Predicted Fatigue Life for the 2024-T351 “Low” Applied Expansion using Three Statistical Distributions, and Compares These to Test Data from Cx4N1-09-B and CxN41-10-B, Along with “Crack Development” Coupon Cx4N1-08-B (2024-T351) – Residual Stress Function Used was Derived from Cx4N1-XX-B (2024-T351) Fatigue-Cracked Coupons, Using the CxA2 (2024-T351) Residual Stress from the Edge of the Hole to 0.04 inch.

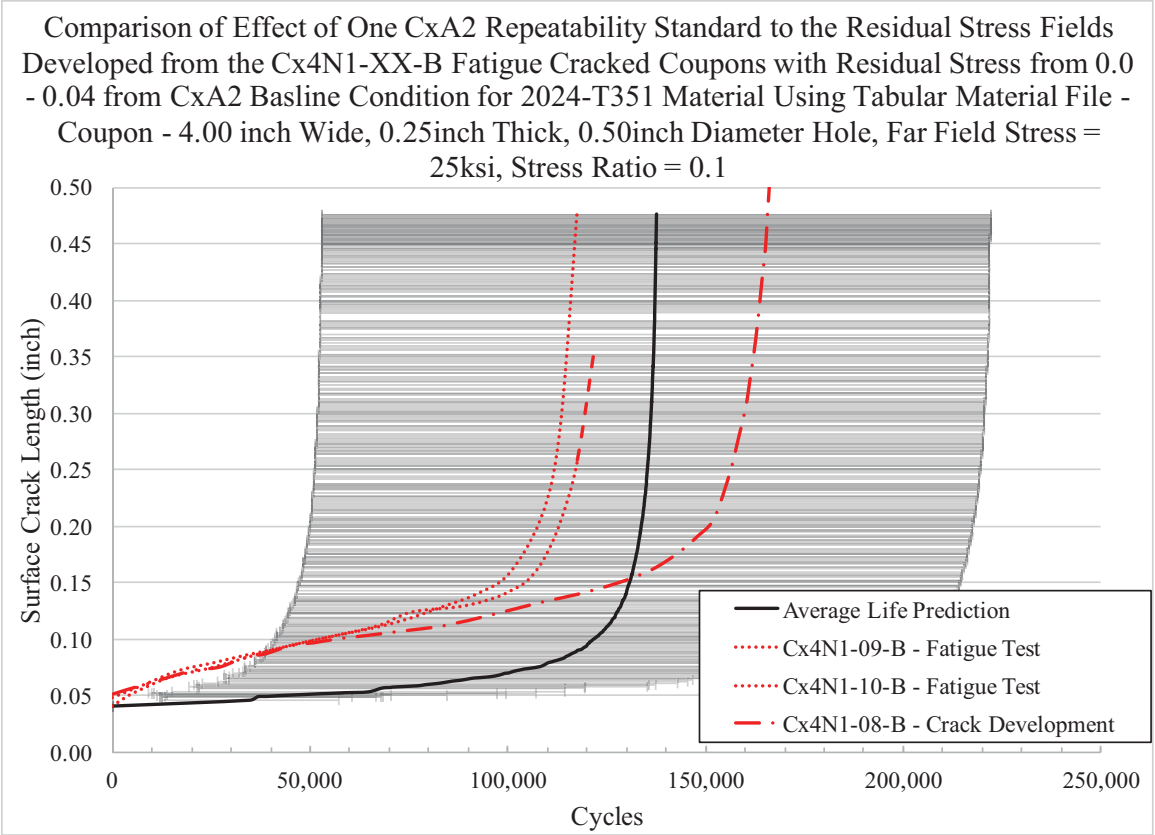

Fig. 939 Fatigue Crack Growth Curve Showing the Average of the Predicted Fatigue Life for the 2024-T351 "Low" Applied Expansion Using the Three Statistical Distributions, and Applies a Confidence Bound Using One Standard Deviation and Compares These to Test Data from Cx4N1-09-B and CxN41-10-B, Along with "Crack Development" Coupon Cx4N1-08-B (2024-T351) – Residual Stress Function Used was Derived from Cx4N1-XX-B (2024-T351) Fatigue-Cracked Coupons, Using the CxA2 (2024-T351) Residual Stress from the Edge of the Hole to 0.04 inch.

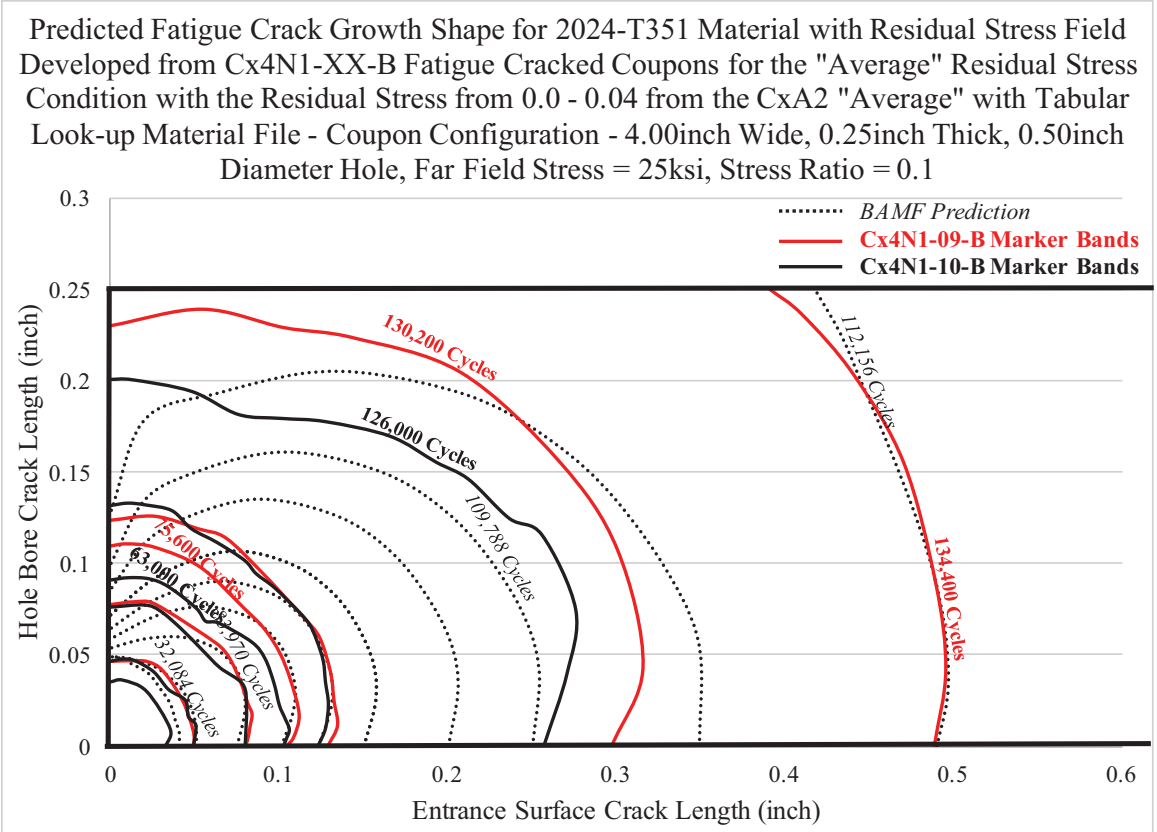

Fig. 940 Comparison of Fatigue Crack Growth Evolution, as Provided by Marker Banding and Through Prediction via BAMF Using the “Average” Residual Stress Distribution for the Left Side of the Hole for the CxA2 (2024-T351) Condition from 0.0 – 0.04 inch from the Edge of the Hole and Then the “Average” Residual Stress Distribution as Developed from the Cx4N1-XX-B (2024-T351) Cracked Coupon Condition.

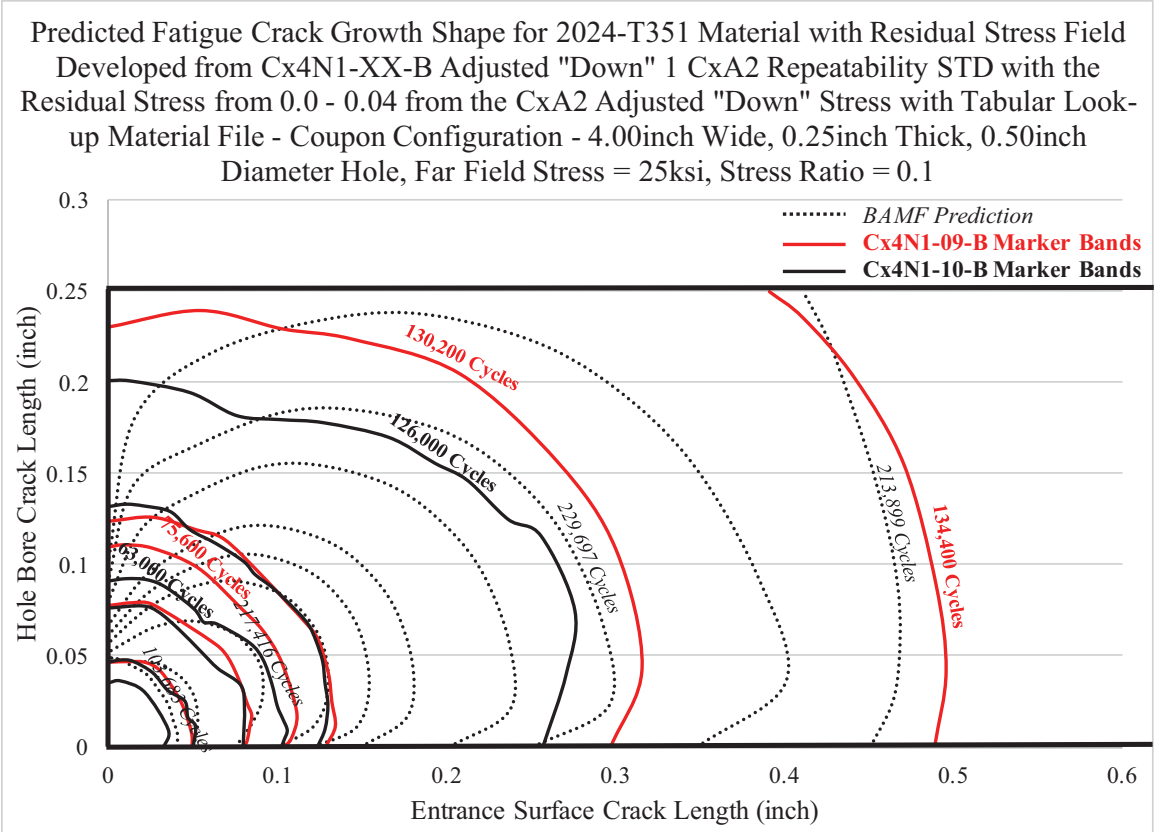

Fig. 941 Comparison of Fatigue Crack Growth Evolution, as Provided by Marker Banding and Through Prediction via BAMF Using the One “Down” Residual Stress Distribution for the Left Side of the Hole for the CxA2 (2024-T351) Condition from 0.0 – 0.04 inch from the Edge of the Hole and Then the One “Down” Residual Stress Distribution as Developed from the Cx4N1-XX-B (2024-T351) Cracked Coupon Condition.

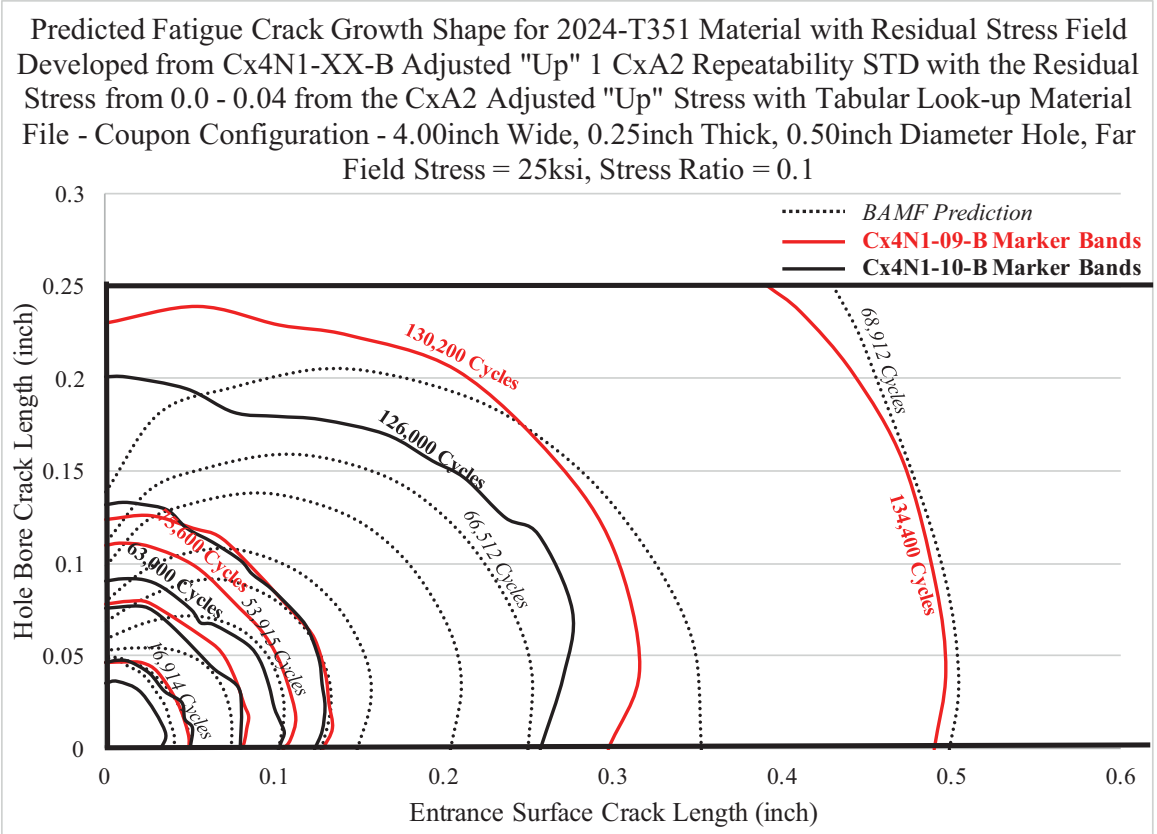

Fig. 942 Comparison of Fatigue Crack Growth Evolution, as Provided by Marker Banding and Through Prediction via BAMF Using the One “Up” Residual Stress Distribution for the Left Side of the Hole for the CxA2 (2024-T351) Condition from 0.0 – 0.04 inch from the Edge of the Hole and Then the One “Up” Residual Stress Distribution as Developed from the Cx4N1-XX-B (2024-T351) Cracked Coupon Condition.

Table 20 Life Predictions Using BAMF Showing Predicted Life Using Cx4N1-XX-D (7075-T651) Cracked Coupons and CxD2 (7075-T651) and Average Test Life of Cx4N1-09-D and Cx4N1-08-D and Cx4N1-07-D From the "Crack Development" Coupons for the "Low" Applied Cold Expansion Level in 7075-T651

Predictions Made with 4N1 Functions and 0.00 - 0.04 as the Baseline CxD2 (7075-T651) Function					
Coupon Type	Material Model	Residual Stress Distribution	Cycles	Average Predicted Life (cycles)	Average Test Life (cycles)
CxD2	APES	Average	125,738	183,226	136,767
		1STDDwn	171,256		
		1STDUp	252,684		

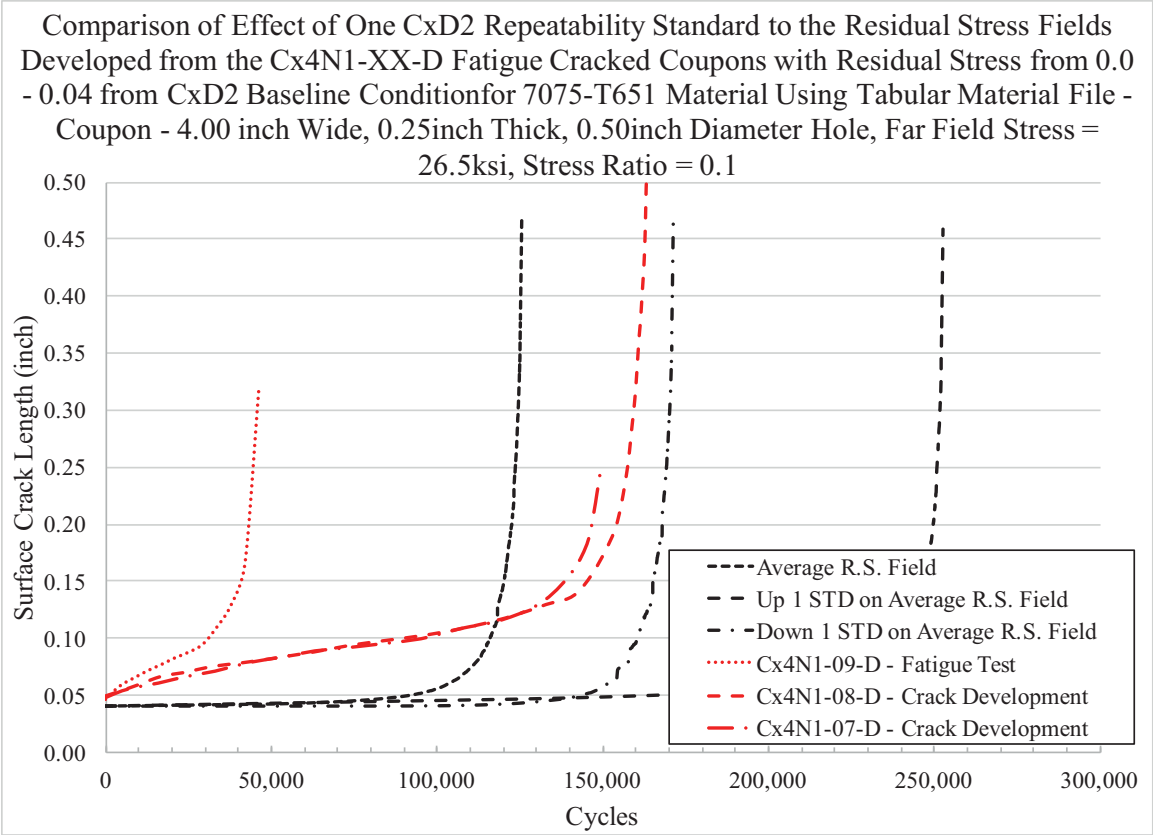

Fig. 943 Fatigue Crack Growth Curve Showing the Predicted Fatigue Life for the 7075-T651 “Low” Applied Expansion Using Three Statistical Distributions, and Compares These to Test Data from Cx4N1-09-D, Along with “Crack Development” Coupons Cx4N1-07-D and Cx4N1-08-D (7075-T651) – Residual Stress Function Used was Derived from Cx4N1-XX-D (7075-T651) Fatigue-Cracked Coupons, Using the CxD2 (7075-T651) Residual Stress from the Edge of the Hole to 0.04 inch.

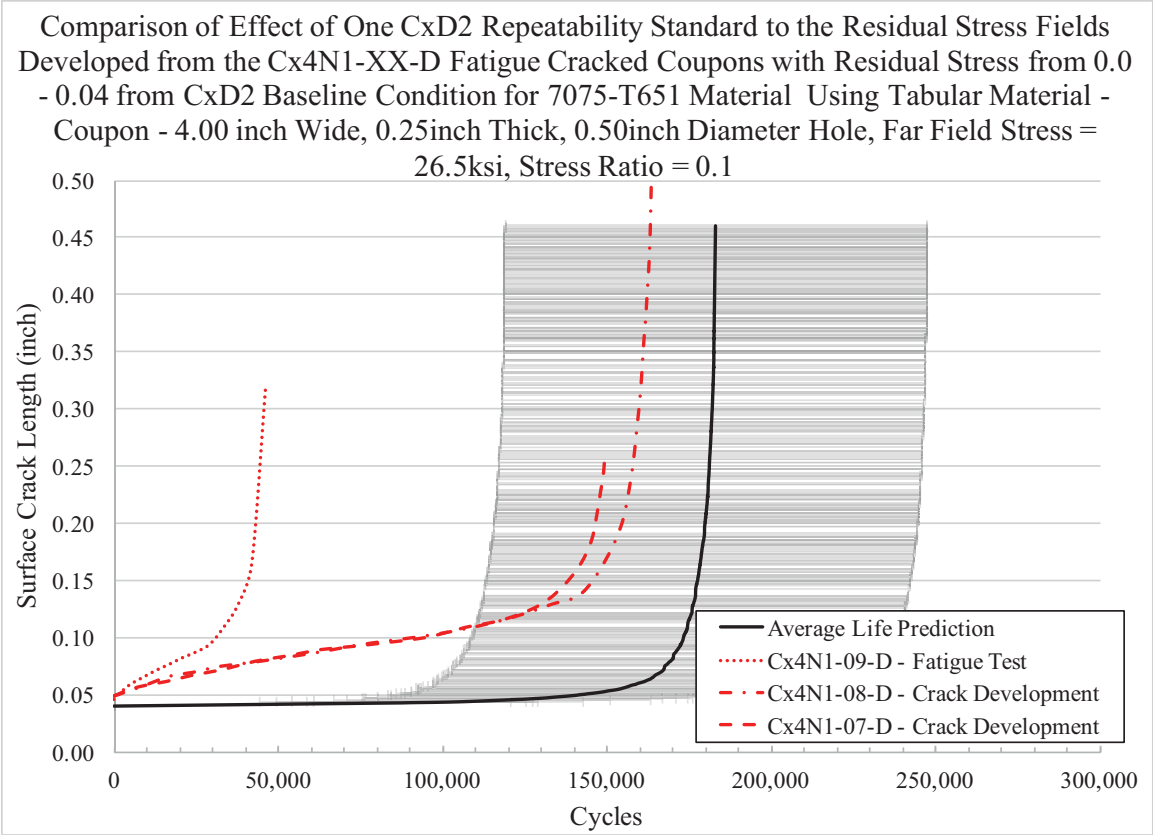

Fig. 944 Fatigue Crack Growth Curve Showing the Average of the Predicted Fatigue Life for the 7075-T651 "Low" Applied Expansion Using the Three Statistical Distributions, and Applies a Confidence Bound Using One Standard Deviation and Compares These to Test Data from Cx4N1-09-D, Along with "Crack Development" Coupon Cx4N1-08-B and Cx4N1-07-D (7075-T651) – Residual Stress Function Used was Derived from Cx4N1-XX-D (7075-T651) Fatigue-Cracked Coupons, Using the CxD2 (7075-T651) Residual Stress from the Edge of the Hole to 0.04 inch.

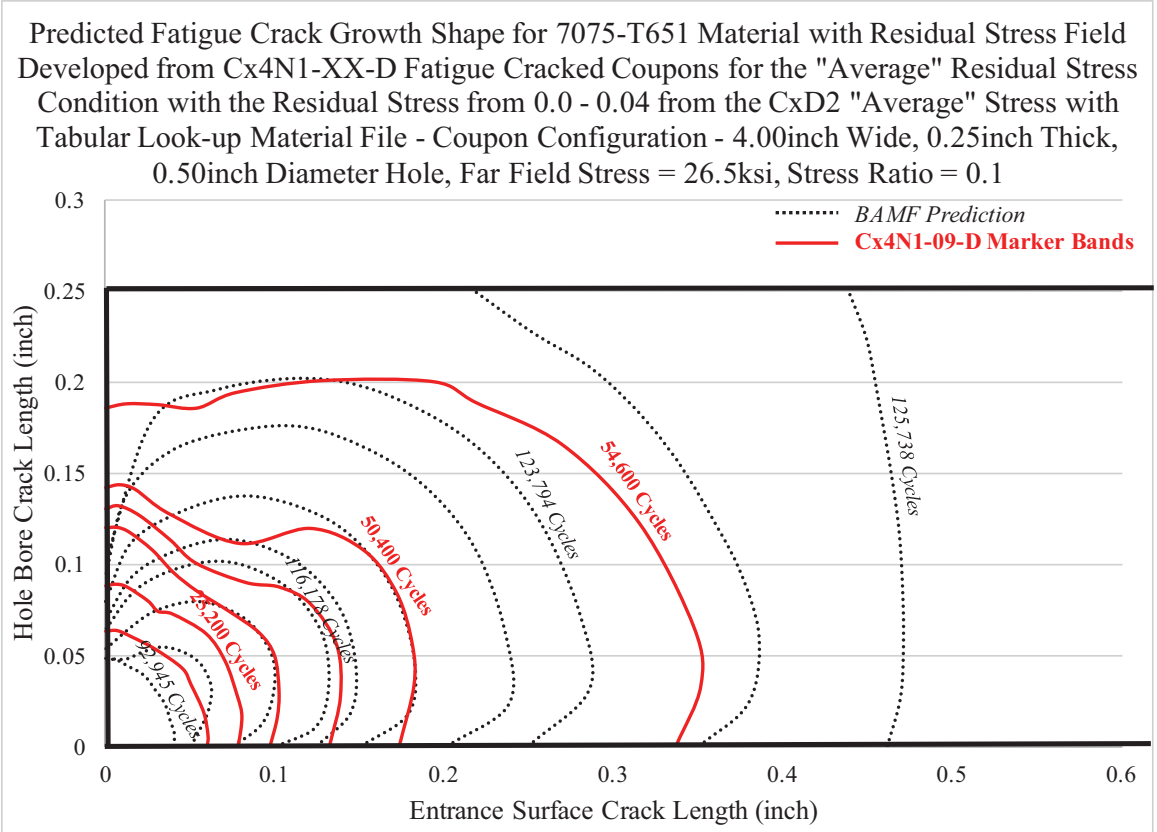

Fig. 945 Comparison of Fatigue Crack Growth Evolution, as Provided by Marker Banding and Through Prediction via BAMF Using the “Average” Residual Stress Distribution for the Left Side of the Hole for the CxD2 (7075-T651) Condition from 0.0 – 0.04 inch from the Edge of the Hole and Then the “Average” Residual Stress Distribution as Developed from the Cx4N1-XX-D (7075-T651) Cracked Coupon Condition.

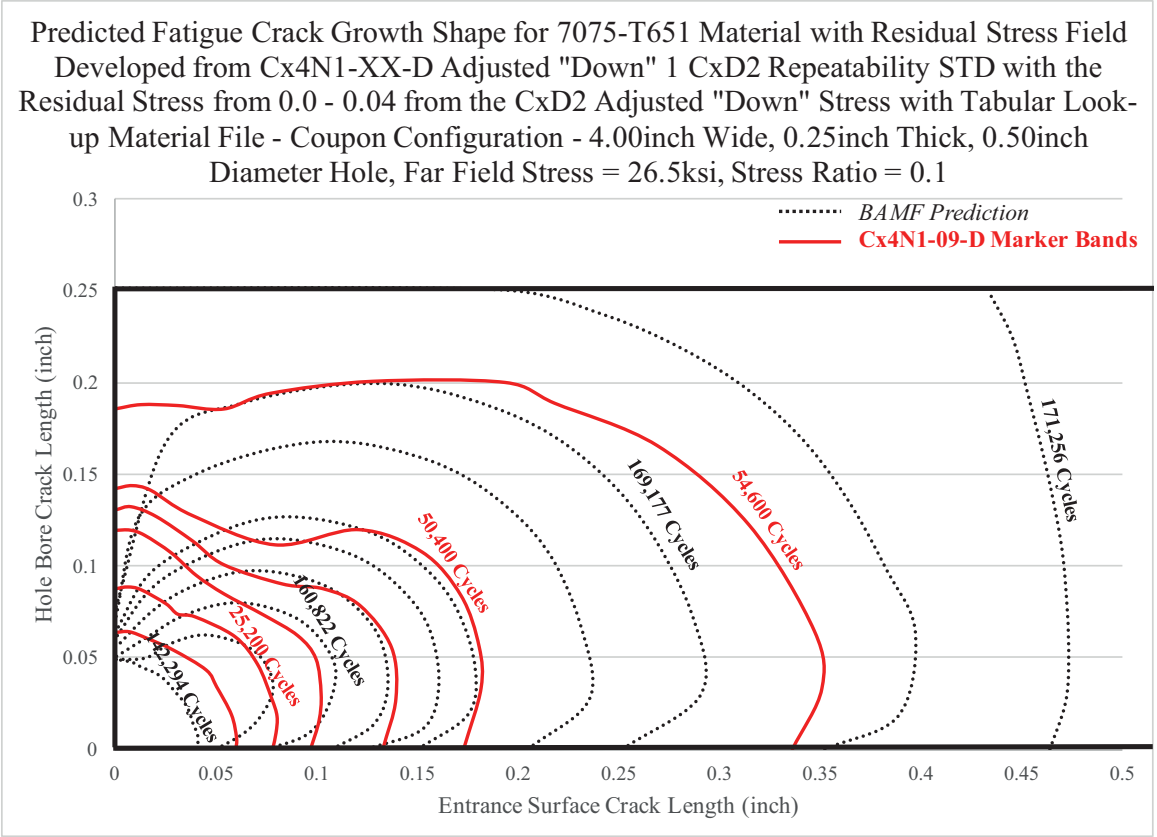

Fig. 946 Comparison of Fatigue Crack Growth Evolution, as Provided by Marker Banding and Through Prediction via BAMF Using the One “Down” Residual Stress Distribution for the Left Side of the Hole for the CxD2 (7075-T651) Condition from 0.0 – 0.04 inch from the Edge of the Hole and Then the One “Down” Residual Stress Distribution as Developed from the Cx4N1-XX-D (7075-T651) Cracked Coupon Condition.

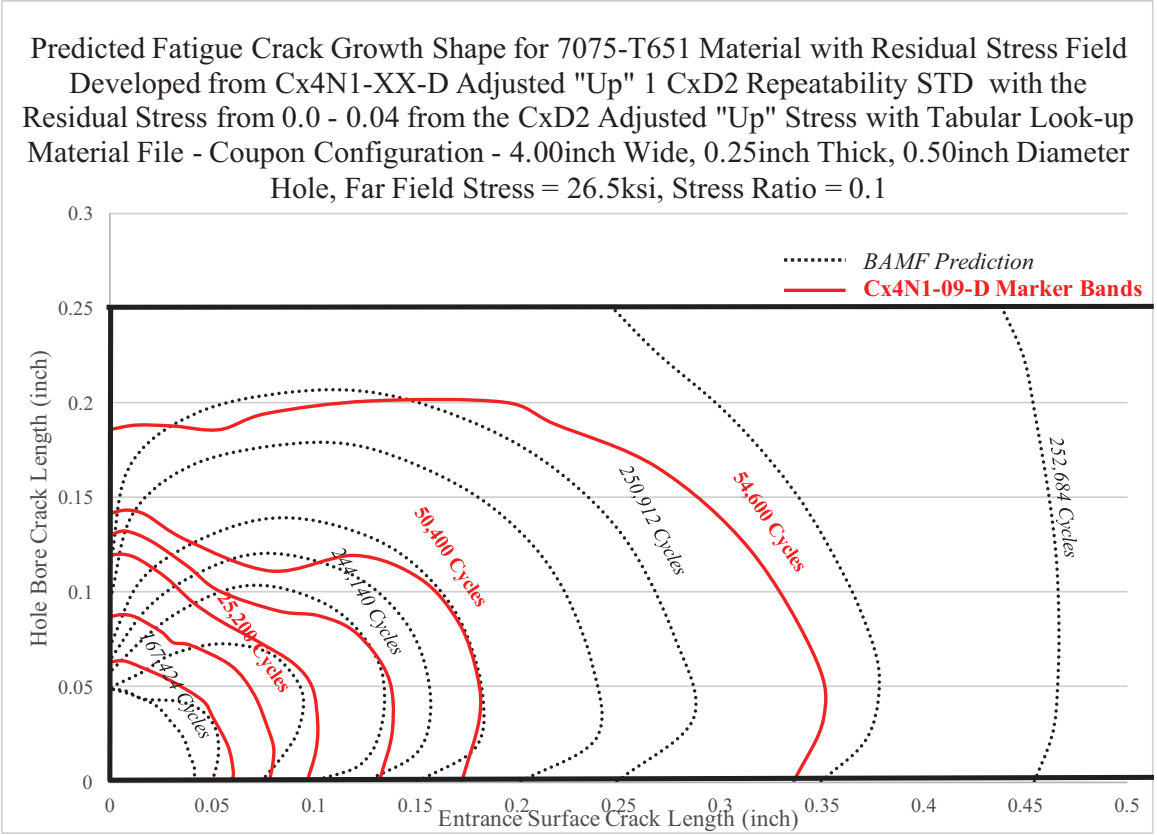

Fig. 947 Comparison of Fatigue Crack Growth Evolution, as Provided by Marker Banding and Through Prediction via BAMF Using the One “Down” Residual Stress Distribution for the Left Side of the Hole for the CxD2 (7075-T651) Condition from 0.0 – 0.04 inch from the Edge of the Hole and Then the One “Up” Residual Stress Distribution as Developed from the Cx4N1-XX-D (7075-T651) Cracked Coupon Condition.

Table 21 Breakdown of Residual Stress Functions Used in the Piecewise, Bivariant "Loaded Crack" Traction Stress Which was Imposed in StressCheck® Using the Cx4N1-01-02-B (2024-T351) Condition from 0.0 – 0.09 inch

Plot Number	Residual Stress from Faituge Cracked Coupons	Distance Applied
1	Residual Stress for -01-02 (0.08inch) Crack Length	0.00 - 0.09inch
2		
3	Residual Stress for -03-04 (0.10inch) Crack Length	0.09 - 0.1125inch
4	Residual Stress for -05-06 (0.125inc) Crack Length	0.1125 - 0.1875inch
5	Residual Stress for -07 (0.25inch) Crack Length	0.1875 - 0.375inch
6	Residual Stress for -08 (0.5inch) Crack Length	0.375 - 0.75inch

Table 22 Life Predictions Using BAMF Showing Predicted Life Using Cx4N1-XX-B (2024-T351) Cracked Coupons and Average Test Life of Cx4N1-09-B and Cx4N1-10-B (2024-T351) for the “Low” Applied Cold Expansion Level in 2024-T351

Predictions Made with 4N1 Functions and 0.00 - 0.09 as Cx4N1-01-02-B (0.08inch Crack) Functions					
Coupon Type	Material Model	Residual Stress Distribution	Cycles	Average Predicted Life (cycles)	Average Test Life (cycles)
CxA2	APES	Average	127,956	154,693	129,600
		1STDDwn	270,965		
		1STDUp	65,158		

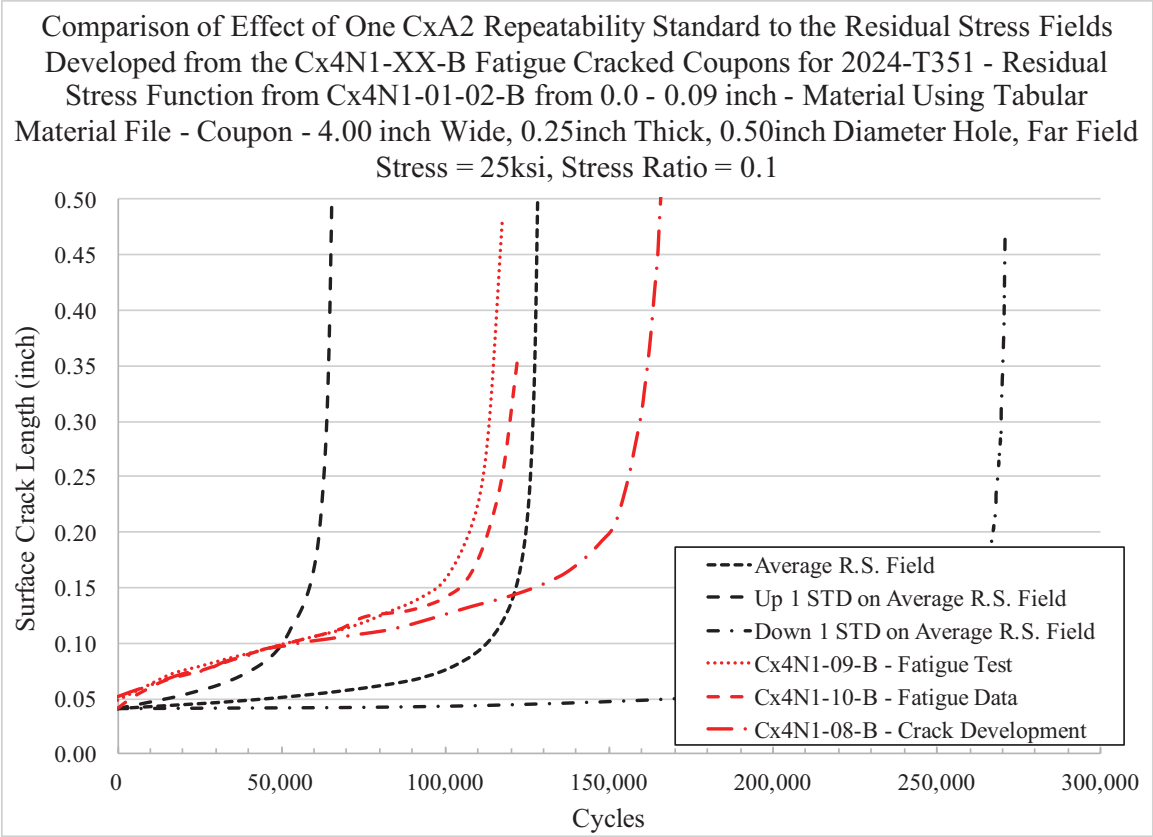

Fig. 948 Fatigue Crack Growth Curve Showing the Predicted Fatigue Life for the 2024-T351 “Low” Applied Expansion Using Three Statistical Distributions, and Compares These to Test Data from Cx4N1-09-B and CxN41-10-B, Along with “Crack Development” Coupon Cx4N1-08-B (2024-T351) – Residual Stress Function Used was Derived from Cx4N1-XX-B (2024-T351) Fatigue-Cracked Coupons, Applying the Cx4N1-01-02-B (2024-T351) Residual Stress from 0.0 – 0.09 inch away from the Edge of the Hole.

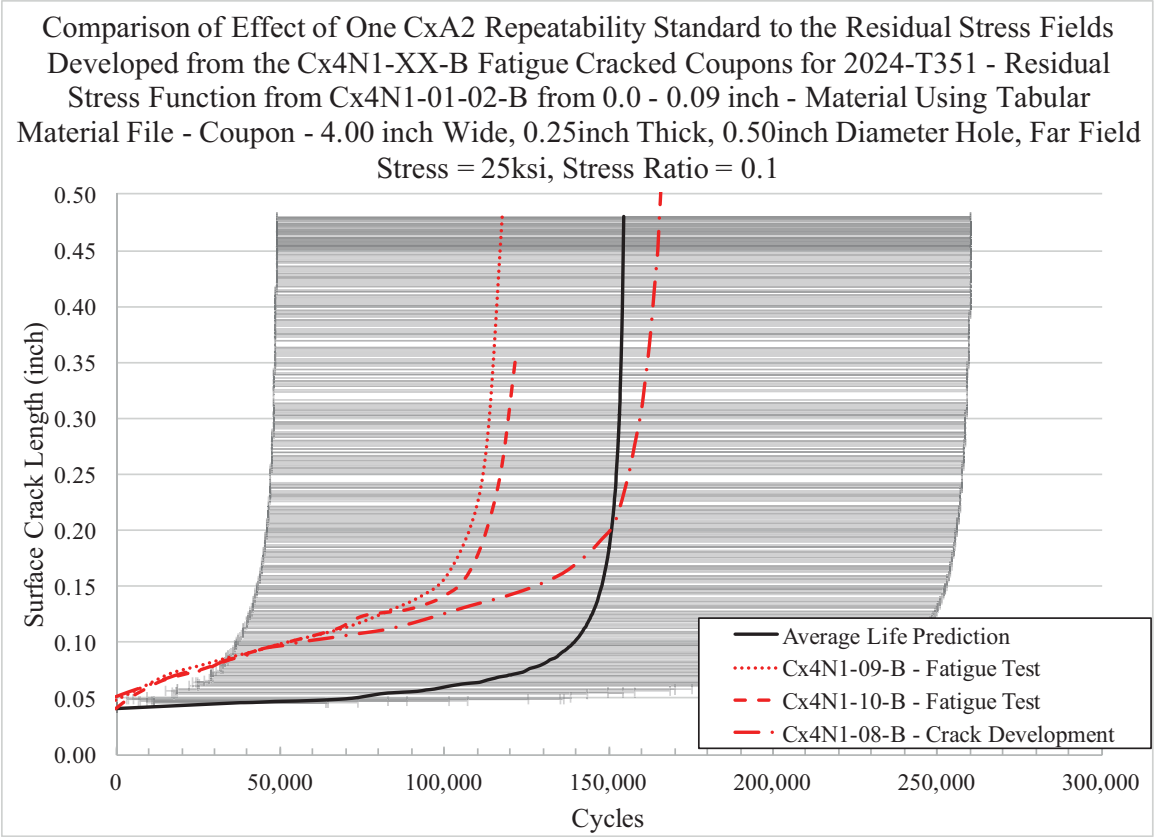

Fig. 949 Fatigue Crack Growth Curve Showing the Average of the Predicted Fatigue Life for the 2024-T351 “Low” Applied Expansion Using the Three Statistical Distributions, and Applies a Confidence Bound Using One Standard Deviation and Compares These to Test Data from Cx4N1-09-B and CxN41-10-B, Along with “Crack Development” Coupon Cx4N1-08-B (2024-T351) – Residual Stress Function Used was Derived from Cx4N1-XX-B (2024-T351) Fatigue-Cracked Coupons, Applying the Cx4N1-01-02-B (2024-T351) Residual Stress from 0.0 – 0.09 inch away from the Edge of the Hole.

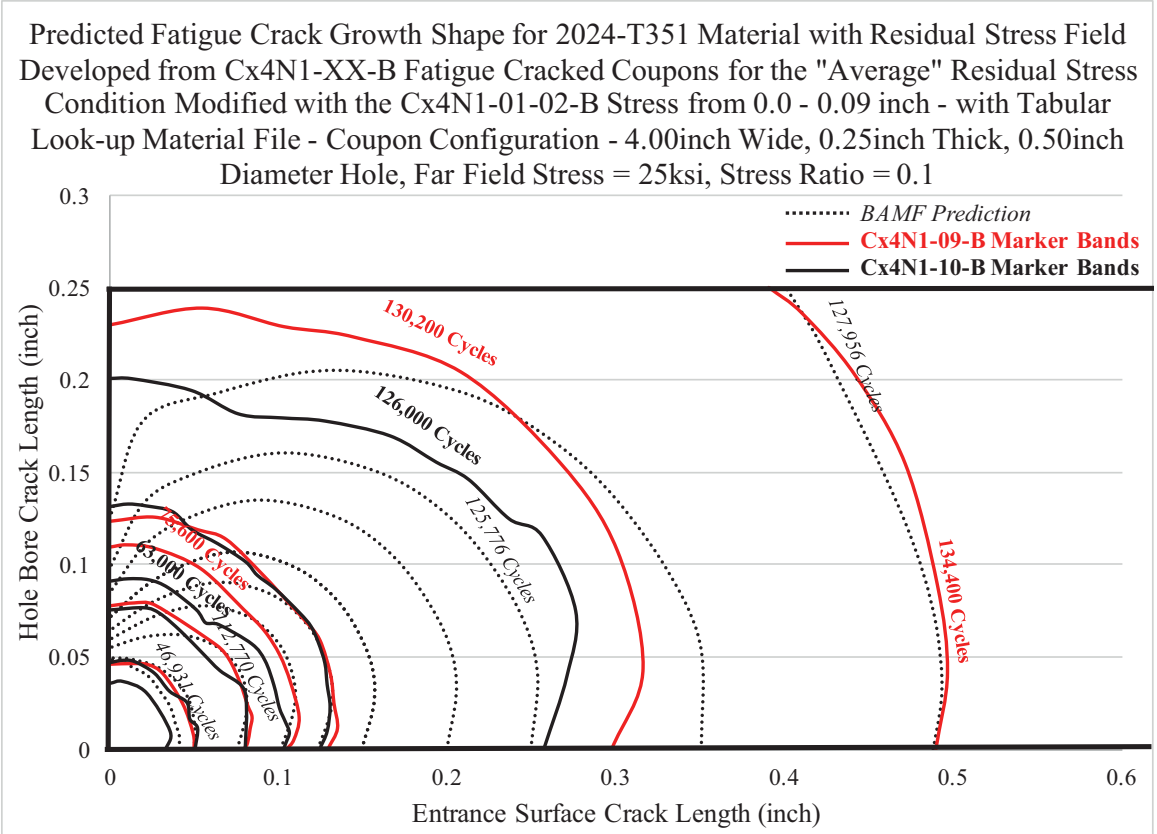

Fig. 950 Comparison of Fatigue Crack Growth Evolution, as Provided by Marker Banding and Through Prediction via BAMF Using the “Average” Residual Stress Distribution the Cx4N1-XX-B (2024-T351) Cracked Coupon Condition, Imposing the “Average” of the Cx4N1-01-02-B (2024-T351) Cracked Condition from 0.0 – 0.09 inch from the Edge of the Hole.

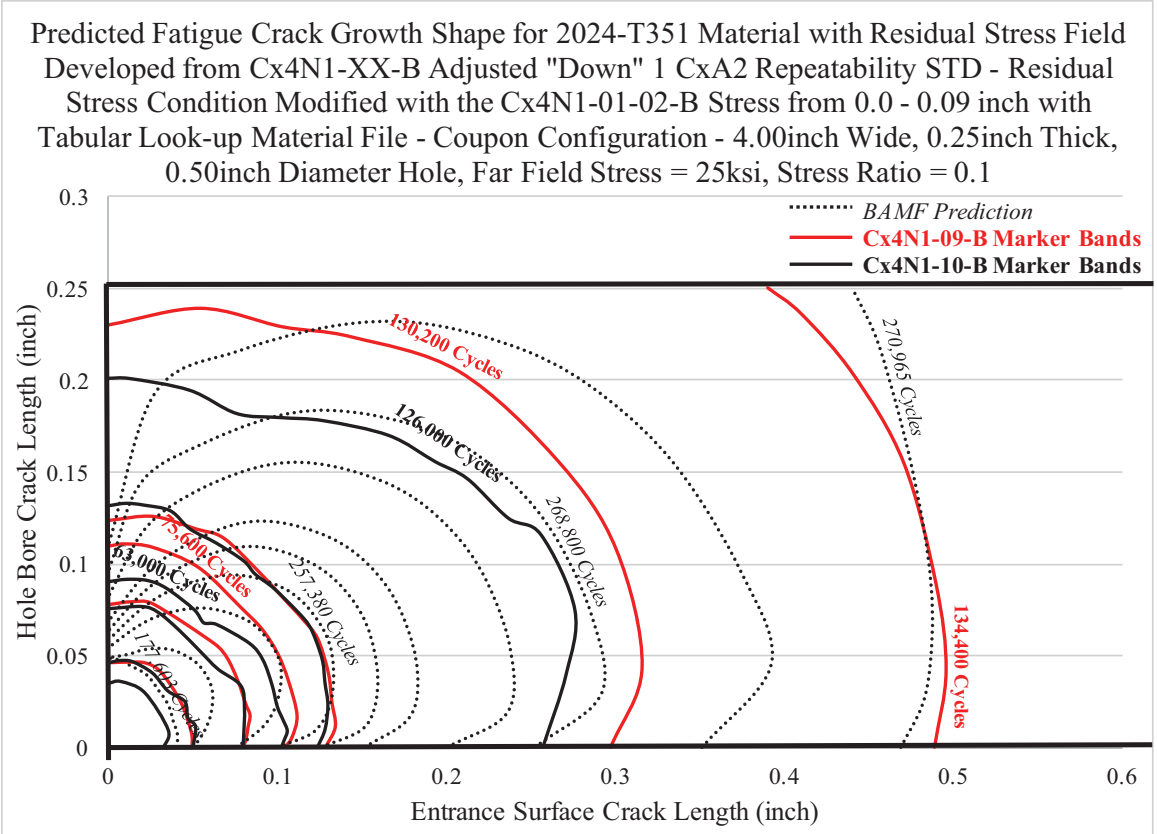

Fig. 951 Comparison of Fatigue Crack Growth Evolution, as Provided by Marker Banding and Through Prediction via BAMF Using the One “Down” Residual Stress Distribution the Cx4N1-XX-B (2024-T351) Cracked Coupon Condition, Imposing the “Average” of the Cx4N1-01-02-B (2024-T351) Cracked Condition from 0.0 – 0.09 inch from the Edge of the Hole.

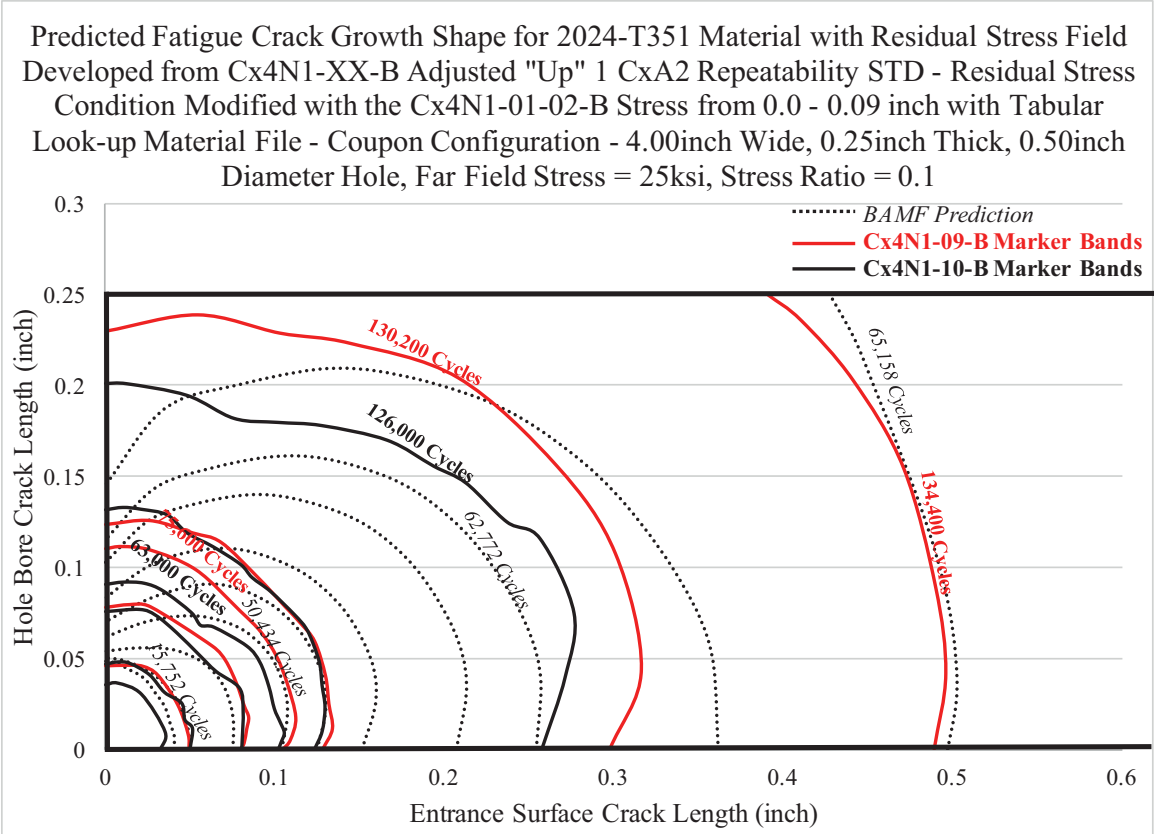

Fig. 952 Comparison of Fatigue Crack Growth Evolution, as Provided by Marker Banding and Through Prediction via BAMF Using the One “Up” Residual Stress Distribution the Cx4N1-XX-B (2024-T351) Cracked Coupon Condition, Imposing the “Average” of the Cx4N1-01-02-B (2024-T351) Cracked Condition from 0.0 – 0.09 inch from the Edge of the Hole.

Table 23 Life Predictions Using BAMF Showing Predicted Life Using Cx4N1-XX-D (7075-T651) Cracked Coupons and Average Test Life of Cx4N1-09-D and Cx4N1-08-D and Cx4N1-07-D from the "Crack Development" Coupons for the "Low" Applied Cold Expansion Level in 7075-T651

Predictions Made with 4N1 Functions and 0.00 - 0.09 as Cx4N1-01-02-D (0.08inch Crack) Functions					
Coupon Type	Material Model	Residual Stress Distribution	Cycles	Average Predicted Life (cycles)	Average Test Life (cycles)
CxD2	APES	Average	64,314	100,988	136,767
		1STDDwn	80,492		
		1STDUp	158,157		

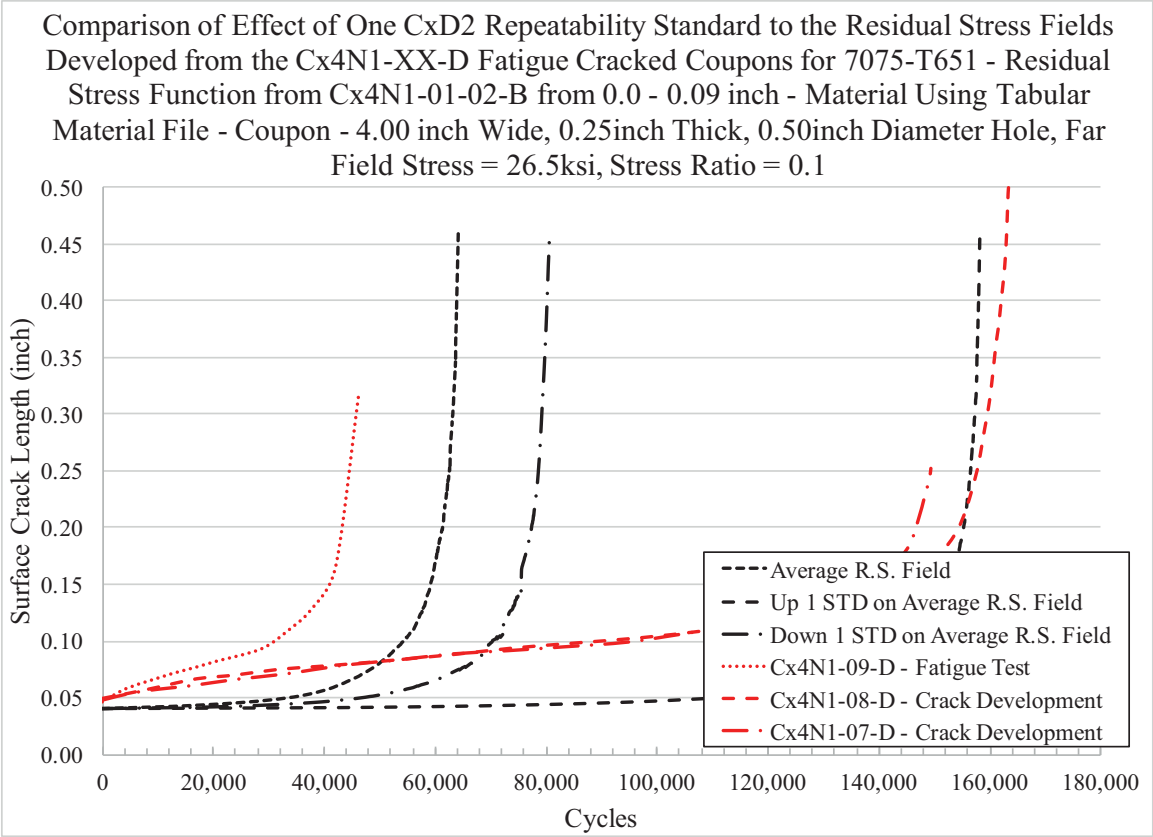

Fig. 953 Fatigue Crack Growth Curve Showing the Predicted Fatigue Life for the 7075-T651 “Low” Applied Expansion Using Three Statistical Distributions, and Compares These to Test Data from Cx4N1-09-D, Along with “Crack Development” Coupons Cx4N1-07-D and Cx4N1-08-D (7075-T651) – Residual Stress Function Used was Derived from Cx4N1-XX-B (2024-T351) Fatigue-Cracked Coupons, Applying the Cx4N1-01-02-D (7075-T651) Residual Stress from 0.0 – 0.09 inch away from the Edge of the Hole.

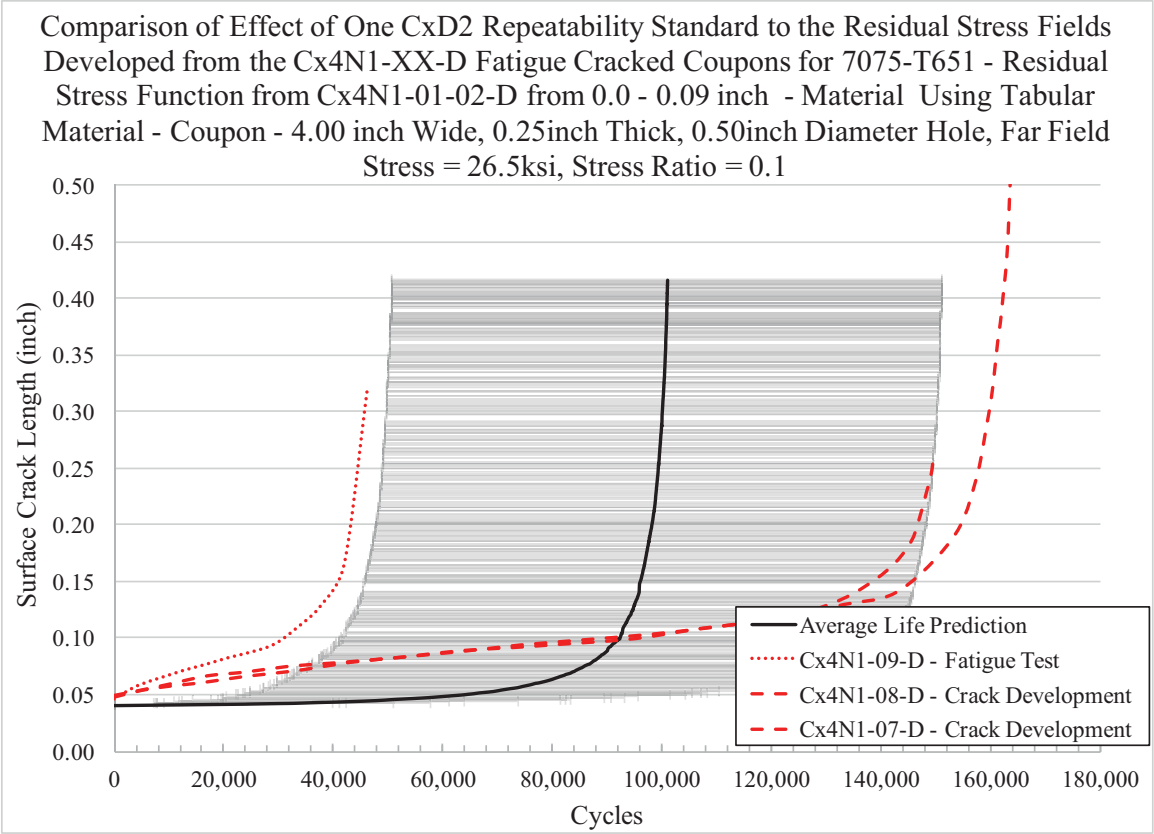

Fig. 954 Fatigue Crack Growth Curve Showing the Average of the Predicted Fatigue Life for the 7075-T651 "Low" Applied Expansion Using the Three Statistical Distributions, and Applies a Confidence Bound Using One Standard Deviation and Compares These to Test Data from Cx4N1-09-D, Along with "Crack Development" Coupons Cx4N1-08-B and Cx4N1-07-D (7075-T651) – Residual Stress Function Used was Derived from Cx4N1-XX-B (2024-T351) Fatigue-Cracked Coupons, Applying the Cx4N1-01-02-D (7075-T651) Residual Stress from 0.0 – 0.09 inch away from the Edge of the Hole.

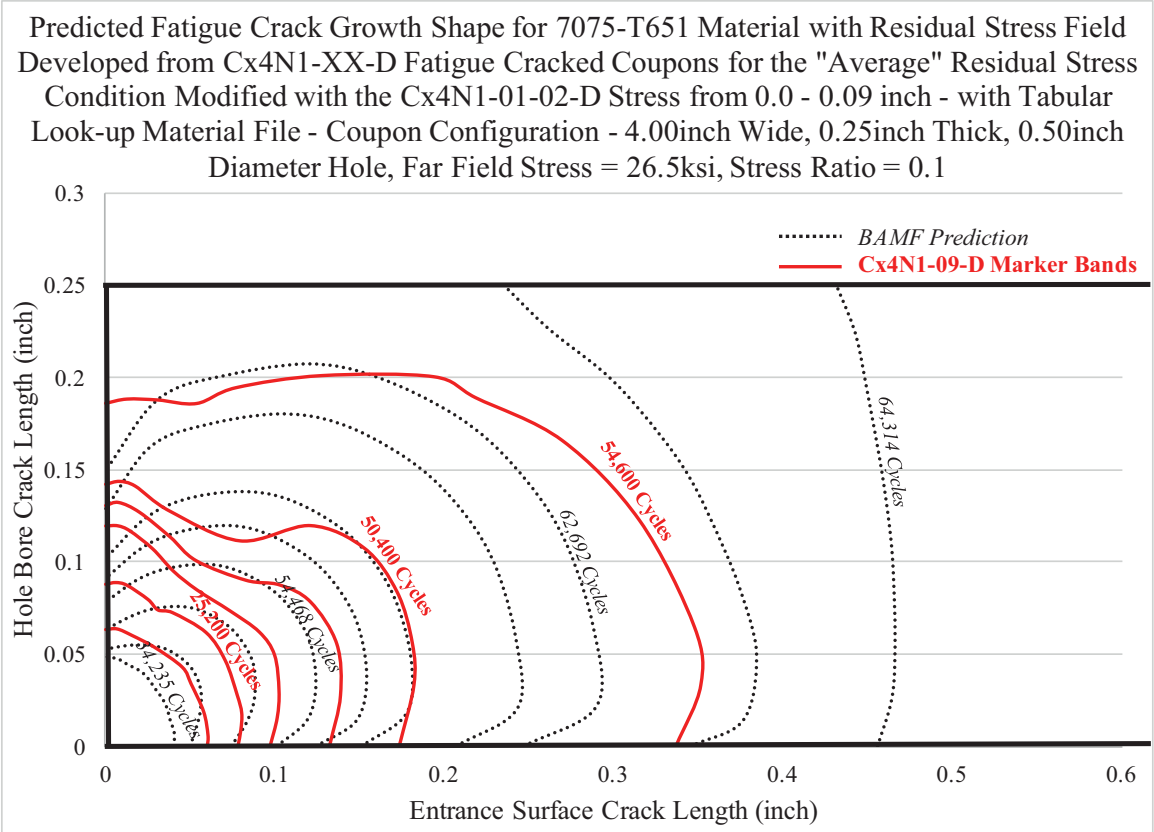

Fig. 955 Comparison of Fatigue Crack Growth Evolution, as Provided by Marker Banding and Through Prediction via BAMF Using the “Average” Residual Stress Distribution the Cx4N1-XX-D (7075-T651) Cracked Coupon Condition, Imposing the “Average” of the Cx4N1-01-02-D (7075-T651) Cracked Condition from 0.0 – 0.09 inch from the Edge of the Hole.

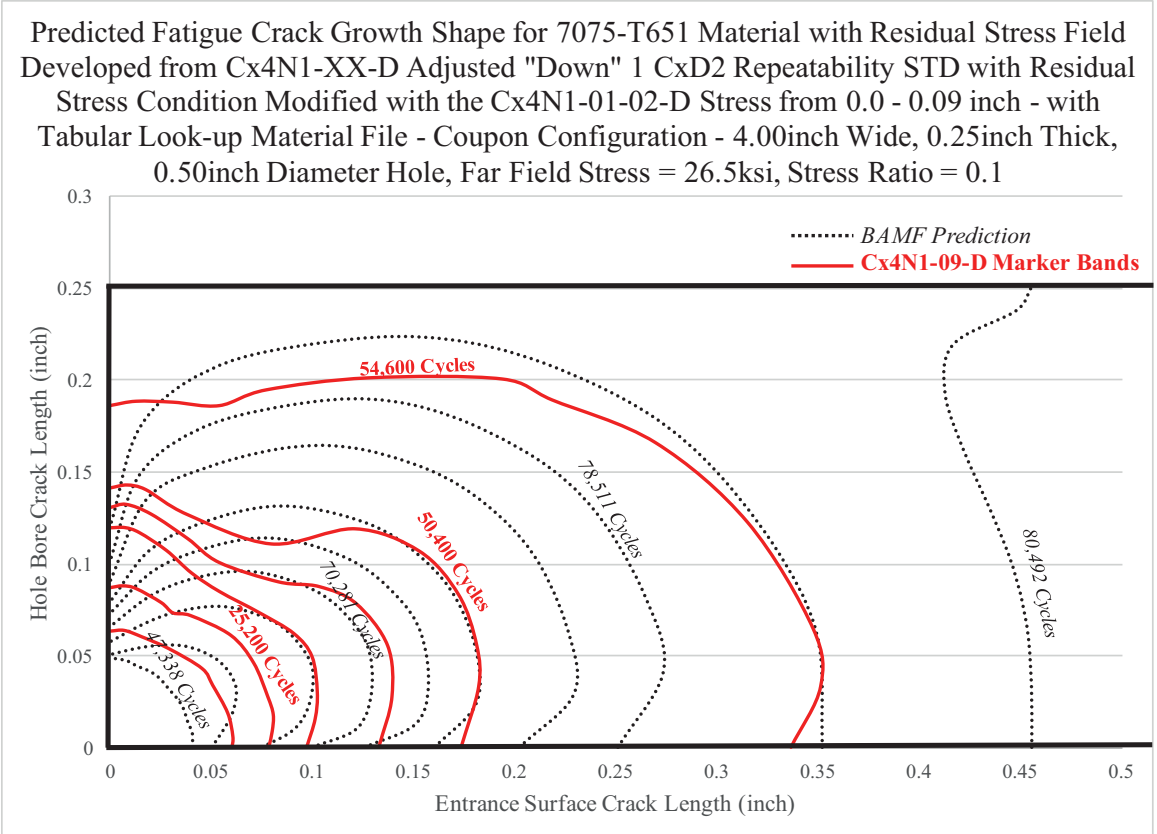

Fig. 956 Comparison of Fatigue Crack Growth Evolution, as Provided by Marker Banding and Through Prediction via BAMF Using the One “Down” Residual Stress Distribution the Cx4N1-XX-D (7075-T651) Cracked Coupon Condition, Imposing the “Average” of the Cx4N1-01-02-D (7075-T651) Cracked Condition from 0.0 – 0.09 inch from the Edge of the Hole.

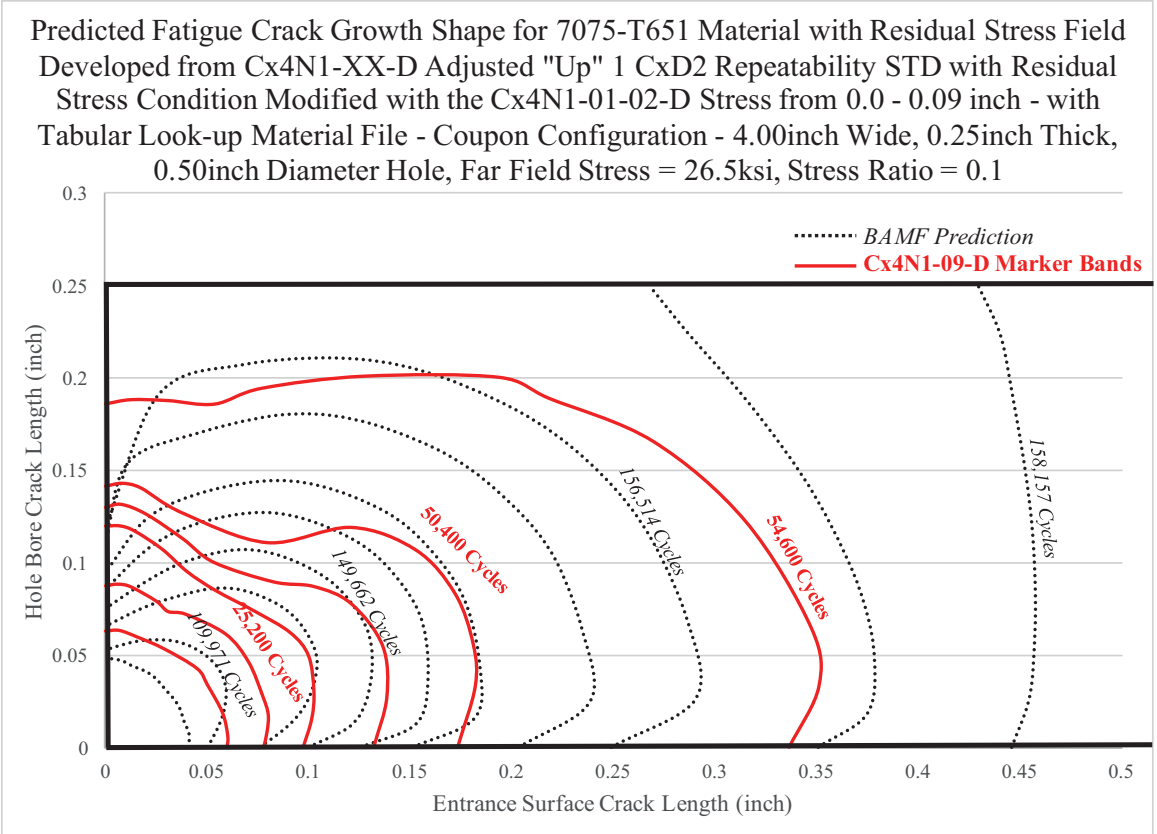

Fig. 957 Comparison of Fatigue Crack Growth Evolution, as Provided by Marker Banding and Through Prediction via BAMF Using the One “Up” Residual Stress Distribution the Cx4N1-XX-D (7075-T651) Cracked Coupon Condition, Imposing the “Average” of the Cx4N1-01-02-D (7075-T651) Cracked Condition from 0.0 – 0.09 inch from the Edge of the Hole.

Table 24 Comparison of Influence of the Piecewise, Bivariant, High Order Polynomial Function Used for the 2024-T351 Fatigue Life Prediction of the “Low” Applied Expansion Level

Comparison of Predicted Fatigue Life Using Different Residual Stress Functions			
Coupon Type	Residual Stress Function	Average Predicted Life (cycles)	Average Tested Life (cycles)
CxA2	CxA2 Baseline	131,630	129,600
	Cx4N1-XX-B with CxA2 from 0.0 - 0.04	137,991	
	Cx4N1-XX-B with CxA2 from 0.0 - 0.09	154,693	

Table 25 Comparison of Influence of the Piecewise, Bivariant, High Order Polynomial Function Used for the 7075-T651 Fatigue Life Prediction of the “Low” Applied Expansion Level

Comparison of Predicted Fatigue Life Using Different Residual Stress Functions			
Coupon Type	Residual Stress Function	Average Predicted Life (cycles)	Average Tested Life (cycles)
CxD2	CxD2 Baseline	599,629	136,767
	Cx4N1-XX-D with CxD2 from 0.0 - 0.04	183,226	
	Cx4N1-XX-D with CxD2 from 0.0 - 0.09	100,988	

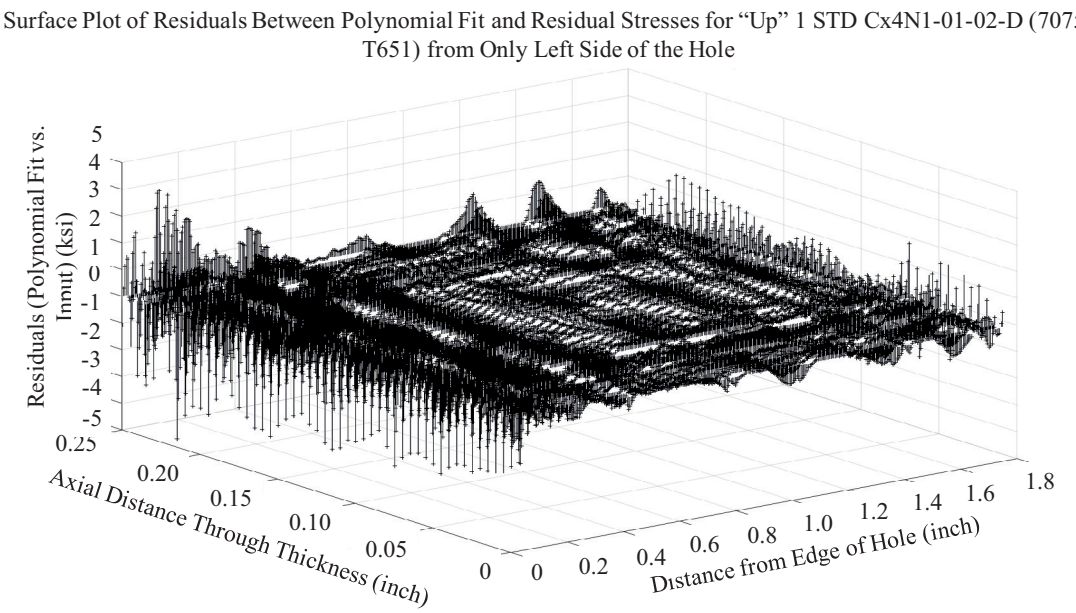

Fig. 958 Surface Plot of the Residual (Difference between the Actual Residual Stress Data and the Fit) at Each Defined Location (Grid Spacing at 0.005 inch x 0.005 inch) for the Average Residual Stress between Coupons Cx4N1-01-D and Cx4N1-02-D (7075-T651) Shifted One Standard Deviation "Up."

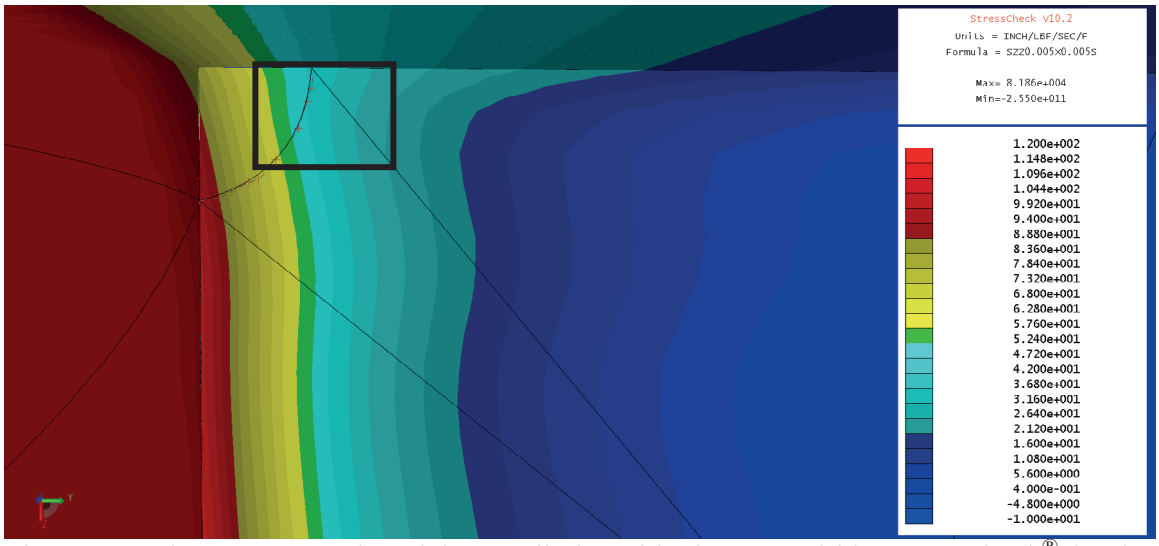

Fig. 959 Surface Contour Plot of the Applied Residual Stress within StressCheck® for the Combined Residual Stress Field of the Cx4N1-XX-D (7075-T651) Condition with the Average Residual Stress Applied, for the Condition Where from 0.0 – 0.04 inch away From the Edge of the Hole the Cx4N1-01-02-D (7075-T651) Residual Stress Field was Applied.

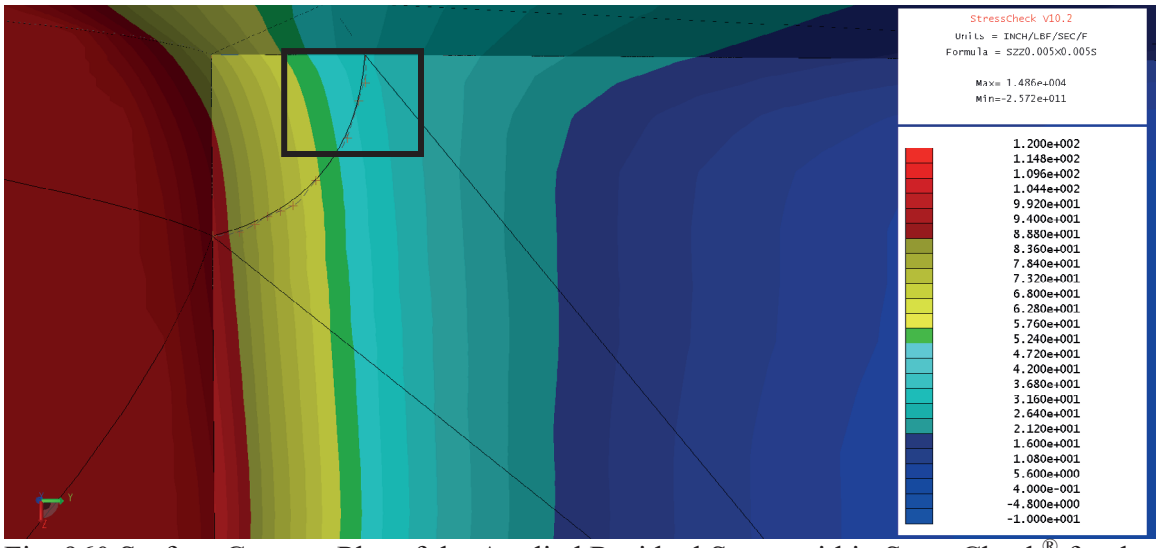

Fig. 960 Surface Contour Plot of the Applied Residual Stress within StressCheck® for the Combined Residual Stress Field of the Cx4N1-XX-D (7075-T651) Condition with the One "Up" Residual Stress Applied, for the Condition Where from 0.0 – 0.04 inch away From the Edge of the Hole the Cx4N1-01-02-D (7075-T651) Residual Stress Field was Applied.

Table 26 Output from the First BAMF Iteration from the Life Prediction for the 7075-T651 Coupon Configuration with the "Average" Residual Stress Field Applied, with the Integration of the Residual Stresses from Cx4N1-01-02-D (7075-T651) from 0.0 – 0.04 inch from the Edge of the Hole

X Location (inch Down Bore of Hole)	Y Location (inch Away From Edge of Hole)	Applied Stress Intensity (ksi√inch)	Residual Stress Intensity (ksi√inch)	Total Stress Intensity (ksi√inch)
0.04	0.00	16.16	-15.62	0.54
0.04	0.01	15.57	-14.86	0.71
0.04	0.01	16.49	-15.67	0.82
0.04	0.02	15.67	-14.69	0.98
0.03	0.03	15.92	-14.93	0.99
0.03	0.03	16.61	-15.70	0.91
0.02	0.04	16.04	-15.28	0.76
0.02	0.04	16.25	-15.72	0.53
0.01	0.04	17.87	-17.91	-0.04
0.01	0.05	17.39	-17.77	-0.38
0.00	0.05	17.68	-18.55	-0.87

Table 27 Output from the First BAMF Iteration From the Life Prediction for the 7075-T651 Coupon Configuration with the one "Up" Residual Stress Field Applied, with the Integration of the Residual Stresses from Cx4N1-01-02-D (7075-T651) from 0.0 – 0.04 inch from the Edge of the Hole

X Location (inch Down Bore of Hole)	Y Location (inch Away From Edge of Hole)	Applied Stress Intensity (ksi√inch)	Residual Stress Intensity (ksi√inch)	Total Stress Intensity (ksi√inch)
0.04	0.00	16.16	-15.39	0.78
0.04	0.01	15.57	-14.79	0.78
0.04	0.01	16.49	-15.72	0.77
0.04	0.02	15.67	-14.98	0.69
0.03	0.03	15.92	-15.33	0.59
0.03	0.03	16.61	-16.15	0.46
0.02	0.04	16.04	-15.76	0.29
0.02	0.04	16.25	-16.15	0.09
0.01	0.04	17.87	-18.21	-0.34
0.01	0.05	17.39	-17.93	-0.54
0.00	0.05	17.68	-18.58	-0.90

12 CONCLUSION FROM QUANTIFICATION OF THE EFFECT OF A FATIGUE CRACK ON THE RESIDUAL STRESS FIELD INTRODUCED BY THE COLD EXPANSION PROCESS

As the military and the civil aerospace industries experience an overall decrease in their budgets for the development and production of new aircraft, there is an ever-increasing need to maintain the aging metallic aircraft within their fleets. However, this need must be balanced with defined safety and structural integrity requirements defined within each governing organization. One method that has been explored for many years is the application of engineered residual stresses to fatigue and fracture critical components. These include processes such as shot peening, glass-bead peening, laser shock peening (LSP), low plasticity burnishing (LPB), and the Cx of critical fastener holes. It has been demonstrated that these residual stress/strain inducing processes can have a beneficial influence on the durability and damage tolerance of a processed part.[160]

However, the analytical capability to quantify the induced residual strain/stress field with confidence, and the ability to introduce that quantified residual stress/strain field within alinear elastic fracture mechanics, analytical framework has lagged behind the ability to process a critical part. Over the past decade advances have been made in the ability to quantify an imposed residual stress field and capture the benefit through improved understanding and toolsets. These residual stress determination methods

include both destructive and nondestructive methods. Many of these methods have been used to quantify the residual stress/strain field that is introduced into materials and components.[161] The contour method is one that has received much attention as of late due to the data spatial resolution and its ability to be employed on a wide variety of component shapes and provide a three-dimensional characterization of the residual stress state. As in all processes, the contour method has limitations, but for many of the fracture mechanics-based challenges the contour method is the residual stress determination method of choice.

In addition to the ability to quantify the imposed residual strain/stress field advances in FEA have allowed for the introduction of these residual stress/strain fields into the calculation of SIFs along a simulated fatigue crack front. Further, the ability to couple FEA software with fatigue crack growth software, have allowed for the use of advanced, tabular look-up material models, to be used to allow for a more accurate prediction of the fatigue crack growth behavior under constant amplitude and spectrum loading. Programs like BEASY, and the advanced plug-in capability with BAMF allow for not only the power that comes from coupling FEA-based SIF calculations, and advanced material models, but it allows for a more accurate prediction of the fatigue crack growth shape evolution, through the use of multipoint crack fronts.

These advances in residual stress determination and modeling have led the aerospace design and sustainment community to the point in which questions are being asked of what next is required to implement the effects of the full-field residual stress/strain field in the calculation of initial and recurring inspection intervals.[162,163] One of these critical questions is whether a fatigue crack that has nucleated/formed at a Cxed

hole and the propagated away from the edge of the hole, causes a change to that initially imposed residual stress/strain field. This question has direct consequences to the state of the art because currently the residual stress/strain field is imposed into a FEA simulation is developed from a nonfatigue cracked body. Thus if there is a change in the residual stress/strain field by the presence and propagation of a fatigue crack this will not be accounted for within the calculations of SIFs along the crack front and thus the life prediction has the potential to be inaccurate.

The purpose of this research was to quantify the effect of a fatigue crack on the residual stress field that is introduced by the Cx process in two common aerospace aluminum alloys, 2024-T351, and 7075-T651. In order to accomplish this a basic contour method data reduction code was further developed to process displacement data related to the determination of residual stresses at Cx holes. A series of baseline, uncracked coupons were developed for both alloys and processed via the contour method in order to provide a statistically-based quantification of the residual stress distribution at a Cxed hole processed to the "low" end of the applied expansion range (3.16%). Another series of coupons, in both alloys, were developed which were exact replicates of the baseline condition. These coupons were then loaded under fatigue until a fatigue crack had propagated to a defined length along the Cx mandrel entrance surface. Replicates of specific crack sizes were produced in order to gain some limited level of statistical representation of the modified residual stress field. Surface fatigue crack lengths ranged from 0.08 inch to 0.50 inch. These coupons were then processed via the contour method in the exact same manner, and residual stresses were determined for each of the individual fatigue-cracked coupons. These residual stresses were then compared to the

baseline, uncracked condition to determine statistical difference between the two groups.

In order to gain a greater understanding of the influence of the fatigue crack on the residual stress field, a series of fatigue crack growth predictions were performed using the baseline, uncracked and the fatigue-cracked residual stress fields. These predictions were then validated by comparison to a series of fatigue tests performed for each aluminum alloy. In addition to the overall life prediction comparison, each fatigue coupon was marker banded to allow for a comparison of the fatigue crack growth shape evolution.

Through this body of research, it was statistically quantified that a fatigue crack does change the residual stress field introduced by the Cx process. This is true for both of the aluminum alloys that were investigated, however the change is not the same in each alloy. When the modified residual stress field is included in the fatigue life prediction the solution is more accurate than without the inclusion of this information. However, with or without the inclusion of the modified residual stress state, the fatigue crack growth evolution is similar and does not match that demonstrated in fatigue test. This is an area in which further research is required. If it the state of the art were able to accurately predict both the fatigue life, from the defined starting fatigue crack size, and the crack shape, this would allow for the development and implementation of more focused inspection methods for the detection of fatigue cracks in material with these types of deep engineered residual stresses. In addition, if the crack shape and the life were to be more accurately predicted it would be possible to extend recurring inspections and thus reduce the overall lifecycle costs and increase aircraft availability.

12.1 Development of Residual Stresses via the Contour Method for Baseline, Uncracked Cold Expanded Condition via the Contour Method for CxA2 (2024-T351) and CxD2 (7075-T651)

The contour method is a very helpful in approximating the residual stress state within a body. It should be noted that like many residual stress determination methods the contour method does not "fundamentally measure" residual stress. Similar to a strain gage where strains are used to calculate stresses, localized surface deformations are fundamentally measured and then used to calculate the stress state within a material, part, or component. The contour method is able to provide a two-dimensional (2D) residual stress "map" along the cut plane. There has been limited work on the quantification of the spatial uncertainty associated with the residual stresses developed by the contour method.

This body of work builds upon the published spatial repeatability and single measurement uncertainty for the contour method and applies these methods to the complex residual stress field around both an uncracked, and a fatigue-cracked Cxed hole. Although this work expanded on the previously published work regarding these two forms of uncertainty there continues to be very limited statistical methods that allow for the development of statistically based conclusions quantifying the difference in 2D fields. For a single point the Student-T test can be done, to a stated confidence level to quantify statistical difference between two populations. This type of method has not been extended to lines or planes in which one would like to quantify difference. There are additional complications when it comes to residual stress fields, and their applications within engineering problems. This main problem resides in the fact that not all points within the residual stress field have an equal influence on the fatigue crack growth life of

a part. As demonstrated through this work, the most influential area of these residual stress fields is within the first 0.10 inch radius from the edge of the hole. Therefore, even though one might develop a method for quantifying statistical difference that difference might not have a significant impact on the end usage of the data.

As the application of engineered residual stresses progress additional questions of influence will be asked. For instance, does the installation and presence of an interference fit fastener modify the residual stress state at a Cx hole? Or does service usage change the residual stress state at a Cx hole? These essential questions can not be answered unless there are sufficient statistical methods developed to enable confidence in the answer developed. Then it may be possible to determine if the answer to these questions has a significant influence on the end goals of the application of engineered residual stresses.

12.2 Single Measurement Uncertainty of Residual Stresses for the Baseline, Uncracked Cold Expanded Condition via the Contour Method for CxA2 (2024-T351) and CxD2 (7075-T651)

A method by which the single measurement uncertainty associated with an individual geometric and residual stress configuration has been provided and was followed for all of the baseline, uncracked 2024-T351 and 7075-T651 coupons. The method produces two uncertainty metrics, “model” or “function” and “displacement.” This method for defining uncertainty is a means by which one can quantify the uncertainty associated with the data reduction process contained within the given contour method.

12.2.1 Single Measurement Uncertainty of CxA2 (2024-T351) Coupons

The single measurement uncertainty was quantified for each of the CxA2 (2024-T351) baseline, uncracked coupons. An example of the “model” or “function” spatial uncertainty and the “displacement” uncertainty are provided for coupon CxA2-1 (2024-T351) in Fig. 961 through Fig. 963. These two individual spatial uncertainties are then RSS to develop a “total” spatial uncertainty. This type of “stacking” of uncertainties is akin to that which is done for tolerance stack-ups in assemblies for manufacturing. This is provided in Fig. 964 and Fig. 965. These contour plots provide one example of what was developed for all five of the CxA2 (2024-T351) coupons. As can be seen in Fig. 961 the majority of the “total” single measurement uncertainty is driven by the “model” or “function” uncertainty. This uncertainty is almost an order of magnitude greater than that which is to represent the “displacement” uncertainty, as shown in Fig. 963. The “displacement” uncertainty is intended to capture the effects of surface roughness and wire-induced errors but due to the method by which this is defined, has a very limited ability to capture outliers from these processes. It is possible that a more robust method for capturing this could be investigated in the future. The “model” or “function” uncertainty has some ability to capture the uncertainties associated with the fit, but can be limited to one's ability to find the “best” fit and how far away from that fit one may choose to go to capture the effect of being off from this best fit. No lower limit was placed on the process used and there appears to be limited technical reasoning as to why this floor should be set.

It can be seen in Fig. 964 and Fig. 965 that the maximum “total” uncertainty was found to be located on the Cx mandrel exit surface, away from the edge of the hole. The

magnitude of this maximum was ± 13 ksi, and the minimum uncertainty was < 1 ksi.

12.2.2 Single Measurement Uncertainty of CxD2 (7075-T651) Coupons

The same method was used to quantify the single measurement uncertainty for each of the CxD2 (7075-T651) coupons. The same three individual spatial uncertainty contour plots are provide for coupon CxD2-1 (7075-T651) in Fig. 966 through Fig. 970. Unlike that developed for the CxA2-1 (2024-T351) coupons the highest regions of spatial uncertainty for the CxD2-1 (7075-T651) is near the edge of the hole. In addition the maximum level of uncertainty was ±36 ksi with a minimum again <1 ksi. It should be noted however that the 7075-T651 coupons had a much tighter region of spatial uncertainty, even though the maximum level of uncertainty was almost three times as high. This could be due to the plastic response of the material, and related to the yield strength and plastic zone size.

12.3 Repeatability Uncertainty of Residual Stresses for the Baseline, Uncracked Cold Expanded Condition via the Contour Method

Within the baseline, uncracked dataset there were five of the 2024-T351 coupons and three of the 7075-T651. From these replicates it was possible to determine at every output, nodal location an average residual stress and the standard deviation about the mean. The repeatability uncertainty would therefore represent more of the process uncertainty and although there is some amount of data processing uncertainty that is included in determining the repeatability uncertainty, the repeatability uncertainty helps to quantify the spatial uncertainty associated with the Cx process. It should be noted that all of the coupons that were developed for this program were developed and

manufactured to hit a very high tolerance requirements and thus induce a very specific level of applied expansion. Therefore, the repeatability uncertainty that was developed represents a very narrow band of the allowable Cx applied expansion and thus cannot be assumed to represent the spatial uncertainty at any Cxed hole.

12.3.1 Repeatability Uncertainty of CxA2 (2024-T351) Coupons

For the CxA2 (2024-T351) material configuration there were five replicates produced. From this work it was determined that the repeatability uncertainty ranged in the 2024-T351 alloy from <1 ksi to 13 ksi, as shown in Fig. 971 and Fig. 972. The maximum repeatability uncertainty was focused at the Cx mandrel exit surface, both at the edge of the hole and also along the exit surface. There was also a region on both sides of the hole at the Cx mandrel entrance surface that had a higher level of uncertainty than that which was calculated through the center of the hole or within the part. Through the core of the part the level of repeatability uncertainty is almost all less than ±4 ksi. However, when these residual stresses are integrated into a fatigue crack growth prediction the spatial uncertainties that are near the edge of the hole, and at the Cx mandrel entrance surface become the most influential on the predicted life. The spatial uncertainties at the Cx mandrel exit surface, although the highest had little influence on the overall life prediction developed with these residual stresses included. This is because by the time the fatigue crack reaches the influence of these residual stresses there is less than .1% of the total fatigue life left, and thus they have almost no ability to influence the total life, when the fatigue crack growth prediction starts with an initial flaw at the Cx mandrel entrance surface.

12.3.2 Repeatability Uncertainty of CxD2 (7075-T651) Coupons

The CxD2 (7075-T651) coupon configuration had three replicates produced, thus there was less statistical power associated with the residual stresses that were developed for these coupons than those which were produced for the 2024-T351 coupon configuration. The spatial repeatability uncertainty for the CxD2 (7075-T651) coupon configuration is provided in Fig. 973 and Fig. 974. It can be seen from Fig. 974 that the 7075-T651 coupon configuration had the highest level of spatial uncertainty at the Cx mandrel exit surface corners. Like the single measurement uncertainty the maximum level of uncertainty was ±36 ksi. This was much higher than that determined in the 2024-T351 material but the spatial dispersion of the uncertainty for the 7075-T651 was much less than that calculated for the 2024-T351 coupons. The data showed that the 7075-T651 coupons had an average spatial uncertainty that was less than that determined for the 2024-T351 coupons. Thus it could be said that the 7075-T651 coupons were more repeatable than the 2024-T351 condition. However, at this time there are established statistical methods that can be used to compare two three-dimensional (3D) fields to determine statistical difference. An average uncertainty is one method that could be used, and was for these purposes.

12.4 Development of Residual Stresses via the Contour Method for Fatigue-Cracked Cold Expanded Condition via the Contour Method for Cx4N1-XX-B (2024-T351) and Cx4N1-XX-D (7075-T651)

In order to quantify the effect of a fatigue crack on the residual stress field introduced by the Cx process a series of replicate coupons were developed and fatigue cracks were nucleated/formed in them on the Cx mandrel entrance surface and then

propagated to a range of lengths, from 0.08 inch to 0.50 inch. These coupons were then processed via the contour method in the exact same way as the baseline, uncracked coupons. This would allow for a comparison to be made between the baseline, uncracked coupons and these which had fatigue cracks nucleated/formed and propagated in them. The fatigue loading was all constant amplitude (25 ksi for the 2024-T351 coupons and 26.5 ksi for the 7075-T651 coupons), at a R = 0.1. Residual stresses were able to be compared at the exact same nodal locations to allow for a direct comparison between coupon configuration and crack size within the cracked coupon subset.

12.4.1 General Trends of Residual Stress Data for Cx4N1-XX-B (2024-T351) Coupon Configurations

The Cx4N1-XX-B (2024-T351) coupons had fatigue cracks that were developed to a range of crack sizes, as shown in Table 28. Replicates for three out of the five defined fatigue crack conditions were developed. All of these coupons were Cxed to the "low" end of the applied expansion level (average of 3.24%), as shown Table 28. The developing of the cracks was performed at a far-field stress of 25 ksi and a R = 0.1. All of the fatigue cracks were nucleated/formed at the Cx mandrel entrance surface, and for all of the residual stress plots, this was done on the left side of the hole.

The residual stress data shows that the presence of the fatigue crack had a direct influence on the residual stress field produced by the Cx process. This effect can be seen most clearly in the through-thickness line plots produced. An example of this effect can be seen in the Cx4N1-01-02-B (2024-T351 coupon with an average fatigue crack of 0.08005 inch). Fig. 975 provides this evidence for the Cx4N1-01-02-B (2024-T351) condition, as compared to the baseline, uncracked condition, CxA2 (2024-T351). The

fatigue crack that was developed in these two coupons extended to an average Cx mandrel entrance surface length of 0.08005 inch and as can be seen in Fig. 975 there is a clear statistical difference between the two averages at a distance from 0.05 inch to 0.10 inch away from the Cx mandrel entrance surface. With the fatigue crack being the only difference between these two replicate sets of coupons, it can be concluded that the presence of the fatigue crack induced this shift in the residual stress.

To further show this effect, if the Cx4N1-05-06-B (2024-T351) coupons are plotted in the same manner, as shown in Fig. 976. This line plot also shows a clear shift towards a less compressive residual stress in the average residual stress in the fatigue-cracked condition, as compared to the average CxA2 (2024-T351) baseline, uncracked condition. Fig. 977 further demonstrates that at a fatigue crack of approximately 0.50 inch at the Cx mandrel entrance surface the residual stress is dramatically shifted in a more tensile direction, as compared to the CxA2 (2024-T351) uncracked, baseline residual stress field. When the Cx4N1-XX-B (2024-T351) coupons are all combined and compared to the baseline, uncracked residual stress field condition developed in the CxA2 (2024-T351) condition one can see a clear trend in a shift of the residual stress towards a less compressive, more tensile between 0.05 inch and 0.15 inch. The through-thickness residual stress line plots seem to provide this evidence in the most clear manner as shown in Fig. 978 through Fig. 981. The trend seems to collapse towards 0.15 inch away from the edge of the hole, however it can still be seen that the -08 (0.50 inch fatigue crack) is still shifted above the CxA2 (2024-T351) average with one standard deviation.

12.4.2 General Trends of Residual Stress Data for Cx4N1-XX-D (7075-T651) Coupon Configurations

A series of identically processed coupons were produced in 7075-T651 aluminum plate. The fatigue crack growth matrix for these Cx4N1-XX-D (7075-T651) coupons is provided in Table 29. All of these coupons were Cxed to the "low" end of the applied expansion range, using the same process as the 2024-T351 material coupons. However they had a slightly higher level of applied expansion, with an average of 3.28% vs. the 3.24% shown in Table 28 for the 2024-T351 material. This difference is within the tolerance of the measuring tools.

The Cx4N1-XX-D (7075-T651) coupons did not have the same general trend as that demonstrated in the Cx4N1-XX-B (2024-T351) coupon configuration. The Cx4N1-XX-D (7075-T651) material did not show a correlated trend in the shift of the residual stress, as a function of fatigue crack size. Instead all of the fatigue-cracked coupons showed a similar shift in the residual stress field. This is more clearly shown again in the through-thickness residual stress line plots. For the Cx4N1-01-02-D (7075-T651) coupons, as shown in Fig. 982, one can see that there is a clear shift in the residual stress field of the fatigue-cracked coupons, as compared to the average CxD2 (7075-T651) coupon condition, and unlike the shift that is shown in the 2024-T351 material, this shift seems to penetrate through the thickness of the coupon. The Cx4N1-05-06-D (7075-T651) coupon configuration shows a very similar shift, completely through the thickness, as is shown in the 0.08 inch fatigue-cracked condition. This is shown in Fig. 983. The 0.50 inch fatigue crack condition, as shown in Fig. 984, also shows this complete shift of the residual stress field, through the thickness of the part.

Another difference that should be noted is that the standard deviation of these

Cx4N1-XX-D (7075-T651) is much smaller than that shown for the 2024-T351 coupons. It is unsure at this point why this is. The same process was followed for all of the steps within the residual stress determination process and the plotting of the data and so there must be some distinct characteristic of the 7075-T651 alloy that enables the residual stress field to be introduced in a more consistent manner, as compared to the 2024-T351 alloy. One potential reason for this difference could be due to the difference in yield strength between the two, and thus the size of the plastic zone developed for each crack size.

When all of the Cx4N1-XX-D (7075-T651) coupons are placed together and compared to the CxD2 (7075-T651) baseline, uncracked condition, as shown in Fig. 985 through Fig. 988, it can be seen that this overall shift in the residual stress field occurs for the range of fatigue crack sizes developed and propagated in the coupons. This general trend is quite different from the residual stress field produced for the Cx4N1-XX-B (2024-T351) coupon condition.

12.5 Integration of Statistically-Based Residual Stresses from Baseline, Uncracked Cold Expanded Coupons for CxA2 (2024-T351) and CxD2 (7075-T651) into Fatigue Crack Growth Predictions, as Compared to Fatigue Test Life and Crack Shape Evolution

With the ability to develop a statistical representation of the residual stress field, based on the average determined residual stress and the repeatability standard deviation, it was possible to develop residual stress fields that were adjusted “up” or “down” from that average residual stress field. This was done node-by-node, with each location having an average residual stress and a standard deviation calculated. Thus it was possible to determine a statistical representation of the possible residual stress field that would be

introduced into a hole by the Cx process used for all of these coupons. This would then allow for a statistical representation of the predicted fatigue life, using an average residual stress, and then the upper and lower bound of one standard deviation on the residual stress field that would be introduced.

With five replicates of the CxA2 (2024-T351) produced and three for the CxD2 (7075-T651) it was possible to have a reasonable statistical representation of the residual stress field. It was known that the information developed from this limited population did not represent a statistically significant number of coupons, but for residual stress determination coupons, this number was quite a bit higher than most populations. For all of the life predictions the same material model was used. Initial predictions used multiple material models, along with the three statistically-based residual stress field, but this became too difficult to manage. It was noted, however, that the material model has a significant influence on the fatigue life prediction and should be investigated further to help clarify the importance of gather "accurate" data in specific ranges of the da/dN vs. ΔK material files. In addition, all of the fatigue crack growth predictions were developed in BAMF, which is a plug-in between StressCheck® and AFGROW. BAMF continues to grow in capability, however it is a superb piece of software and allows for a much faster total life prediction as compared to other similar codes, like BEASY™. BAMF allows for the development of models in a range of shapes and geometries through StressCheck®. All of the residual stress data was introduced via the "Contour Integral Method for Loaded Cracks (CIM-LC)," which is a crack face traction stress. This form of an applied residual stress was very functional for the application of contour method data, which are planar in nature.

However, in order to apply the residual stress data developed via the contour method, the data field had to be fit using a bivariant, high-order polynomial. This by nature introduces additional errors due to miss-fit. These errors can not always be quantified so this is an area within the current state of the art that needs to be improved.

For all of the residual stress equations developed for this work, a fifteenth order bivariant polynomial was used, which is the highest level that StressCheck® can take currently. In addition to this a sensitivity study was performed to determine the level of polynomial fit that would minimize the error in the fit. This error was manifested in the maximum difference between the fit and the actual data, at the specific points along the surface. This residual was plotted and enabled further investigation if needed. However, it is unknown what the fit is like between those stress locations. Therefore, it was determined that a spatial density of 0.005 inch was needed to minimize the errors produced between each nodal stress location. Thus another area of research that is needed is to determine the level of residual stress density that must be developed if a high-order, bivariant polynomial is going to be used to develop residual SIFs.

The effect of the statistical distribution of the residual stress on the fatigue life for baseline, uncracked condition, for both materials is provided.

12.5.1 Comparison of Predicted Crack Growth Curve Shape and Crack Shape Evolution Using Baseline, Uncracked Residual Stress Condition from CxA2 (2024-T351) for the "Average", One "Up", and One "Down" Statistical Distribution as Compared to Fatigue Test Data

The CxA2 (2024-T351) coupon condition represents the "legacy" methods that represent what would have been done prior to the collection of information contained within this thesis. These residual stresses represent the "low" applied Cx condition.

With five replicates of this residual stress condition developed it was possible to calculate an average and repeatability standard deviation. This repeatability standard deviation was calculated for each nodal location and thus three residual stress were able to be calculated at each location, the average, “up”, and “down” one standard deviation. These three residual stress fields were then used to develop a high-order bivariant polynomial, which represented these fields within StressCheck®. It can be seen in Fig. 989 that the single standard deviation on the average residual stress life is able to capture all three of the fatigue test datasets that were developed. It could therefore be said that the CxA2, baseline, uncracked residual stress fields, with the material model used, were able to predict a life that that was accurate to within one-standard deviation of the average.

There was a significant difference in the fatigue life produced by the “up” and the “down” residual stress fields, an order of 4 times. This spread is not uncommon in fatigue data, and especially with residual stresses from the Cx process are introduced.

12.5.2 Comparison of Predicted Crack Growth Curve Shape and Crack Shape Evolution Using Baseline, Uncracked Residual Stress Condition from CxD2 (7075-T651) for the “Average”, One “Up”, and One “Down” Statistical Distribution as Compared to Fatigue Test Data

The CxD2 (7075-T651) coupons were also used to develop a fatigue series of fatigue life predictions using the same statistical technique as defined for the CxA2 (2024-T351) coupons. From the residual stress data of the three replicates, an average and standard deviation was developed at each residual stress location. From this data three residual stress traction high-order, bivariant polynomials were developed to represent the average, “up” and “down” one standard deviation. A single tabular look-up material model was used for all of these fatigue life predictions. The predictions were

made for a constant amplitude loading, with a far-field stress of 26.5 ksi, and a Stress Ratio (R) = 0.1. Fig. 990 provides the comparison of the predicted fatigue life, using the three statistical residual stress distributions, as compared to test. It can be seen in Fig. 990 that the life prediction is very sensitive to the statistical distribution of the residual stress field, unlike that shown in the 2024-T351 material. All of the predictions using the residual stresses developed from the baseline, uncracked CxD2 (7075-T651) condition over-predict the fatigue life, significantly. The "up" one standard deviation is able to come the closest but still an does not provide a conservative[†] estimation of the life. The one standard deviation on the average residual stress does allow for a prediction that would account for all three of the fatigue lives produced, thus allowing some ability to use the one standard deviation approach to capture the fatigue life but this approach would not be based on the integrated residual stress field, and thus could cause significant problems if applied.

One plot that provides some significant information regarding the area of most interest for the difference in the predicted life, is the dc/dN (crack growth) vs. c (Cx mandrel entrance surface crack length). This plot is provided in Fig. 991. From Fig. 991 it can be seen that the greatest difference in crack growth rate is right at the very beginning of the life prediction, from the IFS to less than 0.05 inch. Thus the greatest difference in the life predictions is focused on the residual stresses right at the edge of the hole, or within the first 0.05 inch away from the edge of the hole. This is often where the contour method is said to have "difficulties" determining the residual stresses. One of the

[†] The term conservative in this context means that the predicted life is greater than the tested life, to some defined or arbitrary level.

goals of this work was to quantify these “difficulties” through the development of a spatial repeatability and single measurement uncertainty. This would provide a statistically developed understanding of where the contour method, for a Cx hole provided residual stresses within a given statistical bound. Through using this method, it was possible to develop a fatigue life prediction that captured the upper and lower bounds of the fatigue test data.

12.5.3 Note on the Predicted Fatigue Crack Growth Curve Shape Versus the Test Demonstrated Shape

It can be seen from Fig. 989 and Fig. 990 that all of the fatigue life predictions developed, using all three of the residual stress statistical distributions, were not able to accurately predict the fatigue crack growth curve shape from the IFS to approximately 0.10 inch away from the edge of the hole, at which time the rate increases to an almost vertical line. Currently there is no understanding as to why this is. It is possible that this increased rate is due to something like crack closure that forces the crack tip open, when it is near the edge of the hole, due to the high level of residual compressive stress. Work is under way to focus in on this area of the crack growth curve to determine what causes this dramatic difference in the predicted versus the actual. The inconsistencies between the predicted rate and the actual rate could also be due to a lack of accurate residual stresses near the bore of the Cxed hole. The current residual stress field shows that the residual stress state near the bore of the hole contains the highest level of compressive residual stresses. It is known that the contour method has higher levels of uncertainty near the edge of parts or other geometric changes. Through this work it was hoped that through capturing the spatial repeatability uncertainty it would be possible to show that at

the lower bound of the residual stress it would allow for a more accurate prediction of these crack growth rates. However, this was not demonstrated. Therefore, it could be that the contour method is just not able to accurately, within one standard deviation, provide the residual stress state near the bore of the hole.

It was hoped that the inclusion of the effect of the fatigue crack on the residual stress would allow for a more accurate understanding of the residual stress state as the crack propagates away from the bore of the Cxed hole. Through the quantification of this effect and the inclusion of it in a prediction it was hypothesized that the predictions for both materials would become more aligned with test. And for the crack growth life this was true, but for the crack shape evolution, and the crack growth rate near the bore of the hole, this did not turn out to be true.

12.6 Integration of Statistically-Based Residual Stresses from Fatigue-Cracked, Cold Expanded Coupons for Cx4N1-XX-B (2024-T351) and Cx4N1-XX-D (7075-T651) into Fatigue Crack Growth Predictions, as Compared to Fatigue Test Life and Crack Shape Evolution

The goal of this dissertation was to determine if a fatigue crack had an influence on the residual stress field that is introduced into two common aluminum alloys (2024-T351 and 7075-T651) through the Cx process. Through the work performed within this dissertation it has been determined that a fatigue crack does have a statistically significant influence on the residual stress field introduced by the Cx process into these two common aerospace alloys. The follow-on question to this would be; "*Is there a significant difference on the fatigue life prediction and fatigue crack shape prediction when used for a given case?"* Like in the baseline, uncracked conditions, a statistical distribution was developed for all of the fatigue-cracked conditions, except for the -07 (0.25 inch Cx

mandrel entrance surface crack length) and -08 (0.50 inch Cx mandrel entrance surface crack length) coupon configurations. However, for the conditions that had replicates, only two were manufactured and had residual stresses developed. Therefore, an average residual stress was developed for each of the conditions that had replicates produced and for the configurations that did not, the actual values were used.

The repeatability standard deviation was again applied, from the baseline conditions, CxA2 (2024-T351) and CxD2(7075-T651), to develop the upper and lower bound of the one standard deviation. This was performed for each of the groups of crack sizes, -01-02, -03-04, -05-06, -07, and -08. Thus for each residual stress statistical distribution five individual residual stress spatial distributions were developed. Then for each of those the same process was used to produce the bivariant, high-order polynomial function. This time however that function was made up of six individual function, thus creating a piecewise, bivariant fifteenth-order polynomial function. The functions were bounded by a semi-circular condition that was designed to replicate the crack size and shape that was found in the marker banded Cx coupons in the past. The "P-shape" crack front that has also been documented was too difficult to replicate with the constraints within the function call-in within StressCheck®. It was also shown after the fatigue tests of these "low" Cx coupons that the cracks grew in a more semi-circular shape than the "P-shape" shown in the past for higher applied expansion Cx holes.

These piecewise functions were then integrated into StressCheck® as the same type of CIM-LC, crack face traction as was used in the baseline fatigue crack growth predictions. All of the predictions used the same material file as was used in the baseline predictions, and the same far-field stresses were applied for the 2024-T351 and 7075-

T651 coupon conditions. This was done to ensure that the only difference that was introduced into the prediction was the quantification of the effect of the fatigue crack on the residual stress field, as determined by the contour method developed and executed for all of the coupons within this body of work.

12.6.1 Comparison of Predicted Crack Growth Curve Shape and Crack Shape Evolution Using Fatigue-Cracked Residual Stress Condition from Cx4N1-XX-B (2024-T351) for the "Average", One "Up", and One "Down" StatisticalDistribution as Compared to Fatigue Test Data

The three residual stress statistical bounds of the residual stress field, average, the upper and lower single standard deviation were used to predict the same fatigue condition as done using the baseline, uncracked residual stresses from the CxA2 (2024-T351) configuration. The predicted versus the tested for these three residual stress distributions is provided in Fig. 992. This fatigue life prediction shows that all three of the test fatigue lives fall within the single standard deviation bound about the average predicted fatigue life. In addition to this the lower bound and the average residual stress distribution are both able to predict a fatigue life that is less than that demonstrated by all three of the test demonstrated fatigue lives. This provides additional confidence that the when the effect of the fatigue crack is included in the fatigue crack growth prediction the average residual stress is still able to predict the fatigue life in a conservative but beneficial manner. This is the case for the baseline condition as well.

When compared to the fatigue life predictions using the baseline, uncracked residual stress fields, the addition of the effect of the fatigue crack does little to change the shape of the curve or the life. Thus, showing that for this aluminum alloy the fatigue life prediction does not seem to be highly effected by the inclusion of the effect of the

fatigue crack.

12.6.2 Comparison of Predicted Crack Growth Curve Shape and Crack Shape Evolution Using Fatigue-Cracked Residual Stress Condition from Cx4N1-XX-D (7075-T651) for the "Average", One "Up", and One "Down" Statistical Distribution as Compared to Fatigue Test Data

In addition to the 2024-T351 material, the same method was applied for the Cx4N1-XX-D (7075-T651) coupons. The same material file, far-field stress, and Stress Ratio (R) were used for these predictions as was used in the baseline, CxD2 (7075-T651) predictions. Three residual stress statistical distributions were again developed using the repeatability standard deviation developed from the three CxD2 (7075-T651) coupons. This fatigue life prediction, as compared to test is shown in Fig. 993. This presents a dramatically different prediction capability as compared to that from the baseline, uncracked CxD2 (7075-T651) condition, as shown in Fig. 990. From this plot it is possible to see some of the fatigue life spread that comes from these coupons, all manufactured and Cxed in the exact same manner, but it also shows that with the inclusion of the effect of the fatigue crack the predicted fatigue life become much more inline with the fatigue tested lives. The use of the average residual stress field distribution produces a fatigue life that is slightly longer than that of the longest fatigue tested coupon. The lower bound residual stress distribution is able to be conservative for two of the three fatigue lives, and the standard deviation on the average predicted fatigue life dramatically decreases to ± 75,000 cycles from almost 600,000 cycles in the CxD2 (7075-T651) condition.

This demonstrates that the inclusion of the effect of the fatigue crack on the residual stress field imposed in the 7075-T651 material by the Cx process makes a

significant impact on the accuracy of the fatigue life prediction, bringing the average fatigue life prediction from almost 600,000 cycles to just over 180,000, with the average test demonstrated fatigue life for this condition being almost 130,000 cycles.

In an effort to investigate a sensitivity to the effect of extending in towards the hole more the effect of the fatigue crack, two additional series of predictions were produced. The first applied the residual stress field from the Cx4N1-01-02-D (7075-T651) coupon configuration from the edge of the hole out to 0.08 inch from the edge of the hole. In all of the previous predictions the first 0.04 inch had the baseline CxD2 (7075-T651) residual stress field. The second extended the Cx4N1-01-02-D (7075-T651) coupon configuration from the edge of the hole out to 0.09 inch from the edge of the hole. In doing this the predicted fatigue life using the average residual stress field for the first condition went from 126,000 cycles to 64,000 cycles. This life becoming half of the average test demonstrated fatigue life. When the residual stress field from the -01-02-D condition was extended out to 0.09 inch away from the edge of the hole the average residual stress field predicted a fatigue life just below 65,000 cycles, again compared to the average test demonstrated fatigue life of 129,000 cycles. This helped demonstrate that the most influential zone of residual stress is within that first 0.08 inch, from some of the other evidence shown herein that looks to be more like within the first 0.05 inch. Thus showing that it maybe possible to that the most important data to develop when looking at the influence of a fatigue crack on the residual stress field, when that residual stress field will be imposed into fatigue crack growth coupons, with a starting IFS around 0.05 inch would be to developed data for fatigue-cracked coupons at crack sizes less than 0.10 inch.

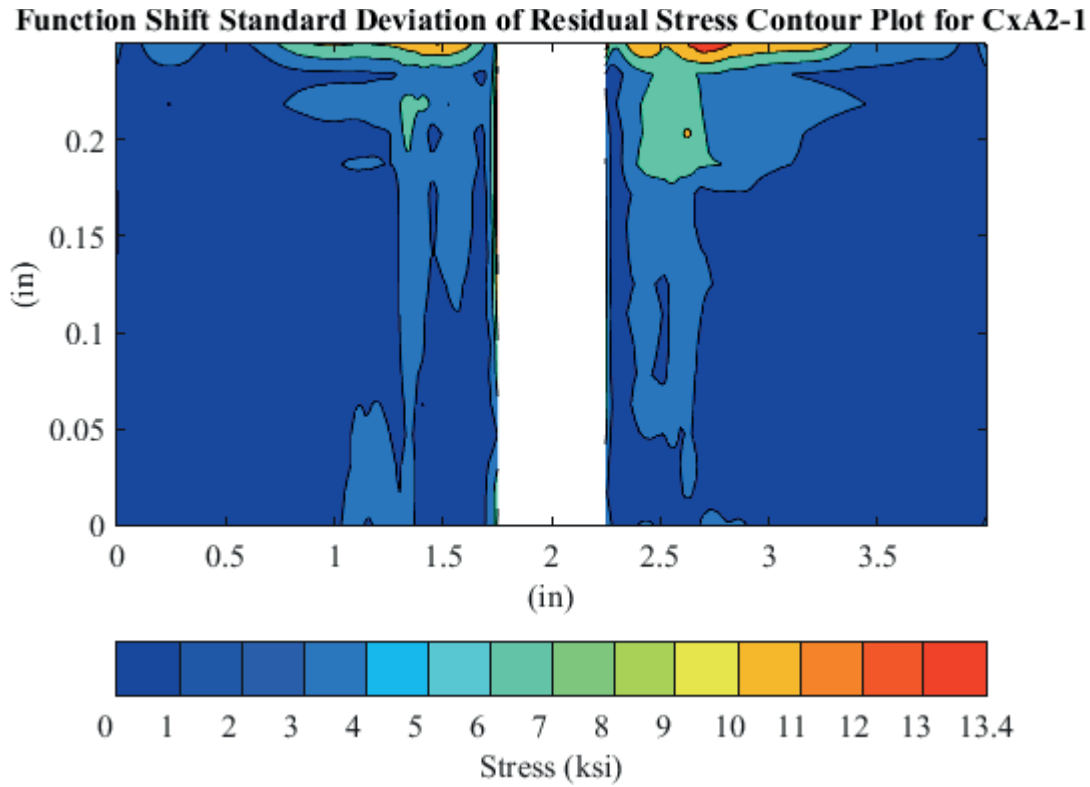

Fig. 961 Contour Plot of the Spatial “Function” or “Model” Residual Uncertainty Associated with Coupon CxA2-1 (2024-T351).

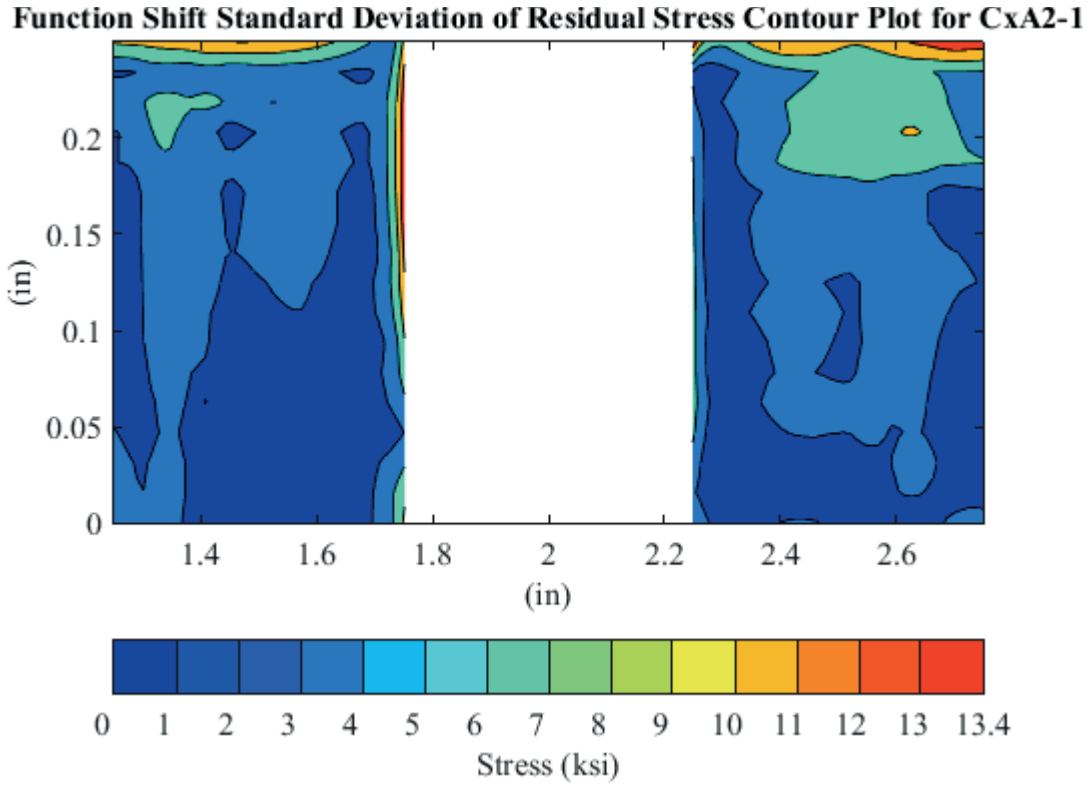

Fig. 962 Contour Plot of the Spatial “Function” or “Model” Residual Uncertainty Associated with Coupon CxA2-1 (2024-T351) – Zoomed in next to Hole.

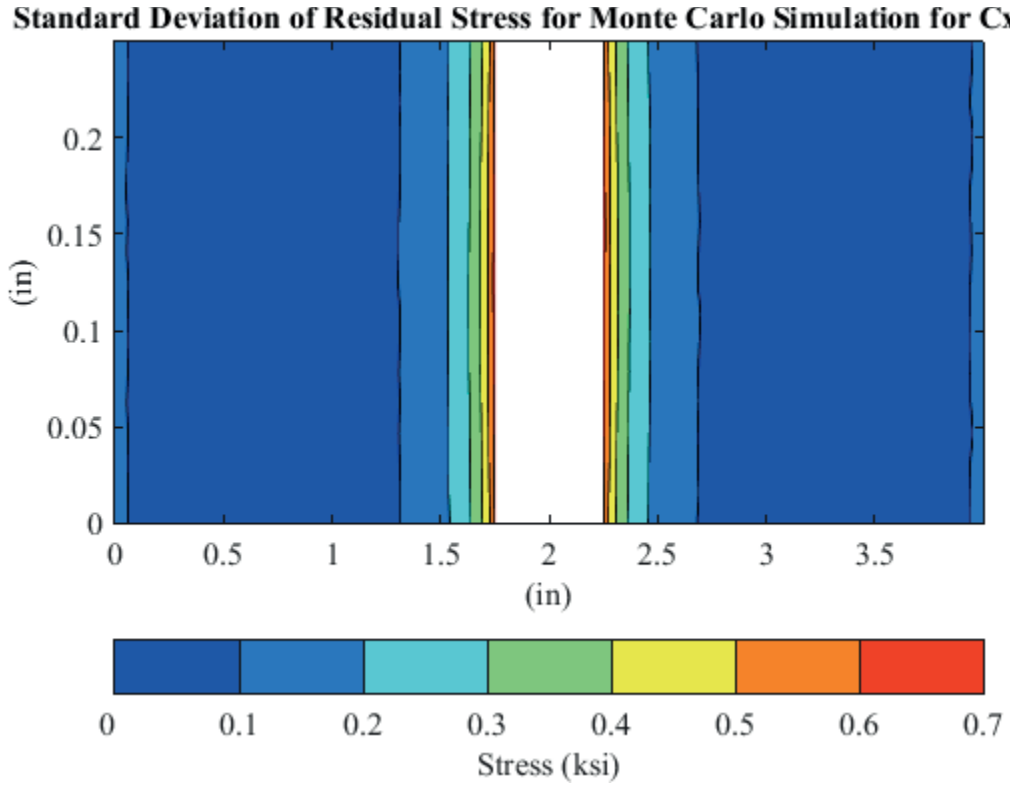

Fig. 963 Contour Plot of the Spatial "Displacement" Residual Stress Uncertainty Developed via Monte Carlo Simulation for Coupon CxA2-1 (2024-T351).

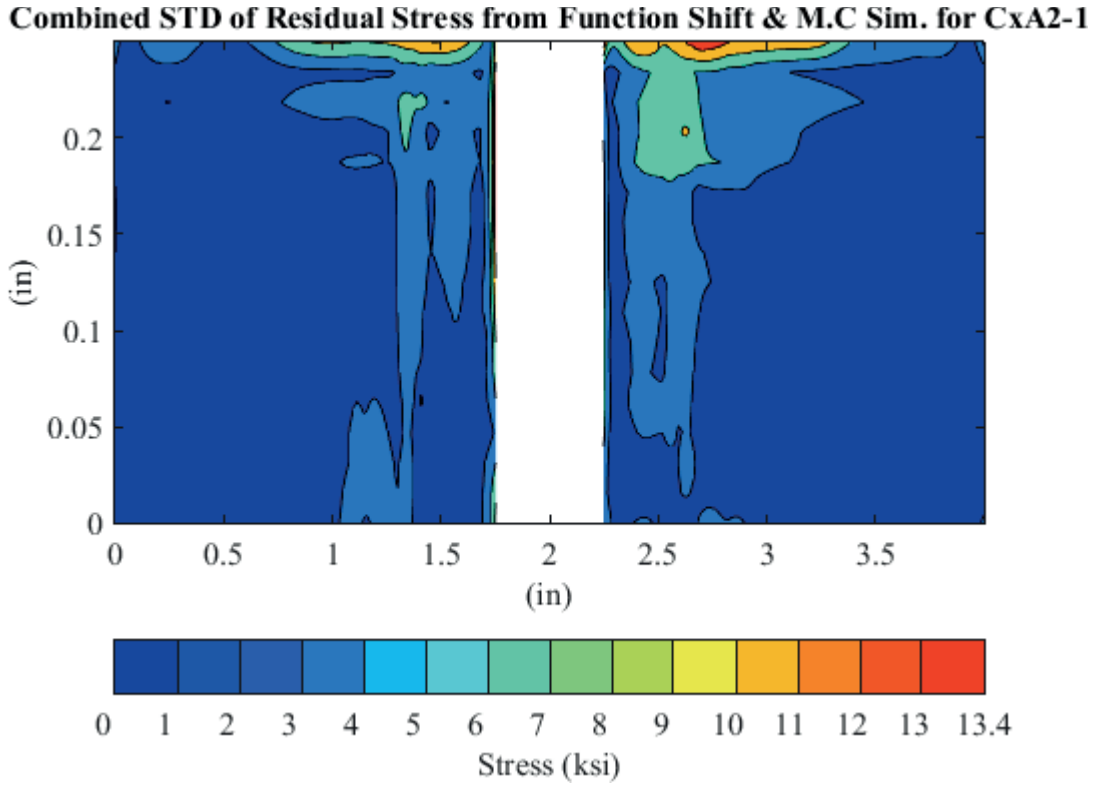

Fig. 964 Contour Pot of the Spatial "Total" Residual Stress Single Measurement Uncertainty Associated with Coupon CxA2-1 (2024-T351).

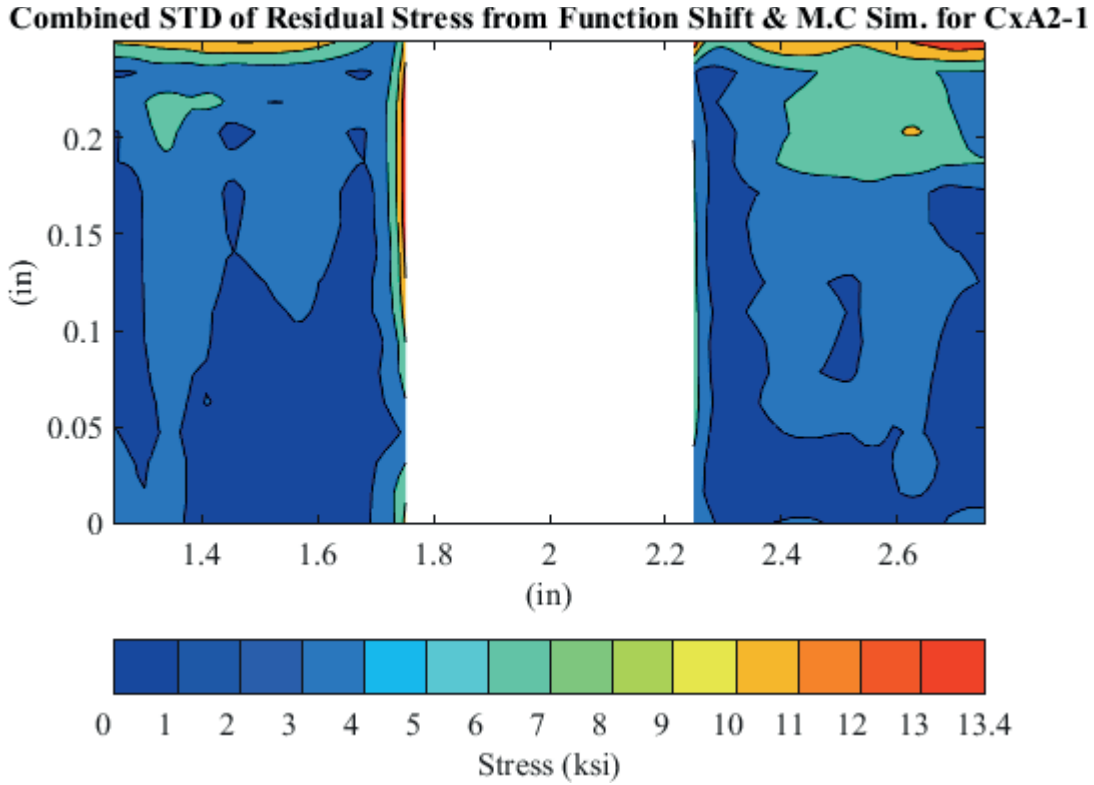

Fig. 965 Contour Pot of the Spatial "Total" Residual Stress Single Measurement Uncertainty Associated with Coupon CxA2-1 (2024-T351) – Zoomed in next to Hole.

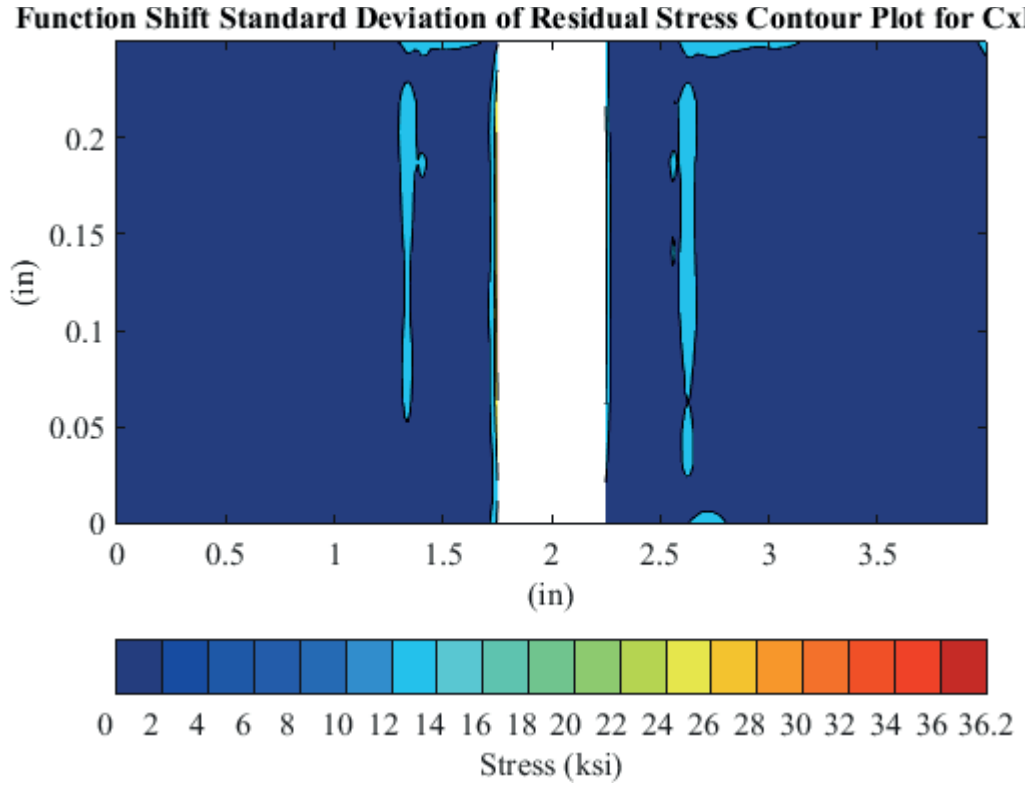

Fig. 966 Contour Plot of the Spatial “Function” or “Model” Residual Uncertainty Associated with Coupon CxD2-1 (7075-T651).

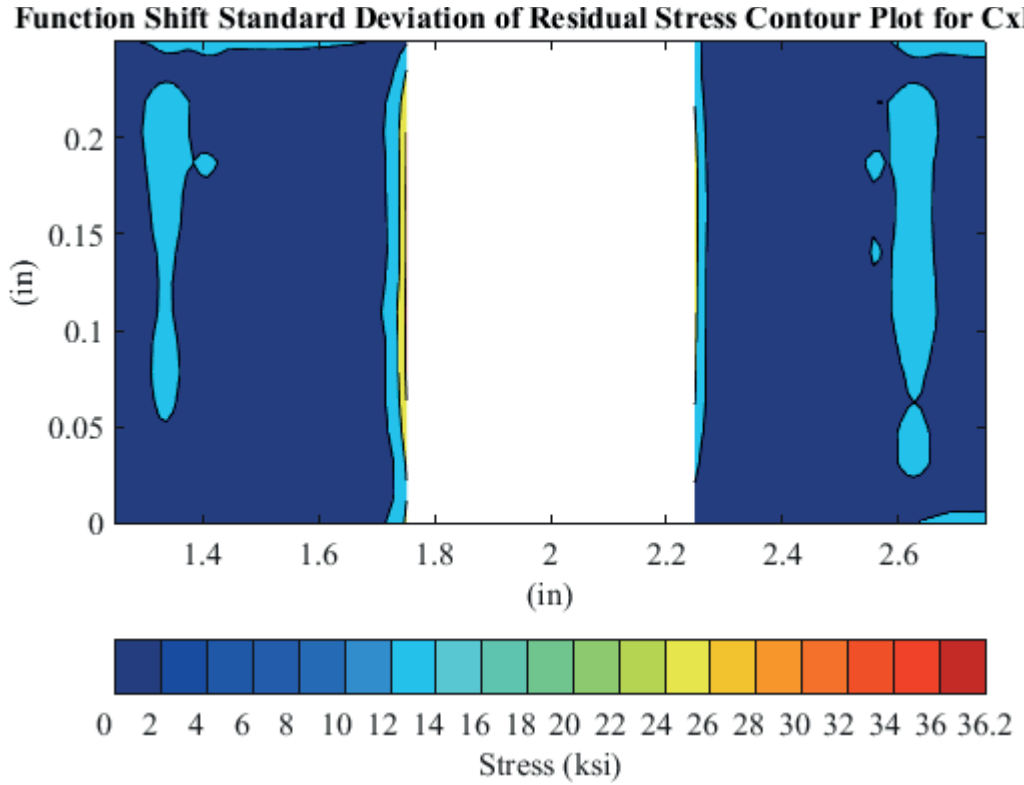

Fig. 967 Contour Plot of the Spatial “Function” or “Model” Residual Uncertainty Associated with Coupon CxD2-1 (7075-T651) – Zoomed next to Hole.

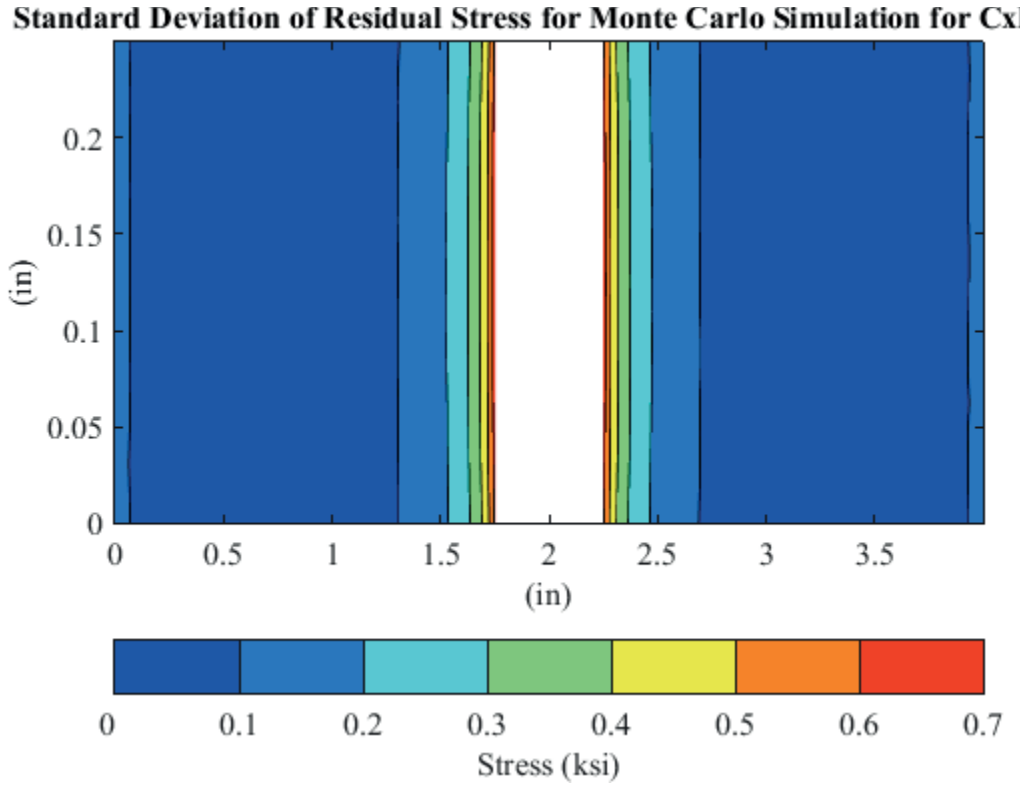

Fig. 968 Contour Plot of the Spatial "Displacement" Residual Stress Uncertainty Developed via Monte Carlo Simulation for Coupon CxD2-1 (7075-T651).

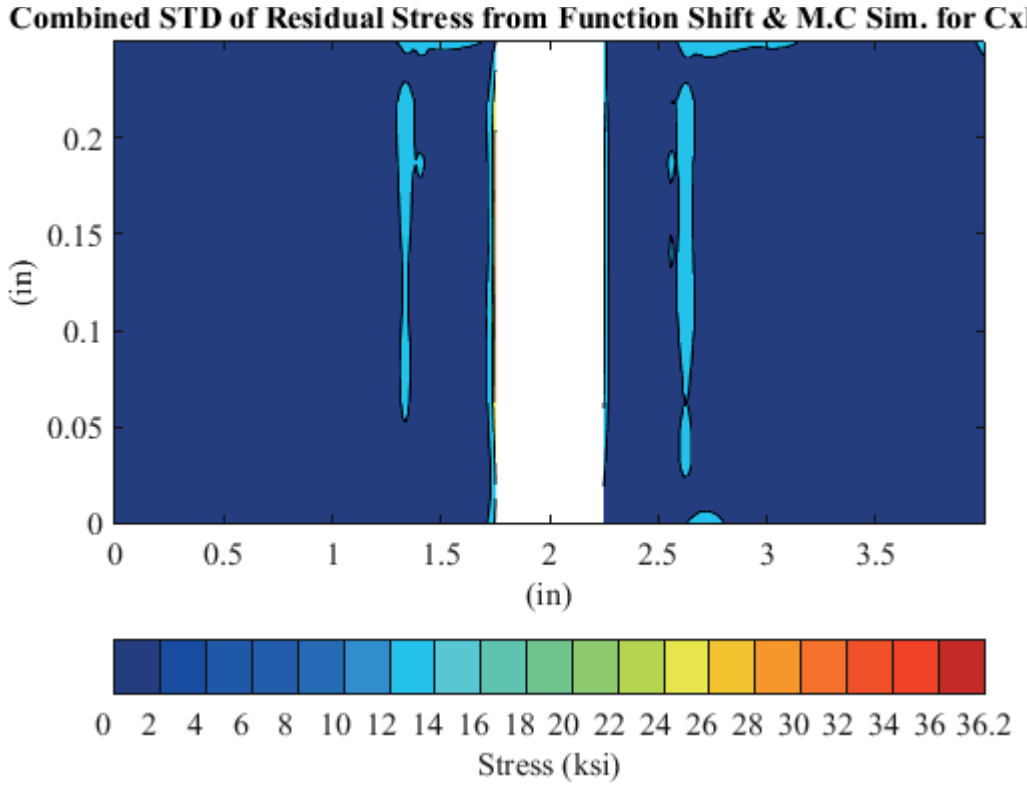

Fig. 969 Contour Plot of the Spatial "Total" Residual Stress Single Measurement Uncertainty Associated with Coupon CxD2-1 (7075-T651).

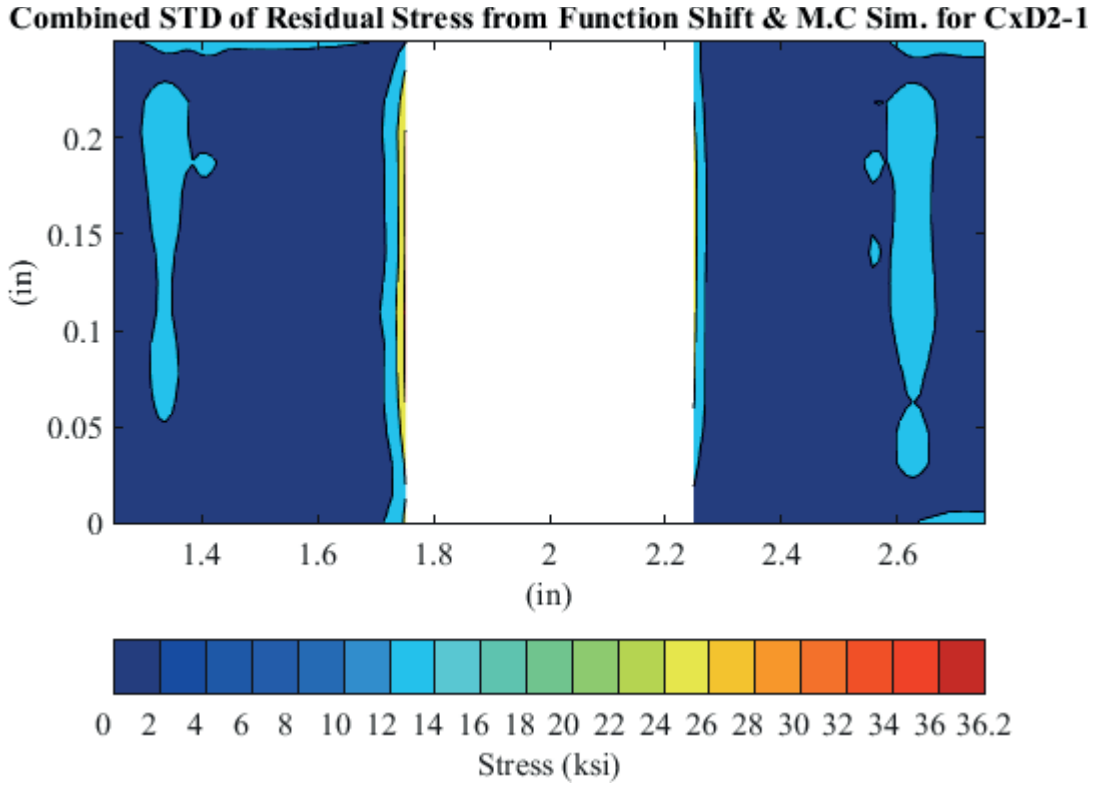

Fig. 970 Contour Plot of the Spatial "Total" Residual Stress Single Measurement Uncertainty Associated with Coupon CxD2-1 (7075-T651) – Zoomed in next to Hole.

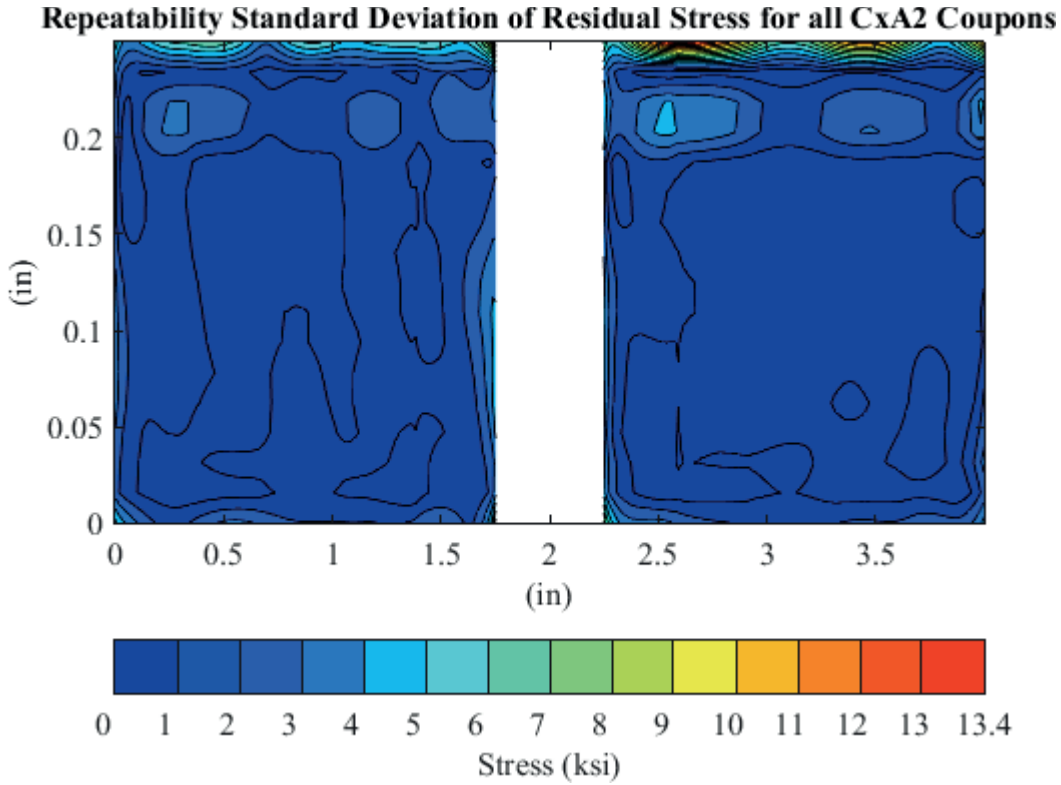

Fig. 971 Contour Plot of the Baseline, Uncracked CxA2 (2024-T351) Spatial Repeatability Uncertainty.

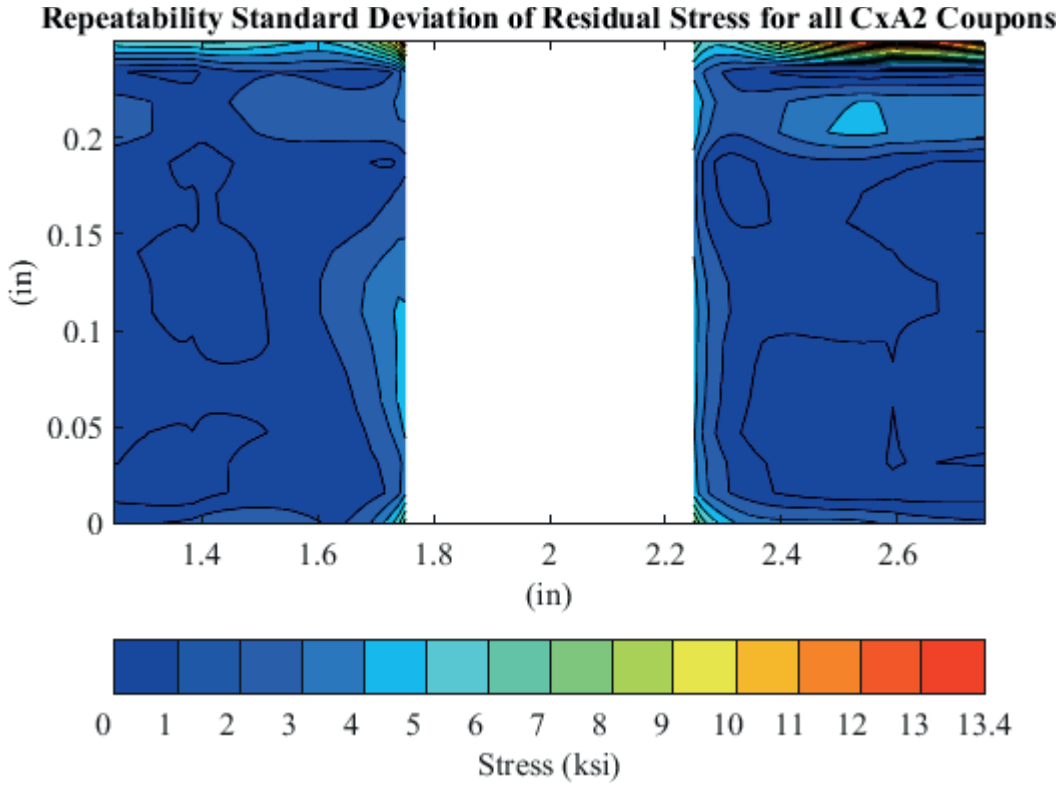

Fig. 972 Contour Plot of the Baseline, Uncracked CxA2 (2024-T351) Spatial Repeatability Uncertainty – Zoomed in next to Hole.

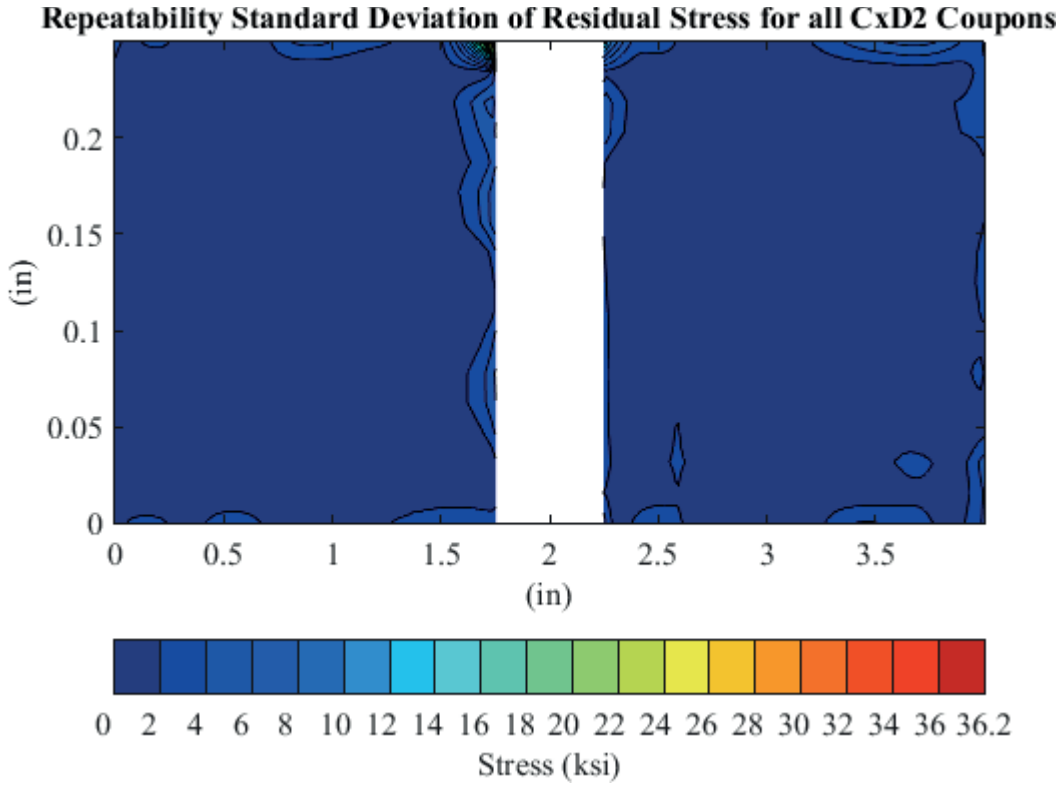

Fig. 973 Contour Plot of the Baseline, Uncracked CxD2 (7075-T651) Spatial Repeatability Uncertainty.

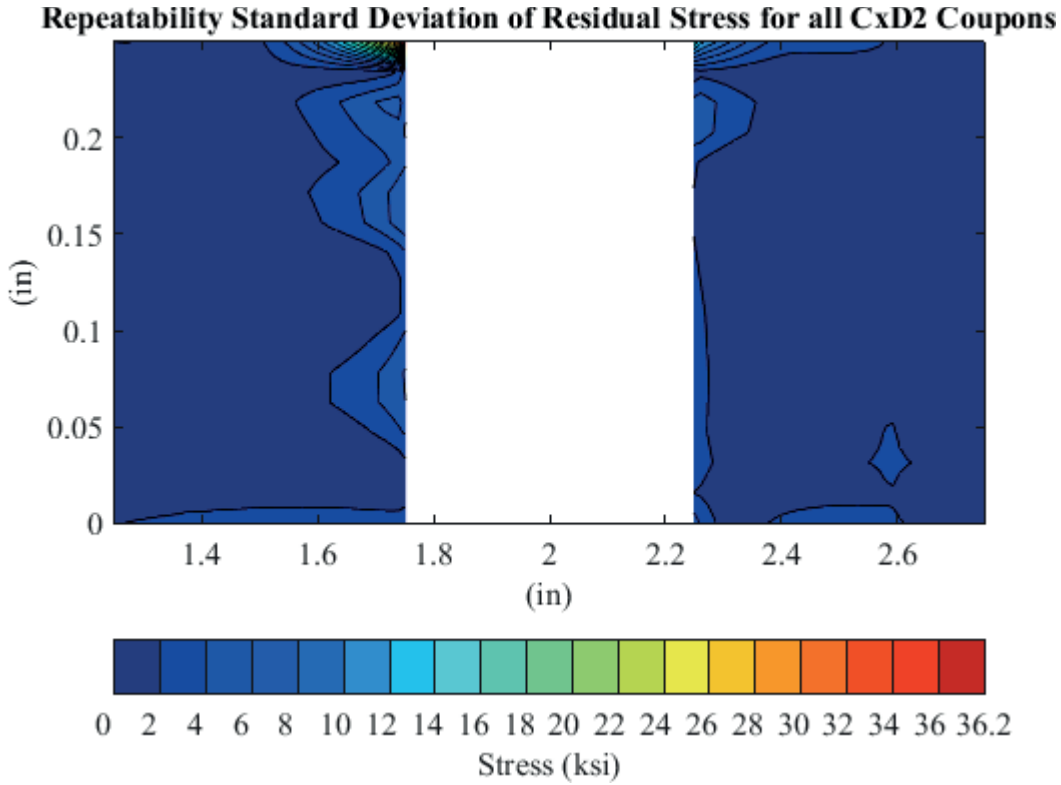

Fig. 974 Contour Plot of the Baseline, Uncracked CxD2 (7075-T651) Spatial Repeatability Uncertainty – Zoomed in next to Hole.

Table 28 Matrix of Cx4N1-XX-B (2024-T351) Fatigue-Cracked Coupons Showing Fatigue Crack Lengths and Other Essential Metrology Features

4N1-XX-B (2024-T351) Coupons							
Specimen ID	**Defined Mandrel Entrance Surface Crack Length (inch)**	**Mandrel Entrance Face Crack (inch)**	**Gauge Width (inch)**	**Gauge Thickness (inch)**	**Initial Ream Diameter (CMM) (inch)**	**% CX**	**Final Ream Diameter (inch)**
4N1-01-B	0.08	0.0797	4.0000	0.2545	0.4771	3.23%	0.4990
4N1-02-B		0.0798	4.0030	0.2550	0.4768	3.29%	0.4997
4N1-03-B	0.1	0.0974	4.0025	0.2548	0.4772	3.21%	0.4997
4N1-04-B		0.0962	4.0022	0.2555	0.4771	3.23%	0.4990
4N1-05-B	0.125	0.1259	4.0027	0.2557	0.4771	3.23%	0.4980
4N1-06-B		0.1214	4.0023	0.2555	0.4770	3.25%	0.4990
4N1-07-B	0.25	0.2515	4.0020	0.2555	0.4770	3.25%	0.4995
4N1-08-B	0.5	0.4974	4.0013	0.2550	0.4770	3.25%	0.4995
AVERAGE			***4.0020***	***0.2552***	***0.4770***	***3.24%***	***0.4992***
STDEV			***0.0009***	***0.0004***	***0.0001***	***0.03%***	***0.0006***

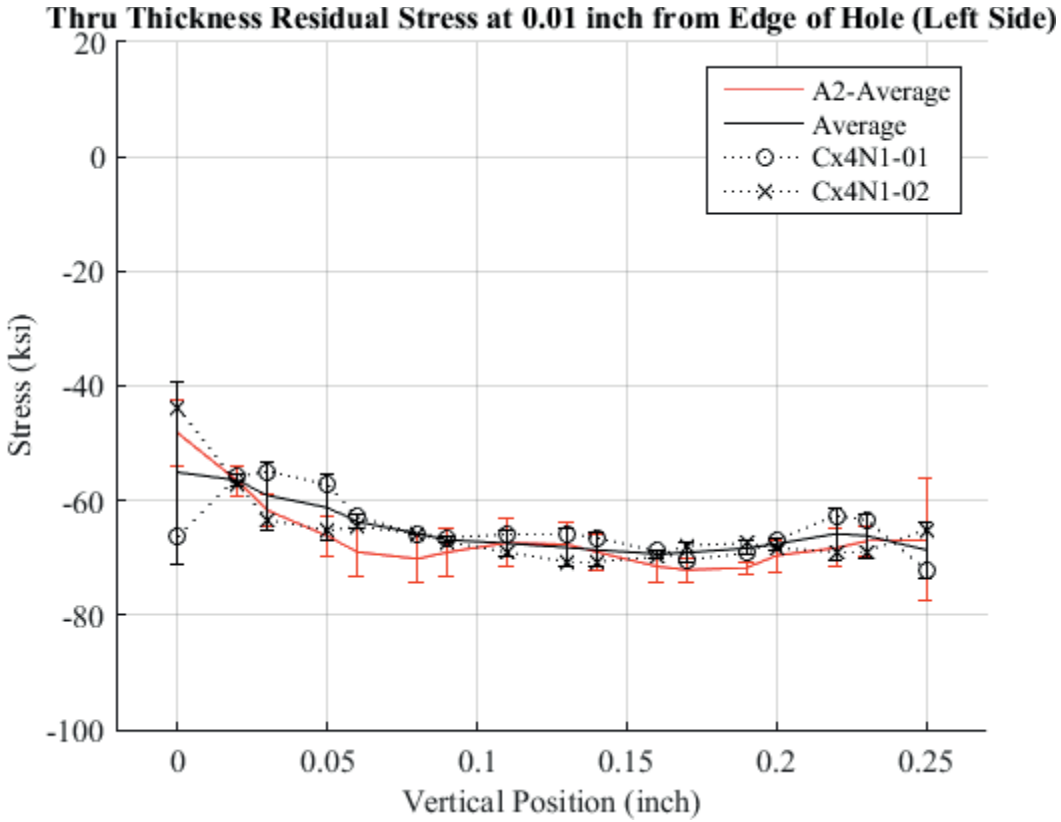

Fig. 975 Through-Thickness Line Plot of the Residual Stress for Cx4N1-01-02-B (2024-T351 with an Average Fatigue Crack Size of 0.08 inch), and the Average of the Two, with One Standard Deviation of the Average, Compared to the CxA2 (2024-T351) Average Residual Stress at 0.05 inch away from the Edge of the Hole, with Error Bars for the CxA2 (2024-T351) Average Being the Repeatability Standard Deviation.

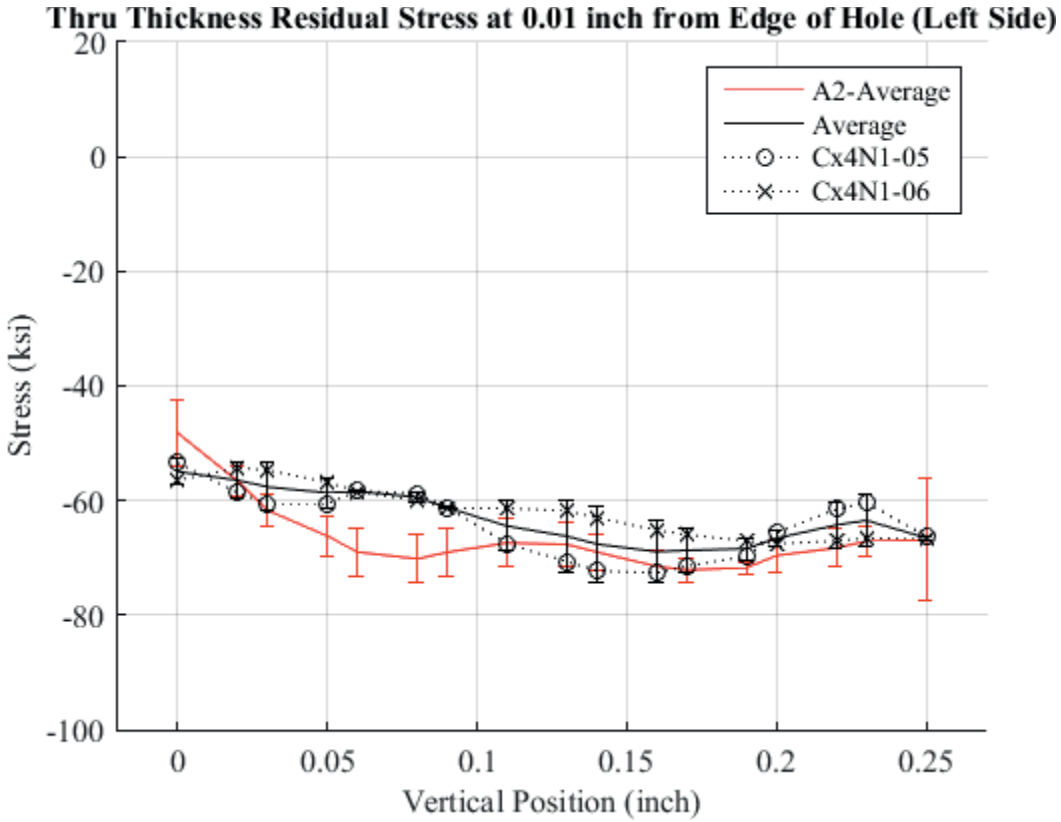

Fig. 976 Through-Thickness Line Plot of the Residual Stress for Cx4N1-05-06-B (2024-T351 Coupons with an Average Fatigue Crack Size of 0.125 inch), and the Average of the Two, with One Standard Deviation of the Average, Compared to the CxA2 (2024-T351) Average Residual Stress at 0.05 inch away from the Edge of the Hole, with Error Bars for the CxA2 (2024-T351) Average Being the Repeatability Standard Deviation.

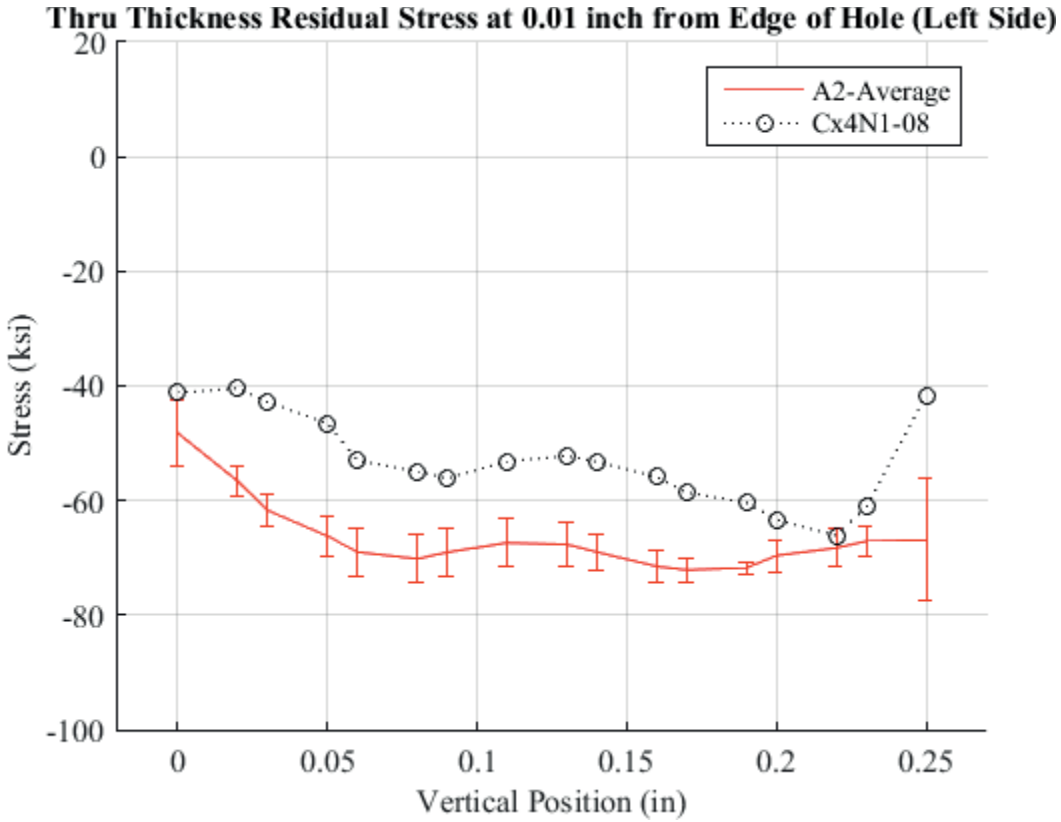

Fig. 977 Through-Thickness Line Plot of the Residual Stress for Cx4N1-08-B (2024-T351 Coupons with a Fatigue Crack Size of 0.4974 inch), Compared to the CxA2 (2024-T351) Average Residual Stress at 0.05 inch away from the Edge of the Hole, with Error Bars for the CxA2 (2024-T351) Average Being the Repeatability Standard Deviation.

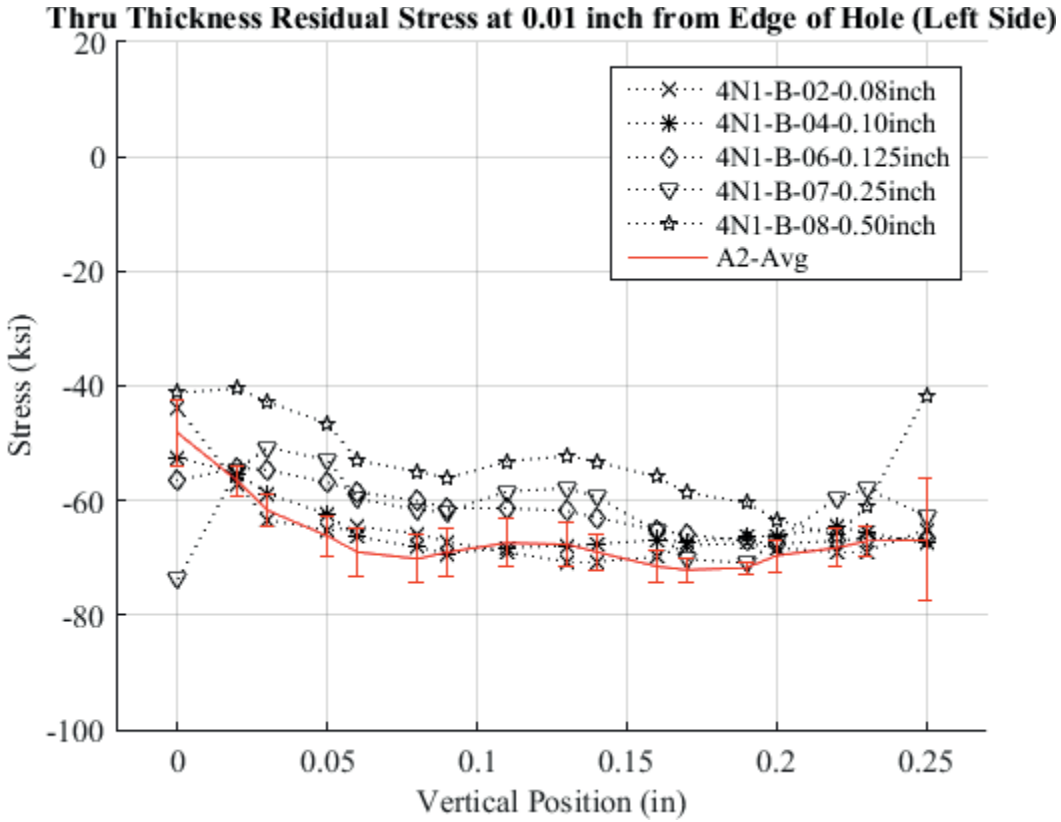

Fig. 978 Through-Thickness Line Plot of the Residual Stress for Cx4N1-02-04-06-07-08-B (2024-T351), Compared to the CxA2 (2024-T351) Average Residual Stress at 0.01 inch away from the Edge of the Hole, with Error Bars for the CxA2 (2024-T351) Average Being the Repeatability Standard Deviation.

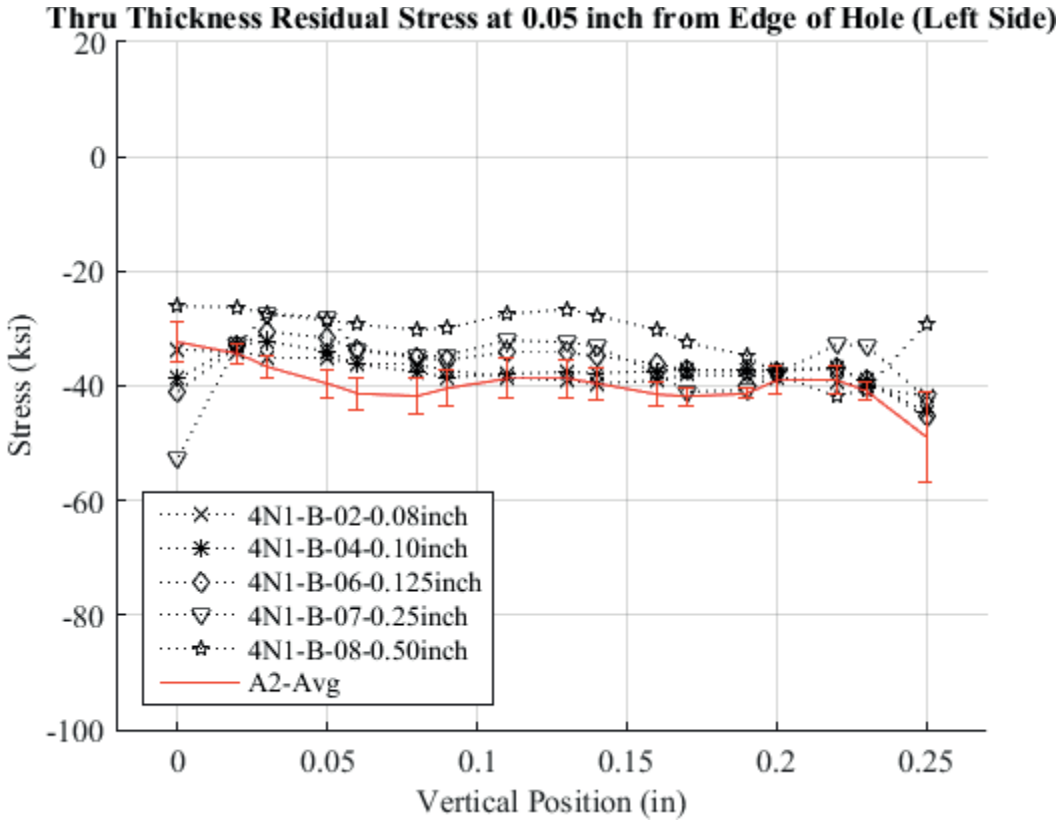

Fig. 979 Through-Thickness Line Plot of the Residual Stress for Cx4N1-02-04-06-07-08-B (2024-T351), Compared to the CxA2 (2024-T351) Average Residual Stress at 0.05 inch away From the Edge of the Hole, with Error Bars for the CxA2 (2024-T351) Average Being the Repeatability Standard Deviation.

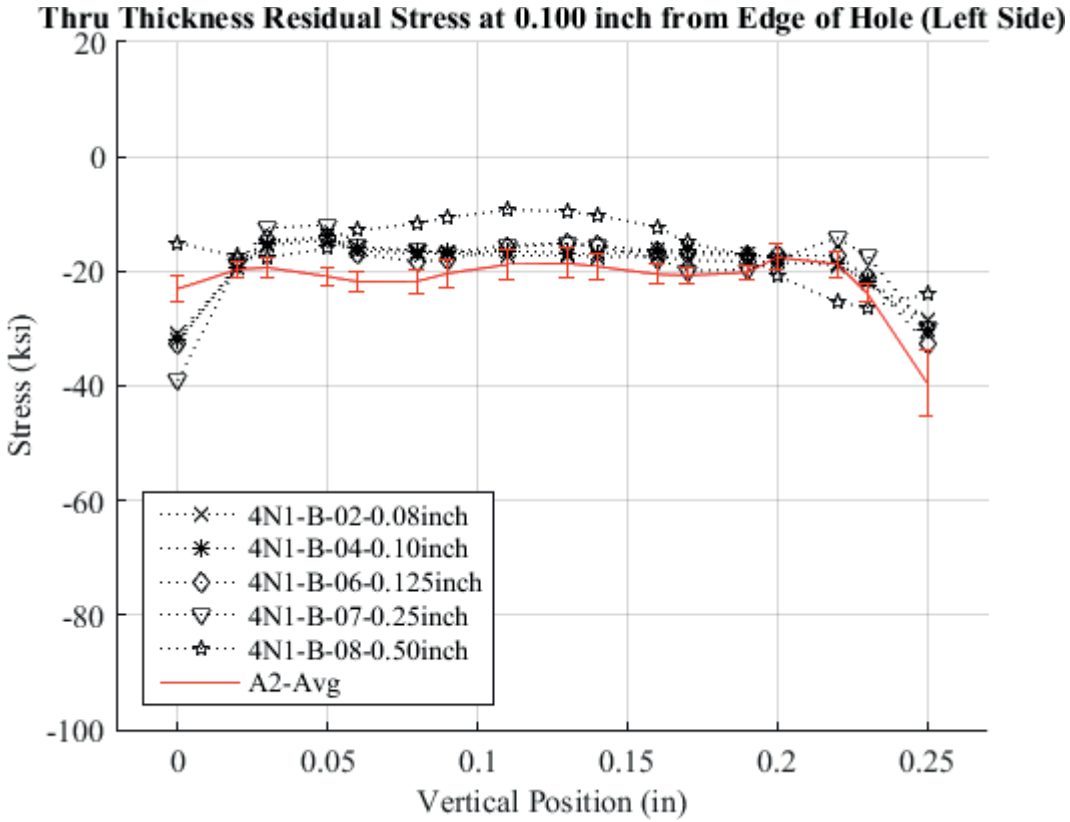

Fig. 980 Through-Thickness Line Plot of the Residual Stress for Cx4N1-02-04-06-07-08-B (2024-T351), Compared to the CxA2 (2024-T351) Average Residual Stress at 0.10 inch away from the Edge of the Hole, with Error Bars for the CxA2 (2024-T351) Average Being the Repeatability Standard Deviation.

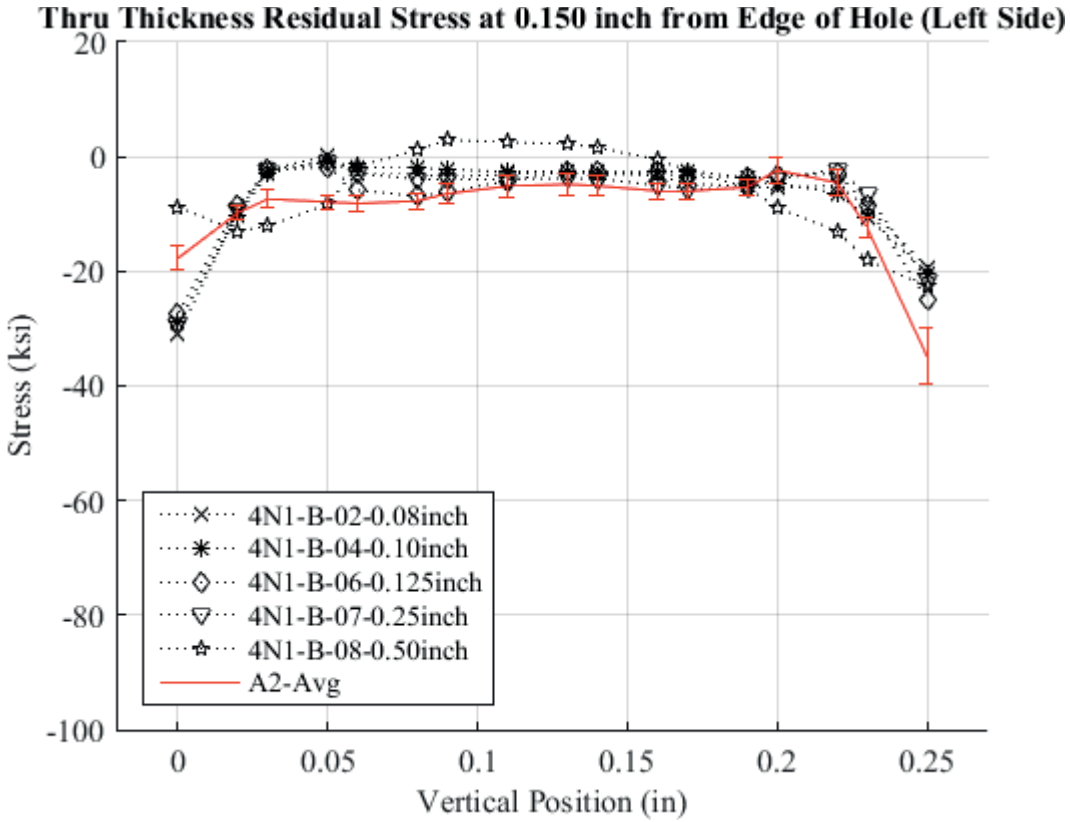

Fig. 981 Through-Thickness Line Plot of the Residual Stress for Cx4N1-02-04-06-07-08-B (2024-T351), Compared to the CxA2 (2024-T351) Average Residual Stress at 0.15 inch away from the Edge of the Hole, with Error Bars for the CxA2 (2024-T351) Average Being the Repeatability Standard Deviation.

Table 29 Matrix of Cx4N1-XX-D (7075-T651) Fatigue-Cracked Coupons Showing Fatigue Crack Lengths and Other Essential Metrology Features

4N1-XX-D (7075-T651) Coupons							
Specimen ID	**Defined Mandrel Entrance Surface Crack Length (inch)**	**Mandrel Entrance Face Crack (inch)**	**Gauge Width (inch)**	**Gauge Thickness (inch)**	**Initial Ream Diameter (CMM) (inch)**	**% CX**	**Final Ream Diameter (inch)**
4N1-01-D	0.08	0.0793	4.0028	0.2495	0.4766	3.34%	0.4988
4N1-02-D		0.0807	4.0023	0.2510	0.4768	3.29%	0.4990
4N1-03-D	0.1	0.0972	4.0017	0.2508	0.4769	3.27%	0.4993
4N1-04-D		0.1015	4.0015	0.2500	0.4770	3.25%	0.4985
4N1-05-D	0.125	0.1253	4.0020	0.2505	0.4769	3.27%	0.4992
4N1-06-D		0.1235	4.0027	0.2507	0.4770	3.25%	0.4980
4N1-07-D	0.25	0.2505	4.0020	0.2505	0.4767	3.31%	0.4983
4N1-08-D	0.5	0.5017	4.0022	0.2512	0.4769	3.27%	0.4992
AVERAGE			***4.0021***	***0.2505***	***0.4769***	***3.28%***	***0.4988***
STDEV			***0.0005***	***0.0005***	***0.0001***	***0.03%***	***0.0005***

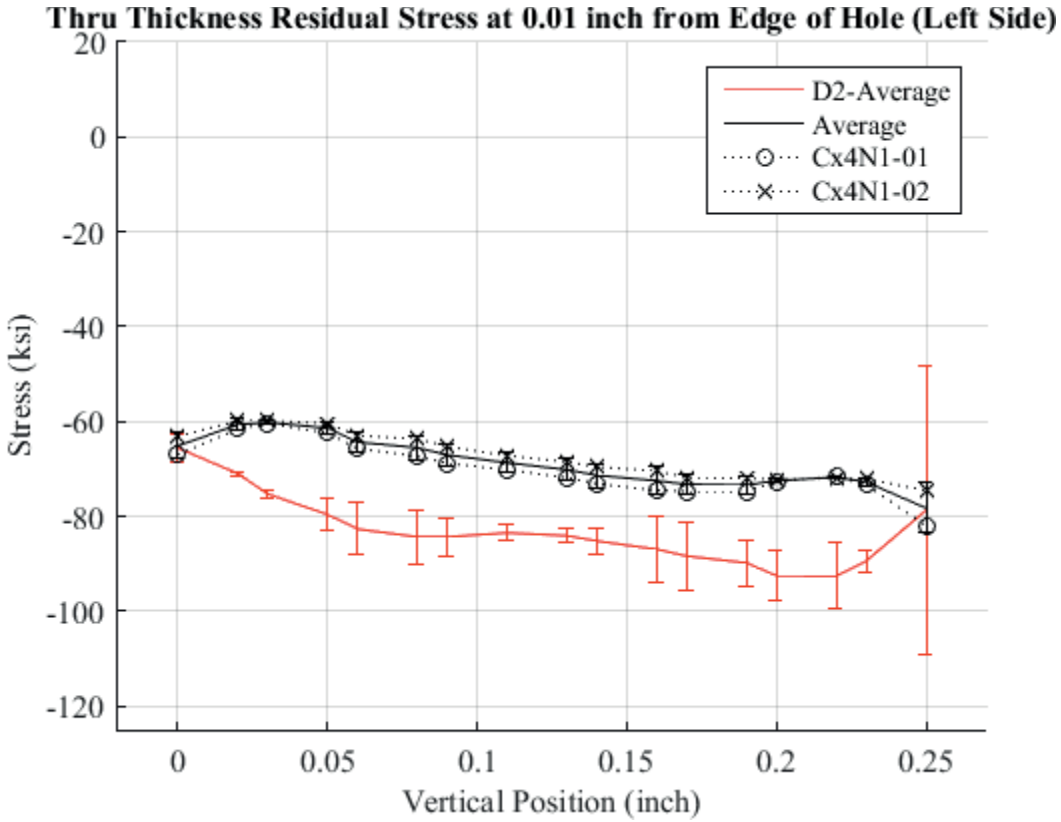

Fig. 982 Through-Thickness Line Plot of the Residual Stress for Cx4N1-01-02-D (7075-T651 with an Average Fatigue Crack Size of 0.08 inch), and the Average of the Two, with One Standard Deviation of the Average, Compared to the CxD2 (7075-T651) Average Residual Stress at 0.05 inch away from the Edge of the Hole, with Error Bars for the CxD2 (7075-T651) Average Being the Repeatability Standard Deviation.

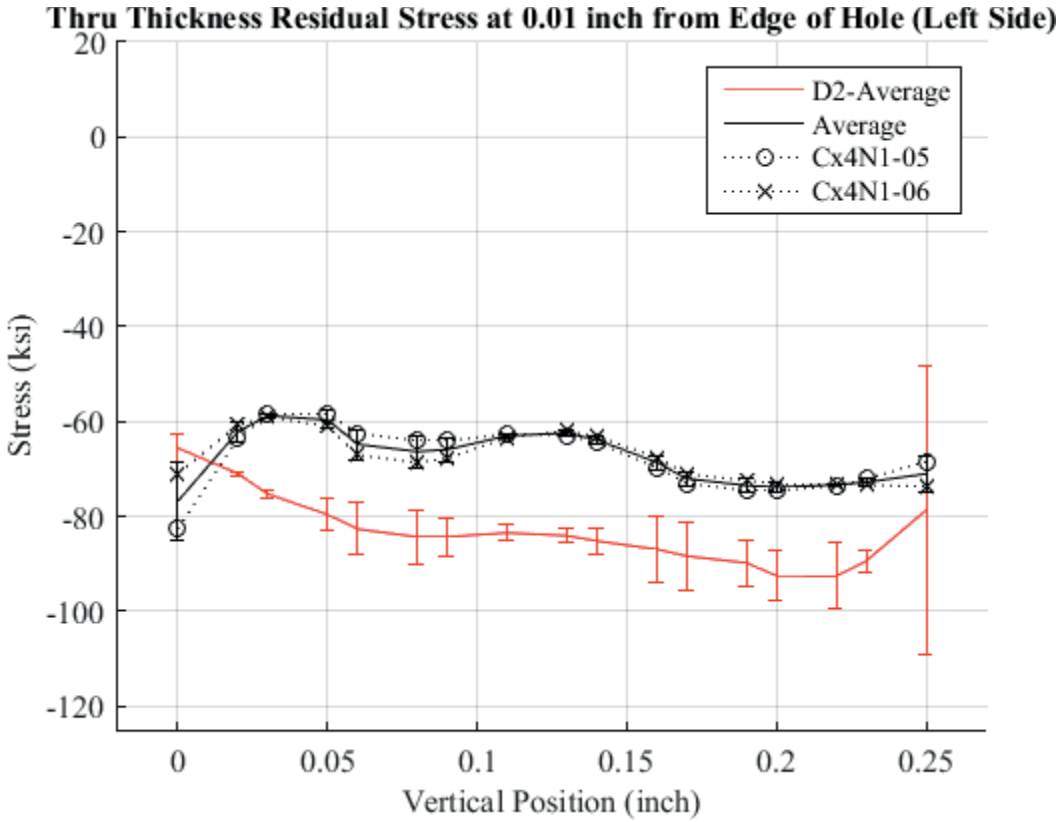

Fig. 983 Through-Thickness Line Plot of the Residual Stress for Cx4N1-05-06-D (7075-T651 Coupons with an Average Fatigue Crack Size of 0.125 inch), and the Average of the Two, with One Standard Deviation of the Average, Compared to the CxD2 (7075-T651) Average Residual Stress at 0.05 inch away from the Edge of the Hole, with Error Bars for the CxD2 (7075-T651) Average Being the Repeatability Standard Deviation.

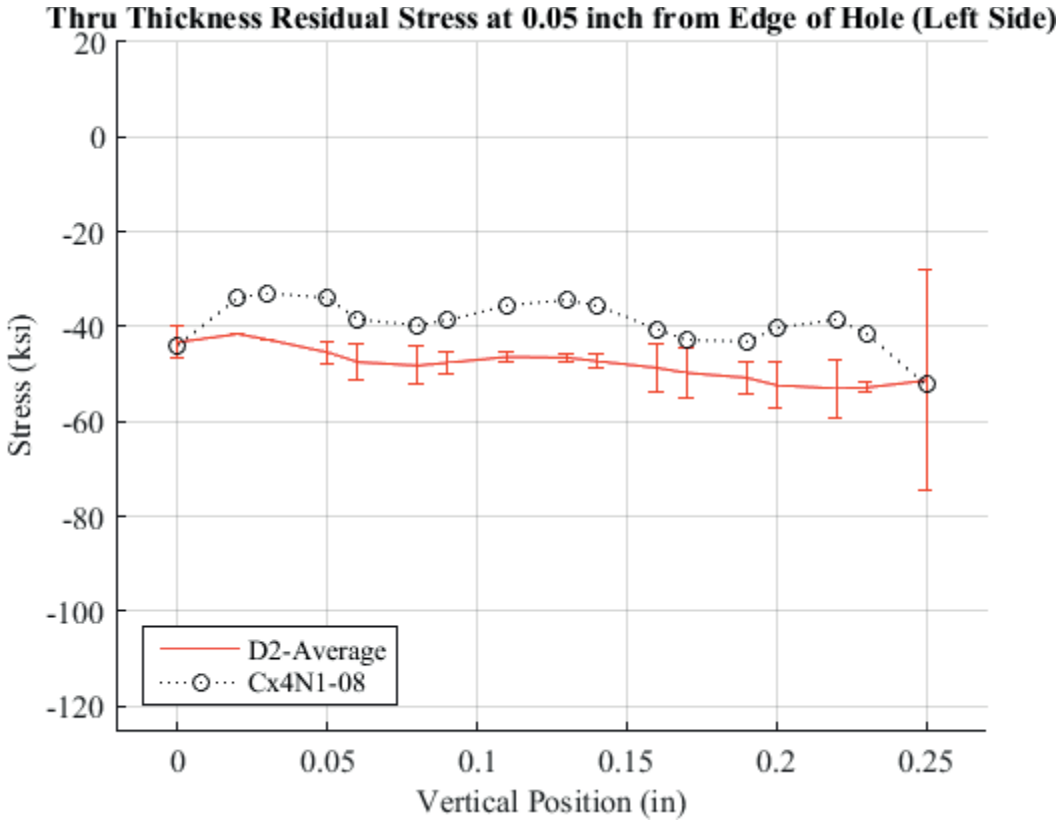

Fig. 984 Through-Thickness Line Plot of the Residual Stress for Cx4N1-08-D (7075-T651 Coupons with a Fatigue Crack Size of 0.5017 inch), Compared to the CxD2 (7075-T651) Average Residual Stress at 0.05 inch away from the Edge of the Hole, with Error Bars for the CxD2 (7075-T651) Average Being the Repeatability Standard Deviation.

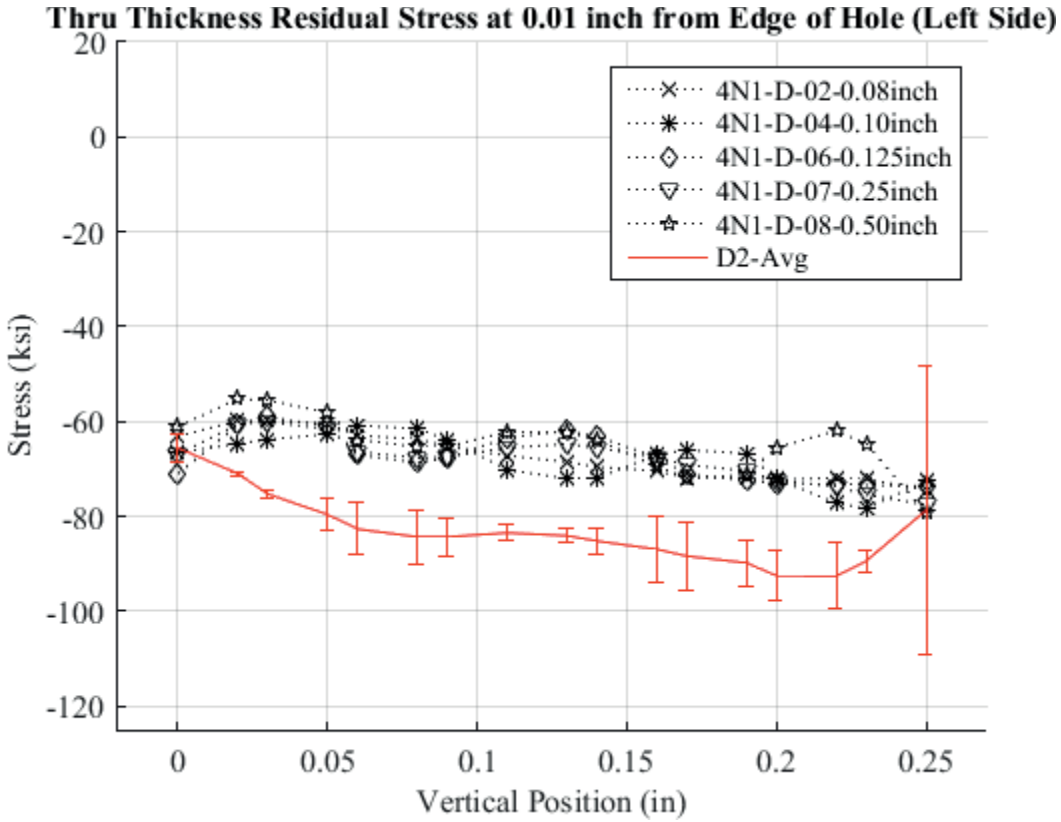

Fig. 985 Through-Thickness Line Plot of the Residual Stress for Cx4N1-02-04-06-07-08-D (7075-T651), Compared to the CxD2 (2024-T351) Average Residual Stress at 0.01 inch away from the Edge of the Hole, with Error Bars for the CxD2 (7075-T651) Average Being the Repeatability Standard Deviation.

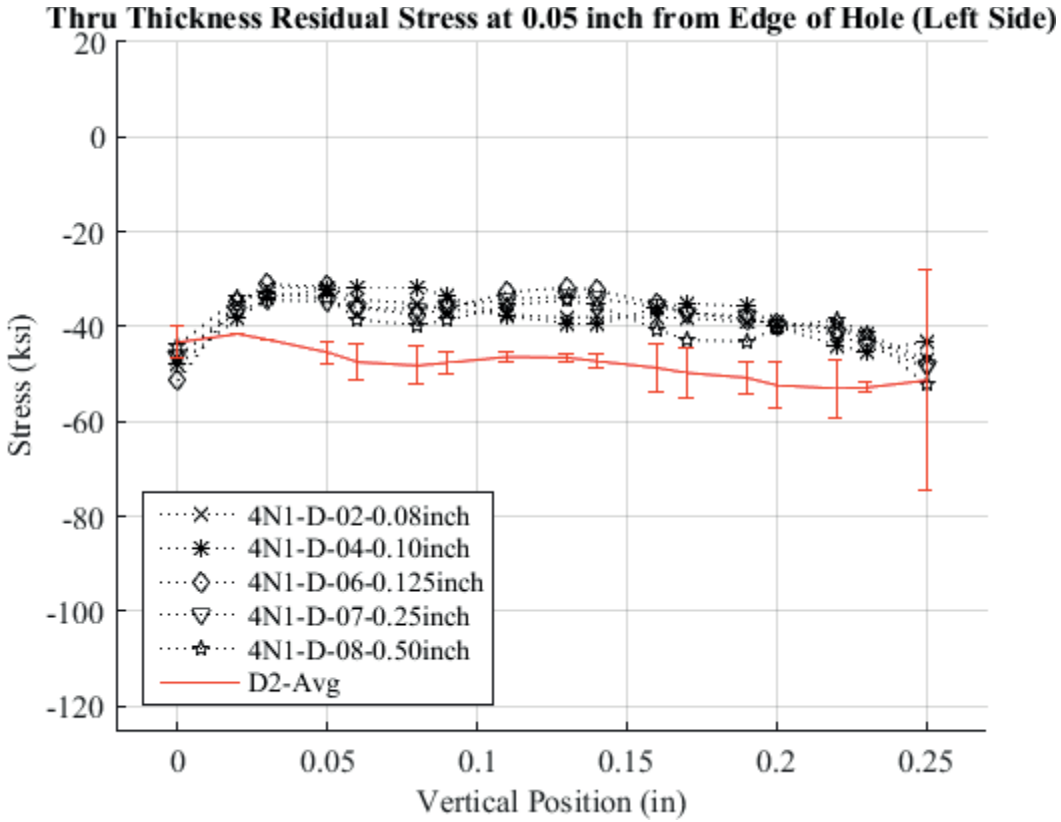

Fig. 986 Through-Thickness Line Plot of the Residual Stress for Cx4N1-02-04-06-07-08-D (7075-T651), Compared to the CxD2 (2024-T351) Average Residual Stress at 0.05 inch away from the Edge of the Hole, with Error Bars for the CxD2 (7075-T651) Average Being the Repeatability Standard Deviation.

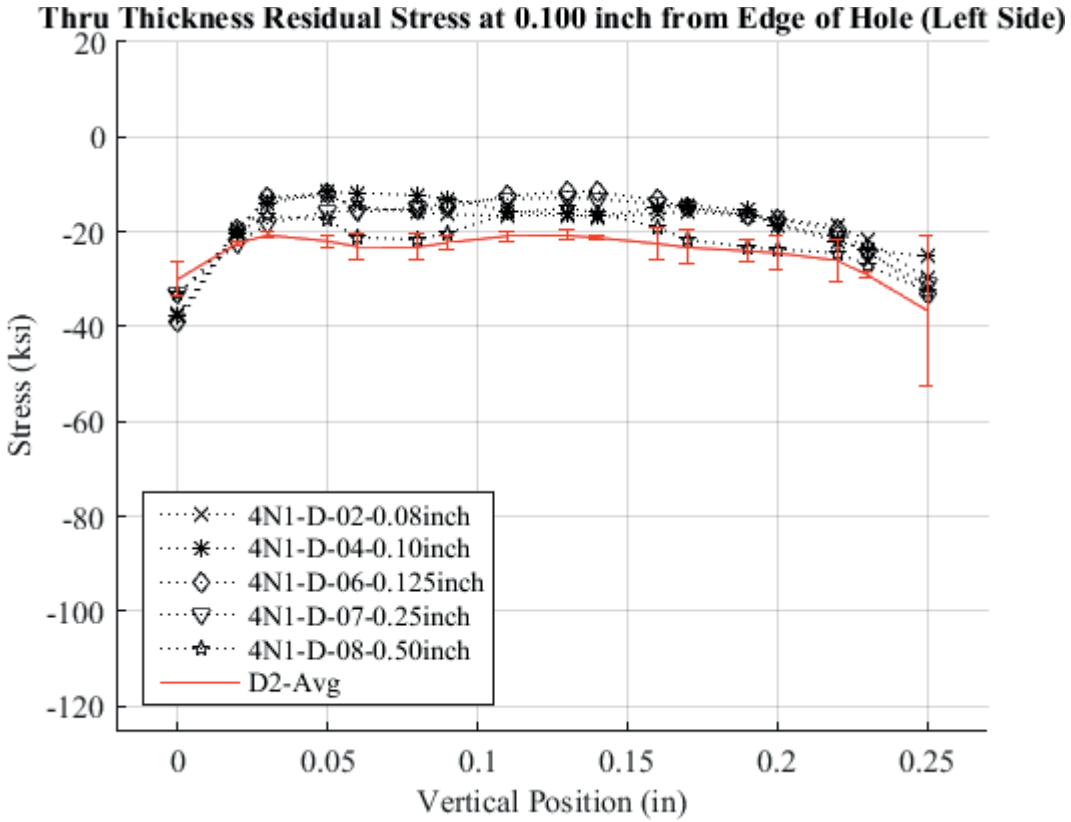

Fig. 987 Through-Thickness Line Plot of the Residual Stress for Cx4N1-02-04-06-07-08-D (7075-T651), Compared to the CxD2 (2024-T351) Average Residual Stress at 0.10 inch away from the Edge of the Hole, with Error Bars for the CxD2 (7075-T651) Average Being the Repeatability Standard Deviation.

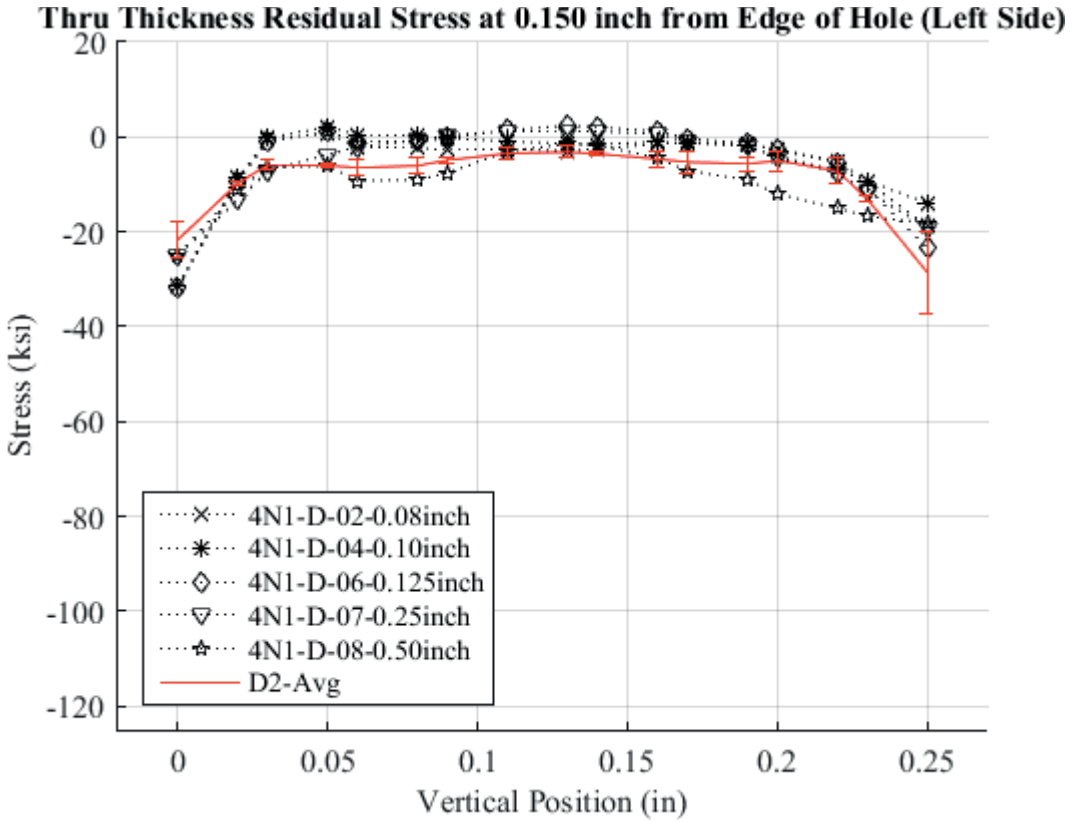

Fig. 988 Through-Thickness Line Plot of the Residual Stress for Cx4N1-02-04-06-07-08-D (7075-T651), Compared to the CxD2 (2024-T351) Average Residual Stress at 0.150 inch away from the Edge of the Hole, with Error Bars for the CxD2 (7075-T651) Average Being the Repeatability Standard Deviation.

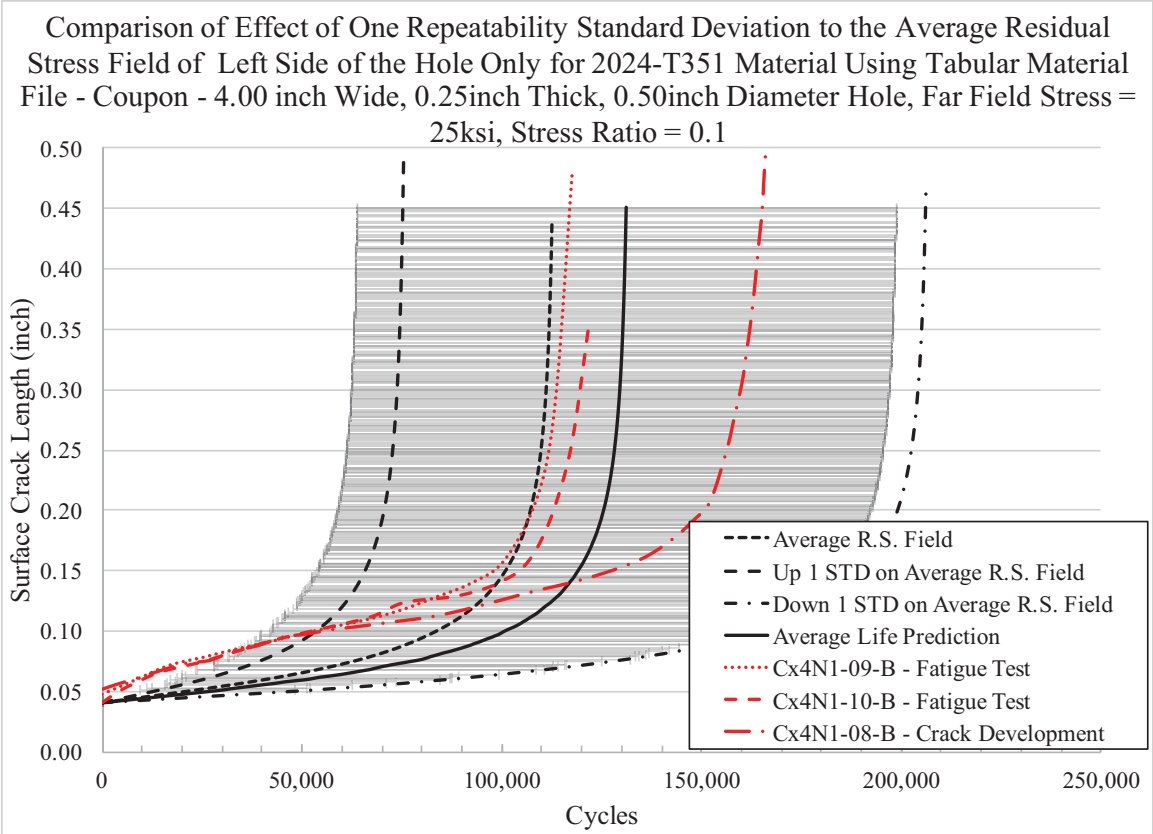

Fig. 989 Fatigue Life Prediction Using the Residual Stress Conditions Developed from the CxA2 (2024-T351) Baseline, Uncracked Condition, Comparing Predicted Life and Curve Shape to Fatigue Test Data.

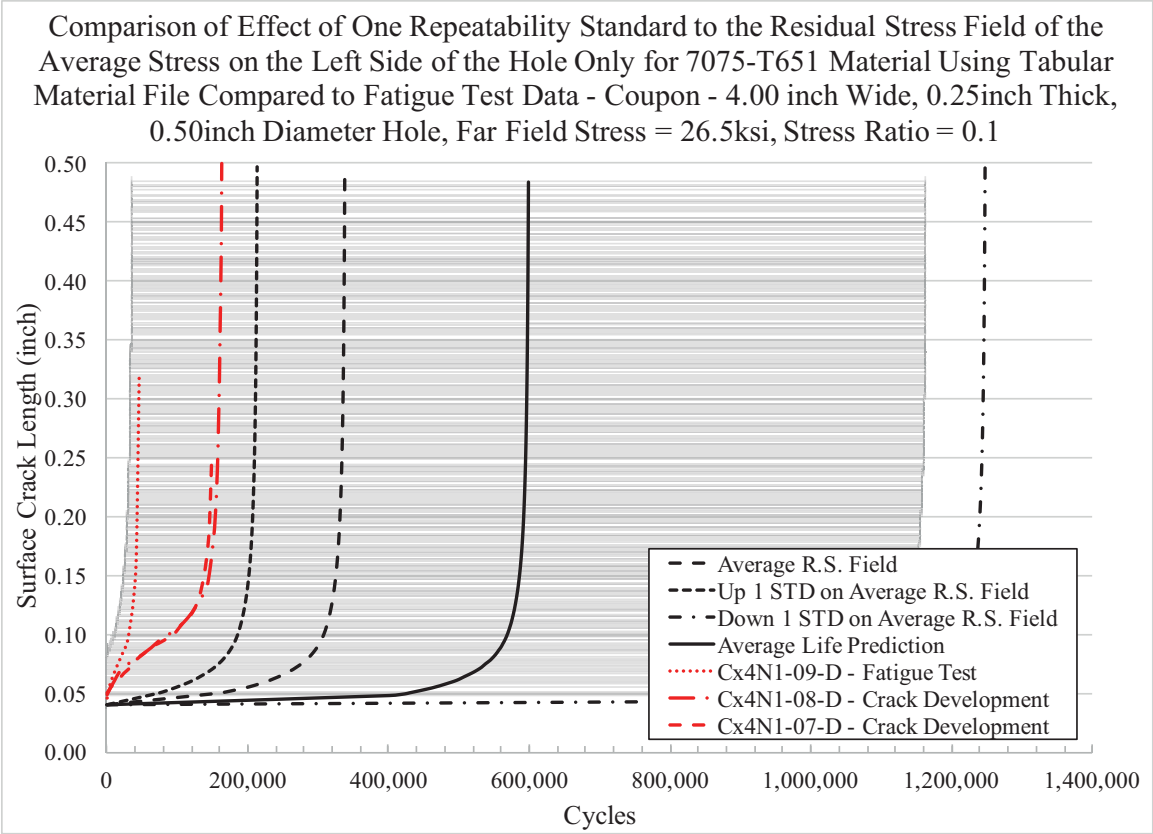

Fig. 990 Fatigue Life Prediction Using the Residual Stress Conditions Developed from the CxD2 (7075-T651) Baseline, Uncracked Condition, Comparing Predicted Life and Curve Shape to Fatigue Test Data.

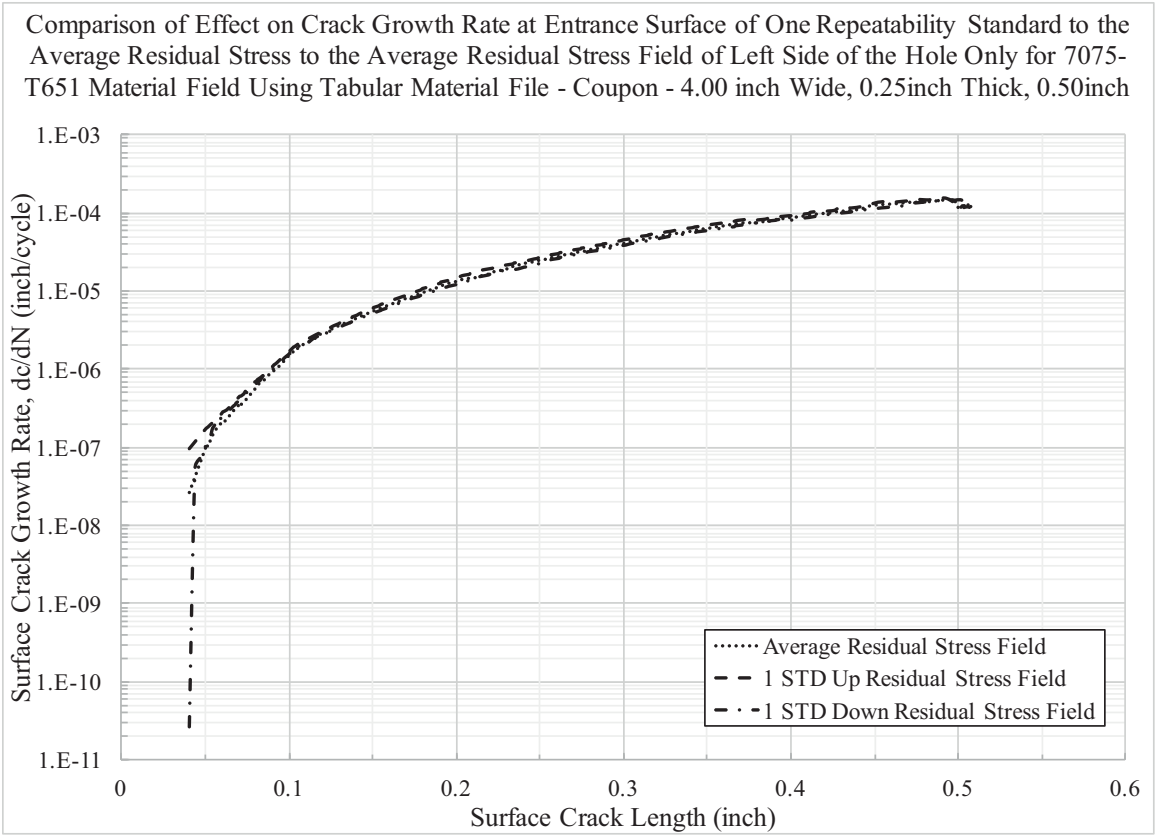

Fig. 991 Plot of the Cx Mandrel Entrance Surface dc/dN (Crack Growth Rate) Versus c (Cx Mandrel Entrance Surface Crack Length) for the Fatigue Life Predictions Using the Baseline, Uncracked CxD2 (7075-T651) Residual Stress Statistical Bounds.

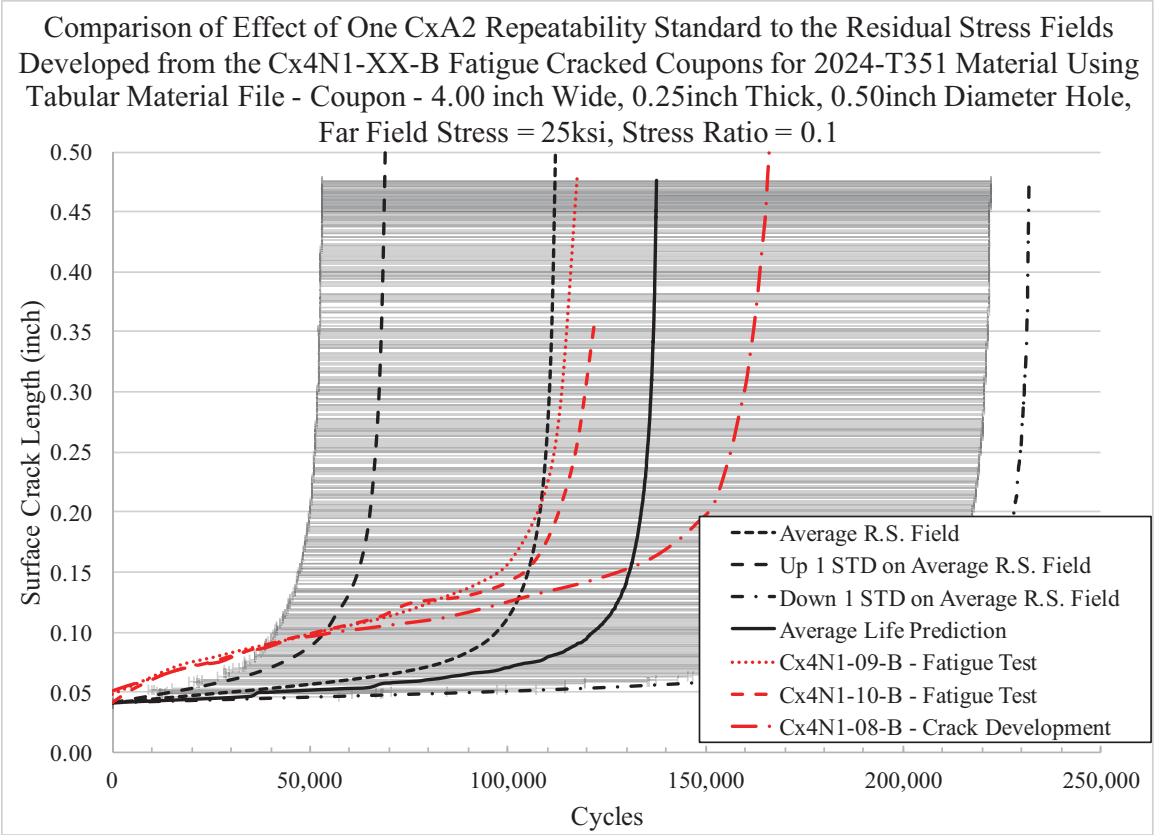

Fig. 992 Fatigue Life Prediction Using the Residual Stress Conditions Developed from the Fatigue-Cracked Coupons Cx4N1-01-08-B (2024-T351) for the Average, Upper and Lower One Standard Deviation Residual Stress Field, Comparing Predicted Life and Curve Shape to Fatigue Test Data.

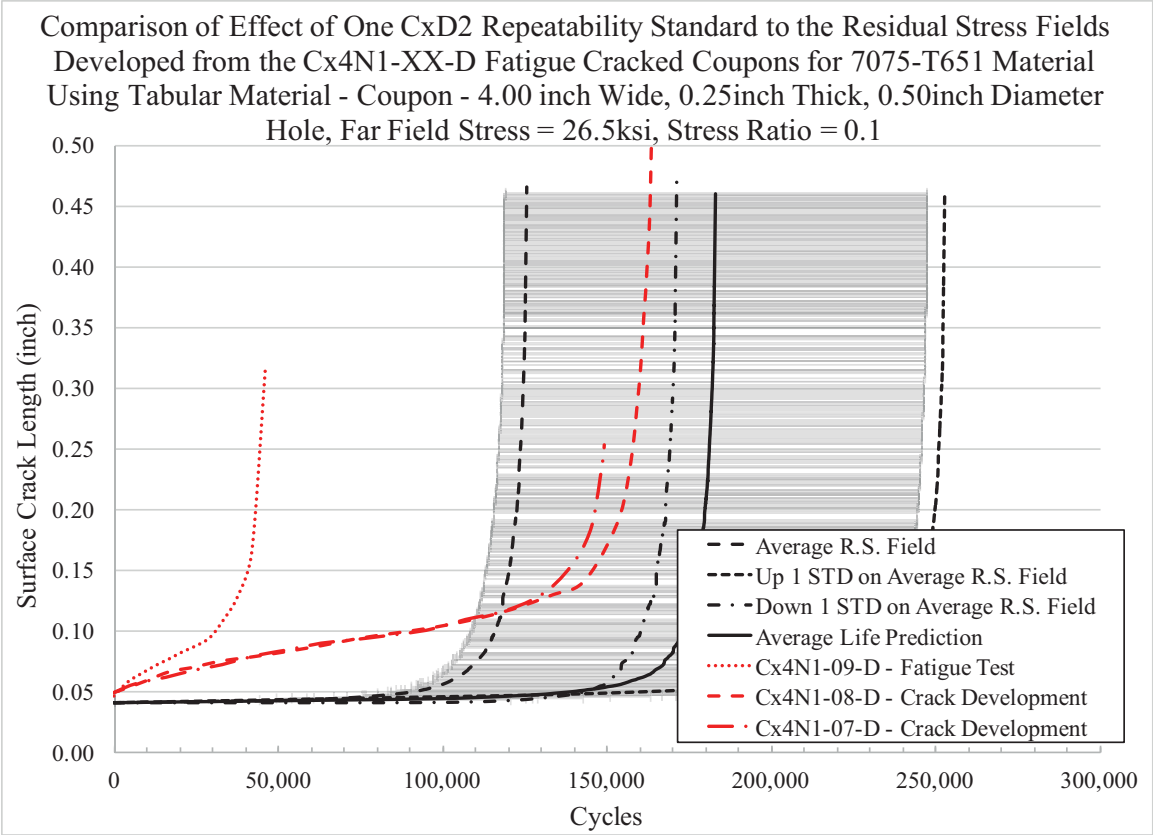

Fig. 993 Fatigue Life Prediction Using the Residual Stress Conditions Developed from the Fatigue-Cracked Coupons Cx4N1-01-08-D (7075-T651) for the Average, Upper and Lower One Standard Deviation Residual Stress Field, Comparing Predicted Life and Curve Shape to Fatigue Test Data.

13 CONCLUSIONS AND RECOMMENDATIONS FROM QUANTIFICATION OF THE EFFECT OF A FATIGUE CRACK ON THE RESIDUAL STRESS FIELD INTRODUCED BY THE COLD EXPANSION PROCESS

13.1 Development of an International Standard for Contour Method to Develop Residual Stresses

The contour method is one of the more recent techniques developed to determine the residual stress distribution with a given body. Developed and first published in 2001 by Dr. Mike Prime, it allows for some incredibly power conclusions to be made based on the information provided.[164,165] However, due to the complexity of the de-noising, smoothing, and fitting processes used to take the measured displacements and convert them to boundary conditions for a FEA simulation, there is the real possibility that significant intra- and interlaboratory uncertainty can result associated with the residual stress information produced by this method. Within this dissertation only the data processing section of the contour method was investigated, developed and implemented to determine residual stresses from provided displacements. In addition to this very complex mathematical and statistical aspect of the contour method, the actual cutting of the part suggests new technical challenges. It is well known that as the wire enters and exits the part cutting artifacts can be introduced influencing the level of uncertainty of the determined residual stresses. Techniques such as "sacrificial layering" has been explored in an effort to minimize these effects that can and do occur during the metrology phase of

the contour method.[166]

With all of these complex aspects associated with the contour method there is currently no standard practice by which an individual can use to develop residual stresses via the contour method. The best that is available is a journal paper discussing the aspects of the contour method in general terms.[167]

This lack of a standardized process, or protocol, has the potential to complicate the acquisition of these residual stresses. It is therefore recommended that efforts be put into place to establish either a standard for the development of residual stresses via the contour method, or that there be some type of qualification plan standardized by which a provider of these residual stresses may become "certified" in some way to allow there to be confidence in the data produced. For organizations around the world that develop residual stresses via the contour method the idea of a "standard" for the development of residual stresses is very disturbing. Each organization that is in the business of determining and selling residual stresses has proprietary methods that have been developed to provide them with a competitive edge in the global market. This type of competition is healthy and is needed to enable the technology to further develop. The purchaser of these datasets, however, currently has no understanding of the uncertainty associated with the data coming out of a single organization, for a given geometry and residual stress distribution. They know even less as to what the interlaboratory uncertainty would be for that same geometry and distribution.

13.2 Quantification of Spatial Residual Stress Data Density on the Development of Residual Stress Fitting Function for Implementation into StressCheck®

An area of future research that is needed is to determine the level of residual stress density that must be developed if a high-order, bivariant polynomial is going to be used to develop residual SIFs. Through this work it was determined that if the spatial density was less than the spatial separation of the nodes along the crack front, that the residual stress fit would bounce and caused significant shifts in the calculated SIF and the final life prediction. A sensitivity study should be performed to capture the optimal fit for the residual stress data and to also check any additional sources of uncertainty this process may introduce. For this work the final residual stress data from the FEA was linearly interpolated from a 0.015 inch grid spacing to a grid spacing of 0.005 inch. This process has the potential to introduced additional uncertainties into the residual stress data used within the FEA. Others have developed residual stresses at a grid density of 0.005 inch from their FEA simulation. For the work that was done here all of the FEA simulations connected with the contour method used brick elements that function very well for these types of calculations, but it was not possible to get the mesh density to that close to the spacing of the crack front nodes.

13.3 Sensitivity Study Using Different Material Models for Fatigue Crack Growth Properties

Through this research it was again noted that material model has a significant influence on the fatigue life prediction and should be investigated further to help clarify the importance of gather “accurate” data in specific ranges of the da/dN vs. ΔK material files. In an effort to gain greater understanding of the area of the da/dN vs. ΔK curve

where most of the fatigue growth occurred, plots were developed, plotting da/dN vs. ΔK versus the surface and bore crack lengths. The purpose of this was to allow for future efforts to be performed tailoring material files to focus in on these areas. However, this becomes very problematic for spectrum loading. For these types of loading conditions a range of Stress Ratios (Rs) are required to be developed and if the spectrum includes low and high loads, then it may be required that focus be made at even farther down in the da/dN vs. ΔK range, or up higher towards instability. For the work performed herein the majority of the life was focused in the dc/dN range from 10^{-7} to 10^{-5} cycles per inch. This range of crack growth rates is not commonly referred to as "near threshold". However, if there are slight differences in material files in these ranges, this can have the potential to cause a significant shift in the correlated crack growth rate and thus shift the life significantly. Thus a focused sensitivity study with different material models would be a powerful way to quantify these effects and give some guidance on the future development of material files when used in life predictions with engineered residual stresses, like those introduced by the Cx process.

13.4 Perform Interlaboratory Round Robin on Contour Method to Determine the Interlaboratory Uncertainty Associated with the Method

One starting point to help establish an understanding of the contour method's interlaboratory uncertainty is to perform an interlaboratory round robin across a range of residual stress determination companies or organizations. Through this it may be possible to establish one aspect of the total uncertainty associated with this residual stress determination method. It is recommended that the round robin be broken into phases to enable there to be specific aspects of the contour method that can be isolated and

quantified.

13.5 Development of a Standard Method for the Viewing of 2D Residual Stress Contour Plots

The research focused on within this body of work developed residual stresses for a range of conditions, including two materials, baseline uncracked coupons, and coupons at a range of fatigue crack sizes. Developing residual stresses for this many different configurations, and then having a desire to compare them presented significant problems in trying to relay 3D data in a 2D presentation space. Through the work here it was determined that line plots at a range of spatial distances away from the edge of the hole and through the thickness provided the most useful information with trying to determine differences in these 3D fields. However, this becomes very cumbersome, and has the potential to miss information that is present between these spaces, or that could be recognized through a more global view of the residual stress fields.

In most of the published resources there was a common trend to provide a contour plot of the entire spatial field and then break out specific line plots at locations of interest, however this leaves the user with a wide range of options when trying to present the data. The development of a standard for the presentation of 3D residual stress data would be very helpful to provide viewers and users of this data with a more standard approach to viewing and interpreting the information contained there-in. In some ways the number of plots that are contained within this dissertation were inserted to help reinforce this point. However, the data contained in each slice of this 3D field is of great value in determining responses to the question of difference between datasets.

13.6 Development of Methods for the Quantification of Statistically-Based Difference between Two 2D and (3D) Fields

The question of difference between two 2D or 3D data fields continues to puzzle statisticians to this day. The ability to determine statistical difference is well defined for a single point with replicates.[168] One can simply do a T-test, with a specified level of confidence, to determine statistically whether differences exist between datasets. However, this method has not been able to break through to its application to a line or a surface. It is possible to perform a T-test at every point along that line, determining for each point whether or not they are different, but when do those differences in points constitute a difference in the two surfaces being compared.

It is therefore recommended that research be pursued to investigate, quantify, and standardize spatial statistical methods whereby it would be possible to state, with confidence, that two lines or planes are different. The statistical quantification of these differences is essential as the aerospace structural management industry move towards defining methods for integrating the effects of engineered deep residual stress processes into the determination of initial and recurring inspection intervals for fatigue and fracture critical structures. Through the statistical quantification of these fields it will be possible to integrate them into statistically-based prediction method, instead of those based on fatigue tests and destructive tear down evaluations.[169]

13.7 Research into Additional Methods for the Application the Contour Integral Method for Loaded Cracks (CIM-LC) for Piecewise, Bivariant High Order Polynomial Functions Representing Residual Stress from the Cold Expansion Process

This research did not investigate different shape CIM-LC functions that could be used to represent the fatigue crack growth evolution at a Cxed hole. It is possible that one could use functions that are broken up by straight lines running through the thickness or by elliptical shaped functions. For fatigue cracks that have been developed and propagated at higher applied expansion levels a more unique shaped P-shape crack has been documented. Thus it is possible that a spline could be used as the shape function by which the residual stress would be adjusted due to the effect of the fatigue crack. For this work a rather simplistic semi-circular shape was selected as the predicted fatigue crack shape that would be developed within the part, and thus most closely represent the shape of the crack that was in the body through the thickness at the time when each coupon was cut for the contour method.

In order accomplish this it would be recommended that fatigue tests be performed at different stress levels, loading sequences, applied expansions and other influential factors, with the inclusion of marker bands to determine the shapes of fatigue cracks as they nucleate/form and then propagate away from the edge of Cxed hole. This evidence would allow for a level of confidence in the establishment of a standard equation or series of equations that would be used, if it is necessary to apply a correction for the effect of the fatigue crack on the residual stress, in the application of the residual traction stress at the crack front.

13.8 Perform Similar Residual Stress Determination Methods on Similar Coupon Designs to Cross-Verify the Findings from the Contour Method

All of the residual stresses determined within this body of work were developed through the use of the contour method. This is just one residual stress determination method that is available to quantify the through-thickness residual stress field at a Cxed hole. Other methods such as X-ray Diffraction (XRD) and Neutron Diffraction are potential options for the quantification of the residual stress field at Cxed holes, and then to perform a similar exercise to develop fatigue cracks within replicate coupons and determine the influence of that fatigue crack on the residual stress field. There are significant limitations on the specimen geometry for these methods, along with the cost of using a facility which has these residual stress determination techniques. The time associated with these measurement techniques also limits the quantity of specimens which could be included in the experiment, however through the use of these other techniques it could be possible to cross-correlate specific points within the test matrix that is contained within this body of work.

The use of multiple residual stress determination techniques to quantify the residual stresses within a body can provide confidence in each method, however it is essential that the spatial uncertainty also be quantified for each method used in this cross-comparison. This uncertainty quantification is often lacking or is not presented in the published findings and is key to developing confidence in one or more of the techniques used. This type of method could be used to again look at the effect of a fatigue crack on the residual stress field introduced by the Cx process in these two aluminum alloys. Doing so would help to build confidence that the effects quantified in this work should be considered when future implementation of deep engineered residual stresses into the

calculations for initial and recurring inspection intervals for fatigue and fracture critical structural applications.

13.9 The Expansion of the Test Matrix to Develop Fatigue Cracks in Different Thickness Materials, Applied Expansions, Hole Off-sets, and Develop Fatigue Cracks Using Different Loading Sequences

The research program contained herein was to answer the question of whether or not a fatigue crack has an influence on the residual stress field introduced by the Cx process in just two aluminum alloys. The evidence from this work shows that the effect of the fatigue crack on the residual stress field is not the same for the two alloys. The evidence show that these two alloys have very different effects from the presence of the fatigue crack. It is therefore recommended that additional research be performed in other alloys in which the Cx process is often performed to help its improve the fatigue performance.

In addition to adding additional materials, forms, or heat treatments to the matrix it would be very important to look at the other end of the applied expansion range, within the applicable specification. All of the work performed herein was done at the "low" end of the applied expansion range for a 0.50 inch final reamed diameter hole. This was done to look at the conservative[‡] case where the tolerance stack-up introduced a residual stress field which was not as highly compressive as it would be if the mean or high end of the applied expansion level was able to be produced.

It has been shown that spectrum, maximum spectrum stress, or spectrum with

[‡] The term conservative within this context means that not all of the potential benefit of the Cx process was taken advantage of, thus potentially reducing the fatigue benefit offered by the Cx process for the researched conditions applied herein.

high levels and numbers of cycles with compression have the ability to dramatically effect on the residual stress field introduced by the Cx process.[170,171,172,173] In addition to this the edge margin of a fastener hole that is to be Cxed has an impact on the boundary constraint at that hole and thus has been shown to have an influence on the residual stress field introduced and may also effect the manner in which a fatigue crack influences that imposed strain/stress field.[64,174,175]

The list of additional factors that can influence the residual stress field introduced by the Cx process is extensive. Thus it is recommended that an experimental test matrix of influential factors be developed that includes material, applied expansion, edge margin, thickness, hole diameter, loading sequence (constant amplitude and spectrum) levels of compressive overloads within the sequence, fastener installation (hole fill), and load transfer (high and low levels of load transfer). Within this large design of experiments a range of fatigue cracks could be developed, from the research contained herein it would be recommended that these crack sizes not exceed 0.125 inch on the Cx mandrel entrance surface. These coupons would then have the residual stress determined and with the use a more robust set of spatial statistical methods, and additional baseline, uncracked residual stress fields, it would be possible to quantify the effect of each factor on the spatial residual stress field.

13.10 Perform Additional Residual Stress Determinations on the 7075-T651 Alloy in Order to Determine if the Baseline, Uncracked Data is Inaccurate or if the Fatigue Crack has Significant Impact on Field, as Determined Herein

This researched highlighted a significant difference in the effect of a fatigue crack on the residual stress field introduced by the Cx process in two common aerospace

aluminum alloys. The 7075-T651 alloy exhibited a response that was not expected. From the residual stresses determined by the contour method the material seemed to have no residual stress response that correlated to the evolved fatigue crack size. This was dramatically different from that demonstrated in the 2024-T351 alloy. The 2024-T351 response seemed to be more of what was expected, in that it had a correlated shift in the residual stress field as a function of fatigue crack size. Thus it is recommended that additional focused research be performed on the 7075-T651 material to determine if this response was unique for the process developed and implemented herein. Historically the 7075-T651 material has been the most difficult to accurately predict fatigue behavior on when it has been Cxed.[176] From this research it would seem that as the effect of the fatigue crack is integrated into the fatigue life prediction it is possible to obtain a more accurate life prediction. This provides some additional level of confidence that the effect, determined by the contour method developed for this research, is somewhat accurately quantified.

13.11 Investigation into Differences in the Fatigue Crack Growth Rate Near the Edge of the Hole (from the Edge to Approximately 0.10 inch)

All of the fatigue life predictions developed using the baseline, uncracked and the fatigue-cracked residual stresses could not accurately represent the test demonstrated fatigue crack growth rate near the edge of the hole. Each of the predictions showed a nearly flat growth rate from the IFS to about 0.125 inch away from the edge of the hole on the Cx mandrel surface. However, all of the fatigue tests demonstrated a much faster crack growth rate from the edge of the hole to approximately 0.08 inch, and then the rate

would drop off and finally it would go critical and the rate would be exponential. Therefore, the sensitivities highlighted earlier should be further investigated.

APPENDIX: SUPPLEMENTAL MATERIAL

1. Appendix A – Modified Thompson Tau Matlab Code for the Removal of Statistical Outliers

2. Appendix B – Residual Stress Line Plots for Baseline Uncracked Coupons – CxA2 (2024-T351)

3. Appendix C – Total Single Measurement Uncertainty Contour Plots for Baseline Uncracked CxA2 Coupons

4. Appendix D – Total Single Measurement Uncertainty Contour Plots for Baseline Uncracked CxD2 Coupons

5. Appendix E – Residual Stress Line Plots Comparing Single Measurement Uncertainty for CxA2 Coupons to Repeatability Uncertainty

6. Appendix F - Residual Stress Line Plots Comparing Single Measurement Uncertainty for CxD2 Coupons to Repeatability Uncertainty

7. Appendix G – Macro Images of Post Wire EDM Cut per the Contour Method for Coupons Cx4N1-XX-B (2024-T351) and Cx4N1-XX-D (7075-T651)

8. Appendix H – Residual Stress Crack Face Traction Equations for CxA2 (2024-T351) Coupons for StressCheck® Implementation (Left Side Only)

9. Appendix I – Residual Stress Crack Face Traction Equations for CxD2 (7075-T651) Coupons for StressCheck® Implementation (Left Side Only)

10. Appendix J – Contour Plots of Applied Residual Stress within StressCheck® (Left Side Only)

11. Appendix K – Residual Stress Fit Surface Plots and Residual Fits for Cx4N1-XX-B (2024-T351) Coupons

12. Appendix L – Residual Stress Fit Surface Plots and Residual Fits for Cx4N1-XX-B (2024-T351) Coupons

13. Appendix M – Residual Stress Fit Surface Plots and Residual Fits for Cx4N1-XX-D (7075-T651) Coupons

14. Appendix N – Residual Stress Crack Front Traction Equations for all of the Cx4N1-XX-D (7075-T651) Coupons for StressCheck® Implementation

15. Appendix O – Contour Plots of Applied Residual Stress within StressCheck® (Left Side Only) for Fatigue Cracked Cx4N1-XX-B (2024-T351) Coupons

16. Appendix P – Contour Plots of Applied Residual Stress within StressCheck® (Left Side Only) for Fatigue Cracked Cx4N1-XX-D (7075-T651) Coupons

REFERENCES

[1] Department of Defense. *DoD Joint Service Specification Guide, Aircraft Structures*, (JSSG-2006). USA: ASC/ENSI; 1998.

[2] United States Air Force. *Air Force Material Command. Department of Defense Standard Practic, Aircraft Structural Integrity Program (ASIP), Report Number MIL-STD-1530D*. USA: USAF-ASC/ENI; 2008.

[3] Fatigue Technologies Inc. *FTI Process Specification 8101D Cold Expansion of Holes Using the Standard Split Sleeve System and Countersink Cold Expansion (CsCx™).* USA: Fatigue Technologies Inc.; 2002.

[4] Phillips, J.L. *Sleeve Coldworking Fastener Holes*, *Vol. I, AFML-TR-74-10*. USA: Air Force Materials Laboratory; 1974.

[5] Fatigue Technologies Inc. *Extending the Fatigue Life of Metal Structures, Materials Testing*. USA: Fatigue Technologies Inc.; 1991.

[6] Rufin, A.C. Extending the Fatigue Life of Aircraft Engine Components by Hole Cold Expansion Technolgy. J. Engng. Gas Turb. Power. 1993;115: 165–171.

[7] McClung, R.C. A Literature Survey on the Stability and Significance of Residual Stresses During Fatigue. Fatigue Fract. Engng. Mater. Struct. 2007;30: 173–205.

[8] Sha, G.T., Cowles, B.A., Fowler, R.L. Fatigue Life of a Coldworked Hole. In: *Proceedings of the Emerging Technologies in Aerospace Structures Design, Structural Dynamics and Materials Proceedings, The Aerospace Conference – Century 2 – Emergying Technology Conference*. San Francisco: 1980.

[9] Ball, D.L. Elastic-Plastic Stress Analysis of Cold Expanded Fastener Holes. Fatigue Fract. Engng. Mater. Struct. 1995;18: 47 – 63.

[10] Armen, H., Levy, A., Eidinoff, H.L. Elastic-Plastic Behaviour of Coldworked Holes. J. Aircraft. 1984;21: 193 – 201.

[11] Gong-Fan, S., Young, C., Yan, C. Cold Expanding of Holes Improves Fatigue-Life of Aluminum Alloy Components, In: *Proceeding of an International Conference Fatigue Prevention and Design.* Amsterdam: 1986.

[12] Buch, A., Berkuvits, A. Effect of Cold-Working by Hole Expansion on Fatigue Life of AlZn-Alloy Lugs under Maneuver Loading, In: *Proceeding of an International Conference Fatigue Prevention and Design.* Amsterdam: 1986.

[13] Ball, D.L., Lowry, D.R. Experimental Investigation on the Effects of Cold Expansion of Fastener Holes. Fatigue Fract. Engng. Mater. Struct. 1998; 21: 17 – 34.

[14] Chakherlou, T.N., Vogwell, J. The Effect of Cold Expansion on Improving the Fatigue Life of Fastener Holes. Eng. Failure Anal. 2002;10: 13 – 24.

[15] Chandawannich, N., Sharpe, W.N. An Experimental Study of Fatigue Crack Initiation and Growth from Cold Worked Holes. Eng. Fract. Mech. 1979;1: 609 – 620.

[16] Chang, J.B. Prediction of Fatigue Crack Growth at Cold-Worked Fastener Holes. J. Aircraft. 1977;14: 903 – 908.

[17] Lai, M.O., Oh, J.T., Nee, A.Y.C. Fatigue Properties of Holes with Residual Stresses. Eng. Fract. Mech. 1993;45: 551 – 557.

[18] Lai, M.O., Siew, Y.H. Fatigue Properties of Cold Worked Holes. J. Mat. Processing Tech. 1995;48: 533 – 540.

[19] Kokaly, M.T., Ransom, J.S. Predicting Fatigue Crack Growth in the Residual Stress Field of a Cold Worked Hole. J. of ASTM Int. 2005;2: 119 – 131.

[20] Kokaly, M.T., Ransom, J.S., Jude, B.S., Retis, H., Reid, L. Observations and Analysis of Fatigue crack Growth from Cold Worked Holes. In: *Proceedings of the 8th Joint FAA/DoD/NASA Aging Aircraft Conference*. Palm Springs: 2005

[21] Jones, K.W., Dunn, M.L. Predicting Corner Crack Fatigue Propagation from Cold Worked Holes. Eng. Fract. Mech. 2009;76: 2074 – 2090.

[22] Newman, J.C., Raju, I.S. Stress Intensity Factor Equations for Cracks in Three-Dimensional Bodies Subjected to Tension and Bending Loads. In: Chapter 9, *Computational Methods in the Mechanics of Fracture*. Amsterdam: Elsvier Science Publishing B.V; 1986.

[23] Pavier, M.J., Poussard, C.G.C., Smith, D.J. A Finite Element Simulation of the Cold Working Process for Fastener Holes. J. Strain Anal. 1997;32: 287 – 300.

[24] Papanikos, P. Meguid, S.A. Three-Dimensional Finite Element Analysis of Cold Expansion of Adjacent Holes. Int. J. Mech. Sci. 1998;40: 1019 – 1028.

[25] Chakherlou, T.N., Vogwell, J. The Effect of Cold Expansion on Improving the Fatigue Life of Fastener Holes. Engng. Failure Anal. 2003;10: 13 – 24.

[26] Kang, J., Johnson, W.S., Clark, D.A. Three-Dimensional Finite Element Analysis of the Cold Expansion of Fastener Holes in Two Aluminum Alloys. J. Engng. Mater.

Technoo. 2002;124: 140 – 145.

[27] Zhang, Y., Edwards, L. Fitzpatrick, M.E. Finite Element Simulation of Hole Cold Expansion Process in EN8 Steel Plate. In: *Proceedings of the UK ABAQUS User Group Conference*. UK: 2002.

[28] Herman, R. Three-dimensional Stress Distribution around Cold Expanded Holes in Aluminum Alloys. Eng. Fract. Mech. 1994;48: 819 – 835.

[29] Ozdemir, A.T., Edwards, L. Measurement of the Three-Dimensional Residual Stress Distribution Around Split-Sleeve Cold-Expanded Holes. J. Strain Anal. 1996;31: 413 – 421.

[30] Priest M. *The Experimental Characterisation of Residual Stresses and Fatigue crack Growth in the Vicinity of Cold Worked Holes in Al 2024-T351*. Ph.D. Thesis, Mechanical Engineering Department, University of Bristol, Bristol: 1997.

[31] Stefanescu, D., Bouzina, A., Dutta, M., Wang, D.Q., Fitzpatrick, M.E., Edwards, L. Comparison of Residual Stress Measurements Using Neutron and X-ray Diffraction around a Cold Expanded Hole. J. Neutron Res. 2002;9: 399 – 405.

[32] Zhang, Y., Fitzpatrick, M.E., Edwards, L. Measurement of the Residual Stresses Around a Cold Expanded Hole in an EN8 Steel Plate Using the Contour Method. Mater. Sci. Forum. 2002;404 – 407: 527 – 532.

[33] Stefanescu, D. Measurement and Prediction of Fatigue Crack Growth from Cold Expanded Holes Part 1: The Effect of Fatigue crack Growth on Cold Expansion Residual Stresses. J. Strain Anal. 2004a;38: 25 – 39.

[34] Stefanescu, D. Measurement and Prediction of Fatigue crack Growth from Cold Expanded Holes Part 2: Prediction of Fatigue crack Growth from Cold Expanded Holes. J. Strain Anal. 2004b;39: 41 – 53.

[35] Oxford University Press. *The Compact Edition of the Oxford English Dictionary – Complete Text Reproduced Micrographically*. Oxford University Press, New York: 1971.

[36]Houghton Mifflin Company. *Webster's II New Riverside University Dictionary*. Houghton Mifflin Company, Boston: 1994.

[37] Savage, C.W. *The Measurement of Sensation – A Critique of Perceptual Psychophysics*, University of California Press, Berkeley: 1970.

[38] Campbell, N.R. Symposium: Measurement and Its Importance for Philosophy. In: *Proceedings of the Aristotelian Society, Supplement 17*. London: 1938: 126 – 127.

[39] Oxford University Press. *Oxford English Dictionary*, "determine, v", OED Online,http://www.oed.com.ezproxy.lib.utah.edu/view/Entry/51244?redirectedFrom=determine (accessed December 11, 2017).

[40] Wilson, E.O. *Consilience*. Vintage Books, a Division of Random House, New York: 1998.

[41] Bueckner, H.F. A Novel Principle for the Computation of Stress Intensity Factors. Z. Angew. Mathematik und Mechanic. 1970;50: 529 – 546.

[42] Rice, J.R. Some Remarks on Elastic Crack-tip Stress Fields. Int. J. Solids Structs. 1972;8: 751 – 758.

[43] Pavier, M.J., Poussard, C.G.C., Smith, D.J. Effect of Residual Stress around Cold Worked Holes on Fracture under Superimposed Mechanical Load. Engng. Frac. Mech. 1999;63: 751 – 773.

[44] Fitzpatrick, M.E., Fry, A.T., Holdway, P., Kandil, F.A., Shackleton, J., Suominen, L. *Measurement Good Practice Guide, No. 52 – Determination of Residual Stresses by X-ray Diffraction – Issue 2*. National Physical Laboratory, Middlesex: 2005.

[45] SAE Fatigue Design and Evaluation Committee. *Residual Stress Measurement by X-ray Diffraction – SAE J784a*: Report of Iron and Steel Technical Committee. Society of Automotive Engineers (SAE), Warrendale: 1971.

[46] Prevey, P.S. X-Ray Diffraction Residual Stress Techniques. In: *Metals Handbook 10*. American Society for Metals, Metals Park, Lambda Research Inc., Cincinnati: 1986.

[47] DeWald, A., Hill, M., VanDalen, J., Pilarczyk, R., Andrew, D., Thomsen, M., Carlson, S., Marosok, D. Residual Stresses from Cold Working of Aircraft Fastener Holes. In: *Proceedings of the 2013 Aircraft Structural Integrity Program (ASIP) Conference*, Bonita Springs: 2013

[48] Mills, T., Post-Domasky, S.P., Pilarczyk, R., Andrew, D., Hodges, J. Modeling Fatigue Performance at Cold Worked Fastener Holes. In: *Proceedings of the 2013 Aircraft Structural Integrity Program (ASIP) Conference*, Bonita Springs: 2013

[49] Shang-Xian, W. Shape Change of Surface Crack During Fatigue Crack Growth. Eng. Fract. Mech. 1985;22: 897 – 913.

[50] Lin, X.B., Smith, R.A. Fatigue Shape Analysis for Corner Cracks at Fastener Holes. Eng. Fract. Mech. 1988;59: 73-87.

[51] Seog Oh, C., Park. P., Hak Huh, Y., Gyu Ko, S., Young Hwang, D., Mo An, H. Fatigue Crack Growth Behavior of Corner Cracks under LBH Loading. Key Eng. Mater. 2005;297-300: 128 – 136.

[52] Andrew, D., Pilarczyk, R., Feiger, J., Smith, L. Influence of ‘a’ Crack Tip Material Properties on Corner Crack Shape and Aspect Ratio. In: *Proceedings of the 2015 AFGROW Workshop*, Layton: 2015.

[53] Chandawanich, N., Sharpe, W., N. An Experimental Study of Fatigue Crack Initiation

and Growth from Coldworked Holes. Engng. Frac. Mech. 1979;11: 609 – 620.

[54] Carlson, S.S. *Experimentally Derived Beta Corrections to Accurately Model the Fatigue Crack Growth Behavior at Cold Expanded Holes in 2024-T351 Aluminum Alloys*. Masters Thesis, University of Utah, Salt Lake City: 2008.

[55] Pell, R.A., Braver, P.W., Mann, J.Y., Sparrow, J.G. Fatigue of Thick-Section Cold-Expanded Holes with and without Cracks. Fatigue Frat. Engng Mater. Struct. 1989;12: 553 – 567.

[56] Mills, T.B., Honeycutt, K.T., Prost-Domasky, S.A., Brooks, C.L. *Integrating Residual Stress Analysis of Critical Fastener Holes into USAF Depot Maintenance*, Report Number A3G-2015-185420, Air Force Life Cycle Management Center, Hill AFB: 2015.

[57] Pilarczyk, R. T., Sedgwick, H., Stowe, G. Integration of Finite Element Models to Determine Stress Intensities for Crack Growth Analysis with Load Re-Distribution, In: *Proceedings of the 2011 Aircraft Airworthiness & Sustainment Conference*, San Diego: 2011.

[58] Engineering Software Research & Development (ESRD). *StressCheck® Master Guide*, Release 10.2, St. Louis: 2015

[59] Chen, T., Xiao, Z.G., Zhao, X.L., Gu, X.L. A Boundary Element Analysis of Fatigue Crack Growth for Welded Connections under Bending. Eng. Frat. Mech. 2013;98: 44 – 51.

[60] Neves, A., Niku, S.M., Baynham, J.M.W., Adey, R.A. Automatic 3D Crack Growth Using BEASY. In: *Proceedings of the 19th Boundary Element Method Conference*, Computational Mechanics Publications, Southampton: 1997.

[61] Mellings, S.C., Baynham, J.M.W., Adey, R.A. Advances in Crack Growth Modelling of 3D Aircraft Structures. In: Bos, M., eds. *Proceedings of the 25th International Committee on Aeronautical Fatigue (ICAF), Bridging the Gap between Theory and Operational Practice*, New York: Springer Science + Business Media; 2009.

[62] Wawrzynek, P., Carter, B. *FRANC3D/NG Reference Manual*, Cornell Fracture Group (http://cfg.cornell.edu), New York: 2007.

[63] Galyon, S.E., Saravanan, R., Arunachalam, R., Greer, J., Hammond, M., Fawaz, S.A. Three Dimensional Crack Growth Prediction. In: Bos, M., ed. *Proceedings of the 25th International Committee on Aeronautical Fatigue (ICAF), Bridging the Gap between Theory and Operational Practice*, New York: Springer Science + Business Media; 2009.

[64] Andrew, D.L. *Investigation of Cold Expansion of Short Edge Margin Holes with Pre-Existing Cracks in 2024-T351 Aluminum Alloy*. Masters Thesis, Mechanical Engineering Department, University of Utah, Salt Lake City: 2011.

[65] Warner, J.W. *Cold Expansion Effects on Cracked Fastener Holes Under Constant*

Amplitude and Spectrum Loading in the 2024-T351 Aluminum Alloy. Masters Thesis, Mechanical Engineering Department, University of Utah, Salt Lake City: 2012.

[66] Vallieres, G.M., Duquesnay, D.L. Fatigue Life of Cold-Expanded Fastener Holes with Interference Fit Fasteners at Short Edge Margins. Fatigue Fract. Engng. Mater. Struct. 2014;38: 1 – 9.

[67] Backman, D., Rutledge, R., Yanishevsky, M. Experimental Measurements of Strain Changes Around Fastener Holes During Cold-Expansion. In: *Proceedings of the 2006 SEM Annual Conference & Exposition on Experimental and Applied Mechanics,* St. Louis: 2006.

[68] Ozdemir, A.T., Edwards, L. Relaxation of Residual Stresses at Cold-Worked Fastener Holes Due to Fatigue Loading. *Fatigue Frat. Engng Mater. Struct*. 1997;20: 1443 – 1451.

[69] Toparli, M., Ozel, A., Aksoy, T. Effect of the Residual Stresses on the Fatigue Crack Growth Behaviour at Fastener Holes. Mater. Sci. Engng. A: Structural Materials: Properties, Microstructure and Processing. 1997;A225: 196 – 203.

[70] Almer, J.D., Cohen, J.B., Winholtz, R.A. Effects of Residual Macrostresses and Microstresses on Fatigue Crack Propagation. Mat. Mater. Trans. A: Physical Metallurgy and Materials Science. 1998;29A: 2127 – 2136.

[71] Wang, D.Q., Edwards, L. Neurton Diffraction Determination of the Complete 3D Residual Stress Distribution Surrounding a Cold Expanded Hole. In: *Proceedings of the 4th European Conference on Residual Stresses*, Cluny en Bourgogne: 1998.

[72] Pilarczyk, R.T. *Experimentally Derived Beta Corrections to Predict Fatigue crack Growth at Cold Expanded Holes in 7075-T651 Aluminum Alloy*. Masters Thesis, Mechanical Engineering Department, University of Utah, Salt Lake City: 2008.

[73] Mills, T.B., Prost-Domasky, S.A., Pilarczyk, R., Andrew, D., Hodges, J. Modeling Fatigue Performance at Cold Worked Fastener Holes. In: *Proceedings of the 2013 Aircraft Structural Integrity Program (ASIP) Conference*, Bonita Springs: 2013.

[74] DeWald, A., Hill, M., VanDalen, J., Pilarczyk, R., Andrew, D., Thomsen, M., Carlson, S., Marosok, D. Residual Stresses from Cold Working of Aircraft Fastener Holes. In: *Proceedings of the 2013 Aircraft Structural Integrity Program (ASIP) Conference*, Bonita Springs: 2013.

[75] Prime, M.B. Cross-Sectional Mapping of Residual Stresses by Measuring the Surface Contour after a Cut. J. Eng. Mater. Tech. 2001;123: 162 – 168.

[76] Prime, M.B., Gonzales, A.R. Contour Method: Simple 2-D Mapping of Residual Stresses. In: *Proceedings of the 6th International Conference onf Residual Stresses*, IOM Communications, London: 2000: 617 - 624

[77] Bueckner, H. The Propagation of Cracks and the Energy of Elastic Deformation. Trans.

Am Soc. Mech. Eng. 1958;80: 1225 – 1230.

[78] Bueckner, H. Novel Principle for the Computation of Stress Intensity Factors. Zeitschrift fuer Angewandte Mathematik & Mechanik. 1970;50: 529 – 546.

[79] Bueckner, H. Field Singularities and Related Integral Representations. In: Sih, G.C., ed. *Methods of Analysis and Solutions of Crack Problems, Vol. 1*, Noordhoff, Leyden: 1973: 239 – 341.

[80] Kelleher, J., Prime, M.B., Buttle, D., Mummery, P.M., Webster, P.J., Shackleton, J., Withers, P.J. The Measurement of Residual Stress in Railway Rails by Diffraction and Other Methods. J. Neutron Res. 2003;11: 187 – 193.

[81] Brown, D.W., Holden, T.M., Clausen, B., Prime, M.B., Sisneros, T.A., Swenson, H., Vaga, J. Critical Comparison of Two Independent Measurements of Residual Stress in an Electron-Beam Welded Uranium Cylinder: Neutron Diffraction and Contour Method. Acta. Mater. 2011;59: 864 – 873.

[82] Prime, M.B., DeWald, A.T. The Contour Method. In: Schajer, G.S., ed. *Practical Residual Stress Measurement Methods*, West Sussex John Wiley & Sons West Sussex: 2013.

[83] Prime, M.B., Sebring, R.J., Edward, L.M., Hughes, D.J., Webster, P.J. Laser Surface-Contouring and Spline Data-Smoothing for Residual Stress Measurement. Exp. Mech. 2004;44: 176 – 184.

[84] Prime, M.B. The Contour Method: Capabilities, Limitations, and Recent Advances. In: *Proceedings of the 4th Residual Stress Summit*, Lake Tahoe: 2010.

[85] Hosseinzadeh, F., Kowal, J., Bourchard, P.J. Towards Good Practice Guidelines for the contour method of Residual Stress Measurement. J. Eng. 2014;2014: 453 – 468.

[86] Cheng, W., Finnie, I., Gremaud, M., Prime, M.B. Measurement of Near Surface Residual Stresses Using Electric Discharge Wire Machining. ASME J. Eng. Mater. Technol. 1994;116: 1 – 7.

[87] Kunieda, M., Lauwers, B., Rajurkar, K.P., Schumacher, B.M. Advancing EDM through Fundamental Insight into the Process. CIRP Ann. Manuf. Technol. 2005;54: 64 – 87.

[88] Cheng, W., Gremaud, M., Finnie, I., Prime, M.B. Measurement of Near Surface Residual Stresses Using Electric Discharge Wire Machining. J. Eng. Mater. Technol. 1994;116: 1 – 7.

[89] Spedding, T.A., Wang, Z.Q. Parametric Optimization and Surface Characterization of Wire Electrical Discharge Machining Process. Precis. Eng. 1997;20: 5 – 15.

[90] Traore, Y., Bouchard, P.J., Francis, J.A., Hosseinzadeh, F. A Novel Cutting Strategy

for Reducing Plasticity Induced Errors in Residual Stress Measurements Made with the Contour Method. In: *Proceedings of the American Society of Mechanical Engineers*, Pressure Vessels and Piping Division (Publication) PVP, Proc. ASME Pressure Vessels and Piping Conf. – Materials and Fabrication, Baltimore: 2011.

[91] Hosseinzadeh, F., Ledgard, P., Bourchard, P.J. Controlling the Cut in Contour Residual Stress Measurements of Electron Beam Welded Ti-6Al-4V Alloy Plates. Exp. Mech. 2012;53: 829 – 839.

[92] Bourchard, P.J., Ledgard, P., Hiller, S., Hosseinzadeh, F. Making the Cut for the Contour Method. In: *Proceedings of the 15th Int. Conf. on Experimental Mechanics*, Porto: 2012.

[93] Traore, Y. *Controlling Plasticity in the Contour Method of Residual Stress Measurements*. Ph.D. Dissertation, The Open University, Milton Keynes: 2013.

[94] Hosseinzadeh, F., Bouchard, P.J., Kowal, J. Surface Profile Measurement for the Contour Method. In: *OU/MatsEng/019*, Issue 1, The Open University, Milton Keynes: 2011.

[95] Prime, M.B., Sebring, R.J., Edwards, J.M., Hughes, D.J., Webster, P.J. Laser Surface-Contouring and Spline Data-Smoothing for Residual Stress Measurements. Exp. Mech. 2004;44: 176 – 184

[96] Johnson, G. *Residual Stress Measurements Using the Contour Method*. Ph.D. Dissertation, University of Manchester, School of Materials, Manchester: 2008.

[97] MathWorks. Language Fundamentals Toolbox: User's Guide (R2015R). In: *Language Fundamentals, Matrices and Arrays, Array Creation and Concatenation, Meshgrid*. Natick: Retrieved August 2, 2016.

[98] MathWorks. Polynomial Function Toolbox: User's Guide (R2015R). In: *Language Fundamentals, Matrices and Arrays, Array Creation and Concatenation, Meshgrid*. Natick: Retrieved August 2, 2016.

[99] Prime, M.B., Kastengre, A.L. The Contour Method Cutting Assumption: Error Minimization and Correction. In: *Proceedings of the SEM Annual Conference & Exposition on Experimental and Applied Mechanics* Indianapolis: 2010.

[100] Thompson, W.R. On a Criterion for the Rejection of Observations and the Distribution of the Ratio of Deviation to Sample Standard Deviation. Ann. Math. Stat. 1935;6: 214-219.

[101] Wheeler, A.J., Ganji, A.R. *Introduction to Engineering Experimentation.* Upper Saddle River: Pearson Education, Inc; 2004.

[102] Abernethy, R.B., Benedict, R.P., Dowdell, R.B. ASME Measurement Uncertainty. J. Fluids Eng. 2001;107: 161 – 164.

[103] ASTM International. *Standard Practic for Dealing with Outlying Observations*, E178-08. West Conshohocken: ASTM International; 2008.

[104] Klawikowski, S.J., Zeringue, Cl, Wootton, L.S., Ibbott, G.S., Beddar, S. Preliminary Evaluation of the Dosimetric Accuracy of the In Vivo Plastic Scintillation Detector OARtrac System for Prostate Cancer Treatments. Phys. Med. Biol. 2014;59: N27 – N36.

[105] Shen, Q., Yang, R. Thompson-Tau Outlier Detection Method for Detecting Abnormal Data of Listed Pharmaceutical Companies in China. In: *Proceedings of the 8th International Symposium on Computational Intelligence and Design*, Hangzhou: 2015.

[106] Pagliaro, P., Prime, M.B., Swenson, H., Zuccarello, B. Measuring Multiple Residual-Stress Components Using the Contour Method and Multiple Cuts. Exp. Mech. 2010;50: 187 – 194.

[107] Prime, M.B. Contour Method Advanced Applications: Hoop Stresses in Cylinders and Discontinuities. In: Proulx T. ed. *Engineering Applications in Residual Stress*, The Society of Experimental Mechanics: 2011: 13 – 28.

[108] Brown, D.W., Holden, T.M., Clausen, B., Prime, M.B., Sisneros, T.A., Swenson, H., Vija, J. Critical Comparison of Two Independent Measurements of Residual Stress in an Electron-beam Welded Uranium Cylinder: Neutron Diffraction and the Contour Method. Acta. Mater. 2011;59: 864 – 873.

[109] Prime M.B., Sebring, R.J., Edwards, J.M., Baumann, J.A., Lederich, R.J. Contour Method Determination of Parent Part Residual Stresses Using a Partially Relaxed FSW Test Specimen. In: *Proceedings of the SEM X Int. Congress and Exposition on Experimental and Applied Mechanics*, Costa Mesa: 2004.

[110] Farin, G. *Curves and Surfaces for CAGD – A Practical Guide*, 5th Edition. San Diego: Academic Press, - A Harcourt Science and Technology Company; 2002.

[111] Prautzsch, H., Boehm, W., Paluszny, M. *Bézier and B-Spline Techniques*. New York: Springer-Verlag Berlin Heidelberg; 2002.

[112] MathWorks. Curve Fitting Toolbox: User's Guide (R2015R). In: *Curve Fitting Toolbox, Splines, Construction, Spap2.* Natick: Retrieved August 2, 2016.

[113] Battelle Memorial Institute. *Metallic Materials Properties Development and Standardization (MMPDS), Report Number MMPDS-06.* Columbus: Battelle; 2011: 3-95.

[114] Battelle Memorial Institute. *Metallic Materials Properties Development and Standardization (MMPDS), Report Number MMPDS-06.* Columbus: Battelle; 2011: 3-508.

[115] Sandia National Laboratory. Metrics for Quadrilateral Elements https://cubit.sandia.gov/public/15.1/help_manual/WebHelp/mesh_generation/mesh_quality_assessment/quadrilateral_metrics.htm, Retrieved May, 11, 2017

[116] Özdemir, A.T., Edwards, L. Through-Thickness Residual Stress Distribution after the Cold Expansion of Fastener Holes and its Effect on Fracturing. J. Eng. Mater. Technol. 2004;126: 129 – 135

[117] Hill, M.R., Olson, M.D. Repeatability of the Contour Method for Residual Stress Measurement. Exp. Mech. 2014;54: 1269 – 1277

[118] Olson, M.D. *Contour Method Advances for Uncertainty Estimation and Multiaxial Residual Stress Mapping*. Ph.D. Dissertation, University of California, Davis: 2015.

[119] Aerospace Industries Association of America. *Fastener – Recommended Shank, Hole and Head-to-Shank Fillet Radius Limits for,* Spec Number NAS618. Washington, D.C.: Aerospace Industries Association of America, Inc; 1992.

[120] Taylor, J.R. *An Introduction to Error Analysis*, *2nd Edition*. Sausalito: University Science Books; 1997.

[121] Coleman, H.W., Steele, W.G. *Experimentation, Validation, and Uncertainty Analysis for Engineers, 3rd Edition.* Hoboken: John Wiley & Sons, Inc.; 2009.

[122] Bell, S. *Measurement Good Practice Guide: A Beginner's Guide to Uncertainty of Measurement*. Teddington: National Physical Laboratory; 1999.

[123] Olson, M.D., DeWald, A.T., Prime, M.B., Hill, M.R. Estimation of Uncertainty for Contour Method Residual Stress Measurements. Exp. Mech. 2014;55: 577 – 585.

[124] Prime, M.B., Hill, M.R. Uncertainty, Model Error, and Other Selection for Series-Expanded, Residual-Stress Inverse Solutions. J. Eng. Mater. Technol. 2006;128: 175 – 185.

[125] Hammersley, J.M., Handscomb, D.C. *Monte Carlo Methods*. Norwich: Fletcher & Sons Ltd; 1964.

[126] Battelle Memorial Institute. *Metallic Materials Properties Development and Standardization (MMPDS), Report Number MMPDS-06.* Columbus: Battelle; 2011: 9-81.

[127] Nikon. *Nikon Measuring Microscope MM-40/60 Series (with Metallurgical Microscope) Instruments, Document Number E110E 99.2.TF.2*. Melville: Nikon; 2010: 32.

[128] Oh, C.S., Park, P., Huh, Y.H., Ko, S.G., Hwang, D.Y., An, H.M. Fatigue crack Behavior of Corner Cracks under LBH Loading. Key Eng. Mat. 2005;297-300: 128 – 136.

[129] Lin, X.B., Smith, R.A. Fatigue Shape Analysis for Corner Cracks at Fastener Holes. Eng. Fract. Mech. 1997;59: 73 – 87.

[130] Shang-Xian, W.U. Shape Change of Surface Crack During Fatigue Growth Eng.

Fract. Mech. 1985;22: 897 – 913.

[131] Andrew, D.L., Pilarczyk, R.T., Feiger, J., Smith, L. Influence of 'a' Crack Tip Material Properties on Corner Crack Shape and Aspect Ratio. In: *Proceedings of the 2015 AFGROW Workshop*. Layton: 2015.

[132] Hammersley, J.M., Handscomb, D.C. *Monte Carlo Methods*. New York: Meuthuen & Co., London, and John Wiley & Sons; 1964.

[133] Taylor, J.R. *An Introduction to Error Analysis – The Study of Uncertainties in Physical Measurements, 2nd Edition*. Sausalito University Science Books; 1997.

[134] Schajer, G.S., Ruud, C.O. Overview of Residual Stresses and Their Measurement. In: Schajer, G.S., ed. *Practical Residual Stress Measurement Methods*. West Sussex: John Wiley & Sons, Ltd.; 2013.

[135] Hodges, J.L., Carlson, S. Integration of Incremental Crack Front Evolution into the Structural Integrity Process: Examples, Experimental Comparisons, and Lessons Learned. In: *Proceedings of the 2014 USAF Aircraft Structural Integrity Program (ASIP) Conference*, San Antonio: ,2014.

[136] Hodges, J.L. BAMF – Implementing Advanced Solutions to Determine Inspection Times. In: *Proceedings of the 2013 Holistic Structural Integrity Process (HOLSIP) Workshop*, Salt Lake City: 2013.

[137] Spradlin, T.J., Hodges, J.L. Predictive Crack Growth Techniques for Laser Peening Process Development. J. Eng. doi: 10.1049/joe.2015.0110. 2015: 1 – 6.

[138] Hodges, J.L. Next Generation Crack Growth Predictions – Coupled Finite Element Modeling and Crack Growth. In: *Proceedings of the 2011 Aircraft Structural Integrity Program (ASIP) Conference*, San Antonio: 2011.

[139] Hodges, J.L. MuPMuC BAMF Updates and Improvements. In: *Proceedings of the 2016 Holistic Structural Integrity Process (HOLSIP) Workshop*, Salt Lake City: 2016.

[140] Riberio, R.L., Hill, M.R. Residual Stress from Cold Expansion of Fastener Holes: Measurement, Eigenstrain, and Process Finite Element Modeling. J. Eng. Mater. Tech. doi:10.1115/1.4037021. 2017;139: 1 – 13.

[141] Stuart, D.H., Hill, M.R., Newman, J.C. Correlation of One-Dimensional Fatigue Crack Growth at Cold-Expanded Holes Using Linear Fracture Mechanics and Superposition. Eng. Frac. Mech. 2011;78: 1389 – 1406.

[142] Actis, R., Watkins, M., Prost-Domasky, S., Hodges, J. Computation of SIFs for Cracks in Cold-Worked Holes. In: *Proceedings of the 2013 Aircraft Structural Integrity Program (ASIP) Conference*, Bonita Springs: 2013.

[143] Mills, T., Prost-Domasky, S., Pilarczyk, R., Andrew, D., Hodges, J. Modeling Fatigue

Performance at Cold Worked Fastener Holes. In: *Proceedings of the 2013 Aircraft Structural Integrity Program (ASIP) Conference*, Bonita Springs: 2013.

[144] Lei, Y., O'Dowd, N.P., Webster, G.A. Fracture Mechanics Analysis of a Crack in a Residual Stress Field. Int. J. Fract. 2000;3: 195 – 216.

[145] Pereira, J.P., Duarte, C.A. The Contour Integral Method for Loaded Cracks. Int. J. Numer. Metho. Biomed. Eng. 2006;22: 421 – 432.

[146] Carlson, S.S., Stanfield, M. Application of Uncertainty Quantification for Residual Stress Measurement at a Cold Expanded Hole. In: *Proceedings of the 2016 AFGROW Workshop*, Layton: 2016.

[147] Augustin, P. Simulation of Fatigue Crack Growth in the High Speed Machined Panel Under the Constant Amplitude and Spectrum Loading. In: *Proceedings of the 25th International Conference on Aeronautical Fatigue (ICAF) Symposium*, Rotterdam: 2009.

[148] Forman, R.G., Shivakumar, V., Cardinal, J.W., Williams, L.C., McKeigham, P.C. *Fatigue Crack Growth for Damage Tolerance Analysis Report Number DOT/FAA/AR-05-15*. US Department of Transportation, Federal Aviation Administration, Washington, D.C.: 2005.

[149] Skinn, D.A., Gallagher, J.P., Berens, A.P., Huber, P.D., Smith, J. *Damage Tolerant Design Handbook Report Number WL-TR-94-4052*. University of Dayton Research Institute, Dayton: 1994.

[150] Gallagher, J.P., Giessler, F.J., Berens, A.P. *USAF Damage Tolerant Design Handbook: Guidelines for the Analysis and Design of Damage Tolerant Aircraft Structure, Rev. B*. University of Dayton Research Institute, Dayton: 1984.

[151] Clark, D.A., Johnson, W.S. Temperature Effects on Fatigue Performance of Cold Expanded Holes in 7050-T7451 Aluminum Alloy. Int. J. Fatigue. 2003;25: 159 – 165.

[152] Chapra, S.C., Canale, R.P. *Numerical Methods for Engineers – with Software and Programming Applications, 4th Edition*. New York: McGraw Hill; 2002.

[153] Schijve, J. The Application of Small Overloads for Fractography of Small Fatigue Cracks Initiated under Constant-Amplitude Loading. Int. J. Fatigue. 2015;70: 63 – 72

[154] Bater, S.A., Molent, L., Wanhill, R.J.H., (2009). Marker Load for Quantitative Fractography of Fatigue Cracks in Aerospace Alloys. In: Bos, M., ed. *Proceedings of the 25th International Committee on Aeronautical Fatigue (ICAF), Bridging the Gap between Theory and Operational Practice*, New York: Springer Science + Business Media; 2009.

[155] Fawaz, S.A. *Fatigue Crack Growth in Riveted Joints*. Dissertation, Delft University of Technology, The Netherlands: 1997.

[156] Wanhill, R.J.H. *Damage Tolerance Engineering Property Evaluation of Aerospace*

Aluminum Alloys with Emphasis on Fatigue crack Growth, Report Number NLR-TR-94177L. The Netherlands: National Laboratory of the Netherlands; 1994.

[157] Mussert, K.M. *Fracture Surface Marking of Alclad 2024-T3 Sheet, Report Number NLR-CR-94456C.* The Netherlands: National Laboratory of the Netherlands; 1994.

[158] Mills, T.B., Honeycutt, K.T., Prost-Domasky, S.A., Brooks, C.L. *Verification of Cold Working and Interference Levels at Fastener Holes, Phase I, Report Number FA8650-08-M-3842*. St. Louis: APES, Inc; 2009.

[159] Prost-Domasky, S.A., Honeycutt, K.T., Mills, T.B., Brooks, C.L. *Verification of Cold Working and Interference Levels at Fastener Holes, Phase II, Report Number FA8650-09-C-3941*. St. Louis: APES, Inc; 2012.

[160] McClung, R.C. A Literature Survey on the Stability and Significance of Residual Stresses During Fatigue. Fatigue Fract. Engng. Mater. Struct. 2007;30: 173 – 205.

[161] Schajer, G.S. The Contour Method. In: Schajer, G.S., ed. *Practical Residual Stress Measurement Methods*, West Sussex John Wiley & Sons West Sussex: 2013.

[162] McClung, R.C., Popelar, C.F., McFarland, J., Bhamidipati, V., James, M.A., Watton, J.D., Hill, M.R., DeWald, A.T., Ball, D.L. Predicting Fatigue Crack Growth in Forgings with Bulk Residual Stresses. In: *Proceedings of the 2014 Aircraft Structural Integrity Program (ASIP) Conference*. San Antonio: 2014.

[163] Ball, D.L., Dubowski, D.M., Spradlin, T.J. Inclusion of Forging Residual Stresses in Large Component Structural Design. In: *Proceedings of the 2016 Aircraft Structural Integrity Program (ASIP) Conference*. San Antonio: 2016.

[164] Prime, M.B., Gonzales, A.R. Contour Method: Simple 2-D Mapping of Residual Stresses. In: *Proceedings of the 6th International Conference on Residual Stresses*. Oxford: IOM Communications; 2000: 617 - 624

[165] Prime, M.B. Cross-Sectional Mapping of Residual Stresses by Measuring the Surface Contour after a Cut. J. Eng. Mater. Tech. 2001;123: 162 – 168.

[166] Toparli, M.B., Fitzpatrick, M.E. Development and Application of the Contour Method to Determine the Residual Stresses in Thin Laser-Peened Aluminum Alloy Plates. Exp. Mech. 2016;56: 323 – 330.

[167] Hosseinzadeh, F., Kowal, J., Bourchard, P.J. Towards Good Practice Guidelines for the Contour Method of Residual Stress Measurement. J. Eng. 2014;doi: 10.1049/joe.2014.0134: 1 – 16.

[168] Rumsey, D.J. *Statistics for Dummies*, *2nd Edition*, Hoboken: Wiley Publishing, Inc.; 2011.

[169] Tuegal, E.J., Babish, C.A. Continuing Airworthiness and the Airframe Digital Twin.

In: *Proceedings of the NATO AVT-222 Workshop: Contining Airworthiness of Ageing Aircraft Systems*, Brussels: 2014.

[170] Warner, J. W. *Cold Expansion Effects on Cracked Fastener Holes under Constant Amplitude and Spectrum Loading in the 2024-T351 Aluminum Alloy*. Masters Thesis, Mechanical Engineering Department, University of Utah, Salt Lake City: 2011.

[171] Newman, J.C., Daniewickz, S.R. Predicting Crack Growth in Specimens with Overloads and Cold-Worked Holes with Residual Stresses. Eng. Frac. Mech. 2014;27: 252 – 266.

[172] Ozdemir, A.T. *Residual Stresses and Fatigue Performances at Cold Expanded Fastener Holes*. Ph.D. Thesis, The Open University, Milton Keynes: 1993.

[173] Warner, J.W., Clark, P.N., Hoeppner, D.W. Cold Expansion Effects on Cracked Fastener Holes under Constant Amplitude and Spectrum Loading in the 2024-T351 Aluminum Alloy. Int. J. of Fatigue. 2014;68: 209 – 216.

[174] Vallieres, G.M., Duquesnay, D.L. Fatigue Life of Cold-Expanded Fastener Holes with Interference-Fit Fasteners at Short Edge Margins. Fatigue Fract. Engng. Mater. Struct. 2014;38: 574 – 582.

[175] Andrew, D.L, Clark, P.N., Hoeppner, D.W. Investigation of Cold Expansion of Short Edge Margin Holes with Pre-Existing Cracks in 2024-T351 Aluminum Alloy. Fatigue Fract. Engng. Mater. Struct. 2013;37: 406 – 416.

[176] Carlson, S.S., Stanfield, M. Application of Uncertainty Quantification for Residual Stress Measurements at a Cold Expanded Hole. In: *Proceedings of the 2016 AFGROW Workshop*. Layton: 2016.